SSD19

19TH INTERNATIONAL CONFERENCE ON SOLID STATE DOSIMETRY

ABSTRACTS

HIROSHIMA, JAPAN

Conference Sep 15-20, 2019

Dosimetric Consideration for Children in Radiation Therapy and Diagnosis

Saveta Miljanić
Ruđer Bošković Institute, Zagreb, Croatia

Highlights There is well established evidence that radiation therapy is making a crucial contribution to long-term survival of childhood cancers, but it is also causing a high evidence of secondary cancers among survivors of childhood cancer. The measurement of out-of-field doses (including concomitant imaging doses) for paediatric population is important for input to epidemiological studies and risk estimations.

Key words paediatric radiotherapy, out-of-field dose, epidemiological studies,

Background and Objectives The introduction of advanced techniques and technology in radiotherapy (RT) has greatly improved ability to deliver highly conformal tumor doses while minimizing the dose to adjacent organs at risk. Despite these huge improvements, there remains a general concern about doses to normal tissues that are not the target of the radiation treatment. Treatment planning systems (TPSs) become highly inaccurate outside the treatment field necessitating a measuring or some other means of assessing the dose[1)]. Progres in cancer therapy for children have produced impressive prospects for long term survival. As shown in Figure 1, for example, five-year survival for all childhood cancers has increased from 40% during 1971-1975 to 82% during 2006-2010 in Great Britain. As patients live longer after treatment the complication of great concern is the risk for developing a second malignancy, which can develop years or decades after treatment. The incidence of second cancers is much higher in children, due to three major factors[2)]: First, children are more sensitive to radiation-induced cancer than are adults by a factor of at least 10. Second, stray radiation is more serious for children than for adults, simply because of the small body of the child. Third, the question of genetic susceptibility arises because many childhood cancers involve a germline mutation that may confer susceptibility to radiation-induced cancer.

Epidemiological studies have shown that some late malignancies can develop in tissues located in the field and also out-of-field and a complete dose specifications primarily to paediatric and young adult treatment is needed. The complete dose description (the synthesis of therapy and imaging doses from all the treatment and imaging modalities) is ideally required. Out-of-field (stray radiation) doses are required for a complete description of organ doses to radiotherapy patients for estimation of risks of second cancer and other late effects.[3)]

The new modalities of photon therapy treatment delivery, such as Intensity Modulated Radiotherapy (IMRT) and Tomotherapy, have the advantages of a more conformal target dose distribution therefore come at a cost of a higher dose "radiation bath", where radiosensitive organs and tissues remote from the target volume may receive doses sufficiently large to lead to a significant probability of cancer induction. Furthermore, there is increasing use of imaging techniques for both verification and fraction-by-fraction guidance of dose delivery (image guided radiotherapy – IGRT), involving repeated computed tomography (CT) imaging throughout the course of treatment, using kilovoltage or megavoltage x-rays. Finally, proton radiotherapy and ion beam facilities are now available and the same rationale for the determination of out-of-field doses for this modality applies.

For input to epidemiological studies complete dose description is employed. These data will also be important in the development, testing and validation of analytical models for calculating out-of-field doses. Such models are useful since it is impracticable to measure ou-of-field doses under all possible combinations of treatment parameters. Accordingly, epidemiological studies and mathematical models of out-of-field doses demand increasingly comprehensive dosimetry throughout the body.[4)]

Out of field and concomitant imaging doses In photon radiotherapy, doses outside the target volume are caused by (i) scatter from the main beams within the patient (ii) scatter from the collimators and (iii) leakage radiation from the accelerator treatment head. At effective accelerating potentials of >8 MV, fast neutrons are also produced in the treatment head and enhance out-of-field doses. Sources of out-of-field doses are described in details in AAPM TG-158[1)]. In proton therapy (generally hadron therapy) there is a fundamental difference between the passive scattering beam lines and the scanning beam lines in terms of out-of-field dose. In passive beam delivery systems there are a number of filters and collimators in which secondary radiation is produced, while in active scanning systems, beam interactions with the patients themselves are in principle the only significant of secondary radiation.[5)]

Numerous studies of out-of-field dose measurements are now available. In AAPM TG-158[1)] data presented were combined from several investigations to identify different regions of out-of-field doses (with the references of others overviews for measured and calculated data).

On the other hand, paediatric studies that report out-of-field organ doses are rare and EURADOS WG9 (Radiation Dosimetry in Radiotherapy) has organized the multi-centre study of out-of-field doses determination in paediatric radiotherapy treatments, using various photon and proton radiotherapy techniques.

Although imaging diagnostic dose is not generally considered part of stray RT doses, its presence is highly relevant to out-of-field dose; it is rapidly increasing and causing concern for

long-term risk in the population. In most cases imaging during therapy accounts for less than 20% of the stray therapeutic radiation, but with the extensive applications of IGRT with daily portal imaging or cone-beam CT using MV X-rays, whole body exposures, whole-body exposures of up to 100 mGy per day are possible, thus exceeding those caused by scattered radiation from the therapeutic beam.[3)]

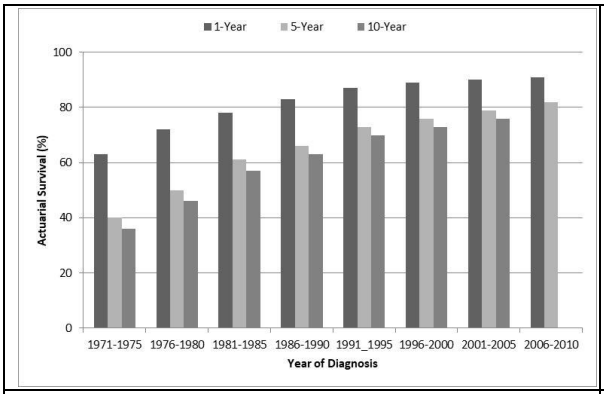

Figure 1. One-, five- and ten year survival for all childhood cancers in children (aged 0-14), UK, (Source:Cancer Research UK https://www.cancerresearchuk.org/)

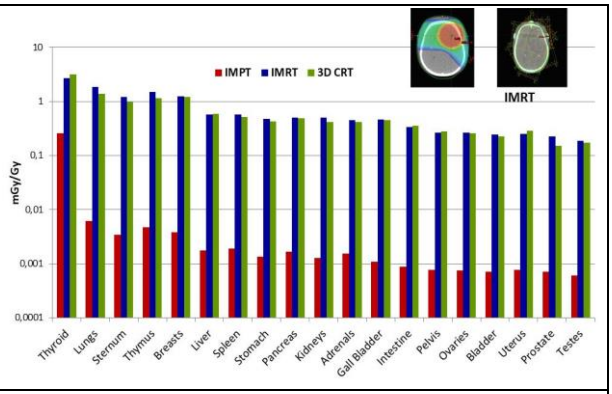

Figure 2. Comparison of the photon organ doses for proton (IMPT) and photon beams (IMRT, 3D CRT) for spherical brain tumour with a diameter of 6 cm measured in 10 year phantom.

EURADOS WG9 measurements campaigns For photon RT, dosimeters were irradiated at the Maria Sklodowska-Curie Memorial Institute of Oncology using 6 MV photon beams for Intensity Modulated Radiotherapy (IMRT) and 3D Conformal Radiotherapy (3D CRT). In Zagreb, dosimeters were irradiated by Gamma Knife in the Clinical Hospital Centre Zagreb and craniospinal irradiation in University Clinical Hospital Sestre milosrdnice, Zagreb (3D-CRT, 6 MV photon beam for brain and 6 MV+18 MV for spinal cord). For proton therapy the Intensity Modulated Proton Therapy (IMPT) using pencil beam scanning was accomplished at the Bronowice Cyclotron Centre in Krakow (IBA Proton Therapy System-Proteus 235). In all treatments (except craniospinal) a spherical brain tumour with a diameter of 6 cm was simulated. For organ dose measurements CIRS anthropomorphic phantoms (5 and 10 year-old and additional 1 year old in proton irradiation) were used.

Several types of dosimeters from different institutions were applied: thermoluminescent, LiF based MTS-7 and MCP, optically stimulated luminescent, OSL type Luxel and radiophotoluminescent, RPL types GD-352M and GD-302M. In proton therapy additionally MTS-6, bubble detectors and PADC track detectors were used for neutron dose evaluation.

Some EURADOS results of out-of-field dose measurements and analysis for paediatric RT have already been published[4),6),7)] and presented[8)] and some others are in preparation.
As an example in Figure 2. comparison of the photon organ doses for proton (IMPT) and photon beams (IMRT, 3D CRT) is shown for 10 year phantom[8)].

Conclusion Radiotherapy gives us the opportunity to study late effects of human irradiation in a very large worldwide patient cohort, with planned, controlled and documented irradiations and a wide range of doses to out-of-field organs from approximately 10 mGy–60 Gy. The basic technology for whole body dosimetry is available, with established, commercially available anthropomorphic phantoms and established dosimetry. Out-of-field dosimetry in anthropomorphic phantoms can be time consuming and limited to a relatively few clinical treatment reconstructions, bearing in mind the very large number of clinical treatment possibilities. However, some simplification of dosimetry methodology is possible and proposed[4)].

References

1) Kry, F. et al., 2017. AAPM TG 158: Measurement and calculation of doses outside the treated volume from external-beam radiation therapy. Med. Phys. 44, 391-429.
2) Hall, E. J., 2006. Intensity modulated radiation therapy, protons, and the risk of second cancers. Int. J. Radiation Oncology Biol. Phys.65, 1-7.
3) Newhauser, W. D., Durante, M., 2011. Assessing the risk of second malignancies after modern radiotherapy. Nature Reviews/Cancer, 11, 438-448.
4) Harrison, R., 2017. Out-of-field doses in radiotherapy: Input to epidemiological studies and dose-risk models. Physica Medica. 42, 239-246.
5) Nuclear Physics European Collaboration Committee (NuPECC), Report 2014: Nuclear Physics for Medicine.
6) Majer, M. et al., 2017. Out-of-field dose measurements for 3D conformal and intensity modulated radiotherapy of a paediatric brain tumour. Radiat. Prot. Dosim. 176, 331-340.
7) De Saint-Hubert, M. et al., 2018. Out-of-field doses in children treated for large arteriovenous malformations using hypofractionated gamma knife radiosurgery and intensity-modulated radiation therapy. Radiat. Prot. Dosim. 181, 100-110.
8) Miljanić, S. et al., 2016. Whole body doses from photon and proton radiotherapy of brain tumors in paediatric patients. Proceedings of the 11th International Workshop on Ionizing Radiation Monitoring, Takayoshi Y. (ed). Oarai: Chiyoda Technol Corporation. 251-259.

Quantum Radiation Imaging for Biomedical Applications

Hiroyuki Takahashi
Institute of Engineering Innovation, School of Engineering, The University of Tokyo, Tokyo 113-8656, Japan

Highlights Positron emission tomography and other radiation imaging techniques provide biological functions and molecular information. We are developing new sensor technologies and studying new imaging methods, which can be used for new cancer diagnostics and high-resolution tracer imaging, as well as new dosimetry applications.

Key words radiation, scintillation detectors, imaging, time over threshold method

Background and Objectives Gamma-ray diagnostics methods such as PET and SPECT have been used for long time. However, the spatial resolution of the conventional gamma-ray imaging system suffers from limitations arising from both the detector and frontend circuit. Therefore, we plan to overcome the difficulty by developing a novel detector and frontend electronics. Furthermore, we are now challenging a new diagnostic method using a coincidence method [1].

Materials and Methods We plan to improve spatial resolution of the gamma-ray imaging techniques and develop a compact Time-over-Threshold (ToT) signal processing system. In principle, ToT system can be applied to any kind of spectroscopy system and it directly converts analog signal into a digital signal through a single stage comparator. Although the nornal ToT method suffers from linearity, recently we invented the dynamic Time over Threshold method, which can be a general-purpose spectroscopy detector. We assembled and fabricated a prototype system. And the details of the system and performance will be provided. Recently we introduced a new concept of temporal/spatial correlation type tomography method based on incident angular resolving detectors such as electron-tracking type gamma cameras which can identify incident gamma-ray direction. This tomography method utilizes the correlation between multiple photons and provides the radioactivity concentration in the body with high resolution, high sensitivity, and high signal to noise ratio. We will study basic characteristics of this revolutionary gamma-ray imaging approach and try to fabricate a hemisphere scanner and explore the new principle. We plan to demonstrate molecular imaging with the In-111 labelled peptide through the two photon emission nuclide detection scheme (we call this DPECT) for establishing a new gamma-ray diagnostic technique for the multiple

gamma photon emitting nuclide such as Sc-44. Establishment of a novel gamma-ray imaging principle and high-resolution molecular imaging beyond PET. Fig.1 shows a comparison between imaging methods.

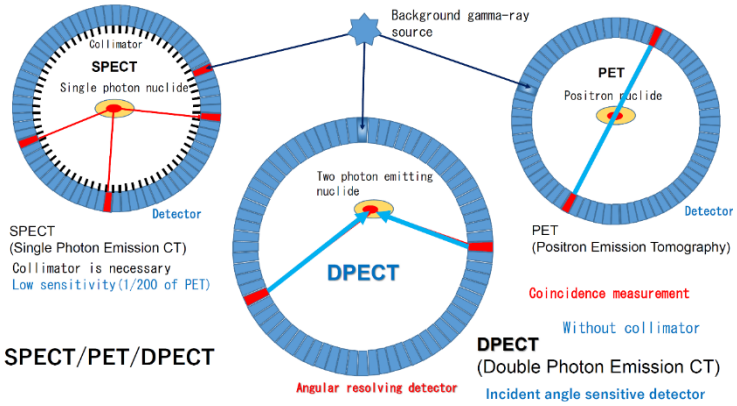

Figure 1 Comparison of SPECT/PET/DPECT

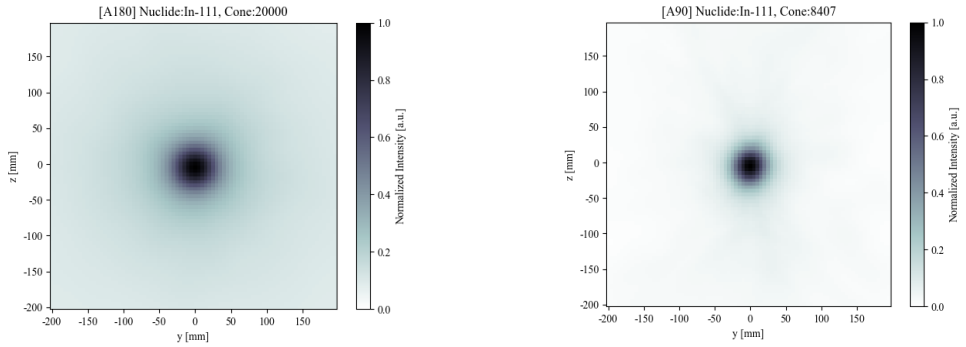

Figure 2. Synthesized Compton camera images without coincidence (left) and with coincidence (right).

Results and Discussion PET requires 10^6 line of responses (LORs). Figure 1 shows a simulation result about two Compton camera images. A synthesized coincident image is greatly improved.

Conclusion Even one event provides one drug position in case if we use electron tracking method. This implies a very high sensitivity of molecular imaging. Hopefully, this method can also be used for radioisotope identification and dosimetry.

References

1) Shimazoe, K. et al.: Double Photon Emission Coincidence Imaging using GAGG-SiPM pixel detectors, JOURNAL OF INSTRUMENTATION, vol.12, C12055, DEC 2017

External Dose-Rate Measurements Based on Smartphones CMOS sensors

Alessia Mafodda[1]*, Clemens Woda[1]
[1] *Helmholtz Zentrum München, Institute of Radiation Medicine, Neuherberg, Germany*

Highlights Main goal of this scientific investigation is the characterization of two applications ("RadioactivityCounter and "GammaPix") that enable dose-rate measurements with an ordinary smartphone, using the CMOS sensor of the built-in camera as a radiation detector.

Key words External dosimetry, smartphone application, dose-rate measurements, citizen measurements, nuclear emergency

Background and Objectives Technological enhancement in personal devices such as the new generation smartphones contributed to enable lay people to conduct their own radiation measurements. In fact, there are some applications available on the market that turn a smartphone into a dose-rate meter using the Complementary Metal Oxide Semiconductor (CMOS) sensor of the camera as a radiation detector. The working principle behind is that CMOS sensor is sensitive to visible light but can detect ionizing radiation when shielded with adhesive black tape[1)]. After covering the camera, the user may run a measurement that consists of a video record where every interaction of radiation (photons) with the chip is observed as an intense signal in a certain pixel (bright spot). The dedicated software analyses each video frame by counting the number of spots, and the sum of detected particles in selected time periods is given as number of counts. Two widely spread applications, available for both Android and iOS operating systems, were considered useful for testing: "GammaPix" (full version) and "RadioactivityCounter". In order to assess the reliability of data produced by such apps, determination of the dynamic range, response time, dose-rate responses, characterization of energy and angular dependence are outlined. The present work is carried out in the framework of the project CONFIDENCE („COping with uNcertainties For Improved modelling and DEcision making in Nuclear emergenCiEs ") within the Joint European Project CONCERT.

Materials and Methods The experiment has been carried out on 14 different smartphone models in order to investigate the variability in sensitivity of the CMOS sensor and the quality of app-specific calibration values. Irradiations were performed at room temperature at the

Secondary Standard Dosimetry Laboratory of the Helmholtz Zentrum München (HMGU) with calibrated ^{137}Cs and X-ray sources, the latter with ISO narrow spectrum qualities from N30 to N300.

Results and Discussion More efforts were put into evaluating the "RadioactivityCounter" app since "GammaPix" resulted in underestimating the nominal reference values on most of the phones by at least an order of magnitude. Dose-rate responses were investigated from 2 to 1000 μGy h^{-1} and were influenced by the noise level of the camera sensors. In fact, a distinction can be drawn between models showing a low counting threshold value n ($n<10$) and those with high n values ($n>10$). A low noise level often characterized phones in the high price range (over 200 €) and equipped with camera of good quality, with just one cheap model as exception. Phones with $n<10$ have shown a linear trend in dose-rate responses starting from 5 μGy h^{-1}, and extending the integration time to one hour resulted in slightly improve the linearity also at low dose-rates (down to 2 μGy h^{-1}). However, during such long time measurements, many "zero" values were recorded leading to an overall very skewed distribution in counts. On the other hand, phone models with noise level higher than 10, showed a linear trend in dose-rate responses from 50 μGy h^{-1}, suggesting that the sensor optical specifications are not optimized for detecting ionizing radiations at low dose-rates. Even though these phones resulted to be "blind" below that threshold, one minute based counts were more normally distributed. If assessing the background in a low dose-rate, shielded environment leads to an improvement in detecting dose-rates lower than 10 μGy h^{-1} is currently investigated and will be discussed. Characterization of the energy dependence of the CMOS sensor was performed for all phone models: a strong over-response of up to a factor of 15 for a photon energy of around 60 keV was observed. In addition, the relative response of the back and front camera was compared for four models, leading to the conclusion that there was no difference in the response when either camera sensor was facing the source. Further investigations were performed on four phones irradiated from different angles and data showed an overall variation of the measured signal at maximum about 10%, whereas a sharp decrease in the detector response was observed for an angle of incidence of 90°.

Conclusion Based on the results obtained so far, reliable measurements at natural environmental radioactivity level are difficult to assess with most of the phones tested, while high level of contamination could be identified.

References

1) O. Van Hoey et al. 2016. Radiation Protection Dosimetry 168, 314-321

Entrance surface dosimetry with radiophotoluminescent polymer films

F. d'Errico[1,2], L. Abegão[2], S. O. Souza[3], A. Chierici[1,2], L. Lazzeri[1],
M. Puccini[1], S. Vitolo[1], Y. Miyamoto[4], H. Nanto[5], T. Yamamoto[4]
[1]*Università di Pisa, Scuola di Ingegneria, Pisa, Italy*
[2]*Yale University, School of Medicine, New Haven, CT - USA*
[3]*Universidade Federal de Sergipe, São Cristovão, SE - Brazil*
[4]*Oarai Research Center, Chiyoda Technol Corporation, Oarai, Ibaraki, Japan*
[5]*Kanazawa Institute of Technology, Nonoichi, Ishikawa, Japan*

Highlights Thin polymer films loaded with luminescent materials have been developed for entrance surface dosimetry in radiation protection and clinical applications. Most notably, the films can be shaped as gloves and measure extremity doses without interfering with the tactile sense. Their photon energy dependence improves when worn under shielding gloves.

Key words thin dosimetric films, extremity dosimetry, radiophotoluminescence

Background and Objectives In a wide international cooperation, thin dosimetric films are developed for radiation protection and clinical dosimetry applications. After initial attempts to manufacture weavable fibers for textiles, our efforts focused on thin membranes[1)]. These were initially produced with a solvent-evaporation technique, which required careful selection of organic solvents in order to avoid affecting the luminescent properties of the dispersed grains. Currently, tissue-equivalent polyethylene films are used to embed a variety of luminescent materials, particularly radiophotoluminescent (RPL) glass grains[2)].

Materials and Methods Our film manufacturing technique relies on either pressure casting or bubble blowing of linear low-density polyethylene LLDPE/RPL blends. RPL grains and LLDPE are pre-mixed and sent through a co-rotating twin-screw extruder producing a homogenized filament. The latter is then quenched by cool-air blowing and cut into small pellets. In order to produce films, pellets are then either compressed at high temperature (>100 °C) and high pressure (>100 bar) between two metal plates lined with Teflon, or they are molten, extruded through a die and inflated to form a thin film bubble. Results presented here refer to thin cast sheets containing dispersed grains of RPL glass. The equipment used for the readout of the films is a laboratory system comprising a high-intensity LED source of UV radiation, optical lenses and filters, spectrometer, power meter, and a silicon-photomultiplier.

Results and Discussion Our first tests involving RPL grains dispersed in thin polyethylene layers confirmed that the grains retain their luminescence properties, as shown in Figure 1.

However, our readout system is not optimal and it detects light scattered by the polyethylene film. The use of Chiyoda Technol equipment is expected to fully resolve this issue.

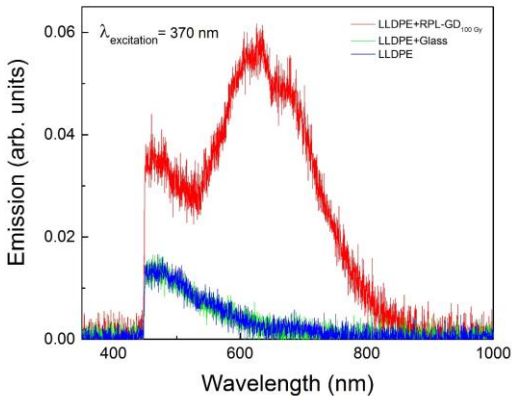

Figure 1. Emission of RPL-loaded films and films with plain glass or no glass.

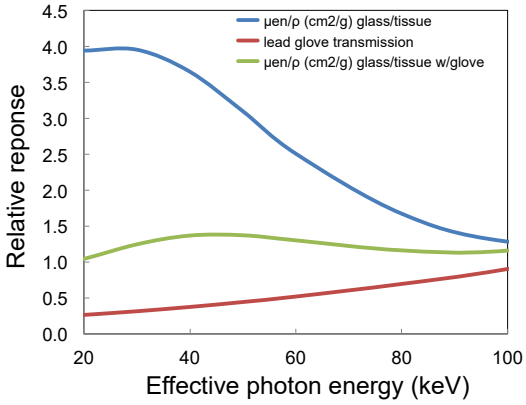

Figure 2. Filtering action of shielding gloves reducing the over-response.

Our films with dispersed RPL grains can be shaped in the form of thin gloves and worn by interventional radiologists under the protective gloves they usually wear for shielding and to prevent biological contamination. These protective gloves are doubly beneficial for RPL dosimetry: first, the filtering action of the gloves compensates for the over-response of unfiltered RPL glass to low energy photons (Figure 2).; moreover, they also thermally insulate the RPL grains keeping them at body temperature and thus expediting signal buildup.

Conclusion Our thin films may significantly impact extremity dosimetry, particularly in interventional radiology. A major advantage of the films is that they do not affect the tactile sense of radiologists, contrary to the use of dosimeter chips on their fingertips. Additional applications are possible in clinical radiation therapy dosimetry. For example, patient entrance doses from high-energy electrons used in Intraoperative Radiation Therapy (IORT) can be recorded by replacing the membranes placed at the end of the IORT applicators with RPL films. In addition, the polyethylene base of the film can be loaded with appropriate lithium or boron compounds in order to make the RPL grains respond to slow neutrons. In particular, if boron compounds are used, films can be used to measure the “boron dose” delivered to patients undergoing melanoma treatments with Boron Neutron Capture Therapy.

References

1) Souza SO, d'Errico F, Azimi B, Alves AVS, Valença JVB, Barros VSM, Cascone MG, Lazzeri L. OSL films for in-vivo entrance dose measurements. Rad Meas. 2017; 106: 643.
2) Yamamoto T. RPL Dosimetry. AIP Conf Proc 2011; 1345: 217.

How to Use Active Personal Dosemeters in Interventional Fields in Hospitals: Results from Laboratory and Workplace Field Tests

F. Vanhavere[1], E. Carinou[2], I. Clairand[3], O. Ciraj-Bjelac[4], M. Ginjaume[5], O. Hupe[6], Z. Knezevic[7], M. Sans Merce[8]

[1]*SCK-CEN, Belgian Nuclear Research Centre, Mol, Belgium*

[2]*Greek Atomic Energy Commission, EEAE, Agia Paraskevi, Attiki, Greece*

[3]*IRSN, Institute for Radiological Protection and Nuclear Safery, Fontenay-Aux-Roses, France*

[4]*Vinca Institute of Nuclear Sciences, University of Belgrade, Belgrade, Serbia*

[5]*UPC, Universitat Politècnica de Catalunya, Barcelona, Spain*

[6]*Physikalisch-Technische Bundesanstalt (PTB),38116 Braunschweig, Germany*

[7]*Ruder Boscovic Institute RBI, Zagreb, Croatia*

[8]*CHUV, Centre Hospitalier Universitaire Vaudois, Lausanne, Switzerland*

Highlights A series of tests have been performed on active personal dosemeters (APD), with the emphasis on their use in interventional radiology/cardiology radiation fields. The results lead to some recommendations and attention points, mainly focused on the influence of pulsed fields and the lead apron backscatter.

Key words radiation, dosimetry, medical staff, personal dosemeters, pulsed radiation

Background and Objectives Considering that occupational exposure in medicine is a matter of growing concern, active personal dosemeters (APD) are increasingly used. During the European ORAMED project(1), several APDs were tested specifically for the use in hospitals. New facts and developments have become available during the last decade, including new types of dosemeters and standardization of tests for pulsed radiation fields. Therefore, it was decided within EURADOS WG12 to perform a new study. This paper will give an overview of the tests performed, and on the recommendations that resulted from these tests.

Materials and Methods The outline of the work plan included the following actions:

1. To perform an extensive survey to collect all relevant issues for the use of APDs in medical imaging applications of ionising radiation (2).
2. To perform a series of tests of APDs in standard continuous and pulsed fields.
3. To test the influence of lead aprons on the calibration and use of APDs (3).
4. To perform tests in hospitals with fixed set-ups using interventional equipment, and with medical staff wearing APDs together with reference passive dosemeters.

Results and Discussion

Results of task 1 are already published (2). This survey revealed several difficulties linked to

the use of APDs, in particular regarding their reliability in pulsed X-ray fields widely used in hospitals. For task 2, the dose rate linearity for pulsed radiation was determined by performing measurements at the pulsed X-ray facility of PTB, Braunschweig, Germany. It is noticeable that all dosemeters show a worse measurement behaviour when the dependence on the dose rate is determined with pulsed or continuous radiation. These measurements have shown that the manufacturers' data regarding the measuring ranges of a dosemeter are only valid for continuous radiation. For task 3, it was found that, for passive dosemeters, the influence on the dosemeter's response to the lead or lead equivalent was within the range 15%–38% for the x-ray qualities. This effect is smaller, of the order of 10%, when lead-free garments are used, and much smaller, within 1%–10%, for most of the APDs used in the study. For task 4, a selection of APDs was irradiated in the pulsed reference fields at PTB and in realistic exposure scenarios at the Städtische Klinikum Braunschweig. In many exposure situations, the response of the APDs was within 20 % of the reference dose value. We also tried to have an overview of differences between active and passive dosimetry in routine practice in hospitals, where all kinds of procedures and parameter settings are used and without an accurate knowledge of the field parameters. This was done for 3 types of APDs, comparing the results of the active and passive devices. From our tests we can conclude that comparing active and passive dosemeters is not straightforward in routine operations. In our experiments we found that APDs show consistently lower values than passive dosemeters during standard IR/IC procedures.

Conclusion From all these tests, a series of conclusions could be drafted, including:

- The APDs that are to be used in hospitals must be chosen taking into account their characteristics to be adequate for the intended use.
- If the dosemeter is to be used in pulsed fields, the user must be aware that the dosemeter may indicate incorrect values. Large underestimations can take place in direct and even in scattered beams, with more influence the higher the instantaneous dose rate.

References

1) Use of Active Personal Dosemeters in Interventional Radiology and Cardiology: Tests in Laboratory Conditions and Recommendations – ORAMED Project, Clairand, I, et al., Rad. Meas. Volume 46 (11), 1252-1257, 2011.
2) Use of Active Personal Dosemeters in Hospitals: EURADOS survey, Ciraj-Bjelac O. et al., Journal of Radiological Protection, Volume 38 (2), 702-715, 2018.
3) Effect of the radiation protective apron on the response of active and passive personal dosemeters used in interventional radiology and cardiology, M. Ginajume, et al. J. Radiol. Prot. Volume 39, 97–112, 2019.

EURADOS Intercomparison for Calibration Methods using KIT *H**(10) Area Dosemeters

C. Naber[1]*, H. Dombrowski[2], C. Hranitzky[3]
[1]*Karlsruhe Institute of Technology, 76344 Eggenstein-Leopoldshafen, Germany*
[3] *Physikalisch-Technische Bundesanstalt, 38116 Braunschweig, Germany*
[2]*Seibersdorf Labor GmbH, 2444 Seibersdorf, Austria*

Highlights The international intercomparisons for calibration methods of passive dosemeters IC2017calm and IC2018calm were organized by EURADOS to study the precision of calibrations of participating dosimetry services and institutes.

Key words EURADOS, intercomparison, calibration, TLD, area dosemeter

Background and Objectives In 2017 and 2018, the intercomparisons for calibration methods of passive dosemeters IC2017calm and IC2018calm were organized by the European Radiation Dosimetry Group (EURADOS) within the working group for environmental dosimetry (WG3). The accredited dosimetry laboratory of the Karlsruhe Institute of Technology (KIT) was chosen as coordinating laboratory. Their *H**(10) TLD dosemeters were provided to the participating institutes. The German national metrology institute Physikalisch-Technische Bundesanstalt (PTB) was the reference laboratory by performing the reference irradiations within the same strict time schedule as the participants to establish the traceability to PTB's primary standards.

Materials and Methods The coordinator supplied 10 dosemeters to each participant together with an irradiation form to gather basic data. The KIT area dosemeters are made of PMMA with a spherical outer shape. Two TLD-700 thermoluminescence detector chips are located at the center of the dosemeter. Because of this geometry, this dosemeters have an isotropic angular response. The participants were asked to irradiate 5 dosemeters with 3 mSv (in 2017) and 10 mSv (in 2018) in terms of ambient dose equivalent, *H**(10). The radiation quality to be used was Cs-137 gamma radiation which is most widely utilized for dosemeter calibrations. 5 dosemeters were not supposed to be irradiated and served to measure the transport dose. To limit the transport dose, the irradiations had to be carried out within a pre-defined period of time. After returning the dosemeters to the coordinator, all dosemeters were read out at the same time with a TOLEDO 654 reader to minimize systematic sources of uncertainty. This strict procedure was required to finally neglect fading influences.

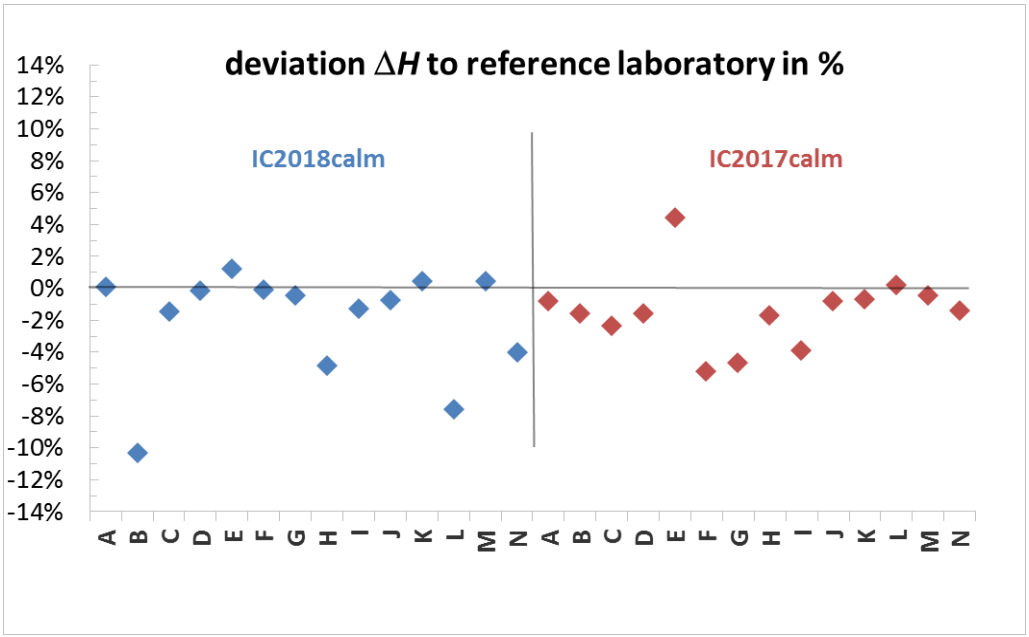

Figure 1. Results of all participants (anonymous reporting numbers according to the certificates) of the intercomparisons IC2017calm and IC2018calm.

Results and Discussion 14 institutions participated in IC2017calm and also 14 institutions participated in IC2018calm, whereby approximately half of them participated in both intercomparisons. For each participant the relative deviation of the reported irradiation dose and the actually measured dose were quoted in a EURADOS certificate. Almost all participants' results were within an acceptable range of -10 % to +10 % around the reference value. About two third of the participant's results deviated by no more than 2.5 % from the reference value, which is based on the PTB calibration irradiations.

Conclusion Both intercomparisons showed similarly good results of the precision of the calibrations of the participating European dosimetry services and institutes. It is planned to perform another intercomparison in 2020 with an extended programme.

A new sensitization method combining CO_2 and UV treatments in a two-phase etching protocol for improved neutron dosimetry with CR-39 track detectors

Daniel A. A. de Vasconcelos[1]*, Riccardo Ciolini[1], Francesco d'Errico[1,2].
[1]*Università di Pisa, Scuola di Ingegneria, Largo Lucio Lazzarino 1, Pisa, Italy*
[2]*Yale University, School of Medicine, New Haven CT 06511, USA*

Highlights Under optimized conditions, CO_2 and UV treatments combined in an original two-phase etching technique increase the total number of tracks by more than 230 % in nuclear track detectors, and the maximum diameter of the tracks by more than 60 %, compared to the standard routine processing.

Key words CR-39, CO_2 treatment, UV treatment, neutron dosimetry, two-phase etching.

Background and Objectives CR-39 is a widely used etched-track detector, however it still presents limitations that require R&D. Particularly difficult is counting automatically the smallest recoil proton tracks, which can be erased by chemical etching procedures due to their limited dimensions[1)]. In this context, detector processing techniques yielding tracks of larger sizes are extremely valuable and warrant further investigation.

In this work, we combined two common sensitization techniques, a post-irradiation treatment with CO_2 under pressure and a UV exposure treatment, in a two-phase etching technique. The main idea was to partially open the tracks, with an optimized CO_2 treatment, before the first etching, allowing UV light to interact directly with the inner walls of the track, hoping to thus enhance the effects of the UV treatment. Then, after the UV treatment, a second etching concludes the process.

Therefore, this study proposes an original approach, combining both sensitization treatments and a two-phase etching technique in order to obtain a "super-additive" effect.

Materials and Methods To investigate this hypothesis, 10 x 10 mm^2 CR-39 plates manufactured by Radosys® Ltd were irradiated on phantom using a ^{241}AmBe neutron source, delivering a $H_p(10)$ of 1 mSv. Fast neutron converter sheets of high-density polyethylene were used. The procedure was divided in 4 steps: 1) CO_2 treatment under a partial pressure of 2.4 MPa for 16 h, 2) first etching lasting 1, 2 or 3 h, 3) 254 nm UV exposure for 48 or 72 h, and 4) final etching of 3, 2, or 1 h (the total etching time was always 4 h). The detectors were etched in a Radosys® Nano etching unit in a 6.25 N solution of NaOH kept at 90 °C. The track analysis

was performed on a Radosys® Radometer 2000 track reader.

Results and Discussion Figure 1a and Figure 1b show the results of the 48 h and 72 h UV treatments, respectively. For both treatments, an increased time of the first etching also increases the total number of tracks, while the range of track sizes remains the same. The two regions where the number of tracks increased the most, are virtually the same for both treatments, with peaks at around 16-18 µm and 24-26 µm. One of the 72 h UV treatments was not displayed because it created deformed tracks that could not be measured.

Figure 1c shows a comparison between the best treatment condition we found, the routine treatment followed by Radosys Ltd. (CO_2 treatment under pressure of 0.6 MPa for 6 days) and the CO_2 treatment conditions used in this work, alone. All were done with a total etching time of 4 h. The two-phase etching technique increased the total number of tracks by up to 230% and their maximum diameter by around 60%.

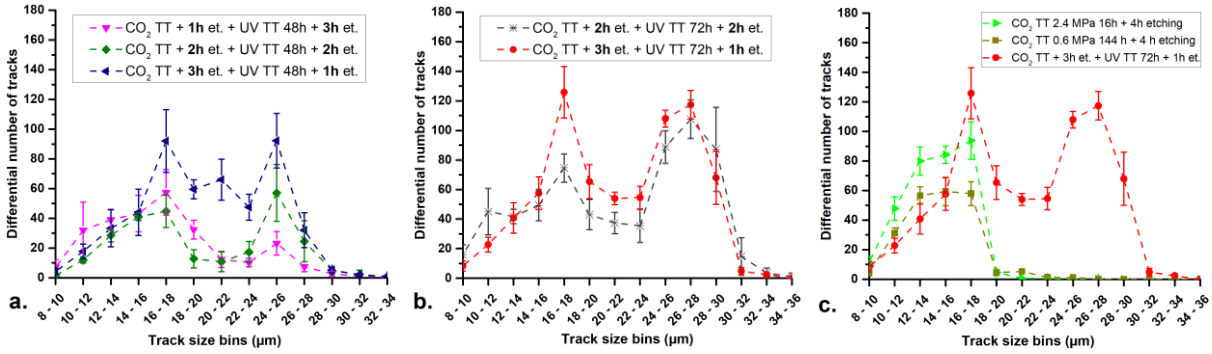

Figure 1. Differential track size distributions of the two-phase etching technique for a UV treatment of a. 48 h and b. 72 h, and the c. comparison between our best treatment condition, the routine approach followed by Radosys and a CO_2 treatment alone, with the conditions used in this study.

Conclusion In this work, we developed an original sensitization method combining CO_2 and UV treatments in a two-phase etching technique that increases both the total number of tracks and their maximum diameter significantly, when compared to the routine treatment protocol followed by Radosys. This method can be used for improved neutron dosimetry and, ultimately, we believe for full scale neutron spectrometry applications and LET-based spectrometry of cosmic radiation.

References

1) Hulber, E., Selmeczi, D., 2005. Counting recoil proton tracks on PADC without a pre-etching step. A novel approach for neutron dosimeter application. Radiat. Meas. 40, 616–619.

Extending information relevant for personal dose monitoring gained from glow curves of passive solid state dosemeters using artificial neural networks

Florian Mentzel[1]*, Kevin Kröninger[1] , Lars Röhrig[1], Luisa Speicher[1],
Marie-Luise Steil[2], Robert Theinert[1], Jörg Walbersloh[3]

[1]*Lehrstuhl für Experimentelle Physik 4, TU Dortmund, Germany*
[2] *Leibnitz-Universität Hannover, Germany*
[3]*Materialprüfungsamt NRW, Germany*

Highlights We present studies using artificial neural networks to investigate the time- and temperature-resolved photon counts from thermoluminescence dosemeters that can yield accurate information not only about the irradiation dose, but also about the time of the irradiation, the number of irradiation fractions and the radiation type. Applied to personal dose monitoring, this introduces additional value to the use of passive dosemeters.

Key words personal dose monitoring, glow curve analysis, artificial neural networks, fading time analysis

Background and Objectives The analysis of glow curves from thermoluminescence dosemeters is subject to extensive investigations in the field of solid state dosimetry [1]. The *Lehrstuhl für Experimentelle Physik 4* at the *TU Dortmund University* develops, in cooperation with the *Materialprüfungsamt NRW*, multivariate glow curve analysis techniques using artificial neural networks (ANNs). This approach allows for the extraction of information far beyond the estimation of the irradiation dose, e.g. the time of the irradiation, the number of irradiation fractions within the monitoring interval and the radiation type. This additional information can add a great value to passive dosimetry in the future.

Materials and Methods The detectors used are produced by the *Materialprüfungsamt NRW* based on LiF:Ti,Mg for their monitoring service [2]. Our investigations are based on both, measurement data and artificial glow curves from empirical simulations using parameter interpolation [3]. In total, more than 3,500 measured glow curves and over 100,000 simulated glow curves are used for the training of the ANNs. Throughout the studies, ANNs as described in Ref. [4] are used for a multivariate analysis of measured and simulated glow curves. We present results obtained using the described data and ANNs including brief information about

the optimization process and performance comparisons with alternative algorithms, e.g. random forests.

Results and Discussion Within the scope of laboratory experiments, the methods presented yield very precise results for determining the irradiation dose, the irradiation time and the radiation type. The irradiation time can be estimated with an uncertainty of less than four days within a monitoring interval of one month using a shallow ANN. Deeper ANNs trained on simulation data allow for the estimation of irradiation doses without fading time corrections with an uncertainty of less than 10% without a individual detector calibration. A differentiation between alpha particles and beta or gamma irradiation exhibits an automatic detection rate of up to 100% using sufficiently high irradiation doses. The estimation of the number of irradiations has been performed on simulation data only showing promising results for a transition to real measurement data with future measurements. The transition to field experiments for the application in real personal dose monitoring is presented and discussed.

Conclusion The information obtained from the glow curve of passive solid state dosemeters can be extended by using ANNs. In addition to the irradiation dose, the time of the irradiation and the radiation type can be accurately reconstructed in the scope of laboratory experiments. Some of the techniques presented here can be transferred to routine personal dose monitoring, which would add a great value to passive solid state dosemeters.

References

1) Y. Horowitz et. al., “Thermoluminescence Theory and Analysis: Advances and Impact on Applications", Encyclopedia of Spectroscopy and Spectrometry (Third Edition), 444-451, Academic Press (2017)
2) J. Walbersloh and F. Busch. “A thin-layer LiF thermoluminescence dosemeter system with fast readout for the use in personal dosimetry services”, Radiation Protection Dosimetry 170.1-4 (2016), pp. 191–194.
3) F. Mentzel et. al. “A machine learning approach to glow curve analysis”, Radiation protection dosimetry, 2019
4) C. Bishop, “Pattern recognition and machine learning”, Springer Science + Business Media, 2006

EURADOS Intercomparisons for Individual Monitoring Services: Results of the 2016 and 2018 Whole Body Dosemeters Intercomparison for Photon and Beta radiations

Stadtmann H.[1*], McWhan A.[2], Figel M.[3], Grimbergen T.W.M [4],
Romero A. M.[5], Dobrzynska W.[2], Gärtner Ch.[1]
[1] Seibersdorf Labor GmbH, Austria
[2] Cavendish Nuclear Limited, United Kingdom
[3] Helmholtz Zentrum Muenchen, Germany
[4] Mirion Dosimetry Services, the Netherlands
5 CIEMAT, Spain

Highlights This paper presents the organization details and the analysis of results of the Eurados intercomparisons 2016 and 2018 for whole body dosemeters in photon and beta fields.

Key words Intercomparison, external radiation dosimetry, whole body dosemeter

Background and Objectives With the aims of encouraging and facilitating the participation of Individual Monitoring Services (IMS) in personal dosemeter intercomparisons, EURADOS (the European Radiation Dosimetry Group) started to organise a self-sustained programme of regular intercomparisons in 2008. Since then, six intercomparisons for whole-body dosemeters and two for extremity dosemeters in photon and beta fields, and two intercomparisons for whole body dosemeters in neutron fields, have been successfully performed[1)]. This paper presents the organization details and results of the 2016 and 2018 intercomparison for whole body dosemeters in photon and beta radiation fields

Materials and Methods The 2016 and 2018 intercomparisons for whole body dosemeters (IC2016 and IC2018) were performed in terms of the dose quantities $H_p(10)$ and $H_p(0,07)$ for photon and beta radiations. For both intercomparisons, the irradiation plan was defined so that participants can obtain information of their dosimetry systems on characteristics such as linearity, reproducibility, energy and angular dependence, and response to mixed irradiations. Irradiation laboratories were selected on the basis of their accreditation, previous experience in similar tasks and price. Registration process, communication and data exchange was done in an on-line platform, easy to use and secure, that allows the participants to monitor the status of their dosimetry systems in real-time and to download all relevant information and documents. The results were analysed according to the performance criteria established in the standard ISO

14146 (2000): “Criteria and performance limits for the periodic evaluation of processors of personal dosemeters for X and gamma radiation”, commonly known as the ‘trumpet curve’.

Results and Discussion In total 103 different systems from 86 participating laboratories and 36 countries took part in IC2016. The number of systems increased up to 121 from 101 IMS and 40 different countries in IC2018. Participating dosimetry systems mainly used film, thermoluminescence (TL) and optically stimulated luminescence (OSL) detectors, but also dosemeters based on other techniques: radiophotoluminescence (RPL), direct ion storage (DIS) or active personal dosemeters (APD). A summary of results is shown in Figure 1.

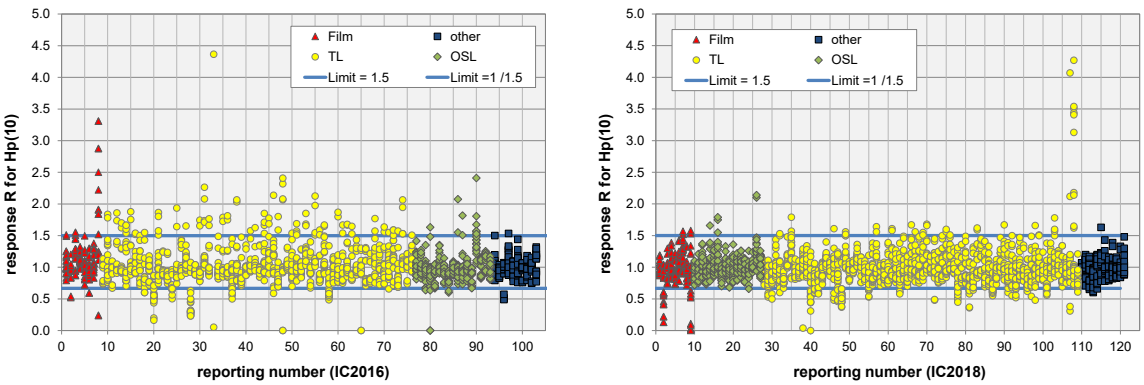

Figure 1. Response for $H_p(10)$ for each participant system in IC2016 and IC2018

Conclusion Most of participants complied with the criteria of the standard ISO 14146 in both intercomparisons. Response to mixed radiation was satisfactory even for the radiation quality beta plus gamma tested in IC2016. The angular irradiations produced the highest number of outliers

The participation in intercomparisons gives IMSs the opportunity to show compliance with their own quality management system, compare results with other participants and develop plans for improving their dosimetry systems. The increasing number of participants confirms the need and usefulness of participation in intercomparisons for dosimetry services.

References

1) EURADOS Reports for previous intecomparisons can be downloaded at http://www.eurados.org/en/Documents_Publications/Reports_documents

Results of the EURADOS 2017 Intercomparison for Whole Body Neutron Dosemeters (IC2017n)

Sabine Mayer[1]*, Marie-Anne Chevallier[2], Elena Fantuzzi[3], Michael Hajek[4], Marlies Luszik-Bhadra[5], Rick Tanner[6], David Thomas[7] and Filip Vanhavere[8]

[1]*Paul Scherrer Institute, Department of Radiation Safety and Security, Forschungsstrasse 111, 5232 Villigen PSI, Switzerland*
[2]*IRSN, BP 17, 31 avenue de la Division Leclerc, 92260 Fontenay-aux-Roses, France*
[3]*ENEA-Radiation Protection Institute, via Martiri di Monte Sole, 4 - 40129 Bologna, Italy*
[4]*IAEA, Vienna International Centre, PO Box 100, 1400 Vienna, Austria*
[5]*PTB, Bundesallee 100, D-38116 Braunschweig, Germany*
[6]*PHE, CRCE, Chilton, Didcot, Oxon OX11 0RQ, UK*
[7]*NPL, Hampton Road, Teddington, TW11 0LW, UK*
[8]*SCK-CEN, Belgian Nuclear Research Centre, Boeretang 200, 2400 Mol, Belgium*

Highlights IC2017n was the second EURADOS intercomparison exercise for neutron dosemeters after IC2012n. Previous proficiency tests for neutron personal dosimetry at an international level have been performed irregularly every 8 to 10 years only.

Key words Neutron dosimetry, neutron dosemeter, EURADOS, intercomparison

Background and Objectives The European Radiation Dosimetry Group (EURADOS) has carried out a number of different intercomparison exercises in the past that qualify as proficiency tests for different dosimetry systems and types of radiation. In 2017 and 2018, the second EURADOS intercomparison for neutron dosemeters (IC2017n) took place. The intercomparison concerns the performance of neutron dosemeters intended to measure neutron personal dose equivalent, $H_p(10)$, as provided by individual monitoring services.

Materials and Methods The neutron dosemeters included in the exercise were restricted to those routinely used in individual monitoring of occupationally exposed workers. No systems under development were allowed. The irradiations were performed at two accredited European laboratories which are both National Primary Metrology Laboratories for ionizing radiation: National Physical Laboratory (NPL, United Kingdom) and Physikalisch-Technische Bundesanstalt (PTB, Germany). All irradiations were carried out according to the irradiation

plan in Table 1.

Quality at irradiation laboratory	$H_p(10)$ (mSv)	# of dosemeters	Irrad. lab
^{252}Cf at 0°	0.3 1.5 12	4 4 4	NPL
^{252}Cf at 0° and ^{137}Cs	1.5 1.0	4	PTB
^{241}Am-Be(α,n) at 0°	1.5	4	NPL
^{252}Cf at 45°	1.5	2	NPL
^{252}Cf (D_2O moderated) at 0°	1.2	4	PTB
^{252}Cf (D_2O moderated) behind a shadow block	1.0	2	PTB
# of irradiated dosemeters		28	

Table 1. Irradiation plan

Results and Discussion 32 participants registered for the intercomparison, with 33 dosimetry systems. The summary of all reported results can be seen in Figure 1. The presentation will report on and discuss the results of the IC2017n exercise.

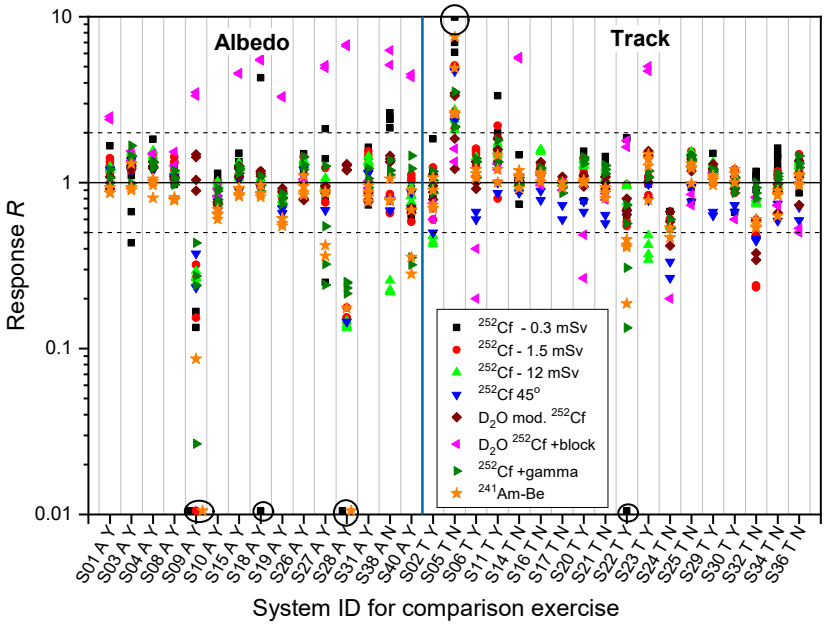

Figure 1. Summary of all reported response values.

Conclusion The intercomparison results can assist participants in demonstrating compliance with the criteria defined in international standards giving performance requirements for neutron dosimetry. They allow comparisons of individual results with those of other participants and, if required, help in developing action plans for improving their own systems.

Passive detector responses at spark discharge simulating lightning discharge in laboratory conditions

D. Kyselová[1, 2*], I. Ambrožová[1], M. Kákona[1, 2], J. Mikeš[3], M. Sommer[1, 2], V. Štěpán[1], O. Ploc[1]

[1]*Department of Radiation Dosimetry, Nuclear Physics Institute of the Czech Academy of Sciences, Prague, Czech Republic*

[2]*Department of Dosimetry and Application of Ionizing Radiation, Faculty of Nuclear Sciences and Physical Engineering, Czech Technical University in Prague, Prague, Czech Republic*

[3] *Faculty of Electrical Engineering, Czech Technical University in Prague, Prague, Czech Republic*

Highlights

Preliminary measurements indicate that passive detectors show a significant increase in their response when exposed at high current and high voltage generators simulating lightning discharge in laboratory conditions.

Keywords

aircraft dosimetry, Terrestrial Gamma-Ray Flashes, Terrestrial Neutron Flashes, lightning generators, spark discharge, passive detector

Background and Objectives

Short, high-energy atmospheric phenomena in thunderstorms such as Terrestrial Gamma-Ray Flashes (TGFs) and Terrestrial Neutron flashes (TNFs), originating in a strong electric field of thunderstorms[1), 2)], can raise radiation exposure of aircraft crews. Routinely, the effective dose of aircraft crews is evaluated using special computer programs[3)]. However, these programs don't take contributions by TGFs and TNFs into account. Previous experiments on the ground and in space, complemented by computer simulations, concluded that effective dose obtained by aircraft crew from a TGF in close proximity can reach 100 mSv[4), 5)]. Based on the measurements of the MCAL instrument at the AGILE satellite[6)], the energy range of photons in TGF is assumed to be up to 40 MeV.

The detection of such phenomena at flight altitude is complicated due to their rare occurrence and requires the deployment of new detector devices for continuous radiation monitoring onboard commercial aircraft.

The electric and radiation environment in thunderclouds has so far not been fully reproduced in laboratory conditions – however, parts of the evolution of the lightning discharge can be approximated using special high voltage and high current generators[7)].

The presence of gamma emission has been previously recorded at high voltage generators using detectors with NaI[8), 9)], BaF_2[9), 10)], $LaBr_3(Ce)$[7), 9)] and plastic scintillator elements[8)].

The combination of challenging electromagnetic conditions and short time gamma emission is well suited for testing of active detectors that are considered for long-term measurements onboard commercial aircraft. Susceptibility of the active detectors to electromagnetic interference can be assessed by parallel measurements with passive detectors.

In this work, a method proposed for improved assessment of the added effective dose to aircraft crew due to short, high-energy atmospheric phenomena is presented together with preliminary results of the first stage – monitoring of radiation environment at high voltage and high current generators using passive detectors.

Materials and Methods

It is expected that testing of passive detectors at the high current and high voltage generators will verify the suitability of active radiation detectors that are used or shall be deployed onboard aircraft and unmanned aerial vehicles. It is not possible to simulate both parts of lightning discharge (current and voltage) in laboratory conditions at once, therefore we used separately two types of generators. As the first step, we prepared experiments with atmospherical lightning impulse waveform 1.2/50 microseconds and also the high current impulse with the waveshape 10/350 microseconds. Parameters of individual discharges were monitored during the whole period of measurements.

Thermoluminescent dosimeters (TLD) and track-etched detectors (TED) were chosen for the first round of tests. Specifically, three types of TLD (CaSO4:Dy, MTS–6, and MTS–7) and TED Harzlas TD–1 were selected. This combination was chosen with respect to the detection of photon and neutron radiation components.

A packet, containing five detectors of each TLD type and one TED, was prepared for measurement. These packets were placed in a defined distance, close to the expected radiation origin in high current and high voltage laboratories. Passive detectors for measurement of the background were placed elsewhere in the building.

Results and Discussion

The experiment at the high current generator is still ongoing. Preliminary data from the high voltage generator show an increase in the TLD response compared to the background. The higher signal for MTS–6 can indicate the presence of thermal neutrons. Further measurements at high voltage generator will be realized to verify these results.

Conclusion

Description of the method proposed to improve estimation of the contribution from TGF and TNF to the effective dose of the aircraft crew, together with the results of the first round of measurements at high current and high voltage generators will be presented.

References

1) DWYER, J. R., et al. Space Sci. Rev., 2012, 173.1–4: 133–196. doi:10.1007/s11214-012-9894-0.
2) DWYER, J. R.; UMAN, M. A. Phys. Rep., 2014, 534.4: 147–241. doi: 10.1016/j.physrep.2013.09.004
3) SCHUHMACHER, H. Radiat. Prot. Dosim., 2011, 144.1–4: 599–604. doi:10.1093/rpd/ncq588.
4) DWYER, J. R., et al. J. Geophys. Res.: Atmos, 2010, 115.D9. doi:10.1029/2009JD012039.
5) TAVANI, M., et al. Nat. Hazards Earth Syst. Sci., 2013, 13.4: 112. doi:10.5194/nhess-13-1127-2013.
6) MARISALDI, M., et al. Phys. Rev. Lett., 2010, 105.12: 128501. doi: 10.1103/PhysRevLett.105.128501.
7) KOCHKIN, P, et al. Plasma Sources Sci. Technol., 2016, 25.4: 044002. doi:10.1088/0963-0252/25/4/044002.
8) DWYER, J. R., et al. J. Geophys. Res.: Atmos, 2008, 113.D23. doi:10.1029/2008JD010315.
9) NGUYEN, C. V., et al. J. Phys. D: Applied Physics, 2008, 41.23: 234012. doi: 10.1088/0022-3727/41/23/234012.
10) RAHMAN, M., et al. Geophys. Res. Lett., 2008, 35.6. doi:10.1029/2007GL032678.

Microdosimetry of Cosmic Ray Shower atop Mount Zugspitze in Bavaria Germany using a TLD Microdosimeter

Bhaskar Mukherjee[1, 2], Clemens Woda[1], Vladimir Mares[1]
[1]*Helmholtz Zentrum München, German Research Center for Environmental Health, Germany*
[2]*School of Physics (A28), The University of Sydney, NSW 2006, Australia*

Highlights (a) Interaction of high-energy protons from galactic origin with the air molecules in the Earth's atmosphere generates Cosmic Ray Shower (CRS). (b) The CRS is composed of neutrons, electrons, protons, photons, muons and pions of diverse energy and intensity distributions. (c) A TLD-microdosimeter (LiBe-14) based on LiF and BeO TLD chip was developed. (d) LiBe-14 microdosimeter was used to assess the ambient dose equivalent of the CRS at "Kugel Alm" Laboratory located atop mount Zugspitze at the Environmental Research Station (UFS Schneefernerhaus; 2650 m above sea level).

Key words Cosmic-ray-shower, ambient dose equivalent, TLD-Microdosimeter

Background and Objectives An extended range Bonner Sphere Spectrometer (ERBSS) is comprised of a multitude of polyethylene moderator spheres of diameter: 6.4, 7.6, 8.9, 10.2, 11.4, 12.7, 14, 15.2, 17.8, 20.3, 22.9, 25.4, 27.9, 30.5, 38.1 cm and a high-pressure ^{3}He proportional counter (SP9 Centronic Ltd), which is responsive primarily to thermal neutrons, and almost insensitive to other components of the CRS including electrons, photons, muons and pions. This ERBSS has been assessing the cosmic ray neutron spectra at "Kugel Alm" continuously since 2005[1)]. Authors have used a novel TLD-based microdosimeter[2)] with a view to estimate the ambient dose equivalent contributed by the entire CRS.

Materials and Methods Three sets of LiBe-14 microdosimeters were attached (Date: 26 Sept 2018) to the 30.5 cm (12 inch) diameter Bonner sphere (emulating a ICRU sphere) located in the neutron-laboratory hut made of weatherproof wooden structure (Figure 1). The 1st and 2nd sets were retrieved on 27 Nov 2018 and 23 Jan 2019 respectively and evaluated using a Risø TL-OSL-DA12 reader following the protocol given elsewhere[2)]. The microdosimetric quantities including ambient dose equivalent H*(10): mSv, average LET: keV/µm and Quality factor: Q were calculated as functions of TL-glow curve area ratio ($r = A_{BeO}/A_{LiF}$) of LiF (TLD-700) and BeO chips[2)].

Results and Discussion The CRS induced ambient dose equivalent relevant to 1st

(Exposure: 62 d) and 2nd batch (Exposure: 116 d) was evaluated to be 124.3 and 225.9 µSv respectively (Figure 2). The 3rd batch will be retrieved on 23 March (Exposure: 174 d).

Figure 1. The "Kugel Alm" Neutron Laboratory at UFS Environmental Research Station Zugspitze (2650 m a.s.l.) operated by Helmholtz Zentrum München. The 30.5 cm (12 inch) diameter polyethylene Bonner sphere with three attached LiBe-Microdosimeters (**x x x**) is shown in the inset (Photos: V. Mares and B. Mukherjee).

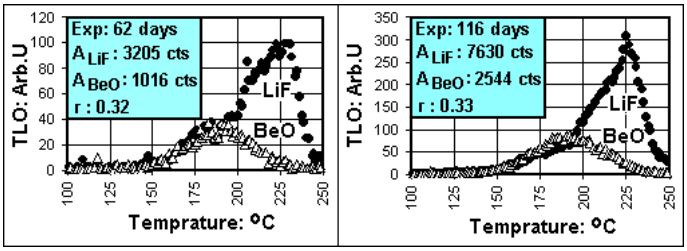

Figure 2. TL glow curves of LiF and BeO dosimeter pairs (Figure 1) exposed to secondary cosmic rays atop mount Zugspitze. The main results are shown in the inset.

Conclusion We have demonstrated the feasibility of a novel LiF and BeO based Microdosimeter (LiBe-14) for the dosimetry of cosmic ray shower induced radiations atop mount Zugspitze. This technique circumvents the High Temperature peak Ratio (HTR) method of dose assessment[3].

References

1) Leuthold, G., Mares, V., Rühm, W., Weitzennegger, E., Paretzke, H.G. Long-term measurement of cosmic ray neutrons by means of a Bonner Sphere spectrometer at mountain altitudes- first results. Radiat. Prot. Dosim. 126 (2007) 506-511.
2) Mukherjee, B. A novel microdosimeter using LiF and BeO thermoluminescence dosimeter pairs for clinical and aerospace applications. Radiat. Meas. 72 (2015) 31-38.
3) Horowitz, Y.S., Satinger, D., Fuks, L., Oster, L., Podpalov, L. On the use of LiF: Mg, Ti thermoluminescence dosimeters in space- a critical review. Radiat. Prot. Dosim. 106 (2003) 7-24.

Current Status and Future Prospect of RPL Glass Dosimeter

Takayoshi Yamamoto[1, 2 *], Yuka Yanagida-Miyamoto[1], Toshiyuki Iida[2] and Hidehito Nanto[3]

[1]*Oarai Research Center, Chiyoda Technol Corporation, Ibaraki, Japan*

[2]*Osaka University, Osaka, Japan*

[3]*Kanazawa Institute of Technology, Ishikawa, Japan*

Highlights The glass dosimeter (GD) which utilizes the phenomenon of radio-photoluminescence (RPL) is applied to various fields in addition to the individual monitoring. Especially, in order to contribute to restoration of the contaminated area in Fukushima the bead-type and sheet-type glass dosimeters have been developed and utilized to observe the distribution of radioactive contaminants. The new glass material that is resistant to severe environment of high temperature has been developed.

Key words radiophotoluminescence, glass dosimeter, bead-type, sheet-type, severe environment

Background and Objectives The silver-doped phosphate glass is utilized as a reliable passive dosimeter because the glass irradiated with an ionizing radiation emits visible lights (orange and blue) by exciting it with the UV light. This phenomenon is called radio-photoluminescence and utilized as the individual and environmental dose monitoring. The accumulated information of radiation dose would never disappear even if the luminescence centers are repeatedly excited by UV light. Moreover, the fading phenomena are practically negligible, such as less than 1 % a year.

At present, performance of the glass dosimeter progresses remarkably together with the highly developed electronics and it is widely adopted as a practical dosimeter ranging from 10μGy to 10 Gy in Japan, France and Switzerland.

A large number of radioactive materials have been spread out far around the site of Fukushima Nuclear Power Plant due to the serious accident on March 11 in 2011. The situation is still so tragic and the radiation level is still so high that a lot of residents who had lived in the contaminated area before the severe accident could not go back to their own home yet. Furthermore, in order to protect the workers and the liquidators who are engaged in the demolition and decontamination task against the circumstance of high-dose-rate (several hundreds mSv/h～several Sv/h), high temperature and high humidity, it is necessary to develop such radiation dosimeter as can withstand those severe

environments. Then it becomes possible to grasp the distribution of both contamination due to radioactive materials and dose rate in those working fields. The purpose of this project is to develop practical dosimetry methods adaptable to various working environments by improving the glass dosimeter currently in use.

Materials and Methods The applicable field of the glass dosimeter has spread out and led to the development of new dosimeter useful for both restoration and recovery from Fukushima accident. By making use of the characteristic that the dose can be visualized with the glass dosimeter the Ag-doped phosphate glass has been crushed to beads of 0.045～0.1 mm in diameter.

(1) Bead-type glass dosimeter

Dispersing and spraying nearly globular glass dosimeters of nearly 0.1 mm in diameter to the passage, the ditch and the wall of housings, we can easily visualize the spatial distribution of radio-photoluminescence emitted from them by irradiating with the UV light from a safety zone of low-dose-rate. Then, we can grasp the distribution map of radioactive contamination.

(2) Sheet type glass dosimeter

Such dosimeters as flexible and possible to cut and paste can easily be obtained by applying bead-type glasses to plastic sheets. Then, it becomes possible to measure the doses of those places difficult to measure such as narrow gap of plumbing by bandaging. In Fig. 1 is shown the X-ray image on the sheet type GD through Cu mesh collimator. The emission of orange color is observed from the area irradiated with X-rays and it is clear that the spatial resolution depends on the diameter of glass bead.[1)]

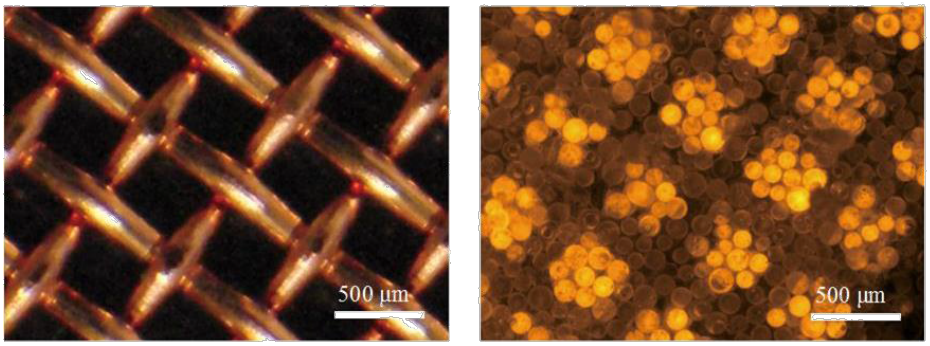

(a) (b)

Fig . 1 (a) photograph of a Cu mesh used for radiation shielding and (b) RPL image from the sheet-type RPL glass dosimeter irradiated with X-rays.

Results and Discussion We are developing such dosimeters as have those characteristics of both low fading under high temperature and high accuracy under high humidity circumstances to decrease radiation exposure to the liquidators working in such severe environment. These dosimeters will largely contribute to obtain useful information for optimizing both working procedure and time and also be useful to evaluate the result of decontamination task for restoration of residential area. We have newly developed the Ca-Na phosphate glass and its temperature dependence is shown together with the usual Al-Na one in Fig. 2. [2)] Though the RPL intensity from Ca-Na glass is smaller in 10 % than that of Al-Na glass, the former glass can withstand higher temperature (550 K) than the later one.

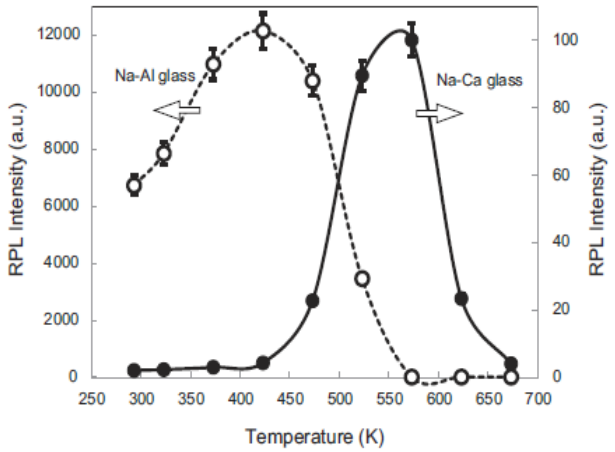

Fig. 2. Temperature dependence of different-type glasses

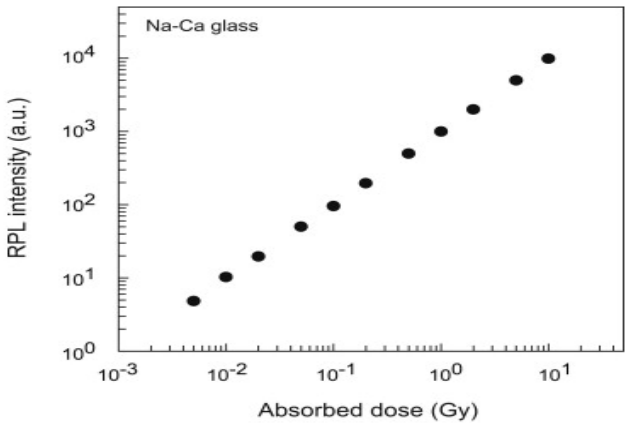

Fig. 3. Dose dependence of new-type glass

Conclusion We have established the technique for producing similar glass beads of approximately 0.1 mm in diameter by crushing the Ag-doped phosphate glass. By spreading the beads on the plastic sheet we have succeeded in producing homogeneous glass sheet, which would be useful for drawing distribution map of radiation dose. We have found out a combination of ingredient of the glass dosimeter that could withstand the severe environment of contaminated area with radioactive materials.

It is necessary to investigate more deeply the dose-rate dependence of the glass dosimeter as well as LET one. It has been reported[3] that the output of luminescence dosimeter decreases with increasing LET under constant absorbed dose. This effect might be due to the recombination of high-density electrons and holes generated in a narrow region. Similar phenomena could be observed when irradiated with the high-dose-rate radiation. For example, it might be interesting to observe the RPL from the glass irradiated with extremely thin electron beam of high density. It might also be interesting to add different materials other than silver to the glass to expect the luminescence of different color from orange and blue. Then a latent color image could be realized by vaporizing several materials on the surface of the glass through proper masking.

The usual phosphate glass could be sensitive to neutrons by adding a little bit of ^{6}Li or ^{10}B due to nuclear reactions and it would be useful for neutron dosimetry.[4] The RPL nearly real-time dosimeter is being developed for mainly medical use. The sheet-type glass would be processed to the gloves for extremity dosimetry in case of the interventional radiology procedures and handling of radioisotopes in nuclear medicine.

Acknowledgements The authors would like to express their gratitude to Prof. Shimizu K., Dr. Ihara Y., Mr. Sugiyama M., Mr. Koguchi Y. and Mr. Sato N. for valuable contribution. This study was supported by Japan Science and Technology Agency.

References

1) Nanto H., Yanagida Y., Sugiyama M., Koguchi Y., Ihara Y., Iida T., Shimizu K., Ikeguchi T., Hirasawa K., Takei Y. and Yamamoto T. 2017. Sensors and Materials **29**, 1439-1445.

2) Sato F., Zushi N., Nagai T., Tanaka T., Kato Y., Yamamoto T. and Iida T. 2013. Radiat. Meas. **53-54**, 8-11.

3) Hajek M., Berger T., Fugger M., Furstner M., Vana N., Akatov Y., Shurshakov V. and Arkhangelsky V. 2006. Radiat. Prot. Dosim. **120**, 446 – 449.

4) Maki D., Nagai T., Sato F., Kato Y., Yamamoto T., Iida T. 2011. Radiat. Meas. **46**, 1543-1546.

Harmonically modulated optically stimulated luminescence (HM-OSL) – principles and application

A. Mandowski[1]*, E. Mandowska[1], K. Maternicki[1], R. Kieszkowski[1], R. Smyka[1], M. Biernacka[1], R. Majgier[1]

[1]*Jan Dlugosz University, Czestochowa, Poland*

Highlights New OSL technique is presented – the harmonically modulated optically stimulated luminescence (HM-OSL). During HM-OSL the stimulating light changes sinusoidally. The OSL response is also sinusoidal. The phase shift between stimulation and OSL is related to several trap parameters. The HM-OSL method was implemented in the Helios OSL reader.

Key words optically stimulated luminescence (OSL), harmonically modulated optically stimulated luminescence (HM-OSL), traps, recombination centers.

Background and Objectives The optically stimulated luminescence (OSL) phenomenon is increasingly being used in dosimetry of ionizing radiation. In the OSL method, the dose of absorbed ionizing radiation can be indirectly determined by recording the radiation recombination of charge carriers (usually electrons) that were captured by the traps during irradiation. The OSL detectors are usually crystalline dielectric materials with a wide band gap. Therefore traps, corresponding to the localized energy levels within the band gap, are usually associated with defects or dopants in the crystal structure.

Materials and Methods We propose the method of measuring the optically stimulated luminescence with optical stimulation realized by the harmonic modulation of light intensity $\Phi(t)$ according to the formula (1):

$$\Phi(t) = \Phi_B + \Phi_A \sin\left(\omega t + \varphi_0\right) \tag{1}$$

where Φ_B and Φ_A denote the base intensity and the amplitude of modulation, respectively, wherein $0 \le \Phi \le \Phi_B$, ω describes the stimulation frequency, φ_0 is an initial phase, while the detector's luminescence response, i.e. the registered OSL signal, is essentially nonlinear:

$$\mathscr{L}(t) = \mathscr{L}_B + \mathscr{L}_A \sin\left(\omega t - \varphi_L\right) \tag{2}$$

however, in a small range of time, when the relative loss of carriers from the traps is much smaller than one, It was assumed that the $\mathscr{L}_A$ and $\mathscr{L}_B$ components change much slower

than the harmonic factor. The frequency and depth of modulation is selected according to the OSL material and detector. The basic measurement parameter is the magnitude of the phase shift φ_L between two sinus-shaped curves, as shown in Fig. 1.

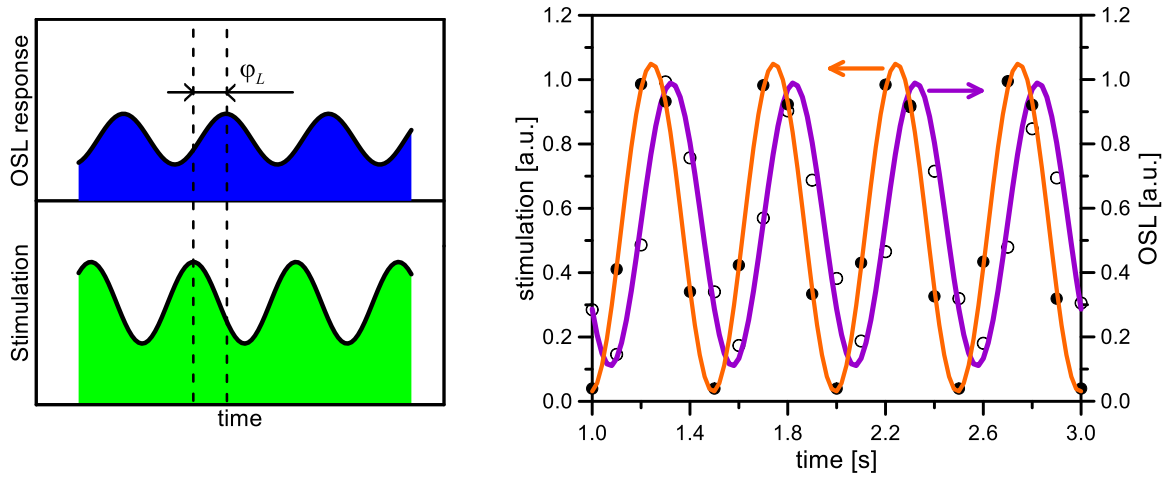

Figure 1. a) Left diagram - the idea of the HM-OSL method. Measured parameter is the phase shift between the stimulation and the OSL response. b) Right diagram - HM-OSL measurement performed on NaCl pellet

Results and Discussion Parameters shown in eq. (2) can be calculated in the frame of a specific model – e.g. localized or delocalized model. For the simplest delocalized model the phase shift is given by

$$\tan(\varphi_L) = \frac{\omega}{Bm_0} = \omega\tau_R \tag{13}$$

where B is the recombination coefficient and m_0 is the concentration of holes in recombination centers.

Conclusion A new stimulation method is presented which gives the possibility to determine some additional parameters of traps and recombination centers, e.g. the lifetime of charge carriers in excited state (transport band) with respect to recombination. The HM-OSL method was implemented as a novel measurement technique in the Helios OSL reader.

Design of a new Al_2O_3:C OSL sensor for extremity and lens of eye

Marc Million[1], Brahim Moreno[1] Mark Akselrod[2]
[1]*Landauer-Europe, 9, rue Paul Dautier, Velizy-Villacoublay, France*
[2]*Landauer, Stillwater Crystal Growth, 723 1/2 Eastgate St, Stillwater, USA*

Highlights A new sensor based on Al_2O_3:C has been designed based on the Bragg-Gray cavity theory to improve its energy response. An optimization of the physical parameters using Monte Carlo modeling is presented along with a comparison with experimental results. The metrological performance versus IEC 62387 requirements is also discussed.

Key words Optically stimulated luminescence, aluminum oxide, radiation dosimetry, extremity, lens of eye.

Background and Objectives Non-tissue equivalent sensor such as Al_20_3:C is generally considered to be not appropriated for extremity dosimetry (finger ring, wrist, lens of eye). The main difficulty is a complexity of implementation of multi-element sensor having several filters in a small volume needed to reconstruct the irradiation conditions and correct for the soft photon energy overresponse. A new approach to correct the photon energy response of an Al_2O_3:C OSL sensor is based on the Bragg-Gray cavity theory. The first goal was to validate of the new approach using Monte Carlo modeling. Additionally, the work focused on optimizing the sensor design considering technological limitations and instrumentation capability in order to develop a ring and a lens of eye dosimeters able to meet the requirements of the IEC 62387. The presented design leads to a new type of extremity dosimeter with one-dimensional dose profile capability.

Materials and Methods The sensor design is based on a diluted mixture of small grain size of Al_2O_3:C powder and a tissue-equivalent binder. The size of the grain and the proportion of the binder strongly impact the energy response. It was also demonstrated the implementation of a thin film filter based on a high Z material such as copper to address the issue of the photon response at very low energies below 30 keV. This study involved optimization of the following parameters: Al_2O_3:C powder grain size, mass ratio of the binder to powder and the metal filter thickness and geometry by using physical modeling. The Monte Carlo modeling was performed using MCNP6. Geometrical approximation has been done for the shape of grains, the grain size distribution and the distribution of grains in the binder. These approximations will be discussed. Experimental tests have been done to validate the model and to prove the approach.

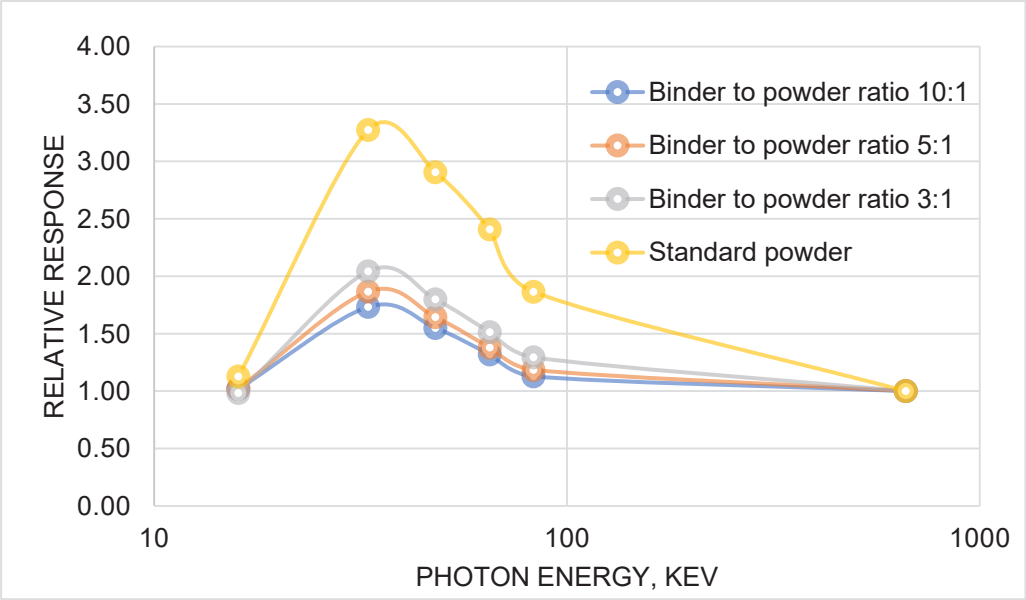

Figure 1. Energy response for OSL film with 2 μm and 13 μm powder with different powder to binder ratio

Results and Discussion The results of the modeling and experimental data are consistent even some discrepancies have been identified. These discrepancies do not affect strongly the overall approach. The results of the investigation have demonstrated that by using the appropriated grain size, binder to sensitive material ratio and thin metal film it is possible to design a sensor whose performances can meet the IEC 62387 criteria for energy and angular response. The design of the sensor requires the use of our latest OSL reader design with higher luminescence sensitivity. Using new instrumentation, it is possible to meet the requirement of the IEC 62387 to report dose from 0.1 mSv. It is a general threshold considered as appropriated by the individual monitoring laboratories and regulators for extremity and lens of eye dosimetry.

Conclusion It has been demonstrated that with the median grain size of 2 μm and the powder to binder mass ratio of 1:5 it is possible to correct the energy response of the Al_2O_3:C and at the same time to achieve the low limit of detection of 0.1 mSv. Using our latest generation of the OSL reader, such sensor design can meet the IEC 62387 performance criteria for extremity dosimetry.

Novel Disk-Shaped OSL Dosimeter Having Smaller Angular Dependence

Sota GOTO[1,2], Hiroaki HAYASHI[1], Emi TOMITA[1], Takashi ASAHARA[1], Natsumi KIMOTO[1], Yuki KANAZAWA[3], Hidetoshi YAMAGUCHI[2], Morihito SHIMIZU[2]

[1]*Kanazawa University, Kanazawa, Ishikawa, Japan*
[2] *National Institute of Advanced Industrial Science and Technology, Tsukuba, Ibaraki, Japan*
[3]*Tokushima University, Tokushima, Tokushima, Japan*

Highlights To improve angular dependence of a passive-type OSL dosimeter, we fabricated a novel disk-shaped dosimeter which consists of two sensitive regions. The angular dependence of our dosimeters improved without significant loss of the detection efficiency from the results of simulation and experiment.

Key words Angular dependence, OSL, Dosimetry, Diagnostic X-rays

Background and objectives An optically stimulated luminescence (OSL) dosimeter is widely used for personal dosimeter in medical dosimetry for low-energy X-rays. When we use this dosimeter, angular dependence of the OSL dosimeter can be one of the causes of systematic error, and it may lead to underestimation of exposure doses. In our previous study[1)], we found that the angular dependence of a commercial OSL dosimeter, which consisted of a disk-shaped OSL element, has a relatively large angular dependence, and recently we noticed that the beam hardening effect caused the large angular dependence. In this study, we developed the novel disk-shaped OSL dosimeter with the aim of reducing angular dependence.

Materials and methods The commercial OSL dosimeter is a φ5 mm disk, mainly composed of Al_2O_3:C, as shown in Figure 1, (a-1) and (b-1). Additionally, we fabricated two novel shaped dosimeters as shown in Fig. 1; (a-2) and (b-2) represent doughnut-shaped dosimeters having a φ3 mm hole; (a-3) and (b-3) is a composite disk-shaped dosimeter having two sensitive regions, a φ3 mm disk and φ5 mm ring.

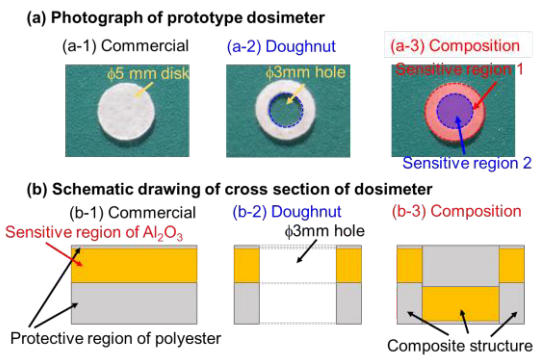

Figure 1 Photographs (a) and schematic drawings (b) of the commercial and two novel OSL dosimeters.

In order to obtain angular dependence and detection efficiency of above dosimeters, we performed a simulation study using Monte-Carlo simulation code EGS5[2]. In the simulation, incident angle of X-ray to dosimeter was set at 15 degree-increments ranging from 0 to 345 degrees using an 80 kV X-ray, and absorbed dose to the OSL dosimeter was calculated at each incident angle. We also measured the angular dependence and the detection efficiency of the present dosimeters using diagnostic X-ray equipment based on a previous study[1].

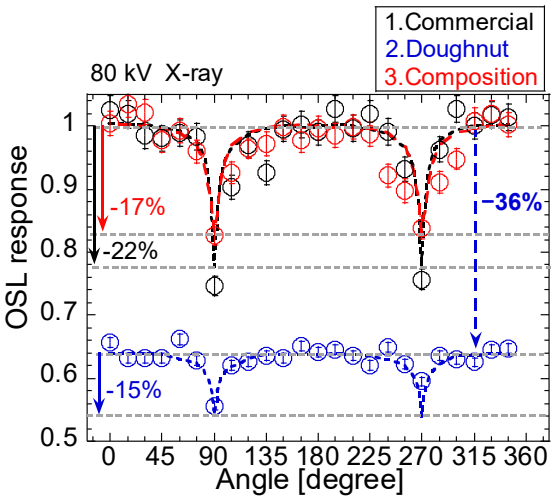

Figure 2 OSL response of the three types of OSL dosimeters at each angle. Newly proposed dosimeter (number 3) has good characteristics.

Results and discussion Figure 2 represents the OSL response at each angle for each of the three types of OSL dosimeters. The results of simulation and experiment are indicated by the broken line and broken circle, respectively. In Fig.2, reduction rate of the OSL dosimeter response for 0 to 90 degrees was evaluated as angular dependence. The angular dependence of the commercial dosimeter was 22%. On the other hand, the angular dependence of the doughnut-shaped dosimeter was improved by 7%. However, detection efficiency for X-ray was decreased by 36% compared to the commercial dosimeter. From the results of the composite disk-shaped dosimeter, the angular dependence improved by 5% without decrease in original efficiency. These simulation results were consistent with the experimental results.

Conclusion In order to improve the angular dependence of a commercial OSL dosimeter, we propose a novel-shaped OSL dosimeter. Using Monte-Carlo simulation and experimental results, we verified the angular dependence and detection efficiency of our dosimeter, and found that the composite disk-shaped OSL dosimeter had good characteristics.

References

1) Hayashi, H. et al., 2015. Procedure to measure angular dependences of personal dosimeters by means of diagnostic X-ray equipment. Med. Imag. Inf. Sci. 32 (1), 8–14.
2) Hirayama, H., et al., The EGS5 Code System. SLAC Report Number: SLAC-R- 730, KEK Report Number, 2005-2008. Hubble, J.H., 1982.

Spatial radiation dosimetry based on various OSL materials embedded into silicone elastomer matrix

M. Sądel, P. Bilski, M. Kłosowski, M. Sankowska
Institute of Nuclear Physics Polish Academy of Sciences, PL-31342 Krakow, Poland

Highlights

A new approach to the spatial radiation dosimetry based on optically-stimulated luminescence (OSL) is presented. By embedding OSL-active particles into a transparent silicone elastomer matrix, the favorable dosimetric properties of an OSL material are exploited towards spatial OSL dosimeter. The new dosimeter formula, carry the advantages known from personal dosimetry: which is its reusability as they can be reset e.g. by an intense light field (bleaching) as well as storage ability as the dose following irradiation can be stored with extended periods of time.

Key words

OSL, Lithium fluoride (LiF:Mg,Cu,P), Lithium magnesium phosphate ($LiMgPO_4$), dosimetry

Background and Objectives

In modern radiotherapy techniques (RT), e.g. proton therapy, the dose is planned using complex, spatial dose distributions. Because of the complexity of RT techniques, proper quality assurance is generally considered as a necessary prerequisite before each patient treatment. Therefore, there is an unmet need to provide a comprehensive spatially resolved measurement of dose distributions. These also implies the developments of new kind of techniques and materials. The basic dosimetric tools in RT are ionization chambers. However, luminescent detectors such as thermo- and optically stimulated luminescence (TL/OSL) are widely applied, especially for personal dosimetry and phantom measurements. LiF:Mg,Cu,P (MCP), is a very well-known TL material. However, it was recently proved that it can also serve as an OSL tool, giving substantial signal sensitivity, compared to other kinds of OSL materials like Al_2O_3:C or BeO [1,2]. Moreover, by using an optimized, with respect to the optical response, dopant concentrations and annealing procedure, its OSL sensitivity can be enhanced even more than 60 % compared to the MCP used in standard TL applications [3]. On the other hand, $LiMgPO_4$ (LMP) became in the last few years one of the most extensively studied new OSL luminescent material. Its promising properties; a high radio-sensitivity and a broad linear response range, allow for considering of the LMP as the potential alternative for the commercially available OSL dosimeter [4]. Thus, taking into account the attractive OSL technique properties which

enhanced its application for dosimetry purposes, and new promising OSL materials, in this study we introduced a novel approach to the spatial radiation dosimetry based on OSL method and MCP and LMP materials embedded into the flexible silicone material host.

Materials and Methods

The OSL materials used is lithium fluoride LiF:Mg,Cu,P and $LiMgPO_4$. The silicone matrix is a commercially available SYLGARD® 184 Silicone Elastomer Kit from Dow Corning. The dosimeters, in form of flat sheets made of a polymer with optically active OSL grains, were obtained by mixing homogeneously dry MCP and LMP particles into a silicone matrix which acts as a flexible host. The samples were irradiated with alpha, beta, gamma, X-rays and protons to different doses and read-out using the CCD camera under stimulation of blue LEDs diodes (470 nm).

Results and Discussion

By investigating prototype dosimeters, direct measurements of the spatial dose distributions were verified. The presentation will show the results in which the numerous 2D/3D OSL dose distributions of various radiation fields (alpha, beta, gamma, X-rays and protons), as well as characterization of the basic dosimetric parameters like sensitivity, linearity, dose-response, repeatability and fading effect, have been investigated.

Conclusion

We proposed a new and reusable method for verification of spatial dose distribution based on the OSL method and promising dosimteric materials. A new system has the potential to verify complex RT dose distributions with high spatial resolution while maintaining the attractive properties know from OSL dosimetry.

Acknowledgements

This project is carried out within the Homing/2017-4/38 program of the Foundation for Polish Science co-financed by the European Union under the European Regional Development Fund.

References

[1] Bilski. P., et al., (2014). Radiat. Meas. 71; 61- 64.
[2] Sadel. M., et al., (2017) J. Phys.: Conf. Series 847; 012067.
[3] Sądel, M., et al., (2019). Radiat. Meas. doi: https://doi.org/10.1016/j.radmeas.2019.02.014
[4] Kulig D., et al., (2017). Radiat. Meas. 106; 94-99.

Latest advances in FNTD technology and instrumentation

Mark Akselrod*, Vasiliy Fomenko and Jonathan Harrison

Landauer, Division of Fluke Health Solution, Stillwater, Oklahoma, USA

Highlights The next technological breakthrough in tools for radiation protection, medical dosimetry and radiobiology research was achieved with Fluorescent Nuclear Track detectors (FNTD) that have some important advantages in measuring neutrons, high energy heavy charge particles (HCP) and even electrons and photons. Second generation of FNTD reader with improved image quality and 30 times faster scanning was developed.

Key words radiation detectors, dosimetry, neutrons, heavy charge particles, aluminum oxide crystals, fluorescence.

Background FNTD technology [1] is based on new aluminium oxide crystals and fluorescent laser scanning confocal microscopy. Detectors are made of Al_2O_3:C,Mg crystals (Fig. 1) having high concentration of single and double oxygen vacancies associated with impurities and forming aggregate defects with unique optical properties. These colour centres undergo radiochromic transformation which remains thermally stable up to 600ºC and are insensitive to ambient light. Unlike Plastic Nuclear Track Detectors (PNTDs) FNTDs do not require chemical etching before imaging. Completely optical imaging of tracks is performed in fluorescent contrast (Fig. 2) and non-destructive readout can be repeated multiple times without erasure, although FNTDs can be erased and reused after bleaching with pulsed UV light.

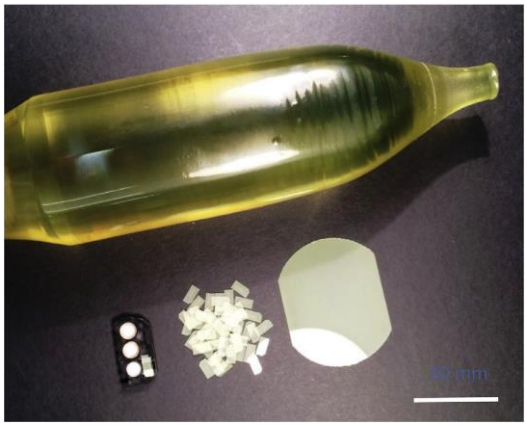

Figure 1. Al_2O_3:C,Mg crystals, polished wafers and FNTDs cut to size.

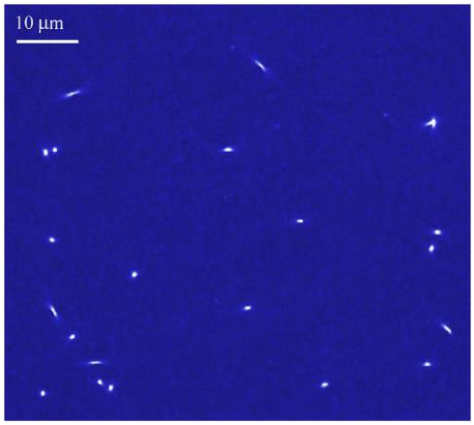

Figure 2. Fluorescent image of recoil proton tracks after AmBe neutron irradiation

Figure 3. First generation commercial FNTD reader

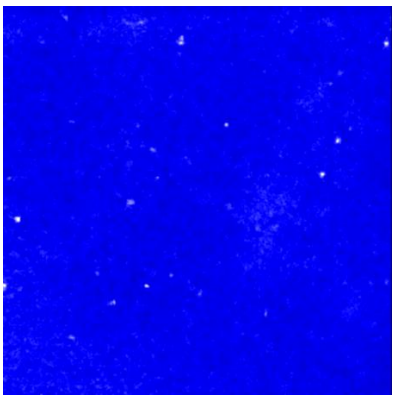

Figure 4. Fluorescent image of delta electron track after irradiation with 0.1 mSv 40 keV X-ray photons.

FNTD instrumentation Two types of fully automatic table-top FNTD readers (Fig. 3) were developed for radiobiology research laboratories and neutron dosimetry services. The readers allow one to load 216 detectors on a tray, their engraved IDs are automatically recognized and fluorescent images are acquired and processed. The readers are characterized by robust and compact optical design, fast data acquisition electronics and a user-friendly software interface. Recently we developed a 2nd generation FNTD reader prototype with 30 times faster readout which allows one to read a larger detector area with improved counting statistics without sacrificing the image quality and prohibitively increasing the readout time.

Radiological characteristics Products of nuclear reactions between neutrons and a neutron converters produce easily detectable fluorescent tracks. Converters containing a high content of hydrogen, like polyethylene, for fast neutrons and ^{6}Li-containing glass for thermal and intermediate energy neutrons are used. The neutron doses in a wide range from 0.1 mSv to 30 Sv were measured. 3D stacks of images obtained in each location allow one to reconstruct trajectories of individual ions and obtain 3D dose profile for neutron energy determination. Latest progress in FNTD technique allowed us to detect and count delta electrons produced by photon doses as low as 0.1 mSv (Fig. 4).

Conclusion The latest progress in FNTD crystal growth, new optical instrumentation, smart image processing and examples of applications in radiation protection, medical dosimetry and radiobiology research will be discussed.

Reference 1. M. Akselrod and J. Kouwenberg, *Fluorescent nuclear track detectors – Review of past, present and future of the technology,* Radiat. Meas. (2018) **117** 35–51.

MBD-2 – A Direct Reading Multi-Functional Dosimeter for Emergency Response, Military and Occupational Dosimetry

M. Vuotila[1], L. Soisalo[1], A. Vuoti[1], K. Spero[2], D. Jarrow[2], J. Fellinger[3]
[1]*Mirion Technologies (Rados) Oy, Turku, Finland*
[2]*Mirion Technologies (MGPI) Smyrna, USA*
[3]*Mirion Technologies (Canberra) Rüsselsheim, Germany*

Highlights The MBD-2 Personal Dosimeter is a device which incorporates the benefits of passive radiation detection with active, self-reading and recording functionality but without alarm indication capability. It is a wrist worn watch-type of dosimeter suitable for photon and neutron dose measurements. Data transfer is achieved via **N**ear **F**ield **C**ommunication (NFC) or **B**luetooth **L**ow **E**nergy (BLE) communication to a smart device (phone, tablet, laptop).

Key words Direct Reading Dosimeter, Direct Ion Storage Technology, photon and neutron detection

Background and Objectives For emergency response situations, for usage in harsh environmental conditions and for military applications a robust, direct reading, simple to use dosimeter is required. Such dosimeters must cover wide energy ranges for both photon and neutron radiation, a large dose rate range and is suitable for applications in pulsed radiation fields as well. The intention of the development of the MBD-2 was to provide a real time situational awareness in the field of use in addition to integrating of the various detection technologies into one configurable device A dose recording and management system requires minimum user interference and should be based on widely used standardized communication technologies such as NFC and BLE.

Materials and Methods The MBD-2 Personal Dosimeter is a device which incorporates the benefits of passive radiation detection with active, self-reading and dose-recording functionality. It uses Direct Ion Storage (DIS), solid state Pin Diode and MOSFET detector technology passive detectors. In the MBD-2 a total of six separate detector elements are integrated – three elements for photon measurements and three elements for neutron measurements. The outline of this watch-type dosimeter is presented and discussed.
The internal electronics provide self-indicating measurement display, digital memory, data logging, on-board diagnostic testing during startup and use of the device and both BLE and NFC read-only wireless communication. All data resides in non-volatile memory for

dose-of-record processing so there is no any danger of losing stored data or configuration settings on main battery failure.

Results and Discussion The radiological performance of the MBD-2 will be summarized for the different applications scenarios. Special attention is given the performance of the dosimeter under harsh environmental conditions and in pulsed and high dose-rate radiation fields. Finally a comparison of the dosimetric properties with the requirements of the relevant IEC and ANSI standards for occupational dosimeters is given.

Conclusion The MBD-2 Personal Dosimeter fulfils all requirements of a direct-reading dosimeter for emergency response, military-tactical and occupational dosimeter.

Development of a prototype thermal neutron dosimeter based on a color-based quasi-digital neutron/gamma discrimination

Gabriele Zorloni[1]*, Francesca Cova[2], Marco Caresana[1], Anna Vedda[2]
[1]*Politecnico di Milano, Milan, Italy*
[2]*Università degli Studi di Milano-Bicocca, Milan, Italy*

Highlights In this study, we propose an original approach for particle discrimination in a mixed radiation field using scintillators. The method relies on the possibility to identify the point of interaction in a phoswich detector from the emission spectra of the produced scintillation light, using optical filters as passive selectors. As a proof of concept, we developed a compact prototype thermal neutron active dosimeter for mixed neutron/γ fields.

Key words n/γ discrimination; phoswich detectors; neutron dosimetry.

Background and Objectives The last 10 years advancements in solid state inorganic scintillators science brought to the development of a wide variety of new materials for radiation detection[1)], thus opening to the possibility of exploring new applications and detection methods. This study aims to take advantage of some of these new scintillators characteristics, by developing a prototype dosimeter as a proof of the principle for an original particle discrimination approach. Instead of using pulse shape discrimination[2)], this instrument relies on the possibility of discriminating particle basing on the color of the emitted scintillation light of a phoswich arrangement, by using two optical filters as passive selectors, and two independent SiPMs. The objective of this work is the preliminary demonstration of the feasibility of this novel technique for performing neutron/γ discrimination.

Materials and Methods For our demonstration, we exploit the different scintillation emissions of $Lu_3Al_5O_{12}$:Pr (LuAG)[3)] and $Gd_3Al_2Ga_3O_{12}$:Ce (GGAG)[3)] single crystals (5x5x1 and 5x5x0.1 mm^3 thick each) in a phoswich detector geometry. Each crystal is coupled to one SiPM through optical filters (one long-pass, the other short-pass, selective to only one scintillator out of the two), thus obtaining a four-slice, two-SiPMs arrangement. In Fig. 1(a), left y axis, are shown the measured RL spectra of the two crystals, and on the right y axis the two filters transmittances. While both crystals are sensitive to γ rays, only the Gd-rich GGAG slice is sensitive to neutrons. Due to the low GGAG thickness, the recoil electrons after the background γ interaction should deposit energy in both scintillators (*i.e.* coincidence signal). After neutron capture on Gd, the emitted high energy γ rays (2 MeV on average) escape from the system, but the internal conversion electrons (30-70 keV on average) are fully stopped in the GGAG, thus causing an anticoincidence signal. An anticoincidence algorithm is therefore

used to perform particle discrimination: the GGAG channel will collect a true neutron signal if i) the signal amplitude falls within a 20-100 keV window, and ii) the signal in the LuAG channel is below a defined voltage threshold; if the LuAG signal falls above the threshold, any observed neutron count is flagged as a γ induced signal and consequently rejected.

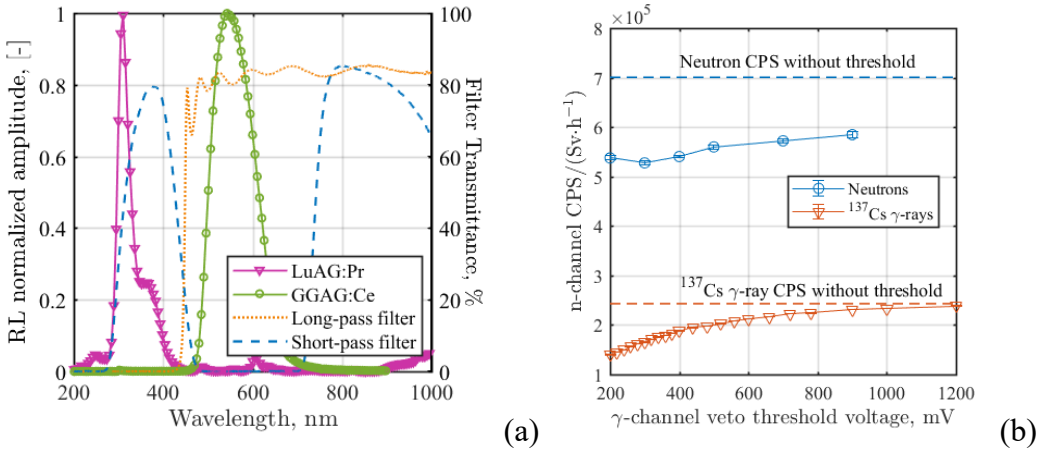

Figure 1. (a): normalized RL spectra of the two crystals (left axis), and filters transmittance (right axis), as a function of the wavelength. (b): GGAG channel counts per unit H*(10) due to neutrons and photons independently, as a function of the LuAG channel veto threshold. Dashed lines correspond to the counts recorded without employing the anticoincidence logic.

Results and Discussion In Fig. 1(b) are shown the counts recorded in the electronic chain of the GGAG sensitive SiPM, *i.e.* the neutron counter, as a function of the LuAG veto trigger threshold, collected independently irradiating the instrument with ^{137}Cs γ rays and with thermal neutrons. The rejection of γ rays increases as the veto threshold decreases, thus demonstrating the feasibility of the color-based approach. Even if the results are still preliminary, in particular because of the non-optimized setup, they seem promising, since improvements of the instrument are under investigation. Nevertheless, we demonstrated that a color-based emission technique is feasible to be applied for particle discrimination purposes.

Conclusion Our findings represent a novel paradigm in particle discrimination research showing how compact detectors composed by novel materials, coupled together in engineered geometries, can display attractive properties related to both their composition and to their geometrical arrangements, leading to novel specific functionalities, providing useful insights for the future engineering of radiation detectors for dosimetry and other applications.

References

1) C. Dujardin *et al.,* IEEE Trans. Nuc. Sc, PP (2018), 1, doi: 10.1109/TNS.2018.2840160.
2) G.F. Knoll, Radiation Detection and Measurement, 3rd edition, Wiley and Sons, Inc., 1999
3) M. Nikl *et al.,* Adv. Opt. Mat. 3 (2015) 463, https://doi.org/10.1002/adom.201400571.

The MIDAS dosimeter/particle monitor of charged particles and neutrons for space environment

C.P. Lambropoulos[1,5]*, C. Potiriadis[2] , G. Theodoratos[1], I. Kazas[3], C. Papadimitropoulos[2], D. Loukas[3], I. Glikiotis[1], P. Paschalis[4], E. Dimovasili[4], M. Kokavesis[1], S. Dimopoulos[1], A. Delakoura[1], S. Pappas[1], G. Dimitropoulos[1]

[1]*ADVEOS microelectronics PC, Chalandri, Attiki, Greece,*

[2] *Greek Atomic Energy Commission, Agia Paraskevi, Attiki, Greece*

[3] *Institute of Nuclear Physics, NCSR Demokritos, Agia Parskevi, Attiki, Greece*

[4]*Department of Physics, University of Cyprus, Nicosia, Cyprus*

[5]*University of Athens, Athens, Greece*

Highlights Radiation doses received by astronauts outside the geomagnetic field are a main risk factor for human space exploration. Determination of LET spectra is necessary in the standard paradigm of risk assessment for mixed radiation fields[1)], because it allows calculation of dose equivalent, while identification of ions by species (or at least by group) is required, if the risk assessment tools developed by NASA are used. The MIDAS device is developed with purpose to achieve mass <50 g, volume < 5 x 5 x 1 cm^3 and power consumption <10 mW for an instrument capable to determine the fluence spectrum as a function of charge and energy of the impinging particles, at least for those species with the most significant contribution to dose in space. In addition it is capable to measure fast neutron spectra for use either in the ISS environment or as radiation monitor.

Key words semiconductor detectors, space dosimetry, neutron and ion particle dosimetry

Background and Objectives The radiation sources of concern are Galactic Cosmic Rays and Solar Particle Events. A complete description of a mixed radiation field is provided by the fluence spectrum as a function of charge and energy of the impinging particles, because with these data, in principal, any dosimetric quantity (absorbed dose, LET, lineal energy) can be calculated. Consequently, devices that could make it possible to infer this spectrum at the point of interest, at least for the most significant particles from a radiological point of view, raise the interest of the space weather community.

Materials and Methods MIDAS sensing element is a cube with dimensions 10 mm x 10 mm x 10 mm. A plastic scintillator cube with neutron/gamma discrimination capability and dimensions 7 mm x 7 mm x 7 mm is enclosed in a Titanium box whose five out of six faces are covered by stacks of 2 layers of silicon pixel detectors with in-pixel signal processing

electronics. The remaining one face is covered by a silicon photomultiplier which collects the light signal produced in the scintillator material. The silicon photomultiplier signal is readout, the tail/total integrals are computed in an analog fashion and the result is digitized. The Titanium shield prevents protons with kinetic energy up to 18 MeV produced by the elastic scattering of the neutrons inside the scintillator to induce signal in the silicon detectors. The silicon detectors are CMOS active pixel sensors manufactured in a quadruple well standard process with > 2000 Ohm cm substrate resistivity. The anode of the sensing diode is formed by the high resistivity p-type substrate and the cathode by a deep (some um) n-type well. The diode is reverse biased with -28 V. The pixel size is 107 um. The thickness of the fully depleted Si layer is 50 um. The in-pixel transistors reside on shallow n and p type wells isolated from the cathode. The pixel electronics have been designed with capability to process charge from 0.5 fCb up to 6 pCb generated by the energy deposited by a single track. The device response has been simulated with the aid of GEANT4. Prototypes of the neutron and the charged particles sub-systems have been manufactured and they are under evaluation.

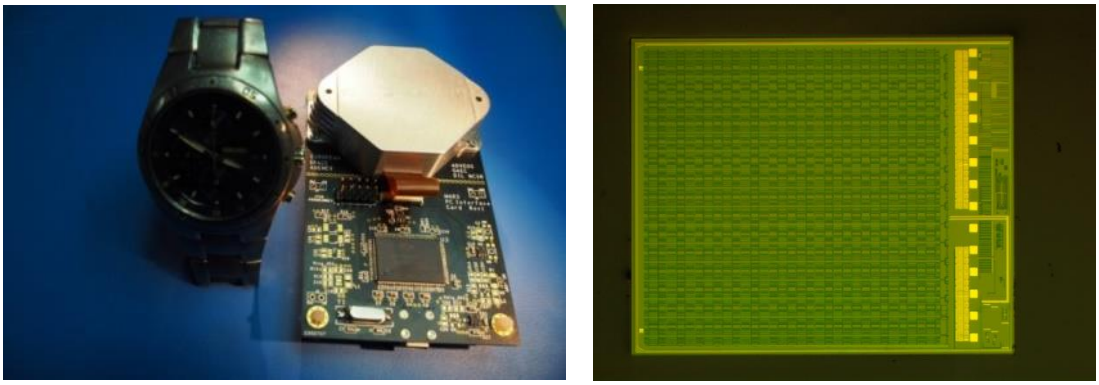

Figure 1: The prototype of the device (left). The active pixel sensor chip (right).

Results and Discussion The results of the simulation study indicate that it is possible to discriminate all the important ions with the aid of appropriate variables constructed by the data which the instrument provides. The experimental tests of the neutron measurement sub-system show that the spectrum of a ^{252}Cf source is measured correctly. The evaluation of the charged particle sub-system (the active pixel sensor) is underway and the active pixel sensor's functionality has been verified partially.

Conclusion We will present the progress in the development of an instrument capable to provide particle fluence spectra for mixed radiation fields found in space. The instrument has the dimensions of a wristwatch which means two orders of magnitude reduction in dimensions, mass and power from current instruments with similar capabilities.

References

1) ICRP Publication 123, Ann. ICRP 42(4), 2013.

Characterization of a pixelated silicon microdosimeter in microbeams of light ions

A. Pola[1], S. Agosteo[1], D. Bortot[1], A. Fazzi[1], D. Mazzucconi[1]*, S. Galer[2], K. J. Kirkby[3,4], M. J. Merchant[3,4], H. Palmans[2,5]

[1]*Politecnico di Milano, Milano, Italy*

[2]*National Physical Laboratory, Teddington, United Kingdom*

[3]*The University of Manchester, Manchester, United Kingdom*

[4]*The Christie NHS Foundation Trust, Manchester, United Kingdom*

[5] *MedAustron, Wiener Neustadt, Austria*

Highlights Characterization of a pixelated silicon telescope using a microbeam. The low energy tail of the spectrum is due to partial collection of the charge. This solid state telescope is a suitable device for measuring the microdosimetric quantities of light-ion beams.

Key words Silicon monolithic telescope, microbeam, microdosimetry

Background and Objectives The effectiveness of radiotherapy is strictly related to the energy deposited by the radiation beam at the cellular level. For this purpose, the microdosimetric approach was proposed for characterizing therapeutic hadron beams[1)]. The monolithic silicon telescope (MST) has demonstrated very good performance in measuring microdosimetric spectra of a light-ion beam if compared with reference TEPCs (Tissue Equivalent Proportional Counters)[2)]. The purpose of this work is to characterize a segmented MST by irradiations with charged particle beams of micrometric spot size available at the Ion Beam Centre - University of Surrey. The aim is to study the dependence of the detector response (charge collection efficiency and pulse height variation) on the irradiated position, together with the impact of performance on the obtained microdosimetric distributions.

Materials and Methods The device used is a Si-micro-telescope composed of a surface stage about 2 μm in thickness segmented in a matrix of micrometric cylindrical elements about 9 μm in diameter. Each element is surrounded by a guard about 14 μm in diameter which confines the charge collection. This stage is coupled to a deeper stage about 500 μm in thickness which measures the residual energy of ions impinging on the detector. The Surrey Ion Beam Centre hosts a 2 MV Tandetron, which includes the microbeam beamline exploited for this experiment. Measurements with three particle beams were performed: 2.5 MeV protons, 9.96 MeV carbon ions and 4.5 MeV lithium ions. The microbeam spot size (about 1.5 μm in FWHM)

was used to irradiate different regions of the device locally in order to study their charge collection efficiency. FLUKA simulations were also carried out for comparison with experimental data.

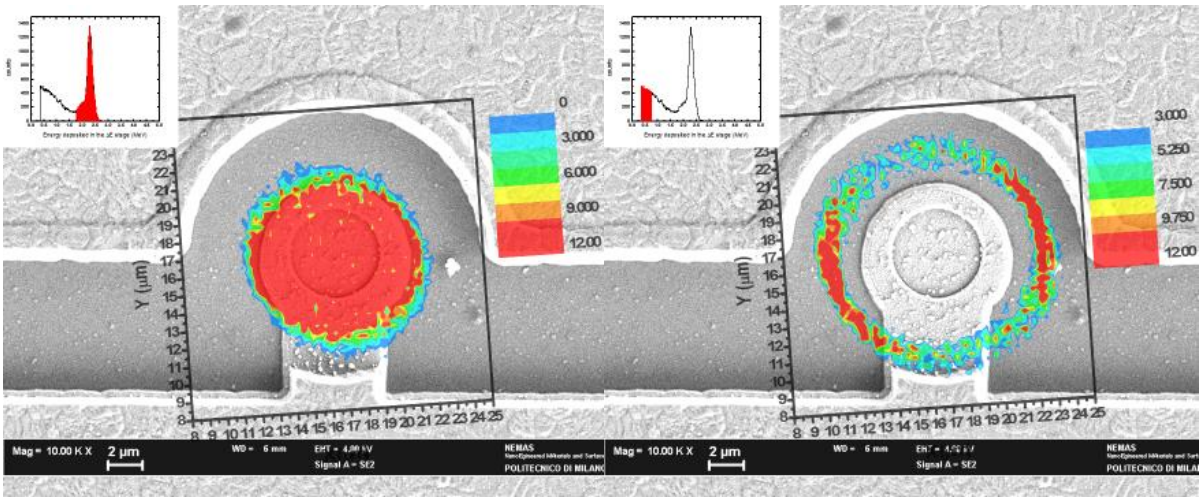

Figure 1. Correlation between irradiated position and corresponding differential spectrum of the energy acquired by the ΔE stage of the microdosimeter.

Results and Discussion Two examples of a SEM image of one segment of the ΔE stage overlaid with the corresponding 2D map of the microbeam position are shown in Figure 1. These plots show the correlation between the irradiated region and the corresponding energy measured by the microdosimeter (differential spectra at top left). The obtained results suggest that the low energy tail of the ΔE stage spectrum is due to the partial collection of the charge generated by events between the sensitive region and the guard ring. This result is confirmed by FLUKA simulations. Nevertheless, this behavior demonstrates a negligible effect (lower than about 10% in terms of total dose) on the microdosimetric dose distribution.

Conclusion The characterization of the response of the segmented silicon microdosimeter with charged particle microbeams highlights a partial charge collection outside the sensitive volume. However, since the obtained microdosimetric distribution is only slightly affected, this solid state telescope is a suitable device for measuring the microdosimetric quantities of light-ion beams.

References

1) Menzel, H.G. et al. Int. J. Radiat. Biol. 57 (4), 865-883 (1990).
2) Agosteo, S. et al. Radiat. Meas. 45 (10), 1284-1289 (2010).

* *Corresponding author*: davide.mazzucconi@polimi.it

Tailor-Made 3D Dosimeter Based on 3D Printing Technology

Takeshi Fujiwara[1]*, Ichiro Kawamura[2], Yutaka Fujimot[2], Masanori Koshimizu[2], Go Okada[3], Keisuke Asai[2]

[1]*National Institute of Advanced Industrial Science and Technology (AIST), Tsukuba, Japan*

[2]*Tohoku University, Sendai, Japan*

[3]*Kanazawa Institute of Technology, Kanazawa, Japan*

Highlights We succeed in fabricating tailor-made 3D dosimeter with radiochromic material and 3D printer. We propose the novel method to precisely copy the shape of personal internal organs with our 3D printed dosimeter, and use for the more accurate and safe radiotherapy.

Key words 3D print, dosimeter, radiochromic, radiotherapy

Background and Objectives The demand of radiotherapy is increasing rapidly. On the other hand, new and complex radiotherapy has been developed such as IMRT, SBRT and particle therapy. For quality assurance of those new generation radiotherapies, we propose a new personalized tailor-made 3D dosimeter based on 3D printing technology.

Materials and Methods First, 3D X-ray CT data is taken for modelling data of the 3D dosimeter. Here, we consider as those modelling data for the tailor-made dosimeter is available because every patient takes X-ray CT before radiotherapy. Figure 1 shows the schemes which a sample are converted into 3D copy. Achieved X-ray 3D CT data are converted into STL data for 3D modelling and printed with commercialized 3D printer. [1,2)]

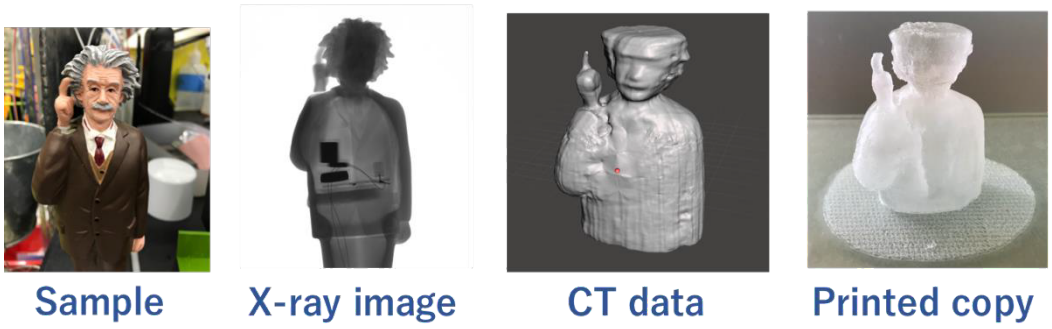

Figure 1. Illustration of the Peace Memorial Park next to the Conference venue.

Results and Discussion First, radiochromic filament are developed with PMMA pellets and 6-nitro-BIPS additives. After optimizing those parameters, such as temperature and fabrication speed, we succeed in producing custom radio-sensitive filament. After all, we fabricated a 3D printed model with this radiochromic material. The radiochromic filament and the printed test model were irradiated with 10 kGy X-rays, and the Figure 3 shows those samples after irradiation. Irradiated part was colored obviously which could be easily observed with naked eyes.

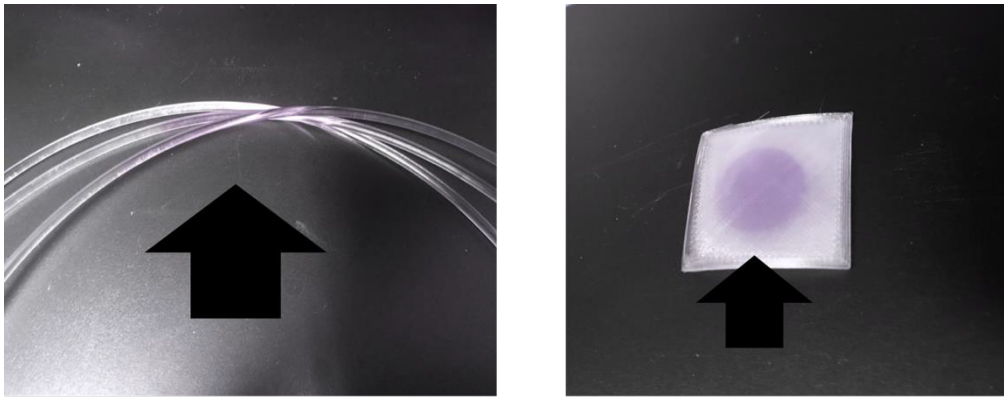

Figure 2. Photographs of radiochromic filaments and 3D printed sample after X-ray irradiation

Conclusion We succeed in fabricating first 3D printed dosimeter based on radiochromic material. In the conference we will introduce the detail of fabrication process and the readout scheme.

References

1) Takeshi Fujiwara, et al., 2019 JSAP spring conference
2) I. Kawamura, et al., 2019 JSAP spring conference

Microdosimetric modeling of radiation-induced luminescence

Alessio Parisi [a,b], Olivier Van Hoey [a], Patrice Mégret [b], Filip Vanhavere [a]

[a] *Belgian Nuclear Research Centre SCK•CEN, Mol, Belgium*
[b] *University of Mons, Faculty of Engineering, Mons, Belgium*

Highlights This talk presents the recently developed Microdosimetric d(z) Model able to describe and predict the relative efficiency of luminescent detectors for measuring different radiation qualities by studying the changes in the microscopic pattern of energy deposition through an analysis of the simulated microdosimetric specific energy probability distributions in nanometric targets. The model was tested for different types of luminescent detectors, showing a very good agreement with experimentally determined efficiency data.

Keywords Luminescent detectors, Microdosimetric d(z) Model, PHITS

Background and Objectives Because of their safe, light, small and passive nature, radiation detectors based on the luminescence technique are commonly used for dose assessment in space and hadron therapy facilities. However, radiation measurements in these complex radiation environments require an in depth knowledge of the detector's efficiency for measuring a wide range of particles and energies. Consequently, during the years a lot of effort has been placed on the experimental investigation of the relative efficiency of luminescent detectors by means of calibrated ion beam exposures at ground level particle accelerators. The latter quantity (η_{rel}) is defined as in Equation 1 as the intensity of the luminescence signal S per unit of absorbed dose D for the radiation under investigation over the same quantity for a reference radiation.

$$\eta_{rel} = \frac{(S/D)_{radiation}}{(S/D)_{reference\ radiation}} \quad (1)$$

It was concluded that this relative efficiency is not a unique function of the LET of the incident radiation, but depends strongly also on the particle type [1, 2]. This happens because, in order to have the same LET, two different particles must have different velocities: the heavier the particle, the higher the velocity. Consequently, the heavier particle will produce δ-rays with higher energies (so longer range in matter) which will deposit their energy in a radially less dense way around the track of the charged particle [3].

Unfortunately, the experimental determination of the relative efficiency of luminescent

detectors through irradiations in charged particle accelerators is time consuming and very expensive. Furthermore, due to experimental limitations, it is often not possible to irradiate the detectors with very high energies, less common isotopes or exotic particles. In addition, the efficiency determination at low energies is biased with associated large uncertainties in range, LET and dose. However, a complete characterization of the efficiency of these detectors is needed, especially for space applications where particles with a really broad energy spectrum and exotic isotopes are present.

Therefore, this lecture deals with the development and validation of the Microdosimetric d(z) Model able to describe and predict the efficiency of luminescent detectors for measuring different radiation qualities. Firstly, the theoretical background, the assumptions behind the model and its methodology are reviewed in detail. Afterwards, the results of the model are benchmarked through a comparison with experimentally determined efficiency values. In addition, a systematic investigation on the effect of simulation parameters on the calculated efficiency values is included in the discussion. Finally, some immediate applications of the model are shortly presented.

Materials and Methods The Microdosimetric d(z) Model [4, 5] shares with Olko's model [3] the hypothesis that a luminescent detector is being composed by many independent structures, called targets, which act as sensitive volumes for the radiation-induced luminescence. The key idea of the Microdosimetric d(z) Model is that the relative efficiency of luminescent detectors can be correlated with the microscopic pattern of energy deposition in nanometric targets quantified by means of microdosimetric specific energy distributions. The dimension of these radiation sensitive structures is not known a priori and represents the only free parameter of the model. Differences with Olko's model can be found in the formalism used in evaluating the relative efficiency, the assessment of the microdosimetric probability distributions, the specific energy response function and the reference radiation. Furthermore, in this work, the particle slowing down within the detector and the creation of secondary particles were considered in the Monte Carlo simulations.

In the Microdosimetric d(z) Model, the relative luminescence efficiency of the detectors is evaluated using Equation 2, where *d(z)* is the dose probability distribution of the specific energy and *r(z)* is the specific energy response function.

$$\eta_{rel} = \frac{\left[\int_0^{+\infty} d(z)\, r(z) dz\right]_{radiation}}{\left[\int_0^{+\infty} d(z)\, r(z) dz\right]_{reference\ radiation}} \qquad (2)$$

The dose probability distribution of the specific energy *d(z)* has been assessed performing computer radiation transport simulations with the Monte Carlo Particle and Heavy Ion Transport code System (PHITS) [6]. On the other hand, the specific energy response function *r(z)* is determined by analyzing the experimentally assessed dose response of the detectors to sparsely ionizing radiation such as high energy photons. More details on the assessment of *d(z)* and *r(z)* can be found in references 4 and 5.

Results and Discussion As an example, using Equation 2, the relative efficiency of LiF:Mg,Ti (MTS) thermoluminescent detectors for measuring heavy ions and photons was assessed as function of the a priori unknown size of the radiation sensitive structure. For both charged particles (Figure 1) and photons (Figure 2), a comparison with experimentally determined efficiency data showed a very good agreement in case of calculations performed in a simulated target size of 40 nm [4, 5]. Similar conclusions were drawn in case of LiF:Mg,Cu,P (MCP) detectors [4, 5]. The determined site size is in agreement with the charge migration distance during the recombination stage (40-47.5 nm) and the characteristic lithium fluoride crystallite size determined through X-ray diffraction (31 nm).

Conclusion The Microdosimetric d(z) Model can be reliably used to assess detector efficiencies for a large number of combinations of particles (photons, electrons, thermal neutrons, exotic particles, antimatter…), energies and detectors, also for mixed fields such as space or hadron therapy.

References

1) Horowitz, Y.S., 1981. Physics in Medicine & Biology, 26, p.765-824.
2) Berger, T. and Hajek, M., 2008. Radiation Measurements, 43, pp.146-156.
3) Olko, P., 2007. Radiation measurements, 41, pp.S57-S70.
4) Parisi, A., 2018. PhD Thesis, University of Mons.
5) Parisi et al., 2019. Radiation Measurements, 123, pp.1-12.
6) Sato, T. et al., 2018. Journal of Nuclear Science and Technology, 55, pp.684-690.

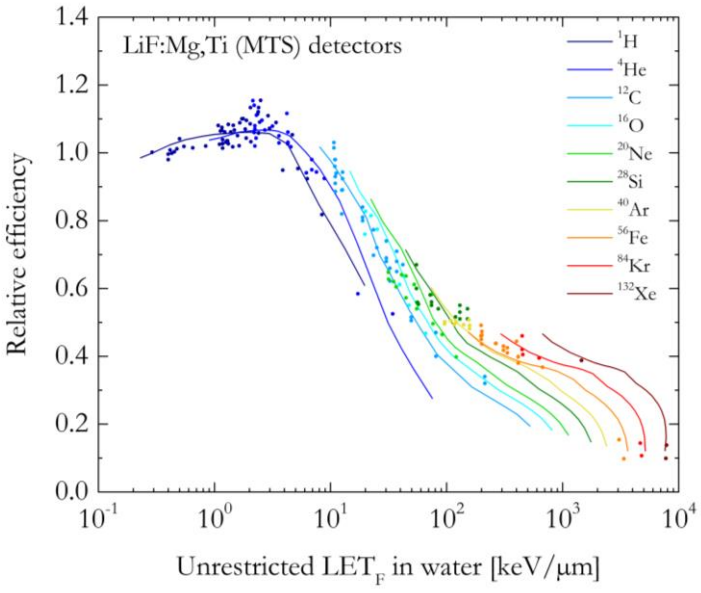

Figure 1. Relative luminescence efficiency of LiF:Mg,Ti (MTS) detectors for measuring ions from ^{1}H to ^{132}Xe: comparison between experimental data (dots) and the results of Microdosimetric d(z) Model (lines) for a simulated target size of 40 nm.

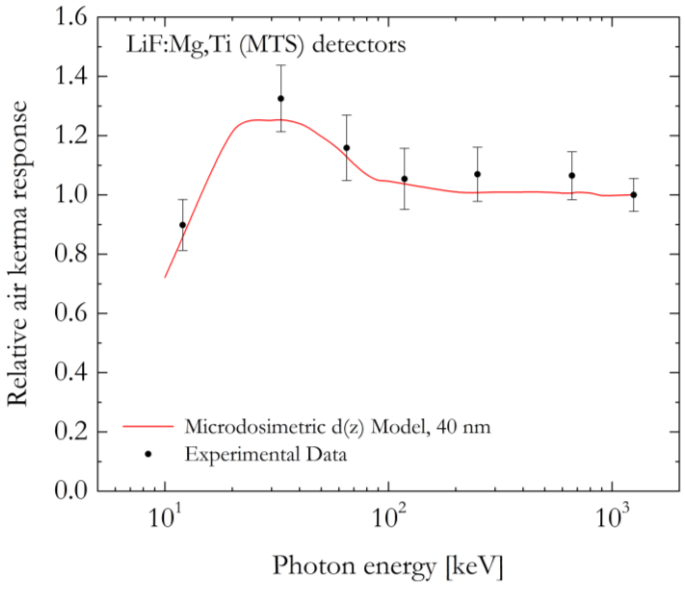

Figure 2. Relative photon air kerma response of LiF:Mg,Ti (MTS) detectors: comparison between experimental data (dots) and the results of Microdosimetric d(z) Model (lines) for a simulated target size of 40 nm.

Quantum tunneling processes in luminescence materials: applications in retrospective dosimetry, temperature sensing and thermochronometry

Vasilis Pagonis[1]*, George Kitis[2] , George S. Polymeris[3]
[1]*McDaniel College, Westminster, USA*
[2]*Aristotle University, Thessaloniki, Greece*
[3]*Ankara University, Ankara, Turkey*

Highlights New experimental data are presented for both natural and laboratory made dosimetric materials, and they are fitted using a quantum tunneling model for luminescence processes. New analytical equations are derived, which are useful metrics in the research areas of retrospective dosimetry, temperature sensing and thermochronometry.

Key words retrospective dosimetry, quantum tunneling, thermochronometry, temperature sensing

Background and Objectives Quantum tunneling is an important luminescence mechanism in both natural and laboratory made dosimetric materials; it is associated with localized transitions, instead of delocalized transitions taking place via the conduction and valence bands. Examples of laboratory made materials with quantum tunneling mechanisms are rare earth doped lanthanides like $YPO_4:Pr_3^+,Dy_3^+$, persistent luminescence phosphors like $SrAl_2O_4:Eu^{2+},Dy^{3+}$, and borates like MgB_4O_7:Dy, Na (see for example the review by Bos[1)]). Examples of natural ubiquitous materials with tunneling are apatites and feldspars.

The objectives of this paper are: (a) Show that the luminescence mechanism in all these materials can be described *quantitatively* using a model based on random distributions of charges (b) Discuss possible applications of thermoluminescence signals in three different research areas: retrospective dosimetry, temperature sensing and thermochronometry studies (Bos [1)],Yukihara et al., 2018 [2)].

Materials and Methods. Figure 1 shows a set of experimental TL glow curves recorded using the display glass of a mobile phone (sample N3109c of category A display glass), with the experimental details given in Discher and Woda[3)]. The sample was preheated to temperatures T_{STOP} indicated in the figure, before measuring the TL glow curve. Figures 2 and 3 show new experimental TL data from the dosimetric material MgB_4O_7:Dy,Na (MBO), with the details of the experimental setup given in Kitis et al[4)]. Figure 2 shows the effect of irradiation temperature, and Figure 3 shows the results of isothermal experiments. Figure 4

shows experimental TL from a preheated geological feldspar sample, with the details given in Pagonis et al[5].

Results and Discussion The solid lines in Figs.1-4 show fitted curves to the experimental data, using the tunneling model and the Monte Carlo method in Pagonis et al.[5], based on the random distribution model by Jain et al[6]. New analytical equations are derived in the model for the variation of the temperature of maximum TL intensity as a function of the preheat temperature and preheat times. These equations can be very useful metrics in the areas of retrospective dosimetry, temperature sensing and low temperature thermochronometry.

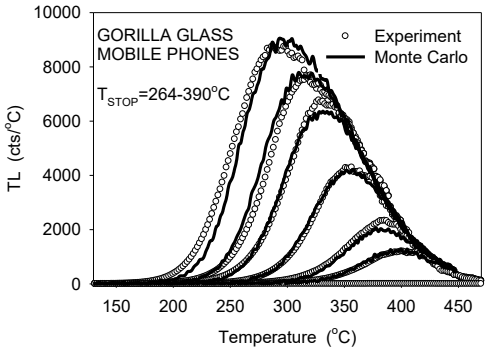

Fig.1

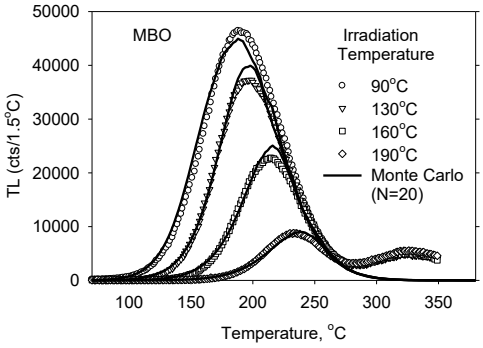

Fig.2

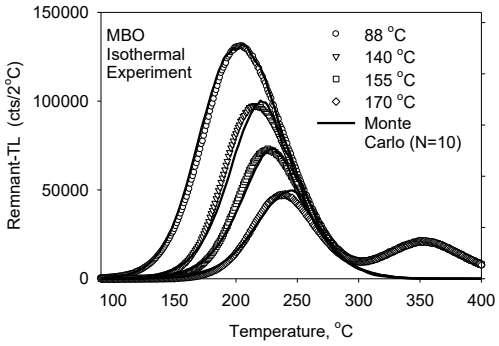

Fig.3

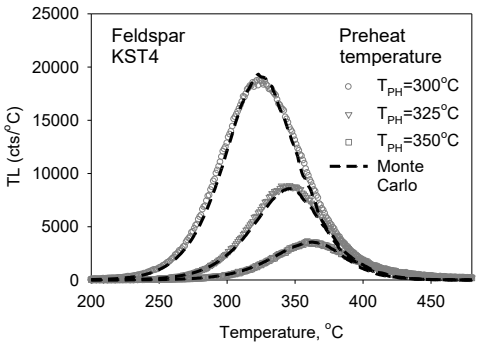

Fig.4

Conclusion The model provides excellent description of all experimental data. The underlying common physical mechanism is the presence of random distributions of charges in the material, and tunneling processes taking place via the excited state of the electron traps.

References

1) A. Bos. Materials 2017, 10, 1357; doi:10.3390/ma10121357.
2) E.G. Yukihara et al. Radiat. Meas. 120, 15 (2018), 274-280.
3) Discher M. and Woda, C. 2013. Radiat. Meas. 53-54, 12 – 21.
4) Kitis et al., 2016. Radiat. Meas. 84,15-25.
5) V. Pagonis et al, 2019. J. Lumin. 207, 266-272.
6) M. Jain et al, 2012. J. Phys.: Condens. Matter 24, 385402.

Infra-red photoluminescence, a step change in trapped charge dating

M. Jain[1]*, R. Kumar[1], E. Sellwood[1], E. Sahiner[1,2], M. Kook[1]

[1]*Center for Nuclear Technologies, Technical University of Denmark, DTU Risø Campus, Roskilde, Denmark*

[2]*Institute of Nuclear Sciences, Ankara University, Beşevler, 06100, Ankara, Turkey*

**Corresponding author; Email: maja@dtu.dk; Telephone: +45 5017 3624*

Highlights

Infrared photoluminescence (IRPL), a new method of trapped charge dating based on non-destructive probe of trapped electrons.

Key words

Infrared photoluminescence, imaging, bleaching, K-feldspar

Background and objectives

Dosimetry and dating techniques based on luminescence rely upon charge detrapping by photon/phonon interactions with the crystal, and subsequent radiative recombination of the opposite charge carriers. Numerical models of localised transition in feldspar suggest that radiative intra-defect transitions (excitation-relaxation) within the main electron trapping state (the principle trap) is the dominant luminescence generation mechanism (Jain et al., 2012, 2015); however such transitions are overlooked in the typical anti-Stokes measurements performed in OSL. Recently our group [1] has discovered two dose-dependent Stokes-shifted emissions in feldspar at ~880 and ~950 nm (excitation at ~830 nm), named infra-red photoluminescence (IRPL) (Prasad et al. 2017; Kumar et al., 2018). These signals derive from radiative relaxation of the excited state of the principle trap with a lifetime of about 30μs.

IRPL shows a dose response similar to that of OSL, but since it does not not involve electron-hole recombination, the signal can be read out non-destructively (especially at cryogenic temperatures). In addition, because IRPL can be measured even from traps remote from recombination centres, it includes a very stable, steady-state component (i.e. one that does not suffer from anomalous fading). IRPL has the potential for:

1) providing direct assessment of thermal and optical stabilities, as well as the behaviour of trapped electrons during different laboratory protocols.
2) High resolution imaging (Sellwood et al., 2019): each defect emits light at the rate of thousands of photons per second (depending on the excitation rate). This provides an unprecedented sensitivity for 2D and 3D mapping of defect distribution and examining charge transfer.

The purpose of our investigations is to establish next generation luminescence dating techniques and obtain a better understanding of luminescence mechanisms in feldspar using IRPL as the tool.

Materials and methods

Samples used in this study are K-feldspar ($KAlSi_3O_8$). Excitation and emission spectra were recorded on Risø Station for Cryogenic Luminescence Research (COLUR) consisting of Horiba Fluorolog-3 spectrofluorometer upgraded to include X-ray irradiator, a temperature controlled closed-loop He cryostat (8-300 K), and multiple excitation and detection ports. We also use the Risø TL-OSL reader with pulsed laser excitation, and IRPL detection through a combination of bandpass interference filters (880/10nm or 950/50nm) and appropriate NIR photomultiplier tubes or an imaging camera (Kook et al., 2018).

Results and Discussion

Here we present new results on the potential of IRPL to 1) understand behaviour of the principle trap under different thermal and optical conditions, 2) understand and solve the long standing problem of anomalous fading in dose measurement, and c) understand spatial correlation between trap distribution and chemical composition.

Conclusion

New understanding of the behaviour of electron traps, and recombination mechanism in feldspar.

References

Jain, M., Guralnik, B., & Andersen, M. T. (2012). Stimulated luminescence emission from localized recombination in randomly distributed defects. Journal of physics: Condensed matter, 24(38), 385402.

Jain, M., Sohbati, R., Guralnik, B., Murray, A. S., Kook, M., Lapp, T., ... & Buylaert, J. P. (2015). Kinetics of infrared stimulated luminescence from feldspars. Radiation Measurements 81, 242-250.

Kook, M., Kumar, R., Murray, A. S., Thomsen, K. J., & Jain, M. (2018). Instrumentation for the non-destructive optical measurement of trapped electrons in feldspar. Radiation Measurements 120, 247-252.

Kumar, R., Kook, M., Murray, A. S., & Jain, M. (2018). Towards direct measurement of electrons in metastable states in K-feldspar: Do infrared-photoluminescence and radioluminescence probe the same trap? Radiation Measurements 120, Pages 7-13.

Prasad, A.K., Poolton, N.R.J., Kook, M., Jain, M. (2017). Optical dating in a new light: A direct, non-destructive probe of trapped electrons. Scientific Reports 7, 12097. DOI: 10.1038/s41598-017-10174-8

Sellwood, E.L., Guralnik, B., Kook, M., Prasad, A.K., Sohbati, R., Hippe, K., Wallinga, J., Jain, M. (2019) Optical bleaching front in bedrock revealed by spatially-resolved infrared photoluminescence. Scientific Reports, DOI: 10.1038/s41598-019-38815.

Role of ionizing radiation on the formation of defects within LiF:Mg

Guerda Massillon-JL[1], Conrad S.N. Johnston[2], and Jorge Kohanoff[2]

[1]*Instituto de Física, Universidad Nacional Autónoma de México, 04510 Coyoacan Mexico City, México*

[2]*Atomistic Simulation Centre, Queen's University Belfast, Belfast BT7 1NN, Northern Ireland, United Kingdom*

Highlights For more than 70 years, defects responsible for the thermoluminescent (TL) glow-curve have been studied experimental and theoretically without a complete understanding. For the first time, a quantum approach based on first principle is used to investigate the role of ionizing radiation on the formation of defects induced by Mg and Ti interstitials in LiF. The results indicated that most of the defects that might be responsible for the complex TL glow curve are created by ionizing radiation.

Key words radiation dosimetry, Hybrid density functional theory, defect formations, ionizing radiation, LiF:Mg,Ti

Background and Objectives. LiF:Mg,Ti is the most commonly thermoluminescent (TL) dosimeter used in several applications. Nevertheless, the basic processes that give rise to the TL-response when exposed to high ionization-density radiation-fields, e.g. low-energy, is not yet well understood [1]. During the last 3 years, we have used a novel approach to solid-state dosimetry based on fundamental quantum mechanics. Electronic structure calculations of defect states induced by Mg interstitials in LiF as well as the localization of secondary electrons produced during the radiation interaction have been investigated from first-principles.

Materials and Methods. In this work, the PBE0 hybrid functional [2] that combines 25% Hartree–Fock (HF) exchange and the PBE semi-local functional has been used. Formation energies of various charged defects as well as the thermodynamic transition level to determine their stability were calculated.

Results and Discussion The results suggest that before irradiation there are only Mg interstitial defects, which distort the LiF lattice by creating an empty space in which electrons can be trapped during irradiation (see Figure 1). Besides the generation of secondary electrons

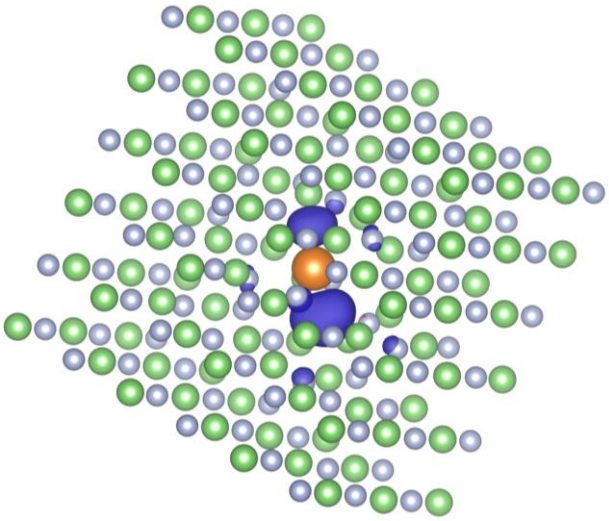

FIG.1 Spin density isosurface of the LiF:Mg+e^-. The grey, green and orange symbols represent the F, Li and Mg atoms, respectively. The blue surface (value 0.0065 e/Å^3) represents the spin density [3].

(and holes), the irradiation can simultaneously create Li and F vacancies, remove a Li atom nearby a Mg interstitial, creating a Mg-Li_{vac} defect; substitute a Li atom by a Mg one to induce a LiF-Mg-Li_{sub} defect and create a Li vacancy plus a Mg substitutional to form a LiF-Mg-Li_{sub}-Li_{vac} defect which will also capture secondary electrons.

Conclusion. The LiF:Mg and LiF:Mg-Li_{vac}+e^- as well as the LiF-Mg-Li_{sub} and LiF-Mg-Li_{sub}-Li_{vac}+e^- defects are very close in energy. We have also seen that the Li vacancy does not play a relevant role in the defect formation [3].

Acknowledgments

We acknowledge computational support from the UK national high-performance computing (HPC) service, ARCHER, for which access was obtained via the UKCP consortium and funded by EPSRC grant ref EP/ K013564/1 and from UNAM HPC service, Miztli, through grant ref. LANCAD-UNAM-DGTIC-334. This project is partially supported by Royal Society grant NA150212 and PAPIIT-UNAM grant IN115117.

References

[1] Massillon-JL G, Cabrera-Santiago A, Minniti R, O'Brien M and Soares C 2014 *Phys. Med. Biol.* **59** 4149

[2] Perdew J P, Ernzerhof M and Burke K 1996 *J. Chem. Phys.* **105** 9982

[3] Massillon-JL G, Johnston C S N and Kohanoff J 2019, *J. Phys. Cond. Matter*, **31** 025502

Radiophotoluminescence from Ag-doped Alkali-phosphate Glass in Real Time, During Irradiation with a LINAC X-ray Beam

Stephen W.S. McKeever[1]*, Sergey Sholom[1], Nishan Shrestha[1] and David M. Klein[2]
[1]*Department of Physics, Oklahoma State University, Stillwater, Oklahoma, USA*
[2]*Oklahoma Cancer Specialists and Research Institute, Tulsa, Oklahoma, USA*

Highlights The real-time response of radiophotoluminescence (RPL) from Ag-doped alkali-phosphate glass during irradiation with high-energy pulsed X-rays from a LINAC is reported. The non-linear growth of RPL versus irradiation time is correlated with the build-up effect for RPL in this material.

Key words Radiophotoluminescence, dosimetry, Ag-doped alkali-phosphate glass

Background and Objectives Radiophotoluminescence (RPL) from Ag-doped alkali-phosphate glass is an established dosimetry method for personal and medical dosimetry[1)]. A characteristic of the RPL signal from this material is the slow build-up of the signal following irradiation[2)]. The objective of the present study is to examine the RPL signal during irradiation using a high-dose-rate, pulsed LINAC X-ray source in an effort to further understand the build-up properties while also exploring the potential of this material as a real-time *in-vivo* dosimeter for use in radiotherapy.

Materials and Methods The samples used in this study were GD-302M glass dosimeters from Chiyoda Technol Corporation, Japan. The composition of the glass is: P: 31.55 wt. % , O: 51.16 wt. % , Al: 6.12 wt. % , Na: 11.00 wt. % , and Ag: 0.17 wt. %. The samples are rods of dimensions 1.5 mm diameter and 12 mm length. The X-ray source was a 6MV/10MV/18MV LINAC. RPL measurements were taken using a 355 nm, 50 mW laser of 1 ns pulse width and a frequency of 10 kHz. The laser pulses were directed down a silica fiber via a dichroic mirror to a GD-302M rod mounted co-linearly with the fiber at the fiber's distal end. RPL emission from the GD-302M rod was directed back along the same fiber, via the dichroic mirror, to a photomultiplier tube. Signals due to radioluminescence and Cherenkov light were eliminated by synchronizing the RPL measurements with the LINAC X-ray pulses such that RPL was measured only between X-ray pulses. The LINAC pulses were 3 μs wide with a frequency of 400 Hz. The timing utilized was such that 20 individual RPL measurements were made between each LINAC pulse. After 100 LINAC pulses, *i.e.* 2000 separate RPL measurements, the RPL signals were summed, background subtracted, and displayed as a single data point every 0.25 s. A subsidiary silica fiber was used to monitor the LINAC on and off periods using the Cherenkov light from the fiber.

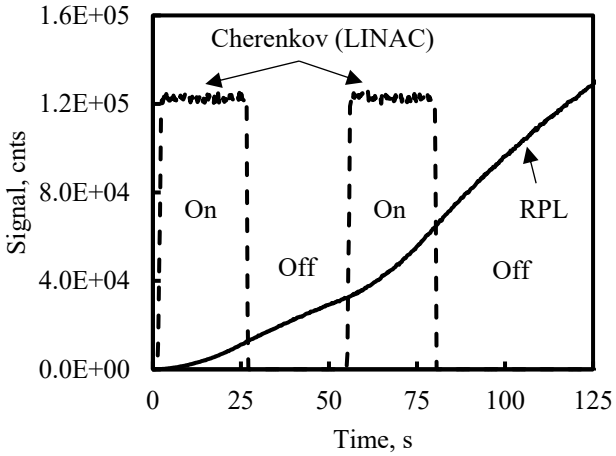

Figure 1. RPL during (On) and after (Off) LINAC irradiation showing the supralinear growth of the RPL signal in irradiation On periods, and the sublinear build-up in the Off periods. Two On periods and two Off periods are shown. The LINAC On periods were monitored using Cherenkov light from a subsidiary silica fiber.

Results and Discussion Figure 1 shows an example of real-time RPL growth during the irradiation period, followed by the continued sublinear growth of the RPL following the irradiation period. The supralinear growth during the irradiation period is caused by a convolution of the intrinsic growth of RPL with dose and the function describing the build-up of the RPL signal. The continued growth after the LINAC irradiation is due to build-up alone. The build-up is a result of the formation of Ag_2^+ dimers after irradiation; Ag^{2+} ions may also contribute.[2] From a consideration of the mathematical functions describing these effects it is possible to devise a correction algorithm for the RPL growth during real-time exposure.

Conclusion The non-linear growth of RPL from Ag-doped alkali-phosphate glasses in real-time during irradiation may be understood from a consideration of the phenomena that give rise to the build-up effect observed after irradiation. Mathematical analysis of the data suggests a correction algorithm may be found to correct for this non-linearity.

Acknowledgements This work was funded by Chiyoda Technol Corporation, Japan, and the State of Oklahoma, USA.

References

1) Yamamoto, T., 2011. In *Concepts and Trends in Medical Radiation Dosimetry*, AIP Conf. Proc., 1345, Rosenfeld, A.B., Kron, T., d'Errico, F., Moscovitch, M. (eds.), 217-230.
2) S. W. S. McKeever, S. Sholom, N. Shrestha, 2019. *Observations regarding the Build-Up Effect in Radiophotoluminescence of Silver-Doped Phosphate Glasses.* Radiat. Meas. 123, 13-20.

Bleaching and dose response studies on Al-hole Electron Spin Resonance (ESR) signals in sedimentary quartz

Alida Timar Gabor[1,2*], Khalif Benzid[1]

[1]*Interdisciplinary Research Institute on Bio-Nano-Sciences, Babeş-Bolyai University, Cluj-Napoca, Romania*

[2]*Faculty of Environmental Science and Engineering, Babeş-Bolyai University, Cluj-Napoca, Romania*

Highlights

Residual dose correction mandatory in ESR dating using Al-hole signals-ESR residuals of Al-hole signals yield hundreds of Gys.

Al-hole residuals increase exponentially with preceding given dose. Mechanism of Al-hole bleaching by electron-hole recombination is supported.

Al-hole signals measured at 90 K are heavily interfered by signals form intrinsic defects (peroxy radicals)

A sum of a single saturating exponential function and a term proportional to the square-root of the accumulated dose describes well the dose response curve of Al-hole signals

Key words sedimentary quartz, ESR dating, Al-hole, dose response curve, residual, bleaching

Background and Objectives The main electron spin resonance (ESR) signals used for dating derive from defects relating to the Al-hole and Ti centres. Al-hole centres are abundant in quartz and the dose response curve of these signals grows to high doses allowing in theory equivalent doses in the kGy range to be measured. Yet, there are some major challenges that confront researchers in this field: (i) The saturating exponential function is the most used to quantify physically the evolution of Al-hole centers with accumulated dose. While this function fits well the experimental data in the low dose range the model fails to describe well the behaviour in the high dose range. The mechanisms behind this observation are not well understood. (ii) The accurate quantification of residual dose contained within the signal is as yet poorly constrained. The physical mechanism for Al-hole bleaching, and consequently understanding the nature of the signal which is being used for dating, is inadequately understood, leading to potential flaws in the fundamental assumptions used. Here we work towards a better understanding of the processes responsible for Al-hole dose response, as well as for developing corrections for the residual of this signal in ESR dating of samples of sedimentary quartz.

Materials and Methods We chose to work with sedimentary quartz samples of different grain sizes from different locations (sand from Australia and loess from Romania, Ukraine and USA) that had been previously securely dated by OSL. Quartz was extracted according to standard OSL preparation techniques, under subdued red light. ESR analyses were carried out using an X band Bruker EMX plus spectrometer equipped with a variable temperature unit.

Results and Discussion Our results demonstrate that both Al-hole as well as the more easily bleached Ti signals yield residual doses, with the Al-hole signals indicating equivalent doses of about 500 Gy, substantially older than expected for the known OSL equivalent doses of a few Gy to tens of Gy. The decay of Al-hole signal as function of bleaching time can be represented by an exponential function with significant residual values. We investigate the dependence of residual magnitude of the Al-hole ESR signal as a function of previous given dose and observe an exponential increase of residual signal with dose. This result is interpreted as supporting evidence that the bleaching mechanism of Al-hole signal is electron-hole recombination with electrons released by light from optically sensitive traps.
We show that even after performing residual subtraction the equivalent doses obtained by Al-hole ESR dating overestimate the expected equivalent doses. By EasySpin simulation of the spectra recorded at 90K we are showing that Al-hole signals are heavily interfered by signals form intrinsic defects (peroxy radicals, ascribed to the bridging oxygen hole centers (OHCs) and non-bridging oxygen hole centers (NBOHCs)). As such we suggest the use of the measurement of the amplitude of the first electronic transition around ~2.06 in order to construct the dose response curve in order to minimize the influence of theses interfering signals. The use of a sum of a single saturating exponential function and a term proportional to the square-root of the accumulated dose is investigated for describing the dose response curve.

Conclusion We consequently reinforce the application of multiple centres ESR dating and recommend that: (i) the dose dependence of Al-hole residuals to be tested before applying bleaching corrections, and (ii) modern analogues, when available, maybe used in parallel with natural bleached samples for quantifying the values of residuals for Al-hole signals (iii) the interference of peroxy signals in Al-hole measurement needs to be taken into account (iv) a function comprising of a sum of a single saturating exponential function and a term proportional to the square-root of the accumulated dose can be used for a more accurate equivalent dose estimation of equivalent doses using Al-hole signals.

The LnTn method: a new method for determining equivalent doses for luminescence dating of sediments

Bo Li[1,2]*, Zenobia Jacobs[1,2], Richard .G. Roberts[1,2]
[1]*Centre for Archaeological Science, School of Earth, Atmospheric and Life Sciences, University of Wollongong, Wollongong, NSW 2522, Australia*
[2]*ARC Centre of Excellence for Australian Biodiversity and Heritage, University of Wollongong, Wollongong, NSW 2522, Australia*

Highlights A new method of determining equivalent dose (D_e) for luminescence dating of sediments is presented. This method overcomes the D_e underestimation problem associated with conventional methods when dating old samples.

Key words LnTn, standardised growth curve, equivalent dose

Background and Objectives Recent studies have suggested that rejecting a large number of 'saturated' grains may result in a significant underestimation in the final D_e due to the truncation of the full D_e distribution (Duller, 2012; Gliganic et al., 2012; Li et al., 2016; Thomsen et al., 2016; Guo et al., 2017). To avoid this problem, Li et al. (2017) proposed a new method, the so-called LnTn method, that involves analysing L_n/T_n distributions and establishing standardised growth curves (SGCs) (Roberts and Duller, 2004; Li et al., 2015) for different grains or aliquots. In this new method, no grains are rejected because they are 'saturated', so a full and untruncated distribution of the L_n/T_n ratios is obtained, which allows reliable D_e estimation beyond the conventional limit of ~$2D_0$ using the standard single-aliquot regenerative-dose procedure. However, there is no systematic investigation of the distribution pattern of LnTn signals, which is critical for developing suitable statistical models to estimate the mean values of the distribution. In this study, we investigated the distribution of LnTn signals and test several statistical models designed for D_e estimation.

Materials and Methods We investigated the LnTn method by modelling various samples of different ages and simulated the resulting single-grain D_e distributions using a Monte Carlo method. The results obtained using the LnTn method are compared with those obtained using conventional methods.

Results and Discussion Our results suggest that the distributions of LnTn signals and D_e values differ: the former are negatively skewed, while the latter are positively skewed. As a result, the arithmetic mean of the LnTn distribution will result in the underestimation of D_e. Such issues can be overcome by using the normalized median absolute deviation (nMAD) to 'trim' the negative tail of the LnTn distribution. We show that this method can also be applied to partially bleached and post-depositionally mixed samples.

Conclusion The LnTn method is a robust method for determining D_e values for luminescence dating of sediments. It relies on the establishment of standardised growth curves, and has the potential to date old samples with D_e values beyond $2D_0$ on the corresponding dose response curve.

References

1) Duller, G.A.T., 2012. Improving the accuracy and precision of equivalent doses determined using the optically stimulated luminescence signal from single grains of quartz. Radiation Measurements 47, 770-777.
2) Gliganic, L.A., Jacobs, Z., Roberts, R.G., Dominguez-Rodrigo, M., Mabulla, A.Z.P., 2012. New ages for Middle and Later Stone Age deposits at Mumba rockshelter, Tanzania: Optically stimulated luminescence dating of quartz and feldspar grains. Journal of Human Evolution 62, 533-547.
3) Guo, Y.-J., Li, B., Zhang, J.-F., Yuan, B.-Y., Xie, F., Roberts, R.G., 2017. New ages for the Upper Palaeolithic site of Xibaimaying in the Nihewan Basin, northern China: implications for small-tool and microblade industries in north-east Asia during Marine Isotope Stages 2 and 3. Journal of Quaternary Science 32, 540-552.
4) Li, B., Roberts, R.G., Jacobs, Z., Li, S.H., 2015. Potential of establishing a 'global standardised growth curve' (gSGC) for optical dating of quartz from sediments. Quaternary Geochronology 27, 94-104.
5) Li, B., Jacobs, Z., Roberts, R.G., 2016. Investigation of the applicability of standardised growth curves for OSL dating of quartz from Haua Fteah cave, Libya. Quaternary Geochronology 35, 1-15.
6) Li, B., Jacobs, Z., Roberts, R.G., Galbraith, R., Peng, J., 2017. Variability in quartz OSL signals caused by measurement uncertainties: Problems and solutions. Quaternary Geochronology 41, 11-25.
7) Roberts, H.M., Duller, G.A.T., 2004. Standardised growth curves for optical dating of sediment using multiple-grain aliquots. Radiation Measurements 38, 241-252.
8) Thomsen, K.J., Murray, A.S., Buylaert, J.P., Jain, M., Hansen, J.H., Aubry, T., 2016. Testing single-grain quartz OSL methods using sediment samples with independent age control from the Bordes-Fitte rockshelter (Roches d'Abilly site, Central France). Quaternary Geochronology 31, 77-96.

Beta dose heterogeneity in sediment samples measured using a Timepix pixelated detector: implications for single-grain OSL dating

Xiao Fu[1,2]*, Anna Romanyukha[2,3], Bo Li[2,4], Mariana Sontag Gonzalez[2], Nathan Jankowski[2,4], Stuart George[3,5], Susanna Guatelli[3,6], Mike Morley[2], Zenobia Jacobs[2,4], Anatoly Rosenfeld[3,6], Richard G. Roberts[2,4]

[1] *School of Earth Sciences, Zhejiang University, Hangzhou 310027, China*
[2] *Centre for Archaeological Science, School of Earth, Atmospheric and Life Sciences, University of Wollongong, Wollongong, NSW 2522, Australia*
[3] *Centre for Medical Radiation Physics, School of Physics, University of Wollongong, Wollongong, NSW 2522, Australia*
[4] *ARC Centre of Excellence for Australian Biodiversity and Heritage, University of Wollongong, Wollongong, NSW 2522, Australia*
[5] *Space Radiation Analysis Group, NASA Johnson Space Center, Houston, Texas 77058, USA*
[6] *Illawarra Health and Medical Research Institute, University of Wollongong, Wollongong, NSW 2522, Australia*

* Email: fuxiao@zju.edu.cn

Highlights Timepix analysis allows spatially-resolved beta dose rates to be estimated for intact sediment samples; Beta dose rates of archaeological and geological samples were studied using this technique and compared with single-grain D_e values; Beta dose rate heterogeneity contributes about 10–20% to the observed spread in D_e values for the samples studied.

Key words Timepix, OSL dating, archaeological and geological samples, beta dosimetry

Background and Objectives Single-grain (SG) optically stimulated luminescence (OSL) dating has been used increasingly in Quaternary and archaeological studies to determine the depositional age of sediments. To appropriately interpret the SG equivalent dose (D_e) distribution of a given sample and ultimately derive a reliable burial dose using a suitable statistical model, understanding the source of the scatter in D_e values is essential. Beta dose rate heterogeneity is one of the major potential sources of D_e overdispersion, but beta dosimetry of sediment samples at high spatial resolution has rarely been measured at the SG scale. Studies have typically used bulk-sample measurement techniques (such as ICP-MS and beta counting) to estimate the sample-average beta dose rates. These techniques yield dose rates applicable to a large sample volume and conceal information about beta dosimetry at the SG level. Recently, Romanyukha et al. [1] proposed a novel technique employing pixel detectors to derive spatially resolved beta dose rates for intact samples at sub-millimetre resolution using a Timepix hybrid pixelated detector. This semiconductor detector consists of an array of 256 × 256 pixels, each 55 × 55 μm in size. Individual pixels can record the tracks and energies produced by particles

impinging on the detector, such as alpha particles and electrons, and the particle types can be recognised from the shapes of the track clusters. Romanyukha et al. developed a measurement procedure applicable to resin-impregnated sediment samples, and tested it on an artificial micro-stratified sample. They identified the beta-particle contribution to the dose rate with sub-millimetre spatial resolution, and proposed that this technique held promise as a means of deriving spatially-resolved beta dose rates at the SG scale for real and intact sediment samples.

Materials and Methods In this study, we apply Timepix to five archaeological and geological sediment samples collected at two cave sites (one in Indonesia and the other in Russia) and a lake-bordering dune in Australia. The samples differ significantly in their inherent radioactivity and contrasting sedimentary contexts. Of key interest is the beta dose rate inhomogeneity at the SG scale within each of these samples, which were collected intact and then resin-impregnated, and the extent to which this contributes to the measured SG D_e distributions. From each sample, we prepared a sub-sample with an approximate volume of 10 × 60 × 6 mm3 (cave sediments) or 10 × 10 × 6 mm3 (dune sediments) for Timepix analysis, and extracted quartz or K-feldspar grains from the sediments immediately surrounding the Timepix sample for SG (or small aliquot, SA) D_e measurement. The beta dose rate distribution of each sample was obtained by converting the beta particle count rates measured using the Timepix into dose rates using a calibration curve derived using an international standard [1]. These dose rate distributions were compared with the corresponding SG (or SA) D_e distributions to assess the relative contribution of beta dose rate inhomogeneity to the observed spread in D_e values, and the relation of both to the micromorphology of the sediment samples.

Results and Conclusions Our results show that the Timepix analysis allows determination of beta dose rate distribution at sub-millimetre scale for intact sediment samples. The beta dose rates of sediment samples from sites in Australia, Indonesia and Russia exhibit non-uniform spatial distributions, and can be positively skewed, negatively skewed or symmetric in shape. The overdispersion in total dose rate caused by beta dose rate heterogeneity is about 10–20% for our samples. We conclude that Timepix can provide important information for interpreting SG OSL dating results for archaeological and geological samples.

References

1) Romanyukha, A.A., Cunningham, A.C., George, S.P., Guatelli, S., Petasecca, M., Rosenfeld, A.B., Roberts, R.G., 2017. Deriving spatially resolved beta dose rates in sediment using the Timepix pixelated detector. Radiation Measurements 106, 483–490.

L Band Electron Paramagnetic Resonance Tooth Dosimetry using affected Cattles' Teeth in Fukushima

Ichiro Yamaguchi[1]*, Kazuhiko Inoue[2], Masahiro Natsuhori[3]

[1]*National Institute of Public Health, Saitama, Japan*
[2] *Tsurumi Dental University, Kanagawa, Japan*
[3] *Kitasato University, Aomori, Japan*

Highlights The positive Electron Paramagnetic Resonance (EPR) signals possibly due to radiation exposure were nondestructively detectable among affected Cattle in Namie town, Fukushima even by using L Band Electron Paramagnetic Resonance Tooth Dosimetry.

Key words Electron Paramagnetic Resonance, L band, tooth dosimetry, cattle, Fukushima

Background and Objectives Electron Paramagnetic resonance (EPR) tooth dosimetry is an established method to evaluate the radiation dose by measuring stable unpaired electrons produced by radiation exposure and remained in a tooth. The X-band EPR method has also been applied to retrospective dose assessment of atomic-bomb survivors, nuclear disaster of Chernobyl nuclear power plant, nuclear bomb test, radiological accident, using extracted teeth. In the case of radiation emergency, an L-band (1.0-1.2GHz) EPR apparatus has been developed for in-vivo measurement as triage targeting a tooth. This method becomes available for retrospective dose assessment and for triage in terms of emergency radiation medicine. The nuclear power plant accident influenced animals also, so that the environmental study group started research activities from September 2012, and has analyzed and evaluated the various influences of radiation exposure on affected cattle. Currently it has been collected about more than 160 cattle data managed by 10 livestock farmers such at Namie Town and Okuma Town, Fukushima Prefecture. Among these researches, we measured the radiation doses to cattle by using L band EPR tooth dosimetry targeting the affected cattle in Namie and Okuma Town as the alternative dose reconstruction.

Materials and Methods Teeth were collected from cattle those has been stayed continuously after the earthquake in the former evacuation zone of Fukushima Prefecture more than 6 years. After picking up the maxillary incisor teeth from the jawbone portion of the damaged calf, it was washed with tap water. Then with the design knife, soft tissue was removed as much as

possible, and its lip side was used for the measurement. Teeth were precisely positioned using a custom-made bite block that located each tooth within the central homogeneous region of the magnet (Small Dipole Permanent Magnet for L-Band EPR, Model: BFMP-415/170-D, Resonance Research, Inc., MA, USA). The EPR spectra were acquired using standard parameters of 20 scans, including a scan range of 2.5 mT, a scan time of 3 and a modulation amplitude of 0.4 mT. This process was repeated for a total of 3 datasets at each dose, as well as at baseline. ^{15}N-PDT, also known as perdeuterated tempone was sealed in a glass vial and was placed in close proximity to the surface loop and used as a reference standard, as well as to monitor EPR signal detection and the amplitude of magnetic field modulation. The spectra from each of the collected datasets were analyzed using non-linear least-squares fitting to estimate the peak-to-peak signal amplitudes of the radiation-induced signals, and of ^{15}N-PDT. A standard tooth irradiated by the ^{137}Cs source was provided from the EPR Center for the Study of Viable Systems at Dartmouth for the comparison.

Results and Discussion Positive radiation induced signals (RIS) were not detectable among all samples at Okuma Town. On the other hand, positive RIS were detectable among all samples at Namie Towns indicating above 1.3 ± 0.3 Gy. Considering the weathering effect, the cumulative ambient radiation dose (1cm dose equivalent) during 6 years since March 2011 was estimated about 1 Sv including initial radiation dose at Omaru area of Namie town, Futaba county, Fukushima prefecture. The cumulative dose to a cow in Okuma Town is estimated to be around 160 mSv because it is estimated at 14% compared with the Omaru area. L band EPR tooth dosimetry shows consistency with these dose estimations.

Conclusion Radiation exposures to cattle stayed continuously after the TEPCO Fukushima Dai-ichi nuclear disaster in Namie that are former evacuation zone of Fukushima Prefecture were confirmed by EPR tooth dosimetry using L band. However, these radiation doses were not detectable for cattle in Okuma.

Acknowledgements Authors thank the farmers for donating the teeth of cattle for scientific research and support of Ms. Satoko Mikawa and Dr. Harold M Swartz.

References

1) Amber Harshman, Shin Toyoda, Thomas Johnson. Suitability of Japanese wild boar tooth enamel for use as an Electron Spin Resonance dosimeter. Radiation Measurements. 116, 46-50, (2018).

Fabrics for short term dosimetry following a radiological emergency: results of a blind test

Lily Bossin[1,2,3]*, Ian Bailiff[1], Ian Terry[2], Rick Tanner[3], Jon Eakins[3], Liz Ainsbury[3]

[1]*Durham University, Department of Archaeology, Durham, UK*

[2] *Durham University, Department of Physics, Durham, UK*

[3]*Public Health England, CRCE, Chilton, Didcot, Oxon, UK*

Highlights Fabrics were used to reconstruct dose following a blind gamma irradiation using luminescence techniques; An indicative accuracy sufficient for medical triage in a radiological emergency was obtained; The use of fabrics potentially provide spatial mapping of dose; Advantages of this approach are the wide availability of fabrics and prompt processing of samples.

Key words Fabrics, emergency dosimetry, TL, fortuitous dosimeters

Background and Objectives Individual dose assessment is desirable in the response to radiological accidents to support medical triage. Luminescence techniques have been successfully applied to assess radiation dose using alumina substrate resistors, such as those found in modern mobile phones. However, their suitability in actual emergencies has been debated (e.g., reluctance of general public to donate costly phones; the trend of decreasing component size). Extension of the range of suitable materials as surrogate dosimeters has been investigated using fabrics[1),2)]. This paper reports on the outcome of a blind test performed to simulate a radiological emergency, where a multi-assays approach was adopted, deploying alumina substrate resistors (OSL), glass displays (TL), dicentric chromosome assay, radiation transport simulations and fabrics (TL) to obtain estimates of the absorbed dose and compare the performance of each technique and assess their respective strengths.

Materials and Methods Three types of polymer-based fabric, a mobile phone (Nokia Lumen 520) and a tube of human blood were positioned on an anthropomorphic phantom. The blind irradiation was carried out using a ^{60}Co source placed below the phantom, resulting in a heterogeneous radiation field (calibrated dose: 2.52±0.09 Gy and 0.58±0.04 Gy at the waist and eye levels of the phantom respectively). Dose assessments with surface mount resistors extracted from the mobile phone used fast and full mode OSL protocols[3)]; TL procedures were applied to the phone glass display[4)]; dicentric chromosome assay was applied to the blood sample. Fabric samples were cut from different locations (8-12 samples/fabric)

and the absorbed dose was evaluated using a TL measurement procedure.

Results and Discussion The estimates of dose to fabrics accurately recovered the blind dose administered (e.g., 2.59±0.17 Gy for Fabric 1 at the nearest calibrated position 2.52±0.09 Gy). The values of dose determined using fabric samples at different locations on the phantom were consistent with the irradiation geometry, following an inverse square law with distance from the source. Good agreement between the values of dose were obtained at the location that included fabric, the mobile phone and blood sample. The results indicate that potentially all dosimeters would have performed well in a triage mode, sorting the patient into the right category of triage (i.e., high dose, >2 Gy).

Conclusion The results of this blind test confirmed the potential of the class of fabrics tested to be used as a surrogate dosimeter material and to provide sufficiently accurate e estimates of gamma dose to support triage during a radiological emergency. Such fabrics offer the advantage of 1) enabling spatial mapping of gamma dose on the wearer, 2) prompt dose assessment (ca 15 min between receipt of a sample and a dose estimate) and 3) wide availability with samples more readily obtained. Future work will concentrate on further viability testing and then, if appropriate, development of practical guidance for use of fabrics.

References

1) Sholom, S., & McKeever, S. W. S. (2014). Emergency OSL dosimetry with commonplace materials. *Radiation Measurements*, *61*, 33-51.
2) Bossin, L., Bailiff, I. K., & Terry, I. (2017). Luminescence characteristics of some common polyester fabrics: Application to emergency dosimetry. *Radiation Measurements*, *106*, 436-442.
3) Bassinet, C., Woda, C., Bortolin, E., Della Monaca, S., Fattibene, P., Quattrini, M. C., ... & Kouroukla, E. (2014). Retrospective radiation dosimetry using OSL of electronic components: results of an inter-laboratory comparison. *Radiation Measurements*, *71*, 475-479.
4) Discher, M., & Woda, C. (2013). Thermoluminescence of glass display from mobile phones for retrospective and accident dosimetry. *Radiation Measurements*, *53*, 12-21.

Investigation of the dose-response in re-irradiated fingernails and combined effect of drying time-temperature to the ESR signal

Chryzel Angelica B. Gonzales*[1,2,3], Hiroshi Yasuda[2], Seiko Hirota[2], Kentaro Miki[4], Akito Saito[4], Jolan E. Taño[1,2,3] and Yasushi Nagata
[1]*Graduate School of Biomedical and Health Sciences, Hiroshima University, Japan*
[2]*RIRBM, Hiroshima University, Japan*
[3]*Phoenix Leader Education Program (Hiroshima Initiative) for Renaissance from Radiation Disaster, Hiroshima University, Japan*
[4] *Department of Radiation Oncology, Hiroshima University Hospital, Japan*

Highlights Individual variability in the dose-response curves in re-irradiated fingernails was observed. Increasing drying temperature and time generates strong ESR signals.

Keywords ESR, EPR, fingernail, retrospective dosimetry

Background and Objectives The use of fingernails as a potential dosimetric tool remains to be of interest due to a number of advantages, including high sensitivity, facile sample collection, and *in-situ* measurement. Although significant progress in the development of fingernail analysis using electron spin/paramagnetic resonance (ESR/EPR) spectrometry has been reported[2,3)], this remains to be an immense challenge for radiation accident dosimetry purposes. The objective of the present work is to investigate the dose-response of fingernails after irradiation, and to examine the combined effect of drying time and temperature to the ESR signal.

Materials and Methods Six healthy adults of Asian type (3 males and 3 females) provided fingernail samples for this study. The pool of samples from the right/left hands of each donor was divided into 4 sets: 3 sets for irradiation and 1 set for control. The mass of each set is of 20 mg. In periods between harvesting and subsequent procedures (e.g. irradiations and measurements), samples were stored in darkness inside a vacuum desiccator (VE-ALL 1-8-989-01, AS ONE, Japan) at room temperature and were given no additional cuts or any pre-treatments. All experimental exposures were carried out with a Gammacell40 Exactor Low Dose Rate Research Irradiator (Best Theratronics Ltd., Japan) at a dose rate of 0.813 Gy/min. The doses were set to 35 Gy and 70 Gy. The re-irradiation (i.e. second irradiation) of the samples taken from the 6 donors were conducted 6 months after the first irradiation. ESR measurements were performed at room temperature on an X-band spectrometer (JES-FA 100, JEOL Inc., Japan) equipped with ES-UCX2 standard cavity. The peak-to-peak amplitude of the central spectral line was considered the magnitude of the ESR signals in the samples.
In addition to the study investigated above, additional experiment was undertaken to examine the time-temperature dependence of fingernail samples with 1-hr water treatment. Samples investigated in this experiment were collected from one donor only. The pre-treatment of the samples began by 1-hr soaking to distilled water followed by drying inside a heat dryer sterilizer (MOV-112 S-PJ, PHC Holdings Corporation, Japan). The drying time with the corresponding temperatures were as follows: (a) 1-hr at 100°C, 80°C, 60°C, 40°C and (2) 30 mins at 100°C, 80°C, 60°C, 40°C. Note that the storage conditions and spectral measurements for this experiment were applied in the same way as described above.

Results and Discussion Figure 1 shows the dose-response curves in the first and second irradiation of vacuum-stored fingernail samples taken from 6 adult donors. Each data point is an average of measurements on three samples and measured at 5 mins after the irradiation process. Preliminary unpublished results of own research for the first irradiation as well as the present work for the second irradiation showed distinctive behavior in the dose-response curves among the 6 adult donors. Donors 3-6 (D3-D6) demonstrated responses at 70 Gy with comparable ESR intensities during the first and second irradiation. However, in the case of D1-D2, a clear indication of a significant decrease from both doses was seen. Efforts to investigate this phenomenon are currently underway.

Figure *2* shows the combined effect of drying time and temperature in unirradiated samples with 1-hr water treatment. According to this plot, the ESR signals were greatly affected when heated to 2 different drying time at different temperatures. Further, the underlying influence of the drying conditions to the ESR signals reveals the increasing ESR peaks is directly linked with the increasing heating temperatures and therefore have different thermal stabilities. This effect, however, requires additional validation in unirradiated fingernail samples.

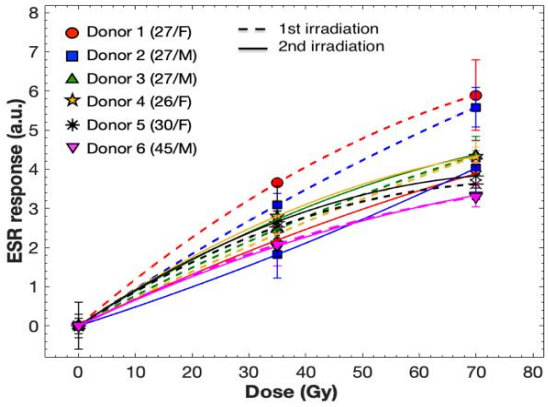

Figure 1. Dose-response curves of vacuum-stored samples irradiated to ϒ-rays from the Cs-137 source.

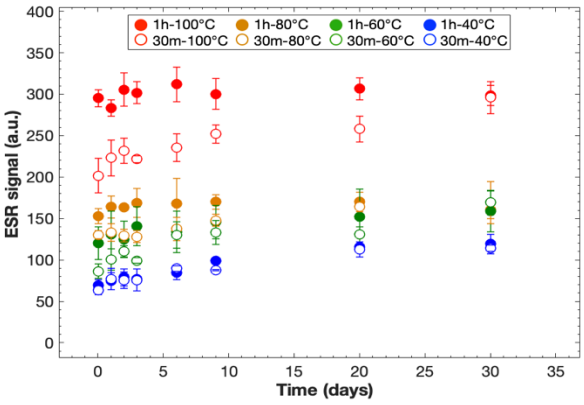

Figure 2. Time-temperature dependence results in unirradiated fingernail samples with 1-hr water treatment.

Conclusion The results presented in this study showed a significant individual variability in the dose-response curves in between the first and second irradiation. At 70 Gy, the measured ESR response from the samples of D3-D6 were essentially similar in intensities for both irradiations. A slight increase in the ESR response at 35 Gy from the same donors was also observed during the second irradiation. However, it was not the case for D1-D2 which demonstrated a much lower response in the second than in the first irradiation. Moreover, it was also found that the ESR peaks were greatly affected by the time-temperature dependence. These confounding factors bring forth a confluence of the several challenges in the application of fingernail ESR dosimetry.

References

1) Trompier F, Romanyukha A, Reyes R, Vezin H, Queinnec F, Gourier D. 2014. *Radiat Environ Biophys* **53** 291–303. doi:10.1007/s00411-014-0512-2.
2) Sholom S, McKeever S. 2017. *Radiat Phys Chem* **141** 78–87. doi:10.1016/j.radphyschem.2017.06.009.

Features of PHITS in Terms of Detector Response Simulations

T. Sato[1]*, T. Ogawa[1], D. Satoh[1], Y. Matsuya[1], T. Kai[1]
Japan Atomic Energy Agency, Tokai, Ibaraki, Japan

Highlights Particle and Heavy Ion Transport code System, PHITS, is a general purpose Monte Carlo code that can simulate the motion of various particles over wide energy ranges, using several nuclear reaction models and data libraries. This paper summarizes the features of specific functions useful for detector response simulations implemented in PHITS

Key words PHITS, Monte Carlo, particle transport, detector response

Background and Objectives Responses of radiation detectors depend not only on the deposition energy but also the profiles of particles imparting the energy such as their stopping power. Thus, evaluation of detector responses for various particles is desirable for the precise radiation measurements in complex fields such as those in heavy ion therapy facilities and in spacecraft. Monte Carlo particle transport simulation codes can play an important role in the evaluation because it is impractical to experimentally determine the detector responses for all types of radiations that exist in those fields. Particle and Heavy Ion Transport code System, PHITS[1)], is one of the most successful codes applicable to that purpose. Several specific functions useful for detector response simulations are implemented in the code, and their features are summarized in this paper.

Material and Methods Features of the following four functions are described in this paper:

1. event generator mode for evaluating charged particles and residual nuclides emitted from neutron-induced nuclear reactions below 20 MeV[2)],
2. microdosimetric function for calculating the probability densities of deposition energies in microscopic sites[3)],
3. track-structure mode to evaluate the profiles of each ionization and excitation event, and
4. conversion function from deposition energy to detector response with consideration of energy resolution of the detector based on user-defined programs.

Results and Discussion Item 1 is indispensable for calculating detector responses for neutron irradiations because event-by-event information on the deposition energy cannot be deduced from the conventional method for estimating neutron dose, i.e. the kerma approximation. Items 2 and 3 were originally developed for radiation biophysics simulations

such as estimation of relative biological effectiveness (RBE) in charged particle therapy[4], but recent studies suggested that they are also useful for detector response calculations[5,6]. This is because the responses of radiation detectors, particularly for scintillators, depend on the microscopic pattern of ionizations and excitations due to the quenching effect, which can be more properly represented by the probability densities of deposition energies in microscopic sites rather than LET. Item 4 is useful for calculating the response functions of detectors whose energy resolution and/or quenching effect are well evaluated. As an example, Figure 1 shows the frequency distributions of deposition energies and light outputs of 5-inch liquid organic scintillator irradiated by 100 MeV proton calculated by PHITS.

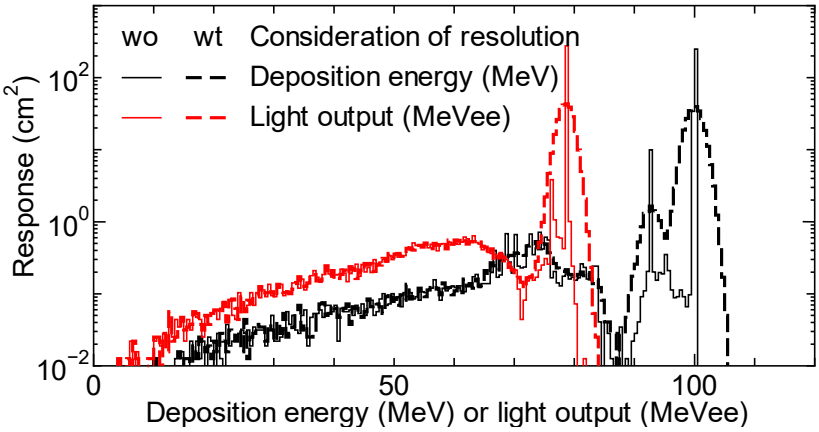

Figure 1. Examples of detector responses calculated by PHITS. Black and red lines are the frequency distributions of deposition energies and light outputs, respectively, while dash and solid lines are those with and without considering the detector resolution, respectively.

Conclusion PHITS has been used by more than 4,000 researchers all over the world for various research fields including detector response simulations. More detailed features of the code particularly for the microdosimetric function and track structure mode will be presented at the meeting.

References

1) T. Sato et al., J. Nucl. Sci. Technol. 55, 684-690 (2018).
2) T. Ogawa et al., Nucl. Instr. Meth. A 763, 575-590 (2014).
3) T. Sato et al., Radiat. Prot. Dosim. 122, 41-45 (2006).
4) T. Sato et al., Radiat. Res. 171, 107-117 (2009).
5) T. Ogawa et al., PLOS ONE 13(8), e0202011 (2018).
6) A. Parisi et al., Radiat. Prot. Dosim. DOI:10.1093/rpd/ncy272 (2018).

Unified Interaction Model simulation of the effect of optical excitation on the TL dose response of LiF:Mg,Ti (TLD-100)

D. Ginzburg[1], I. Eliyahu [2], L. Oster[3], G. Reshes[3]; Y.S. Horowitz[1]; S. Biderman[3], D. Sibony[1,3], G. Amit[2]
[1]*Ben Gurion University of the Negev, Beer Sheva, Israel*
[2]*Soreq Nuclear Research Center, Yavne, Israel*
[3] *Sami Shamoon College of Engineering, Beer Sheva, Israel*

Highlights The intent of this research is to modify the TL dose response of composite peak 5 via excitation following irradiation at appropriate photon excitation energies and to obtain a linear dose response up to at least 30 Gy.

Key words TL dose response, optical bleaching, LiF:Mg,Ti

Background and Objectives LiF:Mg,Ti (TLD-100) is used to determine patient doses from 1-5 Gy in radiation therapy and up to 30 Gy in intraoperative electron radiation therapy. Unfortunately, the dose response is non-linear above ~ 1 Gy reaching values of increased efficiency as high as 1.5 at 10 Gy and 1.9-2.0 at 30 Gy . An additional complication is the dependence of the normalized TL dose response, f(D), on gamma/electron energy as shown in Figure 1 for 100 keV and 8 keV photons. To correct for this behavior, stringent calibration and correction procedures are required for precision applications in clinical dosimetry. The intent of this research is to modify the TL dose response of composite peak 5 via excitation following irradiation at appropriate photon excitation energies and to obtain a linear dose response up to at least 30 Gy.

Methods The photon excitation alters the concentration of the trapping centers (TCs), the competitive centers (CCs) and the luminescent centers (LCs). Preliminary experimental results following 3.6 eV and 4.3 eV photon excitation have been successful in increasing the ratio of peak 5a to peak 5 [1]. This is a positive result since peak 5a, produced by electron-hole geminate recombination, is expected to result in a more linear dose response than peak 5 (an e-only configuration), which is produced by conduction band/valence band charge carrier migration and subject to competitive processes.

Results and Discussion The Unified Interaction Model (UNIM) [2] simulations shown below in Figure 2 are intended to demonstrate the effect of photon excitation and point in the direction of the optimum choice of photon energy and fluence.

In the UNIM the number of TL photons, F(D), created in the sample due to e-h recombination is given by eq'n (1) [1,2].

$$\mathrm{F(D)} = ksn_e(\mathrm{D}) + (1-ks)n_e \sum_{i=1}^{3} \int_{r_0}^{r_{\max}} g(R_i) \cdot e^{-\frac{R_i}{\lambda(\mathrm{D})}} \cdot P_i(n_h, R_i, \mathrm{D}) dR_i \quad (1)$$

The parameter, s, is equal to $n_{e\text{-}h}/n_e$, where $n_{e\text{-}h}$ is the concentration of e-h occupied TC/LC pairs and n_e is the e-only concentration, can also be treated as a function of dose. This ratio is one of the main factors influencing the dose response. Increasing values of s lead to a more linear dose response as shown below in Figure 2.

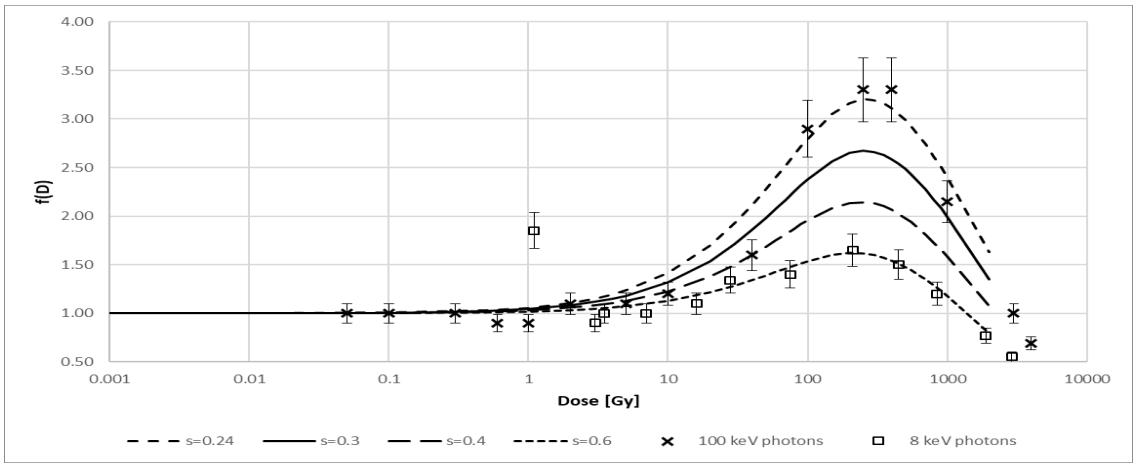

Figure 1. The normalized TL dose response as a function of photon energy. ks (eq'n (2) refers to the ratio of $n_{e\text{-}h}/n_e$. The concentration of e-h population to e-only.

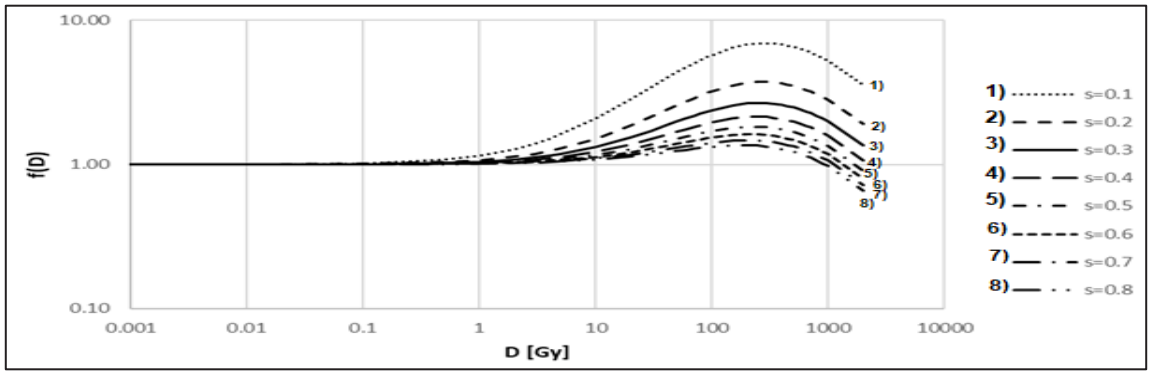

Figure 2. UNIM simulation of the dose response of composite peak 5 as a function of s.

Conclusion High values of s can lead to a value of f(D=30 Gy) of approximately unity and may be achieved by the appropriate choice of photon energy in the vicinity of the 3.8 eV and 4.3 eV optical absorption bands which are correlated with the TC/LC complex [3].

References

1) Ginzburg,D., Oster,L., Eliyahu,I., Reshes,G., Biderman,S, and Horowitz, Y.S., Manipulation of the dose response of composite glow peak 5 in the Thermoluminescence of LiF:Mg,Ti (TLD-100) via optical excitation post irradiation: Potential for improved dose response linearity beyond 1 Gy. Radiat.Prot.Dosim., https://doi.org/10.1093/rpd/ncy206
2) Lavon, A., Eliyahu, I., Oster, L and Horowitz, Y.S., The modified unified interaction model:incorporation of dose dependent localised recombination, Radiat. Prot. Dosim., 163(3), 362-372 (2015).
3) Biderman, S., Druzhyna, S, Galina, R., Eliyahu, I., Oster,L. and Horowitz, Y.S., Investigation of the energy spectrum and dose response of optical absorption bands in 4N single crystal LiF and LiF:Mg,Ti (TLD-100), Radiat. Meas., 106, 30-34 (2017).

A simplified analysis of the recombination mechanism in LiF:Mg,Ti (MTS-N) near peak 5

E. Mandowska[1]*, A. Mandowski[1]
[1]*Jan Dlugosz University, Czestochowa, Poland*

Highlights Recombination mechanism in LiF:Mg,Ti detectors (MTS-N) was studied based on spectrally resolved thermoluminescence (SR-TL) measurements. It was found that in the vicinity of the peak 5 of MTS-N detectors the recombination does not obey the pure localized nor pure delocalized mechanism.

Key words spectrally resolved thermoluminescence (SR-TL), LiF:Mg,Ti (MTS), localized transitions, delocalized transitions, traps, recombination centers.

Background and Objectives LiF:Mg,Ti crystal is one of the most popular thermoluminescence (TL) detectors of ionizing radiation. These crystals are grown in various laboratories. Popular LiF:Mg,Ti detectors are produced also at the Institute of Nuclear Physics in Krakow (Poland) under commercial name MTS-N. Other name is TLD-100. In recent years many papers were devoted to the mechanism of trapping and recombination processes leading to the formation of the main dosimetric peak (peak 5) in this material[1)]. Nevertheless, the elemental recombination mechanism is still not well known.

Materials and Methods Basic theoretical models predict delocalized[2)] (LT), localized[3)] (DT) or semi-localized (SLT) recombination route[4)] for the recombination processes in various solids. The different routes may occur simultaneously during TL readout. Usually, it is difficult to distinguish these mechanisms. Recently, Mandowska[5)] suggested the use of spectrally resolved thermoluminescence (SR-TL) and/or other spectrally resolved measurements for the identification of localized and delocalized processes. For this purpose the formalism of *Z*-functions was proposed. Here we present a simplified analysis applied to LiF:Mg,Ti.

Results and Discussion The function Z_4[5)] may be used for the investigation of LT and DT. For LT this function depends linearly on time and for DT Z_4 is monotonic. The study of monotonicity (in contrast to a specific functional form) may be particularly useful when, for example, we do not have full separation into spectral components and experimental data show a large statistical dispersion. It is worth noting, that in this case it is possible to simplify the Z_4[5)] function. The monotonicity of the function Z_4 will be preserved when we abandon the logarithm and the normalization of the intensity of luminescence, which is used in this

function. These simplified function is marked with the symbol Z_{4M} and for constituent components presents monotonic function - increasing or decreasing. TL emission spectrum of MTS give information about the structure of recombination centers. Using deconvolution of the TL spectra into Gaussian peaks in the energy domain we obtained two peaks with maxima at 404 nm (3.07 eV) and 472 nm (2.63 eV) corresponding to two recombination centers.

To study recombination processes, we calculate two partial glow curves (I_{R1}, I_{R2}) associated with two designated RCs and finally examine the monotonicity of the Z_{4M} ($Z_{4M}=I_{R1}[T(t)]/I_{R2}[T(t)]$) function (Figure 1). In spite of large statistical fluctuations, the running average shows a weak growing trend, which agrees with DT processes. An important exception is the distinctive dip around 460 K. In this area, the function Z_{4M} is evidently non-monotonic.

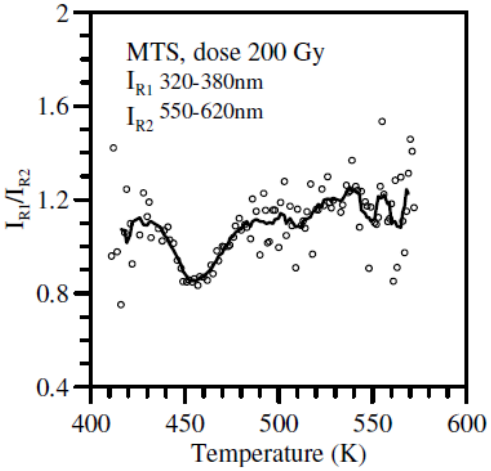

Figure 1. Quotient of two spectral components I_{R1}/I_{R2} (function Z_{4M}) calculeted from SR-TL. Empty circles show the results obtained from experiment. The continuous line represents the running average.

Conclusion There is strong evidence that recombination mechanism in the vicinity of peak 5 is non LT and non DT but most likely SLT.

References

1) Y.S. Horowitz, L. Oster, D. Satinger, S. Biderman, Y. Einav, Radiat. Prot. Dosim. 100, (2002) 123-126.
2) J.J. Randall, M.H.F. Wilkins, Proc. R. Soc. Lond. Ser. A 184 (1945) 366–389.
3) P.L. Land, J. Phys. Chem. Solids 30 (1969) 1693–1708.
4) A. Mandowski, J. Phys. D: Appl. Phys. 38 (2005) 17–21.
5) E. Mandowska, J. Lumin. 188 (2017) 313-318.

A Monte-Carlo study of the Fading of the TL and OSL signals in the presence of deep-level competitors

R. Chen[1*], V. Pagonis[2]

[1]*Raymond and Beverly Sackler School of Physics and Astronomy, Tel-Aviv University, Tel-Aviv 69978, Israel*
[2]*Physics Department, McDaniel College, Westminster, MD21157, USA*

Highlights The fading of thermoluminescence (TL) and optically stimulated luminescence (OSL) has been studied within the framework of a model with deep-level competing traps, using Monte-Carlo simulations.

Key words: Optically stimulated luminescence, thermoluminescence, exponential and non-exponential decay, Monte-Carlo method, fading

Background and Objectives. In a previous paper[1)], the issue of the evaluated lifetimes of thermoluminescence (TL) and optically stimulated luminescence (OSL) has been studied for the one-trap-one-recombination-center (OTOR) case, using the Monte-Carlo simulation. It was shown that under these circumstances, the decay curve of the electron occupancy along thousands of years may not be exponential. Therefore, a lifetime determined from the results at short periods of time may not apply at longer periods of time. The decay at longer times was found to be slower than exponential and thus, one may observe longer lifetimes than predicted by the evaluated trapping parameters. In the present work we demonstrate that with a more complex model, namely, when an additional deeper trap is involved, the probability of getting an exponential decay of the signal is much larger.

Materials and Methods. We have studied the fading of OSL and TL signals with different times elapsing between excitation and read-out, using a Monte-Carlo procedure. The rate at which electrons are raised thermally from the traps into the conduction band is very small at ambient temperature and the average number of electrons in a grain is significantly smaller than unity. Therefore, the excited electrons should be considered one at a time. Thus, the Monte-Carlo simulation appears to be more appropriate than solving the relevant simultaneous differential equations since in the latter case, the concentration in the conduction

band would be a fraction of an electron. It should be noted that in practically all materials, more than one trapping state takes part in the luminescence process. Therefore, it is more realistic to add to the basic OTOR model at least one competing trap. In this case, one cannot choose arbitrarily the concentrations of the trapped carriers at the beginning of decay but rather, the relevant set of equations is solved for the excitation period and the final distribution of carriers is used for the fading stage. Also, the final occupancies of traps and centers at the end of the long fading are used as initial values for the pulsed-OSL or TL stage.

Results and Discussion. In the previous work, we showed that in the OTOR model, the fading may not be exponential and therefore, the half-life of the decay cannot be defined uniquely. Here, we have found that with a significant deep-trap competitor, the extrapolation leading to the evaluation of the long-term stability of the signal is more viable since the decay is much closer to be exponential with a sizeable competitor. An example is shown in Fig. 1.

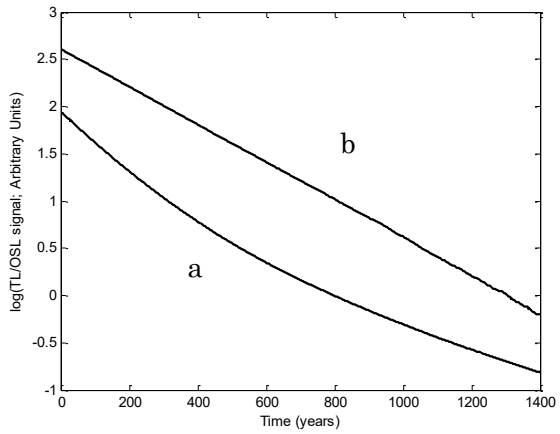

Figure 1: The OSL signal as a function of decay time. (a) with negligible competitor. (b) with large competitor.

Conclusion. The results are compatible with previously existing evidence that the chances of having a TL peak with first-order characteristics are significantly larger in cases where a large deep trap, acting as a competitor, is present. Since in most cases competing traps are prevalent, one may assume that the fading is exponential and the concepts of mean lifetime and half-life are valid.

References

1) Chen, R., Pagonis, V., 2015. Study of the stability of the TL and OSL signals. Radiat. Meas. 81, 192-197.

Radial Electron Fluence around Ion Tracks as a Physical Parameter to Describe the Detection Thresholds of Etched Track Detectors

Tomoya Yamauchi[1]*, Tamon Kusumoto[2], Shogo Okada[3], Satoshi Kodaira[2], Hisaya Kurashge[4], Ziad EL Bitar[5], Masato Kanasaki[1], Keiji Oda[1], Quentin Raffy[5], Abdel-Mjid Nourreddine[5], Remi Barillon[5]

[1]*Graduate School of Maritime Sciences, Kobe University, Hyogo, Japan*

[2]*Radiation Measurements Research Team, National Institute of Radiological Sciences, National Institutes for Quantum and Radiological Science and Technology, Chiba, Japan*

[3]*High Energy Accelerator Research Organization, KEK, Ibaraki, Japan*

[4]*Organization for Advanced and Integrated Research, Kobe University, Hyogo, Japan*

[5]*Institut Pluridisiplinaire Hubert Curien, Strasbourg, France*

Highlights Progress is presented on the studies of Radial Electron Fluence around Ion Tracks, *REFIT*, which has been proposed to describe the detection thresholds of etched track detectors, including the relationship with former experimental results.

Key words *REFIT*, Detection threshold, Etched track detector

Background and Objectives In an earlier study, we proposed the new physical parameter of Radial Electron Fluence around Ion Tracks, *REFIT*, to describe the detection threshold of poly(allyl diglycol carbonate), PADC, which has been considered as the most sensitive etched track detector[1)]. *REFIT* is defined as the density of secondary electrons passing through the surface of a cylinder of a given radius coaxial with an ion trajectory. In the present study, the status of the studies on *REFIT* for PADC and another polymeric etched track detector is discussed.

Materials and Methods As a etched track detectors, PADC and Polyethylene terephthalate, PET, were exposed to protons and heavy ions at the Heavy Ion Medical Accelerator, HIMAC, Chiba of the Japanese National Institute of Radiological Sciences, NIRS, in Japan. Detection thresholds of each detector and for each ion were determined by systematic etching tests. The value of *REFIT* was calculated using Geant4-DNA toolkits. We used the "G4EmDNAPhysics" physics constructor installed in Geant4-DNA ver. 10.3.p01, in which the discrete processes including ionization, electronic excitation, vibrational excitation, elastic scattering and molecular attachment for electrons were taken into account, for energies down to 7.4 eV.

Results and Discussion The PADC consists of a combination of a radio-sensitive section built from ether and carbonate ester, and a relatively radio-tolerant one made of a

polyethylene-like network formed during the polymerization. Experimental results from electron beams and gamma rays indicate that a single electron can cleave the ether but cannot break the carbonate ester. At least two electrons are needed to hit the radio-sensitive section to damage the carbonate ester. Furthermore, the etching tests have revealed that at least two radio-sensitive sections should be destroyed in the radial direction of ion tracks for them to become etchable. Even if the notion of local dose remains relevant, the concept of electron fluence presents several advantages over the first. Figure 1 shows the *REFIT* for indicating ions as a function of the radial distance from the ion trajectory. Values of *REFIT* at a radius of 1 nm for each ion were of the same order and concordant with the experimentally obtained Multi-hit model for low *LET* radiations.

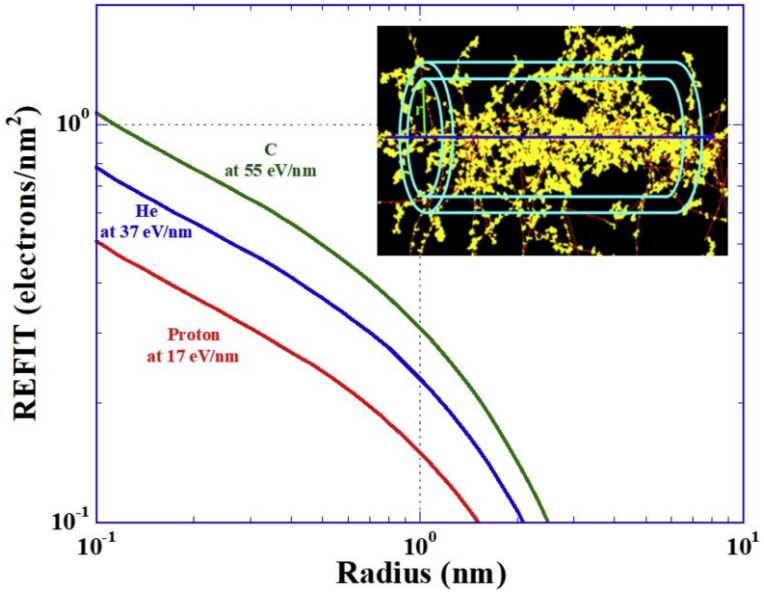

Figure 1. The values of *REFIT* are calculated at the detection thresholds for protons, He and C ions in PADC. The inset sketch is a simulation result of the secondary electrons (red trajectories) around the C ion trajectory at 46 MeV/u (dark blue line on the axis of light blue cylinders). The yellow points show the interaction points[1].

Conclusion We have proposed *REFIT* as a new candidate physical parameter to describe the detection thresholds of etched track detectors. It has been confirmed that *REFIT* is able to describe the detection thresholds of PADC and PET.

References

1) Kusumoto et al., Radial electron fluence around ion tracks as a new physical parameter for the detection threshold of PADC using Geant4-DNA toolkit, *Radiation Measurements* 118, 50-53 (2018). https://doi.org/10.1016/j.radmeas.2018.08.015

The effect of charge imbalance on luminescence production

M. Autzen[1*], A. Murray[1], G. Guérin[2],M. Jain[3], and J.-P. Buylaert[1,3]
[1]*Nordic Luminescence Laboratory for Luminescence Dating, Aarhus University, DTU Risø campus Roskilde, Denmark*
[2] *UMR 5060 CNRS-IRAMAT-CRP2A, CNRS-University Bordeaux Montaige, Maison de l'archéologie, 33607 Pessac Cedex, France*
[3]*Centre for Nuclear Technologies, Technical University of Denmark, DTU Risø campus, Roskilde, Denmark*

Highlights High dose irradiation of quartz with 100/200 keV electrons shows a cumulative effect on the luminescence sensitivity, irreversible unless heated to high temperatures (500-700ºC). We attribute at least part of these observations to the accumulation of negative charge in the phosphor grains.

Key words Radiation transport modelling, Charge Imbalance, Luminescence Dosimetry

Background and Objectives Current luminescence theory and associated production models start from the assumption that phosphors are irradiated under conditions of charge neutrality/balance. However, net charge build up during irradiation of insulators is a well-known phenomenon, and given that the dimensions of phosphors are often much larger than the mean free path or range of the incident radiation (or secondary particles), it appears very unlikely that this assumption is met in practice. We present experimental evidence suggesting that the net charge accumulated by ~50 µm quartz grains during electron beam irradiation affects their luminescence production and sensitivity, and might ultimately prevent further absorption of dose.

Materials and Methods Radiation transport modelling code (using Geant4: Allison *et al*., 2006[1]) was used to predict the degree of charge imbalance experienced by sand-sized quartz and feldspar grains in radiation geometries commonly used in luminescence dating. These results were used as input to luminescence production equations (Bailey, 2004[2]); this allows us to predict the effect that an excess of charge is likely to have on luminescence production and sensitivity. Experiments were carried out using sensitized silt-sized quartz grains (40-60 µm) irradiated in a Comet EBLab-200 electron beam using 100 and 200 keV electrons. The

luminescence measurements were carried out on a Risø TL/OSL DA-20 reader equipped with $^{90}Sr/^{90}Y$ beta source.

Results and Discussion

Modelling shows that quartz grains of all sizes (5 – 1000 µm) acquire an excess negative charge as a result of irradiation with electrons; when exposed to a natural 'infinite matrix' beta spectrum from U, Th and K, for the same dose the excess is larger for small grains than for larger grains. By modifying the luminescence production equations to allow for an initial excess of electrons, it is predicted that the luminescence production and sensitivity follow a saturating exponential until all electron traps are filled, after which both should decrease linearly as the hole population decreases. This is supported by our experimental observations for both 100 and 200 keV electron irradiations. However, the observed decrease in luminescence and sensitivity is not linear; rather it appears to asymptote towards a constant response independent of exposure to the electron beam. We tentatively attribute this behavior to the onset of reflection of the incoming electrons as the charge retained in the sample produces an increasing electric field sufficient to divert, and ultimately stop, the incident electron beam (Blaise and le Gressus, 2018[3]) and so prevent the deposition of further charge and dose.

Conclusion

Based on both modelling and experiment, we argue that electron irradiation in quartz affects its luminescence production and sensitivity as a result of a buildup of net charge within the crystal. This phenomenon continues until the sample has reached a potential equal and opposite to that of the incoming electron beam, after which no further absorption of energy or charge can occur. It is known that electron traps in quartz have stabilities of the order of 10^8 years, and so at least some of the excess charge is very likely stable on that timescale.

References

1) J. Allison, *et al*. (Geant4 Collaboration), Geant4 developments and applications. *IEEE Transactions on Nuclear Sciences* 2006:**53**:270-278.
2) R. M. Bailey, Paper I – simulation of dose absorption in quartz over geological timescales and its implications for the precision and accuracy of optical dating *Radiation Measurements* 2004:**38**:299-310
3) G. Blaise and C. Le Gressus, Electron-trapping and energy localization in insulating materials. Technological impact of space charge electron-beam characterization. *AIP Advances* 2018:**8**:095228

Real-time and Direct Measurements of BNCT Neutron Beam at KURRI and NCC Facilities Using DAD-BNCT.

Masashi Takada[1]*, Nunomiya Tomoya[2], Akihiro Masuda[3], Tetsuro Matsumoto[3], Satoru Endo[4], Hiroki Tanaka[5], Satoshi Nakamura[6], Masaru Nakamura[7], Kei Aoyama[2], Tetsuro Ueda[1], Masashi Ooyauchi[1], Takashi Nakamura[2,8]

[1]*Dept. of Appl. Phys., National Defense of Academy in Japan, Yokosuka, Japan*

[2]*Fuji Electric Co. Ltd., Hino, Japan*

[3]*National Metrology Inst. of Japan, Nat'l Inst. of Adv. Ind. Sci. and Technol., Tsukuba, Japan*

[4]*Hiroshima University, Hiroshima, Japan*

[5]*Institute for Integrated Radiation and Nuclear Science, Kyoto University, Kumatori, Japan*

[6]*National Cancer Center, Tokyo, Japan*

[7]*Cancer Intelligence Care Systems, Inc, Tokyo, Japan*

[8]*Cyclotron and Radioisotope Center, Tohoku University, Sendai, Japan*

Highlights BNCT neutron beams can be measured in real time, directly, and easily using the neutron detector (DAD-BNCT) based on combination of thin silicon sensor and thin LiF radiator. The DAD-BNCT can measure thermal neutrons produced at KURRI and NCC BNCT neutron beams, up to $1x10^9$ (n/cm^2/s), separately from gamma rays with high dose rates around 500 mGy/h. The DAD-BNCT presents good linear response to neutron flux, and also, could be used to monitor BNCT beams.

Key words silicon sensor, neutron, gamma ray, BNCT, real-time detection, high flux

Background and Objectives Neutron fluxes of BNCT have been measured using neutron activation technique with Gold foils, however, we cannot acquire the neutron fluxes in real time. Real-time measurements of BNCT neutron beams are required at the BNCT facilities. The BNCT radiation fields consists of gamma rays around 500 mGy/h and thermal neutron fluxes around $1x10^9$ (n cm^{-2} s^{-1}). The neutron detector have to measure neutrons separately from gamma rays under these radiation fields. Some detection techniques were being developed but have not yet completed due to some problems.

Materials and Methods We have developed simple real-time neutron detector (DAD-BNCT: Direct Active Detector for BNCT) based on combination of a thin-silicon sensor[1)] and thin LiF neutron converter. Experiments of measuring BNCT neutron beam were performed at both National Cancer Center and Kyoto University Research Reactor. Several

characterization of the DAD-BNCT were experimentally obtained. The DAD-BNCT can separate neutron events from gamma rays, completely, at these BNCT fields.

Results and Discussion Experimental pulse height is plotted in figure. Neutron capture peak is observed around 600 ch, clearly, and separated from gamma ray events. Good lineal responses to neutron flux were measured up to $1x10^9$ (n cm^{-2} s^{-1}). Neutron damage have never been observed. The DAD-BNCT can be operated without bias voltage. We can provide simple neutron monitor to BNCT facilities. Also, neutron depth profile was measured and compared with the other results using activation techniques. The experimental results shows good agreement with the others

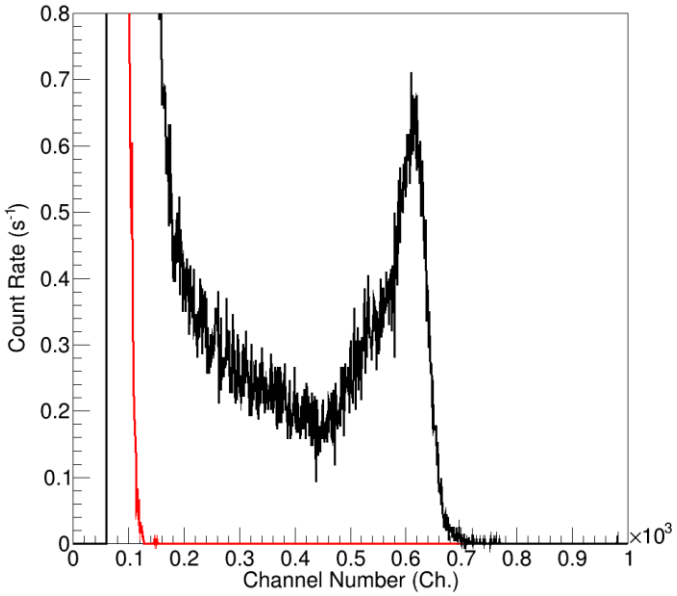

Conclusion BNCT neutron beams can be measured in real time, simply and directly using the DAD-BNCT. Using the DAD-BNCT the facilities can monitor beam fluxes in real time.

References

1) M.Takada, T.Nunomiya, T.Matsumoto, A.Masuda, Y.Watanabe, K.Aoyama, T.Nakamura, M.Takada, Neutron Detection Efficiency and Response Functions of a Thin Neutron Silicon Sensor with Low Gamma-Ray Sensitivity, Radiation Measurements, 2017.

Measurement of Stray Neutrons with Electronic Neutron Dosimeter in Scanning Ion Beam Therapy

Vladimir Mares[1], Sebastian Trinkl[2], Martin Dommert[3], Thomas Tessonnier[4,*], Marek Wielunski[1], Werner Rühm[1], Katia Parodi[4, 5]

[1]Helmholtz Zentrum München, Neuherberg, Germany; [2]Federal Office for Radiation Protection, Neuherberg, Germany; [3]Physikalisch-Technische Bundesanstalt, Braunschweig, Germany; [4]Heidelberg University Hospital, Heidelberg, Germany; [5]Ludwig-Maximilians-Universität München, Garching, Germany; [*]Current address: Centre François Baclesse, Caen, France

Highlights The neutron personal dose equivalent, $H_p(10)$, was measured with an electronic neutron dosimeter (ELDO) at different positions around a PMMA phantom at the Heidelberg Ion-Beam Therapy Center (HIT), Germany. The PMMA phantom was irradiated with a mono-energetic beam of protons, helium ions, carbon ions and oxygen ions delivered to the fixed horizontal quality assurance (QA) beam line. Pencil beam scanning (PBS) dose delivery technique was used.

Key words ion beams radiation therapy, secondary neutrons, electronic neutron dosimeter

Background and Objectives Over the last decade ion beam cancer therapy has made considerable progress. While proton and carbon ions are commonly used in particle therapy, use of helium and oxygen ions is also considered and investigated. It is well known that due to nuclear reactions of the primary high-energy ions with the beam line components, the patient's body, and the components in the treatment room, a considerable secondary radiation, mainly neutrons, is created during irradiation. Resulting secondary radiation dose deposited in the healthy patient tissue surrounding the tumour may lead to late health effects of the therapeutic treatment, because of developing secondary malignancies.

Materials and Methods In our work we focus on the measurement of neutron personal dose equivalent, $H_p(10)$, at different positions around the PMMA phantom in the quality assurance (QA) room equipped with a horizontal beam line at the Heidelberg Ion-Beam Therapy Center (HIT), Germany. Two different energy layers with a field size of 11 x 11 cm^2 within a 30 x 30 x 30 cm^3 PMMA phantom were irradiated with mono-energetic protons (75 MeV/u; 140 MeV/u), helium ions (76 MeV/u, 140 MeV/u), carbon ions (139 MeV/u; 264 MeV/u) and oxygen ions (163 MeV/u, 313 MeV/u) resulting in similar Bragg-peak depths of about 4.8 cm and 14 cm, respectively.

For this experiment an electronic neutron dosimeter (ELDO)[1,2] developed at Helmholtz Zentrum München (HMGU) was used. ELDO consists of 4 Si PIN-diodes with LiF or

polyethylene (PE) converters encapsulated in Pb or Cd: one fast-sensor (with PE) operating in the 1 MeV – 200 MeV neutron energy range, two Delta-sensors (with LiF) operating between 50 keV and 2 MeV, and one Albedo-sensor (with LiF) sensitive to thermal neutrons (< 50 keV). Each sensor is sensitive to a specific neutron energy range and has its own calibration factor.
Additionally, the neutron energy spectra at different positions around the PMMA phantom were measured with an extended range Bonner sphere spectrometer (ERBSS) with spherical ^{3}He proportional counters (SP9 Centronic Ltd) and 15 PE spheres with diameters from 2.5" to 15". The response of this ERBSS system to high-energy neutrons is enhanced due to two additional 9" PE spheres with Pb shells[3].

Results and Discussion It was found that secondary neutron production per primary ion expressed here in terms of $H_p(10)$ and H*(10) values have a strong energy and angular dependence for all ion species under study. The neutron H*(10) normalized per primary ion varies by a factor of 50 among the different ion species in beam direction, for the same energy layer.

Conclusion In the present work $H_p(10)$ values obtained with the HMGU electronic neutron dosimeter are compared to the H*(10) results measured with the ERBSS spectrometer. The results obtained indicate sufficiently good agreement for radiation protection purposes. A strong difference in secondary neutron production per primary ion was found for different ion species and energies.

References

1) Wielunski, M., Schütz, R., Fantuzzi, E., Pagnamenta, A., Wahl, W., Palfalvi, J., Zombori, P., Andrasi, A., Stadtmann, H., Schmitzer, C., Study of the sensitivity of neutron sensors consisting of a converter plus Si charged-particle detector, Nucl. Instrum. Methods A, 517 pp. 240–253 (2004)
2) Wielunski, M., Brall, T., Dommert, M.; Trinkl, S., Rühm, W., Mares, V., Electronic neutron dosimeter in high-energy neutron fields, Radiat. Meas. 114, 12-18 (2018)
3) Mares, V. and Schraube, H.; High energy neutron spectrometry with Bonner spheres. Proceedings, The IRPA Regional Symposium on Radiation Protection in Neighbouring Countries of Central Europe, Prague, Czech Republic, September 1997, 543-547 (1998).

Acknowledgements We would like to acknowledge staff of the Heidelberg Ion-Beam Therapy Center (HIT) for giving us the opportunity to perform spectrometry measurements. We would like to give special thanks to Stephan Brons from HIT for his professional on-site support.

Characterisation of novel 1- and 2-dimesional silicon diode arrays for range and spot size verification in spot-scanning proton therapy

E. Debrot[1], D. Mundy[2], M. Petasecca[1], S. Guatelli[1], C. Beltran[2], A.B. Rosenfeld[1]*
[1]*Centre for Medical Radiation Physics, University of Wollongong, Wollongong, Australia*
[2]*Department of Radiation Oncology, Mayo Clinic, Rochester, Minnesota, United States*

Highlights Silicon diode array detectors implemented in various modalities for fast and high resolution beam profiling and range determination for clinical proton therapy beams.

Key words silicon dosimetry, relative dosimetry, proton therapy, range verification.

Background and Objectives Spot scanning particle beams used for radiation therapy feature steep dose gradients and small beam geometries[1]. These characteristics result in added complexity and increase the importance for precision in quality assurance practices. In this study the 1D silicon Dose Magnifying Glass (DMG) detector array is characterised for range determination for the scanning proton beam at the Mayo Clinic in Rochester, MN. The DMG is used in several modes for range determination and in conjunction with the 2D DUO detector array for spot size measurement.

Materials and Methods The DMG detector consists of a single silicon wafer with dimensions 0.5 x 4.0 x 51.4 mm^3 and an array of 256 silicon diode sensitive volumes with a pitch of 200 µm. The small geometry of the detector allows for high spatial resolution dose profiling and fast range determination in a single acquisition. The DUO detector consists of two orthogonal linear arrays each with 256 active silicon sensitive volumes at a pitch of 200 µm on a silicon wafer with active area 52 x 52 mm^2 and a thickness of 350 µm. The DMG was used to measure proton range while the DUO was positioned normal to the incident beam direction.
The DMG was used in three modes for range verification: (i) to measure proton range in silicon by placing the long axis of the detector parallel to the beam central axis (fig. 1A) and delivering a single monoenergetic spot. (ii) Proton range "in Perspex" was measured with the DMG placed in a custom Perspex phantom with the detector positioned at an angle of 30° relative to the scanning beam central axis thereby varying the depth of each sensitive volume. In this case a flat field at the depth of the Bragg peak was delivered by scanning the beam over the detector. (iii) A single central axis spot was delivered to the DMG setup in the angled phantom with the DUO immediately upstream and aligned with it's arrays centered on the vertical and horizontal axes of the beam. The lateral beam profile obtained with the DUO was used to scale the depth dose curve measured with the DMG to account for variation in proton fluence across the beam

spot.

Results and Discussion Bragg peak profiles for proton energies up to ~110 MeV (with range in silicon up to the length of the DMG) could be resolved (fig. 1B) and corresponding proton range values were determined. The measured range was found to be consistent and reproducible for independent setups. Beam divergence, in combination with the small volume of the detector resulted reduced resolution of Bragg peaks for beam energies with ranges in the distal end of the detector.

The DMG angled phantom setup allowed Bragg peaks to be measured over the entire range of clinically available energies at the Mayo Clinic proton center (~70 - 230 MeV) with the introduction of Perspex blocks upstream of the phantom for setup (ii).

Setup (iii) shown in fig. 1E, resulted in changes in the Bragg profile measured with the DMG at varying depths in Perspex (fig. 1F). The lateral beam profile of the Gaussian shaped beam spot measured using the DUO (fig. 1G) was used to scale the depth profile for variance in proton fluence.

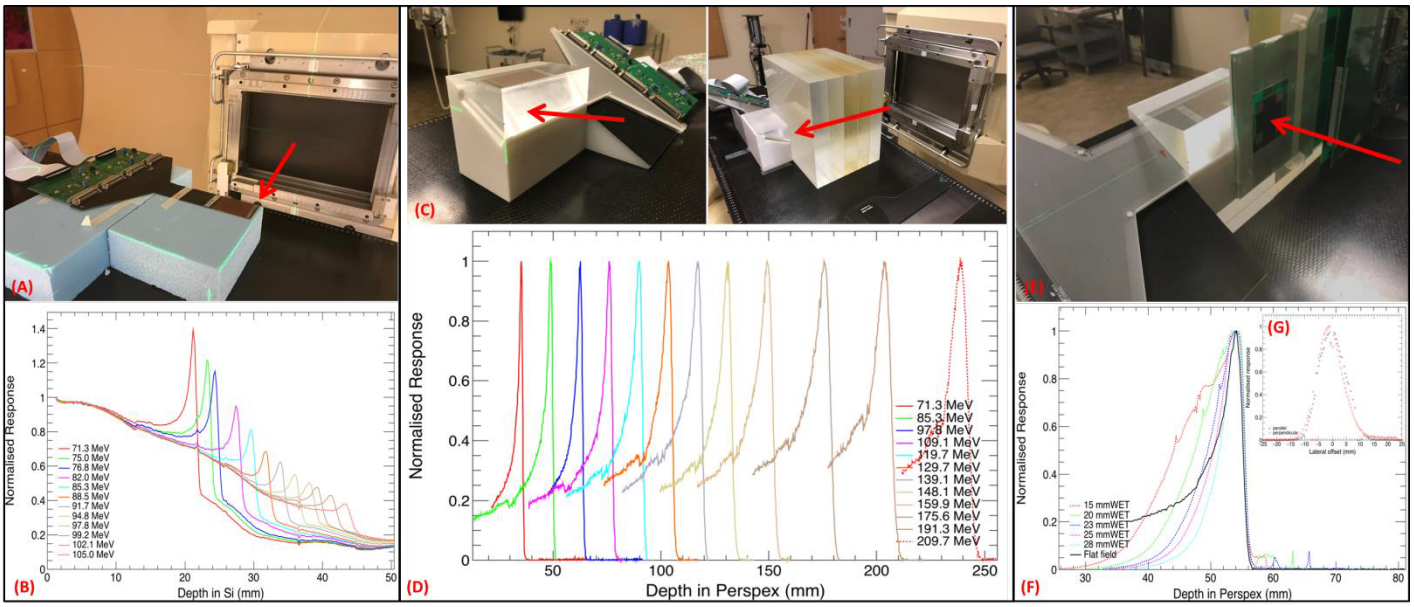

Figure 1. Experimental setup of DMG-256 detector and measured Bragg peak profiles in silicon for single monoenergetic proton pencil beams delivered at isocenter in mode (i), subfigures **A** and **B** respectively. Mode (ii) DMG-256 angled phantom setup (**C**) and measured Bragg peaks "in Perspex" using scanned flat field (**D**). Mode (iii) setup with DUO detector and angled phantom (**E**), depth (**F**) and lateral (**G**) pencil beam profiles with changing WET in Perspex. Red arrows indicate the incident proton beam direction.

Conclusion The DMG and DUO detectors are fast and effective tools for beam profiling and range verification in proton therapy. The small volume and multichannel instantaneous readout of this system is advantageous for fast beam profiling and range versification.

References

1) Mirandola, A. *et al.* (2015) 'Dosimetric commissioning and quality assurance of scanned ion beams at the Italian National Center for Oncological Hadrontherapy', *Medical Physics*, 42(9), pp. 5287–5300.

High-resolution fibre-optic dosimetry in microbeam radiation therapy

James Archer[1*], Enbang Li[1], Anatoly Rosenfeld[1] Michael Lerch[1]
[1]*Centre for Medical Radiation Physics, University of Wollongong, Wollongong, Australia*

Highlights Plastic scintillator fibre-optic dosimeters have been tested for their applicability in synchrotron radiation therapy. Microbeams have been resolved with a 10 μm resolution probe. Sensitivity remains a challenge for this method of dosimetry.

Key words scintillators, relative dosimetry, optical fibres

Background and Objectives Synchrotron microbeam radiation therapy (MRT) is a novel type of pre-clinical external beam radiation therapy that uses highly collimated planes of synchrotron X-rays to deliver a very high dose inside the beams. Inside the microbeams a dose rate upwards of 100 Gy/s can be delivered, necessary to prevent dose blurring in target tissue. As the microbeam widths are typically around 50 μm, with peak-to-peak separation of 400 μm (as implemented at the Imaging and Medical BeamLine (IMBL) at the Australian Synchrotron), a dosimeter must have a spatial resolution less than these lengths to be able to resolve the microbeams. We present the progress made towards a scintillator fibre optic dosimeter that is capable of performing MRT beam quality assurance.

Materials and Methods The scintillator fibre-optic dosimeters uses BC-400 plastic scintillator as the radiation conversion material. This dosimeter design has been demonstrated to be water-equivalent, linear in dose response, energy independent and highly radiation hard [1], [2]. The peak emission wavelength is 423 nm. A sheet of scintillator was polished to a set thickness and optically coupled to the end of a 10 m length of 1 mm diameter core fibre-optic. The fibre-optic was connected to a SenSL MiniSM Silicon Photomultiplier (SiPM). This fibre-optic dosimeter (FOD) can provide relative dosimetry, and can be calibrated against a reference source (such as ionization chamber) to provide absolute dose.
The optimal one-dimensional spatial resolution of the FOD probes is defined by the scintillator thickness along the fibre axis. The resolution in the other two axes is defined by the fibre core diameter; 1 mm. Scintillator thicknesses of 100 μm [3], 50 μm [4], 20 μm [5] and 10 μm (with 10-20% tolerance) have now been tested. The sensitive dosimetric volume of the probes can be as small as 0.0079 mm^3. Testing of the probes was performed on the IMBL at the Australian Synchrotron. Each probe was scanned horizontally, in edge-on configuration, through a microbeam array of width 30 mm and different field heights, allowing the entire

intrinsic microbeam profile to be measured. Calculation of the full-width at half-maximum of the microbeams allows the spatial resolution of the probe to be evaluated. Percent depth dose (PDD) measured with and without the microbeam collimator in place (providing a broad beam) was acquired and can be compared directly with ionisation chamber data.

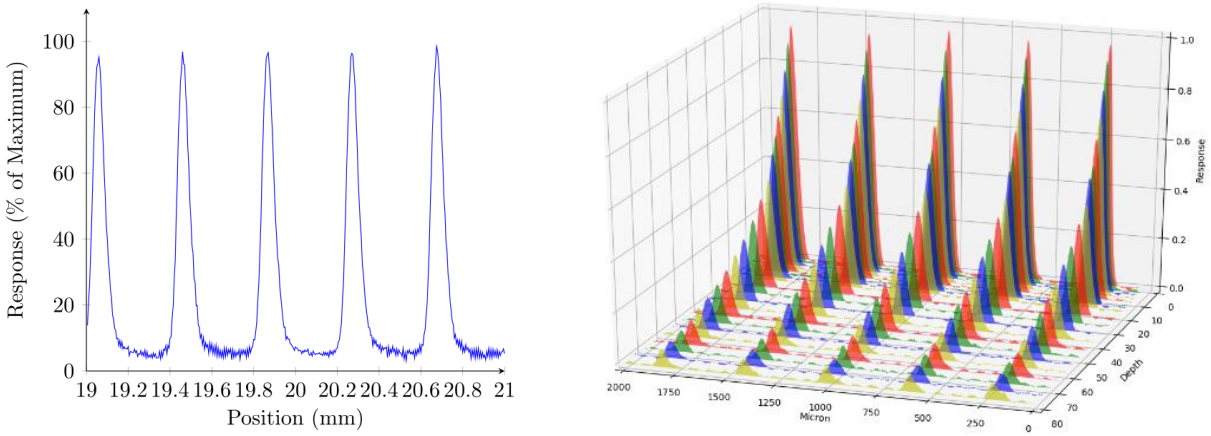

Figure 1. Left: 50 μm microbeam profile. Right: 10 μm microbeam PDD.

Results and Discussion Fig. I. shows microbeams measured with the 50 μm and 10 μm probes. FWHM measurements generally agree with other dosimetric devices of similar spatial resolutions (silicon strip detectors). The PDD results show that there is a consistent 20% overresponse at depths less than 30 mm from the surface, when compared to ionization chamber data. This overresponse is less significant when the FOD probe is scanned face-on relative to the field, along the direction of the beam.

Conclusion In the development of high spatial resolution FOD dosimeters, we have improved the spatial resolution down to 10 μm, the highest resolution scintillator dosimeter found in the literature. Results are comparable for other dosimetry tools of a similar spatial resolution. Methods to improve the sensitivity is currently being explored to allow accurate dosimetry of lower dose rate synchrotron X-ray beams.

References

1) AS Beddar, TR Mackie, and FH Attix, Physics in Medicine and Biology, 1992, 37, 1883.
2) AS Beddar, TR Mackie, and FH Attix, Physics in Medicine and Biology, 1992, 37, 1901.
3) J Archer, E Li, M Petasecca, *et al*, Medical Physics, 2017, 44(5), 1965.
4) J Archer, E Li, M Petasecca, *et al*, Scientific Reports, 2017, 7, 12450.
5) J Archer, E Li, M Petasecca, *et al*, Journal of Synchrotron Radiation, 2018, 25(3), 826.

High-resolution dose profiles measurements for Leksell Gamma-Knife Model C and Icon with a stereotactic diode, micro-diamond detector and ionisation chamber

L. Luketin[1]*, H. Hrsak[1], M. Majer[2], Z. Heinrich[1], R. Harrison[3], L. Stolarczyk[4]
[1]*University Hospital Centre Zagreb, Croatia*
[2]*Rudjer Boskovic Institute, Zagreb, Croatia*
[3]*University of Newcastle upon Tyne, United Kingdom*
[4]*Institute of Nuclear Physics, PAN (IFJ-PAN), Krakow, Poland*

Highlights Leksell Gamma Knife dose profiles measured with the small volume point detectors show excellent agreement with the profiles measured in the standard reference geometry with the radiochromic dosimetry film

Key words dose profiles, Leksell Gamma Knife, small field dosimetry

Background and Objectives Leksell Gamma-Knife (LGK) radiosurgery is a highly precise method for treatment of small intracranial lesions with high single radiation dose. The quality assurance program (QA) for Gamma-Knife includes periodical checks of size and position of each collimator dose distributions from which complex clinical distributions are composed[1)]. This is done by measuring dose distributions profiles in three orthogonal planes (usually along x, y and z-axis of Gamma-Knife unit). As radiochromic film emerged as a reliable and practical dosimetry instrument with high spatial resolution, near tissue equivalence and weak energy dependence[2)], the early idea of Gamma-Knife profiles scanning with point detectors was abandoned and replaced by film dosimetry. However, small volume detectors such as semiconductor diode and micro-diamond are often used for dosimetry of small radiosurgery beams, because of a small measuring volume (thickness of several tens of 1 μm and diameter equal or less than 1 mm) and therefore high spatial resolution. In this work, we propose the method for high-resolution dose profiles measurements for LGK Model C and Icon, using following small volume point detectors: stereotactic diode, micro-diamond detector and small ionisation chamber.

Materials and Methods The small field dosimetry in radiotherapy is one of the research tasks of the Working group 9 (WG9) of the European radiation dosimetry group (EURADOS), under which this work was done. The dose profiles were measured with the p-type stereotactic diode detector Diode SRS (PTW, Freiburg, Germany), single crystal diamond detector microDiamond (PTW, Freiburg, Germany), small-volume ionisation chamber PinPoint (PTW,

Freiburg, Germany) and EBT3 radiochromic film (ISP, Wayne, USA). Measurements were performed in a non-reference geometry where spherical phantom with detector was moved from one measuring point to another using the patient positioning system, with the resolution of 0.2 mm (Figure 1).

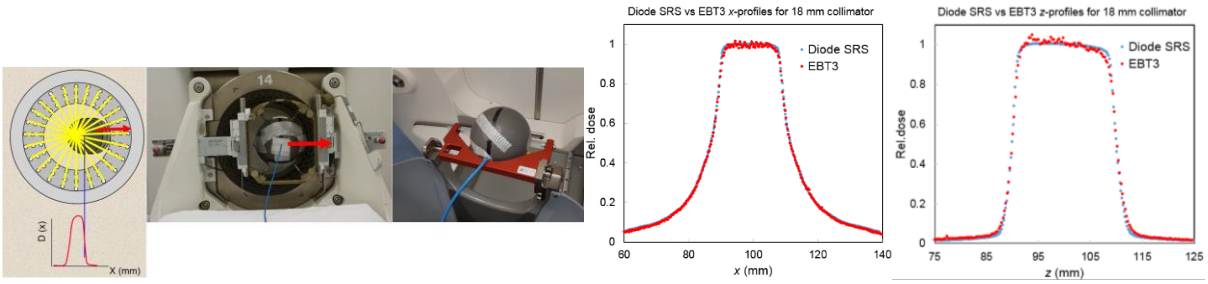

Figure 1. Dose profile scanning for the Gamma Knife composite dose distribution

The method was validated by comparison of profiles simulated in a non-reference geometry of phantom against the profiles simulated in a reference geometry using the Leksell Gamma Plan (LGP) treatment planning system and by comparison of profiles measured with EBT3 film with phantom in reference geometry against the profiles measured with the Diode SRS, microDiamond and PinPoint detector in a non-reference geometry (Figure 1).

Results and Discussion A small difference between simulated profiles in ref. and non-ref. geometry was observed on the plateau of the largest profiles, while x-profiles simulated in non-ref. geometry showed excellent agreement with the x-profiles simulated in ref. geometry. This indicated that the non-reference geometry in which the phantom is travelling along x, y or z-axis, instead of being in the centre of the LGK unit, is a suitable for accurate dose profile scanning with point detector. No volume averaging of the measured signal was observed for the Diode SRS and microDiamond detectors, while for PinPoint detector this effect was not negligible.

Conclusion Diode SRS and microDiamond detectors represent a good choice for the Gamma-Knife dosimetry because of high spatial resolution and good signal response and in conjunction with the patient positioning system they can provide high resolution and volume averaging free dose profile measurement for the Leksell Gamma Knife.

References

1) Maitz AH, Wu A, Lunsford LD, Kondziolka D, Bloomer WD. Quality assurance for Gamma Knife stereotactic radiosurgery. Int J Radiat Oncol Biol Phys 1995;32(5):1465-71.
2) [6] Devic S, Seuntjens J, Sham E, Podgorsak EB, Schmidtlein CR, Kirov AS, et al. Precise radiochromic dosimetry using a flat-bed document scanner. Med Phys 2005;32(7):2245-53.

Graphite calorimetry for quantifying ionization quenching in plastic scintillators in proton dosimetry

Jeppe Brage Christensen[1*], Guillermo Garrido Hernández[2], Anne Vestergaard[3], Stine S. Korreman[3,4] and Claus E. Andersen[1]
[1]*Center for Nuclear Technologies, Technical University of Denmark, Roskilde, Denmark*
[2]*Department of Physics and Astronomy, Aarhus University, Aarhus, Denmark*
[3]*Danish Centre for Particle Therapy, Aarhus University Hospital, Aarhus, Denmark*
[4]*Department of Clinical Medicine, Aarhus University, Aarhus Denmark*

Highlights The response of plastic scintillators and ionization chambers, unlike calorimeters, depend on the linear energy transfer (LET). We propose a graphite calorimeter to investigate the quenching in scintillators and the effect of the LET from all particles.

Key words Quenching, graphite calorimetry, scintillator dosimetry, proton therapy

Background and Objectives Plastic scintillator detectors (PSDs) are attractive for dosimetry due to a prompt signal read-out, a good water equivalence and a sub-mm size. Dosimetry with scintillators suffer, however, from a non-linear luminescence response relative to the energy deposition. The reduced luminescence, termed ionization quenching, is known to depend on the local energy deposition. The quenched luminescence signal is traditionally corrected relative to an ionization chamber measurement which in turn requires corrections for ionic recombination. Such recombination corrections in a scanned proton beam are cumbersome if possible at all: protocols as the TRS-398[1)] recommends the recombination in a high-intensity scanned beam to be corrected with calorimetry. Consequently, the present work investigates the possibility of constructing a graphite calorimeter to examine the quenched luminescence signal from the PSD during proton irradiation.

Materials and Methods A cylindrical graphite calorimeter (⌀ 16 mm×4 mm) is suspended in vacuum in a (30×30×30 cm^3) PMMA phantom as outlined in figure 1(a), where the thickness of the PMMA wall of the phantom is 26 mm. The graphite, coupled to thermistors, enables an accurate, quenching-free measurement of any energy deposition. A hole is drilled in a replica of the center graphite cylinder to contain a sub-mm sized PSD (BCF-12). The fiber-coupled PSD is connected to a photomultiplier tube and data acquisition software. Thus, the quenched scintillator measurement is compared directly to the energy deposition in the graphite calorimeter, where the range of the primaries is varied with solid water slabs. A TOPAS Monte Carlo model of the proton beam line at the Danish Centre for Particle Therapy and experimental setup is used to score the fluence- and dose-averaged linear energy transfer (Φ-LET and D-LET, respectively) in the graphite and the PSD.

Results and Discussion The calculated calorimetric and scintillation response during irradiation with a 120 MeV proton beam is shown in figure 1(b) as a function of the width of the solid water slabs. An inevitable drawback of the graphite cylinder and the PSD is the volume averaging, in particular pronounced at the distal edge. Nonetheless, the increasing LET from the entrance region to the Bragg peak permits an assessment of theoretical

quenching models[2-3]. An example of such a quenched luminescence response is included in figure 1(b) using a theoretical approach[3]. The secondary high-LET ions, especially those liberated in the graphite, constitute several percentage of the dose and must be accounted for[3]. While the response of the PSD and an ionization chamber vary with the high-LET secondary ions, the calorimeter response is LET-independent. Consequently, the Monte Carlo model enables an investigation of whether Φ-LET or D-LET is the better predictor for the quenched luminescence signal. Such an approach would not be feasible with an ionization chamber measurement, which however is less prone to volume averaging.

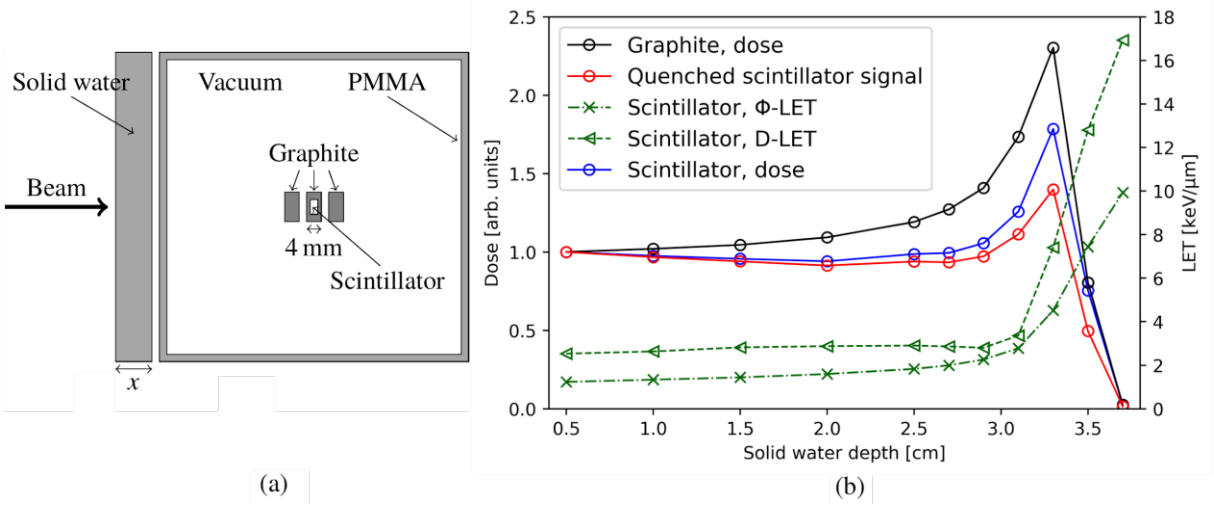

Figure 1. (a) The graphite calorimeter suspended in vacuum in a PMMA phantom. The center graphite cylinder is used to determine the absorbed dose to graphite white the two surrounding graphite cylinders are used to control the temperature changes. A PSD can be inserted in a replica of the center graphite piece. (b) Monte Carlo simulations of the dose in the graphite calorimeter and the scintillator. The Φ-LET and D-LET are scored in the scintillator volume is related to the calculation of the quenched luminescence signal.

Conclusion The LET-dependent response of a PSD requires correction relative to a LET-independent detector as a graphite calorimeter. The combination of a PSD, a graphite calorimeter, and a Monte Carlo simulation of the experiment enables an investigation of how the LET from primary and secondary particles affects the luminescence response in a PSD in an ion beam.

References

1) IAEA (2000) Absorbed Dose Determination in External Beam Radiotherapy, TRS-398, Vienna.
2) Birks JB (1951) Scintillations from organic crystals: specific fluorescence and relative response to different radiations, *Proc. Phys. Soc.* **64** 874
3) Christensen JB and Andersen CE (2018) Relating ionization quenching in organic plastic scintillators to basic material properties by modelling excitation density transport and amorphous track structure during proton irradiation, *Phys. Med. Biol.* **63** 19501

Radiation security and safety in Africa

M L Chithambo

Department of Physics and Electronics, Rhodes University, PO BOX 94, Grahamstown 6140, South Africa

Highlights The issue of safety and security involving nuclear and other radioactive material in Africa will be discussed.

Keywords Nuclear, radioactivity, safety, Africa, IAEA

Introduction Radiation sources are used for research, medical and a myriad other applications across Africa. Although policies have been formulated at national or institutional level to safeguard against deleterious effects of exposure to radiation, new emerging threats such as nuclear terrorism have called attention to the need for training in international best practice in this area. This talk will look at contemporary efforts to strengthen regulations for nuclear security against threats from misuse of nuclear and radioactive material in Africa. We will touch on threats possible, and describe the operation of a nuclear power plant to exemplify how issues of nuclear safety and radioactive waste are addressed.

The world-wide forum for scientific and technical cooperation in nuclear technology is the International Atomic Energy Agency (IAEA). The IAEA is an autonomous organisation which is independent of but cooperates with the United Nations. The principal objective of the IAEA is *to accelerate and enlarge the contribution of atomic energy to peace, health and prosperity throughout the world*. Thus far, the IAEA has 165 member countries 40 of which are from Africa. The IAEA plays a central role in developing educational and scientific programmes used to promote nuclear and radiation safety. African countries, as other members of the IAEA, are party to guidelines on nuclear security standards and their implementation as developed by the IAEA.

Range of threats involving nuclear and radioactive material In order to properly understand efforts to prevent the unlawful use of nuclear and other radioactive materials, it is important to appreciate the types of threats involved. There are a number of threats identified by the IAEA where nuclear or radioactive material could be used in criminal activities such as the following [1]

a) Developing nuclear explosive devices
b) Nuclear material being used to fabricate an improvised nuclear explosive device
c) Use of radioactive material to build a radiological dispersal device
d) Wilful dispersal of radioactivity through vandalism at sites where nuclear and other radioactive material are kept or of such material in transit

Physical and operational aspects We will exemplify the question of nuclear safety and security in Africa by citing the operational aspects of a nuclear power plant, for example, the Koeberg Nuclear Power station, the only commercial one in Africa [2]. From this, it should be apparent as to the types of nuclear and radioactive material that regulatory bodies must deal with to avoid their illicit use.

The generation of power using nuclear reactors is discussed in several texts e.g. [3] and a typical fuel cycle is shown in Fig. 1 [4]. Nuclei close to ^{56}Fe have very high binding energy per nucleon [3]. This energy can be released as heat by forming nuclei whose mass is close to that of ^{56}Fe by either of two routes; from heavy nuclei through fission or from light nuclei by fusion. The generation of nuclear power is based on induced fission. The fuel exploited for nuclear power generation is uranium dioxide. Some isotopes of uranium, for example, ^{238}U require an energetic neutron to induce fission. Others like ^{235}U have nuclei that can be induced to fission even by a zero energy neutron. For nuclear power generation based on fissile uranium, uranium-bearing ore is mined and milled (leaving tailings or residue after the milling) and then undergoes chemical treatment to extract uranium in the form of ammonium diuranate ($(NH_4)_2U_2O_7$). The purpose is to end up with uranium oxide concentrate U_3O_8 upon further treatment. The main isotopes of naturally occurring uranium are ^{235}U at 0.72% and ^{238}U at 99.2%.

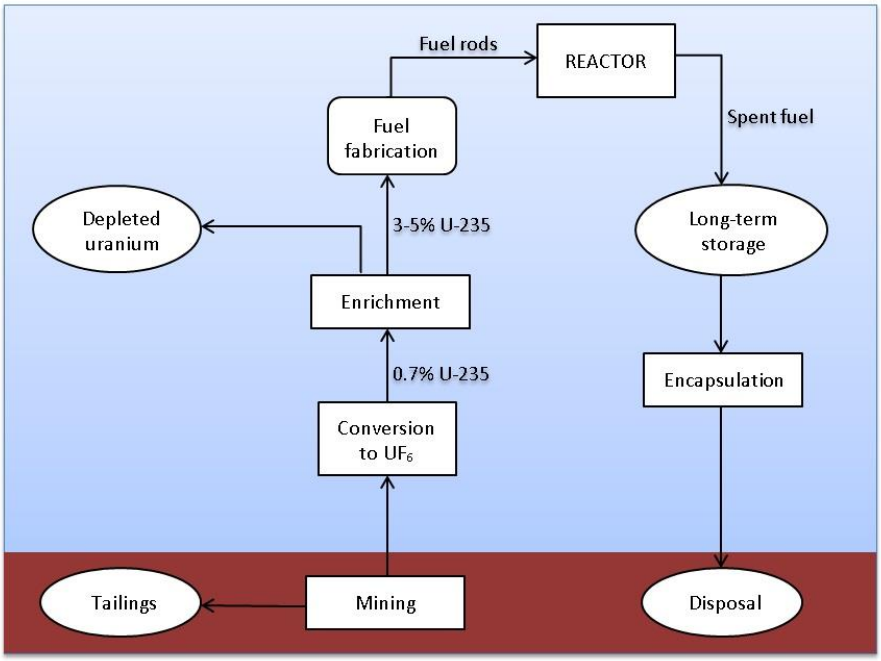

Fig. 1 An open fuel cycle [4].

Uranium oxide has the same isotopic ratio as naturally occurring uranium. Because of this, an incident neutron is more likely to interact with ^{238}U than with ^{235}U and thus U_3O_8 cannot be used as a fuel for reactors. To enable sustained fission, the amount of ^{235}U is artificially enriched to between 3 and 5%. The total energy released in induced fission is 205 MeV [3]. Of this, 178 MeV becomes available as heat. The remainder is attributed to long-lived fission products in the β decay chain. This waste constitutes a health and security hazard. The heat released during fission is harnessed to convert water to steam which drives turbines to move generators to produce electricity.

Treatment of waste There are three types of radioactive waste produced at a typical nuclear power plant that one can list, namely, low-level waste, intermediate-level waste and spent fuel. Low level waste consists of operational materials like glassware and some such with only traces of radiation. Intermediate-level waste are items such as spent filter cartridges. High-level waste is the spent fuel and is initially stored under water to remove the heat and as a way

of shielding against radiation. After re-processing, this will be sealed to be disposed of at geological depths.

Training and education Nuclear security issues relating to the prevention of malicious use of nuclear material and other radioactive substances and their associated facilities are described in the IAEA Nuclear Security Series of publications and other training programmes. The publications are issued under the following categories

a) *Nuclear Security Fundamentals* – these contain principles of nuclear security and are used as the basis for security recommendations
b) *Recommendations* – these outline best practices that should be adopted by IAEA member states
c) *Implementing Guides* – clarify the recommendations and suggest ways to implement them
d) *Technical Guidance* - these are materials like reference manuals, training guides, and service Guides

A list of nuclear security activities are shown in Fig. 2 [1]. We will detail how this architecture is used in ensuring safety and security of nuclear and radioactive material in Africa.

Deter, dissuade	Protect, secure	Assess threat	Detect	Assess alarm/ alert	Interdict	Manage crime scene	Protect evidence	Analyse evidence	Attribute	Return item	Prosecute

Prevention	**Detection**	**Response**

Fig. 2. A range of nuclear security activities [1].

The enduring importance of this architecture can be understood in the context of statistics [5] that show that by 2006 states had reported a total of 1080 incidents of unauthorized and unregulated activities involving nuclear and other radioactive material. Of these, about 25% were on nuclear material and about 70% on other radioactive material.

References

1. Nuclear security systems and measures for the detection of Nuclear and other Radioactive material out of Regulating Control, Implementing Guide, IAEA Nuclear Security Series No. 21.
2. Koeberg Nuclear Power Station, general information brochure, Generation Stakeholders Management and Communications Department, 2011, Eskom, South Africa.
3. Cottingham, W.N., Greenwood, D.A. 1986. An introduction to nuclear physics. Cambridge University Press.
4. Hore-Lacy H, 2003. Nuclear Energy in the 21st Century. World Nuclear University Press.
5. Combating illicit trafficking in nuclear and other radioactive material, IAEA Technical Guidance Reference Manual, IAEA Nuclear Security Series No. 6.

Development of a UAV based spectro-dosimetric system for radiological surveillance

Maksym Luchkov*, Stefan Neumaier
Physikalisch-Technische Bundesanstalt (PTB), Braunschweig, Germany

Highlights The unmanned airborne monitoring system on the basis of a $CeBr_3$ spectrometer is being developed to meet the need for a fast acquisition of metrologically sound data on a large-scale ground contamination following a radiological emergency.

Key words radiation monitoring, dosimetry, UAV, "Preparedness"

Background and Objectives In the framework of the EMPIR project 16ENV04 "Preparedness"[1,2], PTB is developing a spectrometer based dosimetric system that can be operated while being attached to an unmanned aerial vehicle (UAV). The monitoring system has the aim of the minimization of emergency workers' exposition to ionizing radiation in the case of a nuclear or radiological incident, as UAV can cover a large area not only faster than a ground squad but also keep operators distant from a contaminated region.

Materials and Methods The dosimetric system consists of a $CeBr_3$ scintillation detector which records spectra every two seconds into a database alongside with global position, height above ground and temperature data. The system also sends this information via peer-to-peer radio communication to a ground station where spectra are converted into dose rate information. The conversion function from spectra to dose was obtained by a Monte Carlo simulation (GEANT4) of the detector response.

Results and Discussion The paper presents the results from several measurement campaigns: aerial tests locating a 'point' source of Tc^{99m} and ground tests with an uncollimated free field irradiation facility aiming to determine the system performance in the controlled environment. The 'point' source location was calculated from counts in a 143 keV photopeak using the regularized statistical image reconstruction method. The ground campaign results showed good agreement of the measured dose rates with the reference values of 60 to 400 nSv/h, with standard deviations in the order of 10-30 % at just two seconds per measurement.

Conclusion The remarkable performance of the dosimetric system demonstrates the

ability of metrologically accurate two-second long dose rate measurements with the well-characterized $CeBr_3$ spectro-dosemeter. The next step is the extensive aerial testing of the dosimetric system against well-known radiation fields. Finally, the system must be able to calculate surface activity concentrations from the recorded spectra.

References

1) The EMPIR project “Preparedness”, http://www.preparedness-empir.eu (accessed on 20 March 2019).
2) Neumaier S, Dombrowski H, Kessler P, Luchkov M, Vargas A, Bell S, Bogucarskis K, Kovar P. Metrology for the mobile detection of ionizing radiation following a nuclear or radiological incident – The EMPIR project “Preparedness”. Arh Hig Rada Toksikol 2019;70:85-91. (accepted for publication March 2019)

Occupational radiation dose to the lens of the eye for physicians from neurovascular interventional radiology procedures

M.E. Lian[1], H.Y. Tsai[1]*, S.L. Chang[1, 2]

[1]*Institute of Nuclear Engineering and Science, National Tsing Hua University, Hsinchu 300, Taiwan*

[2]*Radiation Protection Association R.O.C., Hsinchu 300, Taiwan*

Highlights The complexity and machine settings of neurovascular interventional radiology (NIR) procedures result in significantly high occupational exposure to physicians. However, there is a lack of actual measurement and assessment of eye lens dose in recent studies in NIR procedures. In this research, clinical measurements of $H_p(3)$ and $H_p(0.07)$ provide not only the direct dosimetry to the eye lens but also the correlation between eye lens dosimeters and additional over-apron neck personal dosimeters for the estimation of eye lens dose when only $H_p(0.07)$ is available in clinical practices.

Key words eye lens dosimeter, neurovascular interventional radiology, personal dose equivalent, dosimetry

Background and Objectives In 2012, International Commission on Radiological Protection (ICRP) has revised the equivalent dose to the lens of the eye for occupational exposure from 150 mSv per year to 20 mSv per year, averaged over five consecutive years, with a maximum of 50 mSv in a single year[1)]. According to the radiological occupation categories provided by International Atomic Energy Agency (IAEA)[2)], workers in the medical field, especially in fluoroscopy guided interventional procedures, are exposed to relevant levels of radiation and should be carefully concerned. Physicians tend to receive an extended radiation exposure for the complexity and machine settings from neurovascular interventional radiology (NIR) procedures, but there is a lack of actual measurement and assessment of eye lens dose in recent studies. IAEA also recommends that separate monitoring for eye lens dose near the eyes or over the trunk shielding is necessary when the protective equipment is used for the trunk and the personal dosimeter is placed behind the protective equipment. This research aimed to observe the occupational radiation dose to the lens of the eye obtained from NIR procedures by direct measurement using the EYE-D^{TM} near the eyes and estimate the eye lens dose from the additional over-apron neck personal dosimeter for the absence of the dedicated eye lens dosimeter.

Materials and Methods A dedicated eye lens dosimeter (EYE-D^{TM}, RadCard, Krakow,

Poland), consisting of a thermoluminescence dosimeter (TLD) pellet (MCP-N, ^{natural}LiF: Mg, Cu, P) and a polyamide capsule, was occupied for direct dosimetry. Dose calibration and energy dependence of TLD were operated in the National Radiation Standard Laboratory (NRSL), Taiwan. Lens doses were measured at NIR departments over a 3-month period by using dosimeters eventually calibrated to personal dose equivalent at 3 mm depth, $H_p(3)$. Additional over-apron neck personal dosimeters, measuring personal dose equivalent at 0.07 mm depth, $H_p(0.07)$, were also issued to NIR physicians at the same time for observation of the correlation to the EYE-D^{TM}. A review of radiation protection practices at these facilities was also carried out.

Results and Discussion The reproducibility and the homogeneity of dosimeters are within 4% and ±10%, respectively. Energy dependence of the dosimeter in low-energy regions is more severe than that in high-energy regions (relative to N80). Complication of NIR procedures and inappropriate usages of radiation protection equipment result in an obviously high dose of occupational exposure to the lens of the eye of NIR physicians. The eye lens dose would be overestimated by the additional over-apron neck personal dosimeter, but there was a good correlation between dose measured by the EYE-D^{TM} and dose measured by the additional over-apron neck personal dosimeter.

Conclusion Estimated annual dose to the lens of the eye for NIR physicians has the potential to exceed the revised ICRP limit when the radiation protective equipment is not properly used. The eye lens dosimeter and the additional over-apron neck personal dosimeter show a good correlation for eye lens dose estimation when dedicated eye lens dosimeter is absent.

References

1) ICRP, 2012 ICRP Statement on Tissue Reactions / Early and Late Effects of Radiation in Normal Tissues and Organs – Threshold Doses for Tissue Reactions in a Radiation Protection Context. ICRP Publication 118. Ann. ICRP 41(1/2)
2) IAEA, 2013. Implications for Occupational Radiation Protection of the New Dose Limit for the Lens of the eye. https://doi.org/10.13140/2.1.2586.1122

The response of the Glass Badge system for mixed irradiation

Michiko Ube[1]*, Satoshi Ueno[1], Naoki Takashima[1], Wakako Shinozaki[1], Yasuhiro Koguchi[1]
[1]*Chiyoda Technol Corporation, Ibaraki, Japan*

Highlights The responses of the Glass Badge (GB) system for mixed irradiations were assessed. The responses for 14 877 mixed irradiation combinations with two different radiation qualities were evaluated. It was confirmed that the calculated dose with the GB system was sufficient for practical use. The GB system was met the requirement of IEC 62387 standard.

Key words RPL, Glass Badge, dosemeter, mixed irradiation

Background and Objectives The individual monitoring service with the GB system have been provided by Chiyoda Technol Corporation since 2000. The radiophtoluminescence (RPL) glass detector is used for photon and beta radiation. The RPL glass detector is made of a silver-activated phosphate glass, which can be readout the RPL signal proportional to the dose by excitation of ultraviolet (UV) light. For a constant energy response to photons over a wide energy range, five different filters are set with the RPL glass detector: two different thickness of the plastics, aluminum, copper, and tin (Figure 1). The two plastic filters and an aluminum filter are also used to measure beta radiation. If the GB is used in the mixed field of photon and beta radiation, the RPL signal is sum of the signals with photons and beta radiations. The algorithm of the GB system includes the branch to determine if there is a beta radiation incidence. In this study, the responses of the GB system for mixed irradiations were assessed.

Materials and Methods The response for mixed irradiation was evaluated according to the method described in the IEC 62387:2012 standard, which is the international standard for passive dosimetry systems of photon and beta radiation. The signals of mixed irradiation were simulated using the sum of signals with two different radiation qualities (photons of 12 keV to

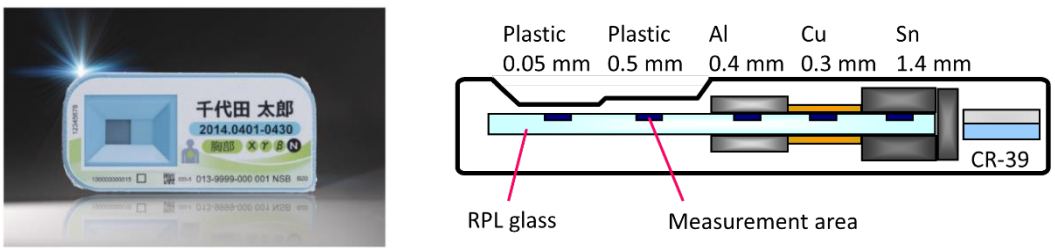

Figure 1 The photo and cross-sectional view of the Glass Badge

6.4 MeV and beta radiations (^{85}Kr and ^{90}Sr/^{90}Y)). The signals for each radiation quality were gained with energy and angular response test of the IEC standard. The mixing ratio were changed 1:9, 2:8, … up to 9:1 and the total dose were 10.0 mSv for any combinations. The responses for 14 877 mixed irradiation combinations were evaluated.

Results and Discussion Table 1 shows some examples of responses of the mixed irradiation. It was found that the responses for most conditions were within ±20 %. For some combinations (e.g. ^{137}Cs : ^{90}Sr/^{90}Y = 9:1), signals were not distinguished between photon and beta radiation, even if the total $H_p(0.07)$ can give good evaluation of the irradiated dose.

Table 1. The examples of combinations and calculated dose for mixed irradiation

Combinations for mixed irradiation			Calculated $H_p(0.07)$ with GB system (mSv)		
Radiation quality		Ratio	Photon	Beta radiation	Total
^{137}Cs	^{85}Kr	9 1	10.0	—	10.0
		5 5	5.2	5.0	10.2
		1 9	1.0	9.7	10.8
	^{90}Sr/^{90}Y	9 1	10.2	—	10.2
		5 5	5.2	5.7	10.9
		1 9	1.0	9.7	10.7
	N-15 (12 keV)	9 1	10.8	—	10.8
		5 5	11.0	—	11.0
		1 9	11.4	—	11.4
	N-60 (48 keV)	9 1	10.7	—	10.7
		5 5	10.6	—	10.6
		1 9	10.6	—	10.6

Conclusion It was confirmed that the calculated dose with GB system was sufficient for practical use. The GB system were met the requirement of IEC 62387 standard.

References

1) IEC 62387:2012, Radiation protection instrumentation – Passive integrating dosimetry systems for personal and environmental monitoring of photon and beta radiation
2) Daisuke Maki, et al, Development of The New Glass Badge, Radiation Protection Dosimetry, 337–345 (2016)

ARADOS: Asian network for radiation dosimetry

Osamu Kurihara[1]*, Wi-Ho Ha[2], Cao Qinjian[3]
[1]*National Institutes for Quantum and Radiological Science and Technology, Chiba, Japan*
[2]*Korea Institute of Radiological and Medical Sciences, Seoul, Korea*
[3]*China Institute of Radiation Protection, Shanxi, China*

Highlights Asian Radiation Dosimetry Group (ARADOS) was established in 2015 with a main purpose to promote collaborations on the relevant activities among Asian countries. Members of ARADOS discussed its missions and structure in past annual meetings and several collaborative study projects have been launched in the last years. Strategies to further activate ARADOS are now being considered for the next step.

Key words Asia, network, radiation, dosimetry, harmonization, collaboration

Background and Objectives Asian Radiation Dosimetry Group (ARADOS) was born through discussion on a proposal by Dr. Wi-Ho Ha of KIRAMS among members of Korea, China and Japan at the first meeting in 2015. He suggested that it was necessary to establish a similar network to European Radiation Dosimetry Group (EURADOS) among Asian countries. Since then, annual meetings have been organized by hosting institutes of Korea, China and Japan in turn, and several collaborative studies have been launched.

Mission and Structure of ARADOS Main missions of ARADOS were discussed in the first meeting at KIRAMS and were then decided as follows: 1) enhancement and harmonization of radiation dosimetry capabilities in Asian countries; 2) exchange of the relevant techniques and activities of each participating institutes; and 3) preparation of the joint response of radiation dosimetry services in radiological/nuclear (RN) accident. The third mission came from experiences of the 2011 Fukushima nuclear disaster in Japan with a consideration of the fact that the coastal area of East Asia is the densest NPP area in the world. The structure of ARADOS was discussed in the second annual meeting at CIRP in 2016. As a result, only the chairperson (Dr. O. Kurihara) and the secretary (Dr. Wi-Ho Ha) were elected. The board members or other administrative members were not decided because ARADOS was still at the beginning stage. Four working groups (WG) were established: WG1 for internal dosimetry, WG2 for external dosimetry, WG3 for biological dosimetry and WG4 for computational dosimetry. Study items are proposed by members of each WG. Currently, two intercomparison

exercises on direct thyroid measurement (WG1) and chromosome analysis (WG3) have been ongoing.

Annual Meeting The annual meeting of ARADOS has been continued since 2015. The last 4th ARADOS meeting in 2018 was hosted by KIRAMS and KHNP/RHI of Korea. Two distinguished European scientists were invited in this meeting for giving their presentations and suggestions to ARADOS's activities. The annual meeting has been a great opportunity to share recent topics of each country and have direct communication between researches. The number of participants has been increasing year by year (Figure 1).

Figure 1. The 4th ARADOS annual meeting at Seoul on October 16-18, 2018.

Future work The framework of ARADOS has been built. So what should we do next? One important task is to open the webpage on ARADOS as a communication channel for persons and new collaborating institutes that are interested in our activities and inviting. On the other hand, ARADOS has currently no scheme to gather funds from participants or sponsors. The cost for the annual meeting has been covered by a hosting institute. Difficulties have also been recognized in transporting materials (e.g., a radioactive source) to other counties in the intercomparison exercises because of distance, cost and regulations of each country. These issues need to be discussed among ARADOS members in near future with reference to experiences of EURADOS for 37 years since its establishment. However, looking on the bright side, members of ARADOS are relatively young and have a lot of potentials.

Dose reconstruction using surrogate dosimetry materials: the potential of fabrics

I.K. Bailiff

Luminescence Dosimetry Laboratory, Durham University, Durham DH1 3LE, UK

Highlights The prompt measurement of dose to individual members of the public exposed during a radiological emergency is critical to medical triage. An assessment is made of the luminescent properties of polymer-based fabrics used in the manufacture of clothing and accessories and their potential to be deployed as dosemeters.

Key words Dose reconstruction, radiological emergencies, luminescence, surrogate dosimetry materials

Background and objectives

Quartz grains extracted from ceramic tiles taken from buildings in Hiroshima were used in the 1960s to measure gamma dose due to the atomic bomb detonation. This approach was further developed to support dose reconstruction studies of several important radiological emergencies affecting populated areas (e.g., Bailiff et al., 2016). Recently, attention has turned to developing techniques capable of providing prompt estimates of gamma dose on a spatially localised scale to support medical triage for individuals exposed in the event of a radiological emergency (e.g., a malicious attack). For such measurements materials that can function as 'fortuitous' or 'surrogate' dosimeters that are usually located close to the body, such as personal possessions, have been sought. Amongst a range of materials examined using luminescence techniques, components within mobile phone devices have attracted the most attention, in particular the alumina substrates of surface-mount resistors and inductors. However, miniaturization of components, combined with an anticipated reluctance of owners to relinquish their phones in an emergency, have prompted the continued search for alternative materials. Natural and synthetic polymer-based woven materials in various forms are widely used in the manufacture of clothing and accessories, and some have been found to be capable of measuring absorbed dose using OSL techniques (Sholom and McKeever, 2014). The clothing materials tested have been generally found to possess characteristics that limit their potential for use in emergency dosimetry, although other fibrous materials such as banknotes (Sholom and McKeever, 2014; Mrozik et al., 2017) appear to have superior characteristics. The main detracting issues with clothing fibres include highly variable intrasample sensitivity, significant fading within a short timescale and a strong 'native' signal in unirradiated fabric.

Where CW OSL measurements are performed (typically using a blue or green LED stimulation source and with a 300-400 nm detection window). Cathodoluminescence measurements with various types of fabric (Bossin et al., 2017) have indicated multiple emission bands extending from the UV to the deep red, some of which may participate in OSL recombination. However, the use of other detection windows to explore the use of longer wavelength emission is limited by the bright fluorescence of polymer fibres (Fig. 1) that obliterates a relatively weak time-dependent OSL signal. Although in the case of one example of a polyester-cotton fabric (Bossin et al., 2017), both fluorescence and the native signal were eliminated by measurement of infrared stimulated luminescence (IRSL), this characteristic was not found in other fabrics tested. The general variability in luminescence response of polymer-based materials (fabrics and shoe soles) suggests that additives may play an important role in determining the luminescence characteristics of fabrics. This paper examines approaches taken to examine the sources of luminescence in fabrics and the potential role of additives introduced during their manufacture and identifies those additives that can help to realise the potential of using clothing and accessories to provide a wider spatial range of dose determinations for radiation exposed individuals.

Fig. 1: PL emission spectrum (470 nm stim.) Mixed fibre fabric

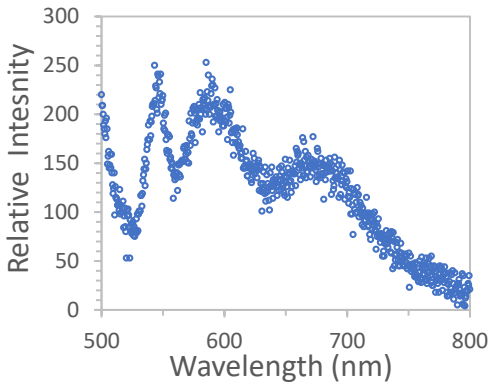

Conclusion

Identification of additives with luminescence properties can potentially can lead to a better understanding of their role in the luminescence observed with fabric samples taken from clothing and the possibility of selective measurement of components with preferred dosimetric properties.

References

Bailiff, I. K., Sholom, S., McKeever, S., 2016. Retrospective and emergency dosimetry in response to radiological incidents and nuclear mass-casualty events: A review. Radiat. Measts 94, 83-139.

Bossin, L., Bailiff, I. K., Terry, I., 2017. Luminescence characteristics of some common polyester fabrics: Application to emergency dosimetry. Radiat. Measts 106, 436-442.

Mrozik, A., Kulig, D., Marczewska, B., Bilski, P., 2017. Dose estimation based on OSL signal from banknotes in accident dosimetry. Radiat. Measts 101, 1-6.

Sholom, S., McKeever, S., 2014. Emergency OSL dosimetry with commonplace materials. Radiat. Measts 61, 33-51.

TL investigation of glasses from mobile phone screen protectors for radiation accident dosimetry

Céline Bassinet*, Wendy Le Bris
IRSN, Fontenay-aux-Roses, France

Highlights The dosimetric properties of glasses extracted from screen protectors for mobile phones are investigated using thermoluminescence. Their potential use as fortuitous retrospective dosimeters in the event of a radiological accident is discussed.

Key words retrospective dosimetry, radiation accident, thermoluminescence, glass screen protector, mobile phones

Background and Objectives In the event of a radiological accident, if data from conventional personal dosimetry does not exist, fortuitous retrospective dosimeters could be used to estimate the dose received by the victims. The dosimetric properties of materials found on the victims or in their vicinity are widely investigated in this aim. Previous studies using thermoluminescence (TL) technique [e.g. 1-4] have shown that glass from display screen of mobile phones is very promising for this application. Glass from mobile phone touchscreens was also studied using TL and phototransferred thermoluminescence (PTTL) [5-6]. It has the advantage that it may be replaced without destroying the phone. In addition, mobile phone screens are often protected against physical damage using a screen protector. Most of these additional sheets of material are glass and they can be easily removed. In the present work, their TL dosimetric properties are studied.

Materials and Methods Several models of mobile phone glass screen protectors were studied. TL measurements were performed using an automated reader. Glass dosimetric properties were investigated, such as intrinsic background dose, sensitivity, measurement reproducibility, dose response and signal stability.

Results and Discussion The majority of glass screen protectors are sensitive to ionizing radiation, but their TL signal intensity is lower than the one of glasses obtained from mobile phone display screens. Preliminary results of dose recovery tests will be compared with the ones obtained using display screen glass and touchscreen glass.

Conclusion The potential use of glasses extracted from mobile phone screen protectors as fortuitous retrospective dosimeters in the event of a radiological accident will be discussed.

References

1) Bassinet, C., Trompier, F., Clairand, I., 2010. Radiation accident dosimetry on glass by TL and EPR spectrometry, Health Phys. 98 (2), 400-405.
2) Bassinet, C., Pirault, N., Baumann, M., Clairand, I., 2014. Radiation accident dosimetry: TL properties of mobile phone screen glass. Radiat. Meas. 71, 461-465.
3) Discher, M., Woda, C., 2013. Thermoluminescence of glass display from mobile phones for retrospective and accident dosimetry. Radiat. Meas. 53-54, 12-21.
4) Discher, M., Woda, C., Fiedler, I., 2013. Improvement of dose determination using glass display of mobile phones for accident dosimetry. Radiat. Meas. 56, 240-243.
5) Discher, M., Bortolin, E., Woda, C, 2016. Investigations of touchscreen glasses from mobile phones for retrospective and accident dosimetry. Radiat. Meas. 89, 44–51.
6) McKeever, S.W.S., Minniti, R., Sholom, S., 2017. Phototransferred thermoluminescence (PTTL) dosimetry using Gorilla® glass from mobile phones. Radiat. Meas. 106, 423-430.

A EURADOS inter-laboratory comparison on retrospective dosimetry using OSL/TL of electronic components and display glass from mobile phones

C Woda[1]*, C Bassinet[2], O Grand[2], M Discher[3], S Della Monaca[4], E Bortolin[4], P Fattibene[4], MC Quattrini[4], S Sholom[5], SWS McKeever[5], Z Čemusová[6], D Ekendahl[6], O Van Hoey[7], L Bossin[8], I Bailiff[8], E Kouroukla[9], JS Eakins[9], L Ainsbury[9], L Waldner[10], T Geber-Bergstrand[10], I Veronese[11], A Galli[12,13], L Panzeri[13], M Martini[13], J Lee[14], JL Kim[14]

[1] *Helmholtz Zentrum München, Institute of Radiation Medicine, Neuherberg, Germany*

[2] *Institut de Radioprotection et de Sûreté Nucléaire (IRSN), Fontenay-aux-Roses, France*

[3] *University of Salzburg, Department of Geography and Geology, Salzburg*

[4] *Istituto di Superiore di Sanità, Rome, Italy*

[5] *Oklahoma State University, Department of Physics, Radiation Dosimetry Laboratory, Stillwater, OK 74078, USA*

[6] *National Radiation Protection Institute, Prague, Czech Republic*

[7] *Environment, Health and Safety Institute, Belgian Nuclear Research Center (SCK•CEN), Mol, Belgium*

[8] *Durham University, Department of Archaeology, Durham, UK*

[9] *Public Health England, CRCE, Chilton, Didcot, Oxon, UK*

[10] *Lund University, Medical Radiation Physics, Malmö, Sweden*

[11] *Università degli Studi di Milano, Dipartimento di Fisica, Milano, Italy*

[12] *CNR-IBFM, Segrate (MI), Italy*

[13] *INFN and Università degli Studi di Milano-Bicocca, Dipartimento di Scienza dei Materiali, Milano, Italy*

[14] *Korean Atomic Energy Research Institute, Daejeon, Korea*

Highlights Uncertainty for OSL on resistors around 25 % (1 sigma); TL method on display glass validated for arbitrary phone sample; ISO 13528 useful for statistical analysis

Key words Retrospective dosimetry, fortuitous dosimeters, inter-laboratory comparison

Background and Objectives The risk of a mass-casualty scenario due to the accidental or intentional exposure of the population to ionizing radiation has led to considerable research effort in the past decade to identify and characterize personal items that can be used as fortuitous dosimeters using either luminescence methods (OSL/TL) or EPR. Inter-laboratory comparisons (ILCs) are an indispensable tool for standardization and to test, whether a measurement protocol on a proposed material works independent of the analyzing laboratory. ILCs have so far been

carried out within the EURADOS WG10 network on electronic components from smartphones, namely for OSL of resistors, EPR of touchscreen glass and TL of display glass[1-3]. The latter was restricted to using the same (bought) phone model with favourable dosimetric properties of the glass. The present study extends the previous ILCs to test the TL method on display glass for arbitrary phone samples, to assess and reduce (if feasible) the uncertainty for OSL on resistors, and to test the TL method on resistors. The ILC was a joint exercise with biological dosimetry labs, organized in the RENEB network, and the same doses were chosen for both physical and biological dosimetry.

Materials and Methods 12 laboratories participated in the ILC - ten from Europe, one from the USA and one from Korea. Three phones per laboratory were irradiated with doses < 1 Gy, 1-2 Gy and >2 Gy, respectively, using a linear accelerator at IRSN. An unirradiated phone was provided as a fourth sample. For OSL on resistors, the time difference Δt between administering the calibration dose and measuring the corresponding OSL signal was set variously as: 1) as short as possible, 2) one day, and 3) the same value as for the LINAC irradiation (for which the fading will cancel out). The TL method was tested on both etched and unetched glass. ISO 13528[4] was used for estimating the means and standard deviations and for identifying outliers.

Results and Discussion For OSL of resistors, an overall uncertainty of ~ 25% (1 sigma) was observed for both the full and fast mode protocols[1] and for Δt as short as possible. For the full mode protocol[1] some reduction in uncertainty was seen when increasing Δt, whereas no such trend was noticed for the fast mode protocol[1]. The TL method was validated for arbitrary display glass samples. An improvement in performance could be observed with etched samples. The TL method on resistors could not be fully validated but its potential was demonstrated. Occasional outliers occurred with all assays and methods. Major sources of uncertainty and the strengths and limitations of the ISO methods will be discussed.

Conclusion The present ILC gave insight into the uncertainty and achievable accuracy for the OSL method of resistors. Through the validation, two independent methods of dose measurement per smartphone are now available for implementation in a dosimetry network to increase measurement capacity in the case of a mass-casualty incident.

References

1) Bassinet et al. (2014). Radiat. Meas. 71, 475-479.
2) Fattibene et al. (2014). Radiat. Environ. Biophys. 53, 311-320
3) Woda et al. (2016). Presentation at SSD18, Munich, 3-8 July.
4) ISO 13528: Statistical methods for use in proficiency testing by interlaboratory comparison

OSL dosimetry with protective glasses of modern smartphones: a fiber optics non-destructive approach

Sergey Sholom [1]*, Stephen W.S. McKeever [1]
[1]*Department of Physics, Oklahoma State University, Stillwater, Oklahoma, USA*

Highlights Protective glasses of modern smartphones were tested with an optically stimulated luminescence (OSL) technique. An optical fiber was used to deliver the stimulation light to the glass and collect the emission back. This enables the potential for the prompt dose evaluation without disassembly of the phone. The current sensitivity of this technique is several Gy depending on the phone manufacturer and model.

Key words Optically stimulated luminescence, smartphones, fiber optics, protective glass.

Background and Objectives Modern smartphones are currently extensively tested as potential emergency dosimeters (*e.g.* surface mount resistors are examined with OSL or thermoluminescence (TL) while display and protective glasses are tested with both TL and electron paramagnetic resonance)[1)]. To date, all dosimetry techniques with phones are destructive and require disassembly of the phone, which could be inconvenient in emergency situations. The objectives of the current work were to test a potential non-destructive dosimetric approach in which the phone's back protective glass (usually made from the Gorilla Glass®) is optically stimulated using fiber optics to deliver the stimulation light and to collect and transport the OSL signal to a photomultiplier tube (PMT).

Materials and Methods Back protective glass (i.e. glass from the rear of the phone) is present on many modern smartphones to support wireless charging. They are usually protected from exposure to environmental light by a phone case. These glasses were collected from several smartphones of different models and were tested with OSL. For purposes of these initial studies the glasses were mechanically separated from the phones and then cut into aliquots of the size 5 x 5 mm^2. Samples were exposed to different doses with a $^{90}Sr/^{90}Y$ beta source at the dose rate 0.3 Gy/s and recorded with OSL at different times after exposure. Stimulation of OSL was with a green (532 nm) laser operating in pulse mode at a frequency of 4 kHz; OSL emission was collected between the laser pulses in the blue wavelength region using a Semrock 468 nm short-pass filter. Stimulation and emission beams were separated using an appropriate dichroic mirror. This arrangement minimized the influence of very strong stimulation light on detection of the weak OSL and is similar in design to that previously described by Klein *et al.*[2)], but utilizing different optical components.

Results and Discussion Figure 1 (a) shows the OSL curves from two representative back

glasses exposed to a 60 Gy beta dose and measured immediately after exposure. These curves were recorded with a PMT duty cycle of 0.85 (*i.e.* the ratio of the time when the OSL is collected by the PMT to the period of laser pulses). A prominent radiation-induced OSL signal (RIS) is seen from these samples, corresponding to a minimum detectable dose (MDD) of about 1 Gy. Other tested samples demonstrated quite variable RISs with values of the MDD in the range 1-20 Gy. Figure 1 (b) shows the dependence of the RIS on the PMT duty cycle obtained for samples of the Xperia phone exposed to 60 Gy. The maximum signal-to-noise ratio was observed for the duty cycle of ~0.85.

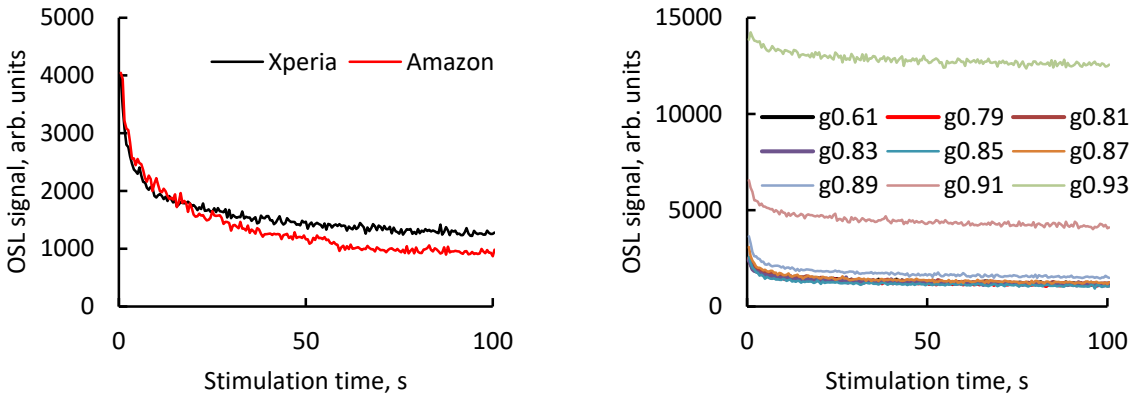

a b

Figure 1. OSL responses (a) from two different back glasses (from a Sony Xperia and an Amazon smartphone) exposed to 60 Gy beta dose, and (b) from the Sony Xperia glass exposed to 60 Gy and recorded for different duty cycles.

Conclusion Back glasses of modern smartphones have been tested as prompt emergency dosimeters using a fiber optics OSL technique. The current sensitivity of this technique is in the range 1-20 Gy (for samples measured immediately after exposure). The results reveal the potential of OSL as a non-destructive dose measurement technique for some types of modern smartphone.

Acknowledgments This work was funded by a grant from Oak Ridge Associated Universities (Grant # G10001987), and the State of Oklahoma.

References

1) S. W. S. McKeever, S. Sholom, J. R. Chandler, 2019. *A comparative study of EPR and TL signals in Gorilla® Glass*. Radiat. Prot. Dosim., doi:10.1093/rpd/ncy243.
2) D. M. Klein, E. G. Yukihara, S. W. S. McKeever, J. S. Durham, M. S. Akselrod, 2006. *In situ long-term monitoring system for radioactive contaminants.* Radiat. Prot. Dosim., 119, 421–424.

Comparison of Experiments and Simulations using OSL from phones, TLDs and Monte Carlo Calculations on a Gamma-Irradiated Phantom

Elena Bakhanova[1]*, Vadim Chumak[1], Sergey Sholom[2], Stephen W.S. McKeever[2], Josh R. Chandler[3], and H.L. Hall[3]

[1]*National Research Center for Radiation Medicine, Kyiv, Ukraine*

[2]*Department of Physics, Oklahoma State University, Stillwater, Oklahoma, USA*

[3]*Department of Nuclear Engineering, Institute for Nuclear Security, University of Tennessee, Knoxville, USA*

Highlights Dosimetry of a gamma-irradiated phantom exposed in different geometries. Dose estimation using MC simulations and comparison with experimental measurements using external smartphones and internals TLDs. Calculations of conversion factor for dose from smartphones to dose to internal organs.

Key words Optically and thermally stimulated luminescence dosimetry, smartphones, LiF-100 TLDs, MCNP, Monte Carlo, human phantom, dose conversion factors.

Background and Objectives Modern smartphones have been proposed as emergency dosimeters for the general population in the event of large-scale, acute exposures due to malevolent acts or radiological accidents.[1,2)] Since such measurements determine the dose to the phone and not to the exposed person, it is important to assess how such measurements relate to the doses to internal body organs. Results of Monte Carlo simulations of doses under varying exposure conditions[3)] demonstrate strong dependence of conversion factors on phone positions. In this work, we compare experimental physical phantom measurements of organ doses (using TLDs), external dose measurements (using smartphones and Al_2O_3:C (Luxel) as reference dosimeters), and computational estimates of both phone and organ doses using MC calculations for a mathematical phantom.

Materials and Methods An Alderson torso phantom filled with LiF TLD-100 detectors in order to measure doses to critical organs was exposed to a ^{137}Cs gamma source in several standard geometries (front - PA, rear - AP and lateral - LAT), together with smartphones (Samsung S6) located on the side, rear and front of the phantom. Doses to the smartphones were assessed using OSL from surface mount resistors.[2)] The irradiations took place at the Oak Ridge National Laboratory, TN, USA. All reference, TLD and phone OSL doses were measured at OSU several days after irradiation. Monte Carlo simulations were made at NRCRM using MCNP-4B and an anthropomorphic ADAM phantom with a simplified phone model positioned according to above irradiation experiments.

Results and Discussion The OSL doses for phones determined with SMRs were in good coincidence with corresponding reference doses measured with Luxel OSL dosimeters. They were in the range 16-123 % compared with the corresponding nominal dose, while TL internal doses were in the range 13-101% depending on geometry of exposure and the location. Conversion factors from SMR doses to the corresponding internal doses were in the range 0.12-4.0, which reflects the large variety of combinations of exposure geometry, phone location and TLD location within the phantom.

Conversion factors were also calculated with Monte Carlo simulations for the same geometries of exposure and the same phone locations, using corresponding experimental values as benchmark data to optimize and adjust the parameters used in the calculations. Finally, the Monte Carlo method was used for calculation of the conversion factors for the main radiosensitive organs for different geometries of exposure.

Conclusion Experimental values of conversion factors from OSL doses for phones to internal doses inside a phantom can be used to optimize the Monte Carlo calculations of these factors. This approach may lead to reliable conversion factors for different internal organs and different geometries of exposure for possible use in the post-accident triage.

Acknowledgments This work was funded at OSU by a grant from the Oak Ridge Associated Universities and the State of Oklahoma, and at UT by a grant from the National Nuclear Security Administration (NNSA), U.S. Department of Energy (DOE). The views expressed are those of the authors and do not necessarily reflect those of the DOE or NNSA.

References

1) I.K. Bailiff, S. Sholom and S.W.S. McKeever, 2016. *Retrospective and emergency dosimetry in response to radiological incidents and nuclear-mass casualty events: A review*. Radiat. Meas. 94, 83-139.
2) C. Bassinet et al., 2014. *Retrospective radiation dosimetry using OSL of electronic components: Results of an inter-laboratory comparison*. Radiat. Meas. 71, 475-479.
3) J.S. Eakins and E. Kouroukla, 2015. *Luminescence-based retrospective dosimetry using Al_2O_3 from mobile phones: a simulation approach to determine the effects of position.* J. Radiol. Protect. 35, 343-381.

Challenges and opportunities in radiotherapy and radiobiology radiation measurements

Gabriel O. Sawakuchi[1]*
[1]*Department of Radiation Physics, The University of Texas MD Anderson Cancer Center, Houston, Texas, USA*

Highlights Solid-state detectors have favorable features with potential to develop the next generation of detectors for applications in complex radiation fields generated by new radiotherapy technologies.

Key words radiotherapy, radiobiology, solid-state detectors, absorbed dose, linear energy transfer

Background and Objectives Radiotherapy (RT) delivery technologies have dramatically evolved in the past decade. New techniques such as stereotactic body RT (SBRT), intensity modulated particle therapy (IMPT) using proton or C-ion beams and magnetic resonance image guided RT (MRgRT) enabled delivering high doses to the tumor with unprecedented accuracy in geographical tumor targeting. However, due to their small and complex radiation fields, these new techniques imposed unique challenges to radiation detectors. This talk will review the challenges and opportunities of RT dosimetry with emphasis on how solid-state detectors (SSDs) could have a positive impact on helping to answer basic questions of RT radiobiology.

Materials and Methods Ionization chambers are the gold standard for relative and absolute absorbed dose measurements in RT. However, inherent limitations of ionization chambers such as large volume and use of high voltages make them sub-optimal for some RT applications. Various SSDs are routinely used in RT clinics to complement ionization chambers. Radiochromic films and diodes in the form of detector array systems are widely used for quality assurance of patient plans and to test linac performance. Thermoluminescent dosimeters, optically stimulated luminescent dosimeters, radiophotoluminescent dosimeters, MOSFETs and diodes are widely used for monitoring surface or intracavitary absorbed doses in patients. Other SSDs that are commercially available for clinical applications in RT include diamond detectors and plastic scintillators, which are mainly used for relative dose measurements. To a lesser extent than the other mentioned SSDs, alanine and Fricke are used for absolute absorbed dose measurements in RT by primary standards dosimetry laboratories

and various forms of polymer gels are under intense development.

Advancements in RT delivery technologies allowed us to deliver highly conformal dose distributions to complicated 3D target volumes using strategies to purposely create heterogeneous dose distributions with sharp dose gradients (e.g., simultaneous integrated boost), all in a complex radiation environment with the presence of a strong magnetic field in the case of MRgRT, or a spectrum of ionization densities in the case of IMPT. Particularly, particle beams produce a spectrum of particles with a wide range of linear energy transfer (LET) values. Because LET is directly related to the biological response, in particle beams both the absorbed dose and LET are important radiation quantities that are directly related to cell kill and both should be measured.

Results and Discussion SSDs have many favorable features including but not limited to biocompatibility, small sizes, variety of shapes, variety of electron densities, capability of measuring quantities beyond absorbed dose such as LET and microdosimetric quantities, and potential to provide high spatial and temporal resolutions. These features could be used to develop the next generation of RT detectors for applications in new RT delivery technologies. Particularly, there are basic questions in particle therapy radiobiology that SSDs could help to answer. We have been using fluorescent nuclear track detectors to measure LET of proton beams and to investigate the types of DNA damage, the DNA repair pathways and the mechanisms of cell death induced by C-ion clinical beams, which create a complex radiation environment composed of multiple particles with a wide range of LET values.[1, 2]

Conclusion Further development of SSDs will help to improve radiation measurements in new RT modalities including absorbed dose measurements under the presence of strong magnetic fields, absorbed dose measurements in small radiation fields (< 2 cm × 2 cm), LET and absorbed dose measurements in particle therapy beams, LET measurements in radiation biology experiments and measurements of microdosimetric quantities.

References

1 C.H. McFadden, T. Hallacy, D.B. Flint, D.A. Granville, A. Asaithamby, N. Sahoo, G.O. Sawakuchi, "Time-Lapse Monitoring of DNA Damage Colocalized With Particle Tracks in Single Living Cells," Int. J. Radiat. Oncol. Biol. Phys. **96**, 221-227 (2016).

2 G.O. Sawakuchi, F.A. Ferreira, C.H. McFadden, T. Hallacy, D.A. Granville, N. Sahoo, M.S. Akselrod, "Nanoscale measurements of proton tracks using fluorescent nuclear track detectors," Med. Phys. **43**, 2485-2490 (2016).

Recent development of solid state microdosimetry and its applications in proton therapy

Linh T. Tran[1], Benjamin James[1], David Bolst[1], Dale Prokopovich[1,2], Susanna Guatelli[1], Dirk Wagenaar[3], Stefan Both[3], Benjamin Clasie[4], Marco Povoli[5], Angela Kok[5] and Anatoly Rosenfeld[1*]

[1]*Centre for Medical Physics, University of Wollongong, NSW, Australia*
[2]*Australia's Nuclear Science and Technology Organisation, Lucas Heights, NSW, Australia*
[3]*University Medical Centre Groningen, University of Groningen, Netherlands*
[4] *Department of Radiation Oncology, MGH, Boston, MA, USA*
[5]*SINTEF, Oslo, Norway*

Highlights: A proton pencil-beam scanning (PBS) and passive double scattering (DS) systems at the proton therapy centres at Massachusetts General Hospital (MGH), USA and University Medical Center Groningen (UMCG), Netherlands have been characterised using 3D silicon microdosimeter. Recently measured dose mean lineal energy values $\overline{y_D}$ at UMCG were compared to LET_d values calculated for delivered plan by Raystation (v5.99) treatment planning system (TPS) in a head and neck anthropomorphic phantom and the relative biological effectiveness (RBE) of the beam are presented.

Key words: Proton beam scanning, LET_d, dose mean lineal energy, RBE

Background and Objectives: Radiotherapy with proton and ion beams is advantageous compared to X-ray radiotherapy due to the highly localised energy deposition, allowing for conformal dose distributions. Both proton and ion beams have a finite range in matter which allows for increased sparing of healthy tissue. Unlike ion beams, protons do not produce projectile fragments beyond the Bragg peak (BP). Nevertheless, inelastic reactions with tissue create a small number of secondary protons, neutrons, gamma rays and heavier recoil nuclei. The distribution of these secondary products changes with depth. The secondary proton production mainly contributes to the halo around the primary proton beam while the secondary neutrons cause an enhanced dose equivalent downstream of the SOBP irradiating normal tissue [1]. The objective of this work was to provide comprehensive microdosimetric quality assurance (QA), in comparison with the TPS, of the MGH and UMCG facility beamline using the 3D SOI microdosimeter developed at CMRP.

Materials and Methods: The silicon microdosimeter provides extremely high spatial resolution and can be used for in-field and out-of-field measurements in both passive scattering and PBS deliveries. The response of the microdosimeter was studied in passive and scanning proton beam at MGH and UMCG, respectively. Fig 1 shows the experimental setup in head & neck CIRS -731 HN phantom at UMCG.

Results and Discussion: Fig 2a shows the dose mean lineal energy, $\overline{y_D}$ measured using the SOI microdosimeter irradiated by the 131.08 MeV pencil proton beam as a function of depth in water. The $\overline{y_D}$ value was around 2 keV/µm in the plateau region, then approximately 3 to 5 keV/µm in the proximal part of the BP, and increasing dramatically to 9 to 10 keV/µm at the end of the BP [2]. Fig 2b shows a comparison of $\overline{y_D}$ obtained with the SOI microdosimeter for brain case in CIRS head phantom to LET_d calculated by Raystation. The microdosimeter was placed 3 cm off the central axis. Good agreement was seen between the measured $\overline{y_D}$ and calculated LET_d for brain, nasal and neck case in the head phantom. RBE values will be presented in the full paper.

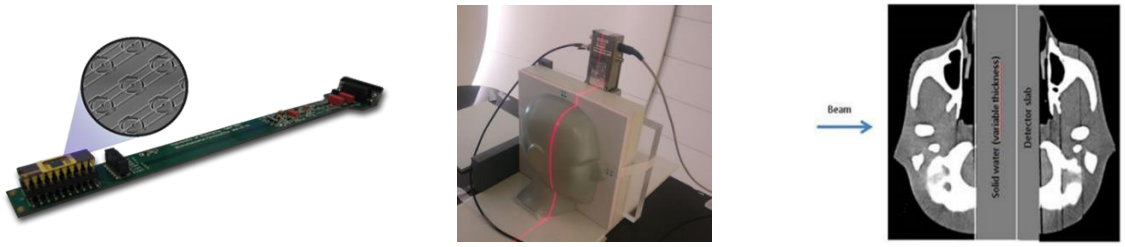

a) b) c)

Figure 1: a) MicroPlus probe with SOI microdosimeter b) Set up of head & neck phantom and c) CT scan of head & neck phantom with inserted PMMA slab and sheath for MicroPlus probe at the UMCG.

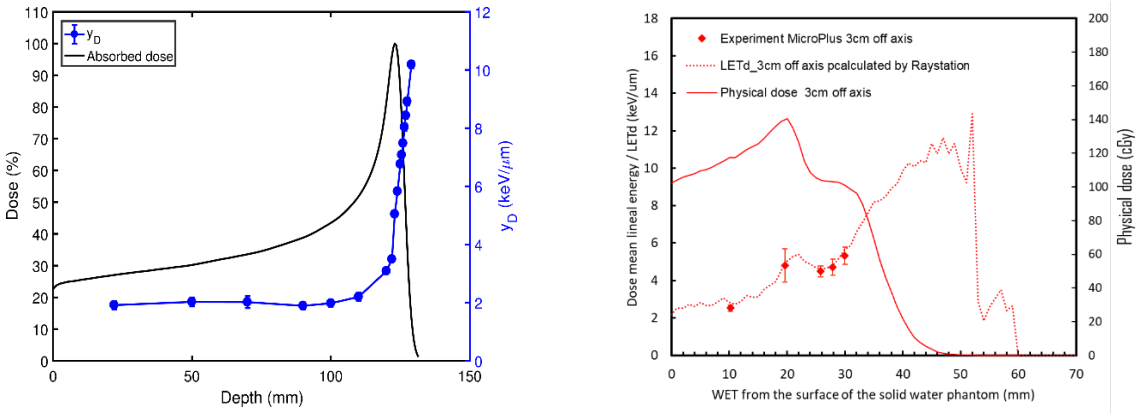

a) b)

Figure 2: a) Dose-mean lineal energy ($\overline{y_D}$) obtained using the SOI microdosimeter as a function of depth in water for a proton PBS spot at MGH facility, b) Comparison of $\overline{y_D}$ obtained with the SOI microdosimeter for brain case in CIRS head phantom to LET_d calculated by Raystation.

Conclusion: This work presented an application of MicroPlus probe for fast QA of $\overline{y_D}$ in passive and scanning proton beams with high spatial resolution. It will be demonstrated that derived RBE_D exceed generaly accepted 1.1 and reached up to 1.7 in a distal part of PBS spot. The accuracy of the TPS calculated LET_d distributions vary within the beam, however its clinical relevance remains to be further studied in treatment site and irradiation geometry specific conditions before clinical adoption.

References

[1] Wayne D Newhauser and Rui Zhang "The physics of proton therapy", Phys. Med. Biol. 60 (2015) R155–R209

[2] Linh T. Tran, *et. al*. (2017), Characterisation of proton pencil-beam scanning using a high spatial resolution solid state microdosimeter, Med Phys. 2017 Nov; 44(11):6085-6095

3-D Clinical Small Field Dosimetry

Cheng-Shie Wuu[1]*, Yi-Fang Wang[1], Olga Dona[1], John Adamovics[2]
[1]*Department of Radiation Oncology, Columbia University, NY, NY, USA*
[2]*Department of Chemistry, Rider University, Lawrenceville, NJ, USA*

Highlights There has been a rapid increase in the use of small fields in modern radiotherapy techniques such as stereotactic radiosurgery (SRS) and stereotactic radiotherapy (SBRT). The dosimetry of megavoltage small fields can be challenging due to lateral charged particle disequilibrium, detector volume averaging effect, and high dose gradients. 3-D radiochromic plastic dosimeter, PRESAGE, can be used to acquire small-field beam data as well as patient-specific IMRT/VMAT QA precisely and accurately.

Key words 3-D dosimetry, small field dosimetry, PRESAGE, optical CT scanner

Background and Objectives Modern radiotherapy such as stereotactic radiosurgery (SRS) and stereotactic body radiotherapy (SBRT) may use relatively small fields (5 mm to 3 cm) to achieve desired dose distribution. An accurate dose verification of small-field treatment delivery is therefore crucial. The measurements of small fields beam data, including output factors, percentage depth dose (PDD), and lateral beam profile, are required for the commissioning of treatment planning systems. However, the dosimetric characterization of small fields is difficult due to the potentials for lateral charged-particle disequilibrium, partial source occlusion with the consequence of reduced output, and partial volume averaging effects. Currently IMRT and VMAT patient-specific QAs are performed with ion chamber or diode arrays because of their ease of use and reliability. The main disadvantages of a 2-D detector arrays are that they do not offer full 3-D dose information and the detector spacing is too large (7 mm) for small field dosimetry. The objective of this study is to demonstrate that an accurate and precise measurement of small-field 3-D dose distribution can be obtained using radiochromic PRESAGE dosimeters in conjunction with a single-beam optical CT scanner.

Materials and Methods In this study, radiochromic plastic dosimeters, PRESAGE®, were used for clinical small-field dose measurements. Six small cylindrical phantoms (6 cm diameter × 7 cm length) were irradiated with 6 MV MLC-delimited square fields: 6 x 6 mm^2, 8 x 8 mm^2, 1 x 1 cm^2, 1.2 x 1.2 cm^2, 1.6 x 1.6 cm^2, and 2 x 2 cm^2. Five cylindrical phantoms (10 cm diameter x 11 cm length) were employed for clinical small-field IMRT/VMAT dose verification. The readouts of irradiated PRESAGE dosimeters were performed with a single laser beam

optical CT scanner. Five IMRT or VMAT plans, with field sizes ranging 1 – 4 cm, were selected for dose verification. For comparative dosimetry radiochromic EBT3 films, positioned in a 30 x 30 x 10 cm^3 solid water phantom, were used for PDD, lateral beam profile, and 2-D dose distribution measurements. EBT3 films were positioned at 1.5 cm depth for MLC-delimited small square field measurements, and at 5 cm depth for all IMRT/VMAT dose measurements.

Results and Discussion Both EBT3 films and PRESAGE dosimeters are used in this study for dose verification of small-field dosimetry calculated from Eclipse Acura XB. The lateral beam profiles of 6 x 6 mm^2 to 2x2 cm^2 MLC-delimited field sizes, shows an excellent agreement in the full width of half maximum (FWHM) and in the penumbra region between EBT3 and PRESAGE, and a slightly worse agreement in the penumbra between the PRESAGE and the Acura XB calculation. This difference in the penumbra region, between measured results and calculation, may be due to inaccurate small-field modelling of the planning system, but also possibly due to geometric uncertainty of MLC positioning. For small-field IMRT/VMAT plans radiochromic film provides a good 2-D dosimetric verification as it has probably the highest intrinsic resolution of detectors, which are relatively water equivalent and no energy dependence for MV beams, and has been recommended for small field dosimetry (1). In one VMAT SRS case, the PTV has an equivalent spherical dimension of 1 cm and a volume of 0.5 cc. EBT3 film was used for patient specific pre-treatment QA, and the gamma index pass rate was 97.4% with 2% DD (dose difference) and 1 mm DTA (distance to agreement) gamma criteria. PRESAGE measurement resulted in a 98% pass rate at the plane along the isocenter and a 97.1% pass rate at the plane 8mm from the isocenter, providing additional information on dose verification.

Conclusion 3-D radiochromic plastic dosimeter, PRESAGE, can be used to acquire small-field megavoltage beam dosimetric parameters precisely and accurately. Both EBT3 film and PRESAGE dosimeter can be used for dose verification of small-field IMRT/VMAT in modern radiotherapy techniques. However, our results indicate that PRESAGE is a suitable 3-D dosimeter for special IMRT QA when additional dosimetry information is required for clinical decision,

References

1) Wilcox EE and Daskalov GM 2007 Med. Phys. **34** 1967-74

4 MV X-ray detection using a novel condenser dosimeter with disposable silicon-diode substrates in radiation therapy

Satoshi Yamaguchi[1*], Eiichi Sato[2], Hirobumi Oikawa[1], Hisao Kakuhara[1], Koyo Kikuchi[1], Hisanori Ariga[1]

[1]*Department of Radiology, Iwate Medical University, Iwate, Japan*

[2]*Department of Physics, Iwate Medical University, Iwate, Japan*

Highlights We developed an integral condenser dosimeter with a surface-mounted silicon X-ray diode, Patient-skin doses using 4 MV radiotherapy can be measured, Integral doses measured corresponded well to those of ionization chamber with small SDs.

Key words Si X-ray diode, condenser dosimeter, disposable USB-A substrate, skin-insulated substrate, radiation therapy

Background and Objectives To measure patient-skin doses in radiation therapy, we developed a novel integral condenser dosimeter with a disposable USB-A mini-substrate consisting of a condenser and a silicon X-ray diode (Si-XD)[1)]. The Si-XD is a high-sensitivity photodiode selected for detecting X-rays. We measured the integral doses of 4 MV X-rays from a commercially available medical linear accelerator using the substrate.

Materials and Methods The condenser dosimeter consists of a USB-A mini-substrate and a microcomputer dock (Figure 1). The substrate is a surface-mounting type to insulate skins from the circuit and consists of a 0.22-μF condenser, a Si-XD (S1087-01, Hamamatsu) with photosensitive dimensions of 1.3 × 1.3 mm^2, and a 10-kΩ resistor. The Si-XD is shaded using a 25-μm-thick aluminum tape, and penetrating X-ray photons through the tape are detected using the Si-XD. The condenser in the substrate is charged to 3.30 V using the dock before X-ray exposing. The charging voltage is reduced by photocurrents flowing through the Si-XD during the X-ray exposing. After the exposing, the substrate is inserted into the dock again, and we measured the voltages using an analog to digital converter in the dock. The dock is connected to a personal computer (PC), and the condenser charging and the measuring voltages are controlled by the PC. A Farmer-type ionization chamber (N30013, PTW) was used to convert the discharging voltages into absorbed dose to water (Gy). The integral dose measurements was performed using a medical linear accelerator (Clinac iX, Varian Medical Systems) and 4 MV X-ray beams with outputs ranging from 25 to 250 MU, the dose rates was 250 MU/min, and the irradiation-field sizes were 10 × 10 cm^2. To measure the X-ray dose, the Si-XD surface of the 5-mm-thick substrate was set at a depth of 10 cm in a solid water

phantom slab (WD, Kyoto Kagaku) with a physical density of 1.02 g/cm^3. The source to surface distance (SSD) in the setup was 90 cm.

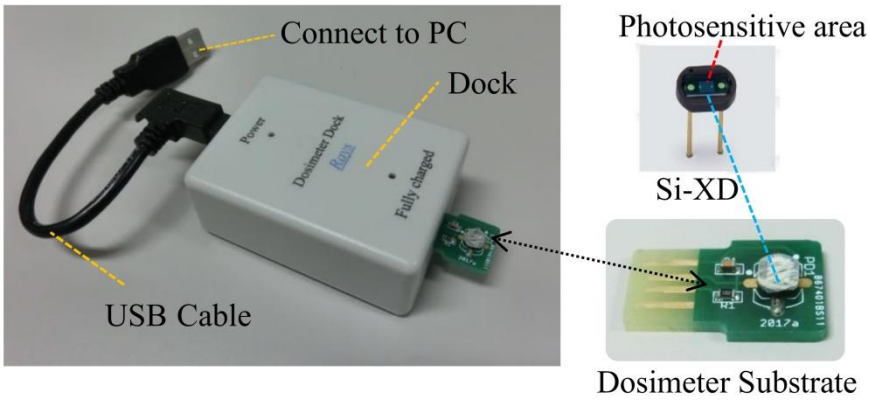

Figure 1. Condenser dosimeter consisting of a microcomputer dock and a substrate

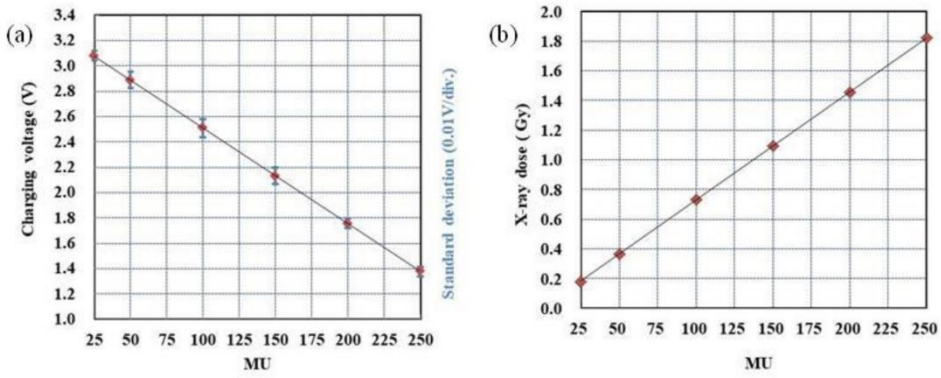

Figure 2. Measurement of the X-ray dose using the condenser dosimeter. (a) Condenser charging voltages with changes in MU and (b) MU dependence of the integral doses determined by one-point calibration.

Results and Discussion The measured X-ray doses were proportional to decreases in the charging voltage (Figure 2), and the calibrated doses corresponded well to those obtained using the ionization chamber.

Conclusion We developed a low-priced condenser dosimeter with Si-XDs. The results suggest that the dosimeter is useful for measuring patient-skin doses during the course of radiation therapy.

References

1) Satoshi Y, Eiichi S.: Product development of a condenser dosimeter using a skin-insulated USB-A-substrate with a silicon X-ray diode. Radiol. Phys. Technol. doi:https://doi.org/10.1007/s12194-018-00493-4.

LET AND RBE OF THERAPEUTIC PROTON BEAMS MONITORED WITH MICRODOSEMETERS

P. Colautti[1], V. Conte[1], A. Selva[1], A. Bianchi[1,3], G.Cirrone[2], G.Petringa[2], S.Agosteo[4], D.Mazzucconi[4], D.Bortot[4], A.Pola[4], L.Cazzola[4].

1. LNL-INFN, Legnaro, Italy. 2. LNS-INFN, Catania, Italy. 3. SCK•CEN, Mol, Belgium. 4. Politecnico, Milano, Italy

Highlights. A mini-TEPC without gas flow measures $\bar{y}_D$ and μRBE of a therapeutic proton beam. The $\bar{y}_D$ values are equal to $\overline{LET}_D$ calculated values. The μRBE values are almost the same as the RBE values. The detector response does not change over time.

Key words. Microdosimetry, mini-TEPC, LET, RBE, therapeutic proton beam.

Background and Objectives. The RBE of therapeutic proton beams increases significantly towards the distal edge of the SOBP, despite a constant RBE value of 1.1 is used in clinical situations. An accurate monitoring of the RBE change with depth could significantly increase the therapeutic gain. The RBE values are generally expressed as a function of the linear energy transfer (LET_∞ or simply LET) of the mono-energetic ion beam. The complex therapeutic radiation field is characterized by the averaged dose-mean LET value ($\overline{LET}_D$) of the total radiation field. This work presents the microdosimetric characterization of the CATANA 62 MeV clinical proton beam performed with TEPCs and silicon microdosimeters. The capability of microdosimetric quantities to model both $\overline{LET}_D$ and RBE is discussed.
The study develops in the framework of the research projects *Neptune* and *Mirto*.

Materials and Methods. A mini-TEPC has been used, which is a modified version of the one that had measured at the therapeutic Centre of Nice [1] and works without gas-flow. The modification simply aims to improve the pumping out of residual gases, hence the washing efficiency. After a careful degassing, detector was filled with propane at 454 mbar. At such a pressure, the simulated site size is 1 μm. The $\overline{LET}_D$ of the total radiation field (primary and secondary ions) has been calculated with a new code based on Geant4 [2]. The RBE values have been taken from the literature [3].

Results and Discussion. Microdosimetric measurements have been performed at the therapeutic Centre CATANA (62 MeV of protons) in two shift two months apart, without any gas refilling in between. Data collected in the two shifts do not show any significant difference. Figure 1 shows the comparison of the dose-mean lineal energy $\bar{y}_D$ values with the

$\overline{LET}_D$ values at different depths in a water phantom (left side of the figure). The microdosimetric-calculated RBE values (μRBE, 5% of uncertainty) and the radiobiological RBE values (10% of uncertainty) are plotted in the right side of the figure. The $\bar{y}_D/\overline{LET}_D$ mean ratio is 0.89±0.04 in the proximal edge, 1.04±0.05 in the SOBP and 1.1±0.2 in the distal edge. The μRBE/RBE mean ratio is 0.95±0.04.

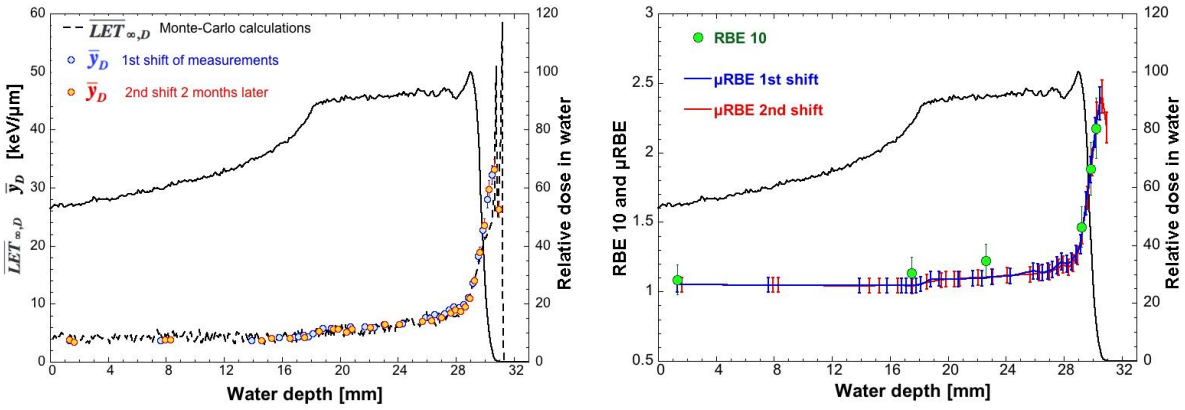

Figure 1. Left side: $\overline{LET}_D$ (dashed line), $\bar{y}_D$ (blue and red circles) and the relative absorbed dose (line) at different depths in a water phantom. Right side: RBE10 (green circles), μRBE (blue and red bars) and the relative absorbed dose (line) at different depths in a water phantom.

Conclusion. The $\bar{y}_D$ values, measured with a mini-TEPC of 0.9mm internal diameter working without gas-flow, are consistent with a new algorithm for $\overline{LET}_D$ calculation with GEANT4 for the 62 MeV-proton therapeutic beam of CATANA. Moreover, the mini-TEPC models very well the therapeutic beam RBE-variation with the depth. Comparison between mini-TEPC and solid-state-detector recent results is also presented.

References

1) De Nardo L. et al. Microdosimetric assessment of Nice therapeutic proton beam biological quality. *Physica Medica* 2004; XX: 71-77.

2) Cirrone G.A.P. et al. Clinical and research activities at the CATANA facility of INFN-LNS: from the conventional hadrontherapy to the laser-driven approach. *Frontiers in Oncology 2017, doi: 10.3389/fonc.2017.00223.*

3) Chaudhary P. et al. Relative biological effectiveness variation along monoenergetic and modulated Bragg peaks of a 62 MeV therapeutic proton beam: a preclinical assessment. *IJROBP 90, 27-35, 2014.*

A review on the OSL of BeO in light of recent discoveries: the missing piece of the puzzle?

Eduardo G. Yukihara*
Department of Radiation Safety and Security, Paul Scherrer Institute, Villigen PSI, Switzerland, eduardo.yukihara@psi.ch

Highlights This presentation reviews the data on the optically stimulated luminescence (OSL) of BeO in light of the recent discovery of strong thermally transferred OSL (TT-OSL) in this material. We discuss how the existing contradictions may be solved by the new information available and present a model for BeO that takes into account these findings.

Keywords optically stimulated luminescence, thermally transferred optically stimulated luminescence, dosimetry, dose re-estimation

Background and Objectives The OSL of BeO, a material used commercially in OSL dosimetry, has long puzzled researchers. On the one hand, optical stimulation seems to affect mostly the thermoluminescence (TL) peaks at ~75 °C (peak 1) and ~200 °C (peak 2), leaving the TL peak at ~340 °C (peak 3) almost unchanged, which would suggest peaks 1 and 2 as the main sources of trapped charges responsible for the OSL signal. On the other hand, the OSL signal seems to be stable up to temperatures >250 °C, which contradicts the first assumption. The recent discovery of thermally transferred OSL (TT-OSL) in BeO[1)] may be the missing piece to complete this puzzle. In this presentation we discuss the discovery of TT-OSL in BeO and present its main properties. We also show how this phenomenon can help explain the OSL mechanism in BeO.

Materials and Methods TL, OSL and TT-OSL measurements of 4.5 mm × 4.5 mm × 0.5 mm BeO chips (Thermalox 995, Materion Corporation) were carried out using a lexsyg smart extended reader (Freiberg Instruments GmbH, Freiberg, Germany). The OSL measurements used blue light emitting diodes (LED) for stimulation (centered at 458 nm, 100 mW/cm^2) and Hoya U-340 filters (Hoya Corporation) and a BP 365/50 EX filter (Delta Optical Thin Films A/S, Hørsholm, Denmark) in front of a UV-VIS photomultiplier tube (PMT, model 9235QB, ET Enterprises Ltd., Uxbridge, UK) for detection. Irradiations were performed using a built-in ^{90}Sr/^{90}Y source (1.53 GBq activity on 6 February 2018, Eckert & Ziegler, Germany).

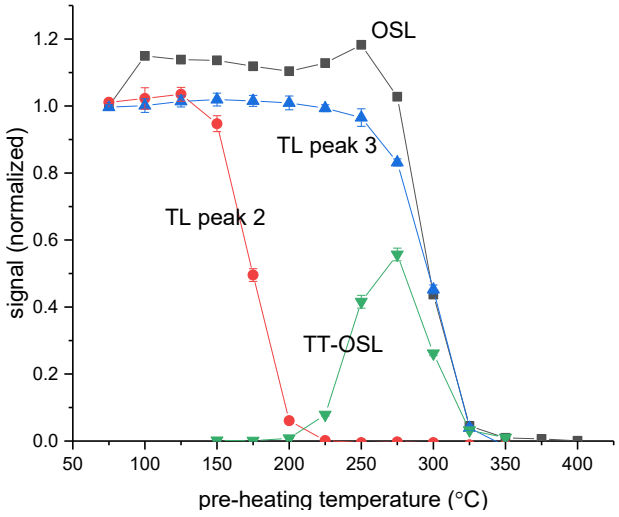

Fig. 1 Stability of the OSL signal, TL peak 2 and TL peak 3 of irradiated BeO with pre-heating temperature, as well as induction of TT-OSL signal with the pre-heating for a BeO sample that was previously irradiated and bleached.

Results and Discussion The results demonstrate that, after a first OSL readout, TT-OSL can be induced in BeO by heating the chips to a temperature at around ~200-350 °C, with a maximum for heating to ~275 °C (at 5 °C/s) (Figure 1). The induced signal has an intensity >50% of the original OSL signal and can be used to re-estimate the dose even after the original OSL signal has been completely bleached. The TT-OSL signal is proportional to the dose of radiation and the TT-OSL decay under optical stimulation is identical to the decay of the OSL signal. Investigations on the dose response, thermal stability and kinetics of the process support the assumption that the TT-OSL is due to a thermally stimulated transfer of charges from optically inactive trapping centers to optically active trapping centers, both with thermal stability coinciding with TL peak 3.

Conclusion The discovery of the TT-OSL in BeO provided a missing piece of the puzzle to understand the OSL mechanism in this material. The data support the assumption that the main source of charges for the OSL signal have similar stability as the TL peak 3 (~340 °C), but the TL is not affected by light because of the presence of an optically inactive trapping centers in the same temperature region. Some of the charges from the optically inactive trapping center can be transferred to the optically active trapping center, leading to the recuperation of the OSL, i.e., to TT-OSL.

References

1) E. G. Yukihara, Observation of strong thermally transferred optically stimulated luminescence (TT-OSL) in BeO. Radiat. Meas. 121, 103-108 (2019).

Designing phosphors for dosimetry with tailored properties: an investigation using doped MgO

L.C. Oliveira[1]*, O. Baffa[1]

[1]*Departamento de Física, FFCLRP-Universidade de São Paulo, 14040-901 Ribeirão Preto-SP, Brazil*

Highlights TL and OSL signals of MgO doped with various lanthanides were investigated. A recombination mechanism for the TL and OSL signal in MgO was proposed.

Key words radiation, optically stimulated luminescence, thermoluminescence, lanthanides, dosimetry

Background and Objectives Our ability to design new phosphors for dosimetry and imaging of ionizing radiation with tailored properties by intentionally introducing defects remains limited. Designing and developing such materials require a clear understanding of the role of defects in the TL process. A better understanding of the role of defects on the TL mechanism is essential for a more effective development of TL materials that meets specific applications, for example, for thermometry of explosions[1,2]. A deeper understanding on the mechanisms of trapping and releasing of charge in luminescent materials can also be beneficial for the development of new OSL materials for dosimetry application.

The empirical model proposed by Dorenbos[3] can be used as a guide to develop new TL and OSL materials. The model allows ones to predict the energy level of a divalent Ln^{2+} within the band gap, provided the energy of charge transfer of the valence band to one Ln^{3+} and the band gap of the material are known.

The objective of the current investigation was to: (i) identify potential new OSL materials for personal and medical dosimetry applications, including that for 2D dose mapping, and (ii) to provide some insights into the mechanisms involved in the TL and OSL of MgO obtained by doping it with several lanthanide combinations and those with lithium.

Materials and Methods We systematically investigated undoped and lanthanide (Ln) doped MgO with diverse combinations: MgO:Ce, Ln; MgO:Tb, Ln; with Ln=Eu, Yb, Tm, Sm, Dy , and also these combinations with Li 3% mol. Samples were synthesized by Solution Combustion Synthesis method. We characterize TL and OSL signals using a Risø TL/OSL-DA-15 reader. Radioluminescence (RL) and TL emission spectra were performed in a custom-built reader consisting of an X-ray source and a CCD spectrophotometer. TL spectrum was obtained using the same RL system, but now applying a heating ramp to the

irradiated sample.

Results and Discussion TL curves, measured at 5 K/s, are summarized in Figure 1. Our investigation suggests that Ce^{3+} and Tb^{3+} are recombination centers. They show their characteristic spectrum under thermal or optical stimulation. Inversely, Sm^{3+}, Tm^{3+} and Yb^{3+} are probably electrons traps. Li enhanced the RL, TL and OSL signal in several folders, in MgO samples that contain Ce^{3+} as luminescent centers.

a) b)

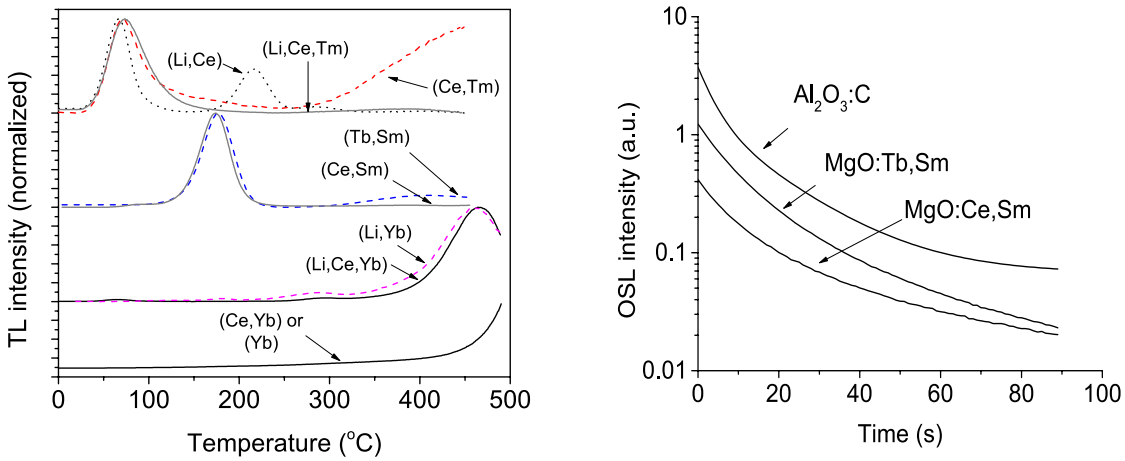

Figure 1. In a) the representative TL curves of doped MgO, measured at a heating rate of 5 °C s^{-1}, normalized to the maximum intensity of each curve. In b) OSL signal of MgO:Tb,Sm and MgO:Ce,Sm. OSL signal from commercial Al_2O_3:C was included for comparison.

Conclusion Using a systematic approach, we successfully identified/developed MgO-based OSL materials with high sensitivity to ionizing irradiation equivalent to commercially available detectors, but with distinct luminescent properties.

Diverse TL were obtained by doping MgO with different combinations of Ln. The calculated activation energies of TL showed the characteristic trend predict by the Dorenbo's model.

References

1) E. Yukihara, A. Coleman, B. Doull, J. Lumin., 146 (2014) 515-526.

2) M.E. Manfred, N.T. Gabriel, E.G. Yukihara, J.J. Talghader, Radiat. Prot. Dosim., 139 (2010) 560-564.

3) P. Dorenbos, J. Phys. Condens. Matter, 15 (2003) 8417.

Phosphor Development for radiation dosimetry

Bhushan Dhabekar, N.S. Rawat and D.K. Koul
Radiological Physics and Advisory Division, Bhabha Atomic Research Centre, Mumbai, India

Highlights The paper discusses dosimetric characterization of various phosphors developed at Bhabha Atomic Research centre (BARC).

Key words Radiation dosimetry, $LiMgPO_4$:Tb,B (LMP), $LiMgPO_4$:B (LMP-N), $LiCaAlF_6$:Eu,Y (LCAF), Al_2O_3:C

Background and Objectives During the last two decades OSL has emerged as one of the most widely studied techniques in the field of radiation dosimetry, like personnel and environmental monitoring, space dosimetry, real-time in vivo dosimetry for radiotherapy, mammography and CT dosimetry. The inherent advantages of OSL technique has resulted in paradigm shift from TL to OSL based dosimetry. It is estimated that more than one-third of the radiation workers worldwide are monitored with OSL dosimeters (~1.7 million users of OSL system out of estimated more than 5 million users of personal dosimetry badges) [1]. Motivated by this BARC has also undertaken OSL based dosimetric programme for various radiological applications. Presently, the most widely used phosphor for different OSL based application is carbon doped alumina. Unlike TL, development of commercial grade OSL phosphor has been a grey area. However, several attempts have been made to develop phosphors other than Al_2O_3:C for OSL based dosimetric applications.

Materials and Methods $LiMgPO_4$:Tb,B (LMP) and $LiMgPO_4$:B phosphor (LMP-N) is synthesized by solid state reaction between LiOH, $Mg(NO_3)_2.6H_2O$ and $NH_4H_2PO_4$ in air along with appropriate dopants. While $LiCaAlF_6$:Eu,Y phosphor (LCAF) is prepared by melt technique. For OSL measurements, Polytetrafluoroethylene (PTFE), based discs (10 mm dia, 0.6 mm thick with phosphor to PTFE ratio 1:3) were used. All OSL measurements were carried out using an automatic Riso TL/OSL-DA-15 reader system.

Results and Discussion

LMP: It was developed and characterized by Dhabekar et al. [2]. The OSL sensitivity of this phosphor is about 1.8 times that of Al_2O_3:C. The linearity of over the range of nine orders of magnitude of dose range is unique to this phosphor. The phosphor also possesses other excellent dosimetric properties like reproducibility, reusability, detection threshold of 0.5 μGy, easy synthesis technique as compared to Al_2O_3:C etc. [3]. The only drawback of this phosphor is

long term fading, which limits its use in dosimetry, particularly when the time of exposure to radiation is not known. The studies carried out by Menon et al. (2018) has shown that in LMP, the second TL peak around 160 °C is responsible for long term fading of OSL signal and it is basically thermal in nature. By modifying the nature of dopants, it has been successfully demonstrated that the nature of TL glow curve can be altered so that the intensity of the second peak and hence fading of OSL signal can be reduced. The new phosphor LMP-N retains all virtuous OSL characteristics of LMP, limiting the degree of fading. By using appropriate protocols for fading correction one can consider this phosphor for various dosimetric applications for a wide range of doses.

LCAF: Rahangdale et al. (2015) were the first to report this phosphor with OSL sensitivity of about 8 times than that of commercial Al_2O_3:C, with minimum detectable dose of 4.7 µGy. Dhabekar et al. (2017) could enhance the OSL sensitivity of this phosphor to more than 20 times that of commercial Al_2O_3:C, with minimum detectable dose of 0.5µGy. The phosphor has been found responsive to wide dose range, few tens of µGy to 100 Gy. The developed phosphor has also been characterized for the kinetics responsible for its luminescence properties, neutron dosimetry and environmental dosimetry.

Conclusion The indigenously developed LMP, LMP-N and LCAF possess excellent dosimetric properties. PTFE based dosimetry grade OSL discs have been developed for various dosimetric applications. In light of the luminescence properties of these phosphors they seem to be good candidates for OSL based applications.

References

1) A. S. Pradhan, J.I. Lee, J.L. Kim, J. Med Phys. 41 (2016) 81
2) Bhushan Dhabekar, S.N. Menon, E. Alagu Raja, A.K. Bakshi, A.K. Singh, M.P. Chougaonkar, Y.S. Mayya, Nucl. Instrum. Methods Phys. Res. B 269 (2011) 1844
3) N.S. Rawat, Bhushan Dhabekar, K.P. Muthe, D.K. Koul and D. Datta, Nuclear Instruments and Methods in Physics Research B 397 (2017) 27
4) S.N. Menon, B.S. Dhabekar, Sonal Kadam and D.K. Koul, Nuclear Inst. and Methods in Physics Research B 436 (2018) 45
5) S.R. Rahangdale, U.A. Palikundwar, S.P. Wankhede, B. Dhabekar, S. Kadam, S.V. Moharil, J. Lumin.167, (2015) 80
6) Bhushan Dhabekar, N.S. Rawat, N. Gaikwad, Sonal Kadam and D.K. Koul, Radiation Measurements 107 (2017) 7

Characterization of electron traps in a natural aluminosilicate (feldspar) by low temperature photoluminescence excitation-emission spectroscopy

Raju Kumar*, Myung Ho Kook, Mayank Jain

Center for Nuclear Technologies, Technical University of Denmark, DTU Risø Campus, Roskilde, Denmark

**Corresponding author: Raju Kumar (mail id: rajcelos.isp65@gmail.com)*

Highlights New approach to obtain optical trap depth and excited states of the principal trap in feldspar. UV resonance in the excitation spectra indicates the existence of a deep electron trap.

Keywords Luminescence dosimetry, infrared photoluminescence, wide bandgap materials, feldspar, low temperature optical spectroscopy.

Background and Objectives Feldspar is the most widespread mineral in the Earth's crust and is commonly used for dating. The main dosimetric trap (principal trap) can be measured using visible or IR stimulated luminescence (IRSL or OSL). Recently, Infrared photoluminescence (IRPL) method has been developed to probe the principal trap in feldspar[1,2]. Unlike OSL which involves electron-hole recombination, IRPL is emitted due to radiative relaxation of the excited state of the principal trap without involving any recombination center. OSL is not ideal for characterizing trap properties in feldspar such as optical trap depth since the electron can diffuse through the band tail states. Furthermore, by its very nature OSL does not allow measurement of excited energy levels, number density and distribution of the electron traps. Since IRPL is the emission of light due to internal transitions within the electron trap (i.e., electrons never leave the trap) it overcomes the challenges faced by OSL. IRPL also provides improved signal-to-noise ratio compared to OSL because of the possibility for repeated excitation of the same trapped electron, thereby making it ideal for high-resolution spectroscopic studies. The objective of this study is to:

1) Determine the electron trapping sites in feldspar.
2) Quantify the trap depth(s).
3) Revisit the phenomenological model (both kinetics and charge transport) in the light of new IRPL measurements.

Materials and Methods Three different Potassium feldspar ($KAlSi_3O_8$) mineral samples were used in this study. Excitation and emission spectra were recorded using COLUR (Risø Station for Cryogenic Luminescence Research[3]). An 830nm (1.49 eV) laser was used to excite the samples, and two IRPL emissions were recorded with a CCD detector using 850 nm LP, and 925 nm LP filters at 7 K.

Results and Discussion All three samples show two IRPL emission bands at ~1.30 eV (955 nm) and ~1.41 eV (880 nm) with different relative intensity across samples. IRPL excitation spectra at 7 K for the 1.30 eV emission consists of three major resonant peaks at 1.45 ± 0.02 eV, 2.05 ± 0.03 eV, and 3.5 ± 0.2 eV (Figure 1). On the other hand, excitation spectra for the 1.41 eV emission at 7 K consists of two resonant peaks at 2.3 ± 0.2 eV, and 3.5 ± 0.2 eV. All the peaks grow in intensity with X-ray dose. Resonant excitation close to 2.0 eV (~2.05 eV for 1.30 eV and ~2.3 eV for 1.41 eV emission) represents transition into the conduction band, thus clearly defining the optical trap depth in K-feldspar for the first time. There also exists an intense UV resonance at around 3.5 eV; this likely represents photo-transfer from a deep trap or center into the principal trap.

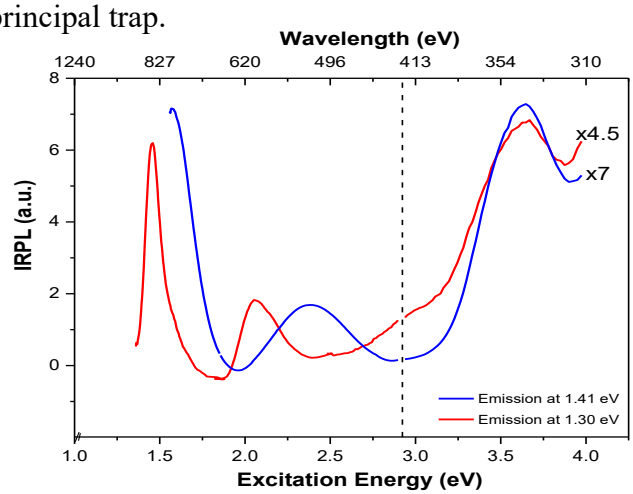

Figure 1: Excitation spectra at 7 K for the IRPL emissions at 1.41 eV and 1.30 eV, measured in a K-feldspar (R48). The UV excitation bands have been scaled w.r.t. the intensities of the Vis-NIR excitation bands (plotted to the left of the dashed line).

Conclusion IRPL has given a clear picture of trapping states in feldspar for the first time. We observe two dose-dependent NIR resonances (~1.30 eV (955 nm) and ~1.41 eV (880 nm)) in the emission spectra of K-feldspar. The excitation spectra corresponding to these suggest that the principal trap occurs at two different sites experiencing slightly different crystal fields. The trap responsible for the 1.41 eV emission has higher optical trap depth than the trap giving rise to the 1.30 eV emission. There occurs a charge transfer into the principal trap from a deep unknown trap; this could be useful for regenerating the trap population.

References

1. Prasad, A. K., Poolton, N. R., Kook, M., & Jain, M. (2017). Optical dating in a new light: A direct, non-destructive probe of trapped electrons. *Scientific reports*, *7*(1), 12097.

2. Kumar, R., Kook, M., Murray, A. S., & Jain, M. (2018). Towards direct measurement of electrons in metastable states in K-feldspar: Do infrared-photoluminescence and radioluminescence probe the same trap?. *Radiation Measurements*.Volume 120,2018, Pages 7-13, ISSN 1350-4487.

3. Prasad, A.K., Lapp, T., Kook, M., Jain, M., 2016. Probing luminescence centers in Na rich feldspar. Radiat. Meas. 90, 292–297.

Perspective of silicate materials for dosimetry applications

José Fernando Diniz Chubaci[1]*, C. D. Gonzales-Lorenzo[1], H. S. Javier-Ccallata[2], G. S. Goveia[1], D. G. Fidelis[1], R. Gennari[1] S. Watanabe[1]

[1]*LACIFID, Institute of Physics, University of São Paulo, São Paulo, Brazil*

[2]*Facultad de Ciencias e Ingeniería, Universidad Tecnológica del Perú (UTP), Arequipa, Perú*

Highlights: TL, PL and optical absorption of calcium silicate produced in our Laboratory was studied. The results indicate that calcium silicate undoped or doped with silver could be suitable for use as TL, OSL or RPL dosimeters.

Key words: silicates, radiation, dosimetry, photoluminescence, thermoluminescence.

Background and Objectives: Recently, great effort has been dedicated for the development of luminescent phosphors using transition metal and rare earth as emission centers. Phosphate glass doped with silver, first introduced by Yokota and Nakajima in 1961, exhibits radiation dose dependent photoluminescence (PL). Silicates are the most abundant, the most interesting and the most complicated class of minerals. According to geologists 90% of the crust of the earth is made of silicates. The silicates can be organized by their chemical composition and their crystal structure. Calcium silicate is one of a group of compounds that can be produced by reacting calcium oxide and silica in various ratios. Calcium oxide acts as a stabilizer for the silica. Calcium silicate ($CaSiO_3$) is a white free-flowing powder with such physical and chemical properties that can be applied in cases of high mechanical capacity, resistance to humidity and fire, chemical inertia and not abrasive or corrosive to other materials. Recently, our research group has been working with silicates for a comprehensive study of the physical characteristics of this class of minerals for potential application as ionizing radiation sensors. Natural or laboratory produced silicate crystals and glasses are very sensitive to the exposure of ionizing radiation. Different silicate compositions and structures ranging from crystals to glasses have been used as ionizing radiation sensors. Natural or laboratory produced silicate crystals has shown to be very sensitive thermoluminescence (TL) material. Photoluminescence emission measurements from silicate glasses has shown increasing response to increasing radiation doses. In this work, calcium silicate was produced as polycrystals by the devitrification method and as glass for the investigation as possible dosimeter for ionizing radiation.

Materials and Methods: The mixture of calcium oxide and silica were heated at temperatures up to 1500ºC during two hours for melting and uniformization. For the polycrystal production the crucible was kept in the furnace during 24 hours for slow cooling and for the glass the crucible was taken from the furnace and the melt turned into a substrate for a quenching process. The calcium silicate was produced undoped and doped with silver to emulate the same silver oxireduction process that can be seen in silver doped phosphate glass. For the detection of radiation doses, chips of calcium silicate were produced compressing 50 mg of the powder (80-180 μm grains sieved from the polycrystals or the glasses) with a pressure of 11 ton/cm^2 and then sintering at 1200°C for one hour. Slabs from the glass blocks were taken for optical absorption and photoluminescence measurements. These chips and slabs proved to be very sensitive to low dose of the order of mGy and high doses in the region of kGy. UV-VIS-NIR optical absorption, thermoluminescence (TL) and photoluminescence (PL) were studied for these samples.

Results and Discussion: The undoped chips of calcium silicate showed prominent TL peaks at 120°C and at 270°C when irradiated with gamma radiation. Photoluminescence from the undoped chips and from the undoped glass slabs showed a clear emission band centered at 693 nm with dose dependence from few Gy up to kGy when excited at 450 nm. The silver doped glass slabs showed an emission band at 580 nm when excited at 370 nm independent of the silver concentration. The intensity of the 580 nm band for the silver doped glass was much higher than that at 693 nm of the undoped sample. The excitation of the undoped samples is compatible with that used for optically stimulated luminescence. The 580 nm band excited at 370 nm resemble that of the silver doped metaphosphate glass.

Conclusion: The results found in this work for thermoluminescence and photoluminescence measurements indicates that calcium silicate undoped or doped with silver could be suitable for use as TL, OSL or RPL dosimetry. Mechanism of gamma radiation interaction and luminescence emission from the calcium silicate material will be discussed in this work. We are working to find best production condition and possible application of this material as ionizing radiation sensors. (This work is partially supported by FAPESP (Proc. 2014/03085-0), CNPq and ONR-G)

References

1) Gonzales-Lorenzo, Carlos D.; Watanabe, S.; Cano, Nilo F.; Ayala-Arenas, Jorge S.; Bueno, Carmen C. - Synthetic polycrystals of $CaSiO_3$ un-doped and Cd, B, Dy, Eu-doped for gamma and neutron detection. Journal of Luminescence, v. 201, p. 5-10, 2018.

Highly sensitive novel silica-based materials for radiation detection

R.E. Shaw[1,2], C.A.G. Kalnins[1,2], N.A. Spooner[1,2,3], C. Whittaker[1,2], J.E. Moffatt[1], G. Tsiminis[1], E. Klantsataya[1], S. Grimm[4], K. Schuster[4], D. Litzendorf[4], A. Matthes[4], K. Wondraczek[4], D. Ottaway[1,2,] H. Ebendorff-Heidepriem[1,2]

[1]*University of Adelaide, Institute for Photonics and Advanced Sensing and School of Physical Sciences, Adelaide, SA, 5005, Australia.*

[2]*Australian Research Council Australian Copper Uranium Transformation Research Hub, Adelaide, SA, Australia.*

[3]*Defence Science and Technology Group, Edinburgh, SA, 5111, Australia*

[4]*Fibre Optics, Leibniz Institute of Photonic Technology, Jena, Germany*

Highlights The radiation response of rare earth doped silica glasses fabricated using powder sintering (REPUSIL) and melt quenching (termed SAL) were investigated. Extreme sensitivity was observed and rare earth doped glasses were identified for a range of radiation detection applications.

Key words ionizing radiation, dosimetry, silica, rare earths, fibres, sensors

Background and Objectives Silica glasses doped with rare earth ions are potential ionising radiation dosimeter materials that are suitable for drawing into optical fibres for distributed sensing applications. High sensitivity dosimetry requires fibres with large cores to maximise detection volume. Large core single material fibres can be reliably fabricated using glass made from the reactive powder sintering of silica (REPUSIL) [1], and a melt quenching technique (termed SAL) [1]. Photoluminescence transitions from rare earths can greatly enhance sensitivity in luminescence based radiation detection techniques such as thermoluminescence, radioluminescence and optically stimulated luminescence (OSL). Key luminescence and dosimetric properties of a range of rare earth doped silica materials produced using the techniques REPUSIL [2] and SAL [3] have been characterised.

Materials and Methods Absorbance, photoluminescence, and thermoluminescence were measured to determine optimal stimulation wavelengths, signal filtering methods and the most suitable candidates for optical fibre sensors. Radioluminescence (scintillation) and OSL are the fundamental mechanisms enabling radiation detection in optical fibres. The most sensitive dopant for fibre fabrication was determined by measuring radioluminescence, OSL and dose response to alpha and beta particle sources and low energy x-rays.

Results and Discussion It was found that cerium and thulium doped REPUSIL and cerium, thulium and terbium doped SAL glasses are promising candidates for low dose optical fibre dosimetry. Samples showed intense luminescence signals in response to both photo-stimulation and irradiation from alpha and beta particle sources. Thulium doped SAL samples showed potential as fluorescent nuclear track radiation detectors. Terbium doped SAL demonstrated twice the OSL response as previously reported terbium doped fluoride phosphate samples [4]. Thermoluminescence showed untrapping of electrons below 200 °C, making samples naturally biased against false positives, hence ideal for passive sensors with high duty cycle applications such as monitoring shielding on radiation sources and facilities. A high intensity response was seen from holmium doped SAL above 3 Gy beta particle dose indicating potential as dosimeters in the 3 Gy – 33 Gy range. Cerium doped REPUSIL showed an order of magnitude higher intensity radioluminescence response for low energy x-rays when compared to cerium doped SAL and previously reported polymer scintillation fibres [5].
Both rare earth doped REPUSIL and SAL spectroscopic measurements indicate emission in the 300 to 500 nm region, very well matched for photon detection with bialkali photomultiplier tubes.

Conclusion Rare earth doped silica fabricated using the SAL and REPUSIL techniques were characterized for their luminescence response to alpha and beta particle irradiation and low energy x-rays. Each rare earth and/or fabrication technique showed advantages for a variety of applications such as high and low dose dosimeters, radiation detectors for medical diagnostics, monitoring radiation sources and facilities and passive sensors.

References

[1] Schuster, K., et al. (2014). "Material and technology trends in fiber optics." Advanced Optical Technology **3**(4): 447-468.
[2] Shaw, R. E., et al. (2018). "Luminescence effects in reactive powder sintered silica glasses for radiation sensing." Journal of the American Ceramics Society: 1-17.
[3] Shaw, R. E., et al. (2019). “Luminescence effects in lanthanum aluminium silicate glasses for radiation sensing.” Pending publication.
[4] Kalnins, C. A. G., et al. (2016). "Enhanced radiation dosimetry of fluoride phosphate glass optical fibres by terbium (III) doping." Optical Materials Express 6(12): 3692-3703.
[5] C. A. Whittaker, et al. (2019). “Evaluating the energy dependence of various polystyrene based plastic scintillators.” Radiation Measurements **122**; 57-62.

Dose Estimation of Electrons and Positrons from ^{64}Cu using Fluorescence Nuclear Track Detector

Tamon Kusumoto[1]*, Sumitaka Hasegawa[1], Norhan Omar[2], Michel Fromm[2], Ryo Ogawara[1], Takeshi Kai[3], Yusuke Matsuya[3], Teruaki Konishi[1], Satoshi Kodaira[1]

[1] *National Institute of Radiological Sciences, National Institutes for Quantum and Radiological Science and Technology*

[2] *Université de Bourgogne Franche-Comté, Besancon, France*

[3] *Japan Atomic Energy Agency, Tokai, Japan*

Highlights Absorbed doses from ^{64}Cu are evaluated using Fluorescence Nuclear Track Detector (FNTD).

Key words FNTD, ^{64}Cu, Auger electron, Dosimetry

Background and Objectives

Recently, radiation therapies have been recognized as effective candidates for the cancer treatment. Among them, the targeted radioimmunotherapy using radiolabeled copper (II) (diacetyl-bis N4-methylthiosemicarbazone) (^{64}Cu-ATSM) is underdevelopment as a new generational cancer treatment [1)]. ^{64}Cu decays by emission of β^- (0.573 MeV), β^+ (0.656 MeV) and electron capture (41%) with half-life of 12.7 h. The specific feature of ^{64}Cu is the emission of auger electrons, which has been expected to be effective to kill cancer cells. The therapeutic effectiveness of ^{64}Cu-ATSM for hypoxic cancer cells has been demonstrated so far but the absorbed dose from ^{64}Cu has not been quantitatively evaluated. To establish a dose evaluation method of electrons, we, in the first step, have conducted the dosimetry of ^{64}Cu.

Experiments

Fluorescence Nuclear Track Detector (FNTD) (Landauer, Ltd.) with a thickness of 90 μm was employed for the dosimetry. The fluorescence intensities were measured using confocal laser scanning microscope (FV-1000, Olympus Co.). FNTD was excited by a laser with a wavelength of 635 nm and then we read the luminescence intensity at 668 nm.

An aqueous copper nitrate solution (FUJIFILM), which was labeled by ^{64}Cu, was used as an electrons source. The radioactivity was 684 kBq at 10:30 on December 20th, 2018. We removed aqueous copper nitrate solution at 13:00 on January 28th, 2019.

Results and Discussion

Figure 1 shows the depth dependence of relative fluorescence intensity, that is proportional to the absorbed dose. Inset photos are confocal microscopic images of FNTD. The fluorescence intensity at deeper layer could be darker due to the optical light absorption of both excited and emitted lights. The changes in the intensity are calibrated by gamma exposures. The relative intensity decreases monotonically with increasing the depth. At 0 μm in depth, the high absorbed dose is predominantly attributed to auger electrons, characteristic X-rays, β^- and β^+. Furthermore, the continuous slowing down approximation range of β^- in FNTD is 0.85 cm calculated by E-STAR program[2]. This implies that we should consider the influence to the normal tissues by β^- and β^+.

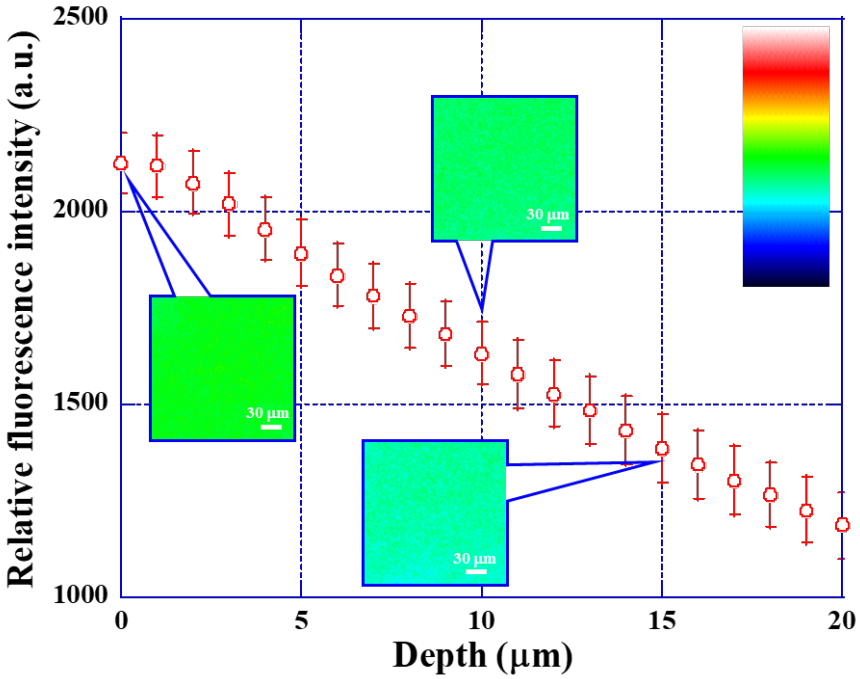

Figure 1. Depth dependence of relative fluorescence intensity. Inset photos are confocal microscopic images.

Conclusion

We clarified depth dependence of fluorescence intensity measured by FNTD. We are addressing to evaluate the ^{60}Co equivalent dose in water at each depth. Additionally, the results obtained present work will be compared to that using a Monte Carlo simulation.

References

1) McMillan et al., J. Radiat. Res. 5 (2015) 784.
2) Berger et al., ESTAR (2005).

Comparative study of dose distribution with conventional mammography and microdose using radiophotoluminescent glass dosimeters (RPL)

Meire Ogussuko[1], Sonia .H. Tatumi[1]*, José F.D. Chubaci [2], Kellen A.C. Daros [3], Shigueo Watanabe[2]

1 Federal University of São Paulo, Baixada Santista Campus, São Paulo, Brazil
2 Institute of Physics, University of São Paulo, São Paulo, Brazil
3 Federal University of São Paulo, São Paulo Campus, Brazil

Highlights RPL dosimeters were applied mammograph diagnostic doses for the improvement of radiation protection of patients. Two-dimensional dose distribution graphs were plotted, using RPL dosimeters, to observe the uniformity of the field emitted by conventional and microdose mammography equipments.

Key words Microdose mammography, RPL dosimeter, glass dosimeters, diagnostic dosimeters

Background and Objectives The rapid detection and diagnosis of breast cancer is essential for the treatment and cure of patients, making the mammography examination mandatory for women with a family history of the disease or over 40 years of age. Currently, we have several equipment that use the microdose system, offering a mammography examination with high precision and low dose of X radiation, providing greater speed and comfort to the users. In the literature few works about Dose Ace system for diagnostic dose measurements can be found, although it is very important in radiology, especially in diagnostic field, to know the absorbed doses in patient to estimate the hazard. It is known that doses delivered to patients can vary due to different X-ray equipment and infrastructure conditions, which affect the image quality, entrance surface dose, etc. RPL dosimetry has been used for this type of evaluation and many authors conclude that they are well appropriate to these types of tests (Knezevic´ et al, 2011).
The objective of this study is to compare the dose distribution between conventional and microdose mammograph using radiophotoluminescent glass dosimeters (RPL), for the improvement of radiation protection of patients.

Materials and Methods Philips SI microdose mammography equipment and 60 radiophotoluminescent glass dosimeters doped with silver, GD-351 type, FD-7 series, by Dose Ace (Chiyoda Technol Corporation), were used to evaluate the dose distribution in polymethylmethacrylate phantons (PMMA) on the surface (skin entry) and between the acrylic layers and compare to the dose distribution on conventional mammography using Hologic's digital mammography equipment, Lorad M-IV

Results and Discussion RPL dosimeters were placed on the surface of the phantom and between the layers of acrylic. Two-dimensional graphs were made with obtained doses and they are analyzed. Comparing the graphs, obtained in two dimensions, it was observed a greater uniformity in the results obtained by the microdose than in the conventional mammography, as expected. The average of the measurements made with 15 dosimeters on the surface of the phantom with the conventional mammography was 15.0 ± 0.6 mGy and with the microdose 2.6 $\pm$ 1.2 mGy. The average of the measurements performed between the acrylic layers with the conventional mammography was 2.3 ± 0.6 mGy and by microdose 0.8 ± 0.1 mGy demonstrating uniformity and lower dose offered by the microdose system.

Conclusion The uniformity in the dose range of mammography experiment using RPL dosimetry systems satisfied the comparations requirements. The difference in the average dose and uniformity results, were observed with conventional and microdose equipment's, using RPL system on phantom. Correlation between doses in the primary beam measured on surface and between acrylic layer (6 cm) was evaluated. Based on the obtained dose values the reduction of dose, improved by microdose equipment, was quantitatively verified.

References

1) Z. Knezevic´, N. Beck, D. Milkovic, S. Miljanic, M. Ranogajec-Komor. 2011. Characterisation of RPL and TL dosimetry systems and comparison in medical dosimetry applications Radiation Measurements, 46,1582-1585.

Acknowledgements The research work was partly supported by the São Paulo Research Foundation (FAPESP) within a research grant nº. 2014/03085-0.

Secondary radiation doses in paediatric phantoms for proton radiotherapy- EURADOS WG9 intercomparison

Željka Knežević[1*], Liliana Stolarczyk[2,3], Iva Ambrozova[4], Maria Davídková[4], Carles Domingo[5], Marijke De Saint-Hubert[6],-Renata Kopeć[2], Marija Majer[1], Imma Martínez-Rovira[5], Saveta Miljanić[1], Natalia Mojżeszek[2], Ondrej Ploc[4], Maite Romero-Expósito[5], Sebastian Trinkl[7], Roger Harrison[8], Pawel Olko[2],

[1]Ruđer Bošković Institute, Zagreb, Croatia

[2]Cyclotron Centre Bronowice, Institute of Nuclear Physics, PAN (IFJPAN), Kraków, Poland

[3]Medical Physics Department Skandionkliniken von Kraemers Allé Uppsala

[4] Nuclear Physics Institute of the CAS, Řež, Czech Republic

[5]Departament de Física, Universitat Autònoma de Barcelona, Bellaterra, Spain

[6]Belgium Nuclear Research Center (SCK-CEN), Mol, Belgium

[7]Federal Office for Radiation Protection, External and Internal Dosimetry, Biokinetics

[8]University of Newcastle upon Tyne, Newcastle upon Tyne, United Kingdom

Highlights Out of field doses of scattered radiation in proton radiotherapy are lower in comparison to different photon radiotherapy techniques for the same delivered tumour dose

Key words secondary radiation, spot scanning proton therapy, paediatric phantoms,

Background and Objectives

Proton therapy potentially reduces acute and late side effects of treatment in comparison to conventional radiotherapy, which is particularly important when treating paediatric cancer patients. EURADOS WG 9 (Radiation Dosimetry in Radiotherapy) performed a measurement campaign to study secondary radiation generated by a proton scanning beam (PBS). The main aim of this study is to characterize secondary neutron and gamma radiation fields inside child anthropomorphic phantoms with different solid state detectors and compare the results with measured secondary doses (1,2) during different photon therapy modalities for similar case of brain treatment in children.

Materials and Methods

Proton irradiations were carried out at the CCB IFJ PAN (Krakow, Poland) using a Pencil Beam Scanning (PBS) technique (IBA, Proteus 235). Measurements of secondary gamma and neutron radiation were performed inside three phantoms which represents 1, 5 and 10-year old children. Unwanted doses were measured with different detectors based on thermoluminescence (TL) MTS-7: ^{7}LiF(Mg,Ti), MTS-6: ^{6}LiF(Mg,Ti) and MCP-n: LiF(Mg,Cu,P) and radiophotoluminescence (RPL): GD-352M and using poly-allyl-diglycol carbonate (PADC) track etched detectors and two types bubble detectors (BD). For all three phantoms treatment

of brain tumor was simulated. Target volume was 65 cm^3 with the isocentre in the head of the phantom. Doses following intensity modulated proton therapy (IMPT) were compared with different photon radiotherapy techniques (IMRT, 3D-CRT, GK) (1,2)

Results and Discussion For IMPT non-neutron organ doses are higher in the 5-year old phantom compared to the 10-year old phantom due to increased proximity of organs to the target, while measured neutron organ doses were higher in the 10-y old phantom. The mean stray non-neutron doses for the 5-year phantom (treatment dose of 1Gy) measured 15-45 cm from the isocentre ranged from 0.47 mGy to 0.15 µGy. Neutron doses are a factor of 3 lower than secondary non-neutron doses close to the target but become a factor of 3 higher than secondary non-neutron doses further away from the target. IMPT results in lower secondary doses compared to different photon therapy techniques by one order of magnitude close to the target and more than two order of magnitude further away from the target (see Figure).

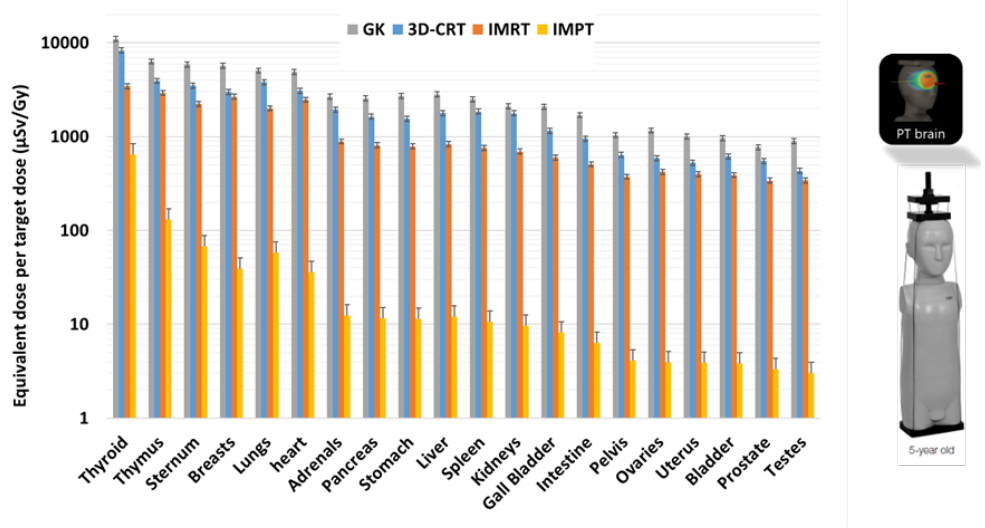

Figure 1 Comparison of stray radiation in 5-year old phantom for IMPT (total dose) and 3D-CRT, GK and IMRT

Conclusion

A combination of several detector types was used to study the total secondary organ doses in proton radiotherapy which showed to be significantly lower in comparison to the different photon radiotherapy techniques for the same delivered tumour dose.

References

1) M. Majer et al. Out-of-field dose measurements for 3D conformal and intensity modulated radiotherapy of a paediatric brain tumour. Radiat. Prot. Dosim. 176, 331-340 (2017).
2) M. De Saint-Hubert et al, Out-of-field doses in children treated for large arteriovenous malformations using hypofractionated gamma knife radiosurgery and intensity-modulated radiation therapy. Radiat. Prot. Dosim. 181 100-110 (2018).

Silver nanoparticles application for enhancement of efficiency in OSL detectors based on Brazilian natural calcium fluoride

Reway, A[1], Machado, T[1], Umisedo, NK[2], Yoshimura, EM[2], Bezerra Jr, AG[1], Malthez, ALMC[1]
[1]*Federal University of Technology - Parana, Curitiba, Brazil*
[2]*University of Sao Paulo, Sao Paulo, Brazil*

Highlights Light emission in radiation detectors can increase due to nanoparticles presence. OSL detectors based on Brazilian natural CaF_2 with silver nanoparticles (Nps-Ag/CaF_2) were produced. It was observed an enhancement of OSL intensity from CaF_2 detectors with Nps-Ag.

Keywords OSL radiation detector, silver nanoparticles, Brazilian natural calcium fluoride

Background and Objectives Nanoparticles (Nps) have been widely applied in several areas, as health, pharmacology, biomedical sensors and power industries. Especially in the power generation, silver Nps (Nps-Ag) were used to enhance the efficiency of light conversion in solar cells by a deposition of a thin layer of Nps-Ag in the surface of the photoactive layer. In this review, the authors described that Localized Surface Plasmon (LSPR) effect and a large optical path, carrying in an increasing of light interaction with electrical field of active surface, are responsible by increasing of light absorption[1]. Guidelli et al. related an increasing of Optically Stimulated Luminescence (OSL) intensity from Ag/ZnO and Au/ZnO core-shell Nps[2]. Calcium fluoride (CaF_2) are employed, in both natural and synthetic forms, mainly as thermoluminescent detectors. As natural CaF_2 detectors present light sensitivity, several studies indicate that detectors based on natural form can be used with OSL technique[3]. Taking in account the dosimetric properties of CaF_2 detectors with OSL technique and the increasing of luminescent emission due to presence of Nps-Ag, the aim of this study was the production and characterization of CaF_2 detectors, based on Brazilian natural fluorite, with NPs-Ag.

Materials and Methods In this study, flexible OSL detectors sheets were produced using a cold technique developed at Federal University of Technology – Parana (UTFPR), consisting in a mixture of CaF_2 crystal powder and a semi-organic matrix[4]. Nps-Ag in acetone solution were obtained by ablation process. The samples of Nps-Ag/CaF_2 and CaF_2 based pellets were cut off from the stripes with and without NPs-Ag, resulting in 24 pellets. The layer deposition was done with spray or drops (samples 1 to 4, 5 to 8 and 9 to 12 received 1, 2 and 3 sprayed and samples 13 to 15, 16 to 18, and 19 to 21 were deposited 1, 2 and 3 drops). A set without Nps-Ag was kept for comparison (samples 22 to 24). The OSL measurements were carried out

in a Risø TL/OSL reader equipped with a built-in $^{90}Sr/^{90}Y$ beta source, blue LED for stimulation and a photomultiplier tube feed with 1225V behind a Hoya U340 filter.

Results and Discussion The presence of Nps-Ag enhancement the sensitivity of CaF_2 detectors (Figure 1). Moreover it was observed that deposition by drop it is more effective, as sprayed is not localized in an area (dispersion). The sensitivity increasing can be attributed to the LSPR and longer light path. In addition, it was not observed enhancement in sensitivity with more than 2 drops, indicating that is a limit to deposition.

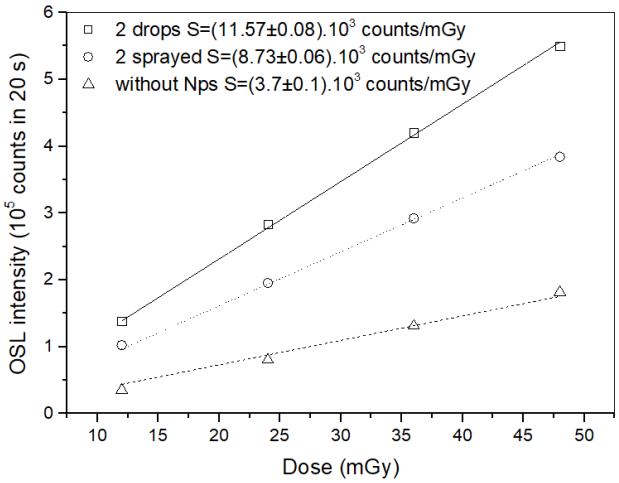

Figure 1. OSL intensity in function of dose from CaF_2 detectors with and without Nps-Ag. Linear fit of data (lines) provided the sensitivity value (S) with R-square higher than 0.999.

Conclusion The presence of the nanoparticles increases the sensitivity of CaF_2 detectors up to 3 times when compared to those without Nps-Ag, reproducibility and linear dose response.

References

1) SANTOS, J.F.L. et al. Ressonância de plasmon de superfície localizado e aplicação em biossensores e células solares. Química Nova, 39 (9), 2016, 1098-1111.
2) GUIDELLI, E. J., BAFFA, O., CLARKE, D., R. Enhanced UV Emission from Silver/ZnO and Gold/ZnO Core-Shell Nanoparticles: Photoluminescence, Radioluminescence, and Optically Stimulated Luminescence. Nature, 2015.
3) MALTHEZ, A. L. M. C. et al. OSL dosimetric properties and efficiency of Brazilian natural calcium fluoride pellets. Applied Radiation and Isotopes, 135, 2018, 166-170.
4) MALTHEZ, A., L., M., C. et al. Low- cost flexible OSL detector leaf for 2D radiation. Book of abstracts of ISRP-14, 2018.

Experimental Evaluation of Thermal Neutron Distribution in Water Phantom in BNCT Irradiation Field Using an Optical Fiber-Based Neutron Detector

Akihisa Ishikawa[1]*, Atsushi Yamazaki[1], Kenichi Watanabe[1], Sachiko Yoshihashi[1], Akira Uritani[1], Yukio Tsurita[1], Kazuki Tsuchida[1], Yoshiaki Kiyanagi[1]

[1]*Department of Applied Energy Engineering, Nagoya University, Furo-cho, Chikusa-ku, Nagoya, Japan*

Key words BNCT, optical fiber-based neutron detector, moderator-based neutron energy spectrometer

Background and Objectives Boron neutron capture therapy (BNCT) involves administering a boron agent to the patient and allowing it to accumulate in their tumor cells. The patient is then externally irradiated with neutrons to induce $^{10}B(n, \alpha)^{7}Li$ reactions in these cells, which are selectively attacked by alpha particles and ^{7}Li ions because of their short ranges of 9 μm and 4.5 μm respectively. One of the key issues in BNCT is to confirm the energy spectrum information of the neutron beam or the thermal neutron distribution. Our group is developing an optical fiber-based neutron detector[1)] for evaluation of the neutron irradiation field in BNCT. The thermal neutron distribution in a patient is a quite important information for treatment planning and dose evaluation and depends on the neutron energy spectrum. In this study, we evaluate the thermal neutron distribution in water phantom placed in the BNCT irradiation field of the Nagoya University Accelerator-driven Neutron Source (NUANS) by using the developed optical fiber-based neutron detector. We compare the experimental result to the simulation result calculated by Particle and Heavy Ion Transport Code System (PHITS).

Materials and Methods The NUANS consists of a Dynamitron accelerator with a maximum proton energy of 2.8 MeV and a maximum current of 15 mA, a lithium target and a MgF_2-based beam shaping assembly (BSA). The neutrons produced by $^{7}Li(p, n)^{7}Be$ nuclear reactions are decelerated and moderated by the BSA. The overview of the experimental setup is shown in Fig. 1. The thermal neutron distribution is measured by scanning the optical fiber-based detector in the water phantom and compared with the simulation results calculated by PHITS. The optical fiber-based detectors used the small-size Eu:$LiCaAlF_6$ or LiF/Eu:CaF_2 eutectics scintillators.

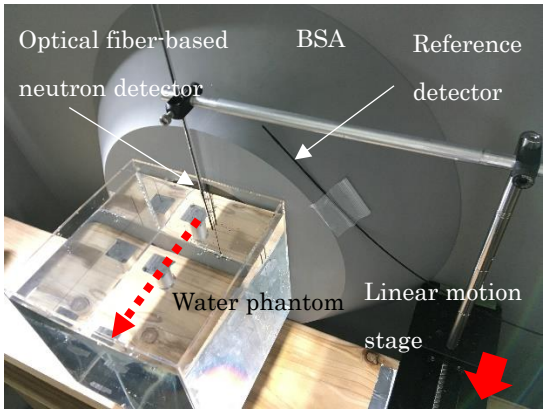

Fig. 1 The overview of the experimental setup. The thermal neutron distribution was measured along the red dotted arrow by the optical fiber-based detector.

Results and Discussion Figure 2 shows the thermal neutron distribution in the water phantom measured by the optical fiber-based detector. The simulation results calculated by PHITS were also plotted, which were standardized by the peak value. We found that the experimental results agreed well with the spectrum simulated by PHITS.

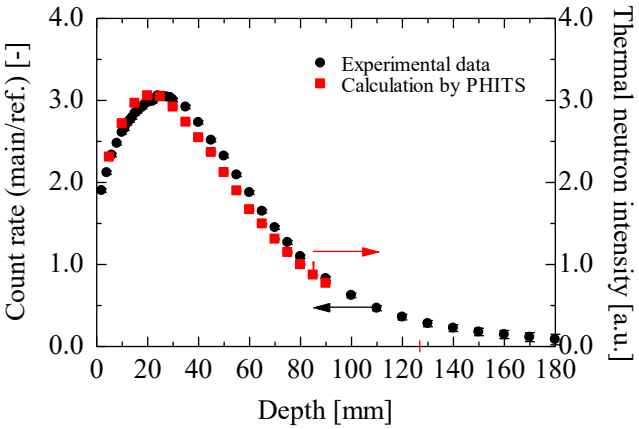

Fig. 2 The results of the measurement and the simulation of the thermal neutron distribution in the water phantom.

Conclusion We experimentally evaluated the thermal neutron distribution in the water phantom by using the optical fiber-based detector. The experimental results agreed well with the results simulated by PHITS.

References

1) K. Watanabe et al., "Development of an optical fiber type detector using a Eu:LiCaAlF$_6$ scintillator for neutron monitoring in boron neutron capture therapy", *Nucl. Instrum. Methods Phys. Res. Sec. A*, **802**, 1–4 (2015).

3D Track information from neutron irradiated FNTDs

A. Stabilini[1,2]*, M. S. Akselrod[3], V. Fomenko[3], J. Harrison[3], S. Greilich[4,5], E.G. Yukihara[1]

[1]*Department of Radiation Safety and Security, Paul Scherrer Institut, 5232 Villigen PSI, Switzerland*

[2]*Department of Physics, Universität Basel, Klingelbergstrasse 82, 4056 Basel, Switzerland*

[3]*Landauer Inc., Crystal Growth Division, 7231/2 Eastgate St., Stillwater, OK 74074, USA*

[4]*Medical Physics in Radiation Oncology, German Cancer Research Center (DKFZ), 69120 Heidelberg, Germany*

[5]*National Center for Radiation Research in Oncology (NCRO), Heidelberg Institute for Radiation Oncology (HIRO), 69120 Heidelberg, Germany*

Highlights FNTDs (Fluorescence Nuclear Track Detector) exposed to fast neutrons were analyzed by acquiring a stack of images using a 2D-galvo FNTD reader. These stacks of images were processed to reconstruct the 3D recoil proton trajectories, providing ultimately an effective delta electron signal filtering and offering additional information on the exposure conditions.

Key words FNTD, Neutron dosimetry, Passive detector

Background and Objectives FNTDs are passive solid-state detectors made of Al_2O_3:C,Mg crystal which show unique features for ionizing radiation detection, namely the ability to record individual charged particle tracks, which can be imaged by confocal laser scanning microscopy (CLSM). Neutron dosimetry is possible using neutron converters and imaging the neutron-induced recoil protons on a single layer, 2 µm beneath the crystal surface(1). Due to their spatial resolution and the possibility to scan several layers of the crystal, FNTDs were also used in hadron therapy to detect the fluence and reconstruct the trajectories of proton and carbon radiotherapy beam, as well as in radio-biological cell survival experiments. The objective of the study is to investigate how much information can be obtained by 3D track-spot detection and trajectories reconstruction for neutron dosimetry.

Materials and Methods FNTDs were coupled with polyethylene converters and exposed, in different layouts, to reference neutron sources. Subsequently, multiple stacks of 2D images were acquired using a custom built FNTD reader(2). The enhancement and the correction of the images as well as the detection and measurements of the radiation-induced track-spots were performed with ImageJ. The track-spots linking was accomplished by the ImageJ plugin version of TrackMate. The reconstructed tracks were then linearly fitted to obtain the trajectories.

Results and Discussion Figure 1 shows an example of the reconstructed tracks of FNTDs irradiated at the same dose and using the same neutron source but at 0°, 30° and 60° angles from the perpendicular to the surface. One can easily distinguish the two irradiations performed at an angle by analyzing the reconstructed tracks. For each reconstructed trajectory several parameters including range, polar and azimuthal angles were estimated. Although the neutron diffusion in the converter and the proton recoil process introduce scattering in the particle direction of propagation with respect to the primary field, a statistical analysis comprising all the trajectories recorded by a detector can provide the relative position of a directional neutron source. Future work will be devoted to perform Monte Carlo simulations aiming at developing a refined model for quantitative assessments based on the inferred trajectories parameters.

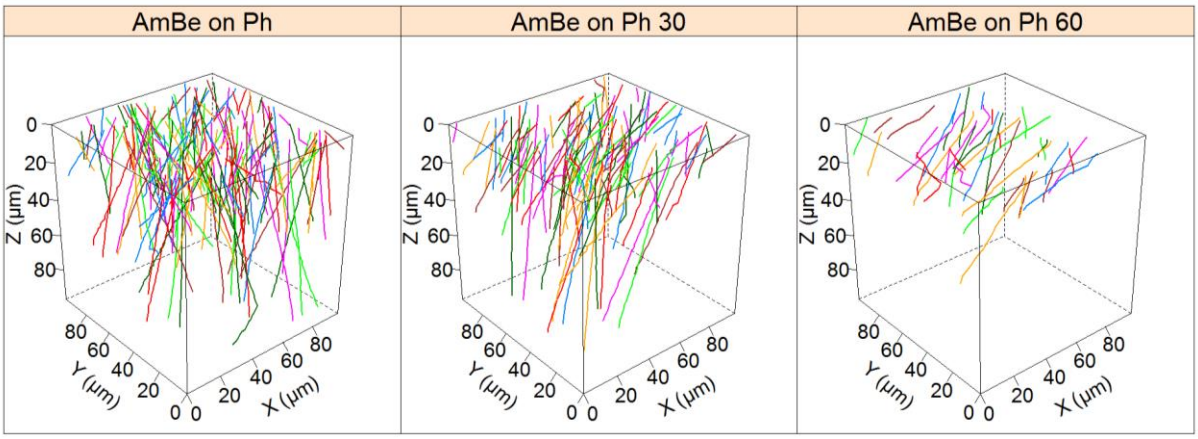

Figure 1. Reconstructed recoil proton tracks of neutron irradiated FNTDs exposed perpendicularly and at angles of 30° and 60°.

Conclusion We carried out an experimental study, based on the 3D imaging of FNTD detectors, aimed at reconstructing the trajectories of recoil protons from fast neutrons irradiations. The analysis offers a method to discriminate between recoil protons and delta electron signal, not available in the faster single-layer acquisition. Moreover, the statistical analysis of the reconstructed trajectories gives evidence of detector irradiations performed at an angle: such information can be used to correct for the geometrical efficiency and, furthermore, could be an indicator of a single intense exposure.

References

1. Akselrod, G. M., Akselrod, M. S., Benton, E. R. and Yasuda, N. A novel Al2O3 fluorescent nuclear track detector for heavy charged particles and neutrons. Nuclear Instruments & Methods in Physics Research B. **247**(2), 295-306 (2006).

2. Akselrod, M. and Kouwenberg, J. Fluorescent nuclear track detectors - Review of past, present and future of the technology. Radiation Measurements. **117**, 35-51 (2018).

Development of plastic scintillators containing a phosphor with aggregation-induced emission properties.

Arisa Magi[1]*, Masanori Koshimizu[1], Yutaka Fujimoto[1], Keisuke Asai[1].
[1]*Tohoku University, Miyagi, Japan*

Highlights We report plastic scintillators containing organic phosphors with aggregation-induced emission (AIE) properties. The optimum phosphor concentration was investigated upon changing the concentration of the phosphor. All of the as-prepared samples emitted scintillation light. Interestingly, the photoelectric peaks of the pulse height spectra were confirmed in the samples to which a large amount of phosphor were added.

Keywords Scintillator, Plastic scintillator, AIE characteristics

Background and Objectives With the growing demand for scintillators exhibiting excellent fast responsiveness, plastic scintillators are considered to have great potential for radiation detection. An ideal plastic scintillator should also have a high scintillation light yield to accurately measure γ-ray radiation. However, it has been reported that the scintillation light yield decreases when the phosphor is added in excess, which can be attributed to the concentration quenching effect. Molecules showing aggregation-induced emission (AIE) properties have been recently discovered, whose luminescence significantly increases upon aggregation, which are expected to overcome the previous problems observed with organic phosphors. Of the various luminescent substances available, 1,1,2,2-tetraphenelethene (TPE) was adopted in our study. TPE has a simple molecular structure and exhibits a significant AIE effect. Upon adopting a propeller-like conformation, TPE effectively prevents any direct π-stacking interactions, which tends to induce non-radiative recombination and a red shift in its photoluminescence, as observed in ordinary crystals [1]. In this study, a plastic scintillator containing TPE was prepared and its X-ray detection characteristics were analyzed.

Materials and Methods Polystyrene was dissolved in tetrahydrofuran and 0.10, 0.50, 1.0, 2.0, 4.0, and 6.0 mol% of TPE was added and dispersed. The resulting samples were dried at room temperature. The excitation and photoluminescence spectra were measured on an F-7000 spectrometer (Hitachi High-Technologies). The radioluminescence spectra were measured using an X-ray tube operated at 40 kV and 40 mA equipped with a charge-coupled device (CCD)-based detector (XGD 2300-HK, Rigaku). The pulse height spectra were measured using ^{137}Cs γ-ray irradiation (50 kBq).

Results and Discussion

Figure 1 shows photographs of the plastic scintillators prepared in this study. When the amount of phosphor added was 0.1–1.0 mol%, the samples were colorless and transparent. On the other hand, when the phosphor content was ≥2.0 mol%, the samples were white. Figure 2 shows the excitation and a photoluminescence spectra recorded for the scintillators prepared in this study. Upon excitation at ~367 nm the samples emit light at 500 nm. This was attributed to the emission of TPE. Figure 3 shows the radioluminescence spectra. The emission spectra were similar to the luminescence spectra.

Figure 4 shows the pulse height spectra and the data obtained for 0.50 mol% b-PBD. B-PBD is often chosen as the phosphor added to scintillators. As far as the data shown in Fig. 4 are concerned, TPE seems to be inferior to b-PBD, but it is a noteworthy feature that the AIE characteristics are concentration dependent.

Conclusions As a new attempt to develop plastic scintillators, we have developed plastic scintillators containing a phosphor with AIE characteristics. As a result, it was found that the samples to which the aggregation-inducing phosphor was added at high concentration were hardly affected by the concentration quenching effect when compared with a conventional b-PBD phosphor. Therefore, it is possible to develop a plastic scintillator with a large amount of light emission.

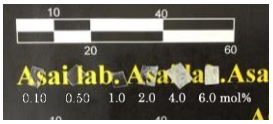

Figure 1. The plastic scintillators prepared in this study with the TPE loading indicated from left to right.

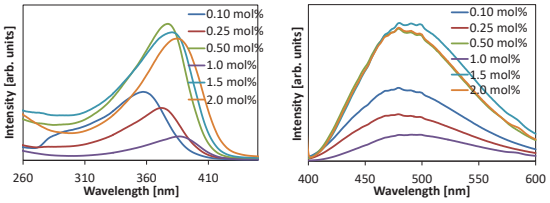

Figure 2. The excitation and photoluminescence spectra recorded for the scintillators prepared in this study.

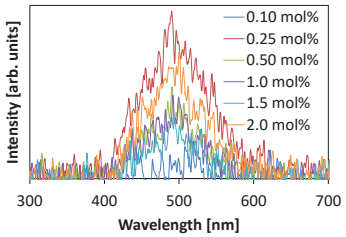

Figure 3. The radioluminescence spectra recorded for the scintillators prepared in this study.

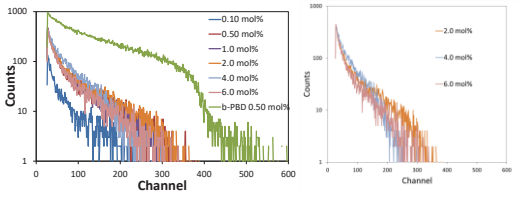

Figure 4. The pulse height spectra recorded for the scintillators prepared in this study [^{137} Cs γ-ray irradiation (50 kBq)].

References

[1]Zhao, Z., Lam, J. W. Y., Tang, B. Z. *J. Mater. Chem*. **2012**, *22*, 23726.

Beam loss monitors for heavy ion accelerators based on neutron detection

Issatov A.T.[1,2]*, Kabytayeva R.K.[1,2], Kalagin I.V.[1], Mitrofanov S.V.[1], Teterev Yu.G.[1]

[1] *Flerov Laboratory of Nuclear Reactions, Joint Institute for Nuclear Research, Dubna, Russia*

[2] *L.N.Gumilyov Eurasian National University, Astana, Kazakhstan.*

Key words beam loss monitors, neutron detection, heavy ion accelerators.

Background and Objectives The development of modern heavy-ion accelerators is associated with an increase in beam intensity. Accordingly, with high-intensity heavy-ion beams, the actual problem is beam diagnostics by non-destructive methods, because using of contact methods for beam diagnostics is impossible due to the high power of the beam.

The beam diagnostics by non-destructive methods can be implemented on the basis of radiation detection resulting from the interaction of a heavy ion beam with accelerator construction materials.

Materials and Methods This paper describes a beam diagnostics method based on neutron registration. Neutron detectors are installed along beam line and measure the neutron flux formed as a result of the interaction of ions with the structural materials of beam line. Thus, one can quite accurately determine the place of ion loss and optimize the settings of the accelerator.

Neutron detectors SNM-16 based on He3 gas are used to neutron registration. The advantage of this detector is insensitivity to gamma radiation. Water is used as a moderator.

Figure 1. Neutron detector SNM-16 based on He3 gas.

TL calcium silicate detectors for proton and carbon beam dosimetry

Carlos Gonzales-Lorenzo[1*], Shigueo Watanabe[1], Satoshi Kodaira[2], Luana Nascimento[3]

[1]*Institute of Physics, University of São Paulo, Brazil*
[2]*Radiation Measurement Research Section, National Institute of Radiological Sciences, Chiba, Japan.*
[3]*SCK·CEN Belgian Nuclear Research Centre, Boeretang 200, Mol, Belgium*

Highlights

Chips of $CaSiO_3$ have been produced for ion accelerated detection.

Irradiations with 290 MeV/n Carbon and 160 MeV proton.

TL response, after irradiation, presented two prominent peaks at 120 °C and 270 °C.

Doses from proton and carbon ions were compared with gamma doses from Cs(137) source.

Keywords Thermoluminescence, $CaSiO_3$, Protons, Carbon, Ion accelerator.

Background and Objectives

Different natural and laboratory produced silicate crystals have shown to be very sensitive TL materials, between them, synthetic polycrystals of calcium silicate $CaSiO_3$ have shown to be a sensitive detector for gamma and neutron radiation [1, 2]. In addition, the use of different ion accelerator dosimeters has been studied, such as Al_2O_3:C+, of seeing potential use in radiotherapy. [3]. In this work, synthetic polycrystals of $CaSiO_3$ in pellets form have been irradiated to proton and carbon ion accelerator and their TL response studied keeping in mind their use or not as ion accelerate detector.

Materials and method:

These polycrystals were produced by the devitrification method, in which, compounds of CaO and SiO_2 in stoichiometric proportion were mixed and carried out to the furnace at 1500 °C for two hours [2]. In addition, chips of $CaSiO_3$ have been produced compressing powder with a pressure of 11 ton/cm^2 and then sintering at 1200 °C for one hour. These chips are shown in Fig. 1(a). The calibration of chips was carried out irradiating them with Cs(137) γ rays as shown in Fig. 1(b). Each chip has 6mm diameter and 1mm thickness. Finally, these chips were irradiated at 160 MeV proton beam and 290 MeV/n carbon ion beam from an upper synchrotron of HIMAC (Heavy Ion Medical Accelerator in Chiba, Japan) at NIRS (National Institute of Radiological Sciences).

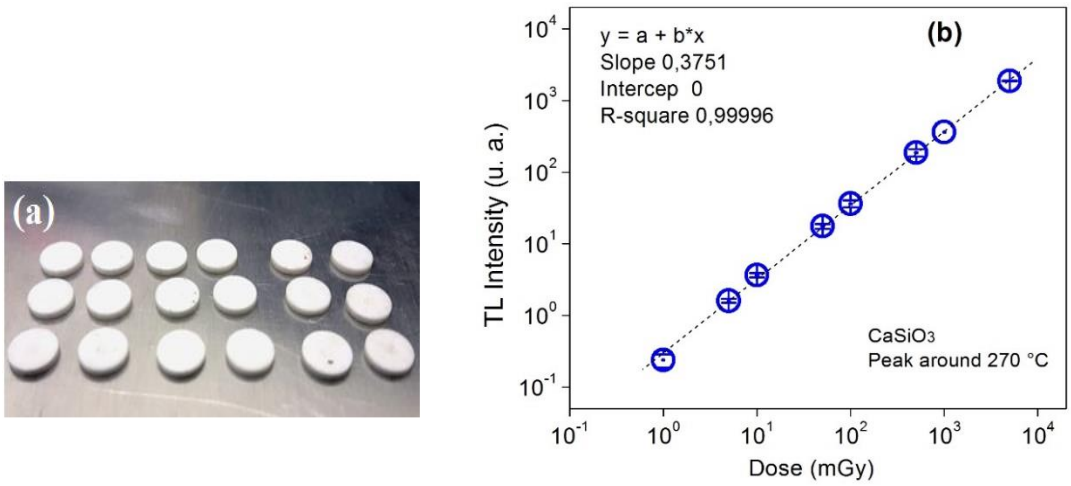

Fig. 3a: (a) Pellets of $CaSiO_3$, (b) TL vs dose γ-rays.

Results and discussion:

These chips of calcium silicate presented a prominent peak at 120 °C, and at 270 °C when irradiated with accelerated heavy ions. The dose read out in Harshaw TL reader presented a good agreement with doses found using a gamma source (Cs-137) in the case of proton beams and slightly less in the case of carbon beam due to the LET dependency. For detection of radiation doses involving accelerated proton and carbon beam, a nuclear reaction and Coulomb barrier effect are involved. The interaction of these accelerator ions with the detectors will be discussed at the meeting.

Conclusion:

In this work, pellets of $CaSiO_3$ polycrystals have been produced for ion accelerated detection. $CaSiO_3$ detectors are suited for that proposal. $CaSiO_3$ is sensitive to low doses of the order of mGy, therefore it can be used in radiotherapy or nuclear medicine.

References

[1] S. Watanabe, N. Cano, Lucas S. Carmo, R. Barbosa, J. Chubaci, High- and very-high-dose dosimetry using silicate minerals, Radiation Measurements, Volume 72, 2015, Pages 66-69, ISSN 1350-4487.

[2] C. Gonzales-Lorenzo, S. Watanabe, N. Cano, J. Ayala-Arenas, C. Bueno, Synthetic polycrystals of $CaSiO_3$ un-doped and Cd, B, Dy, Eu-doped for gamma and neutron detection, Journal of Luminescence, Volume 201, September 2018, Pages 5-10, ISSN 0022-2313.

[3] L.F. Nascimento, F. Vanhavere, S. Kodaira, H. Kitamura, D. Verellen, Y. De Deene, Application of Al_2O_3:C+fibre dosimeters for 290MeV/n carbon therapeutic beam dosimetry, Radiation Physics and Chemistry, Volume 115, 2015, Pages 75-80, ISSN 0969-806X.

Fast Neutron – Gamma ray Dosimetry via Combined TL and OSL Measurements on LiF:Mg,Ti (TLD-700 and TLD-600)

D. Sibony[1] , I. Eliyahu[2] , L. Oster[3], G. Reshes[3] , Y.S. Horowitz[4] , S. Biderman[3], D. Ginsburg[5] and G. Amit[2].

[1] *Nuclear Engineering Unit, Ben Gurion University of the Negev, Beersheva, Israel*
[2] *Soreq Nuclear Research Center, Yavne, Israel*
[3] *Physics Unit, Sami Shamoon College of Engineering, Beersheva, Israel*
[4] *Physics Department, Ben Gurion University of the Negev, Beersheva, Israel*
[5] *Biotechnology Department, Ben Gurion University of the Negev, Beer Sheva,*

The accurate and separate measurement of fast neutron and gamma dose in mixed radiation fields is an important area of application in a great many disciplines but remains problematic. The "needle in the haystack" group named above has decided to take up the challenge by the combined use of thermoluminescence (TL) and optically stimulated luminescence (OSL) of LiF:Mg,Ti dosimeters.

The underlying physical basis of the technique is the fact that the OSL of the F_2 and F_3 centers in LiF:Mg,Ti is enhanced following high ionization density (HID) irradiation (heavy charged particles and neutrons) due to the 2-hit nature of these centers. These centers following irradiation are composed of two trapped electrons bound to two or three adjacent anion centers respectively. On the other hand, the TL mechanism giving rise to glow peak 5 in the glow curve is known to arise from a 1-hit trapping center (TC) based on Mg trimers coupled to Ti-OH. This type of TC is highly sensitive to low ionizing density radiation (gamma rays and electrons) and relatively insensitive to HID irradiation. This is the basis of the superior discrimination between HID and LID radiation in combined OSL/TL measurements. Typical TL and OSL spectra are shown below

TL glow curve and OSL spectrum from LiF:Mg,Ti

Glow peak 5 arises from the thermal release of electrons from traps associated with the 3.8 eV and 4.3 eV optical absorption bands. **The α glow curve has been multiplied by 1000**

The OSL of irradiated pure and doped LiF is attributed to the excitation of intrinsic F_2 and F_3^+ centers at 2.78 eV 2.7 eV respectively

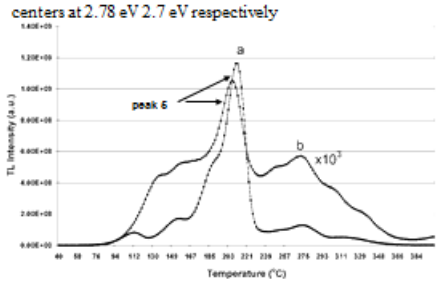

Glow curve (a) β (D =120 Gy) and (b) 4.7 MeV α (fluence, f = 2.5 x10⁹ cm⁻²).

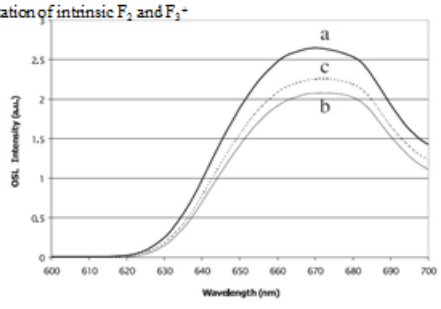

F_2 emission stimulated by laser (2.7 eV) : a) β (D =10 Gy); b) 5 MeV neutrons (D =10 Gy); c) 4.7 MeV α (f = 3 x10⁹ cm⁻²).

We have also demonstrated experimentally that the OSL measurement does not significantly deplete the associated traps so that the subsequent TL measurement can be made on the same sample. The dual measurement on the same sample thus avoids the experimental uncertainties

associated with sample-to – sample dissimilarities and should result in improved accuracy and precision.
In previous work we have clearly demonstrated the potential of combined optically stimulated luminescence (OSL) and thermoluminescence (TL) for neutron–gamma dosimetry [1-3], however the minimum measurable dose in the OSL measurements was limited to approximately 1-2 Gy due to high instrumental background arising from stray light during measurement. In the current research using a Freiburg TL/OSL reader and supported by the PAZY Foundation a MMD of ~ 0.2 Gy should be achievable.

A certain difficulty not previously addressed has been the discovery of a slight supralinearity in the OSL gamma induced dose response between the lowest MMD and 30 Gy. Above 30 Gy the supralinearity strongly increases as does the TL dose response so that the technique requires a solution to this problem for dosimetric applications > 30 Gy. On a positive note the dose response following gamma irradiation for both OSL and TL up to 30 Gy can be fitted with a linear phenomenological function of the following form within the experimental uncertainties.

$$S_\gamma = a_\gamma + b_\gamma D_\gamma \qquad (1)$$

Where S_γ is the intensity of the OSL or TL signal and a_γ and b_γ are calibration constants to be measured experimentally. We have determined that the value of a_γ is negative for both gamma induced OSL and TL due to the slight "true" supralinearity. Since the neutron dose response is "purely" linear ($a_n = 0$ for both OSL and TL) only two calibration constants are involved so that the separate measurement of neutron and gamma dose requires the accurate measurement of six calibration constants. These are currently being determined. Further improvements in the MMD and the non-linearity can be achieved using sensitized materials [4] and deconvolution of the TL glow curves [5] and these are the subject of current investigations

References

1. Oster, L., Horowitz, Y.S. ,and Druzhyna, S., Thermally and Optical stimulated luminescence in LiF:Mg,Ti:Application to mixed high/low ionization density radiation dosimetry, Bull. Russian Acad. of Sciences, 30, 9-13 (2016).
2. Oster, L. , Druzhyna, S. and Horowitz, Y.S., Optically stimulated luminescence in LiF:Mg,Ti:Application to solid state radiation dosimetry, Nucl. Instrum. Meths., A648, 261-265 (2011).
3. Oster, L., Druzhyna, S., Orion, I. and Horowitz, Y.S., Study of combinations of tL/OSL single dosimeters for mixed high/low ionization desnity radiation fields, Radiat. Meas., 56, 320-323 (2013).
4. Horowitz, Y.S., and Shachar, B.B., Sensitized TLD-700 for neutron-gamma ray dosimetry at radiation protection dose levels, Radiat. Prot. Dosim., 33, 263-266 (1990).
5. Horowitz, Y.S. and Youssian, D., Estimation of gamma dose in neutron dosimetry using pea k4 to peak 5 ratios in LiF:Mg,Ti (TLD 100/600). Radiat. Prot. Dosim., 77, 151-158 (1998).

Acknowledgements: This research is supported by the PAZY Foundation

Multi-Sample Integrated TL/OSL Reader System

D. R. Mishra and D. Datta
Radiological Physics and Advisory Division,
Bhabha Atomic Research Centre, Mumbai 400 085, India

Highlights A low cost multi-sample integrated thermo luminescence/optically stimulated luminescence (TL/OSL) reader (MS-ITOR) has been developed for various application. This reader system can handle 36 aliquots at a time. Apart from measuring the TL and OSL the reader has in-built irradiation and optical bleaching facilities.

Key words α -Al_2O_3:C, LiMgPO $_4$:Tb,B, OSL, Radiation Dosimetry, TL

Background and Objectives TL and OSL phenomena have been applied in various applications, like medical dosimetry, personnel monitoring, environment monitoring and geological/ archeological dating. The need of low cost multi-functional TL/OSL reader system remains basic to carry out these applications. Only few such type of reader systems exist commercially. Considering this, a multi-sample integrated TL/OSL reader (MS-ITOR-1) system has been developed, as shown in Figure 1a.

Materials and Methods The developed MS-ITOR-1 reader system can handle 36 sample materials at a time with pneumatically operated on board Sr^{90} beta source. By selecting appropriate carousel two element eighteen OSL cards can, also, be read in the present system. The system has provision for bleaching of the sample (Figure 1b). The 470 nm (40mW/cm^2) and 810 nm (100mW/cm^2) LEDs are provided for OSL stimulations, stabilized using OSD-5 optical diode in feedback path. In TL mode sample can be heated lineally up to 500°C with programmable heading rates from 0.1K/s to 20K/s under inert nitrogen flushed environment. The non-linear stimulation OSL mode (NL-OSL) is also available in the developed system.

Results and Discussion The system has been characterized with different phosphors, α-$Al2O_3$: C, $LiMgPO_4$:Tb,B (LMP), LiF_2 and $CaSO_4$:Dy. Figure 2 shows the CW-OSL dose response of the OSL signal in case of α-$Al2O_3$:C recorded with the present system. The reader was characterized for different dosimetric parameters, like minimum detectable dose (MMD), reproducibility, sensitivity and dose response. All these parameters were found to be satisfactory for dosimetric applications.

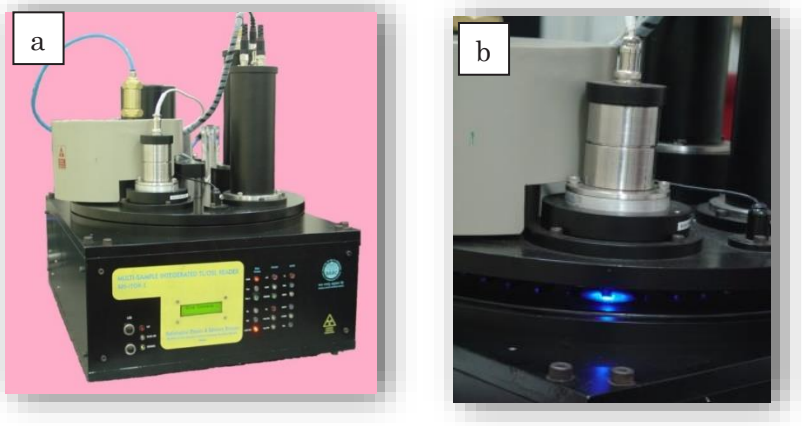

Figure 1. (A) MS-ITOR-1 system, (B) optical bleaching section.

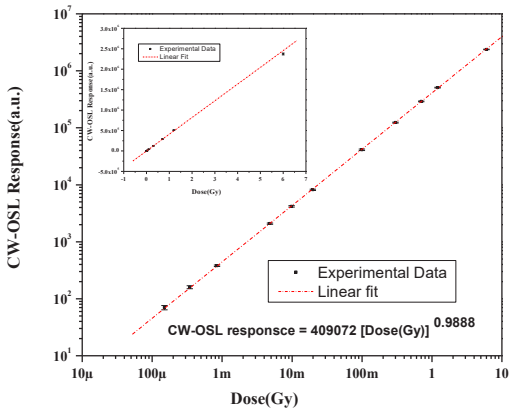

Figure 2. CW-OSL dose response of commercial dosimetric grade α-Al_2O_3:C power pasted on SS Dick for 32mW/cm^2 @470 nm stimulation light irradiated with inbuilt beta source.

Conclusion The MS-ITOR-1 is found to be reliable and cost effective system for basic research and stimulated luminescence, TL and OSL, based applications.

References

1) L. Bøtter-Jensen : The automated Risø TL dating reader system, Nucl. Tracks Radiat. Meas., 14 (1988), pp. 177-180.

TSL and OSL properties of Eu-doped $LiMgAlF_6$

Takayuki Yanagida*, Takumi Kato, Noriaki Kawaguchi
Nara Institute of Science and Technology, Nara, Japan

Highlights Different concentrations of Eu doped $LiMgAlF_6$ samples were synthesized by the spark plasma sintering method. Eu-doped $LiMgAlF_6$ showed an intense thermally stimulated luminescence (TSL).

Key words radiation, dosimetry, ceramics, Eu^{2+}, $LiMgAlF_6$

Background and Objectives Dosimeter materials have been investigated to develop novel and efficient dosimeters. In luminescence-based dosimeters, thermally stimulated luminescence (TSL), optically stimulated luminescence (OSL) and radiophotoluminescence (RPL) materials are used. In this work, as a new dosimeter material, we introduce Eu-doped $LiMgAlF_6$ produced by the spark plasma sintering (SPS) method.

Materials and Methods Eu 0 (undoped), 0.01, 0.1, 1, 2 and 5% doped $LiMgAlF_6$ ceramic samples were synthesized by the SPS method, and the dopant concentration was calculated with respect to Mg. Raw materials were EuF_3, LiF, MgF_2 and AlF_3, and the purity was 3N. After the sintering process, the surfaces of the samples were polished to achieve the same sample size. Finally, we got the samples with the size of 10 mmϕ × 2 mmt. The phase was checked by XRD (Rigaku, MiniFlex600).

After the synthesis, optical characterizations were done. Photoluminescence (PL) emission-excitation contour graphs were measured by Quantaurus-QY (Hamamatsu), and PL decay times were evaluated by Quantaurus-τ (Hamamatsu). In order to investigate an intrinsic luminescence, undoped $LiMgAlF_6$ was studied at Synchrotron facility (UVSOR).

Following optical characterizations, scintillation properties under X-ray irradiation were studied since scintillation and storage of carriers occur at the same time in luminescent materials[1-3]. Scintillation emission spectrum and decay curve were evaluated by our original setups[4,5]. Then, TSL glow curves were measured by TL2000 (Nanogray), and the irradiated X-ray dose was from 0.1 to 100 mGy. The dose was measured by the ionizing chamber (TN30013, PTW). The TSL emission spectrum was evaluated by using our original setup after 1 Gy X-ray irradiation. The OSL spectrum was observed after 1 Gy X-ray exposure, and the stimulation source was 590 nm LED.

Results and Discussion Figure 1 right shows TSL glow curves of Eu-doped $LiMgAlF_6$ samples after 100 mGy X-ray irradiation. All the samples showed a similar shape in the glow curve. Since the intensity of the undoped sample was very weak, we plotted only Eu-doped samples. Figure 1 center exhibits dose response of Eu-doped $LiMgAlF_6$, and all the samples had a good linearity from 0.1 to 100 mGy. Because the intensity was so strong, we could not evaluate TSL under higher irradiation dose due to the saturation of the reader. Figure 1 right depicts OSL spectra upon 590 nm stimulation after 1 Gy X-ray irradiation. The emission peak observed here at 380 nm was generated from 5d-4f transition of Eu^{2+}, which was confirmed by optical characterizations. Throughout the present work, we confirm that Eu-doped $LiMgAlF_6$ had a function of dosimeter material.

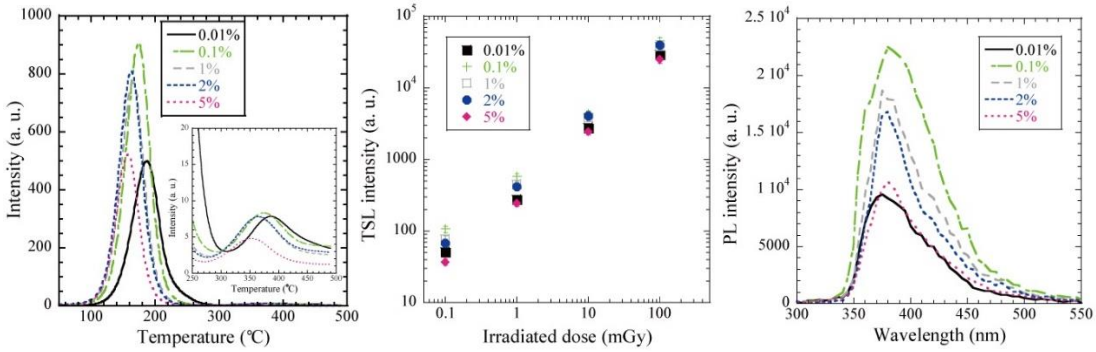

Figure 1. TSL glow curves after 100 mGy X-ray exposure (left), dose response (center), and OSL spectra upon 590 nm stimulation (right) of Eu-doped $LiMgAlF_6$.

Conclusion We synthesized Eu-doped $LiMgAlF_6$ by the SPS method, and evaluated optical, scintillation, TSL and OSL properties of them. Throughout the present work, we confirm that Eu-doped $LiMgAlF_6$ had a function of dosimeter material.

References

1) T. Yanagida, J. Lumin. 169 544 (2016).
2) T. Yanagida, Y. Fujimoto, K. Watanabe, K. Fukuda, N. Kawaguchi, Y. Miyamoto, H. Nanto, Rad. Meas., 71 162 (2014).
3) T. Yanagida, G. Okada, N. Kawaguchi, J. Lumin., 207 14 (2019).
4) T. Yanagida, K. Kamada, Y. Fujimoto, H. Yagi, T. Yanagitani, Opt. Mat., 35 2480 (2013).
5) T. Yanagida, Y. Fujimoto, T. Ito, K. Uchiyama, K. Mori, Appl. Phys. Exp., 7 062401 (2014).

Design and testing of a high-resolution infrared photoluminescence (IRPL) imaging system for large rock samples

E.L.Sellwood*, M.Kook, R.Kumar, M.Jain

Center for Nuclear Technologies, Technical University of Denmark, DTU Risø Campus, Roskilde, Denmark

**Corresponding author; Email: el.sellwood@gmail.com; Telephone: +45 5017 3624*

Highlights

An instrument has been designed to image the recently identified Stokes-shifted IR-photoluminescence emission for routine measurements on large rock slices. Using samples of K-feldspar, appropriate routine measurement protocols were established and demonstrated.

Key words

Infrared photoluminescence, imaging, bleaching, K-feldspar

Background and objectives

For reliability and further improvements in luminescence geochronology, we need a better understanding of the linkages between luminescence, mineralogy and micro-dosimetry. Imaging of optically stimulated luminescence (OSL) with an Electron Multiplying CCD (EMCCD) camera can allow rapid, high sensitivity measurement and high resolution spatial luminescence data to be obtained, which can help form these links in our understanding. Infrared-photoluminescence (IRPL; Prasad et al., 2017) allows non-destructive, direct probing of the principal trap population in feldspars. Unlike OSL, IRPL can give images with unprecedented sensitivity and spatial resolution, and makes it possible to draw direct correlations between the chemical impurities and IRPL intensities (Sellwood et al., 2019). It is thus necessary to develop instrumentation and measurement protocols for imaging IRPL, as well as for OSL. This work presents a full conceptual design of such an instrumentation alongside a demonstration of its use on multiple large K-feldspar samples.

Materials and methods

The imaging system is built upon that used by Sellwood et al., (2019), with an 830 nm laser stimulation for both IRPL and IRSL and an 1020 nm LED for imaging the samples position. Images are captured with an Evolve 512 OEM EMCCD camera, coupled with 2 × 925 nm long-pass interference filters and a 950 Δ50 nm bandpass filter for IRPL detection (Kumar et al., 2018). A combination of BG39 and BG3 filters is used for the complimentary OSL imaging. The IRPL and OSL emissions from three samples of K-feldspar (orthoclase, amazonite and anti-perthite), as well as a sample of granite were imaged and used for calibration of the instrument, defining measurement protocols and an investigation into IRPL bleaching.

Results and Discussion

We present a detailed design of the IRPL imaging set-up and a demonstration of its measurement capabilities. The main aspects of design are:

1) Ability to image both IRPL and IRSL with uniform illumination and detection.
2) An adjustable imaging area up to ~5 x 5 cm, granting measurement of samples of variable sizes and shapes.
3) Normalisation of IRPL sensitivity variations across the sample without the need for an ionising radiation source.

Carefully designed protocols with defined pre-heats, stimulation durations, and normalisation steps allowed both investigations into the emission centres and links to chemistry, and enabled rapid data acquisition for rock surface dating. Image analysis protocols were designed to reduce noise, and define appropriate background subtraction and signal normalisation for the desired application. Overall performance is demonstrated with an investigation into the bleaching behaviours of IRPL in rock slabs using different wavelengths (IR, blue, green and UV)

Conclusion

We present a new instrumentation for the imaging of IRPL and OSL from rocks and minerals. The high-resolution data assists our understanding of trapped-charge processes which occur in feldspars, and their direct links to chemistry. The rapid measurement procedure on large samples benefits applications such as OSL rock surface dating, and lays pathway to the development of a high sensitivity portable dating instrument.

References

Kumar, R., Kook, M., Murray, A.S., Jain, M., 2018. Towards direct measurement of electrons in metastable states in K-feldspar: Do infrared-photoluminescence and radioluminescence probe the same trap? Radiat. Meas. https://doi.org/10.1016/j.radmeas.2018.06.018

Prasad, A.K., Poolton, N.R.J., Kook, M., Jain, M., 2017. Optical dating in a new light: A direct, non-destructive probe of trapped electrons. Sci. Rep. 7, 12097. https://doi.org/10.1038/s41598-017-10174-8

Sellwood, E.L., Guralnik, B., Kook, M., Prasad, A.K., Sohbati, R., Hippe, K., Wallinga, J., Jain., M., 2019. Optical bleaching front in bedrock revealed by spatially-resolved infrared photoluminescence. Sci. Rep.

2D semiconductor devices for high-resolution real-time dosimetry in modern radiotherapy: results in the last 3 years and outlook

Giordano Biasi[1], Marco Petasecca[1], Vladimir L. Perevertaylo[2], Michael L.F. Lerch[1], Tomas Kron[3] and Anatoly B. Rosenfeld[1]

[1]Centre for Medical Radiation Physics, University of Wollongong, Australia, [2]SPA-BIT, Kiev, Ukraine, [3]Department of Physical Sciences, Peter MacCallum Cancer Centre, Melbourne, Australia and Sir Peter MacCallum Cancer Institute, University of Melbourne, Australia

Highlights novel semiconductor devices for real-time sub-mm resolution dosimetry
Key words small-field dosimetry, QA, 2D semiconductor detector

Background and Objectives Modern radiotherapy uses small fields and exquisite image-guidance techniques to deliver highly-conformal dose distributions. Quality assurance (QA) requirements are more stringent than in conventional radiotherapy and accurate dosimetry is challenging [1]. Over the past few years, the Centre for Medical Radiation Physics has pursued the design and characterization of novel dosimeter prototypes with the potential to address the shortcomings of currently available devices.

Materials and Methods The MP512, the Duo and the Octa (Figure 1) are semiconductor dosimeter prototypes first proposed in 2014, 2017 and 2018, respectively. They have real-time read-out provided through a flexible printed circuit board (PCB). Their 512 diode-sensitive volumes are uniformly distributed with a 2 mm pitch over the 2D active area in the MP512, are on 2 perpendicular arrays with a 0.2 mm pitch in the Duo and are on 4 star-like arrays with a $0.3-0.43$ mm pitch in the Octa. In the present work, we assessed these prototypes in radiation fields produced with megavoltage photon beams and delivered with the most common medical linear accelerators. We cross-checked results for consistency using commercially available dosimeters (film dosimetry, PTW microDiamond, PTW SRS diode, IBA SFD diode) and Monte Carlo simulations.

Results and Discussion We optimized the amount of air gap on top of the active area of the dosimeters, to minimize corrections required to relate their readings to dose in small fields [2]. We characterized the directionally-dependent response of the MP512 and proposed a correction methodology to make it a suitable candidate to QA arc deliveries [3]. Applying the methodology, the MP512 was capable of dose reconstruction during arc deliveries with adaptive multi-leaf collimator (MLC) tracking [4]. Owing to their higher resolution, the Duo

and the Octa were selected to be assessed for dosimetry in very small fields ($5-30$ mm across) and were shown to be accurate [5], [6]. Flattening filter free beams were not detrimental to the performance of the Octa [6], [7]. Based on these results, the Duo was proposed to QA stereotactic-dedicated fixed cones [8] and the Octa was proposed to QA a CyberKnife® system [9]. Above assessments were preparatory to the design of a novel system, composed of the Octa and a homogeneous PMMA phantom, dedicated to QA stereotactic treatments of the spine (Figure 2). These treatments are typically non-coplanar arc deliveries, and for QA spatial resolution is more important than absolute dose accuracy [10]. Assessment of this novel system is ongoing.

Conclusion The present work demonstrated that, in the context of available QA dosimeters, and specifically of semiconductor arrays, the MP512, the Duo and the Octa represented a significant step forward in terms of both temporal (pulse-by-pulse real-time) and spatial resolution. Assessment of their potential for streamlining existing QA procedures is ongoing.

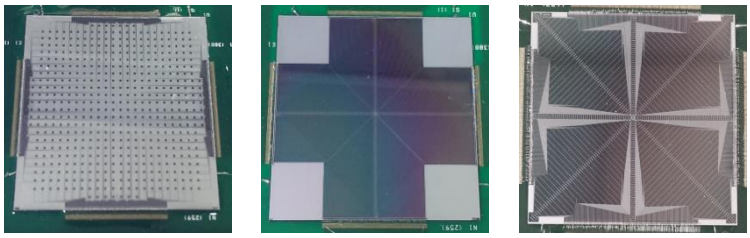

Figure 1. Semiconductor dosimeters with a 2D active area (approx. 5 cm × 5 cm) and real-time pulse-per-pulse read-out proposed by the Centre for Medical Radiation Physics over the past few years. From left to right: the MP512, 2 mm pitch; the Duo, 0.2 mm pitch; the Octa, $0.3-0.43$ mm pitch.

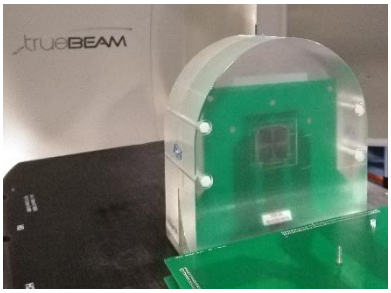

Figure 2. The Octa and its flexible PCB carrier into a phantom dedicated to QA treatments of the spine. Real-time assessment of 2D dose distributions with sub-mm resolution in sagittal and transverse planes would be possible.

References

[1] ICRU, *Report 91*, 2017. [2] Utitsarn *et al.*, *J. Phys. Conf. Ser.*, vol. 777, no. 1, 2017. [3] Stansook *et al.*, *Med. Phys.*, vol. 44, no. 8, 2017. [4] Duncan *et al.*, *J. Appl. Clin. Med. Phys.*, vol. 19, no. 4, 2018. [5] Al Shukaili *et al.*, *Med. Phys.*, vol. 44, no. 2, 2017. [6] Biasi *et al.*, *Phys. Medica*, vol. 45, 2018. [7] Biasi *et al.*, *IEEE Trans. Nucl. Sci.*, vol. 65, no. 9, 2018. [8] Al Shukaili *et al.*, *J. Appl. Clin. Med. Phys.*, vol. 19, no. 4, 2018. [9] Biasi *et al.*, *J. Appl. Clin. Med. Phys.*, vol. 19, no. 5, 2018. [10] Kron *et al.*, *J. Phys. Conf. Ser.*, vol. 777, no. 1, 2017.

Glow curve analysis of TL detectors using robust statistical methods

Stadtmann H.*, Hranitzky C.
Seibersdorf Labor GmbH, Austria

Highlights This paper presents a new automatic algorithm for TL Glow Curve (GC) categorization. Possible irregular GCs can be automatically identified by this new procedure. The presented algorithm can be routinely used for quality control measures in individual monitoring services.

Key words TL detector, LiF:Mg;Ti, glow curve analysis, quality control

Background and Objectives Commercial hot gas TLD readers used in individual monitoring services (IMS) are designed to process a high number of thermo-luminescent (TL) detectors within a short time period. Heating rates of several tens °C per second and short processing times are therefore routinely applied. Although hot gas readers often apply linear time temperature profiles (with a constant gas heating rate) the actual temperature of the processed TL chip deviates strongly from this linear profile (1, 2). Due to small differences in the heat transfer of different TL detectors the exact position of the glow curve varies for different detectors. This fact complicates the use of standard computed glow curve analysis (GCA) procedures (e.g. based on regions of interest – ROI) for routine glow curves.

Materials and Methods Two element LiF:Mg;Ti TL detector cards routinely used in the individual monitoring service (IMS) of the Seibersdorf Labor GmbH were used in this study. A simple GCA procedure for quality control purposes based on few glow curve (GC) characteristic parameters like medians and percentiles derived from statistical analysis were introduced and tested. The multi-dimensional presentation of single glow curves with respect to these parameters allows the categorization of GCs.

Results and Discussion The described procedure is now tested at our IMS. For this purpose hundred thousands of routinely derived GCs were analyzed. The multi-dimensional presentation of single GCs with respect to the derived GC parameters allows the categorization of all GCs.

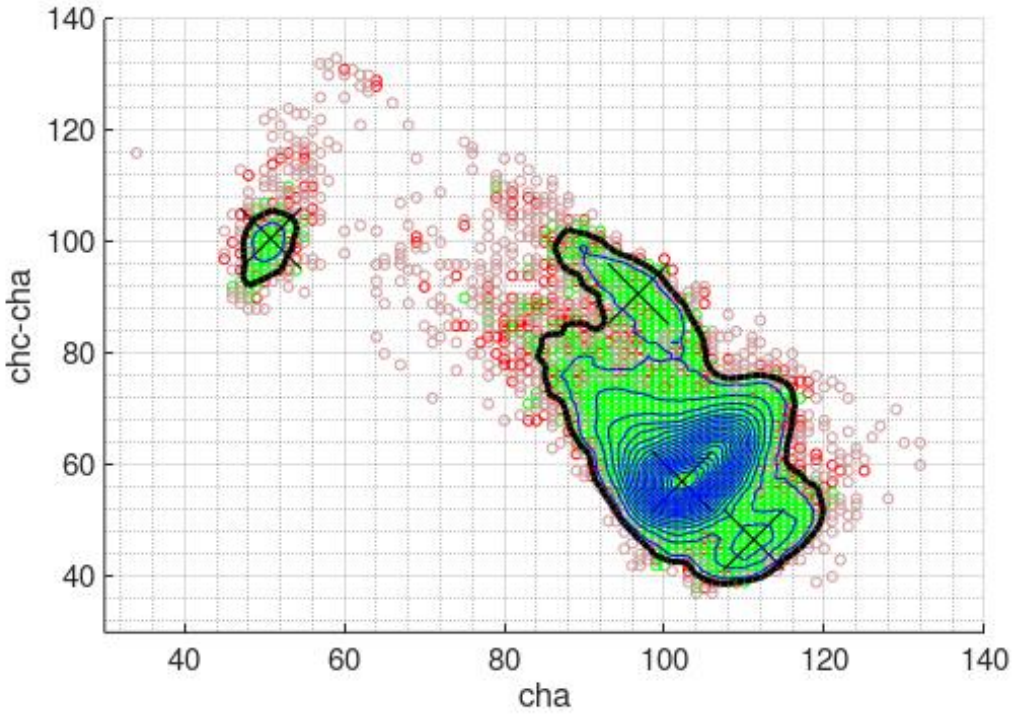

Figure 1. Two-dimensional presentation of 15000 single glow curves with respect to two GC parameters (cha, chc) and its categorization (green and red)

Conclusion The described procedure allows to tag GCs in an automatic way and find possible irregular GCs. The algorithm can be routinely used for quality control measures in individual monitoring services.

References

1. H. Stadtmann, C. Hranitzky, and N. Brasik: *Study of real time temperature profiles in routine TLD read out—influences of detector thickness and heating rate on glow curve shape*. Radiat Prot Dosimetry. 119 (1-4): 310-313, **2006**
2. H. Stadtmann, A. Delgado, and J. M. Gómez-Ros: *Study of Real Heating Profiles in Routine TLD Readout: Influences of Temperature Lags and Non-linearities in the Heating Profiles on the Glow Curve Shape*. Radiat Prot Dosimetry () 101 (1-4): 141-144. **2002**

Evaluation of dead-layer thickness of SSD for SHE research

Hayato Numakura[1]*, Fumiko Horikawa[2], Kouji Morimoto[3], Satoshi Ishizawa[1,3], Mirei Takeyama[2], Fuyuki Tokanai[2]

[1]*Graduate School of Science and Engineering, Yamagata University, Yamagata, Japan*

[2]*Fuculty of Science, Yamagata University, Yamagata, Japan*

[3]*RIKEN Nishina Center for Accelerator-Based Science, Saitama, Japan*

Highlights The precise energy measurement of an α particle using a silicon semiconductor detector (SSD) is very important to identify whether the α particle is emitted through the decay chain of superheavy elements (SHEs) with atomic numbers Z>103. The measurement of the total kinetic energy (TKE) of fission fragments generated through the decay of SHEs is also reliable because a high TKE indicates that fission occurred from a very heavy nucleus. It is necessary to evaluate the dead-layer thickness of the SSD to correct the measured energy to the initial energy of an α particle or the TKE of the fission fragment. To evaluate the dead-layer thicknesses of SSDs, energy spectra were first investigated using ^{241}Am by irradiating α-rays at incident angles of 0, 25, and 45° for three types of SSD. The dead-layer thicknesses of the SSDs were deduced by comparing the peak shifts related to the incident angle of 0° with those obtained by a computer simulation using the particle and heavy ion transport code system (PHITS).

Key words dead-layer thickness, silicon semiconductor detector, superheavy element

Background and Objectives The elements with atomic numbers Z>103 are called superheavy elements (SHEs). Nihonium (Nh, Z=113) has been successfully synthesized and studied by a cold fusion reaction using a gas-filled recoil ion separator (GARIS) at RIKEN[1)]. Following its successful synthesis, a search for a new element with Z=119 using actinide-based fusion reactions (hot fusion) has been started using GARIS-II at RIKEN. As shown in Fig. 1, a silicon semiconductor detector (SSD) box (Si box) was installed at the focal platen of the GARIS as one of the detection systems together with time-of-flight (TOF) detectors. The Si box consists of five

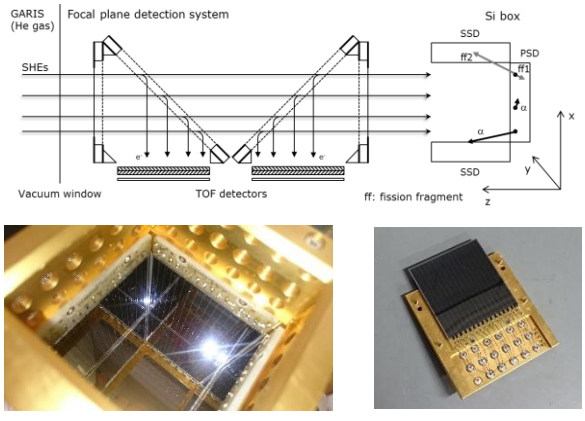

Fig. 1. Schematic side view of GARIS focal plane detection system. The Si box consists of five identical SSDs. One of the SSDs facing incoming SHEs is position-sensitive with 16 strips.

SSDs. One of the SSDs faces the direction of incoming SHEs and is used as a position-sensitive detector (PSD). The produced SHE is implanted into the PSD, where information on the SHE and its subsequent α-decay and/or spontaneous fission (SF) is obtained. The α particle or fission fragment emitted at backward angles relative to the PSD is detected by the four other SSDs or escapes from the Si box. As mentioned in Highlights, the evaluation of the dead-layer thickness of SSDs is important to precisely measure the energy of charged particles emitted from the PSD.

Materials and Methods The dead-layer thickness of an SSD can be estimated by determining the relationship between the measured energy E and the incident angle θ of α-rays. The relationship can be written by the following equation:

$$E = E_0 - \frac{dE}{dx} \times \frac{h}{\cos\theta} \quad , \qquad (1)$$

where E_0 is the initial energy of the α particle, dE/dx is the stopping power, and h is the dead-layer thickness. To evaluate the dead-layer thickness of an SSD, the energy spectra were first investigated using ^{241}Am by irradiating α-rays at incident angles of 0, 25, and 45°. Three types of SSD were used for the measurements. Two of them were newly developed by Hamamatsu Photonics Co., Ltd., and other was CANBERRA PIPS.

Results and Discussion Fig. 2 shows the energy spectra obtained using the SSD of Hamamatsu Photonics at the incident angles of 0, 25, and 45°. The peak channel is shifted to a lower channel with increasing incident angle. In the experiment, the α-rays enter into the SSD at the incident angle θ with a certain spread $\delta\theta$. In addition, since dE/dx is a function of energy, the measured energy E does not have a constant value for the measurement. Thus, the dead-layer thickness was deduced by comparing the shifts with those obtained by the PHITS simulation[2]. A dead-layer thickness of approximately 250 nm was determined from the above analysis.

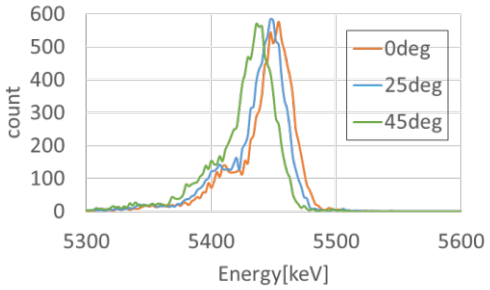

Fig. 2. Energy spectra of α-rays from a ^{241}Am.

Conclusion In this conference, we will present the evaluation of the dead-layer thickness of several SSDs for the study of SHEs.

References

1) K. Morita et al., J. Phys. Soc. Jpn. 73 (2004) 2593
2) T. Sato et al., J. Nucl. Sci. Technol. 55 (2018) 684

Uncertainties due to the body size for the radioiodine measurements using a newly developed thyroid monitor

Hiroshi Yoshitomi[1]*, Sho Nishino[1], Yoshihiko Tanimura[1], Masa Takahashi[1]
[1]*Japan Atomic Energy Agency, Ibaraki, Japan*

Highlights The effect of the body size on the detection efficiency of a newly developed thyroid monitor was estimated by Monte Carlo simulations using several voxel phantoms. The discrepancy from the efficiency in calibration was found to be 30 % at the maximum.

Key words thyroid monitor, voxel phantom, spectrometer

Background and Objectives In case of a nuclear reactor accident, a large amount of radioiodine, mostly ^{131}I, can be released in the environment, which causes internal exposure both to the members of the public and to the emergency workers. We have proposed a portable thyroid monitor using gamma-ray spectrometers with shielding[1)] for assessing the thyroid dose in such a situation. Although this monitor will be properly calibrated, any differences between the phantoms used in calibration and the monitored subjects can affect the accuracy of the measurement. This study aims to investigate the influence of the anatomical features of the subjects on the detection efficiency.

Materials and Methods The proposed thyroid monitor including two $LaBr_3$(Ce) detectors was precisely modelled for the simulations (Figure 1). To mimic the wide variety of subjects, eight different voxel phantoms (ICRP AM[2)], ICRP AF[2)], Otoko[3)], Onago[4)], JM-103[5),6)], JF-103[5),6)], CHILD[7)] and BABYNEW[7)]) were used. For more detailed investigation of the difference among individuals, the JF-103, CHILD and BABYNEW phantoms were also modified to vary thyroid volume and the thickness of the overlying tissue. All the simulations were performed using the Monte Carlo code, PHITS 2.8.8. The detection efficiency was obtained from the calculated 365 keV peak counts of two $LaBr_3$(Ce) detectors, divided by the activity of ^{131}I uniformly distributed in thyroid gland

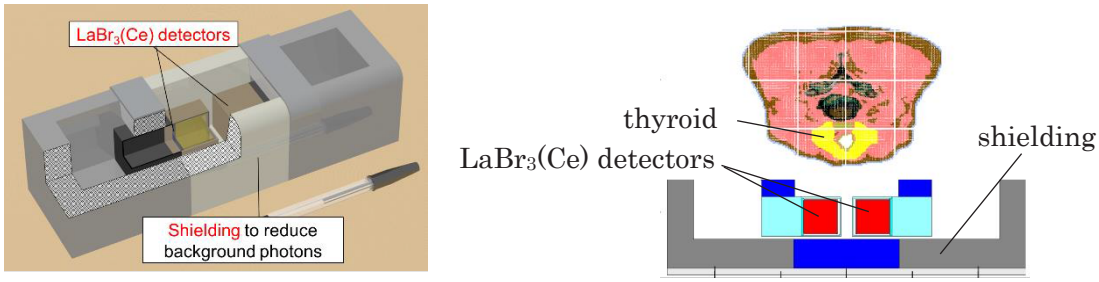

Figure 1. Illustration of the proposed thyroid monitor (left) and the cross-sectional view of the simulation model using JF-103 (right)

Results and Discussion This monitor is calibrated based on the voxel phantoms (ICRP AM, CHILD and BABAYNEW) using the representative point method with simplified physical phantoms[8]. Any differences between the phantom used in calibration and the monitored subject can cause uncertainty in the measurements. Thus, the influence on the results of the measurement should be assessed. Although anatomical features, such as the thyroid shape and the dimensions, between ICRP AM and another adult voxel phantom are different, the differences in efficiency were found to be within 24 % (Table 1). For JF-103 with high resolution and the smallest neck diameter, the thickness of overlying tissue (1.8-11.9 mm) or thyroid volume (6.7-29.0 cm^3) was varied, taking the normal range of their dimensions for the Japanese adult into account. Efficiency decreased with the thickness of overlying tissue but the difference in efficiency between ICRP AM and modified JF-103 was still within ±30 %. In contrast, no major difference was observed over the changes of the thyroid volume. Hence, thickness of overlying tissue is considered to be a major impact factor as changing source-to-detector distance. The effect of these factors on the measurement of the child or baby will be also discussed in the presentation.

Table 1. Characteristics of various adult voxel phantoms and calculated efficiencies

Voxel phantom	ICRP AM	ICRP AF	Otoko	Onago	JM-103	JF-103
Thyroid volume (cm^3)	19.2	16.3	9.5	5.5	19.1	16.0
Thickness of overlying tissue (mm)	8.5	10.6	15.9	8.0	12.0	1.8
Efficiency ($\times 10^{-3}$ cps/Bq)	6.86	7.76	5.68	7.72	6.71	8.48
(Difference)	-	(+13 %)	(-17 %)	(+12 %)	(-2 %)	(+24 %)

Conclusion The detection efficiency depends on the body size such as the thickness of overlying tissue, but the difference was found to be 30 % at most for the proposed configuration and calibration of the thyroid monitor.

Acknowledgement This work is supported by Grant from Nuclear Regulation Authority, JAPAN.

References

1) S. Nishino, *et.al.* European IRPA Congress 2018
2) ICRP Publication 110, Ann. ICRP 39(2), 1-164 (2009)
3) K. Saito, *et. al*. Radiat. Environ. Biophys., 40, 69-76 (2001)
4) K. Saito, *et. al*. Jpn. J. Health Phys., 43(2), 122-130 (2008)
5) K. Sato, *et. al.* JAEA-DATA/Code 2010-009
6) K. Sato, *et. al*. JAEA-DATA/Code 2011-013
7) N. Petoussi-Hens, *et.al.* Phys. Med. Biol., 47(1), 89-106 (2002)
8) H. Yoshitomi, *et. al*. AOCRP-5, PP28 (2018)

Basic Study of Effective Energy Measurements Method using Stacked Thermoluminescence Dosimeters

Hitomi Takagi[1], Shin Yanagisawa[1], Yusuke Koba[2], Kiyomitsu Shinsho[1]

[1]*Tokyo Metropolitan University, Tokyo, Japan*
[2]*National Institute of Radiological Sciences, Chiba, Japan*

Highlights We studied a new effective energy measurement method using stacked thermoluminescence dosimeters (TLDs). We were able to obtain the decay curves through analyzing the relationship between the absorber depth and the absorbed dose, because the stacked small TLD plates have two functions as an absorber and a dosimeter. Given the importance of calculating the effective energies, the further study of this method would be of value to the field of radiation exposure dose management.

Key words TLD, energy dependence, Monte Carlo

Background and Objectives Interventional radiology delivers high radiation doses to interventional staff. Recently, we focused on the occupational dose to the lens of the eye, because the epidemiological studies clarified that radiation-induced cataract has been observed at a lower dose threshold than previously considered by ICRP 103. So, it has become more necessary to manage the occupational dose to the lens of the eye. 3-mm dose equivalent (Hp(3)) is the personal dose equivalent at a depth of 3mm in soft tissue and is used for measuring the lens dose. In this measurement, dose equivalent conversion factors are used and they depend on incident photon energy. However, to measure the energy is difficult technically, so new measurement methods have been required. We considered that we could calculate the incident photon energy from the absorbed dose ratio of each element by using a stack of TLDs. Therefore, we investigated the absorbed dose of stacked TLDs by simulations.

Materials and Methods In Monte Carlo simulations, Particle and Heavy Ion Transport Code System (PHITS) Version 3.01 was used. [1)] The TL materials used were Cr doped Al_2O_3 and ^7LiF. The Cr doped Al_2O_3 TLD was composed of Al_2O_3(>99.5wt%) and Cr_2O_3(0.05wt%); The Effective atomic number (Z_{eff}) of Cr doped Al_2O_3 is 11.14 and the density is 3.70 g/cm^3. Z_{eff} of ^7LiF is 8.20 and the density is 2.64 g/cm^3. The geometry of the simulations is shown in Fig. 1. Three TLDs were stacked. The size of a TLD is φ3.0 mm and the thickness is 0.7

mm. The sources were 30, 40, 60, 80, 120 and 662 keV mono energy photons. Cutoff energy was 1 keV. The statistics errors were 1% or less. The absorbed doses for each TLD were calculated.

Results and Discussion Figure 2 shows the relationship between the absorbed dose ratio (D_1 / D_2) and the incident energy of Cr doped Al_2O_3. The ratio (D_1 / D_2) decreased with increasing incident photon energy. It considered that photons which transmitted element 1 increase as incident photon energy increases. Therefore the energy given to element 1 decreased. The ratio at 30 keV was 1.17 times higher than the ratio at 120 keV.

Conclusion The incident photon energy correlates with the absorbed dose of each element. Therefore, we can conclude that we can calculate approximate effective energy from a gained absorbed dose ratio. The further study of this method would be of value to the field of radiation exposure dose management.

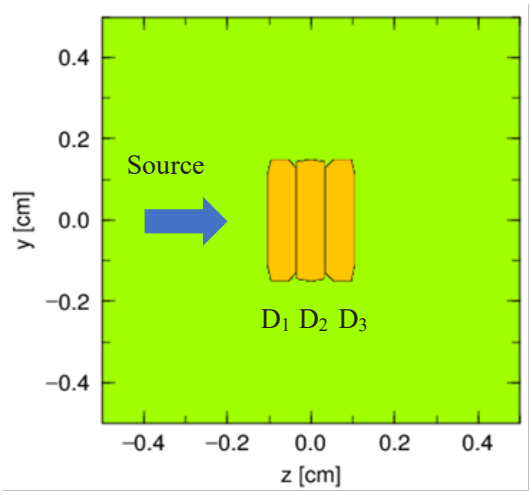

Fig. 1 Geometry of the calculations

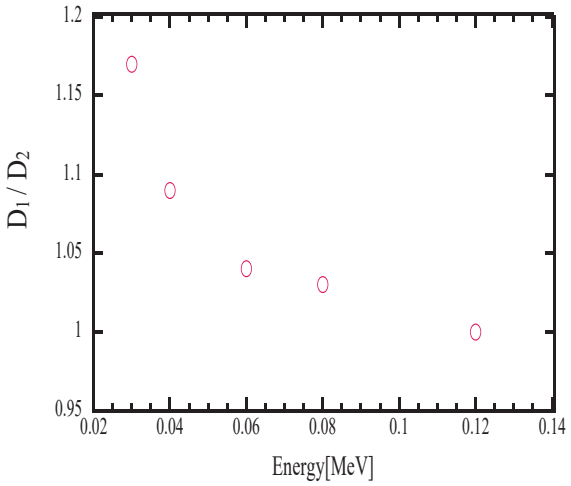

Fig. 2 The relationship between the absorbed dose ratio (D_1 / D_2) and the incident photon energy of Cr doped Al_2O_3

References

1) T. Sato, et al., Particle and Heavy Ion Transport Code System, PHITS, Version 2.52, J. Nucl. Sci. Technol., 50:9, 913–923, 2013.

X-ray-, heavy-particle-, or neutron-induced thermoluminescence of Tb^{3+}- or Dy^{3+}-doped $CaO–Al_2O_3–B_2O_3$-based glasses

Ichiro Kawamura[1*], Hiroki Kawamoto[1], Yutaka Fujimoto[1], Masanori Koshimizu[1], Go Okada[2], Yusuke Koba[4], Ryo Ogawara[4], Takayuki Yanagida[3], Keisuke Asai[1],

[1] *Tohoku University, Miyagi, Japan*

[2] *Kanazawa Institute of Technology, Ishikawa, Japan*

[3] *Nara Institute of Science and Technology, Nara, Japan*

[4] *National Institutes for Quantum and Radiological Science and Technology*

Highlights In this study, Tb^{3+}- or Dy^{3+}-doped $CaO–Al_2O_3–B_2O_3$ glasses were prepared with ^{n}B, ^{10}B, and ^{11}B, and thermoluminescence (TL) properties irradiated with X-ray, heavy particles, or neutron were investigated. X-ray- or heavy-particles-induced TL properties of ^{10}B glass was similar to that of ^{n}B or ^{11}B glass, but neutron-induced TL properties of ^{10}B was not similar to that of ^{11}B glass.

Key words neutron, glass, $CaO–Al_2O_3–B_2O_3$, thermoluminescence, $^{10}B(n,\alpha)^{7}Li$

Background and Objectives Borate-based glass with ^{10}B used for window glass of a nuclear reactor facility. ^{10}B has a large reaction cross-section to thermal neutrons and is excellent in neutron capture ability. When ^{10}B absorbs neutron, α particles (He ions), ^{7}Li, and γ-ray are emitted ($^{10}B(n,\alpha)^{7}Li$ reaction). We intend to develop a new neutron dosimeter material by using this property. We previously investigated TL properties of Tb^{3+}-doped $CaO–Al_2O_3–B_2O_3$-based glass irradiated with X-ray and reported that this glass shows good response to X-ray[1)]. In this study, we fabricated Tb^{3+}- or Dy^{3+}-doped glasses using ^{n}B, ^{10}B, and ^{11}B, and investigated TL properties after irradiation with X-ray, heavy particles, or neutron.

Materials and Methods Glasses were prepared according to a conventional melt quenching method using an alumina crucible at atmospheric pressure in air. High purity $CaCO_3$ (4N), H_3BO_3 (4N), Al_2O_3 (4N), Tb_4O_7 (3N), and Dy_2O_3 (3N) powders were used as starting materials. The concentration of rare-earth-dopants was 1.0–5.0 mol%. The mixture in the alumina cubicle was melted at 1100°C for 20 min and quenched to room temperature. ^{10}B glass and ^{11}B glass fabricated in the same way with $H_3{}^{10}BO_3$ and $H_3{}^{11}BO_3$. These glasses were irradiated with X-ray (our laboratory), heavy particles (HIMAC) or neutrons (NASBEE) and measured TL photons (the range of 300–700 K, the heating rate of 0.5 or 1.0 K/s).

Results and Discussion Figure 1 shows TL grow curves of Tb^{3+}-doped ^{10}B glass and ^{n}B glass irradiated with X-ray. In both glasses, TL peaks were observed at 380 K. This result suggests X-ray-induced TL of ^{10}B glass is similar to that of ^{n}B glass, and it is expected that γ-ray induce TL of them.

Figure 2 shows TL grow curves of Dy^{3+}-doped ^{10}B glass and ^{11}B glass irradiated with α-ray. In both glasses, TL peaks were observed at 390 K. This result suggests α-ray-induced TL of ^{10}B glass is similar to that of ^{11}B glass.

Figure 3 shows TL grow curves of Tb^{3+}-doped ^{10}B glass and ^{11}B glass irradiated with neutron. TL intensity of ^{10}B glass was much greater than that of ^{11}B glass (8 times at 414 K and 26 times at 549 K). This result suggests that α-ray and γ-ray from ^{10}B (n,α) reaction induced TL of ^{10}B glass.

Figure 4 shows TL grow curves induced by α-ray and γ-ray from ^{10}B(n,α) reaction. These data are obtained by subtracting TL of ^{11}B glass from that of ^{10}B glass after neutron irradiation. TL intensity increased as the irradiation increased. This result suggests this glass can be applied to a new neutron dosimeter.

Conclusion TL properties of Tb^{3+}- or Dy^{3+}-doped $CaO–Al_2O_3–B_2O_3$ glasses with ^{n}B, ^{10}B, and ^{11}B irradiated with X-ray, heavy particles, or neutron were investigated. X-ray- or heavy-particles-induced TL properties of ^{10}B glass was similar to that of ^{n}B or ^{11}B glass, but neutron-induced TL properties of ^{10}B glass was not similar to that of ^{11}B glass. This glass has is expected to be applied a new neutron dosimeter.

References

1) H. Ohno et al., *Opt. Mater.*, in press.

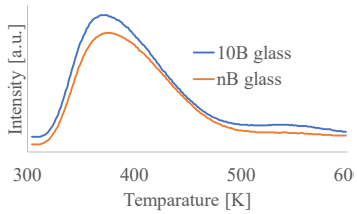

Fig. 1. TL grow curves of Tb^{3+}-doped glasses irradiated with X-ray (1 Gy).

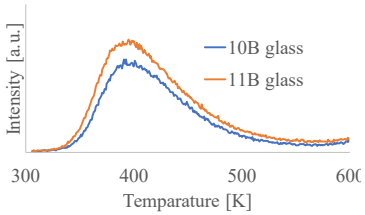

Fig. 2. TL grow curves of Dy^{3+}-doped glasses irradiated with 150 MeV/n He ion (10 Gy).

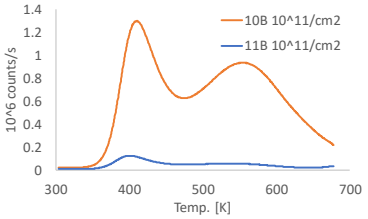

Fig. 3. TL grow curves of Tb^{3+}-doped glasses irradiated with neutron (10^{11} neutrons/cm^2).

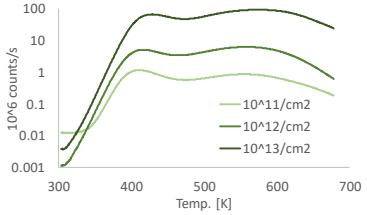

Fig. 4. TL grow curves induced by α-ray and γ-ray from ^{10}B(n,α) reaction (10^{11}, 10^{12}, or 10^{13} neutrons/cm^2).

scCVD diamond membranes for microdosimetry in particle therapy

I. A. Zahradnik[1]*, J. Davis[2], J. Vohradsky[2], Z. Pastuovic[3], D. A. Prokopovich[2,3], P. Barberet[4], S. Saada[1], D. Tromson[1], L. De Marzi[5], M. T. Pomorski[1], A. B. Rosenfeld[2]

[1]CEA-LIST, LCD and LCAE, Diamond Sensors Laboratory, 91191, Gif-sur-Yvette, France
[2]CMRP, Centre of Medical Radiation Physics, University of Wollongong, Australia
[3]ANSTO, Centre Accelerator Science and Nuclear Stewardship, Lucas Heights, Australia
[4]CNRS, CENBG, Chemin du Solarium, 33175 Gradignan, France
[5]Institut Curie, CPO, Centre de Protonthérapie d'Orsay, 91400, Orsay, France

Highlights The DIAμDOS guard-ring microdosimeter prototypes have been fabricated at the Diamond Sensor Laboratory of the CEA in France. The characterization of the diamond detectors has been performed with the use of ion microbeam facilities at AIFIRA in France and ANSTO in Australia. The DIAμDOS detector has been evaluated by means of experimental measurements at CPO in France and experimental results supported by GEANT4[1)] simulations.

Key words CVD diamond membranes, microdosimetry, particle therapy, GEANT4, IBIC

Background and Objectives Particle therapy enables tumors cells to be more effectively destroyed than conventional therapy with photons. In microdosimetry, precise measurements of the lineal energy of particles are used to predict the relative biological effectiveness (RBE) of clinical beams. This motivates the development of a novel type of solid-state tissue-equivalent diamond microdosimeter to obtain a state-of-the-art tool for measurements in clinical conditions.

Materials and Methods The DIAμDOS guard-ring microdosimeter prototypes are based on thin scCVD diamond membranes. These membranes of less than 10 μm thickness were obtained by using techniques described in [2)]. On the top side of the diamond, using photolithography followed by a chemical wet etch process, multiple μSVs have been formed (Figure 1a).

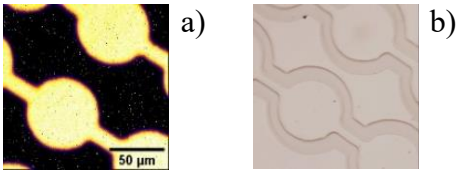

Figure 1. a) Response of diamond microdosimeter to a raster scan at -20 V bias with a 2 MeV p microbeam b) microscope image of the exact same spatial region.

The responses of the diamond detectors to single projectiles have been investigated with the IBIC technique. The active µSVs were irradiated using a raster scanning method and the CCE, radiation hardness, the µSVs spatial definition and pulse-height spectra measured. A Geant4[1), 3)] simulation was developed for this study to calculate the energy deposition distributions of clinical proton beams within the diamond microdosimeter.

Results and Discussion

The IBIC results confirm the isolation of charge collection within the µSV regions and its linear response to a wide range of ions and thus applicability for microdosimetry (Figure 1b & 2a). Preliminary simulations with proton beams have shown typically expected characteristics of a 100 MeV therapeutic proton beam (Figure 2b), such as an increase in lineal energy at higher energies and thus higher RBE values in the distal part for the Bragg peak (inset).

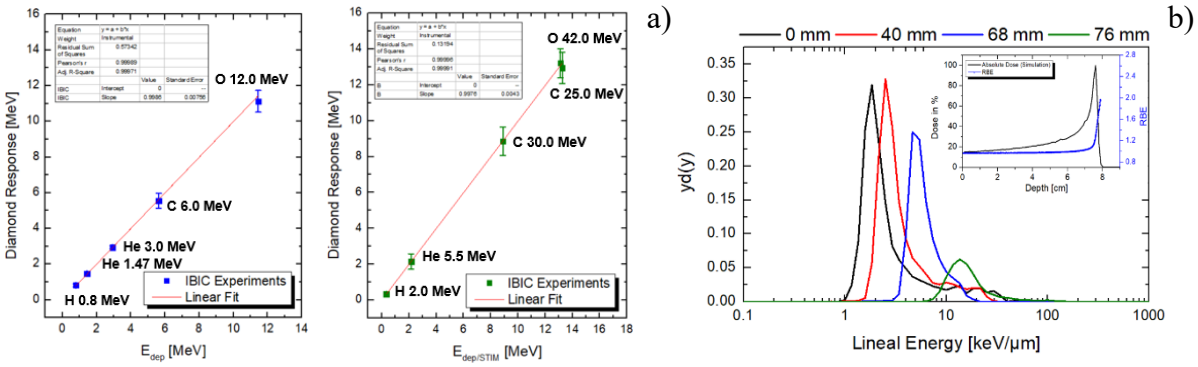

Figure 2. a) Linear response of the DIAµDOS guard-ring detector for stopping (left) and crossing (right) particles. b) GEANT4 simulation of microdosimetric spectra for 100 MeV proton beam in different depths (inset: depth-dose distribution and RBE distribution based on the simulated microdosimetric spectra).

Conclusion These results show a similar behavior of the scCVD diamond membrane based microdosimeters as for known measurements obtained from TEPC[4)] and silicon microdosimeters[5)], which demonstrates the great potential of DIAµDOS guard-ring for microdosimetry and finally its ability to measure microdosimetric quantities in clinical ion beams.

References

1) S. Agostinelli et al., *Nucl. Instrum. Methods B.* **2003**, 506,250.
2) I. A. Zahradnik et al., *Phys. Status Solidi A*. **2018**, 215, 22.
3) J. Davis et al., *IEEE Trans. Nucl. Sci.***2014**, 61, 1544.
4) M. Farahmand et al., *Nu. Ins. Met. Ph. Res. A.* **2003**, 509, 262.
5) A. Rozenfeld, *U.S. Patent No. 8421022 B2.* **2006**.

Thickness correction of an Alanine/EPR dosimeter response in a 40kV x-ray beam

Jakob G. Hjørringgaard[1]*, Arne Miller[1], Christina Ankjærgaard[1], Mark Bailey[1]
[1]*Center for Nuclear Technologies, Technical University of Denmark, Roskilde, Denmark*

Highlights The response to dose of commonly used solid state dosimeters show a strong energy dependence in the low energy range. Here we explore the alanine/EPR response to dose-to-water for a low filtered 40kV x-ray beam, and correct for the dose gradient within the 2.7mm thick dosimeter.

Key words dosimetry, low energy x-rays, alanine, EPR

Background and Objectives The use of low energy x-radiation in both the health sector and the industry requires improvements on transferable dosimetry systems. This issue is further complicated by the energy dependence in the most commonly used solid-state dosimeters e.g. alanine pellets. Here we investigate the effect of dosimeter geometry in establishing the alanine/EPR dosimeter response to dose to water in a 40kV x-ray beam.

Materials and Methods A 50kV 1mA VF-50J tube (Varian Medical Systems)[1)] with a reflective tungsten target was used for irradiations of dosimeters. This tube has a very low inherent filtration and thus the beam quality is characterized by a low half-value layer (HVL) in aluminum of 0.077mm. The spectral distribution of the x-ray beam has been calculated using the EGSnrc Monte Carlo (MC) code[2)] and validated by HVL measurements. A PTW 23344 parallel plate ionization chamber placed at the surface of a designated PMMA phantom is used to measure the absorbed dose to water. The alanine pellets are placed in a cavity of a PMMA slab to mimic the ion chamber geometry. The EPR signal of the irradiated pellets is measured on a Bruker EMX spectrometer.

Results and Discussion Figure 1 shows the response curves of the alanine/EPR dosimeter to dose to water. From the ratio of the slopes we obtain a reduction of ~65% in dose-to-water response for the 40kV x-ray beam compared to a cobalt-60 source, while data from the literature suggest a ~34% decrease for a 40kV beam[3)]. MC calculations of the depth-dose distribution in the dosimeter volume show a decrease of approximately 75% through the 2.7 mm thickness of the dosimeter. A correction for this thickness effect is sought by calculating the ratio of the accumulated dose in the pellet to the accumulated dose assuming uniform dose distribution

normalized to the surface value. Applying this correction factor of 1.92 to measured response (see Figure 1) results in a 32% decrease, similar to the literature value.

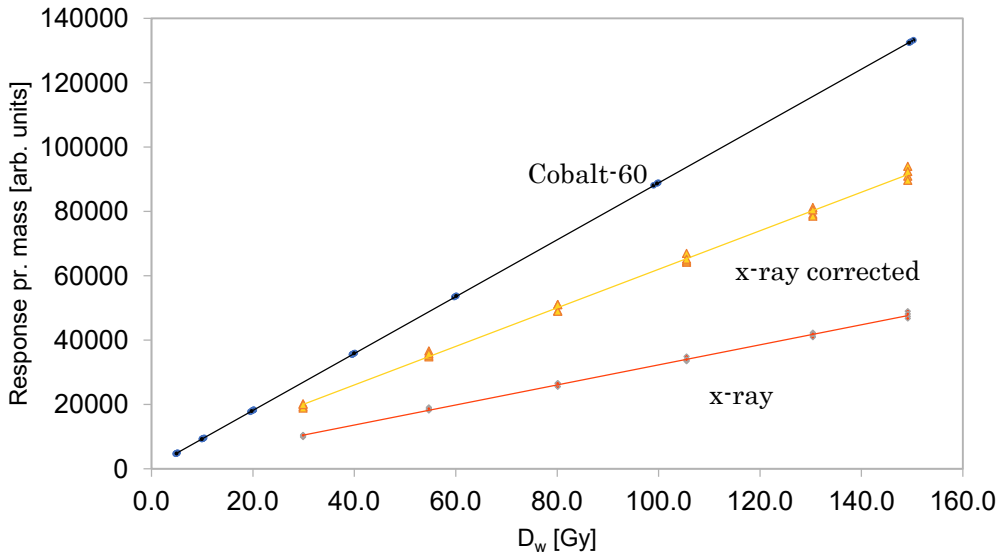

Figure 1. Response curve of the alanine/EPR dosimeter for cobalt-60 (black), 40kV x-rays (red) and geometrically corrected response to 40kV x-rays (yellow).

Conclusion The alanine/EPR response to dose-to-water was investigated for a 40kV x-ray tube with low inherent filtration. Because of a large dose gradient within the dosimeter volume a correction to uniform dose distribution was applied resulting in a decrease in response, when compared to cobalt-60, that is similar to published data. Further work includes investigations on the alanine/EPR response, and geometrical correction, dependence on characterizing factors of the beam (e.g. peak energy and HVL).

References

1) Andersen, C.E., Bøtter-Jensen, L., Murray, A.S., A mini X-ray generator as an alternative to a 90Sr/90Y beta source in luminescence dating. Radiation Measurements 37 (2003) 557–561.
2) Kawrakow, I., Mainegra-Hing, E., Rogers, D.W.O., Tessier, F., Walters, B.R.B., The EGSnrc Code System: Monte Carlo simulation of electron and photon transport. Technical Report PIRS-701, National Research Counsil Canada (2017).
3) Anton, M., & Büermann, L. (2015). Relative response of the alanine dosimeter to medium energy x-rays. Physics in Medicine and Biology 60 (15), 6113-6129.

An Inter-comparison of Personal Electronic Dosimeters Used in Canadian Nuclear Industry

Jason Sun[1]*, Neil Leroux[1]
[1] *Canadian Nuclear Laboratories, Chalk River, Canada*

Highlights An inter-comparison of personal electronic dosimeters used by various nuclear facilities was performed. The overall results suggest that these active dosimeters have achieved the same dose responses as those passive dosimeters at each facility for legal dose records.

Key words nuclear industry, personal electronic dosimeters, inter-comparison

Background and Objectives Personal electronic dosimeters are commonly referred to as personal alarming dosimeters (PADs) in Canadian nuclear industry. Since PADs provide dose and dose-rate readings instantly, they are widely used for dose control purposes in radiation research laboratories and nuclear power plants. PADs usually have lower detection limits, provide audible alarms, and can transfer dose data easily over computer networks. In Canada, like in many other countries, so far only passive dosimeters, e.g., thermoluminescent dosimeters (TLDs), are considered as qualified legal dosimeters. On the other hand, the latest technological development in PADs demonstrates that many active dosimeters can be as reliable, and as accurate, as those passive dosimeters. For convenience and efficiency, there is a hope in Canadian nuclear industry that readings from PADs could also be used as legal dose records, as long as these dosimeters pass the required tests, established by the Canadian Nuclear Safety Commission (CNSC), in its S-106 (R1) Standard[1)].

Materials and Methods As a pilot project, funded by the CANDU Owners Group (COG), an inter-comparison of PADs used by various nuclear facilities was recently performed. The same irradiation protocol and passing criteria, used for the annual COG whole-body TLD inter-comparison, were applied in the evaluation of PADs' responses in terms of the personal dose equivalents, $H_p(10)$ and $H_p(0.07)$. The irradiation to the sample PADs was performed using 33, 161, and 205 *keV* (mean energy) Narrow-spectrum series X-rays, ^{60}Co and ^{137}Cs gamma rays, $^{90}Sr/^{90}Y$ and ^{85}Kr beta sources, as well as the mixtures of them. The delivered doses were randomly chosen in the industry-agreed ranges, covering daily operational situations. A slab phantom, constructed of polymethylmethacrylate (PMMA) walls and filled with water[2)], was placed behind the PADs for each irradiation. The condition of charged

particle equilibrium (CPE) at the dosimeter positions was maintained for the gamma irradiation.

Results and Discussion This presentation provides the details of the PAD inter-comparison study. The overall results, in terms of the Mean Bias and Standard Deviation for each test case, as adopted from the ANSI N13.11-2009 Standard[3)], clearly suggest that these sample PADs have achieved the same dose responses as those TLDs used at each facility.

Conclusion The results from this work would lead to the first step towards the legalization of personal electronic dosimeters in Canada.

References

1) CNSC S-106, Revision 1, Technical and Quality Assurance Requirements for Dosimetry Services, 2006.
2) ISO 4037-3, X and Gamma Reference Radiation for Calibrating Dosemeters and Doserate Meters and for Determining Their Response as a Function of Photon Energy—Part 3: Calibration of Area and Personal Dosemeters and the Measurement of Their Response as a Function of Energy and Angle of Incidence, 1999.
3) American National Standard for Dosimetry, N13.11, Personnel Dosimetry Performance Criteria for Testing, 2009.

Silicon based transmission detectors for real time beam monitoring and quality assurance of microbeam radiation therapy

J. A. Davis[1,2], A. Dipuglia[1], A. Cullen[1], J. Paino[1], S. Guatelli[1,2], M. Petasecca[1,2], A. B. Rosenfeld[1,2] and M. L. F. Lerch[1,2]

1. Centre for Medical Radiation Physics, University of Wollongong, Australia
2. Illawarra Health and Medical Research Institute, University of Wollongong, Australia

Highlights The transmission silicon strip detector is a dual purpose device capable of providing real time dosimetric data in addition to beam monitoring for rapid response in case of incident during treatment. The effect of a 375 μm thick transmission detector upon the depth dose response within solid water and a water tank was measured with a pinpoint ionisation chamber. The experimental results were found to be in agreement with Monte Carlo simulation results for three different beam filtration configurations corresponding to three different mean energies. The amount of perturbation (1-5%) of the beam due to the thick transmission detector directly corresponds to the mean energy and thus beam filtration used. Silicon based transmission detectors are deemed to be a suitable material of choice given accurate compensation of the known beam attenuation during the treatment planning.

Key words radiation, dosimetry, transmission, energy dependence, microbeam

Background and Objectives Typical Quality Assurance (QA) procedures in radiotherapy are reliant upon the assumed consistency in the beam conditions. For conventional radiotherapy fluctuations in photon fluence and spectra will likely have a negligible impact upon treatment delivery, however for microbeam radiation therapy, changes in the beam characteristics can have a huge impact upon treatment safety and efficacy[1)]. Transmission detectors are dual purpose dosimeters, allowing for real time QA in addition to monitoring beam characteristics and providing a mechanism for rapid response in case of undesirable scenarios. Previous investigations have focused upon the real-time capability of the transmission detector in measuring characteristics pertinent to MRT, i.e. microbeam full width half maximum[2,3)]. In this study, the effect of the transmission detector upon pre-treatment QA is investigated using a combination of experimental and simulation techniques.

Materials and Methods Experimental measurement were performed in Hutch 2B of the AS IMBL for a 3T wiggler field, and for three different filter configurations. In configuration one, the additional filtration is Cu/Cu (2.28mm Cu), whereas, configuration two, the additional filtration is Cu/Al (1.14 mm Cu/1.14mm Al) and finally configuration three, the additional filtration is Al/Al (2.28mm Al). The mean energy of the x-ray spectrum will change from ~40keV with Al/Al to ~95keV for Cu/Cu. Dose measurements are performed with a PTW PinPoint 31014 ionisation chamber (IC) in water tank with dimensions 200x200x140 mm^3 for broad beam measurements and the PTW microdiamond for microbeam measurements. A PTW UniDOS webline electrometer is used for readout of the integral dose after each translation of the detector through the field. The experimental set-up is modelled in its entirety with Geant4 to allow for a comparison of theoretical and experimental measurements. For brevity, only Geant4 results for the 3T Cu/Cu configuration (broad beam) with and without the 375 µm thick transmission detector will be presented here.

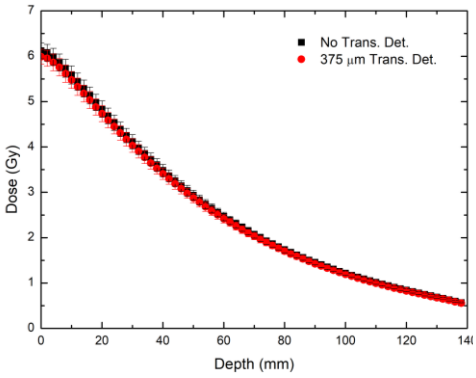

Figure 1- Geant4 simulation broad beam depth-dose response (left) and micro beam peak/valley depth dose response results (right) in 3T Cu/Cu mode with and without transmission detector.

Results and Discussion The depth dose simulation results in the 3T (Cu/Cu) configuration in the water tank is depicted in Figure 1. The results demonstrate an average decrease in dose due to the 375 µm thick transmission detector is (1.99 ± 0.14)%. Full simulation and experimental results will be presented at the SSD19 conference.

Conclusion Geant4 simulation predicts an average of (1.99 ± 0.14) % loss in response with depth. This is in reasonable agreement with the experimental results of was (1.40 ± 0.36) % as determined by the PinPoint IC.

References

1) E. Bräuer-Krisch, et al., Physica Medica, vol. 31, no. 6, pp. 568–583, 2015.
2) J. Kalliopuska, et al., Radiation Measurements, vol. 46, no. 12, pp. 1643–1645, 2011.
3) M. Povoli, et al., Journal of Instrumentation, vol. 10, no. 11, p. P11007, 2015.

Organic Semiconductors for Ionising Radiation Dosimetry

Jessie Posar[1], Jeremy Davis[1], Paul Sellin[2], Matthew Griffith[3], Olivier Dhez[4]
Michael Lerch[1], Anatoly Rosenfeld[1], Marco Petasecca[1]

[1]*University of Wollongong, Australia*

[2]*University of Surrey, UK*

[3]*University of Newcastle, Australia*

[4]*ISORG, 60 Rue des berges, Parc Polytec — Immeuble Tramontane, 38000 Grenoble, France*

Highlights The response of organic photodetectors for use in medical radiation therapy including, dose linearity, energy dependence and dose rate dependence, is characterised. Prior exposure to ionizing radiation (40kGy) increases device sensitivity.

Key words organic semiconductor, radiation, dosimetry.

Background and Objectives. The primary aim of this work is to demonstrate the feasibility of using organic semiconductor technology developed for large area photodetectors in the energy harvesting market for dosimetry in radiotherapy applications. Photodetectors based on organic semiconductors have recently gained momentum in the field of radiation detection due to their relatively inexpensive production costs and simple large area printing fabrication. Organic photodetectors are constructed of acceptor and donor materials, similar to many solid state detectors currently available and used in clinical practice [1]. The most common donor material for organic solar cells is the conjugated polymer poly(3-hexylthiophene) (P3HT) blended with fullerene derivative phenyl-C_{61}-butyric acid methyl ester (PCBM) as the acceptor [2], [3]. Their ability to be manufactured on flexible substrates and with materials that are tissue-equivalent are attractive properties that are presently not available in any real-time devices for ionising radiation dosimetry. Dosimeters for medical applications must withstand a minimal radiation dose of 500Gy/year, and also exhibit a reproducible measurement response [4]. In order to be able to assess the potential of this thin-film photodetector technology in the area of radiotherapy dose verification, we characterised the response to radiation under different clinically relevant conditions for commercial organic photodiode samples produced by ISORG (Grenoble – France) with an area of 1x1cm^2 and fabricated on a flexible PET substrate.

Materials and Methods. Samples were tested prior to and following irradiation up to a total dose of 40 kGy by a cobalt-60 gamma source (dose rate = 1.2 kGy/h). The OPDs response was tested by exposing the samples to ionizing radiation in two modalities: by direct interaction (radiation interacts with OPD substrates directly) and by indirect interaction (radiation is also converted into optical photons with a peak emission wavelength of 420nm by a plastic scintillator (BC400, Saint-Gobain Crystals)). Direct and indirect detection of high energy photons and electrons was tested at the Illawarra Cancer Care Centre at Wollongong Hospital in Australia using medical linear accelerator and X-ray tube (Philips RT 250). Two reverse bias configurations were set up to apply 0 or 2 V across the detector. Dose linearity measurements

were performed for both 6MV photons and 6MeV electrons at calibration conditions of source to surface distance (SSD) of 100cm and depth in a water equivalent plastic phantom of 1.5cm with a field size of 10x10 cm^2. The response of the detector, relative to an ionization chamber positioned in the calibration conditions, was tested under different irradiation dose rates by varying the source to surface distance from 90 cm up to 300 cm. Measurements with an Orthovoltage X-ray machine were conducted in order to broadly explore the energy dependence of the OPD in the incident photon energy range of 29.5keV to 129.4keV.

Results and Discussion Response of samples equipped with 2mm plastic scintillator or without scintillator were observed to be linear with both photon and electron beams from 25 to 500 Gy at 600MU/min. Unexpectedly, Co-60 pre-irradiated samples increase their response as a function of the total irradiation dose as shown in Fig.1b. Exposure to high doses seems to increase the conductivity of the organic compound allowing charge to flow more readily (Fig.1b). Fig.1c shows the dose rate dependence of samples measured both with (2mm) and without (0mm) a plastic scintillator. The different responses of these configurations suggests that direct interaction of ionizing radiation with the organic substrate produces a carrier transport mechanism which is intrinsically different from optical photons. This is also confirmed by the analysis of the temporal behavior of the device, where a "priming effect" has been observed in devices with direct radiation interaction.

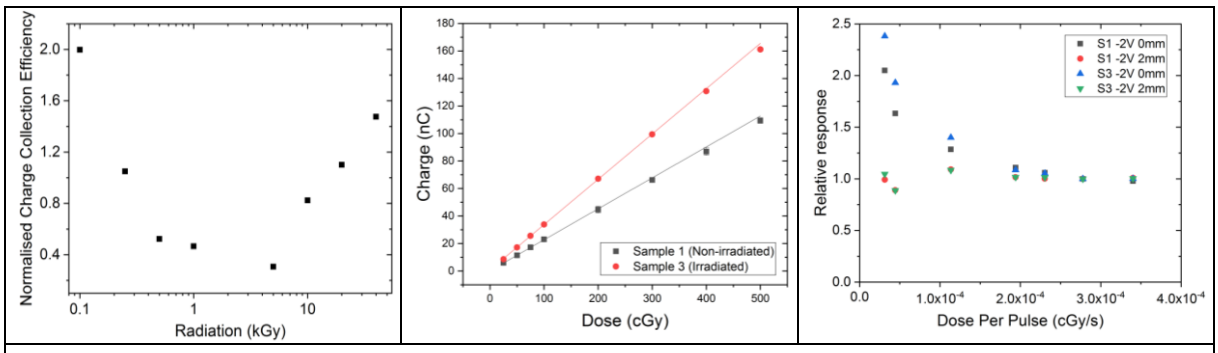

Fig.1. Example of a) the radiation hardness of OPDs (sample3) with 409nm, normalized before irradiation; b)Irradiation effect on linearity for indirect detection (2mm) and 0V ;c) Dose rate dependence of non-irradiated (sample1) and irradiated (sample3) device.

Conclusion The direct and indirect detection of ionizing radiation was measured for both pristine and pre-irradiated organic semiconductor photodetectors. Their linearity to both 6MV photons and 6MeV electrons, radiation hardness and dose rate dependence show that organic semiconductors are a promising candidate for fabrication of flexible, inexpensive and large area devices for ionizing radiation dosimetry.

References

[1] H. Kohler, Anna, Bassler, *Electronic Processes in Organic Semiconductors.* Wiley-VCH, 2015.

[2] B. C. Thompson and J. M. J. Fréchet, *Angew. Chemie Int. Ed.*, vol.47, no.1, pp.58–77, 2008.

[3] R. A. B. Devine, et al., *IEEE TNS*, vol.57, no. 6 PART 1, pp. 3109–3113, 2010.

[4] J. W. Kingsley, S. J. Weston, and D. G. Lidzey, *IEEE J. Sel. Top. Quantum Electron.*, vol. 16, no. 6, pp. 1770–1775, 2010.

A new readout system for radiophotoluminescent (RPL) glass dosimeters up to 1 MGy

J. Trummer[1, 2]*, H. Vincke[2]
[1]*Institute for Radiation Physics, Lausanne University Hospital, Lausanne, Switzerland*
[2]*CERN, Geneva, Switzerland*

Highlights A new RPL readout system has been developed to obtain dose in the range between 1 Gy and 1 MGy. The system combines the measurement of the emitted RPL light with a transmission measurement to cover the aforementioned dose range.

Keywords radiation, dosimetry, RPL glass, high dose readout system

Background and Objectives The High Level Dosimetry group at CERN, Geneva, Switzerland monitors the dose to equipment in the accelerator complex, mainly with RPL glass dosimeters. The annual cumulative absorbed doses encountered close to high-energy accelerators at CERN can reach levels up to MGy.
The RPL dosimeter is a small phosphate glass cylinder doped with silver. Electrons freed in the glass during irradiation, will form colour centres and well-defined luminescence centres.
During the dose readout process, the luminescence centres are excited with UV light which subsequently results in the emission of orange light. The creation of colour centres changes the colour of the glass from transparent to yellow, brown and finally almost black. Colour centres absorb some of the exciting UV as well as the emitted orange light. Due to the increased absorption of UV light and of emitted luminescence light, the dose-response function increases monotonically until a maximum and then decreases (Figure 2, blue diamonds). Conventional systems rely on the measurement of the emitted luminescence light and do not extend above 500 Gy. One readout value corresponds two dose values, one in the low and one in the high dose region. The maximum readout value lies at approximately 1 kGy.
The new readout system combines two measurements of different properties to determine the dose value unequivocally in the range from 1 Gy to 1 MGy. The second property analysed is the light transmission coefficient of the dosimeter as a function of dose received by the RPL dosimeter.

Materials and Methods The reader is configured to measure the light from the excited luminescence centres and to execute a light transmission measurement. The first light source is a high power UV-LED with a wavelength of 365 nm. It is used to excite the RPL light in the

dosimeter and irradiates the dosimeter perpendicular to its cylinder axis. The emitted orange RPL light is measured by a SiPD from above the dosimeter. A filter attached in front of the SiPD cuts off any light with a wavelength below 612 nm (orange light). The second light source is a high power LED with a blue wavelength of 440 nm. It is used for the transmission measurement. The light beam is directed along the cylindrical symmetry axis onto the front face of the cylinder. The attenuated light is measured at the cylinder's back face with a SiC photodiode (Figure 1). A ruby is used as a reference for machine stability. The dosimeters are FD7 glass rods (GD-301 model) from Chiyoda Technol, Japan.

A series of RPL was irradiated at Risø HDRL, Denmark and at BGS, Germany to predefined dose values and measured with the new system.

Results and Discussion The result of the measurement with the new system is shown in Figure 2. The result of the transmission measurement decides if the interpolation of the dose is done on the low dose or the high dose branch of the RPL light curve. In addition, the results of the transmission measurement are used to evaluate the dose value directly in the region of the maximum of the RPL light curve, where its uncertainty is very high. Daily measurements of the ruby rod and an aperture have determined the system to be stable. Room temperature was also varied between 17 °C and 27 °C. Fluctuations are less than 5%. Above 1 MGy the dose-response curves become very flat. Nevertheless a reasonable estimation of the dose can be given up to a range of several MGy.

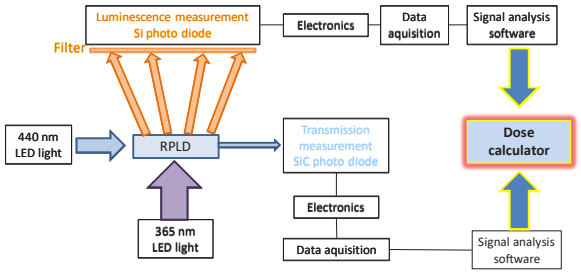

Figure 1. Schematic of the RPL readout system

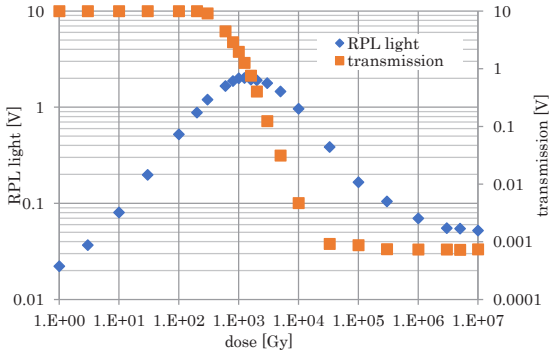

Figure 2. Dose-response curves for UV triggered RPL light emission (blue diamonds) and blue light transmission (orange squares)

Conclusion A new system to measure dose received by RPL glass dosimeters has been built and characterised. Through the combination of two measurements of two independent properties of the irradiated RPL dosimeter, it is possible to cover a dose range of 1 Gy to 1 MGy.

X-ray detection properties of heavy-metal-doped plastic scintillators synthesized by solvent evaporation

Kei Kagami[1]*, Masanori Koshimizu[1], Yutaka Fujimoto[1], Syunji Kishimoto[2], Rie Haruki[2], Fumihiko Nishikido[3], Keisuke Asai[1]

[1]*Tohoku University, Miyagi, Japan*

[2]*High Energy Accelerator Research Organization, Ibaraki, Japan*

[3]*National Institute of Radiological Science, National Institutes for Quantum and Radiological Science and Technology, Chiba, Japan*

Highlights

- Bismuth-doped plastic scintillators were successfully fabricated.
- The maximum value of detection efficiency is 2.3%.
- The time resolution hardly depends on the concentration of Bi, and has high values between ~0.2–0.3 ns.

Keywords plastic scintillator, heavy metal, bismuth

Background and Objectives Scintillation detectors are a category of X-ray detectors that have been applied in various fields, including high-energy physics, security, and medical care. With the advances in synchrotron technology, the development of X-ray measurement technology and insurance of detection efficiency toward high-energy X-rays is particularly necessary. Synchrotron radiation technology enables the generation of high-energy and high-brightness X-rays, offering the potential for further advances in science. However, these advantages have not been fully exploited due to the lack of a suitable detector. Herein, we report the development of a scintillation material based on a plastic material doped with heavy-metal nanoparticles that displays good capability for detecting high-energy X-rays. In general, plastic materials emit high time-resolution luminescence due to the emission of organic phosphor; however, their detection efficiencies are inferior due to the low atomic numbers of their constituent atoms. To overcome this hurdle, we doped nanoparticles of a Bi compound into the plastic matrix to increase the

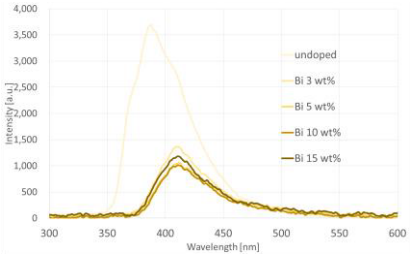

Fig.1 X-ray radioluminescence spectra.

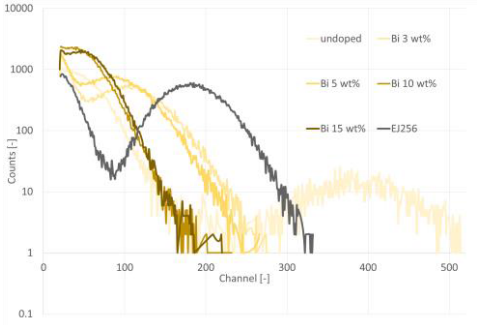

Fig.2 X-ray irradiated pulse height spectra.

detection efficiency for high-energy X-rays while maintaining good time-resolution luminescence. Thus, plastic scintillators with various concentrations of Bi were fabricated via solvent evaporation, and their scintillation properties were measured.

Materials and Methods

To fabricate the Bi-doped plastic scintillators, $BiCl_3$ was dissolved in a solvent mixture of HCl and methanol in a screw vial. Then, polystyrene and the organic phosphor, 2-(4-tert-butylphenyl)-5-(4-biphenylyl)-1,3,4-oxadiazole (b-PBD), were added to the solution. After stirring and completely dissolving all the compounds, samples were prepared after being kept at 57°C for about a week in a constant-temperature dryer. The organic phosphor, b-PBD, was added to the sample at a ratio of 1.0 mol% to the styrene monomer. The weight ratio of Bi to the total mass of the product was varied. The X-ray radioluminescence spectra, pulse height spectra, and time spectra under X-ray irradiation (67.4 keV) of the obtained samples were measured.

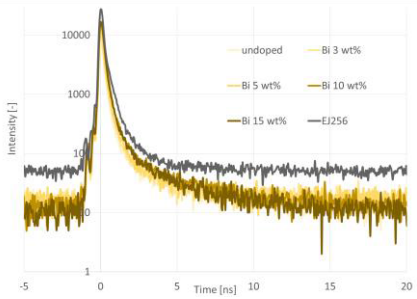

Fig.3 Time spectra.

Table.1 Detection efficiency for 1-mm thickness and time resolution of Bi-doped plastic scintillators.

Sample	Detection efficiency [%] for 1-mm thickness	Time resolution [ns]
none dope	1.7	0.3
3 wt%	2.0	0.2
5 wt%	2.3	0.3
10 wt%	2.3	0.3
15 wt%	2.3	0.3
EJ256	3.4	0.3

Results and Discussion Fig.1 shows the X-ray radioluminescence spectra of the Bi-doped samples. The spectra show broad emission bands that peak between 350 and 550 nm. The peaks of the spectra slightly shifted to the longer wavelength side as the concentration of Bi increased, which can be considered as Mie scattering. Table 1 shows the detection efficiency for 1-mm thickness, calculated using pulse height spectra (Fig.2), and the time resolution values of the Bi-doped samples, determined using the full width at half maximum values of the time spectra (Fig.3). The addition of Bi improved the detection efficiency; however, this quickly ceased due to a decrease in the light yields. The time resolution hardly depended on the concentration of heavy metals, and showed high values of 0.2 to 0.3 ns.

Growth and Scintillation Properties of Ce:$LaCl_3$/$AECl_2$ (AE=Mg, Ca and Sr) Eutectics for X-RAY Imaging Applications

Kei Kamada[1,2], Hiroyuki Chiba[3], Yasuhiro Shoji[2,3], Akihiri Yamaji[3], Shunsuke Kurosawa[1,3], Yuui Yokota[1],Yuji Ohashi[3], Akira Yoshikawa[1,2,3]

[1] *Tohoku University, New Industry Creation Hatchery Center, Sendai, Japan*

[2] *C&A corporation, Sendai, Japan*

[3] *Tohoku University, Institute for Material Reseach, Sendai, Japan*

Highlights Ce doped $LaCl_3$/$AECl_2$ (AE=Mg,Ca,Sr) system eutectics were explored. Ce:$LaCl_3$/$CaCl_2$ showed light output of 9,000 photon/MeV. Scintillation decay time of the Ce:$LaCl_3$/$CaCl_2$ was 26.8 ns (26%) 282 ns (74%).

Key words Scintillator, eutectic, halides, Ce^{3+}

Background and Objectives Scintillators coupled with photodetectors were widely used in radiation imaging applications such medical imaging, security, high energy physics, astrophysics, oil well logging, etc. Currently, submicron-diameter phase-separated scintillator fibers (PSSFs) were reported and they have both characteristics of optical fiber and a radiation-to-light conversion. The PSSFs were realized by a directionally solidified eutectic (DSE) growth in previous research [1]. In PSSFs, the emitted scintillation is confined and transported along the eutectic structure by a total reflection mode, so that light diffusion can be reduced and high-resolution imaging can be achieved. Up to now, research on PSSFs such GAP/α-Al_2O_3[2], and LiF/ CaF_2/$LiBaF_3$ [3] have been already reported by our group.

In order to find good combination of eutectic structure with PSSFs, choice of scintillator materials is important. Here, Ce:$LaCl_3$ scintillator has attracted attention due to its high light yield of over 50,000 photons/MeV and fast decay time of below 20 ns with enough density for low energy X-ray detection even it is hygroscopic[4]. In this research, exploration of PSSFs by directional crystal growth method will be reported. In this study, Ce doped $LaCl_3$/$AECl_2$(AE=Mg, Ca, Sr) eutectics were explored. Investigations of their crystal structure and eutectic phase were performed. Luminescence and scintillation properties were also evaluated.

Results and Discussion White rod with 4 mm diameter and 12-20 mm length was obtained by the BS method. As grown eutectic and 1 mm thick plate after polishing were shown in Fig. 1. The sample showed optical transparency like bundle optical fibers and the background line is visible on the surface through the transparent rods grown in the material. The BEI of the

grown crystals in vertical and transverse cross-section are shown in Fig. 2. The grown eutectic structure showed mixture of rods and plates shape of $LaCl_3$ phase surrounded by $MgCl_2$ and $CaCl_2$ matrix. In the case of $LaCl_3/SrCl_2$, Slorid solution of $(La,Sr)Cl_x$ was observed. Radioluminescence spectra of the grown Ce doped $LaCl_3$/ $AE(Cl,Br)_2$(AE=Mg, Ca, Sr) eutectic measured under X-ray irradiation was shown in Fig. 3. The expected 350 nm emission and 280 nm excitation of Ce^{3+} 4f5d transition have been observed. These results are good agreement of previous reports [4]. Details about eutectic structure, crystal phases, scintillation properties will be reported at my presentation.

Conclusion Ce doped $LaCl_3/AECl_2$ (AE=Mg,Ca,Sr) system eutectics were explored. In the case of AE=Mg,Ca, eutectic with PSSFs structures were observed. Grown eutectics showed 350 nm emission ascribed to Ce^{3+} 4f-5d transition. $Ce:LaCl_3/CaCl_2$ showed light output of 9,000 photon/MeV. Scintillation decay time of the $Ce:LaCl_3/CaCl_2$ was 26.8 ns (26%) 282 ns (74%).

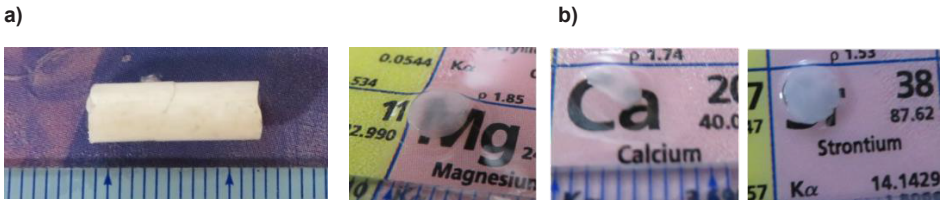

Fig. 3. Photograph of the a) as grown $Ce:LaCl_3/CaCl_2$ eutectic and b) polished sample along he cross section.

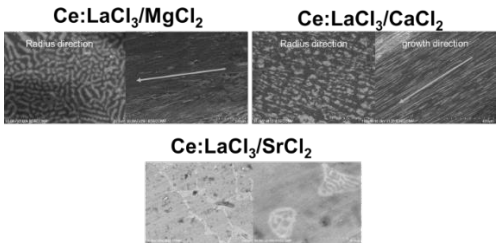

Fig. 2. BEI of the eutectic crystal in transverse cross-section and vertical cross-section.

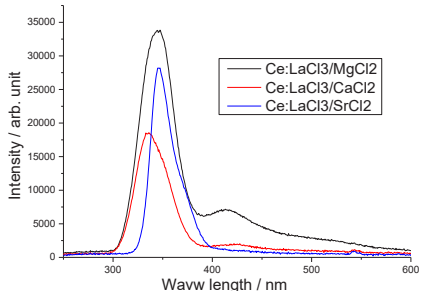

Fig. 2. Radioluminescence spectra of the grown eutectics

References

1) Y.Ohashi, A.Yoshikawa, Y.Yuui, A.Yoshikawa, T.Den, App. Phy. Lett. 102, (2013) 05197.
2) T. Den, T. Saito, R.Horie, Y.Ohashi, N.Yasui, IEEE Trans. Nucl. Sci., 60 (2013) 16.
3) K. Hishinuma Kosuke, K. Kamada, S. Kurosawa, A.kihiro Yamaji Y. Ohashi,, Y. Yokota, A. Yoshikawa, Jpn. J. Appl. Phys. 54 (2015) 04DH04
4) J. T. M. d. Haas and P. Dorenbos, *IEEE Trans Nucl Sci*, 55 (2008)1086-1092

A solid-state microdosimeter for RBE study of ion therapeutic beams and radiation protection for astronauts in space

L. T. Tran[*], *S. Peracchi*[1], *B. James*[1], *D. Bolst*[1], *D. A. Prokopovich*[1,2], *J. Davis*[1], *S. Guatelli*[1], *N. Matsufuji*[3], *A. Kok*[4], *M. Povoli*[4] *and A. B. Rosenfeld*[1].

[1] *Centre for Medical Radiation Physics, University of Wollongong, Australia.*
[2]*Australia's Nuclear Science and Technology Organisation, Lucas Heights, Australia.*
[3]*National Institute of Radiological Science, Japan.*
[4]*SINTEF MiNaLab, Gaustadalleen, Norway.*

Highlights This work studied the microdosimetric distributions and corresponding the relative biological effectiveness (RBE) of different ions, namely ^{12}C, ^{14}N and ^{16}O, using a silicon-on-insulator (SOI) microdosimeter with well-defined 3D sensitive volumes (SV). We demonstrated the possibility of using SOI microdosimeter for $\bar{Q}$ and $H_p(10)$ derivation in a radiation field mimicking Galactic Cosmic Rays outside and inside the International Space Station.

Key words: Heavy ions, cosmic radiation, microdosimetry, SOI, ISS

Background and Objectives: Particle therapy is particularly advantageous for the treatment of solid tumors compared to conventional electron and photon therapy due to a highly localized energy deposition. Heavier ions such as carbon, nitrogen and oxygen have further advantages over protons and lighter ions for treating deep-seated radio-resistant tumors due to an increased relative biological effectiveness (RBE) in the stopping region at the BP, while sparing the normal tissue surrounding the tumor. Heavy ions are also existing in space while space exploration is currently aiming to reach further destinations, increasing astronauts' exposure to hazardous radiation. The dose equivalent, H, is a quantity which expresses the probability that exposure to ionizing radiation will cause biological effects. It is obtained by multiplying the dose by the dose average quality factor, $\bar{Q}$, of the radiation.

Materials and Methods: Microdosimetry is a powerful approach for measuring dose mean lineal energy used to derive RBE as well as evaluate the $\bar{Q}$ of a mixed radiation field typical of space radiation, without knowledge of energy or type of particles. The silicon microdosimeters developed at the Centre for Medical Radiation Physics (CMRP), University of Wollongong provide extremely high spatial resolution and were used to evaluate the RBE of 290 MeV/u ^{12}C, 180 MeV/u ^{14}N and 400 MeV/u ^{16}O ions at Heavy Ion Medical Accelerator in Chiba (HIMAC), Japan as well as determine $\bar{Q}$ in 500 MeV/u Fe ions field upstream of the spacecraft wall. Irradiations were carried out at HIMAC using a beam of 290 MeV/u ^{12}C, 180 MeV/u ^{14}N, 400 MeV/u ^{16}O ions and 500 MeV/u ^{56}Fe. The experiment was performed in water phantom and a free air geometry using the MicroPlus probe with the Mushroom microdosimeter along the central axis of the beam, as shown in Figure 1. For free air geometry, a small 10 mm thick slab of PMMA was put in front of the probe to reproduce the scenario for the ambient dose equivalent Hp(10) estimation. The

spacecraft's wall was modelled with two Al slabs to mimic the radiation environment inside and outside the ISS [1]: the first slab of 7.3 mm represents the real aluminum pressurized shell of the ISS. The thicker slab of 35.95 mm includes an additional layer corresponding to several devices and structures inside the habitable volume of the ISS that provide a further barrier to particle's radiation.

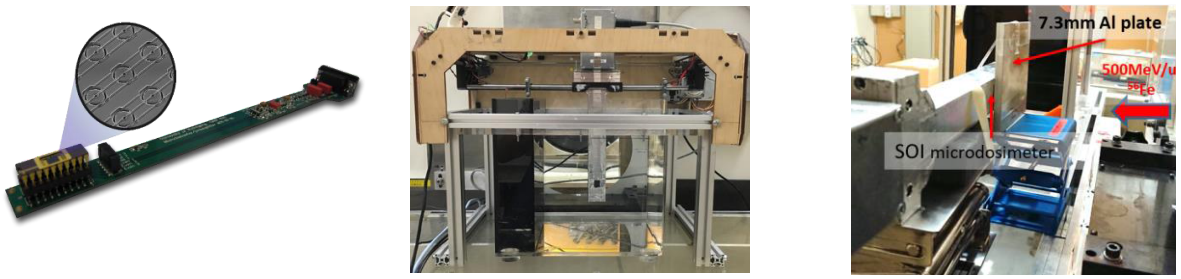

a) b) c)

Figure 1. a) MicroPlus probe connected to the SOI mushroom b) MicroPlus in water phantom c) Free air geometry with Al wall

Results and Discussions: Figure 2a shows the comparison of the Geant4 simulated and microdosimetric measurement based RBE_{10} for the 400 MeV/u ^{16}O beam. This demonstrates that maximum RBE_{10} of 2.94 for Oxygen ions ocurrs slightly earlier than the maximum physical dose. Fig. 2b shows tissue equivalent microdosimetric spectra measured with the 3D Mushroom SOI microdosimeter and their derived $\bar{Q}$ for 500 MeV/u ^{56}Fe ions. The microdosimetric spectrum measured behind 10 mm PMMA does not change significantly with 7.3 mm wall placed in front of the PMMA and it is determined mostly by primary ^{56}Fe ions. For an Al wall thickness of 35.95 mm, the primary ^{56}Fe ions are fully stopped and the radiation field inside of the spacecraft is determined by secondary fragments and neutrons originated from the Al wall (Fig 2b).

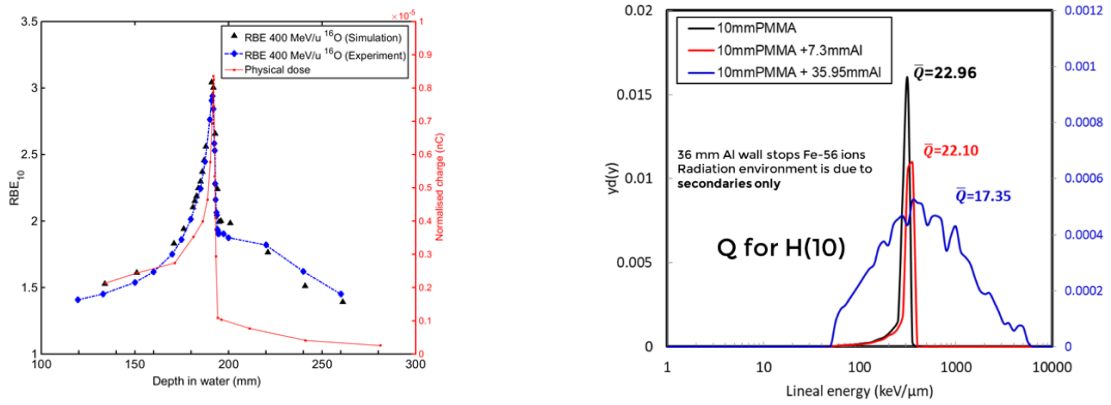

Figure 2. a) RBE_{10} distribution obtained with μ^+ probe as a function of depth in water for the 400 MeV/u ^{16}O pristine BP, b) Microdosimetric spectra obtained during 500MeV/u ^{56}Fe irradiations in free air.

Conclusion: This work presented an application of SOI micodosimeters for RBE evaluation in heavy ion therapy and for $\bar{Q}$ and Hp(10) determination in mimicking GCR radiation environment that can be used for radiation shielding optimization and radiation protection in space

References

[1] R. Destefanis *et al.*, "Space environment characterisation of Kevlar®: good for bullets, debris and radiation too," *Universal Journal of Aeronautical & Aerospace Sciences,* vol. 2, pp. 80-113, 2014.

Measurement and Comparison of Output Factors using Two Detectors for NOVAC7 Intraoperative Radiotherapy Accelerator.

M. Rafiqul Islam[1,2,3], Hiroshi Watabe[1], Andreoli Stefano.[3]
[1] *Division of Radiation and Safety Control, Cyclotron and Radioisotope Center, Tohoku University, Sendai 980-8578, Japan.*
[2] *Institute of Nuclear Medical Physics, AERE, Bangladesh Atomic Energy Commission, Ganakbari, Savar, Dhaka-1349, Bangladesh.*
[3]*Medical Physics Department, ASST Papa Giovanni XXIII Hospital, Piazza OMS, 1, 24127 Bergamo, Italy.*

Highlights NOVAC 7 mobile IntraOperative Radiation Therapy (IORT) that involves the administration of a single dose of radiation to the tumor during surgery. To measure the relative dosimetry like Output Factors, PTW 60019 microDiamond detector exhibited the best performance.

Keywords Intraoperative radiation therapy, NOVAC7, Detectors, Output Factors

Introduction and Objective In recent years, a new type of accelerator specifically designed for Intraoperative radiation therapy (IORT) has been introduced and is currently used in various radiotherapy centers. IORT is an innovative treatment technique that delivers a large single fraction of radiation dose to the tumor bed during surgery. The accurate dose delivery in intraoperative radiotherapy (IORT) tightly depends on the precision of measured dose namely output factors [1)]. The objective of this work was to evaluate and understand the performance of microDimond detector for small field dosimetry in measuring the output factors.

Material and Methods The electron beams considered in this study are generated by the 3D movable NOVAC7 (Hitesys SpA (LT) Italy 1997) system. The NOVAC7 produces pulsed electron beams with four different energies in the range from 3 MeV to 9 MeV, these are denoted with the codes A(3MeV), B(5MeV), C(7MeV) and D(9MeV) by the manufacturer. In this work we used only two high energies C(7MeV) and D(9MeV) due to the energy rang limitation of detectors. The beam collimation is performed through Perspex (PMMA) cylindrical applicators with inner diameters 40,50, 60, 70, 80 and 100 mm, wall thickness 0.5 cm and lengths 69, 67, 67 and 87 cm, respectively. The source-to-surface distance (SSD) is 80 cm, except for the applicator with the diameter of 10 cm for which the SSD is 100 cm [2)]. The output factors were measured for two energies and different applicators with PTW 60017 Diode E and PTW 60019 microDiamond detectors. The PTW 60017 Diode E is well established for dose measurement in small fields for electron beam[3)]. Contrariwise, the water proof PTW 60019 microDiamond is comparatively a new synthetic single crystal diamond detector (SCDD) with 0.004 mm^3 in sensitive volume, a radius of 1.1 mm and thickness of 1µm. The features and advantages of this detector are excellent radiation hardness, temperature independence, synthetic production and consequently a high reproducibility of the dosimetric properties. Working principle of a high purity detector is, incoming ionizing radiation can push electrons

from the valence band to higher energy levels thereby first filling electron traps caused by impurities and then bringing electrons to the conductivity band. A stable current can only be measured though after enough pre-irradiation to fill the traps[4]. For measured the output factors, Detectors were placed inside the water phantom (PTW MP3) at the depth of maximum dose for each combination of energy/applicator size, and the absorbed dose was determined. Obtained results were compared between the two detectors.

Results and Discussion The measured output factors of PTW microDiamond, and PTW Diode E detectors are in good agreement between them. The maximum deviations of output factors for PTW microDiamond +2.74%, and +2.17% for 7 MeV and 9 MeV respectively with respect to the PTW Diode E. Output factor is the ratio of detector reading for the specific applicator to the reading of reference applicator. The Output Factors depend on applicator size and increase with the decrease of applicator size[5]. One of the main aims of our study was to investigate the dosimetric characteristics of solid state detectors for electron Beam. Falco et al. used PTW microDiamond to measure PDD curves, beam profiles and output factors and compared with those obtained by PTW Advanced Markus ionization chamber for NOVAC11[6]. Both synthetic PTW microDiamond and p-type PTW Diode E type detectors are suitable for relative dosimetry output factor measurements for electron energies.

Conclusion Both the diode and microDiamond detectors were shown to exhibit excellent properties for output factor measurements. Based on the results, it may be concluded that the PTW microDiamond could be considered as an accurate tool for output factors measurement of intraoperative electron beam.

Author Disclosure: M Rafiqul Islam: Research Student, Tohoku University, JAPAN.
(and was Medical Physics Resident; ASST Papa Giovanni XXIII Hospital, Bergamo, ITALY.)

References

1) Mojtaba Barzegar, Ali Reza Shirazi, Seyed Rabi Mahdavi, et al. Output Factor Measurement of a Dedicated Intra-Operative Radiotherapy (IORT) Accelerator Using Ethanol Chlorobenzene (ECB) Dosimeter and Comparing the Results with Ionometric Dosimetry and Monte Carlo Simulation. Iran J Radiol. 2017 April; 14(2):e33319.
2) M Pimpinella, D Mihailescu, A S Guerra and R F Laitano. Dosimetric characteristics of electron beams produced by a mobile accelerator for IORT. Phys. Med. Biol. 52 (2007) 6197–6214.
3) Görkem Güngör, Gökhan Aydın, Teuta Z M, et al. Output factors of ionization chambers and solid state detectors for mobile intraoperative radiotherapy (IORT) accelerator electron beams. J Appl Clin Med Phys. 2015;16(2):5017.
4) PTW User Manual for MicroDiamond Type 60019, PTW Freiburg, Germany.
5) Björk P, Knöös T, Nilsson P. Measurements of output factors with different detector types and Monte Carlo calculations of stopping-power ratios for degraded electron beams. Phys Med Biol. 2004;49:4493.
6) Falco M, Marinelli M, Tonnetti A, et al. Characterization of high-dose-per-pulse intraoperative radiation therapy electron beams by using a microdiamond dosimeter. Phys Med. 2016;32:e1–e70.

Lyoluminescence of beta irradiated sodium chloride and halite

M. Biernacka[1]*, E. Mandowska[1], A. Mandowski[1]
[1]*Jan Dlugosz University, Czestochowa, Poland*

Highlights A tailor made equipment was made for advance lyoluminescence (LL) measurements. The LL measurements were applied to recover information about absorbed dose in pure NaCl and halite crystals. Spectral properties of the emission were analyzed.

Key words lyolumiescence (LL), emission spectra, retrospective dosimetry, sodium chloride, halite

Background and Objectives Looking for proper material for retrospective and accidental dosimetry still seems to be an important task. Salt is one of the few materials exhibits a strong intensity of radiation-induced luminescence regardless of whether it is caused by intentional heating (TL), lighting (OSL) or even dissolution of the crystal in water (lyolumiescence , LL)[1)]. The production of the F centers in the crystal of alkali halides responsible for light emission as a result of previous irradiation is well known. However, some unusual behaviors observed in salts as for example the inverse-fading and the regeneration effect indicate a complex nature of the luminescence mechanisms. Moreover, it was observed, that properties of long-lived luminescence of salts from the various origins can strong vary. This fact prompted us to analyze the LL properties for pure sodium chloride and natural halite mineral.

Materials and Methods The investigated materials were sodium chloride pure (99.999%) powder and halite from Klodawa salt mine (Poland). These materials were irradiated by beta Sr^{90}/Y^{90} source. For LL measurements were used the a tailor made equipment based on the Helios reader series (Figure 1). The system is equipped with an optional connection to CCD camera for spectrally resolved measurements.

Results and Discussion The LL reader was built and tested in various conditions. Then, samples made of halite minerals and pure sodium chloride (powder) were prepared. Dose dependence characteristics of the LL response after beta irradiation were made. Irradiated samples were dissolved in distilled water at room temperature with a fixed speed of mixing. It was found that the signal is proportional to the absorbed dose for a wide range of doses. Similar measurements were made using a cooled CCD camera to record emission spectra in the range 200 – 1100 nm.

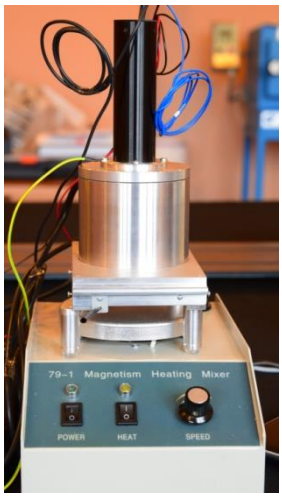

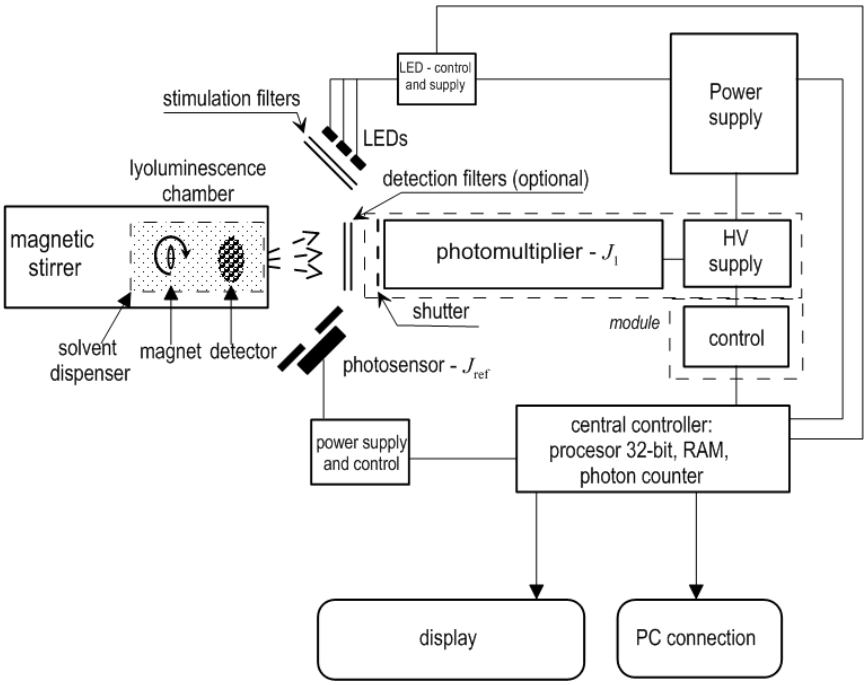

Figure 1. Block diagram of LL measurement system.

Conclusion Dose dependence characteristics of LL signal were done for pure sodium chloride as well as halite minerals. Spectral analysis of the light emitted during the dissolution of these materials brought new information about the spectral bands in these materials. The analysis of LL properties may help us to understand complex luminescence process in these materials that can be useful in the application of salt in dosimetry[2), 3)].

Acknowledgements

The research was partly supported by research project no 2014/15/N/ST10/05148 from the Polish National Science Centre.

References

1) C. D. Kalkar. Lyoluminescence from gamma-irradiated NaCl. International Journal of Radiation Applications and Instrumentation. Part C. Radiation Physics and Chemistry, 34(5) (1989) 729-738.
2) N. A. Atari, K. V. Ettinger, J. H. Fremlin. Lyoluminescence as a possible basis of radiation dosimetry. Radiation Effects, 17(1-2) (1973). 45-48.
3) N. A. Atari, K. V. Ettinger. Lyoluminescent tissue equivalent radiation desimeter. Nature, 247(5438) (1974) 193.

Solid-state, radiofluorogenic polymer dosimeter for recording depth-dose profiles related to radiation processing of surfaces

Skowyra, M.M.[1], Lindvold L.R.[1]
[1]*Center for Nuclear Technologies, Technical University of Denmark, Roskilde, Denmark*

Highlights

- The dosimeter can be cured by the photopolymerisation process in any shape
- Fluorescence response of the dosimeter serves as a tool for measuring depth-dose distributions
- Measured depth-dose profiles can be used as a dose verification in radiation processing of surfaces

Key words radiation-processing, dosimetry, fluorescence, solid-state polymer dosimeter, pararosaniline leuco dye

Background and Objectives Radiation processing is gaining in importance within the various areas such as sterilization of milk cartridges, removal of microorganisms in spices or modification of polymer properties. Characterization of radiation facilities as well as process validation in the mentioned applications are becoming extremely meaningful, hence, there is a need for a dosimetry system, which could verify the efficacy of the radiation procedures. We are developing a solid-state polymer dosimeter for recording both the surface dose and the depth-dose distribution of irradiated material, using low energy electrons. The dosimeter is based on a photo-curable polymer material doped with a radiochromic (*McLaughlin et al, 1977*) and radiofluorogenic dye. Recording the depth-dose distribution is possible by using fluorescence microscopy and image processing of the obtained scans.

Materials and Methods Poly(ethylene glycol) PEGDA (PEGDA-575 g/mol) was a matrix for a pararosaniline leuco dye, which undergoes a transformation from a colourless leuco-dye to a magenta dye, by the effect of ionizing radiation (*ICRU, 2008*). Fig.1. shows reactions taking place during transformation. The properties of the material enable its curing through a photopolymerisation process. Diphenyl(2,4,6-trimethylbenzoyl) phosphine oxide TPO (1.29mM) was used as a photoinitiator (*Bernal-Zamorano, 2018*). The dye (5.56 mM) was dissolved in ethanol (0.77 M), PEGDA-575 (1.68 M) and HEMA (2-Hydroxyethyl methacrylate, 0.74 M) and mixed using vortex mixer (Heidolph Instruments GmbH & CO. KG). Small rectangular samples (3x3x30 mm) were moulded from a silicone rubber mould using a

395 nm LED lamp for curing. The time needed for their curing was 3 minutes; moreover, the process is fully controllable (*Bernal-Zamorano, 2017*). Afterwards the dosimeter was removed from the mould. Irradiations were carried out using low energy electron beams of energies 150 and 200 keV, coming from the electron accelerator (EBLab-200, COMET AG), giving dosimeters the surface dose up to 30 kGy. The irradiated dosimeters were then scanned using a fluorescence microscope and the output images were processed, yielding to dose-depth profiles.

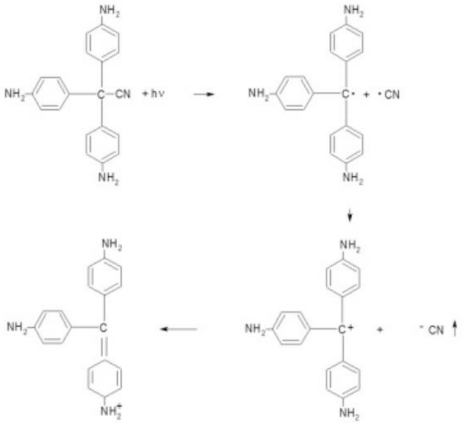

Fig.1. The radiochromic change of pararosaniline leuco dye by the effect of ionizing radiation

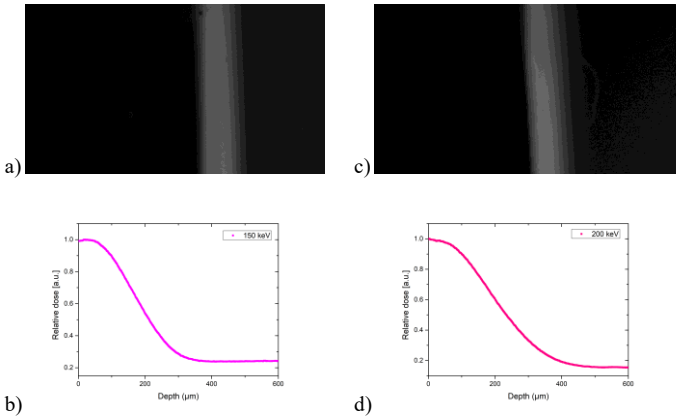

Fig.2. (a) Fluorescence microscope scan of a dosimeter irradiated with 150 keV electrons, **(b)** Dose-depth distribution of (a), **(c)** Fluorescence microscope scan of a dosimeter irradiated with 200 keV electrons, **(d)** Dose-depth distribution of (c)

Results and Discussion Normalized dose distributions as a function of depth are shown in the Fig.2**.** The fluorescence response of the dosimeter is good enough to be used. The quality of produced dosimeter as well as the lightning method during readout affect the dosimeter response.

Conclusion The solid-state dosimeter, which responds to irradiation by the change in its fluorescence response, has been studied. It allows to measure the depth-dose distributions and could be used to verify the efficacy of irradiation procedures. Future studies will focus on using more sensitive two-photon microscopy and performing advanced image processing methods.

References

Bernal-Zamorano, M.R. (2018). *Development and characterization of radiochromic and radiofluorogenic solid state polymer dosimeter material. PhD thesis.* Technical University of Denmark, Center for Nuclear technologies.

Bernal-Zamorano, M.R., Sanders, N.H., Lindvold, L., Andersen, C.E. (2017). *Radiochromic and radiofluorogenic 3D solid polymer dosimeter; effect of the photoinitiator.* Radiation Measurement 106 (2017),192-195.

ICRU (2008). Journal of the ICRU, Vol 8, No 2, Report 80. International Commission on Radiation Units and Measurements.

McLaughlin, W.L.,Miller,A.,Fidan,S.,Pejtersen, K. (1977). *Radiochromic plastic films for accurate measurement of radiation absorbed dose and dose distributions.* Radiat. Phys.Chem.10(2),119-127.

Spectrum estimation of low-energy X-rays radiated from Crookes tube using Peltie type cloud chamber

Masafumi Akiyoshi*, Kenji Yamamoto
Osaka Prefecture University, Sakai, Osaka 599-8570 Japan

Highlights Spectrum of X-rays around 20keV was estimated using high-performance Peltie type cloud chamber. Such low energy X-rays knock out photoelectrons that fly only several mm in air. Measurements of track length in cloud chamber give energy distribution of these photoelectrons. The track length was calibrated by characteristic X-rays from several metals excited by Sr-90 shielded beta-source.

Key words spectrum, low-energy X-ray, radiation track, cloud chamber

Background and Objectives The Crookes tube used in education field sometime radiate quite strong (more than 100mSv/h) X-rays. The dose measurement is relatively difficult because of its low energy. Furthermore, several NaI scintillation detectors that have Be-window to measure low energy X-ray (from 8keV) showed quite low dose than the correct dose. It was arisen from pile-up of many X-rays in short pulse radiated from the Crookes tube that was operated with induction coil. This pile-up effect is significant at spectrum measurement using CZT detector. Pin-hole collimator resolve this pile-up effect, but the count rate must be quite small (several cps) that makes measurement take long time. Unfortunately, the induction coil is driven by mechanical unit, thus profile of output high-voltage pulse was changed with operation time and other external conditions.

Materials and Methods In our laboratory, high-performance Peltie type cloud chamber is developed for reliable demonstration in radiological education [1)2)]. It can be used for observation of beta-ray and photoelectrons from gamma-ray even under stormy weather. The supersaturation layer is designed as very thin (several mm) on a small (40mm) Peltie device, and the thin supersaturation layer can present only a track that runs horizontally to the Peltie device. Thus, this device is suitable to obtain a spectrum of low-energy X-rays.

Results and Discussion In this study, X-rays with peak energy of 15keV showed a histogram of track length with a peak length of 2-3mm, while calculated maximum range of 15keV electron in air is 4.6mm. It may represent geometrical factor of track in supersaturated layer or density of air that contains supersaturated or small drop of ethanol. Accordingly, calibration

curve using known energy X-rays was required. The known energy X-rays were obtained using small Sr-90 shielded beta-source. Beta-rays excite several metal atoms, and then different energy of characteristic X-rays were obtained systematically.

The observation was performed under relatively low dose of X-rays, because high dose of X-rays gives white fog in whole of the chamber and cannot count the tracks. In addition, this device cannot be used for dose measurement. The efficiency is different with weather condition, ethanol vapor pressure and temperatures of Peltie device and top of chamber. Furthermore, the length of tracks were measured manually on video images then counted by manually that limits number of events. Recent improvements in AI and image recognition fields resolve this problem and will give spectrum during the measurement at a field such as radiology.

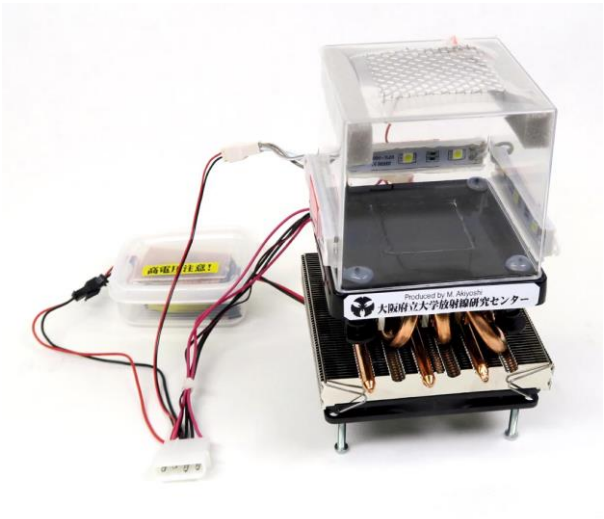

Figure 1. Overview of high-performance Peltie type cloud chamber produced by Osaka Prefecture University.

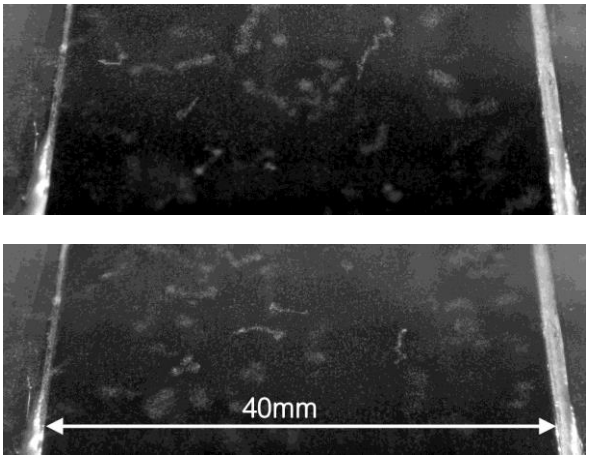

Figure 2. Observed short tracks of photoelectrons emitted by low-energy X-rays from Crookes tube.

References

1) Masafumi Akiyoshi, Practical use of the Peltier-cooling-type high performance cloud chamber in radiological education, Japanese Journal of Radiation Safety Management, 16 (2017) 72-78.
2) Masafumi Akiyoshi, Component engineering for manufacturing the Peltier-cooling-type high performance cloud chamber, Japanese Journal of Radiation Safety Management, 16 (2017) 79-84.

The Precise Measurements of Laser-accelerated Protons from Hydrogen Cluster Targets by CR-39 Track Detectors

Masato Kanasaki[1]*, Kousaku Morii[1], Keita Sakamoto[1], Yuta Takano[1], Takafumi Asai[1], Kazuki Shimizu[1], Satoshi Jinno[2], Tomoya Yamauchi[1], Keiji Oda[1], Yuji Fukuda[3]

[1]*Graduate School of Maritime Sciences, Kobe University, Hyogo, Japan*

[2]*Nuclear Professional School, The University of Tokyo, Ibaraki, Japan*

[3]*Kansai Photon Science Institute, National Institutes for Quantum and Radiological Science and Technology, Kyoto, Japan*

Highlights The laser-accelerated protons from hydrogen clusters are measured by CR-39 track detectors. A step-wise energy moderator is installed in front of CR-39 to obtain the energy spectrum with the resolution of a few MeV. The designed detector unit revealed that the maximum energy and energy spectra depends on the size distributions of the hydrogen clusters.

Key words laser-driven ion acceleration, CR-39, hydrogen cluster

Background and Objectives Recently, to accelerate high-energy ions with the energies more than 100 MeV by the interaction between ultra-short intense laser pulses and target materials, many research groups developed the new targets materials. We have succeeded in developing the micron-size hydrogen clusters[1)], which have possibility to accelerate more than 100 MeV protons in accordance with the Coulomb explosion model[2)]. The hydrogen clusters are generated by expanding the cooled high-pressure hydrogen gas into a vacuum via a conical nozzle, and the size distribution varied with the nozzle temperature. To evaluate the potential abilities of the hydrogen clusters as the targets of laser-driven ion acceleration, it is important to measure the energy spectrum of laser-accelerated protons. In the present study, the ion detector unit using CR-39 was designed to obtain the precise energy spectrum. Note that the CR-39 detectors are the most candidate detector in laser-driven ion acceleration because high-energy electrons and X-rays are generated simultaneously with ions. In addition, the designed detector units revealed that the maximum energy of proton depends on the nozzle temperatures, i.e. the size distribution of hydrogen clusters.

Experiments The ion acceleration experiments using the hydrogen cluster with the nozzle temperature 25, 50, 100 K have been conducted with the J-KAREN-P laser at Kansai Photon Science Institute. The laser pulses were focused with an off-axis parabolic mirror with a focal

length of 2500 mm, giving a peak intensity of 1×10^{20} W/cm in vacuum. In such intensity, the maximum energy of proton can estimate ~7 MeV, because the laser pulse cannot remove all electrons from hydrogen cluster. The ion detector unit, which consists CR-39 and step-wise energy moderators as shown in figure 1, was installed on the laser-propagation direction. The number of etch pits on CR-39 with different thickness of energy moderator provide the energy spectrum. After the 76 laser shots accumulation, the CR-39 sample were chemically etched in a stirred 6 mol/L KOH solution kept at 70 °C.

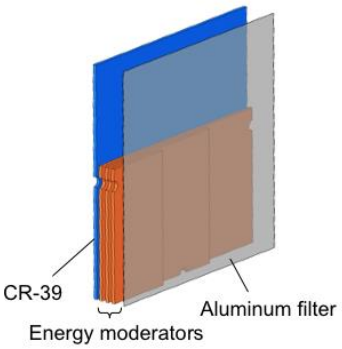

Figure 1. Schematic of the detector unit using CR-39 and energy moderators.

Results and Discussion In order to obtain the precise energy spectrum, the etch pits which overlapped the next energy region exclude from the counts. For example, protons with the energies 0.9~4.7 MeV should be measured by the area with the energy moderator only Al filter, however, more than 4.7 MeV protons, which should be counted on the next energy region, also created the etch pits on the same area. To discriminate such etch pits, therefore, the incident energies of each etch pit for CR-39 were evaluated by the size of etch pits. Based on the careful analysis, the energy spectra were obtained as shown in figure 2. It has been revealed that the energy spectra were different by the nozzle temperature, i.e. the size distributions of hydrogen clusters. The maximum energies and the total number of laser-accelerated proton were increasing with decreasing the nozzle temperature. In the case of nozzle temperature of 25 K, the maximum energy of 11.6 MeV was observed.

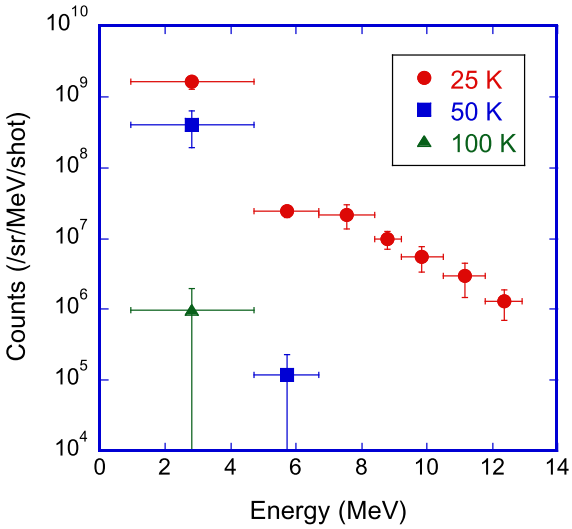

Figure 2. The energy spectra of laser-accelerated protons from hydrogen clusters with the nozzle temperature 25, 50, and 100 K.

References

1) S. Jinno et al., Plasma Phys. Control. Fusion 60 (2018) 044021
2) K. Nishihara et al., Nucl. Instrum. Meth. Phys. Res. A 464 (2001) 98

Development of a Novel Laser Heated Thermoluminescent Dosimeter (LHTLD) for Actual-Time, *in-situ* Dosimetry Measurements

Max Platkov*[1], Marcelo Weinstein[1], Abraham Katzir[2], Daniel Sattinger[1].
[1]*Nuclear Research Center Negev, Beer-Sheba, Israel, 84190*
[2]*School of Physics and Astronomy, Tel-Aviv University, Israel, 6997801.*

Highlights Laser-based Thermoluminescent Dosimetry (TLD) can deliver very high heating rates. It is simple and can be used for measurements in remote locations. Noncontact close-loop temperature control makes more accurate results.

Key words Laser Heated TLD, Middle-Infrared Radiometer, Silver-Halide Fibers.

Background and Objectives TLD is a standard method for determining the radiation dose in different environments. This method involves irradiating a thermoluminescent crystal doped with suitable dopant, and placed in a badge. The crystal is later removed from the badge and heated in a TLD reader in a linear temperature profile with hot nitrogen, thereby inducing the crystal to emit visible radiation. The graph of the intensity of this visible radiation as a function of temperature is called Glow Curve and the area underneath it is proportional to the dose. TLD readers are bulky, stationary and expensive and require removal of the crystal from the measurement site. Our goal is to develop a small and portable reader can perform accurate dose-measurements in actual time, in remote locations without removing the crystal.

Materials and Methods To overcome the challenges inherent to the traditional method we propose a new idea for readout of irradiated crystals, based on lasers and mid-IR transmitting optical fibers. CO_2 laser energy is passed through a suitable AgClBr mid-IR transmitting fiber to heat a doped LiF crystal. The heated crystal then emits black-body infrared radiation that is passed by a second mid-IR fiber to an infrared radiometric detector, and the voltage generated by it is used to determine the temperature. A computer uses this voltage to control the laser heating so that the heating is linear. The heated crystal also emits visible radiation that is transmitted by a visible transmitting fiber to a suitable visible detector. The output of this detector as a function of temperature is again the Glow-Curve. This Laser Heated TLD (LHTLD) is based on lasers and optical fibers which make it more flexible useful in many applications. Several prototypes of this idea were operated successfully by us. The results[1,2]

of measurements with these methods will be presented.

Results and Discussion We constructed several versions of laser based TLD readers[1,2]. These devices are being perfected in terms of design, in order, to achieve our goals. Some intermediate results have been published and include: (1) Widely varying linear heating rates, (2) In standard TLD system the temperature measured is only that of the hot nitrogen. In our system the temperature measurement is a non-contact one and it accurately measures the temperature of the crystal itself , (3) Accurate dose determinations in various ranges.

Conclusion Numerous articles have described the various aspects of standard TLD measurements. We developed a totally different method that is based on laser heating and on suitable optical fibers. The system accurately measures the temperature of crystal and ensures true linear heating. There will be no need to send the irradiated crystal to a remote laboratory where a TLD reader will determine the dose. The use of optical fibers allows to carry out live, repeated measurements in a remote location. The LHTLD system with its laser-heating approach opens up possibilities for miniaturization of the reader.
Our LHTLD approach will be useful for the nuclear industry and environmental protection, where human-accessibility constraints prevent application of standard TLD-based methods. In medicine, the exposure of personnel and patients during CT procedures will be measured, thereby preventing over-exposure. The new fiber-based laser heated TLD reader with noncontact temperature readout will revolutionize many areas of dosimetry.

References

[1] Ditcovski R., Gayer O., Katzir A., “Laser assisted thermoluminescence dosimetry using temperature controlled linear heating”, J. Luminescence 130 (2010) 141–144.
[2] Gayer O., Katzir A., “Laser-fiberoptic non-contact controlled heating of samples for thermoluminescence measurements”, J. Luminescence 113 (2005) 151–155

$TlSr_2Cl_5$: New intrinsically activated crystalline scintillator

Miki Arai*[1],Keisuke Takahashi[1], Yutaka Fujimoto[1], Masanori Koshimizu[1],

Takayuki Yanagida[2], Keisuke Asai[1]

[1]Tohoku Univ., Miyagi, Japan, [2]NAIST, Nara, Japan

Highlights

- Photoluminescence and scintillation properties of $TlSr_2Cl_5$ were studied.
- $TlSr_2Cl_5$ crystals were prepared under vacuum using a self-seeding solidification method.
- $TlSr_2Cl_5$ crystals showed broad emission bands peaking at 450 and 500 nm under X-ray excitation.
- Light yield of $TlSr_2Cl_5$ crystals reached 16,000 photons/MeV under γ-ray irradiation.

Key words Scintillator, Luminescence, $TlSr_2Cl_5$

Background and Objectives A scintillator is a material that emits light by utilizing the energy of incident radiation and is widely used in physical measurements and nuclear medicine diagnosis. An ideal scintillator must have high light yield and effective atomic number (Z_{eff}). Among scintillators that have high light yield, we focused on self-activated scintillators, in particular, those based on thallium because of its high atomic number. There are only a few reports on the interesting scintillation properties of $TlCl–ACl_2$ (A: Divalent cation) crystals [1] [2]. $TlMgCl_3$[1] has a large atomic number (Z_{eff}=71.6) and high light yield (46,000 photons/MeV). In this study, we decided to use Sr as divalent cation. We characterized $TlSr_2Cl_5$ crystals.

Materials and Methods TlCl (99.9%) and $SrCl_2$ (99.9%) powders were used as the starting materials to synthesize $TlSr_2Cl_5$ crystals. The powders were mixed with a ratio of 1:2.03, due to the volatilization of $SrCl_2$, and the crystals were prepared from the melt using the self-seeding solidification method. After the growth, the photoluminescence (PL), X-ray excited radioluminescence (XRL) spectra, pulse-X-ray excited scintillation temporal profiles, and ^{137}Cs γ-ray irradiated pulse height spectra were obtained.

Results and Discussion Figure 1 shows the image of the $TlSr_2Cl_5$ crystals prepared in this study. The crystals were semitransparent and colorless. The XRD patterns showed that most of the peaks were ascribed to $TlSr_2Cl_5$. However, a few peaks corresponding to raw materials were observed. Figure 2 shows the XRL spectra of the $TlSr_2Cl_5$ crystals. Intense emission bands of $TlSr_2Cl_5$ are observed at 450 and 500 nm, which are close to the peak positions of $TlMgCl_3$ [1] and $TlCdCl_3$ [2]. These peaks are characteristic of self-activated thallium-based chloride crystals. We estimate that the emission centers are localized Tl^+ ions or self-trapped excitons. Figure 2 shows the pulse-X-ray excited scintillation temporal profiles of $TlSr_2Cl_5$. Scintillation decay times were estimated to be 21 ns (~3%) and 651 ns (~97%). These decay times for $TlSr_2Cl_5$ are close to that of $TlMgCl_3$[1] and $TlCdCl_3$[2] and are also characteristic of self-activated thallium-based chloride crystals. The ^{137}Cs γ-ray irradiated pulse height spectra for $TlSr_2Cl_5$ and Gd_2SiO_5 (GSO) are shown in Figure 4. The light yields were estimated on the basis of the photoelectron peaks of $TlSr_2Cl_5$ and GSO located in the 492 and 419 channels, respectively. Assuming that the light yield of GSO is 10,000 photons/MeV, which is calibrated by using a Si avalanche photodiode and a ^{55}Fe source, the light yield of $TlSr_2Cl_5$ is estimated to be 16,000 photons/MeV.

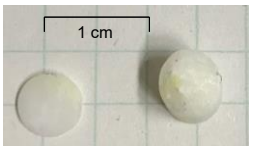

Fig. 1 Photograph of $TlSr_2Cl_5$ crystals.

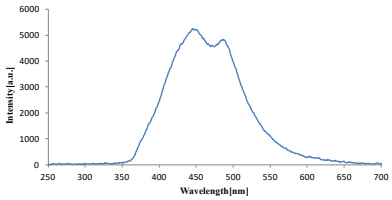

Fig. 2 XRL spectra of $TlSr_2Cl_5$ crystals.

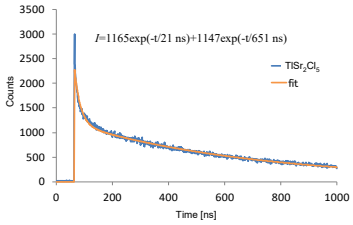

Fig. 3 Pulse-X-ray excited scintillation temporal profiles of $TlSr_2Cl_5$.

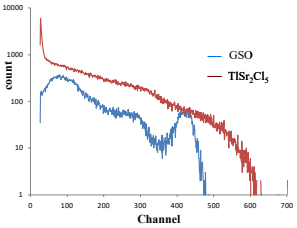

Fig. 4 ^{137}Cs γ-ray irradiated pulse height spectra for $TlSr_2Cl_5$ and GSO.

Conclusion We studied the luminescence and the scintillation properties of the $TlSr_2Cl_5$ crystal, which has a large Z_{eff} value (63.7), for application in X-ray and γ-ray detection. The $TlSr_2Cl_5$ crystal was prepared under vacuum using the self-seeding solidification method. The emission peaks and scintillation decay times of $TlSr_2Cl_5$ are in agreement with those of self-activated thallium-based chloride crystals. We demonstrated good scintillation properties in the crystal such as enough light yield for a photon-counting measurement (~16,000 photons/MeV).

References

[1] Y. Fujimoto, et al., Jpn. J. Appl. Phys. 55 (2016) 090301.
[2] Y. Fujimoto, et al., Radiat. Meas. 106 (2017) 151.

Development of $TlMg(Cl_{1-x}Br_x)_3$ crystals scintillators

Miki Arai*[1], Yutaka Fujimoto[1], Masanori Koshimizu[1],

Takayuki Yanagida[2], Keisuke Asai[1]

[1]Tohoku Univ., Miyagi, Japan, [2]NAIST, Nara, Japan

Highlights

- The photoluminescence and scintillation properties of $TlMg(Cl_{1-x}Br_x)_3$ were studied.
- $TlMg(Cl_{1-x}Br_x)_3$ crystals were prepared under vacuum using a self-seeding solidification method.
- $TlMg(Cl_{1-x}Br_x)_3$ crystals showed emission bands at 420 nm under X-ray excitation.
- The light yields obtained for $TlMg(Cl_{1-x}Br_x)_3$ crystals can reach 45,000 photons/MeV upon γ-ray excitation.

Keywords Scintillator, Luminescence, $TlMgCl_3$

Background and Objectives Scintillators, which are materials that emit light utilizing the energy of incident radiation, are widely used in physical measurements and nuclear medicine. An ideal scintillator must have a high light yield and high effective atomic number (Z_{eff}). We have studied $TlCl–ACl_2$ (A = divalent cation) crystal scintillators because the atomic number of Tl (Z = 81) is large. We have reported that a $TlMgCl_3$ crystal scintillator exhibits a high light yield and a high Z_{eff} = 71.6 [1]. Anion substitution has great potential to improve the scintillation properties of $TlMgCl_3$ because it is known to influence both the photoluminescence and scintilation properties of a variety of materials. We have examined the scintillation properties of the $TlMg(Cl_{1-x}Br_x)_3$ crystals obtained in this study.

Materials and Methods TlCl (99.9%), $MgCl_2$ (99.9%) and TlBr (99.9%) powders were used as the starting materials to prepare two types of $TlMg(Cl_{1-x}Br_x)_3$ crystals. The powders were mixed in a ratio of 1:1:(0.01 or 0.005), and the target crystals were obtained from the melt using a self-seeding solidification method. The photoluminescence (PL), X-ray excited radioluminescence (XRL) spectra, pulse-X-ray excited scintillation temporal profiles, and ^{137}Cs γ-ray irradiated pulse height spectra of the $TlMg(Cl_{1-x}Br_x)_3$crystals were recorded.

Results and Discussion Figure 1 shows a photograph of the $TlMg(Cl_{1-x}Br_x)_3$ and $TlMgCl_3$ crystals prepared in this study. The crystals were semitransparent and colorless. The XRD patterns show many peaks corresponding to $TlMgCl_3$ and a few peaks attributed to Br. Figure 2 shows the XRL spectra recorded for the $TlMg(Cl_{1-x}Br_x)_3$ and $TlMgCl_3$ crystals. Intense emission bands were observed for the $TlMg(Cl_{1-x}Br_x)_3$ crystals at 420 nm, which are identical to the peak position observed for $TlMgCl_3$. This means that the light emitting mechanism of $TlMg(Cl_{1-x}Br_x)_3$ was identical to $TlMgCl_3$. The ^{137}Cs γ-ray irradiated pulse height spectra recorded for $TlMg(Cl_{1-x}Br_x)_3$, $TlMgCl_3$, and GSO are shown in Figure 3. The light yields were estimated on the basis of the photoabsorption peaks observed for $TlMg(Cl_{1-x}Br_x)_3$, $TlMgCl_3$, and GSO located in the 430, 340 and 190 channels, respectively. Assuming that the light yield of GSO is 10,000 photons/MeV, which was calibrated using an Si avalanche photodiode and ^{55}Fe source, the light yields of $TlMgCl_3$ and $TlMg(Cl_{1-x}Br_x)_3$ were estimated to be 42,000 and 45,000 photons/MeV, respectively. This means that light yield of the $TlMg(Cl_{1-x}Br_x)_3$ crystals was higher than $TlMgCl_3$.

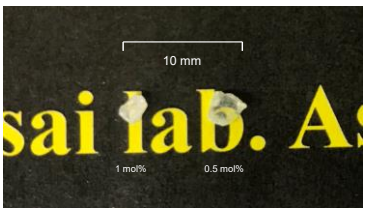

Fig. 1 Photograph of $TlMg(Cl_{1-x}Br_x)_3$ crystals.

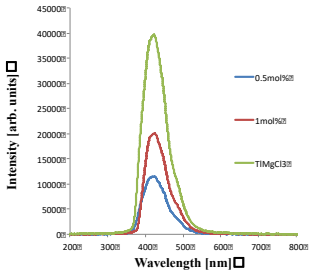

Fig. 2 XRL spectra of $TlMg(Cl_{1-x}Br_x)_3$ crystals.

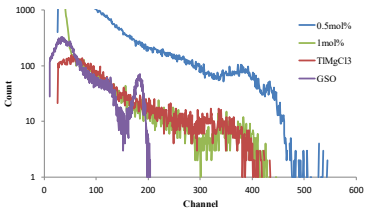

Fig. 3 ^{137}Cs γ-ray irradiated pulse height spectra for $TlMg(Cl_{1-x}Br_x)_3$ and GSO.

Conclusion We have studied the luminescence and scintillation properties of a variety of $TlMg(Cl_{1-x}Br_x)_3$ crystals for application in X-ray and γ-ray detection. The $TlMg(Cl_{1-x}Br_x)_3$ crystals were prepared under vacuum using a self-seeding solidification method. The emission peaks observed for the $TlMg(Cl_{1-x}Br_x)_3$ crystals are identical to $TlMgCl_3$. We have demonstrated that the crystals have good scintillation properties with light yields suitable for photon-counting type measurements (~45,000 photons/MeV).

References

[1] Fujimoto, Y et al., Jpn. J. Appl. Phys. 55 (2016) 090301.

Fast Neutron Flux Evaluation Using Metal Threshold Detectors and Imaging Plate (IP) Transfer Method

H. Uno[1], R. Uemoto[1], M. Uematsu[2], K. Nittoh[2],
T. Kamiyama[3], Y. Kiyanagi[4]
[1]SHI-ATEX Co., Ltd., Saijo, Japan,
[2]Toshiba Technical Services International Corporation, Yokohama, Japan,
[3]Hokkaido University, Sapporo, Japan, [4]Nagoya University, Nagoya, Japan

Highlights A new neutron radiography method was developed for fast neutron measurement, in which β-rays from irradiated threshold detectors such as $^{27}Al(n,\alpha)^{24}Na$ and $^{24}Mg(n,p)^{24}Na$ are transferred and accumulated on X-ray imaging plate (IP).

Key words Imaging plate (IP), Neutron radiography, Threshold detectors, Flux evaluation

Background and Objectives

Neutron radiography method using activation foil detectors and imaging plate (IP) has been developed for thermal and epi-thermal neutron measurement. The method utilizing a set of In, Au, Er, Mn and Cu foil detectors was found to be effective in evaluating neutron spectrum up to 500eV[1)]. This paper describes further development of the method by adding Al and Mg threshold detectors to expand the energy range of neutron spectrum measurement up to 10MeV.

Materials and Methods

Figure 1 illustrates a scheme of fast neutron flux measurements by metal foil irradiation and IP transfer. The β activities produced in the metal foils are converted to luminance data by IP reading system. Applicability of the method to fast neutron flux was examined by comparing IP response from Al and Mg foils irradiated in a $^{9}Be(p,n)$ neutron field with calculation results obtained with Monte Carlo code PHITS. Estimated fast neutron flux above 1 MeV at the foil position was 10^{7} n/cm^{2}s. Irradiation time and IP transfer time were 7.0 hours and 21 hours, respectively.

Results and Discussion

Figure 2 shows arrangement of metal foils (Al, Mg) and distribution of relative luminance (IP response). The position resolution of the measurement was 25 μm/pixel (IP reading pixel size). Standard deviation of pixel-wise luminance was around 2%. Dotted lines in Fig.2 shows results of the PHITS calculation. Relative distribution of the obtained results showed good agreement between IP method and PHITS calculation.

Conclusion

The developed method was found to be applicable to fast neutron measurement. The IP transfer method utilizing both resonance detectors and threshold detectors will be effective in neutron spectrum evaluation for wide energy range.

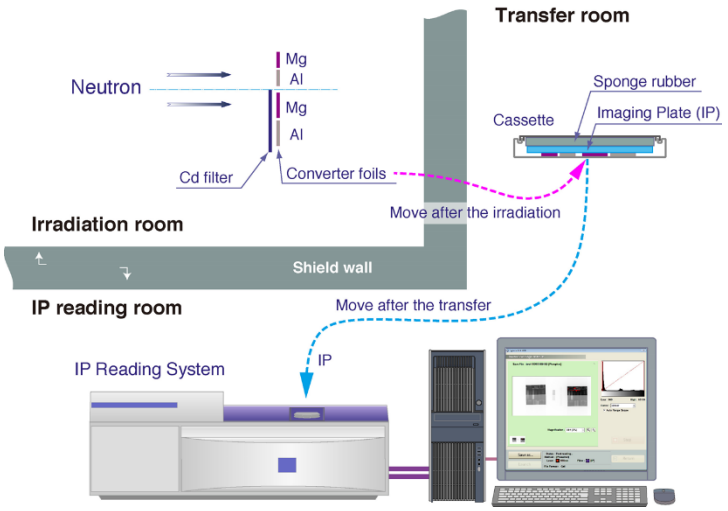

Fig. 1 IP transfer method for fast neutron flux measurement

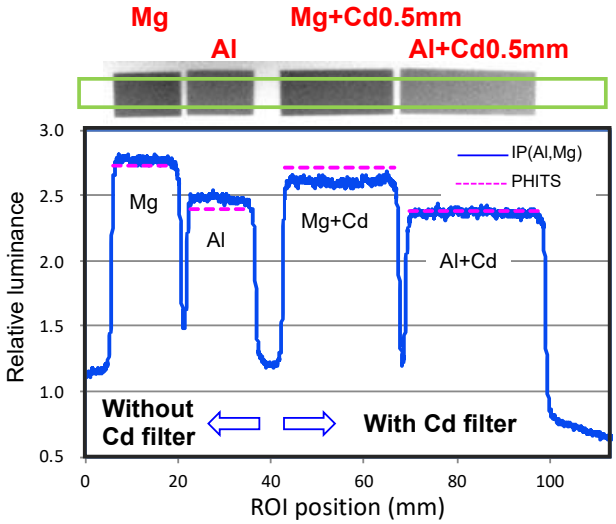

Fig.2 IP response (luminance) obtained from Al and Mg threshold detectors irradiated in ^{9}Be(p,n) neutron field.

References

1) H.Uno, R.Uemoto, K.Nittoh, M.Uematsu, C.Konagai, “Neutron energy spectrum evaluation and radiography using metal foil activation and IP transfer method”,11th World Conference on Neutron Radiography (WCNR-11) in September 2018 in Sydney, Australia [Contribution ID 159]

Production and Study of Flexible OSL detector sheet based on $CaSO_4$:Dy in high temperature silicone matrix

Gasparian, P.B.R.(1), Umisedo, N.K.(2), Yoshimura, E.M.(2), Campos, L.L.(1), and Malthez A.L.M.C.(3)

(1) Instituto de Pesquisas Energéticas e Nucleares – IPEN/CNEN, Sao Paulo, SP, Brazil

(2) Institute of Physics, University of Sao Paulo, Sao Paulo, SP, Brazil

(3) Federal University of Technology - Parana, Curitiba, PR, Brazil

Highlights Flexible OSL detectors with $CaSO_4$:Dy were produced to be used for dose mapping. The matrix of the detector is based in high temperature silicone that allows thermal bleaching. OSL dosimetric properties demonstrate potential application in radiation measurements.

Key words OSL, radiation dosimetry, sheet detector, $CaSO_4$:Dy, dose mapping

Background and Objectives The main difference between Thermoluminescence (TL) and Optically Stimulated Luminescence (OSL) techniques is the employed stimulus, thermal or optical, to luminescent emission[1]. OSL technique presents some advantageous characteristics over TL technique, as simplicity and speed of readout. In addition, with appropriate detector and reader, OSL technique offers the possibility of relatively easy bi-dimensional dose mapping[2]. Calcium sulfate doped with dysprosium ($CaSO_4$:Dy) has been successfully used for personal dosimetry in TL dosimetric systems and its TL properties are well-known[3]. Recent studies highlight the potential of $CaSO_4$ based detectors with different combination of impurities, using TL and OSL techniques[4,5]. The commercially available OSL detector strips with plastic compounds do not allow thermal bleaching which could be required to erase residual signal after high doses. In the case of $CaSO_4$:Dy, it is necessary a thermal bleaching of 300ºC for 15h to erase residual signal after doses higher than 1Gy[5]. Taking into account the advantages of OSL technique, the possibility of relatively easy dose mapping and the potential applicability of $CaSO_4$:Dy with OSL technique for radiation dosimetry, the aim of this study was to produce flexible OSL detector sheets using $CaSO_4$:Dy in a matrix of high temperature silicone which allows thermal bleaching before reuse of the OSL detector sheets.

Materials and Methods The present study was carried using $CaSO_4$:Dy powder, made in IPEN (Instituto de Pesquisas Energeticas e Nucleares, in Brazil). Two different commercially available silicone were used to produce the detector sheets. Both are high temperature silicone,

used mainly for baking pan purposes and other processes involving heating ranging from 280°C to 320°C. Those are resistant to cracking and shrinking, to oil, water and toxic chemicals, and to migration caused by thermal cycling. The sheets were prepared with and without detector for comparison. OSL readouts and irradiations were performed in a Risø TL/OSL reader with blue light stimulation, Hoya U-340 glass filter for detection and a $^{90}Sr/^{90}Y$ built-in beta source.

Results and Discussion Flexible OSL $CaSO_4$:Dy detector sheets were successfully produced (Figure 1). Investigations have shown that it is feasible to obtain homogeneous detector with good reproducibility results (lower than 15%) and linear dose response from 0.1 to 10 Gy. In addition, a thermal treatment at 280°C for 15h was enough to erase the signal storage in the detector after irradiation without changes in its sensitivity.

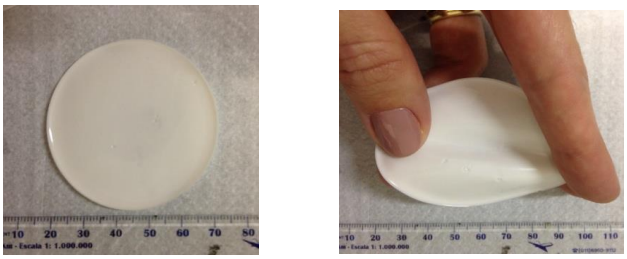

Figure 1. Flexible OSL detector sheet made with $CaSO_4$:Dy in silicone matrix.

Conclusion The results reinforce the potential use of flexible OSL $CaSO_4$:Dy detectors for dose mapping applications.

References

1) Yukihara, E., Mckeever, S., 2011. Optically Stimulated Luminescence: Fundamentals and Applications. John Wiley & Sons Ltd, New Jersey.
2) Yukihara, E. G.; Ruan, C.; Gasparian, P. B. R.; Clouse, W. J.; Kalavagunta, C.; Ahmad, S., 2009. An Optically Stimulated Luminescence system to measure dose profiles in X-ray Computed Tomography. Physics in Medicine and Biology 54, 6337-6352.
3) Campos, L.L., Lima, M.F., 1986. Dosimetric properties of $CaSO_4$:Dy Teflon pellets produced at IPEN. Radiation Protection Dosimetry 14, 333-335.
4) Junot, D.O, Santos, A. G. M., Caldas, L.V.E., Souza, D.N., 2017. International Conference on Luminescence (ICL), Joao Pessoa.
5) Gasparian, P.B.R., Yoshimura, E.M., Umisedo, N.K., Campos, L.L., Malthez A.L.M.C., 2018. Study of the Dosimetric Properties of $CaSO_4$:Dy using OSL technique. International Symposium on Radiation Physics, Cordoba.

Progress in Fluorescent Nuclear Track Detectors Based on Lithium Fluoride Crystals

P. Bilski*[1], B. Marczewska[1], W. Gieszczyk[1], M. Kłosowski[1], M. Naruszewicz[1], M. Sankowska[1], S. Kodaira[2]

[1]*Institute of Nuclear Physics, Polish Academy of Sciences (IFJ PAN), Kraków, Poland*

[2] *National Institute of Radiological Sciences (NIRS) / QST, Chiba, Japan*

Highlights Fluorescent nuclear track detectors (FNTD) based on LiF crystals were successfully used for imaging tracks of various ionizing particles. This was achieved by exploiting photoluminescence of radiation induced F_2 and F_3^+ color centers and a wide-field fluorescence microscope.

Key words radiophotoluminescence, FNTD, lithium fluoride

Background and Objectives At the previous SSD18 conference, the first attempts to exploit radiophotoluminescence of F_2 and F_3^+ color centers in LiF crystals for imaging of radiation induced patterns, aimed on imaging single particle tracks, were reported. Since that time a considerable progress was achieved and the goal of fluorescent detection of single tracks was reached [1-4]. Within the presentation an overview of the so far achieved results will be given.

Materials and Methods LiF single crystals were grown at the IFJ PAN with the Czochralski method. Microscopic observations were conducted using a Nikon Eclipse Ni-U upright fluorescence wide-field microscope with a DS-Qi2 CCD camera. Irradiations of LiF crystal samples with high-energy ions were conducted at the Heavy Ion Medical Accelerator (HIMAC) in Chiba, Japan, within three experimental sessions over years 2017-2018. The following ion species were applied: helium, carbon, neon, silicon and iron. Additionally, radiation from various radioisotope sources was also used.

Results and Discussion The various tested radiation modalities produced in LiF crystals significant radiophotoluminescent signal, enabling imaging of the tracks. The track intensity depends on ionization density, therefore the brightest tracks were obtained for high-LET particles, like iron ions presented in fig.1a. This dependence suggests possibility of extracting some information on ionization density, what will be discussed. Presence of ^{6}Li provides a unique opportunity of detecting products of the well-know (n,α) reaction with thermal neutrons (fig. 1b). Besides heavy particles, the tracks produced by secondary electrons generated by gamma-rays were also detected.

a) 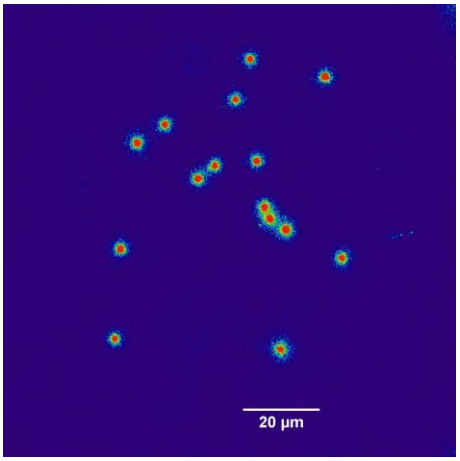

b) 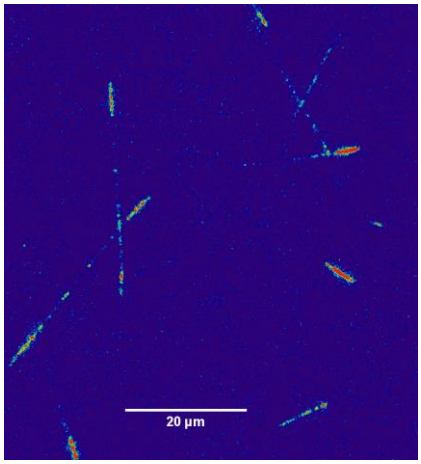

Figure 1. Examples of fluorescent tracks in LiF crystals (colors are false, added for better visualization): a) iron ions, energy=412.5 MeV/nucleon, LET(H_2O)=199 keV/µm; b) products of thermal neutron reactions with ^6Li: alpha particles and tritons .

Conclusion Photoluminescence of F_2/F_3^+ color centers in LiF was exploited for imaging tracks of variety of ionizing particles, showing that LiF may be successfully used as a fluorescent nuclear track detector.

Acknowledgements:
This work was supported by the National Science Centre, Poland (Contract No. UMO-2015/17/B/ST8/02180).

References

1) P. Bilski, B. Marczewska, Fluorescent detection of single tracks of alpha particles using lithium fluoride crystals. Nucl. Instr. Meth. B 392 (2017) 41–45
2) P. Bilski, B. Marczewska, W. Gieszczyk, M. Kłosowski, T. Nowak, M. Naruszewicz, Lithium fluoride crystals as Fluorescent Nuclear Track Detectors. Radiat. Prot. Dosim. 178 (2018) 337-340
3) P. Bilski, B. Marczewska, M. Kłosowski, W. Gieszczyk, M. Naruszewicz, Detection of neutrons with LiF fluorescent nuclear track detectors. Radiat. Meas. 116 (2018) 35-39
4) P. Bilski, B. Marczewska, W. Gieszczyk, M. Kłosowski, M. Naruszewicz, Y. Zhydachevskyy, S. Kodaira. Luminescent properties of LiF crystals for fluorescent imaging of nuclear particles tracks. Optical Materials (2019), doi.org/10.1016/j.optmat.2019.02.014

ezClip - universal BeO detector element for various applications in personal dose monitoring

P. Scheubert[1], R. Eßer[1], H. Hoedlmoser[2], M. Figel[2]
[1] *Dosimetrics GmbH, Munich, Germany*
[2]*Helmholtz Zentrum München, Individual Monitoring Service, Munich, Germany*

Highlights Dosimetrics GmbH München has developed a new detector element based on BeOSL technology. It can be used for extremity dosemeters without compromising the concept of automated bulk processing.

Key words Extremity dosimetry, eye lens, finger ring, OSL, BeO, ezClip

Background and Objectives Meanwhile BeO is an established material in personal monitoring dosimetry [1]. BeO combines tissue equivalency and unequalled luminescence properties [5]. Therefore, BeO is an interesting alternative to other widely used detector materials like Al_2O_3.

Nevertheless, so far its use was limited to whole body dosemeters. For monitoring services it would be desirable, if they could use existing costly infrastructure also to cover extremity dosimetry applications such as finger ring and eye lense dosemeters.

In this publication it will be demonstrated, how this is possible by introducing a single detector element and corresponding holders. A miniaturised detector element consists of the BeO detector crystal molded into a plastic holder. The holder is uniquely coded by a 2D code and a human readable number.

The challenge is to make the complete toolchain of monitoring services reusable. As typically the majority of dose readings is carried out for whole body dosemeters this must be the main focus of optimization. It is desirable that the comparably small number of extremity dosemeters can be evaluated with the same equipment.

Materials and Methods The design was driven by the compatibility aspect. The existing infrastructure of BeOSL reader and eraser devices had to be reused. As well the detector should be compatible with existing TLD finger ring versions. These offer a limited space for the detector element. Special attention was paid to ease of use.

Figure 1. ezClip detector element with carrier and holder. The form factor corresponds to the well-established BeOSL whole body dosemeters.

Results and Discussion Figure 1 shows the realisation variant of the new detector element called ezClip. Results will be presented, that though having a smaller active detector area and additional degrees of freedom (like detector rotation of the detector element in the carrier) the dosimetric properties of the ezClip element make it an attractive extension to existing dosimetry systems. Performance data such as energy and angular response, linearity and coefficient of variation is presented as well as other data that confirms the ezClip's usability.

Conclusion A new BeO single detector element is presented. It can be processed with existing and type tested BeOSL infrastructure. It is very well suited for applications in extremity dosimetry like finger ring and eye lens dosemeters.

References

1) T. Haninger et al, Properties of the BeOSL Dosimetry System in the Framework of a Large-scale Personal Monitoring Service, Radiat Prot Dosimetry doi:10.1093/rpd/ncv425
2) H. Hoedlmoser et al, New eye lens dosemeters for integration in radiation protection glasses, submitted to Rad. Meas. for publication (1/2019)
3) V. Bandalo et al, Performance of the BeOSL eye lens dosemeter with radiation protection glasses, this conference.
4) M. Figel et al, A BeOSL Finger Ring dosemeter, this conference.
5) H. Hoedlmoser et al, Simulation of OSL and TLD dosemeter response for the development of new extremity dosemeters, Rad. Prot. Dosimetry doi: 10.1093/rpd/ncy299 (2018).

Scintillation properties of Pr-dope $Lu_2Si_2O_7$ single crystal

P. Kantuptim[1]*, M. Akatsuka[2], N. Kawaguchi[3], T. Yanagida[4]
Division of Materials Science, Graduate school of science and technology,
Nara Institute Science and Technology, Ikoma, Nara 630-0101, Japan

Highlights This study will firstly report the photo-physical and scintillation properties on different Pr concentrations in $Lu_2Si_2O_7$ single crystals. Photoluminescence (PL) quantum yield (*QY*), scintillation light yield and other properties has been observed. Throughout the systematic studies on these properties, we found the optimum concentration for the Pr doped in $Lu_2Si_2O_7$ for scintillator purpose.

Key words Scintillator, Lu-pyrosilicate, Pr-doped, floating zone method

Background and Objectives Scintillator material is a luminescence material which can convert a high energy photon and particle of the ionizing radiation to the lower energy photons such as ultraviolet and visible light immediately after the absorption of the ionizing radiation. The emitting photons will be collected by photodetector such as photomultiplier tube (PMT) or photodiode (PD) and converted to the electrical signal for radiation detection purpose. The single crystal type scintillators using the rare earth ions as the luminescence center have been commonly investigated. Among luminescence center ions, Pr^{3+} is the one of the highly attractive ions for this purpose from the result of fast scintillation decay time around 10-20 ns (1), and $Lu_2Si_2O_7$ had been used for the host materials due to the high effective atomic number (2). In this study, we investigated Pr differently doped $Lu_2Si_2O_7$ single crystals on optical and scintillation properties. Up to now, Pr concentration dependence in $Lu_2Si_2O_7$ single crystals has not been studied.

Materials and Methods In this study, $Lu_2Si_2O_7$ single crystal doped with Pr was synthesized by the floating zone method. After the crystal growth, the physical property such as photoluminescence (PL) quantum yield (*QY*), PL decay time, scintillation spectra, scintillation decay time profiles, pulse height (PH) spectra and scintillation light yield (*LY*) were evaluated.

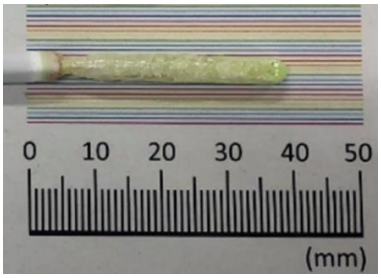

Figure 1. Pr-doped $Lu_2Si_2O_7$ grown by FZ method.

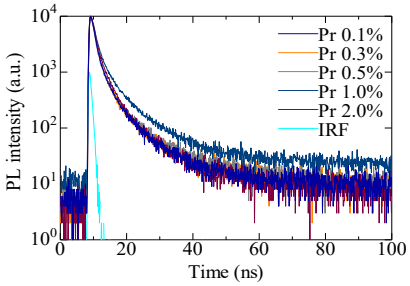

Figure 2. PL decay time profiles.

Results and Discussion Figure 1 shows an example of the appearance of as-grown sample. The PL *QY*s of 0.1, 0.3, 0.5, 1.0, and 2.0 % Pr doped samples resulted 79.4, 52.5, 50.1, 42.4, and 35.4 % respectively. The PL decay time has shown in the figure 2. The decay time was around 6.27-7.98 ns depending on Pr concentration. The scintillation decay time profiles are shown in the figure 3 upon X-ray excitation. The scintillation decay time decreased when the Pr concentration increased from the 157.59 ns (0.1% Pr) to 48.08 ns (2% Pr). The scintillation spectra had shown the emission peak around 300-340 nm, and the emission origin was Pr^{3+} 5d-4f transitions (3). The scintillation light yields were obtained from PH measurement using ^{137}Cs γ-ray source, and 1% Pr doped sample showed the best *LY* of 9700 ph/MeV, as shown in figure 4.

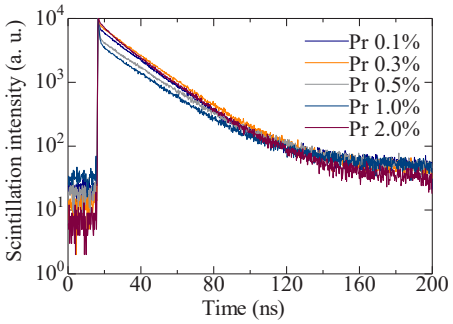

Figure 3. Scintillation Decay time profiles.

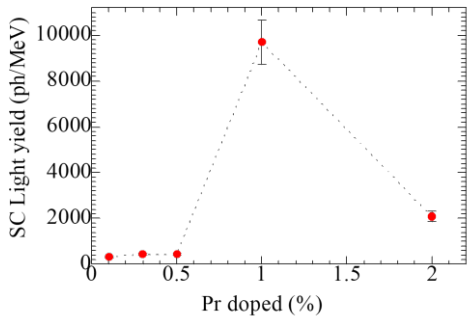

Figure 4. Scintillation light yield as a function of Pr concentration.

Conclusion Optical and scintillator properties of the Pr 0.1, 0.3, 0.5, 1, and 2 % doped $Lu_2Si_2O_7$ have been investigated. The PL *QY* of Pr 0.1% doped one reached 79.4%, and the scintillation *LY* of Pr 1% doped one resulted 9700 ph/MeV. As a conclusion, 1% Pr doping is the optimum concentration of $Lu_2Si_2O_7$ for scintillator purpose.

References

1) Yanagida, Takayuki, et al. "Optical, scintillation and radiation tolerance properties of Pr-doped pyrosilicate crystals." *Japanese Journal of Applied Physics* 57.10 (2018): 106401.
2) Nikl, M., et al. "Pr^{3+} luminescence center in $Lu_2Si_2O_7$ host." *physica status solidi (RRL)–Rapid Research Letters* 3.9 (2009): 293-295
3) Yanagida, Takayuki. "Ionizing radiation induced emission: scintillation and storage-type luminescence." *Journal of Luminescence* 169 (2016): 544-548.

A multipurpose single moderator neutron spectrometer based on solid-state detectors

R. Bedogni[1]*, J.M. Gómez-Ros[1,2], A. Pietropaolo[3], M. Costa[4,5], V. Monti[4,5], A. Pola[6]

[1]*INFN – LNF, via E. Fermi n. 40, 00044 Frascati (Roma), Italy*
[2]*CIEMAT, Av. Complutense 40, 28040 Madrid, Spain*
[3]*ENEA, Dept. Fusion and Technology for Nuclear Safety, via E. Fermi 45, 00044 Frascati, Italy*
[4]*INFN Sezione di Torino, via Pietro Giuria 1, 10125 Torino, Italy*
[5]*Università degli Studi di Torino, Via P. Giuria 1, 10125 Torino, Italy*
[6]*Politecnico di Milano. Dipartimento di Energia. Via La Masa 34. 20156 Milano. Italy*

Highlights This communication describes the different versions of a broad energy range, directional, neutron spectrometer consisting of several solid-state detectors within a single cylindrical moderator. Appropriate choice of detectors and dimensions made it suitable for a wide range of applications.

Key words neutron spectrometry, unfolding, CYSP, single moderator spectrometer

Background and Objectives A multidetector cylindrical single-moderator neutron spectrometer, with energy response from thermal till hundreds of MeV has been developed in the framework of INFN, CIEMAT, ENEA and Politecnico di Milano collaborations[(1-4)]. The neutron spectrum is obtained by unfolding the detectors readings, thus requiring only one exposure to determine all energy components. Because of the collimated structure, the cylindrical spectrometer (Fig. 1) shows a sharply directional response. This communication will describe the different versions of the device and the results obtained from spectrometric measurements in accelerators, cosmic rays, and large-scale neutron research facilities.

Materials and Methods Three versions of the instruments have been produced for different applications. They essentially consist of a collimated HDPE (high-density polyethylene) with seven solid-state thermal neutron detectors located along the cylindrical axis, within a removable HDPE capsule. An external shield made of 5 mm of borated plastic protects the sensitive capsule from lateral contributions over a broad energy range. A lead disk has been inserted between 6th and 7th positions to increase the response to high-energy neutrons.

The original version of the instrument (CYSP)[(1)] uses one-cm^2 windowless p-i-n diodes made sensitive to thermal neutrons through deposition of 30 μm of ^{6}LiF on the sensitive face. A higher sensitivity version (CYSP-HS)[(2,3)] has been developed for measurements in very

low-intensity fields (e.g. the neutron cosmic radiation at ground level) by increasing the sensitive area of the detectors by a factor of 15. A new version of the instrument (CYSP-BEAM) [4] has been build for the spectrometric monitoring of neutron beam-lines in large-scale neutron facilities. It features small sensitive area (one-mm^2) thermal neutron detectors and a specifically designed tight collimator (2.3 cm in diameter).

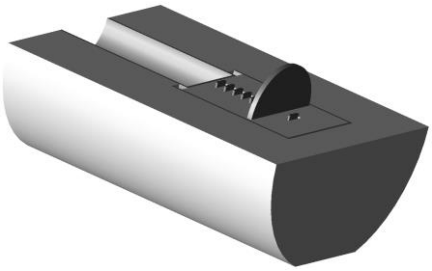

Figure 1. Schematic cut view of the cylindrical spectrometers.

Results and Discussion The neutron spectra and the corresponding integrated quantities have been measured in different workplaces spanning from the ultra low intensity cosmic ray field to accelerator based neutron fields. For instance, the CYSP has been used to determine the neutron spectrum produced in a newly developed high-power liquid Lithium target available at SARAF Israel)[5]. The CYSP-BEAM is being used to measure the neutron spectrum in ISIS (Rutherford Appleton Laboratory, U.K.)[4].

Conclusion New directional neutron spectrometers, based on solid-state detectors and practically insensitive to scattered contributions have been developed. Their wide energy range response and the capability to determine the neutron spectrum with a single exposure made it suitable for measuring time dependant neutron fields.

References

1) J.M. Gómez-Ros et al. CYSP: a new cylindrical directional neutron spectrometer. Conceptual design. Radiat. Meas. 82, 47-51 (2015).
2) J.M. Gómez-Ros et al. The directional neutron spectrometer CYSP: further developments for measuring low intensity fields. Radiat. Meas. 106, 580-584 (2017).
3) R. Bedogni et al. CYSP-HS: a new version of the CYSP directional neutron spectrometer with increased sensitivity. Appl. Radiat. Isotopes 142, 38-41 (2018).
4) R. Bedogni et al. CYSP-BEAM: a multi-detector directional spectrometer for in-beam neutron spectrometry. Nucl. Inst. Meth. A (2019) DOI: 10.1016/j.nima.2019.02.031.
5) R. Bedogni et al. Neutron spectrometry of a liquid Lithium based (p,n) beam at SARAF facility using the broad-energy range directional spectrometer CYSP . Nucl. Inst. Meth. A 902, 144-148 (2018)

Dielectric track detectors in fast neutron measurements and dosimetry

R. Kwiatkowski[1], A. Malinowska[1], A. Szydlowski[2], M. Gierlik[1], J. Rzadkiewicz[1], A. Urban[1]
[1]*National Centre for Nuclear Research (NCBJ), Andrzeja Sołtana 7, 05-400 Otwock, Poland*
[2]*Institute of Plasma Physics and Laser Microfusion (IPPLM), Hery 23, 01-497 Warsaw, Poland*

Highlights The CR-39 track detectors were used to measure neutrons emitted from DT neutron generator. The Monte Carlo simulations of experimental setup were performed. Activation method was used as a complementary diagnostics.

Key words Dielectric Track Detectors, CR-39, Neutron Measurements, Monte Carlo Simulations

Background and Objectives The article presents results of measurements of fast neutrons emitted from DT generator, using track detectors of the CR-39 type, and also activation technique. The neutrons have found varied applications, and neutron generators are one of the most convenient sources of neutrons. In (hot) plasma physics, neutron diagnostics is one of the primary diagnostics used in the experiments. On the basis of the measurements of the flux and spectrum of the emitted neutrons one can determine the properties of hot plasma, and also optimize the system in terms of neutron emission. The main aim of the presented paper was to perform neutron measurements using track detectors and activation methods, and also to compare obtained results with Monte Carlo simulations of the experimental setup.

Materials and Methods The CR-39 type track detectors coupled with various radiators were used to measure neutrons emitted from DT neutron generator. The radiators we used include the standard PE radiator, as well as some metals which, due to the neutron irradiation, emits alpha particles (e.g. Zn, Fe, Ni). The detectors were also shielded with various filters made of materials characterized by lower cross sections for reactions with fast neutrons (i.e. reaction with light ions as one of the products, e.g.: Al, Cu). The filters were meant to block charged particles with energies lower than certain threshold, and thus allowed us to perform rough energy analysis of the ions impinging on the detector surface. Additionally, we used activation method as a monitor of emitted neutron fluxes. The activation samples were chosen to detect fast neutrons, e.g. Fe, Si, Ni and Zn, and gamma-rays, induced by neutrons, were recorded using scintillation probe equipped with $LaBr_3$ crystal. The track detectors after exposure to neutrons were etched in steps, and examined using microscope system with automatic image acquisition. The recorded images were analyzed using specialized software.

Results and Discussion The analysis of tracks and radiation from activation samples allowed us to calculate values of neutron fluxes corresponding to different positions of the detectors. The obtained results showed compliance with the technical specification of the neutron generator. The paper is extension of our previous work[1)], and in this paper we put focus on the Monte Carlo simulations of our experimental setup. The simulations allowed us to calculate response of the used radiators, track detectors and also surrounding, and compare the simulated results with experiment. The different output emission of the used neutron generator and also various neutron energy spectra were tested numerically, and calculations were compared with measured quantities.

Based on the recorded track parameters, it is also possible to calculate linear energy transfer (LET) of the registered particles, and determine the radiation dose of the emitted neutrons[2)].

Conclusion The work presents various techniques for measuring fast neutrons, i.e. using dielectric track detectors equipped with different types of radiators and activation methods. Experimental techniques have been supplemented with careful computer simulations. Using the methods used, it was possible to measure the stream of emitted neutrons and determine the radiation dose from neutrons. The use of computer simulations allowed to compare theoretically calculated values with the measured ones.

References

1) R. Kwiatkowski, et al. Fusion Eng. and Design (2019, in press), https://doi.org/10.1016/j.fusengdes.2019.02.002

2) M. Caresana, M. Ferrarini, M. Fuerstner, S. Mayer, Nuclear Instruments and Methods in Physics Research A 683 (2012) 8–15, https://doi.org/10.1016/j.nima.2012.04.071

Improvements of thermal neutron fields in NIRS accelerator-based neutron source for developments of boron neutron capture therapy

Ryo Ogawara, Tamon Kusumoto, Satoshi Kodaira, Teruaki Konishi and Tsuyoshi Hamano
National Institute of Radiological Sciences, National Institutes for Quantum and Radiological Science and Technology, 4-9-1 Anagawa, Inage-ku, 263-8555 Chiba, Japan

Highlights Thermal neutron fluxes of therapeutic intensities (> 1 × 10^9 cm^{-2} s^{-1}) are required for basic researches of boron neutron capture therapy (BNCT). We developed polyethylene moderators obtaining the thermal neutron fluxes of 1.8 × 10^9 cm^{-2} s^{-1} in NIRS accelerator-based neutron source, named NASBEE facility. Additionally, dose contaminations of fast neutrons and gamma rays are estimated using CR-39 nuclear track detector and optically stimulated luminescence (OSL, Al_2O_3:C) dosimeters.

Key words thermal neutrons, accelerator-based neutron source, CR-39, OSL dosimeter

Background and Objectives Neutron exposure accelerator system for biological effect experiments (NASBEE) facility were constructed to investigate biological effects of around 2 MeV fast neutrons in the National Institute of Radiological Sciences (NIRS), National Institutes for Quantum and Radiological Science and Technology (QST), Chiba, Japan [1]. The thermal neutron flux in ^{9}Be(p, n)^{9}B reactions (4 MeV proton, 600 μA) of NASBEE facility was about 10^7 cm^{-2} s^{-1} using polyethylene (PE) moderators, which reduce velocities of fast neutrons. However, basic researches of BNCT (e.g. subcellular boron-10 distribution, microdosimetry) are required thermal neutron fluxes of therapeutic intensities (> 10^9 cm^{-2} s^{-1}). This work therefore developed thermal neutron fields with the fluxes of > 10^9 cm^{-2} s^{-1} in the NASBEE facility, and dose contaminations of fast neutrons and gamma rays were evaluated using CR-39 nuclear track detector and optically stimulated luminescence (OSL, Al_2O_3:C) dosimeters.

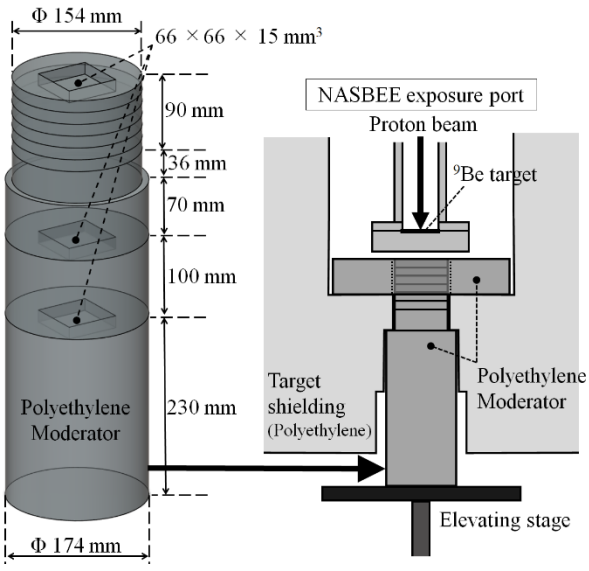

Figure 1. A schematic diagram of NASBEE irradiation port and PE moderators.

Materials and Methods To improve the thermal neutrons fluxes, irradiation samples surrounded with PE moderators were placed at close location from the ^{9}Be target. As shown in Figure 1, one of the 6 disk-shape moderators of 154 mm diameter with 15 mm thickness has square hole of 66 × 66 × 15 mm^3 at its center for a placement of irradiation samples. Thermal neutron fields characteristics (i.e. the fluxes and dose contaminations) can be varied by changing the PE moderator thicknesses placed in front of irradiation samples. Thermal neutron fluxes were estimated by a gold activation method using bare gold foils (5 mm square with 10 μm thickness) and Cd-covered (8 mm square with 0.5 mm thickness) gold foils. CR-39 nuclear track detector (15 mm square with 0.8 mm thickness, TechnoTrack, Chiyoda Technol Corp., Japan) were used for the measurements of secondary particles due to fast neutron interactions. After the neutron exposures for CR-39, 2 hours chemical etching were carried out in 7M NaOH at 70 ℃. Microscopic images of the etch-pits at CR-39 surface were measured using a high-speed imaging microscope (HSP-1000, SEIKO Precision Inc., Japan). OSL dosimeters and its reader system (InLight and microStar, Nagase Landauer, Ltd., Japan) were calibrated by ^{60}Co gamma rays in NIRS/QST. The thermal neutron fluxes and the dose contaminations depending on the PE moderator thickness were measured.

Results and Discussion Figure 2 shows the maximum thermal neutron fluxes of 1.8 × 10^9 cm^{-2} s^{-1} using PE moderator thickness of 30 mm. In this case, etch-pit density of CR-39 and gamma ray doses were 3.9 × 10^7 cm^{-2} C^{-1} and 6.9 Gy C^{-1}, respectively. Dose contaminations of fast neutrons were reduced largely by the PE moderators compared with gamma rays. The ratio of the thermal neutron fluxes and the dose contaminations revealed minimum values with PE moderators of 60 mm (the thermal neutron flux of 1.1 × 10^9 cm^{-2} s^{-1}).

Conclusion Thermal neutron flux of > 1 × 10^9 cm^{-2} s^{-1} was achieved in the NASBEE facility, and neutron field characteristics were evaluated. Exposures of varied thermal neutron fluxes in fixed dose contaminations can be carried out by changing the PE moderator thicknesses and irradiation times. This exposure design is useful for basic researches of BNCT and detector developments.

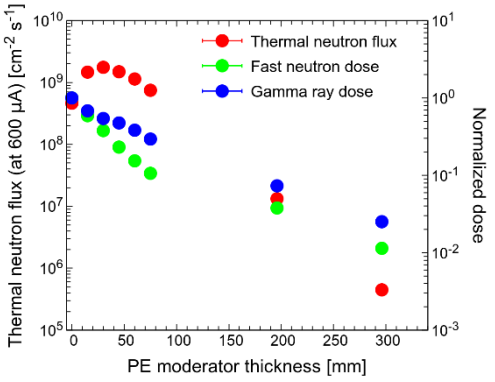

Figure 2. Polyethylene moderator thickness dependence of thermal neutron fluxes and normalized dose

References

1. Mitsuru Suda, et al., *Radiat. Phys. and Chem.* 78, 1216–1219, 2009.

Bulk-density Controlled Thermoluminescence Dosimeters Based on Al_2O_3:Cr Ceramics Aimed at Developing an Anthropomorphic Dosimeter for Photon Radiation Therapy

Shin Yanagisawa[1]*, Yusuke Koba[2], Shigekazu Fukuda[2] and Kiyomitsu Shinsho[1]
[1]*Tokyo Metropolitan University, Tokyo, Japan*
[2]*QST-NIRS, Chiba, Japan*

Highlights We developed new bulk-density controlled thermoluminescence dosimeters (TLDs) based on Al_2O_3 ceramics, aimed at developing an anthropomorphic dosimeter for photon radiation therapy. Their potential was evaluated by measurements of thermoluminescence (TL) properties and theoretical calculations.

Key words radiation therapy, verification, dose distribution, 3D, ceramic

Background and Objectives Although the human body is made up of a lot of elements, it can be classified roughly into three main compositions; air, soft tissue and bone. Therefore, it is ideal to verify the dose distribution in a human body. However, measurements using a solid water phantom are still the most common verification methods of dose distributions.
It has been reported that a stack of tissue-equivalent two-dimensional (2-D) TLDs was able to measure a three-dimensional (3-D) dose distribution[1)]. Recently, we newly developed 2-D bulk-density controlled TLDs to improve their equivalencies to the human body compositions in photon radiation therapy. By controlling the bulk densities of the TLDs, their electron densities were equivalent to those of the human body compositions in photon radiation therapy. We aim to develop an anthropomorphic TLD consisting of only TL phosphors for a 3-D dose distribution verification in photon radiation therapy.

In this study, we performed TL property measurements for photon therapeutic beams and evaluations of equivalencies of the bulk-density controlled TLDs to human body compositions in photon radiation therapy by using Monte Carlo simulations.

Materials and Methods A base 2-D TLD made of alumina ceramics consists of 99.5wt% of aluminum oxide (Al_2O_3) doped with 0.05wt% chromium(III) oxide. Its bulk density and effective atomic number were 3.7 g/cm^3 and 11.14 respectively. The bulk-density control ratios of Al_2O_3 TLDs were 10, 20, 30, 40, 50, 60 and 65%. In those cases, their relative electron densities were 2.94, 2.61, 2.29, 1.96, 1.31 and 1.14 respectively. Their TL intensities and dose responses for 6 MV photon beams were measured by a 2-D TL reader which was a dark box equipped with a CMOS camera and a heater.

For the Monte Carlo simulations, Particle and Heavy Ion Transport Code System (PHITS)[2] Version 3.00 was used. The energies of the therapeutic photon beams were 4, 6 and 10 MV. The deposit energies were scored by PHITS code. The relative electron densities of water equivalent and bone equivalent TLDs were 1.0 and 1.5 respectively. A thirty-centimeter Al_2O_3 cube as a stack of 2-D TLDs was set in the air. The percentage depth dose (*PDD*) curves of Al_2O_3 TLD stacks were compared with those of a water and bone cubes in all simulations. The off-axis ratio (*OAR*) profiles of the TLD stacks were also compared with those of water and bone.

Results and Discussion

The TL intensity decreased as the bulk-density control ratio increased. Each bulk-density controlled TLD had a good linearity for 6 MV X-rays. Fig. 1 shows *PDD* comparisons between the electron-density controlled TLD stacks and the water and bone cubes for the 10×10 cm^2 field. According to Fig. 1, the *PDD* curve of the water equivalent TLD stack was consistent with that of the water cube and the *PDD* curves of the bone equivalent TLD stack was also consi-stent with that of the bone cube in each photon energy. *OAR* curves of each TLD stack were also consistent with those of the water or bone cube.

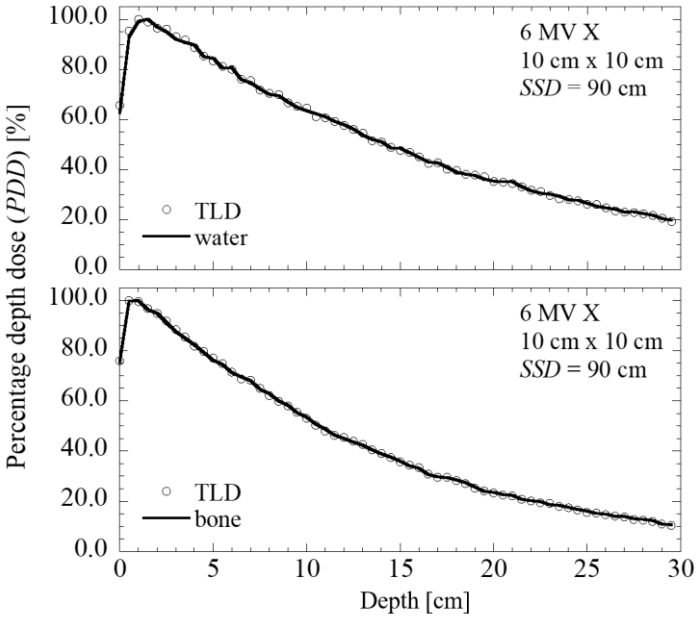

Figure 1. *PDD* comparisons between the bulk-density controlled TLD stacks and the water and bone cubes.

Conclusion We developed relative-electron-density controlled 2-D Al_2O_3 TLDs by controlling their bulk densities and showed that the Al_2O_3 TLDs had good TL properties. The theoretical study suggested that the Al_2O_3 TLDs were equivalent to the human body compositions in photon radiation therapy. The stack of the relative-electron-density controlled 2-D TLDs was expected as an anthropomorphic TLD.

References

1) Shinsho K, *et al.*, Basic characteristic of a prototype tissue equivalent phantom thermolumi-nescence dosimeter (TEP-TLD), Radiat Meas, 46, 1921–1925, 2011.
2) T. Sato, *et al.*, Particle and Heavy Ion Transport Code System, PHITS, Version 2.52, J. Nucl. Sci. Technol., 50:9, 913–923, 2013.

Improvement of the transparency in a PVA-iodide radiochromic gel dosimeter

Shin-ichiro Hayashi[1]*, Kaoru Ono[2], Keisuke Fujino[2], Keisuke Kinoshita[2]
[1]*Faculty of Health Sciences, Hiroshima International University, Hiroshima, Japan*
[2] *High-precision Radiotherapy Center, Hiroshima Heiwa Clinic, Hiroshima, Japan*

Highlights Polyvinyl alcohol-iodide (PVA-I) radiochromic gel dosimeter utilizes the red-coloration due to PVA-iodide complex formed in the gel matrix by irradiation. The transparency is improved significantly by optimizing of the composition and the addition of sucrose without impairing the other desirable properties such as the high sensitivity and the dose-rate-independence. Furthermore, it is also found that the addition of sucrose results in the suppression of auto-oxidation of the gel dosimeter.

Key words radiochromic gel dosimeter, PVA, iodide, complex, sucrose, radiotherapy

Background and Objectives In the past decade, various radiochromic gel dosimeters employing radiation sensitive dyes have been studied to apply to the verification of the complicated three-dimensional (3D) dose distribution in the high precision radiotherapy [1, 2]. Recently, radiochromic gel indicators based on a polyvinyl alcohol-iodide (PVA-I) complex were reported by Miyoshi et al. [3] and Sunagawa et al. [4]. We have developed a novel 3D radiochromic gel dosimeter to base on those indicators [5]. In the present work, the optimization of the composition and the addition of sucrose were examined to improve the transparency of the PVA-I gel dosimeter, and the influence on the dose-response and the stability was investigated.

Materials and Methods PVA-I gel dosimeter prepared in the present study is composed of partially saponified PVA (1.0 wt%), gellan gum (GG, 0.2/0.4 wt%) as a gelling agent, fructose (100 mM) as a reductant, potassium iodide (KI, 50/100 mM), and distilled water (98.6/98.8 wt%). In the case of KI concentration of 50 mM, tribromo acetic acid (TBAA) of 1 mM was added as a sensitizer. Additionally, sucrose was added up to 3.0 M. The prepared gel was subdivided into optical cuvettes, and they were irradiated up to 25 Gy with the different dose rate (100-600 cGy/min) using a 6 MV photon beam of a medical linear accelerator (Varian/BrainLAB Novalis Tx, USA). Absorbances of the samples were measured at 490 nm using an UV-Vis spectrophotometer (UV-1600PC, SHIMADZU, Japan). Absorbance (Abs) was calibrated using a reference cuvette filled with distilled water. The change in the

absorbance (ΔAbs) was obtained by subtracting the absorbance value of a non-irradiated sample from that of the irradiated sample.

Results and Discussion Figure 1(a) shows the sucrose-concentration-dependence on the absorbance of each non-irradiated gel (or background). With decreasing of KI, GG, and both concentrations, the absorbances decreased significantly. It suggests that the interaction between KI and GG causes to the increase of absorbance (or scattering). However, it should be noted that lowering KI and GG concentrations inhibits gelation. On the other hand, with the increase of sucrose concentration, the absorbance decreased further. These results demonstrate that transparency can be improved considerably by the optimization of the basic compositions and the addition of sucrose. Figure 1(b) shows the time-dependence of the background absorbance for 3 days in a gel dosimeter with the lowest absorbance, as an example. With the increase of sucrose concentration, the coloration due to auto-oxidation was suppressed significantly. The optimization of the composition and the addition of sucrose little affected the dose response characteristics.

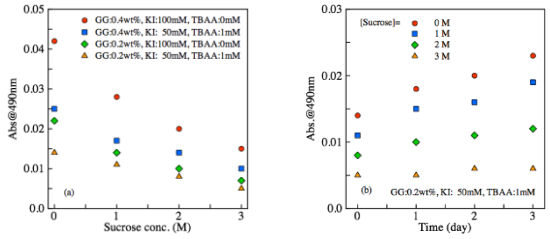

Figure 1. (a): The sucrose-concentration-dependences of the absorbance in each non-irradiated gel dosimeter just after initialization. (b): The time-dependence of one of them for 3 days.

Conclusion It was demonstrated that the transparency of PVA-I gel dosimeter can be improved by the optimization of the composition and the addition of sucrose without impairing the other desirable properties. In addition, it was revealed that the temporal stability of the gel dosimeter was also improved by the addition of sucrose. Further optimization of the composition and evaluation of the other fundamental characteristics are needed. Efforts to address those topics are currently underway.

Acknowledgment This work is supported by JSPS KAKENHI (Grant Number 17K09072).

References

1) Jordan K *et al* 2009 *Phys. Med. Biol.* **54** 6773-6789.
2) Nasr A T *et al* 2015 *Phys. Med. Biol.* **60** 4685-4704.
3) Miyoshi H *et al* 2016 *J. Radioanal. Nucl. Chem.* **308** 469–475.
4) Sunagawa T *et al* 2017 *Mem. Fukui Univ. Technol.*, **47** 105-110. (in Japanese)
5) Hayashi S *et al* 2019 *J. Phys.: Conf. Ser.* (in press).

Prototype Test of Potable Thyroid Dose Monitoring System using Gamma-ray Spectrometers

Sho Nishino[1], Yoshihiko Tanimura[1], Hiroshi Yoshitomi[1], and Masa Takahashi[1]
[1]*Department of Radiation Protection, Nuclear Science Research Institute, Japan Atomic Energy Agency, 2-4 Shirakata, Tokai, Ibaraki 319-1195, Japan*

Highlights The portable thyroid dose monitoring system available in a situation of a severe nuclear accident is in development. In this presentation, the detailed design of the thyroid dose monitor and experimental results using prototype model will be described.

Key words Thyroid dose monitor; Thyroid equivalent dose; Internal exposure;

Background and Objectives In a situation of a severe nuclear accident, a large amount of radionuclides could be released into the environment. Intake of radionuclides by inhalation or ingestion causes internal exposure of people living or working in radiologically affected area. In order to estimate thyroid equivalent dose, individual monitoring based on a radioiodine measurement in thyroid gland should be started immediately after accident because half-lives of radioiodines are short (~8 days for ^{131}I). Therefore, a thyroid monitoring system which is easily installed into evacuation centers and incident command posts should be prepared.

Thyroid Dose Monitor The proposed thyroid dose monitor consists of two gamma-ray spectrometers embedded into a well-type radiation shield as shown in Figure 1 (left). The subject puts their throat on the thyroid monitor from upside, as shown in Figure 1(right). The radioactivity in thyroid is determined from counting rate of ^{131}I 365 keV photo-absorption peak appeared in the energy spectrum, using a pre-determined calibration factor.

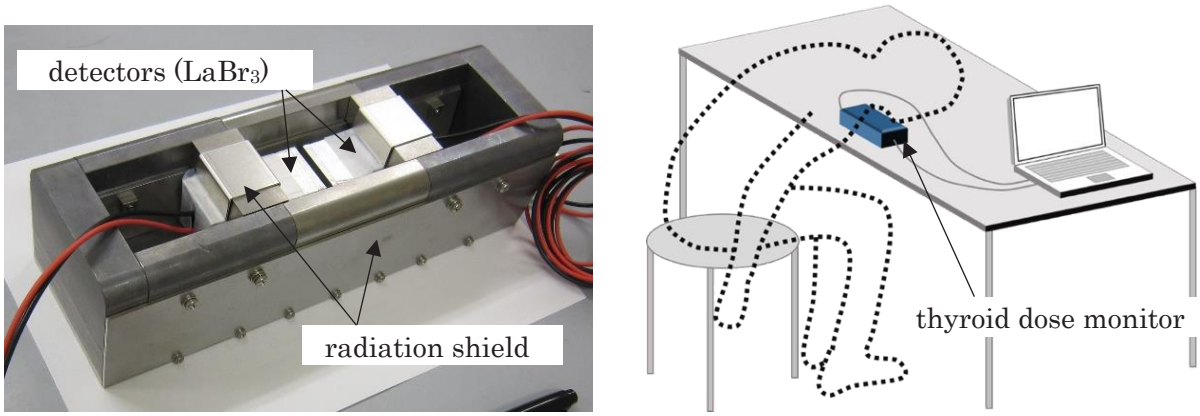

Fig 1. The appearance of the thyroid dose monitor (left) and the attitude of radioiodine measurement using thyroid dose monitor (right).

CdZnTe semiconductor detectors (1.5 cm^3), that have high energy resolution, are adopted for the monitor for radiation-workers who are expected to be measured at areas highly contaminated by various kinds of radionuclides. On the other hand, $LaBr_3$ scintillation detectors (16 cm^3), that give lower minimum assessable thyroid dose thanks to its higher counting efficiency, are adopted for the monitor for members of public. The electric power for the signal processing unit consisting of amplifiers, an analogue-digital converter and a multi-channel analyzer, is supplied from a laptop computer via USB cable. Tungsten (W) heavy alloy and Lead (Pb) are used for radiation shield. W heavy alloy, which has higher shielding efficiency than Pb, is adopted to the shield close to detectors to downsize the monitor.

Prototype Test and Results Performance test using prototype model of the thyroid monitor was performed in the photon reference field established at the Facility of Radiation Standards (FRS) of the Japan Atomic Energy Agency. The monitor showed good shielding performance in high dose rate background condition simulated by ^{137}Cs 662 keV. The minimum assessable thyroid equivalent dose was experimentally evaluated following the technical guideline[1]. As a result, it was confirmed that the monitor can assess thyroid equivalent dose less than 10 mSv even in a high dose rate condition around several 10 $\mu Sv\ h^{-1}$.

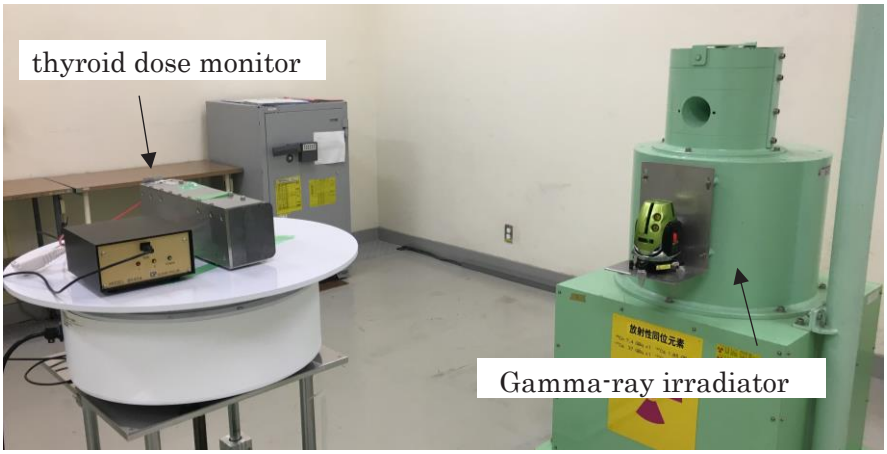

Figure 2 Performance test of prototype thyroid monitor in the photon reference field.

Acknowledgment This work is supported by Grant from Nuclear Regulation Authority, JAPAN.

References

1) Etherington, G. et al., 2017. "CAThyMARA report: Technical guidelines for radio-iodine in thyroid monitoring", OPERRA Deliverable D5.31

An *In-Situ*, Fiber-Optic System for Sub-Surface, Environmental Dose Measurements using Radiophotoluminescence from Ag-doped Alkali-phosphate Glass

Stephen W.S. McKeever[1]*, Sergey Sholom[1], Nishan Shrestha[1] and David M. Klein[1]
[1]*Department of Physics, Oklahoma State University, Stillwater, Oklahoma, USA*

Highlights An *in-situ*, sub-surface environmental monitoring system is described based on radiophotoluminescence (RPL) from Ag-doped alkali-phosphate glass. The system uses a fiber-optic probe encased in a metal or plastic sheath. Once placed in the ground dose measurements can be made *in-situ*.

Key words Radiophotoluminescence, environmental dosimetry, Ag-doped alkali-phosphate glass.

Background and Objectives Potential leakage of radioactive contaminants from low- or high-level, waste-storage sites currently requires periodic soil sampling and subsequent lab-based counting. RPL from Ag-doped alkali-phosphate glass is an established dosimetry method for personal and medical dosimetry.[1)] The objectives of this work were to develop an *in-situ*, sub-surface monitoring system based on RPL from this material and utilizing a fiber-optic-based readout method.

Materials and Methods The samples used in this study were GD-302M glass dosimeters from Chiyoda Technol Corporation, Japan. The composition of the glass is: P: 31.55 wt. % , O: 51.16 wt. % , Al: 6.12 wt. % , Na: 11.00 wt. % , and Ag: 0.17 wt. %. The samples are rods of dimensions 1.5 mm diameter and 12 mm length and were located co-linearly with a silica fiber at the fiber's distal end. The fiber is placed inside a stainless-steel probe. RPL measurements used a 355 nm, 50 mW laser of 1 ns pulse widths and a frequency of 10 kHz. The laser pulses were directed down the fiber via a dichroic mirror to the GD-302M detector. RPL emission from the detector was directed back along the same fiber, via the dichroic mirror, to a photomultiplier tube.

Results and Discussion Figure 1 illustrates prototype probes made from stainless-steel, along with the optical fiber. The probes are similar in design to those used previously for optically stimulated luminescence from Al_2O_3:C.[2)] Laser pulses directed down the probe stimulate RPL emission from the GD-302M detector. Gamma radiation only is detected and this is partially attenuated by the walls of the steel probe. The measured attenuation by the stainless steel probe walls is between ~15-20 %. Build-up of the RPL signal during irradiation is not a problem since the build-up rate is much faster that the RPL growth due to the low environmental dose rate.

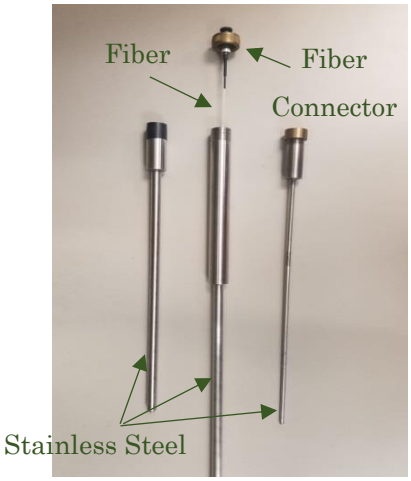

Figure 1. Example stainless-steel probes and fiber inserts. Longest probe shown: ~1m.

With the first configuration of the system a minimum measurable dose (MMD) of ~200 μGy was obtained. At an estimated world-wide environmental dose rate of ~200 μGy per month and an assumed period between monitoring of 1 month, a lower MMD is desired. Experimental results will be described that improve the sensitivity involving the use of PVC probes and an optimized the holder design for locating the GD-302M at the end of the silica fiber.

Conclusion The sensitivity of the prototype, fiber-based, environmental monitoring system developed in this work has the potential for use as an *in-situ*, sub-surface monitoring system. Such a system would remove the need for regular and expensive soil analysis and allow cheap and rapid detection of sub-surface leakage of radioactive waste from contaminated waste storage sites.

Acknowledgments This work was funded by Chiyoda Technol Corporation, Japan, and the State of Oklahoma, USA.

References

1) Yamamoto, T., 2011. In *Concepts and Trends in Medical Radiation Dosimetry*, Rosenfeld, A.B., Kron, T., d'Errico, F., Moscovitch, M. (eds.), 217-230.
2) D.M. Klein, A.C. Lucas, S. W. S. McKeever, 2011. *A low-level environmental radiation monitor using optically stimulated luminescence from Al_2O_3:C: Tests using ^{226}Rn and ^{232}Th sources.* Radiat. Meas., 46, 1851-1855.

Application of Monte Carlo Code and Artificial Intelligence Algorithm to Design and Validate Nested Neutron Spectrometer Using for Accelerator-Based Neutron Source

Sy Minh Tuan Hoang[1*], Gwang Min Sun[2]

[1]*Institute of Fundamental and Applied Sciences, Duy Tan University; Ho Chi Minh City 70000, Vietnam*

[2]*Korea Atomic Energy Research Institute*

111 Daedeok-Daero 989 Beon-Gil, Yuseong-gu, Daejeon, Republic of KOREA

Highlights Designed calculations, simulation, and fabrication of a Nested Neutron Spectroscopy (NNS) have been carried out in this study based on MCNP6 and PHITS codes and a CAD software. With some benefits as light-weight and field portable, cylinders easily be positioned upright on a flat stand, quick configuration for measurements in demanding environments, and able to run in the current mode for high flux environments, the aims of this study is to fabricate the NNS system.

Key words Nested Neutron Spectrometer, Neutron spectrum, Artificial intelligence, MCNP, PHITS.

Background and Objectives The Nested Neutron Spectroscopy (NNS) [1] is an efficient and accurate for measuring neutron fluence in nuclear reactors, accelerator-based neutron sources, and research laboratories that enable the characterization of neutron spectra over 20 MeV and providing an important quality assurance tool for radiation protection. The objectives of this study are to implement the designed calculations, simulation, and fabrication of a Nested Neutron Spectroscopy (NNS). It has some advantaged features in comparison with conventional neutron spectrometers as a convenient single unit package; cylinders can easily be positioned upright on a flat stand, quick configuration for measurements in demanding environments, and large neutron fluence rate measurement range (up to 10^6 $cm^{-2}s^{-1}$).

Materials and Methods The design of the NNS applied a CAD software and Monte Carlo codes (MCNP6 and PHITS) to measure the neutron spectrum generating from proton-induced fast neutron at KIRAM Cyclotron MC-50 (Republic of Korea). At the heart of the NNS are several moderating cylindrical shells, placed one inside the other, providing a lighter-weight compact instrument for neutron field characterization with the routine field use of the well-known BSS method. The nested moderator design allows for quick and easy adjustments of the detector setup by a single operator. Consecutive measurements are completed for each moderator configuration to accurately determine neutron energy distributions from thermal energies to 20 MeV. For higher energies, an optional insert can extend its measurement range

up to 1 GeV.

Results and Discussion The artificial intelligence algorithm was utilized to unfold the energy spectrum of neutron based on the response matrix of 28 energy groups and 35 databases of IAEA spectra. By comparison with the measured spectrum obtained from activation foils, the results of NNS was experimentally validated with the measurement.

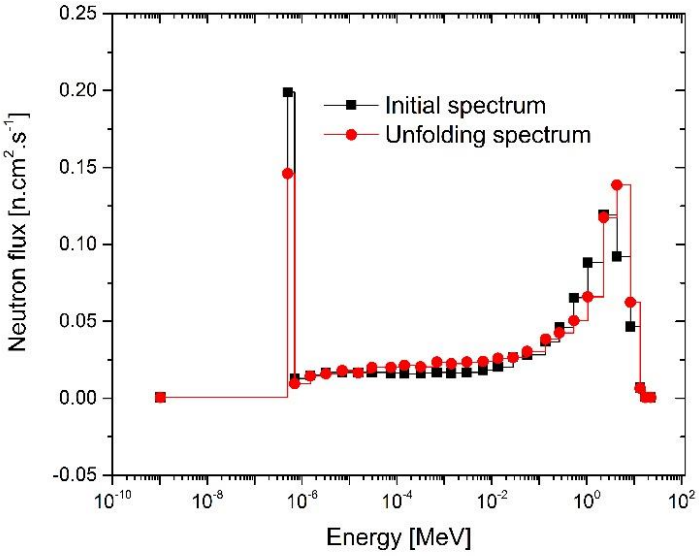

Figure 1. The initial spectrum of a Cf-252 source and the unfolding spectrum using artificial intelligence algorithm.

Conclusion The design of the NNS system to be fabricated including seven cylindrical blocks made of HDPE with the diameter and height respectively from 6.6 cm to 22 cm, and perform matrix calculations the response function of this spectrometer system has been carried out MCNP6 and PHITS codes. In addition, a model of an artificial neural network using tool functions in MATLAB environment has developed a software tool to calculate neutron flux from the original data (scroll solution). The results obtained were initially evaluated as very positive: the spectrum used to test has the exact same shape as the original spectrum; 35 spectra (in 140 spectra of IAEA) used to test the method result in predictable errors of less than 4%. More than 90% of the dose equivalent is calculated using the obtained neutron mass spectra with a deviation of less than 10% compared to the original spectrum.

References

1) Dubeau, J, Hakmana, W.S.S., Atanackovic, J., Yonkeu, A., Archambault, J.P., Radiat Prot Dosimetry. 2012, 150(2), 217-222

Characterisation of Micropatterns written using a Proton Beam in Ag-activated Glass and LiF Crystal observed by Multi- and Single-photon Microscopy

Toshio Kurobori[1]*, Wataru Kada[2], Yuka Yanagida[3], Yasuhiro Koguchi[3], Takayoshi Yamamoto[3], Ivan Sudic[4], Natko Skukan[4], Milko Jaksic[4]

[1]*Kanazawa University, Kanazawa, Ishikawa 920-1192, Japan*

[2]*Gunma University, Kiryu, Gunma 376-8515, Japan*

[3]*Chiyoda Technol Corporation, Oarai, Ibaraki 311-1313, Japan*

[4]*Institut Ruder Boskovic, Bijennicka cesta 54, 10000, Zagreb, Croatia*

Highlights The RPL depth profiles of microscale patterns in Ag-activated glass and LiF crystal written using proton and carbon beams are compared and evaluated using multi- and single-photon microscopes.

Key words Ag-activated phosphate glass, LiF, RPL, Proton beam, Multi-photon microscopy

Background and Objectives Ag-activated phosphate glass is the most widely known radiophotoluminescence (RPL) material and can be used in not only personal, environmental, and clinical dosimeters but also two- and three-dimensional (2D and 3D) dose imaging detectors[1)] and the demonstration of the fluorescence nuclear track detector (FNTD) capabilities.[2)] Very recently, we have reported on the demonstration of microscale patterns in Ag-activated glass written using a focused MeV light ion beam.[3)] These microscale patterns were reconstructed by combining two-photon microscopy equipped with a femtosecond (fs) laser and analytically evaluated by means of lateral/axial dose distributions. Although the penetration depth was in good agreement with the Bragg peak position, but a significant broadening of the depth profiles, especially at the "plateau" region, in the experiment was observed and compared with the SRIM simulation. The purpose of this work is to investigate the origins such a behaviour using both different materials and ion beams with linear energy transfer (LET) values.

Materials and Methods A commercially available LiF crystal and Ag-activated glass with dimensions of approximately 10×10×1.5 mm^3 was used for the optical measurements. The mass density, photon effective atomic number, and refractive index of each material are 2.64 g/cm^3, 8.25 and 1.39 for LiF and 2.61 g/cm^3, 12.57 and 1.52 for Ag-activated glass. A proton beam with an energy of 4.5 MeV/u was used and the irradiation fluence was at (1.43, 4.29, 14.3, 8.9) $\times 10^8$ ions/cm^2. In the case of microscale image observations, multi- and single-photon confocal

microscopes were used. As two-photon excitation(2PE) and one-photon excitation (1PE) sources, fs pulses in the near-infrared (NIR) region generated from a Ti:sapphire laser and 405 nm light emitted from a CW laser diode were used, respectively.

Results and Discussion Figure 1 shows the orange RPL intensity profiles as a function of depth from the surface for (a) LiF and (b) Ag-activated glass, respectively. The inset shows a photograph of the patterns with a 300×350 μm^2 field of view at different fluences in the range (1.43~28.9)×10^8 ions/cm^2 in 4 steps. The 2PE wavelengths were 890 nm for the former and 720 nm for the latter, respectively. For a two-photon microscopy, each axial resolution was about (a) 1.31 and (b) 1.16 μm for a 40×/1.15 numerical aperture (NA) objective lens configuration. Although the Bragg peak position of ~150 μm was in good agreement with the SRIM simulation, but it should be highlighted that in the case of Ag-activated glass a significant broadening like a rectangular depth profile at the "plateau" region and the Bragg peak position with large variance inferred from Fig. 1(b) were observed. The origins of broadening may be considered to different center-formation mechanisms, composition of the materials and their atomic networks within the host. In addition, to confirm such assumptions a carbon beam with an energy of 290 MeV/u beam was also used.

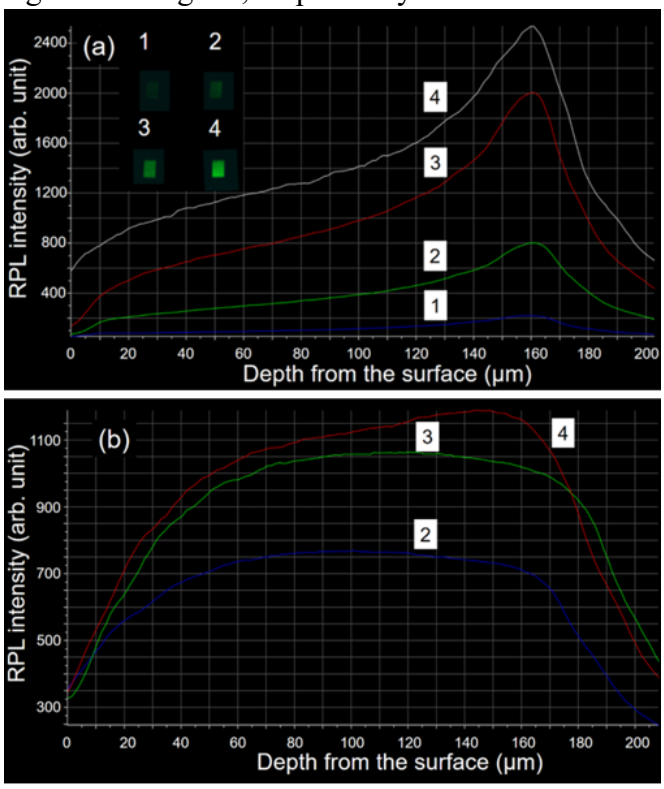

Figure1. Dose distribution profiles as a function of depth from the surface (a) in LiF crystal and (b) in Ag-activated glass.

Conclusion The origins of a significant broadening of the RPL depth profiles were investigated using different RPL materials and HCPs. The dose profiles as a function of the implantation depth were compared visible light 1PE confocal microscopy with NIR light 2PE microscopy.

Acknowledgements Proton irradiation was carried out within the RBI, Zagreb, Croatia.

References 1) Kurobori *et al.*: Jpn. J. Appl. Phys. **55**, 02BC01 (2016). 2) T. Kurobori *et al.*: Nucl. Instrum. Methods Phys. Res., Sect. A **855**, 25 (2017). 3) T. Kurobori *et al.*: Jpn. J. Appl. Phys. **57**, 02CC01 (2018).

Comparison of Ag-activated Glass and Lithium Fluoride Crystal based on Radiophotoluminescence as a Real-time Fiber Dosimetry

Toshio Kurobori[1]*, Yuka Yanagida[2], Yasuhiro Koguchi[2], Takayoshi Yamamoto[2]
[1] *Kanazawa University, Kanazawa, Ishikawa 920-1192, Japan*
[2] *Chiyoda Technol Corporation, Oarai, Ibaraki 311-1313, Japan*

Highlights A real-time fibre-optic-coupled dosimetry system using Ag-activated phosphate glass and LiF crystal based on the radiophotoluminescence phenomena are demonstrated.

Key words Ag-activated phosphate glass, LiF, RPL, real-time dosimetry

Background and Objectives A variety of optical fibre real-time dosimetry systems have been demonstrated providing both accumulated absorbed dose and dose rate using the optically stimulated luminescence (OSL) or scintillation, and the radioluminescence (RL), respectively, as a potentially useful clinical demands of real-time *in-vivo* patient dosimetry applications. Very recently, we have reported on a demonstration of a real-time fibre-optic-coupled dosimetry system using Ag-activated phosphate glass based on the radiophotoluminescence (RPL) phenomena.[1)] However, it was found that the experimental real-time results suggested that the "build-up" and "fading effect" are superimposed both during and after X-ray irradiation and these effects are major difficulties in applying RPL glasses to real-time RPL dosimetry. As for as Ag-activated glass is utilised as a real-time RPL dosimetry, such a "build-up" behaviour cannot be more or less avoided. If other RPL material such as lithium fluoride (LiF) with much lower "build-up" effect is used, it would be possible to realise a real-time RPL dosimetry. In the present work, the performance characterisation using a real-time Ag-activated glass dosimetry is compared with that of a real-time LiF crystal dosimetry.

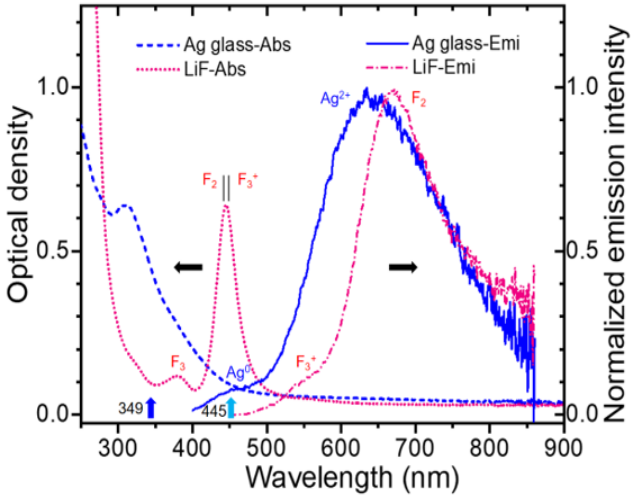

Fig.1 Absorption and luminescence spectra for Ag-activated glass and LiF single crystal.

Materials and Methods A commercially available LiF crystal and Ag-activated glass were used as an RPL dosimetry material. The mass density, photon effective atomic number, and refractive index of each

material are 2.64 g/cm^3, 8.25 and 1.39 for LiF and 2.61 g/cm^3, 12.57 and 1.52 for Ag-activated glass. The heart of the real-time RPL dosimetry system consists of a dichroic mirror, a miniaturised dosimeter, a silica optical fibre, and an excitation laser. As the excitation sources, a Q-switched laser at 349 nm (pulse width τ_p<5 ns, repetition rate f_p<5 kHz) for Ag-activated glass and a high-repetition-rate laser at 445 nm (τ_p <500 ps, f_p <80 MHz) for LiF crystal were used, respectively.

Results and Discussion Figure 1 shows the absorption and the corresponding luminescence spectra in LiF and Ag-activated glass after irradiations. The F-aggregated colour centres (CCs) such as F_2 and F_3^+ centres in LiF and the radiation-induced Ag-related CCs such as Ag^0 and Ag^{2+} centres in Ag-activated glass are mainly used in this work. In the case of Ag-activated glass dosimetry, the GD-302M (Dose Ace) was used. Figure 2 shows a comparison of response curves of a real-time glass dosimetry based on (a) the orange- and (b) blue-RPL for a sequence of pre-dose (PD, non-exposure) and X-ray irradiation region with a dose of 42.2 Gy and then "build-up" and "fading" regions under non-X-ray exposure. The figure shows the integrated RPL area intensity in the wavelength range of 400-500 nm for the blue RPL and in the range of 600-700 nm for the orange RPL as a function of elapsed time. Although the intensity of the blue RPL is much lower than that of the orange RPL, the intensity of the blue RPL rapidly decreases even under X-ray irradiation due to reach the saturation level within a short-time. In the present work, performance characterisation of the real-time Ag-activated glass and LiF crystal dosimetry is compared with that of a real-time plastic scintillation dosimetry.

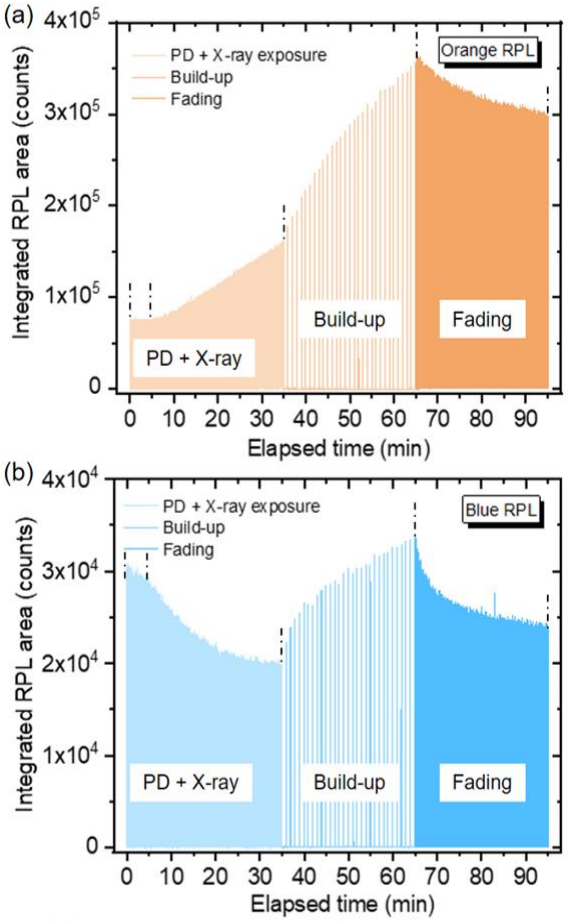

Fig. 2 Response curves of a real-time glass dosimetry based on (a) orange RPL and (b) blue RPL.

Conclusion To realise a reliable real-time RPL dosimetry, inevitable "build-up" and "fading" effects representing major difficulties in applying such RPL materials to real-time dosimetry were investigated and evaluated.

Acknowledgements This work was supported by JSPS KAKENHI Grant Number 17H03519.

References 1) Kurobori: Jpn. J. Appl. Phys. **57**, 106402 (2018).

Conceptual Design of Passive Energoselective Individual Dosemeter Using High Z Detectors

Vadim Chumak[1,2*], Elena Bakhanova[1], Vitalii Voloskyi[1]
[1]*National Research Center for Radiation Medicine, Kyiv, Ukraine*
[2]*Ukrainian Radiation Protection Institute, Kyiv, Ukraine*

Highlights Conceptual design of a passive TL/OSL dosemeter with ability of deconvolution of ambient photon energy composition. Application areas are emergency response (first respondents, military) and other applications where knowledge of incident photon spectrum is essential. The design is substantiated by Monte Carlo calculations and energy spectrum deconvolution algorithm.

Key words Passive dosemeters, optically and thermally stimulated luminescence dosimetry, individual monitoring, energy spectrum, ICRU.

Background and Objectives Traditionally tissue-equivalence of TL/OSL detectors was considered as a great advantage of potential dosimetric materials due to their flat energy response related to biological tissue. However, high effective atomic numbers Z of some materials and, respectively, strong energy dependence may contribute essential data for evaluation of incident photon energies and even for reconstruction/deconvolution of energy spectra. This feature is essential in case of emergency response, when nuclide composition of a source is not originally known – the situation quite common for most military, terrorist attack or radiological accident scenarios. The recent ICRU / ICRP proposal for operational quantities for external radiation exposure adds demand to evaluation of workplace field characteristics, first of all, the energy composition of the photon field. This expands application area of affordable passive energoselective dosemeters also to occupational dosimetry domain.

Materials and Methods In recent years new high Z OSL materials like $YAlO_3:Mn^{2+}$ or Lu_2O_3-based storage phosphors[1, 2)] were introduced and studies as potent detectors possessing significant (up to 50x) energy response in lower energies. This property together with selective filtration by various materials (like Al, Cu, Pb, Sn and their combinations) allow modification of response and, if used in multi-detector systems, deconvolution of incident photon spectra. Such multi-detector systems were proposed and studied earlier[3)] demonstrating reasonable energy resolution of such systems.

Results and Discussion Similar approach is used for development of a conceptual design of an individual dosemeter to be used for emergency and occupational dosimetric monitoring.

Energy and angular response of various detector-filter combinations was modeled by Monte Carlo simulation, some practical dosemeter designs were modeled and studied in this respect. Resulting response functions were incorporated into energy deconvolution algorithm and abilities of spectrum deconvolution were tested with positive outcome.

Conclusion It was demonstrated that the dosemeter comprising several high and low Z detectors would have reasonable weight and dimensions to be used in emergency and occupational dosimetry applications.

References

1) Ya. Zhydachevskii et al., 2016. *Energy response of the TL detectors based on $YAlO_3$:Mn crystals*, Radiat. Meas. 90, 262-264.

2) D. Kulesza et al., 2010. *Lu_2O_3:Tb,Hf storage phosphor,* Radiat. Meas. 45, 490-492.

3) V. Chumak et al., 2017. *Passive system characterizing the spectral composition of high dose rate workplace fields: Potential application of high Z OSL phosphors,* Radiat. Meas. 106, 638-643.

Performance of 2nd-generation FNTD reader in neutron-dose measurements

V. Fomenko(1), J. Harrison(1), M. Moscatel(2), M. Kirr(2), M. Akselrod(1)
[1]*Landauer, Division of Fluke Health Solutions, Stillwater OK , USA*
[2]*Landauer, Division of Fluke Health Solutions, Glenwood IL , USA*

Highlights Performance of a 2nd generation of Fluorescent Nuclear Track Detector (FNTD) reader prototype, utilizing laser line excitation and parallel multipixel fluorescence readout is described. The instrument demonstrated a 30-time increase in the readout speed, compared to the speed of the 1st generation commercial reader and improved image quality. The fluorescent imaging of 32 mm^2 of FNTD area takes about 3 min and provides the sensitivity of 21 tracks/mm^2/mSv for the Am-Be neutrons. Blind tests of the new reader prototype after irradiation with Am-Be neutrons in combination with M30 X-ray photons were performed and have demonstrated compliance with the ISO-14146 standard.

Key words radiation detectors, neutron dosimetry, aluminum oxide crystals, fluorescence.

Background and Objectives The neutron dosimeters based on FNTD technology [1] combine Al_2O_3:C,Mg single crystals with neutron converters and have repeatedly demonstrated good metrological performance. Several iterations of instruments for FNTD readout have been developed. Previously, the FNTD readers were based on the principle of laser scanning confocal fluorescent microscopy when FNTD readout is performed by raster scanning a focused laser beam and collecting the resulting fluorescence on a single-point detector in a confocal arrangement. The neutron dose was estimated from identification and counting the recoil proton tracks. The motivation for the development of a new reader is rooted in the fundamental principles of the counting statistics. The larger the interrogated detector area, the smaller the coefficient of variation of the dose measurement that involves track counting. At the same time, the increased interrogated area leads to longer readout times. Thus, a faster readout is desirable to achieve larger detector readout area and improved counting statistics without sacrificing the image quality and prohibitively increasing the readout time.

Materials and Methods The following advances were utilized in the new reader:

a) Fast CMOS camera for parallel detection of fluorescent signal from FNTD crystals.
b) High power red laser diodes, along with an advanced optical design.

c) New proprietary image processing algorithm for background subtraction, noise reduction and track identification.

Results and Discussion Two types of FNTD packages have been used for the tests: large-area dosimeter packaging with utilized area per one converter of 21 mm^2 and standard Radwatch packaging with the detector surface area in contact with a polyethylene converter of 8.4 mm^2. The dosimeters in both packaging configurations have been irradiated to only Am-Be fast neutrons or in combination with M30 X-ray photons. The dose readout results were quantified against the ISO-14146 standard (2017-08-09 draft), as presented below.

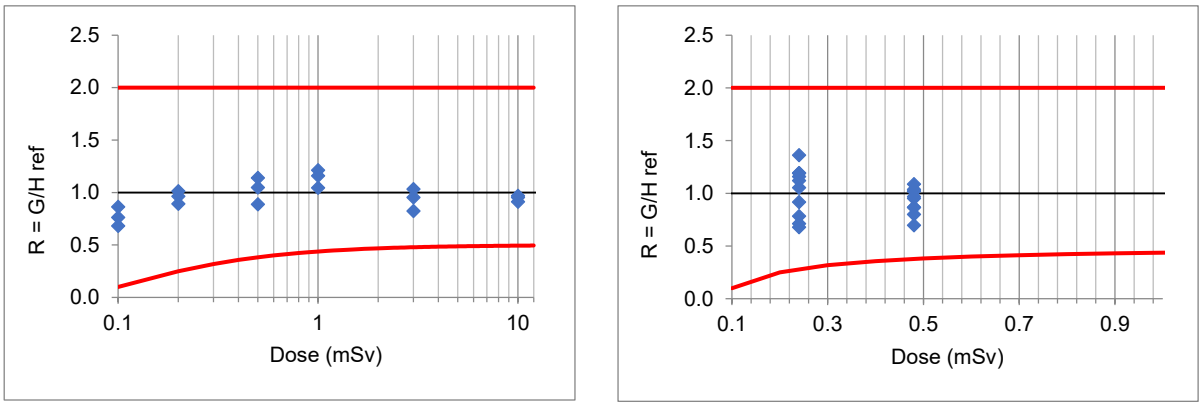

(a) (b)

Figure 1. Normalized response of FNTDs to delivered Am-Be neutron dose measured with the new reader: (a) calibration measurements with large area detectors; (b) Blind test results after mixed neutron and M30 photon dose irradiations of FNTDs in standard packages. Red lines correspond to the performance limits of ISO-14146.

Conclusion The 2nd generation FNTD reader provides faster dosimeter readout, higher image quality and is compliant with the requirements of ISO-14146 standard.

References

1. M. Akselrod and J. Kouwenberg, *Fluorescent nuclear track detectors – Review of past, present and future of the technology,* Radiat. Meas. (2018) **117** 35–51.

Feasibility study on neutron dosimetry under extreme radiation environments using a diamond detector

Xiuqing Xu[1]*, Masayuki Hagiwara[1,2], M. Jauhar Kholili[1], Manobu Tanaka[1,2]

[1] The Graduate University for Advanced Studies, SOKENDAI, Hayama, Japan, [2]High Energy Accelerator Organization, KEK, Tskuba, Japan,

Highlights The responses of a diamond detector to gamma-rays, neutrons and alpha-particles were measured and simulated. We demonstrated that a diamond detector can be used for neutron dosimetry under extreme radiation environments with high-level gamma-ray contamination.

Key words CVD diamond detector, Mixed radiation fields, harsh environments, neutron detector, Fukushima Daiichi nuclear power plant (NPP)

Background and Objectives Mixed radiation fields (neutrons, gamma-rays and so on) are present in many environments including nuclear power plants, nuclear reprocessing facilities, particle accelerators and in medical nuclear facilities. Especially, neutrons and gamma-rays composing these fields are required to be monitored in order to characterize the radiological environments and to avoid the workers from excessive radiation exposure. However, in some harsh environments associated with Fukushima Daiichi nuclear power plant (NPP) after the accident in 2011 and state-of-art high-intensity accelerators such as SuperKEKB, J-PARC and LHC, the real-time monitoring of neutrons and gamma-rays in their caves, that gives diagnostic information in the systems, can be challenging, because high levels of background events[1)]. In 2018, we launched the RIDERS project (Remote Inspection of Debris under Extreme Radiation by Diamond Sensor Integrated with SONAR Systems) to develop a prototype of submerged remotely operated vehicle (ROV) integrated with a neutron detector and sonnars in collaboration with Japanese experts from the High Energy Accelerator Research Organization (KEK), the National Institute Material Science (NIMS) and the National Maritime Research Institute (NMRI), targeting the localization and characterization of the fuel debris at NPP on site. For neutron detector, a thin diamond detector coated by a neutron convertor is selected, because it could measure neutron events associated with the debris apart from huge gamma-ray events by ^{137}Cs widely-dispersed throughout the primary containment vessel (PCV). In this paper, we simulated the response of diamond detectors with different thickness for gamma-rays and neutrons consistent with the Fukushima Daiichi PCV environments, and tested a single-crystal chemical vapor deposition (CVD) diamond detector.

Materials and Methods The responses of diamond detectors were simulated by using the PHITS code[2] for different thickness. To confirm the simulation results, we used a 0.14 mm thick CVD diamond detector with active area of 10 mm^2 and a 95% enriched ^{6}LiF neutron convertor with 1.9 μm thickness. The irradiation tests with several radiation sources; ^{241}Am (α), ^{137}Cs (γ) and ^{241}Am-Be (n) was performed in the radiation calibration facility at KEK.

Results and Discussion Figure 1 shows the calculated results of deposition energies on the diamond detectors with 0.2 mm squares and thickness of 500, 30, 5 μm for irradiation of ^{137}Cs gamma-rays. The sensitivity and deposit energy for the ^{137}Cs gamma-rays decreased with decreasing the detector thickness. The maximum deposition energies were significantly less than the expected deposition energies from the neutron-induced ^{6}Li(n,t)α reaction: E_t= 2.73 MeV, E_α= 2.05 MeV. Besides, the pile-up events will be less impact, because the high count rate capability of diamond detector will be acceptable up to 1 MHz owing the fast mobility characteristics of electrons and holes in diamond. The results of irradiation tests of a CVD diamond detector will be presented in the conference.

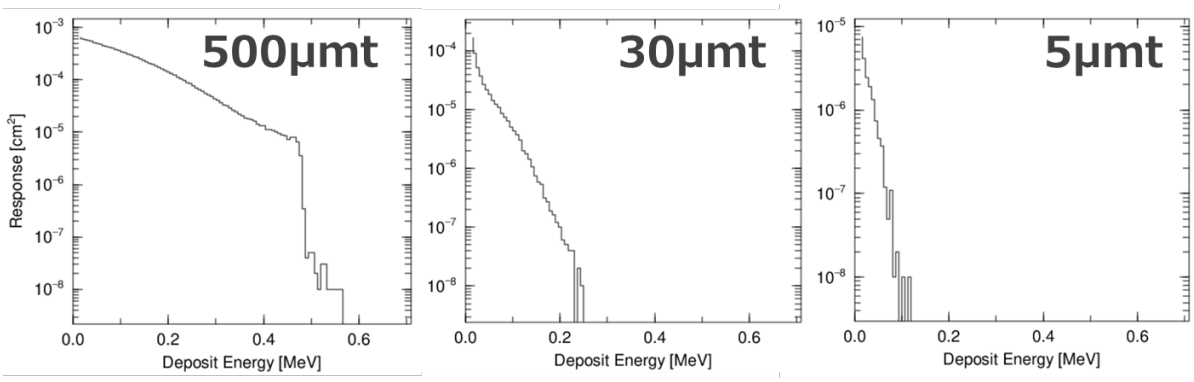

Figure 1. the simulated deposition energies on diamond detectors with difference thickness for ^{137}Cs gamma-rays.

Conclusion The responses of diamond detectors were simulated and measured for gamma-rays, neutrons and alpha-particles. We demonstrated that a thin diamond detector is available for neutron measurement under high-intensity gamma-ray environments using a CVD diamond detector.

References

1) M. Nancekievill, A. R. Jones, M. J. Joyce, B. Lennox, S. Watson, J. Katakura, K. Okumura, S. Kamada, M. Katoh and K. Nishimura: IEEE T Nucl Sci 65 (9), 2565-2572 (2018).

2) T. Sato, Y. Iwamoto, S. Hashimoto, T. Ogawa, T. Furuta, S. Abe, T. Kai, P. Tsai, N. Matsuda, H. Iwase, N. Shigyo, L. Sihver and K. Niita: J. Nucl. Sci. Technol. 55, 684-690 (2018)

Neutron Response Simulation of New Real-Time Personal Dosimeters at the Energy Range between 10 keV and 1 MeV

Yohei Abe[1]*, Masashi Takada[2], Tomoya Nunomiya[1], Kei Aoyama[1], Takashi Nakamura[1,3],
[1]*Fuji Electric Co. Ltd., Hino, Japan*
[2]*Dertment of Applied Physics, National Defense of Academy in Japan, Yokosuka, Japan*
[3]*Cyclotron and Radioisotope Center, Tohoku University, Sendai, Japan*

Highlights Real-time neutron personal dosimeters based on silicon sensor indicate smaller neutron energy response functions than the ICRP dose response curves at the neutron energy range between 10 keV and 1 MeV. Measurement values of these dosimeters are dependent on neutron fields having different energy spectra due to the disagreement between the energy response of dosimeters and the ICRP curves. We have simulated the neutron energy responses using PHITS3 code to improve the energy responses, by considering neutron angular responses in the response functions and reproducing a package of thermal neutron absorber.

Key words silicon sensor, real-time neutron personal dosimeter, simulation, PHITS3 code, angular response, low gamma sensitivity

Background and Objectives Real-time neutron personal dosimeters have been widely used at several radiation fields, such as reactors and accelerators, and then, they will be applied to personal dosimeters of aircrews and workers for boron neutron capture therapies. The neutron personal dosimeters are required to cover a wide energy ranges of neutrons from 0.025 eV to a few tenth MeV. Fast and thermal neutrons are detected by neutron reactions with hydrogens and by neutron capture reactions with boron, respectively. However, at the energy range between a few keV and MeV neutrons are detected via capture reactions of neutrons scattered with human body, called as albedo neutron. The response functions are agreed with the ICRP curves below a few keV and over a few MeV, but the former is smaller values than the later between a few keV and MeV. Dosimeters based on silicon sensor indicate that the measurement values are dependent on neutron fields having different neutron energy spectra due to the disagreement of the dosimeter responses and the ICRP curves. Users require the real-time dosimeters independent of neutron fields. From this background, we have simulated the neutron response functions at the neutron energy range from 1 keV to 1 MeV to produce the real-time neutron dosimeters based on Silicon sensor, independent on neutron fields.

Materials and Methods New neutron dosimeters are based on thin pn silicon diode with 40 μm in thickness. This thin silicon sensor has two advantages of larger and lower detection

efficiencies for fast neutrons and gamma ray, respectively[1]. This gamma-ray responses were experimentally obtained. This neutron sensors can measure gamma rays around 500 mGy/h and higher. The neutron response functions have been simulated using the PHITS3 Monte-Carlo code because of better simulation results than the MCNP6 code[2]. Until now, results of only neutron counts have been accumulated to simulate neutron energy responses; however, in this study, we have considered neutron angular energy response functions of entering the sensor for the response functions. Based on this simulation results, we will reproduce the sensor package, working as thermal neutron absorber, to control neutron energy responses. Also, for higher energy neutrons, we can improve the neutron energy response functions.

Results and Discussion Now, we have simulated the neutron energy response functions of the new real-time neutron personal dosimeters. Figure 1 shows one of the simulation results, plotting tracks of neutron scattered at phantom. Based on the simulation, we can improve the neutron energy response functions of new real-time personal dosimeter.

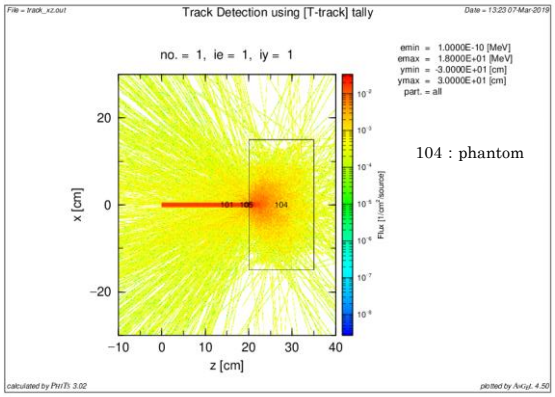

Figure 1. Neutron tracks scattered at phantom.

Conclusion We show new idea to improve the neutron energy response functions between 10 keV to 1 MeV, based on the PHITS3 simulation, considering the neutron angular energy response functions and reproducing the sensor package working as thermal neutron absorber. Using our new real-time personal dosimeters, we can measure personal doses independent on the neutron field.

References

1) M.Takada, T.Nunomiya, T.Matsumoto, A.Masuda, Y.Watanabe, K.Aoyama, T.Nakamura, Neutron Detection Efficiency and Response Functions of a Thin Neutron Silicon Sensor with Low Gamma-Ray Sensitivity, Radiation Measurements, 106, 585-590, 2017.

2) M.Takada, T.Matsumoto, A.Masuda, T.Nunomiya, K.Aoyama, T.Nakamura, Simulated 8 MeV Neutron Response Functions of A Thin Silicon Neutron Sensor, Radiation Protection Dosimetry, 180(1/4), 372-376, 2018.

Background Correction Method for Portable Thyroid Dose Monitor Using Gamma-ray Spectrometer Developed at JAEA in High Dose Rate Environment

Y. Tanimura[1]*, H. Yoshitomi[1], S. Nishino[1], M. Takahashi[1]
[1]*Japan Atomic Energy Agency, Ibaraki, Japan*

Highlights A correction method for the background photons in high dose rate environment was developed to apply to the thyroid dose monitoring using the portable thyroid dose monitoring system developed at the Japan Atomic Energy Agency.

Key words thyroid dose, spectrometer, high dose rate, radio iodine, background photons

Introduction A portable thyroid dose monitoring system using gamma-ray spectrometers has been developed at the Japan Atomic Energy Agency (JAEA) in order to assess the equivalent dose to the thyroid for workers and members of the public in a high dose rate environment at an early stage after a nuclear accident[1)]. The system consists of a couple of gamma-ray spectrometer and a detector shield made of tungsten heavy alloy and lead as shown in Figure 1. The shield has enough thickness to block the background (B.G.) photons entering to the spectrometers from side and bottom. However, the B.G. photons from up above cannot be blocked by the shield and can affect the measurement because there are no shielding material above the spectrometers. This makes it important to correct the B.G. photons for an accurate thyroid dose monitoring in a high dose rate environment.

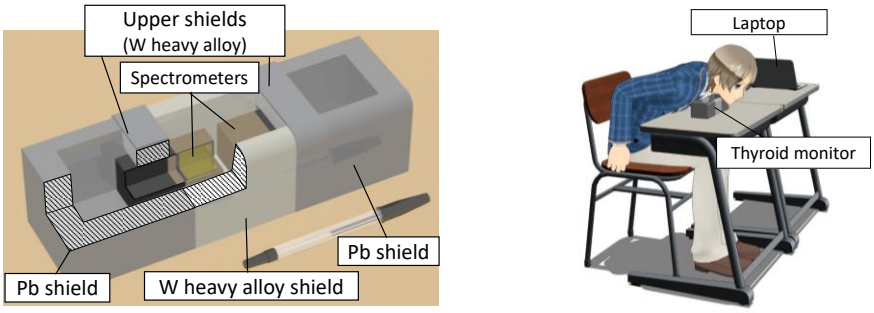

Figure 1. Schematic drawing (left figure) and measurement setup (right figure) of the portable thyroid dose monitoring system.

If the B.G. correction was performed using the measurement data without anything above the spectrometers, the B.G. photons from up above directly entered the spectrometers without any attenuation. As a part of the B.G. photons are reduced by the human body of the subject in the actual thyroid dose measurement, this makes subtraction of the B.G. photons too much and

results in under estimation of the thyroid dose. Therefore, an appropriate correction method for the B.G. photons are required for the accurate monitoring.

In this work, a correction method for the B.G. photons was developed to apply to the portable thyroid dose monitoring system developed at JAEA. In the correction method, cylindrical PMMA phantoms, one of which was used to calibrate the system[2], were employed and set up above the spectrometers in order to mimic the human body.

Methods The system was precisely modelled and its count rates for the B.G. photons were calculated using the PHITS 3.02 code. Three different voxel phantoms[3,4] (ICRP AM, CHILD and BABYNEW) were also included in the calculation models to mimic the human bodies of subjects of different aged. In the calculation the system was irradiated with the isotropic 364 keV gamma-rays from surrounding ^{131}I sources and its peak counts were calculated under three conditions; with the voxel phantom, with a cylindrical PMMA phantom and without the detector shield and any phantom. Then the ratios to the third condition were evaluated for each age group; adult, child and baby.

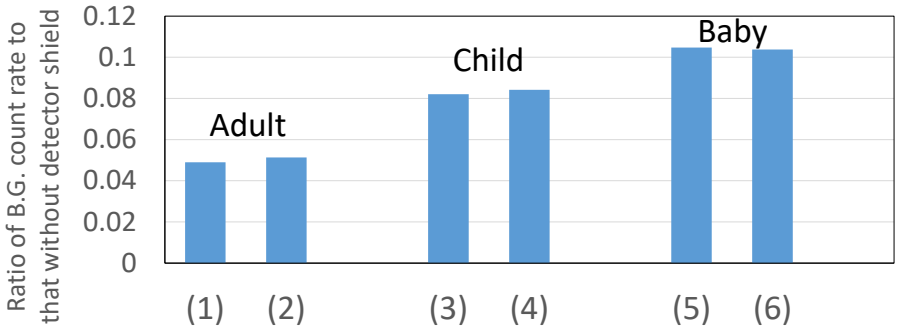

Figure 2. Ratio of the B.G. count rate to that without the detector shield. (1), (3), (5): voxel phantom (adult, child, baby), (2): 20cmΦ×17cm PMMA (vertical), (4): 13cmΦ×12cm PMMA (vertical), and (6): 13cmΦ×12cm PMMA (transverse).

Results and Discussion Figure 2 shows the ratios of the B.G. count rate to those without the detector shield. The ratios with the cylindrical PMMA phantoms are consistent with those with the voxel phantoms. It means that the cylindrical PMMA can be substitute for the human body of the subject in the B.G. photon correction.

Acknowledgment This work is supported by Grant from Nuclear Regulation Authority, JAPAN.

References

1) S. Nishino, *et.al.* European IRPA Congress 2018
2) H. Yoshitomi, *et. al*. AOCRP-5, PP28 (2018)
3) ICRP Publication 110, Ann. ICRP 39(2), 1-164 (2009)
4) N. Petoussi-Hens, *et.al.* Phys. Med. Biol., 47(1), 89-106 (2002)

OSL-dosimetry with BeO. The myOSL-series of portable and stationary equipment

K. Dornich[1], D. Richter[1], I. Słonecka[2], S. Schischke[3]
[1]*Freiberg Instruments GmbH, Freiberg, Germany*
[2]*Central Laboratory for Radiological Protection, Warsaw, Poland*
[3]*RadPro International GmbH, Wermelskirchen, Germany*

Highlights Stationary and portable equipment for OSL dosimetry based on BeO is presented, with an achievable coefficient of variation of 0.66 % for the OSL signal induced by the same dose with more than 100 repeats for a single *MyOSLdosimeter*.

Keywords dosimetric equipment, BeO, OSL

Background and Objectives BeO has a near tissue equivalency and is thus well suited for personal as well as medical dosimetry because of the wide dose range available. Optical stimulation is favored over thermoluminescence and the avoidance of heat allows the use of even portable instrumentation. We here present two new OSL-readers, one designed for rapid mass measurement in personal dosimetry and the other for single element use, both providing facilities for reading and zeroing BeO-elements, in order to allow re-use of the dosimeters at an excellent reproducibility.

Materials and Methods The *myOSLraser* luminescence reader (Figure 1) is developed for the *myOSLdosimeter*, which consists of 2-BeO-elements for Hp(0.07) and Hp(10). The reading as well as the required zeroing is achieved in a single unit for both elements within seconds for a standard dose in personal dosimetry. The zeroing (bleaching) after read-out of the signal used for dose estimation is performed automatically in the same device and thus no separate zeroing equipment is required. In addition to the generally used read-erase-read (RER) mode, where the dosimeter is bleached before re-use, an accumulation mode with no bleaching is available, which allows the re-measurement of the signal before subsequent re-use.

For irradiation purposes the stand alone *myOSLirradiator* is equipped with a Sr-90/Y-90 source (37 MBq). In order to measure large numbers of *myOSLdosimeters* an exchangeable attachment (*myOSLautomatic)* is available (Figure 1), which fits either measurement or irradiation device and allows automated feeding for 200 dosimeters. Management for the

measurement, zeroing and user instruction is achieved by individual dosimeter identification through a bar-code.

An excellent coefficient of variation (0.66 %) of the OSL-signal for more than 100 repeats of a 1 mSv β-irradiation for an individually calibrated *MyOSLdosimeter* is achieved, which shows the excellent properties of the BeO-dosimeters. Such performance is achieved by state of the art stabilization of stimulation and detection in the *myOSLraser* equipment. The *myOSL*-readers and dosimeters comply with IEC-62387.

Optical readout consumes less power and thus facilitates portable use. The *myOSLchip* is a single BeO-element battery operated OSL-reader/eraser. Due to its low weight it is truly portable. The positioning of the single element dosimeter in the *myOSLchip* is manually operated, thus allowing full user control of measurement and bleaching. Individual dosimeter calibration is possible and measurements can also be related to a universal signal-dose response curve. While the number of dosimeters and measurement data managed by the device is restricted in portable mode, full use of the *myOSLdosimetry* software can be made in non-portable operation with external power supply and connection to a PC.

This *myOSLdosimetry* software allows a full scale data management for both devices, including complete measurement and dosing histories, data storage of calculated doses and luminescence measurement, individual dosimeter and device calibration etc. A large number of user defined settings is available which allow, e.g. the definition of units to be displayed or of rejection criteria, like exceeding single or total accumulated threshold doses which are leading to an automated flagging of the specific dosimeter when reached. Reporting functions allow the automated production of individual reports, *myOSLdosimeter* histories etc.

Figure 1: MyOSLraser with automation for reading/bleaching 200 dosimeters.

Simulation of experimental chemical cross sections induced by ions in a polymer (PADC)

Tamon Kusumoto[1], Quentin Raffy[2], Michel Fromm[3], Ziad El Bitar[2], Satoshi Kodaira[1], Tomoya Yamauchi[4] and Remi Barillon[2]*.

[1]Radiation Measurements Research Team, National Institute of Radiological Sciences, National Institutes for Quantum and Radiological Science and Technology, Chiba, Japan
[2]Institut Pluridisciplinaire Hubert Curien, Strasbourg, CNRS UMR 7178, France
[3]UMR CNRS 6249 Chrono-Environnement, Université de Bourgogne-Franche-Comté,
[4]Graduate School of Maritime Sciences, Kobe University, Japan

Highlights Simulation of experimental chemical cross section induced by ions in a poly allyl diglycol carbonate (PADC – CR39) based on the radial dose deposited by secondary electrons removed by the incoming ion.

Key words ion, latent track, chemical structure, radial dose, simulation, Geant4-DNA.

Background and Objectives For many years, we have developed a strong collaboration between Japanese and French teams to understand the chemical structure of a latent track induced by ions in polymers used as nuclear track detectors.

Materials and Methods A systematic work[1] has been made on poly allyl diglycol carbonate (PADC) for ions from H to Xe with LET ranging from 10 to 1200 KeV. μm^{-1}. The chemical cross section for bond breaking of the main PADC functional groups and the creation of OH groups have been determined for these ions. Complementary work was made with γ, X-rays and electrons[2] proving the key role of the energy distribution of the secondary electrons and the density of deposited energy. Additionally a review on the mechanism of chemical modifications on similar compounds was made[3].

Results and Discussion Based on all these data we present an approach based on the radial dose deposited at the nanometer scale by secondary electrons removed by the incoming ion[4] to simulate these experimental chemical cross section. In this work the calculation is based on the use of the Geant4-DNA code. Success and limitation of this method will be discussed.

Reference

[1]Chemical yields for loss of ether and carbonate ester bonds in PADC films exposed to proton and heavy ion beams
Y. Mori, T. Yamauchi, M. Kanasaki, Y. Maeda, K. Oda, S.Kodaira, T. Konishi, N. Yasuda, R. Barillon. Radiation Measurements, 46 (2011), 1147-1153

[2]Elucidation of the Two-Step Damage Formation Process of Latent Tracks in Poly(allyl diglycol carbonate), PADC: Role of Secondary Low-Energy Electrons. T. Kusumoto, M. Fromm, P. Cloutier, AD Bass, L. Sanche, R. Barillon, T. Yamauchi. Journal of Physical Chemistry C, 122 (2018), 21056-21061

[3]Role of intermediate species in the formation of ion tracks in PADC : A review
M. Fromm, S. Kodaira, T. Kusumoto, R. Barillon, T. Yamauchi. Polylmer Degradation and Stability, 161 (2019), 213-224

[4]A first attempt to simulate oxidization effects on latent track structure in PADC combining the radial dose theory and a radio-oxidation kinetic model. R. Barillon, T. Yamauchi, Y. Mori, Q. Raffy. Radiation Measurements, 83 (2013), 1-4

Investigation of fast primary protons and (p,^{11}B) fusion reaction products generated from Plasma Focus facility.

A. Malinowska[1], A. Szydłowski[2], R. Kwiatkowski[1], M.Paduch[2], L.Ryć[2], R.Miklaszewski[2], E.Zielińska[2]

[1]*National Centre for Nuclear Research (NCBJ), Andrzeja Sołtana 7, 05-400 Otwock, Poland*

[2]*Institute of Plasma Physics and Laser Microfusion (IPPLM), Hery 23, 01-497 Warsaw, Poland*

Highlights The proton-boron fusion reaction was investigated within the Plasma Focus facility. The distribution and energies of fast protons emitted during Plasma Focus discharges were determined. The CR-39 track detectors and silicon detector were used to measure emitted alpha particles.

Key words: DPF-1000U facility, fast primary protons, alpha particles, (p, ^{11}B) fusion reaction, PADC track detector.

Background and Objectives: The paper demonstrates the results obtained recently with the polyallyl-diglycol-carbonate (PADC) of the CR-39 type and Si detectors used to measure alpha particles, which are the products of the p + ^{11}B = 3α + 8.7 MeV fusion reaction. This reaction is interesting for scientific community because it offers the possibility of producing energetic alpha particles without neutron generation which may allow the building of a clean nuclear-fusion reactor[1),2)]. The above mentioned reaction has been initiated in the vacuum vessel of the DPF-1000U Plasma Focus facility, which is operated in IPPLM, Warsaw, Poland. Before location of the B target in the discharge chamber we conducted precisely measurements of the parameters of the proton beams emitted from the plasma focus. Especially we determined flux magnitudes, angular and energetic distributions of the generated fast protons.

Materials and Methods To carry-out aforementioned measurements, i.e. characteristics of fast primary protons and α particles produced in the (p + ^{11}B) nuclear reaction we used the PADC detector of the CR-39 TASTRAK type and Si-detector. The CR-39 TASTRAK detector possess many specific advantages which make it a very useful diagnostic tool for registration and experimental analysis of fast particles emitted from high–temperature plasma devices. Described PADC detector can be used both for measurements of fusion reaction products (including neutrons) as well as other fast primary ions emitted from the investigated plasma which can help in understanding of the physical processes occurring in the exploited fusion

machine. The experiment was performed in a few versions i.e. with a solid B-target and with a gaseous B-targets positioned on the discharge axis in different places in relation to the inner electrode face. An attempt was made to find such position in which the fast proton flux was the highest and at the same time the presence of the target doesn't disturb the process of the Plasma Focus discharge. The gaseous target will be formed in different positions using BF_3 gas injected to the chamber by a fast acting gas puff system. The Si detector is used mainly to distinguish (by the time of flight method) pulses of X-rays and fast primary protons emitted from the plasma focus and α particles from (p, ^{11}B) fusion reactions.

Results and Discussion: Up to now we have found, on the basis of nuclear track density recorded by one of the track detector, that around 10^7(p,^{11}B) nuclear reactions have been induced in a solid state ^{11}B target located on the discharge axis of the DPF-1000U facility. However, the paper presents only primary rough experimental results because the experiment is continuously continued and we are still making an effort to optimize the DPF-1000U discharges so that to achieve the highest possible proton beam generation and to find an optimal position of the B-target on the discharge PF-facility axis.

Conclusion: The possibility of using fast primary proton beams generated from the DPF-1000U Plasma Focus facility has been study. Hitherto, around 10^7 (p,^{11}B) nuclear reactions were identified on the basis nuclear track densities recorded by the CR-39 TASTRAK track detector. Before the essential experiment, precisely measurements of the parameters of the proton beams emitted from the plasma focus were conducted using such detectors.

References

1) D. Margarone, A. Picciotto, A. Velyhan, J. Krasa, M. Kucharik, A. Mangione, A. Szydlowski, A. Malinowska, G. Bertuccio, Y. Shi, M. Crivellari, J. Ullschmied, P. Bellutti, G. Korn, "Advanced scheme for high-yield laser driven nuclear reactions", Plasma Phys. Control. Fusion 57 (2015) 014030.

2) A. Picciotto, D. Margarone, A. Velyhan, P. Bellutti, J. Krasa, A. Szydlowski, G. Bertuccio, Y. Shi, A. Mangione, J. Prokupek, A. Malinowska, J. Ullschmied, G. Korn, "Boron-Proton Nuclear Fusion Enhancement induced in silicon targets by Low Contrast Pulsed Laser", Phys. Rev. X. 4, 031030 (2014).

Radon-Thoron level monitoring using pin-hole based twin cup dosimeter & deposition based direct progeny sensors and assessment of dose to general public

Bhupender Singh[1&2], Krishan Kant[*1], Maneesha Garg[2], Ajit Singh[1], BK Sahoo[3], BK Sapra[3], SK Chakarvarti[4]

[1]Department of Physics, Aggarwal College Ballabgarh, Faridabad, Haryana-121004,
[2]Department of Physics, YMCAU&T, Faridabad, Haryana-121006,
[3]RP & AD, Bhabha Atomic Research Centre, Mumbai 400085,
[4]Ex-Natioanal Institute of Technology, Kurukshetra
[*]Corresponding Author: kkant67_@rediffmail.com

Abstract

Radon is a radioactive, carcinogen and naturally occurring gas present in indoor and outdoor environment. In the present paper, radon and thoron concentrations with their decay products has been measured by using passive measurement technique single entry face pin-hole based twin cup dosimeter. The Solid State Nuclear Track Detectors (LR-115 type-II film of sensitive layer of 12µm) were used in dosimeters to register the tracks produced by alpha particles from radon and thoron gases in indoor environment. The DRPS and DTPS (direct radon/thoron progeny sensors) were used for estimation of radon and thoron progenies levels in the indoor environment. The detector in DRPS/DTPS was LR-115 type-II film with appropriate absorber. The estimated radon and thoron level in summer season in area of Faridabad district, Haryana, India varied from 2.5 to 109.1Bqm^{-3} with an average of 16±1.4Bqm^{-3} and from 2.2 to 181.6Bqm^{-3} with an average of 13.2±1.5Bqm^{-3} respectively. The radon and thoron progenies concentrations varied from 0.08 to 13.5Bqm^{-3} with an average of 1.9±0.12Bqm^{-3}and from0.07 to 1.31Bqm^{-3} with an average of 0.21±0.01Bqm^{-3}.The radon, thoron concentration and their progenies level and calculated dose is within the recommended limits of WHO, ICRP and UNSCEAR.

Introduction

Radon and thoron originates from rocks and soil through emanation and exhalation process and reached to environment through leakage or cracks [1]. Radon and thoron gases with their decay products are responsible to more than half of the total natural radiation dose to general public [2]. Radon is considered as second leading cause of lung cancer after smoking [3]. Investigations over the world show a significant increase in the risk of lung cancer due to household radon [4-6]. The decay products are the isotopes of heavy metals Po, Bi & Pb and they have high diffusivities and ability to stick to surface of lungs.

Materials and Methods

Single entry face pin holes twin cup dosimeter has two identical cylindrical diffusion chambers with dimensions (l= 4.1cm,r= 3.1cm). The pin-holes and dimensions of compartments are based on diffusion model of radon and thoron transmission given by Sahoo et.al, [7].The transmission factor for radon into second chamber is about 0.98 and for thoron is about 0.01 as calculated by diffusion model.

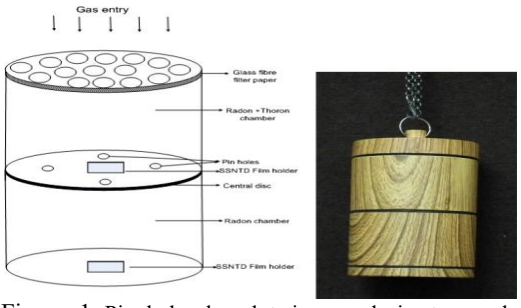

Figure 1 Pin holes based twin cup dosimeter used for measurements of Radon-Thoron gases.

For ^{222}Rn progeny, LR-115 detector with 37µm absorber used to detect 7.67MeV energy α-particles emitted from ^{214}Po, produced by decay of ^{218}Po, ^{214}Pb & ^{214}Bi. For ^{220}Rn progeny, LR-115 detector with 50µm absorber used to detect 8.78MeV energy α-particles emitted from ^{212}Po, produced by decay of ^{212}Pb & ^{212}Bi atoms deposited on Mylar surface. The track recorded in the exposed LR-115 film is related to Equilibrium Equivalent Progeny Concentration (EEC) using the sensitivity factor.

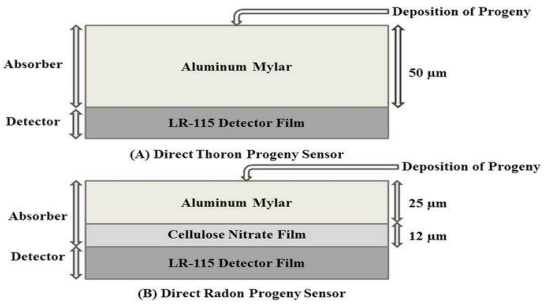

Figure 2 Tools of Measurement of Radon-Thoron progenies level in air (a) DTPS, (b) DRPS

Type	Description of houses
A	Houses with & without Plaster Girder and Stone Slab Roof + Brick Walls + Cement Floor
B	Brick Wall Houses + Thatched Roof
C	Mud Wall Houses + Thatched Roof
D	Traditional Houses with RCC (Concrete) Roof + Plaster Walls + Cement Floor
E	Modern Houses – RCC Roof + Plaster Walls + Marble Floor + Tiles on Walls.

Figure3 Description of dwellings for radon-thoron monitoring in environment of Faridabad district, Haryana, India.

^{222}Rn (Radon) gas concentration (C_R)

$C_R(Bqm^{-3}) = (T_1\text{-}B)/(d.K_R)$ (1)

^{220}Rn (Thoron)gas concentration (C_T)

$C_T(Bqm^{-3}) = (T_2\text{-}d.C_R.K_R\text{-}B)/(d.K_T)$ (2)

^{212}Po concentration

$EETC(Bqm^{-3})=(T_T\text{-}B)/(d.S_T)$ (3)

^{214}Po concentration

$EERC(Bqm^{-3})=(TRn\text{-}B)/(d.S_R)$ (4)

$TRn=T_{DTPS}-(\Pi_{RT}/\Pi_{TT})T_{DRPS}$ (5)

Total inhalation effective dose of radon along with its progeny is calculated by,

$TIDr(mSvy^{-1}) = [(Cr\times0.17)+(EERC\times9)]\times8760\times0.8\times10^{-6}$ (6)

Total inhalation effective dose of thoron along with its progeny is calculated by,

$TIDt(mSvy^{-1})= [(Ct\times0.11)+(EETC\times40)]\times8760\times0.8\times10^{-6}$ (7)

Where, symbols have their usual meanings

Results and Discussion

Table-1: Variation of concentrations of indoor radon, thoron, radon progeny, thoron progeny and dose levels in Summer season in dwellings of Faridabad district Haryana, India.

Parameters	Min	Max	AM±SE
222Rn	2.5	109.1	16±1.4
220Rn	2.2	181.6	13.2±1.5
EERC	0.08	13.52	1.9±0.12
EETC	0.07	1.31	0.21±0.01
TIDr(mSvy^{-1})	0.17	1.77	0.35±0.01
TIDt (mSvy^{-1})	0.03	0.53	0.17±0.01
TID$_{total}$(mSvy^{-1})	0.12	2.15	0.52±0.02

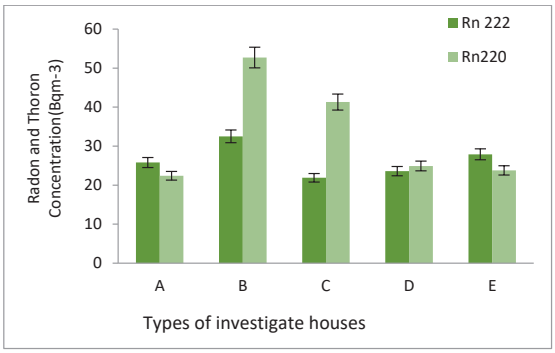

Fig.4. Variation of radon (AM) and thoron (AM) concentrations in different types of dwellings.

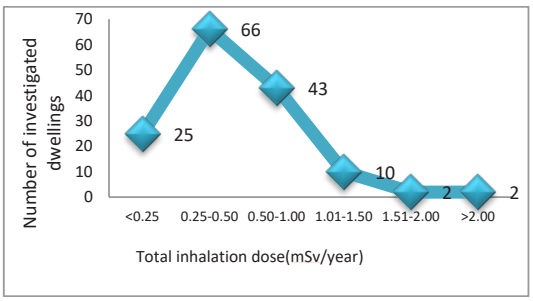

Fig5. Frequency distribution of inhalation dose in Faridabad district of Haryana, India.

The variation of radon and thoron levels might be due to the different geological locations, different ventilation conditions and different building materials used for construction of dwellings as shown in other investigations [8].The level of radon gas was higher in mud and modern dwellings and it might be due to diffusion of high emanation from the minerals in the walls which closed agreement with other study [9].

Conclusion

The level of radon and thoron concentrations was within recommended limit of 300Bqm^{-3} proposed by ICRP, 2011. Progenies level was within safe limits 17Bqm^{-3} and 3Bqm^{-3} for radon and thoron progeny respectively recommended by ICRP, 1993.Dose received by population was within 10 mSvy^{-1} recommended by WHO, 2009.

Acknowledgement

Authors are thankful to Board of Research in Nuclear Science, Bhabha Atomic Research Centre, Mumbai, India for financial assistance vide project no. 36(4)/14/63/2014-BRNS dated 26/02/2016 for carrying out this work.

References

1. WW Nazaroff and AV Nero (1998). Radon and its decay products in indoor air, John Wiley & Sons, New York.
2. UNSCEAR, (2006). United Nations scientific committee on the effects of atomic radiation. Report A/AC.82/-644, Exposures of workers and the public from various sources of radiation, United Nations, New York.
3. WHO (2009). WHO hand book on indoor radon: a public health perspective. Geneva 27, Switzerland: World Health Organization.
4. Vimercati L, Fucilli F et al (2018). Radon Levels in Indoor Environments of the University Hospital in Bari-Apulia Region Southern Italy. Int. J. Environ. Res. Public Health; 15:e694 doi: 10.3390/ijerph15040694.
5. López-Abente G, Núñez O et al (2018). Residential radon & cancer mortality in Galicia, Spain. Sci Total Environ;doi:10.1016/j.scitotenv.2017.08.144.
6. Stanley F.K, Zarezadeh S, et al (2017). Comprehensive survey of household radon gas levels and risk factors in southern Alberta. CMAJ Open; 5:E255–E264. doi: 10.9778/cmajo.20160142.
7.BK Sahoo, BK Sapra, et al (2013). A new pin-hole discriminated ^{222}Rn/^{220}Rn passive measurement device with single entry face. Radiation Measurement; DOI:10.1016/j.radmeas.2013.08.003.
8.Nitin Gupta, Krishan Kant and Maneesha Garg. Radon-thoron and their progeny dosimetry in multi-storeyed malls in Delhi NCR (India) using plastic track detectors. *Int. J. Low Radiation, Vol. 10, No. 4, 2017.*
9. K Kant, Suraj B Upadhyay, GS Sharma and SK Chakarvarti (2006). Radon dosimetry in typical Indian dwellings using plastic track detectors. Indoor Built Environ; DOI:10.1177/1420326X06064091.

Metrological feedback on ISO 21909:2015 and performance assessment of the neutron dose measurement process of LANDAUER EUROPE

MORENO Brahim[1], MILLION Marc[1]
[1]*LANDAUER, Scientific department, Vélizy-Villacoublay, France*

Highlights The framework for testing the performance of neutron dosemeter has evolved. A first feedback on the new ISO 21909 standard will be presented based on experimental measurements obtained with our routine measurement process. An upgrade of our dose estimation algorithm using a Monte-Carlo method will also be discussed.

Key words dosimetry, SSNTD, neutron, metrology, ISO 21909

Background and Objectives In the 2005 version of the ISO 21909, the performance tests and associated acceptance criteria were technology dependent. Part of the work for creating the 2015 version was to have a standard that applies to all neutron dosemeters with the same methodology for performance assessment and the same performance objective. In the process of developing the standard, all tests have been completely redefined. Thus, it was not possible for the authors to use data obtained from type testing against ISO 21909:2005 to fully check the relevance of the new criteria. The work described here is twofold. The first goal is to be part of the effort to provide feedback on the standard from a metrological point of view by using the performance results of our standard neutron dose measurement process against ISO 21909:2015. The second objective is to provide status and description of the work undergone to improve the response of our neutron dose measurement process.

Materials and Methods LANDAUER neutron measurement process is based on the Neutrak dosemeter, a Solid-State Nuclear Track Detector (SSNTD). The type test was performed by the United Kingdom National Physical Laboratory (NPL). This laboratory is one of the few accredited against ISO/IEC 17025 to perform the neutron irradiations required in the ISO 21909:2015 standard. Irradiations spanned from 144 keV to several MeVs for mono-energetic neutrons. The dosemeter was also tested for thermal neutrons and for angle dependency. Improvement on the dose response is built on track morphological criteria such as tracks area and radius. One explored solution is to use morphological criteria as inputs to a modified version of the reconstruction algorithm developed for one of LANDAUER whole body dosemeter (1). Measurements are compared to a response database. This database will be

used to reconstruct the input signal with a Monte-Carlo method in terms of dose and radiation quality.

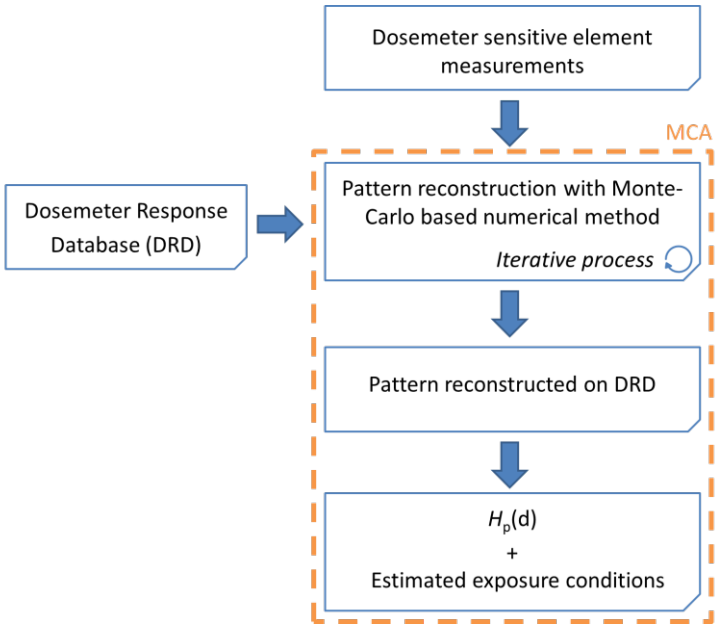

Figure 1: Schematic of the proposed algorithm to reconstruct the neutron dose based on track morphological criteria.

Results and Discussion The use of the standard for assessing the performance of neutron dose measurement processes can be improved. It provides sometimes a worse picture than the actual performance of the system. For instance, for the non-linearity test, the reference for calculating the dose response is built on the average of the $H_M^{C_i}/C_i$ ratios for all dose points. The quantity $H_M^{C_i}$ is the average of the measurements for the conventional true dose C_i. This method artificially increases the uncertainty of the performance criteria. First experimental results fit inside the standard acceptable limits with room to improve the response by using the previously described algorithm.

Conclusion Substantial improvement can be made to the standard, so the type test gives a better assessment of the actual performance of the neutron dose measurement processes. Preliminary results obtained with the new neutron dose algorithm will be presented.

References

1. **Marc Million, Brahim Moreno.** Development of a Multi-Sensitive Element Passive Dosemeter Based on OSL Technology. *Radiation Protection Dosimetry.* 2017, Vol. 174, 3, pp. 377-381.

Radiological aspects on the fuel assembly separator dismantling from VVR-S nuclear research reactor

C. Tuca[1]*, R. Deju[1] and A. Zorliu[1]

[1]*Horia Hulubei National Institute for Physics and Nuclear Engineering, Magurele-Bucharest, Romania*

Highlights The VVR-S nuclear research reactor with thermal neutrons from Romania, used for radioisotopes production and physics research purposes was operated between 1957 and 1997 and finally shut down in 2002 in order to be decommissioned for safety reasons. The separator for fuel assemblies, was dismantled in 2014 using plasma torch technology. The process involved radiological risks for the workers due to the high levels of dose rate. The workers external exposure was monitored continuously and the internal exposure was assessed based on the activity concentration of the aerosols released during the cutting process.

Key words reactor, decommissioning, radiological monitoring, dosimetry, effective dose

Background and Objectives The reactor was operated at nominal thermal power of 2 MW and the maximum thermal neutron flux of $2x10^{13}$ neutrons/cm^{2}s using as fuel the uranium dioxide enriched by 10% ^{235}U isotope and 36.63% ^{235}U isotope. The fuel assemblies were placed in the reactor core into a dedicated aluminum alloy cylinder, the separator which was the most activated component of reactor. The separator dismantling is radiologically monitored to assure the workers and environment protection according to the ALARA principle. For this purpose, there were also implemented the radioprotection measures such as: the construction of a biological concrete shielding around the separator, set-up of HEPA portable filtration systems in the cutting area and the adequate protective gear for the workers.

Materials and Methods Before separator removal from the reactor core (see Figure 1), the internal surface of the inner vessel is scanned for a minute with a FH 40 G digital multi-meter with FHZ 691-10 probe to detect the 3% increases of the dose rate from background. The hot spots were also identified with a LB 123 D-H10 monitor. The external separator surfaces were scanned 30 cm above the reactor block, with FH 40 GL-10 and FHZ 612-10 systems to estimate the potential radiological risks for cutting process. The separator was cut with a Powermax105 plasma jet system (see Figure 2). The external exposure of the workers is monitored using Saphydose Gamma isotropic electronic dosimeters. The ambiental dose rate were monitored with a LB 123 UMo monitor and LB 1231 beta/gamma and LB 1233 alpha/beta probe. The surface contamination monitoring is performed with Thermo Scientific FHT 111 M

contamination monitor located at the Reactor Hall exit door. The activity concentrations of the aerosols released during the process were monitored with FHT 2000 AERD alpha/beta systems. The concentrations were reported to the maximum admissible values for reference beta-gamma (Co-60) and alpha artificial (Am-241) emitters and (Rn-222) [1]. The committed effective dose equivalent is calculated taking into account the external and internal exposure, based on the methodology described in paper [2].

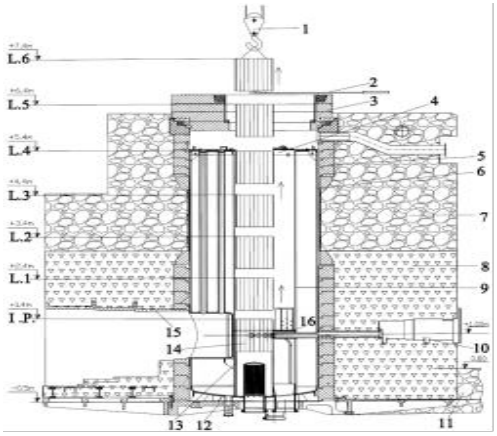

Fig.1. Separator removal: 2 – monitoring system; 13 - inner reactor vessel;14 – separator

Fig.2. Separator cutting

Results and Discussion During the separator removal the external dose rate was insignificant. A potential internal exposure could be in the separator cutting due to the alpha artificial emitters in case that the workers are not protected by the respiratory masks. The highest dose rate was at the extraction of the separator cut pieces from biological shielding and positioning in the waste package as well as the for the clean-up activities. The dose rate of 10.2 μSv/h is slightly higher than the limit (10 μSv/h), but the collective dose of 0.14 man-Sv is quite small comparing with the estimated one, 1man-Sv. The greater contribution in the effective dose was given by the external exposure 56 %. The internal exposure accounts for 44 %.

Conclusion The effective dose for the exposed personnel in the separator dismantling shows that the limit of 20 mSv/h [2] was not overpassed. The workers were not radiologically affected in the separator dismantling process due to the choosing of a proper cutting technology as well as the suitable radioprotection measures implemented.

References

1) Radiological Safety Fundamental Regulations, CNCAN president order no. 752/3.978/136/2018, published in the Romania Official Monitor, Part I no. 517 bis/25.06.2018.
2) C.Tuca, R.Deju, A.Zorliu (2017) Radiological risk assessment for hot cell decontamination, Romanian Journal of Physics, 62 (7-8), Article 812, 2017

Uncertainty and Response Limits of Passive Dosemeters

C. Hranitzky*, H. Stadtmann
Seibersdorf Labor GmbH, 2444 Seibersdorf, Austria

Highlights The upper limits of the measurement uncertainty of passive personal and area dosimetry systems were estimated according to the IEC 62387 dosimetric performance requirements. The corresponding limits of the response of these dosemeters were calculated for 90 % and 95 % confidence probabilities and compared to the ISO 14146 'trumpet curve' criteria for intercomparisons.

Key words passive dosemeter, uncertainty, response, limits, intercomparison, trumpet curve

Background and Objectives Passive radiation protection dosemeters for individual and area monitoring are used for issuing periods between one and several months. The performance and test requirements of these dosimetry systems are described in the international standard IEC 62387:2012 and its modified European edition EN 62387:2016. Using the mandatory response limits for the various influence quantities, the corresponding upper limit of the uncertainty contributions can be estimated. Recommendations for the total uncertainty are not provided in the IEC standard but may be included in the currently discussed new revision. The limits of the dosemeter response and related criteria for evaluating intercomparisons and periodic performance verifications are recommended in the recently revised standard ISO 14146:2018. The objective of the presented work was to present reasonable upper limits of the total uncertainty for personal and area dosimetry systems just fulfilling the IEC 62387 requirements. The resulting response limits as a function of the reference dose were compared to the ISO 14146 response limits, the so-called 'trumpet curves'.

Materials and Methods The upper limits of the total measurement uncertainty of passive area and personal dosemeters were estimated on the basis of a dose model function including the main influences quantities (calibration, statistical variation, dose non-linearity, radiation energy and angle of radiation incidence and environmental influences). The resulting upper limits of the total uncertainty as a function of dose (conventional true dose in terms of personal or ambient dose equivalent) were used to calculate the upper limits of the dosemeter response. To be consistent with the ISO 14146 approval criteria for intercomparisons, 90 % and 95 % confidence probabilities were applied.

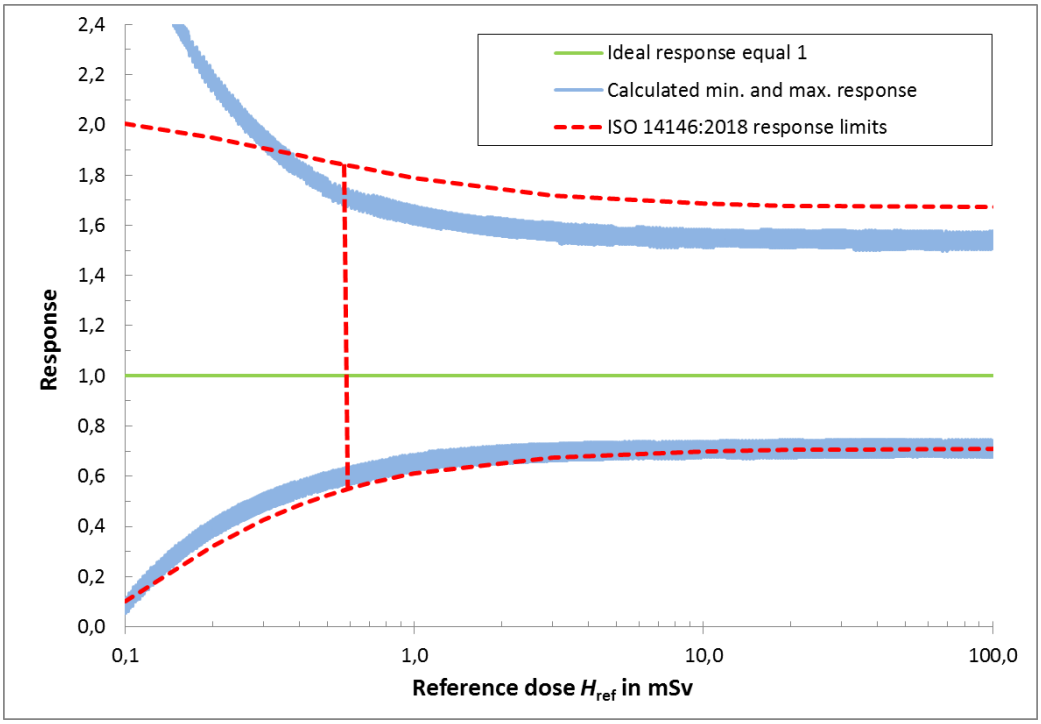

Figure 1. Minimum and maximum values of the dosemeter response at a 90 % confidence level compared to the ISO 14146:2018 response limits as a function of the reference dose. The minimum recommended reference dose of 0.6 mSv (assuming a three-month natural background dose contribution) is also indicated as vertical dashed line.

Results and Conclusion The subtraction of the natural background dose is crucial for the determination of response results in intercomparisons of passive dosemeters. The increased uncertainty and resulting response limits at low dose values due to the background subtraction were investigated for typical intercomparison periods of several months. Finally the range of the uncertainty contribution of the reference dose was considered for the 90 % confidence limits. This range is given in figure 1 as a broadened band of calculated maximum and minimum response values. The ISO 14146 recommendations for the response limits as well as for the minimum reference dose were found to be appropriate.

Dose Rate Measurements in Two Main Cities of Karnataka, India with Distinct Geological Features

Darwish Al-Azmi[1*], Sudeep Kumara[2], Mohan M.P.[2], Karunakara N.[2]

[1]Department of Applied Sciences, College of Technological Studies, Public Authority for Applied Education and Training, Shuwaikh, P.O. Box: 42325, Code 70654, Kuwait. (Email: ds.alazmi@paaet.edu.kw / dalazmi@yahoo.co.uk).
[2]Center for Advanced Research in Environmental Radioactivity (CARER), Mangalore University, Mangalagangothri-574199, India.

Highlights Gamma dose rates were measured using a portable NaI(Tl) dosimeter at two cities of Karnataka State in India. The dose rates in Mangalore and its surrounding were found to be within the normal level. Relative higher gamma dose rates were recorded within Mysore city due to the granite region.

Keywords gamma dose rates, mobile measurements, scintillation dosimeter, Karnataka

Background There are regions in the world, known as high natural background radiation (HNBR) areas, where the outdoor natural background radiation substantially exceed the normal range due to the natural enrichment of certain radioactive minerals. HNBR areas have been reported in several regions worldwide [1)]. High natural background radiation levels have been reported around the coastal regions of Mangalore city in Karnataka State, India, due to the scattered deposits of monazite sand, thus elevated levels of gamma dose rates have been observed accordingly [2,3)]. Also within the same State, high levels of background radiation have been observed in and around Mysore city due to the granite region within the area [4)].
It is of interest to further explore the study to record the gamma dose rates on the roads of the Karnataka State using a portable dosimeter.

Materials and Methods The measurements of the ambient gamma dose rates within Karnataka State, southwestern India, were carried on the asphalt roads of Mangalore and Mysore cities and their surroundings during the period from December 2017 to June 2018 using a portable dosimeter.
The scintillation dosimeter "RIID EYE"; a portable NaI(Tl) gamma spectrometer/dosimeter (Thermo, USA) was used for the measurements. At each location, the mean value of 5 to 7 repeated readings, each of 5-minute sampling interval, was considered as the representative value for the dose rate at the investigated location. This type of measurement criteria was expected to provide a desired accuracy with a confidence level of 95% [5)]. Each location coordinates were recorded using a GPS system. So far, two cities have been covered within this study and it is planned to cover most of the roads of the Karnataka State.

Results and Discussion Measurement of the gamma dose rates on some of the roads of Mangalore and Mysore cities were carried out for 37 locations (Figure 1). The measurements were carried out on the asphalt roads around Mangalore City in Karnataka state in India and its surrounding through the Mysore City. The dose rate values ranged from 39.7-186.2 nSv/h (Figure 2). Higher dose rates were observed around the granitic regions of Mysore city since these granites naturally contain relative higher concentrations of ^{226}Ra, ^{232}Th and ^{40}K [4)].

However, in locations other than the granitic region, the dose rates were found to be similar to the worldwide average value.

Conclusion In spite of the relative high background radiation levels in Mangalore, up-to 530 nSv/h [2], the dose rates on the asphalt roads of the city show normal range. However, some relative higher dose rate values were recorded within Mysore city due to the presence of the granite within the region [4]. The dose rates along the national high way connecting Mangalore and Mysore cities were found to be similar to the worldwide average value.

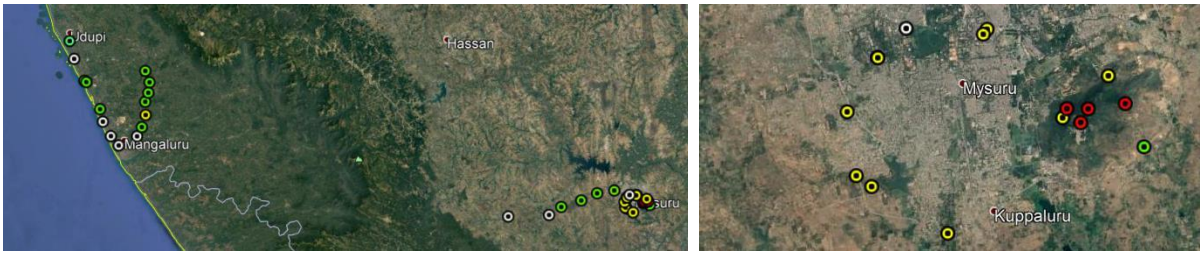

Figure 1. **Left** Map showing Mangalore and Mysore cities and the highway connecting the two cities where the dose rates were measured. **Right:** Expanded view of Mysore city. (Dose rate values are shown in color codes: white: up to 50 nSv/h, green: 51-100 nSv/h, yellow: 101-150 nSv/h and red 151-200 nSv/h).

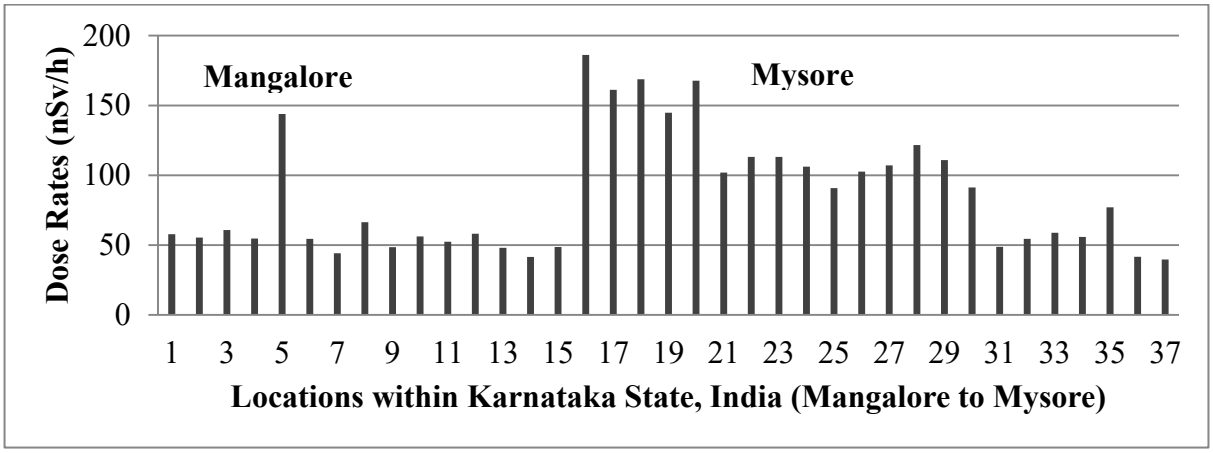

Figure 2. Comparison of dose rates at two different locations; Mangalore and Mysore cities within Karnataka State. High dose rate values correspond to granitic areas of Mysore.

References

1) UNSCEAR. United Nations Scientific Committee on the Effects of Atomic Radiation (UNSCEAR). Report to the General Assembly, vol. 1, Annex. B; (2008).
2) D. Al-Azmi, Sudeep Kumara, M.P. Mohan, and N. Karunakara. Gamma dose rates in the high background radiation area of Mangalore region, India. Accepted paper in the Journal of Radiation Protection Dosimetry (2019).
3) D. Al-Azmi, N. Karunakara, and A. Mustapha. Teaching about natural background radiation. Physics Education 48(4), 506-511 (2013).
4) T.S. Shashikumar, M.S. Chandrashekara, and L. Paramesh. Studies on Radon in soil gas and Natural radionuclides in soil, rock and ground water samples around Mysore city. International Journal of Environmental Sciences Volume 1, No 5, 786-797 (2011).
5) D. Al-Azmi. Outdoor dose rate mapping in Kuwait. Journal of Environmental Radioactivity 169-170, p.109-115 (2017).

Fade study and readout optimization for the routine of a LiF:Mg,Ti thermoluminescent detector

D. M. Sorger[1,2], H. Stadtmann[1], W. Sprengel[2]
[1]*Seibersdorf Labor GmbH, Radiation Protection Dosimetry, 2444 Seibersdorf, AUT*
[2]*Graz University of Technology, Inst. of Material Physics, Petersgasse 16, 8010 Graz, AUT*

Highlights The application of different Time-Temperature-Profiles and the influence of fading in the routines of the individual monitoring services were investigated at Seibersdorf Labor GmbH. Several Harshaw TLD-100 dosimeters have been irradiated and fully read out after different periods of storage. A following fade study with an optimization of the standard procedure was performed.

Key words Thermoluminescence, Time-Temperature-Profile, LiF:Mg,Ti, TLD-100, Fading, Pre-fade, Post-fade, sensitivity loss, signal loss, Personal dosimetry

Background and Objectives LiF:Mg,Ti thermoluminescent dosimeters (TLDs) are frequently used for personal dosimetry by individual monitoring services (IMS) all over the world. Ionizing radiation leads to a signal storage in the TLD which can be deduced as the absorbed dose. This is performed with a controlled heating of the detector element according to a defined time-temperature profile (TTP). The output of this procedure is a time dependent light signal, called glow curve (GC). “Fade is the process of gradually reducing the capability of producing the response due to radiation exposure.” [1)] The fading in LiF:Mg,Ti has been discussed many times in different literature. The main effects of fading are Pre-fade and Post-fade. Pre-fade is characterized by the spontaneous trapping of electrons in the band gaps before irradiation. Post-fade appears after irradiation due to the loss of low energy electrons.[2)] In most IMSs preheating the LiF:Mg,Ti detector element is performed to reduce the fade.

Materials and Methods In case of Harshaw TLD-100 dosimeters, several fading experiments were performed to describe fading during typical storage periods of about a few weeks up to three months. TLDs were read out with several TTPs at different Pre-fade-time to Post-fade-time combinations which included either preheating or non-preheating. The quality of the resulting GCs was analyzed by an elaborated glow curve deconvolution (GCD) process, introduced by Stadtmann, 2017 [3)]. For the experimental investigation, routinely utilized automated TLD readers (Harshaw T8800) and a traceable irradiation facility of the secondary standard dosimetry laboratory (SSDL) of the Seibersdorf Labor GmbH were used.

Results and Discussion The fading experiment covering about the three months interval shows that preheating the TLD-100 crystals does not lead to a significant signal stability. This is owed to the Pre-fade, which does not significantly decrease with preheat in typical times of utilizing the dosimeters. The relative responses of the signal over time is illustrated in figure 1 and the responses are listed in table 1.

Table 1. Relative to the three weeks Pre-fade and four weeks Post-fade signal loss and sensitivity loss of Harshaw TLD-100 during seven weeks of Pre-fade (t_1) and seven weeks of Post-fade (t_2) with the established TTP.

t_1 / Weeks	t_2 / Weeks							
	0	1	2	3	4	5	6	7
0								
1					1.00	1.01	0.99	0.97
2				1.01	1.01	1.00	0.99	0.97
3			1.00	1.00	1.00	0.98	0.98	0.99
4		1.01	1.00	0.98	0.99	0.96	0.96	0.96
5		0.99	0.99	0.96	0.97	0.95	0.95	
6		0.97	0.96	0.94	0.95	0.94		
7		0.96	0.94	0.94	0.95			

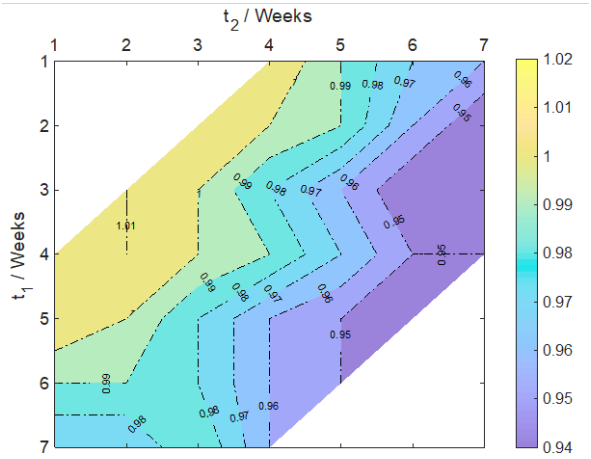

Figure 1. Pre-fade (t_1) and Post-fade (t_2) of Harshaw TLD-100 with the established TTP.

Conclusion A specific testing series of several TTPs for the IMS routine in Seiberdorf Labor GmbH was performed. As a consequence of the results the TTP of the standard procedure will be optimized to achieve shorter readout times and controlled signal fading. Further experiments with adjusted TTPs will follow to refine the optimization and introduce a fade function. These will lead to a comprehensive improvement of the readout process.

References

1) L. Z. Luo. Extensive fade study of Harshaw LiF TLD materials. Radiation Measurements 43 (2008) 365.
2) Doremus, S.W., Higgins, G.A. Pre-Irradiation Fade and Post-Irradiation Fade for LiF:Mg,Ti TLD-600, TLD-700, as a Function of Time. Radiation Protection Dosimetry 54 (1994) 119.
3) H. Stadtmann, G. Wilding. Glow curve deconvolution for the routine readout of LiF:Mg,Ti thermoluminescent detectors. Radiation Measurements 106 (2017) 278.

Determination of Field Neutron Calibration Factors of Harshaw TLD-Albedo Dosimeter in Well-logging Oil Industry

D. Imatouken[1]*, A. Bellal[1], F.Z Abdelaziz[1]

[1]*Service de Dosimetrie Externe, Nuclear Research Center of Algiers, Algiers, Algeria*

Highlights

Determination of neutron exposures configurations encountered in well-logging activities.

In-situ evaluation of neutron correction factors for each irradiation condition.

Implementation of neutron personal dosimetry in Well-logging Oil industry.

Key words: Neutron Dosimetry, Well-logging, In-situ calibration, Neutron factor Correction.

Background and Objectives: In well-logging oil industry we used generally ^{241}AmBe sources and/or 14-MeV neutron generators**.** In this area,the assessment of neutron personal dose depends on the irradiation conditions encountered when performing work with different irradiation situation. The first evaluation of neutron dosimetry systems was introduced by Cummings[1)]. Many source configuration exposures are investigated by this author. In our study, the same configurations are used in order to evaluate, in-situ, the Neutron Correction Factors (NCF) which will be used for the neutron dose calculation.

Materials and Methods: We investigate five neutron source configuration exposures suggested by Cummings. We used Berthold LB 6411 neutron Dose-rate meter and a passive Harshaw TLD-Albedo dosimeter type 8814 Holder with 7776 TLD cards[2)]. The ambient neutron dose H*(10) and the neutron dose rate $\dot{H}^*(10)$ at the irradiation points are determined by Berthold LB 6411. In the same point, the Harshaw TLD-Abeldo dosemiter are exposed at the front of water phantom in order to simulate the irradiation of the workers. All TLD-Cards are read on the Harshaw 6600 reader. The special Time-Temperature- Profil (TTP) has been used in order to minimize the fading effect. For the calculation of the neutron dose, the WinAlgorithms neutron calculation program, provided by Harshaw, are used according to same calculation parameters (Neutron Correction Factor K_n, Cs-137 Relative Response,..)[3)].

Results and Discussion: The result of the investigations on the neutron exposure configurations shows that the most important irradiations are measured during the manipulation of the Am-Be sources (source in air, source in Well-logging tools) or the use of the neutron generator in the calibration tank.(Table 1).

Table 1. Summary of neutron TLD-Albedo dosimeters response.

	Reading (Gu)				Neutron Correction Factors NCF or K_n,	H*(10)
	Element 1	Element 2	Element 3	Element 4		(µSv)
Am-Be source in air	2.7 ± 0.1	2.4 ± 0.1	3.0 ± 0.5	11.3 ± 0.5	1.15	126
Am-Be in well-logging tool	2.8 ± 0.1	2.4 ± 0.2	2.6 ± 0.3	21.9 ± 1.5	0.85	209
Am-Be in well-logging tool calibrator	3.2 ± 0.2	2.8 ± 0.2	3.4 ± 0.6	28.8 ± 7.8	0.36	150
Am-Be Shipping cask	5.7 ± 0.4	4.9 ± 0.4	5.6 ± 0.6	87.3 ± 23.7	0.15	195
Neutron generator in the calibration tank	2.7 ± 0.3	2.4 ± 0.3	3.2 ± 0.3	7.0 ± 0.1	0.38	16

The neutron configuration exposures can be categorized into three quality neutron fields: Thermal neutron field (K_n about 0.15), Thermal and epithermal neutron field (K_n about 0.37) and fast neutron field (K_n about 1.00) accordance to glow curves.

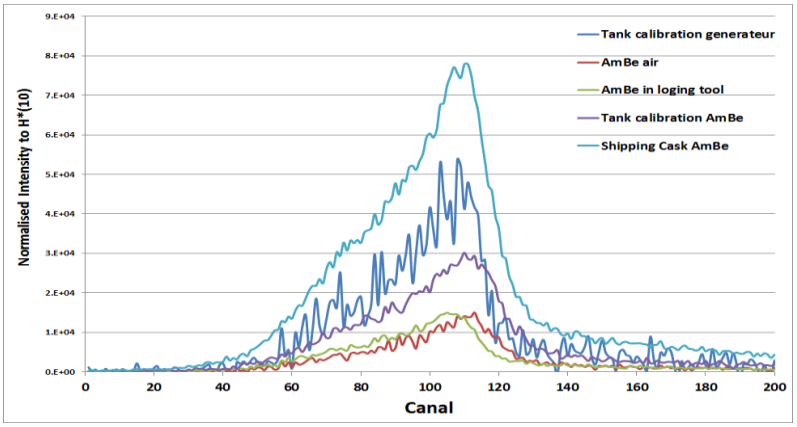

Figure 1. Thermoluminescence glow curves neutron sensitive element normalized to H*(10).

Conclusion: The investigations on the neutron exposures of the worker practicing in the field of the well-logging show that the neutron exposures can be sorted in soft, intermediate and hard neutron fields depends on neutron source configurations. The bests Neutron Correction Factors to be used in order to calculate neutron dose Hp(10) are 0.15, 0.37 and 1.00.

References

1) Cummings, F.M.; Haggard, D.L. & Endres, G.W.R "Evaluation of neutron dosimetry techniques for well-logging operations" Report No.: NUREG/CR-3609 (1985)
2) Imatouken, D "Détermination des facteurs de correction de dose des dosimètres neutrons Albédo du CRNA liés aux expositions professionnelles dans le domaine de Well logging" Internal report. Jully 2017.
3) Thermo Electron Corporation "WinAlgorithms: Dose Calculation Algorithm for Types 8805, 8810, 8814, 8815 Dosimeters: User's Manual" Publication No. ALGM-W05-U-0903-001 (2003).

*dimatoukene@yahoo.com

Computational chemical approach to the separation of Am(III) from Eu(III) using Bis(trifluoromethylphenyl)dithiophosphinic acids: Substituent effect

Doan Thi Thanh Nhan[1,2)], Taiki Kimura[2)] , Satoru Nakashima[1,2,3)]

[1] *Radioactivity Environmental Protection Course, Phoenix Leader Education Program, Hiroshima University, 1-1-1 Kagamiyama, Higashi-Hiroshima 739-8524, Japan*

[2] *Department of Chemistry, Graduate School of Science, Hiroshima University, 1-3-1 Kagamiyama, Higashi-Hiroshima 739-8526, Japan*

[3] *Natural Science Center for Basic Research and Development, Hiroshima University, 1-4-2 Kagamiyama, Higashi-Hiroshima 739-8526, Japan*

Highlights DFT calculation was applied to know the substituent effect on the separation of Am(III) from Eu(III) by bis(trifluoromethylphenyl)dithiophosphinic acids. Optimized strictures revealed that Eu-S and Am-S distances are similar for all complexes, but *m*-,*m*-trifluoromethyl derivative has a relatively larger Am-S distance, while *o*-,*o*- and *o*-,*m*-trifluoromethyl derivatives have the relatively shorter Am-S distance.

Key words spent nuclear fuel, MA/Ln separation, solvent extraction, DFT calculation, substituent effect

Background and Objectives The spent nuclear fuel is composed of short-lived fission products such as lanthanides (Ln) and extremely long-lived minor actinides (MA). MA ions have a high radiotoxicity, while Ln ions have not a long-term hazard. Shortening the half-lives by transmutation after separation of MA has been required as a rational method of disposal of spent nuclear fuel. Solvent extraction is one of the most useful methods for the separation of MA(III) ions from Ln(III) ions. The selectivity of MA(III) ions over Ln(III) ions has been indicated to depend on the kind of donor atom of the ligands used in solvent extraction. For example, O-donor ligands tend to separate Ln(III) ions from MA(III) ions, while N-donor and S-donor ligands tend to separate MA(III) ions from Ln(III) ions.[1)] Density functional theory (DFT) calculations have been applied successfully to understand the coordination geometry, stability and chemical bonding for Eu and Am complexes.[2)]

Bis(trifluoromethylphenyl)dithiophosphinic acids are good ligands to separate Am(III). The *o*-trifluoromethyl, *o*-trifluoromethyl (*o*-,*o*-) and *o*-trifluoromethyl, *m*-trifluoromethyl (*o*-,*m*-) derivatives showed unprecedented selectivity for Am(III) over Eu(III) ($SF_{Am/Eu}$ >100,000), while *m*-trifluoromethyl, *m*-trifluoromethyl (*m*-,*m*-) derivative was far less

selective ($SF_{Am/Eu}$ ~20).[3-5] This shows that the location of the substituent plays a key role in the extraction selectivity. In the present study, we applied DFT calculations to understand the substituent effect.

Materials and Methods All DFT calculations were performed by using the program ORCA 3.0.0.[6] Scalar-relativistic effect was considered using relativistic effective core potential (RECP) method and zeroth-order regular approximation (ZORA) Hamiltonian with segmented all-electron relativistically contracted (SARC) basis sets. The B2PLYP functional was used for single point energy calculations considering the solvation effect of water by a conductor-like screening model (COSMO).

Results and Discussion We obtained optimized structures for *o*-,*o*-, *o*-,*m*-, and *m*-,*m*- complexes. Optimized structures were all tris-type for all complexes for Eu and Am. We performed MO overlap population (MOOP) analysis between metal f-orbital and the donor atoms for the present complexes. There was no significant difference in MOOP analysis among three complexes for Eu complexes and Am complexes. The obtained average Eu-S distances are 2.805, 2.797, and 2.806 Å for *o*-,*o*-, *o*-,*m*-, and *m*-,*m*- complexes, respectively. The obtained Am-S distances are 2.807, 2.805, and 2.814 Å for *o*-,*o*-, *o*-,*m*-, and *m*-,*m*- complexes, respectively. There is not much difference between Eu-S and Am-S distances, suggesting that the present ligands have the Am selectivity. The slightly longer Am-S for *m*-,*m*- complex may reflect the less selective ($SF_{Am/Eu}$ ~20) situation.

Conclusion DFT calculation revealed the similar distance between Eu-S and Am-S, but the relatively longer Am-S distance for *m*-,*m*- complex. The present results may explain the Am selectivity and the difference between *o*-,*o*-, *o*-,*m*- complexes and *m*-,*m*- complex.

References

1) E.g., M. P. Jensen and A. H. Bond, *Radiochim. Acta*, **2002**, *90*, 205.
2) E.g., M. Kaneko, S. Miyashita, S. Nakashima, *Inorg. Chem.*, **2015**, *54*, 7103.
3) J. R. Klaehn, D. R. Peterman, M. K. Harrup, R. D. Tillotson, T. A. Luther, J. D. Law, L. M. Daniels, *Inorg. Chim. Acta*, **2008**, *361*, 2522.
4) D. R. Peterman, M. R. Greenhalgh, R. D. Tillotson, J. R. Klaehn, M. K. Harrup, T. A. Luther, J. D. Law, *Sep. Sci. Technol.*, **2010**, *45*, 1711.
5) F. W. Lewis, M. J. Hudson, L. M. Harwood, *Synlett*, **2011**, 2609.
6) F. Neese, *Wiley Interdiscip. Rev.: Comput. Mol. Sci.*, **2012**, *2*, 73.

First investigations of a new reference workplace field with a high-energy neutron component at PSI

E. Hohmann[1*], R. Galeev[1,2], S. Mayer[1]

[1]*Department of Radiation Safety and Security, Paul Scherrer Institute, Villigen PSI, Switzerland*

[2]*Department of Physics, University of Basel, Basel, Switzerland*

Highlights Workplace field with high-energy neutron component usually available from May to December with a mean availability of 95 % at the Paul Scherrer Institute (PSI).

Key words high-energy neutrons, workplace field, reference

Background and Objectives Neutron dosimeters used for dose monitoring of occupationally exposed workers or positions adjacent to controlled areas are routinely calibrated in fields produced by radioisotope sources. Radiation fields around high-energy particle facilities or at high altitudes often include a significant component of neutrons with energies greater than 20 MeV [1)]. For the calibration of survey instruments and dosemeters foreseen to be used in this environment, reference fields with a high-energy neutron component are necessary. The presented study investigates a suitable radiation field available at PSI.

Materials and Methods The PSI High Intensity Proton Accelerator facility (HIPA) is a cascade of three accelerators that delivers a proton beam with an energy of 590 MeV and a maximal current of 2.2 mA. The beam is transported to the experimental hall, where it passes through two carbon targets used for secondary particle production[2)]. The targets are heavily shielded by blocks of concrete and iron. A collimation system ensures a reproducible position of the beam spot on the targets. In addition, the comparison of the proton current in front and behind the target is used as verification of the correct beam positioning.

This setup provides a steady neutron field with a dominant high-energy component outside the shielding above the targets. Considering normal operation of HIPA, this field is available from May to December with mean availability of 95%.

The neutron field was investigated using a commercial available survey instrument suitable for measurements of high-energy neutrons (WENDI 2) [3)] and an extended range Bonner Sphere spectrometer (ERBSS).

Results and Discussion The data measured with the ERBSS was unfolded using two different methods: Bayesian parameter estimation and maximum entropy unfolding[4)]. The spectral neutron distribution obtained with both methods show reasonable agreement (Figure 1, bottom).

The dose rate calculated from the spectrum and measured with the survey instrument suitable for high-energy neutrons agree within the uncertainties (Figure 1, top).

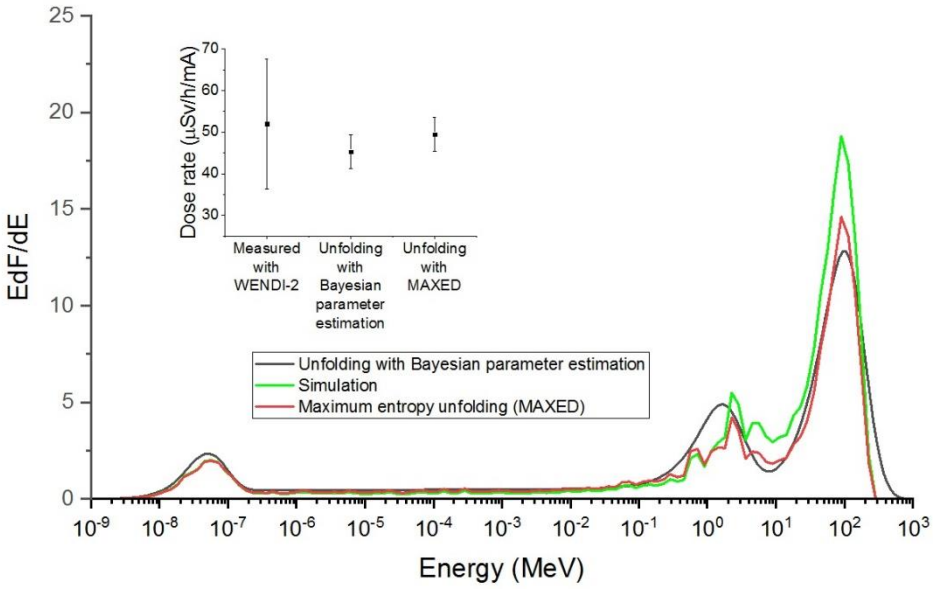

Figure 1. Measured spectral neutron distributions and dose rate.

The stability of the field was investigated by a series of the measurements at the same position for different time periods. The results of each series, normalized to the proton current, are Gaussian distributed with a standard deviation of less than 5%.

Conclusion A workplace field with significant high-energy neutron component is available from May to December at PSI. First measurements confirmed the stability of the field and the suitability of the beam monitoring system used for normalization.

Acknowledgements We want to thank Vadim Talanov (PSI) for providing the Monte Carlo simulations of the HIPA facility.

References

1) Boschung, M., et al.: Field calibration and comparison of personal neutron dosemeter designs based on CR-39 for the use around high-energy accelerators. Radiation Measurements 43(2-6) 1081-1084 (2008).
2) REGGIANI, D.: Extraction, Transport and Collimation of the PSI 1.3 MW Proton Beam. In: Proceedings of HB2012, Beijing, China (2012).
3) OLSHER, R. H., MCLEAN, T.: High-energy response of the PRESCILA and WENDI-II neutron REM meters. Radiation Protection Dosimetry 130 510–513 (2008).
4) REGINATTO, M.: Overview of spectral unfolding techniques and uncertainty estimation. In: Radiation Measurements 45 1323–1329 (2010).

Individual doses recorded during a high productive period of research and development regarding the radiation source applications

Felicia Mihai[1]*, Ana Stoichioiu[1]
Horia Hulubei, National Institute for R&D in Physics and Nuclear Engineering, Magurele, Romania

Highlights In this paper are presented the collective doses recorded during the period 1976 – 1995 for occupational exposed worker from nuclear research area, especially for Horia Hulubei, National Institute for R&D in Physics and Nuclear Engineering, IFIN-HH. The individual doses are also studied in this paper.

Key words collective dose, individual dose, radiation, dosimetry

Background and Objectives In nuclear research area many people were implicated to perform, develop and to discover the application efficiency of the radiation sources. In the studied period the IFIN-HH had a remarkable contribution to the development of the radiation source applications in different nuclear economic areas especially from Romania.

The period 1976 – 1995 was a flame for the nuclear development after founding in 1957 the VVR-S nuclear reactor and U-120 Cyclotron and subsequently many other high energy sources in different departments from IFIN-HH were developed. The individual doses have been recorded any coherently possible since 1976. After this period the occupational exposure doses are much lower1. More and less knowing the radiation effects on human health refer to limit of doses, the radioprotection rules were established in function of the radiation recorded data at that time. The maximum limit of allowed dose per year has been 5 Remi.

Materials and Methods The dosimeter system used in studied period consisted from ORWO film and FD-III-B dosimeter badge. The detection limits reported by dosimetry laboratory from IFIN-HH institute for ORWO dosimetric system were 20 mrem to 10 Remi for x-ray and 40 mrem to 100 Rems for gamma radiation. The collective dose mean value was calculated as following: the cumulated dose values during the year was divided to the number of workers who recorded doses. The most involved research departments in the nuclear economic development were considered in this study. The total number of monitored workers are 850 ÷ 1000 per year.

Results and Discussion In figure 1 are presented the collective dose mean values for the

period 1976-1985. Annually, between 50 and 200 people have accumulated doses. The SIN department accumulated the highest dose values in this period. The workers have manipulated radioactive markers for industry and gamma sources for nuclear medicine.

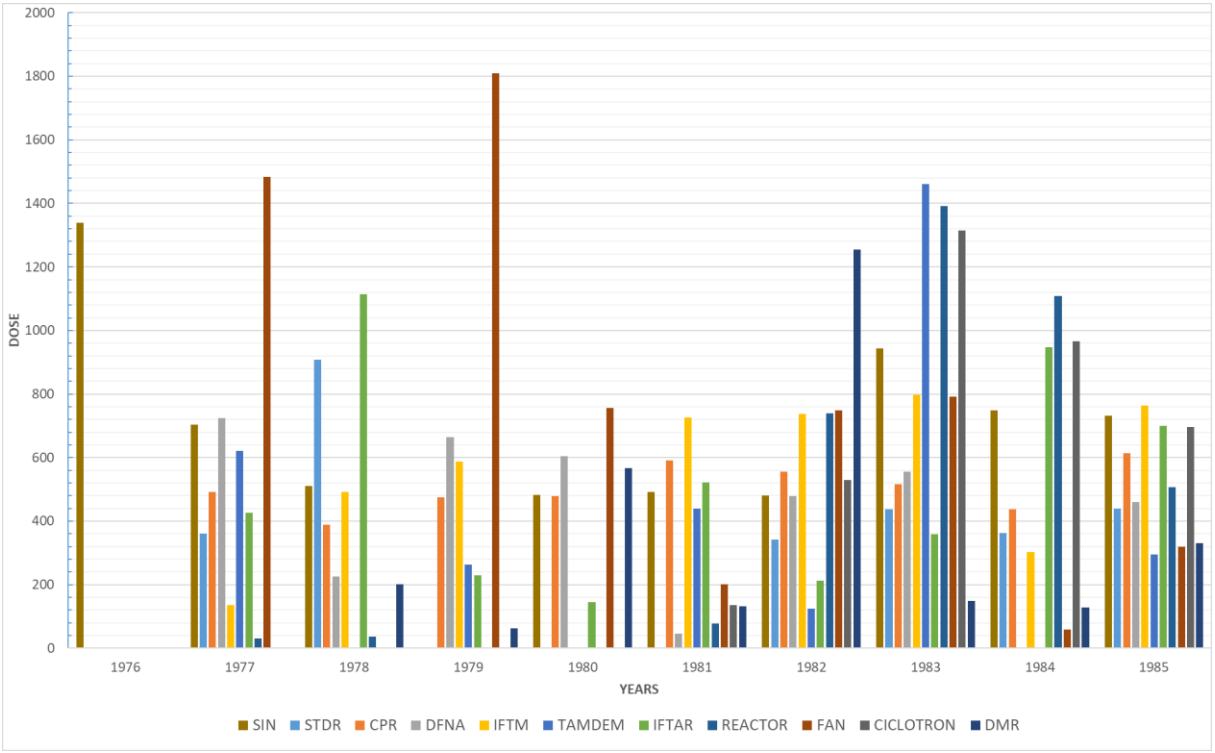

Figure 1. Collective dose mean values for different research departments

Regarding individual doses, approximately 20 persons recorded doses during 10 ÷ 20 years from studied period. The highest individual dose was about 32500 mrems during 19 years.

Conclusion The analyzed period is from the time than many types of radiation sources were explored in different research areas. The data obtained can be used for analysis the risk of radiation exposure on a long term and after a long period of cessation of the working with radiation sources.

References

1) F. Mihai, A. Gheorghiu, E. Udup and A. Stochioiu, Occupational exposure recorded before and after new radioprotection regulations, ICRS-12 & RPSD-2012, Progress in Nuclear Science and Technology, vol. 4, pp.783-787, 2014.

Study of a discriminative technique between radon and thoron in *Radout* detector

Francesco Cortesi[1]*, Stefano Coria[1], Marco Caresana[2]
[1]*Mi.am S.r.l., Piacenza, Italy*
[2]*Department of Energy, Politecnico di Milano, Milan, Italy*

Highlights ^{222}Rn and ^{220}Rn discrimination is investigated using a solid-state nuclear track detector (SSNTD) based passive detector named *Radout* used by Mi.am company. The analysis of track morphological parameters performed by Politrack allows to identify a critical parameter for the discrimination of the two radon isotopes: the recalculated reduced etch rate.

Key words radon, thoron, SSNTD, CR-39, SRIM, reduced etch rate, *Radout*

Background and Objectives Although only ^{222}Rn isotope is commonly considered in radon pollution surveys, there is another isotope, ^{220}Rn, also called thoron, that is relevant and dangerous for human health. In this work these two radon isotopes discrimination is investigated using a solid-state nuclear track detector (SSNTD) based passive detector named *Radout* used by Mi.am company in its routine service of Radon dosimetry.

Materials and Methods Experimental exposures to ^{220}Rn and ^{222}Rn were performed using the detector *Radout*, composed by a conductive polymer made holder plus a CR-39 SSNTD produced by TASL[1]. The CR-39 SSNTDs, placed in the Radout detector, were chemically etched by a sodium hydroxide warm aqueous solution and analyzed by the automatic track detector reader Politrack. The analysis of track morphological parameters performed by Politrack allows to identify a critical parameter for the discrimination of the two radon isotopes: the recalculated reduced etch rate. In order to represent the observed trend of the frequency distribution of this parameter, a computational model was elaborated. The model is composed by two steps. The first step is a time-independent Monte Carlo simulation of the two decay chains considering only alpha-emitter nuclides and it is implemented through TRIM, a subroutine of the well-known SRIM program developed by Ziegler and Biersack[2]. The second step is a track final shape elaboration and it is based on the idea of spherical wave propagation of the etchant along particle trajectory during etching of CR-39, hypothesized by Membrey and Fromm[3], and on the dependence between track etch rate and ionization parametrized by Dörschel[4] and Caresana[5].

Results and Discussion Though the *Radout* detector efficiency is well characterized only for ^{222}Rn exposures and its efficiency for ^{220}Rn isn't studied yet, the comparisons between the reduced etch rate frequency distribution, experimentally and computationally determined, seem to be qualitatively in good agreement. As it is emphasized by figure 1.

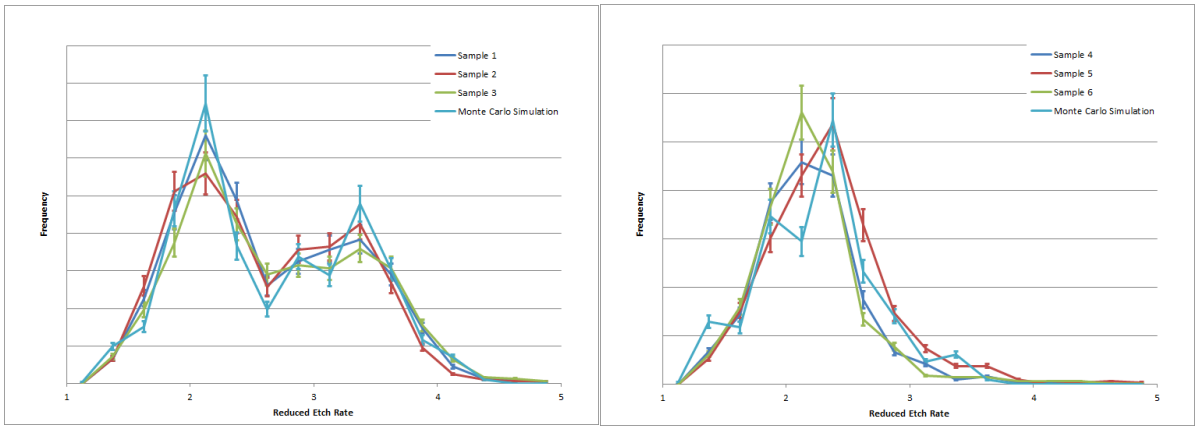

Figure 1. Reduced etch rate frequency distribution for ^{222}Rn (on the left) and ^{220}Rn (on the right)

Conclusion The difference between the track morphological parameters distributions is supposed to be significative to discriminate the exposures of the two isotopes. The experimental exposures and the Politrack analysis of the detectors are compared with a computational program to verify the existence of a critical parameter for the assessment of ^{220}Rn and ^{222}Rn concentrations in a mixed exposure. As result of the analysis the reduced etch rate frequency distribution is considered as the possible discriminative critical parameter.

To unfold the resulting reduced etch frequency distribution, further studies are needed but a first indication of the presence of ^{220}Rn in a ^{222}Rn exposure can be obtained by the analysis of the ratio between the two peaks resulting on the upper surface of the CR-39 detector in the case of ^{222}Rn exposure.

References

1) T. A. Systems, "TASTRAK performance sheet: Alpha-particles," www.tasl.co.uk
2) J. F. Ziegler, J. P. Biersack and U. Littmark, New York: Pergamon, 1985.
3) M. Fromm, M. Membrey, A. Chambaudet and R. Saouli, Nuclear Tracks Radiation Measurements, vol. 19, pp. 163-168, 1991.
4) B. Dorschel, D. Hermsdorf, K. Kadner and S. Starke, Radiation Measurements, no. 35, p. 287–292, 2002.
5) M. Caresana, M. Ferrarini, M. Fuerstner and S. Mayer, Nuclear Instruments and Methods in Physics Research A, no. 683, pp. 8-15, 2012.

Individual Monitoring with BeOSL Dosemeters: New Dosemeters for Extremity and Environmental Dosimetry

H. Hoedlmoser[1]*, M. Greiter[1], V. Bandalo[1], J. Brönner[1], P. Kleinau[1], T. Haninger[1], E. Mende[1], P. Scheubert[2], R. Eßer[2], M. Figel[1]

[1]*Helmholtz Zentrum München, Individual Monitoring Service, Munich, Germany*

[2]*Dosimetrics GmbH, Munich, Germany*

Highlights The Individual Monitoring Service (IMS) at the Helmholtz Zentrum München has developed a new ring dosemeter, a new eye lens dosimeter (ELD) for integration in radiation protection (RP) glasses and a new environmental dosemeter based on BeOSL technology.

Key words extremity dosimetry, eye lens, finger ring, OSL, BeO, environmental dosimetry

Background and Objectives The IMS at the Helmholtz Zentrum München is the largest dosimetry service in Germany and monitors approximately 170 000 customers per month by means of OSL, film and TLD dosemeters. 10 000 customers per month are supplied with extremity dosemeters such as photon and beta rings. In whole body dosimetry, the IMS has transitioned approximately 80 000 customers to the new BeOSL technology[1)]. In extremity dosimetry and environmental dosimetry new solutions based on BeOSL are required to replace older technologies still in use. In collaboration with Dosimetrics the BeOSL portfolio has been extended with three new dosemeter types:

- A new Hp(3) ELD for photon radiation using a standardized integration mechanism for RP glasses[2,3)]
- A finger ring Hp(0.07) dosemeter[4)]
- A new H*(10) environmental dosemeter

Both extremity dosemeters use the new BeOSL detector element “ezClip” compatible with existing BeOSL readers and infrastructure[3)]. The dosemeters were tested according to the requirements of IEC 62387.

Materials and Methods New dosimeter designs were developed using MCNP6 Monte Carlo Models to simulate the energy and angular response functions[4)]. The designs were realized by means of injection molding tools and the radiological characterization of the new dosemeters was carried out at the secondary standard calibration facilities of the IMS in Munich[5)].

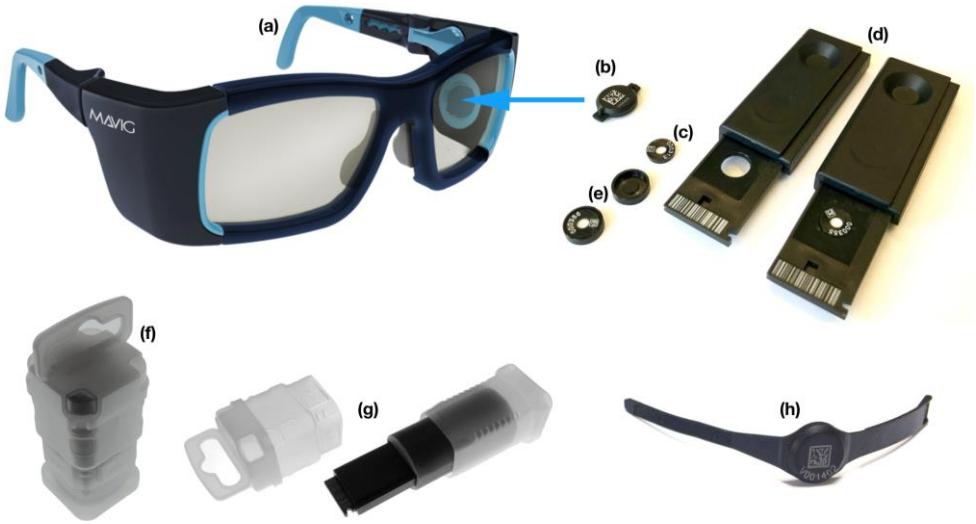

Figure 1. New BeOSL dosemeters: (a) RP glasses with ELD interface, (b) ELD, (c) detector element in (e) detector tray, (d) readout badge, (f) environmental dosemeter, with internal badge (g).

Results and Discussion Figure 1 shows the new dosemeters. For each new type the dosimetric performance is presented in terms of energy and angular response, linearity and coefficient of variation in comparison to the requirements of IEC 62387.

Conclusion A new environmental and two new extremity dosemeters all based on BeOSL technology have been shown to fulfill IEC requirements and PTB requirements for official use in Germany. The dosemeters are currently undergoing the formal certification procedures by PTB Braunschweig.

References

1) T. Haninger et al, Properties of the BeOSL Dosimetry System in the Framework of a Large-scale Personal Monitoring Service, Radiat Prot Dosimetry doi:10.1093/rpd/ncv425
2) H. Hoedlmoser et al, New eye lens dosemeters for integration in radiation protection glasses, submitted to Rad. Meas. for publication (1/2019)
3) V. Bandalo et al, Performance of the BeOSL eye lens dosimeter with radiation protection glasses, this conference.
4) M. Figel et al, A BeOSL Finger Ring dosemeter, this conference.
5) P. Scheubert et al, this conference.
6) H. Hoedlmoser et al, Simulation of OSL and TLD dosemeter response for the development of new extremity dosemeters, Rad. Prot. Dosimetry doi: 10.1093/rpd/ncy299 (2018).
7) V. Bandalo, et al, A Fully Automated Secondary Standard X-Ray Calibration Facility for Personal Dosemeters, Rad. Prot. Dosimetry, doi:10.1093/rpd/ncy187 (2018).

A BeOSL Finger Ring Dosemeter

H. Hoedlmoser [1]*, M. Greiter[1], V. Bandalo[1], J. Brönner[1], P. Kleinau[1], T. Haninger[1], M. Emmerl[1], E. Mende[1], P. Scheubert[2], R. Eßer[2], M. Figel[1]

[1]*Helmholtz Zentrum München, Individual Monitoring Service, Munich, Germany*

[2]*Dosimetrics GmbH, Munich, Germany*

Highlights The Individual Monitoring Service (IMS) at the Helmholtz Zentrum München has developed and characterized a new ring dosemeter for the measurement of Hp(0.07), based on BeOSL technology. The new detector element can be read out by means of standard BeOSL readers and fulfills IEC requirements.

Key words extremity dosimetry, finger ring, OSL, BeO, Monte Carlo simulation

Background and Objectives The IMS at the Helmholtz Zentrum München is the largest dosimetry service in Germany and monitors approximately 10 000 customers per month with extremity dosemeters such as photon and beta rings[1)]. To replace the older TLD technology in the finger ring dosemeter with BeO detectors, new BeOSL detector elements were required and the design of the ring dosemeter body had to be adapted in order to accommodate the different shape of the detector element and to ascertain the opacity oft the material in the BeO OSL stimulation wavelength range. As a first step a ring for the measurement of photon radiation was redesigned and equipped with the new “ezClip” BeOSL detector element[2)] for extremity dosimetry. The ring dosemeters were characterized according to the requirements of IEC 62387.

Materials and Methods The adapted ring design was evaluated using a MCNP6 Monte Carlo Models to simulate energy and angular response functions[3)]. The design changes were realized by means of new injection molding tools and the radiological characterization of the new dosemeters was carried out at the secondary standard irradiation facilities of the IMS in Munich[4)].

Results and Discussion Figure 1 shows the new ring dosemeters in an irradiation situation and an insert with the individual components of the dosemeter and readout badge. Figure 2 shows the energy response measured in the laboratory in comparison to the output of the Monte Carlo Model. Data is presented on dose linearity, coefficient of variation, and the achievable detection limit. Measurement results concerning the opacity of the material of the ring body are shown. The performance of the BeOSL ring is compared to the older TLD version of the ring.

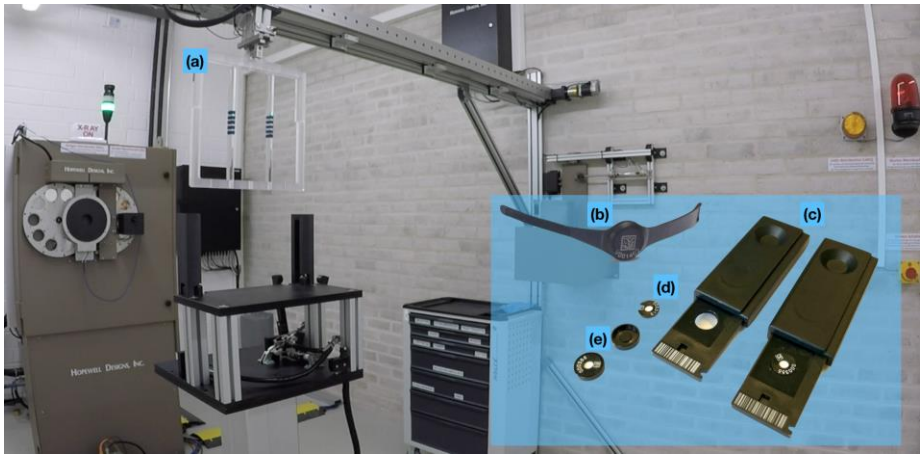

Figure 1. New BeOSL ring dosemeters: (a) irradiation in SSDL, (b) ring body, (d) detector element in (e) detector tray, (c) readout badge.

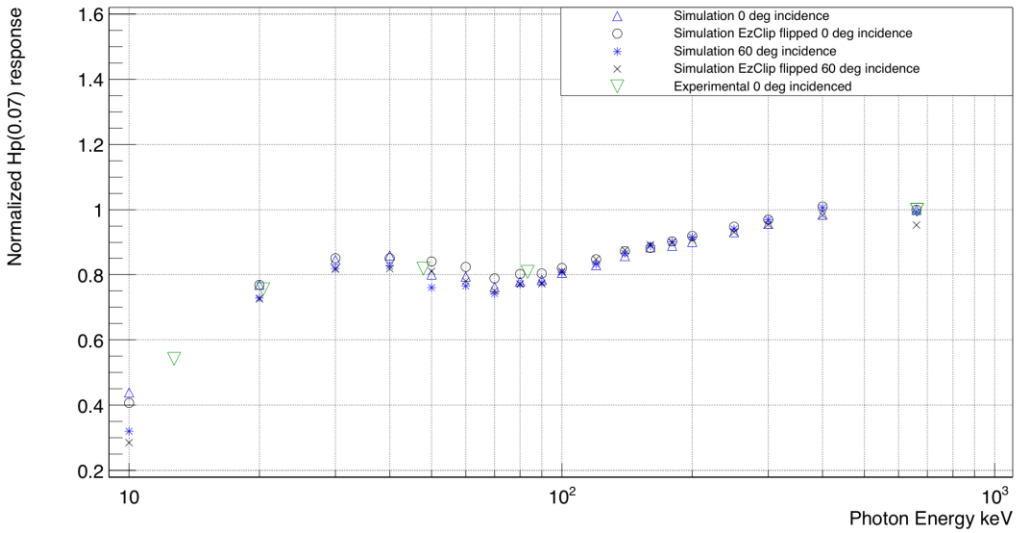

Figure 2. Energy response of the BeOSL ring dosemeters

Conclusion A new ring dosemeter for photon radiation based on BeOSL technology was developed and fulfills the relevant IEC requirements. In comparison to its predecessor using TLD technology both the energy response function and the achievable detection limits are improved.

References

1) H. Hoedlmoser et al, Individual Monitoring with BeOSL Dosemeters: New Dosemeters for Extremity- and Environmental Dosimetry, this conference.
2) P. Scheubert et al, this conference.
3) H. Hoedlmoser et al, Rad. Prot. Dosimetry doi: 10.1093/rpd/ncy299 (2018).
4) V. Bandalo, et al, Rad. Prot. Dosimetry, doi:10.1093/rpd/ncy187 (2018).

Development of Fast Neutron Imaging and Detection Methods with Nuclear Emulsion and its Applications

Hideki Tomita[1*], Kanji Watanabe[1], Yuya Izumi[1], Yoichiro Nakayama[1], Shota Hayashi[1], Kotaro Kanamori[1], Kunihiro Morishima[2], Masahiro Yoshimoto[2], Ryosuke Komatani[2], Tatsuhiro Naka[2], Toshiyuki Nakano[2], Mitsuhiro Nakamura[2], Yoshimune Ogata[3)], Nobuaki Tabata[4)], Eiji Yamashita[4)], Toshiki Kobayashi[4)], Tetsuo Iguchi[1], Mitsutaka Isobe[5,6], Kunihiro Ogawa[5,6], MunSeong Cheon[7], and KSTAR team[7]

[1] *Graduate School of Engineering, Nagoya University, Nagoya, Japan*

[2] *Graduate School of Science, Nagoya University, Nagoya, Japan*

[3] *Radioisotope Research Center Medical Division, Nagoya University, Nagoya, Japan*

[4] *Nagoya Diagnostic Radiology Foundation, Nagoya, Japan*

[5] *National Institute for Fusion Science, Toki, Japan*

[6] *SOKENDAI (The Graduate University for Advanced Studies), Toki, Japan*

[7] *National Fusion Research Institute, Daejeon, Republic of Korea*

Highlights Methods of imaging and detection for fast neutron using advanced nuclear emulsion technique with the automated scanning system were developed. Fast neutron pinhole imaging and collimated detection of fast neutrons were demonstrated.

Keywords fast neutron, nuclear emulsion, pinhole imaging, collimated detection

Introduction A nuclear emulsion plate is known to be useful as fast neutron detection by recording a recoiled proton caused by elastic scattering with a hydrogen atom in an emulsion layer. By recognizing three-dimensional shape and length of a recoiled proton track after photographic development of the emulsion, information of an incident neutron such as its energy and direction can be derived. A large number of recoiled tracks can be analyzed quickly by using an automated scanning system for the emulsion. We have developed imaging and detection methods for fast neutron using advanced nuclear emulsion technique with the automated scanning system [1-4].

Fast Neutron Pinhole Camera As one of the applications of the nuclear emulsion technique, a pinhole camera for fast neutron generated by DD reaction in fusion plasma was developed to measure emission profile of fusion neutrons (see Fig.1 (a)) [1,2]. The camera consisted of a pinhole collimator and a nuclear emulsion plate was installed at the magnetic fusion experimental device KSTAR (Korea Superconducting Tokamak Advanced Research). Emission profile of 2.5 MeV neutrons from the KSTAR plasma was successfully recovered by

the Abel inversion of line integrated distribution obtained by the camera.

Collimated Detection of Fast Neutron We proposed a novel method to measure an incident direction of a fast neutron without any physical collimator with statistical reconstruction in the analysis of recoiled proton tracks (see Fig.1 (b)) [3,4]. Assuming that an averaged energy of an incident fast neutron is pre-estimated, scattering angle in the elastic scattering of the fast neutron can be presumed by simple kinematics with a measured direction and energy of the recoiled proton. The direction of the incident fast neutron can be estimated by overlapping of the cones with the estimated scattering angle projected on a reconstruction plane. Feasibility of the method was investigated by Monte Carlo simulation and experiment using a ^{252}Cf neutron source. In addition, we demonstrated measurements of an averaged incident direction of fast neutrons generated in PET nuclide production at a medical cyclotron at the Nagoya Diagnostic Radiology Foundation.

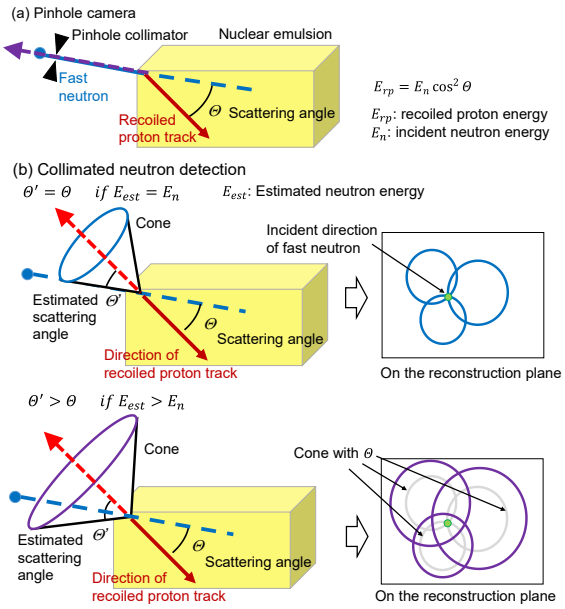

Fig. 1 Principle of fast neutron pinhole imaging and collimated detection methods using a nuclear emulsion plate

Acknowledgments This work is performed with the support and under the auspices of the NIFS Collaboration Research program (NIFS12KOAH029, NIFS15KOAH033, NIFS11KLEH011, NIFS14KLEH036) and Cooperation between Japan and Korea in the Area of Fusion Energy Research and Related Fields. Also, this work is partly supported by the JSPS-NRF-NSFC A3 Foresight Program in the field of Plasma Physics (NSFC: No.11261140328).

References

1) Y. Nakayama *et al.*, "Application of Advanced Nuclear Emulsion Technique to Fusion Neutron Diagnostics", Physics Procedia **80**, 81, (2015).
2) Y. Izumi *et al.*, "Development of fast neutron pinhole camera using nuclear emulsion for neutron emission profile measurement in KSTAR", Review of Scientific Instruments **87**, 11D840 (2016).
3) K. Watanabe *et al.*, "Fast Neutron Imaging Telescope using Statistical Reconstruction in Nuclear Emulsion", JPS Conference Proceedings, **24**, 011023 (2019).
4) H. Tomita *et al.*, "Development of Collimated Fast Neutron Detection without Physical Collimator", 2018 IEEE Nuclear Science Symposium Conference Proceedings, (*submitted*).

Development of Noble Scintillation Paper Functionalized for Detecting ß-Particles

Hirokazu Miyoshi[1]*, Mami Nakamura[1], Akira Yumoto[2], and Yoshinori Itsuki[2]

[1]*Advance Radiation Research, Education, and Management Center, Tokushima University, Tokushima, Japan*

[2]*R&D Department, Awa Paper Mfg. Co., Ltd., Tokushima, Japan*

Highlights Noble scintillation paper functionalized for detecting ß-particles was prepared. The paper had different structures to capture ß-particles from ^{90}Y. Scintillation images were obtained and analyzed.

Key words scintillation, paper, ß-particle, tritium, detection, dosimetry

Background and Objectives Organic scintillators encapsulated in silica nanoparticles by a sol–gel method have been developed[1]. They are used in smear tests and detection of tritium by dropping and dispersing them on polyethylene paper. Their counting efficiency is quite low and they can not be uniformly dispersed on the paper.

Next, scintillator–silica fine powders (FPs) have been developed[2]. Micrometer-size silica FPs are used as platforms for the collection of tritium liquid and fixing scintillator–silica nanoparticles. The dropped tritium liquid is stopped on silica FPs and nearby scintillator–silica nanoparticles are excited by ß-particles of tritium on these platforms. These are used in the fabrication of scintillation paper at Awa Paper Co., Ltd.

In this study, noble scintillation paper was developed using scintillator–silica FPs. The efficiency of the paper with different structures to detect tritium ß-particles was investigated. Finally, the scintillation paper was applied to the dosimetry of ^{90}Sr ß-particles.

Materials and Methods Two types of scintillator–silica FP were prepared. One type is prepared using silica FPs produced as previously reported[2]. The powders were washed 3 times in 200–300 ml of distilled water and dried on a heater at about 90 ºC. The obtained dried powders were separated into sizes of 1 mm and about 300 µm size using different sieves. Scintillation paper was prepared by a conventional papermaking method and a coating method as follows. Scintillator–silica FPs were sandwiched between two pieces of paper or coated on paper uniformly. The other type is prepared using new scintillator–silica powders by a sol-gel method without using silica FPs but using ß-cyclodextrin. The obtained powders were dispersed in ethyl alcohol at 80 ºC and coated on the paper.

Results and Discussion Scintillation paper uses a different type of scintillator–silica, which is widely coated uniformly on the paper. It is easy to dispose and contains no plastic components. Moreover, it is thin, cheap, and easy to change its form.

A $^{90}Sr/^{90}Y$ stick source (Isotrak SIR82901) emitted 2.270 MeV ß-particles from ^{90}Y of the daughter nuclei of ^{90}Sr. The paper was irradiated with ^{90}Y ß-particles. Scintillation images were obtained and analyzed using an Image Quant LAS 4000mini (GE HealthCare Co., Ltd.) in the precision mode for 10 min of collection with high sensitivity. After their images were obtained as tiff files, ImageJ software was used to measure their intensities. Except for the new paper without silica FPs, the scintillation images of ß-particles from ^{90}Y were obtained.

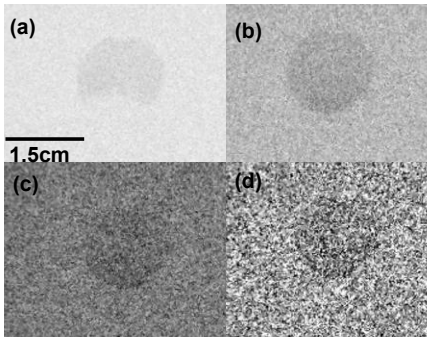

Figure 1 Scintillation images at a, 0.5 cm; b, 1.5 cm; c, 2.5 cm; d, 3.5 cm) of ^{90}Y ß-particles irradiated on scintillation paper

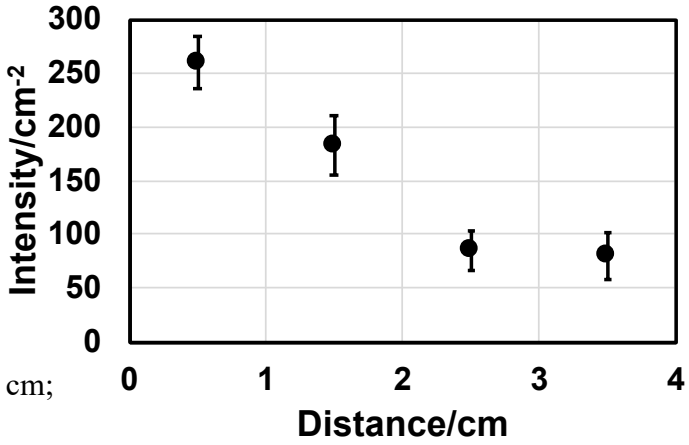

Figure 2 Relationship between scintillation intensity and distance from the $^{90}Sr/^{90}Y$ source

We will discuss our scintillation paper and its application in solid-state dosimetry, considering its structure.

Conclusion Scintillation paper was successfully prepared by a conventional papermaking method and a coating method using scintillator–silica FPs. Scintillation light was observed as CCD images by irradiating ^{90}Y ß-particles.

References

1) H. Miyoshi, T. Ikeda, Preparation of paper scintillator for detecting ^{3}H contaminant, Radiat. Prot. Dosim., 156, (2013) 77–282.
2) H. Miyoshi, M. Hiroura, K. Tsujimoto, N. Irikura, T. Otani, Y. Shinohara, Preparation of new scintillation imaging material composed of scintillator-silica fine powders and its imaging of tritium, Radiat. Prot. Dosim., 174, (2017) 478–484.

Investigation of using a long-life electronic personal dosimeter for monitoring aviation doses of frequent flyers

Hiroshi YASUDA[1]*, Kazuaki YAJIMA[2], Tatsuhiko SATO[3]
[1]*RIRBM, Hiroshima University, Hiroshima, Japan*
[2] *NIRS, National Institutes for Quantum and Radiological Science and Technology, Japan*
[3] *Japan Atomic Energy Agency, Japan*

Highlights Possible application of a recently developed electronic personal dosimeter having a long-life battery for management of aviation doses of frequent flyers was investigated through the measurements onboard selected international flights.

Key words cosmic radiation, aviation, electronic dosimeter, aircraft, JISCARD

Background and Objectives International Commission on Radiological Protection (ICRP) recently published a report on radiological protection in aviation[1)], in which ICRP recommended that frequent flyers in the public people should know self-assessment individual doses and, as appropriate, adjust their flight frequency. However, it is hard for those busy flyers to get their accurate aviation doses through calculations using precise information on many flight profiles (i.e., time-dependent latitudes, longitudes & altitudes). It must be useful if their personal doses in aviation can be monitored in a simple way.

Materials and Methods With the thought above, we have been investigating possible application of a long-life electronic personal dosimeter (EPD) to frequent flyers. In the present study, we focus on a recently developed EPD "D-Shuttle" (Chiyoda Technol Cooperation) which can record both hourly dose rates and cumulative dose up to 400 days without a battery exchanging; the recorded data are read out occasionally with an exclusive portable reader. This dosimeter has advantageous features for the long, portable use such as

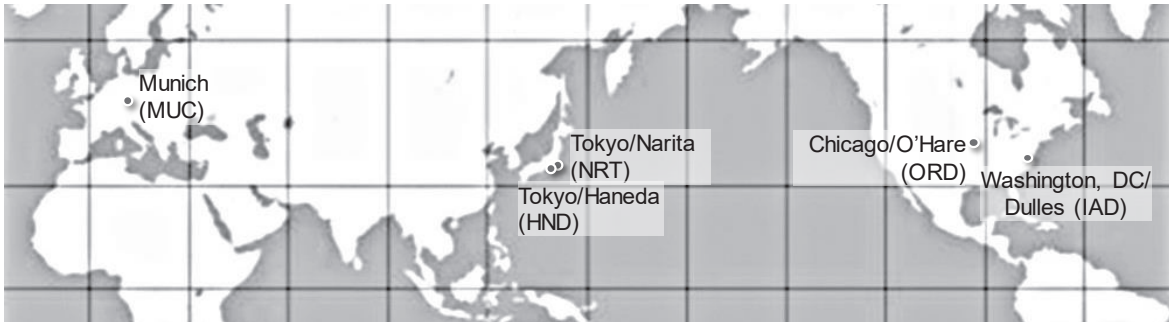

Figure 1. The departure/arrival cities of the four long-haul flights.

light weight (23 g), small size (H68×W32×D14 mm^3), robustness and no electromagnetic wave interference.

One piece of D-Shuttle was carried by the author (HY) in the period of February to June, 2017 in four long-haul flights from Tokyo, Japan to Germany or USA (see Figure 1): Haneda (Japan) to Munich (Germany), Munich to Haneda, Narita (Japan) to Washington, D.C. (USA) and Chicago (USA) to Narita (Japan). The dosimeter was put to a carry-on bag and then placed under a passenger seat in the cabin. The recorded dose rate values were downloaded by using an exclusive reader and then compared with ambient dose equivalent values calculated with a route-dose calculation code JISCARD EX[2)] which incorporates an analytical model which gives the atmospheric radiation spectra immediately[3)].

Results and Discussion The H*(10) dose rates measured with D-Shuttle were significantly lower than the model calculated values in any flights (Table 1); those ratios (measured/calculated) ranged from 19% to 26 %. The number of the percentage tended to be lower for a higher-altitude flight, which is attributable to the very low efficiency of D-Shuttle for neutrons that are the most radiologically-important component of cosmic radiation at aviation altitudes.

Table 1. Comparison of the route doses of four flights measured with D-Shuttle with those calculated with a computer code for aviation dose calculation: JISCARD EX[2)].

Flight route	Departure date (JST)	Measured dose (A) [μSv]	Calculated dose[a] (B) [μSv]	Ratio of A in B
Haneda to Munich	2017-02-26	14.4	75.2	0.19
Munich to Haneda	2017-03-04	14.1	63.7	0.22
Narita to Washington DC	2017-06-18	14.2	54.7	0.26
Chicago to Narita	2017-06-25	13.6	59.2	0.23

[a] Ambient dose equivalent, H*(10), calculated with JISCARD EX.

Conclusion It is expected that the long-life electronic personal dosimeter D-Shuttle would be effectively used for monitoring of the individual aviation dose of a frequent flyer, though some careful corrections of the measured values should be made. While, it is desirable to add a function of detecting cosmic neutrons keeping its portability. Such function should be useful for verification of GLE doses for all passengers as well as aircraft crew.

References

1) ICRP. Publication 132, Ann. ICRP 45(1), 1-48, 2016.
2) Yasuda, H. et al. Radiat. Prot. Dosim. 146, 123–125, 2011.
3) Sato, T. et al., Radiat. Res. 170, 244-259, 2008.

Energy response of CaF_2 detectors using deconvolution of OSL signal

Pagotto, I.[1]*, Malthez, A.L.M.C.[1], Umisedo, N.K.[2], Yoshimura, E.M.[2]
[1]*Federal University of Technology – Parana, Curitiba, Brazil.*
[2]*University of Sao Paulo, Sao Paulo, Brazil.*

Highlights CaF_2 presented changes in the curve shape of OSL emission according to type and energy of radiation. Using parameters of curve deconvolution, the energy range can be estimated from OSL emission.

Key words photon energy response, OSL, deconvolution, calcium fluoride

Background and Objectives Different dosimetric materials or filtration windows are a common way to find the energy range to which personal monitor was exposed. Corrections regarding energy in Optically Stimulated Luminescence (OSL) dosimetric systems are necessary, as energy response of those materials is not always flat[1]. Published studies have shown that OSL emission curve shapes can be different according the beam energy[1,2]. OSL detectors based on Brazilian natural calcium fluoride (CaF_2) presented changes in the emission curve shapes for different types and energies of radiation[3]. Aiming the application of the CaF_2 as OSL detector and to simplify the corrections with respect to energy, in this study the energy response of the CaF_2 detectors was evaluated and shape curves were analyzed. Moreover, a method to identify the energy range based on the exponential parameters using the data from deconvolution curves was proposed.

Materials and Methods Employing a cold process developed at Federal University of Technology – Parana[4], detectors were made using Brazilian fluorite in powder form after suffered a thermal treatment to erase residual signals. The pellets were cut off from detector sheet and selected by sensitivity (similar OSL responses). Readouts were done in a TL/OSL Risø reader with blue LED for stimulation and a Hoya U340 filter for detection window. Doses from 0.5 up to 6.0 mGy using radiation qualities from 43 up to 1250 keV (ISO narrow and RQR beams) and photons from ^{60}Co and ^{137}Cs gamma sources were used. To avoid the influence of fading, the readouts were done 24h after exposure. The Mathematica software, used to make the deconvolution of curves, fitted three exponential functions employing R^2 higher than 0.99.

Results and Discussion CaF_2 detectors present an over OSL response relative to ^{60}Co photons, indicating that shape curves can change according photon beam energy. The parameters of exponentials indicate that is possible to distinguish the energy comparing the evaluated values in parameter table, like Table 1.

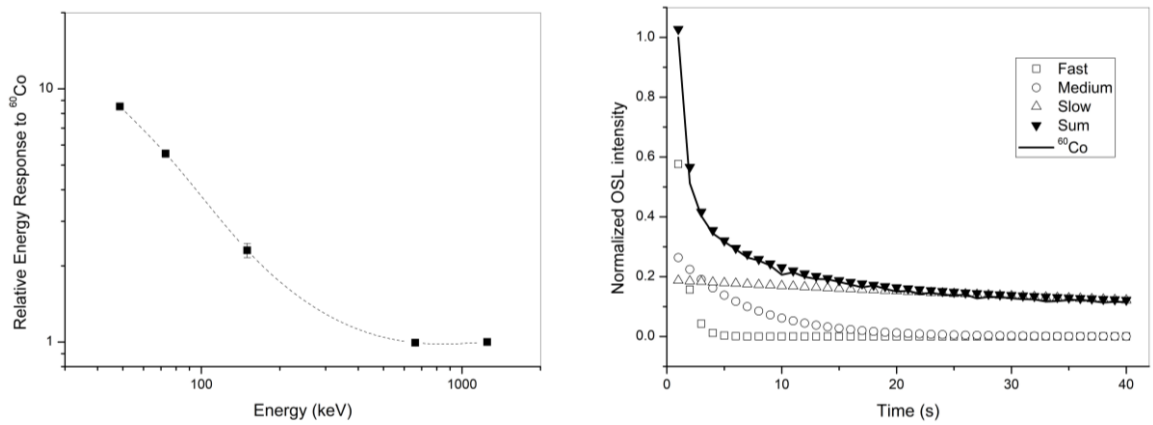

Figure 1. Photon energy response relative to ^{60}Co photon energy (left) and OSL intensity (full line) and exponentials resulting from deconvolution of normalized OSL emission curve (right).

Table 1. Exponential parameters from deconvolution of OSL emission curves to different energies.

Energy (keV)/ Parameters	Fast	Medium	Slow
43.28	1.29 ± 0.03	0.18 ± 0.01	0.023 ± 0.002
73	1.31 ± 0.03	0.17 ± 0.01	0.019 ± 0.002
150	1.30 ± 0.03	0.16 ± 0.01	0.015 ± 0.002
662	1.25 ± 0.03	0.16 ± 0.01	0.011 ± 0.001
1250	1.30 ± 0.03	0.16 ± 0.01	0.011 ± 0.001

Conclusion The application of exponential parameters can be used to determine the energy range through OSL intensity without filters and additional other detectors.

References

1) Malthez, A.L.M.C. et al. Experimental photon energy response of different dosimetric materials for a dual detector system combining TL and OSL. Radiat. Meas.,71, 2014, 133-138.
2) Gasparian, P.B.R., Vanhavere, F., Yukihara, E.G. Evaluating the influence of experimental conditions on the photon energy response of Al_2O_3:C optically stimulated luminescence detectors. Radiat. Meas.,47 (4), 2012, 243-249.
3) Malthez, A.L.M.C. et al. OSL dosimetric properties and efficiency of Brazilian natural calcium fluoride pellets. Applied Radiation and Isotopes, 135, 2018,166–170.
4) Malthez, A.L.M.C. et al. Low-cost flexible OSL detector leaf for 2D radiation measurements. Book of abstracts of the ISRP-14, 2018, 314.

The Testing of Filtered Shallow Dose Dosimeters for the Measurement of $H_p(3)$ towards Eye-lens Dosimetry

Jacques Dubeau[1], Jason Sun[2]*, Neil Leroux[2]
[1] *DETEC, Gatineau, Canada*
[2] *Canadian Nuclear Laboratories, Chalk River, Canada*

Highlights Existing shallow (skin) dose dosimeters, with modifications for the possibility to accurately measure personal dose equivalent $H_p(3)$ for eye dosimetry, were tested on 5 different models. Most models performed suitably well to be considered as potential $H_p(3)$ eye dosimeters.

Key words nuclear industry, eye dosimetry, $H_p(3)$, filtered shallow dose dosimeters

Background and Objectives In 2012, the International Commission on Radiological Protection (ICRP) made available new recommendations on the dose limits to the lens of the eye in its Publication 116. For nuclear energy workers, the annual dose limit was reduced to 20 *mSv* per year, averaged over 5 years, with a maximum dose of 50 *mSv* in any single year. This represents an important reduction of the previous limit of 150 *mSv*. The limit to the general public was left unchanged at 15 *mSv*. These changes were due to new conclusions on epidemiological studies which indicate that the onset of cataracts may occur at doses of 0.5 *Sv* and lower. Most dosimetry services have programs in place to monitor the deep (whole-body) and shallow (skin) doses, $H_p(10)$ and $H_p(0.07)$, but very few are presently equipped to measure the operational quantity of interest relevant to the eye-lens protection, $H_p(3)$, the personal dose equivalent at 3 *mm* depth. Some commercially available $H_p(3)$ dosimeters have begun to appear on the market, but they are mainly designed towards medical applications, i.e., for the dosimetry of X-rays only. The nuclear industry requires X-ray, gamma-ray, beta particle, as well as neutron dosimetry. The work now reported considers photon and beta particle dosimetry.

Materials and Methods It would be advantageous not to burden dosimetry services with a totally new technology. It was thus decided to examine if skin dosimeters now in use could be slightly modified to accurately measure $H_p(3)$. The modification proposed was the addition of a low-Z polycarbonate (Lexan) filter with a thickness of the order of 300 $mg\ cm^{-2}$. Testing was performed on 5 different models of skin dosimeters, currently in use at 4 Canadian nuclear facilities and a United States cancer center. The dosimeters were exposed, on suitable head

phantoms, to X-rays (48, 118, and 165 *keV* mean energies), to ^{137}Cs and ^{60}Co gamma-rays, and to beta particles from a standard $^{90}Sr/^{90}Y$ source. The irradiations were performed at normal incidence, as well as at 20°, 40° and 60° oblique incidences.

Results and Discussion Results of the dosimetric responses of the 5 skin dosimeter technologies, under the stated irradiations conditions, will be presented. Most technologies performed suitably well to be considered as potential $H_p(3)$ dosimeters, pending further type-testing.

Conclusion This work demonstrates that it is possible to use existing shallow dose dosimeters, modified with suitable filtration materials, for the measurement of dose to the lens of the eye, in the nuclear industry.

Acknowledgements The authors thankfully acknowledge the contributions of the following: Jovica Atanackovic (Ontario Power Generation), Lawrence Dauer (Memorial Sloan Kettering Cancer Center), Sampath Hakmana Witharana (New Brunswick Power), and Andrei Hanu (Bruce Power). This work was funded by the CANDU Owners Group (COG).

Optically Stimulated Luminescence of Different Borate Glasses

J.V.B. Valença[1,2]*, I. S. Silveira[2], A.C.A. Silva[3], N.O. Dantas[3], P.L. Antonio[4], L.V.E. Caldas[4], F. d'Errico[5,6], S.O. Souza[2]

[1]*Universidade Federal de Ciências da Saúde de Porto Alegre, Porto Alegre, Brazil*

[2]*Universidade Federal de Sergipe, São Cristóvão, Brazil*

[3]*Universidade Federal de Alagas, Maceió, Brazil*

[4]*Instituto de Pesquisas Energéticas e Nucleares, São Paulo, Brazil*

[5]*Università di Pisa, Pisa, Italy*

[6]*Yale University, School of Medicine, New Haven, CT USA*

Highlights Studying glasses for dosimetric applications offer lots of possibilities, as well as challenges. Different borate glasses were analyzed regarding some important characteristics that may be considered in dosimetric studies using the OSL technique.

Key words: Borate glass, OSL, Radiation dosimetry.

Background and Objectives Over the last decades searching for new luminescent dosimetric materials, as well as better understanding the signal origin from well known TLDs and OSLDs, has increased. Using the optical properties of glasses for application in the field of radiation detection has been quoted as an actual direction of research in the glass science[1]. Borate glasses can present desirable characteristics for personal dosimetry, even though some drawbacks must be overcome to make their use feasible in a practical way.

The main objective of this work was not only to analyze in a comparative way the OSL signal of different borate glass matrixes but also focus on a better understanding of the characteristics regarding the emission intensity and stability. Table 1 shows the produced compositions.

Table 1. Produced borate glass compositions.

$Li_2CO_3 - K_2CO_3 - B_2O_3$ [LKB] mol%	$Li_2CO_3 - M_gO - B_2O_3$ [LMB] mol%	$Li_2CO_3 - CaO - B_2O_3$ [LCB] mol%
$20Li_2O \cdot 10K_2O \cdot 70B_2O_3$ (L10KB)	$20Li_2O \cdot 10MgO \cdot 70B_2O_3$ (L10MB)	$20Li_2O \cdot 10CaO \cdot 70B_2O_3$ (L10CB)
$20Li_2O \cdot 15K_2O \cdot 65B_2O_3$ (L15KB)	$20Li_2O \cdot 15MgO \cdot 65B_2O_3$ (L15MB)	$20Li_2O \cdot 15CaO \cdot 65B_2O_3$ (L15CB)
$20Li_2O \cdot 20K_2O \cdot 60B_2O_3$ (L20KB)	$20Li_2O \cdot 20MgO \cdot 60B_2O_3$ (L20MB)	$20Li_2O \cdot 20CaO \cdot 60B_2O_3$ (L20CB)
$20Li_2O \cdot 25K_2O \cdot 55B_2O_3$ (L25KB)	$20Li_2O \cdot 25MgO \cdot 55B_2O_3$ (L25MB)	$20Li_2O \cdot 25CaO \cdot 55B_2O_3$ (L25CB)
$20Li_2O \cdot 30K_2O \cdot 50B_2O_3$ (L30KB)	$20Li_2O \cdot 30MgO \cdot 50B_2O_3$ (L30MB)	$20Li_2O \cdot 30CaO \cdot 50B_2O_3$ (L30CB)

Materials and Methods Glasses were produced using the typical melt-quenching method. X-ray diffractometry (XRD) and differential thermal analysis (DTA) were used to evaluate

the produced materials. A $^{90}Sr/^{90}Y$ beta source (dose rate of 0.1 Gy/s) built into a Risø TL/OSL reader was used in the irradiation procedures. The OSL signal was analyzed in terms of both the total area under the curve as well as the emission in the very first 0.16 s. The pre-heating processes were applied to study the stability of the signal.

Results and Discussion Regarding the emitted OSL intensity, the composition named as LKB was the most sensitive[2]. Similarities in the decay patterns for the LCB and LMB compositions were found, even though there were differences in the sensitivity, which might be related to the valence of the atoms Mg and Ca. Glasses with the presence of MgO and CaO presented more stability to the environmental moisture. LKB glass samples showed different patterns of sensitivity depending on the parameter used to plot the dose-response curves, as illustrated in Figure 1[3].

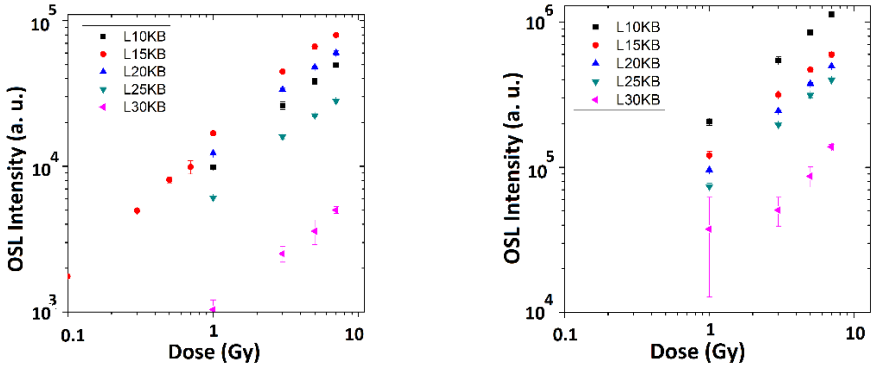

Figure 1. Dose-response curves for the LKB composition considering the total area under the curve (right) and the emission in the first 0.16 s (left).

Conclusion Varying the composition of the borate glasses can influence drastically their sensitivity. Evaluation of parameter used to plot the dose-response curve may present an important influence in the studies involving the association between glasses and optically stimulated luminescence for dosimetric purposes.

References

1) Mauro, J.C.; Philip, C.S.; Vaughn, D.J.; Pambianchi, M.S. Glass Science in the United States: Current Status and Future Directions. **Int J Appl Glass Sci**, v. 5, p. 2–15, 2014.
2) Valença, J.V.B.; Silveira, I.S.; Silva, A.C.A.; Dantas, N.O.; Antonio, P.L.; Caldas, L.V.E.; d'Errico, F.; Souza, S.O. Optically stimulated luminescence of borate glasses containing magnesia, quicklime, lithium and potassium carbonates. **Rad Phys Chem**, v. 140, p. 83-86, 2017.
3) Valença, J.V.B.; Silva, A.C.A.; Dantas, N.O.; Caldas, L.V.E.; d'Errico, F.; Souza, S.O. Optically stimulated luminescence of the $20Li_2CO_3$-(X)K_2CO_3-(80-X)B_2O_3 glass system. **J Lumin**, v. 200, p. 248-253, 2018.

Eye Lens Dosimetry for Workers at Fukushima Daiichi Nuclear Power Station: (1) Laboratory study on the dosimeter position and the shielding effect of full face mask respirators

K. Hoshi[1]*, H. Yoshitomi[1], K. Aoki[1], Y. Tanimura[1], N. Tsujimura[1], and S. Yokoyama[2]
[1]*Japan Atomic Energy Agency, Ibaraki, Japan*
[2]*Fujita Health University, Aichi, Japan*

Highlights To clarify the eye lens dosemeters positioning the shielding effect of full face mask respirators, photon irradiation experiments to various eye lens dosemeters attached on the head phantom was performed at the secondary photon calibration fields of Japan Atomic Energy Agency.

Key words lens of the eye, dosimetry, phantom, Fukushima daiichi nuclear power station

Introduction In 2011, the International Commission on Radiological Protection recommended reducing the occupational equivalent dose limit for the lens of the eye. Since then, there have been extensive discussions and studies on the implementation of the new limit into the radiation protection regulations in Japan. In FY 2017, the Japanese Nuclear Regulatory Agency (NRA) established the Radiation Safety Research Promotion Fund for funding projects on nuclear safety regulation, and adopted the two-year research project entitled “Study on standard eye lens monitoring, suitable dose management and radiation protection for nuclear and medical workers (principal investigator: S. Yokoyama)”. As part of this research project, we conducted the eye lens dosimetry study for workers, specifically engaged in the recovery and decommissioning operations at Fukushima Daiichi Nuclear Power Station. The study is a two-phase study: a laboratory study on the eye lens dosemeter’s characteristics to photons, and a field study executed at actual workplaces at Fukushima Daiichi Nuclear Power Station. This paper summarizes the results of the first-phase study, which was designed to clarify the eye lens dosemeter positioning and the shielding effect of full face mask respirators used at the station.

Materials and Methods Photon irradiation experiments to various eye lens dosemeters attached on the head phantom was performed at the secondary photon calibration field at the Facility of Radiation Standards (FRS) and the Instrument Calibration Facility (ICF) of the Japan Atomic Energy Agency. The dosemeters used were: (1) two kind of $H_p(3)$ dosemeters, namely Dosiris (Chiyoda Technol) and Vision (Nagase Landauer), both of which utilizes a

small LiF TLD, and (2) Glass badge (Chiyoda Technol). Three dosememers of the former two types were placed each on the middle of the eyebrow and both corners of the eye of the head of a RANDO phantom. One glass badge was placed on the forehead of the phantom. Figure 1 shows a photograph of how the dosemeters were placed on the head phantom. Two types of commonly used full face mask respirators are chosen in this study and the comparative measurements were made with and without the masks. Moreover, small disc-shaped $Li_2B_4O_7$ TLD chips were loaded into the phantom at positions corresponding to the lens of the eye to directly evaluate the mask shielding effect to the lens dose. Irradiations were made with three energies, N100, N250, and Cs at two exposure geometry AP and ROT.

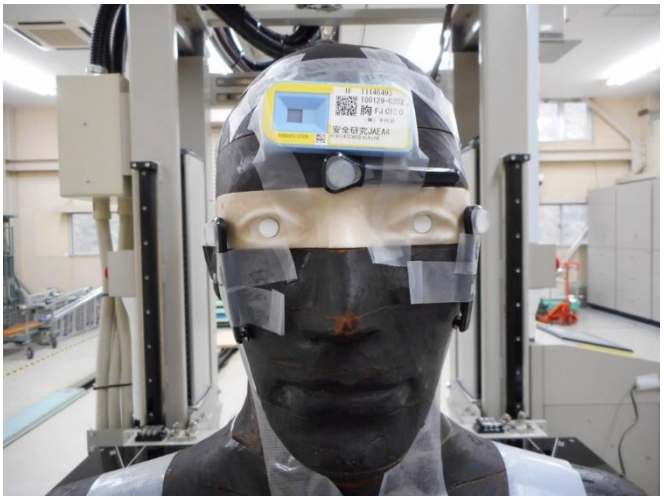

Figure 1 Photograph of how the dosemeters were placed on the head pahtom

Results and Conclusion The results are as follows:

1) No marked difference was observed in readings of the dosemeters attached on the different positions on the head phantom.

2) Two types of full face mask respirators provided insignificant shielding effect for photons of 83 keV to 662 keV.

3) Comparative measurement between AP and ROT geometries suggested that head-mounted dosemeters would generally produce a small angular variation in readings specifically in multidirectional fields as compared to the trunk-mounted dosemeters.

A new concept thyroid monitor using multiple GAGG detectors for population monitoring in a nuclear accident

Kazuaki Yajima[1]*, Eunjoo Kim[1], Kotaro Tani[1], Osamu Kurihara[1]
[1]*National Institutes for Quantum and Radiological Science and Technology, Chiba, Japan*

Highlights A new thyroid monitor using multiple $Gd_3(Al,Ga)_5O_{12}$ (GAGG) detectors with each crystal size of one cubic centimeter has been developed. The GAGG detectors can be placed around the front surface of the human neck to increase the sensitivity for ^{131}I in the thyroid, especially with the intension of measuring infants and small children. The arrangement of 8 GAGG detectors was tested using age-specific phantoms with thyroid shaped container filled with ^{131}I solution, demonstrating that the minimum detectable activity (MDA) of the new monitor was lower than that of a conventional NaI(Tl) spectrometer (a crystal size of 2.54 cm in diameter x 2.54 cm in thickness).

Key words Thyroid monitor, ^{131}I, nuclear accident, exposure, GAGG

Background and Objectives Individual monitoring of large populations potentially exposed to the released radionuclides in a nuclear accident is a very challenging task, in particular regarding thyroid exposure due to intake of short-lived radioiodine (mainly, ^{131}I). In the Fukushima Daiichi nuclear power plant accident in 2011, screening campaigns to identify persons with significant thyroid exposure were conducted using conventional NaI(Tl) survey meters[1)]; however, the number of the subjects were limited for grasping regional distributions of the thyroid doses of residents in Fukushima. One of the difficulties found in such direct thyroid measurements is to place a typical cylindrical detector probe on the front surface of the neck in particular for small children. In this study, we developed a new concept thyroid monitor with multiple GAGG detectors to allow their arrangement suitable for measurements of any subjects and examined its performance.

Materials and Methods The prototype thyroid monitor consists of 8 GAGG detectors, a multi-signal processing unit and a laptop on which a software package for control the detectors and spectral analyses is installed. The exterior view of the monitor is shown in Figure 1. The power supply for the detectors is made via a USB connection of the laptop. Each detector has a one cubic centimeter GAGG crystal connected to a silicon photomultiplier (SiPM), which is installed in an aluminum casing with a size of 1.6 cm x 1.7 cm x 3.5 cm. The gain shift of a pulse due to change of temperature is compensated by a thermometer mounted in each detector. For performance tests of the monitor, age-specific thyroid phantoms recently developed by a

French institute, Institut de Radioprotection et de Surete Nucleaire (IRSN) were used[2]. A thyroid-shaped container installed in each phantom (imitating 5-y, 10-y, 15-y and Adult Male) was filled with standard ^{131}I solution. In experiments, the 8 GAGG detectors were arranged to a 2 x 4 array to be contact with a curved front surface of the neck phantom (Figure 2).

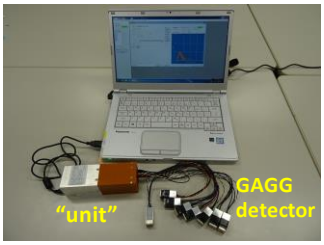

Figure 1. Exterior view of the prototype monitor.

Figure 2. Arrangement of 8 GAGG detectors with 2 x 4 array (left) and an experimental setup using the 5-y neck phantom (right).

Result and Future task The MDA values of the new monitor were calculated based on the Currie's formula[3] under normal background conditions (~0.05 μSv h^{-1}). Peak efficiency (at 365 keV of ^{131}I) used in the formula was determined from the experiments using the neck phantom. Table 1 provides the MDA values of the new monitor for Adult, 15-y, 10-y and 5-y neck phantoms in the case of a counting time of 180 seconds, together with those of a typical NaI(Tl) spectrometer with a crystal size of 2.54 cm in diameter and 2.54 cm in thickness for comparison. As shown, the new monitor was better than the typical NaI (Tl) spectrometer in terms of MDA, despite of the fact that the former was smaller than the latter regarding the total crystal volume (8.0 cm^3 vs. 12.9 cm^3).

The new monitor is still under developing stage. Currently, we plan to produce a jig to fix the optimized arrangement of the GAGG detectors and a shield for the detector assembly for use under elevated background conditions. Further progress of the new thyroid monitor will be presented in the upcoming workshop.

Table 1. MDAs of ^{131}I for the age-specific neck phantoms (counting time: 180 s).

Detector	MDA of ^{131}I (Bq)			
	Adult	15 y	10 y	5 y
New monitor GAGG 2x4 array	31	26	23	19
1" ϕ x 1" NaI(Tl) spectrometer	45	38	35	27

Funding This study has been conducted as a research project commissioned by Nuclear Regulation Authority, Japan during 2017-2019.

References

1) Kim, E. et al., National Institute of Radiological Sciences, NIRS-M-252, 59-66, 2012.
2) Beaumont, T. et al., Phys. Med. Biol. 62, 4673-4693, 2017.
3) Currie, LA., Anal. Chem. 40, 586-593, 1968.

Measurement of Dose Distribution from a Crookes Tube Using TL Dosimeter

Do Duy KHIEM*, Masaya YASHIKI, Hiroto MATSUURA, Masafumi AKIYOSHI
Graduate School of Engineering, Osaka Prefecture University, Osaka, Japan

Highlights The X-ray energy radiated from a Crookes tube is approximately 20 keV. It caused a distribution of $H_p(0.07)$ dose enclosing the Crookes tube at 0.015 – 0.11 mSv in 1 hour. The dose concentrates in the central human body and relatively descend to expanded area.

Key words Crookes tube, TL dosimeter, X-ray exposure, dose distribution, radiation protection

Background and Objectives In Japan, Crookes tubes have been used as fundamental equipment in science education in junior-high schools. Some studies showed that X-ray radiation from the Crookes tubes has very low energy (about 20 keV)[1)], but the dose is remarkably high (up to several hundred mSv/h). However, radiation protection and safety guideline have not been evaluated sufficiently yet. As a result, X-ray radiated from Crookes tube is possible exposure to a teacher and participated student during a demonstration. Due to unstable apllied voltage pulse to Crookes tube, it caused an inhomogeneous X-ray spectrum[2)]. In adition, it does not radiate X-ray as a aligned and expanded radiation field, but gives inhomogenous distribution of dose. In these reasons, a $H_p(10)$ does not give a good approximation of effective dose. In this study, the dose distribution of X-ray in direction surrounding a Crookes tube was estimated using TL dosimeters and obtained $H_p(0.07)$ to estimate air absorbed dose. These results will contribute as a radiation safety database on Crookes tube serving in radiological education in Japan.

Materials and Methods TL dosimeters from Panasonic manufactory are attached on a human body shape which the 2D size is fitted to a junior-high school student. A large number of dosimeters were distributed on the whole body shape to evaluate the spatial distribution of dose. A $H_p(0.07)$ at E1 position on dosimeter represents a skin dose affecting to students. A setting distance was 1m from the Crookes tube to the body shape and exposure time was 1 hour to integrate enough dose to compare.

In addition, the applied voltage from the induction coil was regulated by output power on the induction coil to change X-ray energy and dose. Thus, the X-ray spectrum and the electrical components applying to Crookes tube were also investigated. A CZT detector and a digital oscilloscope were used to estimate X-ray energy and applied voltage from the induction coil (as a power supply of Crookes tube).

Results and Discussion An increase in the output power at the induction coil changed the distribution of the applied voltage, which resulted in a shift in the X-ray energy to higher energy region. X-ray energy distributed at 16 – 20 keV corresponding to an applied voltage at 25 – 40 kV. There was a good correlation in the distribution behavior between the X-ray spectrum and the applied voltage. At PW16 (applied voltage 40 kV and X-ray energy 20 keV), it cause a distribution of $H_p(0.07)$ dose at 0.015 – 0.11 mSv in 1 hour. The dose distributed highest in the aligned direction to Crookes tube (central area) and relatively descend corresponding to the expanded area (Fig. 1).

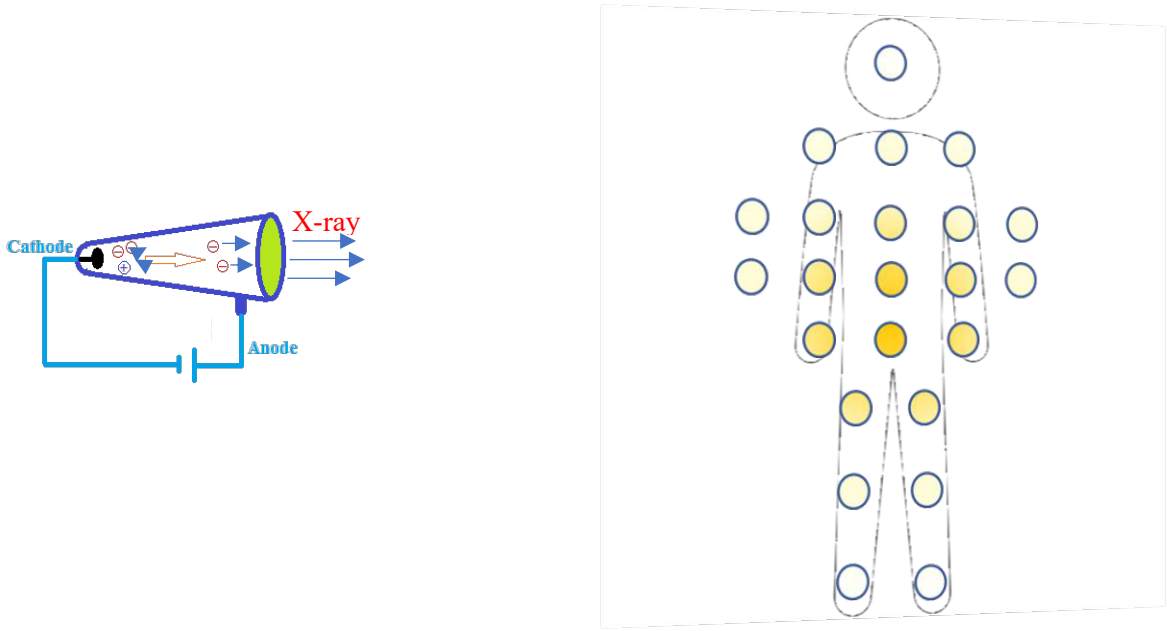

Figure 1. Illustration of the dose distribution from a Crookes tube on a human body shape where the circles designate as the TL dosimeters. The distribution of high and low dose corresponds to the dark and light color on the shape.

Conclusion X-ray at low energy was estimated using a CZT detector and the dose was measured with TL dosimeters. It is approximately 20 keV in energy and causes a distribution dose of $H_p(0.07)$ at 0.015 – 0.11 mSv in 1 hour. This range of dose is lower than in other studies[1,2]. However, it depends on Crookes tube type and operational conditions.

References

1) Ohmori, G.: X-ray exposure in the teaching of science at junior and senior high schools. NIRS-M—105, Japan 107–112 (1995) *(in Japanese).*

2) M. Akiyoshi, et al., Development of evaluation techniques for low energy X-rays from a Crookes tube, Radiation chemistry, 106 (2018) 31-38 (*in Japanese)*.

Monte Carlo simulations with mathematical phantoms to investigate the effectiveness of a whole-body counter for thyroid measurement

Kotaro Tani[1]*, Yu Igarashi[1,2], Eunjoo Kim[1], Takeshi Iimoto[2], Osamu Kurihara[1]
[1]*National Institutes for Quantum and Radiological Science and Technology, Chiba, Japan*
[2]*The University of Tokyo, Chiba, Japan*

Highlights Computational simulations were performed to investigate the availability of FASTSCAN, the whole-body counter widely used after the Fukushima nuclear disaster in 2011, for the population monitoring focusing on ^{131}I accumulated in the human thyroid.

Key words internal dosimetry, thyroid measurement, Monte Carlo simulation

Background and Objectives In vivo measurements for assessing internal dose from incorporated radionuclides into the human body may be conducted in the event of radiological accidents with a large release of radionuclides into the environment. In this context, one of the difficulties experienced after the Fukushima nuclear disaster in 2011 was to implement campaigns to measure radioiodine (mainly ^{131}I) accumulated in the human thyroids for a large number of subjects within a short period of time[1)]. Although the campaigns using conventional NaI(Tl) survey meters were carried out in the accident, the several challenges have been identified, such as measuring under the elevated background levels, gathering the subjects during the accident, securing measurers and so on. On the other hand, many whole-body counter (WBS) units have been introduced in Fukushima to understand the levels of internal contamination with $^{134/137}$Cs in residents. We performed computational simulations using mathematical human phantoms for a FASTSCAN unit (Canberra Inc., USA), the WBC system mostly used in Fukushima, to investigate its availability for the population monitoring (including children) shortly after a similar nuclear disaster.

Materials and Methods The FASTSCAN unit, a standing WBC having two NaI(Tl) detectors (crystal size: 7.6×12.7×40.6 cm^3), was suitably model in the simulations by MCNP (a general Monte Carlo N-Particle transport code version 6.2)[2)]. The counting efficiency of each detector (upper or lower) was calculated for ^{131}I in the thyroid of the age-specific mathematical phantoms (5y, 10y, 15y and Adult)[3)], provided from Dr. Alexander Ulanovsky with his courtesy. The simulation geometry is illustrated in Figure 1.

Results and Discussion Figure 2 shows the results of the calculated counting efficiencies, demonstrating the similar tendency for the 15y and Adult phantom. The counting efficiency of the upper detector was higher than that of the lower one; the ratio of these counting

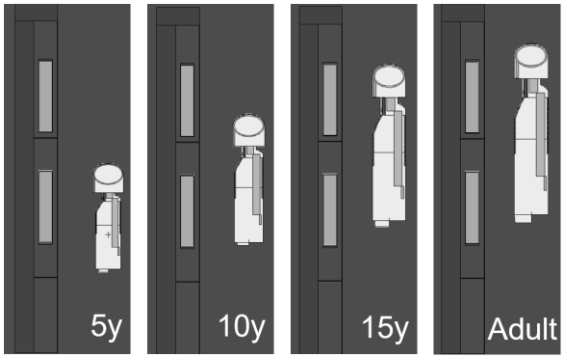

Figure 1. Simulation geometry with the whole-body counter and the phantoms.

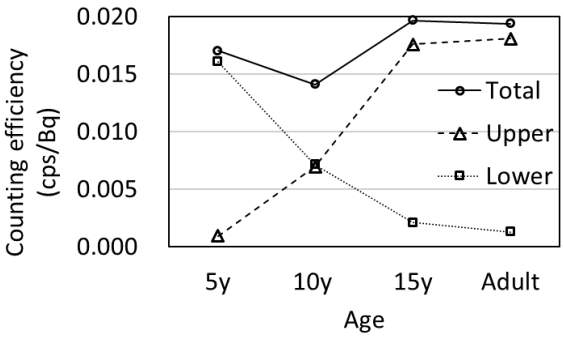

Figure 2. Counting efficiency at 365 keV of whole-body counter to the phantoms.

efficiencies (upper/lower detectors) was more than 8.4. This relationship is opposite for the 5y phantom and the corresponding ratio was 0.059. This reason was explained by the positional relationship between the upper/lower detectors and the thyroids of each phantom (see Figure 1). On the other hand, the total counting efficiencies of the two detectors were similar among the 5y, 15y and Adult phantoms. However, the total counting efficiency for the 10y phantom was decreased by 27% compared with that for the Adult phantom. This is caused by the location of the thyroid of the 10y phantom, which exists between the two detectors regarding the height from the floor. When this phantom stood on a 30 cm height stool as in operations of FASTSCAN units in Fukushima Prefecture for children whose height were lower than 130 cm, the total counting efficiency was almost similar to that for the rest of the phantoms. Although further considerations are necessary, measurements of ^{131}I in the thyroid with FASTSCAN units would have advantages such as a high-throughput monitoring capability and a relatively small age-dependency on the total counting efficiency for ^{131}I. The counting efficiency ratio of the two detectors would be also utilized to distinguish ^{131}I localized in the thyroid from the possible surface contamination. Additional simulation results will be presented in the session together with the relevant data obtained from human measurements after the Fukushima nuclear disaster.

References

1) Kim, E. et al: Internal thyroid doses to Fukushima residents – estimation and issues remaining, J. Radiat. Res. 57(S1), i118-i126 (2016).
2) Werner C. J. (editor): MCNP User's Manual, LA-UR-17-29981 (2017).
3) Ulanovsky, A. V. et al: Modifications to the ORNL phantom series in simulation of the responses of the responses of thyroid detectors Radiat. Prot. Dosim. 79(1-4), 429-431 (1998).

The Experimental Study on Radon Detection Using the CR-39 Track-etching Detectors

Lixia Tian[1*] Meiyu Guo[2]

[1] East China University of Technology, Nanchang, 330013, China
[2] Institute of Metrology, Zhengzhou, 450000, China

Abstract: The plastic solid-state nuclear track detectors become more and more popular in the charged particles detection and environmental monitoring. In this paper, the characteristics of the CR-39 and cellulose acetate are compared , on the basis of the track-etching condition(6.5mol/L, 70℃, 8h) ,the CR-39 detector is calibrated with a calibration coefficient of 0.035 Tc/cm^2/Bq · h/m^3. Based on track-etching system, the Radon concentration of Anyang district and Chengdu city is measured. Some factors affecting the radon concentration are also discussed. The results indicate that radon concentrations in Anyang district are 13.0Bq/m^3～54.2Bq/m^3,while in Chengdu are 14.1Bq/m^3～43.2 Bq/m^3.

*e-mail: tianlixia@ecit.cn

Analyses of MgB_4O_7: Ce,Li in clinical and neutron dosimetry using Optically Stimulated Luminescence Technique

Luiza F. Souza[1]*, Caroline C. Santos[1], Divanizia N. Souza[1], Rogerio M. Vidal[2], Francesco d´Errico[3,4], Susana O. Souza[1]

[1]*Universidade Federal de Sergipe, São Cristóvão, SE, Brazil*

[3]*Instituto do Câncer do Ceará, Fortaleza-CE, Brazil*

[4] *Università di Pisa, Scuola di Ingegneria, Pisa, Italy*

[5]*Yale University, School of Medicine, New Haven, CT, USA*

Highlights MgB_4O_7:Ce,Li detectors presented wide dose-response range required in clinical dosimetry and no significant energy dependence for irradiations with 6 and 10 MV.

Key words OSL dosimetry, new radiation detectors, radiotherapy

Background and Objectives The main challenge for Optically Stimulated Luminescence (OSL) technique has been the lack of materials for some medical applications. Only two materials are commercially available for OSL dosimeters, and both have some limitations. Al_2O_3:C (Landauer Inc.) is the most common, although it is not a good tissue equivalent material. The adoption of BeO (Brush Ceramics Products, Materion Co.) is increasing because of its high sensitivity and effective atomic number (z_{eff}) of 7.2. However, both are not sensitive to neutrons, and thus there is a need for new OSL dosimeters. Borates are of great interest in dosimetry. MgB_4O_7, z_{eff} of 8.4, has been used in thermoluminescent dosimetry. Due to the presence of boron in their chemical compositions, borates are potentially suitable for thermal neutrons dosimetry. Recently some studies showed that MgB_4O_7:Ce,Li is also a good OSL emitter[1]. Therefore, this work aimed to investigate the feasibility of using the MgB_4O_7:Ce,Li as an alternative to being applied in clinical measurements, using OSL technique, as well for thermal neutrons dosimetry. A series of experiments were performed in clinical beams to characterize the MgB_4O_7:Ce,Li, such as reproducibility, dose-response, dose rate dependence, field size dependence, energy dependence, percentage depth dose (PDD) curve and finally the possibility to use the MgB_4O_7:Ce,Li to detect thermal neutrons by OSL.

Materials and Methods The crystals of MgB_4O_7:$Ce_{0.5\%}$,$Li_{0.5\%}$ were prepared through solid state synthesis[1] and the tests were performed with materials in form of pellets, with 3 mm of diameter, 1 mm of thickness, and 10 mg of weight. The irradiations of the pellets were

performed in reference gamma rays source ^{137}Cs (662 keV) and in clinical beams of 6 MV and 10 MV using a Clinac Varian 21EX. For the dose rate dependence, the pellets were exposed to 10 MV photons and doses rates of 200, 300, 400, and 500 cGy/min, at a 100 cm source to surface distance (SSD). For the field size dependence, the samples were exposed to fields of 3×3 cm^2, 5×5 cm^2, 10×10 cm^2, and 20×20 cm^2. The percentage depth dose (PDD) curves were performed in a solid water phantom, with a 10×10 cm^2 field. All the data was compared with the treatment planning system (TPS), obtained with an ionization chamber (IC). The neutrons irradiation was performed at a thermalized neutrons source of $^{241}Am/Be$, with the detectors free in air and placed in a solid water phantom.

Results and Discussion The dose-response of the $MgB_4O_7:Ce_{0.5\%},Li_{0.5\%}$ exposed to 10 MV and 6 MV photon beams showed a broad range from 0.1 up to 20 Gy. The results also showed that OSL response of the MgB_4O_7:Ce,Li saturates above 20 Gy. Moreover, the reproducibility of the OSL readings for the pellets used in the analyses was below 10%.

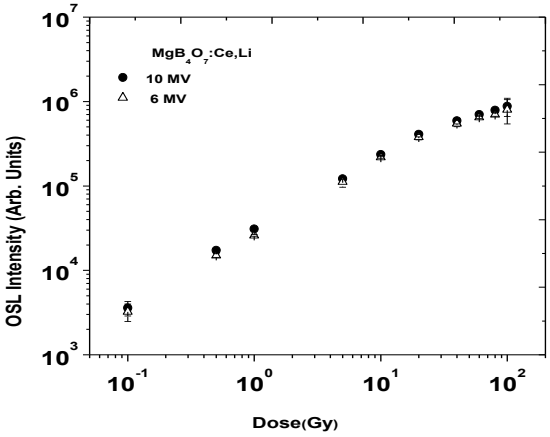

Figure 1. OSL dose-response curves for $MgB_4O_7:Ce_{0.5\%},Li_{0.5\%}$ exposed to 0.1 Gy up to 10 Gy, when irradiated to 10 MV and 6 photon beams.

Conclusion The first results indicated that the detectors presented wide dose-response range, required in clinical beams dosimetry and that no significant energy dependence was seen for irradiations with 6 and 10 MV. The pellets also presented a good reproducibility at the OSL readings (< 10%). Furthermore, the experimental results related to the energy dependence (with more energies), PDD, dose rate, field size dependence as well as the possibility to use this material to detect thermal neutrons will be presented at the conference.

References

1) Souza L.F. et al. Radiat Meas. 2017. 106:196-9.

$LiMgBO_3:Tb^{3+}$ TL phosphor for personnel neutron dosimetry applications

Meghnath Sen*[a,c], Rakesh Shukla[b], V Sathian[a], M. S. Kulkarni [a,c] and A. K. Tyagi [b,c]

a : Radiation Safety Systems Division, BARC, Mumbai-400085, India

b: Chemistry Division, BARC, Mumbai-400085, India

c: Homi Bhabha National Institute, Anushakti Nagar, Mumbai-40094, India

**Corresponding author: meghms@barc.gov.in , Phone no. (O): 022-25590948*

Highlights Tb^{3+} doped $LiMgBO_3$ was synthesized using sol gel method. Its structural characterizations were done using XRD, PL and SEM techniques. It has shown very good thermoluminescence (TL) response for thermal neutrons from graphite moderated ^{241}Am-Be neutron source. The TL signal is stable with low fading rate.

Key words TL phosphor, $LiMgBO_3:Tb^{3+}$, ^{241}Am-Be, personnel neutron dosimetry

Background and Objectives Among the monitoring of various ionizing radiations, personnel neutron monitoring is more important because of its higher relative biological effectiveness as compared to others. Personnel neutron dosimetry is a complex subject and poses several challenges mainly because of the huge dependency of interaction cross section of materials with neutron energy, wide range of neutron spectra and presence of associated photons with neutron radiation. Compared to gamma dosimetry literature reporting TL/OSL based neutron dosimetric applications is less [1-2]. Majority of the work on personnel neutron monitoring has been carried out based on TLD-600 (^{6}LiF: Mg, Ti) and TLD-700 (^{7}LiF: Mg, Ti) respectively [3]. Therefore, there is a great scope to develop new materials for the said purpose. In this context, the present paper reports the synthesis, structural characterizations and TL based neutron dosimetric studies of $LiMgBO_3:Tb^{3+}$. The selection of the material has been done based upon the following aspects: Firstly, the Z_{eff} (effective atomic number) of the material being ~9.1, it is a near tissue equivalent phosphor which is a pre-requisite for any material to act as a personnel dosimeter. Secondly, the host matrix itself contains both Li and B having very high cross section for thermal neutrons which can produce required TL/OSL response in the material through (n, p) and (n,α) interactions respectively.

Materials and Methods The synthesis of $LiMgBO_3:Tb^{3+}$ phosphor was carried out by sol-gel method. The starting chemicals used were $CH_3COOLi.2H_2O$, $Mg(NO_3)_2.6H_2O$, H_3BO_3 and Tb_4O_7 which were dissolved in dilute HNO_3 medium. Required amounts of $C_6H_8O_7$ and

$(CH_2OH)_2$ were mixed in the solution during boiling of the reaction mixture in a hotplate under constant stirring. Once the reaction is completed, bulky and foamy polymeric residue was obtained which after calcination at 850°C for 6h resulted in $LiMgBO_3:Tb^{3+}$.

Results and Discussion The phase formation of the material was confirmed by XRD which matched well with the JCPDS pattern 49-0528 as shown in Fig1. The sharp nature of the peaks indicate well crystallinity of the material. The neutron irradiation was carried out in STAG (Standard Thermal Assembly in Graphite) facility, the primary standard for the thermal neutron fluence rate where thermal neutrons are generated from moderated ^{241}Am-Be fast neutron source. The TL glow curve of neutron irradiated $LiMgBO_3:Tb^{3+}$ has dosimetric peak at 195˚C with shoulder peak near 130˚C as shown in Fig2. The material has very good sensitivity for the neutrons and its TL response varies linearly with neutron dose. Moreover, the TL signal has very good stability with negligible post irradiation fading.

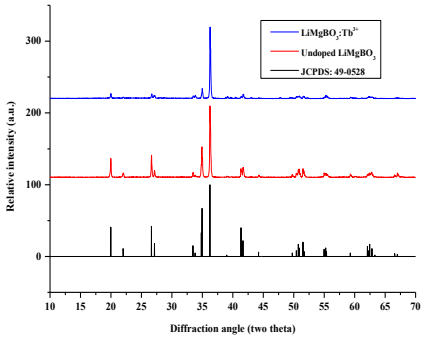

Fig1. XRD pattern of the synthesized material

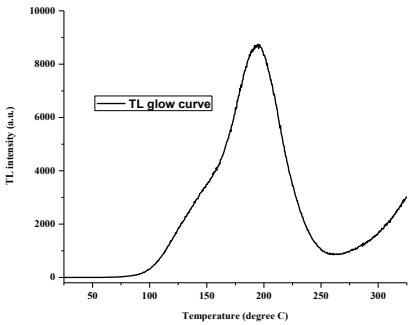

Fig2. TL glow curve of $LiMgBO_3:Tb^{3+}$

Conclusion A neutron sensitive near tissue equivalent $LiMgBO_3:Tb^{3+}$ TL material has been developed. Its TL signal has good stability with very low fading. The material can be useful as a potential candidate for TL based personnel neutron dosimetry applications.

References

1) M.S. Kulkarni et al. "Studies on new neutron-sensitive dosimeters using an optically stimulated luminescence technique" Nuclear Instruments and Methods in Physics Research B 269 (2011) 1465–1470

2) E.G. Yukihara et al. "Development of new optically stimulated luminescence (OSL) neutron dosimeters" Radiation Measurements 43 (2008) 309 – 314

3) A R Laxmanan, "A review on the role of thermoluminescent dosimeters in fast neutron personnel dosimetry", Nuclear tracks and radiation measurements (1982), Volume 6, Issues 2–3, June–September 1982, Pages 59-78

Computational enhancement of scintillation detector capabilities for purpose of monitoring of the artificial gamma activity in the water environment

Michal Fejgl[1], Miroslav Hýža[1]
[1]*National Radiation Protection Institute, Prague, Czech Republic*

Highlights Network of monitoring stations continuously measuring artificial gamma activity in surface water is being built in the Czech Republic. Functionality of the system is based on the failure resistant monitoring stations assembled to a network equipped with central data processing. Stations are automated, autonomous and of a simple construction, therefore failure protected, and their detection capabilities are enhanced by the Noise Adjustment Singular Value Decomposition (NASVD) method, which is used for data processing. This mathematical tool decreases the detection limits, what enables employment of the network not only for the purpose of emergency preparedness but also for normal monitoring with particularly more demanding requests due to detection limits.

Key words NaI(Tl), artificial gamma activity, normal monitoring, accidental monitoring, detection limits, emergency preparedness

Background and Objectives Results of the research project with the aim to develop a network for continuous monitoring of artificial gamma activity in surface water bodies are presented in this contribution. The main results of this project is development of the Station for Continuous Monitoring of Gamma Activity (SAGMA) and of the System for Artificial Gamma Radioactivity Measurement (SCOMO), which consist of several SAGMAs.

SAGMA is constructed as an automatic and autonomous station proposed for monitoring of gamma activity in surface water bodies. Gamma activity determination is based on a submersible NaI(Tl) scintillation detector placed directly in the investigated water body. Benefit of SAGMA is its simple construction, which is failure resistant in conditions of the radiation accident and its consequences as an electric blackout or outage of public services. Electric power supply and data transfer are independent on the local providers. SCOMO is a network build from several SAGMAs placed in spots important for emergency preparedness, with respect to the nuclear facility accident.

Materials and Methods

Particular effort was devoted to suppression of the SAGMA detection limits. Noise Adjustment Singular Value Decomposition Method (NASVD) was used for this purpose. A large reference dataset comprising all year-seasons was collected by SAGMA prototype in the reference environ of the Vltava River in Prague. Vltava water with natural gamma activity fluctuations

was measured continuously (in 10 minutes long real-time windows), this dataset was used for the NASVD algorithm training.

This method is standardly employed in the field of airborne gamma ray spectrometry (1), it enables to supress influence of the background fluctuation. Practical usage of this tool in the river environment brings suppression of detection limits by factors of 3-5. The higher is the background level and the larger is the training set, the stronger is the impact of the NASVD tool. This feature is particularly beneficial during rain events, when the background level is naturally enhanced.

Results and Discussion Minimal detectable activities for determination of ^{131}I and ^{137}Cs by SAMGMA for several integration times were calculated. Integration time 10 minutes is sufficient for reaching of MDA required by the Czech legislation for accidental monitoring, one day long integration time is needed for fulfillment of the legal requirements for normal monitoring.

Comparison of detection capabilities between simple-construction SAGMA and different devices with similar purpose will be presented in the contribution. Summarization of the integral influence of effects such as terrestrial radiation, water composition and cosmic radiation at the locations of each SAGMA within the SCOMO network based on the data collected during the pilot SCOMO operation will be presented in the contribution.

Conclusion A relatively simple measurement setup based on the 3″ x 3″ NaI(Tl) detector combined with the full spectrum NASVD analysis can be used for a reliable and sensitive analysis of artificial radioactivity in the river water. In addition, the independent power supply and diverse connectivity methods allow easy integration to the Emergency Preparedness System of the Czech Republic and strengthen its capabilities**.**

References

1) Minty B., Hovgaard J., 2002. Reducing noise in gamma-ray spectrometry using spectral component analysis. Explor. Geophys. 33 (3),172-176

Compatibility assessment for IEC 62387 standard and improvement of angular dependence of the $H_p(3)$ dosemeter DOSIRIS®

Michiko Ube[1]*, Naoki Takashima[1], Arata Motomura[1], Wakako Shinozaki[1], Satoshi Ueno[1], Yasuhiro Koguchi[1]

[1]*Chiyoda Technol Corporation, Ibaraki, Japan*

Highlights Chiyoda Technol Corporation started eye lens dosimetry service using $H_p(3)$ dosemeter DOSIRIS. Compatibility assessment for IEC 62387 of DOSIRIS was performed, and the characteristics of DOSIRIS met the requirements except for the angular dependence for ^{90}Sr-^{90}Y beta radiation. Angular dependence can be improved by optimization of filter.

Key words DOSIRIS, TLD, $H_p(3)$, IEC 62387, energy and angular dependence

Background and Objectives In 2011, ICRP stated the new dose limit of the equivalent dose for eye lens. Since the $H_p(10)$ and/or $H_p(0.07)$ may not be good estimation of equivalent dose for the eye lens, it is important for some workers to measure $H_p(3)$ with a dosemeter worn close to the eye. The requirements for $H_p(3)$ dosemeters are described in IEC 62387:2012[1)] which is the international standard for personal dosemeters. The conversion coefficients from air kerma to $H_p(3)$ for the slab phantom are also given in this standard. We have performed the compatibility assessment of the $H_p(3)$ dosemeter DOSIRIS for the IEC 62387.

Materials and Methods DOSIRIS is an eye lens dosemeter to measure $H_p(3)$ developed by IRSN (Institut de radioprotection et de sûreté nucléaire). Chiyoda Technol Corporation started the service to measure $H_p(3)$ with DOSIRIS for some radiation workers mainly for medical staff. DOSIRIS has a headband to set it near the eye (Figure1). It contains a ^{7}LiF:Mg,Ti TLD detector in the cap made of 3 mm thickness PP (polypropylene) to measure $H_p(3)$. In this tests, the dosemeters were irradiated on slab phantom according to IEC 62387 standard.

Figure 1 DOSIRIS and TLD element

Results and Discussion Type testing according to IEC 62387 was performed including the tests for energy and angular dependence. The relative responses due to the change of the energy and angle of incidence for photon and beta radiation are shown in Figure 2. The energy and angular responses for photon in the range from 30 keV to 1250 keV meet the requirement. For beta radiation incident from 60 degrees, the response exceed the requirement of the IEC 62387.

To improve the angular dependence for beta radiation, we calculated the response of TLD using Monte Carlo particle transport simulation of PHITS (Particle and Heavy Ion Transport code System) code [2]. By the optimization of the cap thickness of DOSIRIS, the angular response for beta radiation can be improved.

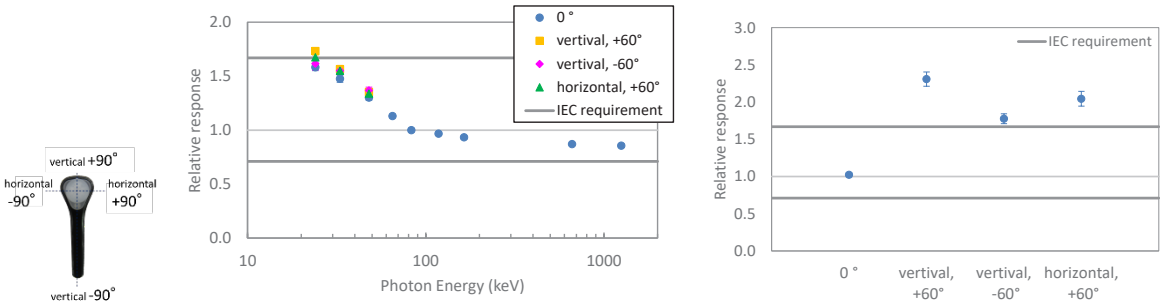

Figure 2. Energy and angular response (left: for photon, right: for ^{90}Sr-^{90}Y beta radiation)

Conclusion The energy and angular response of DOSIRIS for photon fulfilled the requirement of IEC 62387 standard. It was concluded by the calculation that the angular responses for beta radiation can meet the requirement by optimization of the filter thickness of dosemeter.

References

1) IEC 62387:2012, Radiation protection instrumentation – Passive integrating dosimetry systems for personal and environmental monitoring of photon and beta radiation
2) Tatsuhiko Sato, Yosuke Iwamoto, Shintaro Hashimoto, Tatsuhiko Ogawa, Takuya Furuta, Shin-ichiro Abe, Takeshi Kai, Pi-En Tsai, Norihiro Matsuda, Hiroshi Iwase, Nobuhiro Shigyo, Lembit Sihver and Koji Niita, Features of Particle and Heavy Ion Transport code System (PHITS) version 3.02, J. Nucl. Sci. Technol. 55, 684-690 (2018).

Development of a portable and sensitive radioactive detection system for outdoor nondestructive measurement of radioactive cesium in standing trees

Mika Kagaya[1]*, Hideaki Katagiri[2], Ryoji Enomoto[3], Akiko Yamaguchi[4], Hiroshi Muraishi[5], Nofumi Narita[2], Takara Watanabe[6],

[1]*National Institute of Technology, Sendai college, Miyagi, Japan*

[2]*Ibaraki University, Ibaraki, Japan*

[3]*University of Tokyo, ICRR, Chiba, Japan*

[4]*Ibaraki Prefectural Forestry Research Institute, Ibaraki, Japan*

[5]*Kitasato University, Kanagawa, Japan*

[6] *National Cancer Center Hospital East, Chiba, Japan*

Highlights Trees in the large area around the Fukushima Daiichi Nuclear Power Plant were contaminated by radioactive cesium owing to the accident in 2011, damaging mushroom industry using logs. To promote the industry again, no-contaminated safe trees should be selected. Herein, we developed a portable and sensitive radioactive detection system to select the trees before felling. By measuring in the field, we confirmed that the detector could operate in outdoor environments contaminated with low-level radiation, ~0.05 μSv/h.

Key words portable radioactive detection system, ^{137}Cs, 32-keV characteristic X-ray

Background and Objectives A relatively large area in eastern Japan was contaminated by ^{137}Cs as a result of the Fukushima Daiichi Nuclear Power Plant accident. For the contamination in the log, shiitake mushrooms production has been declining in the surrounding area. The Forestry Agency set a maximum concentration limit for radiocesium of 50 Bq/kg[1)] for bed logs to be deemed safe for cultivated shiitake mushrooms (<100 Bq/kg). Previously, we developed a portable and sensitive radioactive detection system for shiitake logs[2)]. However, it cannot measure radioactivity in standing trees, requiring extra manpower and cost for felling before inspection. Hence, herein, we developed a portable and sensitive device that can screen standing trees for ^{137}Cs at a concentration of or above ~50 Bq/kg.

Materials and Methods We measure 32-keV characteristic X-rays from ^{137}Cs instead of 662-keV gamma rays in order to avoid thick and heavy shields. We use a CsI (Tl) scintillator (5×5×1 cm) and a 3-inch photomultiplier tube. The detector was covered by thin Cu shields (Fig. 1). First, X-rays released from a tree including background was measured. Next, we made a background measurement by interleaving Cu plate between the scintillator and the tree at the same place to avoid systematic uncertainty due to position dependence of background. We

obtained a 32-keV peak by subtracting the background spectrum (Fig. 2 (b)).

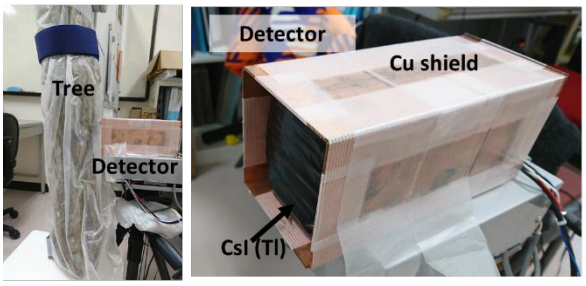

Figure 1: Radioactive detection system

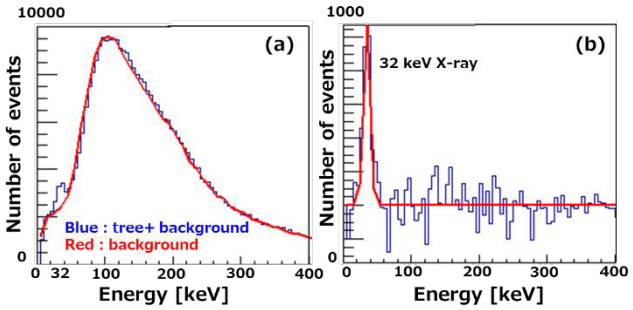

Figure 2: Energy spectrum

Results and Discussion Field measurements were performed in environments with low-level radiation contamination ~0.05 μSv/h. Fig. 3 shows the relationship between concentrations of ^{137}Cs (662 keV) measured using a Ge detector and the number of X-ray events. Based on these results, we confirmed that the proposed detector could measure the low-level concentration of ^{137}Cs in concentrations at or above ~50 Bq/kg, indicating that this method is promising for screening tests for standing trees.

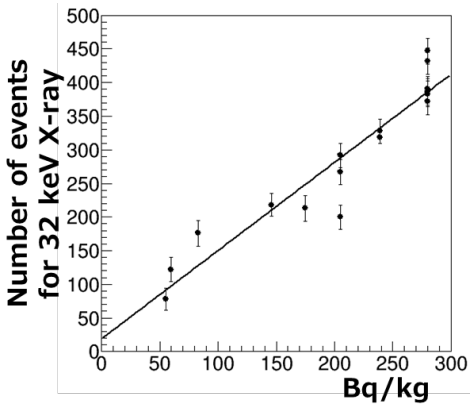

Figure 3: Relationship between concentrations of ^{137}Cs and 32 keV X-ray events

Conclusion In this study, a portable and sensitive radioactive detection system using CsI (Tl) was developed to measure radioactive concentrations of ^{137}Cs nondestructively by detecting 32-keV X-rays. We succeeded to measure the low-level concentration of ^{137}Cs in concentration at or above ~50 Bq/kg in environments with low-level radiation contamination.

References

1) http://www.rinya.maff.go.jp/j/press/tokuyou/120830.html (2012)

2) M. Kagaya et al., "A portable radioactive detection system for outdoor measurement of concentration of radioactive caesium in a mushroom bed log at a low-level contaminated environment", RADIOISOTOPES, (2019), in press.

Application of machine learning for derivation of correction factor for radon exhalation rate

M. Janik[1]*, M. Hosoda[2], S. Tokonami[2]
[1]*QST, Chiba, Japan*
[2]*Hirosaki University, Hirosaki, Japan*

Highlights

Nowadays machine learning (ML) methods provides extremely important tools for intelligent environmental data analysis, processing and visualization. We describe application of ML to environmental sciences in the emphasis to radon exhalation rate.
Nowadays machine learning (ML) methods provide extremely important tools for intelligent environmental data analysis, processing and visualization. We describe the application of ML to environmental sciences in relation to the radon exhalation rate.

Key words

radon, machine learning, exhalation rate

Background and Objectives

Interest in radon is not limited only to its impact on health and its dose to the public, but due to its nature, the techniques to analyze its behaviour can be used in many fields such as radiotherapy, atmospheric physics, geophysics, geohazards, mineral exploration, and even planetary science.
In this study, we focused to radon exhalation from the ground surface. The radon exhalation depends upon a number of variables, such as the radium activity concentration, its distribution in soil grains (soil type, grain size, porosity, temperature and moisture), as well as atmospheric pressure, rainfall and temperature.
The aim of our study was to analyze the influence of rain and derive correction factor on the radon exhalation rate using machine-learning methods (AutoML).

Materials and Methods

In this study, measurements near Sakurajima volcano in southern Japan were performed. The radon exhalation rate values were obtained using the method described by Hosoda et al. [1]
The data contained more than 20,000 measurement sets, i.e. radon exhalation rate, CO_2 flux, pressure, soil temperature at 10, 40 and 100 cm, air relative humidity, air temperature, rainfall,

wind speed and direction, as well as the volumetric water content in the soil for 6 layers from 10 to 100 cm.
Analysis and numerical processing were conducted by applying AutoML (Auto Machine Learning) methods.

Results and Discussion

In the first step, data were pre-processed, for e.g., handling null values before feeding it into the system. In the next step, simple analysis indicated that at least 120 hours were needed to return to the initial radon exhalation rate after rainfall.
Next, the dataset was randomized and divided into three sets: (i) a training set, (ii) a cross-validation set and (iii) a test set. The training and the cross-validation sets were used to train the system, while the test set was used to verify its performance.
Based on these sets, the correction factor for exhalation rate was computed as a function of the CO2 flux and atmospheric pressure using AutoML.

Conclusion

In this study, we performed and analyzed the radon exhalation rate in the soil using an AutoML system. Two significant results were obtained. First, we were able to observe a time lag before radon exhalation values stabilized after rain, secondly, we determined that CO_2 flux and atmospheric pressure were the most important variables (independent of rain) needed to obtain a corrected exhalation rate in dry conditions.

References:

[1] Hosoda, M., Ishikawa, T., Sorimachi, A., Tokonami, S., & Uchida, S., (2011). Development and application of a continuous measurement system for radon exhalation rate. Review of Scientific Instruments, 82(1), 015101. https://doi.org/10.1063/1.3527065

Study on terrestrial background component subtraction from measured pulse height spectrum for environmental radiation measurement using a scintillation spectrometer

Munehiko Kowatari[1]*, Yoshihiko Tanimura[1], Patrick Kessler[2], Annette Röttger[2]
[1] *Japan Atomic Energy Agency, Tokai, Naka, Ibaraki, Japan*
[2]*Physikalisch-Technische Bundesanstalt, Braunschweig, Germany*

Highlights The study investigates the effective subtraction of background components due to terrestrial radionuclides for environmental radiation monitoring using a scintillation spectrometer.

Key words radiological emergency, $CeBr_3$ scintillation detector, terrestrial background,

Background and Objectives In radiological emergency, timely and reliable radiological information such as dose rate or radioactive concentrations due to artificial radionuclides is indispensable to protect general public and the first responder of the situation. The authors have investigated the method for effectively identifying and determining the radioactivity concentration using a scintillation spectrometer[1)]. In this study, the authors demonstrate how influence of terrestrial background (BG) component on measured pulse height spectrum can be minimized to obtain the peaks from gamma rays emitted by artificial radioactivity. In some cases of radiological emergency monitoring, subtraction of BG components was probe to be difficult[2)], because the prior measurement of BG component at the place to be monitored is compulsory. By removing the BG component appropriately from measured pulse height spectrum without any prior BG measurement, the effective minimum detection limit of the spectrometer would be declined.

Materials and Methods In this study, a cylindrical $CeBr_3$ scintillation spectrometer with a 2.54-cm diameter and 2.54-cm height was selected for demonstration. According to the procedure described in ICRU53, pulse height spectrum was measured at the height of 1 m from the ground in the field in Japan Atomic Energy Agency. To determine surface contamination densities on soil for ^{134}Cs and ^{137}Cs, the unfolding method was selected. To estimate and subtract the effect of terrestrial BG components, pulse height spectrum for each natural radionuclides were estimated by performing the Monte Carlo (MC) calculation using the PHITS code. For self-contamination components from the $CeBr_3$ crystal, inherent BG was measured in the underground laboratory operated by the Physicalisch-Technische Bundesanstalt. After

subtracting the BG components from the measured pulse height spectrum, the net pulse height spectrum were de-convoluted by the unfolding method and surface contamination densities on soil for ^{134}Cs and ^{137}Cs were determined according to the ICRU 53.

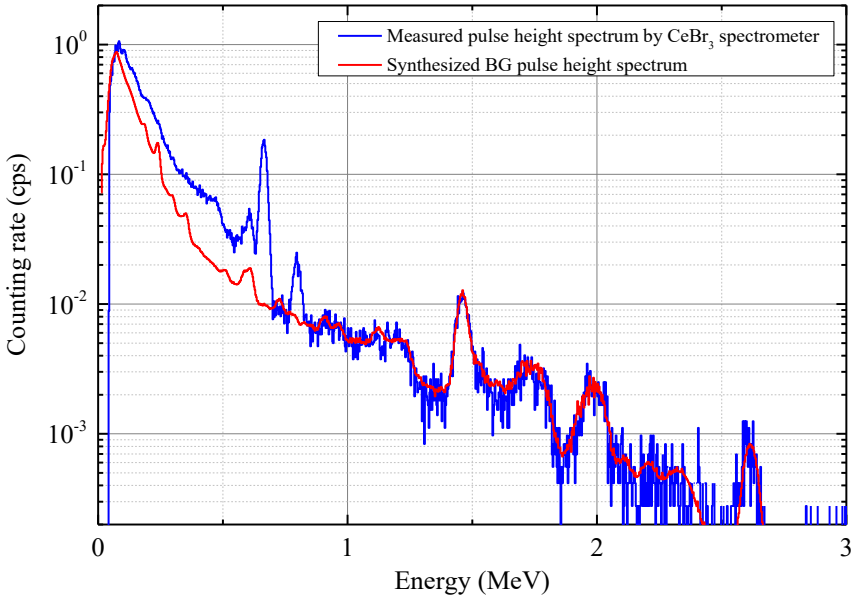

Figure 1. Comparison of measured and synthesized BG pulse height spectrum. The $CeBr_3$ scintillation spectrometer was used for measurement.

Results and Discussion By applying the MC calculation to the estimation of pulse height spectrum by each natural radionuclides and considering the self-contamination of the detector, the pulse height spectrum only due to BG components was successfully reproduced.

Conclusion The study investigates the method for effective subtraction of background components due to terrestrial radionuclides for environmental radiation monitoring using a scintillation spectrometer. By de-convoluting the net pulse height spectrum, surface contamination densities on soil for ^{134}Cs and ^{137}Cs were determined to be 0.32 Bq cm^{-2} and 3.0 Bq cm^{-2}, respectively.

References

1) M Kowatari et al.: Development of a simultaneous evaluation method of radioactivity in soil and dose rate using $CeBr_3$ and SrI_2(Eu) scintillation detectors for environmental monitoring, Progress in Nuclear Science and Technology Volume 6 (2019) pp. 81-85.
2) H Hirayama et al.: Estimation of Radionuclide Concentration in Plume Using Pulse Height Distribution Measured by LaBr3 Scintillation Detector and Its Response to Radionuclides in Plume Calculated with egs5. Transactions of the Atomic Energy Society of Japan, 12(4), (2013) 304-310 (in Japanese).

The prospects of the evaluation of the high LET peaks of thermoluminescence glowcurves in the context of neutron dosimetry

Myriam Heiny[1]*, Frank Busch[2], Kevin Kröninger[1], Robert Theinert[1], Jörg Walbersloh[2]

[1]*Lehrstuhl für Experimentelle Physik 4, TU Dortmund University, Germany*
[2]*Materialprüfungsamt NRW, Germany*

Highlights We present a measurement and an evaluation of high LET thermoluminescence glowcurve peaks and their advantage regarding new prospect in neutron dosimetry.

Key words individual monitoring, thermoluminescence, high LET peaks, neutron dosimetry

Background and Objectives The individual monitoring service at the Materialprüfungsamt Nordrhein-Westfalen (Germany) and the Lehrstuhl für Experimentelle Physik 4 at the TU Dortmund University develop the compact dosemeter system TL-DOS based on thin-layer thermoluminescence detectors [1] as well as an associated glowcurve analysis tool [2]. The system is designed to process different dosemeter types for various measurands with the same readout device. This work focuses on the evaluation of the high LET peaks, and their use in the new developed TL-DOS neutron dosemeter.

Materials and Methods First, a design specification for the thermoluminescence detectors produced by the Materialprüfungsamt NRW based on ^{6,7}LiF:Ti,Mg is defined to meet the requirements of albedo neutron dosimetry. For the dosemeter badge an albedo cassette developed by the TU Dresden [3] is used. The TL-DOS reader, described in [1], is used for the measurement of the thermoluminescence glow curve. This combination takes advantage of a high temperature read out (T_{read} = 653 K). Hence, the deeper traps and the corresponding peaks, so called high LET peaks (see Fig.1), can be measured and evaluated with glowcurve deconvolution. Additionally to neutron induced glowcurves, alpha irradiations from a Am-241 source are used for the study of this high LET peaks.

Results and Discussion The TL-DOS albedo neutron dosemeter was irradiated in different photon and neutron fields, which were both neutron reference fields (PTB Germany) as well as workplace fields. A high sensitivity even at high energy neutron fields is demonstrated from the results. Additionally, some detectors are irradiated with mixed alpha and gamma fields. All measurements are evaluated including the high LET peaks which were considered

and analyzed seperately. The analysis provides additional information about the radiation field, for example the particle type, the composition of mixed fields and the irradiation energy. This information can be especially useful for neutron dosemeters due to their strong energy dependence and their use in mixed gamma-neutron fields [4].

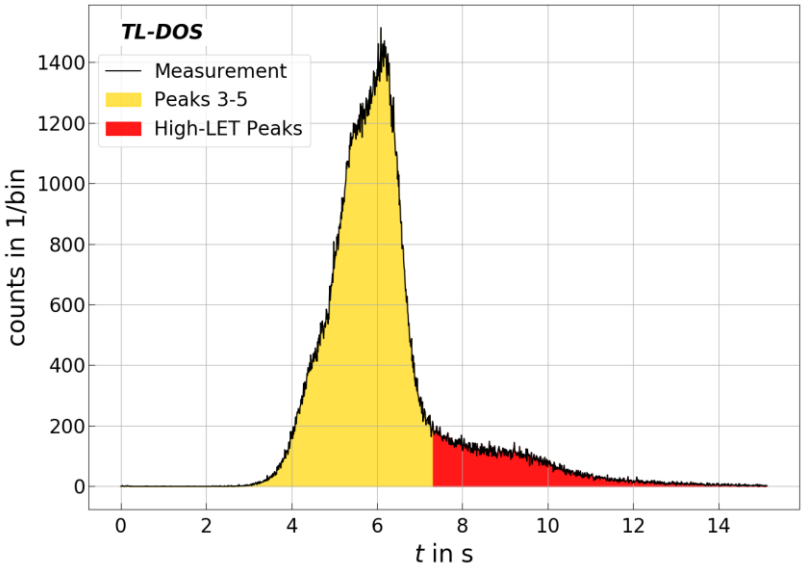

Figure 1. Measured glow curve including the high LET peaks after a neutron irradiation

Conclusion A neutron dosemeter based on the TL-DOS system was developed. The information obtained from the glow curve and the high LET peaks provides advantages and offers new possibilities. We present the current development status and test results as well as future prospects.

References

[1] J. Walbersloh, F. Busch, A thin-layer lif thermoluminescence dosemeter system with fast readout for the use in personal dosimetry services, Radiation Protection Dosimetry

[2] R. Theinert, et al., Computational analysis of thermoluminescence glow curves from thin layer dosemeters, Radiation Measurements

[3] T. Hanninger, J. Henniger, Dosimetric properties of the new TLD albedo neutron dosemeter AWST-TL-GD 04, Radiation Protection Dosimetry

[4] M. Hajek and R. Cruz Suárez, A solution for neutron personal dosimetry in the absence of workplace spectrometry, Radiation Protection Dosimetry

Development of a mechanical resistant fluorite-based pellet to be used in personal dosimetry

Nancy K. Umisedo[1]*, Emico Okuno[1], Francisco Cancio[1], Elisabeth M. Yoshimura[1] and Roseli Künzel[2]

[1]*Institute of Physics, University of São Paulo, São Paulo, SP, Brazil*

[2]*Department of Physics, Federal University of São Paulo, Diadema, SP, Brazil*

Highlights A new fluorite-based pellet has been produced with the objective of substituting the detector currently in use at the Laboratory of Dosimetry of the University of São Paulo.

Key words fluorite, thermoluminescence, dosimetry

Background and Objectives The Laboratory of Dosimetry of the University of São Paulo performs the external individual monitoring of workers exposed to X and gamma rays applying the technique of thermoluminescence (TL)[1)]. Two types of detectors are used in this service: TLD-100 (LiF:Mg,Ti) and pellets of CaF_2:NaCl made with natural green fluorite cold pressed with sodium chloride as agglutinant. Due to the mechanical fragility of these pellets, a new detector has been developed using a commercial adhesive as a binding agent instead of the sodium chloride.

Materials and Methods The fabrication process of the new pellets employs as the binding agent only the activator of a commercial adhesive resistant to high temperature. The proportion used in this project is 100:28 parts per weight of fluorite powder and the activator respectively. After well stirred the resulting creamy consistency mixture is cold pressed using a hydraulic press. The pellets obtained at this point are still fragile and the maximum resistance is reached submitting them to a curing temperature of 100 °C for 24 h. To obtain appropriate thickness (0.9 mm) and a smooth surface, the 5 mm disc shaped samples are rubbed using a sandpaper. Before each use they are thermal treated at 400 °C for 20 min, the same used for the CaF_2:NaCl pellets. Various tests required for a TL dosimeter were performed and some results are presented in this work.

Results and Discussion An important characteristic of the new pellet is the very good mechanical resistance obtained. Differently from the detector currently in use, it is impossible to break them manually. The sensitivity of the new samples is similar to presented by the

CaF_2:NaCl detectors as can be seen in figure 1. In (A) detectors were exposed to the same dose and the adhesive binding agent doesn't show any TL peak. The reproducibility (C.V. = 7%) of TL signal after 10 cycles (thermal treatment, irradiation and readout) is comparable to the value presented by the detectors currently in use.

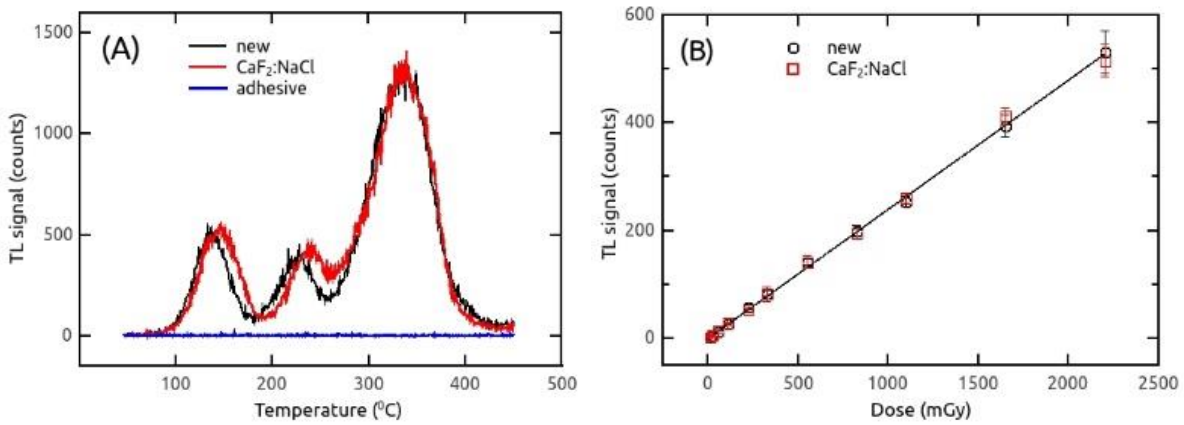

Figure 1. Glow curves (A) at heating rate of 10 °C/s and dose response curve (B) of the new and the CaF_2:NaCl detectors exposed to beta radiation.

Conclusion The mechanical resistance obtained by the use of commercial adhesive as the binding agent probably will extend the lifetime of the new detectors that might be reused many times without replacements of the batches. The similarities of glow curves and the sensitivity between the new and the CaF_2:NaCl pellets indicate advantages for the substitution of the detectors currently in use at the Laboratory of Dosimetry of the University of São Paulo.

References

1) E. Okuno, N.K. Umisedo, F. Cancio, M.A. Aldred and E.M. Yoshimura, Radiat. Prot. Dosim. v. 1-4, p. 1-4, 2017.

Development of omnidirectional Compton camera for visualizing low energy gamma rays from radiopharmaceuticals with high sensitivity

Naofumi Narita[1], Hideaki Katagiri[1], Ryoji Enomoto[2], Hiroshi Muraishi[3], Takara Watanabe[3,4,6], Mika Kagaya[5], Daisuke Kano[6]

[1]Ibaraki University, Ibaraki, Japan, [2]University of Tokyo, Tokyo, Japan

[3]Kitasato University, Tokyo, Japan, [4]Tokyo Metropolitan University, Tokyo, Japan

[5]National Institute of Technology, Sendai College, Miyagi, Japan

[6]National Cancer Center Hospital East, Chiba, Japan

Highlights We developed an omnidirectional scintillator-based Compton camera that visualizes low energy gamma rays radiated from radiopharmaceuticals with high sensitivity. We verified the performance of the detector by measuring the ^{99m}Tc and ^{111}In in a nuclear medicine facility.

Key words Compton camera, scintillator, high sensitivity, omnidirectional, ^{99m}Tc, ^{111}In

Background and Objectives Nuclear medicine imaging is a method of diagnosis that involves imaging the function of a living tissue by administering a radiopharmaceutical to the body, and it is widely applied clinically owing to the spread of single-photon emission computed tomography (SPECT) equipment. Healthcare workers are at risk of radiation exposure because of splashing or missing of radiopharmaceuticals. Thus, to reduce healthcare workers' exposure to radiopharmaceuticals, we aim to develop an environmental monitoring camera that can image low energy gamma rays from radiopharmaceuticals usually used in SPECT such as ^{99m}Tc and ^{111}In.

Materials and Methods We developed an omnidirectional Compton camera based on previous studies[1)2)]. Four scintillation counters are placed at the vertices of a tetrahedron to detect hits. Each scintillation counter comprises a 1-inch thick calcium fluoride scintillator and a photomultiplier tube. The calcium fluoride crystal is a high light-yield inorganic scintillator with relatively low atomic number, thus enabling imaging capability for gamma rays at the energies down to about 100 keV when used in a Compton camera. We performed imaging tests using ^{99m}Tc and ^{111}In in a hospital setting. We also applied a technique that involved rotating the detector to reduce the ghost image of the Compton camera[3)].

Results and Discussion Figure 1-(a) and Figure 2 show the imaging results for 141 keV gamma rays. We successfully imaged ^{99m}Tc (141 keV) placed at the 0° with respect to the horizontal and vertical directions. Figure 1-(b) shows the imaging results when data are collected while the Compton camera is rotated in the horizontal plane, i.e., around the vertical axis. We verified that the ghost image is reduced by rotating the detector. The detection

efficiency was 42 counts per second for 1 μSv/hour dose rate. Our detector identified the direction of the ^{99m}Tc radiation source within approximately 20 seconds for the dose rate of 0.1 μSv/hour. In addition, our detector also succeeded in imaging ^{111}In (171 keV, 245 keV).

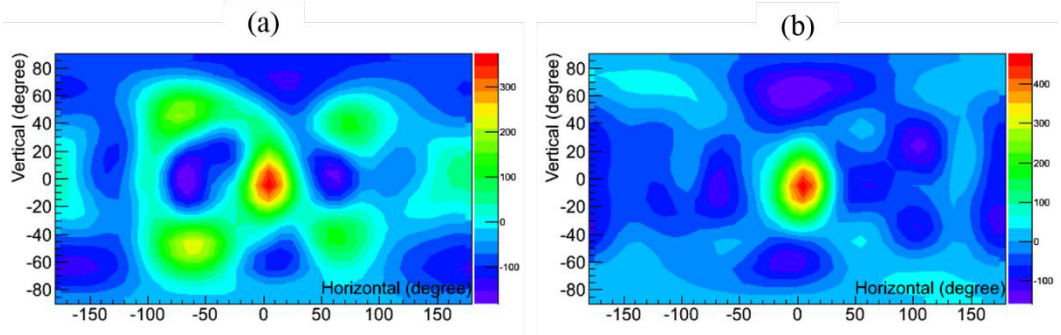

Figure 1. (a) Image of 141 keV gamma rays from ^{99m}Tc. ^{99m}Tc (10.95 MBq) was placed at a distance of 150 cm from the detector, and the radiation was imaged for 370 seconds. (b) Image of 141keV gamma rays when the detector is rotated. The detector was rotated at intervals of 60° from 0° to 180° around the vertical axis. Measurement (imaging) time was 540 seconds.

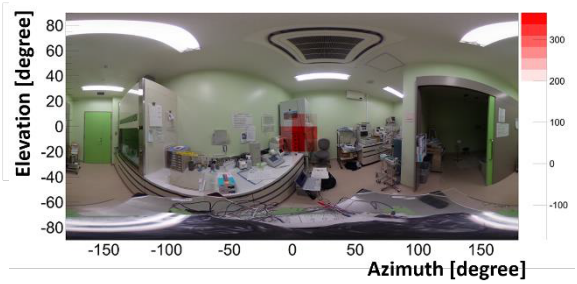

Figure 2. Composition of 141 keV gamma ray image and whole sky photo.

Conclusion We have developed an omnidirectional scintillator-based Compton camera that can visualize ^{99m}Tc (141 keV) with high sensitivity of 42 cps/(μSv/hour). And we have demonstrated that the detector has also acceptance for ^{111}In (171 keV, 245 keV).

References

1) Katagiri H, et al (2018) "Development of an all-sky gamma-ray Compton camera based on scintillators for high-dose environments," J Nucl Sci Technol, 55, 1172-1179.
2) Watanabe T, et al (2017) "Development of an omnidirectional gamma-ray imaging Compton camera for low-radiation-level environmental monitoring," Jpn J Appl Phys, 57, 026401.
3) Muraishi H, Patent application: Radiation detection device, Radiation detection method and program, Patent application2018-177648, 21 September 2018.

Examination of angular dependence of DoseAce with New Holder

Naoki Takashima[1]*, Michiko Ube[1], Satoshi Ueno[1], Edilaine H. Silva[2]
[1]*Chiyoda Technol Corporation, Ibaraki, Japan*
[2]*Belgian Nuclear Research Centre (SCK・CEN), Mol, Belgium*

Highlights In order to improve angular dependence of small a radiophotoluminescence (RPL) glass dosemeter, DoseAce, the holder and filter were reviewed. It was confirmed by irradiation examination that the angular dependence of DoseAce with the new holder was improved.

Key words RPL glass, angular dependence, DoseAce

Background and Objectives DoseAce is a small dosemeter of RPL glass (Figure 1). It is used in medical dose measurement. Since DoseAce has cylindrical shape, angular dependence in vertical direction (rotation around the axis of the cylinder) is small. However, there is large angular dependence in horizontal direction[1)]. It was a problem when it was used in fields where scattered photons are major contributor to dose such as interventional radiology and cardiology. In order to improve the angular dependence, the new holder was designed[2)]. In this study, the evaluation of horizontal angular dependence of DoceAce with the new holder was carried out by irradiation examination.

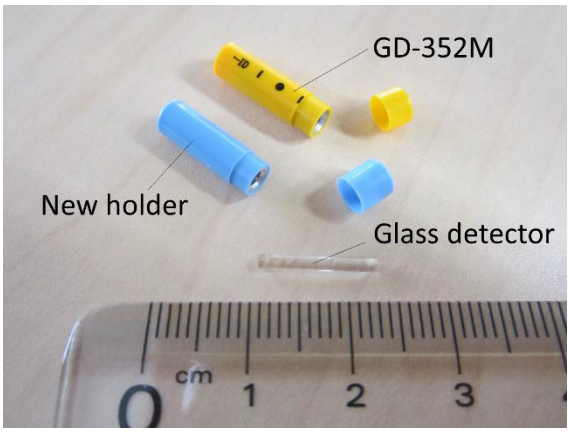

Figure 1.
Holder and detector of DoseAce

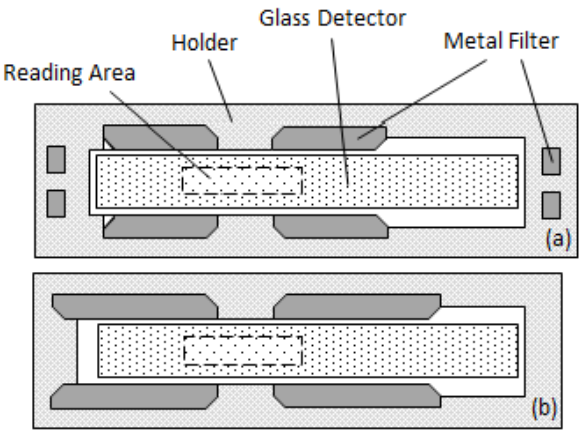

Figure 2. Illustrations of new holder(a) and GD-352M(b)

Materials and Methods Figure 2 shows the illustrations of the new holder and previous one (GD-352M) (AGC Techno Glass, Japan). GD-352M is one of the DoseAce models, and its holder is composed of metal (tin and lead) filters. On the other hand, the new holder changed shape of metal filters. The metal filters on side of the detector were shorten of about 30 %. The additional metal filters which have ring shape were inserted on the top and bottom of the new holder.

The irradiation examination was performed with X-ray narrow spectrum series (N-30, N-40, N-60, N-80, and N-100). The Dose Ace with new holder was irradiated free in air and on the cylindrical phantom (Φ = 20cm × 20cm). GD-352M was irradiated free in air only. Irradiation angles were 0, ±30, ±45, ±60, ±75, and ±90 degrees in horizontal direction of DoseAce.

Results and Discussion

Figure 3 shows the angular dependence for N-60 (E_{eff} = 47 keV) free in air normalized to 0 degrees of Cs-137. The responses of GD-352M for ±90 degrees are high because of no filter on their directions. The response of the new holder is flatter than that of GD-352M. The responses from 60 to 75 degrees increased due to shorten filters, and that from ±90 degrees decreased due to the additional filters.

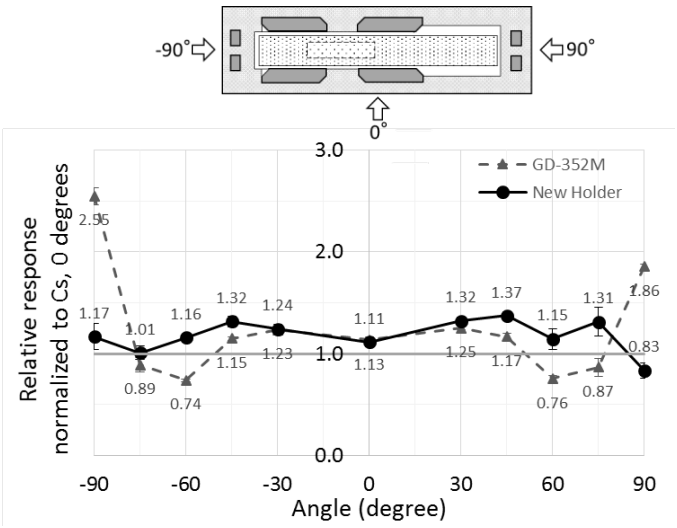

Figure 3. Angular dependence for N-60

Conclusion In this study, the irradiation examination was carried out for DoseAce with new holder in order to improve angular dependence. The result showed that angular dependence for the new holder was flat compared with that of GD-352M. DoseAce with the new holder is expected to apply to scattered photons fields.

References

1) E. H. Silva, et al, Energy and Angular Dependence of Radiophotoluminescent Glass Dosemeters for Eye Lens Dosimetry. Radiation Protection Dosimetry, 1-5 (2016)
2) E. H. Silva, et al, Optimization of a Radiophotoluminescent Glass Dosemater for Occupational Radiology/Cardiology. Radiation Protection Dosimetry, 1-7 (2018).

Gamma dose rate effects in luminescence signals of various dosimetric phosphors

Niyazi Meriç*, Miray Başdoğan#, Gaye Çakal, Engin Aşlar, Eren Şahiner, George S. Polymeris

Institute of Nuclear Sciences, Ankara University, 06100-Beşevler, Ankara, Turkey

Highlights The presence of gamma dose rate effects was investigated on the TL signal of 6 different dosimetric phosphors as well as the OSL signal of 3 of them.

Key words LiB_4O_7:Cu,In, MgB_4O_7:Dy,Na, TLD100 (LiF:Mg,Ti), (CaF_2:N), BeO, quartz, OSL, TL, deconvolution, dose rate, dose response.

Background and Objectives In various dosimetric applications, including age assessment, a dose response curve is constructed, which is used as reference for calculating an unknown accumulated dose. In many cases, the dose rate used for the construction of a dose response curve is quite different than the dose rate of the dose to be measured. Dating stands as an indicative example where the equivalent dose (ED) is accrued quite slowly, over hundreds or even thousands years; nevertheless, for the construction of the dose response curve, the dose rate applied is quite faster. The objective of this paper includes studying the possible effects of the different dose rates in both dose response features as well as signal deconvolution parameters.

Materials and Methods Batches of different, well established, artificial luminescence materials including LiB_4O_7:Cu,In, MgB_4O_7:Dy,Na, TLD100 (LiF:Mg,Ti), (CaF_2:N) and BeO dosimeters were used as luminescence materials in this study. Batch reproducibility was tested using a 0.5 Gy gamma irradiation, assessing all materials' calibration factors. All artificial materials were irradiated using a 130 TeraBq Co-60 gamma ray source, using various dose rates ranging between 0.2 Gy/h and 40 Gy/h, namely covering two orders of magnitude. For all artificial phosphors, dose response curves were constructed using these aforementioned gamma dose rates. For each material, 12 different dose steps were used, ranging between 25mGy and 3.5 Gy. Moreover, a naturally occurring quartz sample of geological origin, which was collected from Nigeria, was also studied, without any previous heating or predose. Quartz was irradiated using a 400 TeraBq Co-60 gamma ray source, using three dose rates, namely 28 Gy/h, 325 Gy/h and 1325 Gy/h. For the quartz sample, dose response curves were

constructed up to 500 Gy; mass reproducibility was within 5%. For all materials, TL was measured, while for the CaF_2:N, BeO and quartz, optically stimulated luminescence (OSL) was also measured, following the appropriate pre-heating. For each material, dose rate, dose and luminescence signal, two independent measurements were performed. All luminescence measurements were carried out using either a Harshaw 3500 TLD reader or a Risø TL/OSL reader (model TL/OSL-DA-20).

Results and Discussion All luminescence signals were deconvolved using the appropriate models. Only the behavior of stable, dosimetric signals was studied. For the possible gamma dose rate effects, the following probes were used:

- The dependence of the results of the deconvolution analysis, such as activation energies of various TL peaks and photo-ionization cross sections of various OSL components, on the gamma dose rate.
- The dependence of the component resolved dose response properties, such as linearity features and lowest detectable dose limit on the dose rate.

Conclusion The TL dose response features of the most artificial luminescence dosimeters do not yield significant dependence on the gamma dose rate. However, slight dependence of the kinetic parameters of specific TL peaks is monitored. The OSL measurements and analysis (as well as the TL in quartz) are currently ongoing.

[#] The present work is based on the master thesis of Miray Başdoğan.

Eye Lens Dosimetry for Workers at Fukushima Daiichi Nuclear Power Station: (2) Field Study using Humanoid Phantom

N. Tsujimura[1]*, K. Hoshi[1], K. Aoki[1], H. Yoshitomi[1], Y. Tanimura[1], and S. Yokoyama[2]
[1]*Japan Atomic Energy Agency, Ibaraki, Japan*
[2]*Fujita Health University, Aichi, Japan*

Highlights To evaluate the relationship between the whole-body and eye lens dosimeters a field study using humanoid phantoms with different dosemeters attached were made at selected locations at the Fukushima Daiichi Nuclear Power Station.

Key words lens of the eye, dosimetry, phantom, Fukushima daiichi nuclear power station

Introduction As part of the research project entitled "Study on standard eye lens monitoring, suitable dose management and radiation protection for nuclear and medical workers" sponsored by the Japanese Nuclear Regulatory Agency, we conducted the eye lens dosimetry study for workers engaged in the decommissioning operation at the Fukushima Daiichi Nuclear Power Station. The study consists of two parts: a laboratory study on the eye lens dosimeter's characteristics to photons and a field study conducted at actual workplaces to evaluate the relationship between the whole-body and eye lens dosimeters. This paper summarizes the results of the second-part study, in which humanoid phantoms with different dosemeters attached were placed at selected locations at the Fukushima Daiichi Nuclear Power Station.

Materials and Methods The field study using two humanoid phantoms took place at an open field between the Unit 2 and 3 reactor buildings. Each phantom consists of a head section (a 20-cm diameter × 20-cm polyethylene cylinder), a neck section (a 12-cm diameter × 8-cm polyethylene cylinder), and a trunk section (a 30-cm × 30-cm × 15-cm PMMA slab). One phantom was affixed on a stepladder and placed stationary; the other phantom was placed on a horizontally-rotating table driven at 1.25 rpm by a motor. The centers of the head and trunk sections were 153 cm and 120 cm above the ground. Dosemeters used were two kinds of eye lens dosemeters, namely Dosiris (Chiyoda Technol) and Vision (Nagase Landauer), a RPL glass dosemeter (Chiyoda Technol), and an electronic dosemeter (Panasonic). The Dosiris, Vision, and glass dosemeters were on the head section; glass and electronic dosemeters were on the trunk section. They were placed both on the front and rear of the sections for surveying the directionality of the photon field. Moreover, during the measurement campaign, the authors (NT, KH, KA, HY, and YT) carried four Vision dosemeters worn: two near the eye (attached to

the temples of their own prescription glasses) and two on the front and back torso, in addition to their dose-of-record passive dosemeters (TLD and OSLD) at the chest. The first and second measurement campaigns were performed on March 8–9, 2018 and December 19–20, 2018, respectively.

Results and Conclusion The readings of the phantom-mounted dosemeters up to ~1.5 mSv were obtained for several hours of irradiation at the location with the highest dose rate. There were no significant differences between $H_p(10)$, $H_p(3)$ and $H_p(0.07)$ values obtained from the dosemeters attached at the same sections. The $H_p(3)$ at the head section was ~20% higher than $H_p(10)$ at the trunk section.

The Vision dosemeters carried by the authors indicated almost same readings both on the front and back torso, demonstrating that the rotational geometry exposure was most likely for workers. Also indicated was that the $H_p(3)$ measured near the eye was slightly higher than that measured at the torso. This occurred probably due to two reasons: first, there were a slight height dependence in the observed ambient dose rate, and second, in rotational exposure geometry the head-mounted dosemeters had a smaller angular response than the trunk-mounted dosemeters. These results will aid in understanding the responses of personal dosemeters of the workers engaged in the decommissioning operations.

Uncertainty of track-etch detectors used in radon surveys

P. Bossew[1], M. Janik[2]
[1]*German Federal Office for Radiation Protection, Berlin*
[2]*QST/NIRS, Chiba, Japan*

Highlights A tentative uncertainty budget of track-etch detectors used in radon in thoron survey is presented. The consequences of uncertainty for decision making related to radon regulation are discussed.

Key words radon, track-etch detector, survey

Background and Objectives Indoor radon is considered a serious hazard to human health, being the second cause of lung cancer after smoking [1]. Therefore, it is increasingly subjected to regulation in various countries. Verifying compliance with regulation requires estimating indoor radon concentration, in the first place by measurement. For large radon surveys involving thousands of measurements, mostly track-etch solid state detectors are used, which are robust, cheap and easy to evaluate. Quality assurance relies on calibration and intercomparison under defined conditions. As possibly implying legal consequences, quality assurance and control of radon measurement is of high importance. This includes understanding data uncertainty.

Materials and Methods The measurement principle of radon measurement by track-etch technique is based on counting alpha tracks in plastic material, which are caused by decay of radon and its progenies in the atmosphere, to which the detector is exposed. Track density is proportional to exposure. Top-down assessment of track-etch data uncertainty pertains to statistical evaluation of detector populations under known equal exposure conditions. To this end, data from exposure experiments and intercomparison exercises are used. Bottom-up approaches intend to establish an uncertainty budget considering its individual components. It is based on knowledge of detector physics and processing routines. For discussion of possible consequences of radon data uncertainty, we refer to European regulation as laid down in the European Basic Safety Standards Directive [2].

Results and Discussion Results of top-down and bottom-up approaches are compared and discrepancies discussed. We then address the consequences of the inevitable presence of uncertainty in practical use. These are relevant (a) in decisions about compliance with radon regulation, for example, whether the long-term radon concentration in a building exceeds a reference level; (b) radon data are used to estimate so-called radon priority areas in

compliance with European radon regulation. We discuss the role of uncertainty of radon data, which may propagate into aggregated quantities, such as regional probability to exceed a reference level or extension of radon priority areas whose definition is based on aggregated radon data. A particular topic is thoron; although not covered by regulation so far, its measurement by track-etch technique involves specific pitfalls. We also address results of the current European project “Metro Radon” [3] which relate to the matter of radon data uncertainty.

Conclusion Although measuring long-term radon concentrations with track-etch detectors is technically simple and cheap and therefore popular, establishing uncertainty budgets is less easy. Uncertainty of radon data may propagate into aggregated quantities on which decisions rely, which may have far-reaching economical consequences.

References

1) Zeeb, H., Shannoun, F. & World Health Organization. (2009). WHO handbook on indoor radon: a public health perspective. World Health Organization. http://www.who.int/iris/handle/10665/44149 (accessed 27 Feb 2019)
2) Council Directive 2013/59/Euratom of 5 December 2013 laying down basic safety standards for protection against the dangers arising from exposure to ionising radiation etc., https://eur-lex.europa.eu/legal-content/EN/TXT/?uri=CELEX%3A32013L0059 (accessed 27 Feb 2019)
3) metroRADON - Metrology for radon monitoring. http://metroradon.eu/ (accessed 27 Feb 2019)

Measurements of Eye Lens Doses for Workers at Fukushima Daiichi Nuclear Power Station

S. Yokoyama*[1], I. Ezaki[2], H. Tatsuzaki[3], S. Tachiki[1], S. Hirao[4], K. Aoki[5], Y. Tanimura[5], K. Hoshi[5], H. Yoshitomi[5], and N. Tsujimura[5]

[1]*Fujita Health University, Aichi, Japan*

[2]*Chiyoda Technol Corporation, Tokyo, Japan*

[3]*National Institutes for Quantum and Radiological Science and Technology. Chiba Japan*

[4]*Fukushima University, Fukushima, Japan*

[5]*Japan Atomic Energy Agency, Ibaraki, Japan*

Highlights To discuss how to monitor and manage the equivalent dose for the lens of the eye of radiation workers at nuclear facilities, the dose was measured at the head and the chest of the radiation workers around water storage tank areas (^{90}Sr/^{90}Y dominant area) and the nuclear reactor buildings (high dose gamma areas) of the Fukushima Daiichi Nuclear Power Station. The relationship between $H_p(10)$ and $H_p(3)$ for the workers in these areas and the doses measured at the head wearing a full-face mask and the chest were clarified.

Key words equivalent dose for the lens of the eye, monitoring, radiation workers, Fukushima daiichi nuclear power station (1F-NPS)

Introduction In March 2018, the content of discussions in the subcommittee on radiation protection of the lens of the eye, the Radiation Council, Japan was summarized and requested all relevant government and agencies to take appropriate actions[1)]. The report indicated that the dose limit to the lens of the eye is appropriate to revise as shown in the following; 20 mSv/year, averaged over defined periods of 5 years, with no single year exceeding 50 mSv. In addition, the report showed that workers exposed to high radiation dose were decommissioning workers at the Fukushima Daiichi Nuclear Power Station (1F-NPS) and medical staff.

In FY 2017(1st, April to 31st March), there were 267 workers with 20 to 50 mSv/year and 48 workers with 50 to 100 mSv/year (The total was about 14,000 workers.) at the 1F-NPS [2)]. In particular, the equivalent dose of the lens seems to be high around disassembly areas of tanks in which ^{90}Sr/^{90}Y contaminated water was stored (beta dominant areas) [3)] and nuclear reactor buildings (gamma dominant areas). From FY 2018, Tokyo Electric Power Company Holdings Incorporated (TEPCO) started voluntarily managing the lens dose for the 1F-NPS workers, with a goal of < 50 mSv/year. To discuss how to manage the dose to the lens for nuclear workers appropriately, we measured the dose on the head and the chest of the workers who are likely to

be exposed to high dose of beta (^{90}Sr/^{90}Y) or gamma rays (^{137}Cs, ^{134}Cs and scattered radiations) at the 1F-NPS.

Materials and Methods The individual dose monitoring for workers at the 1F-NPS was conducted in November and December, 2017 and December, 2018. The subjects were 10 persons working in the disassembly areas of the water storage tanks and 21 persons working around Units 1, 2, 3 and 4 buildings. The doses, $H_p(10)$, $H_p(0.07)$ and/or $H_p(3)$ were measured using passive dosimeters (TLDs, RPLGDs and/or OSLs) wearing on the head inside a full-face mask and the chest inside a protector, when wearing them. Three TLDs were worn at the outside of the left and right eyes, and the center of the forehead in 2017. The dosimeters (RPLGDs or OSLs) were worn at the center of the forehead inside the full-face mask, the neck, the upper arm outside the protector and the chest inside the protector in 2018. In addition, the dose was measured using an electronic dosimeter worn on the upper arm outside the protector. These doses were measured under routine dose monitoring.

Results and Conclusion In the beta dominant areas, the $H_p(3)$ on the head was ~20% of $H_p(0.07)$ at the chest position. The shielding factor released by TEPCO is 70~90%[3]. Although the mask is used to protect internal exposure, it could effectively shield beta rays of ^{90}Sr /^{90}Y. Thus, the dose measured inside the mask should be used for management of the lens dose in the beta dominant areas. In the gamma dominant areas, there were no significant differences between $H_p(10)$, $H_p(3)$ and $H_p(0.07)$ values obtained from the dosemeters at the same sections. The $H_p(3)$ on the head was ~20% higher than $H_p(3)$ measured on the upper arm outside the protector. Using a dose level for a direct measurement (15mSv/year) which is a part of the voluntarily managing by TEPCO, it will be possible to comply the regulations related to the exposure of the lens in the future.

References

1) NRA, On a modality of the radiation protection for the lens of the eye. (in Japanese), http://www.nsr.go.jp/data/000238374.pdf. (accessed on 24 February 2019)
2) TEPCO, Table 16. Cumulative Data of Equivalent Dose to the Lens of the Eye by Fisical Year, https://www7.tepco.co.jp/wp-content/uploads/180427e0109.pdf (accessed on 24 February 2019)
3) FEPC, https://www.mhlw.go.jp/content/11201000/000477103.pdf (in Japanese) (accessed on 24 February 2019)

Acknowledgment

This work was supported by the Radiation Safety Research Promotion Fund.

Redistribution of radioactive cesium in the sloped catchment, 7 years after the nuclear accident: case of Ogi Dam area, Fukushima

Triyono Basuki[1,2], Wiseman Bekelesi[1,2], Masaya Tsujimoto[1,2] , Satoru Nakashima[1,2,3]

[1] *Radioactivity Environmental Protection Course, Phoenix Leader Education Program, Hiroshima University, 1-1-1 Kagamiyama, Higashi-Hiroshima 739-8524, Japan*

[2] *Department of Chemistry, Graduate School of Science, Hiroshima University, 1-3-1 Kagamiyama, Higashi-Hiroshima 739-8526, Japan*

[3] *Natural Science Center for Basic Research and Development, Hiroshima University, 1-4-2 Kagamiyama, Higashi-Hiroshima 739-8526, Japan*

Highlights Radioactive cesium inventory and air dose rate were measured in very sloped catchment. The radioactive cesium was distributed along the gradient elevation, however forest zone still maintained higher radioactive contamination.

Key words radioactive cesium, air dose, redistribution, gradient elevation, land use type

Background and Objectives Radioactive cesium migration in un-disturbed different land-use, especially forest area that remained highly contaminated, attracted more interest as this area can be source of particulate radioactive cesium that migrated to downstream area (Koarahashi et. al., 2012; Laceby et.al., 2016). This work examined the redistribution of radioactive cesium in micro scale sloped catchment after the nuclear accident.

Materials and Methods The study area is in Ogi Dam catchment, Kawauchi village, Fukushima, that is located about 18 km south eastern of Fukushima Daichi Nuclear Power Plant. Air dose measurement by NaI survey meter and soil and sediment core sampling were conducted on March 15~16, 2018 (Fig 1). ^{137}Cs in soil core samples was measured by HP Ge detector.

Results and Discussion The air dose rate and ^{137}Cs inventory were distributed along the gradient elevation which shows higher activity and air dose rate in the middle of slope (Fig 2-1). It probably indicated the occurrence of radioactive cesium movement inside the forest zone. It was confirmed by the air dose rate and ^{137}Cs inventory data classified based on land use type that shows the forest zone has higher radioactive contamination than lower zone (Fig 2-2). Beside the soil, vegetation in forest zone still works as a radionuclide storage. Considering the indication of accumulation of ^{137}Cs in Dam sediment, the radioactive cesium that redistributed to the dam was probably mainly contributed by area other than forest catchment, such as transition zone which is more open and more active zone.

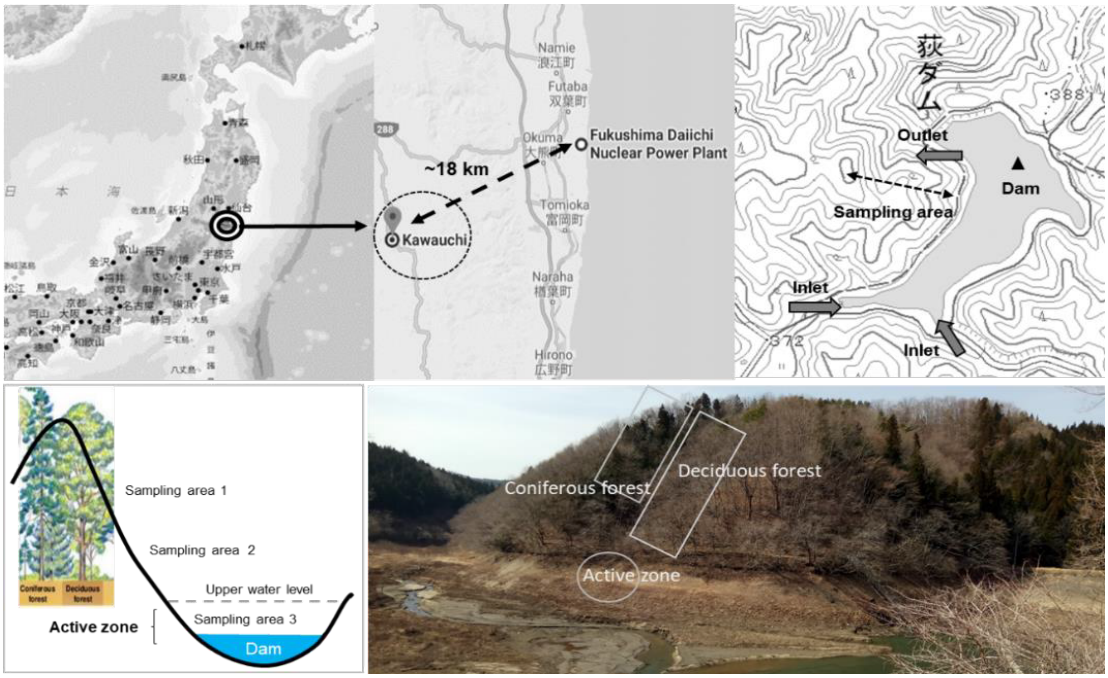

Fig 1. Sampling site, Ogi dam area, Kawauchi Village, Fukushima

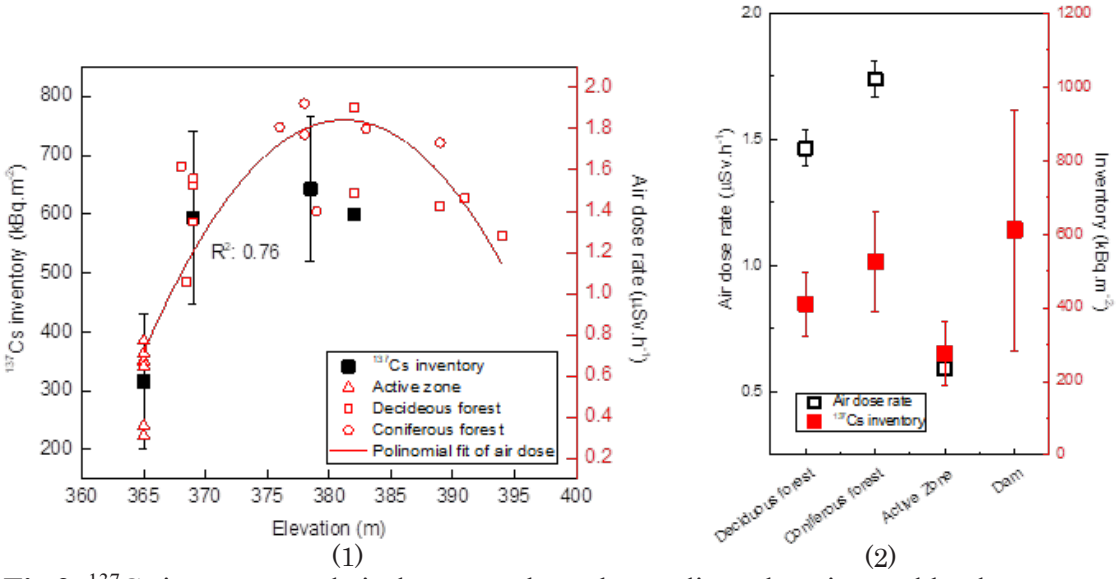

(1) (2)

Fig 2. ^{137}Cs inventory and air dose rate along the gradient elevation and land use type.

Conclusion There was an indication of radioactive cesium migration along the gradient elevation of sloped catchment area. However, forest area of the sloped catchment still retained a higher radioactive contamination. Therefore, the main source of mobile particulate radioactive cesium in sediment was most probably from the active zone of the catchment.

References

1) Jun Koarashi et. al., Science total environment 431 (2012) 392-401
2) Laceby J.P., et. al., Journal of environmental radioactivity 183 (2016) 742-753

Performance of the BeOSL eye lens dosimeter with radiation protection glasses

V. Bandalo[1]*, M. Figel[1], M. Greiter[1] , J. Brönner[1], P. Kleinau[1], T. Haninger[1], E. Mende[1], P. Scheubert[2], R. Eßer[2], M. Furlan[3], M. Schmid[4], H. Hoedlmoser[1]

[1]Helmholtz Zentrum München, Individual Monitoring Service, Munich, Germany

[2]Dosimetrics GmbH, Munich, Germany,

[3]Dosilab AG, Köniz, Switzerland, [4]MAVIG GmbH, Munich, Germany

Highlights A new BeOSL eye lens dosimeter (ELD) for integration in radiation protection (RP) glasses has been investigated in laboratory tests with an Alderson head phantom. The results show both the measurement capabilities of the dosemeters and the protective effect of the glasses. Results are supplemented by data from Monte Carlo Simulations and first clinical applications in radiology.

Key words extremity dosimetry, eye lens, OSL, BeO, radiation protection glasses

Background and Objectives The Individual Monitoring Service (IMS) at the Helmholtz Zentrum München has introduced[1)] a new BeOSL ELD for use with a new mechanical interface for the integration in RP glasses developed in a collaboration with MAVIG GmbH and Dosilab AG. The ELD uses the new BeOSL detector element for extremity dosimetry[2)]. The dosemeters were tested with the MAVIG BR330 RP glasses on an Alderson head phantom. Measurements with and without RP glasses were compared to simplified Monte Carlo Models showing excellent agreement and will be compared to the results of ongoing tests in clinical applications in radiology.

Materials and Methods ELDs were irradiated on the Alderson phantom with and without the RP glasses at the secondary standard calibration facilities of the IMS in Munich[3)]. MCNP6 Monte Carlo Models, which had already been implemented in the development of the dosemeters[4)], were used to simulate energy response with and without the equivalent shielding provided by the RP glasses. In clinical tests, dosemeters have been used with headband adapters and inside the RP glasses. Analysis of the ELD signals was carried out by means of standard BeOSL readers of the IMS[5)].

Results and Discussion Figure 1 shows RP glasses on the Alderson phantom in the laboratory irradiation situation and details of the Dosemeter. Figure 2 shows the measured and simulated response of the dosemeter inside and outside the RP glasses on a phantom. Similar results are expected from the ongoing clinical tests.

Figure 1. Alderson phantom and (a) RP glasses BR330, (b) ELD with BeOSL detector (c).

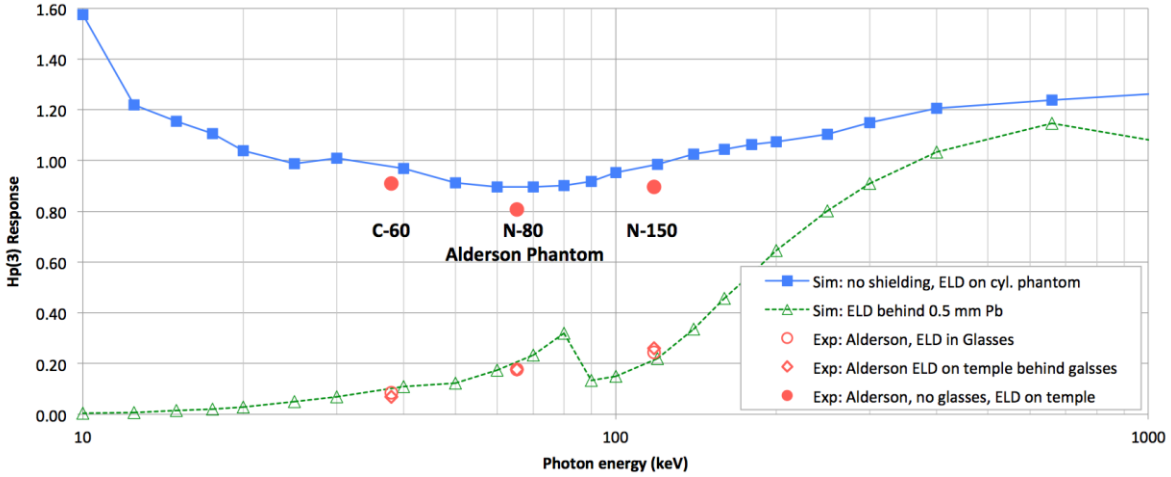

Figure 2 Comparison of ELD response as measured on Alderson phantom and as simulated.

Conclusion The new dosimetry system for eye lens dose consisting of a BeOSL dosemeter integrated into the BR330 RP glasses can measure doses down to 50(?) uSv while the RP glasses efficiently remove between 90 % and 60 % of the eye lens dose in energy ranges as used in interventional radiology.

References

1) H. Hoedlmoser et al, New eye lens dosemeters for integration in radiation protection glasses, submitted to Rad. Meas. for publication (1/2019)
2) P. Scheubert et al, this conference.
3) V. Bandalo, et al, A Fully Automated Secondary Standard X-Ray Calibration Facility for Personal Dosemeters, Rad. Prot. Dosimetry, doi:10.1093/rpd/ncy187 (2018).
4) H. Hoedlmoser et al, Rad. Prot. Dos. doi:10.1093/rpd/ncy299 (2018).
5) T. Haninger et al, Radiat Prot Dosimetry doi:10.1093/rpd/ncv425

Development of a realistic 3D printed Eye Lens Dosimeter using CAD integrated with Monte Carlo Simulation

V.S.M. Barros[1], M. F. dos Santos[1], V. Cassola[1], R. Kramer[1], J.V. Costa[1], M. E. A. Andrade[2], V.K. Asfora[1], H.J. Khoury[1]

[1]*Departamento de Energia Nuclear; Universidade Federal de Pernambuco; Recife, Brazil*

[2]*Faculdade Integrada do Recife FACIPE, Recife, Brazil*

Highlights To propose a new methodology for prototyping and benchmarking based on the Dose Equivalent to the sensitive part of the eye lens; demonstrate the integration of CAD Software and Monte Carlo Simulation in Geant4 with mesh modeling simulation and 3d printing; demonstrate the use of strengths and drawbacks of 3D printing on the fast prototyping of new dosimeters.

Key words Eye lens radiation dosimetry, 3d printing, Monte Carlo

Background and Objectives Revision of the threshold dose for cataract formation and consequently the adoption of a lower the annual dose limit has led to new eye lens dosimeters adapted from extremity dosimeters or developed and characterized. Also, in order to overcome limitations of the ICRU sphere, a new quantity - the *personal absorbed dose to the lens of the eye* - is proposed as a favored approach which simplify the system of radiation monitoring and dose assessment. Concomitantly, fabrication methods such as additive manufacturing (3D printing) has been introduced with a key aspect when applied to radiotherapy and dosimetry of near tissue equivalence of the printing material. It is also important to note that a real eye lens or an anthropomorphic model of an eye lens have an intrinsic angular and energy dependency associated. Therefore, the purpose of this work is to propose a high throughput methodology to design, simulate, print with 3D printing technology an eye lens dosimeter with superior energy and angle dependence in terms of the absorbed dose to the posterior subcapsular cataract-sensitive area of the lens.

Materials and Methods In this work the reference model from which the dosimeter model is based was taken from Behrens et al. [1]. The dosimeter was modelled in SolidWorks (Dassault Systemes) placing a dosimeter crystal (LiF) model at a defined distance from the surface. In the reference model, this distance varies between 3.34 mm at the axis (y=0) and 2.7 mm in the direction of the equators (y= ±4.6 mm). Three dosimeter models with varying depth positions were exported as mesh files and an import function in the Geant4 Monte Carlo simulation code was written to convert the mesh to triangular or quadrangular Geant4

Tessellated solid (no voxelization of the model geometries prior to simulation). The absorbed doses per incident fluence to three dosimeter models were simulated for an anterior–posterior and Lateral (AP and LAT) direction for 41 monoenergetic photon energies between 5 keV and 10 MeV. By comparison of energy and angle dependence with the reference eye model, the detector geometry which presented the best match was printed using stereolitography, which offered the necessary resolution. Printed dosimeters were then irradiated in metrological standard ISO-Narrow series field qualities (ISO 17025:2005) with two LiF:Mg,Ti thermoluminescent dosimeter chips as the sensitive elements.

Results and Discussion Results for the comparison of the monoenergetic energy dependence between the reference eye model [1] and the dosimeter model is shown in Figure 1 for the best matching geometry. An overresponse is observed up to 1.5 MeV at maximum of around +15% due to the choice of LiF as the detector element in the dosimeter model.

(a)

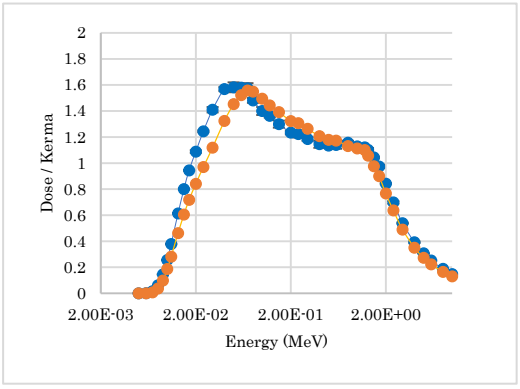

(b)

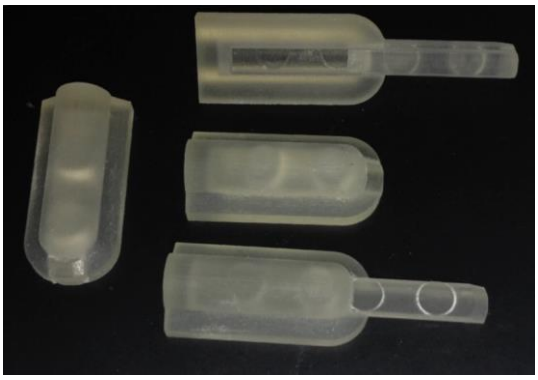

Figure 1. (a) Energy dependence comparison of the reference Monte Carlo model (red) and the dosimeter model B (d=3.0mm) (blue). (b) Printed model using stereolitography.

Conclusion A method for modeling-simulating-prototyping new radiation dosimeters was demonstrated which has throughput of a few days was developed. An eye lens dosimeter with an energy and angular dependence that matches more closely the sensitive are of the lens was developed. These should show a better response to new quantities currently being proposed by ICRU. The analysis of the energy response of detectors modelled with crystals positioned at different depths made possible to determine a sensitivity component for expanded uncertainty evaluation with possible applications to manufacturing maximum tolerances.

References

1) R Behrens, G Dietze,M Zankl. Dose conversion coefficients for electron exposure of the human eye lens. Phys. Med. Biol. 54 (2009) 4069–4087.

Improvement of energy and angular dependence of RPL glass ring dosemeter for photon radiation

Wakako Shinozaki[1*], Michiko Ube[1], Naoki Takashima[1], Miki Hirata[1], Yasuhiro Koguchi[1]
[1]*Chiyoda Technol Corporation, Ibaraki, Japan*

Highlights The response of RPL (Radiophotoluminescence) glass ring dosemeter was improved by optimizing the dosemeter filter based on the Monte Carlo simulation. It was confirmed by irradiation experiments that the dosemeter fulfills the energy and angular criteria of IEC 62387:2012 standard[1)] in the energy range from 24 keV to 1,250 keV.

Key words ring dosemeter, RPL glass, energy dependence, IEC 62387:2012 standard

Background and Objectives The RPL glass ring dosemeter (GR) is one of the dosemeters used in the extremity dose control in Japan. RPL glass has some suitable features for dose measurement such as repeatable readout, uniformity and stability of the sensitivity and very small fading. But RPL glass has strong energy dependence for photon radiations because of the higher effective atomic number than the tissue material. One or more filters are usually used together to make the energy dependence flat.

The conventional GR for photon was consist of one RPL glass element and one tin filter which has a small open square hole on it. Due to this filter, the energy dependence of the GR was improved in the energy range of 30 keV to 200 keV at 0 degrees incident. But for lower energy, around 80 keV and angular incident, the GR still showed insufficient responses and did not meet the criteria of the IEC 62387:2012 standard for passive dosemeter. In this study, the filter constitution of GR was optimized to improve the responses of energy and angular incidences for photons using Monte Carlo simulation and the performance was examined by irradiation tests according to the IEC 62387 standard.

Materials and Methods The PHITS code[2)] was used for the simulation. As the first step, to improve the response to photons from the side (70 to 110 degrees incident), the second tin filter was located on the back of the RPL glass to shield incident photon from greater than 90 degrees. The responses of GR with the second filter were calculated for the incidences from 70, 80, 90, 100 and 110 degrees for the energy of 48 keV at which the response became the highest. In the second step, the responses at 0 and 60 degrees incident were calculated with changing the thickness and the size of square hole of the first tin filter on the front of the RPL glass. Optimized tin filters were determined based on the results of the simulations and the GR with

these filters was tested by irradiation experiments.

Results and Discussion The optimized GR filter configuration is shown in Figure 1. The second filter is added to the back of the RPL glass. Compared with the conventional GR, the first filter is thicker and has a larger hole on it. As a result of the irradiation experiments, it is found that the new GR fulfills the requirements of IEC 62387 in the energy range of 24 keV to 1,250 keV at 0 and 60 degrees as shown in Figure 2 and for side incident.

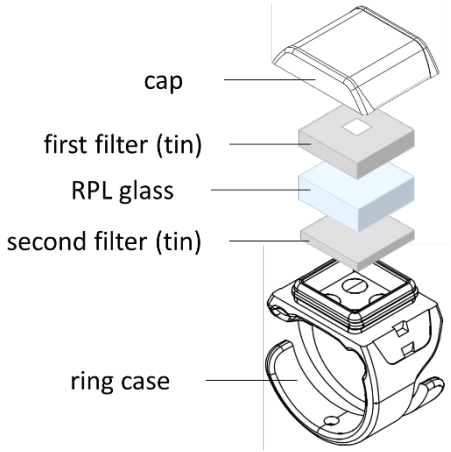

Figure 1 The optimized GR filter configuration

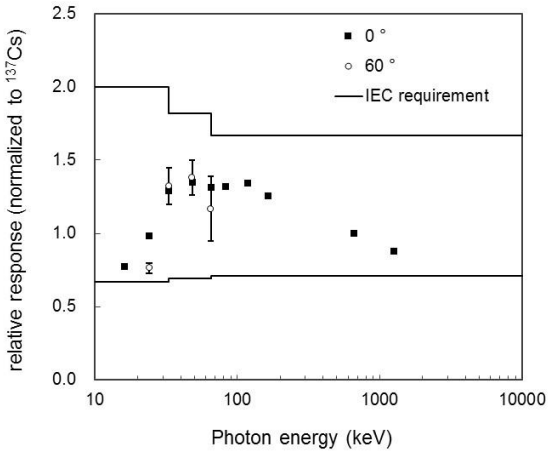

Figure 2 The energy and angular dependence of the GR

Conclusion We succeeded in improving the energy dependence and the response to angular incident by changing the filter configuration of conventional GR for photons.

References

1) IEC 62387:2012, Radiation protection instrumentation – Passive integrating dosimetry systems for personal and environmental monitoring of photon and beta radiation
2) Tatsuhiko Sato, Yosuke Iwamoto, Shintaro Hashimoto, Tatsuhiko Ogawa, Takuya Furuta, Shin-ichiro Abe, Takeshi Kai, Pi-En Tsai, Norihiro Matsuda, Hiroshi Iwase, Nobuhiro Shigyo, Lembit Sihver and Koji Niita, Features of Particle and Heavy Ion Transport code System (PHITS) version 3.02, J. Nucl. Sci. Technol. 55, 684-690 (2018).

Evaluation of Photon and Neutron Dose Distributions in Mixed Radiation Field Using Optically Stimulated Luminescence Dosimeter

Ya Han Tsai[1], Chien Yi Ting[2], Chun Wei Li[1], Hsiao Wen Chiu[3]

[1] *Department of medical imaging and radiological sciences, Kaohsiung medical university, Kaohsiung, Taiwan, R.O.C.*

[2]*Department of Medical Imaging and Radiology, Shu-Zen Junior College of Medicine and Management, Kaohsiung, Taiwan, R.O.C.*

[3]*Department of radiation oncology, Kuo General Hospita, Tainan, Taiwan, R.O.C.*

Highlights Mixed radiations were generated in high-energy radiation field. Equivalent dose of the environment during radiotherapy from neutrons and photons was measured to assess radiation risk of workers and patients using optically stimulated luminescence dosimeters (OSLDs).

Key words: Radiation, Neutron, Dosimetry, OSLD

Background and Objectives

High energy linear accelerator could produce neutrons when the output energy was over 10 MV[1)], which could increase additional dose in patients and workers. The aim of this study was to assess radiation dose from neutrons and photons of workers and patients in different field sizes using optically stimulated luminescence dosimeters (OSLDs) [2)].

Materials and Methods

Neutron and photon doses from a 10 MV photon energy Elekta synergy linear accelerator with different field sizes (10×10 cm^2,15×15 cm^2 and 20×20 cm^2) were measured by using OSLDs placed in a solid water phantom (20×20×20 cm^3) in this study[3)]. Neutron and photon doses were measured at the surface and a depth of 5 cm in the phantom. The doses at the surface and at the depth of 5 cm were investigated when the dose varied gradually from 10 Gy to 100 Gy in a fixed field of 10×10 cm^2 and at the same distance (SSD: 100 cm). The data were collected from three sites, including the dress desk, the mold cabinet and the proximal maze in the treatment room. The radiation dose was measured at two time points, including the moment immediately after irradiation and that five minutes after five minutes.

Results and Discussion

The results showed that field-size increase caused an increase in neutron dose. However, no neutron dose was measured at depth of 5 cm in the phantom. Instead, the photon dose at 5 cm in depth is about 1.16~1.8 times higher than that on the surface. The mean in-field dose was respectively 942.1 mSv, 958.9 mSv and 993.8 mSv in 10×10 cm^2, 15×15 cm^2 and 20×20 cm^2 of field size. The mean out-field dose was 76.7 mSv, 113.6 mSv and 137.8 mSv respectively in 10×10 cm^2, 15×15 cm^2 and 20×20 cm^2 of field size. A significant reduction (respectively 91.9 %, 88.2 % and 86 % in 10×10 cm^2, 15×15 cm^2 and 20×20 cm^2 of field size) was found in out-field dose compared with in-field dose. After irradiation, the highest dose was found at the hospital dress desk, where was also the only place finding neutron radiation at the three investigated sites of the environment. Radiation dose was 100 %, 66.6 % and 99.6 % reduced respectively at the proximal maze, the mold cabinet and the hospital dress desk at five minutes after irradiation.

Conclusion

Neutrons are indeed generated when irradiated by a 10MV linear accelerator. In order to reduce neutron dose, appropriate protection is imperative for patients. At the end of each radiotherapy, the radiologist is suggested to wait for a few minutes to enter the treatment room so as to reduce unnecessary dose.

References

1) Mesbahi A, A Monte Carlo study on neutron and electron contamination of an unflattened 18-MV photon beam. Appl Radiat Isot. 2009 Jan;67(1):55-60.
2) Nascimento LF, D'Agostino E, Vaniqui AC, Saldarriaga C, Vanhavere F, De Deene Y. Characterisation of OSL and OSLN droplets for dosimetry. Radiat Prot Dosimetry. 2014 Oct;161(1-4):116-22.
3) Passmore C, Kirr M. Neutron response characterisation of an OSL neutron dosemeter. Radiat Prot Dosimetry. 2011 Mar;144(1-4):155-60.

Dose Monitoring of Physicians Focused on the Dose to the Eye Lens

Zina Cemusova[1]*, Lucie Sukupova[2], Daniela Ekendahl[1]
[1]*National Radiation Protection Institute, Prague, Czech Republic*
[2]*Institute for Clinical and Experimental Medicine, Prague, Czech Republic*

Highlights In response to a change in legislation, lots of manufacturers started to offer the special type of personal dosemeters designed to measure dose equivalent at the depth of 3 mm ($H_p(3)$), which represents the operational quantity for the dose to the eye lens (D_{eye}). Nevertheless, it has some properties that can limit its usability. What is more, introducing another dosemeter to the equipment of radiation workers may be difficult. These are the reasons why another ways of D_{eye} monitoring are considered.

Key words dose to the eye lens, occupational doses in interventional radiology and cardiology, dose monitoring in hospitals

Background and Objectives The lowering of the limit of the dose to the eye lens from occupational exposure raised the need of the eye lens monitoring[1,2,3]. Questions about the proper way of the monitoring are solved. This study is aimed at workers in interventional radiology and related professions because they belong to one of the most endangered groups from the point of view of the eye lens irradiation.

Materials and Methods The doses were monitored in practice, with a help of a special eye dosemeter[4] and whole-body personal dosemeters[5], for 41 operating physicians from interventional cardiology and radiology, gastroenterological department and a special room for implantations of defibrillators and pacemakers, and 4 nurses from the gastroenterological department. The values measured with the eye dosemeter were compared with the values measured on the neck and chest.

Results and Discussion It can be summarized that the measured personal doses were lower than expected on the basis of the results of similar studies[2,3,6].
The average estimate of the annual eye lens dose was almost 5 mSv (based on $H_p(3)$ measured with the eye dosemeter), where interventional radiologists and cardiologists had rather higher doses and gastroenterologists and physicians from the special implantation room had lower doses. It must be emphasized that no correction factor taking account of shielding with lead

glasses, worn by most of physicians, was applied. So, the values, all measured outside the glasses, are conservative estimates[7].

In most cases, doses measured with a dosemeter on the neck were slightly higher than on the temple and doses measured on the chest were higher than in the neck position.

The correlation between the eye lens dose and the personal dose equivalent at the depth of 0.07 mm ($H_p(0.07)$) measured with the dosemeter on the neck was in agreement with another published data[2,8,9], specifically $H_p(3)= 0.78*H_p(0.07)+ 0.11$.

Conclusion The protective shieldings are effectively used at the workplaces participating in this study. Therefore, the measured occupational doses were low.

It can be concluded that D_{eye} monitoring with a help of a commonly employed whole-body dosemeter seems to be a reasonable way.

References

1) International Commission on Radiological Protection. Statement on tissue reactions. ICRP 4825-3093-1464. ICRP (2011).
2) Covens, P., Berus, D., Buls, N., Clerinx, P. and Vanhavere, F. Personal dose monitoring in hospitals: global assessment, critical applications and future needs. Radiat. Prot. Dosim. 124, 250–259 (2007).
3) Martin, C.J. Personal dosimetry for interventional operators: when and how should monitoring be done? Brit. J. Radiol. 84, 639-648 (2011).
4) Bilski, P. et al. The new EYE-D^{TM} dosemeter for measurements of $H_p(3)$ for medical staff. Radiat. Meas. 46, 1239–1242 (2011).
5) Cassata, J.R., Moscovitch, M., Rotunda, J.E. and Velbeck, K.J. A new paradigm in personal dosimetry using LiF:Mg,Cu,P. Radiat. Prot. Dosim. 101, 27–42 (2012).
6) Vanhavere, F. et al. Measurements of eye lens doses in interventional radiology and cardiology: Final results of the ORAMED project. Radiat. Meas. 46, 1243–1247 (2011).
7) Geber, T., Gunnarsson, M. and Mattsson, S. Eye lens dosimetry for interventional procedures- Relation between the absorbed dose to the lens and dose at measurement positions. Radiat. Meas. 46, 1248–1251 (2011).
8) Clerinx, P., Buls, N., Bosmans, H. and de Mey, J. Double-dosimetry algorithm for workers in interventional radiology. Radiat. Prot. Dosim. 129, 321-327 (2008).
9) Cemusova, Z., Ekendahl, D. and Judas, L. Assessment of eye lens doses in interventional radiology: a simulation in laboratory conditions. Radiat. Prot. Dosim. 170, 256-260 (2016).

Dosimetric properties of non-doped LiF/CaF_2 eutectic

Noriaki Kawaguchi*, Takayuki Yanagida
Nara Institute of Science and Technology, Nara, Japan

Highlights We have developed a non-doped LiF/CaF_2 eutectic for thermoluminescence (TL) dosimetry. While the non-doped LiF/CaF_2 eutectic and a CaF_2 single crystal showed similar luminescence properties, the non-doped LiF/CaF_2 eutectic can be obtained using a simple melt-solidification method with a lower melting temperature than that of CaF_2. The TL intensity of the non-doped LiF/CaF_2 eutectic was higher than that of the CaF_2 single crystal, and the integrated TL intensity of the non-doped LiF/CaF_2 eutectic monotonically increased as a function of X-ray dose from 10 to 1000 mGy.

Key words radiation, dosimetry, thermoluminescence

Background and Objectives Over the past few decades, dosimetric materials showing thermoluminescence (TL), optically-stimulated luminescence (OSL), and radio-photoluminescence (RPL) have been intensively studied. Although many types of materials including crystalline powders, single crystals, ceramics, and glasses have been reported as the dosimetric materials, there were few studies on dosimetric properties of eutectic materials. The eutectic materials can be obtained using the simple melt-solidification method and have been studied as thermal energy storage materials and neutron scintillators. Our group have been interested in eutectic materials also for the dosimetry due to their simple production process; therefore, we studied the TL and OSL dosimetric properties of Eu-doped LiF/CaF_2 eutectics[1]. The Eu-doped LiF/CaF_2 eutectic showed promising dosimetric properties; however, the segregation of Eu ions can be a problem for its production using the melt-solidification method. In this study, we have investigated dosimetric properties of the non-doped LiF/CaF_2 eutectic.

Materials and Methods The non-doped LiF/CaF_2 eutectic was obtained using a simple melt-solidification method. The high purity LiF and CaF_2 powders were mixed with a mole ratio at the eutectic point (LiF:CaF_2 = 80:20) and poured into a carbon crucible. The mixed powders were melted and cooled using a vacuum chamber equipping a carbon heater and a carbon heat insulator under Ar atmosphere. The X-ray induced scintillation spectrum and the

TL glow curves of the obtained sample were measured. To compare the properties, we have also evaluated the non-doped CaF_2 single crystal which was made by Tokuyama Corporation using the Czochralski method.

Results and Discussion The X-ray scintillation spectra of both the non-doped LiF/CaF_2 eutectic and the non-doped CaF_2 single crystal showed broad emission peaks around 300 nm due to the self-trapped exciton of CaF_2. While the scintillation intensity of the eutectic sample is lower than that of the single crystal sample, the TL intensity of the eutectic sample was significantly higher that of the single crystal sample (Fig. 1). An opposite trend in the scintillation and TL intensities can be explained by the concentration of trapping centers. It is considered that the concentration of trapping centers in the eutectic sample is higher than that in the single crystal sample. Both samples showed linear TL responses to X-ray dose in the range from 10 to 1000 mGy (Fig. 2).

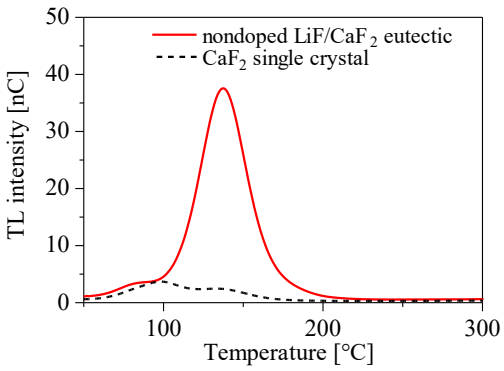

Figure 1. TL glow curves of the non-doped LiF/CaF_2 eutectic and the non-doped CaF_2 single crystal after 100 mGy of X-ray irradiation.

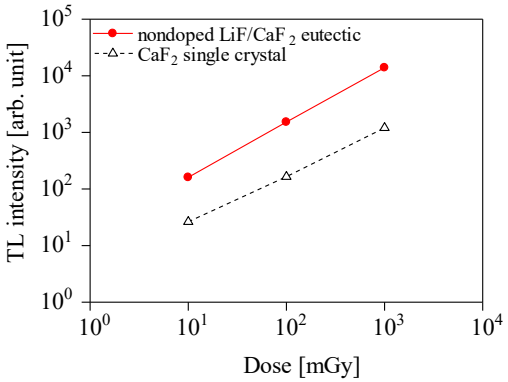

Figure 2. Dose response curves of the non-doped LiF/CaF_2 eutectic and the non-doped CaF_2 single crystal.

Conclusion The non-doped LiF/CaF_2 eutectic, which is obtained by the simple melt-solidification method, shows a higher TL intensity than that of the CaF_2 single crystal. In addition, the TL intensity of the non-doped LiF/CaF_2 monotonically increases as a function of X-ray dose from 10 to 1000 mGy.

References

1) N. Kawano, N. Kawaguchi, K. Fukuda, G. Okada, T. Yanagida, J. Mater. Sci.: Mater. Electron. **29** (2018) 8964–8969.

Radiation-induced luminescence properties of Eu-doped $BaAl_2O_4$ crystals

Daisuke Nakauchi[1]*, Noriaki Kawaguchi[1], Takayuki Yanagida[1]
[1]*Nara Institute of Science and Technology, Japan*

Highlights Eu:$BaAl_2O_4$ single crystals were prepared by the floating zone method, and the ionizing-radiation-induced radioluminescence and storage luminescence properties were evaluated for dosimetry applications.

Key words scintillator, radioluminescence, thermoluminescence, photoluminescence, afterglow, crystal growth

Background and Objectives Luminescent materials have been utilized in radiation detection, and they are classified into two types such as scintillators and storage-type phosphors. Scintillators convert a single quantum of ionizing radiation into thousands of low energy photons immediately, so they have been playing an important role in various fields of radiation detections including medical imaging, security and so on. On the other hand, storage-type phosphors have a function to store and accumulate the incident radiation energy and emit a light with external stimulations of light or heat. Alkaline-earth aluminates are well-known long-lasting phosphors [1], but there is only a few reports on the radiation-induced luminescence. In our previous study, we have shown that Eu-doped $SrAl_2O_4$ crystals show notably high scintillation light yield [2]; therefore, other alkaline-earth aluminates are likely to have good sensitivity against ionizing radiations. In this study, Eu:$BaAl_2O_4$ single crystals were prepared, and the fluorescence and ionizing radiation induced luminescence properties were evaluated for dosimetry applications.

Materials and Methods 0.5, 1, 2 and 3% Eu-doped $BaAl_2O_4$ single crystals were synthesized by the floating zone method. As a raw material, $BaCO_3$ (99.99%), Al_2O_3 (99.99%) and Eu_2O_3 (99.99%) were used and mixed homogeneously. The mixed powder was formed into a cylindrical rod by applying hydrostatic pressure, and then the rod was sintered at 1400 °C for 8 h. As scintillation properties, radioluminescence spectra under X-ray irradiation were measured using our original setup [3]. The X-ray generator (XRB80N100/CB, Spellman) was equipped with an X-ray tube having a W anode target and a Be window. The X-ray tube was operated with the bias voltage of 80 kV and tube current of 1.2 mA. In these analyses, emitted radioluminescence photons from the samples were led to a spectrometer

unit equipped with a CCD (DU-420-BU2, Andor) and a monochromator (SR163, Shamrock) through an optical fiber to measure the spectra. Radioluminescence decay curves were measured using an afterglow characterization system [4]. As storage luminescence properties for dosimetry, the thermoluminescence (TL) glow curve was measured using a TL reader (TL-2000, Nanogray) with a heating rate of 1 °C/s. Prior to these measurements, the samples were irradiated with 40 kV X-rays.

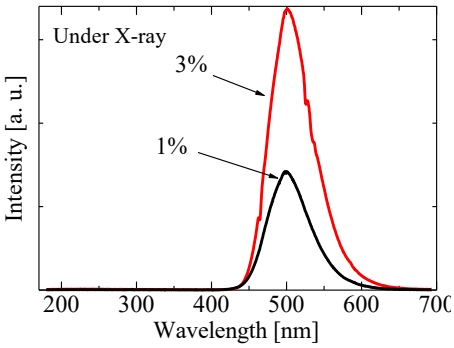

Fig.1 Radioluminescence spectra under X-ray irradiation.

Results and Discussion Figure 1 shows X-ray induced radioluminescence spectra of Eu:$BaAl_2O_4$. The samples exhibit intense radioluminescence with a broad emission band peaking around 500 nm, which are attributed to the 5d-4f transitions of Eu^{2+}. Figure 2 exhibits the radioluminescence decay time profiles of Eu:$BaAl_2O_4$. The decay curves are well-approximated by one exponential function, whose decay time constants are 913 for 1% and 667 ns for 3% Eu-doped samples. As shown in Fig. 3, the TL glow curves are evaluated after 1 Gy X-ray irradiation. The 1% Eu-doped sample exhibits two grow peaks around 100 and 440 °C. In this presentation, photoluminescence, and radioluminescence and afterglow properties will be also reported and discussed with the accumulated luminescence characteristics.

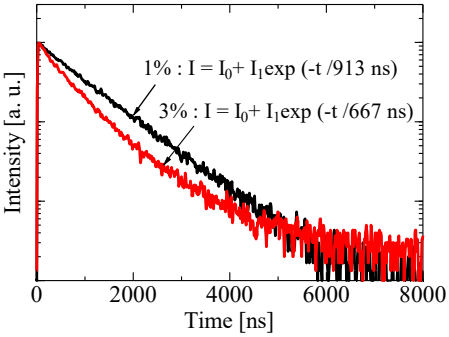

Fig.2 Radioluminescence decay curves under X-ray irradiation.

Conclusion Eu:$BaAl_2O_4$ crystals prepared by the floating zone method show strong radioluminescence signals with a broad peak around 500 nm, which is suitable for uses with Si-photodiode.

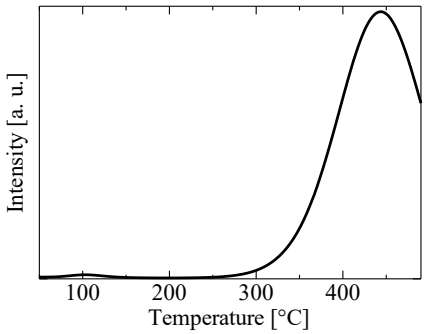

Fig.3 Thermoluminescence glow curves after X-ray irradiation.

References

[1] T. Matsuzawa, J. Electrochem. Soc. 143 (1996) 2670. doi:10.1149/1.1837067.
[2] D. Nakauchi, G. Okada, M. Koshimizu, T. Yanagida, J. Lumin. 176 (2016) 342. doi:10.1016/j.jlumin.2016.04.008.
[3] T. Yanagida, K. Kamada, Y. Fujimoto, H. Yagi, T. Yanagitani, Opt. Mater. 35 (2013) 2480. doi:10.1016/j.optmat.2013.07.002.
[4] T. Yanagida, Y. Fujimoto, T. Ito, K. Uchiyama, K. Mori, Appl. Phys. Express 7 (2014) 062401. doi:10.7567/APEX.7.062401.

LET-dependent thermoluminescence of $Y_3Al_5O_{12}$:Ce

Masanori Koshimizu[1]*, Go Okada[2], Yuho Hirata[3], Daisuke Nakauchi[4], Takumi Kato[4], Noriaki Kawaguchi[4], Kenichi Watanabe[3], Yusuke Koba[5], Yutaka Fujimoto[1], Takayuki Yanagida[4], Keisuke Asai[1]

[1]*Department of Applied Chemistry, Tohoku University, Sendai, Japan*

[2]*Kanazawa Institute of Technology, Kanazawa, Japan*

[3]*Nagoya University, Nagoya, Japan*

[4]*Nara Institute of Science and Technology, Ikoma, Japan*

[5]*National Institutes for Quantum and Radiological Science and Technology, Chiba, Japan*

Highlights The thermoluminescence properties of $Y_3Al_5O_{12}$ (YAG):Ce (Ce concentrations: 0.5, 0.8, and 2 mol%) were characterized after irradiation with heavy charged particles or gamma-rays. The effects of linear energy transfer (LET) were significant for YAG:0.5 mol% Ce. The LET dependence of the glow curve has a trend opposite to that of the gamma-ray dose dependence.

Key words dosimetry, thermoluminescence, linear energy transfer, YAG

Background and Objectives Heavy charged particle beams have long been used for materials modification because of their characteristic interactions with matter. Recently, their applications in radiation therapy have been attracting significant attention. The heavy charged particles produce dense electronic excitation in condensed matter, which results in peculiar chemical reactions, unique biological effects, and the formation of columnar defects. In addition, the response of radiation detectors often depends strongly on the density of the electronic excitation or linear energy transfer (LET).

The LET-dependent response of radiation detectors is considered to be caused by the interaction of excited states; however, the way in which the interaction leads to the LET-dependent response has not been clarified. Recently, we have been investigating the LET effect of phosphor-based radiation detectors, including scintillators and thermoluminescence (TL) materials. We investigated the LET-dependent response of the Ce-doped $LiCaAlF_6$, a TL material, after high-energy He irradiation and estimated the diffusion length of the electron-hole pairs based on the similarity of the LET-dependent properties of the material after He irradiation and its dose-dependent properties after gamma-ray irradiation.[1)] In this study, we analyzed the LET-dependent TL properties of Ce-doped $Y_3Al_5O_{12}$ (YAG).

Materials and Methods Transparent YAG ceramics doped with 0.5, 0.8, or 2 mol% of Ce were used as the samples. TL glow curves were obtained after irradiating the samples at a heating rate of 1 K/s. The irradiation at high LET was performed at HIMAC, NIRS, Japan. The samples were irradiated with 160 MeV H, 150 MeV/n He, and 135 MeV/n C. The LET was enhanced using binary filters. The samples were also irradiated with gamma rays from ^{60}Co at Nagoya University.

Results and Discussion The TL glow curves of YAG doped with 0.5 mol% Ce after (a) gamma ray irradiation at different doses and (b) 160 MeV H irradiation with different binary filter thicknesses are shown in Figure 1. Glow peaks were observed at 410, 460, and 550 K in all the TL glow curves. The relative intensities of the glow peaks strongly depended on the gamma ray doses and LETs. The relative intensities of the glow peaks at high temperatures increased with the LET; a similar trend was observed in Ce-doped $LiCaAlF_6$.[1] In contrast, the relative intensities of the glow peaks at high temperatures decreased with the gamma ray dose. This dose dependence was opposite to that of Ce-doped $LiCaAlF_6$.[1] The opposite LET- and gamma-ray dose dependence trends indicate that the LET dependence cannot be explained solely with the excitation density, and that discussion of the dynamic aspects of the excited states is necessary to elucidate the basic mechanism of the LET dependence.

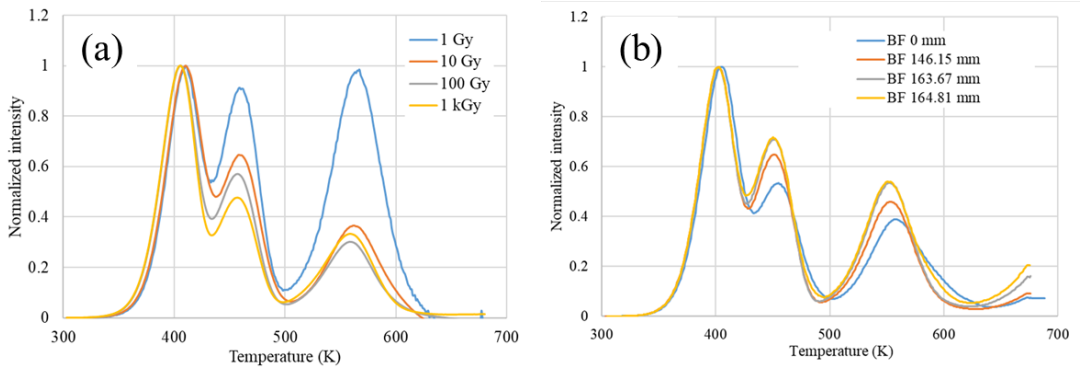

Figure 1. TL glow curves of YAG doped with 0.5 mol% Ce after (a) gamma ray irradiation at different doses and (b) 160 MeV H irradiation with different binary filter thicknesses.

Conclusion The relative intensities of the glow curves in Ce-doped YAG showed opposite LET- and gamma-ray dose dependence trends.

References

1) D. Nakauchi et al., Nucl. Instrum. Methods Phys. Res. B, 409 (2017) 23.

Study of in-water broadening of proton and carbon-ion PBs for the evaluation and compensation of the EBT3 film sensitivity quenching

G. Gambarini[1,2]*, G. Barzon[1], D. Bettega[1,2], L. Bettinelli[1], M. Ciocca[3], A. Mirandola[3]

[1]*Department of Physics, Università degli Studi di Milano, Milano, Italy*

[2]*National Institute of Nuclear Physics (INFN), Section of Milan, Milano, Italy*

[3]*Medical Physics Unit, Centro Nazionale di Adroterapia Oncologica (CNAO), Pavia, Italy*

Highlights Functions describing PB broadening in water and EBT3 film sensitivity quenching were experimentally searched, for both protons and carbon ions. The results allow to perform suitable correction of the acquired dose images.

Key words proton, carbon ion, pencil-beam, dosimeter sensitivity, Bragg peak

Background and Objectives In charged-particle dosimetry, it is well known that in solid, liquid or gel detectors a non-negligible decrease of sensitivity can occur with the increase of the linear energy transfer (LET) of radiation. For this reason, quantitative determinations in Hadrontherapy dosimetry are commonly based on ionization chambers, in whose gaseous active volume there are no significant troubles caused by high LET of radiation. Dose images are often obtained by means films, but only for qualitative information. Considering the great advantage of achieving spatial distributions of absorbed dose, a method for correcting the dose images acquired by Gafchromic films has been proposed and tested in the same laboratory[1,2]. In the suggested method, a correction coefficient is evaluated in each point of the acquired image, taking into account the various pencil beams (BPs) that give a dose contribution in the considered position and the reduction of the detector sensitivity for each of these contributions. Experimental studies are carried out for getting the various parameters necessary for the correction of the acquired dose images.

Materials and Methods The studied detectors are Gafchromic® EBT3 films that were irradiated with protons or carbon-ions in a water phantom, at the Synchrotron of CNAO (Pavia). Optical density images were acquired with laboratory-made instrumentation. The films were calibrated with a properly scanned PB of 173.61 *MeV* protons. In the proposed method[2], the correction coefficient $C(x,y,z)$ is calculated as ratio between the absorbed dose (D_{abs}) and the measured one (D_{meas}), in each point of the image. The MATLAB software in development for calculating the $C(x,y,z)$ matrix utilizes, as input, the data extracted from the treatment plane concerning the PBs used for irradiation, i.e. their energies and incidence coordinates. The calculation algorithms require functions describing the PB broadening and

the film-sensitivity reduction as a function of depth in water for whichever initial energy.

Results and Discussion Irradiations of EBT3 films, with various configurations, were performed with a few PB energies. For protons and carbon ions, 3D distributions of the absorbed dose in water were deduced from experimental results. Formulations describing, as a function of energy and depth, the dose profile along the PB axis and the transversal broadening were attained by means of fitting procedures. The quenching of EBT3 film sensitivity was evaluated as the ratio of the measured dose and the absorbed one. The average value at the depth of the Bragg peak was found to be approximately equal to 0.75 for protons and 0.3 for carbon ions.

Conclusion Also if the calculation of the correction coefficient has large approximations, good results were obtained. Such results have stimulated to carry out additional research to increase the accuracy of the procedure.

References

1) G. Gambarini et al. Correction method of measured images of absorbed dose for quenching effects due to relatively high LET. Radiat. Phys. Chem. 140 (2017) 15–19.
2) G. Gambarini et al. Development of a procedure for quenching-effect correction in images of absorbed dose from protons or carbon ions acquired with Gafchromic EBT3 films. Radiat. Phys. Chem. 155 (2019) 138–145.

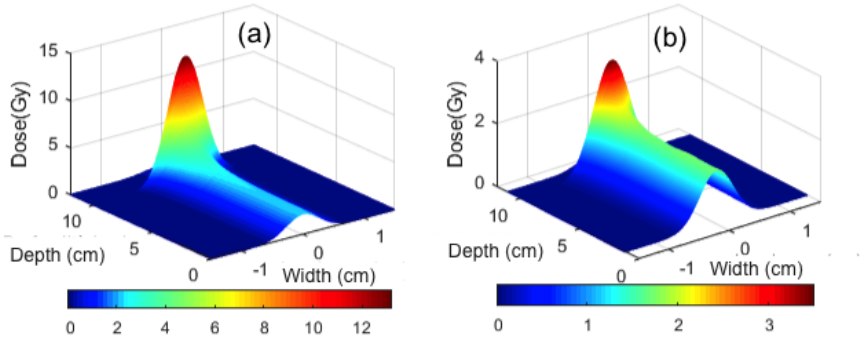

Figure 1. Example of evaluated distributions of the (a) absorbed and (b) measured doses for a PB of carbon ions of 221.44 MeV/n.

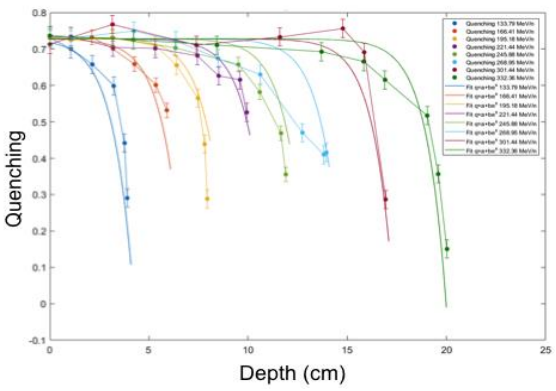

Figure 2. Comparison of experimental values of sensitivity quenching for carbon ions of various energies and the curves evaluated, for the same energies, with the function chosen for describing the quenching effect.

Thermally Stimulated Luminescence of Tin-Doped Borate Glasses

Hirokazu Masai[1]*, Hiromi Kimura[2], Noriaki Kawaguchi[2], Takayuki Yanagida[2]
[1] *National Institute of Advanced Industrial Science and Technology, Ikeda, Osaka, Japan*
[2] *Nara Institute of Science and Technology, Ikoma, Nara, Japan*

Highlights We have examined X-ray-induced luminescence of Sn-doped zinc borate (SZB) glasses prepared in Ar atmosphere. The scintillation intensity of SZB glasses increases with increasing tin concentration while the intensity of thermally stimulated luminescence (TSL) decreases. Clear inverse relationship between scintillation and TSL in SZB glasses is observed.

Key words radiation, thermally stimulated luminescence, tin, glass

Background and Objectives Because glasses have no structural ordering in the long range, the good formability is one of the advantages for practical applications. On the other hand, various kinds of local structures are allowed to be exhibited in random network of glass. Since such local structures can work as trap sites, it is expected that glasses are candidates of storage-type dosimeter. It is recently proposed that there is an inverse correlation between radiation induced scintillation and storage luminescence[1)]. Considering the nature of glasses, examination of the relationship between scintillation and storage luminescence in glasses is worthwhile. In the present study, we examined the relationship in Sn^{2+}-doped zinc borate (SZB) glasses, whose photoluminescence (PL) properties were recently reported[2)]. Since Sn^{2+} species are oxidized during melting in air[2, 3)], we prepare these glass melts in Ar condition.

Materials and Methods The SZB glasses were prepared according to a conventional melt quenching method. Starting chemicals, ZnO, B_2O_3, and SnO, were mixed and melted in Ar atmosphere at 1100°C for 30 min. The glass melt was quenched on a stainless steel plate and then annealed at the glass-transition temperature. As prompt luminescences, PL and X-ray induced scintillation were measured. After X-ray irradiation, we measured TSL glow curves of these glasses with the heating rate of 1 °C/s.

Results and Discussion The obtained SZB glasses were transparent and clear PL due to Sn^{2+} emission centers[4)] was observed by UV irradiation. The scintillation spectra by X-ray irradiation show that the peak areas increase with increasing SnO concentration. Figure 1 shows TSL glow curves of *x*SZB glasses after 1 Gy X-ray irradiation (*x* means concentration

of Sn cations). The glow peak intensity of the 0.1SZB glass is the highest among these glasses, and the intensity decreases with increasing SnO concentration. Figure 2 shows peak areas of TSL and X-ray induced scintillation after 1 Gy irradiation as a function of SnO concentration. There is a clear inverse relationship between these two parameters in the SZB glasses.

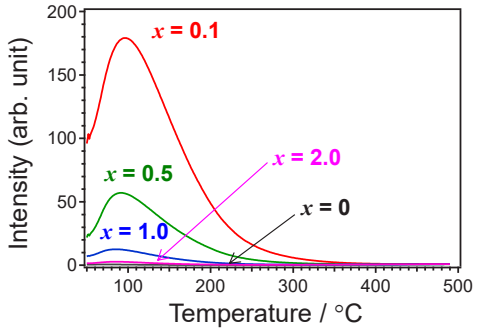

Figure 1. TSL glow curves of *x*SZB glasses after 1 Gy irradiation.

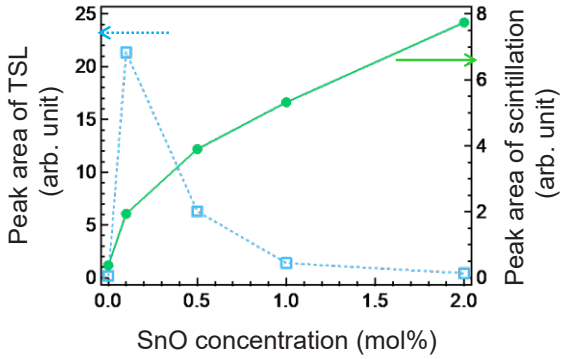

Figure 2. Peak areas of TSL (left) and X-ray induced scintillation (right) after 1 Gy irradiation of *x*SZB glasses as a function of SnO concentration.

Conclusion The X-ray induced scintillation and TSLof SZB glasses were examined. It is found that there is an inverse relationship between the scintillation and TSL in the SZB glasses.

References

1) T. Yanagida, *J. Lumin.* **169,** 544 (2016).
2) H. Masai, *et al. Bull. Chem. Soc. Jpn*. **88,** 1047 (2015).
3) H. Masai, *et al. J. Mater. Chem. C* **2,** 2137 (2014).
4) H. Masai, *et al. Appl. Phys. Express* **3,** 082102 (2010).

TL and OSL solutions for a bi-localized transitions (BLT) system

Arkadiusz Mandowski[1]*
[1]*Jan Dlugosz University, Czestochowa, Poland*

Highlights Equations for a bi-localized system with quasi-equilibrium conditions are considered. The system is solved analytically for TL (thermoluminescence) and OSL (optically stimulated luminescence). TL curve has a double peak structure.

Key words thermoluminescence (TL), optically stimulated luminescence (OSL), traps, recombination centers, spatially correlated systems.

Background and Objectives Recently, it was shown that for a system of T-RC (trap – recombination center) pairs it is more energetically preferred to form small clusters than separate T-RC pairs. Therefore, each localized transition (LT) system will contain certain number of small clusters consisting of several T-RC pairs. The smallest cluster of this type consists of two T-RC pairs. This is the case of bi-localized system of traps. The possible bi-localized transitions (BLTs) could be represented by the following transitions scheme:

$$\begin{array}{ccccc} \Pi_2^0 & \underset{\bar{A}_2}{\overset{2D_2}{\rightleftarrows}} & \Pi_1^1 & \underset{2\bar{A}_2}{\overset{D_2}{\rightleftarrows}} & \Pi_0^2 \\ & & \bar{B}_2\downarrow & & 2\bar{B}_2\downarrow \\ & & H_1^0 & \underset{\bar{A}_1}{\overset{D_1}{\rightleftarrows}} & H_0^1 \\ & & & & \bar{B}_1\downarrow \\ & & & & E_0^0 \end{array} \qquad (1)$$

The $H_m^n(t)$ states have the same meaning as for the semi-localized transitions (SLT), i.e. states with a single electron and a single hole. However, the $\Pi_m^n(t)$ symbol denotes additional BLT states with two charges in RCs. The diagram (1) allows to write kinetic equations for the system, which can be solved numerically. However, using simple quasi-equilibrium arguments it is easy to derive analytical solutions. These solutions were obtained for TL as well for the OSL cases. Analytical formulation allows to analyze in detail all elemental processes leading to TL and OSL.

Materials and Methods The TL solution has a double peak shape. Due to various parameters the peaks may overlap more or less. We present a mathematical proof that for most cases the less overlapping TL peaks obey simple first order kinetics. Much more difficult is the case with strongly overlapping TL peaks. The resulting TL curve is very complex and far from first order kinetics. Two examples are shown in Fig.1. More complex is the case of OSL decay. The two first order components could be separated only for specific parameters.

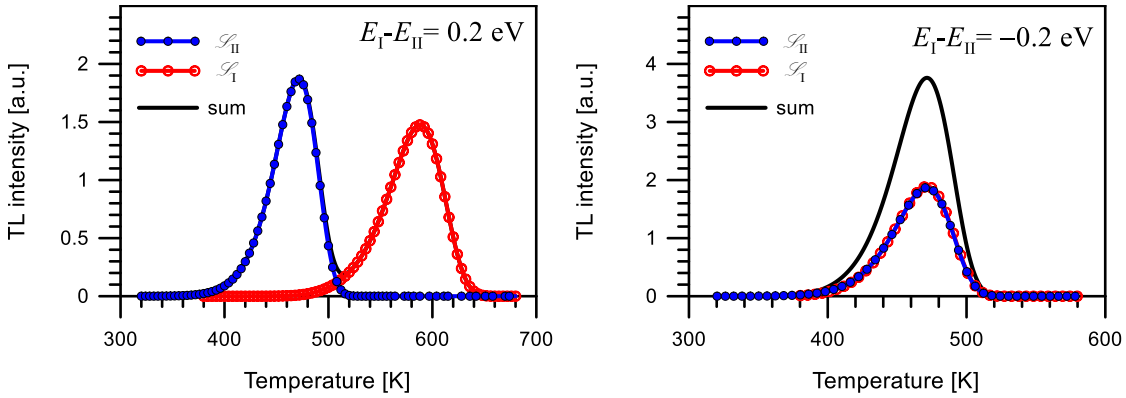

Figure 1. Thermoluminescence resulting from a bi-localized transitions (BLT) system. Two extreme cases are shown. a) the left diagram – the case of less overlapping peaks. b) the right diagram – two strongly overlapping peaks

Conclusion The paper presents kinetic equations for TL and OSL luminescence related to bi-localized recombination. For strongly overlapping TL peaks the kinetic equation has a non first order form. This feature gives the possibility to differentiate the BLT system from the typical LT system. The OSL response of BLT is analyzed under various optical stimulation.

References

1) A. Mandowski. Semi-localized transitions model for thermoluminescence. J. Phys. D: Appl. Phys. **38**, 17-21 (2005)
2) A. Mandowski. Topology-dependent thermoluminescence kinetics. Radiat. Prot. Dosimetry **119**, 23-28 (2006)

On the Mechanisms of Plasmon-Enhanced Optically Stimulated Luminescence

Éder José Guidelli*, Andressa C. A. Assunção, Oswaldo Baffa
Physics Department – FFCLRP – University of São Paulo, Brazil

Highlights Optically Stimulated Luminescence (OSL) intensity is enhanced upon interaction with Localized Surface Plasmons (LSP) but the exact mechanism is still not clear. Our results suggest that trapped electrons optically unreachable can be converted into useful luminescence information *via* plasmonic coupling. As a consequence, higher dosimetric sensitivity and smaller bleaching times are obtained.

Key words Optically stimulated luminescence, plasmon resonance, radiation dosimetry, nanoparticles;

Background and Objectives Localized surface plasmons (LSP) are well known to enhance luminescence emission. The origins of these luminescence enhancements are usually explained based on two mechanisms: (1) the excitation mechanism, due to local-electric field amplification close to the metal surface; and (2) the metal-coupled emission mechanism, due to an energy transfer from the excited luminophore to the plasmons. Here, we investigate the luminescence enhancement caused by silver nanoparticle (AgNP) films, using X-ray irradiated sodium chloride nanocrystals, and Optically Stimulated Luminescence (OSL) to elucidate the mechanisms involved in the Plasmon-Enhanced OSL.

Materials and Methods AgNP films were produced by Layer-by-Layer (LbL) and microwave-assisted (MW) methods. NaCl crystals produced over the AgNP films by dropcast. Samples were irradiated in air, with a dose of 10 Gy, using an X-Ray tube (Magnun - Moxtek, USA) operating at 48kVp and 0.2 mA. Optically stimulated luminescence (OSL) was acquired using an OSL reader developed by our research group. Samples were stimulated with blue (470 nm), green (530 nm) and red (652 nm) LEDs.

Results and Discussion The area of the OSL curve is enhanced around 7-fold in presence of the LbL AgNP film with the higher absorbance tested, compared to the intensity of NaCl crystals deposited on glass (Figure 1 (a)). Fig. 1 also shows that that a more intense plasmon resonance band (at 470 nm) slowed the OSL decays. Mechanisms 1 and 2 cannot explain these results, suggesting that a third mechanism caused OSL enhancement. Furthermore, OSL

regeneration is only observed in absence of the AgNP films, suggesting that electrons trapped in non-optically active traps (small photoionization cross-section) can now contribute to the OSL signal.

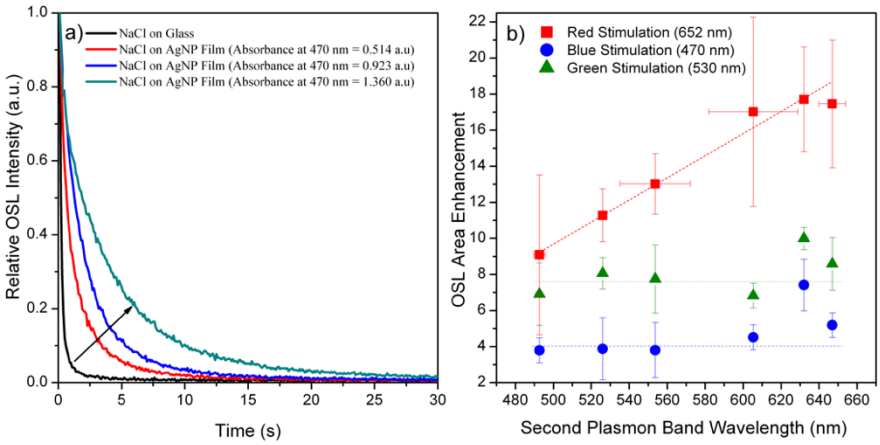

Figure 1. (a) OSL Signal for NaCl crystals deposited on glass and on AgNP films with different plasmon band intensity. (b) OSL area enhancement as a function of the second plasmon band position, upon blue, green, and red OSL stimulations.

To verify this hypothesis, we produced MW AgNP films with one plasmon band peaking at 390 (overlapping with OSL emission) and a second plasmon band with peak position varying from 500-650 nm. Figure 1 (b) reveals that the largest enhancements are observed with the red OSL stimulation, when the stimulation wavelength is well tuned with the film plasmon band but not with the NaCl F center absorption (450 nm). This result reinforces the hypothesis that small photoionization cross-section traps (non-optically active traps) participate in the OSL process under plasmon resonance conditions.

Conclusion Plasmon interaction may transform useless trapped electrons into useful luminescence information, enhancing OSL intensity and dosimetric sensitivity.

Financial Support: Brazilian Agencies CNPq (407471/2016-2) FAPESP (2013/07699-0, 2014/20431-9, 2018/11620-3) and CAPES (Finance Code 001 and 6479 - Acordo de Cooperação Técnica CAPES/USP)

References

1) Guidelli et.al., *Scientific Reports*, **6**, Article number: 36691 (2016)

Anomaly Detection of TLD Glow Curves Using three different machine learning classifiers

Gal Amit[1]*, Hanan Datz[1]
[1]*SNRC, Soreq Nuclear Research Center, Israel*

Highlights A novel method for the detection of glow curves (GCs) anomaly is presented. The method uses machine learning algorithms in order to detect abnormal GCs shapes and categorize them. A high detection performance rate for either 'anomalous' or 'regular' GC shape class of up to 96% is achieved, depending on the algorithm type.

Key words dosimetry, glow curve analysis, machine learning, anomaly detection

Background and Objectives Anomalies in glow curve (GCs) shapes can appear in various forms. If ignored, these anomalies might significantly change dose estimation, and in almost all cases would involve over-estimation. Moreover, many external dosimetry laboratories (EDLs) need to maintain quite busy lines of TLD readings, so they need a fully automatic process that will assist their technicians in classifying anomalous GCs. The proposed novel automatic method can serve as a solution for these two challenges. In addition to that, this automatic way of classifying anomalous Vs. regular GC shapes will also enhance EDLs capabilities in terms of quality control.

Materials and Methods The algorithms developed in this research were developed in the EDL of the Radiation Safety Division at the Soreq Nuclear Research Center, Yavne, Israel. They use both Support Vector Machines (SVMs) and Artificial Neural Networks (ANNs), which have been extensively employed in machine learning classification applications in various fields. The algorithms software was written using a standard MATLAB R2017b[11], and their input was obtained from the software supplied along with Harshaw TLD readers - WinREMS version PL-267328.2.3.0.

A general prescription for the development and application of a machine learning classifying algorithm always includes the following three stages. The first is data tagging, in which each input in a data set is labeled with an appropriate class label, in our case either 'anomalous' or 'regular'. The second stage is a training method which trains the algorithm over this set of tagged input in order to obtain an optimal set of algorithm paramters, and the third stage is predicting the classification of some new data using the trained classifier.

Table I. Predictions of three different classifiers

Algorithm	Real class	Predicted class	
		anomalous	regular
SVM	anomalous	137	66
	regular	18	3433
SVM weighted	anomalous	203	0
	regular	137	3314
ANN	anomalous	124	79
	regular	26	3425

Table II. SVM, weighted SVM, and ANN performance evaluated using different metrics.

	accuracy	sensitivity	F-measure
ANN	0.971	0.611	0.703
SVM	0.977	0.675	0.765
SVM weighted	0.963	1	0.748

Results and Discussion Table **I** presents the predictions of the three developed classifiers: ANN, SVM, and weighted SVM. Table **II** concludes the performances of all three algorithms using different metrics. It can be seen that performance accuracies are higher than 96 percent for all three algorithms. Figure **I** shows some examples of 'anomalous' and 'regular' GCs detected by the algorithm. Later on, a more sophisticated tool based on these current classifiers is planned to be developed in order to categorize different kinds of anomalies.

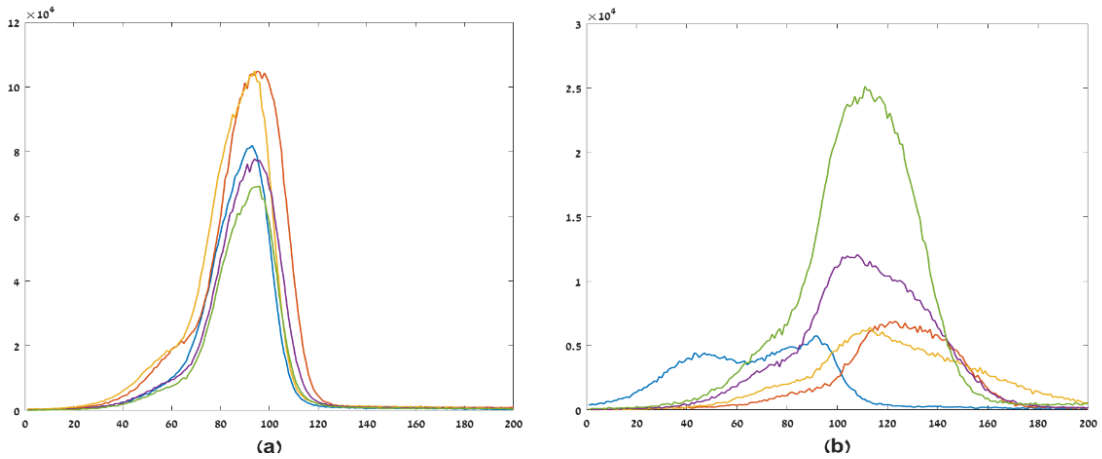

Figure 1. Curves detected by the SVM classification algorithm (a) Some sample regular curves (b) some sample irregular curves.

Conclusion It is clear that all three classifiers have high performance rate in terms of their accuracies, meaning that applying one of them on a busy line of an EDL should improve both its accuracy and its quality control process. There is no conclusive conclusion which algorithm needs to be used for best performance, while this is to be decided considering which parameter is to be optimized most importantly.

Kinetic Simulations of Complex Phenomena following optical absorption, optical excitation and thermal excitation of LiF:Mg,Ti (TLD-100)

I.Eliyahu [1] , L. Oster[3], G. Reshes[3]; Y.S. Horowitz [2]; S. Biderman[3], D. Sibony[2] , D. Ginsburg[2] and G. Amit[2].

[1]*Soreq Nuclear Research Center, Yavne, Israel,* [2] *Ben Gurion University of the Negev, Beersheva, Israel* , [3] *Sami Shamoon College of Engineering, Beersheva, Israel*

The Needle in the Haystack group named above have over the past several years developed an increasingly complex kinetic model to simulate the behavior of the LiF:Mg,Ti system following ionizing irradiation, optical excitation and finally thermal excitation. The kinetic model is based on the migration and recombination of charge carriers (both electrons and holes) in the conduction band and valence band. The uniqueness of the model is that it incorporates spatially correlated trapping centers (TCs) and luminescent centers (LCs) which can lead to geminate (localized) recombination. The inclusion of the spatially correlated TC/LCs has far-reaching consequences both on the glow curve and the dose response. The model in its latest form is shown below. It includes the spatially correlated TC/LC with four possible configurations following irradiation, a non-spatially correlated electron TC also contributing to peak 5, two types of F vacancies; those created in the sample by the irradiation and those initially present in the sample and V_3-V_k transformation as a source of holes.

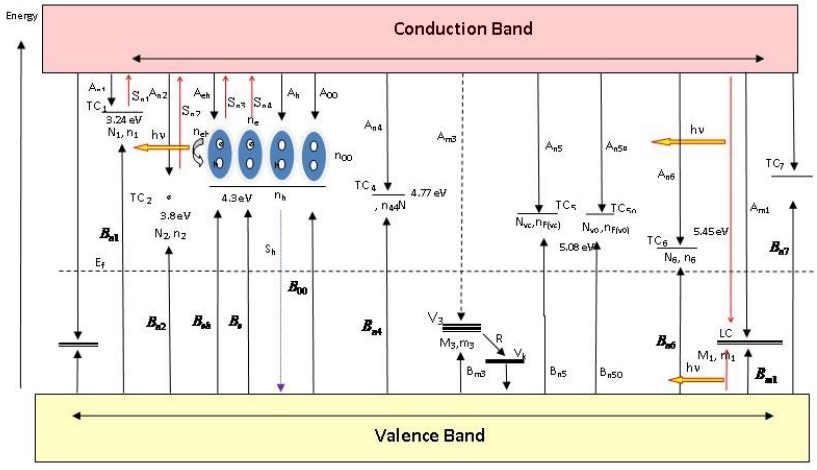

Figure 1. Conduction band/valence band model for the heating stage of LiF:Mg,Ti (TLD-100).

The complexity should come as no surprise since the TL glow curve consists of at least 10 glow peaks between room temperature and 400°C. Along the way several interesting observations and conclusions have been reached based on both the successes and the failures of the simulations. The

simulation of the linear/supralinear dose response as a function of photon/electron energy was achieved by allowing the ratio of the filling rates of the e-h configuration to the e-only configuration to depend on photon energy [1]. However, the simulation of the dependence of ratio of the intensity of glow peak 5a to glow peak 5 as a function of dose also required the introduction of band-tail states to allow semi-localized recombination of the e-only configuration as well [2]. These are not shown explicitly in Figure 1. Kinetic simulation of the effects of 5.08 eV (F band) on the optical absorption energy spectrum required geminate recombination between an excited state of the F center and the V_3 centers and the release of hole via V_3-V_k transformation to explain the decrease in intensity of the OA bands [3]. A somewhat controversial conclusion was reached following the inability to simulate filling rates in the irradiation state and the results of optical bleaching on the optical absorption using identical values of the recombination coefficients [4]. The filling of the traps during irradiation required high values of A (the electron recombination probability) compared to those of B (the hole recombination probability). On the other hand, optical excitation required the opposite to explain the decrease (rather than an increase) of the OA bands. It was suggested that one possible reason was the differences in the electron energy spectra released by ionizing radiation and the optical excitation with the latter composed of a far greater density of ultra-low energy electrons. This, when coupled with the dependence of the recombination cross-sections on electron energy, could explain the necessity for different values of the recombination probabilities. Such a possibility is new to kinetic simulations [5].

The current version of the model will be used to simulate the effects of 3.6 eV, 4.3 eV and 5.08 eV optical excitation on the TL glow curve and the TL dose response of the components of glow peak 5. Interesting experimental results have already been observed including changes in the ratio of glow peaks 5a to 5, an increased intensity of peak 5b and a decrease in the supralinearity of peak 5.

References

[1[. Eliyahu, I., Horowitz, Y.S., Oster, L. and Mardor, I**., A kinetic model incorporating both localized and delocalized recombination:Application to the dependence of the TL dose response on photon energy,** J. Lumin., 145, 600-607 (2014).

[2]. Eliyahu, I., Horowitz, Y.S., Oster, L., and Mardor, I**.," Nanodosimetric kinetic model incorporating localized and delocalized recombination:Application to the prediction of the electron dose response of the peak 5a/5 ratio in the glow curve of LiF:Mg,Ti (TLD-100) "**. Radiat. Meas., 71, 226-231 (2014)

[3]. Eliyahu, I., Druzhyna, S., Horowitz, Y. and Oster, L., **Kinetic simulation of 5 eV optical excitation of irradiated LiF:Mg,Ti (TLD-100):Evidence for V_3/V_K participation leading to hole capture ,** Radiat. Meas., 90 , 27-32, (2016)

[4] Eliyahu, I., Horowitz, Y.S., Oster, L., Druzhyna, S., Biderman, S., and Reshes, G., **Kinetic simulations of optical absorption in LiF:Mg,Ti(TLD-100) following irradiations by ^{137}Cs gamma rays and photon bleaching at energies of 3.1 eV, 4.0 eV and 5.08 eV,** J. Lumin., 187, 313-321 (2017)

[5] Chen, R., and Pagonis, V., **Thermally and optically stimulated luminescence:A simulation response** , p.145, Wiley (2011),

Compensation Effect in Thermally Stimulated Luminescence Kinetics of Irradiated Widegap Materials

I.A. Weinstein, A.S. Vokhmintsev
NANOTECH Centre, Ural Federal University, Mira street, 19, Ekaterinburg, Russia
i.a.weinstein@urfu.ru

Highlights Experimental and theoretical regularities of the compensation effect observed are studied on the example of the analysis of thermally stimulated kinetics in the luminescence mechanisms of irradiated dosimetric materials.

Key words spectrally resolved thermoluminescence, compensation relation, isokinetic temperature, photoluminescence thermal quenching, first-, second- and general-order kinetics, Al_2O_3, hexagonal BN, AlN, activation energy, effective frequency factor

Background and Objectives The fundamental features and regularities of kinetic processes that take place in the temperature ranges of the thermoluminescence (TL) peaks govern the mechanisms of radiation-stimulated charge-carrier redistribution between capture and recombination levels in the forbidden band of widegap dosimetric crystals. An important role is also played by the temperature dependence of the efficiency of radiative transitions whose parameters depend on energy and thermodynamic states of a complex multi-trap system based on optically active centers of the intrinsic and impurity nature. We have previously analyzed the compensation effect in kinetics of the temperature quenching processes of photoluminescence, as well as the mechanisms of thermally stimulated luminescence of TLD-500 dosimetric crystals under conditions of the dominance of dynamic atomic disorder effects. The present work reports on the fundamental features of the compensation relationship between the parameters of various-order kinetic processes in the thermally stimulated luminescence of functional widegap media of solid-state dosimetry.

Materials and Methods The study utilizes original and independent experimental data on spectrally resolved thermally stimulated luminescence of irradiated (gamma, beta, UV, etc) oxygen-deficient alumina crystals (TLD-500), as well as of nominally pure widegap nitrides (AlN, h-BN) in various structural modifications. For conducting the numerical analysis of the TL curves measured, the known formalism of the first-, second-, and general-order kinetic processes was applied. To analyze the temperature dependencies of the photoluminescence in the materials mentioned above, we resorted to the Mott relation with a different number of channels of non-radiative relaxation of excitations.

Results and Discussion When studying the temperature quenching of photoluminescence in TLD-500, the compensation effect was observed associated with a consistent decrease in the

values of quenching activation energy and the pre-exponential factor as the time of UV irradiation of the crystals increased. The effect observable appears to be due to a change in the dynamic vibrational contribution to the total entropy of the crystal lattice. Based on the data obtained, the estimation of the isokinetic temperature was made: T_i = 384 K for F-centers and 394 K for F^+-centers. The resulting difference in the values of T_i is in agreement with the fact that, against T_m in the F–center TL emission band, T_m for the main TL peak of 450 K in the F^+–center emission band is shifted towards higher temperatures.

The TL mechanism of oxygen-deficient α–Al_2O_3 crystals reveals a compensating relationship between the activation energy during emptying traps and the corresponding effective frequency factors. The isokinetic temperature T_i = 442 K for the main peak is shown to be in good agreement with the maximum temperature T_m = 440 K at β-radiation doses above the threshold value. Similar compensating dependencies were also observed in the processes of TL of β-irradiated single crystals and AlN powders. With an increase in the storage time upon irradiation of the samples, the processes studied are found to obey the condition $T_m \rightarrow T_i$. For powders, the position of the maximum was shifted from 450 to 566 K, with T_i = 605 ± 10 K. For single crystals, T_m = 471 ÷ 496 K with T_i = 509 ± 10 K.

The performed formal analysis of the first-, second-, and general-order kinetics equations yields a formal relationship between the values of activation energy and the effective frequency factor, followed by examination using numerical simulation. The paper discusses possible applications of estimates of the isokinetic temperature T_i in the practice of solid-state luminescent dosimetry.

Conclusion

The experimentally and theoretically observed relationship within a simple compensation relation between the activation energy and the effective frequency factor determines the kinetics of thermally stimulated emission of irradiated widegap materials in different spectral bands. For a number of the irradiated oxides and nitrides, compensation relation parameters such as the isokinetic temperature T_i and the pre-exponential factor S_0 have been estimated. The compensation parameter S_0 is established to be not a constant, as it is presumed in the empirical relation; it depends on a heating rate, a temperature maximum of the TL peak, and others. The possible physical meaning of the isokinetic temperature and compensation constant have been interpreted taking into account a change in compositional entropy during thermally stimulated transformations of the thermodynamic state of a multi-trap system in irradiated solids.

Acknowledgments

The work was supported by Act 211 Government of the Russian Federation, contract № 02.A03.21.0006 and Minobrnauki initiative research project № 16.5186.2017/8.9.

Analysis of luminescence properties of electronics components in smart phones based on the trap interaction model

Kisoo Chung[1]*, Chang-Young Park[1], Jungil Lee[2], Jang-Lyul Kim[2], Hyoungtaek Kim[2], Michael Discher[3]

[1]*Gyeongsang National University, Department of Physics, Junju, Korea*

[2]*Korea Atomic Energy Research Institute, Yuseong, Daejeon, Korea*

[3]*University of Salzburg, Department of Geography and Geology, Salzburg, Austria*

Highlights Several kinds of luminescence from electric components of mobile devices induced by irradiation (RL), thermal stimulation (TL), optical stimulation (OSL) and their combinations (PTTL, TA-OSL etc.) were studied in both aspects of experimental and theoretical.

Key words RL, TL, OSL, PTTL, TA-OSL, dosimetry, glow curve deconvolution

Background and Objectives Luminescence properties of electrical components detached from the modern mobile devices such as smart phones have been paid attention for the purpose of dose retrieval in situation of radiation emergency[1)]. But, the luminescence mechanism has not been deeply understudied and still the research works are staying somewhat an empirical viewpoint. This is due to the complexity and the disorder of the substance material differs from the dosimetric material such as Al_2O_3:C. In this study, polycrystalline alumina substrates of surface mount register and capacitor in smart phones were measured under various stimulation sequence and analyzed with the deconvolution program based on the extended trap interaction model[2)].

Materials and Methods Versatile system[3)] was used for measuring the various kinds of luminescence. The system sequentially measured luminescence under the complex set of conditions such as radio-luminescence (RL), thermoluminescence (TL), optically stimulated luminescence (OSL) and their sequential or concurrent combinations (photo-transferred TL (PTTL), thermally assisted OSL(TA-OSL) etc.). Meanwhile, in order to identify luminescence mechanism from the glow data taken by the system were deconvoluted with computer program called as 'LumiAnal'. Which had been developed by our research group based on so called trap interaction model[4)]. This model permits not only the interchange of electrons through the conduction band also the interchange of holes through the valence band unlike ordinary trap interaction model. 'LumiAnal' is realization of the algorithm and can be adapted when three types of stimulations (RL, TL, OSL) are applied concurrently and/or sequentially.

Results and Discussion For the preliminary study, three kinds of stimulations were sequentially applied to an alumina substrate. X-ray (MAGNUM 50kV, 10W) for 100 ~ 1000 s

(RL mode), thermal stimulation from room temperature up to 400 °C (TL mode), optical stimulation with 470 nm blue LED (Luxeon V) for 50~150 s (OSL mode), and thermal stimulation after photon transferring with 470 nm LED up to 400 °C (PTTL mode) were applied sequentially. The experimental sequence was as follows; RL from alumina substrate by applying X-ray irradiation for 1000 s - TL with 5 °C/s - illumination and OSL with blue LED for 100 s on the temperature of 200 °C - PTTL with 5 °C/s[5]. The results are shown in Figure 1.

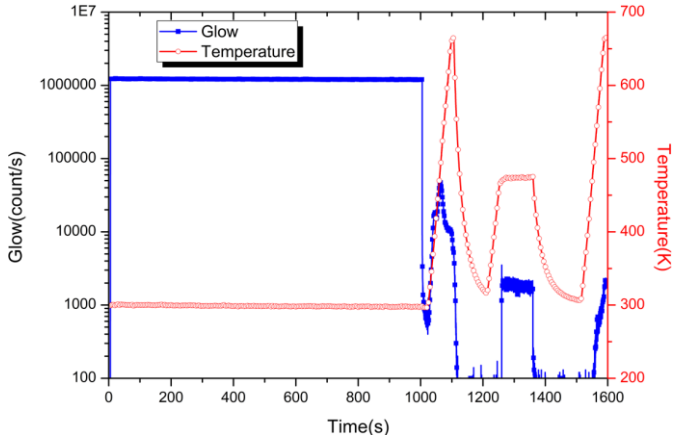

Figure 1: Sequential luminescence of RL-TL-OSL-PTTL from alumina substrate detached from a smart phone.

Conclusion The sequential glow curves of alumina substrates were reasonably deconvoluted with four main TL dosimetric traps (MDT; up to 400 °C) and more than one deep trap which can be stimulated by photon flux. The four MDTs have their activation energy of 0.55, 0.59, 0.75 and 0.83 eV, respectively.

References

1) Discher, M. and Woda, C., 2013. Thermoluminescence of glass display from mobile phones for retrospective and accident dosimetry, Radiat. Meas. 53-54, 12–21.
2) Chung, K.S. et al., 2012. A computer program for the deconvolution of the thermoluminescence glow curves by employing the interactive trap model, Radiat. Meas. 47, 766–769.
3) Park, C.Y. et al., 2018. An Integrated System for Radioluminescence, Thermoluminescence and Optically Stimulated Luminescence Measurements, J. Radiat. Protect. & Research. 43, 160-169.
4) Chung, K.S. et al., 2015. An algorithm for the integrated deconvolution of radioluminescence and thermally/optically stimulated luminescence glow curves, Radiat. Meas. 79, 7-12.
5) Bossin, L. et al., 2018. Phototransferred TL properties of alumina substrates, Radiat. Meas. 120, 41-46.

Luminescence properties of $LiGaO_2$ crystal and its potential application in dosimetry

L.Trinkler[1], A.Trukhin[1], J.Cipa[1], B.Berzina[1], V.Korsaks[1], Mitch M.C.Chou[2]
[1]Institute of Solid State Physics, University of Latvia, Riga, Latvia
[2] Center of Crystal Research, National Sun Yat-sen University, Kaohsiung, Taiwan

Highlights Photoluminescence and thermostimulated luminescence of $LiGaO_2$ crystal was studied in 10-500 K temperature region after UV irradiation. Luminescence mechanisms were elucidated. TL peak at 350 K and the corresponding emission spectrum in visible region makes $LiGaO_2$ potentially applicable as material for TL dosimetry.

Key words lithium metagallate; thermostimulated luminescence; photoluminescence

Background and Objectives Lithium metagallate $LiGaO_2$ (LGO) is a wide band (Eg ~ 6 eV) material [1], nowadays used as lattice-matched substrate for semiconductor epilayers. Taking into account its prospective properties, the application range could be much larger, including also dosimetry area. The task of the present study is elucidating of the luminescence mechanisms in nominally pure LGO crystal induced by irradiation with UV light and manifested in the processes of photoluminescence (PL) and thermally stimulated luminescence (TL), as well as estimation of its potential application in TL dosimetry.

Materials and Methods LGO has a wurtzite-derived structure. Belonging to the space group $Pna2_1$ determines polarity along the c axis. LGO samples (10x10x1 mm) were cut off the large β $LiGaO_2$ crystal. In PL and TL measurements a deuterium lamp conjugated with a monochromator or an ArF pulsed laser 193 nm were used as UV light sources. Luminescence light was detected through a spectrophotometer by a CCD camera or by a photomultiplier tube. Luminescence kinetics were measured using an oscillograph and a PMT. PL and TL measurements were done in 10-300 K, 60-400 K, 290-600 K temperature ranges.

Results and Discussion PL emission spectrum consists of several main luminescence bands: 280 nm (4.4 eV), 340 nm (3.65 eV), 540 (2.3 eV) and 700 nm (1.77 eV). The 280 nm emission band is excited in an exciton band peaking at 206 nm (6.0 eV) and in the band-to-band region (> 6 eV), other emission bands have their own excitation bands in the energy gap region, besides all of them are excited also in the band-to-band region [2].
The complex study of dependence of spectral properties on intensity of the excitation light

and kinetic measurements allowed conclusion that all PL emission bands of LGO are due to donor-acceptor pair (DAP) recombination. Presumption about the atomistic nature of the DAPs causing the 280 and 340 nm bands: Ga-O and Li_i-O, correspondingly, is based on comparison with the PL of Al_2O_3 doped with Ga and Li [3].

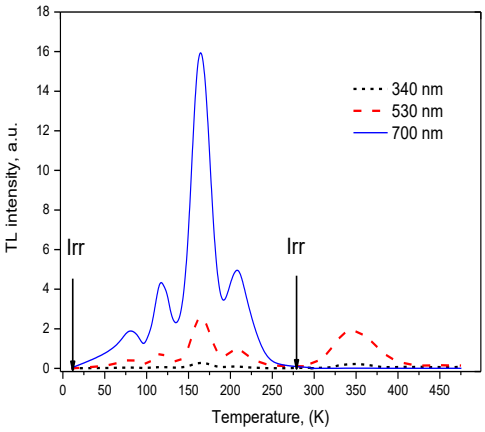

Fig.1. TL curve of $LiGaO_2$ after irradiation with 193 nm laser at 10 and 290 K for 20 min.

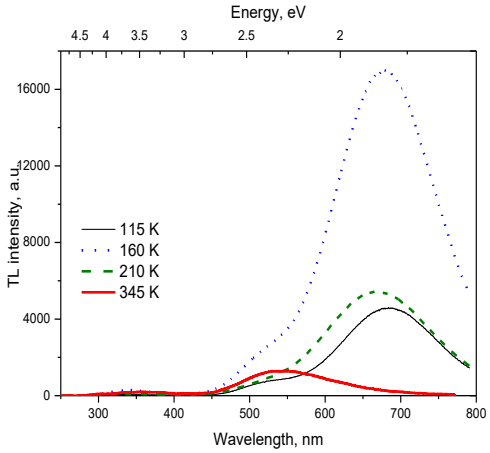

Fig.2. TL emission spectra in different TL peaks after irradiation with 193 nm laser.

TL response of LGO is produced after irradiation with X-rays and UV light. The main attention was devoted to the UV light induced TL process, selecting the excitation wavelengths from the band-to-band region and particular PL excitation bands. For all irradiation wavelengths the TL curve contains peaks at 70, 120, 170, 210 and 350 K (Fig.1). TL emission spectrum contains the same bands, which are observed in the PL: 340, 540 and 700 nm (Fig.2); their relative yield depends on irradiation wavelength and temperature.

Conclusion We have studied luminescence properties of $LiGaO_2$ crystal and elucidated luminescence mechanisms. TL studies are in progress, however even now it is clear that TL peak at 350 K and the corresponding emission spectrum in visible region makes $LiGaO_2$ potentially applicable as material for TL dosimetry.

References

1) S. Tumėnas, P. Mackonis, et al., Applied surface science, 421 (2017) 837.
2) L.Trinkler, A.Trukhin, et al., Optical materials, 69 (2017) 449.
3) L.Trinkler, A.Trukhnin, M.M.C.Chou, Latv. J. Phys. Techn. Scienc, 6 (2018) 4.

Acknowledgement The present research has been sponsored by the Latvian Council of Science, Grant No. lzp-2018/1-0361.

Comparison of the Optical Absorption and Thermoluminescence in LiF:Mg,TI (TLD-100) following irradiation by high energy protons and $^{90}Sr/^{90}Y$ beta rays

G. Reshes[1] , I. Eliyahu [2] , L. Oster[1], Y.S. Horowitz [3]; S. Biderman[1], D. Sibony[1,3], G. Amit[2] , D. Ginsburg[3] , P. Olko[4], P. Bilski[4], J. Swakon[4], T.Horwacik[4]

[1]*Sami Shamoon College of Engineering, Beer Sheva, Israel*
[2]*Soreq Nuclear Research Center, Yavneh Israel*
[3]*Ben Gurion University of the Negev, Beer Sheva*
[4]*Institute of Nuclear Physics, Polish Academy of Sciences, Krakow, Poland*

Key words Optical absorption, TL, proton and beta irradiation, LiF:Mg,Ti

Background and Objectives Proton radiotherapy is an emerging technique of increasing popularity [1,2] . Since LiF:Mg,Ti (TLD-100) thermoluminescence (TL) is one of the applicable dosimetric techniques an understanding of the similarities and differences in the radiation induced physical mechanisms following proton (heavy charged particle-HCPs) and beta/gamma irradiation is obligatory since HCPs can alter the radiation induced mechanisms due to enhanced defect creation. In this research we report on the optical absorption (OA) characteristics of TLD-100 samples following both beta ray and 20-, 40- and 58 MeV proton irradiation.

Methods, Results and Discussion The optical density is a measure of the concentration of the various electron traps following irradiation and sets the stage for the creation of the TL glow curve upon thermal excitation. Figures 1 and 2 show the OA energy spectrum following irradiation by beta rays and 20 MeV protons.

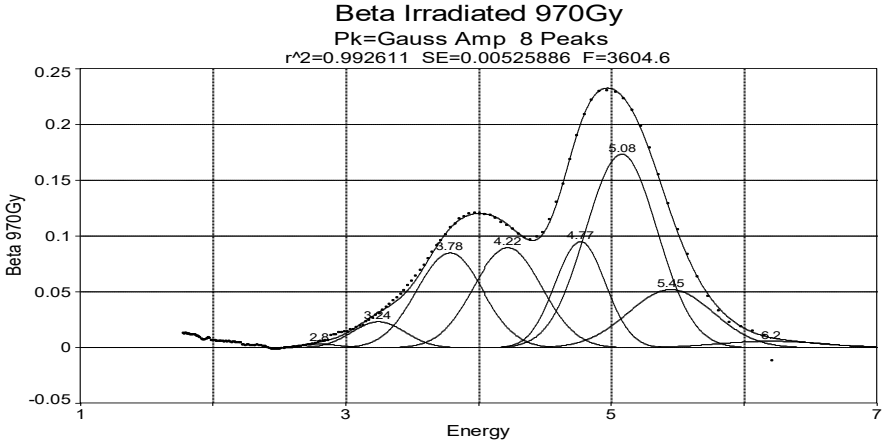

Figure 1. OA energy spectrum following beta irradiation to 970 Gy.

Inspection of the two spectra reveal that the same major OA bands are observed for both irradiations. The 3.8 and 4.3 OA bands are those correlated with the trapping centers (TCs) giving rise to TL composite peak 5 and it is comforting to note that their relative strengths and the absolute value of the OD per Gy are identical in the two spectra within a few %. The major difference between the two spectra is in the OD of the F band at 5.08 eV; (0.17

and 0.30 following beta and proton irradiation respectively. The increased OD of the F band is expected and is due to the creation of vacancies in the samples by the radiation [3]. On the other hand, the 35% higher OD of the 5.45 eV band following proton irradiation is somewhat of a surprise. The TC associated with this OA band is the competitor to peak 5 TL so its increased OD could be relevant to the simulation of the dose response following proton irradiation. An alternative explanation lies in the possibility that the created vacancies following proton irradiation are somewhat different from those initially present in the sample leading to an increase in the width of the F band. An increased width of the F band would lead to a decreased OD of the 5.45 eV OA band. This possibility requires further investigation by a renewed analysis of the data in ref. [3].

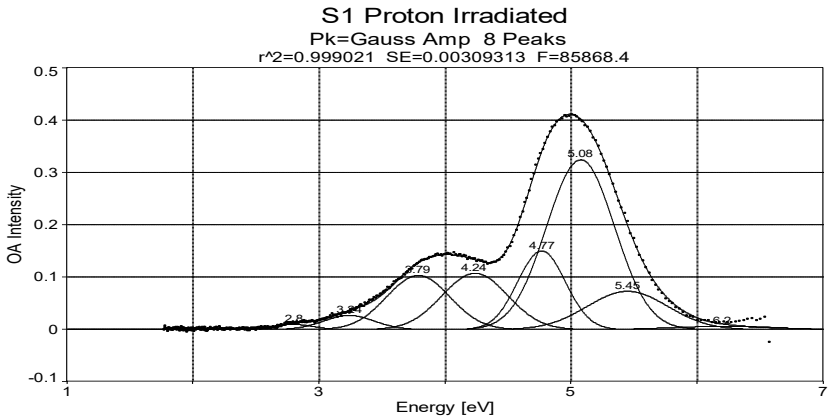

Figure 2. OA energy spectra following 20 MeV proton irradiation to a level of dose of 1124 Gy.

It is further interesting to note that in the TL glow curves the ratio of peak 5a to peak 5 is slightly higher (1.29 ± 0.13) for the 20 MeV protons at 0.164 ± 0.01 (1 SD) compared to 0.127 ± 0.008 (1 SD). This difference is consistent with the understanding that peak 5a (formed from an electron –hole (e-h) configuration is more likely to be formed following by the protons due to the higher ionization density. The effect is not observed for peak 4 which is formed by a hole-only configuration (single charge carrier). It is somewhat disappointing that the increased population of the e-h configuration is not observed as a change in the relative strengths of the 3.8 eV and 4.3 eV bands which might have revealed clues as to their identity (e-only vis-a-vis e-h). It may be that the increased relative intensity of peak 5a is due to charge transfer during heating.

References

1) L.Stolarczyk, T.Cywicka-Jakiel, T. Horwacik, P. Olko, J. Swakon and M.P.R. Waligorski, Evaluation of risk of secondary cancer occurrence after proton radiotherapy of ocular tumours, Radiat. Meas., 1944-1947 (2011).
2) B. Mukherjee, C. Fuentes and J. Lambert, Out-of-field dosimetry and 2nd cancer risk assessment of child patients under proton therapy using a tLD based microdosimter, Radiat. Meas., 106, 336-340 (2017).
3) I. Eliyahu, Y.S. Horowitz, L. Oster, I. Mardor, S. Druzhyna, and S. Biderman, Kinetic modeling of Fluorine vacancy/F center creation in LiF:Mg,Ti including vacancy interstitial recombination:evaluating the factors leading to the lack of supralinearity in the optical absorption F center concentration dose response, Nucl. Instrum. Meth., B343, 15-25 (2015).

Optical and thermoluminescence properties of thulium doped $KMgF_3$ polycrystal

Lituania Pérez Cruz[1,2*], Epifanio Cruz Zaragoza[1], David Díaz[2], Enrique Camarillo García[3], José Manuel Hernández Alcántara[3], and Héctor Octavio Murrieta Sanchez[3]

[1]*Instituto de Ciencias Nucleares, Universidad Nacional Autónoma de México, A.P. 70543, 04510 Ciudad de México, México*

[2]*Posgrado en Ciencias Químicas, Facultad de Química, UNAM, Ciudad Universitaria, Av. Universidad 3000, 04510 Ciudad de México, México*

[3]*Instituto de Física, Universidad Nacional Autónoma de México, A.P. 20364, 01000 Ciudad de México, México*

Highlights Ionizing radiation induced color centers in $KMgF_3$:Tm fluoroperovskite. UV and blue emission from thulium doped-polycrystal was observed. $KMgF_3$:Tm [1 mol %] displays several thermoluminescent (TL) peaks in an aceptable temperature range suitable for ionizing radiation dosimetry.

Key words Perovskite, $KMgF_3$:Tm, F centers, thermoluminescence, emission

Background and Objectives $KMgF_3$:Tm phosphor was recently studied as a new material for Optically Stimulated Luminescence dosimeter [1]. Following the investigation on this phosphor material like a dosimeter, polycrystals samples were characterized by XRD. Their absorption, emission and TL properties under gamma and beta radiation were investigated to identify the dopant ion participation. The correlation between F centers and the glow curves at different gamma doses was analyzed. The TL response of $KMgF_3$:Tm as a function of the beta and gamma dose, reproducibility and fading of their signals were obtained.

Materials and Methods Fluoroperovskite powder samples were synthesized by solid-state reaction of equimolar amounts of KF, MgF_2 and TmF_3 impurity. Polycrystals were grown by the recrystallization process from powder samples. Phase and crystallinity of the material were analyzed by Powder X-Ray Diffraction using a Brüker Phase Diffractometer. Absorption spectra were measurement with a Cary 5000 Varian spectrophotometer with double-beam as direct absorption. Photoluminescence spectra were recorded using a Spectrofluorometer FluroMax-4 of Horiba Scientific with a continuous Xenon light source.
Thermoluminescence measurements were performed under a nitrogen atmosphere with a

Harshaw 3000 TLD system using a linear heating rate of 2 °C/s. The polycrystals were expose to $^{90}Sr/^{90}Y$ beta source and with gamma radiation using a ^{60}Co Gammabeam 651PT Nordion irradiator. Optical absorption and emission spectra were carried out on polished polycrystals with 1.5x4x6 mm size.

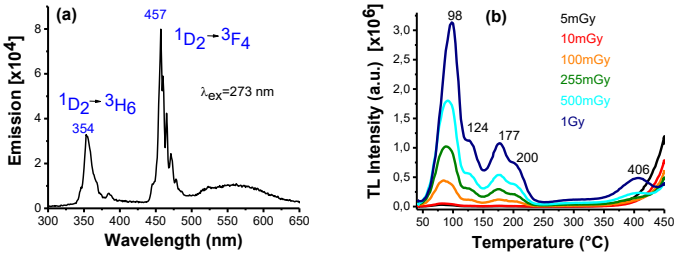

Figure 1. (a) Emission spectrum of $KMgF_3$:Tm [1.0 mol %] polycrystal irradiated at 5 kGy with gammas of ^{60}Co, (b) glow curves using beta radiation from $^{90}Sr/^{90}Y$.

Results and Discussion The F, F_2 and F_3 color centers were generated by ionizing radiation in the $KMgF_3$:Tm [1.0 mol %] phosphor, this fact is more evident at higher doses of gamma radiation (>100 Gy). It seems that the color centers mainly and thulium dopant emissions at 457 nm ($^1D_2 \rightarrow {}^3F_4$) and 354 nm ($^1D_2 \rightarrow {}^3H_4$) (Figure 1a), contribute to the TL glow curve. The F band at 273 nm on the optical absorption spectra is the most stable color center in this fluoroperovskite phosphor. The TL glow curve was formed by five peaks and that the TL peak at higher temperature ($T_{max\sim}$ 419 °C) is probably due to the thulium impurity. The TL response of $KMgF_3$:Tm as a function of the beta and gamma doses were analyzed between 0.05-1 Gy (Figure 1b) and 0.1-10 kGy, respectively, in the first case a linear response over that dose range was observed.

The presence of thulium gave more stability to the glow curve respect to the undoped fluoroperovskite, that was improved in their reproducibility (SD = 0.135) signal. Post-irradiation heat treatment to the first peak at 83°C of the glow curves can reduce the shallow traps signal contribution and a significant improvement in the TL fading was obtained.

Conclusion $KMgF_3$:Tm phosphor was synthesized and it characterized by XRD. The absorption and emission spectra suggest that the thulium impurity and F centers contribute to forming the glow curve. The TL analysis showed that $KMgF_3$:Tm phosphor polycrystal is suitable for radiation dosimetry at low doses.

References

1) Luis Camargo, Lituania Pérez Cruz, Epifanio Cruz-Zaragoza, Segundo Martínez Ovalle and Julián Marcazzó, 2018. OSL properties of $KMgF_3:Tm^{3+}$ for dosimetric applications as OSL dosimeter. Applied Radiation and Isotopes 141, 219-223.

F- and F^+-band radioluminescence and the influence of annealing on its emission spectra in Al_2O_3:C,Mg

M.L. Chithambo, J. M. Kalita, A. Finch[1]

Department of Physics and Electronics, Rhodes University, Grahamstown, South Africa

[1]Department of Earth & Environmental Sciences, University of St Andrews, Irvine Building, St Andrews, Fife, KY16 9AL, UK

Highlights The F and F^+ bands associated with radioluminescence in Al_2O_3:C,Mg are affected by thermal quenching but the behaviour for the F^+ band depends on prior annealing.

Key words radioluminescence, Al_2O_3:C,Mg, emission bands, annealing

Background and Objectives Radioluminescence spectra of aluminium oxide co-doped with carbon and magnesium (Al_2O_3:C,Mg), the subject of this study, is seen to consist of emission bands near 330, 410 and 700 nm. Under optical stimulation, the bands at 330 and 410 nm stand out [1] whereas under thermoluminescence, the discernible bands are near 325, 410 and 485 nm [2]. When α-Al_2O_3 is co-doped by C and Mg, the supposed replacement of Al by Mg induces a number of electron centres some of which are linked to the said bands. The canonical forms of these defects are oxygen vacancies aggregated with Mg^{2+}, namely, F^+(Mg) or a combination of two F^+(Mg)-centres, that is, F_2^{2+}(2Mg) or the F^{2+}(2Mg), a product of dissociation of F_2^{2+}(2Mg)-centres [3]. Stimulated luminescence emitted near 410 nm is attributed to intra-centre transitions at an F centre following electron capture at an F^+ defect, whereas hole capture at an F centre or, equivalently, electron capture at an α centre accounts for the emission at 330 nm. Systematic investigation of the F^+ band under stimulated emission is hampered by its transience. The aim of this study is to side-step this limitation by exploiting prompt emission under radioluminescence. We report the effect of measurement and annealing temperature on the F^+ and F band emissions in Al_2O_3:C,Mg.

Materials and Methods Samples used were α-Al_2O_3:C,Mg parallelepipeds of size 8 x 4 x 0.5 mm (Landauer Inc., USA). Sample were annealed at 600, 700, 900 and 1200°C for 15 min or used *as received*. Radioluminescence was measured in vacuum either at room temperature or under heating to 400°C using a high sensitivity luminescence spectrometer [4]. Samples were X-ray irradiated *in-situ* using a Philips MCN-101 X-ray tube at a rate of 1.8 Gy min^{-1}. The luminescence was detected over the wavelength range of 250 to 850 nm.

Results and Discussion The radioluminescence of Al_2O_3:C,Mg shows emission bands near

330, 420 and 700 nm. The intensity of the bands is affected by annealing temperature as noted in measurements made between 30 and 400ºC. In Al_2O_3:C,Mg annealed at 1200ºC, the radioluminescence intensity of the 420 nm band changes little between 30 and 150ºC but decreases consistently thereafter up to 260ºC in a manner consistent with thermal quenching (Figure 1(a)). Results for the same band from samples annealed at 600ºC and those from unannealed samples show similar behaviour. The dependence of the F^+ band on measurement temperature depends on the annealing temperature. The F^+ band is independent of measurement temperature in Al_2O_3:C,Mg annealed at 600ºC but not when the sample is annealed at 1200ºC where the change for the F^+ emission resembles that shown in Figure 1(b) for the unannealed material.

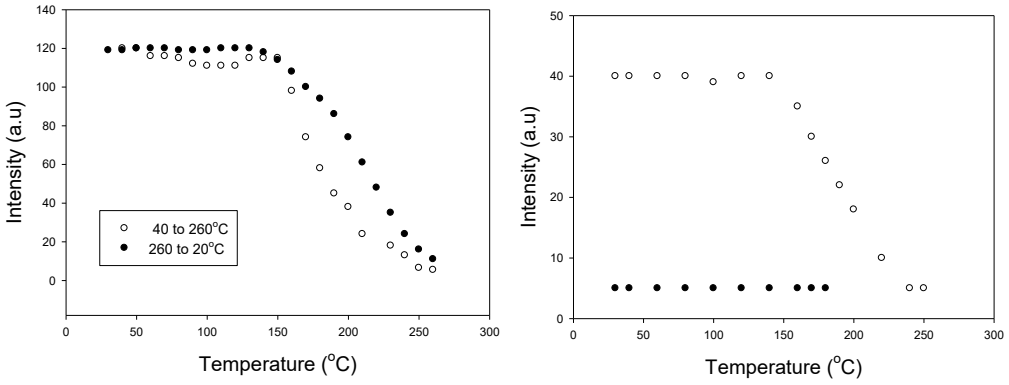

(a) (b)

Figure 1. The temperature dependence of the 420 nm radioluminescence in Al_2O_3:C,Mg annealed at 1200ºC (a) and of the 330 nm band (solid circles) and the 420 nm band (open circles) in Al_2O_3:C,Mg annealed at 600ºC (b).

Conclusion The radioluminescence emission band at 420 nm is affected by thermal quenching regardless of prior annealing whereas the temperature dependence of F^+ radioluminescence depends on prior annealing. The defect dissociations involved in these processes will be discussed.

References

1) Denis, G., Rodriguez, M.G., Akselrod, M.S., Underwood, T.H., Yukihara, E.G., 2011. *Radiat. Meas.* 46, 1457-1461.
2) Kalita, J., Chithambo, M.L., 2018. *J. Lumin.* 196, 195-200.
3) Akselrod, M.S., Akselrod, A.E., Orlov, S.S., Sanyal, S., Underwood, T.H., 2003. *J. Fluores*. 13, 503–511.
4) Luff, B.J., Townsend, P.D., 1993. *Meas. Sci. Technol*. 4, 65-71.

Excitation density effects on the scintillation properties of $CdWO_4$

Masanori Koshimizu[1]*, Satoshi Kurashima[2], Atsushi Kimura[2], Mitsumasa Taguchi[2], Takayuki Yanagida[3], Yutaka Fujimoto[1], Keisuke Asai[1]

[1]*Department of Applied Chemistry, Tohoku University, Sendai, Japan*

[2]*National Institutes for Quantum and Radiological Science and Technology, Takasaki, Japan*

[3]*Nara Institute of Science and Technology, Ikoma, Japan*

Highlights We recorded the scintillation temporal profiles of $CdWO_4$ under different linear energy transfers (LETs). The LET dependence was analyzed from the viewpoint of quenching due to excited state interaction.

Keywords linear energy transfer (LET), scintillation temporal profile, excited state interaction, cadmium tungstate

Background and Objectives It has long been known that the responses of scintillators depend strongly on linear energy transfer (LET), which is an important factor in the detection of heavy charged particles. This LET-dependent response was formulated more than fifty years ago by Birks [1], although the formulation was a phenomenological one focusing only on the scintillation efficiency or light yield. To elucidate the basic process of the excited state dynamics responsible for this LET-dependent response, analysis of the dynamical aspect is necessary.

Recently, we analyzed these dynamics using LET-dependent scintillation temporal profiles, which were obtained using pulsed ion beams [2]. For scintillators that contain rare-earth ions as luminescence centers, LET-dependent energy transfer processes or competition with quenching due to excited state interaction have been inferred from the LET-dependent rise in the temporal profiles [3–5]. In contrast, in a self-activated scintillator ($Bi_4Ge_3O_{12}$), quenching due to the excited state interaction plays an important role in both the formation and decay of the excited states [6], which may be common to other self-activated scintillators. To verify this hypothesis, in this study, we analyzed the LET-dependent scintillation properties of another self-activated scintillator, $CdWO_4$ (CWO).

Materials and Methods Scintillation temporal profiles were obtained using pulsed beams of 20 MeV H^+, 50 MeV He^{2+}, and 130 MeV C^{5+}. Heavier ions deposit energy at high LETs under the experimental conditions used in this study. The scintillation from CWO was detected using a photomultiplier tube, and the detection signals were averaged and recorded as scintillation temporal profiles using a digital oscilloscope.

Results and Discussion Figure 1 shows the rise and decay parts of the scintillation temporal profiles of CWO. The rise and decay were faster at higher LETs. This LET-dependent behavior can be explained in terms of quenching due to excited state interaction, because the scintillation light yield decreased with an increase in the LET. The rise and decay parts correspond to the formation and radiative decay of the excited states prior to the scintillation, respectively. Hence, the observed LET-dependent temporal scintillation profiles can be explained in terms of the competition between the quenching due to excited state interaction and the formation or radiative decay of the excited states.

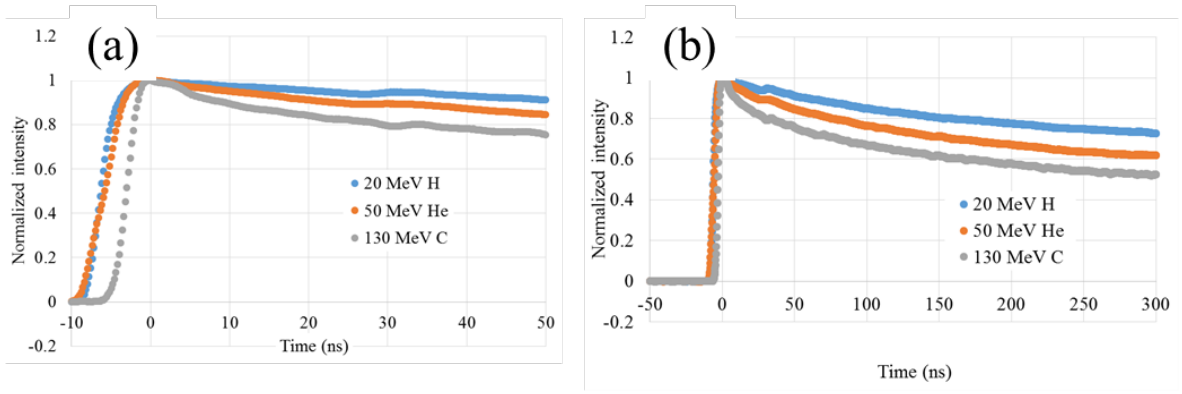

Figure 1. (a) Rise and (b) decay parts of scintillation temporal profiles of CWO under irradiations of pulsed beams of 20 MeV H^{+}, 50 MeV He^{2+}, and 130 MeV C^{5+}.

Conclusion The quenching due to excited state interaction plays an important role in both the formation and decay of the excited states in CWO.

References

1) J. B. Birks, “The Theory and Practice of Scintillation Counting”, Pergamon, New York (1964).
2) M. Koshimizu, et al., Rev. Sci. Instrum., 86 (2015) 013101.
3) T. Yanagida, et al., Nucl. Instrum. Methods Phys. Res. B, 365 (2015) 529.
4) M. Koshimizu, et al., J. Lumin., 169 (2016) 678.
5) T. Yanagida, et al., Nucl. Instrum. Methods Phys. Res. B, 409 (2017) 27.
6) M. Koshimizu, et al., Nucl. Instrum. Methods Phys. Res. B, 409 (2017) 19.

Luminescence of non-bridging hole centers as a marker of particle irradiation of α-quartz

L. Skuja[1], N. Ollier[2]*, K. Kajihara[3]

[1]*Institute of Solid State Physics, University of Latvia, 8 Kengaraga str., LV1063, Riga, Latvia*

[2]*Laboratoire des Solides Irradiés CEA-CNRS Ecole Polytechnique, 91128 Palaiseau, France*

[3]*Department of Applied Chemistry for Environment, Graduate School of Urban Environmental Sciences, Tokyo Metropolitan University, 1-1 Minami-Osawa, Hachioji, Tokyo 192-0397, Japan*

Highlights Oxygen dangling bonds ("non-bridging oxygen hole centers", NBOHCs), are peculiar to amorphous state of SiO_2 and cannot be induced in α-quartz by purely ionizing irradiation. Their presence in quartz normally is an indication of particle-induced damage. Here were detected NBOHCs for the first time in high-dose electron-irradiated α-quartz crystal. Their presence may signal the formation of nucleation centers in crystal structure as the first step to radiation-induced amorphization just below the amorphization threshold.

Key words: point defects, PL, electron irradiation, NBOHC, silica, quartz

Background and Objectives

Silica is omnipresent in nature being a constituent of the earth mantle. SiO_2, often in the form of crystalline quartz is therefore important in dosimetric dating in geology. Luminescent radiation-induced defects in quartz are of interest in this aspect. On the other hand, silica-based glasses provide the backbone of many of today's rapidly expanding photonics applications, which serve diverse fields such as optical communications, electronics, sensor technologies, medicine, and materials processing. Point defects in silica, created during the manufacturing or by irradiation are detrimental for most applications and have been extensively studied.

Among multiple point defects which are known in SiO_2, there are several types, which occur *only* in amorphous state. They are usually of "dangling bond" type, which exist on the internal surfaces of nanosized voids, present in amorphous SiO_2, and absent in quartz. Defects of this type cannot be induced in α-quartz by purely ionizing irradiation (e.g., γ-rays), capable of creating only separate Frenkel defects (vacancies-interstitials). Thus the presence of dangling bond defects in crystalline SiO_2 indicates that a stronger damage by particle (neutrons, ions) irradiation has occurred.

The most generic and widespread dangling bond-type defect in amorphous SiO_2 is NBOHC. It has a red photoluminescence (PL) band at 1.9 eV. It is absent in γ-irradiated α-quartz, however,

present in neutron-irradiated quartz [1]. Recently we observed the onset of this PL in quartz crystals, exposed to high-dose electron irradiation close to the amorphization threshold [2]. The purpose of this work is to check the spectroscopic parameters of NBOHC PL in quartz and to evaluate the applicability of this PL for dosimetric purposes.

Materials and Methods

High purity synthetic α-quartz samples (Asahi Glass/Tokyo Denpa) were irradiated by 2.5 MeV electrons using SIRIUS Pelletron linear accelerator (LSI) with fluences between 1.2×10^{18} and 3.0×10^{19} e^-/cm^2, electron flux 5.5×10^{13} $e–/(cm^2$ s) (dose rate 51 MGy/h) and sample temperature 60 °C. They were compared to α-quartz crystal irradiated by 1×10^{19} fast (E>1 MeV) neutrons/cm^2 and to γ-irradiated crystals and glasses. PL and Raman spectra and PL kinetics were measured at T between 295 K and 14 K.

Results and Discussion

In previous studies, a near-resonance excitation in the 2 eV region was used to detect the PL of NBOHCs. This required high-resolution spectrometers and may be less useful for practical applications (e.g., dosimetry). Here we report the detection of NBOHC's in e-irradiated and n-irradiated α-quartz under excitation by 4th harmonic of Nd-YAG laser (266 nm). In this case the NBOHC PL emission can be separated from excitation by a simple long-pass filter. It was observed both in e- and n-irradiated crystals with similar PL decay constants in the range of ~10 μs. Differently from the case of NBOHCs in silica glass, a strong increase of PL at low T was observed (×80, ×14 and ×5 in e-irradiated, n-irradiated quartz and glass, respectively). The UV- excited PL showed the characteristic narrow vibrational structures in e-irradiated quartz, broadened ones in n-irradiated quartz and they were absent in SiO_2 glass.

A broadening of the NBOHC emission band was also observed in densified irradiated silica glass inferring the presence of an additional component around 2.18 eV [3].

Conclusion

266 nm excited luminescence of oxygen dangling bonds (NBOHC) in can serve for detecting of particle irradiation dose of α-quartz.

References

[1] L. Skuja, K. Kajihara, M. Hirano, H. Hosono, Nucl. Instr. and Meth. Phys, Res. B286 (2012) 159–168.

[2] L. Skuja, N. Ollier, K. Kajihara, K. Smits, J. Non-Crystalline Solids, 505 (2019) 252–259.

[3] N. Ollier, K. Piven, C. Martinet, T. Billotte, V. Martinez, D.R. Neuville, M. Lancry, Journal of Non-Crystalline Solids. 476 (2017) 81–86.

The peculiarities of F center photoluminescence kinetics in anion-deficient corundum in the 200-700 K temperature range

Rinat Abashev[1,2*], Alexander Surdo[1,2], Igor Milman[1,2]
[1]*Institute of Metal Physics UB RAS, Ekaterinburg, Russia*
[2]*Department of Experimental Physics, Ural Federal University, Ekaterinburg, Russia*

Highlights Specific changes have been discovered in the photoluminescence kinetics of F centers in anion-deficient corundum crystals over the temperature range of 200-700 K. In the intervals $290 \le T_{meas} \le 370$ K and $420 \le T_{meas} \le 700$ K, the fast component τ_{fast} equal to the F center lifetime in excited state τ_F has a slow component with τ_{slow} occurring alongside it. The contribution of the slow component and its time constant are maximal at the beginning and minimal at the end of each of these intervals.

Key words Anion-defective corundum, F center photoluminescence (PL), PL decay kinetics in F-centers, thermoluminescence

Background and Objectives A study [1,2)] of F center luminescent properties in anion-deficient corundum (α-$Al_2O_{3-\delta}$) crystals over a temperature range of 4-550 K has revealed significant temperature-dependent changes in the photoluminescence (PL) decay kinetics of these centers. Along with the frequently mentioned component with the time constant τ_F=36 ms at T=4-350 K characterizing F center lifetime in excited state, a slower component with τ_{slow} =50-170 ms was discovered. In [1)] it was revealed at T=4-40 K and was associated with the presence of two excited triplet states in the F center. In [2)], the slow component was not detectable in the kinetics, and its contribution to the PL yield in the range 300-550 K was estimated by the almost-constant offset in the 100 ms time window. The emergence of the slow component in [2)] was due to phosphorescence caused by F center photoionization with subsequent capture and release of electrons from traps responsible for the 310 and 450 K thermoluminescence (TL) peaks. The objective of this study was, therefore, to investigate systematically PL decay kinetics in F centers in α-$Al_2O_{3-\delta}$ samples over expanded time and temperature ranges, compare them with TL data and present a mathematical and physical model of these processes.

Materials and Methods As objects of the study, we chose anion-deficient crystals of corundum (α-$Al_2O_{3-\delta}$). The PL spectra and PL decay kinetics were studied using a Cary Eclipse spectrofluorimeter. The PL decay kinetics in F centers were studied under excitation

by radiation with $h\nu_{ex}$=5.9 eV over a temperature range of 80-700 K and time interval of 0-1 s with a maximum resolution of 0.1 ms.

Results and Discussion Figure 1 shows temperature-dependent changes in the fast and slow components of F center PL decay kinetics for $h\nu_{em}$=3.0 eV and $h\nu_{ex}$=5.9 eV (curves 1-3). For comparison purposes, we imposed on it a TL curve (curve 4) measured at a heating rate of β=0.3 K/s, which is about equal to the average stepwise heating rate in F center PL decay kinetics studying. As can be seen from it, the fast component with $\tau_{fast}=\tau_F$ is constant over T_{meas}=225-380 K, then it starts reducing at $T_{meas}\geq$380 K and reaches zero at T_{meas}=510 K (curve 1). One of the slow components in the kinetics starts manifesting itself as a pedestal on the low-temperature side of the main peak (curve 2). Rough estimation of τ_{slow} in this area at, for example, T_{meas}=410 K provides a value of ~10±7 s. At T_{meas}=430 K peak maximum and on its high-temperature side, the value of τ_{slow} gets stable, being ~1.7±0.3 s. Further on, as T_{meas} is increased to 650 K, i.e. immediately before the electron-type TL peak at 720 K, the value of τ_{slow} goes down to zero. A similar behavior of the dependence $\tau_{slow}(T_{meas})$ is observed between the low-temperature peak at 260 K and the main peak in the region 290-370 K (curve 3), which are also of electron type.

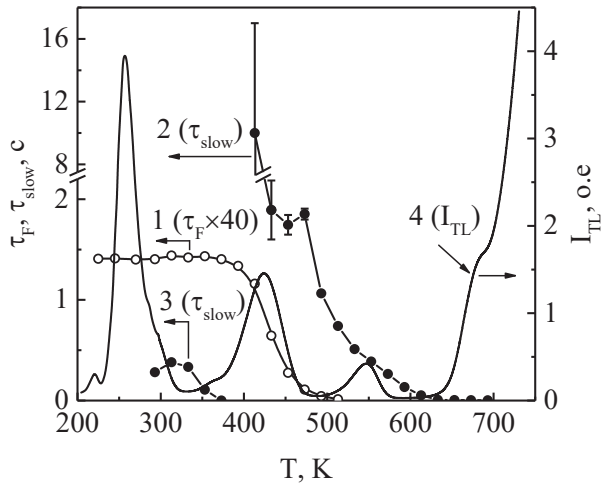

Figure 1 – The temperature dependence of the fast $\tau_{fast}=\tau_F$ (1) and slow τ_{slow} (2, 3) PL components in F centers for $h\nu_{em}$=3.0 eV and $h\nu_{ex}$=5.9 eV in an α-$Al_2O_{3-\delta}$ sample, and the TL curve measured at β=0.3 K/s (3)

Conclusion The reported pattern manifesting itself as certain stabilization of $\tau_{slow}(T_{meas})$ in the high-temperature parts of the 260 K and 430 K peaks suggests that a certain dynamic equilibrium occurs between the emptying and filling of corresponding traps. The data show that the equilibrium under discussion is upset towards the filling of corresponding electron-type peaks in the low-temperature parts as well as between such peaks, which is supported by the proposed mathematical and physical models.

References

1) Brewer J.D., et al. 1980. Phys. Rev. B. 22. I. 10. P. 4900-4906.
2) Akselrod M.S., et al. 1998. J. Appl. Phys. V. 84. P. 3364–3373.

Simulation of thermoluminescence dose response in cluster systems with deep traps

S.V. Nikiforov [1], A.S. Merezhnikov[1], V. Pagonis[2]
[1] *Ural Federal University, Ekaterinburg, Russian Federation*
[2] *Physics Department, McDaniel College, Westminster, USA*

Highlights

An improved Monte Carlo method for calculating TL in a cluster system is proposed.
New cluster TL model with deep electron trap is analyzed by Monte Carlo method.
TL dose dependencies are simulated for the first time in a cluster system.
The heating rate effect on superlinearity of TL dose response was found using the model under study.

Key words Thermoluminescence kinetics; Cluster system; Monte Carlo method; Deep traps; TL dose response

Background and Objectives Nonlinear dose dependences of thermoluminescence (TL) are found in a number of luminescent materials. Theoretically, dose response is studied in the framework of TL kinetic models, which simulate the process of charge transfer between different energy states. One of the promising fields is the simulation of the charge transfer process in cluster systems [1,2]. In such systems, the influence of deep traps in the clusters on the nonlinearity of TL dose response has not been studied.
The aim of this work is to simulate the TL dose response in a system with clusters containing both TL-active and deep traps.

Materials and Methods We have considered a new cluster TL model, consisting of luminescence centers and clusters of defects, including TL-active and deep electron traps. In order to obtain the dose dependences of the TL output, the irradiation, relaxation, and heating stages were simulated. TL curves were calculated using the Monte Carlo method [1]. In this paper, the calculation algorithm was significantly optimized by reducing the required amount of random number generations.

Results and Discussion The TL dose dependences were studied at different heating rates with initially unfilled deep traps (fig.1). As shown in the figure, at relatively low doses, the TL output increases linearly. At high doses, the region of superlinearity is observed to change into

saturation. An important feature of TL dose response, is the dependence of the TL output and superlinearity value on the heating rate. This phenomenon is directly related to the presence of cluster defects in the system, In this case, with an increase in the heating rate, the nonlinearity of the dose response decreases, and the TL output increases at low doses. In addition, the influence of various model parameters on the shape of TL dose dependences, and in particular on the linearity range, are discussed in the paper.

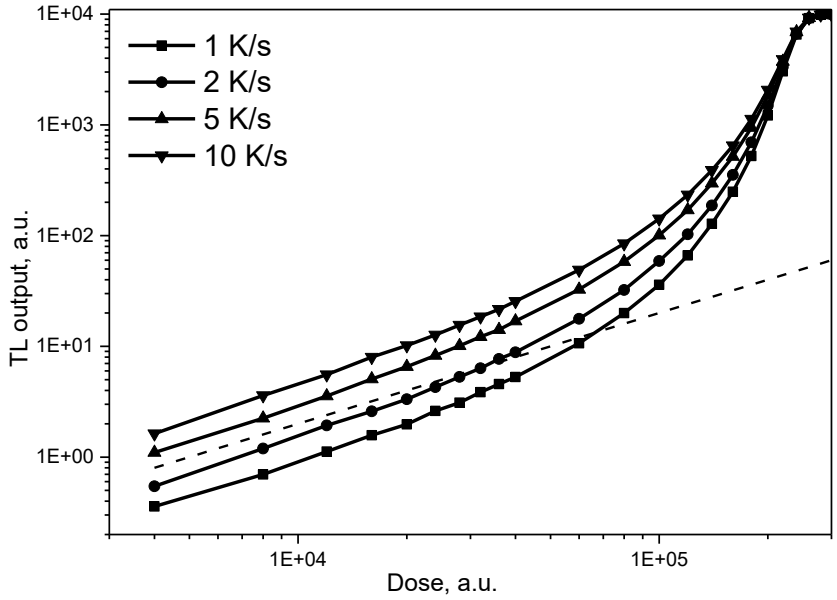

Figure 1. TL dose dependencies calculated at different heating rates. The dotted line corresponds to the linear dependence

Conclusion In the present paper, the simulation of the TL dose dependences in the system with clusters containing TL-active and deep traps was performed for the first time. The features of the influence of various model parameters on the shape of TL dose dependences are established.

References

1) Mandowski, A. and Swiatek, J., 1992. Philos. Mag. B 65, 729–732.
2) Pagonis, V., and Chen, R., 2015. Radiat. Meas. 81, 262-269.

Slow OSL component in quartz separated by TM-OSL method

Alicja Chruścińska*, Piotr Palczewski
Institute of Physics, Faculty of Physics, Astronomy and Informatics, Nicolaus Co-pernicus University, Grudziadzka 5/7, 87-100 Torun, Poland

The TM-OSL method applied to separate the slow OSL component in quartz
Parameters of trap responsible for the slow component
Dose response curve of the slow component observed in TM-OSL measurements

optically stimulated luminescence, thermally modulated OSL, trap spectroscopy, quartz

Recently, the possibility to exploit the deepest traps in quartz is becoming more and more interesting in the field of OSL dating of geological sediments. The hope for extending the dosimetric range, and thus the age range, is one reason and the other is a need of finding traps which have parameters suitable for thermochronometric applications[1-2]. The range of OSL dating using the fast component signal in quartz allows credible dating up to last 100 - 150 ka (doses in the range 100 - 250 Gy) but some troubles with age underestimation are reported for samples older than 40 ka (doses ~ 100 Gy) recently[3]. A chance for age range extending is seen in the slow OSL component S[4], in the Isothermal TL (ITL) signal measured at 310 °C[5] or Thermally Transferred-OSL (TT-OSL) signal[6] and finally in the Violet Stimulated Luminescence (VSL)[7]. It was showed for all the above listed kinds of signal that they have a dose saturation level of an order of magnitude higher than the signal related to the fast OSL component in quartz. A similar dose dependence has been observed recently for one of the OSL components seen in the thermally modulated OSL measurements (TM-OSL) with the stimulation light wavelength of 450 nm and heating rate of 0. 1 K/s[8]. The TM-OSL method is used here for the effective separation of this OSL component from other slow components in quartz and for determining the parameters of trap that is responsible for the signal.
TM-OSL is a method developed recently for advanced investigations of traps which are the source of OSL signals. It is based on optical stimulation during linear heating of the sample. Such stimulation enables direct estimation of trap parameters such as the optical depth and those that describe the strength of coupling between the trap defect and the crystal lattice. It also improves radically the selectivity of trap emptying[9]. It was shown that the shape of TM-OSL curves depends on three experimental parameters: 1) the energy of photons used for stimulation, 2) the photon flux density used for the stimulation as well as 3) the heating rate (see Fig. 1). All these factors can be used in order to better separate the OSL signal originating

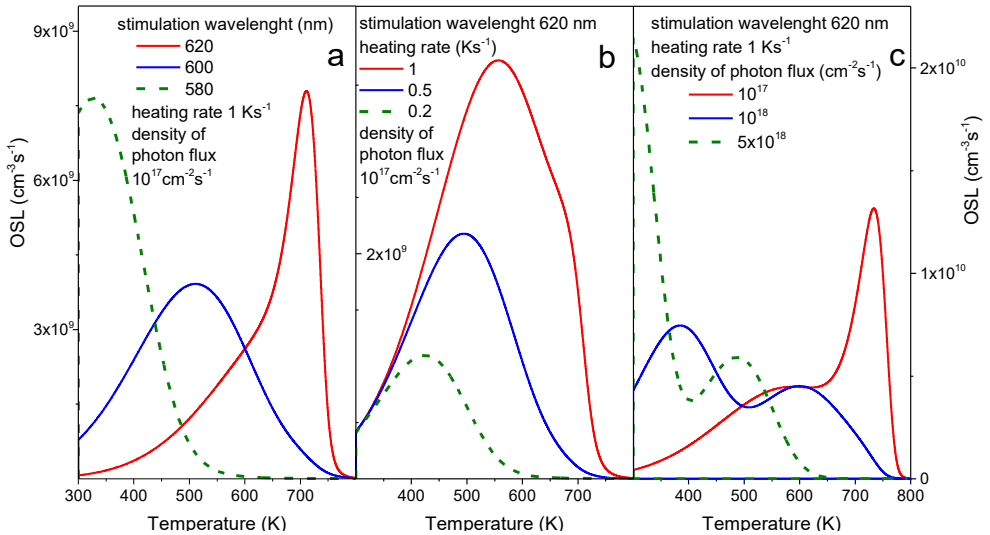

Figure 1. Simulated TM-OSL curves obtained for a trap having the optical depth of 2.45 eV for different stimulation light wavelengths (a), for different heating rates (b), and for two traps having the optical depths 2.4 and 2.5 eV for various photon flux densities (c) and the stimulation wavelength 620 nm.

from different kinds of defects. Here, this method is used for detailed investigations of deep traps in three quartz samples separated from sediments in a way commonly used in dating. The samples have significantly different intensities of the tested OSL component. The component observed previously using 450 nm with heating rate of 0.1 K/s is measured now with much higher photon flux density using 470nm and heating rate of 1 K/s. The trap parameters obtained for the tested TM-OSL component and its growth curve are compared with the earlier results obtained for the above mentioned kinds of signal in quartz which have the dose saturation level significantly higher than the signal related to the fast OSL component. The suitability of the signal for OSL dating age extension is shown.

1) B. Guralnik et al., Quat. Geochronol. 25, (2015), 37–48.
2) G. King et al., Chem. Geol. 446, (2016), 3-17.
3) A. Timar-Gabor & A. Wintle, Quat. Geochron. 18, (2013), 34-40.
4) J.S. Singarayer, Radiat. Meas. 32, (2000), 873–880.
5) M. Jain et al., Anc.TL 23, (2005), 9–24.
6) G. Adamiec et al., J. Phys. D: Appl. 41, (2008), 135503.
7) C. Ankjærgaard et al., Quat. Geochronol. 18, (2013), 99-109.
8) P. Palczewski & A. Chruścińska, Radiat. Meas. 121 (2019), 32-36.
9) A. Chruścińska & N. Kijek, J. Lum. 174, (2016), 42-48.

Acknowledgements This work has been financed by the grant of the National Science Centre, Poland, No. 2016/21/B/ST10/01867.

Preliminary study on dosimetric characteristics of different types of smartphone screen protective films using EPR

Byeong Ryong Park, Jae Seok Kim, Wi-Ho Ha*, Seongjae Jang

NREMC, Korea Institute of Radiological and Medical Sciences, Seoul, Republic of Korea

Highlights The dosimetric characteristics of three types of smartphone screen protective films were confirmed by electron paramagnetic resonance (EPR) spectroscopy. The tempered glass (TG) film showed similar characteristics to the touchscreen glass so that it could be used as a dosimetry sample instead of touchscreen glass in radiation accident.

Key words Electron paramagnetic resonance, Electron spin resonance, Retrospective dosimetry, Radiation accident, Screen protective film

Background and Objectives In case of radiation accident, rapid and accurate assessment of the exposed dose is important to determine the prognosis of the medical condition of exposed patients and establish treatment plans. EPR dosimetry is one of the physical dose assessment methods. It can be used for assessing the external exposure using biological materials, such as tooth enamel and nail, and various personal belongings of overexposed patients. In recent years, EPR dosimetry studies on touchscreen glass of smartphone among personal belongings have been actively performed internationally[1]. A lot of smartphone users use a protective film to protect the touchscreen. Most initial protective films were made of polyethylene terephthalate (PET) as raw material, but the newest films are mainly made of TG or thermoplastic polyurethane (TPU). If it is possible to assess the exposed dose using protective films instead of a touchscreen glass, there is an advantage that the expensive smart phones could not be damaged. Therefore, in this study, the feasibility of dosimetry using protective film was confirmed by measuring the EPR spectra, linearity of response function, and fading of different types of protective films.

Materials and Methods Three types of commercially available touchscreen protective films made of different materials (PET, TG, and TPU) were used in this experiment. EPR measurements were conducted on an X-band Bruker Elexsys E500 spectrometer with a Bruker ER4122SHQE resonator used 5 mm diameter sample tube at the room temperature. Each protective film was irradiated from 1 to 30 Gy (1, 2.5, 5, 10, 15, 20, 25, and 30 Gy) using additive dose method to confirm the radiation induced signal (RIS) and response function. Fading was measured for five months after irradiation. Irradiation of all samples was

conducted with a Biobeam8000 irradiator (STS Steuerungstechnik &. Strahlenschutz GmbH, Germany) used a ^{137}Cs gamma ray source.

Results and Discussion The PET film showed no significant RIS. TG and TPU film were able to identify RIS and the coefficient of determination (R^2) of response function was higher than 0.97. However, TPU film showed the same shape in background signal (BKS) and RIS, a larger BKS and a relatively low increase rate in RIS. Signal intensity of TG film decreased by approximately 10% for one day, 20% for one month, and 35% for five months after irradiation, while that of TPU film was stable for five months. Overall, the TG film showed similar characteristics to the touchscreen glass.

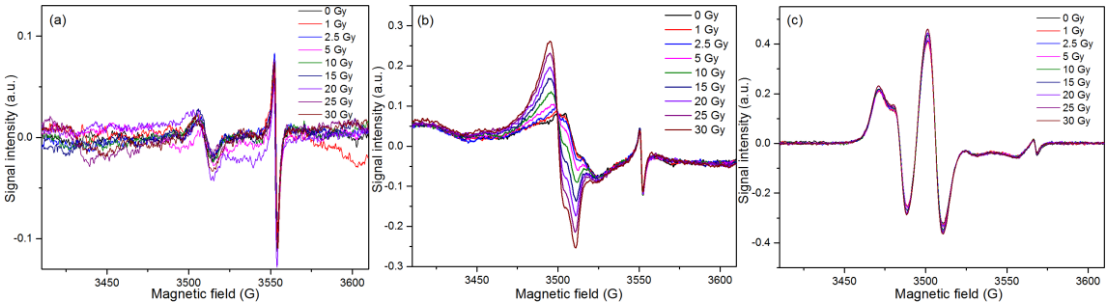

Figure 1. EPR spectra of gamma ray irradiated three types of smartphone screen protective films: (a) PET, (b) TG, and (c) TPU films.

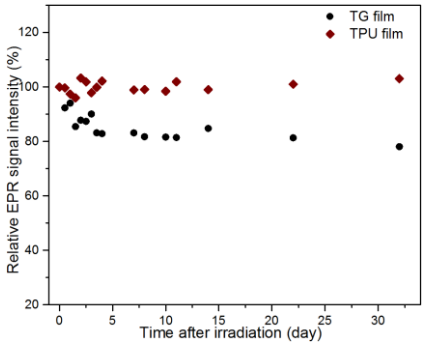

Figure 2. Normalized signal intensity change of TG and TPU films for one month after irradiation at 30 Gy.

Conclusion It has been confirmed that EPR dosimetry using TG film is possible. The RIS signals of TPU film are stable for several months, but the processing of large BKS signals remains a problem. Further studies are currently ongoing for each film, such as minimum detectable dose and signal differences according to film manufacturer.

References

1) Fattibene, P. et al. EPR dosimetry intercomparison using smart phone touch screen glass. Radiat. Environ. Biophys. 53, 311–320. https://doi.org/10.1007/s00411-014-0533-x. (2014)

Retrospective Electron Paramagnetic Resonance (EPR) Dosimetry of Radiation Accidents Using Environmental Biological Samples

C.C. Lu [1]*, F.N. Wang [1], H.H. Lin [2,3], J.P. Lin [4], L.H. Lai [4]

[1]*Department of Biomedical Engineering and Environmental Sciences, National Tsing Hua University, Hsinchu, Taiwan*

[2]*Medical Physics Research Center, Institute for Radiological Research, Chang Gung University/Chang Gung Memorial Hospital, Taoyuan, Taiwan*

[3]*Department of Radiation Oncology, Chang Gung Memorial Hospital, TaoYuan, Taiwan*

[4]*Department of Medical Imaging and Radiological Technology, Yuanpei University of Medical Technology, Hsinchu, Taiwan*

Highlights: Ox bone, clam shell, cyclina shell, chitin, tooth, and fingernail can be used as the environmental dosimeters. Linear dose-response curves of ox bone, clam shell, cyclina shell, chitin, tooth, and fingernail are presented. The grain size and storage temperature of the materials on the sensitivity of EPR spectra are examined.

Keywords: electron paramagnetic resonance, retrospective dosimetry, human tissue, shell, chitin

Background and Objectives: In response to large-scale radiological incidents and nuclear mass-casualty events, it is essential to develop a retrospective dosimetry framework towards the estimation of the environmental dose for a risk assessment. Electron Paramagnetic Resonance (EPR) dosimetry provides measurements of absorbed dose in a variety of materials through the measurement of the radiation damage therein induced. Therefore, materials contained in creatures from sea or land can be collected and potentially used as environmental dosimeters for a retrospective dose analysis. Here, we propose the retrospective dose assessment based on the use of EPR measurement of free radicals from environmental biological samples.

Materials and Methods: The biological samples include human tissue (enamel and fingernail), ox bone, cyclina shell, clam shell, and chitin from squid (Figure 1). All materials are first dehydrated and ground to the powder with different sizes. EPR spectra of all materials, irradiated with different doses range from 5Gy to 50Gy using 6MV linear accelerator, were obtained from the calculation of peak-to-peak amplitudes.

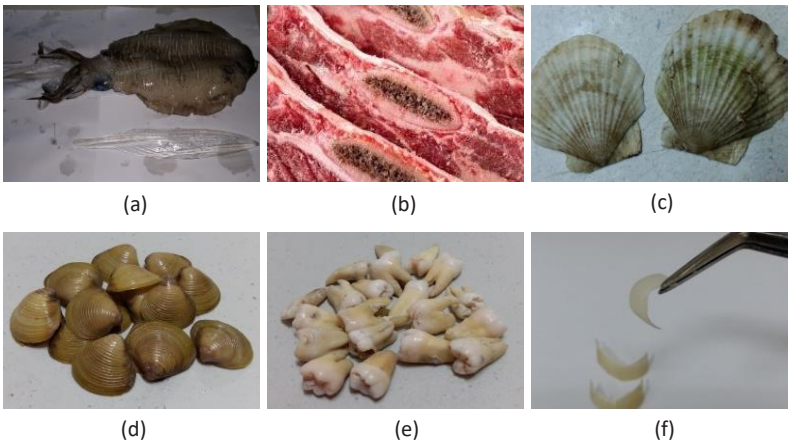

Figure 1. Biological samples of (a) ox bone, (b) chitin, (c) cyclina shell, (e) clam shell, (d) tooth and (f) fingernail.

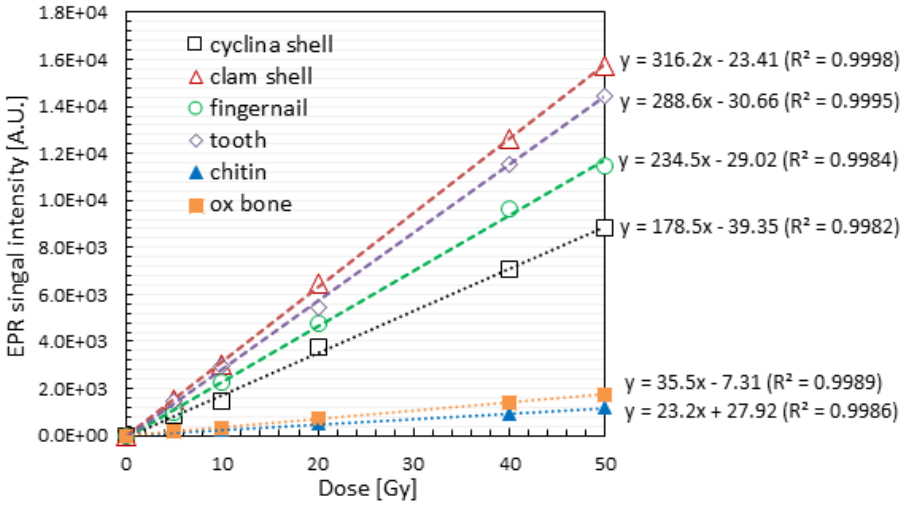

Figure 2. Dose response curve for the six biological samples.

Results and Discussion: The dose-response curve of EPR signals versus irradiated dose for the six materials shows a good linearity (R^2~0.99) (Figure 2). For the grain-size experiment, the ox bone and tooth with 0.5 mm, the chitin with 0.1 mm and the others with 1 mm have the strongest signal. For the storage-temperature experiment, the optimal temperature of storage is at -20°C for tooth, fingernail, ox bone and chitin, at 45°C for clam shell and cyclina shell where the signal fading is minimal.

Conclusion: We conclude that the developed dose-response curves of the six materials can help a fast, rough retrospective dose reconstruction under the environment when radiation accidents occur.

Luminescence dating of old loess samples. Which is the most suitable laboratory protocol for obtaining accurate chronologies?

Daniela Constantin[1]*, Anca Avram[1, 2], Alida Timar-Gabor[1,2]

[1]*Interdisciplinary Research Institute on Bio-Nano-Sciences, Babes-Bolyai University, Cluj-Napoca, Romania*

[2]*Faculty of Environmental Sciences and Engineering, Babes-Bolyai University, Cluj-Napoca, Romania*

Highlights The natural signals emitted by polymineral fine grains (post-IR $IRSL_{290}$ and post-IR $IRSL_{225}$ protocols) and by 63-90 µm quartz SAR-OSL, enter field saturation for samples immediately below the Eemian palaeosol (500 Gy, 400 Gy and 300 Gy, respectively). Although the laboratory dose response curves on 4-11 µm quartz grow beyond 5000 Gy, accurate ages are obtained only for samples from the last interglacial-glacial cycle (<240 Gy). The measurable range of doses for each signal depends on the degree of overlap between the natural and laboratory dose response curves.

Key words luminescence dating, loess, quartz, feldspars

Introduction The loess-paleosol sequences in the Middle and Lower Danube Basin are amongst the thickest and most complete available in Europe. At the site of Batajnica in the southern Carpathian (Middle Danube) Basin, Northern Serbia, previous stratigraphy, geochemistry and magnetic susceptibility investigations identified 5 loess-paleosol alternations, the lowermost being correlated to MIS 15. Thermoluminescence ages have been reported but in depth state of the art absolute dating is lacking.

Materials and Methods In order to establish a luminescence chronology for this site, samples have been collected from the uppermost loess layer as well as from the boundaries of the three uppermost paleosols. The Single Aliquot Regenerative (SAR) protocol has been applied to 4-11 µm and 63-90 µm quartz grains. Feldspar infrared stimulated luminescence (IRSL) emitted by 4-11 µm polymineral grain was measured using the post IR-$IRSL_{225}$ and post IR-$IRSL_{290}$ techniques. Natural growth curves have been constructed for each signal using the samples collected from the paleosols boundaries. Expected ages have been estimated based on magnetic susceptibility data correlated with the SPECMAP palaeoclimatic model.

Results and Discussion Quartz yielded reliable OSL ages for the samples with equivalent doses up to 220 Gy (80 ka). Post-IR $IRSL_{225}$ ages are consistent with the quartz OSL ages for this interval. For samples with equivalent doses beyond 220 Gy (~40 ka) the post-IR $IRSL_{290}$ protocol overestimates systematically the expected depositional moment. The overestimation of the post-IR $IRSL_{290}$ ages is caused by the overestimation of the measured equivalent dose, as confirmed by dose recovery ratios and results on a sample collected just above a potential tephra layer in the uppermost loess unit (L1), that very likely correlates with the Campanian Ignimbrite/Y5-ash layer ($^{40}Ar/^{39}Ar$ dated elsewhere to 39.3 ± 0.1 ka).

The natural 63-90 µm quartz signals reach field saturation and interpolate above the 85% saturation threshold of the laboratory dose response curves for samples beyond the Eemian interglacial (De > 300 Gy). Natural and laboratory dose response curves on 63-90 µm quartz deviate at ~ 300 Gy. The laboratory signals emitted by the 4-11 µm quartz grow beyond 5000 Gy while the corrected natural signals interpolate well below the curvature, even for a sample collected below the S3 paleosol (expected age and equivalent dose based on magnetic susceptibility data ~ 300 ka; De ~ 1170 Gy). Yet, the OSL ages on 4-11 µm quartz highly underestimate the expected depositional moment starting with samples below the S1 paleosol (>240 Gy). Natural and laboratory dose response curve on 4-11 µm quartz deviate from the natural growth curve at ~ 200 Gy and saturates at higher doses. Starting with the samples collected below the S1 paleosol (> 500 Gy), the natural post-IR $IRSL_{290}$ signals reach field saturation and are interpolated above the 85% saturation threshold of the laboratory dose response curves. For a sample collected below S3 paleosol (expected age and equivalent dose based on magnetic susceptibility data ~ 300 ka; De ~ 1350 Gy), the natural corrected post-IR $IRSL_{290}$ signal is interpolated above the laboratory dose response curve. This systematic overestimation of the measured equivalent dose using the post-IR $IRSL_{290}$ is reflected in the difference between the growth of the natural and laboratory signals. The laboratory and natural field saturation levels of post-IR $IRSL_{225}$ signals limits the range of the accurate ages to the last glacial-interglacial cycle samples (> 400 Gy). The growth of the natural and laboratory signals overlap up to ~ 800 Gy.

Conclusion The natural signals emitted by polymineral fine grains (post-IR $IRSL_{290}$ and post-IR $IRSL_{225}$) and 63-90 mm quartz SAR-OSL enter saturation for samples immediately below the Eemian palaeosol. Although the laboratory dose response curves on 4-11 mm quartz grow beyond 5000 Gy, accurate ages are obtained only for samples from the last interglacial-glacial cycle.

This work has received funding from the European Research Council (ERC) under the European Union's Horizon 2020 research and innovation programme ERC-2015-STG (grant agreement No [678106] awarded to ATG).

Infrared luminescence dating of Spituk Lake sediments in the Indus River Valley, Ladakh, India

Dipak K. Panda and Debabrata Banerjee*
Physical Research Laboratory, Navrangpura, Ahmedabad, India
**Corresponding Author: deba@prl.res.in*

Highlights: We present infrared stimulated luminescence (IRSL) ages of Spituk Lake deposits in Ladakh, India. The IRSL ages for seven samples from the Spituk section range from 105 to 170 ka, and suggest that deposition in the Spituk area began at ~170 ka after damming of the Indus River. These ages are substantially older than ~50,000 years BP reported previously by Phartiyal et al (2005). The uppermost unit in this section marks a change in climate and fluvial activity and the IRSL ages suggest that lake existed for another ~70 ka, and later disappeared due to breaching of the dam at ~100 ka.

Keywords: OSL, Ladakh, Spituk Lake, Indus River, IRSL

Background and Objectives: The major tectonic features in the Higher Himalaya comprise the Indus Tsangpo Suture Zone, the Shyok Suture Zone and the Karakoram Fault. Many sedimentary deposits are preserved in the form of terraces, fans, lake and moraines, and represent archives of paleoclimatic changes during the late Quaternary. The Indus River flows along NW-SE tending Karakoram Fault and along the Indus Tsangpo Suture Zone which marks the boundary between the Asian and the Indian continental plates. The present work aims at infrared stimulated luminescence dating of Spituk Lake deposits to decipher the timing of formation of the Spituk Lake in Ladakh. The Spituk section is the best preserved >50 m high Quaternary section which represents deposits of fluvial, glacial and lacustrine environments.

Materials and Methods: The feasibility of infrared stimulated (IRSL) luminescence dating of 63-150 μm quartz-rich grains was investigated in 7 samples collected from Spituk, Ladakh. Although HF etching was performed during chemical processing of the samples, all aliquots exhibited significant IR and post-IRIR signals. Hence, a modified SAR protocol (Murray and Wintle, 2000) was to estimate the infrared stimulated luminescence (IR_{60}) equivalent doses following the procedures outlined in Buylaert et al. (2012). The same preheat conditions were applied prior to the measurement of the natural and regenerative dose as well as the test dose. The first IR stimulation was carried out at 60°C for 200 s, followed by the second stimulation

at 290°C. External dose rates for the samples were calculated from the activity concentrations of decay chains ^{238}U, ^{232}Th and ^{40}K measured using high resolution gamma spectrometry (HPGe).

Results and Discussion: The lower units in the Spituk section were observed to be fine sandy, whereas the middle layer has a thick clay representing a lacustrine environment. The uppermost layers contain gritty sand and coarse sand layers, suggesting a fluvial environment. The IRSL luminescence ages for the seven samples from the Spituk section range from 105 to 170 ka. The IRSL age at the bottom of the Spituk section is ~170 ka, and suggests that deposition in the Spituk area began at ~170 ka after damming of the Indus River. These ages are substantially older than ~50,000 years BP reported previously by Phartiyal et al (2005). The uppermost unit in this section marks a change in climate and fluvial activity and the IRSL ages suggest that lake existed for another ~70 ka, and later disappeared due to breaching of the dam at ~100 ka in marine isotope stage (MIS) 5.

References

Murray, A.S. and Wintle, A.G., 2000. Radiation Measurements, 32, 57-73.
Buylaert, J P et al., 2012. Boreas, 41, 435-451.
Phartiyal, B et al., 2005 Geomorphology, 65, 241-256.

Dating sediments from Paranaguá Barrier, Paranaguá by EPR method

E. E. Cuevas Arizaca[1 5]*, Silva R.J.[1] Faria Pereira L.F. [1] Rojas R.[2] Cano N.F[2]. Baria Ribeiro R. [3] Chubaci, J.F.D. [1] Ferreira Guedes, C. C. [4] T.K.G. Rao[1] S. Watanabe[1]

[1] *Instituto de Física, Universidade de São Paulo, Brazil*

[2] *Universidade Federal de São Paulo, Santos, Brazil*

[3] *Instituto de Pesquisas Energéticas Nucleares, Brazil*

[4] *Departamento de Geologia, Universidade Federal de Paraná, Brazil*

[5] *Universidad Católica de Santa Maria, Arequipa, Perú.*

Highlights.

Sediment dating by EPR was successfully performed. Signal of E'_1 center was used.

Key words: Sediments, Quartz, EPR, Dating.

Background and Objectives.

The extensive sea coast of Brazil is characterized by mountains and coastal plane. The coastal planes are supposed to be of Quaternary and its formation is due to factors such as rainfall, wind, climate, etc., but the sea level fluctuation in the past is a very important cause. There are various dates based on radiocarbon method; ages determined by this method allowed to construct curves of variation of sea level in Holocene. For the Pleistocene period practically no dating data is available except for Villwock et a (1986) that discuss from stages of sea level variation, but restrict to coastal plane in the state of Rio Grande do Soul. The four stages have been designated Barrier I, II, III and IV.

In the state of Paraná, there are three sand terraces. One of them close to the port of Paranaguá, and called Paranaguá Barrier, which is a large one. 20 km wide. 25 km long and 5 to 10 m of height. It is purpose of this work to date Paranaguá Barrier to find its formation age.

Materials and Methods

Samples for dating have been collected from sea coast in four levels from the top called PR1, PR2, PR3 and PR4. For the EPR measurements we used 150 mg of quartz and regenerative protocol was utilized. The annealing temperature was 470 ºC and the samples were irradiated with gamma radiation, with doses 5 up to 300 Gy. Samples were pre-heated at 330 ºC.

Results and Discussion

Annual dose rates (Dan) have been estimated using uranium, thorium and potassium concentrations. These concentrations were derived from gamma spectroscopy Ikeya et al (1993). These results are presented in Table 1.

The results of the regenerative method for accumulated dose are shown in Fig. 1b. Typical signal of E'_1 center is presented in Fig. 1a. Its intensity is found to increase with the dose. From Fig 1b the accumulated dose was determined.

.

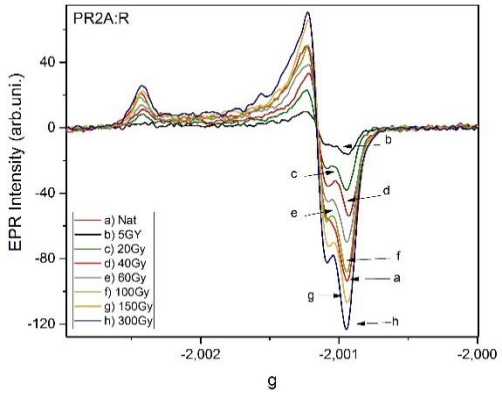

Fig 1a. The signal of E'_1 center with gamma ray dose of 5 up to 300 Gy.

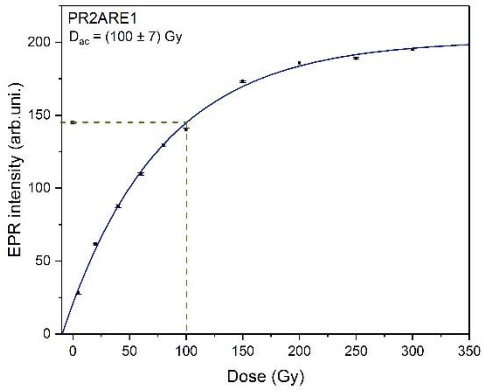

Fig 1b. EPR intensity as a function radiation dose.

Table 1.

Sample	Dan (mGy/y)	Dac (Gy)	Dan (mGy/y)	Age (ky)
PR1	0,75 ± 0,01	79 ± 6	0,75 ± 0,01	106 ± 8
PR2	0,88 ± 0,02	100 ± 7	0,88 ± 0,02	114 ± 9
PR3	0,96 ± 0,02	62 ± 7	0,96 ± 0,02	64 ± 7
PR4A	0,88 ± 0,02	98 ± 9	0,88 ± 0,02	111 ± 10

Conclusion

The results of the present study indicate that for the samples examined ages are around 100.000 years B.P.

References

Villwock J.A., Tomazelli L.J. Loss E.L., Dehnhard E.A., Horfilho N.O., Bachi F.A., (1986) Geology of the Rio Grande do Sul Coastal Province, Brazil. Quaternary of South America and Antarctic peninsula. Vol. 4. Pp 79-97.

Ikeya M, (1993) New Applications of Electron Spin Resonance Dating, Dosimetry and Microscopy.

Dose determination using spectrally-resolved luminescence: implications for dating

E. Şahiner[1,2]*, R. Kumar[1], M. Kook[1], G.S. Polymeris[2] , N. Meriç[2] and M. Jain[1]

[1]*Center for Nuclear Technologies, Technical University of Denmark, DTU Risø Campus, Roskilde,4000, Denmark*

[2]*Institute of Nuclear Sciences, Ankara University, Beşevler, 06100, Ankara, Turkey*

**Corresponding author; Email: sahiner@ankara.edu.tr*

Highlights Equivalent dose dependence on emission wavelength is resolved both within and across the main emission bands of quartz and feldspar using an automated spectrometer. This is the first systematic dating study using spectrally-resolved OSL/TL.

Keywords Spectrally-resolved luminescence, Optically Stimulated Luminescence (OSL), Thermoluminescence (TL), Radiation dosimetry, Luminescence dating, Equivalent Dose (ED)

Background and Objectives TL and OSL are widely used in solid state dosimetry and archeological/geological dating. Typically, luminescence dosimetry involves measuring light in a chosen emission band using appropriate optical filters in front of a photomultiplier tube or a charged couple device (CCD). This approach leads to high sensitivity but at the cost of non-detection of photons in the other emission bands. For basic studies, it is desirable to collect the entire emission spectrum of the dosimeter so as to evaluate the relative performance of different emission bands. Spectrally resolved data is especially important when overlapping emission bands have very different responses to irradiation or/and athermal fading, leading to inaccuracies in measurement of dose or the kinetic parameters. Furthermore, it becomes easier to discriminate black body radiation from luminescence emission at high temperatures. Although there have been attempts to measure wavelength multiplexed luminescence[1,2,3], spectrometry remains under-utilized in luminescence dosimetry and dating. In this study, we report on spectrally-resolved OSL (SR-OSL) and TL (SR-TL) measurements from natural quartz and K-feldspars for developing improved dating protocols.

Materials and Methods A Risø TL/OSL reader with a spectrometer attachment was used for all the measurements presented here. The spectrometer is attached to a thermoelectrically cooled Electron multiplying CCD (EMCCD) camera system. A complete detail on this system has been previously presented by Prasad et al.[4] The SAR method was used on samples which were extracted from sediments relying on conventional OSL dating protocols. We investigate the dependence of different parameters on emission wavelength, from UV (300 nm) to near-IR (1000 nm).

Results and Discussion In order to find out the appropriate emission wavelength interval for dose estimation, dose-dependent spectra from different feldspar and quartz samples of known age were examined at a resolution of 20 nm. Figure 1 shows an example of a typical SR-TL from a natural K-Feldspar extracts; there are two main emissions bands. Based on such data we evaluate ED, dose recovery, preheat plateau, recycling and recuperation by using a SAR protocol. The dose response from SR-TL and SR-OSL were further evaluated by comparing with the standard PMT measurements.

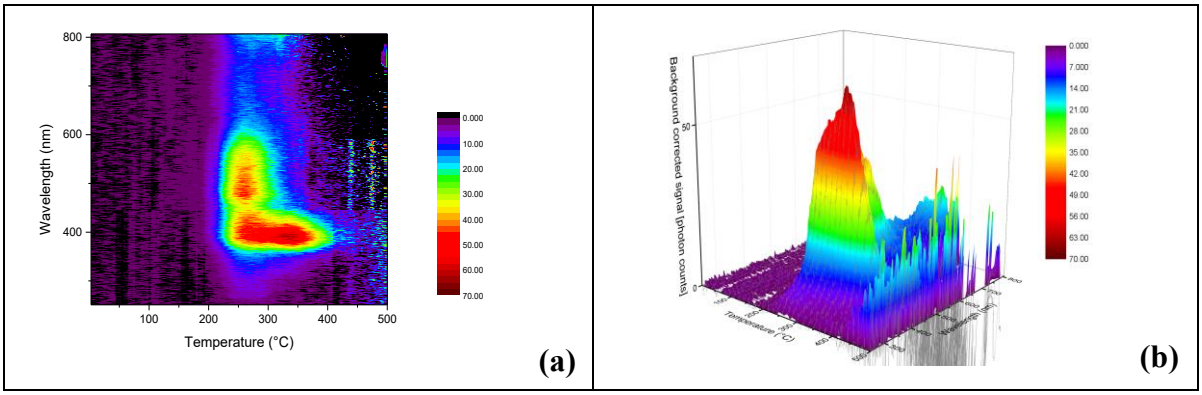

Figure 1. TL glow curve emission spectra for natural K-rich Feldspar, including ~300 Gy natural doses: (a) 2D plot (b) 3D plot

Additionally, correlation of anomalous fading of feldspar with emission wavelength was examined using infra-red stimulation at different temperatures and compared with the corresponding ED values. Our data suggest that spectrally-resolved luminescence gives important insight into dosimetric behavior of quartz and feldspar and greater accuracy in regions with overlapping emission peaks.

Conclusion This study demonstrates the novelty of a multi-spectral approach in luminescence dating methods to obtain more accurate dose estimates in quartz and feldspar.

Acknowledgements The corresponding author (E. Şahiner) has been supported by the TÜBİTAK fellowship with grant No: 1059B191700876

References

1) Luff, B. J., & Townsend, P. D. (1993). High sensitivity thermoluminescence spectrometer. Measurement Science and Technology, 4(1), 65.
2) Vokhmintsev, A. S., Minin, M. G., Henaish, A. M. A., & Weinstein, I. A. (2015). Spectrally resolved thermoluminescence measurements in fluorescence spectrometer. Measurement, 66, 90-94.
3) Finch, A. A., Wang, Y., Townsend, P. D., & Ingle, M. (2019). A high sensitivity system for luminescence measurement of materials. Luminescence.
4) Prasad, A. K., Lapp, T., Kook, M., & Jain, M. (2016). Probing luminescence centers in Na rich feldspar. Radiation Measurements, 90, 292-297.

Thermoluminescence characteristics of SIM cards used in mobile communication providers in Korea for emergency dosimetry

Hyoungtaek Kim[1]*, Min Chae Kim[1,2], Jungil Lee[1], Michael Discher[3], Clemens Woda[4],Insu Chang[1], Seung Kyu Lee[1], Jang-Lyul Kim[1], Kisoo Chung[5]

[1]*Korea Atomic Energy Research Institute, 989-111 Daedeok-daero, Yuseong-gu, Daejeon, 34057, Korea*

[2]*Hanyang University, 222, Wangsimni-ro, Seongdong-gu, Seoul, 04763, Korea*

[3]*University of Salzburg, Department of Geography and Geology, Salzburg, Austria*

[4]*Helmholtz Zentrum München, Institute of Innovative RadiotherapyRadiation Medicine, Neuherberg, Germany*

[5]*Gyeongsang National University, Department of Physics, Junju, Korea*

Highlights Characteristics of thermoluminescence of SIM cards in South Korea for accident dosimetry were identified.

Key words Emergency dosimetry, SIM cards, TL, OSL

Background and Objectives Thermoluminescence (TL) and optically stimulated luminescence (OSL) methods using mobile phone materials such as a glass and resistor have been widely studied for emergency dosimetry[1,2)]. However, these materials are accompanied with pretreatment processes like sample extraction, washing and etching[1,2)], which is a bottleneck for rapid triage in case of radiation accidents and terrorism that causes mass casualties. A SIM card in a mobile phone considered as one type of chip card has a high degree of signal decay in several days after irradiation due to an anomalous fading[3)]. However, if an in-situ measurement is required within one or two days, SIM cards are expected to be suitable for a dose reconstruction of mass samples because of fast sample extraction and no pretreatment processes[3)]. In the previous study, different TL glow curves were found depending on a type of SIM cards[4)]. Therefore, characterizations such as zero dose and signal fading based on classification should be studied in advance. In this study, TL and OSL signals of SIM cards distributed in Korea were investigated. TL glow curves of SIM cards according to different combinations of filter and detector were measured to optimize the detection range.

Materials and Methods The SIM cards used in this experiment are currently distributed by mobile communication providers in Korea like SK Telecom (SKT), Korea Telecom (KT) and LG Telecom (LGT). The target material is a UV-cured epoxy for encapsulation of a chip. The epoxy is expected to contain a certain amount of silica[3,4)] depending on the type, and the chemical component analysis using an energy dispersive X-ray spectroscopy (EDS) will be carried out. A SIM card was cut into 5x5 mm^2 and placed on a sample cup after removing a

plastic cover with a metal contact facing to the bottom. The model of TL reader was a Riso-DA20 including a filter and detector changer. The filters were varied from a U-340(7.5 mm), blue filter pack (2 mm Schott BG-39 and 3 mm Schott BG-3), Brightline HC 340/26 (2mm) and without any filter. The detectors can be selected as either a blue sensitive PMT (ET PDM9107-CP-TTL) or a red sensitive PMT (Hamamatsu H7421-40).

Results and Discussion Unfortunately, dosimetric properties of the SIM card distributed by SKT were not observed up to 2 Gy irradiation. For the SIM cards of KT and LGT, the glow curves of radiation induced signal were identical with a peak temperature of 80 ºC but the background signal of as-received samples were different in terms of the intensity as well as the peak temperature like in figure 1. Both SIM cards showed a very high background signal beyond 100 ºC which results in a limitation to use stable signals over signal fading. Therefore, optimizations of signal integration and detection window are required. The combination of the blue sensitive PMT without any filter showed the maximum intensity for 1 Gy irradiation. The signal fading and zero dose distribution will be acquired depending on the type of SIM cards.

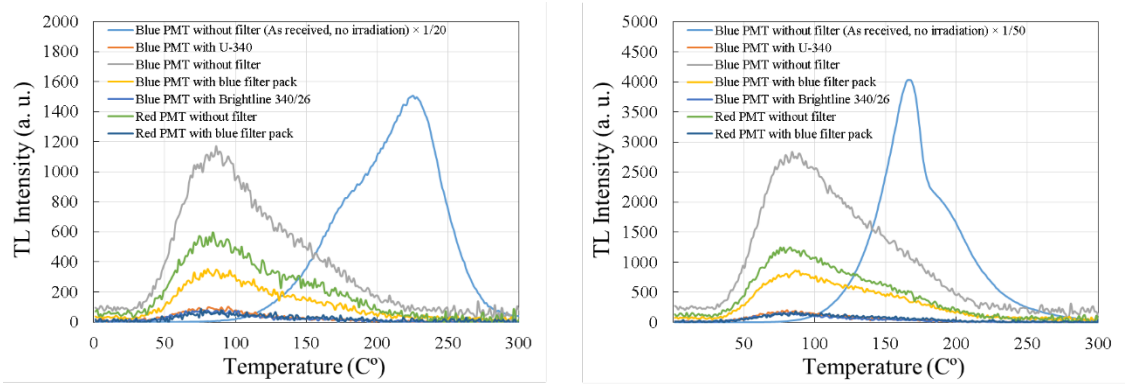

Figure 1. TL glow curves of 1 Gy irradiated (after 300 ºC preheat) and as-received SIM cards distributed from (a) KT and (b) LGT with different filter and detector combinations

References

1) Discher M. and Woda C., Thermoluminescence of glass display from mobile phones for retrospective and accident dosimetry, Radiat. Meas., vol 53-54, 12 – 21, 2013.

2) Lee J.I. et al., On the use of new generation mobile phone (smart phone) for retrospective accident dosimetry, Radiat. Phys. and Chem., vol 116, 151-154, 2015.

3) Woda C. et al., On the use of OSL of wire-bond chip card modules for retrospective and accident dosimetry, Radiat. Meas., vol 44, 548 – 553, 2009.

4) Kandemir A. et al., Thermoluminescence studies of SIM card chips used in mobile communication providers in Turkey, Radiat. Phys. and Chem., vol 149, 84-89, 2018.

Measurement of Radiation Exposure Dose using Resistor Elements in Electronic Personal Dosimeters

H.J. Yu[1]*, J.T. Lee[1], M.J. Kim[2]
[1]*Korea Institute of Nuclear Safety, Daejeon, Korea*
[2]*RADPION Inc., Daejeon, Korea*

Highlights Analysis of the thermoluminescence (TL) signal and inherence physical characteristics of resistor elements in the electronic personal dosimeter (EPD) was performed. Then the estimated accident dose was derived by using measurement of TL from resistor extracted from the EPD and verified the results.

Key words EPD, resistor, TL, retrospective dosimetry, industrial radiography

Background and Objectives When radiation accident is occurred in the industrial radiography field, the exposed dose can be evaluated by reading a personal dosimeter such as TLD, OSLD, etc. In some cases, the workers did not wear personal dosimeter at the moments of the accident. In order to evaluate the exposed dose to the workers, retrospective dosimetry using TL/OSL of resistor elements from electronic device is usually performed. The radiation workers in industrial radiography field must wear active dosimeter such as EPDs in addition to the cumulative dosimeter in Korea. In order to examine the feasibility of resistor elements in EPD as a new marker of retrospective dosimetry, we analyzed the TL signal and inherence physical characteristics of resistor extracted from the EPD. Then we derived estimated accident dose and verified the results.

Materials and Methods The model of EPD we used in this study was CLOVER, which is most widely used in Korea. Resistor elements were extracted from the circuit board of CLOVER and cleaned with acetone and ethanol. All the experiments were performed in the red-light environment. RISO TL/OSL reader (DA-20) was used to measure TL signal and absorbed dose to resistor was obtained by using SAR-TL method[1)]. To identify the dosimetric characteristics dose response curves were measured according to the temperature region of interest. Sensitivity variations of the sample were also identified with repeated measurement. The accident dose can be calculated by subtracting the zero-dose from the irradiated dose and dividing it by f and C[2)]. Where f is fading correction factor and C is over estimation factor. Finally, the estimated accident dose was verified with 1Gy irradiated sample in standard radiation field.

Results and Discussion TL signal obtained from the resistor of EPD and dose response curve is shown in figure 1. Considering the intensity of signal, life-time, and linearity of dose response curve, etc., the use of the signal in the temperature from 100 to 200 degrees was the most reliable for retrospective dosimetry. The value of factors produced in this study and the estimated accident dose with 1Gy irradiated sample in standard radiation field are summarized in Table 1. Accident dose was calculated around 10% lower than the standard irradiation dose.

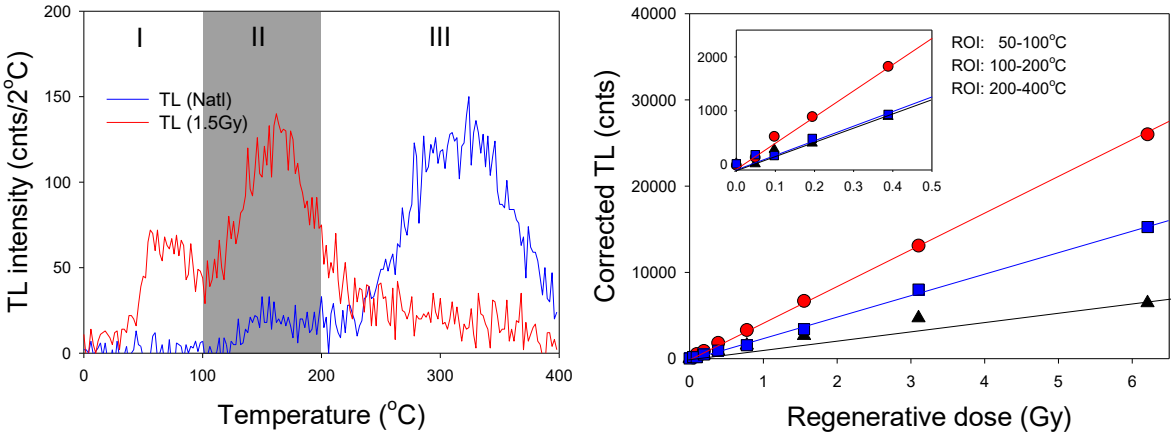

Figure 1. TL glow curve(left) and dose response curve(right) from resistor of EPD

Table 1. The year and location of the past SSD conferences

ED_{irr}(Gy)	ED_{zero}(Gy)	f	C	ED_{acc}
0.96±0.10	0.06±0.07	0.59±0.01	1.73±0.09	0.89±0.02

Conclusion Based on the results, the resistor extracted from EPD was judged to have good dosimetric properties. It is expected that the dose assessment method using resistor of EPD could be used as a new supplementary means for the retrospective dosimetry in industrial radiography field.

References

1) Murray, A.S., Wintle, A.G., 2003. The single aliquot regenerative dose protocol: potential for improvements in reliability, Radiation Measurements 37, 377-381.
2) Woda, C., Fiedler, I., Urso, L., Kaiser, J.C., 2011. Retrospective dosimetry for the population in emergency situations

Sources of variation in beta dose rate to coarse grains in sliced samples of heterogeneous composition

I.K. Bailiff
Department of Archaeology, Durham University, Durham DH1 3LE, UK

Highlights Computational modelling of beta dose rate in heterogenous materials

Key words Radiation, dosimetry, beta dose, single grains, heterogenous materials

Background and Objectives The development of experimental approaches suitable for the dating of strongly heterogeneous materials using luminescence techniques with single grain resolution has proved challenging. In particular, the assessment of the beta component of the dose rate is problematic because of the lack of spatially resolved techniques capable of measuring dose rate on a sub-mm scale. There is a need for computational tools to complement and guide the development of indirect (e.g., image plates and spatially-resolved semiconductor detectors) and direct (i.e., solid-state dosimetry) measurement and computational (Martin et al, 2015) approaches under development. Recent work (Bailiff, 2018) has investigated the effect of grain truncation caused by cutting during the slicing of solid samples (ceramic or resin encapsulated sediment) using radiation transport simulations. In that study (luminescent) detector grains were located in a matrix containing a uniform distribution of lithogenic radioactive sources. In this paper a similar computational approach has been taken to investigate the effect on the beta dose rate to detector grains by introducing into the modelled sample matrix spatially constrained concentrations of radionuclides in the form of mineral grains (e.g., potassic feldspar, zircon).

Materials and Methods

Dosimetry models were constructed for use with the general-purpose radiation transport code MCNP. The simulations provided a calculated precision of 1–2% in most cases (after 10^6-10^{10} particle histories), although this level of uncertainty does not reflect the larger uncertainties that would be encountered with experimentally determined quantities. The models comprised a simulated sample matrix of sufficient size (e.g., several mm radius) to obtain an infinite medium volume (IMV) for a detector grain located at the centre of the matrix. Spherical grain sources containing a uniform distribution of one type of lithogenic source (either ^{238}U, ^{232}Th or ^{40}K) were introduced into the matrix at various distances from the detector grain. The models are used to examine the effect on the beta

dose rate of proximity of the grain sources to the detector grain and the non-uniformity of the dose within the detector grains; the additional effects of truncation of detector grains caused by slicing the sample matrix are examined.

Results and Discussion The modelling simulations provide explicit dose rate data as a function of separation for individual grain source-detector pairs and, when applied to multiple grain sources distributed within an IMV, yielded β dose rate distributions to a quartz coarse grain detector at the centre of the volume. the distributions indicate the expected asymmetry in the distribution of β dose rate, but this applies to small coarse grains (~60 μm radius) and the simulations predict that the asymmetry diminishes with increasing detector grain size. The effects of the truncation of detector grains on the assessment of beta dose located within an IMV where the dominant source of beta dose is from grain sources is also assessed. Use of experimental data obtained with sliced ceramic samples are included in the analysis.

Conclusion The results obtained are used to illustrate the potential issues and difficulties that are encountered in attempting to estimate dose rate to individual coarse grains within a radiogenically heterogeneous material.

References

1) Bailiff, I.K., 2018. An examination of beta dose attenuation effects in coarse grains located in sliced samples. Radiation Measurements 120, 188-194.
2) Martin, L., Mercier, N., Incerti, S., Lefrais, Y., Pecheyran, C., Guérin, G., Jarry, M.,Bruxelles, L., Bon, F., Pallier, C., 2015. Dosimetric study of sediments at the beta dose rate scale: characterization and modelization with the DosiVox software. Radiat. Meas. 81, 134–141.

Thermoluminescence and Infrared Light Stimulated Luminescence Dosimetric Characteristics of Limestone ($CaCO_3$)

J.M. Kalita[1,2]*, M.L. Chithambo[1]

[1]*Department of Physics and Electronics, Rhodes University, Grahamstown, South Africa*

[2]*Department of Physics, Assam down town University, Guwahati, India*

Highlights Stimulated luminescence properties of limestone ($CaCO_3$) collected from the Mawsmai Cave, India have been studied using thermoluminescence (TL) and infrared light stimulated luminescence (IRSL) techniques. The radiation dosimetric features of the sample have been assessed.

Key words Limestone ($CaCO_3$), thermoluminescence (TL), infrared stimulated luminescence (IRSL), radiation dosimetry

Background and Objectives Limestone is a sedimentary rock composed of calcium carbonate ($CaCO_3$). Limestone has numerous industrial applications including as a building material, a chemical feedstock for the production of lime and as a soil conditioner. However, there are only few studies concerning potential application of limestone in luminescence dating using stimulated luminescence[1)].

In contrast to limestone, another variety of calcium carbonate, calcite has attracted much attention in luminescence dosimetry due to its excellent luminescence properties[2)]. In this work, we study thermoluminescence (TL) and infrared stimulated luminescence (IRSL) of limestone under beta irradiation and assess its dosimetric characteristics.

Materials and Methods Samples used were limestone collected from Mawsmai Cave, India (latitude: 25°18′00″N, longitude: 91°42′00″E). The samples were cleaned and ground to fine powder. X-ray diffraction (XRD) and energy dispersive X-ray fluorescence spectroscopy (XRFS) analyses were carried out using a Phillips X'Pert Pro Powder X-ray Diffractometer and an Axios, PANalytical spectrometer respectively. TL and IRSL were measured using the RISØ TL/OSL DA-20 Luminescence Reader from samples irradiated at ambient temperature using a $^{90}Sr/^{90}Y$ beta source at a dose rate of 0.1028 Gy/s. The luminescence was detected by an EMI 9235QB photomultiplier tube through a Schott BG 39 filter (transmission band 330–690 nm). All measurements were carried out in a nitrogen atmosphere to prevent spurious signals from air. For all measurements, 40 mg of sample was used for each aliquot. IRSL measurements were carried out in a continuous-wave mode using a set of 870 nm infrared LEDs set at 130 mW/cm^2 optical power density.

Results and Discussion XRD analysis indicates that the sample is crystalline and has rhombohedral crystal structure. The XRFS analysis shows that the concentration of CaO is 33.45%. Apart from the CaO, minor concentration of SiO_2 and MgO are also found.

The TL measured at 1 ºC/s from A sample irradiated between 10 and 1000 Gy shows three glow peaks, P1 at 76 ºC, P2 at 150 ºC and P3 at 239 ºC (Figure 1(a)). Peaks P1 and P2 shift to 96 ºC and 180 ºC with the dose whereas P3 shows no such behaviour. The activation energy of peaks P1, P2 and P3 are estimated using initial rise method as ~0.66, 0.44 and 1.00 eV respectively. The dosimetric characteristics were studied for peaks P1 and P3. The TL intensity of P1 increases uniformly with the dose from 10–1000 Gy whereas that of P3 shows two different uniform regions within 10–100 Gy and 100–1000 Gy respectively.

The IRSL measurement carried out at 25 ºC shows an ill-shaped decay curve (Figure 1(b)). Like the TL peak P3, the IRSL intensity also increases with dose in two different uniform regions within 10–100 Gy and 100–1000 Gy. Later the residual TL measured after the measurement of IRSL shows similar response as that under the conventional TL.

Analysis of the TL fading shows that peak P1 decreases by 88% and whereas P3 by 14% within 12 hours after irradiation.

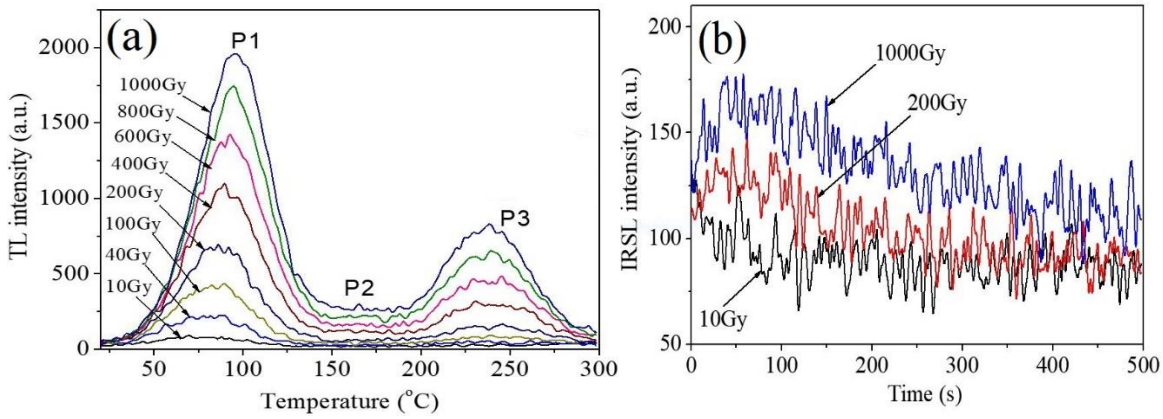

Figure 1. (a) TL glow curves and (b) IRSL decay curves of limestone irradiated to different doses.

Conclusion TL and IRSL properties of limestone mineral have been studied under beta irradiation. The dosimetric characteristics such as dose response and fading were studied. This study shows that the mineral can be used as natural radiation dosimeter.

References

1) K. Ninagawa, T. Kitahara, S. Toyoda, K. Hayashi, H. Nishido, M. Kinjo, T. Kawana, Quat. Sci. Rev. 20 (2001) 829–833.
2) J.M. Kalita, G. Wary, Nucl. Inst. Meth. Phys. Res. B 383 (2016) 93–102.

Characteristic study of radiation induced signal of Korean fingernails using EPR dosimetry

Jae Seok Kim, Byeong Ryong Park, Wi-Ho Ha*, Seongjae Jang

NREMC, Korea Institute of Radiological and Medical Sciences, Seoul, Republic of Korea

Highlights Human fingernails were used to evaluate the exposed dose in a radiation accident situation. The characteristic of radiation induced signal in Korean fingernails were researched by the EPR dosimetry.

Key words EPR dosimetry, Retrospective dosimetry, Radiation accident, Fingernail

Background and Objectives In a radiation accident situation, an accurate and rapid retrospective dosimetry for effective medical triage is needed to evaluate the radiation dose. Korea Institute of Radiological and Medical Science (KIRAMS) as the first responding agency against a radiation accident in Korea, Korean fingernails have being researched by KIRAMS for evaluating the radiation dose with EPR dosimetry. Among of the EPR signal in fingernails, the characteristic of radiation induced signal (RIS) was analyzed with respect to the linearity of dose response, individual response, and fading[1), 2)]. These characteristics of RIS in fingernail are important factor for improving an accurate and rapid fingernails-EPR dosimetry.

Materials and Methods The used fingernails in this study were collected from healthy individuals of various ages. Figure 1 shows the specific procedure from the sample preparation to the RIS measurement for reducing the uncertainty of irradiation and measurement. After measuring the RIS in samples, the linearity of dose response and the individual response of the RIS were analyzed from 1 to 50 Gy (1, 2, 10, 25, and 50 Gy). The fading of the RIS was measured five times within ten days.

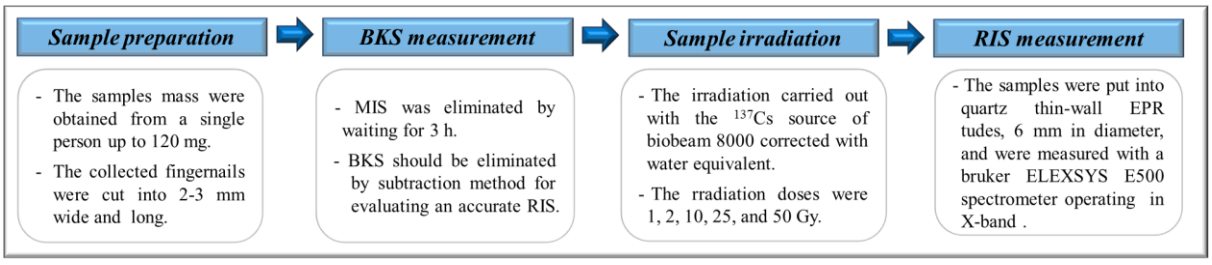

Figure 1. Procedure for evaluating the characteristic of the RIS in Korean fingernails.

Results and Discussion Figure 2 shows the characteristic of RIS in Korean fingernails-EPR signals according to the linearity of dose response, fading, and individual response. Figure 2(a) shows the linearity between irradiation dose and intensity of EPR signal. These results were found that Korean fingernails have the linear relationship for irradiation doses ranging from 1 to 50 Gy. The coefficients of determination (R^2) are 0.9984, 0.9937, and 0.9999 at each of samples. Figure 2(b) shows the individual responses against irradiation dose. The normalized results can be seen that the standard deviation of the individual response was decreased according to increasing the irradiation dose. Figure 2(c) shows the fading of the RIS in using one donor's samples. It can be seen that each of the relative standard deviation (RSD) from 1 to 50 Gy is 50.47, 24.66, 15.27, 5.99, and 5.51% at each of doses.

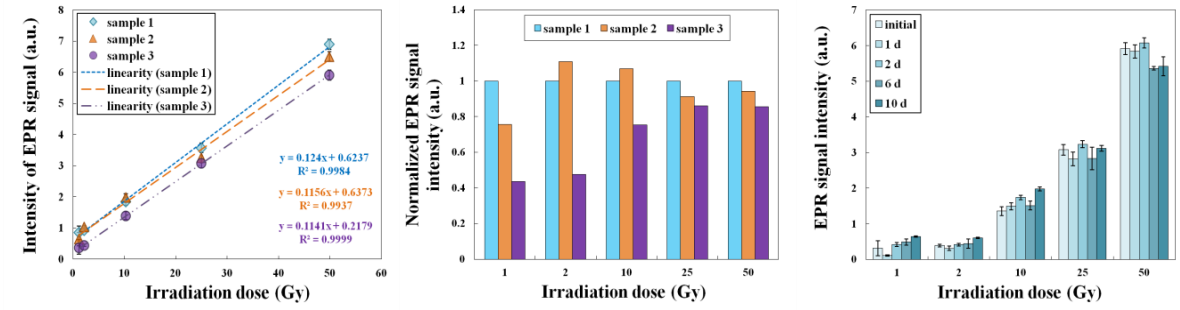

(a) (b) (c)

Figure 2. The characteristic of RIS in Korean fingernail-EPR signal: (a) the linear relationship between irradiation dose and intensity of EPR signal, (b) the individual responses according to irradiation dose, and (c) the fading of RIS in the irradiated samples within 10 d.

Conclusion These preliminary studies were carried out to evaluate the characteristics of RIS on the sample's EPR response. The linearity of dose response will be applied to determine the exposed dose using the dose response curve of RIS in the fingernails. The individual response and fading should be considered as a correction factor for an accurate dose assessment. These results of characteristic of RIS will be applied to produce an accurate and rapid protocol for Korean fingernail-EPR dosimetry.

References

1) Trompier, F., Romanyyukha, A., Kornak, L., Calas, C., LeBlanc, B., Mitchell, C., Swartz, H., Clairand, I., 2009. Electron paramagnetic resonance radiation dosimetry in fingernails. Radiat. Meas. 44, 6-10.
2) Ricardo, A. R., Trompier, F., Romanyukha, A., 2012. Study of the stability of EPR signals after irradiation of fingernail samples. Health Phys. 103(2), 178-180.

RFID based electronic chip cards – retrospective dosimeter for Individual dose assessment

Jakathamani S[1,2], Annalakshmi O[2], Mathiyarasu R[2]., Jose M. T[1,2], Venkatraman B[1,2]
[1]*Homi Bhabha National Institute, Mumbai, India*
[2]*HSEG, IGCAR, Kalpakkam, India.*

Highlights OSL (Optically Stimulated Luminescence) dosimetric properties of silica chip present in RFID (Radio Frequency IDendification) based identity cards were studied for emergency retrospective dosimetry. The protocol for retrieval of the absorbed dose was developed using SAR (Single Aliquot Regenerative Dose).

Key words Accident dosimetry, OSL, SAR protocol

Background and Objectives Retrospective dosimetry is an important aspect of radiation related accident investigations. As per the report from IAEA[1)] retrospective dosimetry consists of the measurements conducted for dose reconstruction purposes when information provided by conventional dosimetry methods is inadequate or unavailable. This is being carried out using a variety of techniques including Thermoluminescence (TL), Optically Stimulated Luminescence (OSL), Electron Paramagnetic Resonance (EPR), Chemiluminescence etc. Mostly, electronic components extracted from electronic devices are reported for accident dosimetry applications using TL and OSL[2)]. In this work, we investigated the OSL dosimetric properties of silica (without epoxy encapsulation) extracted from RFID based electronic identity cards and established a protocol for using it as a retrospective dosimeter for the estimation of dose to individuals.

Materials and Methods The silica(inset of fig.1(a))part from RFID based electronic cards were extracted mechanically without epoxy encapsulation. OSL measurements were carried out for silica part alone using an automated RISO TL/OSL reader-DA-20 equipped with blue LEDs (470 nm ± 30 nm) for stimulation, delivering approximately 72 mW/cm^2 at the sample position and a Thorn EMI 9235 bialkali photomultiplier combined with a 7.5 mm U-340 Hoya filter (290-370 nm) for detection of light from sample. The irradiations were carried out using built-in ^{90}Sr/^{90}Y beta source in RISO reader and ^{137}Cs gamma source. The OSL decay curves were analyzed using the light output in the first 1 s for determination of dose due to external radiation and average data during the last 5 s of stimulation is used as background.

Results and Discussion In order to check the radiation sensitivity, silica extracted from RFID based ID cards was irradiated to a dose of 5 Gy using built-in beta source and the recorded OSL decay curve is shown in the inset of fig.1 (a). The response of the silica chip to different doses of beta radiation was studied and the dose response curve is shown in fig. 1(a). The result shows that the response is linear from 100 mGy to 15 Gy. The minimum detectable dose was estimated to be 100 mGy from the standard deviations of the OSL output of un-irradiated silica. The linearity of the response was also checked with gamma dose from ^{137}Cs source. In order to study the fading percentage of OSL signal, the identity cards (as a whole) were irradiated with 3 Gy of gamma dose at different periods of time using ^{137}Cs and stored in dark. The OSL measurements were carried out on a single day and from the results it was observed that the signal faded around 15% in the first 24 hours and upto maximum of 60% in one week and thereafter the signal is stable. The protocol for dose reconstruction was developed using SAR and the dose was estimated with an accuracy of around 10 - 20% using different test doses. Fig. 1(b), shows the dose retrieval (dose reconstruction) of 1 Gy using SAR protocol with 5 Gy test dose normalization.

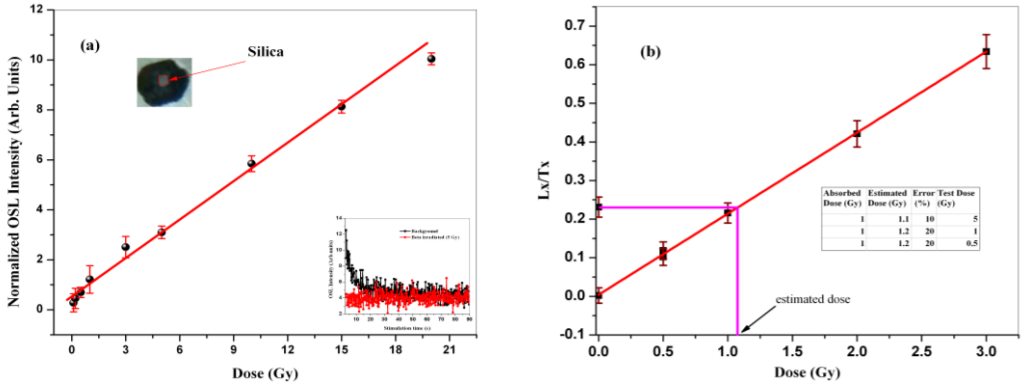

Figure 1: (a) Dose response of silica chip (b) Dose reconstruction – SAR protocol

Conclusion OSL technique has been applied to reconstruct the radiation dose from an irradiated RFID based identity card. From the current studies it is evident that RFID based ID cards can be used for radiation dose estimation in case of emergencies with appropriate correction factors for fading. Further work is being carried out in improving the accuracy of the dose estimation after the exposure with appropriate correction factor for fading.

References

1) R. V. Griffith: Retrospective Dosimetry needs from an IAEA perspective, Radiation Protection Dosimetry Vol. 77, No. 1/2, pp. 3–9 (1998) Nuclear Technology Publishing.
2) Clemens Woda, Irene Fiedler, Thomas Spöttl: On the use of OSL of chip card modules with molding for retrospective and accident dosimetry, Radiation Measurements 47 (2012) 1068-1073.

Physical characteristics of zero-dose in TL/OSL retrospective dosimetry using resistor component within electric personal dosimeter

Jeongtae Lee[1]*, Hyungjoon Yu[1], M.J. Kim[2]
[1]*Korea Institute of Nuclear Safety, Daejeon, Republic of Korea*
[2]*RADPION Inc., Daejeon, Republic of Korea*

Highlights Resistor TL/OSL zero-dose is very important to TL/OSL retrospective dosimetry using electric personal dosimeter (EPD). We evaluated the zero-dose for the resistor TL/OSL signal, respectively. We also examined the thermal and optical dependence of the zero-dose.

Key words Zero-dose, resistor, TL/OSL, thermal dependence, optical dependence

Background and Objectives In Korea, it is mandatory for radiography radiation workers to wear an active electronic personal dosimeter (EPD) as well as a passive dosimeter. For those radiation workers, a certain situation which could make their dosimeter not to be reliable rarely occurs, such as dropping TLD near sources, failure of EPD record. The record of EPD may be unreliable in a certain condition such as pulsed radiation field, high or low energy field, high dose rate field[1)]. In that case, TL/OSL retrospective dosimetry using resistor component within cell phone has been used as an alternative tool to assess personal dose[2)]. However, using private cell phone was considered somewhat impractical due to some difficulties such as the uncertainty of carrying cellphone, etc. Meanwhile, EPD has resistor components in the same manner, even more and bigger compared to those of cell phone. Based on these findings, the study on the development of the dosimetry specialized in radiography field was carried out[3)].
In the study of TL/OSL retrospective dosimetry, zero-dose (residual dose measured from non-radiation-induced background signal) is critical factor to assess personal dose accurately. Especially the magnitude and fluctuation of zero-dose is closely related to the minimum measurable dose (MMD). In this study, we researched the physical characteristics of zero-dose of resistor component within EPD.

Materials and Methods In order to calculate the zero-dose of resistor component within EPD, the model CLOVER (ADR-20, ILJIN Radiation Engineering Co, Ltd) was selected as sample, which is the most widely used in radiography field in Korea. Resistor components were extracted from the front and back side of the PCB and grouped into 8 regions. Spatial distribution of zero-dose was figured out by applying simplified SAR-TL/OSL method. The

thermal and optical dependence of the zero-dose were also measured from the REEL resistors (Type 1608, 1.6x0.8 mm^2) used in manufacturing the EPD.

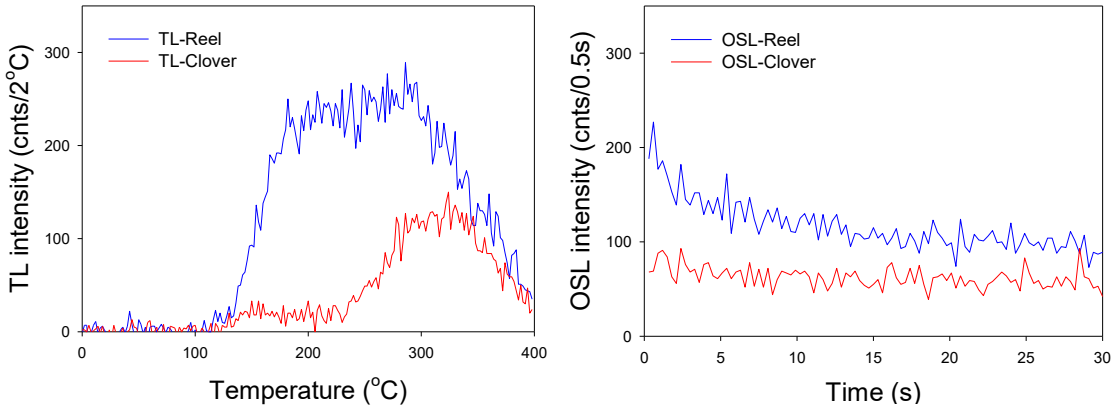

Figure 1. Comparison between TL/OSL signals measured from EPD and REEL resistor.

Results and Discussion In this study, we found that the mean TL/OSL zero-doses of resistor component within EPD were distributed as 31~100 mGy (TL ROI: 100~200ºC) and 9~17 mGy (OSL ROI: 0~1.5s). However, there was no difference of zero-dose between each side of PCB. Also, we found that zero-dose is much sensitive to heat rather than light. It indicates that the soldering heat in manufacturing process is one of the significant factors to determine the zero-dose of resistor components.

Conclusion We figured out that the OSL signal of resistor components within CLOVER EPD has high sensitivity to heat and light, and because of this, low and stable zero-dose distribution. Therefore, we concluded that the retrospective dosimetry of OSL is much reliable than that of TL. The physical characteristics of zero-dose of resistor components within EPD is expected to contribute to the accurate assessment of personal dose of radiation workers.

References

1) Intercomparision of personal dose equivalent measurements by active personal dosimeter(TECDOC-1564), IAEA
2) Beerten, K., Woda, C., Vanhavare, F., 2009. Thermoluminescence dosimetry of electronic components from personal objects. Radiat. Meas. 44, 620-625.
3) Kim, M.J., Gil, J.K, Sung, K.S., 2018. Preliminary study for the dosimetric characteristics of electric devices within electric personal dosimeter (KINS/HR-1693), Korea Institute of Nuclear Safety.

Retrospective dosimetry using optically stimulated luminescence of smart chip card

Jungil Lee[1]*, Hyoungtaek Kim[1], Min Chae Kim[1,2], Michael Discher[3], Clemens Woda[4], Insu Chang[1], Seung Kyu Lee[1], Jang-Lyul Kim[1], Kisoo Chung[5]

[1]*Korea Atomic Energy Research Institute, 989-111 Daedeok-daero, Yuseong-gu, Daejeon, 34057, Korea*

[2]*Hanyang University, 222, Wangsimni-ro, Seongdong-gu, Seoul, 04763, Korea*

[3]*University of Salzburg, Department of Geography and Geology, Salzburg, Austria*

[4]*Helmholtz Zentrum München, Institute of Innovative RadiotherapyRadiation Medicine, Neuherberg, Germany*

[5]*Gyeongsang National University, Department of Physics, Junju, Korea*

Highlights Optically stimulated luminescence properties of smart chip cards were identified.

Key words retrospective dosimetry, smart chip cards, OSL

Background and Objectives When an unexpected radiation accident or terrorism is happened, various techniques for retrospective dosimetry such as chromosomes analysis in blood samples[1)], electro paramagnetic resonance (EPR) measurement on tooth samples[2)], thermoluminescence (TL) and optically stimulated luminescence (OSL) measurement on personal belongings[3)], and computational calculation[4)] can be performed to restore a dose on a patient. Each technique can be applied complementarily depending on a time and geometry of exposure. The TL/OSL method proven to be capable of rapid and accurate dose assessment can[3,5,6)] be take the first order for a triage. In the previous studies, a chip card showed a high possibility of accurate dose reconstruction with a minimum detectable dose (MDD) less than 10 mGy for OSL measurements and around 100 mGy for infrared stimulated luminescence (IRSL) measurement[5-7)]. In the present study, measurement optimization using a different stimulation light (UV, blue, green and Infrared) and detection window (combination of filter and detector) for recently distributed smart chip card was carried out.

Materials and Methods The smart chip card model applied in the experiment was a SEL 4442 chip contact IC card which is available in an online market. In addition, check and credit cards actually used in the market will also be tested. An encapsulation filler material of a smart chip is a UV-cured epoxy compound which contains silica and showed dosimetric properties for OSL[5-7)]. The samples were mounted on a sample cup and measured in a Riso-DA20 TL/OSL reader. The reader was upgraded with a filter and detector changer. An ET PDM9107-CP-TTL PMT for blue detection window (160 - 630 nm) and a Hamamatsu H7421-40 for red detection

window (300 - 720 nm) are selectable. A filter set can be consist of one of U-340 (7.5 mm), blue filter pack (2 mm Schott BG-39 and 3 mm Schott BG-3), Brightline HC 340/26 (2mm). An Optical stimulation was achieved by one of blue LED (470 nm, 80 mW/cm^2), Green LED (525 nm, 40 mW/cm^2), IR LED (850 nm, 300 mW/cm^2) and violet laser (405 nm, 100 mW).

Results and Discussion In figure 1, the OSL decay curves of 1 Gy irradiated and non-irradiated smart chip card were represented. Signal distribution of zero dose and long term stability of OSL signal will be measured according to the measurement configurations.

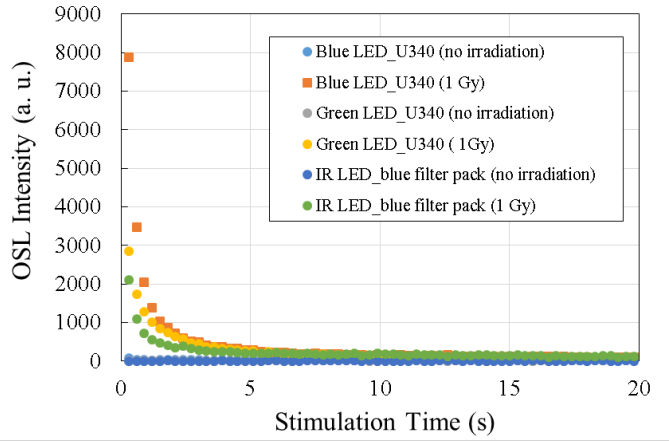

Figure 1. OSL decay curve of 1 Gy irradiated and non-irradiated smart chip card (SEL 4442 chip contact IC card)

References

1) Snigiryova, G., Braselmann, H., et al., 2009. Retrospective biodosimetry of Chernobyl clean-up workers using chromosome painting and conventional chromosome analysis, Int. J. Radiat. Biol. 71, 119-127
2) Skvortsov, V.G., IIvannikov, A., et al., 2000. Application of EPR retrospective dosimetry for large-scale accidental situation, Appl. Radiat. Isotopes, 52, 1275-1282
3) Discher M. and Woda C., Thermoluminescence of glass display from mobile phones for retrospective and accident dosimetry, Radiat. Meas., vol 53-54, 12 – 21, 2013.
4) Eakins, J.S., Kouroukla, E., 2015. Luminescence-based retrospective dosimetry using Al2O3 from mobile phones: a simulation approach to determine the effects of position, J. Radiol. Prot., 35, 343–381.
5) Mathur V.K. et al., Radiation sensitivity of memory chip module of an ID card, Radiat. Meas., vol 42, 43 – 48, 2007.
6) Woda C. et al., On the use of OSL of wire-bond chip card modules for retrospective and accident dosimetry, Radiat. Meas., vol 44, 548 – 553, 2009.
7) Woda C. et al., On the use of OSL of chip card modules with molding for retrospective and accident dosimetry, Radiat. Meas., vol 47, 1068 – 1073, 2012.

EPR dosimetry study of Hiroshima atomic bomb victims

Kassym Zhumadilov[1,4 *], Alexander Ivannikov[2], Valeriy Stepanenko[2], and Masaharu Hoshi[3]

[1] L.N. Gumilyov Eurasian National University, Munaitpasova 13, Astana 010008, Kazakhstan
[2] A.F. Tsyb Medical Radiological Research Center, 4, Korolev str., Obninsk, 249036, Russia;
[3] Hiroshima University, 734-8553, Japan.
[4]National Research Nuclear University "MEPhI" (NRNU "MEPhI", Moscow, Russian Federation)

Highlights The method of electron paramagnetic resonance (EPR) dosimetry has been applied to human tooth enamel to obtain individual absorbed doses of victims of Hiroshima atomic bombing.

Key words EPR dosimetry, tooth enamel samples, Hiroshima, victims

Background and Objectives EPR dosimetry is one of the tools for retrospective individual dose reconstruction. This method can help to estimate the individual absorbed doses more than 50 years after the exposure event. EPR measures the number of radicals created by ionizing radiation exposure in tooth enamel.
Materials and Methods Only 3 teeth samples were collected from this region. According to our information there is no any dental x-ray was applied to patients. A tooth samples were cut to its buccal and lingual parts. Enamel was mechanically separated from dentine using hard alloy dental drills and diamond saws.
Results and Discussion It was found that the excess doses obtained after subtraction of natural background radiation for one person is background, second is 133 mGy and third is 243 mGy. Positions of teeth were 1, 2 and 4, therefore only lingual part was used for analysis. But for this case we cannot exclude with 100 % probability the influence of sunlight's to these samples. Another problem is the lack of samples, because not so many victims of black rain area are alive.
Conclusion Possibly, high dose of 243 mGy in tooth enamel of radiation is due to exposure from atomic bomb.

References

Zhumadilov K.S. et al. 2005. Tooth enamel EPR dosimetry: selecting optimal spectra registration parameters and effects of sample mass on sensitivity. J. Radiat. Res. 46, 435-442.
IAEA, 2002. IAEA-TECDOC-1331, Vienna.

Production mechanism of E_1' center by brittle fracture with fault displacement

Kiriha Tanaka[1]*, Jun Muto[1], Yasuo Yabe[1], Toshitaka Oka[1], Hiroyuki Nagahama[1]
[1]*Tohoku university, Miyagi, Japan*

Highlights ESR intensity for E_1' center increased linearly on new surfaces of quartz grains formed by brittle fracture. This result implies that E_1' center can be increased by various fault motions without frictional heating: brittle fracture of seismic fault movement fault creep, landslide and so on. E_1' center can also be an index of displacements of such fault motions.

Key words ESR fault dating, E_1' center, displacement, microwave power dependency

Background and Objectives Fault dating using an electron spin resonance (ESR) is a method to estimate an age of the last fault movement or fault formation. This method is based on a premise that trapped unpaired electrons in defects in quartz are accumulated by natural radiation and annealed by a fault movement (Ikeya et al., 1982). This premise has not been understood completely yet (Yang et al., 2019). Hence, we performed shear tests with different displacements using a low-velocity rotary shear apparatus and examined ESR characteristics.

Materials and Methods We used silica sands bought from APPIE, Japan, as starting quartz gouges. The silica sand is 45-300 μm in diameter and contains of 95 % SiO_2 and impurities of 5 %. Shear tests were conducted for starting gouge with normal stress of 1.0 MPa, slip rate of 0.76 mm/s and displacement up to 1.41 m. ESR measurements were performed for starting and sheared gouges at room temperature and microwave power of 0.01 mW. ESR measurements with microwave power from 1.0×10^{-4} to 25 mW were also performed and spin-lattice (T_1) and spin-spin (T_2) relaxation times were calculated according to Poole (1983) to assess microwave power dependency quantitatively. Microstructural observation was performed for starting and sheared gouges using a scanning electron microscope (SEM).

Results and Discussion Figure 1a showed that ESR intensity for E_1' center increased with displacement and reached 130 %. Figure 1b showed that microwave power dependency of E_1' center in quartz gouge got close to that of E_1' center on the surface of quartz with increasing displacements. Relaxation times T_1 and T_2 of gouges decreased linearly from 5.1×10^{-8} to 4.4×10^{-8} s and from 9.3×10^{-4} to 4.1×10^{-4} s, respectively, with increasing displacements. Effect of heating on E_1' center is negligible because maximum temperature rise at grain contacts is estimated to be about 150 K (Smith and Arnell, 2013). Moreover, SEM observation clarified grain size reduction of gouges after tests. Therefore, brittle fracture generates new grain

surfaces in quartz gouges and E_1' centers were produced on the surfaces. Shear test conditions in this study are close to the condition of stable fault sliding at the shallow depth without frictional heating such as fault creep and landslide. Our result implies that E_1' center in intra-fault material can increase by fault creep and/or landslide as well as brittle fracture of seismic fault movement, hence it can be an index of displacements of such fault motions.

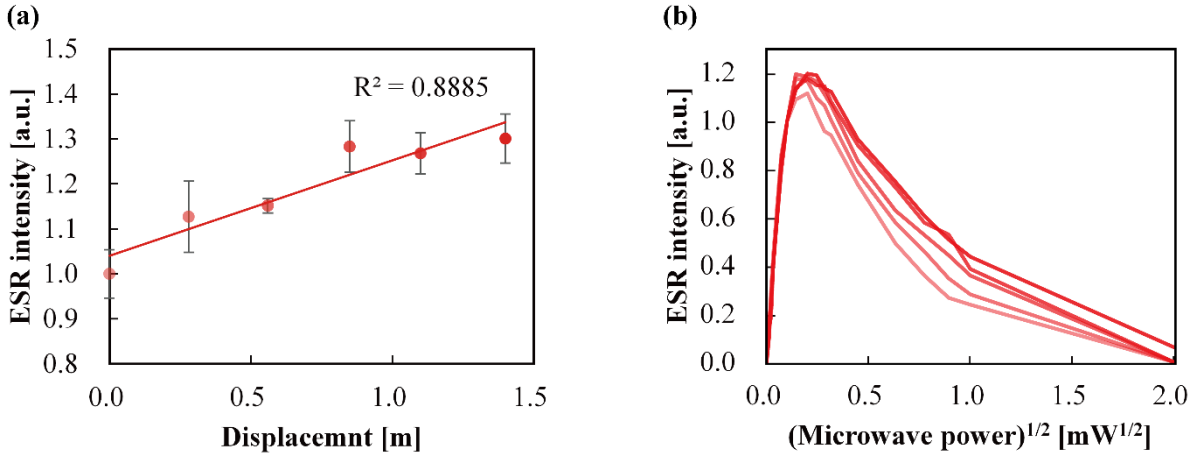

Figure 1. ESR characteristic change of E_1' center. (a) The relationship between the ESR intensity for E_1' center and fault displacements. (b) The relationship between ESR intensity for E_1' center and microwave power and red color represents displacements from 0, 0.28, 0.57, 0.86, to 1.13 m from lighter to darker, respectively.

Conclusion We performed shear tests for starting gouge with a normal stress of 1.0 MPa, a slip rate of 0.76 mm/s and displacements up to 1.41 m. ESR intensity for E_1' center increased linearly by brittle fracture with increasing displacements. The mechanism is presumed to be that brittle fracture generates new grain surfaces in quartz gouges and E_1' centers were produced on the surfaces. E_1' centers in intra-fault material seem to be affected by various fault motions without frictional heating and it can be an index of displacements of such fault motions.

References

1) Ikeya, M., Miki, T., Tanaka, K., 1982. Dating of a fault by electron spin resonance on intra-fault materials. Science, 215, 1392-1393.

2) Yang, H.L., Chen, J., Yao, L., Liu, C.R., Shimamoto, T., Thompson J.J.A., 2019. Resetting of OSL/TL/ESR signals by frictional heating in experimentally sheared quartz gouge at seismic slip rates. Quaternary Geochronology, 49, 52–56.

3) Poole, C.P., 1983. Electron spin resonance: A comprehensive treatise on experimental techniques. John Wiley and Sons Inc, 780pp.

4) Smith, E.H., Arnell, R.D., 2013. A new approach to the calculation of flash temperatures in dry, sliding contacts. Tribology Letters, 52, 407–414.

Luminescence investigations on memory cards from mobile phones for their use as fortuitous dosimeters

Knuth Scheiff, Alessia Mafodda, Clemens Woda*
Institute of Radiation Medicine, Helmholtz Zentrum München, Neuherberg, Germany

Highlights Memory cards from mobile phones have potential as fortuitous individual dosimeters; two OSL emissions at 330 and 370-390 nm; linear dose-response to several Gy; assessment of detection limit and signal fading

Key words Fortuitous dosimeter, TL, OSL, retrospective dosimetry, radiological or nuclear emergency

Background and Objectives Retrospective dosimetry using personal objects carried on or close to the human body has been intensively studied in the past decade due to the threat or risk of unplanned exposure of the general population with ionizing radiation. Mobile phones, being widespread among the population, seem to be particularly promising in this respect and many electronic materials found in the phones have been the subject of several investigations using either Thermoluminescence (TL), optically stimulated luminescence (OSL) or electron paramagnetic resonance (EPR): Touchscreen glass of modern smartphones, display glass, Integrated Circuits (ICs), surface mount resistors and inductors (see e.g.[1)] and references therein). One drawback of many of these materials and methods is the necessity to destroy the phone for the measurement, implying a possible low acceptability by the population. Sampling of comparatively low-cost, easily replaceable items, leaving the phone intact and functional, could be an improvement and in this study memory cards (micoSD cards) are investigated as such a potential candidate.

Materials and Methods Several tens of memory cards from different producers have been collected for analysis. TL and OSL measurements are carried out on intact cards and on the chemically extracted filler material[2)]. A Risoe TL/OSL-DA-20 and a Lexsyg Research (Freiberg Instruments) automated luminescence reader is used, the latter additionally equipped with a emission spectrometry unit, consisting of an Andor Technology iDus 420 Series CCD camera and a Shamrock 163 spectrometer.

Results and Discussion Preliminary results indicate that the OSL emission spectrum of the molding compound of the memory cards consists of a main emission peaking at 330 nm and a

second one at 370-390 nm. Considerably higher intensity per unit dose of the OSL signal was observed, when stimulating with blue LEDs (~ 470 nm) and detection in the UV (270-370 nm) than when stimulating with green LEDs (~ 530 nm) and detecting either in the UV or blue wavelength range (Fig .1). An increase in sensitivity to radiation of the OSL signal is seen for several cycles of dosing and readout. By using a single aliquot regenerative dose (SAR) protocol with test-dose normalization[3)], the effect of sensitivity changes could be reduced and a linear dose response observed until several Gy. The OSL signal can be thermally erased by heating up to 300°C but the shape of the pulse-annealing curve seems to vary between samples. Preliminary estimates of the detection limit of intact cards are in the order of tens of mGy, immediately after irradiation. Similar to the OSL signal of ICs, resistors and inductors, the OSL signal of memory cards is not stable but fades with time since irradiation. A detailed fading study, correlation between TL and OSL and results of trial irradiation on intact cards in mobile phones using a ^{137}Cs source will be presented.

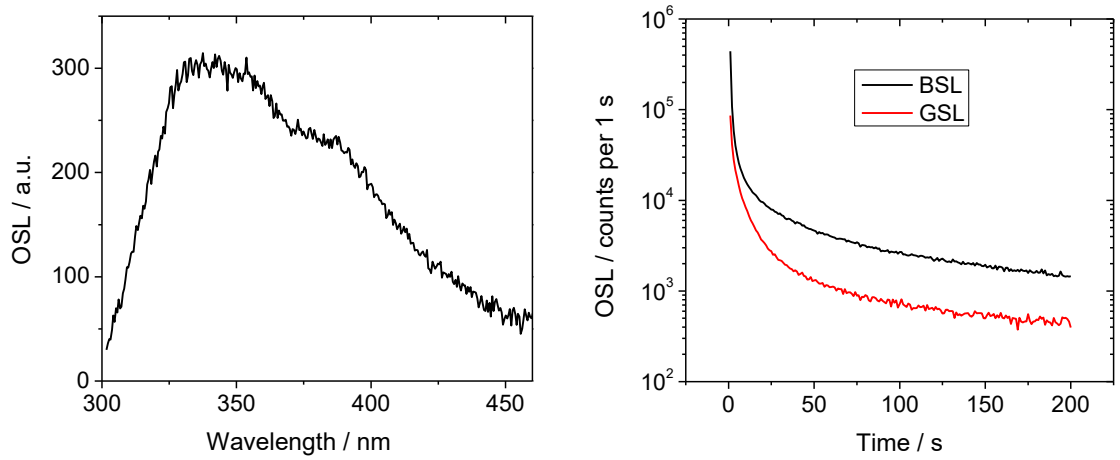

Fig. 1: OSL emission spectrum (left) and OSL decay curve (on filler material) with blue (BSL) and green LEDs (GSL) after irradiation with a dose 1 Gy and measuring in the 340-390 nm detection window.

Conclusion Based on the results obtained so far, memory cards, used in many modern smartphones, have a potential as fortuitous dosimeters for estimating individual doses following a radiological or nuclear incident.

References

1) Bailiff, I., Sholom,S. and McKeever, S.W.S., 2016. Radiat. Meas. 94, 83-139.
2) Woda, C., Fielder, I. and Spöttl, T., 2012. Radiat. Meas. 47, 1068-1073.
3) Murray, A.S. and Wintle, A.G., 2003. Radiat. Meas. 37, 377-381.

New Approaches for Teeth Retrospective Dosimetry based on Pulsed Electron Spin Resonance Techniques

Lotem Buchbinder[1,2]*, Hanan Datz[1], Aharon Blank[2]

[1] *Radiation Safety Division, Soreq Nuclear Research Center, Yavne, Israel*

[2]*MR Lab, Schulich Faculty of Chemistry, Technion - Israel institute of technology, Haifa, Israel*

Highlights Pulsed Electron Spin Resonance (P-ESR) technique for tooth-based dosimetry shows great promise in providing direct estimate of spin concentration without a-priori knowledge of the measured tooth volume. The proposed technique could be used as a basis for accurate retrospective dosimetry.

Key words Radiation, Dosimetry, Retrospective, ESR, Relaxation time, DEER, Teeth

Background and Objectives Electron Spin Resonance (ESR) of teeth enamel has been applied for retrospective dosimetry for many years. The common approach makes use of continuous–wave ESR (CW-ESR), which provides dosimetric data solely based on the magnitude of the ESR signal. This approach is prone to many problems, ranging from instrumental signal instability to unknown biological variability of the enamel amount in a given tooth. One possible way to overcome these issues is to apply pulsed- rather than CW-ESR approach. P-ESR can provide much richer information about the properties of the paramagnetic defects in the tooth, such as their relaxation times or the strength of the magnetic interaction between them. These parameters can be directly correlated with the concentration of the paramagnetic defects, and thus directly provide the dosimetry data (which is known to be linearly correlated with defects' concentration). However, while P-ESR techniques have been around for many years, only a few studies have employed it to teeth dosimetry, primarily due to issues, such as short relaxation times at room temperature and poor sensitivity.

In higher doses and higher spin concentrations, spins are closer to one another and have stronger interactions. Therefore, we focus on two phenomenon with measurable quantities that are influenced by these interactions and accessible by P-ESR. The first is spin-spin relaxation time, T_2, involving dipole interaction between spins. Our hypnosis is that the higher concentration the faster energy exchange will be, due to spins' proximity in the lattice, resulting in a shorter relaxation time. The spin dipole interaction can also be directly measured using advanced P-ESR techniques, such as Double Electron-Electron Resonance (DEER). The so-called DEER relaxation curve can provide the average distance between the interacting spins.

Materials and Methods Measurements were carried out with a miniature dielectric resonator using a home built P-ESR system, operating at ~10 GHz. A dedicated probe-head (Figure 1) was constructed to provide adequate spin sensitivity for samples irradiated with 1000 Gy down to ~ 10 Gy. Special miniature gradient coils incorporated into the probe-head to reduce dead time by stepping quickly the magnetic field and thus cope with the problem of short relaxation times of the measured tooth radicals. Relaxation processes studies carried out using the Hahn echo pulse sequence. The relaxation process is characterized by a signal that decays at a rate characterized by defined by the time constant T_2. This time constant is a fundamental property of the sample, often depending on spin concentration. However; it is not dependent on possible static field heterogeneity, which is an instrumental artefact. A second method, 3-pulse DEER method uses two separate microwave frequencies to study dipolar interaction.

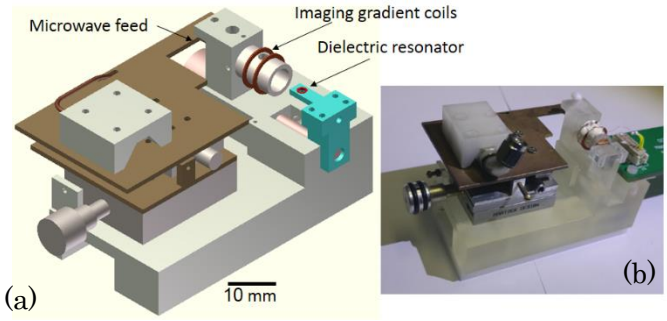

Figure 1. (a) Drawing of the teeth measurements probe with imaging capabilities.
(b) Assembled prototype of the new teeth probe.

Results and Discussion The relaxation time, T_2, was measured for several teeth, irradiated with various doses and was found to be in the order of few hundreds of nanoseconds. Data was analysed using MatLab script and UPENWin to obtain the T_2 & full distribution of T_2. The general trend is for T_2 to decrease as a function of the irradiation dose, due to increased spin-spin interaction. DEER experiments using irradiated quartz show a rapid decay with increased dose with good correlation to theory.

Conclusion Spin-spin relaxation time measurements show a trend which indicate that lower doses have a longer T_2, this could allow to estimate spin concentration. Initial DEER measurements with irradiated Quart show slower decay in lower doses. Both of these techniques show for the first time the use applicability of Pulsed ESR for dose estimation without dependence on the sample volume.

Phototransferred thermoluminescence measurements of glass extracted from modern mobile phones

Michael Discher[1]*, Clemens Woda[2], Jungil Lee[3], Hyoungtaek Kim[3], Kisoo Chung[4], Andreas Lang[1]

[1]*University of Salzburg, Department of Geography and Geology, Salzburg, Austria*
[2]*Helmholtz Zentrum München, Institute of Radiation Medicine, Neuherberg, Germany*
[3]*Korea Atomic Energy Research Institute, Radiation Safety Management Division, Yuseong, Daejeon, Republic of Korea*
[4]*Gyeongsang National University, Department of Physics, Junju, Republic of Korea*

Highlights: The PTTL method for an additional independent measure on the glass material extracted from mobile phones is tested as a tool for retrospective dosimetry.

Key words: Emergency dosimetry, glass extracted from mobile phones, PTTL, TL

Background and Objectives: Different investigations have shown that components of mobile phones are suitable as emergency dosimeters in case of radiological incidents. For physical dosimetry, components can be read out using optically stimulated luminescence (OSL), thermoluminescence (TL) and phototransferred thermoluminescence (PTTL) methods to determine the absorbed dose for retrospective dosimetry.

Among the variety of items investigated, a promising material is glass (i.e. watch glass, display glass, touch screen glass). Its dosimetric properties have been studied in detail for touch screen glass [4; 6] and display glass of modern mobile phones [1-3; 5; 7]. The studies show that for unexposed glass samples a native signal, so-called zero dose signal, is observed which significantly limits the low-dose sensitivity. Employing a labor-intensive sample preparation procedure can reduce the zero dose signal. Generally, the TL signal of glasses is also not stable over time and a fading correction has to be applied for an accurate dose reconstruction.

The PTTL method uses deep radiation-sensitive traps for dose reconstruction and consists of 1) preheating the sample to a certain temperature, 2) exposing the sample to UV light and 3) measuring the luminescence signal of electrons transferred to shallower traps, that were emptied during preheating.

In a recent investigation the PTTL signals of a specific touch screen glass were studied and indicate higher thermal stability that corrections for fading of the PTTL signal may not be needed [6].

Results and Discussion: For preliminary measurements, touch screen and display samples were extracted from two different mobile phones. The PTTL signals of background (as received,

no irradiation) and PTTL signals of previously irradiated samples (2 Gy beta dose) were obtained after preheating to 400°C and 365 nm UV light exposure for 20 minutes (see Fig. 1). The signal shape is similar to the shape of the PTTL signals reported in [6].

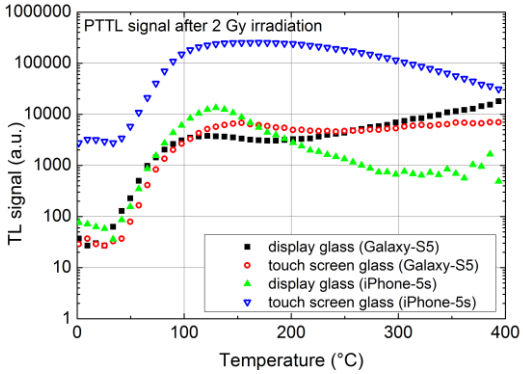

Fig. 1: PTTL glow curves of irradiated touchscreen and display glass samples of two modern mobile phones after preheating to 400°C and exposure to UV light.

Conclusion: Further dosimetric investigations, in terms of signal fading, confounding signals, detection limit, luminescence emission spectrometry and dose recovery tests, are carried out with more glass samples of different modern mobile phones (touch screen and display glass) to support the results obtained so far for a specific type of touch screen glass. The PTTL method on glass has the potential of detecting an almost stable signal and may serve as an additional independent measure on the glass material extracted from mobile phones.

References:

[1] Bassinet C. et al., 2014. Radiation accident dosimetry: TL properties of mobile phone screen glass, Radiat. Meas 71, 461 – 465.

[2] Discher M. and Woda C., 2013. Thermoluminescence of glass display from mobile phones for retrospective and accident dosimetry, Radiat. Meas. 53-54, 12 – 21.

[3] Discher M. and Woda, C., 2014. Thermoluminescence emission spectrometry of glass display in mobile phones and resulting evaluation of the dosimetric properties of a specific type of display glass. Radiat. Meas. 71, 480 – 484.

[4] Discher M. et al., 2016. Investigations of touchscreen glasses from mobile phones for retrospective and accident dosimetry. Radiat. Meas. 89, 44 – 51.

[5] Kim, H. et al. in press. Thermoluminescence of AMOLED substrate glasses in recent mobile phones for retrospective dosimetry. Radiat. Meas., DOI: 10.1016/j.radmeas.2019.01.004.

[6] McKeever, S. W. S. et al., 2017. Phototransferred thermoluminescence (PTTL) dosimetry using Gorilla glass from mobile phones. Radiat. Meas. 106: 423-430.

[7] Mrozik A. et al., 2014. Investigation of thermoluminescence properties of mobile phone screen displays as dosimeters for accidental dosimetry. Radiat. Phys. Chem. 104, 88 – 92.

Computational method of dose conversion from a mobile phone display glass to human body with different size of mesh phantoms for emergency dosimetry

Min Chae Kim[1,2], Hyoungtaek Kim[1], Haegin Han[2], Jungil Lee[1,*], Seung Kyu Lee[1], Insu Chang[1], Jang-Lyul Kim[1], and Chan Hyeong Kim[2]

[1]*Radiation Dosimetry Team, Korea Atomic Energy Research Institute, 989-111 Daedeok-daero, Yuseong-gu, Daejeon, 34057, Republic of Korea*

[2]*Department of Nuclear Engineering, Hanyang University, 222, Wangsimni-ro, Seongdong-gu, Seoul, 04763, Republic of Korea*

Highlights Monte Carlo simulation was performed to reconstruct a body dose from a mobile phone dose. Doses were calculated with the different size of mesh phantoms for various exposure conditions.

Key words retrospective dosimetry, emergency dosimetry, thermoluminescence (TL), optically stimulated luminescence (OSL), mesh phantom, Monte Carlo simulation

Background and Objectives A variety of techniques for emergency dosimetry have been conducted to reconstruct an exposed dose using surrounding objects in absence of a dosimeter. Methods for dose reconstruction include techniques such as analysis of chromosomes of lymphocytes in blood[1)], an electron paramagnetic resonance (EPR) of tooth samples[2)], and thermoluminescence (TL) / optically stimulated luminescence (OSL) measurements using materials of mobile phone components such as a resistor, inductor, and display glass[3)]. Among those, the TL/OSL techniques, which have advantages like fast sample preparation and rapid dose reconstruction, are in the limelight in actual accidents. However, since a reconstructed dose from surrounding objects is not corresponded to a human body dose, several studies were carried out to derive dose conversion factors using a Monte Carlo calculation with a human phantom[4,5)]. The previous studies have shown that a human body itself significantly affects to the dose reconstruction of a mobile phone up to 2.7 times for standing posture[4,5)]. These simulations were only calculated for a phantom of one standard size (176 cm/ 73 kg in ICRP reference data). However, an actual size of a human body is various and also affects to the dose conversion factors. In order to use a human phantom matched to the size of a victim, voxel and mesh phantoms having various body sizes in terms of height and weight have been designed[6,7)]. In this study, simulations were performed to provide factors for dose conversion for three different sizes with mesh phantoms (10th, 50th, and 90th percentile of height and weight). In addition, uncertainty from a body size was

derived to get a human body dose, because it is not easy to reflect an actual size of victims for triage in a radiation emergency.

Materials and Methods Monte Carlo simulations were performed using the GEANT4 (GEometry ANd Tracking 4) code. Three sizes of mesh-type reference computational phantoms (MRCPs) for adult male were selected: M_H10W10 (167.2 cm/ 55.9 kg), M_H50W50 (176.5 cm/ 79.3 kg), and M_H90W90 (185.8 cm/ 108.4 kg) in standing posture[6]. A bottom display glass of a mobile phone was defined as a fortuitous dosimeter. The mobile phone was located on the chest, hip, thigh, and hand of phantoms. Iridium-192, Caesium-137, and Cobalt-60 were applied and exposure geometries were employed with anterior-posterior (AP), posterior-anterior (PA), left-lateral (LLAT), right-lateral (RLAT), isotropic (ISO), and rotational (ROT).

Results and Discussion Conversion factors which enable to estimate human body dose from a mobile phone dose will be listed as per difference sizes of the phantom. Variations of phone doses were observed depending on phone positions and body sizes, which were resulted from different shielding effects of different body sizes.

References

1) Snigiryova, G., Braselmann, H., et al., 2009. Retrospective biodosimetry of Chernobyl clean-up workers using chromosome painting and conventional chromosome analysis, Int. J. Radiat. Biol. 71, 119-127
2) Skvortsov, V.G., IIvannikov, A., et al., 2000. Application of EPR retrospective dosimetry for large-scale accidental situation, Appl. Radiat. Isotopes, 52, 1275-1282
3) Lee, J.I., et al., 2017. Thermoluminescence of chip inductors and resistors in new generation mobile phones for retrospective accident dosimetry. Radiat. Meas., 105, 26–32
4) Eakins, J.S., Kouroukla, E., 2015. Luminescence-based retrospective dosimetry using Al_2O_3 from mobile phones: a simulation approach to determine the effects of position, J. Radiol. Prot., 35, 343–381
5) Kim, M.C., Kim, H., et al., 2019. A study on dose conversion from a material to human body using mesh phantom for retrospective dosimetry, Radiat. Meas., under review
6) Lee, H.J., Yeom, Y.S., et al., 2019. Percentile-specific computational phantoms constructed from ICRP mesh-type reference computational phantoms (MRCPs), Phys. Med. Biol., 64, 045005
7) Johnson P B, Whalen S R, et al., 2009. Hybrid patient-dependent phantoms covering statistical distributions of body morphometry in the US adult and pediatric population Proc. IEEE 97 2060–75

Optical dating of the early Neolithic potteries excavated from the Gosan-ri archaeological site in Jeju Island, Korea

M.J. Kim[1]*, J.W. Go[2], M.B. Bang[2], J.H. Choi[3], D.G. Hong[4]
[1]*RADPION Inc., Daejeon, Korea*
[2]*Jeju Cultural Heritage Institute, Jeju, Korea*
[3]*Korea Basic Science Institute, Daejeon, Korea*
[4]*Kangwon National University, Chuncheon, Korea*

Highlights Optical dating was carried out for the early Neolithic potteries collected from the Gosan-ri site. Gosan-ri-type pottery known as the oldest pottery in Korea was manufactured and utilised from the late 8th century BC. Gosan-ri site was formed after the late 10th century BC and had been lasted during about 500 years.

Key words Gosan-ri-type pottery, Gosan-ri site, OSL dating, Neolithic age

Background and Objectives It has been known that the earliest pottery is from the Far East region between 17,300 cal. BP and 15,000 cal. BP. Especially, early potteries from the Russian Far East including Japan and China are mostly plant-fibre-tempered pottery and accompanied with the relics from chronological sequences of Palaeolithic-to-Neolithic age[1)]. On the Korean peninsula, plant-fibre-tempered pottery was only found in the early Neolithic sites on Jeju Island. This pottery is termed 'Gosan-ri-type pottery' (GSTP) in reference to the Gosan-ri site where it was first discovered. However, in spite of the archaeological importance of the Gosan-ri site and GSTP, it could not obtain the reliable absolute ages over the last twenty years, because of the lack of sufficient sample amount and optimum dating method. So, the absolute chronology of the Gosan-ri site as well as GSTP has been controversial issue in the Korean archaeological research.

In the recent excavations at the Gosan-ri site, a number of very important structures and features, including a dwelling pit and large hearth contained many GSTP shards were yielded. These new discoveries are very significant and have great potential to provide reliable absolute ages on the basis of the archaeological context of the Gosan-ri site. In this study, we carried out the OSL dating for GSTP and other Neolithic potteries collected from these newly discovered structures and features in an attempt to determine the an absolute chronology for the Gosan-ri site. Finally, we estimated the period of the formation, occupation and discard at the Gosan-ri site based on a statistical analysis combining the pottery OSL ages resulting from this study with other absolute ages obtained from the Gosan-ri site and its neighbouring places in the previous studies.

Figure 1. The early Neolithic relics excavated from the Gosan-ri archaeological site.

Materials and Methods In order to evaluate the absolute dates of the early Neolithic potteries in the Gosan-ri site, we selected six pottery shard samples including four GSTPs, one appliqué decorated pottery, and one plain coarse pottery. Paleodose was evaluated from the SAR-OSL method and annual dose rate was calculated from the concentrations of the natural radionuclides both sample and its neighbouring soil.

Results and Discussion The pottery OSL age was determined from the ratio of the paleodose to annual dose rate. From the high degree of thermal zeroing during pottery firing process, accurate recovery of paleodose, and the burial conditions, it turned out that the resulting OSL ages are reliable. Also, all pottery OSL ages agreed well with those typological order as GSTP -> appliqué -> plain-coarse[2]. With the Bayesian statistical analysis we concluded that GSTP was manufactured and utilised from the late 8th century BC. Also, the Gosan-ri site was formed after the late 10th century BC and abandoned before the early 5th century BC.

Conclusion We determined the OSL ages for the early Neolithic potteries collected from the Gosan-ri site. These results will corroborate the fact that GSTP is the oldest known Korean Neolithic pottery, and contribute the absolute chronology from the formation to discard of the Gosan-ri site.

References

1) Kuzmin, Y.V., 2013. Origin of old world pottery as viewed from the early 2010s: When, where and why?. World Archaeology 45, 539–56.
2) Go, J.W., Kim, K.J., Bang, M.B., 2014. The Jeju Gosan-ri Site, Jeju Cultural Heritage Institute.

ESR and OSL Dating of mammalian fossils from Mirim Lake, Southen Brazil

Angela Kinoshita[1,2], Renato Lopes[3], Ana Maria G Figueiredo[4], Sonia Tatumi[5], Marcio Yee[5]
Oswaldo Baffa[1*]

[1]*FFCLRP-USP, Universidade de São Paulo, Ribeirão Preto, SP, Brazil*
[2]*USC, Universidade do Sagrado Coração, Bauru – SC, Brazil*
[3]*UFSC, Universidade Federal de Santa Catarina, Florianópolis – SC, Brazil,*
[4]*IPEN, Instituto de Pesquisas Energéticas e Nucleares, São Paulo, SP, Brazil*
[5]*UNIFESP, Universidade Federal de São Paulo, Santos, SP, Brazil*

Highlight: Fossils of mammals found in Mirim Lake, southern Brazil were dated by ESR and OSL, providing consistent results with site stratigraphy and literature data from nearby sites.

Key words: ESR Dating, OSL dating, Mirim Lake

Background and Objectives: On the southeastern bank of the Mirim Lake, in the south of the Coastal Plain of the State of Rio Grande do Sul. Several fossils of a notoungulate *Toxodon platensis*, presumably of the same animal, were found in a layer, 3 meters below the surface of the surrounding terrain during a period of drought, that lowered the water level. Being preserved in their original depositional setting, these remains provided an opportunity for interpreting their depositional history and determining the chronostratigraphic setting of the fossil-bearing deposit. One tooth was selected for ESR dating. From a layer of caliche nodules composed of quartz and feldspar grains embedded in Alpha-type micritic cement, positioned at about 0.5 meter above the fossils, one nodule was selected for dating using optically stimulated luminescence (OSL)

Materials and Methods. The tooth was submitted to a thermal treatment, for separation of enamel and dentine. Then, the enamel was subjected to a 1N HCl acid treatment, in an ultrasonic bath for 3 minutes to extract an outer layer, dried and crushed manually to a powder with particles of 200-400 mesh diameter (38–76 μm). This material was divided into 10 aliquots of approximately 30 mg for irradiation with additive doses. The aliquots (except 1) were irradiated with gamma radiation at dose rate at 634 Gy/hour dose rate, up to a dose of 8 kGy. The spectrum of original and irradiated aliquots, were recorded on the JEOL FA-200 X-Band ESR spectrometer. The peak-to-peak intensity of the dosimetric signal at $g_{\perp}$ (g=2.0018) was associated with the additive dose for the construction of the dose-response curve (DRC) to obtain the equivalent dose (D_e). The enamel, dentine and sediment associated with teeth were

analyzed through Neutron Activation Analysis to determine the concentration of Uranium, Thorium and Potassium. De was converted into age through the DATA software. The cosmic dose rate of 190μGy / year was calculated taking into account latitude, longitude and the depth of the collection site. Sedimentary water was considered at 100%.

The caliche nodule was chemically cleaned with hydrogen peroxide during 24 hours, washed with distilled water, immersed in HF - 10% during 45 min, to remove carbonates and the surface of the quartz, thus removing the ionization from α-particle, washed with distilled water; subsequently, immersed in HCl - 10% for 2 hours, and washed again with distilled water. Finally, to eliminate heavy minerals and feldspar the sample was immersed in Sodiumpolyntungstate (SPT), then pure quartz grains were obtained. OSL measurements were performed on the RISø TL/OSL reader, with blue light excitation (470 nm) and detected in the UV region using U-340 optical filter. The equivalent doses (D_e) was determined by the single- aliquot regenerative-dose protocol. Fourth eight aliquots (~ 3 mg of 180-210 μm) of the sample were used. D_e values have been evaluated using aliquots with recuperation <5% and recycling test between ± 10 %. The samples were irradiated with a ^{90}Sr / ^{90}Y beta source with dose rate of 0.089 Gy/s. The natural radioactive contents (U, Th and K-40) were determined by γ-spectroscopy (high-pure germanium detector- HPGe, Canberra), the contribution of the cosmic radiation was theoretically calculated.

Results and Discussion:

The ESR dating of toxodon tooth provide ages of 68 ± 13 ka and 126 ± 24 ka for Early Uptake and Linear Uptake models respectively. The quartz grains extracted from a caliche nodule provided two groups using finite mixture modeling (FMM) for OSL age, being one of 32.8 ± 5.1 ka and the other of 16.9 ± 2.5 ka. The well-defined chronostratigraphic setting of the fossils found *in situ*, as determined by absolute ESR and OSL datings contribute for the understanding of the geological evolution of the lake shore in light of the Late Pleistocene climate changes.

Conclusion The well-defined chronostratigraphic setting of the fossils found *in situ*, as determined by absolute ESR and OSL dating contribute for the understanding of the geological evolution of the lake shore in light of the Late Pleistocene climate changes.

Partial Financial Support: Brazilian Agencies CNPq (407471/2016-2, 302730/2016-8) FAPESP (2013/07699-0, 2009/02069-2) and CAPES Finance Code 001.

Chronology of coastal dune ridges in Vaigai region, south-eastern Tamil Nadu, India

S.Sathiyaseelan[2], D K Panda[1], D Banerjee[1*], D Ramesh[2] and A D Shukla[1]
[1]*Physical Research Laboratory, Ahmedabad, India*
[2]*Bharathidasan University, Tamil Nadu, India*
[*]*Corresponding Author: deba@prl.res.in*

Highlights: We have tested the applicability of the post-infrared infrared stimulated luminescence dating of 90-150 µm quartz grains in five dune samples collected from a ~3.5 m deep trench near Ramanathapuram, Tamil Nadu. The pIRIR ages are stratigraphically consistent, and suggest aeolian activation began in this region before 60 ka, and continues until 2000 years ago.

Keywords: OSL, Aeolian sands, Tamil Nadu, post-IR IRSL

Background and Objectives: The Quaternary period is a great interest to the geoscientist for inferring the ecological, environmental and climatic changes. Throughout the world, coastal dunes ridges have been systamatically analysed to infer past climatic changes. Studies of coastal processes and evolution have frequently encountered problems in obtaining reliable chronologies for depositional events. There are very few studies exist which attempt at understanding the evolutionary changes of these coastal dunes. The Tamil Nadu coastline has well developed dune sediments which are archives of Quaternary paleoclimates. In the present study an attempt was made to infer the post-infrared infrared stimulated luminescence dating to reconstruct the palaeodepositional environments of coastal dune ridge sediments in Vaigai prodelta region during the Quaternary period.

Materials and Methods: We have tested the applicability of the post-infrared infrared stimulated luminescence dating of 90-150 µm quartz grains in 5 dune samples collected from a ~3.5 m deep trench near Ramanathapuram, Tamil Nadu. Although HF etching was performed, all aliquots exhibited post-IRIR signals. In light of this, a modified SAR protocol (Murray and Wintle, 2000) was used for post-IR IR dating following the procedures outlined in Buylaert et al. (2012). The same preheat conditions were applied prior to the measurement of the natural and regenerative dose as well as the test dose. The first IR stimulation was carried out at 60°C for 200 s, followed by the second stimulation at 290°C. Dose rate measurements were carried

out on dried samples, which were packed and sealed air-tight to prevent radon loss. The samples were stored for one month after sealing to re-establish ^{226}Ra-^{222}Rn equilibrium. External dose rates for the samples were calculated from the activity concentrations of decay chains ^{238}U, ^{232}Th and ^{40}K measured using high resolution gamma spectrometry (HPGe).

Results and Discussion: The pIRIR luminescence ages for the five dune-sand samples range from 2.0±0.3 to 57±6 ka. Alappat et al. (2016) have determined ages of red dune sands in the southwestern coast of Tamil Nadu. Their OSL ages suggested two events of deposition with the sands in the upper part being deposited during 16–13 ka, whereas the indurated layer in another terrace was deposited at 4.5 ka. Previous investigations have shown that monsoon precipitation intensified in the region as early as 14 ka and was dominant until up to 7 ka. During the early Holocene, dune building activity may have stopped or reduced significantly due to reduced sand supply in this region. During lower sea-level stands, aggradation is the dominant process since the continental shelf was exposed for aeolian reworking and may be related to the large scale aggradations during LGM in the river sequences along the west coast of India. The OSL age of 11 ka and 6.5 ka suggest sands were being deposited until ~11 ka and is consistent with previous findings. Jayangondaperumal et al. (2012) have found that coastal red sand in the east coast of India were deposited before 11 ka in association with lower sea level and the near-coastal red sand was deposited during the sea-level high stand at 6 ka. Furthermore, aeolian reactivation continued till 2000 years ago, and previous chronologies can be used to infer that sands from the upper part of the dunes in the southwestern Indian coastline were also deposited during the last ~400 years.

References

Murray A S and Wintle, A G 2000. Radiation Measurements, 32, 57-73.
Buylaert J P et al., 2012. Boreas, 41, 435-451.
Alappat L et al., 2016. German J Geol., 168, 183-198.
Jayangondaperumal, R., et al., 2012. Quart. Research, 77, 468-481.
Thiruvikramji, K.P., Joseph, S. and Anirudhan S. (2008). “Teri’s of Southern Tamilnadu. A Saga of Holocene climate change”, Memoir of Geol. Soc. India No. 74, p. 351-359.

Possible emergency dosimetry using the optically stimulated luminescence (OSL) of fingernails

Seiko Hirota[1]*, Michael Discher[2], Andreas Lang[2], Hiroshi Yasuda[1]
[1]*RIRBM, Hiroshima University, Hiroshima, Japan*
[2]*Salzburg University, Salzburg, Austria*

Highlights Dosimetric properties of optically stimulated luminescence (OSL) from human fingernails are presented and their possible application to retrospective dosimetry of a hand exposure is discussed.

Key words OSL, fingernail, emergency dosimetry, alpha-keratin, fading

Background and Objectives In response to a radiological accident accompanied by significant radiation exposure of the public, it is critical to immediately apply a reliable and practical method for retrospective dosimetry and provide a precise dose soon after the exposure. Here, we focused on using human fingernails as dosimeter as these can be obtained more easily than other biosamples such as tooth and bone.

While electron spin/paramagnetic resonance (ESR/EPR) has been used for determination of the radiation-induced radicals in the biosamples including fingernails[1)], other detection techniques of radiation-induced radicals are not well investigated. Regarding a possible application of OSL from fingernails, study by only one group [2)] can be found at present.

This is surprising as OSL of fingernails for emergency dosimetry should offer a far simpler protocol than can be achieved using ESR.

Materials and Methods Fingernails investigated here were collected from healthy-state donors (Asian and Caucasian type) during routine hygienic procedures. After clipping, fingernails were placed in a sealable plastic bag and stored with silica aerogel where a humidity is around 15 % and a temperature is around 20 degree Celsius.

The fingernail samples were exposed to approx. 100 Gy of beta radiation (source :Sr-90/Y-90) in two luminescence reading devices Lexsyg Smart and Research (Freiberg Instruments, Germany) at the Luminescence Laboratory at Salzburg University, Austria. The continuous wave (CW) OSL signals of the irradiated fingernail samples were measured using the different stimulation wavelength and optical powers: IR (850±20 nm, max. 300 mW/cm²), green (525±20 nm, max. 80 mW/cm²), blue (458±5 nm, max. 100 mW/cm²) and violet (405±3 nm, max. 100 mW/cm²).

Results and Discussion Signals of radiation-induced OSL were observed in the 100-Gy irradiated samples and signal size seems to be proportional to given dose, as shown in Figure 1. Here, the red marked area in Fig. 1a is defined as the background corrected radiation induced signal of OSL signal (RIS-OSL). It is displayed for different applied doses in Fig. 1b. As shown in Fig. 1b a big signal around 0 Gy was observed for some non-irradiated samples. These signals were not regenerated by irradiation and are different in terms of decay rates: half-life of radiation-induced signal is less than 10 seconds and that of signal at 0 Gy is about 20 seconds. A detailed analysis of the OSL decay curve may be helpful to separate both signals. Additionally, in case of some samples, signals increased for a certain period after irradiation. No obvious signal of mechanical-induced OSL was observed.

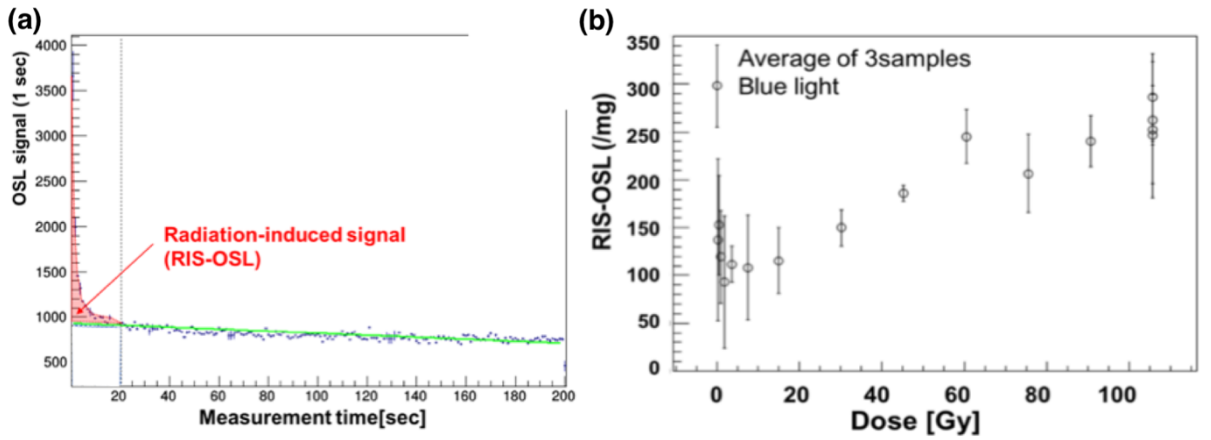

Figure 1. (a) Selected OSL emission patterns of human fingernails 5 hours after and (b) dose-response curve just after irradiation of β-rays.

Conclusion These results obtained in our study indicate that fingernail-OSL may be used for retrospective dosimetry of significant radiation exposure in a radiological accident, that the main prerequisite will be the quantification of the OSL properties of individual fingernails (sensitivity, fading patterns, dose responses, etc) after detailed study and optimization of measurement procedures. It is desirable that the protocol of fingernail-OSL dosimetry for typical accident cases will be standardized for practical applications.

References

1) Trompier F, Romanyukha A, Kornak L, Calas C, LeBlanc B, Mitchell C, Swartz, H, Clairand, I: *Radiat. Meas.* 44 (1), 6–10, 2009.
2) Mishra DR, Soni A, Rawat NS, Bokam G: *Radiat. Environ. Biophys.* 55:255-264, 2016.

Dependence of fingernail ESR signals on radiation quality

Seiko Hirota[1]*, Chryzel A. Gonzales[1], Hiroshi Yasuda[1]
[1]*RIRBM, Hiroshima University, Hiroshima, Japan*

Highlights The time dependent behaviors of electron spin resonance (ESR) signals from fingernails were different between different-quality radiations; this fact should be considered carefully for standardization of fingernail ESR as a retrospective dosimetry for radiological accident.

Key words ESR, fingernail, emergency dosimetry, alpha-keratin, fading

Background and Objectives Application of ESR using bio-substance and personal belongings have been studied to use as a retrospective dosimetry in case of radiological accident[1]. Among these samples, fingernails can be easily harvested and be attached on almost all people in time of accident.

According to previous studies, ESR can detect radiation-induced signals from fingernail which is proportional to radiation dose[2]. However, the instability and fading of signal is one of the issues to use fingernails to estimate personal dose[2]. Additionally, dependence of the signals on radiation quality has not yet been investigated well. It should be needed to address it for practical use of fingernail ESR for real accidents.

Thus, we have been investigating the fading behavior of fingernail signals that could change depending on radiation quality.

Materials and Methods Fingernails investigated in this work were collected from healthy-state donors (Asian type, both male and female). They were cut by using nail clippers in a compound lever style. After clipping, fingernails were stored with silica aerogel where a humidity is approx. 10 % and a temperature is approx. 20 degree of Celsius.

The fingernail samples were exposed to up to approx.100 Gy of gamma source and X-rays. A gamma source is ^{137}Cs equipped in Gammacell exactor 40 (Best Theratronics Ltd.). X-rays are generated by cabinet X-ray system model CP-160 (Faxitron Ltd.) where tube voltages can be set from 10 kV to 160 kV.

The measurements of ESR were carried out by JES-FA100 (JEOL Ltd.) with X-band (approx. 9.4GHz) in approx. 20 degree of Celsius and approx. 40 % of humidity. The signal intensity is defined as a peak to peak amplitude of ESR spectrum in a range between 3rd and 4th peaks of manganese markers, which was measured with following condition: 1mT modulation width, 7.5mT sweep width and 30 seconds sweep time.

Results and Discussion As shown in Figure 1 (left), signal intensities keep increasing after 6 months from irradiation by using X-rays (tube voltage was 160 kV). This tendency is different from that in case of gamma-rays found in a previous study [2]. If this tendency is confirmed, fingernail dosimetry for X-rays can be apply for not only radiological accident but also usual dose monitoring of medical personnel who has possibility to be exposed to X-rays. However, in short time, in both case of X-ray and gamma-ray irradiations, both rising and falling trend can be seen (Figure1 middle and right). The detail time structure should be invesitigated to make clear what happens in side fingernail and realize standization of fingernail ESR dosimetry.

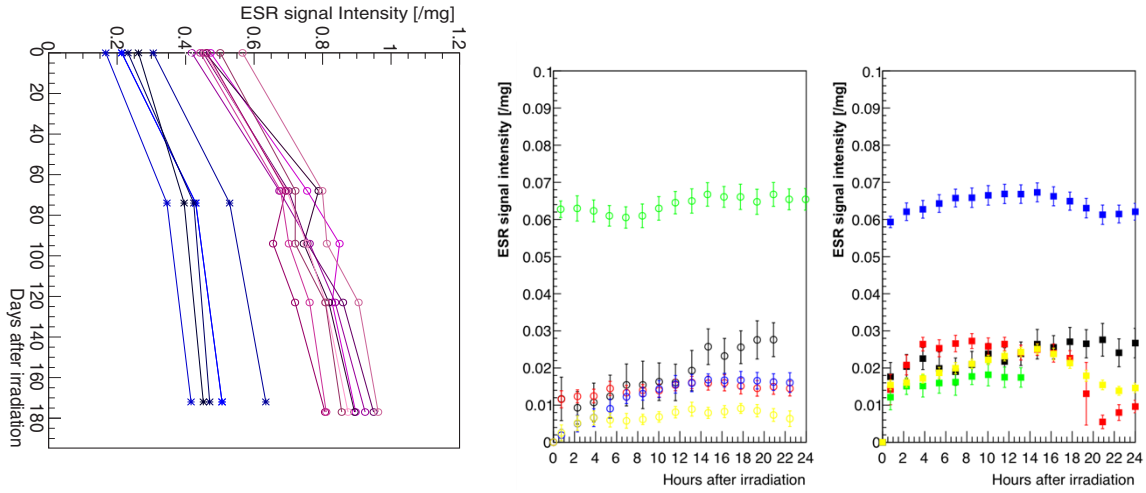

Figure 1. Left: Time dependence of signal intensity in 15 samples which is irradiated by X-rays (tube voltage was 160 kV). Accumulated dose for 10 samples (open circle, magenta color) were 100 Gy and that for other 5 samples were 55Gy (asterisk, blue color). The horizontal axis shows excess of signal intensity due to radiation. Middle and Right: Time changes of fingernail signals for 24 hours after gamma-ray irradiation (middle) and X-ray irradiation (right) with 3 Gy accumulated dose. The same color indicates the same donor. The Middle is a case of gamma-rays and the right is a case of X-rays (tube voltage is 160kV).

Conclusion The unique, increasing trend of fingernail ESR signal for long period up to few months was observed. Further investigations on both short- and long-term trends of fingernail ESR signals in relation to radiation quality are needed.

References

1) B.G.Dalgarno J.D.Mcclymont : *Appl. Radiat.* 40 (10-12), 1013-1020, 1989.
2) F.Trompier, A.Romanyukha, L.Kornak, C.Calas, B.LeBlanc, C.Mitchell, H.Swartz,I.Clairand: *Radiat. Meas.* 40 (1) , 6-10, 2009

High-dose dosimetry with Ag-doped phosphate glass: applicability assessment with different techniques

Sergey Sholom [1]*, Stephen W.S. McKeever [1]
[1]*Department of Physics, Oklahoma State University, Stillwater, Oklahoma, USA*

Highlights Ag-doped phosphate glass was assessed as a potential high-dose dosimeter using radiophotoluminescence (RPL), optical absorption (OA), thermoluminescence (TL) and electron paramagnetic resonance (EPR). OA and EPR responses demonstrated a monotonic increase with dose and, with the proper calibration, may be used for dosimetry up to several hundreds of kGy.

Key words Radiophotoluminescence, optical absorption, thermoluminescence, electron paramagnetic resonance, high-dose dosimetry, Ag-doped phosphate glass

Background and Objectives Ag-doped phosphate glass is a well-known RPL dosimeter for application in the dose range from tens of μGy up to several hundreds of Gy.[1)] At the same time, little is known about properties of this dosimeter in the high-dose range. The objectives of this work were to test radiation-induced signals from Ag-doped phosphate glass in the kGy dose range using different physical techniques.

Materials and Methods The samples used in this study were GD-450 glass dosimeters from Chiyoda Technol Corporation, Japan. The composition of the glass is: P: 31.55 wt. % , O: 51.16 wt. % , Al: 6.12 wt. % , Na: 11.00 wt. % , and Ag: 0.17 wt. %. The original glass plates were cut to aliquots of the size 4.5 x 7 mm^2 to fit the size of EPR tubes and TL sample discs. The following equipment was used: Cary 5000 spectrophotometer (OA spectra), Horiba Fluorolog 3 (RPL emission), Risø TL/OSL DA-15 reader (TL glow curves) and Bruker EMX spectrometer (EPR spectra). Samples were exposed using a $^{90}Sr/^{90}Y$ beta source in the dose range 0-300 kGy; all samples were annealed after irradiation at 200 °C for few minutes to eliminate all unstable signals.

Results and Discussion Figure 1 shows the dose-response relationships for signals observed with OA and EPR. OA curves (plot a) are plotted for different wavelength regions while EPR dependences (plot b) are shown for different components of the Ag^{2+} signal (at g=2.07 and g=2.37).[2)] It is seen in this figure that the dose-response relationships are monotonic for the tested dose range, which means that they can be used for dose assessment after proper calibration. The dose-response curves of signals tested with other techniques (i.e. RPL and TL) as well as the response for other EPR signals were non-monotonic (they had a maximum in the range 1-10 kGy, above which the signals decreased) and therefore they cannot be used

in high-dose dosimetry.

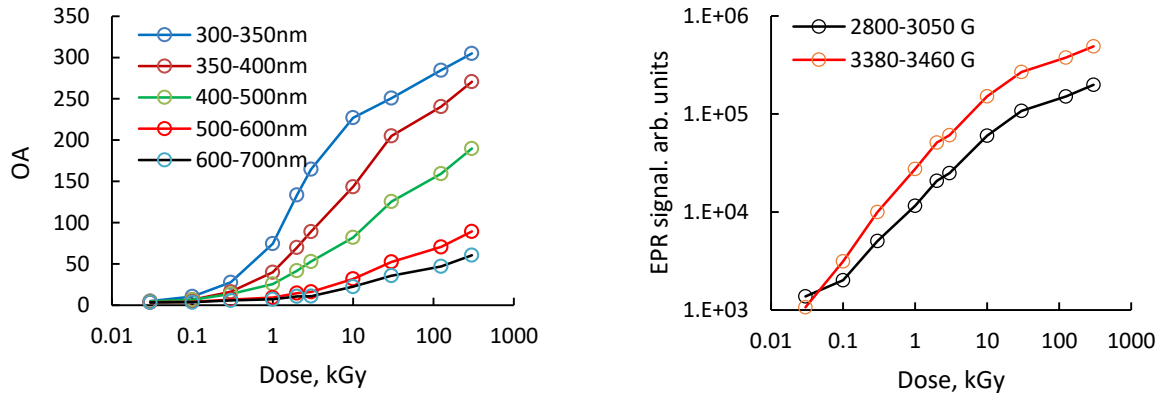

a b

Figure 1. Dose-response relationships: (a) optical absorption for different wavelength regions; (b) different components of the Ag^{2+} EPR signal

Conclusion The dose-response curves for Ag^{2+} EPR signals in Ag-doped phosphate glass as well as the OA coefficients for this material in different wavelength ranges demonstrate a non-linear, monotonic increase with dose in the range up to several hundreds of kGy. This suggests that this glass may be used in high-dosimetry applications after the proper calibration.

Acknowledgments This work was funded by Chiyoda Technol Corporation, Japan, and the State of Oklahoma, USA.

References

1) E. Piesch, B. Burghardt, 1994. *Photoluminescence dosimetry: the alternative in personnel monitoring*. Radioprotection 29, 39-67.
2) S. W. S. McKeever, S. Sholom, N. Shrestha, 2019. *Observations regarding the Build-Up Effect in Radiophotoluminescence of Silver-Doped Phosphate Glasses.* Radiat. Meas. 123, 13-20.

Optically stimulated luminescence (OSL) ages determinations of Holocene fluvial terraces system, Central Amazon

Sonia H. Tatumi[1*], Márcio Yee[1], Juan C. R. Mittani[1], Emílio A. A. Soares[2], Eliezer S. Gonçalves Júnior[3], Marcel S. Passos[4]

1 Federal University of São Paulo, Baixada Santista Campus, São Paulo, Brazil
2 Department of Geosciences, University of Amazonas, Manaus, Amazonas-Brazil.
3 National Mining Agency, Amazonas State Unit, Manaus, Amazonas-Brazil.
[4] University of Brasília, Brasília, Federal District-Brazil.

Highlights The present study shows a geochronological novel data of the Solimões-Amazonas river system's Holocene lower terrace, range between the Manacapuru and Madeira river mouths, Central Amazonia. To improve the precision of the young ages sediments, comparisons between the ages found by central age (CAM), minimum age (MAM) and finite mixture model (FMM) models were made and ages between 2.9 to 9.7 kyears were evaluated.

Key words Optically Stimulated Luminescence, Amazon Basin, River Terrace, Holocene.

Background and Objectives Nowadays, OSL dating has been used, as a viable option to radiocarbon, in order to conduct chronological studies of Quaternary deposits in Brazil (Rossetti et al, 2017, Sant'Anna, et al, 2017) mainly on account of the organic matter destruction, due to the strong tropical weathering, as well as the wide temporal range reached by OSL. Thereby, due to the benefits of the method, OSL has provided a great support for paleoenviromental reconstructions in the Amazonian region, and the fuller understanding of the Solimões-Amazonas system's Late Pleistocene and Holocene fluvial dynamics. The present study presents a novel geochronological data pertaining to the Solimões-Amazonas river system's Holocene lower terrace, range between the Manacapuru and Madeira river mouths, Central Amazonia.

Materials and Methods OSL curves were measured using an automated TL/OSL reader, model RisØ-DA20. The luminescence was detected in UV region using a U-340 filter.

The single-aliquot regenerative dose (SAR) protocol, on coarse grains of quartz, was employed for D_e evaluation, according to Murray and Wintle (2000). For natural radioisotopes determination, gamma spectroscopy measurements were made with high-purity Germanium (HPGe) detector, Canberra 373 model. Samples with ages dispersion less than 20% were calculated using the central age model (CAM). Samples with dispersion greater than 20% had their ages determined by the minimum age model (MAM) (Galbraith and Roberts, 2012). To improve the precision of the young ages sediments, comparisons between the ages found by CAM and MAM and finite mixture model (FMM) models were performed.

Results and Discussion An example of OSL shine down curve and radial plot are shown in Figure 1, OSL signal with fast decay behavior was observed, suggesting that these quartz grains are easily to bleach. The experimental shine down curves were deconvoluted using general order equation. The results showed age dispersions between 13 to 29%. The ages results obtained ranged from 5,600 to 142,700 years, which is consistent with sediment deposition during the latest Mid-Late Pleistocene to mid-Holocene.

Conclusion The results indicated that 78% of the ages determined by FMM agree with those obtained by CAM. FMM is a useful tool to further verify discrete components of D_e distributions in the sample, which can be relate to different deposition periods. In addition, a theoretically study of OSL components was made fitting the CW-OSL decay curve with general order kinetic equation and OSL curve could be deconvoluted in three individual components. The ages obtained (2.9 to 9.7 kyears) in the present study for the lower terrace of the Solimões-Amazonas river system showed compatibility with those reported in previous studies, highlighting its final development in the Holocene.

References

1) Rossetti, D.F., Valeriano, M. M., Gribel, R., Cohen, M.C.L. Tatumi, S.H. Yee, M., 2017, Geomorphology, 295, 406-418.
2) Sant'Anna, LG, Soares, E. A , Riccomini, C., Tatumi, S.H., Yee, M., 2017.Quaternary Science Reviews 170, 82-97
3) Murray, A.S., Wintle, A.G., 2000. Radiation Measurements, 32(1):57-73.
4) Galbraith, R.F., Roberts, R.G., 2012. Quaternary Geochronology, 11:1-27

Acknowledgements The research work was partly supported by the São Paulo Research Foundation (FAPESP) within a research grants nº.2009/02069-2, 2016/02262-0.

Electron spin resonance dosimetry using tooth enamel of Japanese macaque

Toshitaka Oka[1,2], Atsushi Takahashi[3], Kazuma Koarai[2], Yasushi Kino[2], Tsutomu Sekine[1,2], Yoshinaka Shimizu[4], Mirei Chiba[4], Toshihiko Suzuki[4], Jun Aida[4], Ken Osaka[4], Keiichi Sasaki[4], Yusuke Urushihara[5], Masatoshi Suzuki[6], Hisashi Shinoda[4], Manabu Fukumoto[7,8]

[1]*Institute for Excellence in Higher Education, Tohoku University, Miyagi, Japan*
[2]*Graduate School of Science, Tohoku University, Miyagi, Japan*
[3]*Tohoku University Hospital, Miyagi, Japan*
[4]*Graduate School of Dentistry, Tohoku University, Miyagi, Japan*
[5]*Graduate School of Medicine, Tohoku University, Miyagi, Japan*
[6]*Institute for Disaster Reconstruction and Regeneration Research, Tohoku University, Miyagi, Japan*
[7]*Department of Molecular Pathology, Tokyo Medical University, Tokyo, Japan*
[8]*Institute of Development, Aging and Cancer, Tohoku University, Miyagi, Japan*

Highlights Detection limit of the electron spin resonance (ESR) dosimetry using tooth enamel of Japanese macaque, extracted by a novel enamel-dentine separation technique, was estimated to be ~40 mGy. The external exposure dose for Japanese macaques collected in Fukushima prefecture were estimated.

Key words electron spin resonance (ESR), electron paramagnetic resonance (EPR), Fukushima nuclear power plant accident, detection limit

Background and Objectives Releases of the radioactive materials from the Fukushima Daiichi Nuclear Power Plant due to its accident result in an external/internal exposure to people and animals. We attempted to utilize electron spin resonance (ESR) spectroscopy to estimate the external exposure dose, but the detection limit of the ESR was thought to be a few hundred mGy. Therefore, the improvement of the detection limit of ESR was required. We constructed two dose response curves with two ESR spectrometers, and estimated the external exposure dose for Japanese macaque collected in Fukushima prefecture.

Materials and Methods Tooth enamel of Japanese macaque was extracted by a novel enamel-dentine separation technique using the difference of the density of enamel and dentine.

The extracted enamel were irradiated by ^{60}Co gamma-ray at Takasaki Advanced Radiation Research Institute, National Institutes for Quantum and Radiological Science and Technology (Japan), and dose response curves were constructed by two different ESR spectrometers of RE-2X (JEOL, Japan) and MS 400 (Magnettech, Germany). The external exposure doses were estimated and compared using these dose response curves. Observed spectra were deconvoluted by 'EPR dosimetry' programme [1] to extract the intensity of CO_2 radical.

Results and Discussion Detection limit for both ESR spectrometers are ~40 mGy, which are extremely lower than our previous result of ~170 mGy for Japanese deciduous tooth, were observed. One of the important point for the improvement of the detection limits is how to remove the impurity from the tooth. In this work, we removed the black points on the surface of the tooth by a hard-alloy drill and extracted the high quality enamel by using a novel enamel-dentine separation technique. In some cases, ESR signals were overlapped with a broad ESR peak maybe due to the radicals of metal, we cannot analyse the intensity of CO_2 radical; the chemical treatment reported in the previous studies [2,3] were effective to remove such broad peak.

The external exposure dose of several Japanese macaque were estimated to be comparable to or lower than the detection limit of ~40 mGy at present. Dose estimation of other macaque collected in a highly-contaminated area in Fukushima prefecture will be presented at the conference.

Conclusion Two precise dose response curves were constructed and the detection limit of both ESR spectrometers were estimated to be ~40mGy. We attempted to estimate the external exposure dose of several Japanese macaque collected in Fukushima prefecture, but the high-exposed macaque were not found at present.

References

1) A. A. Koshta, A. Wieser, E. A. Ignatiev, S. Bayankin, A. A. Romanyukha, M. O. Degteva, New computer procedure for routine epr-dosimetry on tooth enamel: description and verification, Applied Radiation and Isotopes 52 (2000) 1287–1290.
2) Use of electron paramagnetic resonance dosimetry with tooth enamel for retrospective dose assessment, IAEA-TECDOC-1331, IAEA, Vienna, Austria, 2002.
3) A. Wieser, P. Fattibene, E. A. Shishkina, D. V. Ivanov, V. De Coste, A. Güttler, S. Onori, Assessment of performance parameters for EPR dosimetry with tooth enamel, Radiation Measurements 43 (2008) 731–736.

Comparison of luminescence properties of various porcelain-based items from Turkey towards their effective use in accidental retrospective dosimetry

Y.K. Kadioğlu[1,*], S. Geranmayeh[2], E Aşlar[2], E. Şahiner[2], G.S. Polymeris[1,2], N. Meriç[1,2]

[1] *Earth sciences Application and research Center of Ankara University (YEBIM), Gölbasi 06830, Ankara, Turkey*

[2] *Institute of Nuclear Sciences, Ankara University, Beşevler 06100, Ankara, Turkey*

Highlights Towards the effective use of porcelain samples to accidental retrospective dosimetry applications, new experimental data are presented, including a comparison of luminescence features among various porcelain-based items collected from Turkey.

Key words Porcelain, TL, OSL, XRD, accidental dosimetry.

Background and Objectives The TL properties of porcelain have been investigated since the early 1980s and are well understood in the context of dating using conventional TL[1,2)]. Porcelain has been shown to be a promising material for retrospective dosimetry, using mostly the pre-dose measurement of either the 110 °C TL peak or the 230 °C TL peak[3)]. Very few studies have been devoted to the OSL properties of porcelain[4)]. The objective of the present study includes the investigation of the usability of various porcelain-based items which are commonly found around a house in everyday life, using both luminescence techniques.

Materials and Methods Various porcelain based items were collected for the present study, including a sugar bowl, an ashtray, a porcelain breaker, an artificial dental porcelain, an electric fuse and the seal of a porcelain moneybox. For each sample, grain sizes within the fractions 90 – 140 μm were selected. The presence of porcelain was verified using both XRD and Raman techniques. All luminescence measurements were carried out using a Risø TL/OSL reader (model TL/OSL-DA-20). The following luminescence properties were studied for all aforementioned items, for both:

- TL glow curve shapes, number of TL peaks after deconvolution,
- TL and OSL repeatability - reproducibility,
- Deconvolution parameters such as of various TL peaks and photo-ionization cross sections of various OSL components,

- Component resolved dose response properties, such as linearity features and lowest detectable dose limits, for both TL and OSL,
- Stability
- Pre-dose features (for TL mostly).

Results and Discussion Special emphasis was devoted to the TL peaks of 110 °C and 230 °C. In general, the samples collected from all porcelain-based items yield many prevalent properties, such as the presence of both aforementioned TL peaks with similar activation energies and stability. On the contrary, the sensitization patterns as well as the dose response properties of these aforementioned TL peaks are sample dependent. For one among the porcelain samples of the present study, pre-dose sensitization could not be monitored for either TL peaks. In some cases, extra peaks can be monitored, depending on the pre-treatment. The OSL analysis is currently ongoing.

Conclusion Similarities and differences for the TL properties of the 110 °C and 230 °C TL peaks of various porcelain-based items collected from Turkey were pinpointed. Each sample should be treated independently, as there are not many prevalent features.

References

1) D. Stoneham, Nucl. Tracks, 10 (6) (1985) 509-512.
2) D. Stoneham, Radiat. Meas. 24 (1995) 499-505.
3) Y. Göksu et al., Appl. Radiat. Isot., 49 (1–2) (1998) 99-104.
4) C.I. Burbidge, Mediterr. Archaeol. Archaeom. 10 (2010) 53–60.

IMPLEMENTATION OF EYE-LENS DOSIMETRY IN POLAND

Agnieszka Szumska*, Maciej Budzanowski, Izabela Milcewicz-Mika, Renata Kopeć

Institute of Nuclear Physics Polish Academy of Sciences, Krakow, Poland

Highlights Improvement of eye lens dosimetry and potential for high ocular radiation doses to interventional radiology and cardiology staff.

The obtained dosimetry data could be used for epidemiological studies to assess retrospectively eye lens dose.

Key words eye lens dosimetry, TLD

Background and Objectives The eye lens is one of the most sensitive organ for radiation injury and exposure leads to radiation induced cataract. It has been seven years from the ICRP Statement on tissue reactions containing the recommendations for an equivalent dose limit for the lens of the eye of 20 mSv in a year for workers, and has been 6 years since Laboratory of Individual and Environmental Dosimetry provided eye lens doses measurement. Reduction of the limit for occupational exposure for the lens of the eye needs adequate approaches for eye protection and eye dose monitoring.

Materials and Methods The most accurate method for monitoring the equivalent dose to the lens of the eye is to measure the personal dose equivalent Hp(3) with a dosimeter worn as close as practicable to the eye. To measure eye lens doses in terms this quantity a dedicated dosimeter and the appropriate method has been developed in the largest dosimetry service in Poland. In measurements MTS-N (LiF: Mg,Ti) thermoluminescence detectors were used.

Results and Discussion Results of measurements of Hp(3) from eye lens dosimeters (over 3000 readouts), issued in the years 2012–2018 were reported.
The frequency distribution of eye lens dose measurements performed using special dedicated dosimeters, via their Hp(3) operational values, over 3-month periods, after subtraction of natural background in 72% cases are below 0.1mSv. In case new operational quantity Hp(3) the percentage of workers, which exceed the new limit are 2%.
Our data show great differences on ratio between eye lens doses and doses on skin.

Conclusion The obtained dosimetry data could be used for epidemiological studies to assess retrospectively eye lens dose.

No meaningful correlation could be established between eye lens doses and skin doses.

Eye-lens dosimetry was introduced and implemented in Poland as a routine and accredited measurement for the PN-EN-ISO/IEC 17025 standard and became a routine method with fulfilled new requirements.

Measurement of the eye lens radiation exposure in interventional urology using Al_2O_3:C OSL dosimeters

Authors:

S. Medici [1,2], A. Pitzschke [1], J. Damet[1,3]

[1] Institute of Radiation Physics, Lausanne University Hospital, Lausanne, Switzerland

[2] European Organization for Nuclear Research (CERN), Geneva, Switzerland

[3] Department of Radiology, University of Otago, Christchurch, New Zealand

Purpose:

The aim of this work was to measure the eye lens radiation exposure of the medical staff during interventional urology procedures using optically stimulated luminescence (OSL) dosimeters made out of Al_2O_3:C.

Methods:

The measurements were carried out for six medical staff members performing 33 common fluoroscopically-guided urology procedures with an over-couch X-ray system. The personal dose equivalents Hp(0.07) were measured at the eye level using Landauer OSL NanoDot® dosimeters and at the chest level with Landauer OSL Inlight® dosimeters placed over the protective apron. The Inlight dosimeters were used to determine the average photon energy to which each staff member was exposed. Energy correction factors were applied to the NanoDot and Inlight dosimeters results to cope with the high over-response of the Al_2O_3:C detector material at photon energies below 100 keV. The ratio of the dose measured close to the eye lens and on the chest was determined and the annual eye lens dose was estimated based on the workload in the service.

Results:

During the procedures, the X-ray tube voltage of the fluoroscopy installation ranged between 63 and 124 kVp and the average delivered kVp, weighted by the dose-area-product (DAP), was 96 kVp. The measured photon energy ranged between 30 – 40 keV, a typical value for scattered radiation field around a patient. At these energies, Al_2O_3:C is known to strongly over-respond due to its higher effective charge (Zeff ≈ 11.3) [1] with respect to soft biological tissue (Zeff ≈ 7.8) [2]. In our case, we found an over-response by a factor of 2 – 5, so that proper energy response correction was mandatory. The average eye lens dose per procedure measured for the physician and the instrumentalist nurse were 78 ± 24 µSv and 38 ± 18 µSv, respectively. The eye lens dose per DAP was 8.4 ± 17.5 µSv/(Gy·cm^2) for the physician and 4.1 ± 8.7 µSv/(Gy·cm^2) for the instrumentalist nurse. The eye to chest dose ratios were 0.9 ± 0.4 and 2.6 ± 1.6 for the physician and instrumental nurse, respectively. The annual estimated eye lens dose for both staff members was in the range of 7 – 8 mSv [3].

Conclusions:

Al_2O_3:C based OSL dosimeters can be used for staff exposure studies in the medical field, however their strong energy dependence is challenging. For the determination of the energy correction factors, we found it useful to combine NanoDot dosimeters for point-like dose measurements and Inlight dosimeters for additional photon energy determination. The clinical results showed that the eye lens to chest dose ratio greatly varied according to the staff function. The dose equivalent measured by the personal dosimeter worn on the chest may underestimate the eye lens dose of some medical staff members. The annual eye lens doses were in the order of 10 mSv.

References

[1] E. G. Yukihara and S. W. S. McKeever, Optically Stimulated Luminescence: Fundamentals and Applications, Wiley, 2011.

[2] A. Pedro, D. T. Burns, A. E. Nahum, J. Seuntjens and F. H. Attix, Fundamentals of Ionizing Radiation Dosimetry, Wiley, 2017.

[3] S. Medici, A. Pitzschke, N. Cherbuin, M. Boldini and J. Damet, "Eye lens radiation exposure of the medical staff performing interventional urology procedures with an over-couch X-ray tube," *Physicia Medica,* vol. 43, pp. 140-147, 2017.

Dose reassessment by using phototransferred thermoluminescence (PTTL) phenomenon to the high sensitive MCP thermoluminescent detectors and application in dosimetry

A. Sas-Bieniarz, M. Budzanowski, I. Milcewicz-Mika, E. Pyszka, R. Kopeć
Institute of Nuclear Physics, Polish Academy of Sciences, Kraków, Poland

Highlights Possibility of dose reassessment by using phototransferred method to the height sensitive thermoluminescent MCP-N detectors applied to environmental and eye lens dosimetry.

Key words thermoluminescence (TL) dosimetry, LiF: Mg,Cu,P (MCP-N) detectors, phototransferred thermoluminescence (PTTL), dose reassessment

Background and Objectives Dose reassessment in film, OSL and RPL dosimetry is well known and standard method in contrary to TL dosimetry. Erasure of the TL signal on detector readout is considered as the main disadvantage of TL dosimetry, as post-readout dose reassessment is then impossible in principle. By using the phototransferred thermoluminescent (PTTL) method which consists of the first readout, UV exposure and the second readout it is possible to reassess doses in TL dosimetry. This method was applied to reassess doses in individual dosimetry at Laboratory of Individual and Environmental Dosimetry IFJ PAN (polish acronym: LADIS) by using LiF: Mg,Ti (MTS-N) detectors. The next step was to applied this method to height sensitive MCP-N detectors used for environmental and eye lens dose measurement.

Materials and Methods Standard MTS-N (LiF: Mg,Cu,P) sintered detectors (4.5 mm diameter and 0.9 mm thickness used in environmental and in eye lens dosemeters) were applied. Some of them have been used in routine control for 16 years long. The TL detectors were read in automatic RE2000 (Rados Oy, Finland) readers. After readout the PTTL method was applied to dose reassessment for MCP detectors. Detectors were subjected to UV radiation (254 nm length) and read once again. The influence of UV irradiation conditions and the second readout parameters on The PTTL signal were checked.

Results and Discussion The response of MCP-N detectors to UV radiation is significantly lower than MTS-N detectors. Due to adjusting readout parameters it is shown that PTTL

response of MCP-N detectors is linear and it is also like in case of MTS-N detectors possible to reassess doses. The standard and the second readout after applying the PTTL method of the same MCP-N detector exposed to 20 mSv of Cs-137 gamma-rays are presented in Figure 1.

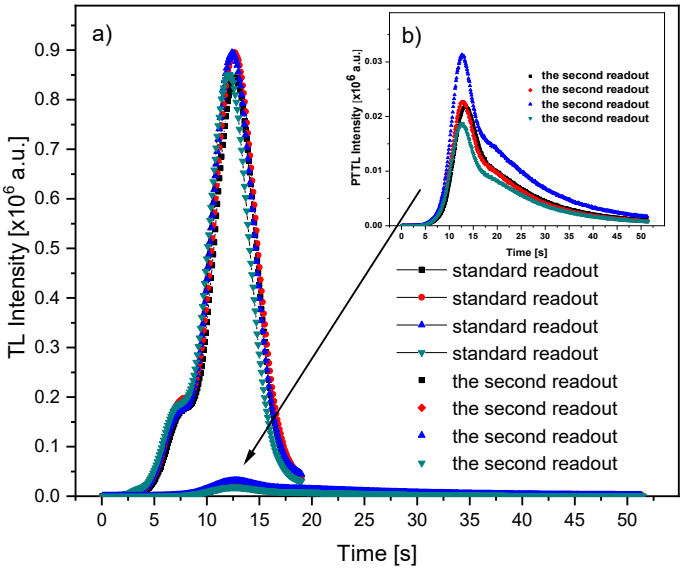

Figure. 1. a) Glow curves of the first readout and of the second PTTL-stimulated readout of MCP-N detectors exposed to 20 mSv of Cs-137 gamma-rays; b) the second PTTL readout.

Conclusion The obtained results may suggest that due to applying the PTTL method to MCP-N detectors it is possible to reassess dose and check the measurement correctness. It is especially required in case when the dose exceeded the annual dose limit.

References

1) Sas-Bieniarz A., Budzanowski M., Bubak A. and Kopeć R. (2014) Application of phototransferred theromluminescence (PTTL) for dose re-assessment in routine dosimetry using MTS-N (LiF: Mg, Ti) thermoluminescent detectors, Radiat. Meas. 71, 447-450
2) Sas-Bieniarz A., Budzanowski M., Bubak A. and Kopeć R. (2016) Application of PTTL method for dose reassessment in extremity dosimetry, Radiat. Prot. Dosim. 170, 204-207
3) Moscovitch M., Benevides L., Romanyukha A., Hull F., Duffy M., Voss S., Velbeck K.J., Nita I., Rotunda J.E. (2011) The applicability of the PTTL dose re-analysis method to the Harshaw LiF: Mg, Cu, P material, Radiat. Prot. Dosim. 144, 161-164

Radiation Safety Survey of Veterinary Radiology Diagnosis and Nuclear Medicine in Taiwan

Yu-Ting Ma[1] , Hsin-Wei Liu[1] , Fang-Yuh Hsu[1,2,*] , and Ching-Han Hsu[1]

[1]*Department of Biomedical Engineering and Environmental Science, National Tsing Hua University, Hsinchu, Taiwan*

[2]*Nuclear Science and Technology Development Center, National Tsing Hua University, Hsinchu, Taiwan*

Highlights The features of X-ray tube and assessed doses for relative person and working environments for X-ray diagnostic imaging and nuclear medicine processes were investigated in this paper. More than 250 veterinary hospitals using X-ray machines and a hospital performing veterinary nuclear medicine in Taiwan were assessed.

Key words veterinary X-ray, veterinary nuclear medicine, personnel dose assessment, radiation protection, radiation safety inspection

Background and Objectives The pet care in veterinary hospitals play a more and more important role, nowadays in Taiwan. Pets are more often send to veterinary hospitals for the X-ray examination, or for nuclear medicine inspection than before. Radiation doses and risks for the people including veterinary doctors, X-ray operators and pet breeders are highly concerned due to they may be also exposed by radiation in different levels while the pets are performing the X-ray examination, or nuclear medicine inspection. In particular, pet breeders usually need to stay next to pets in the X-ray room to help collect diagnostic imaging.

Materials and Methods The features of X-ray tube, such as leakage amount of X-ray, thickness of inherent filter and tolerance of field size, and also evaluated the doses to the pet breeder or helper, whom may stay inside the X-ray room when performing X-ray imaging for pets were investigated. Besides, the personnel doses and working environment doses for performing veterinary nuclear medicine were also assessed. A solid-plastic survey meter of scintillation detector was used for measuring the doses in veterinary X-ray diagnosis as well as in nuclear medicine processes.

Results and Discussion More than 250 veterinary hospitals using X-ray machines and a hospital performing veterinary nuclear medicine in Taiwan were investigated. In the results of this paper, features of X-ray tubes and assessed doses for relative person and working

environments were reported.

Conclusion This paper investigated the features of X-ray tube and assessed doses for relative person and working environments for X-ray diagnostic imaging and nuclear medicine processes. Provide good information to the radiation safety authorities and improve the effectiveness of radiation protection control in Taiwan.

References

1) Code of Practice & Safety Guide: Radiation protection in veterinary medicine, Radiation protection series publication no.17. Australian Radiation Protection and Nuclear Safety Agency, 2009.
2) EPA (Final Draft) Radiation Guideline 6: Compliance requirements for ionizing radiation apparatus used in diagnostic imaging (part 6: veterinary science – radiography and fluoroscopy), The NSW Environment Protection Authority (EPA), Sydney, 2016.
3) IAEA Safety Standards Series No. GSR-Part3: Radiation protection and safety of radiation sources: International basic safety standards, general safety requirements. International Atomic Energy Agency (IAEA), Vienna, 2014.
4) IAEA Draft Safety Report: Radiation protection and safety in veterinary medicine, International Atomic Energy Agency (IAEA), Vienna, 2018
5) National Council on Radiation Protection and Measurements (NCRP), Radiation Protection in Veterinary Medicine, NCRP Report no. 148, 2004.
6) The 1991 Recommendations of the International Commission on Radiological Protection. ICRP Publication 60, 1991.
7) The 2007 Recommendations of the International Commission on Radiological Protection. ICRP Publication 103, 2007.
8) US.NRC 10 CFR Part 35.75, Release of individuals containing unsealed byproduct material or implants containing byproduct material. United States Nuclear Regulatory Commission, 2007.

Radiation Dose Evaluation on Shielding Vest Wearing Exposure Experiments

Hidenori Kawano[1], Kenichi Hozumi[2], Asami Tsurumaki[1],
Hideo Hirayama[2], Yoshihito Namito[2], Hidemichi Ohashi[1], Yukio Sakamoto[1]
[1]ATOX, [2]High Energy Accelerator Research Organization

Highlights For the estimation of dose reduction effect by shielding vest, exposure tests by ^{137}Cs source and X-ray generator were done using water phantom covered with shielding vest made of heavy metal. That effect including of photon energy dependence was also surveyed by the Monte Carlo simulations.

Key words shielding vest, exposure test, Monte Carlo simulation, dose evaluation

1 Exposure Test

1-1 Configuration of Test

Personal dosimeters were settled in front, rear and lateral sides of the water phantom for breast and abdominal region, and inside and outside of shielding vest which covered the phantom shown in Fig.1. The shielding vest was BIO RUBBER, RSM E-400 and the thickness equivalent of lead is 0.44 mm according to maker's catalog. Irradiation geometries were Anterior Posterior (front), Posterior Anterior (rear), and rotational. Photon sources were ^{137}Cs and X-ray generator (100 kV, 0.1 mA, Tungsten target).

1-2 Experimental Results

Table 1 shows the ratios of indicated values of dosimeters at far side from source to those at near side in the case of dosimeters settled at front side. The reduction factors of ambient dose equivalent are 12 – 17 % for ^{137}Cs gamma-ray, and 98 – 99% for X-ray, respectively. The ratios of indicated values for Posterior Anterior irradiation are smaller than those for Anterior Posterior and rotational irradiations. This is caused from the scattered photons with low energy which is large attenuation by shielding vest.

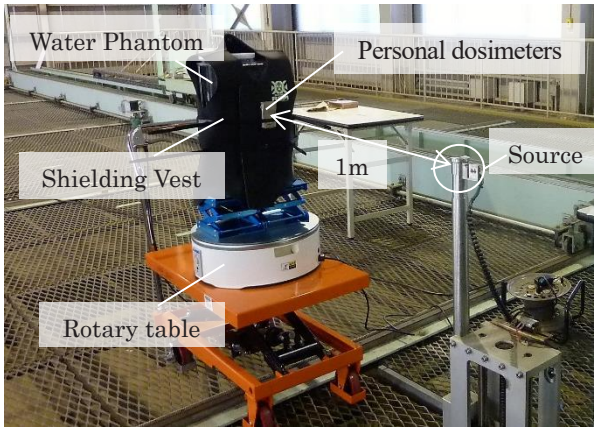

Fig.1 Set up of Exposure Test

Table 1 The ratios of indicated values※ of dosimeters

Irradiation geometries	^{137}Cs gamma-ray	X-ray
Front	0.83	0.010
Rear	0.69	0.063
Rotational	0.88	0.020

※ [outside / inside] for front and rotational irradiation and [inside / outside] for rear irradiation

2 Monte Carlo Simulations

According to the maker's catalogue, a material of shielding vest has 4.4 % of ambient dose equivalent reduction effect for ^{137}Cs gamma-ray. On the other hand, our exposure test by using of water phantom shows over 12 % dose reduction effect. This difference is surveyed by Monte Carlo Simulations.

2-1 Simulation Model

A water phantom was approximated by a rectangular solid. A shielding vest with 0.44 mm thickness of lead covered water phantom excluding front side, and a thickness for front side was double of normal thickness because of an overlap of shielding vest. Ambient dose equivalents at air region with same volume as personal dosimeters were evaluated by Particle and Heavy Ion Transport Code System, PHITS[2].

2-2 Simulation Results

Fig. 2 shows the dose reduction factors obtained by Mote Carlo simulations as a function of incident photon energy with experimental data. Dose reduction effect is remarkable for photon energy under 200 keV. Simulation results are in good agreement with measured ones for ^{137}Cs gamma-ray, but in not good agreement with ones for X-ray. This discrepancy is caused by the elemental composition of materials in shielding vest.

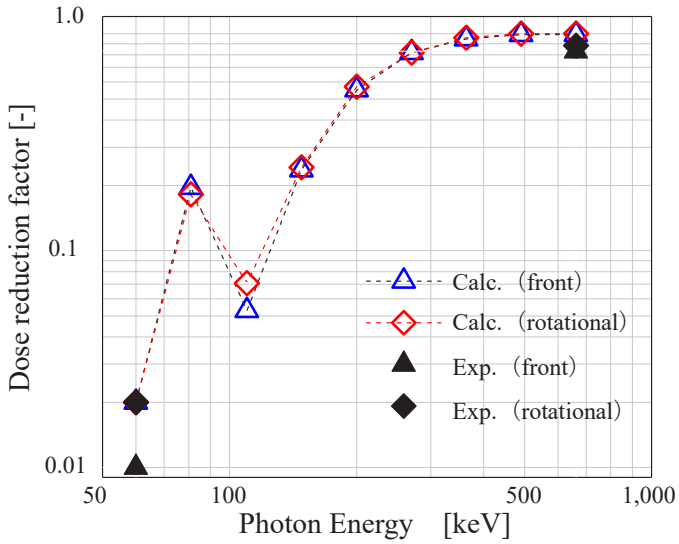

Fig. 2 Energy dependence of dose reduction effect of shielding vest

3 Conclusion

We got ambient dose equivalent reduction effect of 12 – 18 % for ^{137}Cs gamma-ray, and that of over 90 % for lower energy X-ray from experiments. There are many lower energy photons via transmission and scattering by buildings and structures for main source of ^{137}Cs. The large dose reduction effect is expected by wearing shielding vest, where the contribution of lower energy photon is dominant of dose. The Monte Carlo simulations show good agreement with experimental results

for ^{137}Cs gamma-ray, and poor agreement with those for lower energy X-ray. Much considerations are needed for elemental compositions of shielding vest and radiation behavior simulation in water phantom.

References

1) H. Kawano et al., Radiation Dose Evaluation on Shielding Vest Wearing, ATOX Technical Report, No.9, 22-23 (2017)
2) T. Sato et al., Particle and Heavy Ion Transport Code System PHITS, Version 2.52, J. Nucl. Sci. Technol. 50:9, 913-923 (2013)

Quality Control of blood irradiators using an alanine/EPR dosimeter

HyoJin Kim[1], Hyun Kim[1], Sung Jin Noh[1], Yeong-Rok Kang[1]*

[1]*Research Center, Dongnam Inst. of Radiological & Medical Sciences (DIRAMS)*

Highlights For the quality control of blood irradiators, a jig for irradiation of alanine dosimetry is produced, and the dose distribution and uncertainty of blood irradiator container are evaluated using EPR spectroscopy.

Key words radiation, dosimetry, alanine, EPR, blood irradiator

Background and Objectives This study aims to establish quality control of blood irradiators using an alanine dosimeter and to secure dosimetry reliability. Regular quality control is necessary for the quality assurance of a blood irradiator. For blood irradiation, the Food and Drug Administration (FDA, USA) recommends a minimum radiation dose of 25 Gy in the center and 15 Gy in the periphery. Approximately 48 medical institutions in South Korea own and use blood irradiators; however, quality control for blood irradiators is insufficient. For dosimetry using alanine dosimeters, the measurement of dose to assure the dose delivery system are performed by a dosimetry devices (alanine dosimeter jig) developed in this study. Further, the dose evaluation and distribution in the container were verified, and the uncertainty was evaluated.

Materials and Methods For the quality control of blood irradiators, a gamma ray irradiator (Biobeam-8000, STS GmbH, Germany) embedded with a ^{137}Cs beam source of approximately 2,200 Ci, installed in the Dongnam Institute of Radiological and Medical Sciences, was used. A dedicated jig for blood irradiator was fabricated to measure the water absorbed dose and dose distribution using an alanine dosimeter inside the blood irradiator (Fig. 1). Furthermore, the standard dose curve was acquired by irradiating 1–30 Gy, using a cobalt irradiator. The blood irradiator dose was evaluated using an alanine dosimeter. The amount of radicals produced for the radiation dose of the irradiated alanine pellets was measured by EPR (Electron paramagnetic resonance) spectroscopy (ELEXSYS E500, Bruker, Germany).

Results and Discussion The size of the EPR signals was measured according to the radiation dose of the alanine pellets using the blood irradiator. As the dose was increased from

1 Gy to 30 Gy, the size of the EPR signals increased proportionately. As the radiation dose increased, the linear regression equation result of the reaction curve for peak-to-peak of the EPR signals was $Y = 0.0081*X-0.004$, and the determination coefficient R^2 showed a linearity of 0.99 or greater. The dose distribution results confirmed that the dose was higher in the periphery than in the center of the blood irradiator, and the dose difference between the top and bottom parts was verified. The dose distribution in the container of the blood irradiator is shown in Fig. 2. For accurate verification, we plan to investigate the dose distribution using a glass dosimeter.

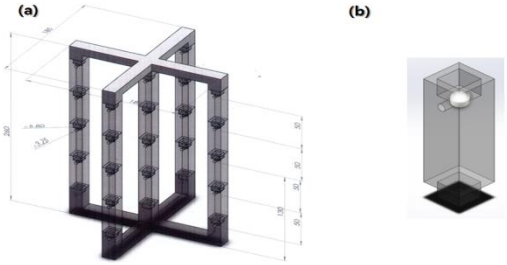

Fig. 1 (a) Jig for blood irradiator (b) Part of the jig with alanine inserted

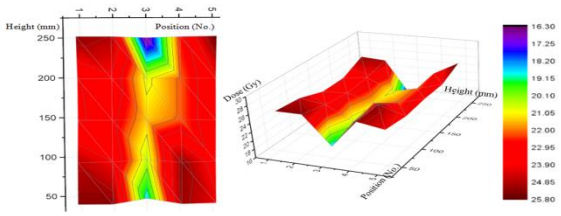

Fig. 2 Dose distribution of all positions of the container in the blood irradiator

Conclusion This study proposed a reliable irradiation method based on the dose of each position during irradiation in the blood irradiator through the measurement of dose linearity and dose distribution of the blood irradiator. Furthermore, a jig for quality control of blood irradiator was developed, which facilitated the evaluation of the dose of blood irradiator using a device-type dosimeter. The linearity of the EPR spectrum from 1 to 30 Gy irradiated from the blood irradiator was verified and the basis of quality control using a blood irradiator jig was prepared.

Acknowledgments This work was supported by a grant from the Government Research Foundation of DIRAMS grant funded by the korea government(MISP) (50496-2019)

References

[1]Chen FD, Covas, DT, Baffa O: Dosimetry of blood irradiation using an alanine/ESR dosimeter. Appl Radiat Isot 55:13-16 (2001)

Exposure doses estimation to uranium personnel of the mining enterprise and the population of Akmola region, Kazakhstan using tooth enamel EPR method

Kassym Zhumadilov[1,6*], Alexander Ivannikov[2], Artem Khailov[2], Sergei Orlenko[2], Baurzhan Abyshev[1], Valeriy Skvortsov[2], Valeriy Stepanenko[2], Shin Toyoda[3], Polat Kazymbet[4], Masaharu Hoshi[5]

[1]*L.N. Gumilyov Eurasian National University, Munaitpasova 13, Astana 010008, Kazakhstan*
[2]*A.F. Tsyb Medical Radiological Research Center, 4, Korolev str., Obninsk, 249036, Russia*
[3]*Department of Applied Physics Faculty of Science Okayama University of Science, 700-0005, Japan*
[4]*Institute of Radiobiological Research, Astana 010008, Kazakhstan*
[5]*Hiroshima University, 734-8553, Japan*
[6]*National Research Nuclear University "MEPhI" (NRNU "MEPhI", Moscow, Russian Federation)*

Highlights Tooth enamel samples from staff of the uranium mining enterprise in comparison with the population of the control territory have been investigated by the EPR dosimetry method.

Key words tooth enamel EPR dosimetry, Stepnogorsk, uranium mining

Background and Objectives The extraction of uranium often leads to a significant accumulation of radioactive materials in the environment. To assess the radiation impact of uranium mining enterprises on the personnel of enterprises and the population of the adjacent territories, the personnel of the Shantobe uranium mine and the population of Stepnogorsk (Akmola region, Northern Kazakhstan) were examined by the EPR dosimetry method.
Materials and Methods A special study has been carried out to develop a method for isolating the possible contribution of internal irradiation from alpha-emitting isotopes. The radiation induced signal (RS) from the incorporated alpha emitting isotopes is formed in the surface layer of the enamel from the adjacent soft tissues. Proposed method is based on the comparison of the amplitude of RS in the sample after bleeding of the enamel surface layer.
Results and Discussion On the basis of the measurements performed, a statistical analysis of the obtained values of the added doses obtained by the EPR method of dosimetry for tooth enamel separately for population groups and personnel was carried out. For the population of Stepnogorsk (50 teeth samples) the average dose was 4 +/- 11 mGy, of 51 mGy. For the personnel of the Shantobe uranium mining enterprise (30 teeth samples) the average dose value is 95 +/- 20 mGy, a variation of 85 mGy. For some samples of personnel, an assessment of the possible contribution of AI by comparing RS in samples before and after etching of the surface layer was carried out.
Conclusion A higher average dose value and a larger variation for personnel are probably due to the contribution of occupational exposure. Probably, part of this contribution is due to internal irradiation from alpha sources in the soft tissues of the body. This work was supported by the Ministry of Education and Science of Kazakhstan (№ AP05135470 agreement № 132).

References

IAEA, 2002. IAEA-TECDOC-1331, Vienna.
Zhumadilov K.S. et al. 2005. Tooth enamel EPR dosimetry: selecting optimal spectra registration parameters and effects of sample mass on sensitivity. J. Radiat. Res. 46, 435-442.

Impact of dosimeter type on recorded occupational radiation dose

Michael Gilhen and Tomas Kron
Department of Physical Sciences, PeterMacCallum Cancer Centre, Melbourne, Victoria, Australia

Highlights Peter MacCallum Cancer Centre (Peter Mac) is a dedicated oncology hospital providing nuclear medicine, radiation therapy, and radiology services. It also includes a large research department that uses X-ray devices and unsealed radioactive material. Currently, approximately 28 % of Peter Mac staff is monitored for personal dose equivalent (Hp10). In 2007 the type of dosimeter and provider was changed from a thermoluminescent detector (TLD) to optically stimulated luminescence detector (OSL) dosimeter. An examination of the Peter Mac occupational radiation dose register showed a marked decrease in the average Hp10 when use of the OSL dosimeter commenced.

Key words thermoluminescent detector, optically stimulated luminescence detector, personal dose equivalent

Background and Objectives The personal dose equivalent records have recently been consolidated from the current and previous dosimetry providers into a single electronic record keeping system. Personal dose equivalent records date back over 30 years to 1987 and contain the entire dose history of over 5000 employees.
The dose register was examined to see if there was any difference in the average radiation dose to employees when the type of dosimeter was changed in 2007 from a dysprosium doped calcium sulphate ($CaSO_4$:Dy) thermoluminescent detector (TLD) to a aluminum oxide (Al_2O_3) optically stimulated luminescence detector (OSL) dosimeter. The TLD dosimeters were provided and analyzed by the Australian Radiation Protection and Nuclear Safety Agency (ARPANSA) and had a minimum detectable dose of 70 µSv. The OSL dosimeters are Landauer Luxel dosimeters that have a minimum detectable dose of 10 µSv. The database examination was undertaken with the view that there should be little difference in the average dose to employees, as both types of dosimeter were analysed to estimate personal dose equivalent (Hp10) and work practices with ionizing radiation did not change significantly.

Materials and Methods A commercial radiation safety record keeping software package (Historion, Cybermynd, Melbourne, Australia) was used to consolidate electronic radiation dose records from two separate sources Radiation doses from 1987 to 2006 we obtained in csv format from the. The csv files we uploaded into Historion via the data import tools.

Radiation doses from 2007 to the present day were imported direct from the Landauer customer portal via the Historion data import tool. The average personal dose equivalent measured by all dosimeters issued from 2004 – 2009 was calculated and compared to see if there were any differences due to a change in dosimeter type. Control dosimeters were excluded from the analysis.

Results and Discussion The average personal dose equivalent measured with the ARPANSA TLD dosimeter was 146.2 (2004) 142.2 (2005) and 133.0 (2006) µSv. The average personal dose equivalent measured with the Landauer dosimeter was 31.4 (2007), 31.9 (2008) and 22.6 (2009) µSv. Figure 1 shows a reduction in the personal dose equivalent measured by the dosimeters.

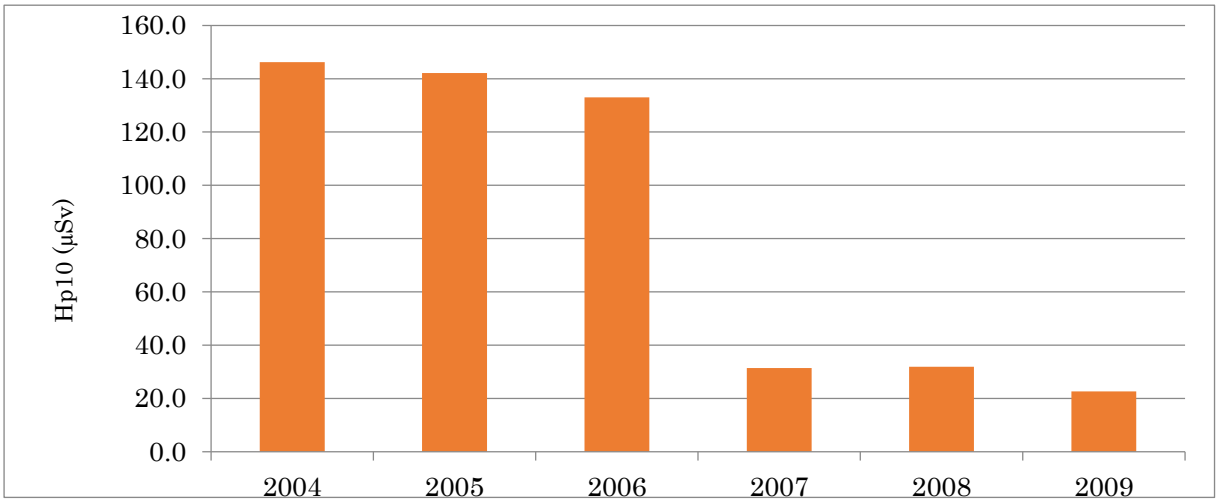

Figure 1. Average personal dose equivalent measured by dosimeters issued to employees

The average dose for 2004 – 2006 was 140.5 µSv and for 2007 – 2009 was 28.7 µSv. Measured radiation doses were reduced by 79 % when using OSL rather than TLD as a personal dosimeter.

Conclusion The reduction in dose between dosimeter types is somewhat surprising given that work practices did not change significantly during the monitoring periods assessed. Possible causes for these differences and the impact on managing occupation radiation doses is discussed.

A New Standard Sample to be Used in ESR (EPR) Tooth Enamel Retrospective Dosimetry

S. Toyoda[1]*, M. Murahashi[1], A. Ivannikov[2]
[1]*Department of Applied Physics, Okayama University of Science, Okayama, Japan*
[2]*A. Tsyb Medical Radiological Research Center, Obninsk, Russia*

Highlights Instead of using a set standard samples of irradiated tooth enamel, tempol is shown to be useful in ESR (electron spin resonance, or EPR) retrospective dosimetry to determine the doses given to tooth enamel.

Key words dosimetry, ESR, EPR, tooth enamel, standard

Background and Objectives ESR (electron spin resonance, same as EPR, electron paramagnetic resonance) dosimetry is an established method for obtaining retrospective radiation doses with using permanent tooth enamel[1)]. As it is known that the sensitivity to the absorbed dose of the dosimetric CO_2^- radical in tooth enamel is uniform[2)], the calibration method is usually employed to the enamel sample to obtain the retrospective dose, where the dose is obtained as the dose value corresponding to the signal intensity in the calibration line. Each laboratory working on ESR dosimetry, therefore, has to have a set of standard samples of irradiated tooth enamel to be measured in order to draw the calibration line. However, the sets of calibration samples have never been compared with each other. In the present paper, we would like to propose a separate standard sample, other than tooth enamel, with stable radicals to be used as a standard.

Materials and Methods Tempol was used in the present study. Tempol was diluted by benzene to $1x10^{-6}$ mol/l for ESR measurement, where the spin number in the solution in the sample tube in known. The three hyperfine lines of an ESR spectrum were integrated twice to obtain the area which corresponds to the spin number. Calibrating the measurement sensitivity within the cavity with using the Mn marker, the spin number of the dosimetric CO_2^- radical in a tooth enamel sample irradiated to 1.0 Gy was obtained.

Results and Discussion A spin concentration of $8.7x10^{16}$ spin/kg was obtained in that enamel sample, which corresponds to the G value (spin number per absorption of 100 eV of radiation energy) of 1.40. When tempol is adopted as the standard with this G value, any laboratory in the world can determine the dose to human tooth enamel as long as the laboratory has tempol

and has the technique to determine the spin concentration, without a set of tooth enamel standard samples. It is further necessary to examine and to agree among the laboratories the precise G value for CO_2^- radical in tooth enamel.

Conclusion We would like to propose tempol to be used as a standard for ESR tooth enamel dosimetry.

References

1) ISO (2013) Radiological protection – Minimum criteria for electron paramagnetic resonance (EPR) spectroscopy for retrospective dosimetry of ionizing radiation – Part 1: General principles, International Standard, ISO 13304-1.
2) Wieser, A., El-Faramawy, N., Meckbach, R. (2001) Dependencies of the radiation sensitivity of human tooth enamel in EPR dosimetry, Appl. Radiat. Isot. 54, 793-799.

Retrospective Radiation Doses to Cattle by Fukushima Dai-ichi Nuclear Power Plant Accident: ESR Tooth Enamel Dosimetry

A. Todaka[1]*, S. Toyoda[1], M. Murahashi[1], M. Natsuhori[2], K. Okada[3], S. Ito[4]

[1]*Okayama University of Science, Okayama, Japan*

[2]*Kitasato University, Aomori, Japan*

[3]*Iwate University, Morioka, Japan*

[4]*Fazenda da Esperanca, Fukushima, Japan*

Highlights The method of ESR (EPR) dosimetry is applied to cattle tooth enamel to obtain retrospective radiation doses by Fukushima Dai-ichi Nuclear Power Plant accident in 2011. The obtained doses are up to 1.2 Gy, being roughly consistent with the accumulated environmental dose rates. The study shows that mammal tooth enamel is useful in ESR dosimetry.

Key words accidental radiation doses, ESR, tooth enamel, cattle

Background and Objectives Radionuclides were released to the environment by the Fukushima Dai-ichi Nuclear Power Plant accident. It is an important issue to estimate the radiation doses to animals in order to know the impact of the accident to the environment. In the present study, we employed ESR dosimetry to apply to tooth enamel of cattle, the method of which has already been established for human tooth enamel. Stable CO_2^- radicals, to be detected by ESR, are created in tooth enamel made of hydroxyapatite by radiation, being accumulated through life.

Materials and Methods Tooth samples were extracted from the jaw of the cattle. We used two teeth of each cattle. Total of 20 Japanese cattle from 4 to 12 years old raised ranches in Okuma-Ikeda , Namie-Omaru, and Namie, which are located in contaminated areas. The teeth were removed from the jaws and cut in halves with a saw. Dentin was removed by dental drills, and soaked in a 20% KOH solution at 60°C with ultrasonic. After being washed and dried, the samples were crushed to less than 1 mm with sieves. The ESR measurements were performed for the samples, and the intensities of the dosimetric CO_2^- radical signal were obtained by a computer program to extract that component from the spectrum.

Results and Discussion The dose responses of the CO_2^- signal to gamma ray doses were examined with 12 tooth samples of 6 cattle. The slope of the line best fitted to the

obtained dose response corresponds to the sensitivity. It was found that the sensitivity varies only 9 % where no dependences were observed on the ages, ranches, and estimated given doses. Assuming that the sensitivity is constant for all cattle, the given retrospective doses were obtained by dividing the signal intensity by this sensitivity where the maximum dose was 1.2 Gy. These dose values were then compared with the integrated environmental dose rate monitored at Omaru ranch where the changes of the dose rate with time were integrated for the period from the formation of the cattle tooth enamel until the cattle was provided for examination. As results, these estimated values are roughly consistent with the those obtained by the ESR measurements for the samples of the Omaru ranch. As for the samples of the Okuma ranch, there are samples, the obtained doses of which are below the detection limit, while some show high values that do not match the integrated values. All latter cattle have records of moving from other ranches. Most probably, these cattle were exposed to radiation in those ranches before moving.

Conclusion The sensitivity of the ESR signal due to CO_2^- radical varies 9 % among cattle, therefore, the calibration method can be applied to cattle tooth enamel to obtain the retrospective doses. ESR doses were obtained to be up to 1.2 Gy for the cattle raised in the ranches located in the area contaminated by Fukushima Dai-ich Nuclear Power Plant accident. Those values for cattle in Omaru ranch are consistent with the integrated radiation doses. The present study showed that ESR dosimetry is useful for the tooth enamel of cattle as well as for that of human.

Proficiency Testing and Dose Comparison for External Personnel Dosimeters Evaluation in Taiwan

Yi-Chun Lin[1], Min-Chi Chiu[1]*, Chin-Chi Chen[1], Chun-Liang Chen[1], Ming-Chen Yuan[1], Chien-Hau Chu[1], Teng-Hung Tsou[1], Tseng-Te Huang[1]

[1]*Health Physics Division, Institute of Nuclear Energy Research, Taoyuan City, Taiwan(R.O.C.)*

Highlights All the categories of performance of current 8 tested laboratories meet the ANSI/HPS N13.11-2009(R2015) criteria and the reanalysis results were suggested to be an important step of an accreditation procedure for the personnel dosimetry system in Taiwan.

Key words Personal dose equivalent $H_p(d)$, Performance testing, Personnel dosimeters, Monte Carlo method, Radiation safety

Background and Objectives In the radiation safety field, the execution of personnel dosimetry proficiency testing is always performed by the National Radiation Standard Laboratory (NRSL) of the Institute of Nuclear Energy Research (INER) in Taiwan. Nowadays, the 10th external personnel dosimetry performances have been conducted according to the Taiwan Accreditation Foundation (TAF) criteria, TAF-CNLA-T08(3) — technical criterion for accreditation of personnel external dose evaluation laboratory, and the conformity assessment concept is based on the U.S. test criteria — the ANSI/HPS N13.11-2001 standard. In response to the latest release of ANSI/HPS N13.11-2009(R2015), the purpose of this paper is to study the dose assessment ability and criterion update feasibility through the personnel dose equivalent data reanalysis of the 10th proficiency testing for improvement of measurement quality and traceability of individual dosimetry evaluation laboratories in Taiwan. In addition, the dose evaluation of personnel dosimeters to measure the personal dose equivalent, $H_p(d)$ in realistic irradiation field is also demonstrated. The measured values of $H_p(d)$ were compared to calculated values using Monte Carlo method in the requested spectra.

Materials and Methods From 2016 to 2017, the 10th proficiency testing was smoothly completed under full cooperation among NRSL and the 8 tested laboratories using 5 different types of detectors. These personnel external dosimetry laboratories evaluated the domestic doses of radiation-related matters for radiation safety. The used dosimeters were of the 4 thermolummescent dosimeter (TLD) types of HARSHAW, Panasonic, RADOS and Thermo, and 1 optically stimulated luminescence dosimetry (OSLD) type LANDAUER. The nearly 3

times of dose data were reevaluated with ANSI/HPS N13.11-2009(R2015) which defines different testing items, numbers of dosimeters, radiation source types and stricter limitations than the 2001 version. For calibration field using ^{137}Cs photon, X-ray, ^{90}Sr beta, and ^{252}Cf neutron sources with the dosimeters placed at PMMA phantom, the reference values of $H_p(d)$ were determined from air kerma, absorbed dose and neutron fluence in photon, beta and neutron beams, respectively, and also directly calculated using MCNP6 code.

Results and Discussion The results showed that tolerance level (L), absolute of bias (|B|) and standard deviation (S) for all the categories of performance of 8 tested laboratories met the latest ANSI/HPS N13.11 criteria. The performance quotients of 4 laboratories were below 20% and the others were below 30% which showed that the technical competence of each laboratory was pretty good. Besides, the dose evaluation of personnel dosimeter showed general agreement in measured calculated and reference values.

Conclusion With the ANSI/HPS N13.11 standard evolving from the 2001 version, all the participants were able to pass the proficiency testing based on ANSI/HPS N13.11-2009(R2015). The reanalysis results of performance testing were suggested to be an important step of an accreditation procedure for the personnel dosimetry system in Taiwan. For the different irradiations, the relative response to photon, beta and neutron produced by INER are also satisfactory. Following this, we will conduct as soon as possible additional dose evaluation of extremity rings and lens of eye dosimeters for radiation safety applications.

References

1) ANSI/HPS N13.11-2009(R2015). American National Standard for Dosimetry – Personnel Dosimetry Performance – Criteria for Testing.
2) M.S. Lin, J.H. Lee, C.M. Chou, I.J. Chen and S.M. Hsu. Performance testing and dose verification for extremity ring dosimetry. Radiation Measurements 45 (2010).

LET assessment for RBE modeling in proton therapy beams using pairs of differently doped thermoluminescent detectors

Alessio Parisi [a], Sabina Chiriotti [a], Marijke De Saint-Hubert [a], Olivier Van Hoey [a], Lara Struelens [a], Patrice Mégret [b], Charlot Vandevoorde [c], Philip Beukes [c], Evan Alexander de Kock [c], Julyan Symons [c], Jaime Nieto Camero [c], Jacobus Slabbert [c], Emily Debrot [d], David Bolst [d], Linh Tran [d], Anatoly Rosenfeld [d], Tomasz Horwacik [e], Hubert Jabłoński [e], Leszek Malinowski [e], Tomasz Nowak [e], Pawel Olko [e], Jan Swakoń [e], Filip Vanhavere [a]

[a] *Belgian Nuclear Research Centre SCK•CEN, Mol, Belgium*
[b] *University of Mons, Faculty of Engineering, Mons, Belgium*
[c] *iThemba LABS, Cape Town, South Africa*
[d] *Centre for Medical Radiation Physics, University of Wollongong, Wollongong, Australia*
[e] *Institute of Nuclear Physics, Polish Academy of Sciences (IFJ PAN), Krakow, Poland*

Highlights A new methodology is presented for assessing linear energy transfer (LET) and relative biological effectiveness (RBE) in proton therapy beams using thermoluminescent detectors. The assessed LET and RBE values were compared with respectively the results of Monte Carlo computer simulations and of an in vitro cell survival study, showing good agreement.

Keywords Proton therapy, thermoluminescent detectors, LET, RBE, PHITS

Background and Objectives Recent evidence suggests the inadequacy of using a constant RBE factor of 1.1 in proton therapy treatment planning, especially in the distal edge region where values up to 3 were reported [1]. This RBE increase is mostly caused by the higher protons' LET when close to their stop in matter. In this work, a new methodology for assessing LET and RBE in proton therapy beams using thermoluminescent detectors is presented.

Materials and Methods The method is based on the different LET response of two different lithium fluoride thermoluminescent detectors (^{7}LiF:Mg,Ti MTS-7 and ^{7}LiF:Mg,Cu,P MCP-7) for measuring charged particles. The relative efficiency of the two detector types was predicted using the recently developed Microdosimetric d(z) Model [2] in combination with the Monte Carlo code PHITS. Afterwards, the expected ratio of the response of the two detector types was correlated with the fluence- (LET_F) and dose- (LET_D) mean values of the unrestricted proton LET in water. Finally, using the obtained proton LET_D values as input, the RBE can be assessed using a phenomenological LET-vs-RBE model of cell survival [1]. The aforementioned

methodology was benchmarked by exposing the detectors at different locations within a spread out Bragg peak (SOBP, range ~ 120 mm, modulation ~ 50 mm, max energy ~ 200 MeV) of the clinical proton beam at iThemba LABS (Cape Town, South Africa) and within a pristine Bragg peak (range ~ 30 mm, max energy ~ 60 MeV) at IFJ PAN (Krakow, Poland). The assessed LET_F and LET_D values were compared with the results of Monte Carlo simulations using GEANT4 (iThemba LABS) or PHITS (IFJ PAN). In addition, in the first case (iThemba LABS) the RBE change within the proton SOBP was calculated using the experimentally assessed LET_D values as input for the RBE model of Paganetti et al., 2014 [1] and compared with the results of a colony survival study employing Chinese Hamster Ovary (CHO) cells.

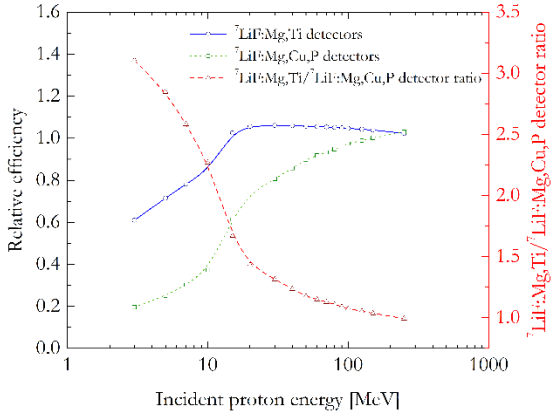

Figure 1. Relative efficiency of ^{7}LiF:Mg,Ti detectors, ^{7}LiF:Mg,Cu,P detectors and their ratio plotted as function of the proton energy.

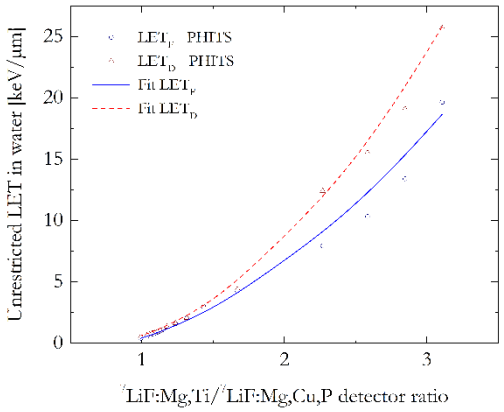

Figure 2. Correlation between the expected detector ratio and the unrestricted proton LET_F and LET_D in water.

Results and Discussion In both experimental campaigns, the experimentally assessed LET values were found to be in agreement with the results of radiation transport simulations, generally within 10%. In addition, the RBE was found to vary from around 1.1 in the plateau region up to approximately 1.9 at the distal edge of the proton SOBP at iThemba LABS. A very good agreement was found between the RBE values assessed by employing the proposed methodology and the results of the in vitro study, with an average relative deviation around 6%.

Conclusion This work proved the feasibility of a cheap, safe and easy-to-use method for assessing the LET and modeling RBE within clinical proton beams in the framework of cancer therapy applications.

References

1) Paganetti, 2014. Physics in Medicine & Biology, 59(22), p.R419.
2) Parisi et al., 2019. Radiation Measurements, 123, pp.1-12.

Radiological properties of Coumarin derivative fluorescent gel dosimeter

Anri Mochizuki[1]*, Takuya Maeyama[1]
[1]*Kitasato University, Kanagawa, Japan*

Highlights Gel dosimetry has attracted attention as a useful tool for dose verification in advanced radiotherapy because gel dosimeters can be used as phantoms in the same way as the phantoms used in an actual radiotherapy treatment chain. This study evaluates the effects of scavengers of water decomposition radicals on fluorescent degradation yield of a nanoclay-based radio-degradation fluorescence gel using 7-diethylamino-4-methylcoumarin (7D4MC). Results of this study revealed that OH radicals are the most important factor in a reaction employing 7D4MC. Oxygen is the second most important factor, whereas hydrated electrons do not significantly affect the reaction.

Key words Gel dosimeter, radio-degradation fluorescence gel, Nanoclay, X-ray

Background and Objectives Recently, high-precision radiotherapy that focuses high doses of radiation on the tumor and decreases the damage to normal tissue is becoming popular. Gel dosimetry has attracted attention for dose verification in advanced radiotherapy. In a recent study, we introduced a nanoclay gel-based dosimeter that uses fluorescent dyes. There are two types of such gels, including a radio-fluorogenic gel (RFG)[1)], whereby a fluorescent dye is produced when a non-fluorescent dye such as coumarin-3-carboxylic acid (CCA) reacts with radicals formed via the radiolysis of water; in contrast, the other type of gel is a radio-degradation fluorescence gel (RDG), whereby a non-fluorescent dye is produced when a fluorescent dye such as rhodamine 6G (R6G) or 7-diethylamino-4-methylcoumarin (7D4MC) reacts with the radicals. Moreover, we investigated the diffusion suppression of cationic dyes in nanoclay gel and observed that 7D4MC exhibited higher sensitivity than R6G as RDG[2)]. The objective of this study is to evaluate the effects of scavengers of water decomposition radicals on fluorescent degradation yield.

Materials and Methods The effects of scavengers of water decomposition radicals were evaluated by comparing the dose dependence of the fluorescence intensity under different preparation conditions. A standard sample comprises 1-μM 7D4MC and 1.0-wt% nanoclay. As shown in Table 1, preparation conditions were changed by adding several scavengers of water decomposition radicals to the standard sample. The samples that change the gases were

prepared by bubbling them with argon gas or N_2O gas inside a glove box. The prepared samples were irradiated using an industrial X-ray machine (250 kVp, 8 mA, with a 1-mm-thick Al filter; Rigaku Radioflex 250CG, Japan) at a dose rate of 1.43 Gy/min. Two or three days after irradiation, fluorescence measurements of the irradiated samples were obtained using an F-4500 Spectrofluorometer (Hitachi, Japan).

Table 1. Preparation conditions of samples

No.	Gas	Additive
1	Air	-
2	Air	50 mM *t*-BuOH
3	Ar	-
4	N_2O	-
5	Air	1 mM K_2SeO_4

Results and Discussion *t*-BuOH, N_2O, and K_2SeO_4 quickly react with OH radical, hydrated electron (removing oxygen), and hydrated electron, respectively. Fig. 1 summarizes the degradation yields of 7D4MC under different preparation conditions. Compared with sample No.1 in Table 1, the sensitivity of sample No. 2 decreased suddenly, thereby elucidating that OH radicals are the most important factor in reactions involving 7D4MC. The sensitivity of sample No. 3 that removes oxygen also decreased. Therefore, oxygen is considered to be the second most important factor in the reaction of 7D4MC, after OH radicals. Moreover, the yield of sample No. 4 was lower yield than that obtained under standard conditions by eliminating the effects of oxygen. Conversely, the results of No. 4 were higher than results of No. 3 because OH radicals are produced by the reaction of N_2O with hydrated electrons. The results of No. 5, which included the addition of K_2SeO_4 increased because the hydrated electrons do not contribute to the degradation yield of 7D4MC. In addition, SeO_3^- that was produced by the reaction of K_2SeO_4 with hydrated electron reacted with 7D4MC in the same way OH radicals do.

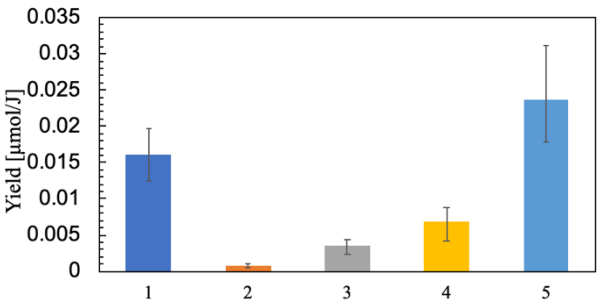

Figure 1. Average degradation yields of 7D4MC under different preparation conditions.

Conclusion In this study, we evaluate the effects of scavengers of water decomposition radicals on the fluorescent degradation yield of a nanoclay-based RDG using 7D4MC. To summarize the results, OH radicals were found to be the most important factor in the reaction of 7D4MC. Oxygen was found to be the second most important factor, whereas hydrated electrons had almost no effect on the reaction.

References

(1) T. Maeyama and S. Hase. Radiat. Phys. Chem. 151, 42-46, 2018. (2) T. Maeyama, A. Mochizuki, T. Takanashi. Journal of Physics: Conference Series, 2018. in press.

Application of linear energy transfer measurement system in therapeutic proton beams

CY Chien[1*], CH Sung[2], HH Chen[3,4], HC Huang[3,4], SL Chang[1], HY Tsai[1]

[1]*Institute of Nuclear Engineering and Science, National Tsing Hua University, Hsinchu City, Taiwan*

[2]*Department of Medical Imaging and Radiological Sciences, College of Medicine, Chang Gung University, Taoyuan, Taiwan*

[3]*Department of Radiation Oncology, Chang Gung Memorial Hospital, Linkou, Taoyuan City, Taiwan*

[4]*Graduate Institute of Clinical Medical Sciences, College of Medicine, Chang Gung University, Taoyuan City, Taiwan*

Highlights Linear energy transfer (LET) measurement system with thermoluminescent dosimeter (TLD) has been developed in our previous study. The aim of this research is to apply the LET measurement system to patient-specific treatment fields of pediatric cancers and glioblastoma multiforme in proton therapy with TLD.

Keywords thermoluminescent dosimeter, linear energy transfer, proton therapy, patient-specific treatment field, pediatric cancer, glioblastoma multiforme

Background and Objectives Over the last few years, there has been growing interest in proton beam therapy. To determine the biological dose of treatment planning in proton therapy, it is common practice to multiply the physical dose by a constant relative biological effectiveness (RBE) of 1.1. However, it has been suggested that this practice is no longer appropriate because the RBE is expected to be greater than 1.1 in the distal part of the proton range. Since the linear energy transfer (LET) is one of the reasons affected RBE, it is necessary to measure LET in proton therapy to replace constant RBE to variable RBE. In our previous study[1)], we successfully developed the LET measurement system in proton therapy with TLDs. In consideration of the importance of the LET in treating a variety of cancers, pediatric cancers and glioblastoma multiforme (GBM) are chosen in this research because the radiocarcinogenic risk for pediatric patients is significantly higher than for the elderly as well as the prognosis for GBM is poor. Due to these reasons, we decide to use the patient-specific treatment fields of pediatric cancers and GBM. Hence, the main aim of this study is to apply the LET measurement system to patient-specific treatment fields of pediatric cancer and GBM in proton therapy with TLD.

Materials and Methods We measured the absorbed dose and LET by TLDs in high-density polyethylene (HDPE) phantom in the patient-specific treatment fields of pediatric cancer and GBM, which include the nominal energy, the range at the central axis, spread-out Bragg peak (SOBP) width and water-equivalent depth. The absorbed dose was measured and compared the results with those predicted by the clinical treatment planning system. The results of the average LET acquired by the LET measurement system with TLDs were compared with the results obtained using TOPAS Monte Carlo simulations (version 3.0.1).

Results and Discussion Comparing the measured and clinical results of the absorbed dose, TLDs provided good agreement with the clinical treatment planning system. For measurements of the average LET in the patient-specific proton therapy treatment fields, the results measured using TLDs also agreed with the TOPAS Monte Carlo LET values.

Conclusion The performed investigations confirmed the promising properties of the LET measurement system with TLDs for application in therapeutic proton beams. Further applications could be the evaluation of the absorbed dose and LET in an anthropomorphic phantom irradiated by therapeutic proton beams.

References

1) Sung, C.H., Chen, H.H., Lin, Y.C., Wu, S.W., Huang, H.C., Chang, S.L., Tsai, H.Y., 2018. Linear energy transfer measurement system development with TLD-100. In: Presented at the American Association of Physics in Medicine (AAPM). 60th Annual Meeting in Nashville, TN from July 29–Aug 2.

Localized dose dependence of DNA double strand break region in human cells irradiated by SPICE microbeam

D. Ohsawa* and T. Konishi
Department of Basic Medical Sciences for Radiation Damages, National Institute of Radiological Sciences, National Institutes for Quantum and Radiological Science and Technology, 4-9-1 Anagawa, Inage-ku, Chiba, 263-8555, Japan

Highlights SPICE microbeam profile was measured using FNTDs. Localized dose distribution by the SPICE microbeam irradiation was calculated using the measured beam profile. Correlation between the localized dose distribution and DNA double strand break region was investigated using human lung normal WI-38 cells.

Key words microbeam; target irradiation; FNTD; beam size; localized dose distribution; confocal laser microscope; immunofluorescence; γ-H2AX

Background and Objectives Single Particle Irradiation system to Cell, SPICE, at the National Institute of Radiological Sciences (NIRS) is an advanced outstanding cell irradiation system capable of a single-proton single-cell irradiation with high throughput and without losing accuracy [1]. It delivers a focused vertical microbeam of 3.4 MeV protons with an approximately 2 μm in diameter to the targeted cell nucleus or cytoplasm. Such advantages of the SPCIE have motivated further investigations on the cellular response to different DNA damage complexities induced by ionizing radiation. For reliable analysis, precise information both on number of protons to hit the targeted cells and thereby localized dose distribution is essential. Previously, we reported an accurate and systematic investigation of the SPICE microbeam size using the FNTD [2]. In the present study, as a second step, we discuss the localized dose distribution and correlation with DNA double strand break (DSB) region, visualized by immuno-staining against γ-H2AX, in human lung normal WI-38 cells irradiated by SPICE microbeam.

Materials and Methods

1. Measurement of the SPICE microbeam profile using FNTD

Details of the SPICE have already been described [1]. Al_2O_3: C, Mg FNTDs were used for the measurement of SPICE micorbeam profile [2]. A FNTD, of which the size is 8×4×0.5 mm^3 and one surface is polished to optical grade, was adhered to the polypropylene surface in the cell dish with the polished surface down and irradiated from underneath with 1-1,000 protons per position in a grid pattern with a grid-point distance of 200 μm. After the irradiation, the FNTD was observed by a 60× oil immersion objective lens (NA: 1.35) equipped in a confocal laser scanning microscope (Fluoview1000, Olympus Co., Japan). Z(optical axis)-stack of images can be obtained by binding up all the image slices (104 or 146 slices) each separated by slice distance (0.87 or 0.55 μm). Image processing such as segmentation and analysis of image statistics for specified regions of interest was performed using ImageJ/Fiji. The beam profiles at the FNTD surface were well approximated by 2-dimensional normal functions over a wide range of the number of the protons per position (50~1,000p/pos), and their spreads (standard deviations), σ_{Long} and σ_{Short}, for long and short axis direction, ranged from 0.60 × 0.46 to 0.76 × 0.60 μm, depending on the number of

protons per position.

2. Calculation of the localized dose distribution

Localized dose distribution in a cell nucleus was numerically simulated using the beam profile obtained by irradiating 50~1,000 protons per position on the FNTD; in this simulation, radial dose distribution of a single proton track in water was calculated with existing amorphous track structure models (Chatterjee model and Kramer & Kraft model), and incident positions of the protons are randomly distributed to follow the corresponding beam profile.

3. Irradiation and immunofluorescent staining of cells

The size and intensity of the DNA DSB region were measured using WI-38 cells (lung fibroblast, ATCC number: CCL-75) and fluorescent antibodies against phosphorylated histone protein H2AX, γ-H2AX. Phosphorylation of the histone protein H2AX occurs early after irradiation in a Mbp-region surrounding a DNA DSB site and the antibodies against γ-H2AX thus enable us to detect DSBs in cells and are widely used as a biomarker for it. The WI-38 cells were irradiated at the center of the nucleus with 50~500 protons and fixed 1 hour after the irradiation. After the fixation, the cells were immuno-stained with anti-γ-H2AX antibody followed by the Alexa488 fluorescent secondary antibody to detect the position of DBSs, and also counterstained with DRAQ5 to detect the position of cell nuclei and observed by a 60× water immersion objective lens (NA: 1.00) equipped in the same microscope as the FNTD, in which the image slices were obtained by scanning along the Z axis with slice distance of 0.87 μm from the upper to the lower edge of the cell nucleus.

Results and Discussion Calculated dose distributions consist of sharp peaks due to core and a broad convex profile due to penumbra, and owing to the short penumbra range of 3.4 MeV proton, the SPICE microbeam was found to have a sharply defined dose distribution without low dose tails. On the other hand, the sizes of the localized DSB region identified as fluorescent γ-H2AX spots were observed to be rather larger than that of the dose distribution, indicating that induction of DSB in the targeted cell nuclei were enhanced beyond the localized dose distribution.

Conclusion We successfully evaluated the localized dose distribution as a function of the number of the incident protons per position. It was found that the sizes of localized DSB region, which were identified as fluorescent spots of γ-H2AX, were rather larger than the localized dose distribution. This result indicates that induction of DSB in the targeted cell nuclei were visualized beyond the beam size region.

References

1) Konishi, T et al. (2013). SPICE-NIRS Microbeam: a focused vertical system for proton irradiation of a single cell for radiobiological research. J. Radiat. Res., 54, 736-747.
2) Ohsawa, D et al. (2018, July). Analysis of SPICE Microbeam Profile Using Fluorescent Nuclear Track Detector (FNTD). Poster session presentation at the meeting of 16th International Conference on Nuclear Microprobe Technology and Applications, University of Surrey, Guildford, UK.

Dosimetric characteristics of an optical CT scanned genipin-gelatin gel dosimeter for radiotherapy applications

D Ramm
Royal Adelaide Hospital, Adelaide, Australia
University of Adelaide, Adelaide, Australia

Highlights A genipin gel dosimeter was shown to have potential as a clinical radiotherapy dosimeter for relatively high doses and small gel volumes.

Key words gel dosimetry, 3D, optical CT, radiotherapy

Background and Objectives The genipin-gelatin gel dosimeter is a radiochromic gel dosimeter previously developed for measurement of radiotherapy 3D dose distributions[1]. This gel dosimeter has some desirable properties such as; low toxicity, good spatial stability, good water equivalence, and dose response through optical absorption. The main drawbacks are low dose sensitivity and high initial optical density. Studies of basic properties of genipin gel have been conducted[2], but detailed considerations of 3D optical scanning of this gel has not been reported. In this work, characteristics of genipin gel were assessed from 3D optical CT scans to quantify some aspects of dosimetric performance for radiotherapy dose verifications.

Materials and Methods Genipin gel was prepared similarly to previously[1)2)], with minor adjustments of component concentrations. Gel samples were scanned in 3D with an in-house fluid-less optical CT at 594 nm and resolution of 0.3 x 0.3 x 1.0 mm^3[3]. Gel dosimeter size was 5 cm diameter and 6 cm length. Gel samples were irradiated using a Varian Truebeam linear accelerator 6MV FFF beam at 1400 MU/min. Doses of 30 Gy and 15 Gy were delivered under reference conditions, providing near uniform dose in the gel axial planes and decreasing dose with depth beyond the build-up region. The gel measured percentage depth dose (PDD) curves were compared to ion chamber reference data. Uniformity and signal to noise ratio (SNR) were computed for each axial slice.

Results and Discussion A genipin gel sample is shown in figure 1(a), positioned on the optical CT scanner. Figure 1(b) shows the reconstructed dose data used to provide the PDD shown in figure 1(c). Agreement of gel PDD was within ± 2 % of ion chamber reference data beyond the build-up region. SNR was 70 ± 15 at 30 Gy and 45 ± 7 at 15 Gy, while non-uniformity was 2.4 ± 0.5 % and 3.0 ± 0.5 % for 30 and 15 Gy respectively. These results

are substantially inferior to those achieved previously with ferrous-xylenol-gel (FXG) at only 4 Gy[3]. Typical values for SNR and non-uniformity were 250 and 1.2 % respectively. Nevertheless these results provide indication that genipin gel may be a useful 3D dosimeter at dose levels approaching 30 Gy with a 5 cm diameter gel.

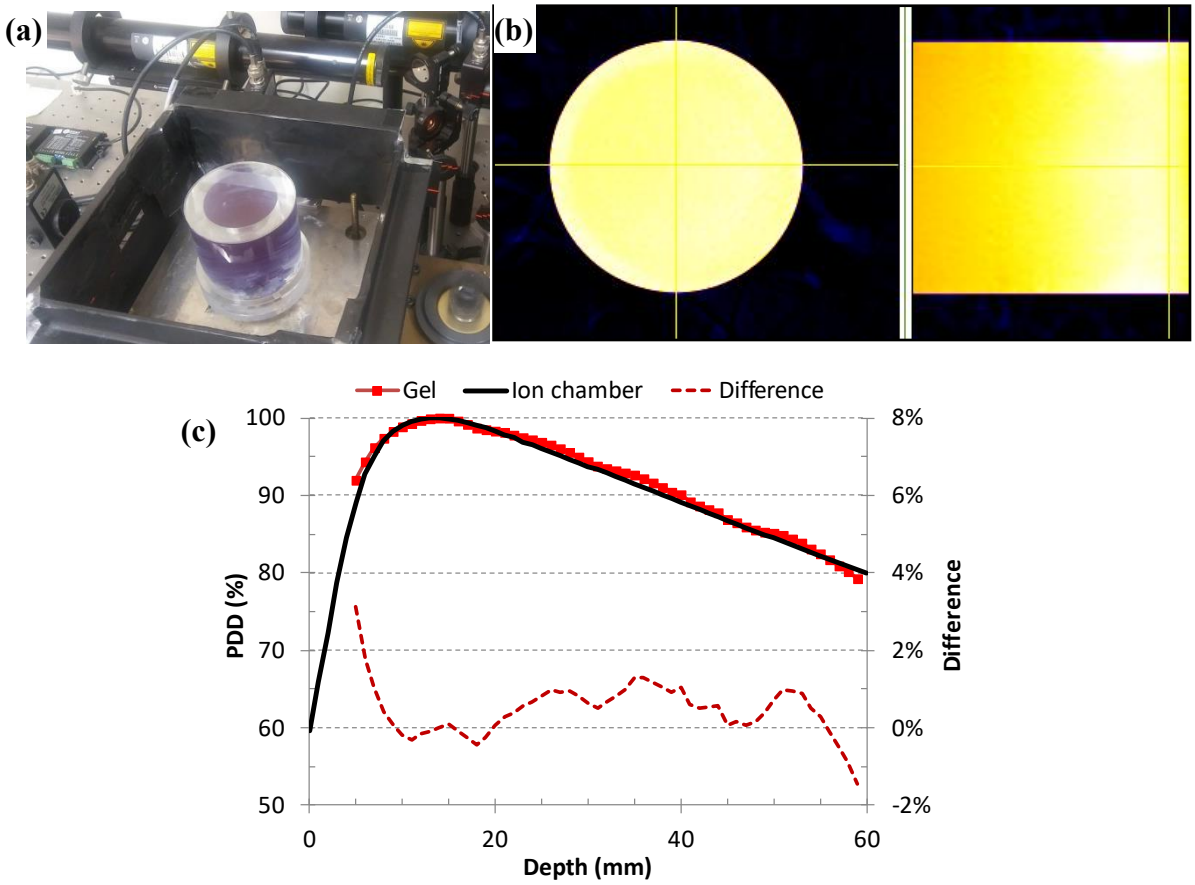

Figure 1. (a) Genipin gel sample on the optical CT scanner. (b) Reconstructed gel dose in axial and transverse planes, irradiated to 30 Gy. (c) PDD extracted from the 3D dose data.

Conclusion Genipin gel performance was adequate to indicate that when combined with suitable optical CT scanning, doses and gel size, it may be a useful radiotherapy dosimeter.

References

1) Jordan K 2008 Zero diffusion radiochromic genipin-gelatin dosimeter *Med. Phys.* **35** 3413
2) Davies J B, Bosi S G, Baldock C 2013 Dosimetry aspects of a non-diffusing genipin-gelatin gel *Rad. Phys Chem.* **83** 19-27
3) Ramm D 2018 A fast dual wavelength laser beam fluid-less optical CT scanner for radiotherapy 3D gel dosimetry II: dosimetric performance *Phys. Med. Biol.* **63** 045020

Development of a Clinically Applicable Rectum Dosimeter for Brachytherapy using an Optically Stimulated Luminescence Dosimeter

Emi Tomita[1], Hiroaki Hayashi[1], Takashi Asahara[1], Natsumi Kimoto[1], Sota Goto[1], Yuki Kanazawa[2], Yasufumi Shitakubo[3], Kanako Sakuragawa[3], Hitoshi Ikushima[2,3], Tohru Okazaki[4], Takuya Hashizume[4]

[1]*Kanazawa University, Ishikawa, Japan*
[2]*Tokushima University, Tokushima, Japan*
[3]*Tokushima University Hospital, Tokushima, Japan*
[4]*Nagase Landauer, Ltd., Ibaraki, Japan*

Highlights We propose a novel rectum dosimeter made from a piece of OSL sheet and a catheter to measure absorbed doses of rectum during high-dose-rate ^{192}Ir brachytherapy for cervical cancer. The dosimeter can be analyzed in a similar way as a commercial type dosimeter by inserting the disk punched out from the sheet into commercial type dosimeter cases. We will demonstrate availability of our dosimeter in an actual clinical situation.

Key words Brachytherapy, Rectum dosimeter, OSL dosimeter, Actual dosimetry

Background and Objectives High-dose-rate brachytherapy is one of the clinical treatment options for cervical cancer. Currently, dose calculation algorithms such as TG-43[1)] has been proposed by AAPM and it is generally installed into a therapeutic planning system used in current clinical radiotherapy. In contrast, an actual dosimetric system using semiconductor detectors such as MOSFET has been reported[2)] as a way to manage absorbed doses of an organ at risk (OAR). In this study, we focused our attention on an optically stimulated luminescence (OSL) dosimeter[3)] which is not expensive and can save irradiation information, and developed a novel disposal rectum dosimeter.

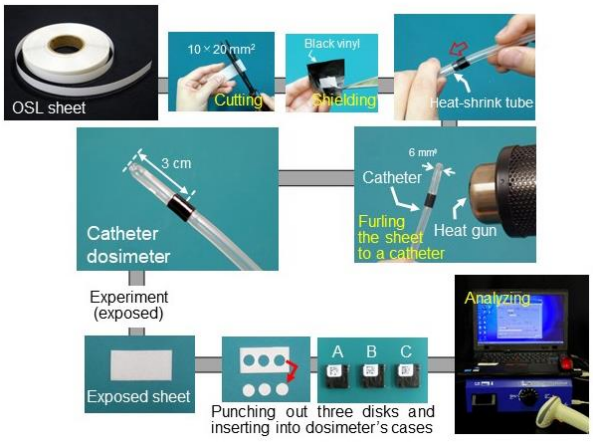

Figure 1. The procedure to fabricate and analyze the rectum dosimeter

Materials and Methods Figure 1 shows the procedure to fabricate and analyze the rectum dosimeter. The proposed dosimeter was made from an OSL sheet and a catheter (ϕ=6 mm). We used a heat-shrink tube to furl the sheet to the catheter. After exposure, the OSL sheet was removed from the catheter, and three disks were punched out. Then, we analyzed the OSL disks by inserting them into commercial type dosimeter cases. With the aim of applying our dosimeter to clinical situations, we performed experiments using clinical irradiation systems. First, an experiment to obtain a dose calibration curve of our dosimeter was performed. Second, the uncertainty of our dosimeter was evaluated. Finally, after permission from the IRB was obtained, we performed actual dosimetry of rectum in clinical brachytherapy.

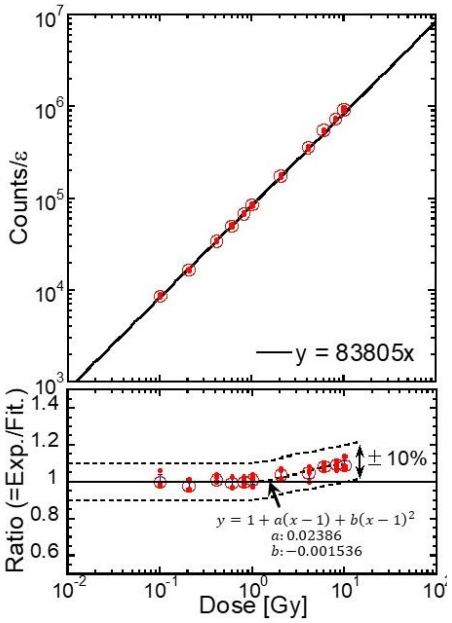

Figure 2. A dose calibration curve for the rectum dosimeter

Table 1. Results of clinical dosimetry

ID	Planned dose [Gy]	Measured dose [Gy]
A	3.53	3.58±0.54
B	6.40	6.63±0.99
C	4.67	4.76±0.71

Results and Discussion Figure 2 shows a dose calibration curve of the rectum dosimeter. Relationship between reference dose and response of the dosimeter was clarified with the dose range of 0.1 to 10.0 Gy. From the calibration curve, we determined the uncertainty of our dosimeter was +/-10%. The uncertainty can be explained by angular dependence and repeatability of the dosimeter. In the clinical study, our rectum dosimeter could appropriately measure absorbed dose (Table 1).

Conclusion We proposed a novel rectum dosimeter made from an OSL sheet and a catheter, and obtained a dose calibration curve with the dose range of 0.1 to 10.0 Gy within an uncertainty of 10%. Furthermore, we demonstrated actual dosimetry using the dosimeter.

References

1) R. Nath, et al., Dosimetry of interstitial brachytherapy source: recommendations of the AAPM Radiation Therapy Committee Task Group No. 43, Med. Phys. 22(2), 1995, 209-234.
2) K. Tanderup, et al., In vivo dosimetry in brachytherapy, Med. Phys. 40(7), 2013, 070902.
3) PA. Jursinic, Characterization of optically stimulated luminescent dosimeters, OSLDs, for clinical dosimetric measurements, Med. Phys. 34(12), 2007, 4594-4604.

Assessing doses and risks of the patient after cervical cancer radiotherapy

Po-Chen Kuo[1,2,5] , Cheng-Ching Yu[2], Fang-Yuh Hsu[3,4*] , Jeng-Fong Chiu[5], Min-Chi Chiu[5], Pai-Chia Lin[5] , Tung-Ho Chen[5], Chen-Yuan Chen[1,6]

[1]*Department of Radiotherapy Oncology, Chang-Gung Memorial Hospital, Keelung Lake View Branch, Keelung, Taiwan.*

[2]*Department of Radiological Technology, Yuanpei University, Hsinchu, Taiwan.*

[3]*Nuclear Science and Technology Development Center, Tsing Hua University Hsinchu, Taiwan.*

[4]*Department of Biomedical Engineering and Environmental Sciences, National Tsing Hua University, Hsin-chu, Taiwan.*

[5]*Department of Radiation Oncology and Cancer Center, Taipei Medical University Hospital Cancer Hospital, Taipei, Taiwan.*

[6]*Department of Radiotherapy Oncology, Chang-Gung Memorial Hospital, Linkou Branch, Taoyuan, Taiwan.*

Highlights This study assessed the health risks for the patients after cervical cancer radiotherapy. After performing the treatments of IMRT and brachytherapy for the patients with different cervical cancer sizes, the effective doses were assessed and reported in the results. The total induced secondary cancers risks (for tissues outside the treatment fields) induced by the treatments of cervical cancer were assessed. According to the results, the treatment parameters such as field sizes and total monitor units were the main factors of affecting the probability of secondary cancer risk.

Key words cervical cancer, brachytherapy self-made phantom, intensity modulated radiotherapy, volumetric modulated arc therapy, secondary cancer risk

Background and Objectives In recent year, the average incidence age of cervical cancers is decreased in Taiwan. Radiotherapy is one of the clinically recommended treatments of cervical cancer. Due to the control rate of tumor treatment is increased, and patients' survival rate is improved, therefore, for clinical radiotherapy patients, it's important to verify the effective dose and assessment the probability of out-field second cancer risk of the whole body after the treatment.

Materials and Methods In this work, a Rando phantom and a selfmade pelvic phantoms

were used for simulating the cervical cancer patients treated by the radiotherapy externally and internally, respectively. The individual organ doses were estimated by means of the TLD-100 chips for different treatment plans design that externally include intensity-modulated radiotherapy (IMRT) and volumetric-modulated arc therapy (VMAT) techniques, and combined the internal brachytherapy. For risk assessment, the method for assessing effective dose as well as the risk coeificients recommend by ICRP 103 report were used.

Results and Discussion This study considered total dose of 5040 cGy given by teletherapy (IMRT and VMAT) combined with a total dose of 2400 cGy by brachytherapy to assess the effective doses and secondary cancer risks. For large tumor, the mean effective dose of 427.50 ± 4.59 (mSv) and 269.60 ± 2.04 (mSv) were estimated for IMRT combined brachytherapy and VMAT combined brachytherapy, respectively. The mean risks of inducing secondary cancer were 2.14 ± 0.03 (%) and 1.35 ± 0.01 (%) for using IMRT combined brachytherapy and VMAT combined brachytherapy, respectively. For small tumor, the mean effective dose of 57.50 ± 0.35 (mSv) and 52.40±0.46 (mSv) were estimated for IMRT combined brachytherapy and VMAT combined brachytherapy, respectively. The mean risks of inducing secondary cancer were 0.29 ± 0.01 (%) and 0.26 ± 0.01 (%) for using IMRT combined brachytherapy and VMAT combined brachytherapy, respectively.

Conclusion According to the results of this study, the field sizes and total monitor units were the main factors of affecting the probability of secondary cancer risk. A more comprehensive consideration is recommended to make to provide better life quality for patients after radiotherapy in their long-term survival period, by means of the proper setting of dose criterion for critical organs of treatment plan.

References

1) Hall EJ, Phil D. Intensity-modulated radiation therapy, protons, and the risk of second cancers. Radiation Oncology 2006; 65 (1):1-7
2) Anil K., et al. Second Cancers Among 104760 Survivors of Cervical Cancer: Evaluation of Long-Term Risk. J Natl Cancer Inst 2007; Vol.99, Issue21, 1634-43.
3) Abe T., et al. Assessing cumulative dose distributions in combined radiotherapy for cervical cancer using deformable image registration with pre-imaging preparations. Radiat Oncol. 2014; 9: 293.

Dosimetric comparison of pediatric PET/CT tests

Fernanda Guerra Paiva[1]*, Priscila do Carmo Santana[2], Arnaldo Prata Mourão Filho[1,3]
[1]*Department of Nuclear Engineering, Federal University of Minas Gerais, Brazil*
[2]*Medical School, Federal University of Minas Gerais, Brazil*
[3]*Biomedical Engineering Center, Federal Center for Technological Education of Minas Gerais, Brazil*

Highlights High radiation doses associated with PET/CT, compared with conventional exams have raised health care.
Evaluation of absorbed and effective dose to children of 2 and 10 years.

Key words PET/CT, Dosimetry, Computed Tomography

Background and Objectives Positron Emission Tomography (PET) associated with Computed Tomography (CT) scanning is becoming increasingly important in noninvasive imaging studies and in the monitoring of children with known or suspected malignant diseases [1, 2]. These compound tomographic scanners allow the fusion of functional images obtained from the administration of radionuclides, such as ^{18}F, and anatomical images generated by X-ray beam attenuation from CT [3-5]. Although the immediate benefit to the individual patient may be substantial, relatively high radiation doses associated with PET/CT, compared with conventional exams have raised health care. This is especially concerning for children, who are more sensitive to radiation-induced carcinogenesis and have many remaining years of life for the development of cancer [6].

Materials and Methods In this study, the absorbed and effective doses generated by the CT scan and incorporated by the administration of the radionuclide ^{18}F-FDG were evaluate in the most radiosensitive organs. To evaluate the CT dose, radiochromic film strips (Gafchromic XR-QA2) [7,8] were placed into two pediatric body phantoms, similar to children of 2 and 10 years, built by PMMA volumes, as shown in Figure 1. The CT protocol performed was the standard pediatric whole-body scanning used in the service where the study was done.

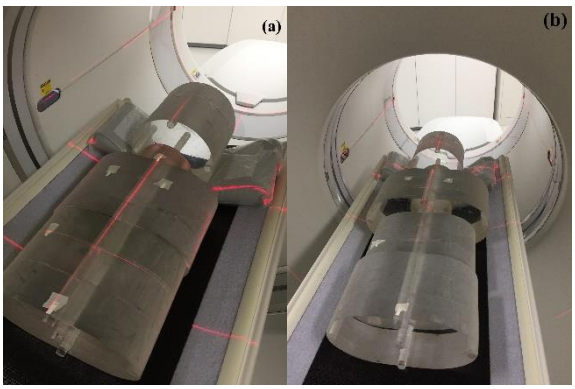

Figure 1. Pediatric PMMA phantoms. 2 years old (a) and 10 years old (b).

The activity of the radiopharmaceutical ^{18}F-FDG to be injected may vary according to the patient mass and the detector sensitivity. The Effective Dose was evaluated using the biokinetic model proposed by the International Commission on Radiological Protection (ICRP) number 106 [9]. The protocol used was 3.33 MBq.kg^{-1} (0.09 mCi.kg^{-1}), this amount is commonly used in the service were the study was done, and it was multiplied by the mass of each phantom, 12 kg for the 2 years old and 31 kg for the 10 years old.

Results and Discussion The absorbed doses from CT scan were approximately on average 19% higher in the 10-year phantom. This can be explained by the scan distance, which was 50.35 cm for the 2-year phantom and 73.9cm for the 10-year phantom. For the 2-year phantom, the organs that presented the highest absorbed dose from CT scan were thyroid and bone marrow. In the 10-year phantom, the highest absorbed doses were found in the esophagus and bone marrow. The highest values were found in the central region of the phantom, that can be explained by the scattered radiation. Different values are due to the variations in the format and size of the phantoms. Analyzing the effective dose from ^{18}F, the bladder had a higher value for both ages, explained by the excretion route of the radiopharmaceutical.

References

1) STAUSS, J. et al. Guidelines for 18F-FDG PET and PET-CT imaging in paediatric oncology. European journal of nuclear medicine and molecular imaging, v. 35, n. 8, p. 1581-1588, 2008.
2) JADVAR, Hossein et al. PET and PET/CT in pediatric oncology. In: Seminars in nuclear medicine. WB Saunders, 2007. p. 316-331.
3) CZERNIN, Johannes; SCHELBERT, Heinrich. PET/CT imaging: facts, opinions, hopes,

and questions. The Journal of Nuclear Medicine, v. 45, p. 1S, 2004.

4) GERBAUDO, Victor H. (Ed.). A Case-based Approach to PET/CT in Oncology. Cambridge University Press, 2012.
5) FLUX, Glenn et al. The impact of PET and SPECT on dosimetry for targeted radionuclide therapy. Zeitschrift für medizinische Physik, v. 16, n. 1, p. 47-59, 2006.
6) GELFAND, Michael J.; LEMEN, Lisa C. PET/CT and SPECT/CT dosimetry in children: the challenge to the pediatric imager. In: Seminars in nuclear medicine. WB Saunders, 2007. p. 391-398.
7) ALNAWAF, Hani et al. Absorption spectra response of XRQA radiochromic film to x-ray radiation. Radiation measurements, v. 45, n. 1, p. 129-132, 2010.
8) ISP. (2010). International specialty products. Gafchromic XR catalogue. 8p.15.
9) ICRP. (2008) Radiation dose to patients from radiopharmaceuticals. Addendum 3 to ICRP Publication 53. ICRP Publication 106. Approved by the Commission in October 2007. Ann ICRP;38(1-2):1–197.

MgB_4O_7-laden polymer films for neutron entrance skin dosimetry

F. d'Errico[1,2], M. Ibba[1], R. Ciolini[1], L. Lazzeri[1], L.F. Souza[3], S. O. Souza[3]
[1]*Università di Pisa, Scuola di Ingegneria, Pisa, Italy*
[2]*Yale University, School of Medicine, New Haven, CT USA*
[3] *Federal University of Sergipe, São Cristóvão, Brazil*

Highlights The technology of thin polymer films has been developed for clinical and radiation protection dosimetry of neutron entrance doses in mixed radiation fields.

Key words polymer films, MgB_4O_7, optically stimulated luminescence

Background and Objectives Both clinical procedures and industrial processes exist when neutron entrance doses must be assessed within intense mixed fields of gammas and neutrons. In a particularly successful application of boron neutron capture therapy, skin melanoma is treated with large doses of thermal neutrons that should be assessed directly at the entrance in boron-loaded skin tissue. In the nuclear power cycle, manufacturing fresh fuel and reprocessing spent rods require operations inside glove boxes where the operators' hands are exposed to such mixed fields. Measurements of these entrance doses are quite complex. Attempts have been made to develop extremity dosemeters for neutrons based on track etch detectors or on thermoluminescent pellets, but the detector chips in these devices interfere with the tactile sense of the operators. For this reason, we have sought the development of extremely thin and flexible polymer films loaded with neutron sensitive luminescent materials
Materials and Methods Optically stimulable MgB_4O_7:Ce,Li was produced by solid-state synthesis, mixing stoichiometric amounts of MgO and H_3BO_3 and then sintering the product at 900 °C. Films loaded with grains of MgB_4O_7:Ce,Li were then manufactured with various technologies: solvent-evaporation techniques, pressure casting or bubble blowing of polymer blends. The solvent-evaporation technique is a relatively easy technique and it allows the rapid production of small test-samples; however, it requires a careful selection of organic solvents in order to avoid affecting the luminescent properties of the dispersed grains. Pressure casting and bubble blowing require much more complex equipment, but they can produce large sheets of thin films uniformly loaded with the materials of interest.
Results and Discussion The solubility of MgB_4O_7:Ce,Li powder samples was tested with a variety of solvents used in manufacturing polymer-films. In particular, it was verified that acetone and benzene are solvent perfectly compatible with polyvinyl chloride (PVA) and MgB_4O_7:Ce,Li used to make the films. The presence of crystalline phases was confirmed by

X-ray diffraction and by comparing the OSL signal emitted by the powders before and after the solubility tests. Films were then produced with different percentages and grain sizes of MgB_4O_7:Ce,Li, in turn synthesized using natural boron, boron-10 or boron 11. The films were then irradiated with 70 kV X-rays and in a thermal neutron irradiator consisting of two 16 Ci Am-Be sources moderated by paraffin producing a neutron flux of 2.15 10^4 n/(cm^2 s) at the reference position in the center of the apparatus. Results are shown in Figures 1 and 2.

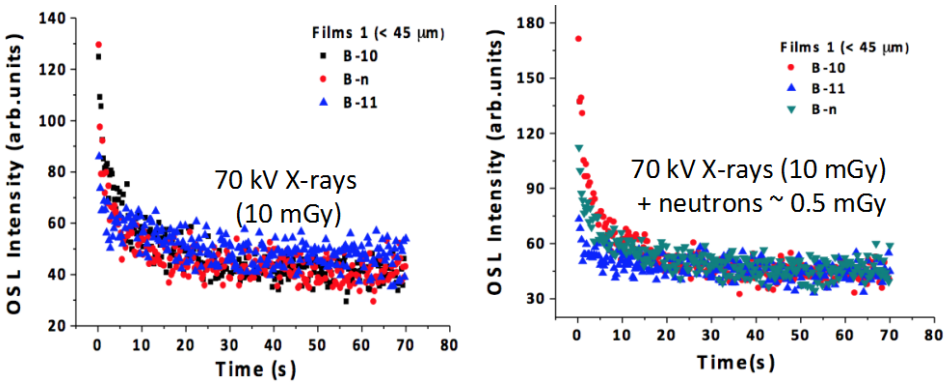

Figure 1. OSL signal from MgB_4O_7:Ce,Li produced with natural boron, boron-10 or boron 11 and irradiated with 70 kV X-rays or X-rays plus thermal neutrons.

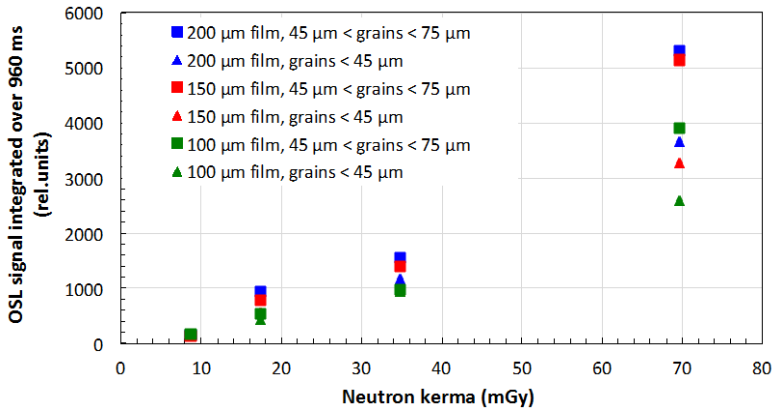

Figure 2. OSL from MgB_4O_7:Ce,Li made with boron-10 and irradiated with thermal neutrons.

Conclusion The MgB_4O_7-laden polymer films produced in this work are suitable for photon and neutron measurements. They provide high sensitivity and they can be used for measurements of thermal neutrons in clinical BNCT procedures as well as for albedo dosimetry in radiation protection applications.

References

1) Souza, L.F., Silva, A.M.B., Antonio, P.L., Caldas, L.V.E., Souza, S.O., d'Errico, F., Souza, D.N. Dosimetric properties of MgB4O7:Dy,Li and MgB4O7:Ce,Li for optically stimulated luminescence applications. Radiation Measurements 106,196-199 (2017).

Evaluation of L-Alanine Response to Photon and Electron Beams using ESR Spectroscopy

Han-Ki Jang[1*], Ki-Tek Han[1], Woo-sang Ahn[2], Wook Jae Yoo[1], Jeho Min[1]
[1]*Korean Association for Radiation Application, Jeongup, Korea*
[2]*Gangneung Asan Hospital, University of Ulsan College of Medicine, Gangneung, Korea*

Highlights In this study, we evaluated characteristics of L-alanine response to photon and electron beams, such as linearity, repeatability, and dependence for radiation energy and dose rate.

Key words ESR, alanine, electron, photon

Background and Objectives Electron spin resonance(ESR) is one of the physical detection methods and has been used at various fields related to radiation dosimetry. Especially, an alanine/ESR system is the most well-known substance as a free radical dosimeter. Also, it is recommended by the International Atomic Energy Agency(IAEA) as a standard for high-dose measurements through the IAEA-TECDOC-1188[1)]. In this study, we evaluated L-alanine response to apply the alanine/ESR system to therapeutic radiation.

Materials and Methods We used a clinical linear accelerator(CLINAC) installed in a domestic hospital. Irradiation doses were set to 1 to 10 Gy for the energies of 6, 12 and 20 MeV electron beams and 4, 6, 10 and 15 MV photon beams to evaluate the response of the alanine/ESR system to the photon and electron beams. And, the experiment was performed after setting the dose rate range from 100 to 600 MU/min using 6 MV photon and 12 MeV electron beams in order to evaluate the dependence on the dose rate. In the case of alanine samples, we used two types of alanine sample manufactured by Bruker and Magnettech, respectively.

Results and Discussion First of all, the beam stability test was performed using an ion-chamber to improve the reliability of the result before alanine sample irradiation. As a result, the beam stability according to the dose was very good with R-square value more than 99.9999%. Also, the relative standard deviation(%RSD) of the result for dose rate was obtained to be less than 0.2%. Next, a phantom was fabricated for accurate beam irradiation and the alanine sample was inserted in the phantom. Using this phantom, we irradiated reference dose to the alanine samples and then analyzed with ESR spectroscopy. As a result, the responses of

alanine/ESR were increased linearly by increasing doses of photon and electron beams (Figure 1 and 2). Finally, response curves were compared to confirm energy dependence of the system. It is confirmed that there is a difference according to energy in the 1 ~ 10 Gy range. In the case of dose rate dependence, %RSD for all results was obtained with less than 5% as shown in figure 2. Therefore, the dose rate dependence was judged to be insignificant.

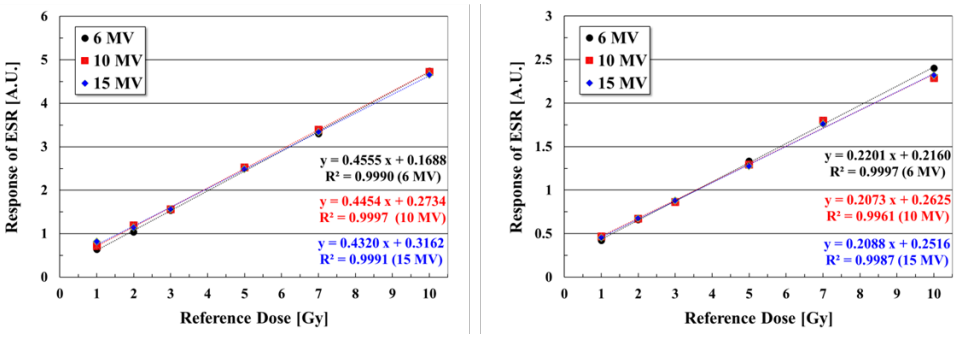

Figure 1. Response of L-alanine for photon beam(left: Magnettech, right: Bruker)

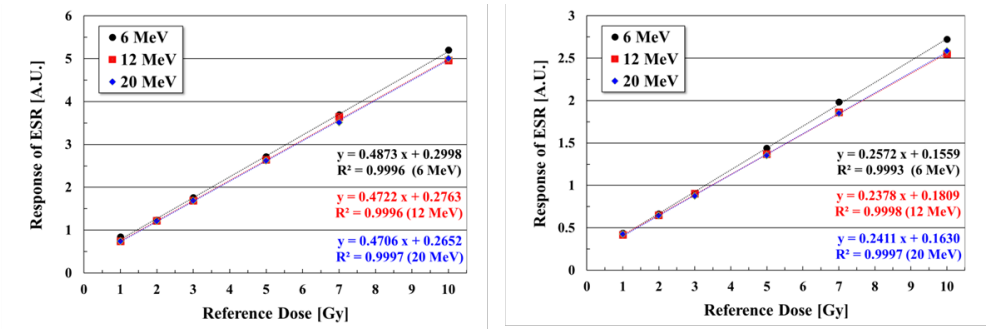

Figure 2. Response of L-alanine for electron beam(left: Magnettech, right: Bruker)

Conclusion In this study, we evaluated L-alanine response to apply the alanine/ESR system to therapeutic radiation. It was confirmed that the dependence of radiation energy and dose rate was insignificant in the range of 1 to 10 Gy. Further studies are planned to measure response of L-alanine response to high-dose rates above 1,000 MU/min of each sources will be performed

Acknowledgement This work was supported by the National Research Foundation of Korea(NRF) grant funded by the Korea government (No. 2015M2C5 A1041691 and No. 2018R1D1A1B07049703)

References

1) IAEA, Assessment and management of ageing of major nuclear power plant components important to safety: In-containment instrumentation and control cables, IAEA-TECDOC-1188(2000) 1:39.

COMPARISON BETWEEN TWO LABLLED EDTMP RADIOPHARMACEUTICAL WITH 153SM AND 177LU

Hesham MH Zakaly[1,3]*, Mostafa Y. A. Mostafa[1,4], M Zhukovsky[1,2]

[1] *Ural Federal University, Yekaterinburg 620002, Russia*
[2] *Institute of Industrial ecology UB RAS, 620990, Ekaterinburg, Russia*
[3] *Al-Azhar University, Assuit Branch, Physics Department, 71524 Assuit, Egypt*
[4] *Minia University, faculty of Science, Department of Physics, El-Minia, Egypt*

Key words radiation, dosimetry, SSD, conference, Hiroshima

Background and Objectives ^{177}Lu and ^{153}Sm are perspective radionuclides in terms of applying in nuclear medicine. High-energy beta particles and the relatively half-life of the radionuclide are used to achieve an effective palliative treatment of bone metastases. The technology-targeted delivery of the radionuclide to the pathological area is used to minimize radiation exposure to healthy organs and tissues. This result is achieved by the rapid delivery of the radiopharmaceutical to the tumor cells. For example, different complexes are used for bones cancer treatment like ^{153}Sm-EDTMP and ^{177}Lu-EDTMP. This complex is concentrated in the skeleton in proportion to osteoblastic activity. Pathological foci, where the accumulation is intense, can be visualized in studies in the gamma camera which allows scintigraphy of the patient and monitor the treatment process. In this work, the effect of the drug carrier EDTMP (i.e. ethylene diamine tetramethylene phosphate) on the ionic form of ^{177}Lu and ^{153}Sm is presented.

Materials and Methods The absorbed doses in different organs and tissues of 177Lu and 153Sm in ionic form and labelled with EDTMP are determined by IDAC-Dose 2.1 (Internal Dose Assessment by Computer) software. WinAct software is used to calculate cumulative activity1,2. 177Lu and 153Sm are lanthanide radionuclide which actively accumulates in the liver and bone when uses in ionic form. In the case of labelling with EDTMP, the distribution and elimination of the drug occur according to the kinetics of the carrier, (i.e. ethylene diamine tetramethylene phosphate). The using of osteotropic (Describing any drug etc. that is attracted to, and targets bone) complex allows creating a large dose in the pathological areas and minimizing damages in healthy organs and tissues. –

Results and Discussion ^{177}Lu and ^{153}Sm labelled with EDTMP are decreasing the liver dose

absorption and increasing the bone surface absorption for more effective treatment and minimize side effect. The effective dose per administered activity was estimated to be 0.189 mSv/ MBq for ^{177}Lu-ionic form, 0.232 mSv/MBq for ^{153}Sm-ionic form and 0.242 mSv/MBq for ^{177}Lu-EDTMP and 0.139 mSv/MBq for ^{153}sm-EDTMP. Figure 1 shows the direct effect of EDTMP in absorbed dose distribution for different organs and tissues. Also, even in ionic form the distribution of ^{177}Lu is better than ^{153}Sm more absorbed in bone surface, red bone marrow, and kidney with low absorption in live [1,2].

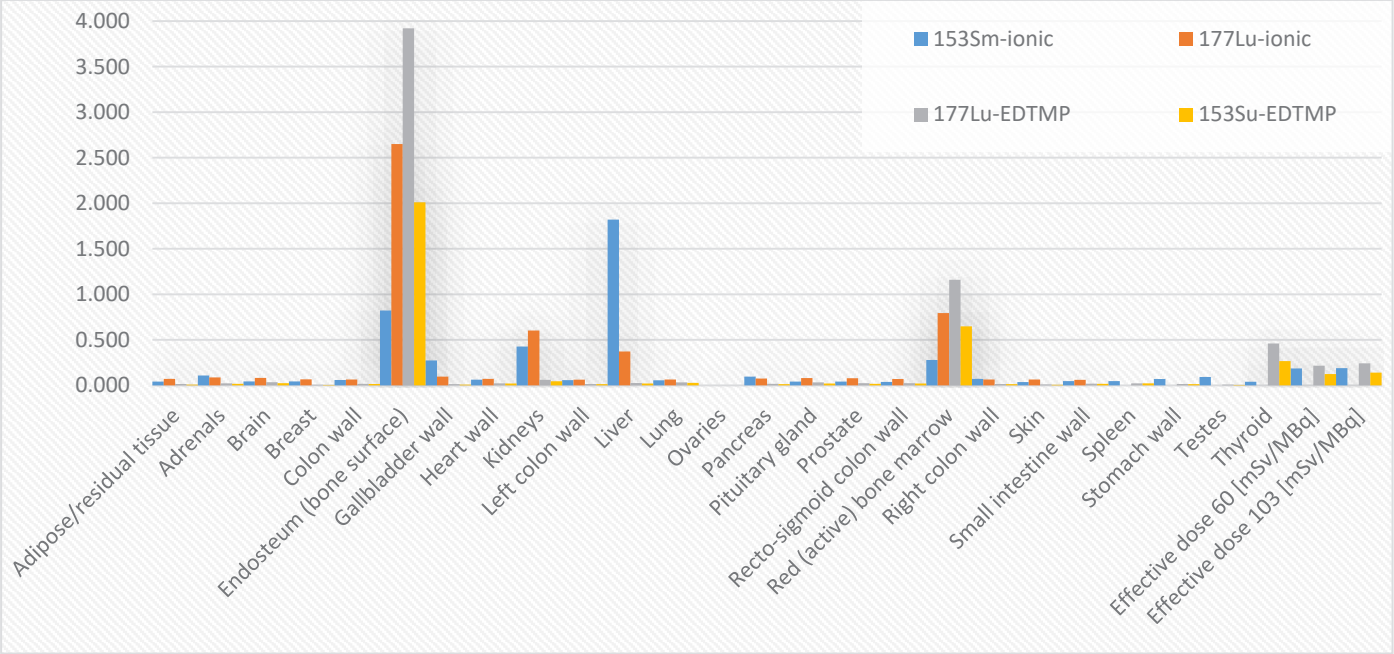

Figure 1. Absorbed Dose in (mSv/MBq) in different organs and tissues

References

1) M.Y.A. Mostafa, H.M.H. Zakaly, and M. Zhukovsky, Radiol. Phys. Technol. (2019).
2) M.V. Zhukovsky & Hesham M.H. Zakaly, Radiat. Appl. IN Press, (2019).

Development of postal dosimetry service using an alanine dosimeter in Japan

Hidetoshi Yamaguchi[1]*, Morihito Shimizu[1], Yuichiro Morishita[1],
Kuniyasu Okudaira[2] and Hiroshi Oguchi[3]
[1]*National Metrology Institute of Japan (NMIJ), AIST, Ibaraki, Japan*
[2]*Nagoya University Hospital, Aichi, Japan*
[3]*Nagoya University, Aichi, Japan*

Highlights The NMIJ is developing a postal dosimetry service using an alanine dosimeter. The NMIJ's alanine dosimeter responses were investigated in Co-gamma ray, electron and carbon beams. The postal dosimetry service will be used for radiation therapy, radiation processing and radiation monitoring at accelerator facility.

Key words alanine, postal dosimetry, radiation therapy, electron beams, calibration line

Background and Objectives Alanine dosimeter is a useful dosimeter for quality assurance and quality control of radiation processing and radiation therapy in high-dose range: 1 Gy -100 kGy. National Metrology Institute of Japan (NMIJ) is developing a postal dosimetry service using an alanine dosimeter for various radiation beam (Fig. 1). Alanine dosimeter response depends on radiation beam quality and geometry of the dosimeter[1,2)]. In the present study, we investigated the response for Co-gamma rays and high-energy electron beams to verify radiation quality dependence and linearity between dose and signal in the NMIJ's alanine dosimetry system.

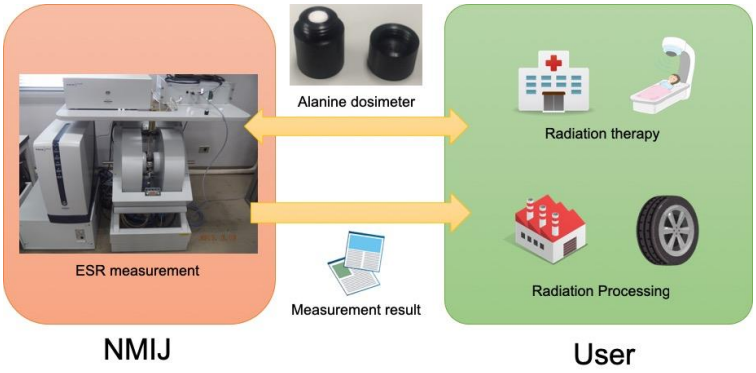

Figure 1. Postal alanine dosimetry service. The NMIJ measures the dose of the alanine dosimeter irradiated at user radiation facilities and reports measurement result to users.

Materials and Methods Alanine dosimeters were irradiated with Co-gamma ray and 16 MeV

high-energy electron beam from a clinical linac (Varian, CL-iX). The delivered dose to the alanine dosimeter was set in the range between 20 to 50 Gy in order to make a calibration line. The delivered dose was measured by a calibrated ionization chamber before the irradiation.

Results and Discussion The calibration lines for the gamma rays, electron beams and carbon beams measured in our previous work[3] are shown in Fig. 2. The alanine dosimeter response for the electron beam is 2 % lower than that for the gamma ray. For the carbon beam which has very high-LET (Liner Energy Transfer), the response is 26 % lower than that for Co-gamma ray. The response might strongly depend on the LET of the radiation beam. However, as each calibration line shows linearity between dose and measured signal, dosimetry service for the radiation quality can be performed by the NMIJ.

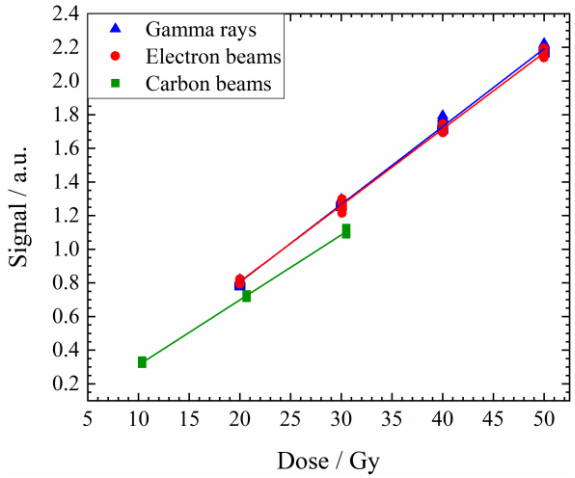

Figure 2. Calibration lines for gamma rays, electron beams and carbon beams.

Conclusion The alanine dosimeter response was investigated for the gamma ray and the high-energy electron beam. The response depended on the LET of the radiation beams. In the future, we will carry out the evaluation of the alanine dosimeter response in high-energy photon beams and proton beams and extend dose range to 1 Gy - 100 kGy.

References

1) Anton, M., et al. "Difference in the relative response of the alanine dosimeter to megavoltage x-ray and electron beams." Phys. Med. Biol. 58.10 (2013): 3259.
2) Zeng, G. G., et al. "An experimental and Monte Carlo investigation of the energy dependence of alanine/EPR dosimetry: II. Clinical electron beams." Phys. Med. Biol. 50.6 (2005): 1119.
3) Hidetoshi, Y., et al. "Feasibility study of alanine dosimeter for carbon-beam dosimetry." World Congress on Medical Physics and Biomedical Engineering 2018. IFMBE Proceedings, vol 68/3. (2019): 565

Application of radiophotoluminescent glass dosimeter to radiotherapy dosimetry audit

Hideyuki Mizuno[1], Shigekazu Fukuda[1], Taku Nakaji[1], Akifumi Fukumura[1], Wataru Yamashita[2], Nobuhiro Takase[2], Masahiro Hoteida[2], Yousuke Sasaki[2], Hiroaki Okuyama[2], Tota Ushiroda[2], Katsuhisa Narita[2]

1 National Institute of Radiological Sciences, QST
2 Association for Nuclear Technology in Medicine

Background and Objectives

Radiophotoluminescent glass dosimeter (RPLD) has been used in Japan as dosimeter of postal dose audit in external radiotherapy. Due to its advantages of compactness, repeatable readout, good precision and small fading[1)], RPLD become a suitable dosimeter for the audit. In Japan, the permanent auditing system using RPLD for external radiotherapy was launched in 2007. Currently, in multicenter clinical studies conducted in the framework of the Forum for Nuclear Cooperation in Asia (FNCA), the RPLD is also used as a dosimeter for brachytherapy dosimetry audit.

Material

The glass dosimeter (DOSE ACE, ASAHI TECHNO GLASS CORPORATION; ATG) is silver-activated phosphate glass. Its weight composition is as follows: 11.0% Na, 31.55% P, 51.16% O, 6.12% Al and 0.17% Ag [14]. Its dimensions are 1.5mm in diameter and 12mm in length. A solid-state laser (ultraviolet wavelength) is used for reading. On its reading, 10 to 20 pulses of laser are irradiated per second, and the average value is obtained. In order to suppress variations in light emission amount depending on slight position fluctuation including rotation of the element, sensitive setup of the element is necessary. In addition, the whole reading process is repeated for 5 times, to improve the statistics.

Dosimetry audit for external radiotherapy

RPLD elements are embedded in a solid phantom (Tough water phantom, manufactured by Kyoto Science Co., Ltd.), and it is set to be the reference condition of linear accelerator, and the reference dose (1 Gy) is irradiated. Phantom and RPLD are sent to the radiotherapy hospital according to their request. After irradiation, those are sent back to NIRS to evaluate the dose irradiated to the RPLD. For the dose evaluation, the following equation is used.

$$D_{\mathrm{w},i=}(M_i \cdot SCF_i - M_{0,i'} \cdot SCF_{i'}) \cdot N_{D,r} \cdot f_{\mathrm{en}} \cdot f_{\mathrm{P}} \cdot f_{\mathrm{lin}}$$

where

$M_{0,i'}$ is the background value of the i'-th RPLD;
SCF_i is the individual sensitivity correction factor of the i-th RPLD;
$N_{D,r}$ is the calibration coefficient for the reference radiation quality;
f_{en} is the correction factor for the radiation quality;
f_{P} is the correction factor for phantom material;
f_{lin} is the correction factor of nonlinearity.

Dosimetry audit for brachytherapy

The use of RPLD as a dose auditing tool for image-guided brachytherapy performed as a multicenter clinical study of cervical cancer has been studied. We are planning an end-to-end test that enables validation including the same flow as the actual patient, such as CT acquisition and treatment plan, rather than simple source intensity measurement. Although the beam quality is close to the cobalt irradiation field that calibrates the RPLD, it is affected by the dose gradient caused by the distance from the source close, and it is necessary to consider the volume effect. The phantom photograph produced is shown in the figure below. It was manufactured so that the RPLD element can be inserted into the evaluation points which are clinical dose evaluation points, point A right and left, and representative points of risk organs, bladder and the rectum (ICRU reference point). Currently we are doing Monte Carlo simulation for basic data verification and beam quality correction.

Conclusion

RPLD is a useful solid state dosimeter for the external dosimetry audit in radiation therapy.

References

1) Mizuno H, Fukumura A, Fukahori M, Sakata S, Yamashita W, Takase N, et al., Application of a radiophotoluminescent glass dosimeter to nonreference condition dosimetry in the postal dose audit system. Med Phys. 2014 Nov;41(11):112104. doi: 10.1118/1.4898596.

Optical evaluation about polymer gel dosimeter in carbon ion beams

Hiraku Kawamura[1, 2]*, Takaoki Takanashi[2], Hiroshi Yoshii[3], Tsugufumi Matsuyama[3], Yoshie Izumoto[3] and Hitoshi Sato[4]

[1]Gunma Prefectural College of Health Sciences, Maebashi, Japan, [2]RIKEN, Wako, Japan, [3]National Instruments for Quantum and Radiological Science and Technology, Chiba, Japan, [4]Ibaraki Prefectural University of Health Sciences, Inashiki, Japan

Highlights Optical evaluation method of polymer gel dosimeter irradiated to 400 MeV/n carbon-ion beam was researched. Regarding absorbed carbon dose to optical response, increasing the absorbed dose to irradiated gels, optical signal intensities were increased. When the prepared gels were irradiated to form carbon Bragg curve, the result of the scanned original optical computed tomography system was indicated dose concentration region.

Key words optical evaluation, polymer gel dosimetry, carbon therapy, HIMAC

Background and Objectives Gel dosimeters as polymer gels and radiochromic gels, chemical dosimeters, are three-dimensional dosimeters that can spatially hold chemical reactions caused by radiation and are expected to be applied in radiation therapy that irradiates from various directions and irradiates them according to the shape of the tumor in clinical radiotherapy. In the future of this dosimeter, it will be used as a clinical QA tool.

Proton and carbon therapy, called particle therapy are spread in world. It is possible to set only to irradiate target volume including tumors in the deep of the body using Bragg peaks which are these features.

It has been reported that the gel dosimeter located in high LET region such as Bragg peak shows sensitivity loss because of radical recombination. However, detailed examinations are needed that there were few reports that is still because there are few carbon line facilities.

Polymer gel dosimeter was irradiated with carbon beams in HIMAC (Heavy Ion Medical Accelerator in Chiba). The irradiated gels were evaluated to degree and distribution of polymerization related to radiation dose using original optical computed tomography (OCT) system. In the present study, we attempted to describe an availability of three-dimensional dose measurement using the optical tomographic apparatus in gel dosimetry.

Materials and Methods 1. Dose response of PAGAT gel dosimeter in carbon beams: PAGAT polymer gels sealed 20 ml cylindrical PET container were irradiated with 2, 4, 6 Gy in 400 MeV / u carbon beams, respectively. The irradiated gels were scanned with the

constructed OCT (Fig. 1). The wavelength of the scanned laser was 632.8 nm, and a PIN photodiode was used as a detector. A mechanism for translation and rotation the irradiated gel dosimeter with the step motor and the chuck at the upper part was constructed, and the lateral movement and the rotation operation were operated by the stage controller. The gel dosimeter was placed in a water bath, the light intensity of transmitted the gels container was measured while moving the gel dosimeter with pass and rotational motion, and the result was reconstructed as images using Filtered-Backprojection (FBP) from 360° data. The region of interest (ROI) was set in the image, and the signal value was measured.

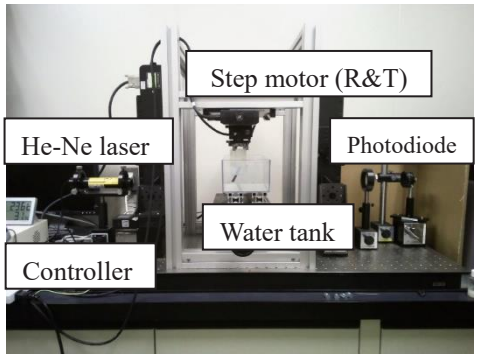

Figure 1.OCT system

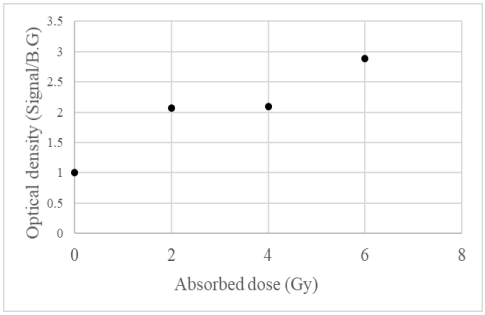

Figure 2. Dose to optical density relationship in carbon beams

2. Dose distribution images of Bragg peak: The prepared PAGAT gel dosimeter was placed in a 300 ml cylindrical container and the sample was irradiated with 400 MeV / u carbon beams so that the Bragg peak was at about half of the container. Dose evaluation using OCT after irradiation was performed in the same procedure as in 1.

Results and Discussion The results of the measurement 1 are shown in Fig. 2. The optical response to irradiated gels were increased with respect to the absorbed dose. Clear linearity could not be confirmed.

The obtained results of the measurement 2 are shown in Fig. 3. It was shown that it is possible to show the Bragg peak position from the resulting image.

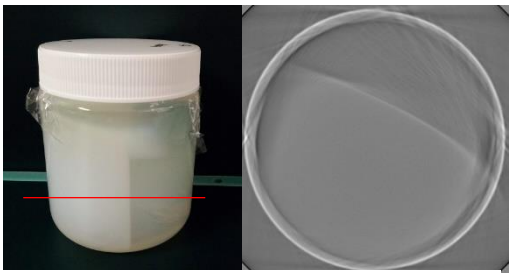
Figure 3. Irradiated gel container (Left) and reconstructed sectional image (reconstructed position is red line).

Conclusion Carbon beam irradiation was performed on polymer gel dosimeter, and dose response characteristics and Bragg peak appearance were attempted by OCT instead of conventional MRI, R_2 method. Even in optical CT, the measured value increased with increasing of the absorbed dose, and a tomographic image consistent with the Bragg peak was obtained.

Applicability of 2,3-dihydro-2-spiro-4′-[8′-aminonaphthalen-1′(4′ H)-on]perimidine to dosimeters

H. Kawamoto*, M. Koshimizu, Y. Fujimoto, K. Asai
Graduate School of Engineering, Tohoku University, Sendai, Japan

Highlights Recently, radiotherapy has been attracting a great deal of attention. In radiotherapy, dosimeters that have high tissue equivalence and are capable of accurate dose measurement are required to reduce the risks to patients. This study focused on a photochromic reaction, and investigated the applicability of the photochromic compound 2,3-dihydro-2-spiro-4′-[8′-aminonaphthalen-1′(4′H)-on]perimidine (PNO-p) to dosimeters. PNO-p was found to undergo a photochromic reaction when exposed to X-ray irradiation. In addition, the X-ray sensitivity increased with increasing the concentration of PNO-p and doping with an organic phosphor.

Key words photochromism, dosimetry, radiotherapy, organic dosimeter

Background and Objectives Radiotherapy is a method of cancer treatment that has attracted attention for its ability to reduce the stress on the body caused by surgical procedures. One of the most important aspects of radiotherapy is the correct measurement of dose distribution to reduce the risk of side effect to patients. In addition, dosimeters used in radiotherapy require high tissue equivalence. Although heavy metals such as Ag are currently used in medical dosimetry, in this work, we focused on photochromism. Photochromism is a reversible isomerization reaction caused by the absorption of a photon. This property could allow the repeatable measurement of dose distribution using an organic material with high tissue equivalence if such a reaction could be induced by ionizing radiation.

In a previous paper [1], the photochromic reaction of 2,3-dihydro-2-spiro-4′-[8′ -aminonaphthalen-1′(4′H-on]perimidine (PNO-p) was induced by irradiation with UV-light. In this reaction, the closed form of PNO-p, which has an absorption peak at 398 nm, changed to its open form, which has an absorption peak at 520–590 nm. In this study, we investigated the response of PNO-p to X-ray irradiation and the effect of doping with an organic phosphor 2-(4-tert-butylphenyl)-5-(4-biphenylyl)-1,3,4-oxadiazole (b-PBD) on this response.

Materials and Methods Polystyrene (PS) was dissolved in tetrahydrofuran (THF). Subsequently, a solution of PNO-p dissolved in THF was added to the PS solution. The proportion of PNO-p to styrene monomer units was 0.25, 0.50, or 1.0 mol%. Additionally, b-PBD dissolved in THF was added to the polymer/PNO-p solution. The proportion of b-PBD to

the styrene monomer unit was 0.25 or 0.50 wt%. Finally, the solvent was allowed to evaporate at 313 K for 3 days, and we obtained the PS film containing PNO-p and b-PBD. The films were irradiated with X-rays to 30 kGy; the optical absorption spectra were measured before and after irradiation with X-ray and UV-light.

Results and Discussion Fig. 1 shows the absorption spectra of a PS film containing 1.0 mol% PNO-p. The intensity of the absorption peaks at 400–460 nm was decreased after UV-light and X-ray irradiation. Additionally, the intensity of the absorption peak at 550–650 nm increased with UV-light and X-ray irradiation. Based on these results, the PNO-p in the PS film undergoes a photochromic reaction when irradiated with X-rays. Fig. 2 shows the dose dependence of the increase in the absorbance of the PS films containing PNO-p. The absorbance of the PS film containing a high concentration of PNO-p changed more significantly at lower doses than that of the low concentration film. This result suggests that the sensitivity to X-ray irradiation increases with increasing PNO-p concentration. Fig. 3 shows the dose dependence of the increase in the absorbance in PS films containing 1 mol% of PNO-p and b-PBD. The change in absorbance was larger in the PS films containing PNO-p and b-PBD than in the film without b-PBD. This result suggests that b-PBD acts as a sensitizer.

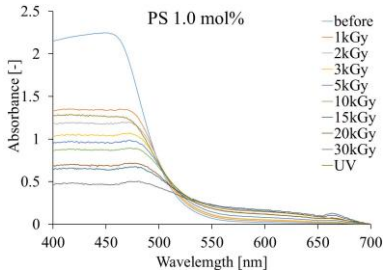

Fig. 1 Absorption spectra in PS film containing 1 mol% of PNO-p.

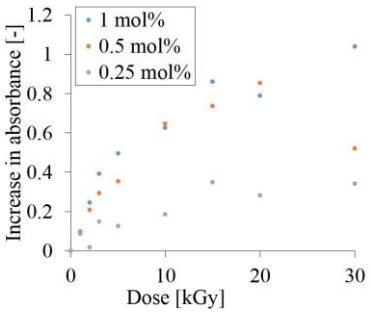

Fig. 2 Dose dependence of the increase in absorbance.

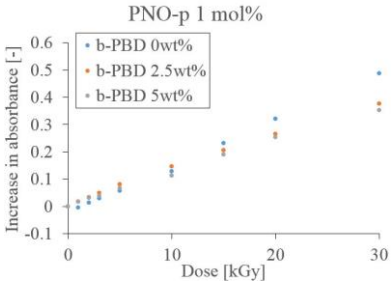

Fig.3 Dose dependence of the increase in absorbance in b-PBD doped-PS films.

Conclusion We focused on photochromic compound PNO-p and investigated the isomerization reaction that occurred when it was irradiated with X-rays. The results confirmed that PNO-p underwent a photochromic reaction in response to X-ray irradiation. In addition, the sensitivity of the fabricated PNO-p/PS films to X-rays increased with increasing concentration of PNO-p and with doping of the organic phosphor b-PBD. These results suggest the applicability of the photochromic compound PNO-p to dosimeters.

References

1) R. Davis, N. Tamaoki, Org. Lett. 7 (2005) 1451-1464.

Elucidation of radiophotoluminescence center formation process from activation energy and formation temperature

H. Kawamoto[1]*, M. Koshimizu[1], Y. Fujimoto[1], G. Okada[2], T. Yanaida[3], H. Masai[4], K. Asai[1]

[1]*Graduate School of Engineering, Tohoku University, Sendai, Japan*

[2]*Kanazawa Institute of Technology, Nonoichi, Japan*

[3]*Nara Institute of Science and Technology, Ikoma, Japan*

[4]*The National Institute of Advanced Industrial Science and Technology, Ikeda, Japan*

Highlights To elucidate the radiophotoluminescenece (RPL) center formation process in Ag-doped phosphate glasses, the temperature dependence of RPL intensities was measured. The Ag^0 formation starting temperatures were found to be 100 K, 100 K, and 25 K and the activation energies of Ag^0 formation were 51 meV, 56 meV, and 43 meV in Ag-doped phosphate glass having Na and Al (Na–Al/Ag), Na and K (Na–K/Ag), Al and K (Al–K/Ag), respectively. Electrons are trapped at negative ion vacancies before being transferred to Ag^+ such that the activation energy increases with increasing distance between electron trapping sites and Ag^+.

Keywords radiophotoluminescence, Ag-doped phosphate glass, dosimeter

Background and Objectives Radiophotolumienscence (RPL) is an emission phenomenon caused by photoexcitation of luminescence center (RPL center) formed by irradiation with X-rays. The RPL process does not have the recombination process of electron–hole pairs formed by X-ray irradiation and further, the RPL center can be initialized by annealing. Because of these characteristics, RPL dosimeters can read and measure radiation doses repeatedly. Ag-doped phosphate glasses are used in RPL dosimeters. The RPL center formation process has been studied with optical and electron spin resonance measurements, whereas electron–hole pairs are generated by irradiation with X-rays. Some electrons are trapped at Ag^+ and form Ag^0. On the other hand, some holes transfer to Ag^+ and form Ag^{2+} after being trapped at PO_4^{3-} tetrahedrons. However, the RPL center formation process is not understood so that the elucidation of the RPL center formation process is needed for development and improvement of RPL dosimeters.

In this study, the starting temperatures and activation energies of RPL center formation in Ag-doped phosphate glasses having different cations were considered. To obtain the required data, RPL intensities of samples irradiated at room and at cryogenic temperatures were measured.

Materials and Methods Commercially available Ag-doped phosphate glass having Na and Al (Na–Al/Ag) were used. The Na–K/Ag and Al–K/Ag were synthesized with melt

quenching method with a Ag concentration of 0.1 mol%. The temperature dependence of RPL intensity was measured using two procedures. In the first procedure, samples were irradiated with X-rays at 25 K. Subsequently, the samples were heated from 25 K to 300 K at intervals of 25 K and the RPL spectrum was measured at each temperature. In the second procedure, samples were heated at 300 K for 1 h after being irradiated with X-rays at room temperature. Subsequently, the samples were cooled from 300 K to 25 K and the RPL spectra were measured at each temperature. Based on the measurements, the activation energy and starting temperature of RPL center formation could be estimated.

Results and Discussion Table 1 shows activation energies, starting temperatures, and thermal energies at the starting temperature of Ag^0 formation. Activation energies were larger than the thermal energies for all samples, which means that electrons are trapped at other sites before being transferred to Ag^+. The first ionization energies of Al, Na, and K are 5.99 eV, 5.14 eV, and 4.34 eV, respectively. Thus, activation energies are not correlated with the first ionization energies of the cation. Therefore, electrons are most likely trapped at negative ion vacancies. Fig. 1 shows the relationship between activation energy of Ag^0 formation and mean molecular volume. The activation energy increased with increasing mean molecular volume. On the basis of this result, it is probable that the increase in activation energy is caused by an increased distance between the electron trapping sites and Ag^+.

Conclusions In Na–Al/Ag, Na–K/Ag, Al–K/Ag, activation energies of Ag^0 formation are 51 eV, 56 eV, and 43 meV, respectively. Activation energies are larger than the thermal energies at the starting temperature of Ag^0 formation. Therefore, electrons are trapped at negative ion vacancies before being transferred to Ag^+. On the basis of relationship between the activation energy and mean molecular volume, the activation energy increased with increasing distance between the electron trapping sites and Ag^+.

Table 1. Starting temperatures (T_S), activation energies (E_A), and thermal energies (E_T) of Ag^0 formation.

Sample	T_S [K]	E_A [meV]	E_T [meV]
Na–Al/Ag	100	51	8.2
Na–K/Ag	100	56	8.2
Al–K/Ag	25	43	2.0

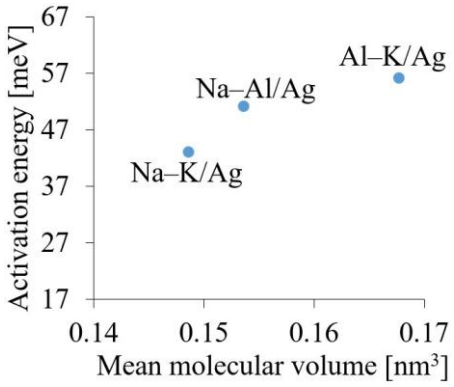

Fig. 1. Experimentally-determined activation energies of Ag^0 formation plotted versus mean molecular volume for several materials.

Gold Nanoparticle Effects on Sensitivity and Dose Enhancement

Lima, S. L.*, Guidelli J. E., Baffa O.

Departamento de Física – DF, Faculdade de Filosofia Ciências e Letras de Ribeirão Preto

Universidade de São Paulo – USP

Highlights: Gold Nanoparticles have a complex effect on dose enhancement and dose sensitivity that deserves more detailed studies. Using different animoacids and gold nanoparticles concentration DEF and sensitivity was studied.

Key words: ESR (Electron Spin Resonance), DEF (Dose Enhancement Factor) Radiation Dosimetry and Nanocomposits.

Background and Objectives The insertion of AuNps (gold nanoparticles) in an alanine dosimeter matrix is a viable alternative for dosimetric signal amplification due to its high atomic number (Z). DEF (Dose Enhancement Factor) is estimated by the ratio of the intensity of the sample signal containing AuNps, by the signal strength of the pure sample. Some physical factors may influence the dosimetric gain of the material, such as beam energy of radiation, variations of mass percentages of gold and the influence of applied dose. The sensitivity of the dosimetric material, mainly determined by its chemical structure, could influence the dose increase value, since a more sensitive material would be able to produce more free radicals for a given dose. To understand more about these influences, we studied different amino acids and compounds, namely: Alanine, 2-Methyl-Alanine, Asparagine and Monosodium Glutamate by varying the NpsAu concentration and the radiation dose applied.

Materials and Methods AuNps were incorporated in an amino acid matrix in different proportions (Table 1) by addition of different volumes of the colloidal gold dispersion with 1.1 mol L^{-1}. The mass percentage of gold in the nanocomposites varied from 0.1% to 3% to each amino acid and compound.

Table 1: Mass percentage of the components present in each amino acid sample and its respective sample code.

(% mass)	NpAu (% mass)	Sample Code
100.00	0.00	0.0%NpAu
99.90	0.10	0.1%NpAu
99.50	0.50	0.5%NpAu
99.00	1.00	1.0%NpAu
97.00	3.00	3.0%NpAu

DEFs[1] were experimentally calculated as the quotient of the peak-to-peak amplitude of the central line of the ESR spectra obtained for the irradiated nanocomposites and pure material (Figure 1).

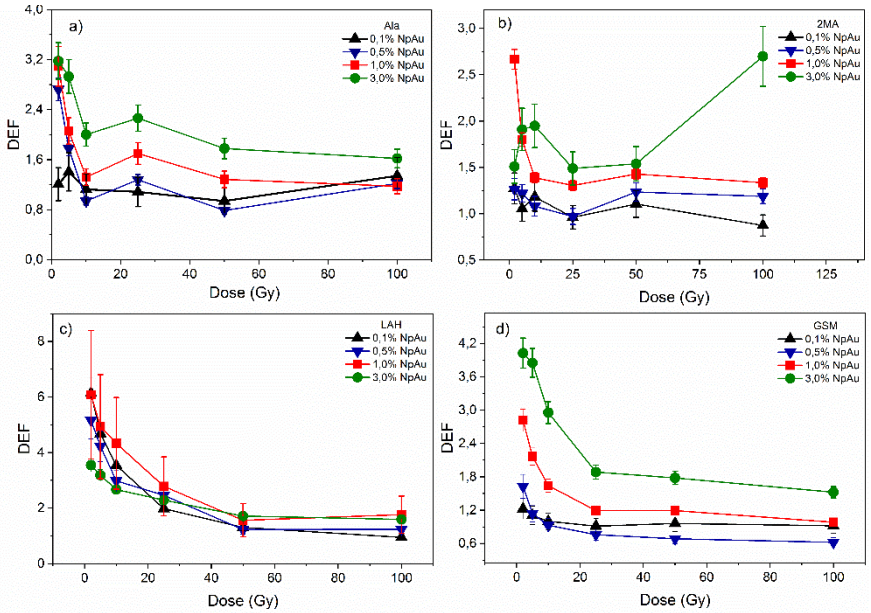

Figure 1. Dose enhancement effect of the amino acids and compound, (a): alanine, (b): 2-methylalanine, (c), asparagine and (d) monosodium glutamate respectively.

Results and Discussion Differently from what we expected, the order of gain in dosimetric sensitivity occurred in the opposite way, the higher the sensitivity of the dosimetric material, the lower the gain, following the decreasing order: Asparagine, Monosodium Glutamate, Alanine and 2-Methyl-Alanine. In addition, dose dependence was observed. As the dose increases the dosimetric gain decreases for all materials. Comparing a dose of 2 Gy and 100 Gy at a concentration of 1% NpAu, the dose / dosimeter gain reduced about 43%, 50%, 50%, and 65% for Alanine, 2-Methyl-Alanine, Asparagine and Monosodium Glutamate respectively.

Conclusion The net result of DEF is a combination of several factors: sensitivity for radical formation, recombination of radicals, increase of interaction with radiation, among others. DEF dependence with dose appears to be related with radical recombination.

Financial Support: Brazilian Agencies CNPq (407471/2016-2) FAPESP (2013/07699-0) and CAPES Finance Code 001

References

1) E. J. Guidelli and O. Baffa, Potential application of metal nanoparticles for dosimetric systems: Concepts and perspectives, *AIP Conf. Proc.*, 2014, **1626**, 5–14.

Development of radiochromic polymer films based on photochromic diarylethenes for X-ray detection

Ichiro Kawamura[1*], Masanori Koshimizu[1], Yutaka Fujimoto[1], Hiroki Kawamoto[1], Keisuke Asai[1]

[1]*Tohoku University, Miyagi, Japan*

Highlights We fabricated organic films containing a diarylethene-type photochromic compound and investigated their isomerization behavior upon X-ray irradiation to develop a tissue-equivalent and non-disposable radiation imaging element. The effect of adding the organic phosphor was also studied. The results show that absorbance of 400–600 nm increased upon X-ray irradiation. Irreversible reaction was also observed, and photochromic reaction can be sensitized by the addition of 2-4(-*tert*-butylphenyl)-5-(4-biphenylyl)-1,3,4-oxadiazole.

Key words photochromism, diarylethene, dosimetry

Background and Objectives One of the major benefits of radiotherapy is that it reduces physical stress caused by surgical procedures; thus, it has potential for further research in various fields, including medicine. In radiotherapy, estimation of accurate dose distribution is of prime importance. Hence, dosimeter materials are desired which have properties similar to those of biological tissues, i.e., an organic substance from the viewpoint of energy absorption characteristics of radiation. We aim to develop a radiation imaging element using an organic photochromic material. Photochromism is defined as the reversible isomerization of a single chemical species between two isomers having different absorption spectra, which occurs without changing the molecular weight after photon absorption. If this transformation is caused by ionizing radiation, photochromism can be applied to radiation imaging. In this study, we used a diarylethene-type photochromic compound, 1,2-bis[2-methylbenzo[b] thiophen-3-yl]-3,3,4,4,5,5-hexafluoro-1-cyclopentene (BMTH). The open-ring isomer absorbs 258 nm while the closed-ring isomer absorbs 516 nm; both have excellent thermal stability[1)]. Therefore, it is expected that back reaction hardly occurs. We investigated the isomerization caused by X-rays using absorption spectroscopy. In addition, we investigated the effects of adding the organic phosphor, 2-4(-*tert*-butylphenyl)-5-(4-biphenylyl)-1,3,4-oxadiazole (b-PBD).

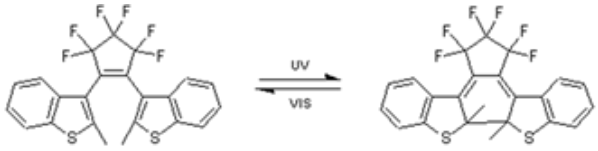

Fig. 1. Schematic of the isomerization of BMTH.

Materials and Methods Poly(methyl methacrylate) (PMMA), BMTH, and b-PBD were dissolved in tetrahydrofuran. All samples were stirred and evaporated to form films. The films were irradiated with X-rays, and the absorption spectra before and after irradiation were measured.

Results and Discussion Figure 2 shows the absorption spectra of PMMA film containing BMTH (1.0 wt%) before and after X-ray irradiation. The absorbance of 400–600 nm increased as irradiation increased. This result shows that a reaction proceeds by X-ray irradiation.

Figure 3 shows the absorption spectra of PMMA film containing BMTH (1.0 wt%) and b-PBD (0–5 wt%) before and after X-ray irradiation. The absorption of 450–550 nm increased with the addition of b-PBD. This result shows that the fluorescence of b-PBD induced a reaction.

Figure 4 shows the change in absorbance of PMMA film containing BMTH (1.0 wt%) and b-PBD (0 or 5 wt%) without irradiation. Reversibility improved by the addition of b-PBD. This result shows that the fluorescence of b-PBD induced photochromic reaction.

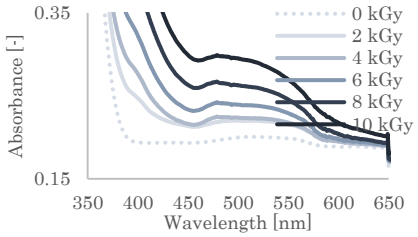

Fig. 2. Absorption spectra of PMMA film containing BMTH before and after X-ray irradiation.

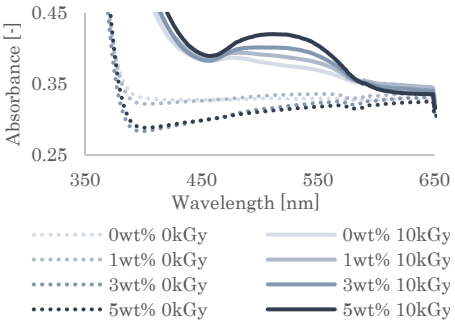

Fig. 3. Absorption spectra of PMMA film containing BMTH and b-PBD before and after X-ray irradiation.

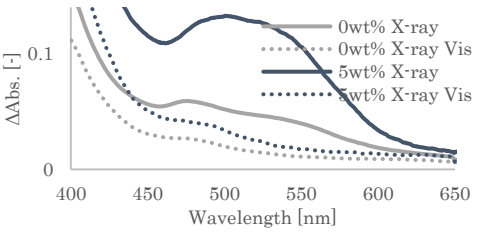

Fig. 4. Change in absorbance of PMMA film containing BMTH and b-PBD without irradiation.

Conclusion We investigated the isomerization behavior of BMTH upon X-ray irradiation. The absorbance of 400–600 nm increased upon X-ray irradiation, while an additional irreversible reaction was also observed. These results indicate that BMTH undergoes a photochromic reaction and another reaction upon direct excitation by X-rays. The photochromic reaction was enhanced with the addition of the fluorescence molecule, b-PBD.

References

1) M. Irie et al., *Chem. Rev.*, **114** 12174 (2014)

Image Guidance Protocol for Microbeam Radiation Therapy at the Australian Synchrotron

J.R. Paino[1], M. Barnes[2], E. Engels[1,3], N. Le[1,3] J.A. Davis1,3, M. Tehei[1,3], S. Corde[1,3,4], M.L.F. Lerch[1,3]

1. Centre for Medical Radiation Physics, University of Wollongong, N.S.W., Australia

2. Applied Physics, RMIT University, VIC, Australia

3. Illawarra Health and Medical Research Institute, University of Wollongong, N.S.W., Australia

4. Radiation Oncology Department, Prince of Wales Hospital, N.S.W., Australia

Key words Microbeam radiation therapy, dosimetry, SSD, conference, Hiroshima

Background and Objectives

Microbeam Radiation Therapy (MRT) is a novel radiotherapy modality wherein synchrotron generated X-rays passed through a multi-slit collimator produce an array of quasi-parallel micron scale beams. The resultant spatially fractionated field displays surprisingly high normal tissue dose tolerance and a therapeutic ratio far greater than that of conventional modalities. The unique tissue sparing properties of MRT have found use in the treatment of inoperable and otherwise untreatable tumors, such as glioblastomas. Development of specialized treatment planning and quality assurance is needed to take MRT from its current pre-clinical state into clinical stages. The imaging and aligning process forms a critical component of QA and so it is essential that this process is accurate, repeatable and of minimal dose. As with conventional treatment modalities, the imaging and aligning procedures should aim to maximize dose conformity and minimize dose to sensitive surrounding tissue. In this study, we assess and evaluate the imaging, treatment planning and quality assurance process for small animal applications.

Materials and Methods

To define the intended treatment target, an Inveon PET-SPECT-CT Small Animal Scanner at Monash Biomedical Imaging was used to obtain CT scans of a $9 \times 9 \times 9\ cm^3$ volume with 97μm resolution [1]. The scan consisted of 142 exposures each 200ms with 80 kVp. The CT scan is used to define the target size location with respect to skeletal landmarks.

Dosimetry thus far had not been performed on this CT scanner and so was conducted using pinpoint IC and MOSkin [2] detectors within a $2.5 \times 2.5\ cm^2$ solid water phantom representative of a small

animal head. Results of the MOSkin detector were calibrated to that of the pinpoint IC at equal location. The scanning process was repeated with the MOSkin on the surface of the phantom to determine the surface dose.

Experiments were performed at the Australian Synchrotron on the Imaging and Medical Beamline (IMBL) in hutch 2B. To configure the dynamic MRT stage for performing image-guided MRT, a setup procedure was performed that tied together the desired beamline components for both imaging and treatment [3]. Configuration was performed with the beamline in monochromatic mode at 40 keV. A 1mm fiducial marker placed on the stage provided sufficient contrast to be seen on the resulting image. Stage translation was adjusted until the fiducial's location on the imaging stage was independent of stage rotation. The stage was then scanned to define the field limits and located the beam's center, thereby establishing an effective isocenter. Any target placed on the stage was able to be moved to place the treatment field at the desired location and angle.

Results and Discussion

The dose associated with the μCT scanning process was found to be 7.24 ± 0.01 cGy in the center of a $2.5 \times 2.5\ cm^2$ solid water phantom and 8.63 ± 0.24 cGy at the surface. The CT total imaging process took approximately 30 minutes per subject and provided images for use within hours, allowing for a continuous workflow between imaging and treatment.

The surface dose associated with the 2D X-ray imaging using the X-ray tube in hutch 2B was found to be 2.8 ± 0.4 mGy per image. The planar imaging and alignment process was reproducibly performed in less than 5 minutes.

Film on the exit surface of the cadaver shows target accuracy to within ± 0.3cm verifying that the treatment alignment process provides suitable accuracy for treatment.

Conclusion

In this study a method for small animal imaging and targeting was implemented on the Imaging and Medical Beamline. To achieve this, μCT and planar X-ray images were co-registered. Phantom measurements show the dose associated with the imaging process is acceptably low as to not affect outcomes with CT surface dose of 8.63±0.24 cGy and planar X-ray image dose of 2.8±0.4 mGy. This study confirmed that sufficient tools are already in place within hutch 2B to allow targeting with sub millimeter precision (±0.3mm) and the implementation of simple treatment plans.

References

1) Magota, K., Kubo, N., Kuge, Y., Nishijima, K.I., Zhao, S. and Tamaki, N., 2011. Performance characterization of the Inveon preclinical small-animal PET/SPECT/CT system for multimodality imaging. *European journal of nuclear medicine and molecular imaging, 38*(4), pp.742-752.
2) Butson, M. J., Rozenfeld, A., Mathur, J. N., Carolan, M., Wong, T. P., & Metcalfe, P. E. (1996). A new radiotherapy surface dose detector: the MOSFET. *Medical physics, 23*(5), 655-658.
3) EPSM talk. M. Barnes et. al. (2018). O43 A patient positioning protocol for synchrotron Micro-beam radiotherapy (MRT). EPSM, Engineering and Physical Sciences in Medicine 2017. *Australas Phys Eng Sci Med*(41). pp 278
4) Hall C, Hausermann D, Maksimenko A, et al. Detectors for the Imaging and Medical Beam Line at the Australian Synchrotron. IOP Sci. 2012:17-20. doi:10.1088/1748-0221/8/06/C06011.

Dosimetric Impact of Iodine Content in a Polyvinyl Alcohol-iodide Radiochromic Gel Dosimeter

Kaoru Ono[1]*, Keisuke Fujino[1], Shin-ichiro Hayashi[2], Yukio Akagi[1], Yutaka Hirokawa[1]
[1]*High-precision Radiotherapy Center, Hiroshima Heiwa Clinic, Hiroshima, Japan*
[2]*Faculty of Health Sciences, Hiroshima International University, Hiroshima, Japan*

Highlights The dosimeteric impact of iodine content in a polyvinyl alcohol-iodide (PVA-I) radiochromic gel dosimeter was investigated through depth dose measurements and Monte Carlo (MC) simulations. Results enabled us to conclude that the dose response with iodine content can be ignored in high-energy X-rays used in the field of radiotherapy.

Key words PVA, KI, iodine content, radiochromic gel dosimeter, radiotherapy

Background and Objectives Recently, radiochromic gel indicators based on a polyvinyl alcohol-iodide (PVA-I) complexes that can be reused after annealing were reported by Miyoshi et al.[1)] and Sunagawa et al.[2)]. We have developed to base on those indicators a novel 3D radiochromic gel dosimeter[3)]. The dosimeter is composed of mostly water, with iodine at a high atomic number of 53 partially added. The present study focuses on the dosimetric effect of iodine content in the PVA-I gel dosimeter for high-energy X-rays used in radiotherapy as determined by depth dose measurements and MC simulations.

Materials and Methods First, a base solution (partially saponified PVA (1 wt%), with gellan gum (0.4 wt%) as a gelling agent and distilled water (98.6 wt%) added) was prepared. Next, D(-)-fructose (0.1 M) as a reductant, and potassium iodide (KI = 0.1, 0.2, and 0.3 M) as an iodide source, were added to the base solution, where M denotes molarity (mol/1000gH_2O). Finally, the prepared gels were poured into several tall acrylic containers (2 × 2 × 25 cm^3). The PVA-I gel dosimeters were placed parallel to the beam axis in a water-equivalent phantom at a source-to-surface distance of 90 cm and irradiated with 6-MV X-rays (10 × 10 cm^2) using a Novalis Tx linear accelerator (Varian/Brainlab). A few hours after irradiation, the dosimeters were scanned with an Epson ES-10000G flatbed scanner configured with 72 dpi (~0.35 mm/pixel) and 48-bit RGB (16 bits per channel). The dose-optical density response information was obtained from the blue channel, and the depth dose curves of each dosimeter were converted. In addition, MC simulations (MCNP6) were conducted with the depth-dose and photon-energy spectrum in water and the dosimeters.

Results and Discussion Figure 1 shows the measured depth-dose curves with the PVA-I gel dosimeters in which KI (i.e., iodine) content was varied from 0.1 to 0.3 M. The figure also shows the calculated depth-dose curve with MCNP6 in water. All curves were normalized at a 5-cm depth. The depth-dose curves in the dosimeters agreed with the MC dose calculations in water, which were on average within < 2%, except for in the build-up region. Figures 2(a) and 2(b) show the photon-energy spectrum in water and the dosimeters calculated with MCNP6 at a 10-cm depth. In the high-energy region, little difference was observed between the dosimeters and water. In contrast, the photon fluence was significantly decreased as the iodine content was increased in the low-energy region. These findings reveal that the impact of the dose response with iodine content can be ignored in high-energy radiotherapy X-rays. However, the influence of low-energy X-rays might not be negligible in radiation treatment planning using X-ray computed tomography.

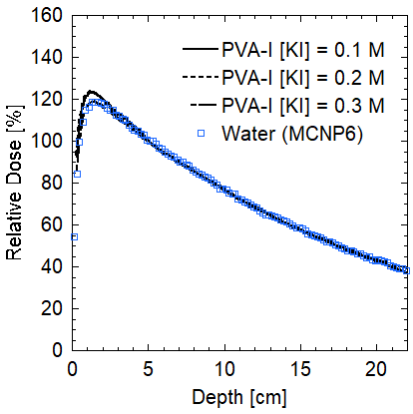

Figure 1. Measured depth-doses by the PVA-I dosimeters, and the MC doses in water.

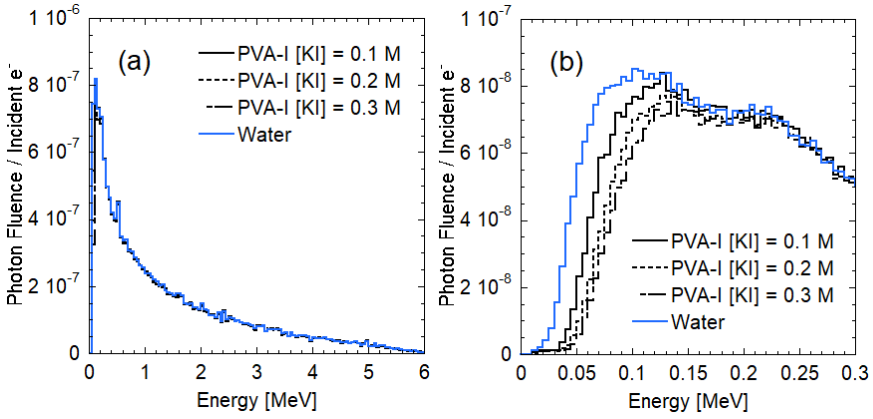

Figure 2. Photon-energy spectrum in water and the PVA-I dosimeters calculated with MCNP6 in high-energy region (a) and low-energy region (b).

Conclusion This study showed that the depth dose in a PVA-I gel dosimeter irradiated with high-energy X-rays is not affected by iodine content. We hope that these findings will contribute to improved 3D dose evaluations that employ radiochromic gel dosimeters.

References

1) Miyoshi H *et al* 2016 *J. Radioanal. Nucl. Chem.* **308** 469–475.
2) Sunagawa T *et al* 2017 *Mem. Fukui Univ. Technol.*, **47** 105-110 (in Japanese).
3) Hayashi S *et al* 2019 *J. Phys.: Conf. Ser.* (in press).

Scintillator screen for measuring dose distribution in scanned carbon-ion therapy

Katsunori Yogo[1]*, Hikaru Souda[2], Akihiko Matsumura[2], and Tatsuaki Kanai[2]
[1]*Nagoya University, Nagoya, Japan*
[2]*Gunma University Heavy Ion Medical Center, Maebashi, Japan*

Highlights A ZnS scintillator with a small LET dependency and camera system is useful for quick and easy measurement of the dose distribution in scanned carbon-ion therapy with high spatial resolution.

Key words silver-activated zinc-sulfide scintillator, carbon-ion pencil beam, linear energy transfer, dose distribution, quality assurance

Background and Objectives Precise measurement of the dose distribution of a carbon-ion pencil beam is essential for safe delivery of treatment in scanned carbon-ion therapy. We develop an easy-to-use and quick dose-measurement tool that employs a silver-activated zinc-sulfide (ZnS) scintillator, which shows a small linear energy transfer (LET) dependency, to measure the dose distribution of a carbon-ion pencil beam with high spatial resolution.

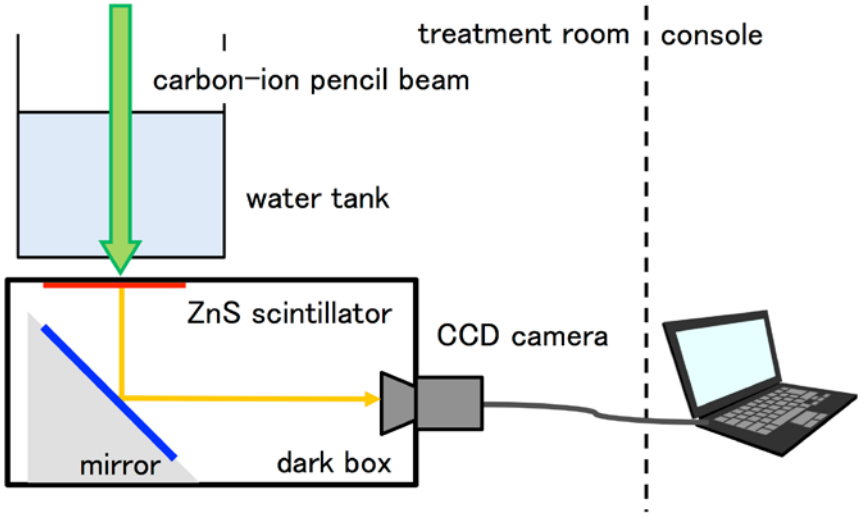

Figure 1. Experimental setup

Materials and Methods A ZnS scintillator sheet was set up perpendicular to the beam axis, and scintillation images were recorded using a charge-coupled device camera [1)] (Figure 1). We used 290-MeV/nucleon monoenergetic carbon-ion pencil beams at the Gunma University

Heavy Ion Medical Center. The thickness of the water tank placed above the scintillator was remotely controlled to adjust the measurement depth. Images were acquired at different water depth, and depth and lateral profiles were analyzed from the images (Figure 2).

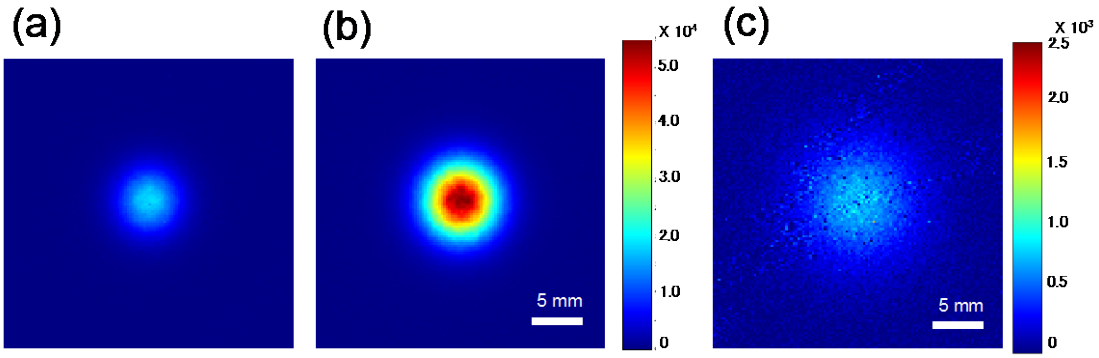

Figure 2. Scintillation images of a pencil beam at (a) the depth of the entrance, (b) the Bragg peak, and (c) the tail with a 290-MeV/u carbon-ion pencil beam. The maximum value of the color bar in (c) is approximately 20 times lower than those in (a) and (b).

Results and Discussion The depth–brightness profile of the ZnS scintillator matched the depth dose measured using an ionization chamber, which was better than that of a conventional Gd-based scintillator. This result is advantageous for measurements using a carbon-ion pencil beam, which consists of primary carbon ions with a much higher LET than a proton. The ZnS scintillator showed good output characteristics, dose linearity ($R^2 > 0.99$), and output reproducibility (deviations below 2%). The ZnS scintillator showed good agreement with the lateral-dose profiles measured using the diode down to ~1% of the central dose. The tool can measure lateral profiles at the depth of the Bragg peak and tail in addition to the entrance. Our tool was realized to measure the dose distribution of the carbon-ion pencil beam with high-spatial resolution.

Conclusion A ZnS scintillator with a small LET dependency and camera system is useful for quick and easy measurement of the dose distribution in scanned carbon-ion therapy with high spatial resolution.

References

1) Yogo K, Tatsuno Y, Tsuneda M, et al. Practical use of a plastic scintillator for quality assurance of electron beam therapy. Phys Med Biol. 2017;62(11):4551–4570.

Practical calibration curve for a small-type OSL dosimeter to measure exposure dose of patients during medical X-ray diagnosis

Kazuki Takegami[1,2]*, Hiroaki Hayashi[2], Natsumi Kimoto[2], Sota Goto[2], Emi Tomita[2], Takashi Asahara[2], Yoshiki Mihara[3], Yuki Kanazawa[4]

[1]*Yamaguchi University Hospital, Yamaguchi, Japan*
[2]*Kanazawa University, Ishikawa, Japan*
[3]*Shimane University Hospital, Shimane, Japan*
[4]*Tokushima University, Tokushima, Japan*

Highlights To manage the exposure dose of patients during diagnostic X-ray examinations, it is necessary to evaluate the dose without taking into consideration complicated conditions related to X-ray photographic settings. In order to develop a practical analysis method in which energy dependence of an OSL dosimeter is considered, we performed some experiments. From the experimental results, we concluded that our calibration curve can be applied to various dosimetric points when we add a systematic uncertainty of 15%.

Key words OSL dosimeter, calibration curve, diagnostic X-ray region, X-ray spectrum

1. Background and Objectives During diagnostic X-ray examinations using X-ray energies of 20-140 keV, the entrance-surface dose (ESD) is a well-known standard index to evaluate the maximum exposure dose of a patient. Ideally, a radiation dosimeter should be calibrated for each photon of energy. In a clinical setting, a dosimeter which is put on the surface of the patient's skin detects not only direct X-rays but also scattered and penetrating X-rays. We previously proposed that the ESD can be measured using an OSL dosimeter (nanoDot™, Landauer, Inc.) without information concerning clinical exposure conditions when we apply an additional systematic uncertainty of 15% [1]. In this study, we performed further experiments in detail, and carried out an evaluation of the uncertainty based on X-ray spectrum measurements [2].

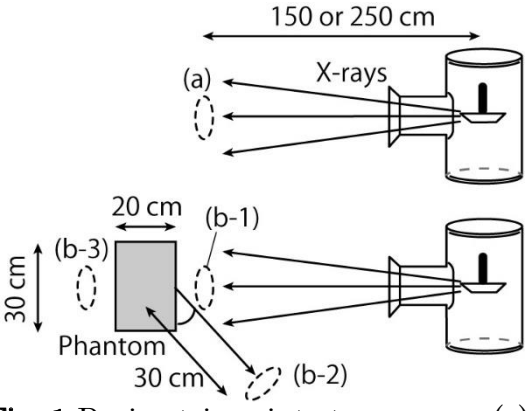

Fig. 1 Dosimetric points to measure (a) air-kerma in free air, (b-1) ESD, (b-2) air-kerma with scattered X-rays, and (b-3) air-kerma with penetrating X-rays.

2. Materials and Methods At first, using diagnostic X-ray equipment (MRAD-A50S/70, TOSHIBA medical systems Co.), we obtained a main calibration curve which was derived from the

relationship between reference air-kerma measured with an ionization chamber (DC300, PTW) and the corresponding responses measured with an OSL dosimeter (see **Fig. 1(a)**); tube voltage was set at 83 kV. Next, we performed experiments for the following three conditions; **(b-1)** ESD, **(b-2)** air-kerma of scattered X-ray and **(b-3)** air-kerma of penetrating X-ray (see **Fig. 1(b)**). The related responses of the OSL dosimeter were measured using a soft tissue-equivalent phantom having a thickness of 200 mm; the tube voltages were 55, 83 and 108 kV. We then compared the results to evaluate deviations from the main calibration curve. Finally, we measured the X-ray spectra with a CdTe detector (EMF-123 type, EMF Japan Co., Ltd.), and evaluated the uncertainty of doses based on considering the X-ray spectra and energy dependence of the OSL dosimeter.

3. Results and Discussion Black circles and line in **Fig. 2** show a main calibration curve under the condition of free air, and the other experimental results were plotted in color. As a result, we determined that the deviation from the main calibration curve is 15%. The results were also consistent with the evaluation of the X-ray spectra. It means that the exposure doses of the patients can be evaluated without taking into consideration error factors during the medical X-ray examinations.

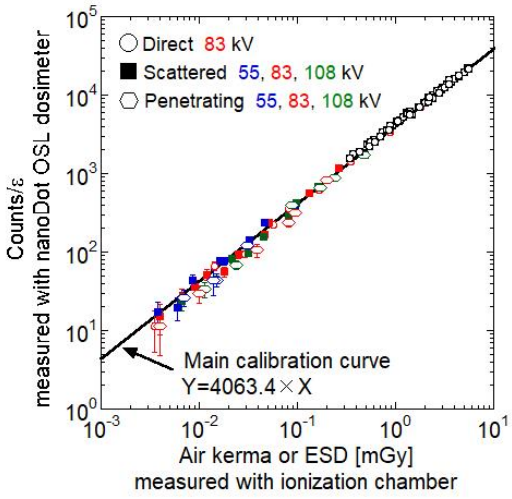

Fig. 2 Proposed calibration curve for air-kerma measurement and results of the other measurements.

4. Conclusion We clarified that our practical calibration curve can be applied to measure exposure dose caused by medical X-ray examination. We didn't need information of X-ray photographic conditions when we adopt an additional uncertainty of 15%. We expected to be able to measure the doses of medical staffs and assistants in a convenient way using our method.

5. References

1) Takegami K, Hayashi H, Okino H, et al. Practical calibration curve of small-type optically stimulated luminescence (OSL) dosimeter for evaluation of entrance skin dose in the diagnostic X-ray region. Radiol. Phys. Technol. 2015;8:286-294.
2) Asahara T, Hayashi H, Goto S, et al. Exposure dose measurement during diagnostic pediatric X-ray examination using an optically stimulated luminescence (OSL) dosimeter based on precise dose calibration taking into consideration variation of X-ray spectra. Radiat. Meas. 2018;119:209-219.

Influence of the Components of a Radiochromic PVA-Iodide Gel Dosimeter on the Thermal and Spatial Stability.

Keisuke Fujino[1]*, Kaoru Ono[1], Shin-ichiro Hayashi[2], Yukio Akagi[1], Yutaka Hirokawa[1]
[1]*High-precision Radiotherapy Center, Hiroshima Heiwa Clinic, Hiroshima, Japan*
[2]*Faculty of Health Sciences, Hiroshima International University, Hiroshima, Japan*

Highlights The temporal and the spatial stabilities of the absorbance on a novel radiochromic polyvinyl alcohol-iodide (PVA-I) gel dosimeter with different polymerization degrees of PVA were investigated. A slight dependence on the temporal change in the coloring and its distribution due to the difference in polymerization degrees of PVA was observed.

Key words PVA, KI, radiochromic gel dosimeter, thermal stability, spatial stability

Background and Objectives In the past decade, various radiochromic gel dosimeters using radiation sensitive dyes have been studied to evaluate three-dimensional dose distribution in radiotherapy[1)2)]. Recently, radiochromic gel indicators based on a polyvinyl alcohol-iodide (PVA-I) complex were reported by Miyoshi et al.[3)] and Sunagawa et al.[4)]. Furthermore, we developed a novel radiochromic gel dosimeter based on the PVA-I complex as well[5)]. In our previous study, we reported that dose properties such as the dose-response and the dose-rate dependency in the PVA-I gel dosimeter scarcely depended on the polymerization degree of PVA[5)]. We subsequently investigated the thermal and spatial stability of the PVA-I gel dosimeter with various polymerization degrees (DP) of PVA in the present study.

Materials and Methods The composition of the PVA-I dosimeter was as follows: PVA (1.0 wt%); Gellan gum (0.4 wt%); distilled water (98.6 wt%); potassium iodide (0.1 M); and D(-)-fructose (0.1 M). The DP of PVA was varied between 500 and 3500. The fabricated gel was subdivided into optical cuvettes, and the samples were classified into two sets according to the storage temperature (5 and 15 °C) during this period. They were irradiated up to 20 Gy using a 6 MV photon beam (Novalis Tx; Varian/BrainLAB). The irradiated samples were read with a flatbed scanner (EPSON ES-10000G) every 24 h for a total of 5 days after irradiation, and the temporal changes of their coloring and the dose distribution were investigated by calculating the net optical densities.

Results and Discussion As an example, the temporal changes of the net optical densities of PVA-I gel dosimeters under each DP at 10 Gy irradiation are shown in Figure 1. Little sequential change of the net optical densities was observed regardless of the storage temperature and the DP of PVA, and the dose response of each DP and storage temperature was also constant during this period. When the samples were stored at 5 ℃, however, they became strongly colored and saturated compared to those stored at 15 ℃. Additionally, when the DP of PVA was 3500, the dose sensitivity was significantly lower than those observed under the other conditions. In terms of spatial stability, the distribution at the boundary plane of the irradiated region proceeded gently, and no clear difference was observed with varying the DP of PVA.

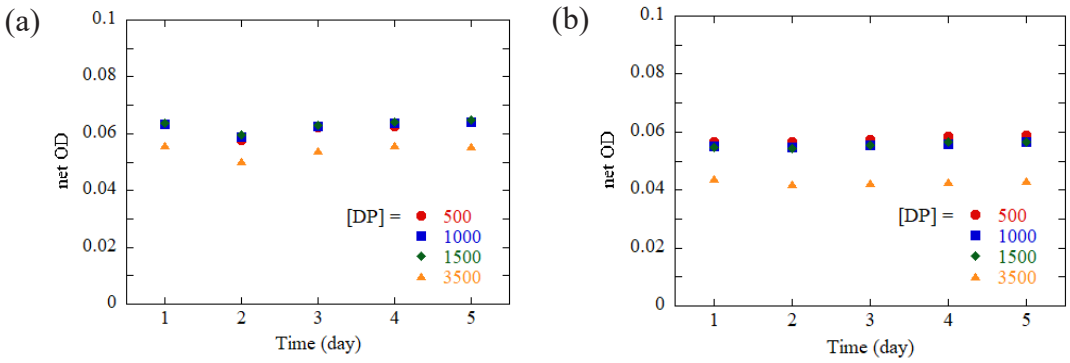

Figure 1. Temporal change of the net optical densities at 10 Gy irradiation under the storage at 5 ℃ (a) and 15 ℃ (b).

Conclusion This study indicates that no significant difference in the thermal and spatial stability of the PVA-I gel dosimeter was apparent among the tested range of DP of PVA (500-3500). However, it is possible that these stabilities may be influenced by using PVA with a higher DP. Efforts to address the topic are currently underway.

Acknowledgment This work is supported by JSPS KAKENHI (Grant Number 17K09072 and 18KK0417).

References

1) Jordan K et al 2009 Phys. Med. Biol. 54 6773-6789.
2) Nasr A T et al 2015 Phys. Med. Biol. 60 4685-4704.
3) Miyoshi H et al 2016 J. Radioanal. Nucl. Chem. 308 469–475.
4) Sunagawa T et al 2017 Mem. Fukui Univ. Technol., 47 105-110. (in Japanese).
5) Hayashi S et al 2019 J. Phys.: Conf. Ser. (in press).

An Investigation of the Radiation Doses in Percutaneous Interventional Procedures for Peripheral Arterial Occlusive Disease (PAOD) Procedures

Kuo-Ting Tang[1],Chien-Yi Ting[2], Wen-shiann Wu[1],Chun-Chih Lin[3]
[1]Division of Cardiology, Chi Mei Medical Center, Tainan, Taiwan,R.O.C.
[2]Department of Medical Imaging and Radiology, Shu-Zen Junior College of Medicine and Management, Taiwan, R.O.C.
[3]Department of Natural Biotechnology/Graduate Institute of Natural Healing Sciences, Nanhua University, Taiwan, R.O.C.

Highlights The study investigated radiation dose of staff undertaking percutaneous interventional procedures for peripheral arterial occlusive disease (PAOD). Optically simulated luminescent dosimeters were used to measure radiation dose and radiation risk was further evaluated in percutaneous interventional procedures.

Keywords: radiation dose, OSLD, peripheral arterial occlusive disease, PAOD, ankle brachial index, ABI

Background and Objectives Peripheral arterial occlusive disease (PAOD) is defined as an ankle brachial index (ABI) less than 0.9 and impairment in perfusion at the popliteal, anterior tibia and anteroposterior tibia arteries due to stenosis or complete obstruction. Recent data indicate that more than 200 million people worldwide suffer from this disease. Radiological diagnosis is the largest contributor to artificial radiation (87%) for PAOD patients. Accordingly, the study aimed to evaluate radiation exposure during percutaneous interventions for peripheral arterial occlusive disease.

Materials and Methods In this study, a stationary floor-mounted under-couch C-arm system (Siemens Artis zee, Washington, DC) was used. The energy range of the X-ray tube was 50–53 kV and the current was 2–4 mA. Three optically simulated luminescent dosimeters (OSLDs) were positioned on the operator, including one pasted on the thyroid region, the second attached to the eye goggles, and the third placed at the gonad region during the percutaneous interventional procedure. Each dosimeter was individually calibrated before measurement. After the procedure was finished, the dosimeters were immediately collected and the data were analyzed in the lab. Evaluation of radiation dose in patient was performed by using an acrylic phantom and OSLDs. A lead shield was mounted against the treatment table. The results were

recorded in a typical digital subtraction angiography (DSA) in a fixed field of view (FOV) for the PAOD protocol. Dose-area products were estimated along with the measured dose. Statistical analysis was performed with paired *t*-test.

Results and Discussion Mean operator radiation doses for the eye lens, thyroid, and gonad were 173.2 ± 0.6, 334.1± 1.9, and 248.5 ± 3.4 μSv, respectively. Radiation exposure for the operator was significantly decreased after shielded with lead [respectively 156.1 ± 0.8, 246.7 ± 1.9 and 36.76 ± 3.5 at eye lens, thyroid, and gonad (P <0.0001)]. A significant dose reduction was found at the lens (173.2 ± 0.6 μGy before treatment vs. 156.1 ± 0.8 μGy after treatment; P<0.001) of the operator. Significant difference was found in equivalent dose at the thyroid (334.1 ± 1.9 μGy before treatment vs. 246.7 ± 1.7 μGy after treatment; P<0.001) and the gonads (248.5 ± 3.4 μGy before treatment vs. 36.76 ± 3.5 μGy after treatment; P<0.001) of the operator/cardiologist after treated with the shield device. Mean equivalent doses at each of the three sites (i.e., gonad, thyroid and lens) were significantly reduced by the radiation-block drape compared to the control group. However, no significant difference was found in dose-area product (what the operator usually used to evaluate the dose) between the two groups (179.9 ± 0.1 mGy.cm^2 before treatment compared to 177.4 ± 2.6 mGy.cm^2 after treatment; P=0.38). Proper radiation shield was found effective to decrease operator's health risk during radiological diagnosis for the PAOD compared to the control group.

Conclusion Radiation exposure to the eye lens, thyroid, and gonad of the operator during percutaneous interventional procedures for PAOD is relatively lower than that of the patient. Radiation exposure by DSA protocol could cause higher dose at the thyroid in the operator than that to the lens, and the operator's gonad close to the main projection field might receive a higher dose. Recanalization procedure for PAOD was found resulting in higher dose to thyroid and gonad than proper shielded, which suggests that shielding is effective to reduce health risk.

References

1) Behrendt, C-A., et al. "Radiation dosage for percutaneous PAD treatment is different in cardiovascular disciplines: results from an eleven year population based registry in the metropolitan area of Hamburg." European Journal of Vascular and Endovascular Surgery 53.2 (2017): 215-222.
2) Mettler Jr, Fred A., et al. "Medical radiation exposure in the US in 2006: preliminary results." Health physics 95.5 (2008): 502-507.

A plastic scintillation dosimeter for MRI-LINAC dosimetry

Levi Madden[1], James Archer[1], Enbang Li[1], Dean Wilkinson[2], Anatoly Rozenfeld[1]
[1]*CMRP, University of Wollongong, Wollongong, Australia*
[2]*ICCC, Wollongong Hospital, Wollongong, Australia*

Highlights

- Single fiber dosimeter
- Temporal and neural network analysis for separation of Cerenkov signal
- Suitable for MRI-LINAC dosimetry

Key words Fiber optic dosimeter, relative dosimetry, plastic scintillators.

Background and Objectives Plastic scintillation dosimeters (PSDs) are comprised of a plastic scintillator volume coupled to a plastic optical fiber. Plastic scintillators possess water equivalence, linear responses with dose and energy independent responses for the radiations produced by clinical linear accelerators (LINACs) [1,2]. The number of photons that a plastic scintillator emits is dependent solely upon the dose deposited in the scintillators volume, permitting relative dosimetry through the measurement of the scintillation signal transmitted through the optical fiber with a photodetector. However, LINAC irradiated plastic optical fibers produce Cerenkov radiation, which are transmitted through the optical fiber and measured by the photodetector [1,2]. The optical signals measured by a photodetector are a combination of scintillation and Cerenkov radiation; only the scintillation signal is proportional to the dose deposited in the scintillator. Methods in PSD-LINAC dosimetry require the measurement of the Cerenkov radiation signals for signal correction; presented are the results of PSD dosimetry using various techniques for Cerenkov radiation signal correction with clinical LINACs [3,4].

Materials and Methods The plastic scintillation dosimeters constructed use cylindrical volumes (2 mm diameter and 0.5 mm length) of BC444 (Saint Gobain) plastic scintillator and Eska CK40 optical fibers. Optical paint (BC620, Saint Gobain) was applied to all fiber optic probes to ensure light tightness of the probes [3,4]. Photomultiplier tubes (RCA 426) were applied for measurement of the optical signals transmitted through the optical fibers, with a digital oscilloscope (Picoscope PS6406D) applied to measure the photomultiplier tubes outputs as time dependent voltage signals [3,4]. The methods applied for signal correction were background subtraction [1,2], algorithmic temporal analysis [3] and neural network temporal analysis [4]. Beam profiles were measured in solid water using a Varian 21iX Clinac at Wollongong hospital. The beam profiles were also measured in solid water using Scanditronix

CC13 ionisation chambers (ICs) for comparison with the PSD measured profiles. The LINAC produced photon beams at beam energies of 6 MV and 10 MV, with a dose rate of 600 MU/min for all measurements.

Results and Discussion

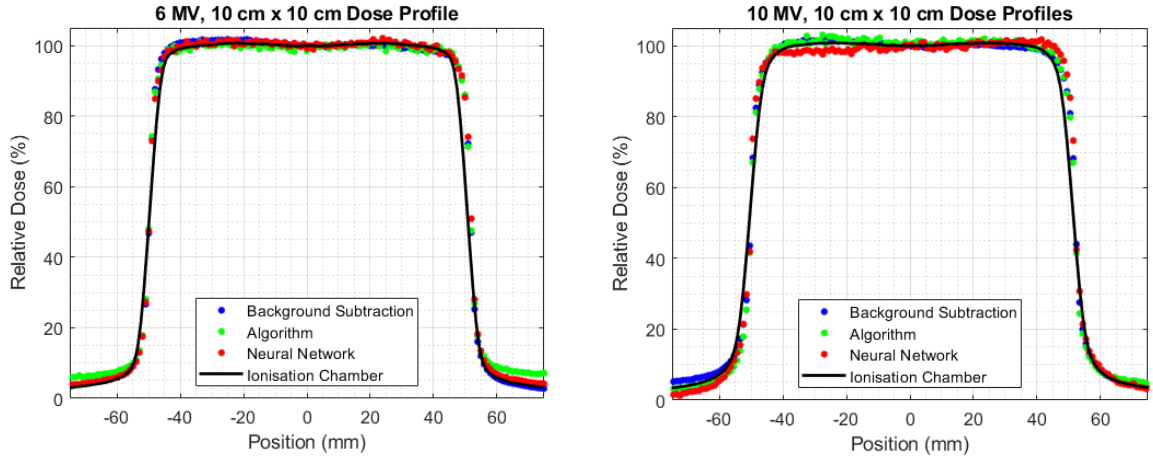

Figure 1: 6 MV and 10 MV beam profiles measured at a depth of 1.5 cm in solid water, source to surface distance of 100 cm and field size of 10 cm by 10 cm.

On average, the background subtraction and neural network analysis measured profiles were within a 1.3% agreement of the IC measured profiles. Algorithmic temporal analysis was on average within a 1.8% agreement of the IC measured profiles. Penumbras measured using the PSD were on average 3.3 mm and 3.8 mm wide for the 6 MV and 10 MV beam, while the corresponding IC measured penumbras were 5.3 mm and 6.4 mm.

Conclusion The presented methods allow for PSDs to be applied for dosimetry with Clinical LINACs. Current work at CMRP (UOW) aims to apply the constructed PSDs in small field dosimetry and MRI-LINAC dosimetry, where the PSDs energy independent response and MRI compatibility make PSDs promising for relative dosimetry.

References

1) AS Beddar, TR Mackie, and FH Attix, *Phys. Med. Biol.*, 1992, **37**, 1883.
2) AS Beddar, TR Mackie, and FH Attix, *Phys. Med. Biol.*, 1992, **37**, 1901.
3) J Archer, L Madden, E Li, D Wilkinson and A Rozenfeld, *Med. Phys.*, 2019, .doi:10.1002/mp.13383
4) L Madden, J Archer, E Li, D Wilkinson and A Rozenfeld, *Phys. Med. Biol*, 2018, **63**, 225004

Radioluminescence results from an Al_2O_3:C+fibre prototype in hadron therapy beams: ^{1}H, ^{4}He and ^{12}C.

L. F. Nascimento[1]*, A. Parisi[1], L. E. C. Rocha[2], S. Kodaira[3], E. G. Yukihara[4], F. Vanhavere[1]

[1]*Belgian Nuclear Research Centre, SCK•CEN, Mol, Belgium* *ldfnasci@sckcen.be

[2] *Centre for Business Network Analysis, University of Greenwich, London, UK*

[3] *Radiation Measurement Research Section, NIRS, Chiba, Japan*

[4] *Department of Radiation Safety and Security, Paul Scherrer Institute, PSI, Switzerland*

Highlights RL from Al_2O_3:C has a lower luminescence efficiency (η) with high LET particles, regardless of the beam type/energy, while η depends on crystal size. We use these results to determine fluence-averaged LET (LET_f) calibration curves in the plateau region of variuous particle beams, so that a combination of measurements from two detectors can be used to calculate unkown LET_f and dose. This method can be applied for daily QC in hadron therapy.

Key words real time dosimetry, hadron therapy beams, LET, RL

Background and Objectives - Hadron therapy (HT) introduces challenges for the dosimetrists, radiobiologists and medical physicists, because of its complicated technical and radiobiological aspects compared to conventional therapy. International agencies and commissions (IAEA, AAPM, ICRU among others) have been working on a worldwide harmonisation for treatment protocols, quality assurance (QA) and quality control (QC). In this work, we present the response from radioluminescence (RL) Al_2O_3:C real time detectors versus average LET for therapeutic high LET beams.

Materials and Methods - We tested several fiber probes: one 'Single Crystal'-type, with one Al_2O_3:C crystal ($2\times1\times1$ mm^3); two '38 µm'-type, with Al_2O_3:C droplet with average crystal size of 38 µm (r= 0.5 mm, l=200 µm); and two '4 µm'-type, with Al_2O_3:C droplet with average crystal size of 4 µm (r= 0.5 mm, l=200 µm). We irradiated the Al_2O_3:C fibers with 160 and 230 MeV proton, 150 MeV/n helium and 290 and 400 MeV/n carbon mono-energetic beams. The fiber probes were positioned in front of a polymethylmethacrylate (PMMA, density=1.19 g cm^{-3}) binary filter with water-equivalent thickness ($mm_{W\text{-}eq.}$). The relative luminescence efficiency η used in this work is defined as the ratio of the luminescence signal to the radiation field k and the luminescence signal to a reference low LET radiation field l (Cobalt), for specific doses $D_{k,l} \xrightarrow{thus} \eta_{k,l} = (RL_k/D_k)\big/(RL_l/D_l)$ (1), being RL_l/D_l pre-determined for each detector type (a_i). Monte Carlo simulations were performed using PHITS version 2.82 to assess LET_f. A simplified geometry of the irradiation setup was used in the simulations including only the PMMA energy degraders.

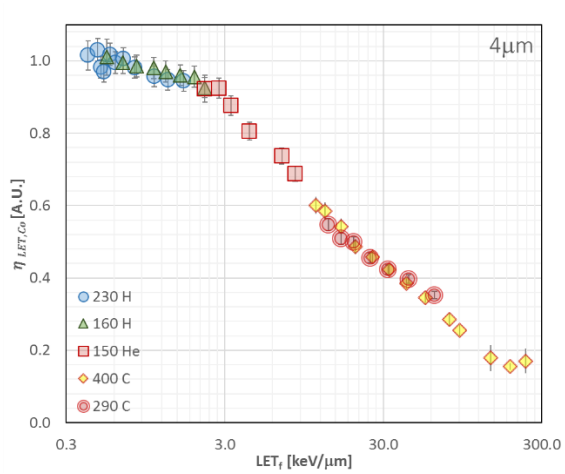

Figure 1. Combination of all the 4um luminescence efficiencies (RL) acquired from different beam types and energies vs LET$_f$.

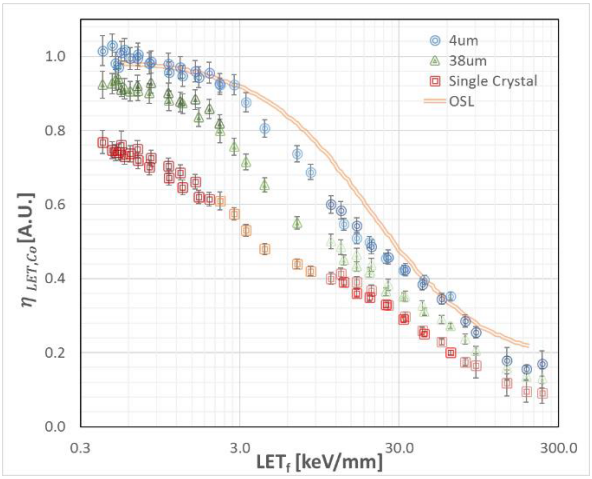

Figure 2. Combination of all luminescence efficiencies from all probe types (RL and OSL[2]) acquired from different beam types and energies vs LET$_f$.

Results and Discussion Figure 1 presents the luminescence efficiency vs LET$_f$ from the 4µm fibre (RL), with results obtained from irradiations with several beam types and energies. If we limit ourselves to irradiations along the plateau region of each Bragg curve (Figure 1), the curves from both proton beams connect to the curve from helium and to the two carbon beams. When combining all the curves from the different detectors (Figure 2), this trend is consistent with previous observed results from OSL Al_2O_3:C [2]. We fitted calibration curves ($\eta_{cal,i}$) for all the detectors (i) and used the fact that the dose is the same:

$$(\eta_{cal,CG} * a_{CG})/RL_{CG} = (\eta_{cal,38um} * a_{38um})/RL_{38um} = (\eta_{cal,4um} * a_{4um})/RL_{4um} \quad (2)$$

Using this equation, the unknown D and LET$_f$ are given by the crossing point of the curves in (2), for different detectors, for various LET.

Conclusion The response of Al_2O_3:C RL detectors are LET$_f$-dependent, which is also observed in solid-state dosimeters in general. Because of the decrease in luminescence efficiencies with LET, doses in heavy charged particle beams cannot be calculated directly from the real time RL measurements. To solve this, we used a combination of two detectors to demonstrate the robustness of our approach. The advantage is that the curves can be obtained very quickly, because the RL is a real time measurement (20 ms time resolution). This method could be further explored for daily QC in HT.

References

[2] E. G. Yukihara *et al.*, Time-resolved optically stimulated luminescence of Al2O3: C for ion beam therapy dosimetry. *Physics in Medicine & Biology* **60**, 6613 (2015).

ImageDosis: 2D real-time *in vivo* dosimetry

Luana de F. Nascimento[1]*, Dirk Verellen[2], Jo Goossens[2], Filip Vanhavere[1], Mark Akselrod[3]

[1]*Belgian Nuclear Research Centre, Boeretang, 200, 2400 Mol, Belgium *ldfnasci@sckcen.be*

[2]*Department of Radiotherapy, Iridium Kankernetwerk; University of Antwerp, MIPRO, Belgium*

[3]*Landauer Inc., Stillwater Crystal Growth Division, Stillwater, OK 74074, USA*

Highlights *in vivo* system capable of accurately measuring the 2D real time dose rate received by the patient and account for the proper patient positioning relative to the LINAC

Key words real time dosimetry, dose rate, radiotherapy, 2D dosimetry, RL

Background and Objectives - Radiotherapy (RT) is a highly complex, multi-step process that requires the input of different experts in planning and delivering the treatment. As RT treatments are continuously evolving, it is important to consider *in-vivo* dosimetry (IVD) as part of RT safety and quality control (QC) measures; several public health committees, societies and associations recommend measuring the dose received by each patient routinely in RT [1]. We suggest a novel technique we called ImageDosis aimed to be a patient safety and QC radiation measurement system based on a 2D radioluminescence (RL) technique for real time IVD. Our goal is to develop a system capable of accurately measuring the two dimensional (2D) real time dose rate received by the patient and account for the proper patient positioning relative to the linear accelerator (LINAC). In this work we present the feasibility study for the idea, presenting the dosimetric characterization of the system and some QA tests.

Materials and Methods - ImageDosis is based on the RL signal from Al_2O_3:C,Mg micro-crystals mixed with a polymer binder, coated as a thin layer on a plastic substrate that can be put on top of a patient/phantom. The system consists of three main components: (1) the radiation detector, (micron-size Al_2O_3:C,Mg matrix); (2) the readout using a high-resolution scientific camera; and (3) proprietary image and signal processing software. The camera, together with the system's signal processing, measures the time-dependent luminescence and translate this signal to a high-resolution frame-by-frame sequence showing the evolution of the dose delivered to the patient/object. The external beam irradiations were performed at the Iridium Kankernetwerk (Belgium) using both an Elekta-Synergy and Varian LINACs, with photons (6, 10 and 15 MV) and electrons (6, 9, 12, 15 and 18 MeV) in FF and FFF mode with dose rates from 0.05 to 24 Gy/min. Squared field sizes ranged from 0.5 x 0.5 cm^2 to 10 x 10 cm^2.

Results and Discussion The RL images shown in Figure 1 and 2 are samples from movies acquired from a 1 minute irradiation recorded at 1 ms sampling rate. Fig 1 shows the 8 x 8 cm^2 field during irradiation with RL coming from the Al_2O_3:C,Mg printed film, while Fig 2 presents two geometries that are more complex.

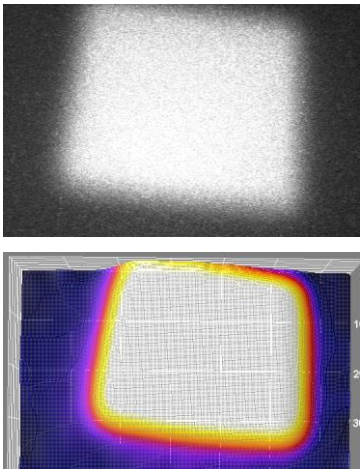

Figure 1. RL emission from Al_2O_3:C,Mg sheets during irradiations in ambient light (field size 8 x 8 cm^2, 600 MU/min)

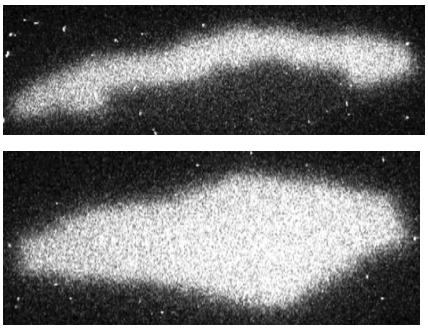

Figure 2. RL signal under IMRT complex geometries

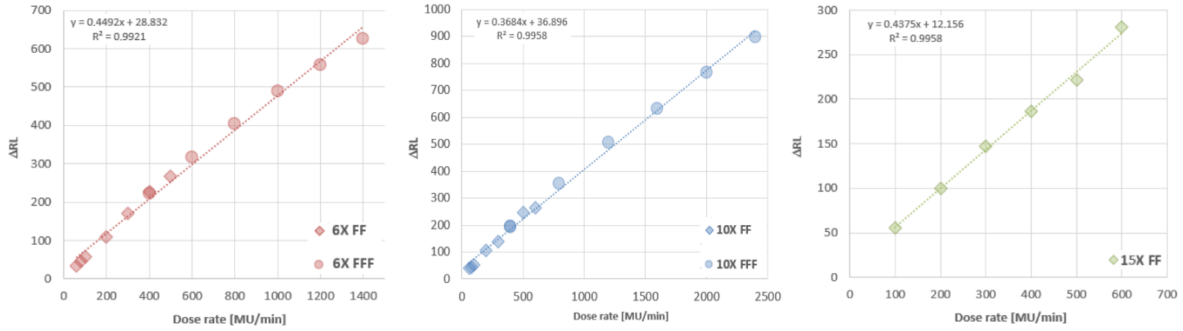

Figure 3. Al_2O_3:C,Mg RL vs dose rate (MU/min) for 6, 10 and 15 MV, in FF and FFF modes.

The quantization of homogeneity and variation in the radiation beam as a function of time gives 0.1 mm^2 spatial resolution, linear dose rate range from 0.05 to 24 Gy/min (FF and FFF modes), time resolution of 20 ms, good agreement (~1%) with the reference ion chamber. The system provides the option to make the plot of intensity values across features in any image, from a point, a line, or area of interest from the image selected. QA test results, using different irradiation modalities, such as Alternating leaves, Picket Fence, Pyramid and detection of errors in phantom position showed good agreement with delivered geometries.

Conclusion We demonstrate the feasibility of a system capable of real time *in-vivo* visual assessment of the radiation field 2D map and distribution of absorbed dose rate, using a luminescent sheet. In this work we provide the prove of concept, showing linear response with dose rate, high spatial and time resolution and good signal to noise ratio in main beam and penumbra region

References

1.Mijnheer, B., et al., *In vivo dosimetry in external beam radiotherapy.* Medical physics, 2013. **40**(7): p. 070903..

Borate vitreous matrix ($80MgB_2O_4–20MgB_4O_7$) tested for clinical radiation dosimetry

Luiza F. Souza[1]*, Gerardo B. Rivera[1,2], Rogerio M. Vidal[3], Susana O. Souza[1], Divanizia N. Souza[1]

[1]*Universidade Federal de Sergipe, São Cristóvão, SE, Brazil*
[2] *Corporación Universitaria del Huila, Neiva-Huila, Colômbia*
[3]*Instittuto do Câncer do Ceará , Fortaleza, CE, Brazil*

Highlights New OSL glass detectors ($80MgB_2O_4–20MgB_4O_7$) presented wide dose-response range required in clinical beams dosimetry.

Key words OSL dosimetry, borate glass, radiotherapy, quality assurance.

Background and Objectives The advances in radiotherapy techniques, such as Intensity Modulated Radiotherapy (IMRT), Volumetric Modulated Arc Therapy (VMAT), and Tomotherapy, require complex quality assurance (QA) protocols and detectors capable of verifying dose with high accuracy and precision. Detectors based on Optically Stimulated Luminescence (OSL) have been an important alternative tool for QA and *in vivo* practices, once that the gold standard detector in these practices, the ionization chambers (ICs), also presents limitations[1]. These passive luminescent detectors have several advantages, which relies on no need for power or cables during the irradiation, high sensitivity, small sizes materials, and reusability. Therefore, this work aimed to investigate the feasibility of using the OSL emitted by borate vitreous matrices as an alternative to be applied in clinical dosimetry measurements. The main features of these matrices are its small size, transparency, structural hardness, low hygroscopicity, tissue equivalence, and wide dynamic range. A series of experiments were performed in clinical beams to characterize the borates, such as reproducibility, fading, dose-response, dose rate dependence, field size dependence, and energy dependence.

Materials and Methods The borate glass matrix ($80MgB_2O_4–20MgB_4O_7$), called here as MBO, was prepared by fusion and a rapid cooling method, using 80% MgB_4O_7 and 20% MgB_2O_4. The glass was co-doped with 0.5 %wt Ce_2O_3 (Sigma, 99.9% purity) and 0.1 %wt $LiCO_3$ (Sigma, 99.9% purity). The detectors were produced in pellets form with 15 mg,

3.17 mm in diameter, and 0.9 mm thickness. The irradiations of the pellets were performed in the reference gamma rays sources ^{137}Cs (662 keV) and ^{60}Co (1250 keV), and in the clinical beams of 6 MV and 10 MV using a Clinac Varian 21EX. For the dose rate dependence, the pellets were exposed to 10 MV photons and doses rates of 200, 300, 400, and 500 cGy/min, at a 100 cm source to surface distance (SSD). For the field size dependence, the samples were exposed to fields of 3×3 cm^2, 5×5 cm^2, 10×10 cm^2, and 20×20 cm^2 and the percentage depth dose (PDD) curves were performed in a solid water phantom, with a 10×10 cm^2 field. All the data was compared with the treatment planning system (TPS), obtained with an ionization chamber (IC).

Results and Discussion The dose-response of the glasses exposed to 10 MV photon beams showed a broad range from 0.1 up to 20 Gy, with a slight overresponse (< 10%) within 0.5 Gy and 3 Gy. The results also showed that OSL response of the MBO glasses saturates above 18 Gy. The standard deviations of the OSL signal in each dose were below 3%, indicating a reproducible signal among the MBO pellets.

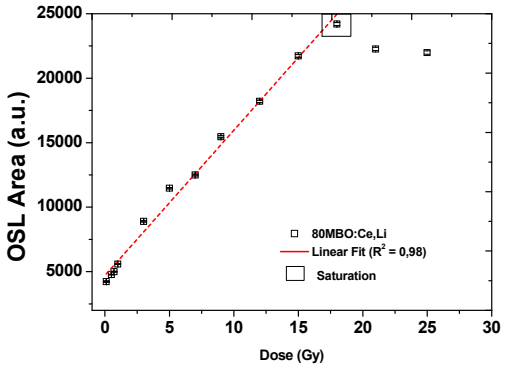

Figure 1. OSL dose-response curves for MBO glasses exposed to 0.1 Gy up to 25 Gy, when irradiated to 10 MV photon beams.

Conclusion The first results indicated that the detectors presented wide dose-response range, required in clinical beams dosimetry. The standard deviation, in each dose, is an indication that the OSL signals of MBO pellets are reproducible. Furthermore, the experimental results related to the fading, energy dependence, dose rate dependence, and PDD will be presented at the conference.

References

1) Alvarez P., Kry S.F., Stingo F., Followill D. TLD and OSLD dosimetry systems for remote audits of radiotherapy external beam calibration. Radiat Meas. 2017. 106: 412-5.

Out-of-field mean photon energy in radiotherapy measured using TLD-300 dosimeters

VM López-Guadalupe[1]*, E López-Pineda[1], A Rodríguez-Laguna[2], MA Poitevin-Chacón[2], and ME Brandan[1]

[1]*Instituto de Física, Universidad Nacional Autónoma de México, Coyoacán 04511, Ciudad de México, Mexico*

[2]*Unidad de Radioterapia, Hospital Médica Sur, Tlalpan 14050, Ciudad de México, Mexico*

Highlights

The glow curve shape of TLD-300 has been quantified by PHR, the peak-height ratio between high- and low- temperature peaks, as a function of photon energy, in the range 16-1250 keV. This has extended previous calibrations done up to 55 keV with diagnostic photons. We've found that the PHR sensitivity to the photon energy becomes negligible at about 700 keV.

TLD-300 dosimeters were exposed in-phantom to out-of-field radiation in a 6 MV linac. Preliminary results indicate mean energy equal to (394±20) keV at 1 cm from the 10x10 cm^2 field edge, and a mean of (316±22) keV, independent of distance, at 3-15 cm from the edge.

Key words Radiotherapy, 6 MV linac, out-of-field energy, TLD-300.

Background and Objectives In radiotherapy, the possible damage to healthy organs and late induction of a new primary cancer requires knowledge of the out-of-field dose and radiation energy[1)]. Recent publications[2,3)] have reported the remarkable sensitivity of the TLD-300 glow curve (GC) to the photon energy in diagnostic applications. Since TLDs are considered suitable for radiotherapy out-of-field dosimetry[1)], this work investigates the use of TLD-300 to evaluate the mean energy of photons in phantom regions located outside a 6 MV linac treatment volume.

Materials and Methods TLD-300 chips were calibrated exposing to ^{99m}Tc (140 keV), ^{18}F (511 keV annihilation gammas), ^{137}Cs (662 keV), ^{60}Co (1250 keV) sources and to a 28 kV Mo/Mo mammography beam. The calibration curve quantifies the dependence of the peak-height ratio (PHR, ratio of the high- and low- temperature GC maxima) on the mean photon energy. Measurements were performed inside a PMMA phantom irradiated with 6 MV photons from a Varian True Beam®. Out-of-field dosimeter exposures took place outside a 10x10 cm^2 field, at the isocenter plane, inside a PMMA phantom, with 4.5 cm buildup and 5 cm backscatter material. Monitor units were 211, and dose estimates indicate that this exposure guarantees a linear dosimeter response. Chips were placed 1-15 cm away from the field edge. TL dosimeters were annealed and read following the same protocol used previously by our group[2,3)].

Results and Discussion Figure 1 shows the calibration curve measured with, at least, 4 dosimeters at each energy (the number was determined by the geometrical conditions of each irradiation). Uncertainties are equal to one standard deviation. As already suggested by calibration at lower energies[2,3], the sensitivity of PHR (that is, the GC shape) to the energy decreases with photon energy, practically disappearing beyond about 700 keV. The measured out-of-field mean energy was (394±20) keV at 1 cm from the field edge, and (316±22) keV (mean value) at 3-15 cm from the edge. Independent Monte Carlo simulations[1,4] have reported that, depending on the accelerator manufacturer and model, the secondary radiation mean energy is expected to be of the order of 200-600 keV and a function of the off-axis distance. Our (preliminary) results for the secondary radiation field are consistent with the Monte Carlo calculations. Currently, we are working on the definition of a more accurate TL protocol that would improve the precision of the method in the range of energies encountered in radiotherapy.

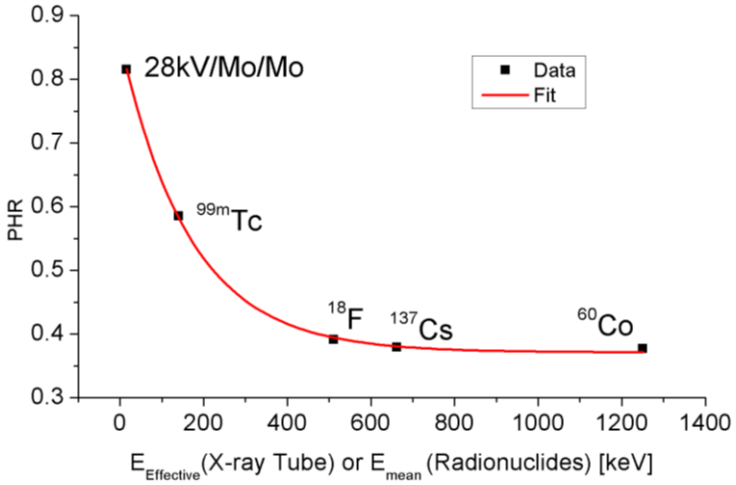

Figure 1. TLD-300 calibration curve. Error bars are comparable to the size of the symbols.

Conclusion The TLD-300 GC is sensitive to the photon field energy up until about 700 keV. We've determined out-of-field mean photon energies at distances between 1 and 15 cm from a radiotherapy field edge, and the results agree with general predictions. A TL protocol more complex than the current one is, probably, required to extend the method to energies of 1 MeV and beyond. We plan to have results on this goal by the conference date.

We acknowledge partial support from DGAPA-UNAM, Grant PAPIIT IN10329.

References

1) SF Kry *et al.*, Med. Phys. 44 (2017) e392.
2) A Gómez-Facenda *et al.*, Radiat Meas 106 (2017) 341-345.
3) ID Muñoz *et al.*, Med. Phys. 45 (2018) 4287-4296.
4) A Skrobala *et al.*, Cancer/Radiothérapie 21 (2017) 352-357.

Perturbations of radiation field behind high-density titanium dental implants irradiated with proton and carbon beams

M. Davídková[1]*, C. Oancea[1, 2, 3], A. Luu[2, 4], G. Mytsin[2], V. Vondráček[5], R. Abdulhadi[6], A. Hamilton[6], S. Kodaira[7], I. Ambrožová[1]

[1]Department of Radiation Dosimetry, Nuclear Physics Institute of the CAS, Prague, Czech Republic; [2]Joint Institute for Nuclear Research, Dubna, Russia; [3]Horia Hulubei National Institute for Nuclear Physics and Engineering, Magurele, Romania; [4]Institute of Physics, Vietnam Academy of Science and Technology, Vietnam; [5]Proton Therapy Center (PTC), Prague, Czech Republic; [6]Quest University Canada, Squamish, Canada; [7]National Institute of Radiological Sciences (NIRS), National Institutes for Quantum and Radiological Science and Technology, Chiba, Japan

Highlights Modified particle fluences behind metallic dental implants and plastic material were detected and perturbations in distribution of absorbed dose were quantified.

Key words Track–etched detectors, metallic dental implants, absorbed dose, LET, ion therapy

Background and Objectives Ion therapy is increasingly used in patients with head and neck cancer, which is a common tumour in humans. For example, oral cavity and oropharyngeal cancer are together the 6th most common cancer in the world [1]. Often, patients with these cancers have metal implants either from reconstruction surgeries or dental procedures. These implants could interfere with the prescribed proton or carbon ion therapy, producing significant range and dose uncertainties. Dosimetric problems introduced by high–density materials in ion therapy are of interest to medical physicists and radiation oncologists. The improved understanding of the macro– and microscopic dosimetric effects may allow choosing for these patients tumor treatment using ion beam directions crossing metallic dental implants.

Materials and Methods Titanium (Ti), most commonly used material for dental implants placed in water-equivalent plastic phantom, was irradiated by an active proton beam scanning (PBS) at PTC [2] and scattered carbon ion beam at NIRS. LET spectra behind water–equivalent nylon-6 with a 65 mm thickness surrounding the 2, 5, 10 and 15 mm inserts of grade–2 and grade–5 Ti were determined using strips of track etched detectors (TEDs) HARZLAS TD-1 (Nagase Landauer Ltd., Japan) with a dimension of 50 mm x 20 mm x 0.9 mm (density = 1.3 g/cm^3). The spectra of LET ranging from 7 to more than 1000 keV/µm were determined from etched TEDs [3] and compared with Monte Carlo simulations using the Geant4 toolkit, version 10.03.p01 [2].

Results and Discussion As a consequence of particles scattered inside the Ti, significant dose enhancement at the border between implants and plastic in the case irradiation by PBS was detected. Our analyses have shown that the number of particles detected in the interval from 7 to 100 keV/µm was increased by 39.5% for grade–5 Ti and 27.5% for grade–2 Ti, respectively, as compared to the number of particles detected in the area without implants. In order to identify the contribution of different particle types to dose, Monte Carlo simulations using Geant4 were performed. The small contribution of secondary particles compared to secondary protons was anticipated. TEDs irradiated behind Ti implants by carbon ion beam are under evaluation. Perturbations of radiation field for the same experimental setup in case of proton and carbon ion beams will be compared.

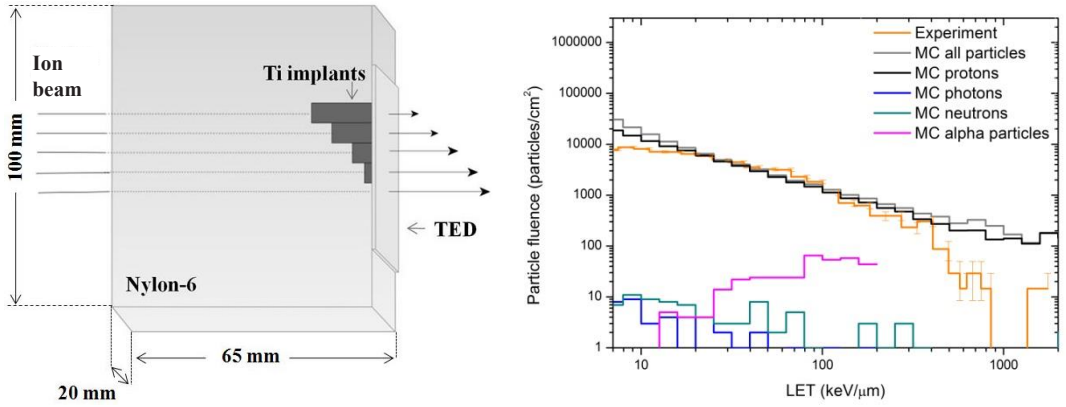

Figure 1. A) Experimental setup for irradiation of Ti implant with thicknesses of 15, 10, 5 and 2 mm x 5 mm x 20 mm placed in a 65 mm x 100 mm x 20 mm nylon–6. B) Comparison of the measured and simulated LET spectra behind 5 mm grade–5 Ti within TED detection interval. [modified from 2]

Conclusion A conglomeration of tracks at the border between the 15 mm dental implant and the plastic material caused by scattered particles inside the Ti alloys was detected. This leads to dose enhancement of up to a factor of 13 in the case of grade–2 Ti, and 12 in the case of grade–5 Ti PBS irradiations. The obtained data are valuable in benchmarking MC–based treatment planning systems that incorporate LET or RBE concepts.

References

1) Warnakulasuriya, S., 2009, Oral Oncol. 45, 309–316
2) Oancea, C., Luu, A, Ambrožová, I, Mytsin, G., Vondráček, V., and Davídková, M., 2018, Phys. Med. Biol. 63, 215020
3) Pachnerová Brabcová, K., Ambrožová, I., Kolísková, Z., and Malušek, A., 2013, Nucl. Instr. Meth. Phys. Res. A, 713, 5–10

Energy spectrum map of the scattered radiation field in interventional radiology with hybrid pixel detector

Marie Nowak[1,2]*, Pierre Carbonez[1,3], Francis R. Verdun[2], Jerome Damet[1,2,3]

[1]*CERN, European Organization for Nuclear Research, Geneva, Switzerland*

[2]*Institut of Radiation Physics, Lausanne University Hospital, Lausanne, Switzerland*

[3]*Dept. of Radiology, University of Otago, Christchurch, New Zealand*

Highlights This work aims to characterise the scattered radiation field in an interventional radiology theatre and to generate a 3D map of energy spectra measured with a Timepix3 hybrid pixel detector. The information on the energy of the radiation field was then used to calculate operational quantities for external radiation exposure using the ICRU conversion factors. This approach brings new tools to better understand the worker's exposition and provides crucial information to improve radiation protection gears. The approach is in line with the redefinition of the operational quantities proposed by the ICRU.

Key words energy spectra, hybrid pixel detector, Timepix3, dose, dosimetry

Background and Objectives Due to the evolution of imaging installations in radiology theatres, along with their complexity and the lack of X-ray spectral characteristics given by the manufacturers, it became more and more difficult to assess the real dose exposure of hospital staff members. The knowledge of the energy spectrum to which the user is exposed would allow a more precise determination of the dose and to optimize radiation protection gears. The 2017 ICRP report also points out the need to adapt operational quantities and proposes to define quantities based on particle fluence. Since 1997, the CERN Medipix team has been developing novel photon detectors that are able to provide spatial, temporal and energy information for each incoming photon. The Timepix3 hybrid pixel detector (HPD) was used to measure the energy spectra of the scattered radiation field in an interventional radiology (IR) theatre. This study presents 3D maps of the energy spectra in the scattered radiation field within an IR hospital theatre. Effective dose and absorbed dose to organs are subsequently calculated using conversion factors[2)].

Materials and Methods A Timepix3 (Medipix, CERN, Geneva, Switzerland) HPD chip was used for this work. The detector has a matrix of 256 x 256 pixels with 55 µm sides and can record up to 40 Mhits/cm^2/s. For each photon detection three parameters are recorded: time over threshold, time of arrival and pixel coordinates. The chip used was fitted with a 500 µm

thick silicon sensor and was coupled with an AdvaDAQ (Advacam, Prague, Czech Republic) readout system. Measurements were carried out in an IR theatre, in a 3 m radius semicircle around the X-Ray tube at four different heights. All collected data were corrected for the detection efficiency and the associated energy spectrum has been reconstructed. Each of these spectra has then been dose-related using the mass attenuation coefficient values present on NIST website[2].

Results and Discussion Figure 1 shows, on the left side, the grid used for measurement with 3 chosen positions in the room: A, B and C. The graphic on the right side presents the energy spectra for different heights at positions A, B and C. We can see that the homogeneity of the spectra is position-dependant. In addition, a shift in energy can be observed between the two different heights. Those energy spectra have then been used to create a 3D map of the scattered radiation field in the room, which allows us to determine the dose rates distribution and thus adapt radiation protection gear accordingly. Finally, the effective dose values can be estimated taking into account the fluence and the energy of the incoming particles as recommended by the ICRP and ICRU.

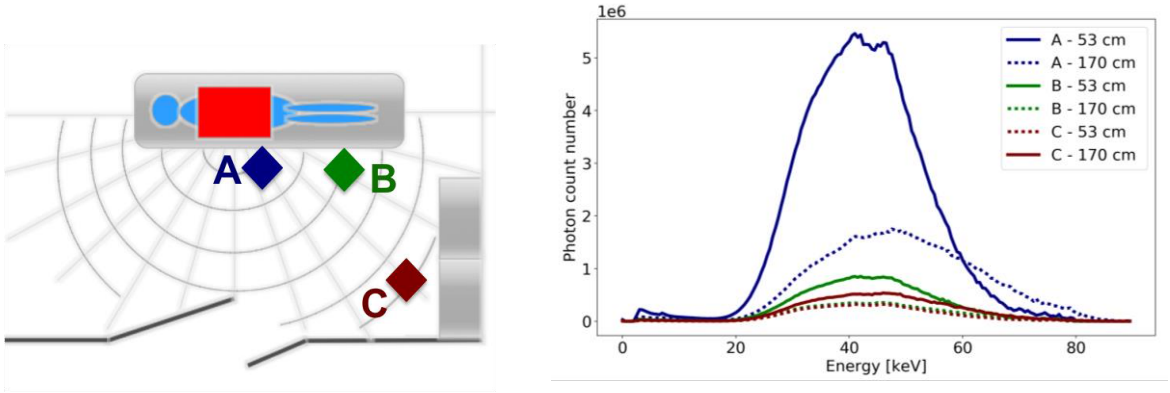

Figure 1. Left: Position of measurement in the room. Right: Energy spectra measured. Solid and dotted lines represent respective heights of 53 and 170 cm.

Conclusion The 3D map of the scattered radiation field allows us to strengthen the collaboration with the medical staff to optimise practices together and identify appropriate radiation protection gear. The dose values obtained in this study are a first step for developing an innovative dose measurement device.

References

1) ICRP: Draft Join Report of ICRU and ICRP for Consultation: Operational quantities for External Radiation Exposure
2) NIST: X-Ray Mass Attenuation Coefficients – Water, liquid, http://physics.nist.gov (accessed on 8 February 2019)

Out-of-field dose measurement in photon and proton craniospinal irradiation of paediatric patients – EURADOS WG9 phantom study

Marija Majer[1]*, Iva Ambrožová[2], Marie Davídková[2], Marijke De Saint-Hubert[3], Željka Knežević[1], Saveta Miljanić[1], Natalia Mojzeszek[4], Vedran Rajevac[5], Liliana Stolarczyk[4,6], Pawel Olko[4], Roger M. Harrison[7]

[1]*Ruđer Bošković Institute (RBI), Zagreb, Croatia*

[2]*Nuclear Physics Institute (NPI), Řež, Czech Republic*

[3]*Belgium Nuclear Research Center (SCK-CEN), Mol, Belgium*

[4]*Cyclotron Centre Bronowice (CCB), Institute of Nuclear Physics (IFJ), Krakow, Poland*

[5]*University Clinical Hospital Centre Sestre milosrdnice (UCHCSM UHT), Zagreb, Croatia*

[6]*Medical Physics Department Skandionkliniken, Upsala, Sweeden*

[7]*University of Newcastle, Newcastle upon Tyne, United Kingdom*

Highlights proton radiotherapy strongly reduces the out-of-field doses in the CS treatment of paediatric patients compared to photon radiotherapy

Key words out-of-field dose measurement, photon and proton craniospinal irradiation

Background and Objectives Out-of-field doses, caused by stray radiation, may increase secondary cancer risk for radiotherapy patients. Children are of particular concern due to high radiosensitivity and long-life expectancy. Therefore out-of-field dose measurement of different radiotherapy techniques is extremely important for risk assessment and radiation protection. Craniospinal (CS) irradiation increased tremendously survival rate for the patients with medulloblastoma which is the most common malignant brain tumour in children. This study, carried out within EURADOS Working Group 9 (Radiation Dosimetry in Radiotherapy), evaluates and compares out-of-field doses for paediatric medulloblastoma treatment using photon and proton CS irradiation.

Materials and Methods Photon and proton irradiations were performed on Siemens Artiste linac at UCHCSM UHT (Zagreb) using 3D conformal radiotherapy (3D-CRT) and at CCB (IFJ, Krakow) using pencil beam scanning (PBS) technique (IBA Proteus 235 gantry) respectively. CS treatments of the same target volume (whole brain and spinal cord irradiation + 0.5 cm margin) in CIRS anthropomorphic phantoms representing 5-year and 10-year old children were performed. For 3D-CRT, 6 MV photon beams were used for brain and 6 MV + 18 MV for spinal cord irradiation. The stray doses were measured with three types of thermoluminescent detectors (MTS-7: ^{7}LiF (Mg,Ti) and MTS-6: ^{6}LiF (Mg,Ti) for 10-year; MCP-n: LiF(Mg,Cu,P) for 5-year) and radiophotoluminescent (RPL) detector type GD-352M. The neutron contribution during PBS was determined with poly-allyl-diglycol-carbonate (PADC) nuclear

track detector in 10-year phantom. For 3D-CRT dosimeters were placed in all out-of-field organs, while for PBS dosimeters were put in the selected radiosensitive organs close to spinal cord.

Results and Discussion For out-of-field doses during 3D-CRT CS radiotherapy excellent agreement between RPL and MCP-n detectors was confirmed: the RPL/MCP ratio for the same point in 5-year phantom was on average 1.02 ± 0.15. Due to the use of 18 MV photon beams, higher doses were measured with MTS-6 than with MTS-7: the highest gamma-equivalent neutron dose per target dose in 10-year phantom were 293 and 181 mGy/Gy for esophagus and TL/spine respectively. Mean organ doses for both phantoms were comparable with exception of pancreas, stomach and four organs (uterus, adrenals, mandible, testes) with a factor 3.5, 2 and 1.5 higher values for 5-year phantom. This finding is expected due to the closer proximity of organs to the central spine axis in the 5-year phantom.

Comparison of stray radiation doses for proton and photon radiotherapy for 10-year phantom is shown in Figure 1. For points in the selected organs shown in Figure 1, gamma doses (RPL) are 2-3 orders of magnitude lower for PBS in comparison to 3D-CRT (MTS-7). For PBS, measured neutron dose equivalents (PADC) are a factor of 5 higher than gamma doses (RPL). In other points (closer to the central spinal axis) of the selected organs (including lungs, thyroid, esophagus), PADC were over-irradiated while measured gamma doses showed a factor 2 to 2000 lower values in comparison to 3D-CRT.

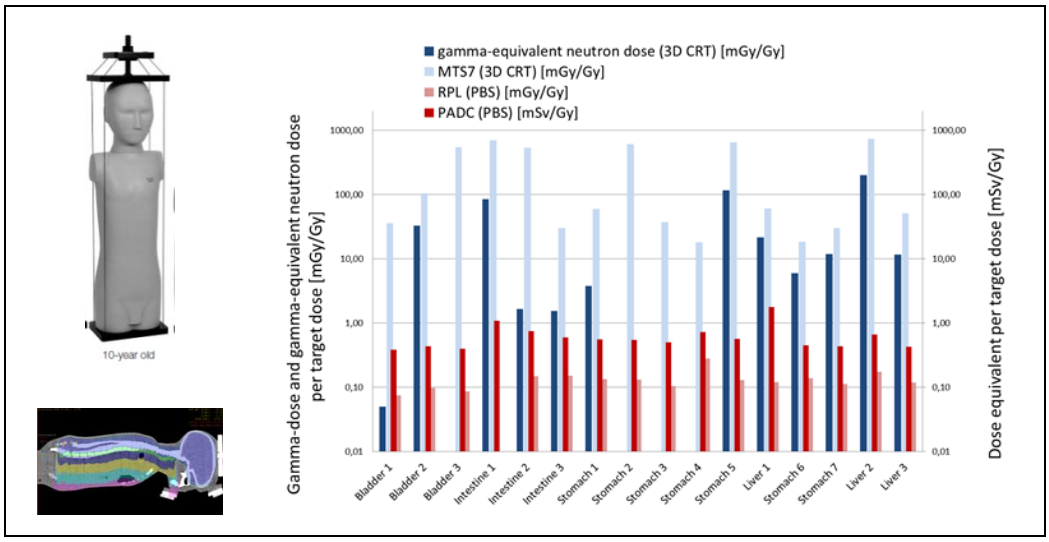

Figure 1. Comparison of stray radiation doses in the selected points of the organs close to spinal cord in 10-year old phantom for 3D CRT and PBS

Conclusion For measured points CS treatment with protons showed lower out-of-field doses for paediatric patients in comparison to photons.

Wiggler to Water: Validating the Model of the Microbeam Radiation Therapy Beamline at the Australian Synchrotron

Andrew Dipuglia[1, 2], Matthew Cameron[1], Iwan Cornelius[1], Jeremy Davis[1,2], Susanna Guatelli[1,2], Stéphanie Corde[1,3], Andrew Stevenson[4], Marco Petasecca[1,2], Anatoly Rosenfeld[1,2], and Michael Lerch*[1, 2]

[1] *Centre for Medical Radiation Physics (CMRP), University of Wollongong, Australia.*
[2] *Illawarra Health and Medical Research Institute (IHMRI), University of Wollongong, Australia.*
[3] *Radiation Oncology Department, Prince of Wales Hospital, Randwick, Australia.*
[4] *Australian Synchrotron, Imaging and Medical Beamline, Melbourne, Australia*
Email: mlerch@uow.edu.au

Highlights Using the Geant4 Monte Carlo toolkit, we have developed a model of the Microbeam Radiation Therapy Beamline at the Australian Synchrotron facility. The resultant photon energy spectrum compares very well with that of a previously benchmarked toolkit, SPECT. Further simulations of dose distributions within a solid water phantom show good agreement with experimentally obtained results. The broad beam and microbeam data are within 3% and 5% respectively for all configurations and all depths studied.

Key Words Microbeam Radiation Therapy, X-Tream dosimetry, Radiation Transport,

Background and Objectives Microbeam Radiation Therapy (MRT) uses high-intensity synchrotron x-rays which are spatially fractionated by a Multi-Slit Collimator to treat tumors [1]. The complex geometries and high intensities of the beam used in MRT demands tools allowing for independent verification of dose distributions delivered to patients to ensure accurate dose delivery and patient safety. The objective of this work is to experimentally validate the first complete Monte Carlo model of the entire MRT beamline at the Australian Synchrotron (AS).

Materials & Method The Geant4 MC model for MRT at the AS is based on a previously benchmarked model of the ID17 beamline at European Synchrotron Radiation Facility (ESRF) [2]. The ESRF model uses Geant4 interfaced with the third party SHADOW code that models synchrotron radiation production in the wiggler. In our model for MRT this dependency was removed so the entire beamline is simulated. We use the Low Energy Livermore polarized physics list with the Geant4 MC toolkit simulation. Stage 1 models the synchrotron radiation production in the insertion device and transports the resulting photons through the MRT beamline where they are then stored in a Phase Space File (PSF). Stage 2 uses the PSF as an input to a second simulation for dose calculations in the vertically scanned phantom. The X-ray photon spectrum incident on a 100 mm x 100 mm x 140 mm solid water phantom is compared to SPECT. The calculated broad beam (BB) depth dose is compared with pin point ionisation chamber and EBT3 film data. Calculated microbeam profiles are also compared with experimental data using EBT3 film and the X-Tream dosimetry system [3,4].

Results & Discussion Fig. 1a shows the generated BB spectra from Geant4 compared to SPEC for both 3T and 2T wiggler field strengths. Fig 1b shows the BB depth dose of Geant4 simulation for a range of depths in RMI457 solid water phantom vs Pinpoint ionisation chamber and EBT3 film for a 3T wiggler with Cu-Cu filtration configuration and 2.014 mm BDA. Fig. 2a shows the two dimensional dose distribution and Fig 2b shows the corresponding 1D dose profiles at 2 cm depth within a RMI457 solid water phantom for a BDA of height 2.014 mm. Fig. 2c shows the G4 MRT absolute dose intensity map of the 5 central microbeams within a 20 mm x 20 mm MRT treatment field. Fig. 2d shows the G4-MRT absolute microbeam peak dose (blue) and valley dose between two microbeams (red) with depth in a solid water phantom. Also shown are equivalent data using the CMRP X-Tream system (SSD) (black) and EBT-3 film (green).

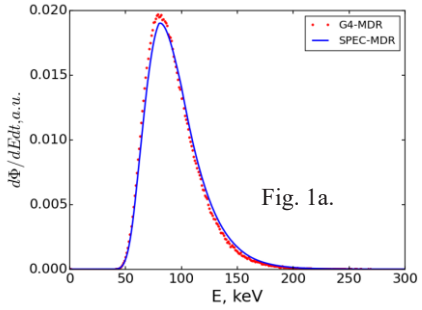

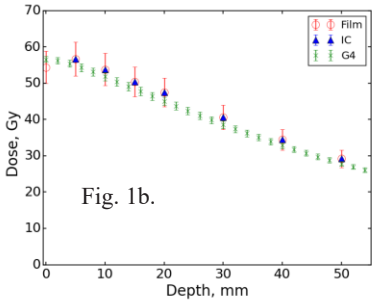

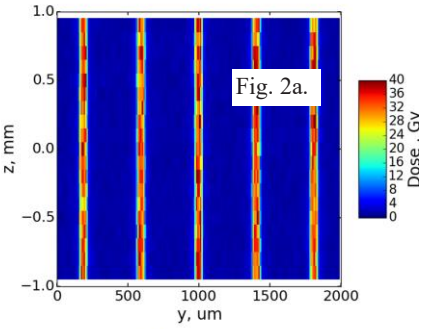

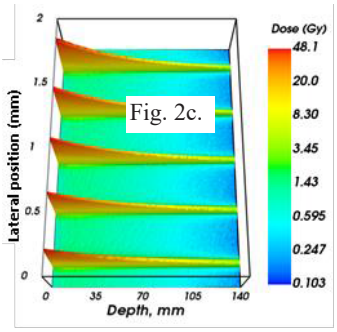

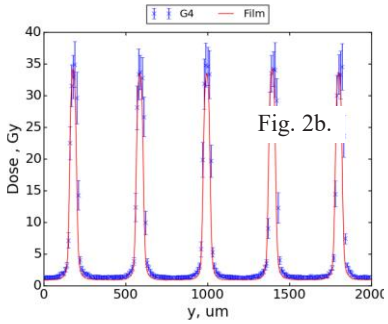

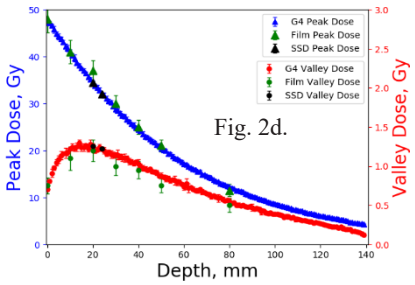

Conclusion The Geant4 based model of the AS MRT beamline has been successfully validated in both BB and MB configurations using wiggler field strengths of 3T and 2T. This work has also begun the generation of a database containing PSF files for each beam configuration and filtration available.

The AS is acknowledged for the use of their experimental facilities and the MASSIVE computing cluster. We acknowledge the financial support of the Australian Government Research Training Program Scholarship, and Australian National Health & Medical Research Council (APP1093256).

References

[1] Slatkin, D., et al.. *Medical Physics*, **19**(6), 1395-1400, (1992).
[2] Stevenson, A. W. et al. *Journal of synchrotron radiation* 24, 939–953 (2017).
[3] Petasecca, M., et al., *JINST*, 7 P07022, (2012)
[4] Lerch et al., *Radiation Measurements*, 46 (12), pp. 1560-1565, (2011).

EPR dosimetry on human fingernails: study of the variability of the endogenous signal

Tkatchenko N.[1], Romanyukha A.[2], R. Reyes[3], Swarts SG.[4], Tipikin DS.[5], Gourier D.[6], Trompier F.[1]
[1]*Institut de Radioprotection et de Sûreté Nucléaire (IRSN), 92260 Fontenay aux Roses, France*
[2]*Naval Dosimetry Center, US Navy, Bethesda, MD, USA*
[3]*Uniformed Services University of the Health Sciences, Bethesda, MD 20814, USA*
[4]*Department of Radiation Oncology, University of Florida, Gainesville, FL, USA*
[5]*In vivo Multifunctional Magnetic Resonance Center (IMMR), West Virginia University, Morgantown, WV, USA*
[6]*PSL Research University, Chimie-ParisTech-CNRS, Institut de Recherche de Chimie-Paris, 75005 Paris, France*

Keywords: EPR dosimetry, fingernails, radiological accident

Background and Objectives
Human fingernails and toenails have been studied for years by means of Electron Paramagnetic Resonance (EPR) spectroscopy to develop a new capability of estimating ionizing radiation doses received by individuals in case of radiological accidents. However, a practical and robust dosimetric protocol does not exist and is still needed.

Materials and Methods
EPR measurements were performed using Q-band spectrometer. Fingernail samples came from 30 different donors (various origins). A first study was done on the endogenous signal variability between donors and between fingers. It was followed by the study of the signal following external parameters: moisture content, temperature, and UV light exposure. The nature of the radical that causes the observed signal was characterized by combining both chemical reactions (acid-base, red-ox) with numerical simulations (Easyspin).

Results
The endogenous signal intensity differs from individuals up to 300 % and a dispersion of 60 % was observed. The signal also showed variation up to 11 % between fingers from the same individual. Harvesting period seemed to have a significant effect on the signal intensity; i.e. up to 20%. Sunlight exposure and especially UVA induced free radicals with the same spectral characteristics. Moisture content within sample impacted EPR signal intensity and water proceeded as a reducing agent. The hypothesis that the endogenous signal comes from an o-semiquinone anion radical was strongly supported by chemical experiments and numerical simulations.

Conclusions
The endogenous signal is a real problem for drawing an universal EPR radio-induced signal intensity curve, usable to estimate absorbed dose for any victim because it overlaps with the radio-induced signal of interest. More investigations are needed in order to discriminate the endogenous signal(s) and promising results have been recently obtained by combining numerical and chemical treatments.

TLD versus MOSFET: a review of utilisation rates of different detectors for *in vivo* dosimetry across a large radiothearpy department

Peta Lonski[1]*, Eujin Chan[1], Tomas Kron[1]
[1]*Department of Physical Sciences, Peter MacCallum Cancer Centre*

Highlights Utilisation rates of TLD and MOSFET detectors for *in vivo* dosimetry were reviewed over a period of two years for two different radiotherapy facilities – one having an on-site TLD reader and the other a MOSFET system. Patient records were categorised according to treatment site. While MOSFETs were considered appropriate as an *in vivo* dosimetry system for most cases at the site with a MOSFET system, in some cases TLDs were requested from the other facility. TLDs were the preferred dosimeter for kilovoltage treatments and out-of-field dose measurements.

Key words TLD, MOSFET, *in vivo* dosimetry, radiotherapy

Background and Objectives *In vivo* dosimetry is routinely employed in radiotherapy for dose verification, quality improvement, and patient safety. For a detector to be useful as an *in vivo* dosimeter it should have minimal energy dependence, a linear dose response, be safe to place on a patient, and provide sufficiently accurate, reproducible, and timely results. TLD and MOSFET are two common methods and both are used across our institution, which comprises five radiotherapy campuses. The aim of this work was to compare utilisation of TLD and MOSFET between two different campuses, one being equipped with a TLD system and the other a MOSFET system.

Materials and Methods *In vivo* dosimetry records were reviewed over a two year time period between May 2015 and July 2017 for two radiotherapy campuses. Campus 1, which comprises six linear accelerators, is equipped with a TLD system using LiF:Mg,Cu,P material[1], and Campus 2, having two linear accelerators, with a MOSFET system. Both campuses treat 3DCRT, stereotactic body radiotherapy ('SBRT'), IMRT and VMAT as well as electron radiotherapy and both provide superficial and deep x-ray therapy ('S/DXRT') services. Campus 1 also provide total body photon and total body electron radiotherapy, while Campus 2 does not. Patient *in vivo* records were grouped by treatment modality and anatomical site for comparison.

Results and Discussion A total of 310 patient TLD records were available from Campus 1 for review. Campus 2 had MOSFET records for 67 patients. Both campuses were able to

perform in-field dose verification for a variety of radiotherapy modalities. Campus 1 was able to perform *in vivo* dosimetry for TBE treatments performed using a rotational technique whereby patients stand on a rotating platform while the beam is on – TLD in this case being preferable for not requiring any cables. In some S/DXRT cases it was noted that Campus 2 requested TLDs from Campus 1 in preference to MOSFETs, which can give unacceptable energy response and additional uncertainties in effective depth for very low energy beams, particularly <80 kVp (Aluminium filtration).

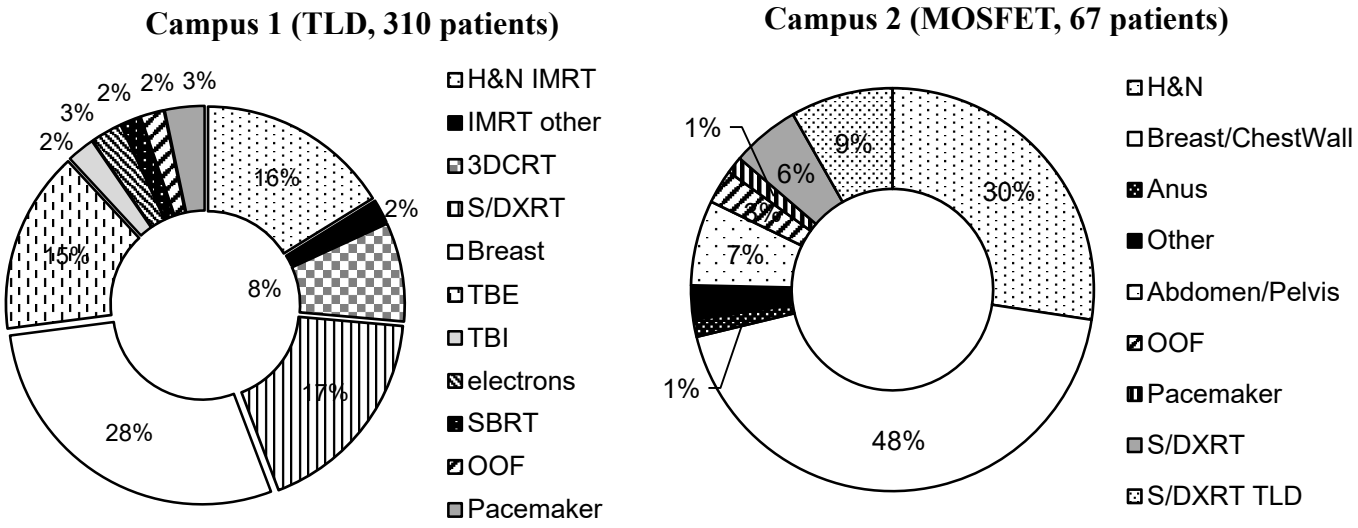

Figure 1 – Percentage of *in vivo* measurements by treatment site, comparing Campus 1 (TLD) with Campus 2 (MOSFET). Campus 2 requested TLDs for 9% of cases, all for S/DXRT treatments.

Conclusion Both TLD and MOSFET dosimeters were found to be appropriate for *in vivo* dosimetry across a large and complex radiotherapy department. In addition, TLDs were used for phantom measurements, research, and area monitoring. MOSFET had the advantage of providing results instantly but in some cases the near tissue equivalence of LiF:Mg,Cu,P proved to be desirable over MOSFET (for instance S/DXRT). Choice of detector for *in vivo* dosimetry should take into account practical considerations as well as dosimetric advantages and disadvantages, and may vary depending on the size, complexity, and types of services offered within a radiotherapy department.

References

1. Kron T. Thermoluminescence dosimetry and its applications in medicine--Part 1: Physics, materials and equipment. Australasian physical & engineering sciences in medicine. 1994;17(4):175-99.

TL performance of the LiF:Mg,Ti in the dosimetry of small fields

Authors: Almeida, S.B.[(1)], Villani, D[(2)].,Menegussi, G[(2)].,and Campos, L.L.[(1)]

[1]*Instituto de Pesquisas Energéticas e Nucleares, CNEN/SP, Brazil*

[2]*Instituto do Câncer do Estado de São Paulo, Brazil*

Highlights: Dosimetric performance of the LiF:Mg,Ti employing the thermolumenecence technique for the application in dosimetry of small fields.

Key words: termoluminecence Dosimetry**,** LiF:Mg,Ti, small field.

Background and Objectives: Radiosurgery plays an important role in the treatment of intracranial lesions and an increasingly adopted approach, one of the hallmarks of this technique is the need to use beams with small diameters, precisely directed at the target volume [1]. This technique consist in the application of high doses of radiation in a small intracranial volume, having a good definition and location by means of stereotactic geometric accessory, through the application of multiple and concentric thin beams. This modality allows to concentrate the radiation in the target volume in such a way that the drop of the peripheral doses is very fast, avoiding in this way that the adjacent structures receive high doses [1,2].

In radiotherapy the new techniques have some difficulties, such as beam dosimetry, geometric characterization and the use of small fields of radiation [3]. In some cases the field sizes are reduced because the lesions are very small, the treatment simulations in the planning have a very important role, in this way, they must be provided with data referring to these small fields. The dosimetry becomes quite complex, since the precision becomes quite questionable, especially when small fields are being used in regions of low density [4,5].

Due to the lack of lateral electronic balance, dose determination in the target volume in small field cases is quite difficult. Another problem for this type of dosimetry is the marked dose gradient at the edges of the field. However, this fact requires that the choice of the radiation detector should be of a relevant size in the dosimetry of small fields [6]. This work aims to study the LiF:Mg,Ti dosimeters performance in the dosimetry of small fields.

Materials and Methods: For this analysis LiF:Mg,Ti dosimeters produced by Harshaw with 3,15 mm side, 0.9 mm thickness and mass of 24,6 mg, previously selected, were used. The irradiation system used was the linear accelerator that belongs to the Instituto do Câncer do Estado de São Paulo (ICESP), with photon energies of 6MV and 9MV and dose range between 1Gy and 25Gy. In addition, for measurements, solid SW water plates of 30x30x1cm³ dimension

were also used. The studied fields sizes were 5x5cm^2, 4x4cm^2 and 2x2cm^2.

Results and Discussion: The dosimeters were selected with sensitivity between ± 3%. The TL response presented non-significant variation. The dose response curves to ^{60}C0 gamma radiation and photon beams of 6 and 9 MV presented a linear behavior in the dose range studied (1Gy to 25Gy). Results obtained in simulated irradiations demonstrated the viability of using LiF:Mg,Ti as dosimeter to the small photon fields.

Conclusion: Dosimetry of small photon fields is an important and rather difficult procedure because the dimensions of the field and the detectors are not sized to facilitate the indicated procedures. LiF:Mg,Ti showed a satisfactory performance for the dosimetry of the studied fields.

Acknowledgments

The authors are thankful for the financial support given by CAPES finance code 001, CNPq, CNEN, granted fellowships and FAPEMIG.

References

1) Morrison,Hood, R., Yin, F. F., Salama, J. K., Kirkpatrick, J., & Adamson, J "Is a single isocenter sufficient for volumetric modulated arc therapy radiosurgery when multiple intracranial metastases are spatially dispersed?." Medical Dosimetry 41.4 (2017): 285-289.
2) Calcina, C. S. G. Características dosimétricas para campos pequenos, visando a implementação de um sistema postal de controle de qualidade na radiocirurgia. Diss. Universidade de São Paulo, 2006.
3) R. Alfonso, P. Andreo, R. Capote, M., et al. A new formalism for reference dosimetry of small and nonstandard fields. Medical Physics vol. 35 (2005).
4) Das, Indra J., George X., et al. Small fields: non-equilibrium radiation dosimetry. Medical physics 35.1 (2008): 206-215.
5) Whyte, Richard I., et al. Stereotactic radiosurgery for lung tumores: preliminary report of a phase I trial. The annals of thoracic surgery 75.4 (2003): 1097-1101.
6) Waligórski, M.P.R. What can solid state detectors do for clinical dosimetry in modern radiotherapy? Radiation protection dosimetry 85. 1-4 (1999): 361-366.

Allium cepa as a biota for natural background radiation levels

Magno N. Xavier[1], Eliane M. D. Maffei[2], Simara S. Campos[2], Roseli F. Gennari[3], Francesco d'Errico[4,5], Susana O. Souza[1*]

[1]*Department of Physics, Federal University of Sergipe, São Cristóvão - SE - Brazil*

[2]*Department of Natural Sciences, Department of Exact and Technological Sciences, State University of Southwest Bahia, Vitória da Conquista - BA - Brazil*

[3]*Institute of Physics, University of São Paulo, São Paulo - SP – Brazil*

[4]*Università di Pisa, Scuola di Ingegneria, Pisa, Italy*

[5]*Yale University, School of Medicine, New Haven, CT USA*

Highlights This work suggests that it is possible to assess the effect of low concentrations of radionuclides in inducing cellular damage using the micronucleus test in *Allium cepa*. Mutations are identified as small nuclei next to the main cellular nucleus making possible the use of *Allium cepa* as a biota for the analysis of radiation effects.

Key words: *Allium cepa*, biota, radio-ecological impact, natural background radiation.

Background and Objectives A field of growing interest in radiation dosimetry is the use of non-human biota, plants, and animals, suitable for the assessment of the radio-ecological impact of events involving radioactivity releases in the environment[1]. Recently, the viability of the method has also been verified to exposures caused in regions of intrinsic radiation background, such as in areas that concentrate on their soil high levels of radionuclides. In contrast to physical methods, the dose itself is not recorded but the effects of the dose at the cellular level are investigated. For this purpose, biological standards that arise after the cells are exposed to the ionizing radiation are evaluated, constituting a biomarker. Among the evaluated standards, we highlight micronuclei, which are the result of mutations, identified as small nuclei next to the main cellular nucleus, but without structural connection with it. When the frequency of damage is statistically higher than the value of the control group, the presence of these structures may indicate a risk factor.

In this work, we investigated the frequency of micronuclei induced by low concentrations of radionuclides causing a radiation background. Our objective was to determine if is possible to use *Allium cepa* as a biota for the assessment of low radiation levels.

Materials and Methods Onion seeds (*Allium cepa*) cultivated in Petri dish were cultivated for 7 days in the presence of different amounts (0.0, 0.25, 0.50, 0.75, and 1.00 g) of a rock containing low levels of radionuclides. Onion cells are utilized as a versatile biomarker since

they report a concordance of 71% to 91.5% with a variety of cytotoxicity tests performed on mammalian cells[2]. The radiometric characterization of the rock was performed by gamma spectrometry. After growing the roots exposed to the radiation backgrounds, spectroscopic analyses in the infrared region were performed to detect changes in the biochemical structure. Damage was evaluated through the micronucleus technique.

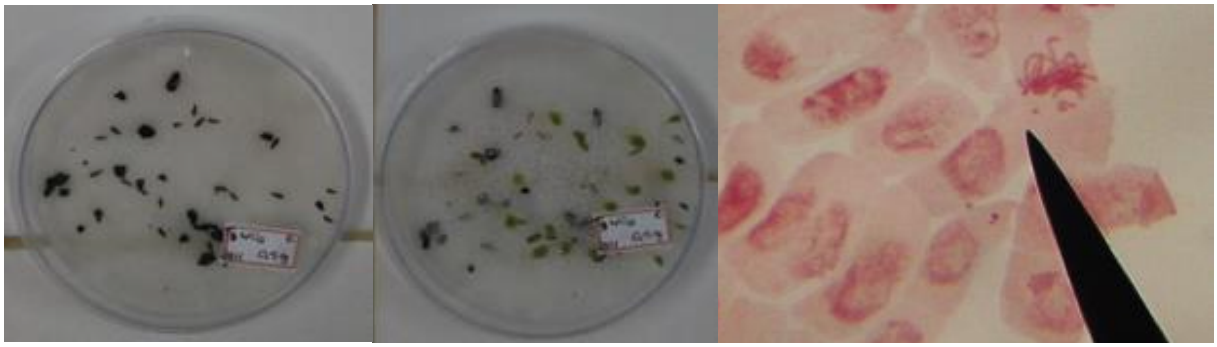

Fig. 1. Procedure for the evaluation of radioinducide micronuclei in the cells.
(1) Seeds sown to germinate, (2) Root growth, (3) Counting micronucleus cells.

Results and Discussion The results of the rock sample experiments indicated activity values consistent with those from regions characterized by low levels of background radioactivity. However, in relation to the control group, all the other samples that were exposed to the rock background radiation presented statistically superior cellular damages. Infrared spectra do not indicate incorporation of uranium or some other element by the onion plant roots.

Conclusion This study demonstrated that it is possible to observe the ability of low concentrations of radionuclides to induce cellular damage in *Allium cepa*, supporting the use of the plants as biota for the analysis of radiation effects.

References

1) Ulanovsky A. Dosimetry for animals and plants: contending with biota diversity. Ann ICRP. 2016;45(1 Suppl):225-38. doi: 10.1177/0146645316630710.
2) Feretti D1, Zerbini I, Zani C, Ceretti E, Moretti M, Monarca S.Allium cepa chromosome aberration and micronucleus tests applied to study genotoxicity of extracts from pesticide-treated vegetables and grapes. Food Addit Contam. 2007 Jun;24(6):561-72.

Three-dimensional measurement of dose distribution of PVA-I radiochromic gel dosimeter using optical CT

Takaoki Takanashi[1]*, Shin-ichiro Hayashi[2]

[1]*3D Gel Dosimeter Research Laboratory, Cluster for Science, Technology and Innovation Hub, RIKEN, Saitama, Japan*

[2]*Faculty of Health Sciences, Hiroshima International University, Hiroshima, Japan*

Highlights The three-dimensional absorbance distribution of the PVA-I radiochromic gel dosimeter irradiated by X-ray using an optical computed tomography apparatus was measured.

Key words PVA-I gel dosimeter, Optical CT

Background and Objectives Research on various gel dosimeters has been conducted as a method of three-dimensional (3D) measurement of radiation[1)]. Because the spin-spin relaxation time of polymer gel dosimeters varies with irradiation, measurement using a magnetic resonance imaging (MRI) is used in general. However, using MRI apparatus at the research site has high barriers in terms of cost and the like. On the other hand, researches have been also conducted to read gel dosimeters using a computed tomography (CT) apparatus using light[2)]. The optical CT (OCT) apparatus measures 3D absorbance and can be used for reading out of not only a polymer gel dosimeter but also a gel dosimeter using coloration of radiochromic agent. In this study, we measured the 3D distribution of absorbance in a polyvinyl alcohol-iodide (PVA-I) gel dosimeter[3)] irradiated by X-ray using an OCT apparatus developed for biological research.

Materials and Methods The gel dosimeter used in this study is composed of a partially saponified PVA (1 wt%), gellan gum (0.4 wt%), potassium iodide (0.1 M), fructose (0.1 M), and water. It was filled in a glass vial (φ18 mm). Irradiation was carried out with 20 Gy at 250 kV and 4.0 mA (1 Gy / min), using industrial X-ray equipment (Rigaku, RadioFlex). After irradiation, immersed in a matching solution (water) and optical CT measurement was carried out at 360 ° 180 projection using continuous spectrum light to obtain a reconstructed image. In addition, after dispensing the same composition sample into the optical cell, irradiating with ^{60}Co, performing 5, 10, 20, 30, 50 and 100 Gy for each, then using an UV-Vis spectrophotometer (UV-1600PC), and the response at the maximum absorption wavelength (λ = 490 nm) was examined. The configuration of the OCT is shown in Fig. 1. Originally the

device was designed for fluorescent mouse brain imaging. A cooled CCD camera that the CCD size is 4/3 inch 16 megapixels (max 4656 x 3522) was used. The depth of field of the telecentric lens (TL) was 11 mm, projection image resolution combined with TL was max 30μm/pixel. Resolution of the rotation mechanism was maximum 0.0025° / pulse. The projection images were reconstructed by filtered back projection (FBP) method on each slice.

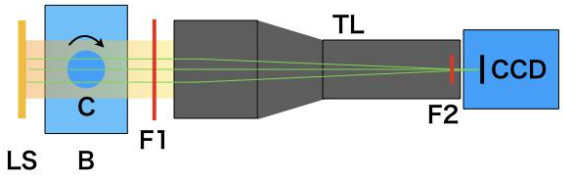

Figure 1. Overview of the OCT including the flat light source (LS), refractive index matching bath (B), rotation stage (C), filters (F1, F2), lens (TL), and CCD camera.

Results and Discussion The dose responses of PVA-I gel measured by spectrophotometer (λ = 490 nm) was linear up to 100 Gy. Fig. 2 shows a sample of a PVA-I gel dosimeter irradiated with X-rays (A), a tomographic image measured using optical CT (B), and a 3D distribution of absorbance prepared by laminating this tomographic image (C). As shown in Fig. 2 (C), the 3D image was acquired, but the irradiated area was not well controlled. Therefore, it is necessary to verify the accuracy of reproduction of dose by other methods (Monte Carlo calculation etc.).

Figure 2. A PVA-I dosimeter irradiated with X-rays in an oblique area (A). Reconstructed tomographic image (B). The 3D image created by stacking the reconstructed tomographic images (C).

Conclusion The change in contrast due to irradiation is disturbed by stray light generated by an obstacle existing in the optical path of a container or a water tank, and it was difficult to obtain a 3D distribution of quantitative absorbance at this stage. In the future, it is required to improve quantitative by changing to a surface light source with reduced diffusion, eliminating stray light such as baffle installation.

Acknowledgment This work is supported by JSPS KAKENHI (Grant Number 17K09072).

References

1) C. Baldock, et al. *Phys. Med. Biol.*, **55** (2010) R1-R63.
2) S.J. Doran and N. Krstajić *J. Phys.: Conf. Ser.*, **56** (2006) 45-57.
3) S. Hayashi et al. *J. Phys.: Conf. Ser.* (in press).

Precise dose calibration method of OSL dosimeter with help of X-ray spectra toward exposure dose evaluation of eye lens

Takashi Asahara[1,2]*, Hiroaki Hayashi[1], Sota Goto[1], Emi Tomita[1], Natsumi Kimoto[1], Takumi Asakawa[1], Kazuki Takegami[1,3], Yuki Kanazawa[4], Tohru Okazaki[5], Takuya Hashizume[5]

[1]*Kanazawa University, Kanazawa, Ishikawa, Japan*

[2]*Okayama University Hospital, Okayama, Okayama, Japan*

[3]*Yamaguchi University Hospital, Ube, Yamaguchi, Japan*

[4]*Tokushima University, Tokushima, Tokushima, Japan*

[5]*Nagase Landauer, Ltd., Tsukuba, Ibaraki, Japan*

Highlights In order to evaluate the exposure dose to the eye lens during clinical X-ray diagnosis, we developed a precise calibration method of an optically stimulated luminescence (OSL) dosimeter. Our procedure took into consideration variations in X-ray spectra and energy dependence of the dosimeter. We present the results of our method using a phantom study.

Key words OSL dosimeter, calibration method, X-ray spectrum, medical dosimetry

Background and objectives The eye lens is a radiation-sensitive organ in which exposure dose needs to be managed, but in a precise sense, the exposure dose to the eye lens can not be directly measured with a personal dosimeter. Here, we focused our attention on the dose evaluation method of the eye lens of an operator during interventional radiology (IVR) using a commercially available small-type OSL dosimeter. This dosimeter can not estimate incident X-ray energy, therefore a calibration factor taking into consideration the energy dependence of the dosimeter should be determined. Recently, we proposed a precise dose calibration method [1]; in this method, a calibration factor for the OSL dosimeter can be determined by the X-ray spectrum and energy dependence of a dosimeter. Figure 1 shows the concept of our method. In this study, we performed a phantom study to apply to our method for a specific situation, in which eye lens exposure dose of medical staff is measured during IVR.

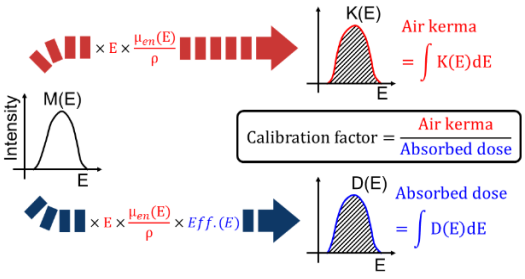

Figure 1 Concept for calibration factor determination method with help of X-ray spectrum.

Materials and methods For determination of the calibration factor of the OSL dosimeter, the X-ray spectrum at the eye lens position of an operator during fluoroscopy was measured with a CdTe spectrometer. In the X-ray irradiation condition, we mimicked a medical X-ray fluoroscopic examination using the IVR equipment installed in a clinic. Using a human dummy and human-equivalent phantom, a phantom experiment was carried out with an exposure time of 30 min and tube voltage of 74 kV. Here, the OSL dosimeters were attached at three dosimetric points around the operator's head: front

side and back side of the protective goggles, and front of the head (eye lens position). In our method to determine proper calibration factors, we needed the X-ray spectra of these dosimetric points. Thus, using the measured X-ray spectrum as an incident beam, we estimated the corresponding three spectra using Monte-Carlo simulation [2]. Protective goggles components were determined by experimentation, and the beam hardening effect caused by the protective goggles and backscattering from head of the operator were considered in this simulation. Then, using the X-ray spectra obtained by the above simulation, we derived the corresponding calibration factors of the OSL dosimeter using the method shown in Fig. 1, and these factors were used to analyze the exposure dose measured with OSL dosimeters.

Results and discussion Figure 2 (a) and (b) show measured and simulated X-ray spectra for dosimetric positions represented in the inset. Figure 2 (c) shows the relationship between the calibration factor of the OSL dosimeter and effective energy of X-ray spectrum. The calibration factor for each dosimetric position varied at values close to the vendor-supplied calibration factor, which was measured with 80 kV X-rays. We found that the vendor-supplied calibration factor can be used for the dose measurement to eye lens without large modifications. In the demonstration, the mean exposure doses to the eye lens without and with the goggles were measured to be 67 μGy and 18 μGy, respectively.

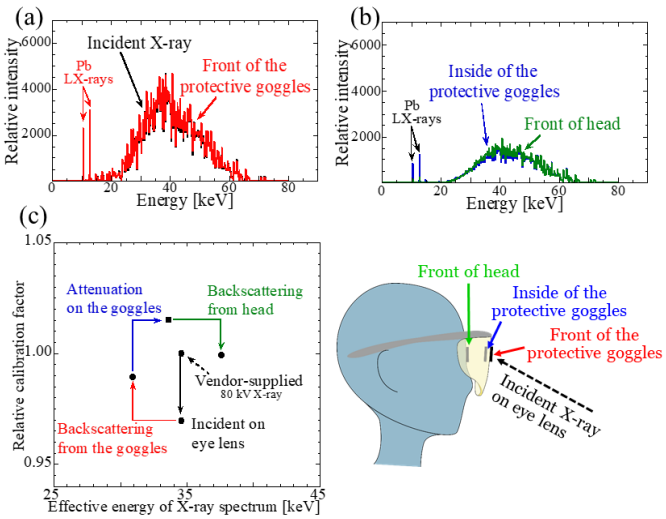

Figure 2 Results to derive calibration factors in the situation represented in the inset. (a) and (b) show measured and simulated X-ray spectra. (c) shows calibration factors as a function of an effective energy of X-ray spectrum.

Conclusion Based on measured and simulated X-ray spectra, calibration factors of an OSL dosimeter were precisely determined. We applied our method to the analysis of a phantom experiment and proved to measure the eye lens doses with OSL dosimeters.

References

1) T. Asahara, H. Hayashi, S. Goto, et al., Exposure dose measurement during diagnostic pediatric X-ray examination using an optically stimulated luminescence (OSL) dosimeter based on precise dose calibration taking into consideration variation of X-ray spectra. Rad. Meas. 119, 2018, 209-219.
2) H. Hirayama, Y. Namito, A. F. Bielajew, et al., The EGS5 code system. SLAC report number: SLAC-R-730, KEK report number: 2005-2008, 2005.

Measurements of neutron dose equivalents during BNCT using fluorescent nuclear track detectors

Takuya Hashizume[1]*, Toshiya Sanami[2], Masayuki Hagiwara[2], Hideaki Monjushiro[2], Taichi Miura[2], Hiroaki Kumada[3], Tohru Okazaki[1], Hiroaki Hayashi[4]

[1]Nagase Landauer, Ltd., Japan, [2]High Energy Accelerator Research Organization, KEK, Japan, [3]Tsukuba University, Japan, [4]Kanazawa University, Japan

Highlights The responses of the FNTD dosimeter to the BNCT neutron beam were measured and simulated. We demonstrated that the FNTD dosimeter can be used as a personal neutron dosimeter during BNCT.

Key words BNCT, FNTD, neutron dose equivalent

Background and Objectives Boron neutron capture therapy (BNCT) is a next-generation cancer therapy based on the nuclear capture reactions between slow neutrons and the boron-10 implanted in tumor cells. During BNCT, exposure of patients not only to the direct neutron beam but also to the neutrons from the outside of the irradiation field should be monitored. To measure neutron dose equivalents outside the irradiation field, foil activation technique of gold or manganese is used. However, this technique requires a complex gamma spectrometer and takes time to get the measurement results. Instead of activation foils, we want to apply a fluorescent nuclear track detector (FNTD [1]) to a passive neutron dosimeter. The FNTD dosimeter with its reader provides a neutron dose automatically and immediately after the irradiation. The responses of the FNTD dosimeter to the BNCT neutron beam have not been reported, and measurable dose range for the neutrons is unclear. In this study, we tested the FNTD dosimeters to measure neutron dose equivalents in a BNCT facility.

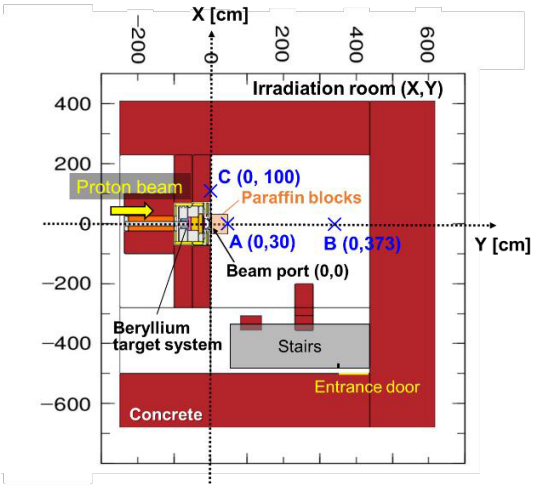

Figure 1. Irradiation arrangements in iBNCT facility

Table 1. Irradiation conditions

Proton energy	7.9 MeV
Irradiateion period	307 s
Beam current	416 mC before the target
Geometry	Paraffin blocks with 30 cm thickness in front of the beam port

Materials and Methods The FNTD dosimeter consists of Al_2O_3:C,Mg single crystals sized 4 × 8 × 0.5 mm^3 and three different converters having 1 mm thickness: high density polyethylene (HDPE) for detecting fast neutrons via (n,p) reactions, Li-glass for detecting slow neutrons via $^6Li(n,\alpha)^3H$ reactions, and Teflon® for evaluating background-tracks. Irradiation with the BNCT neutron beam was performed in the iBNCT (Inaraki BNCT)

facility at Tokai in Japan [2]. Figure 1 shows the irradiation arrangements. In the irradiation room, the FNTD dosimeters were placed at three different positions: 30 and 373 cm on the beam axis, and 100 cm sideways from the beam port (A, B, and C in Figure 1, respectively). In front of the beam port, paraffin blocks with 30 cm thickness were placed to mimic the patient head. Irradiation conditions are summarized in Table 1. After the irradiation, the FNTDs were scanned on 1.08 mm^2 areas at 2 μm depth by an automatic reader (FXR-700N [1]), which has a confocal laser microscopy system, to obtain fluorescence images of neutron-induced charged particle tracks. Then, track densities (*TD*s) [mm^{-2}] corresponding to the three converter areas were evaluated by processing the fluorescence images. In addition, neutron spectra at the three positions were calculated by Monte Carlo simulation code, PHITS (ver. 3.02) to obtain neutron dose equivalents ($H_p(10)$). Using the neutron spectra with the PHITS code, the following dosimetric responses were estimated: the densities, angular distributions, and energy distributions of the neutron-induced tracks. Calibration factors (*CF*s) [mm^{-2} mSv^{-1}] were calculated by dividing the *TD*s with the neutron dose equivalents.

Results and Discussion In Table 2, the measured *TD*s corresponding to the HDPE and Li-glass converter areas (TD_{HDPE} and TD_{Li}) were presented. The background-*TD*s at the Teflon® converter areas were subtracted to calculate TD_{HDPE} and TD_{Li}. Although significant values for TD_{HDPE} was not obtained at any irradiation positions, those for TD_{Li} (77.34~132.11 [mm^{-2}]) were adequately obtained at the all positions. In addition, the rates of calculated track densities (TD'_{Li}/TD'_{HDPE} in Table 2) indicated that tracks were more frequently detected with the Li-glass converters than with the HDPE converters. These results suggest that dose equivalents of the epithermal neutrons for BNCT can be measured with the TD_{Li} values. The *CF*s for the TD_{Li} were 8.03~13.41 [mm^{-2} mSv^{-1}]. Therefore, the *CF* around 10 [mm^{-2} mSv^{-1}] is suitable for neutron dosimetry in this irradiation condition during BNCT.

Conclusion The FNTD dosimeters were tested to measure neutron dose equivalents in the iBNCT facility with help of the Monte Carlo simulation. We demonstrated that the FNTD dosimeter is available for neutron dose measurement during BNCT.

References 1) M. Akselrod et al., Radiat. Prot. Dosim. 161, 86-91 (2014)
2) H. Kumada et al., Plasma Fusion Res. 13, 2406006 (2018)

Table 2. Summary of analyzed data

ID	Position (X,Y)	$H_p(10)$ [mSv]	Measured Track Density (*TD*) [mm^{-2}]		Rate of Calculated Track Density (*TD'*) TD'_{HDPE} : TD'_{Li}	Correction Factor for Li-glass (CF_{Li}) [mm^{-2} mSv^{-1}]
			HDPE (TD_{HDPE})	Li-glass (TD_{Li})		
A	(0,30)	7.61	-8.12 ± 7.00	102.07 ± 10.37	1 : 129	13.41
B	(0,373)	9.63	-0.34 ± 6.01	77.34 ± 8.68	1 : 71	8.03
C	(100,0)	10.47	-4.27 ± 7.35	132.11 ± 11.09	1 : 302	12.62

Measurement of Peripheral out of field dose in High Energy External Electron beam using Gafchromic film

Verma TR[1*], Painuly NK[1], Arun A[1], Adarsh P. P[1]., Gupta R[1], Bhatt MLB[1]
[1]King George's Medical University; UP, Lucknow INDIA
Corresponding Author: teerth05kashi@gmail.com

High lights:

Besides limited range of penetration, electron beam has been questioned for scattered and transmission radiation out of treatment field. This contribute considerable amount of radiation dose to unintended normal tissue. In the present study, Out of filed (OOF) doses showed a trend of decrease with increase in applicators size and electron energy.

Key words:
Electron beam, Scattered dose, Gafchromic film measurement

Background and Objective:
Electron beam radiotherapy is advantageous for superficial cancers because of rapid dose falloff. The applicators are used to reduce as much as possible the escaping of scattered and transmission electrons outside of the intended area. In the present study, peripheral dose outside the electron applicators was measured using Gafchromic film for different field size applicators and energies.

Materials and Methods:
Before the actual measurements, basic data e.g. beam profile, PDD, Dmax etc. of linear accelerator having electron energies 4 MeV, 6 MeV, 8 Mev , 12 MeV, 15 Mev, 18 MeV with applicator size of 6 cm X cm, 10 cm x cm, 14 cm x cm was measured using the Radiation Field Anayliser. Standard Quality assurance test of the LINAC was performed and ensured that all the parameters are under tolerance. In this study, Gafchromic EBT3 film was used for the measurement of the dose. Firstly calibration of the Gafchromic film with dose was done by exposing the gafchromic films of dimension 5x5 cm^2 for doses ranging from 0-8 Gy keeping the gantry angle 0^0. One by one, these films were sandwiched between the PMMA solid water slab phantoms ensuring the thickness of the slabs (anteriorly) equal to the Dmax of the corresponding electron beam.
Slab phantom of dimension 40x40x15 cm^3 maintaining SSD 100 cm was created over the couch. Again, to measure the OOF doses, Gafchromic films of dimension 8x8 cm^2, 12x12 cm^2, 16x16 cm^2 was placed (at SSD=100) during the delivery of 2 Gy using the applicators of size 6x6 cm^2, 10x10 cm^2, 14x14 cm^2 as shown in the Figure (1). This fractionation scheme was chosen to mimic the real patient treatment scenario in which 10 Gy at the rate of 2 Gy per fraction is delivered. The dose evaluation was done using "ImageJ" software.

Results and Discussion:
A bar graph was plotted for dose recorded Vs distance (cm) of these points (i.e. 0.2, 0.4, 0.6, 0.8, 1, 1.2, 1.4 cm away from the field edge) at all the four side of exposed films Figure (2). Highest dose variation was recorded for the 6 MeV beam with applicator size 10 cm^2 ranging from 1.25

Gy at 0.2 cm to 0.52 Gy at a distance of 1.4 cm. Also, the variation in doses for the equidistance points from the field edge (in 90^0, 270^0 towards gantry and out of gantry directions) of same applicator were recorded with maximum variation at 0.2 cm points followed by 0.4 cm points. In this experiment, out-of-field (OOF) dose was recorded at SSD plane only. Alabdoaburas et al. measured OOF doses at 1 cm depth and off-axis distances for different field and electron energies. Electron beam is known for its rapid dose fall-off; however care should be taken as it can cause deleterious effects at very radiation sensitive nearby organs such as lens of the eye. It is now well known that the subcapsular lens epithelium, particularly where it differentiates to lens fibers, is very susceptible to radiation damage. While the current guidelines for the threshold dose to cataract formation ranges from 2-5Gy, recent studies indicate that the dose could be more than 0.5Gy.

Figure (1): experimental Setup showing

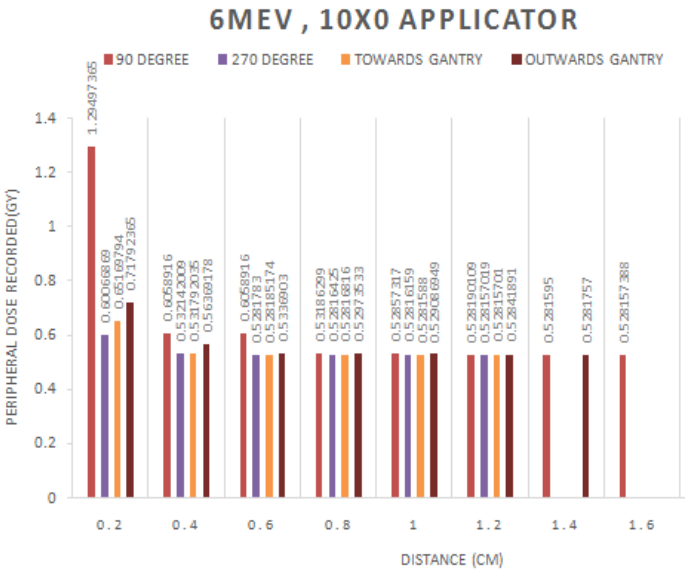

Figure (2): Dose Vs distance of the dose point

Conclusion:

In the present study, authors measured the out of field peripheral dose at the surface. A significant OOF dose was recorded which showed a trend of decrease with increase in applicator size and electron energy. These results can be used in day to day electron beam therapy. Also these results can be used to predict the radiation induced cancer because of radiation dose to normal tissue due to peripheral dose.

References:

- Mohamad M. Alabdoaburas, Jean-Pierre Mege, Jean Chavaudra, Jérémi Vũ Bezin, Attila Veres, Florent de Vathaire, Dimitri Lefkopoulos, Ibrahima Diallo J Appl Clin Med Phys. 2015 Nov; 16(6): 435–448. Published online 2015 Nov 8. doi: 10.1120/jacmp.v16i6.5616
- AAPM TG 158: Measurement and calculation of doses outside the treated volume from external-beam radiation therapy

The Research of IMRT, VMAT, Partial Arc, and Hybrid (3DCRT/IMRT) Techniques for Right Breast Cancer Radiotherapy and Optimization

Y.C. Liu [1,2], C.C. Lu [3]*, H.H. Lin [4,5], J.P. Lin [6], L.H. Lai [6]

[1]*Institute of Nuclear Engineering and Science, National Tsing Hua University, Hsinchu, Taiwan*

[2]*Department of Radiation Oncology, Wei Gong Memorial Hospital, Miaoli, Taiwan*

[3]*Department of Biomedical Engineering and Environmental Sciences, National Tsing Hua University, Hsinchu, Taiwan*

[4]*Medical Physics Research Center, Institute for Radiological Research, Chang Gung University/Chang Gung Memorial Hospital, Taoyuan, Taiwan*

[5]*Department of Radiation Oncology, Chang Gung Memorial Hospital, TaoYuan, Taiwan*

[6]*Department of Medical Imaging and Radiological Technology, Yuanpei University of Medical Technology, Hsinchu, Taiwan*

Highlights: The research about right side breast cancer is studied. VMAT double arc design enhances dose homogeneity and conformality. Partial arc angle design reduces lung overlapped-irradiation area. 70% 3DCRT with 30% IMRT is optimized in dose calculation.

Keywords: VMAT, IMRT, HI, CI, ICRP

Background and Objectives: The purpose of research is to use different breast cancer radiation therapy treatment planning to compare and estimate the optimization, whole body effective dose, and critical organ absorbed dose. The four planning are volumetric modulated arc therapy (VMAT), Partial arc, Hybrid (3DCRT/IMRT), and intensity-modulated radiation therapy (IMRT).

Materials and Methods: The optically stimulated luminescent dosimeter (OSLD) is placed in the Rando-phantom, the organs of absorbed dose can be estimated. Each planning comes with 50.4Gy prescription total dose, and treat critical organ including lung and heart. Dose-Volume histogram (DVH) will be used to show the PTV (V95%), homogeneity index (HI), conformal index (CI), and others of optimized index. The estimation of whole body effective dose uses ICRP 60, ICRP 103 Publication.

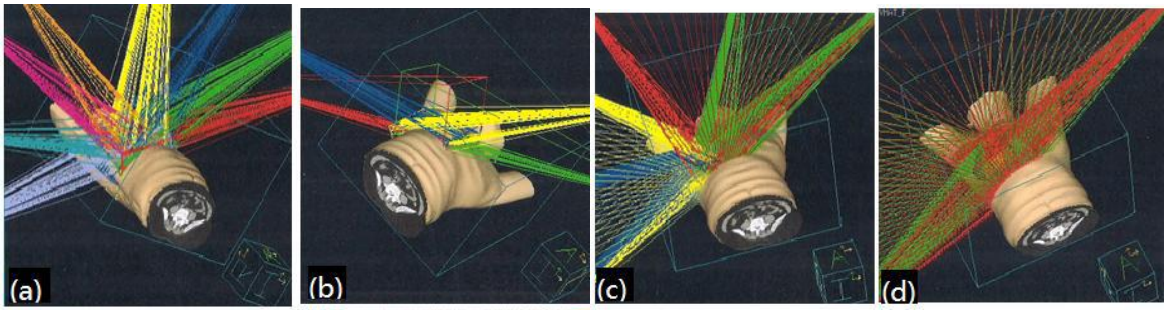

Figure 1. (a)Pure IMRT (b)Hybrid (c)Partial arc (d)VMAT

Table 2. Comparison of parameters for 4 different treatment techniques

Machine parameters	VMAT	Partial Arc	Hybrid (3DCRT/ IMRT)	Pure IMRT
calculation mode	smart Arc	smart Arc	DMPO	DMPO
max number of segment	40	40	25	25
Gantry Angle	Beam 1: 55±10°-235±10° Beam 2: 235±10° -55±10°	Beam 1: 55±10°-335±10° Beam 2: 275±10°-235±10° Beam 3: 235±10°-315±10° Beam 4: 15±10°-55±10°	Beam 1: 3D- 235±10 ° Beam 2: 3D-55±10 ° Beam 3: IMRT-250±10° Beam 4: IMRT-35°	Beam 1: 56° Beam 2: 37° Beam 3: 7° Beam 4: 333° Beam 5: 284° Beam 6: 257° Beam 7: 229° Beam 8: 295°
Collimator Angle	10°	10°	3D:10° 3D:350°	×
Wedge	×	×	×	×
Delivery Time(sec)	234±15	146±11	245±20	300±35
Delivery MU	687±15	519.4±17	319.1±19	427.1±25

Results and Discussion: The result is as followings: the best conformal index (CI) and homogeneity index (HI) are VMAT and Partial arc. The heart absorbed dose (V5%) is lower than 0.07±0.01, VMAT and Hybrid (V10%) are 0%. The mean heart dose lowest is Hybrid1 47Gy±0.02.The dose of left contralateral lung (V5%), the lowest is VMAT (0%). The right ipsilateral lung average dose and V20% are the lowest of VMAT. The left contralateral breast mean dose is about 2Gy. The delivery time, the fastest is Partial arc (146secs), and the slowest is Hybrid (245secs). The Delivery monitor unit (MU), the highest is VMAT (687 MU). The whole body effective dose, for ICRP-60, the highest is 2.01Sv±0.23 (VMAT); for ICRP-103, the highest is 2.89 Sv±0.15 (VMAT). The VMAT lens and skin dose is highest because VMAT belongs to dynamic arc therapy, larger area of low dose scattering is induced by continuous rotation.

Conclusion: To meet both hospital and patient's need, the treatment planning should be designed with consideration of patient's real condition.

Development of an optical fiber type small-size dosimeter for monitoring the dose in the urethra during the carbon ion radiotherapy

Yuho Hirata[1]*, Atsushi Yamazaki[1], Kenichi Watanabe[1], Sachiko Yoshihashi[1], Akira Uritani[1],
Yusuke Koba[2], Naruhiro Matsufuji[2],
Takumi Kato[3], Noriaki Kawaguchi[3], Takayuki Yanagida[3]
[1]*Nagoya University, Aichi, Japan*
[2]*QST, Chiba, Japan*
[3]*NAIST, Nara, Japan*

Highlights The direct dosimetry near the affected region is necessary for safety radiotherapy. For this purpose, we are developing a small-size dosimeter using radiation-induced phosphor and an optical fiber. In this paper, we conducted test experiments assuming that the small size dosimeter is inserted into the urethra.

Key words optical fiber, OSL, carbon ion radiotherapy

Background and Objectives Carbon ion radiotherapy has been applied to treatment of prostate cancer. Since urethra passes through the inside of the prostate, it is desirable to reduce the dose of the urethra when irradiating with the carbon ions. A small-size dosimeter inserted in the urethra makes it possible to directly confirm that the dose to the urethra has been reduced to a safe level. For this purpose, we are developing a small-size dosimeter using radiation-induced phosphor and an optical fiber. In this paper, we fabricated the optical fiber type small size dosimeter and conducted test experiments assuming that the small size dosimeter was inserted into the urethra.

Materials and Methods We fabricated the small-size dosimeter which is adhered a radiation-induced phosphor on a tip of an optical fiber (core dia.: 400 μm). The carbon ions with energy of 350 MeV/u were irradiated to the dosimeters at Heavy Ion Medical Accelerator in Chiba (HIMAC). An ion chamber and the small-size dosimeter were installed in the water. Spread-out Bragg peak (SOBP) was formed by combining the Bragg peaks of different depths in the water. In order to simulate the dose reduction in the urethra, the dose of SOBP was partly reduced. The dose distribution around the virtual urethra position was measured by changing the position of the ion chamber and the small-size dosimeter.

Results and Discussion Figure 1 shows the distribution of the dosimeter responses around the virtual urethra measured with the small-size dosimeter using Eu:BaFBr and Ce:CaF_2. The dose reduction at the virtual urethra position (depth: 85mm) was measured by both of the ion

chamber and the small-size dosimeters. However, the response change of the small-size dosimeters were small compared with the response of the ion chamber. The sensitivity of the small-size dosimeter using the radiation-induced phosphor deteriorates in the high linear energy transfer (LET) region[1]. The dose at the virtual urethral position has been reduced by excluding the carbon ions having the Bragg peak at this position. Since the dose changed with the LET component at the reduced dose region, the response sensitivity of the phosphor deteriorated.

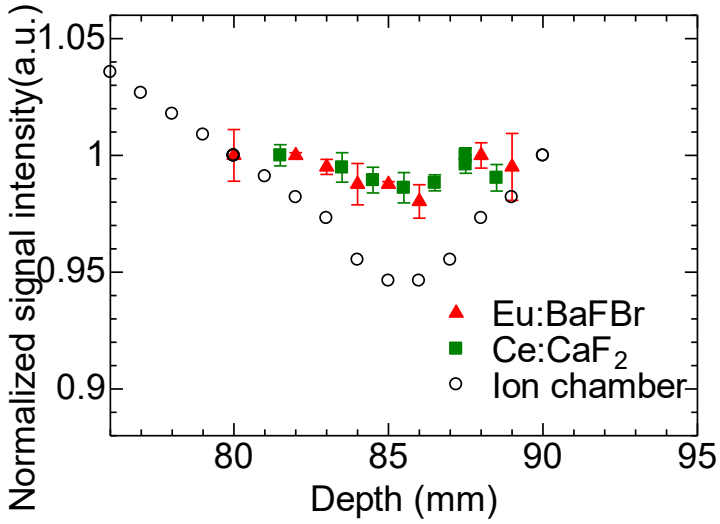

Figure 1 The SOBP around the virtual urethra measured with the ion chamber and the small-size dosimeters.

Conclusion We are developing a small-size dosimeter using the radiation-induced phosphor and the optical fiber for monitoring the dose in the urethra during carbon ion radiotherapy. We conducted the test experiments of the small-size dosimeter by forming SOBP in the water taking into account the reduction of the dose in the urethra. The small size dosimeter could measure the dose reduction in the urethra, but the reduction response was smaller compared with the ion chamber. As future works, we will improve the measurement method to clearly measure the dose change.

References

1) Y. Hirata, *et. al.*, Correction of quenching effect of a small size OSL dosimeter using Eu:BaFBr and Ce:CaF2, Radiat. Meas. (2017). doi:10.1016/j.radmeas.2017.03.043

Colloid-like centers in α-$Al_2O_{3-δ}$, their formation, annealing and effects on luminescence properties

Alexander Surdo[1,2*], Igor Milman[1,2], Rinat Abashev[1,2]
[1]*Institute of Metal Physics UB RAS, Ekaterinburg, Russia*
[2]*Department of Experimental Physics, Ural Federal University, Ekaterinburg, Russia*

Highlights Colloid-like centers in anion-deficient corundum crystals (α-$Al_2O_{3-\delta}$) are formed most efficiently under thermo-optical treatment (TOT) if the F center concentration (C_F) is 10^{17} cm^{-3}, temperature (T_{TOT}) is 1200 K, photon energy ($h\nu_{TOT}$) is 4.0-4.2 eV and supplied optical energy density (W_{TOT}) is 50 - 150 J/cm^2.

Key words thermo-optical treatment of α-$Al_2O_{3-\delta}$, formation and thermostability of colloid-like centers, optical absorption, thermo- and optically simulated luminescence

Background and Objectives It was shown in [1)] that the TOT of α-$Al_2O_{3-\delta}$ crystals with C_F=10^{17} cm^{-3} at T_{TOT}=1120 K, $h\nu_{TOT}$=3.6-4.8 eV and 10 J/cm^2 ≤ W_{TOT} ≤ 20 J/cm^2 effectively turns simple anion-vacancy F type centers into complex divacancy and interstitial centers of F_2 and Al_i types (Figure 1, curves 1-2). Where such conditions are not met, the efficiency of complex center production reduces. The objective of the study was therefore to investigate the TOT effect systematically over a broad range of W_{TOT}, T_{TOT} and C_F with reference to the luminescent and optical properties of α-$Al_2O_{3-\delta}$ crystals.

Materials and Methods As objects of the study, we chose α-$Al_2O_{3-\delta}$ crystals with C_F in the range of 10^{16}-10^{17} cm^{-3}. TOT was performed in the temperature range T_{TOT}=1120-1400 K. Irradiation with ultraviolet light was done using an optical system based on the mercury lamp «DRT-240» under a supplied energy density in the range of W_{TOT}=20-180 J/cm^2. Optical absorption (OA) spectra were examined using a Cary 60 spectrophotometer.

Results and Discussion If we increase W_{TOT} from 30 to 180 J/cm^2 at T_{TOT}=1120 K, centers of not only F type but also F_2 and Al_i types start to disappear (Figure 1, curves 3-4). The OA spectra then show a wide structureless band with a peak at $h\nu_m$=5.3 eV and FWHM=1.0 eV, whose intensity increases with W_{TOT}. At the same time, we can observe a decrease in the intensity of photoluminescence (PL) from F, Al_i and F_2 centers as well as in the thermal luminescence (TL) yield in the main peak at 450 K and in the response of optically simulated luminescence (OSL). For W_{TOT}=150 J/cm^2, the above values decrease more than 1000 times

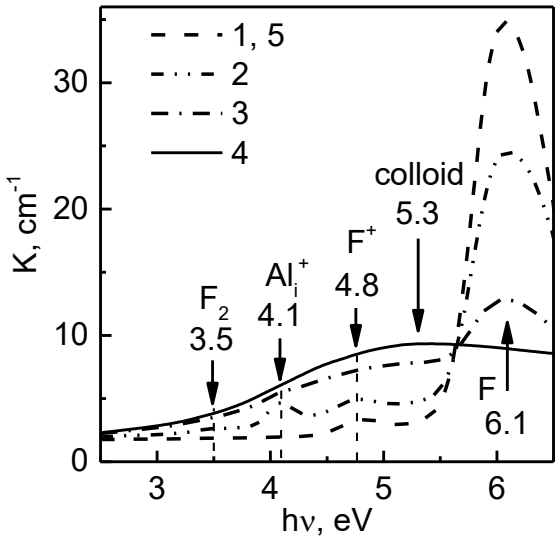

Figure 1. Optical absorption spectra of an α-$Al_2O_{3-\delta}$ sample before (1) and after TOT at T_{TOT}=1120 K under varying W_{TOT}: 15 J/cm^2 (2), 45 J/cm^2 (3), 150 J/cm^2 (4) and subsequent annealing at 1370 K (5)

compared with those in the original samples. For establishing the nature of the defects responsible for the wide OA band, we studied in detail the temperature dependence of its FWHM(T) and $h\nu_m$(T) peak position and the polarization relationships. It has been established that $h\nu_m$ and FWHM do not change in the temperature range of 300-700 K. Nor have we discovered differences in the absorption intensity depending on the crystal's optical axis relative to the plane of polarization of the incident light. Additionally we have studied the efficiency of center transformation under TOT depending on T_{TOT}. It was found that growth in the T_{TOT} and W_{TOT} decreased the value of $h\nu_m$ but insignificantly.

According to [2], all these data together may point to the formation of colloid-like centers in TOT-treated α-$Al_2O_{3-\delta}$ crystals under these parameters similar to those forming in alkali-haloid crystals (AHC) under TOT. Moreover, in contrast to AHC, the annealing of TOT-treated α-$Al_2O_{3-\delta}$ crystals in air at 1300-1400 K restores their original defect structure and optical absorption (Figure 1, curve 5) and luminescent properties. Thus, the concentration and PL response of F centers become similar to such before TOT. At the same time, the OSL yield and the TL yield in the main peak at 450 K recover to the original values.

Conclusion The results of the study open up broad perspectives for modification of TL and OSL properties of α-$Al_2O_{3-\delta}$-based detectors, for example, for developing TLD-500 detectors with a thin (5-25 mg/cm^2) sensitive layer for skin and eye dosimetry. Crystals of α-$Al_2O_{3-\delta}$ with colloid-like centers could be used for creating materials with a gradient change and/or alternation of optical and luminescent properties.

References

1) Surdo A.I., Abashev R.M., Milman I.I., Ivanov V.Yu., 2019. Non-radiation creation of complex centers in wide-gap oxide crystals. Radiat. Meas. (in press)
2) Schwartz K.K., Ekmanis Yu.A., 1989. Dielectric materials: Radiation processes and radiation resistance. Riga, Zinatne. 187 p.

Luminescence of carbon-related centers in irradiated powders of hexagonal boron nitride

A.S. Vokhmintsev, I.A. Weinstein, M.G. Minin, S.A. Shalyakin
NANOTECH Centre, Ural Federal University, Mira street, 19, Ekaterinburg, Russia

Highlights The effects of h-BN micro- and nanopowders high temperature treatment in carbon crucible (1273 – 1873 K) on luminescent properties were studied by the means of photoluminescence (PL) and spectrally resolved thermally stimulated luminescence (TSL) techniques. Energy and kinetic characteristics of TSL processes, activated in the 300 – 873 K temperature range, were studied in the frame of general order kinetics. It was shown that the increase of C_N-centers concentration (carbon atom in the position of nitrogen atom) leads to the raise of 330-nm PL intensity and of high-temperature TSL response at 380-nm band.

Key words spectrally resolved thermoluminescence, h-BN, UV excitation, carbon-related defects, trap, activation energy, general kinetics order

Background and Objectives Hexagonal boron nitride (h-BN) or "white graphite" possesses the set of unique electrophysical characteristics, what makes it a prospective material for optoelectronics, nanophotonics and luminescent dosimetry of ionizing radiation [1]. It is known that carbon is considered to be the main technological impurity in h-BN and can replace regular positions of atoms in the boron and nitrogen sublattice forming the systems of electron and hole levels within the energy gap correspondingly. It is known that traps in h-BN also act as a recombination centers and, to the large extent, determine its emission and dosimetric properties [2, 3]. The goal of the present work is to investigate luminescent properties of irradiated micro- and nanostructured powders of hexagonal boron nitride in as-grown state and after the high-temperature vacuum treatment in the carbon crucible.

Materials and Methods Samples studied in the present work were hexagonal boron nitride micro- (h-BNmicro) and nanopowders (h-BNnano). h-BNmicro sample ("UNICHIM & OP", Russia) demonstrated flake-like morphology with the average particle size 7 ± 3 um and concentration of major impurities of C and O $\leq$ 2 wt.%. h-BNnano sample (Hongwu International Group Ltd., Hong Kong, China) possessed 99.8 % of h-BN particles with 80 – 100 nm size and concentration of C and O $\leq$ 0.5 wt.%. Studied h-BN powders were placed in the carbon crucible and treated in the vacuum furnace under the temperatures T_A = 1273, 1473, 1673 and 1873 K for two hours. Pressure in the furnace chamber was $1.3 \cdot 10^{-2}$ Pa. PL and

spectrally resolved TSL studies were performed using Perkin Elmer LS55 luminescent spectrometer with the high-temperature accessory [4]. PL spectra were analyzed in the 290 – 650 nm range under 210-nm excitation. For the TSL excitation the samples were preliminarily exposed to the monochromatic UV radiation in 210 nm band. TSL emission spectra were recorded in 300 – 600 nm range with 1200 nm/min speed. TL glow curves were measured in 330, 380 and 425 nm bands and 2 K/s rate and analyzed in the frame of general order kinetics.

Results and Discussion PL studies showed that the as-grown samples demonstrated a wide luminescence band within 350 – 500 nm region with ≈420 nm maximum and less intense short-wavelength shoulder at ≈330 nm. For the as-grown h-BNmicro and h-BNnano samples a luminescence at ≈380 nm and ≈425 nm was dominating in the TSL spectrum and was characterized by high- (550 – 600 K) and low-temperature (300 – 350 K) peaks correspondingly. It was found that the PL intensity at ≈330 nm increased and the PL intensity at ≈420 nm band decreased with the elevation of T_A values. At the same time, as a result of the thermal treatment, the TSL response increased for the high-temperature peak in 600 – 750 K range. The values for activation energy of E_a = 1.2 – 1.5 eV and kinetics order of b = 1.0 – 1.2 were calculated for the thermally stimulated processes in all the studied bands.

Conclusion Findings have been discussed using the analysis based on the experimental data of PL and TSL spectroscopy in comparison to the independent studies. It has been concluded that the increase of PL intensity in ≈330 nm band and high-temperature TSL peak in ≈380 nm band in h-BN samples, annealed under the vacuum in the presence of carbon, were caused by the increment of hole C_N-centers concentration.

References

1) Vokhmintsev, A.S., Minin, M.G., Weinstein, I.A., 2016. Application of hexagonal boron nitride micropowder for thermoluminescent dosimetry of UV radiation. Radiation Measurements 90, 205–209.
2) Vokhmintsev, A.S., Minin, M.G., Weinstein, I.A., 2017. Estimation of thermoluminescence kinetic parameters in h-BN by different techniques. Radiation Measurements 106, 55–60.
3) Vokhmintsev, A., Weinstein, I., Zamyatin, D. 2019. Electron-phonon interactions in subband excited photoluminescence of hexagonal boron nitride. J. Lumin. 208, 363 –370.
4) Vokhmintsev, A.S., Minin, M.G., Henaish, A.M.A., Weinstein, I.A., 2015. Spectrally resolved thermoluminescence measurements in fluorescence spectrometer. Measurement. 66, 90–94.

Correlation of individual components observed in TM-OSL measurements with components known from LM-OSL measurements

Alicja Chruścińska[1]*, Grzegorz Adamiec[2], Piotr Palczewski[1]

[1] *Institute of Physics, Faculty of Physics, Astronomy and Informatics, Nicolaus Copernicus University, Grudziadzka 5/7, 87-100 Torun, Poland*

[2]*Institute of Physics CSE, Silesian University of Technology, ul. Konarskiego 22B, 44-100, Gliwice, Poland*

Components of OSL signal in quartz separated by TM-OSL method
Trap parameters obtained by isothermal measurements for individual OSL components
Correlation of traps active in LM-OSL and TM-OSL processes

optically stimulated luminescence, TM-OSL method, trap parameters, quartz

Quartz is a basic natural dosimetric material. Its thermoluminescence (TL) and optically stimulated luminescence (OSL) are extensively used in retrospective dosimetry[1)], dating[2)] and, recently, in thermochronometry[3)]. Identification of the traps responsible for the luminescence has been attempted for a long time but there are still many unknowns. Trap identification is fundamental to understand the signals recorded in different applications for them results to be reliable. This is particularly relevant when the values of trap parameters are directly used in calculations as e.g. in thermochronometry. The methods of OSL applied routinely use light with a constant stimulation energy (continuous wave OSL – CW-OSL) or linearly increasing flux of stimulation photons (linearly modulated OSL – LM-OSL). During such stimulation it proves difficult to separate the signals originating from different traps as the only parameter differentiating individual traps active in the given experiment are their optical cross-sections which depend on experimental conditions such as the stimulating photon length or temperature. Recently, it has been shown that new information about traps can be obtained by increasing the sample temperature during optical stimulation with a constant stimulation energy[4)], enabled by thermally modulated OSL (TM-OSL). This can be implemented in standard OSL readers. This method allows direct estimation of optical trap depth and parameters describing the strength of electron-phonon coupling in the electron transition from the trap to the conduction band. By this kind of stimulation one can reach very deep traps that are not detectable by TL measurements below 500°C. The resolution of the OSL signal from different traps is remarkable. When the experimental parameters are properly selected one can detect the OSL signal from a single kind of trap. This has been recently demonstrated for

quartz[5]. Depending on the sample, three or four components were separated using the TM-OSL method with stimulation light wavelengths 620 nm, 540 nm and 450 nm. The individual components of OSL in quartz were previously investigated by the LM-OSL method[6] and at least six components were resolved when blue light was used for stimulation. In the current work, the components observed in TM-OSL measurements are correlated with those from LM-OSL. Two methods are used: isothermal holding of the samples at different temperatures and the cleaning out of faster OSL components by TM-OSL before the LM-OSL measurements, which results in removing defined peaks from the LM-OSL curve. From the isothermal experiments, the trap depths and the frequency factors are obtained by analysing the lifetimes for different holding temperatures. Such analysis is performed for each component of the LM-OSL curve and also for each TM-OSL component measured for given stimulation energy measured after defined isothermal holding time. In such experiments an advantage of the TM-OSL method over the LM-OSL is clear. The decomposition of LM-OSL curve into components requires the assumption concerning the kinetics of the OSL process related to an individual trap, and the most reasonable for quartz is first order. This approximation, however, is valid in the case of negligible trap competition and for high levels of trap filling. Both conditions cannot be considered as fulfilled especially for longer times of isothermal holding. This leads to the appearance of a larger number of LM-OSL (or CW-OSL) components needed for acceptable result of fitting, which is further complicated by the problems with fitting multiple components to OSL curves[7,8]. In turn, the TM-OSL method relies on measuring the individual components independently, so the intensity of a given component is established experimentally. The correlation of the TM-OSL and LM-OSL components is performed for three sediment quartz samples of a different characteristics.

Acknowledgements

This work has been financed by the grant of the National Science Centre, Poland, No. 2016/21/B/ST10/01867.

References

1) I.K. Bailiff, S. Sholom, S.W.S. McKeever, Radiat. Meas. 94 (2016), 83-139.
2) A.G. Wintle, G. Adamiec, Radiat. Meas. 98 (2017), 10-33.
3) G. King et al., Chem. Geol. 446, (2016), 3-17.
4) A. Chruścińska & N. Kijek, J. Lum. 174, (2016), 42-48.
5) P. Palczewski & A. Chruścińska, Radiat. Meas. 121 (2019), 32-36.
6) J.S. Singarayer, R.M. Bailey, Radiat. Meas. 37 (2003), 451–45.
7) G. Adamiec, Radiat. Meas. 39 (2005), 63-75.
8) Bluszcz, A. and Adamiec G., Radiat Meas. 41 (2006), 886-891

HfO_2 nanocrystals synthetized by precipitation method: morphological and luminescent properties

Alvaro de Farias Soares[1]*, Sonia Hatsue Tatumi [1,2], René R. Rocca[2], Lilia C. Courrol[2]
[1]*Polytechnic School, University of São Paulo, São Paulo, Brazil*
[2]*Federal University of São Paulo, São Paulo, Brazil*

Highlights Hafnium oxide (HfO_2) nanocrystals were successful obtained by precipitation method, with crystallite size of the 25 nm and monoclinic structure. This material showed high TL and OSL response for β and UV irradiations.

Key words nanocrystal, dosimetry, TL, OSL, beta and UV irradiation

Background and Objectives Several luminescence materials are investigated for dosimetry applications, however, only few phosphorus can be applied to UV radiation dosimetry. HfO_2 doped with rare-earth in different structures had been studied, however, there are few works for pure HfO_2 [1], and studies with OSL emissions are scarce. Therefore, the present work studied the morphological and luminescent properties (TL, OSL and PL) of HfO_2, and using β and UV irradiations.

Materials and Methods HfO_2 nanocrystals were synthetized by precipitation method. For morphological analysis of the crystalline structure, X-ray diffraction (XRD) measurements were made with RigakuD'Max 2500PC spectrometer with Cu K_α radiation, in the range of 15-75°. The morphological and composition were obtained with a JSM-6610LV model microscope of the JEOL, coupled with EDS. The crystallite size analysis was performed using the Scherrer equation [2]. In the luminescent analyzes, PL measurements were obtained using a Fluorolog 3 Fluorimeter. TL and OSL emissions were carried out using a RISØ TL/OSL model DA-20 reader, BG-39 optical filter for TL and U340 optical filter for OSL, with β source $^{90}Sr/^{90}Y$ (40 mCi). UV medical lamps were used (UVA Osram 9W, NB-UVB LightTech 9W) and germicide lamp (UVC Osram 9 W). The TL and OSL emissions were theoretically fitted with computerized glow curves deconvolution (CGCD) using general order kinetic [3].

Results and Discussion XRD results prove the crystallinity of the HfO_2 with monoclinic crystalline structure, spatial group P21/c, reference code 01-078-0050 and phosphor name Baddeleyite. The nanoscale was attested by the size of the crystallite, using the Scherrer equation [2] it was found 25.02 ± 0.02 nm, SEM images corroborate with this, and the EDS

proved the purity of the samples (5.8 and 94.2 wt.%. of O and Hf, respectively). In PL, the emission spectrum (λ_{exc} = 300 nm) showed a broad band between 350-550 nm and a peak at 468 nm, which explains the emission in the visible region in TL. The excitation spectrum (λ_{em} = 468 nm) showed that there are at least 4 peaks promoting this emission at 291, 344, 378 and 427 nm. Upon excitation at 254 nm (UVC), the emission spectrum showed a peak at 297 nm, and a band between 300-480 nm; in the case of λ_{exc} = 311 nm (NB-UVB) the emission spectrum has a peak at 352 nm, and a band between 400-550 nm; and for λ_{exc} = 344 nm (UVA), peaks at 377, 385, 468 and 566 nm. TL response after β irradiation, showed that the sample is very sensitive, with peak which grows with the dose, from low doses to high (0.2-50 Gy). CGCD showed the presence of eight peaks composing the curve, with the most intense peaks being located at 136, 99 and 270 °C, in addition, the kinetic order (*b*) varied (1.15-2), and the activation energy (*Ea*) at 0.68, 0.7, 1.05, 1.11, 1.2, 1.3, 1.35, 1.4 eV. For the OSL emission, it was possible to verify the presence of the fast component (t = 0.28 s) for low doses and medium and long components (t = 0.81 and 650 s) for larger doses (> 20 Gy). The HfO_2 also showed good potential application for UV dosimetry, when exposed to UVC irradiation by lamps (peak at 254 nm), there is OSL emission from 30 s of exposure, and grows with the dose. The presence of fast, medium and long components (t = 0.8, 3.6 and 36 s, respectively) were verified. LMOSL measurements were performed after UVC irradiations and showed increase with the dose, after deconvolution four peaks are determined in the curve. Similarly, the sample also showed response to medical therapy lamps, after irradiation by NB-UVB (peak at 311 nm) there is OSL emission with low exposure times (30 s), indicating the possibility of using the material for dosimetry in phototherapy, which use this source mainly in the treatment of skin diseases. For UVA irradiation (band between 315-400 nm), the sensitivity of the sample is lower.

Conclusion Ours results prove that the obtained HfO_2 nanocrystals are promising for use in the area of dosimetry, including for UV irradiation, widely applied in phototherapy medicine.

References

1) Mendonza, J. G. et al. Synthesis and characterization of hafnium oxide films for thermo and photoluminescence applications. Appl. Radiat. Iso., 68, 696-699 (2010).
2) Ramadoss, A.; Krishnamoorthy, K.; Kim, S. J. Novel synthesis of hafnium oxide nanoparticles by precipitation method and its characterization. Mater. Res. Bull., 47, 2680-2684 (2012).
3) Afouxenidis, D. et al. Computerised curve deconvolution of TL/OSL curves using a popular spreadsheet program. Radiat. Prot. Dosim., 149, No. 4, 363-370 (2012).

Comparative studies of thermoluminescent properties of Yttrium- and Lutetium-Aluminum perovskite crystals doped with Sc^{3+} and La^{3+}

A. Mrozik[1]*, W. Gieszczyk[1], P. Bilski[1], S. Witkiewicz[2], Yu. Zorenko[2]
[1] *Institute of Nuclear Physics Polish Academy of Sciences, Krakow, Poland*
[2] *Institute of Physics, Kazimierz Wielki University, Bydgoszcz, Poland*

Highlights: Sc^{3+} and La^{3+} doped perovskite crystals have been grown by micro-pulling-down (MPD) method. Thermoluminescent properties of $YAlO_3$:Sc, $YAlO_3$:La, $LuAlO_3$:Sc, $LuAlO_3$:La crystals with different dopant concentration were examined after alpha and beta irradiation.

Key words: perovskites crystals, micro-pulling-down, luminescence, rare-earths dopants

Background and Objectives: Multicomponent oxide compounds, including perovskites, play an important role in imaging applications as scintillating screens based on the single crystalline films (SCFs). Luminescence properties of Sc and La doped YAP SCF were previously investigated by Zorenko et al.[1)]. The aim of this work is research on thermoluminescent properties of Sc^{3+} and La^{3+} activated perovskite crystals – $YAlO_3$ and $LuAlO_3$ – prepared from the melt by MPD crystal growth method. Stimulated luminescence measurements, such as TL, confirm that these commonly known scintillators also show storage properties. This indicates a potential and perspectives of dosimetric applications of Sc^{3+} and La^{3+} doped YAP and LuAP. The study of both scintillating and storage properties of materials is also of importance in order to understand the luminescence mechanisms and to develop efficient radiation detectors.

Materials and Methods: In this work, the Sc^{3+} and La^{3+} doped YAP and LuAP crystals (with different dopants concentration) were grown from the melt by the MPD method. Starting materials were prepared by mixing the appropriate oxides (Al_2O_3, Y_2O_3 and Lu_2O_3) in stoichiometric proportions. The crystals were grown at the constant growth rate of 0.2 mm/min in the inert gas atmosphere (Ar). The obtained crystals had about 3 mm diameter and several cm lengths. Luminescent properties of the obtained crystals were investigated by TL method. The TL spectra were measured after the samples irradiation with both beta and alpha particles. The influence of dopants concentration on luminescent properties of the obtained crystals has been also investigated. The dosimetric properties of investigated materials (dose response, detection limit and also fading) will be also presented. Comparison of luminescence nature of $YAlO_3$ and $LuAlO_3$ hosts (differences between the band gap energy) will be discussed.

Results and Discussion: The emission spectra of Sc^{3+} and La^{3+} ions in YAP and LuAP matrixes are located in the UV range [1]. In case of YAP:Sc and YAP:La crystals, the glow-curves are different, but dominated by TL components with maxima located below 200 ºC. The obtained results suggest that the influence of dopants concentration on the shape of glow-curves is significant (see Fig.1). In case of Sc^{3+} dopant (0.2 mol. %), the measured glow-curve presents three low temperature components with glow-curve maximum located at around 200 ºC. With increasing Sc^{3+} concentration, proportions between the amplitudes of TL components have been changed and the curve maximum shifts to around 100 ºC. Similarly, proportions between the amplitudes of TL components also strongly depend on La^{3+} concentration. In case of the highest dopants concentration, the amplitude of TL signal is significantly reduced.

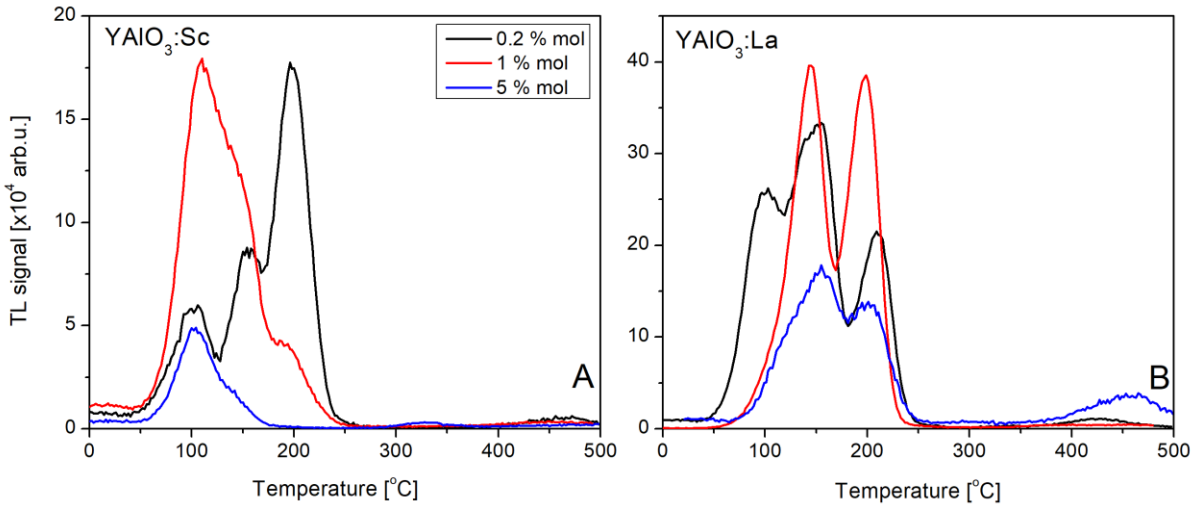

Fig.1. The TSL glow curves of YAP:Sc and YAP:La crystals with different Sc^{3+} (A) and La^{3+} (B) concentration in 0.2-5 mol % range.

Conclusion: Within this work we showed the influence of Sc^{3+} and La^{3+} ions on luminescent properties of YAP and LuAP perovskite crystals grown by micro-pulling-down method. Both the Sc^{3+} and La^{3+} doped samples show the emission in the UV range. The increase of dopants concentration strongly reduces the TL signal and changes proportions between TL components. These and the other obtained results will be discussed in details in the paper.

Acknowledgements: This work is supported by Polish National Science Centre within OPUS 11 program (2017-2020), project No. 2016/21/B/ST8/03200

References

1) Zorenko Yu., Gorbenko V., Voznyak T., Zorenko T., Nikl M., Nejezchleb K., Luminescence of La^{3+} and Sc^{3+} impurity centers in $YALO_3$ single-crystaliline films, J. Lumin. 128,2008, 595-602

RL, OSL and TL spectral measurements of $LiMgPO_4$ crystals doped with rare earths elements

A. Sas-Bieniarz, B. Marczewska, M. Kłosowski, W. Gieszczyk, P. Bilski
Institute of Nuclear Physics, Polish Academy of Sciences, Kraków, Poland

Highlights: Spectral measurements of optically stimulated luminescence (OSL), thermoluminescence (TL) and radioluminescence (RL) were obtained for high sensitive $LiMgPO_4$ (LMP) crystals grown by a micro-pulling-down (MPD) method. Acquired spectra of TL, OSL and RL emission from the studied LMP crystals were comparable.

Key words: OSL, TL, RL, LMP crystals, rare-earths elements, spectrally-resolved measurements

Background and Objectives: LMP crystals are characterised by high sensitivity to ionizing radiation and fast decay of luminescence after the light stimulation. Due to these two features the LMP crystals can be considered as a good alternative to the well-known Al_2O_3 and BeO detectors and can be potentially used for a fiber-coupled real time dosimetry. Investigated LMP crystals were grown from the melt by a MPD method. The obtained RE-doped crystals were tested for their luminescent properties in regard to the possible usage as real-time detectors.

Materials and Methods: Differently doped LMP crystals were grown from the melt by a MPD method. Investigated LMP crystals were doped with terbium, thulium or both these elements simultaneously. Luminescent properties of the obtained crystals were tested using the automatic Risø-TL/OSL-DA20 reader. Spectrally-resolved measurements of the RL, TL and OSL emission were performed using the QE Pro Ocean Optics high sensitive spectrometer equipped with CCD (charge-coupled device) detector.

Results and Discussion: Luminescent properties of LMP crystals depend on the type of doping with rare earths elements. For 515 nm stimulation light the OSL emission spectrum of Tb-doped LMP samples exhibits several characteristic peaks below 500 nm (Figure 1). At this spectral range, the Tm-doped sample presents only one significant peak (Figure 2). Similar features were also observed for RL spectra. The OSL and RL emission spectra measured for each sample are comparable (Figure 3). The highest OSL and RL signal has been measured for Tb- and Tm-doped samples, respectively.

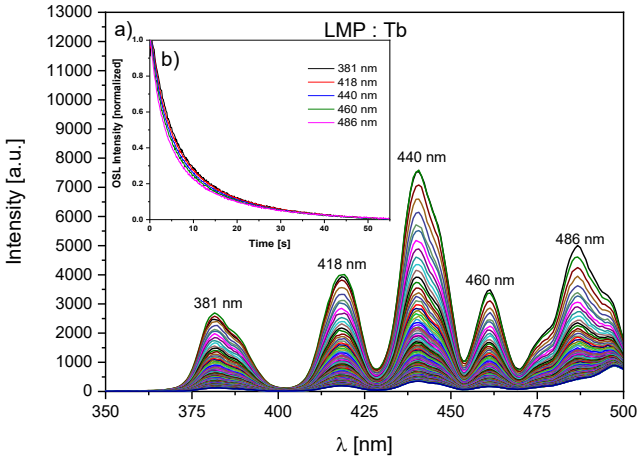

Fig. 1. a) Spectrally-resolved OSL measurements of LMP: Tb obtained in 0.1 s time intervals in 60 s; b) normalized OSL decay curves for all peaks.

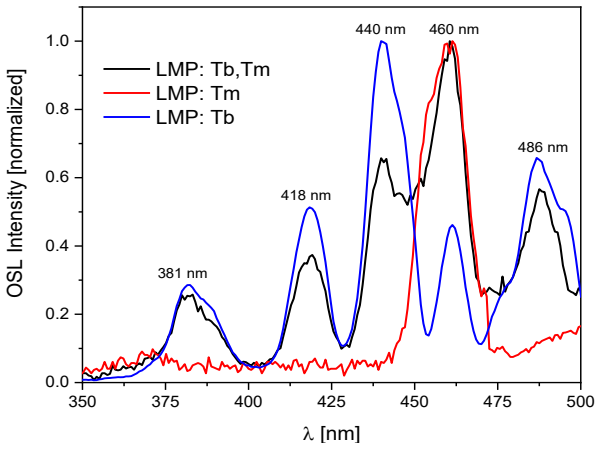

Fig. 2. Normalized OSL spectrally-resolved measurements of LMP doped with different REs elements.

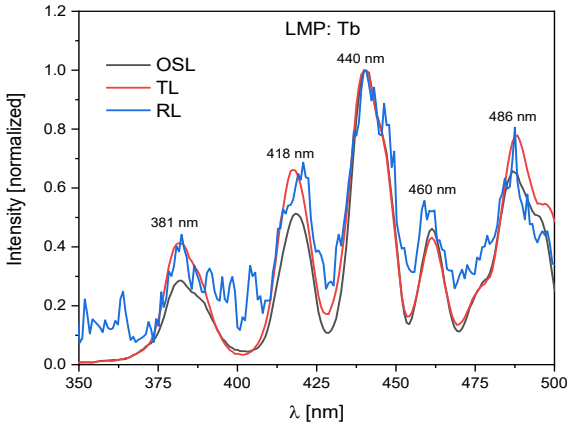

Fig. 3. Normalized OSL, TL and RL spectrally resolved measurements of LMP: Tb.

Conclusion: The obtained results tend to suggest that the RE-doped LMP crystals could be considered as good candidates for real-time detectors. The highest intensity of OSL and RL signal was measured for Tb- and Tm-doped samples, respectively.

Acknowledgements: This work was supported by the National Science Centre, Poland (Contract No. UMO-2016/21/B/ST8/00427).

References

1) D. Kulig, W. Gieszczyk, P. Bilski, B. Marczewska, M. Kłosowski. Radiat. Meas. 85, 88-92 (2016);

2) D. Kulig, W. Gieszczyk, B. Marczewska, P. Bilski, M. Kłosowski, A.L.M.C. Malthez. Radiat. Meas. 106, 94-99 (2017).

Low dose radiation dosimetry using natural blue quartz crystal by TL technique

Betzabel N. Silva-Carrera[1*], Nilo F. Cano[2], E. E. Cuevas Arizaca[3], Massahiro Miyamoto[4] , Heber S. Videira[4], Shigueo Watanabe[5]

[1]*Instituto de Pesquisas Energéticas e Nucleares, IPEN-CNEN/SP, São Paulo, SP, Brazil*
[2]*Instituto do Mar, Universidade Federal de São Paulo, Santos, SP, Brazil .*
[3]*Facultad de Ciencias e Ingenieiras Fisicas y Formales, Universidad Católica de Santa Maria, Arequipa, Perú.*
[4]*Hospital das Clínicas da Faculdade de Medicina da Universidade de São Paulo, HCFMUSP, Brasil.*
[5]*Instituto de Física, Universidade de São Paulo, São Paulo, SP, Brazil .*

Highlights.

This work presents the results of response of blue quartz for low dose radiation detection. These dosimeters were placed on a patient skin undergoing heart, liver and thyroid scintigraphy for 10 minutes the patient ingered a solution of Tc(99m). An unexpected result was obtained; the peak of 230 °C did not appear in the TL glow curve of the blue quartz. Since the 230°C appears prominent when irradiated with gamma radiation of Co(60) or Cs(137). Similar measurements were carried out in other silicate minerals such as aquamarine and tourmaline, these crystals did not present this unexpected behavior.

Key words: Quartz, radiation, dosimetry ,TL.

Background and Objectives.

Quartz is a mineral well known due to multiple use in several human activity. In particular, quartz responds well to radiation dose in relation to its thermoluminescence (TL) properties. Therefore, quartz is considered as an useful material for detection of ionizing radiation. Quartz responds to low (~mGy) as well to high (hundreds of kGy) radiation dose.

Using 0.075 to 0.180 mm diameters grains of quartz, we produced pellets with each pellet subjected to 11 ton/cm^2 pressure and sintering at 1200 ºC for over 60 min. These pellets are rigid and easy to handle. High dose radiation is useful in industrial application; on the other hand low dose radiation are present in medical applications.

We have already carried out detection of gamma rays emitted by Tc(99m). This radioactive element is used in imaging internal organ of human body. A matrix of pellets was prepared to detect gamma rays emitted by Tc (99m). Quartz pellets placed on the surface for 10 min were able to detect the position of the source.

Materials and Methods

Green and Blue quartz varieties of quartz were used because they are very sensitive TL crystals. As above 0.075 to 0.180 mm grains of these quartz have been used to produce pellets with 50 mg mass and size 6mm x 1 mm. Then at the Radiology Institute of Hospital- HCHMSP (University of São Paulo) a matrix of 5x4 pellets was placed on right hand thyroid of a patient and a matrix of 4x3 pellets on left hand for 10 min. To this patient it was given solution of radioactive iodine 131 (I-131) about 11 μCi.

Results and Discussion

Fig. 1. Shows in color TL intensity detected by pellets. Since red color is highest TL it indicates the position of Iodine source captured by some abnormality in the thyroid. further experiments are programmed. This image was produced with the peak of 320 °C.

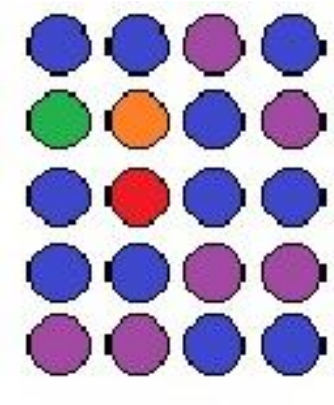

Fig. 1. TL intensity response of quartz pellets, I-131.

Conclusion

The quartz pellets were able to detect low radiation emitted by radioactive iodine captured by some tissue like tumor. They are very sensitive gamma-ray detectors with main prominent TL peaks occurring at 230 °C (Co(60) or Cs(137)) and we are trying to understand why 230°C peak did not be seen when irradiated with Tc(99m) and Iodine source .

References

1. *Álvaro Barbosa de Carvalho Junior et al., Manufacturing polycrystalline pellets of natural quartz for applications in thermoluminescence dosimetry. Materials Research.2012:15(4);1-8*
2. *Álvaro Barbosa de Carvalho Junior et al., Effect of particle size in the TL response of natural quartz sensitized by high dose of gamma radiation and heat – treatments. Materials Research.2010:13(2);2651-271*

Evaluation of Dosimeter Properties of Polycarbonate for Industrial Electron Beam Irradiation

Cyra Jelle G. Calleja[1&2]*, Roy B. Tumlos, Ph.D[1]

[1]*Department of Physical Sciences and Mathematics, College of Arts and Sciences, University of the Philippines Manila, Manila, Philippines*

[2]*The Graduate School, University of Santo Tomas, Manila, Philippines*

Highlights In this study, commercially-available polycarbonate was evaluated for dosimetry application in industrial electron beam irradiation. Polycarbonate exhibited discoloration when irradiated and this change was quantified through spectrophotometry. The study evaluated the dose response, reproducibility, and stability of polycarbonate in high-level doses from a mega voltage electron source.

Key words polycarbonate, dosimeter, absorbance, dose, response

Background and Objectives In electron beam irradiation processing, film dosimetry systems usually of polymer based are used for routine dose measurements to ensure that the irradiation procedure is correctly applied according to specifications and process is carried out within prescribed limits[1)]. However, these dosimetry systems are costly, not widely available, require extensive preparation treatment and handling, and sensitive to humidity. General-purpose commercial polycarbonate, a readily available and inexpensive thermoplastic used in industries, has been observed sensitive to ionizing radiation[2)]. The aim of this study is to determine the feasibility of polycarbonate as a routine dosimeter in industrial electron beam irradiation by evaluating its dosimeter properties - dose response, reproducibility, and stability (before and after irradiation).

Materials and Methods Clear polycarbonate solid sheets with UV protection of 3.0 mm thickness were purchased from the local construction plastic supply store and cut into plates of size 10 x 50 mm. 2.5 MeV ELV-8 Electron Beam Accelerator of the Philippine Nuclear Research Institute (PNRI) was used to irradiate the polycarbonate plates at the doses of 7 kGy, 14 kGy, 28 kGy and 40 kGy. Three polycarbonate plates were used for each dose point for reproducibility. The 7 to 40 kGy dose range was chosen as it is the range typically used in electron beam irradiation processing. To observe the change in the optical property of the irradiated polycarbonate at each dose point, the optical absorbance spectrum of the unirradiated and irradiated plates were obtained at the wavelength range of 380-800 nm using Shimadzu UV-1800 spectrophotometer. To quantify the dose response of polycarbonate, the

specific absorbance of the irradiated polycarbonate plates versus air was measured at the wavelength where the maximum absorbance occurred using the spectrophotometer. The mean specific absorbance of irradiated polycarbonate plates, measured 3 hours after irradiation, is plotted against dose to observe the behavior of the response of the polycarbonate with increasing doses. The unirradiated and irradiated polycarbonate plates were then stored in different environmental conditions for 24 days. The absorbance of each plate samples were re-measured every 48 hours during the storage period and the specific absorbance vs time was graphed to observe the stability of polycarbonate before and after irradiation.

Results and Discussion The clear polycarbonate noticeably changed to yellow-green when exposed to radiation and the color darkens as the dose increases. In the optical absorbance spectrum of irradiated polycarbonate, absorbance peak was observed constantly around 412 nm and was more prominent as radiation increases. This peak wavelength indicated where maximum absorption of light occurred. At this wavelength, the measured specific absorbance of polycarbonate irradiated with a mega-voltage electron source increases with dose in a quadratic manner. The coefficient of variation of the mean dose response of irradiated polycarbonate samples were within 2%. Over the course of 24 days, the variation in the specific absorbance of unirradiated polycarbonate plates stored in different environmental conditions was less than 2%. On the other hand, the response of irradiated polycarbonate plates stored in a light-protected container at room condition decreased by up to 47% on the 6^{th} day decreasing gradually to 65% on the 24^{th} day. In spite of the quick initial fading, the response of irradiated polycarbonate plates stored at room temperature in a light-protected container and in different humidity conditions did not change significantly.

Conclusion At high-level electron doses, the dose response of polycarbonate is quantitative, reproducible and not sensitive to humidity. Before irradiation, polycarbonate does not require extensive preparation and handling, stable and not sensitive to environment. Thus, polycarbonate is a feasible dosimeter for industrial electron beam irradiation.

References

1) International Atomic Energy Agency, Guidelines for the Development, Validation and Routine Control of Industrial Radiation Processes, International Atomic Energy Agency, Vienna, 2013.

2) L. Massey, The effects of sterilization methods on plastics and elastomers. Norwich, NY: William Andrew Pub., 2005.

Dosimeter properties of Sn-doped SiO_2 glasses synthesized by the Spark Plasma Sintering method

Daiki Shiratori*, Hiromi Kimura, Noriaki Kawaguchi, Takayuki Yanagida
Nara Institute of Science and Technology, Nara, Japan

Highlights In this study, we successfully produced a SiO_2 glass at temperature lower than the softening temperature by sintering at 1300 °C using the Spark Plasma Sintering (SPS) method. A very small amount of Sn^{2+} was added as the luminescence center into the prepared SiO_2 glass and the radiation induced luminescence characteristics including the dosimetric characteristics were evaluated.

Key words dosimeter, glass, SiO_2, tin, thermally-stimulated luminescence (TSL)

Background and Objectives A SiO_2 glass has a high transmittance from vacuum ultraviolet to infrared regions and is excellent in low coefficient of thermal expansion and chemical durability. Therefore, SiO_2 glass can be expected as a host material for radiation measurement. However, the softening temperature of SiO_2 glass is as high as 1774 °C, in the case of using a conventional melt quenching method, it is necessary to high-temperature manufacturing process. Generally, such a high temperature process to make glasses is difficult. The SPS method enables us to sinter at low temperature within a short time, and it is possible to manufacture SiO_2 glass at a temperature lower than the softening temperature of it. In this study, SiO_2 glass was prepared by the SPS method, and Sn^{2+} was selected as luminescent center. The reason for chosen Sn^{2+}: In recent years, rare earth free materials are required for phosphors due to the shortage of resources, and Sn^{2+} shows luminescence suitable for the wavelength sensitivity of the photomultiplier tube for a radiation detector.

Materials and Methods We have synthesized Sn-doped SiO_2 glass sample by the spark plasma sintering method. SiO_2 (3N) glass nano-sized powder and SnO_2 (4N) powder was homogeneously mixed with the molar ratio of 100 and 0.005, respectively. The total mass of the mixture was 0.35 g. The mixture was then loaded in a graphite die and sandwiched and sealed by two graphite punches. The sintering temperature was increased from 600 °C to 1300 °C at the rate of 30 °C /min and held for 180 min while applying a force of 5.5 kN. The sintering was performed under vacuum. After sintering, the carbon sheet was removed, and the sample surface was polished. In order to evaluate the obtained sample. In addition to the characteristics as a dosimeter, the basic optical characteristics and various kinds of radiation

induced luminescence properties were measured.

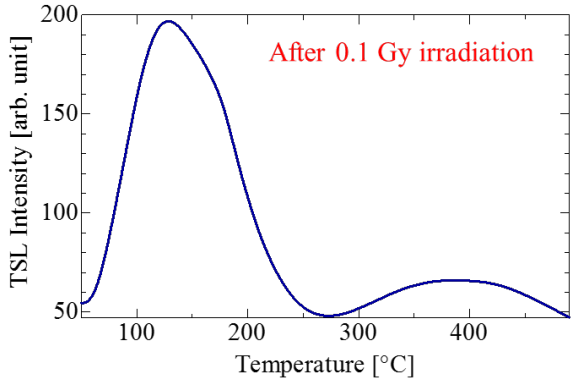

Figure 1. TSL grow curve of the $0.005SnO_2$-$100SiO_2$ glass sample.

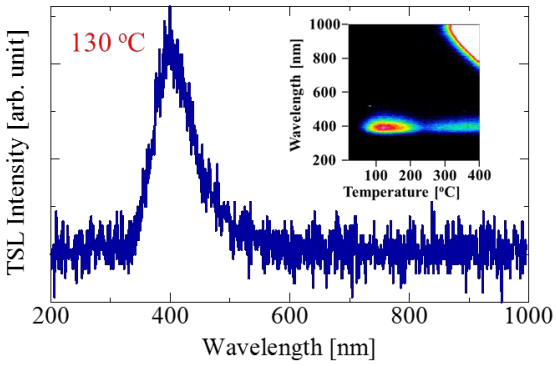

Figure 2. TSL spectra of the glass sample. The sample was stimulated at 130 °C. The inset shows the TSL spectrum at the corresponding temperature.

Results and Discussion The obtained glow curve is illustrated in Figure 1. Prior to the measurements, the glass sample was irradiated with X-rays of 0.1 Gy. The obtained glow curve has two glow peaks around at 130 and 390 °C. Figure 2 displayed the TSL spectrum, which showed the maximum emission intensity when thermally stimulated temperature at 130 °C. The sample showed broad emission centered at around 400 nm. From the emission wavelength, this emission would be attributed to Sn^{2+} [1,2]. The inset exhibits the map of the emission wavelength for each temperature region. The positions of the emission are well consistent with figure 1, and in both cases, the luminescence appeared in around 400 nm. From above results, it is suggested that this sample has at least two kinds of stimulation bands and emission due to Sn^{2+}.

Conclusion Sn-doped SiO_2 glass was prepared by the SPS method, and its dosimeter characteristics were evaluated. The glow curve has two peaks at around 130 and 390 °C, and the low temperature side is dominant. From the TSL spectrum, we confirm broad emission around 400 nm, which is ascribe to Sn^{2+}.

References

1) H. Masai, Y. Ueda, T. Yanagida, O. Go, and Y. Tokuda, Sensors Mater. **28**, 871 (2016).
2) H. Masai, T. Fujiwara, S. Matsumoto, Y. Tokuda, and T. Yoko, J. Non. Cryst. Solids **383**, 184 (2014).

TL and OSL characterization of $CaSO_4$:Mn and $CaSO_4$:Mn,Ag(NP)

Anderson M. B. Silva [1], Danilo O. Junot [2]*, Luiza F. Souza [1], Linda V. E. Caldas [2], Divanizia N. Souza [1]

[1] *Departamento de Física, Universidade Federal de Sergipe, São Cristóvão, SE, Brazil*

[2] *Instituto de Pesquisas Energéticas e Nucleares/Comissão Nacional de Energia Nuclear, São Paulo, SP, Brazil*

Highlights Samples of $CaSO_4$:Mn and $CaSO_4$:Mn,Ag(Np) were produced by means of the slow evaporation route.
X-ray diffraction confirmed the anhydrite crystalline structure of the samples and scanning electron microscopy confirmed the formation of the silver nanoparticles.
The incorporation of silver nanoparticles in the $CaSO_4$:Mn matrix enchances the TL and OSL signal of the samples.

Key words dosimetry, thermoluminescence, optically stimulated luminescence.

Background and Objectives In order to provide control in relation to the possible dangerous effects caused by ionizing radiation, the use of a radiation detector is necessary. Such a device operates from the transfer of energy from the incident radiation to the sensitive material of the detector, being able to produce a response signal, which can be measured. Among the detectors available are the ones that use techniques such as thermoluminescence (TL) and optically stimulated luminescence (OSL). TL/OSL materials have been studied for decades, in order to increase their sensitivity, signal stability and reproducibility, and to provide improvement to their dosimetric properties. According to literature results [1], silver as a co-dopant in the $CaSO_4$ matrix seems to increase the emission intensity of the materials without silver. As there are no reports on the structural and dosimetric characterization of $CaSO_4$:Mn with the incorporation of silver, the aim of the present work was to produce and characterize polycrystals of $CaSO_4$ doped with manganese and co-doped with silver nanoparticles (AgNPs), in order to use them as TL/OSL dosimeters.

Materials and Methods The phosphors were produced by means of the slow evaporation route and characterized by X-ray diffraction (XRD) and by scanning electron microscopy (SEM) techniques. The silver co-dopant was incorporated in the form of nanoparticles and was produced by the method of Lee and Meisel [2] and characterized by ultraviolet-visible (UV-Vis) and XRD vibrational spectroscopy techniques. The composites in the form of pellets

were obtained from the addition of powdered Teflon to the phosphors. The TL and OSL emissions of the new materials produced were investigated in a Risö TL/OSL reader.

Results and Discussion X-ray diffraction analyses showed that samples exhibit only a single phase corresponding to the crystal structure of anhydrite, and they indicated that the prepared AgNPs have a crystalline structure with face centered cubic (FCC) lattice and average crystallite size estimated of 31.5 nm. The UV-Vis spectra presented a characteristic plasmon resonance band of silver nanoparticles, with a maximum around 425 nm. The TL emission curve of $CaSO_4$:Mn presents the main dosimetric peak at approximately 203 °C. The silver co-doped samples introduced an increase in the TL intensity of the silverless material. All samples presented homogeneity and reproducibility coefficients of less than 10%. The OSL analyzes of the composites showed a typical exponential decay curve with a fast decay rate. All of thhe samples exhibited TL/OSL response proportional to the absorbed dose.

Conclusion By incorporating the silver nanoparticles in the $CaSO_4$:Mn matrix, the composites presented more intense TL and OSL signals, besides better response stability. This higher sensitivity of the $CaSO_4$:Mn,Ag(Np) samples may bring great advantages in the response of these materials for use in ionizing radiation dosimetry.

References

1) Junot, D. O.; Couto Dos Santos, M. A.; Antonio, P. L.; Caldas, L. V. E.; Souza, D. N. Feasibility study of $CaSO_4$:Eu, $CaSO_4$:Eu,Ag and $CaSO_4$:Eu,Ag(NP) as thermoluminescent dosimeters. Radiat. Meas., 71: 99-103, 2014.
2) Lee, P.; Meisel, D. Adsorption and surface-enhanced Raman of dyes on silver and gold sols. J. Phys. Chem., 86(17): 3391-3395, 1982.

TL/OSL signal of $CaSO_4$:Eu,Ag samples produced by variations of the slow evaporation route

Danilo O. Junot [1]*, Divanizia N. Souza [2], Linda V. E. Caldas [1]

[1]*Instituto de Pesquisas Energéticas e Nucleares/Comissão Nacional de Energia Nuclear, São Paulo, SP, Brazil*

[2]*Departamento de Física, Universidade Federal de Sergipe, São Cristóvão, SE, Brazil*

Highlights Crystals of $CaSO_4$:Eu,Ag were produced by variations of the slow evaporation route.
The TL emission spectra confirmed the presence of Eu^{3+} and Eu^{2+} in the crystal matrix.
The $CaSO_4$:Eu,Ag(a) and $CaSO_4$:Eu,Ag(b) composites presented the most intense TL and OSL signals and showed a linear and reproducible dose response.

Key words $CaSO_4$ synthesis methods, radiation dosimetry, thermoluminescence, optically stimulated luminescence

Background and Objectives The techniques of thermoluminescence (TL) and optically stimulated luminescence (OSL) are highly sensitive to defects caused by external elements to the crystalline matrix of a luminescent material. The structure of these defects can be controlled by the preparation method [1]. The aim of this work was to produce crystals of $CaSO_4$ doped with europium (Eu) and silver (Ag) nanoparticles, by means of three different preparation routes, and to study their application in radiation dosimetry by the TL and OSL techniques.

Materials and Methods The crystals were produced by variations of the slow evaporation route. In all preparations, calcium carbonate ($CaCO_3$) was used as precursor, and it was incorporated in a solution of sulfuric acid, that was evaporated. Samples of $CaSO_4$:Eu,Ag(a) were obtained using europium oxide and the silver particles, produced by the polyol method, as dopants. For the growth of the crystals of $CaSO_4$:Eu,Ag(b), silver was incorporated in nitrate form, dissolved in water. $CaSO_4$:Eu,Ag(c) phosphorus were synthetized mixing europium oxide in a colloidal suspension of silver nanoparticles dispersed in ethylene glycol. Composites of all samples were obtained from the addition of powdered Teflon to the powdered phosphors. Structural characterization was made by X-ray diffraction measurements and TL/OSL analyses were performed in a Risö TL/OSL reader.

Results and Discussion X-ray diffraction analyses showed that samples exhibit only a single phase corresponding to the crystal structure of anhydrite. Optical characterization confirmed the presence of Eu^{3+}/Eu^{2+} in the crystal matrix. All of the composites present TL response between 130 °C and 230 °C, with the maximum intensity at around 170 °C for silver co-doped samples and 205 °C for the $CaSO_4$:Eu samples. The $CaSO_4$:Eu,Ag(a) samples showed a considerably more intense emission, about 2 times higher than of the $CaSO_4$:Eu samples. No emission related to Ag ions could be observed in the TL emission spectra of the samples. It is clear that the insertion of silver enhances the concentration of Eu^{2+} ions in the $CaSO_4$ lattice. Dosimetric characteristics such as reproducibility, linearity, signal kinetics, and minimum detectable dose were evaluated after the exposure of the samples to a $^{90}Sr/^{90}Y$ source in a dose range from 0.1 to 10 Gy and to a blue-light stimulation. The OSL curves of the samples show a fast exponential decay as the optically active traps are emptied, which indicates that the traps responsible for the OSL emission have high photoionization cross sections for the 470 nm wavelength of the blue LEDs.

Conclusion The $CaSO_4$:Eu,Ag(a) and $CaSO_4$:Eu,Ag(b) composites presented the most intense signals and showed a linear and reproducible dose response, but the $CaSO_4$:Eu,Ag(a) samples showed as best potential material for application in TL/OSL dosimetry.

References

1) J. Azorin. Preparation methods of thermoluminescent materials for dosimetric applications: An overview. Applied Radiation and Isotopes 83, 2014, 187-191.

Al2O3:C Sample Dependence of the Thermoluminescence Phenomena.

D. Imatouken[1 2] *, F.Z. Abdelaziz[1] A. Bellal[1], M. Kechouane[2]

[1]*Nuclear Research Center of Algiers, Algiers, Algeria.*

[2]*Laboratoire de Physique des Materiaux, Universite des Science et Technologie Houari-Boumediene Algiers Algeria.*

Highlights Investigation of sample to sample luminescence phenomena variability with different dose levels.

Key words Tl emission spectra, glow curve shape, Dose dependence, Al2O3:C.

Background and Objectives The luminescence proprieties of Al2O3:C exhibit significant variation from sample to sample. For Thermally stimulated Luminescence (TL), many authors have observed a variety of its sensitivity, peak shape and position. This sample variability is attributed to the fact that the main TL peak in Al2O3:C is produced by the set of several traps and each trap responds differently to irradiation. In this study, we investigate behavior of different luminescence phenomena (TL emission spectra, TL glow curve shape,…) for beta irradiations at different degrees of deep traps filling, ranging from 2 mGy to 100 Gy, in the temperature range from ambient temperature to 450°C..

Materials and Methods Single crystal of Al2O3:C samples were used, purchased at Landauer Inc., Stillwater Crystal Growth Division from USA. The samples characterizations and choices were performed prior annealing, using a small test dose of 2 mGy. The luminescence measurements were performed using Riseo TL/OSL reader (model TL/OSL-DA-20), equipped with a $^{90}Sr/^{90}Y$ beta particles source and Hoya U-340 emission filter. The Ocean optics spectrometer, mounted on TL/OSL reader via optical fibre, is used in order to record emissions spectra from Thermally Stimulated Luminescence (TL). The Photoluminescence spectra are recorded using Perkin Elmer Luminescence Spectrometer Model LS-50B in the range of 200 nm to 450 nm. The TL glow curve from these samples is readout with same Time Temperature Profile but irradiated at different dose level ranging from 0.5 mGy to 100 Gy. Finally, in order to classify the grade of Al2O3:C samples, the delay optically stimulated luminescence is readout using Blue LED simulation during 0.5 s after these 4.5 s without simulation with total 1100 Datapoints

.**Results and Discussion** For Photoluminescence, all selected samples present an emission band at 326.7 nm. This band is identified as an oxygen ion vacancy center with one trapping electron. This center is positively charged (F^+).

The glow curves of thermoluminescence of Al2O3:C irradiated at 10 Gy from room temperature to about 400°C present variability on the shape (Figure 1).

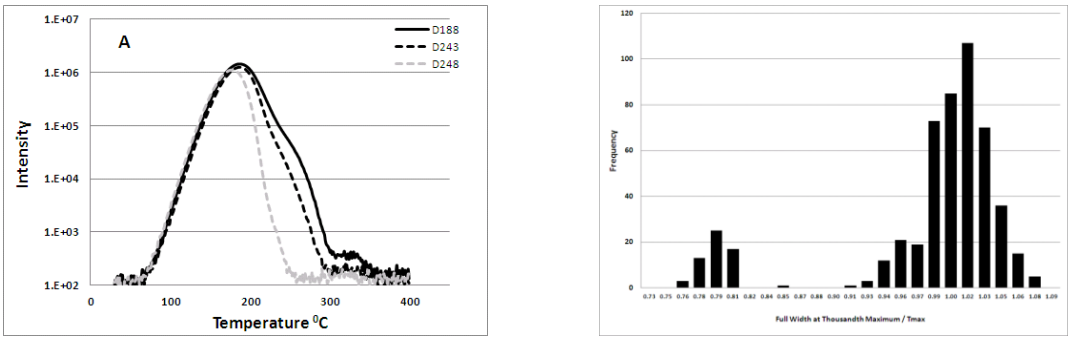

Figure 1. Normalized Thermoluminescence glow curves for some Al2O3:C samples and their shape Factor distribution (500 samples).

The distribution of Full Width at Thousandth Maximum (FWTM) for the normalised intensity at maximum peak temperature (Shape Factor); describe two distributions about 0.79 and 1.01.

The thermoluminescence emission spectra exhibit two emission bands. The predominantly emission band is located at about 205°C with two emission wavelengths (407 nm and 696 nm) and second at 350°C with emission wavelength of 696 nm (Figure 2). The blue emission at 407 nm is the F center emission and the emission at 696 nm is due to the R-line transition in substitutional Cr^{3+} ions (substitute for Al^{3+}).

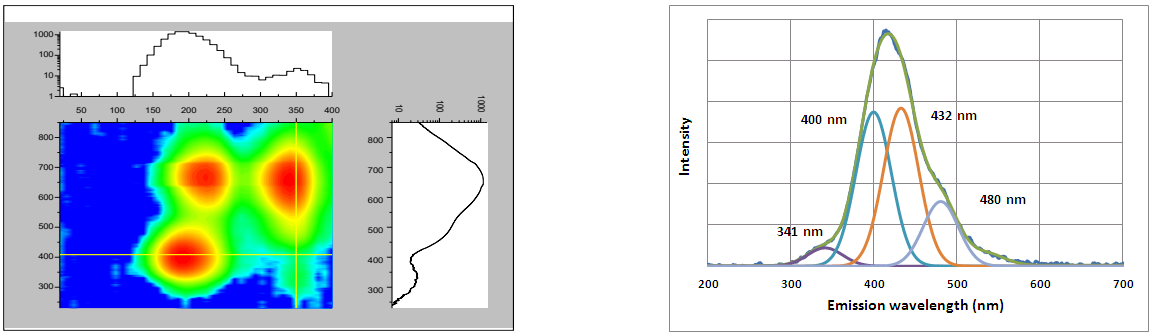

Figure 2. Typical thermoluminescence emission Spectra for Al2O3:C samples and band emissions at temperature of the maximum intensity (10 Gy).

The Analysis of DOSL curves in terms of time resolved decay indicate that no contribution of any shallow traps if the use of preheating temperature of about 120°C. The decay times obtained for selected samples are equal to 35.4 ±3.34 ms. these correspond to lifetime τ_F of excited F centers reported by many authors

Conclusion The experimental results obtained in this study demonstrate that the luminescence of Al2O3:C present greater variation depend on samples. It is important to explore many others analysis techniques such as Radiation Luminescence.

Kinetic Parameters of Thermoluminescence in Al-deficient Aluminum Nitride Crystals

D.M. Spiridonov, D.V. Chaikin, I.A. Weinstein, A.S. Vokhmintsev, N.A. Martemyanov
NANOTECH Center, Ural Federal University, Mira street, 19, Ekaterinburg, Russia

Highlights UV excitation spectra and kinetic parameters of thermally stimulated mechanisms have been studied in aluminum-deficient AlN submicrocrystals using spectrally resolved thermolumoinescence and varying heating rates techniques. The regularities of observed processes and origin of responsible active traps have been discussed.

Key words AlN, spectrally resolved thermoluminescence, SR-TSL, TL excitation spectra, oxygen-related centers, nitrogen vacancy, activation energy.

Objectives The aim of the work was to analyze the features of the spectrally resolved thermoluminescence (TSL) in UV irradiated AlN crystals with aluminum deficit.

Materials and Methods Aluminum nitride crystalline powder has been synthesized by gas-phase method. Grown particles in the form of a hexagonal prisms or a combination of prism with bipyramids had sizes of 0.1 – 2.0 μm. The crystals studied were characterized by aluminum deficit with ratio of Al:N ≈ 0.9:1. The main impurities were O (1.6 at.%) and Si (0.5 at.%).

TSL measurements were performed using the laboratory installation based on Perkin Elmer LS55 spectrometer with integrated high-temperature accessory. Thermoluminescence was recorded at λ_{em} = 415 nm (2.99 eV) emission band within the room temperature (RT) – 773 K range. The samples were irradiated at RT with the monochromatic light of Xe-lamp in UV region of λ_{exc} = 200-330 nm with 5-nm step. Depending on the measurement method the heating rate was varied in the range of r = 0.5 – 9.5 K/s, varying heating rate technique.

Results and Discussion The TSL excitation spectrum was analyzed for r = 2.0 K/s. It was shown that all glow curves were characterized by a wide peak in the temperature range of 300 – 600 K with maximum at T_{max} = 345 ± 5 K and λ_{exc} = 265 nm. As the heating rate increased the maximum shifted to higher temperatures: from T_{max} = 314 K (r = 0.5 K/s) to T_{max} = 368 K (r = 9.5 K / s), see Figure 1.

The quantitative estimation of the kinetics parameters was carried out in the frame of the general order kinetics. It was found the TSL peak was approximated well by one component with activation energy E_a = 0.44 – 0.73 eV, effective frequency factor s = 2.7×10^5 – 1.0×10^{10} s^{-1} and kinetics order b > 2.2. The possible origin of responsible active traps based on V_N nitrogen vacancies was discussed. It was supposed that the calculated values of the kinetics order can point to a high probability recapture of released charge carriers.

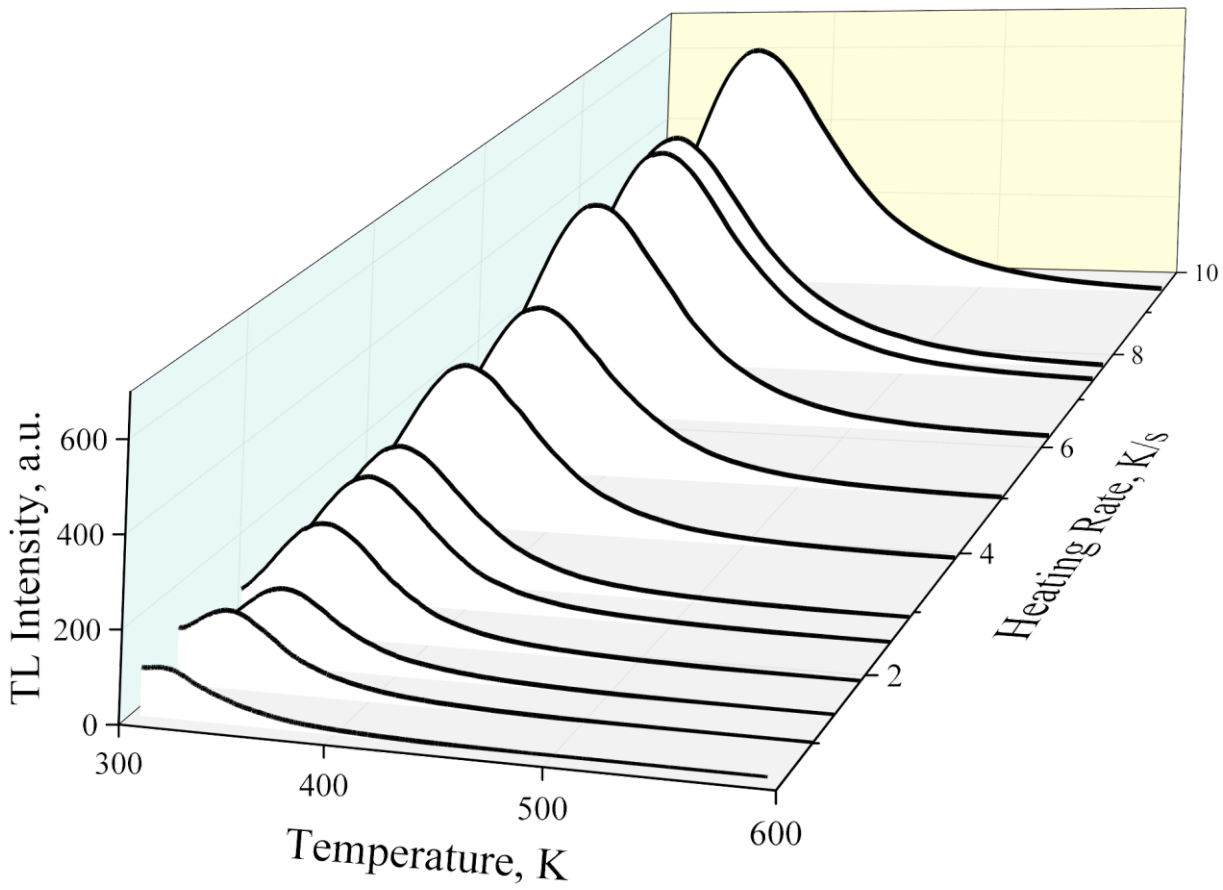

Figure 1. TSL curves measured with use of varying heating rates technique.

Conclusion The analysis of the spectral and kinetic parameters of spectrally resolved thermoluminescence in AlN submicrosized crystals was carried out. The obtained data were compared with the results of independent studies. Conclusions were proposed about the origin of active traps and non-stoichiometry effects on luminescent properties of the synthesized Al-deficient aluminum nitride crystals.

Acknowledgments This work was supported partially by Russian Foundation for Basic Research (project No. 18-32-00550) and Act 211 Government of the Russian Federation, contract № 02.A03.21.0006. Ch.D.V., I.A.W. and A.S.V. thank Minobrnauki initiative research project № 16.5186.2017/8.9 for support.

Production and characterization of green quartz dosimetric pellets

Cuevas Arizaca E. E.[1 3]*, Rojas R. R.[2] Cano N. F[2]. Rondon Rondon M.[3]* Chubaci, J.F.D. [1] T.K.G. Rao[1] Watanabe S.[1]

[1] *Instituto de Física, Universidade de São Paulo, Brazil*

[2] *Universidade Federal de São Paulo, Santos, Brazil*

[3] *Universidad Católica de Santa Maria, Arequipa, Perú.*

Highlights.

Green quartz pellets were produced to measure ionizing radiation.

Study of energy dependence was made.

Key words: Dosimetry, TL, Green quartz.

Background and Objectives.

The quartz crystal is one the most famous materials and extensive researches have been done regarding its TL and OSL properties for applications at dosimetry and geological dating, Rocha et al (2011). As far as we know, no work has been published on dosimeters properties of pellets produced only of green quartz by the sinterization method for low dose radiation detection up to the present. In the present work we have produced and investigated the behavior of green quartz chips subjected to low dose with energy 40 and 80 keV. All samples were irradiated by X-rays their TL glow curves, dose response, fading and reproducibility were evaluated.

Materials and Methods

Green quartz minerals have been purchased for the present work from LEGEP Minerals Ltd. Fig. 1(a) show pictures of fragments. It was crushed and sieved in fine powder and pressed with a pressure of about 11 ton/cm^2 to obtain pellets and then sintering at about 1200 °C for 60 minutes. Each pellet has a mass of about 50 mg and a diameter of 6 mm and 1 mm thickness. These pellets are shown in Fig. 1(b). Grains with size smaller than 0.080 mm were used in x-ray diffraction analysis (XRD).

Results and Discussion

The behavior of the TL glow curves of green quartz pellets as function of 40 keV x-rays for low doses of 0.47 mGy up to 20.12 mGy is shown in Fig. 2a. The glow curves obtained show an intense and dominant TL peak with maximum at 230 °C. The samples were irradiated with different x-rays doses between the range of 0.47 mGy and 20.12 mGy for 40 keV and 0.57

mGy and 12.12 mGy for 80 keV. For each dose a group of 5 pellets were used and the mean values of the TL intensity of the peak at 230 °C were taken and the standard deviations of the mean value were calculated. Analyzing the dose response curves with log axes in the same scale, as observed in Fig. 2b, it can be observed that the TL responses of green quartz pellets samples presents linear behavior in the dose range of 0.47 to 50.00 mGy for 40keV and 0.57 to 12.12 mGy for 80 keV X-rays. These pellets are planned to be used in medicine involving low dose.

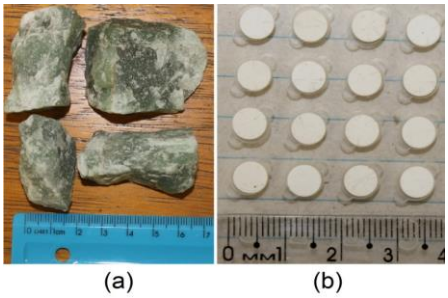

Figure 1. (a) Green quartz minerals. b) Green quartz pellets.

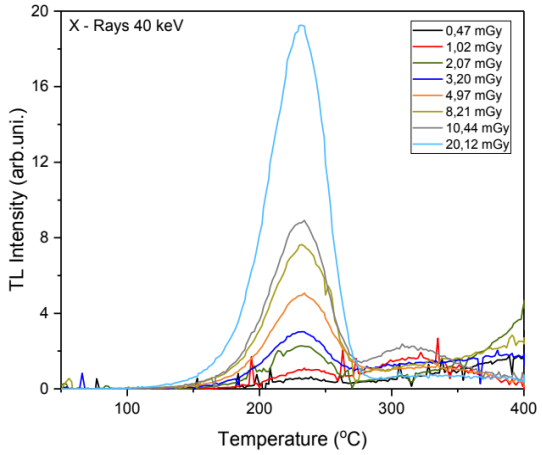

Fig 2a. TL glow curves irradiated at several doses between 0.47 and 20.12 mGy, 40 keV

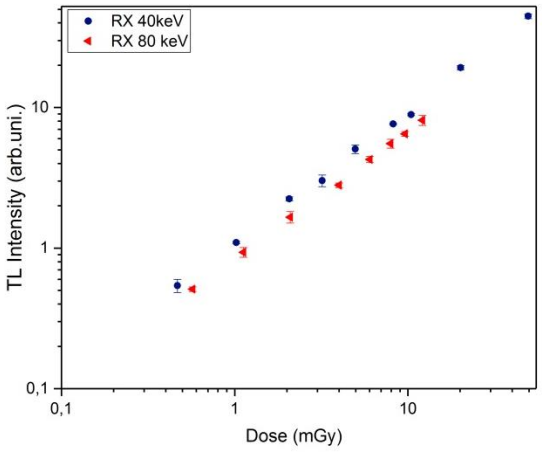

Fig 2b. Dose response curves of green quartz pellets, 40 keV and 80 keV.

Conclusion

The production of green quartz pellets was successful. Our TL analysis shows that green quartz pellets are sensitive to X-rays for low dose, TL intensity increase with the dose and shows energy dependence.

References

Rocha, F.G., Nascimento S.F., Santos, L.H.S., Nunes, M.G., Campos, V.P., Farias, T.M.B., Chubaci, J.F.D., Campos, L.L., 2011. Caracterização de pastilhas dosimétricas de quartzo verde para aplicação em dosimetria clínica.

Thermoluminescence and optically stimulated luminescence properties of a BeO dosimeter with double main dosimetric glow peak structure

Engin Aşlar[1,*], George S. Polymeris[1,2], Eren Şahiner[1], Y.K. Kadioğlu[2], Niyazi Meriç[1,2]
[1] *Institute of Nuclear Physics, Ankara University, 06100-Beşevler, Ankara, Turkey*
[2] *Earth sciences Application and research Center of Ankara University (YEBIM), Gölbasi 06830, Ankara, Turkey*

Highlights Luminescence characterization is attempted for a batch of BeO dosimeters which yield double structured main dosimetric glow curve shape.

Key words BeO, OSL, TL, deconvolution, activation energy, dose response, bleaching.

Background and Objectives Beryllium oxide (BeO) is a luminescent material that was initially recommended as thermoluminescence (TL) dosimeter[1)]. The use of BeO dosimeter has become widespread in personal, medical and environmental dosimetry fields[2,3)], using mostly optically stimulated luminescence (OSL) [4)].

BeO samples that are currently used for TL and OSL measurements are commercially available by Thermalox 995, Brush Wellman Inc., U.S.A. These materials yield a single main dosimetric TL peak at around 185 °C (HR=1°C/s). The objective of this paper includes a luminescence (TL and OSL) characterization of a BeO dosimetric material which yields a double structured main dosimetric peak, similar to the case of Al_2O_3:C [5)]. Comparison with the corresponding properties of the BeO supplied by Thermalox 995 will be also presented.

Materials and Methods A batch of BeO dosimeters were purchased from Radkor, Turkey. Each dosimeter comes in square disc form with dimensions of 4mm and thickness of 1 mm, identical to those by Thermalox 995. SEM-EDS and XRD measurements have proven the presence of BeO as the main phase. However, all BeO dosimeters of this batch yield a double main dosimetric peak within the temperature region 120 – 320 °C; a typical example of TL glow curve is presented in Fig. 1. The TL signal of this aforementioned temperature region consists of two overlapping TL peaks of first order of kinetics. Fig. 1 also presents the respective TL glow curve corresponding to BeO disc by Thermalox 995. The objective of the present work includes studying the following properties:

- TL peaks' characterization using both fractional glow technique (FGT) and deconvolution analysis,

- Post-annealing behavior of TL signal for temperatures ranging up to 800 °C,
- TL glow curve structure dependence on the attributed dose,
- Bleaching ability of each TL peak and possible correlation with the OSL components,
- Component resolved TL and OSL dose responses and lowest detectable dose limits.

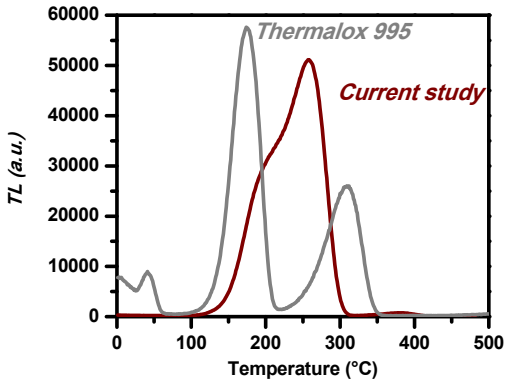

Figure 1. TL glow curves of two different BeO discs; one supplied by Thermalox 995 and one for the BeO subjected to the present study.

Results and Discussion The TL glow curve shape of the BeO of the present study is totally different, compared to the corresponding TL glow curve of the Thermalox 995 BeO; this is also the case for the corresponding traps. Post annealing behavior indicates that the double structure of the TL signal doesn't change throughout the temperature region up to 800 °C. Each deconvolved TL peak yield different dose response features. Nevertheless, the general properties of the OSL components seem to be compatible with those of the OSL of the BeO supplied by Thermalox 995.

Conclusion The TL properties of the BeO subjected to the present study yield major differences, compared to the corresponding TL properties of BeO supplied by Thermalox 995. This is not the case for the general OSL properties.

References

1) G. Scarpa, Phys. Med. Biol. 15 (1970) 667-672.
2) M. Sommer et al., Radiat. Meas. 42 (2007) 617-620.
3) E. G. Yukihara, Radiat. Meas. 46 (2011) 580-587.
4) E. Bulur, Radiat. Meas. 29 (1998) 639-650.
5) G. I. Dallas, Radiat. Meas. 43 (2008) 435-440.

Characterization of ytterbium-doped phosphate glass using the TL and OSL techniques for radiation dosimetry

Felícia D.G.Rocha[1]*, Daniel Villani[1], Vicente de P.de Campos[1], Gabriel Gomes do Nascimento[1], André Luiz Silva Oliveira[1], Diogo Rubio Sant'Anna Das Dores,[2], Zélia M. da Costa[2], Letícia L.Campos[1]

[1]*Instituto de Pesquisas Energéticas e Nucleares, CNEN/SP , Brazil*

[2]*Universidade Federal de Juiz de Fora, Minas Gerais, Brazil*

Highlights Characterization of ytterbium doped phosphate glass samples using the thermoluminescent and optically stimulated luminescence techniques for application in radiation dosimetry.

Key words radiation, thermoluminescence, optically stimulated luminescence, dosimetry

Background and Objectives Thermoluminescence (TL) or thermally stimulated luminescence has been actively developed in the past years due to its reliability, sensitivity and commercial availability and is currently in use with different materials as dosimeters[1)]. Nowadays, TL dosimeters are applied worldwide and play a significant role in dose measurements. The OSL or optically stimulated luminescence technique is also a very important tool for many areas of radiation dosimetry and have recently gained popularity for its use in medical and personnel dosimetry[2,3)]. Recent technological applications have generated much interest in the study of glasses, specially glasses doped with rare-earth ions that are used for optical amplifiers, fibers and lasers[4)]. Thus, in this work, the properties of 0.5 and 3 mol% ytterbium phosphate glass samples were investigated using the thermoluminescent technique and optically stimulated luminescence in order to verify the usefulness of this material for radiation dosimetry. The samples were tested in gamma-radiation beams, and their main dosimetric characteristics were evaluated (TL glow curve, response as a function of absorbed dose, energy dependence and response repeatability).

Materials and Methods The ytterbium phosphate glass samples were produced at Federal University of Juiz de Fora, using the melting-quenching technique. The dopant material Yb_2O_3 used has purity better than 99.99%. The TL measurements were performed using a Harshaw 4500 TLD reader in a nitrogen atmosphere, with a linear heating rate of $10°C.s^{-1}$.

The maximum temperature of 450 °C was reached in each readout cycle. The samples were thermally treated prior and after irradiation in a Vulcan 3-550 PD furnace, at 400 °C for one hour. The OSL measurements were performed on a TL/OSL-DA-20 model RISØ reader. It was used continuous-wave (CW-OSL) mode of illumination of the NICHIA Blue LED array NSPB-500 AS-type at 90% of power. The investigation of TL/OSL properties for the glass samples was evaluated exposing them to a radioactive source of Cs^{137}, with and absorbed dose of 5.0 Gy. To obtain the dose response curve, the samples were irradiated with gamma radiation in a dose range of 1.0 to 20.0 Gy.

Results and Discussion

The TL measurements show useful dosimetric range of the material within 2 to 20Gy of absorbed dose, with presence of three peaks in the glow curve (152±2ºC, 250±5 and 360±5ºC). Compatible results are also demonstrated for the OSL measurements with great sensitivity. The concentration of dopant material is a factor that influences TL and OSL signal intensity, and experimental results show that samples containing 0.5 mol% are ~ 12% more sensitive.

Conclusion The experimental results of this work indicate that Ytterbium-doped phosphate glasses produced at Federal University of Juiz de Fora present thermo (TL) and optically stimulated luminescence (OSL) over the absorbed dose range of gamma radiation showing the feasibility of use for radiation dosimetry.

Acknowledgments

The authors are thankful for the financial support given by CAPES finance code 001, CNPq granted fellowships and FAPEMIG.

References

1) Furetta, C. and Weng, P-S. Operational Thermoluminescence Dosimetry. 1998, World Scientific.
2) Akselrod, M.S., Bøtter-Jensen, McKeever, S.W.S., 2007. Optically stimulated luminescence and its use in medical dosimetry. Radiat. Meas., 41, S78-S99.
3) Yukihara,E.G. and McKeever, S.W.S. Optically Stimulated Luminescence: Fundamentals and Applications. 2011, John Wiley & Sons Ltd.
4) Hraiech, S.C. Bouzidi and M. Férid. Luminescence properties of Er^{3+}-doped phosphate glasses. Physica B: Condensed Matter 522 (2017): 15-21.

THERMOLUMINESCENCE PROPERTIES OF POTASSIUM FLUORIDE

Ogundare F.O[a] and Folley D. E.[b]

[a]Department of Physics, University of Ibadan, Ibadan, Nigeria

[b]Department of Physics and Electronics, Rhodes University,P. O. Box 94, Grahamstown, South Africa

Highlights: Assessing the potentials of potassium fluoride for dosimetry

Keywords: Potassium Fluoride, dosimetry, thermoluminescence

Background and Objectives

Retrospective dosimetry using thermoluminescence (TL) technique requires the use of any material which might have been exposed onsite. Potassium fluoride, a laboratory chemical, is therefore a potential material for retrospective dosimetry if found to possess characteristics expected of a TL material. This study is designed to examine the TL characteristics of this chemical.

Materials and Methods

TL measurements, on the sample at different doses (1 – 20 Gy) and heating rates (0.2 – 4°C/s) , were carried out using a TL/OSL Riso reader. The kinetic parameters of the sample's glow curves were determined using glow curve deconvolution and variable heating rate methods.

Results and Discussion

The glow curves of the fluoride, readout at $1^{o}Cs^{-1}$ for all the doses, exhibited two apparent peaks around 129 ± 1 and 251 ± 2°C. In addition, two shoulders appeared clearly, at high doses (>14 Gy), around 72 and 200°C, indicating the presence of two other peaks. The fact that the temperature of maximum intensity, for each of the two peaks, does not change with dose suggests that the peaks are of first order kinetics. The integrated intensity of the 129°C peak vary linearly with increasing dose, while that of 251°C peak exhibited superlinearity up to 8 Gy and thereafter linearity. The integrated intensity of 129°C peak decreased while that of 251°C peak increased with heating rate. The decrease of the 129°C intensity is attributed to thermal

quenching while the increase of the intensity of 251°C is attributed to inverse thermal quenching. The activation energy of thermal quenching for the 129°C was estimated to be 0.59 eV. Assuming two peaks, the mean activation energy, estimated using the two kinetic analysis methods, for 129°C peak and 251°C peak were 1.03±0.02 eV and 0.85±0.10 eV respectively, the corresponding order of kinetics values are 1.26±0.03 and 1.00. The best fit, especially at high doses, using the GCD method was, however, obtained with four peaks at 72, 110, 206 and 251°C. The activation energy of the 72, 110, 206 and 251°C peaks are, on the average, 0.67±0.03, 1.04±0.01, 0.78±0.07 and 1.46±0.03 respectively.

Conclusion

Potassium fluoride had a relatively simple glow curve consisting of two apparent peaks. Each of the glow peaks exhibited dose-response linearity which qualify the phosphor as potential TL material for dosimetry. Glow curve deconvolution revealed that the glow curve of the sample is made up of four glow peaks.

References

Hernandez-Medina A., Negron-Mendoza A., Ramos-Bernal S., Colin-Garcia M. (2013). The effect of doses, irradiation temperature, and doped impurities in the thermoluminescence response of NaCl crystals. Rad. Meas. 56 369-373

Hunter P. G., Spooner N. A., Smith B. W., Creighton D. F. (2012). Investigation of emission spectra, dose response and stability of luminescence from NaCl. Rad. Meas. 47 820-824

Elashmawy M. (2018). Study of constraints in using household NaCl salt for retrospective dosimetry. Nuclear Instruments and Methods in Physics Research B 423 49-61

Druzhyna S., Datz H. Oster L., Lerch M., Rosenfeld A., Cullen A., Orion I., Horowitz Y. S. (2017). Thermoluminescence dose response of photon irradiated NaCl: Unified interaction model analysis of the dependence of the supralinearity on photon energy. Rad. Meas. 106 455-458

Goksu,H.Y.,2003.Telephone chip-cards as individual dosimeters.Radiat.Meas.37,617–620.

Inrig, E.L.,Godfrey-Smith,D.I.,Khanna,S.,2008.Optically stimulated luminescence of electronic components for forensic, retrospective,and accident dosimetry. Radiat. Meas.43,726–730.

Thermally assisted optically stimulated luminescence (TA – OSL) in BeO dosimeter; the role of thermal quenching.

George S. Polymeris[1,*], George Kitis[2], Engin Aşlar[1], Eren Şahiner[1], Niyazi Meriç[1]
[1] *Institute of Nuclear Physics, Ankara University, 06100-Beşevler, Ankara, Turkey*
[2] *Nuclear Physics Laboratory, Department of Physics, Aristotle University of Thessaloniki, 54124 Thessaloniki, Greece*

Highlights The dependence of the isothermal TA – OSL of BeO dosimeters on the measurement temperature was studied. The TA – OSL dose response features depend strongly on the stimulation temperature.

Key words BeO, TA – OSL, thermal quenching, very deep traps (VDTs).

Background and Objectives Recently, an alternative experimental procedure was suggested in order to measure the signal resulting from very deep traps (VDTs), without heating the samples to temperatures greater than 500 ºC. Thermally assisted optically stimulated luminescence (TA – OSL), this somehow unconventional technique which efficiently combines both optical and thermal stimulation, appears as a promising tool for stimulating electrons from VDTs. For a number of well-established luminescent phosphors, TA – OSL exhibits a number of interesting dosimetric properties; several of them seem to be prevalent, even ubiquitous. TA – OSL of both Al_2O_3:C and quartz has been reported to be effectively applied towards extending the maximum detection dose thresholds. The present study further exploits the applicability of the technique to another well established luminescent phosphor, namely BeO.

Materials and Methods A batch of BeO dosimeters, purchased from Thermalox 995, Brush Wellman Inc., U.S.A., were used for the present study. Each dosimeter comes in square disc form with dimensions of 4mm and thickness of 1 mm. Dosimeters were annealed at 800 °C for 1 h. in order to empty all traps. The TA – OSL signal was measured at the isothermal mode, at a constant elevated temperature, following a TL measurement at 500 °C. The experimental procedure involved two basic protocols. To obtain more information about the thermal behavior of the source traps which cause it, the first protocol was applied in order to study the TA – OSL signal versus the temperature at which the OSL measurement is performed. The results of this protocol will not only show the thermally assisted nature of the signal, but will

also help identifying the optimum measurement temperature. The second protocol was applied in order to investigate the dose response of the TA – OSL signal.

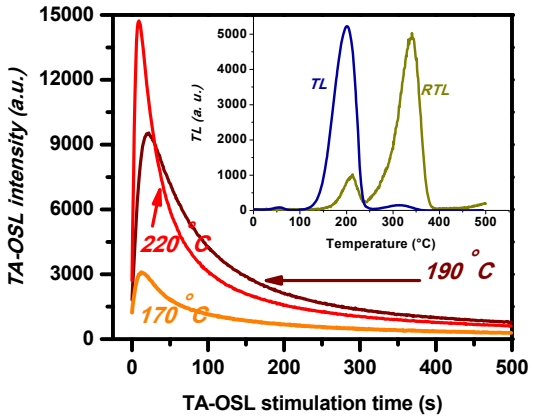

Figure 1. Examples of isothermal TA – OSL measurements in BeO discs; the inset presents a TL and a RTL glow curve after TA – OSL at 190 °C.

Results and Discussion Several isothermal TA – OSL features are studied, including the shape of the TA – OSL curve, the dependence of both shape and intensity on the stimulation temperature, as well as the dose response of the TA – OSL after selecting the optimum stimulation temperature. The intense residual TL (RTL) signal after TA – OSL (inset of Fig. 1) suggests that charge of TA – OSL redistribute via the conduction band. This latter conclusion is also supported by the TA – OSL shape of BeO, which forms a narrow peak for short stimulation times; this latter feature could be easily presented by Fig. 1. Therefore, the TA – OSL curves were fitted using the appropriate transfer luminescence model. Finally, the impact of the complex thermal quenching effect in BeO on both the calculation of the thermal assistance activation energy of TA – OSL as well as the corresponding dose response is also discussed in detail.

Conclusion The TA – OSL properties of BeO are quite interesting; besides Al_2O_3:C, BeO is the second reported phosphor yielding peak shaped TA – OSL curve. The selection of the appropriate measurement temperature becomes crucial for the isothermal TA – OSL dose response features.

OSL characterization of calcium silicate polycrystals.

Gilson S. Goveia[1]*, C. D. Gonzales-Lorenzo[1], J. F. D. Chubaci[1],
S. Watanabe[1], L. F. Nascimento[2]
[1]*LACIFID, Institute of Physics, University of São Paulo, São Paulo, Brazil*
[2]*Belgian Nuclear Research Centre, SCK-CEN, Mol, Belgium*

Highlights The aim of this work is to study the possible application of calcium silicate for OSL dosimetry.

Key words OSL, calcium silicate, dosimetry.

Background and Objectives Calcium Silicate ($CaSiO_3$) with various interesting physical and chemical characteristics such as high mechanical capacity, resistance to humidity and fire, chemical inertia, not being abrasive or corrosive to other materials in which it is applied and can be used in various forms. It is very often used as thermal insulation in passive fire protection systems, once it is safer than asbestos; anti-caking agent in food preparation including table salt; as a sealant; and also, as cement component among many other uses. Calcium Silicate has a fluorescent property that may or may not vary according to the radiation dose received. This work is intended to evaluate the dosimetry characteristics through the technique of widely used Optically Stimulated Luminescence (OSL).

Materials and Methods Calcium silicate was produced by a combination of calcium oxide and silicon oxide in a blend heat treated at 1500ºC for about 2 hours and then submitted to a cooling process of about 100ºC per hour during about 24 hours down to room temperature for the desired crystalline formation. The sample was then removed from the crucible, macerated and sieved to a particle size of 75 micrometer. A batch of approximately 20 mg of calcium silicate was produced and taken for OSL response studies at SCK-CEN, Belgium. The results were obtained using a Risø reader, by making different sequences on different days using blue LED stimulation for 600 seconds (1 point per second) and irradiations with a Sr/Y source (80 mGy/s), with given doses ranging from 0 to 28 Gy.

Results and Discussion OSL results show a linear growth response in both TOSL (Average Total OSL minus background) and POSL (Mean of the 2 first seconds minus the background) with increasing radiation dose. There were four separate dose response tests, both TOSL and POSL had a linear response, as can be seen in the graphs (Figure 1).

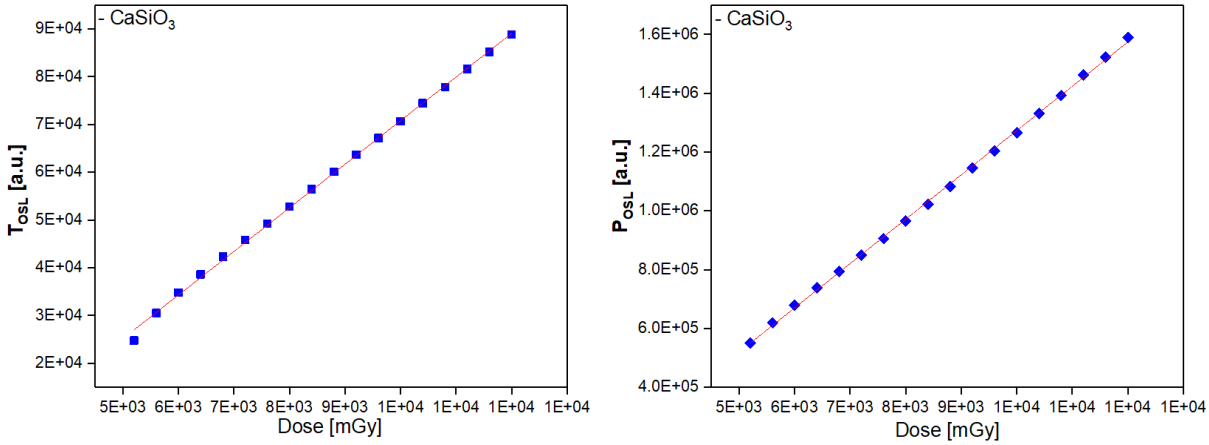

Figure 1. The T_{OSL} and P_{OSL} for increasing radiation dose exposure.

The OSL reading reproducibility test of the samples showed a compatibility of the response curve between the results after 20 rounds. The fading test consisted on measuring the emission of the sample shortly after being irradiated, without exciting it with the LED, i.e., reading the spontaneous emission of the sample, followed by an OSL reading (for both tests the sample was irradiated with 800 mGy). This test showed a fast decay in the OSL reading for the first 300 seconds before reaching a background value, but it may not affect the OSL dose response results as usually the time between irradiation and the reading is longer than the short-time fading effect. The different decay pattern between the fading curve and the OSL may indicate that they have different centers (fading may be caused by a shallow trap). Other tests focused on the reproducibility of readings, light-induced OSL and stability of the OSL signal upon long time storage are in progress.

Conclusion The results show good linearity with the given doses and short-time fading that ceases after 300 seconds. Further studies are under development for general characterization and possible applications in dosimetry. The sample apparently exhibits a stochastic effect characteristic even at the end of each OSL cycle, but this effect is still under investigation. There is the possibility of producing thin films from this material for wider application in dosimetry and further physical characterization. (This work is partially supported by FAPESP (Proc. 2014/03085-0), CNPq and ONR-G)

References

1) Gonzales-Lorenzo, Carlos D.; Watanabe, S.; Cano, Nilo F.; Ayala-Arenas, Jorge S.; Bueno, Carmen C. - Synthetic polycrystals of $CaSiO_3$ un-doped and Cd, B, Dy, Eu-doped for gamma and neutron detection. JOURNAL OF LUMINESCENCE, v. 201, p. 5-10, 2018.

RPL observed in $LiCaAlF_6$:Sm

Go Okada[1]*, Noriaki Kawaguchi[2], Hidehito Nanto[1], Safa Kasap[3], Takayuki Yanagida[2]
[1]*Kanazawa Institute of Technology, Nonoichi, Japan*
[2]*Nara Institute of Science and Technology, Ikoma, Japan*
[3]*University of Saskatchewan, Saskatoon, Japan*

Highlight Sm-doped $LiCaAlF_6$ compound was successfully obtained by the mechanochemical synthesis technique. The obtained material was found to show radio-photoluminescence (RPL) where strong photoluminescence (PL) appears around 700 nm (excitation at 360 nm) after irradiation with X-rays, and the intensity increases with radiation dose.

Keywords Sm, $LiCaAlF_6$, RPL, mechanochemical syntehsis

Background and Objectives $LiCaAlF_6$ is a well-known compound as a phosphor material for laser and scintillator applications. In particular, Ce^{3+}- and Eu^{2+}-doped $LiCaAlF_6$ single crystals show notable scintillation properties, and they are especially used for neutron detections because ^6Li has a large cross-section with neutrons due to the nuclear reaction of $^6Li + n \rightarrow \alpha + T + 4.78$ MeV. The latter material is, in fact, a breakthrough of neutron detectors because the supply of the conventional detection element, ^3He, dramatically decreased, and the market price went up extremely high. Furthermore, the Ce^{3+}- and Eu^{2+}-doped $LiCaAlF_6$ as well as those doped with other rare-earth ions were reported to have thermally- and optically-stimulated luminescence (TSL and OSL) properties; however, as far as we are aware, no reports were found to show radio-photoluminescence (RPL) in this host matrix. RPL is an dosimetric phenomenon which has a great potential to be used as a strong tool of microdosimetry. Therefore, the objective of this research was to develop a $LiCaAlF_6$-based phosphor material which shows RPL for a potential application of neutron microdosimetry.

Materials and Methods Towards the motivation of developing a $LiCaAlF_6$-based RPL material, we have synthesized Sm-doped $LiCaAlF_6$ compound via the mechanochemical technique. The obtained materials with different concentrations of Sm were studied by using several characterization techniques such as X-ray diffraction (XRD), PL excitation/emission, and PL lifetime.

Results and Discussion $LiCaAlF_6$:Sm compound was successfully obtained by the mechanochemical synthesis technique. Fig. 1 illustrates XRD patterns as a function of synthesis time. As confirmed in the figure, the convoluted diffraction patterns of starting compounds are dominantly observed without the mechanochemical process while the diffraction pattern corresponding to $LiCaAlF_6$ becomes evident with the process time. From this observation, we confirmed that $LiCaAlF_6$ compound was successfully obtained. Fig. 2 shows PL spectrum of the obtained sample as a function of X-ray irradiation dose. When the sample is not irradiated, or when the sample is as-prepared, PL predominantly due to the 4f-4f transitions of Sm^{3+} is recognized around 550, 600, and 650 nm. This observation indicates that the Sm ion is activated as luminescent centre and incorporated with the $LiCaAlF_6$ compound. With increasing irradiation dose, the emission around 700 nm increases. The origin of the emission around 700 nm is considered to be due to the 4f-4f transitions of Sm^{2+} as the spectral emission positions are typical. The inset of Fig. 2 demonstrates dose-response curve of integrated PL signal around 700 nm as response, where we confirmed that our material has a sensitivity of at least 100 mGy.

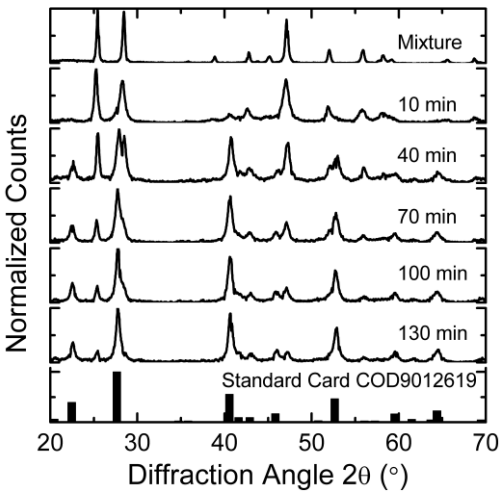

Fig. 1 XRD patterns of mechanochemical processed samples as a function of the processing time.

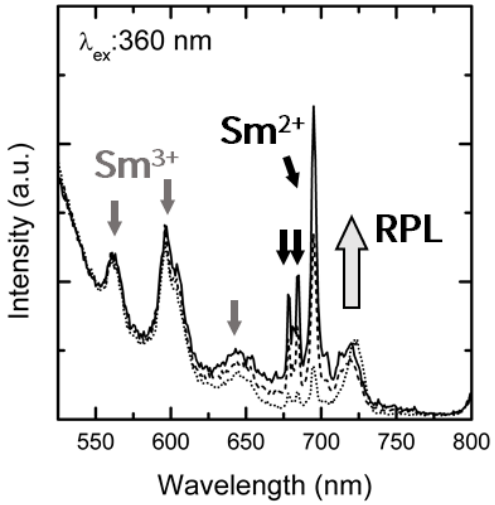

Fig. 2 PL spectrum of $LiCaAlF_6$:Sm as a function of X-ray irradiation dose. The inset illustrates the dose response function of RPL as integrated PL signal around 700 nm induced by irradiation.

Conclusion $LiCaAlF_6$:Sm compound was successfully obtained by the mechanochemical synthesis technique, and we have confirmed that it has RPL properties. Since it is consisted of Li, the material has a great potential to be used for neutron dosimetry.

NIR-emitting Scintillators for Dosimetry

Go Okada[1]*, Noriaki Kawaguchi[2], Hidehito Nanto[1], Takayuki Yanagida[2]
[1]*Kanazawa Institute of Technology, Nonoichi, Japan*
[2]*Nara Institute of Science and Technology, Ikoma, Japan*

Highlight We have synthesized a series of garnet crystals doped with Nd^{3+}, and they were studied as scintillators for dosimetric applications. The materials show strong NIR emission around 1050 nm under both UV-Vis light and X-rays. The NIR emission is useful when the scintillation signal is collected via optical fibre especially under strong radiation dose since the transmission through optical fibre is effective for the NIR light and the signal can be easily separated from Cherenkov radiation coming from interactions of ionizing radiations with the optical fibre, scintillator etc.

Keywords Nd^{3+}, garnet crystals, NIR

Background and Objectives Scintillators are a type of phosphor materials which convert ionizing radiation to low energy photons; therefore, they allow us to utilize conventional photodetectors to detect ionizing radiation indirectly. Over the past decades, a large number of scintillator materials have been developed, and they have been utilized in a wide range of applications in, for instance, medical diagnosis, border security, and science and industry. Despite the long history and large number of applications, the most scintillators show luminescence in the near UV range and visible range. One of the main reasons is considered that a photomultiplier tube (PMT) and Si photodiode have been recognized as a very sensitive photodetector, and they typically have the maximum sensitivity in the near UV and visible ranges, respectively. In recent years, however, a new class of photodetectors having high sensitivity in the near-infrared (NIR) range have been developed, which allows us to extend the choice of scintillator materials. Particularly, NIR-emitting scintillators are attractive when the scintillation light is collected through an optical fibre as illustrated in Fig. 1. Especially when the radiation dose is large, the transmittance medium of optical fibre experiences radiation damage which considerably reduces light

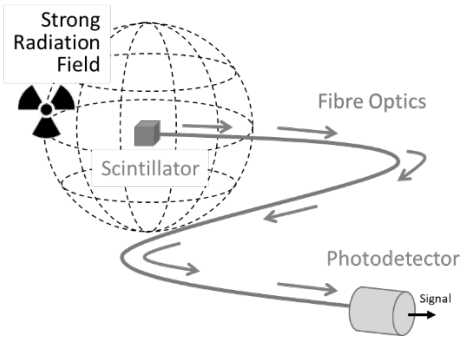

Fig. 1 Configuration of radiation measurement using NIR-emitting scintillator through fibre optics.

propagation efficiency. In addition, Cherenkov radiation is expected to appear in the near UV range, which cannot be separated from scintillation signal if a conventional scintillator is used while NIR light can be easily separated. For these reasons, the motivation of this research is to develop a series of NIR emitting scintillators and then test for radiation measurement, especially to measure large radiation dose from a distant site via an optical fibre.

Materials and Methods A series of garnet crystals were synthesized by the floating zone technique. A small fraction of Nd^{3+} was added to the crystal host as a luminescent activator. The concentration of Nd^{3+} varied as 0.5, 1.0, 2.0, 5.0, and 10.0%, and the tested host materials are $Y_3Al_5O_{12}$ (YAG), $Y_3Al_2Ga_3O_{12}$ (YAGG), $Gd_3Al_2Ga_3O_{12}$ (GAGG), $Lu_3Al_5O_{12}$ (LuAG), and $Lu_3Al_2Ga_3O_{12}$ (LuAGG). For comparison, we have measured scintillation spectrum, scintillation lifetime as well as conventional photoluminescence properties.

Results and Discussion The above mentioned garnet crystals were successfully obtained by the floating zone technique. The materials show strong luminescence under X-ray irradiation as illustrated in Fig. 2. The spectrum consists of sharp line emissions over the visible and NIR regions, and the origin is attributed to the 4f-4f transitions of Nd^{3+}. The scintillation intensity strongly depends on the host material while the photoluminescence quantum yield is reasonably consistent (~60-70%) regardless of the host material. This result suggests that the energy transfer efficiency, which is the efficiency of absorbed radiation energy to the host material to be transferred to luminescent centre, is strongly dependent on the choice of host material.

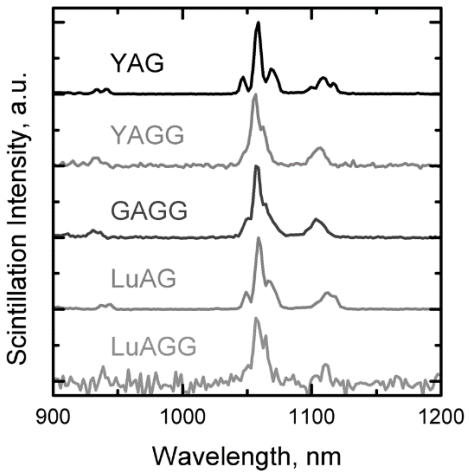

Fig. 2 X-ray induced scintillation spectra of a series of garnet crystals doped with Nd^{3+}.

Conclusion We have synthesized a series of Nd^{3+}-doped garnet crystals as NIR-emitting scintillator with different concentrations of Nd^{3+} and different host materials, and then the luminescent properties were mainly investigated for scintillator applications. Strong luminescence due to the 4f-4f transitions of Nd^{3+} in the NIR range was confirmed in all the samples under X-rays, but it was revealed that the energy transfer efficiency strongly depends on the host material.

Novel Mechanism of Scintillation Enhancement by LED Light using Scintillator–silica Fine Powder Pellet

Hirokazu Miyoshi[1]*, Yoko Utsumi[1], Kazuo Taniguchi[2], Hitoshi Gotoh[3], Tomoya Kurata[4], Miyuki Wakita[4], Miho Sakata[4] and Tohru Maruno[4]

[1]Advance Radiation Research, Education, and Management Center, Tokushima University, Tokushima, Japan, [2]Techno Bridge Co., Ltd., Osaka, Japan, [3]ACTiS Co., Ltd., Tokushima, Japan, [4]NTT-AT Creative Co., Ltd., Tokushima, Japan

Highlights A new mechanism of enhancement of scintillation on scintillator–silica fine powder pellets was proposed on the basis of thermoluminescence glow curves of pellets divided into those irradiated and nonirradiated by LED light.

Key words scintillation, glow curve, LED, pellet, thermoluminescence

Background and Objectives Scintillator–silica fine powders (FPs) were prepared by a previously described method[1]. The obtained powders were pressed at about 6 ton/cm^2 using a tablet molding machine. It has been reported that the detection efficiency was enhanced by LED light (365 or 375 nm) irradiation or radiation[2]. However, the mechanism of scintillation enhancement has not been clarified to date. Upon LED light irradiation, the excited electrons accumulate at an energy level lower than those of scintillators. When ß-particles are irradiated onto a pellet of scintillator–silica FP pellet, the electrons accumulated upon LED light irradiation are released, enhancing scintillation light. To achieve this, the accumulated electrons must transfer to the entire surface of the pellet.

In this study, the glow curve of the thermoluminescence (TL) of the LED-light-irradiated pellet was measured to clarify the lower energy level of electrons and their electron accumulation. We clarified whether the electrons generated transfer to the entire surface by dividing the surface of a pellet into the LED-light- and non-LED-light irradiated areas.

Materials and Methods The prepared scintillator–silica FP pellets were set in a home-made vessel on a heater. Temperature was measured against time using a thermocouple with a USB-type detalogger, and TL intensity was measured as current against time with a photomultiplier tube (PMT) connected to an electroanalyzer (BAS Co., Ltd.). Finally, those times of temperature and current were matched to obtain TL intensity against temperature using Origin J software. The programming rate was about 2 ºC / min. An energy of a trap level (E , approximately 1.0 eV) was estimated by the programming rate method. The transmission of charges from the LED-light-irradiated area to the non-LED-

light-irradiated area was confirmed by dividing the surface of a pellet into these areas and measuring the TL glow curve using a metal vessel or a black paper.

Results and Discussion Figure 1 shows the TL glow curves of scintillator–silica FP pellets. The solid line shows the measurements of the LED-light irradiated area and the dashed line shows those of the non-irradiated area. As shown in the figure, even the non-LED-light irradiated area shows a TL glow curve of almost 70% of that of the LED-light-irradiated area. Figure 2 shows the TL glow curves of the areas of the divided pellets. For the LED light irradiation and measurements, the solid line shows the different area and the same area (dash-dotted line) of the divided pellets on the metal vessel and that on a black paper (dashed line). As shown in the figure, in the case of the metal vessel, even the divided pellet showed large TL grow curves. Otherwise, in the case of the black paper, the TL glow curve clearly decreased. These findings indicate that the electrons generated by LED light irradiation transfer to the entire surface of the pellets.

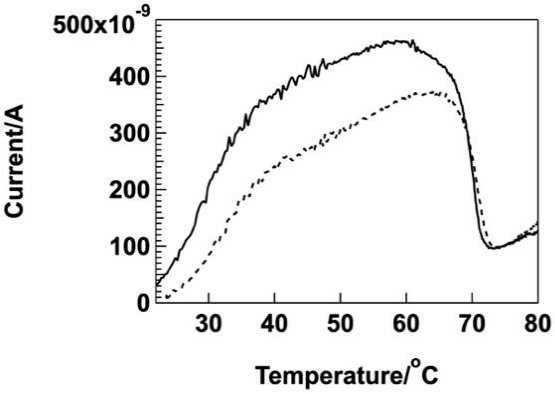

Figure 1 TL glow curves of scintillator–silica FP pellets

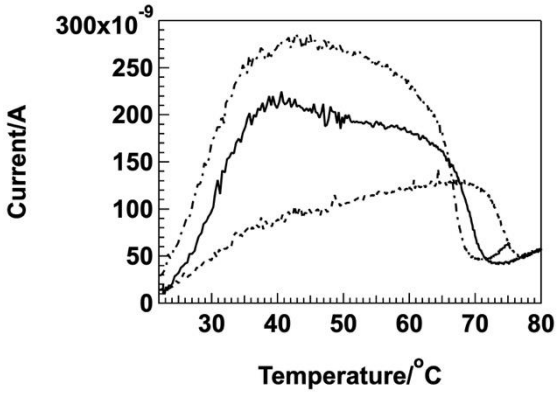

Figure 2 TL glow curves of the scintillator–silica FP pellets divided into LED-light- and non-LED-light irradiated areas

Conclusion The trap level was confirmed from the TL glow curves. The TL glow curves of the two areas of the pellets on the metal vessel and black paper indicated that the generated electrons transfer between the LED-light- and non- LED-light irradiated areas.

References

1) H. Miyoshi, M. Hiroura, K. Tsujimoto, N. Irikura, T. Otani, Y. Shinohara, Preparation of new scintillation imaging material composed of scintillator-silica fine powders and its imaging of tritium, Radiat. Prot. Dosim., 174(4), (2017) 478–484.
2) H. Miyoshi, H. Gotoh, M. Hiroura, Y. Yamanaka, N. Irikura, T. Otani, Y. Yamamoto, Enhancement of counting efficiency for tritium using light-excited scintillator silica pellets, J. Radioanal. Nucl. Chem., 311(3), (2017) 1991–1999.

Optically-stimulated luminescence properties of CsBr:Eu transparent ceramics

Hiromi Kimura[1]*, Takumi Kato[1], Daisuke Nakauchi[1], Masaki Akatsuka[1], Noriaki Kawaguchi[1], Takayuki Yanagida[1]

[1]*Nara Institute of Science and Technology, Nara, Japan*

Highlights Eu-doped CsBr transparent ceramic samples with different concentrations of Eu (0.05, 0.1, 0.5, 1.0 and 5.0 mol.%) were synthesized by the spark plasma sintering (SPS) method. In the OSL properties, the OSL spectra of all the samples showed an emission band peaking at around 450 nm, which was attributed to the 5d-4f transitions of Eu^{2+}.

Key words transparent ceramics, OSL, TSL, CsBr, Eu

Background Storage phosphors have a function to record the radiation dose, and they are often used for ionizing radiation detectors. When the phosphors are irradiated with ionizing radiations such as X- and γ-rays, the phosphors absorbed the radiation energy, and then the electrons and holes are generated. Following the generation process, these carriers are temporarily trapped in carrier trapping centers. The trapped electrons and holes can be released by the stimulation to emit photons. Here, the light emission by the heat and light stimulation is called thermally-stimulated luminescence (TSL) and optically-stimulated luminescence (OSL), respectively. Such phosphors have been utilized in individual radiation monitoring devices and imaging plates (IPs).

Since the late 1990s, Eu-doped CsBr (CsBr:Eu) has attracted much attention as IPs [1)] because it has good properties such as high OSL intensity, short decay time and high X-ray detection efficiency. However, almost all of the studies were done in a form of bulk single crystal [2)], bulk opaque ceramics [3)] and thin film prepared by a vacuum deposition technique [4)]. In recent years, we have reported that the OSL properties were improved in CsBr:Eu transparent ceramic samples compared with those of single crystals [5)]. In this study, we have synthesized CsBr:Eu transparent ceramic samples with various concentrations of Eu using the spark plasma sintering (SPS) methods, and evaluated optical and OSL properties.

Methods CsBr:Eu transparent ceramic samples with different concentrations of Eu (0.05, 0.1, 0.5, 1.0 and 5.0 mol%) were synthesized by the SPS method using Sinter Land LabX-100 in a vacuum. Raw powder of CsBr (>99.99%, Furutachi Chemical) and $EuCl_3 \cdot 6H_2O$ (>99.9%, Furutachi Chemical) were homogeneously mixed using a mortar and pestle, and the added molecular fraction of Eu was with respect to that of Cs. During the sintering, the

temperature was increased from 20 to 450°C at a rate of 45 °C/min and held for 10 min while applying the pressure of 6 MPa. The temperature was measured using a K-thermocouple attached on the graphite die. After the synthesis, the wide surfaces of the ceramic samples were polished by hand using a sandpaper (3000 grits), and the prepared samples were measured diffuse transmittance (SolidSpec-3700, Shimadzu) and OSL spectra (C11367, Hamamatsu Photonics).

Results and Discussion Figure 1 shows diffuse transmittance spectra of the samples. The transmittance of all the samples were approximately ~60%. The transmittance value slightly decreased as the concentration of Eu increased. In all the samples, the absorption of 4f-5d transitions Eu^{2+} were confirmed around 280 and 350 nm [6].

The OSL spectra of the samples upon 630 nm stimulation are indicated in Figure. 2. When the samples were irradiated by X-rays (~1 Gy), the OSL spectra of the samples showed an emission band peaking at around 450 nm, and the emission origin was attributed to the 5d-4f transitions of Eu^{2+}.

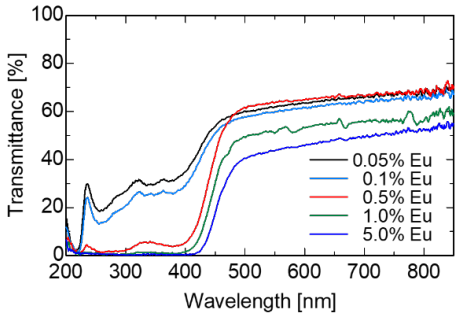

Figure 1. Diffuse transmittance spectra of Eu-doped (0.05, 0.1, 0.5, 1.0 and 5.0 mol%) CsBr transparent ceramic samples.

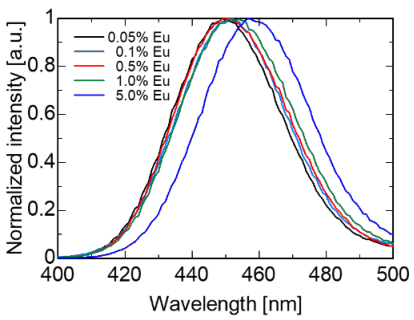

Figure 2. OSL spectra of Eu-doped (0.05, 0.1, 0.5, 1.0 and 5.0 mol%) CsBr transparent ceramic samples.

Conclusion We have synthesized CsBr:Eu transparent ceramic samples with different concentrations of Eu (0.05, 0.1, 0.5, 1.0 and 5.0 mol%) using the SPS methods. All the samples showed a high transmittance in visible range. In the OSL spectra, the samples showed an emission band peaking at around 450 nm, which was due to the 5d-4f transitions of Eu^{2+}.

References

1) P. Hackenschmied, *et al.*, Nucl. Instruments Methods Phys. Res., B **191** (2002) 163.
2) K. Saeki, *et al.*, Opt. Mater. **61** (2016) 125.
3) N.M. Winch, *et al.*, Nucl. Instruments Methods Phys. Res., A **654** (2011) 308.
4) A. Ejiri, *et al.*, Solid State Commun. **110** (1999) 575.
5) H. Kimura, *et al.*, Optik **157** (2018) 421.
6) N. Ganapathi Subramaniam, *et al.*, Mater. Lett. **57** (2003) 2021.

Scintillation and thermoluminescence properties of Tm-doped $CaHfO_3$ crystals.

Hiroyuki Fukushima*, Daisuke Nakauchi, Noriaki Kawaguchi, Takayuki Yanagida
Division of Materials Science, Nara Institute of Science and Technology, Nara, Japan

Highlights

· Tm-doped $CaHfO_3$ crystals were synthesized by the floating zone method with xenon arc lamps. · Scintillation and thermoluminescence properties of Tm-doped $CaHfO_3$ were evaluated. · The Tm-doped samples show thermoluminescence glow peaks at around 75 and 240 °C.

Key words Scintillation, Dosimetry, Thermoluminescence, $CaHfO_3$,

Background and Objectives Storage phosphors are utilized for personal dose monitoring application. Such materials irradiated with ionizing radiation temporarily stores the absorbed energy in a form of electrons and holes at trap levels and emit lights when excited by thermal or optical stimulations. The former storage luminescence is called as thermoluminescence (TL), and the latter one optically stimulated luminescence (OSL). Almost phosphor-type dosimeters are solid state materials such as C-doped Al_2O_3 (McKeever et al., 1996), Ag-doped phosphate glass (Miyamoto et al., 2011) and Tm-doped CaF_2 (Kawano et al., 2018). Recently, we have reported the scintillation properties of Ce-doped $CaHfO_3$ crystals. The afterglow levels of $CaHfO_3$ indicated relatively high value, thus, a strong TL emission could be expected. In this study, Tm-doped $CaHfO_3$ crystals were synthesized by the floating zone method with xenon arc lamps, and the thermoluminescence and scintillation properties were evaluated.

Materials and Methods Undoped and Tm-doped $CaHfO_3$ crystals were synthesized by the floating zone method with xenon arc lamps. As a raw material, CaO (Furuuchi Chemical, 99.99 %), HfO_2 (Furuuchi Chemical, 99.95 %) and Tm_2O_3 (Furuuchi Chemical, 99.99 %) were used and mixed homogeneously. The mixture was formed to a cylindrical rod by applying a water pressure, and then the rod was sintered at 1400 °C for 8 h. The X-ray-induced scintillation spectra were measured by using X-ray generator where a bias voltage and a tube current are 80 kV and 1.2 mA, respectively. The TL glow curve was evaluated after X-ray irradiation of 2 Gy. The increment ratio of temperature was 1 °C/s, and the measurement range was from 25 to 490 °C. The TL emission spectrum was measured by using a spectrometer (QEPro, Ocean).

Results and Discussion Figure 1 shows X-ray-induced scintillation spectra of the undoped

and 1.0 % Tm-doped $CaHfO_3$ crystals. The undoped crystal showed broad emission around 440 nm while the Tm-doped crystal exhibited sharp emissions of Tm^{3+} around 350 ($^1I_6 \rightarrow {}^3F_4$), 360 ($^1D_2 \rightarrow {}^3H_6$), 450 ($^1D_2 \rightarrow {}^3F_4$) and 470 nm ($^1G_4 \rightarrow {}^3H_6$).

Figure 2 shows TL glow peak of 1.0 % Tm-doped $CaHfO_3$ crystal. The TL glow peak appear around 75 and 240 °C, and the emission was similar to other Tm-doped materials (e.g., Kawano et al., 2018).

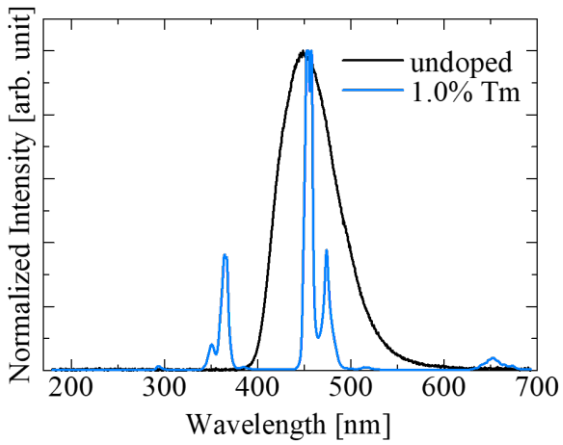

Fig. 1 X-ray-induced scintillation spectra of undoped and Tm-doped $CaHfO_3$ crystals.

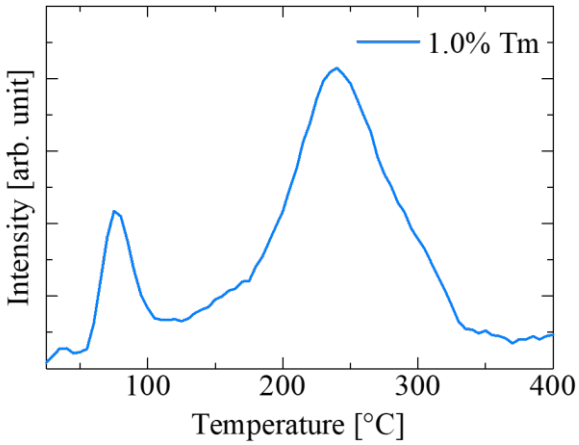

Fig. 2 TL glow curve of Tm-doped $CaHfO_3$ crystal after 2 Gy X-ray irradiation.

Conclusion Scintillation and thermoluminescence properties of Tm-doped $CaHfO_3$ crystals were evaluated for the first time. The X-ray-induced scintillation spectra of Tm-doped $CaHfO_3$ crystal showed sharp emission lines owing to 4f-4f transitions of Tm^{3+}. The TL glow curve showed peaks at around 75 and 240 °C. From these results, Tm-doped $CaHfO_3$ crystal indicated a good potential for scintillation and thermoluminescence materials.

References

Kawano, N., Nakauchi, D., Fukuda, K., Okada, G., Kawaguchi, N., Yanagida, T., 2018. Comparative study of scintillation and dosimetric properties between Tm-doped CaF_2 translucent ceramic and single crystal. Jpn. J. Appl. Phys. 57, 102401.

McKeever, S.W.S., Akselrod, M.., Markey, B.G., 1996. Pulsed Optically Stimulated Luminescence Dosimetry Using Alpha-Al_2O_3:C. Radiat. Prot. Dosimetry 65, 267–272.

Miyamoto, Y., Takei, Y., Nanto, H., Kurobori, T., Konnai, A., Yanagida, T., Yoshikawa, A., Shimotsuma, Y., Sakakura, M., Miura, K., Hirao, K., Nagashima, Y., Yamamoto, T., 2011. Radiophotoluminescence from silver-doped phosphate glass. Radiat. Meas. 46, 1480–1483.

Study on structural and dosimetric properties of Ce and Dy dopped LaAlO3 produced in vegetable oil

Iury Santos Silveira[1]*, Harlley Dantas Hauradou Xavier[1], Carolina Melo de Abreu[1], Divanizia do Nascimento Souza[1]

[1]DFI/UFS, Universidade Federal de Sergipe, São Cristóvão, Brazil

Highlights Production and characterization of crystalline $LaAlO_3$:Ce,Dy with dosimetric properties was tested by means of a green synthesis using Copaiba oil.
The crystallite size of obtained $LaAlO_3$:Ce,Dy was nanometric, and its luminescence properties were maintained in comparation to well-known production routes of these material.

Key words Radiation, Dosimetry, UV Dosimetry, Rare-Earth, Thermoluminescence

Background and Objectives Dosimetric materials with thermoluminescent properties have been studied for more than 60 years. Theirs applications are present in several areas, such as personal, industrial and environmental dosimetry.[1)] Thermoluminescent (TL) dosimeters are mostly oxides, sulfates or sulfates doped with rare earth (RE) ions. The RE ions improve the TL signal. The objective of this work is to produce $LaAlO_3$:Ce,Dy through a variation of the Sol-Gel synthetic route using Copaiba vegetable oil and to study the optical and thermoluminescent properties of this material.

Materials and Methods To the production of lanthanum aluminate it was used: La_2O_3, HNO_3, $Al(NO_3)_3 \cdot 9H_2O$, $Ce(NO_3)_3 \cdot 6H_2O$, Dy_2O_3, Copaiba oil, and 99,8% ethyl alcohol. La_2O_3 and Dy_2O_3 were dissolved in nitric acid and mixed with ethyl alcohol, then the nitrates in their proportions were diluted in alcohol, just as the oil. The solutions were mixed and stirred for 30 minutes after homogenization, then they were heated to 200 °C for drying the alcohol. The final solution was thermally treated at 500 ºC for 5 hours, and later at 800 ºC for 6 hours. After the thermal treatments, the powdered material was macerated, and the characterizations were performed with X-ray Diffraction (XDR), Fourier Transform Infra-red Spectroscopy (FTIR), Scanning Electron Microscopy (SEM), and photoluminescence. Pellets with 3 mm diameter were produced using powdered samples, that were sintered at 900 ° C for 2 hours. The pellets were irradiated with a $^{90}Sr/^{90}Y$ beta source, gamma rays from ^{60}Co, and different wavelengths of ultraviolet light. After irradiation, the dosimetric properties of the pellets were subsequently analyzed by a TL-OSL reader.

Results and Discussion The diffraction results showed agreement between the obtained crystalline phase and the cataloged standards, demonstrating that there was crystal formation. With the FTIR analysis it was possible to identify the La-O and Al-O vibration bands, indicating the presence of $LaAlO_3$ perovskite and confirming the crystalline phase.[2] The optical emission and excitation spectra of pure and doped matrix are similar to those already known.[3] The thermoluminescent properties are also maintained. These results thus indicating that the synthesis using vegetable oil was successful.

Conclusion Synthesis with copaiba oil shown a very effective method in the production of lanthanum aluminate, so that there has been great conversion rate of reactants into product. Moreover, this route does not produce tailings and is healthy for the environment. The optical properties remained as already studied in the literature, indicating that the produced samples preserve their luminescent and dosimetric characteristics.

References

1) V. H. Oliveira; N. M. Khaidukov; E. C. Silva; L. O. Faria; Study of TL properties of $LaAlO_3$:Ce,Dy crystals for UV dosimetry. Radiation Measurments. 46 (2011) 1173-1175.
2) A. Morales-Hernández; J. Zarate-Medina; M.E. Contreras-García; J. Azorín-Nieto, T. Rivera-Montalvo; Synthesis and thermoluminescence of $LaAlO_3:Pr^{3+}$ to UVC radiation dosimetry. Apply Radiation and Isotopes. 118 (2016) 12-17.
3) T. Manohara, S.C. Prashanthaa, H. Nagabhushanab, K. Channakeshavalua, H.P. Nagaswarupaa; Photoluminescence Studies of Rare-Earth-Doped (Ce^{3+}) $LaAlO_3$ nanopoweders prepared by facile combustion route. Materials Today: Proceedings. 4 (2017) 11848–11856.

Characterization of Optically Stimulated Luminescence from LiF:Mg,Cu,P : Towards reusable high-resolution 3D dosimetry

Jacob Søgaard[1]*, Peter S. Skyt[3], Jørgen B. B. Petersen[2], Brian Julsgaard[1], Ludvig P. Muren[2,3], and Peter Balling[1]

[1]*Dept. of Physics and Astronomy & iNANO, Aarhus University, DK-8000 Aarhus C, Denmark*

[2]*Dept. of Medical Physics, Aarhus University and Aarhus University Hospital, DK-8200 Aarhus N, Denmark*

[3]*Danish Centre for Particle Therapy, Aarhus Univ. Hospital, DK-8200 Aarhus N, Denmark*

Highlights Embedding an optically stimulated luminescence (OSL) active dosimeter material as microparticles in a transparent silicone matrix creates a 3D optically accessible dosimeter. Characterization of OSL properties provides crucial information for an efficient 3D readout procedure. The OSL properties of the promising material LiF:Mg,Cu,P are reported.

Key words Optically Stimulated Luminescence (OSL), LiF:Mg,Cu,P (MCP), 3D Dosimetry, Characterization, Reusability

Background and Objectives Radiotherapy is an efficient and well-established method for curing cancer. However, to minimize radiation-induced normal-tissue damage, steep dose gradients along the circumference of the tumor volume are required and can be achieved by new treatment modalities such as proton therapy. Verification of such dose gradients calls for precise 3D dosimetry methods.

The work presented here provides necessary optically-stimulated-luminescence (OSL) characterization results as the foundation for the development of high-precision 3D dosimeters with formable shapes[1)], based on readout of the OSL signal from the well-known thermo-luminescence (TL) material LiF:Mg,Cu,P (MCP). Such dosimeters will be highly relevant in the development phase of new radiotherapy methods and modalities. The proposed procedure has the potential to provide reusable dosimeters, enabling standardized dosimetric verification programs for patients treated with radiotherapy.

Materials and Methods The spectral response of MCP was characterized by stimulating an MCP pellet (Mikrolab, Krakow, Poland) with a blue (460 nm) diode laser. The luminescence was imaged by a f=35 mm quartz lens onto a 250 µm entrance slit of a spectrometer (Princeton Instruments Acton SP2358) equipped with a CCD camera (PIXIS 100BR). The scattered-light signal from the stimulating laser was suppressed in the detection arm by a 400 nm bandpass filter (Thorlabs), and a short-pass filter with cutoff wavelength at 450 nm (OD4,

Edmund Optics) placed between the collecting lens and the spectrometer. The luminescence from pellets irradiated with a dose of 10(1) Gy (CS-137) was recorded as a function of time using a reasonably uniform stimulation intensity (CW-OSL) obtained by imaging the laser light transmitted through a circular aperture onto the pellet with a focusing lens (f=100 mm).
The simplest example of an OSL decay signal is obtained from a material with a single OSL trapping state and follows a single-exponential decay[2]. Assuming that this is the case for MCP, the measured OSL signal was fitted to the function $S(t) = BG + S_0\, e^{-\frac{t}{\tau}}$. In this scheme, the photoexcitation cross-section, σ, of OSL active electrons can be determined from τ as $\sigma = h\nu(\tau I)^{-1}$, where I is the intensity of the stimulating light.

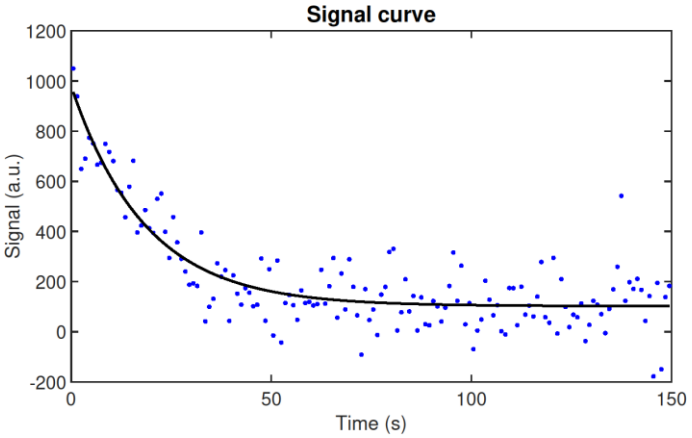

Figure 1.
Example of MCP OSL decay signal with a stimulation intensity of $I = 2.1(8) \cdot 10^2$ mW cm^{-2}.
Fit: $S(t) = BG + S_0 e^{-\frac{t}{\tau}}$, with $BG = 1.0(3) \cdot 10^2$, $S_0 = 9(1) \cdot 10^2$, and $\tau = 18(4)$ s.

Results and Discussion An exponential decay of the OSL signal was observed for MCP, and a photoionization cross-section of $\sigma = 1.1(7) \cdot 10^{-19}$ cm^2 was determined from the data shown in figure 1. The signal was obtained in a spectral window from 380 nm - 430 nm, which is in the vicinity of reported TL signals peaking at 360 nm[3].

Conclusion Our study showed that OSL signals from MCP are stimulated efficiently by a 460 nm laser. The preliminary photoionization cross-section value allows an estimate of scan times in future laser-scanning setups used for 3D readout.

References

1) M. Sadel, E. M. Høye, P. S. Skyt, L. P. Muren, J. B. B. Petersen, and P. Balling, J. Phys.: Conf. Ser. **847**, 012044 (2017), doi :10.1088/1742-6596/847/1/012044.
2) E. G. Yukihara and S. W. S. McKeever, Optically Stimulated Luminescence. John Wiley & Sons, Incorporated, 1. ed., 2011. ISBN: 9780470977057
3) W. Gieszczyk, P. Bilski, B. Obryk, P. Olko, and A. J. J. Bos, Radiat. Meas. 53-54, 22 – 30, 2013, doi: 10.1016/j.radmeas.2013.03.025

Effect of proton generator concentration and annealing temperature on the dose response of a novel radiochromic gel dosimeter

Jolan E. Taño[1,2,3,*], Shin-ichiro Hayashi[4], Seiko Hirota[1],
Chryzel Angelica B. Gonzales[1,2,3], Hiroshi Yasuda[1]

[1]*Department of Radiation Biophysics, RIRBM, Hiroshima University, Hiroshima, Japan*

[2]*Graduate School of Biomedical and Health Sciences,Hiroshima University,Hiroshima, Japan*

[3]*Phoenix Leader Education Program, Hiroshima University, Hiroshima, Japan*

[4]*Hiroshima International University, Higashi-Hiroshima, Hiroshima, Japan*

Highlights Higher proton generator concentration results to the increase of sensitivity of the radiochromic gel dosimeter based on a polyvinyl alcohol-iodide complex. The sensitivity of the gel dosimeter was nearly independent of the annealing temperature.

Key words radiochromic, gel dosimeter, proton generator, radiotherapy, annealing

Background and Objectives Current radiotherapy techniques deliver complex and volumetric treatment plans to the patient. In order to verify the dose delivered, a precise, three dimensional (3D), and tissue equivalent dose evaluation system is desirable. Radiochromic gel dosimeter has a potential of addressing these requirements. The latest studies on radiochromic gels reported about the utilization of polyvinyl alcohol (PVA) doped with an iodide complex with high radiation sensitivity[1-3]. Motivated by these studies, this research aims to develop a novel gel dosimeter composed of PVA crosslinked with glutaraldehyde (GTA) and doped with potassium iodide (KI), then analyze the effects of varying proton generator (glucono-δ-lactone, GDL) concentrations and annealing temperature to the sensitivity.

Materials and Methods The gel samples were produced using ultrapure water, and analytical grade reagents from Wako Pure Chemical Co., Japan. The PVA (partially hydrolyzed, 86~90 mol% saponification) was dissolved in water at 80˚C for 1 hour using a magnetic stirrer. The PVA solution was then allowed to cool down to 25˚C, then, the KI, fructose, GDL, and GTA (25% aqueous) were put into the solution and stirred until a homogeneous solution was achieved. A total of eight sample sets were prepared with different GDL molarities (i.e. 50, 100, 150, 200, 250, 300, 350 and 400 mM). The gel solutions were poured into PMMA cuvettes (10 x 10 x 45 mm^3) with polyethylene cover and annealed inside a dry heat sterilizer (MOV-112 S-PJ, PHC Holdings Co., Ltd., Japan) at various temperatures (i.e. 45˚C, 60˚and 75˚C) for 12 hours to allow gelation. A Gammacell-40 research irradiator (Best Theratronics Ltd., Canada) with low dose rate Cs-137 sources was used to irradiate the samples. The dose rate during the time of measurement was 0.835 Gy/min. The gel samples were irradiated with doses: 10, 20, 40 and 70 Gy, and one sample was maintained unirradiated as control. Absorbance was measured at 490 nm using a UV-vis spectrophotometer (Thermo Fisher Scientific Inc., USA). The dose response sensitivities of the samples were analyzed with respect to the GDL molarity and annealing temperature (AT). The change in absorbance (ΔAbsorbance) is calculated as the difference of the absorbance values of the irradiated [Abs(i)] and the non-irradiated [Abs(n)] samples, respectively:

$$\Delta\text{Absorbance} = \text{Abs(i)} - \text{Abs(n)}$$

Results and Discussion The resulting gel dosimeter was transparent and colorless if unirradiated and converts to a reddish hue after exposing to gamma-rays, as shown in Figure 1. Figure 2 presents the results of the GDL molarity dependence of the formula. The graph shows that the sensitivity of the gel samples correlated linearly with increasing GDL concentration for the dose range of 10 to 70 Gy. Also, high dose response linearity was observed with average R^2=0.99 from all samples. The result of the AT dependence test is shown in Figure 3. The graph shows that the sensitivity of the gel dosimeter was nearly independent of the AT, though it should be noticed that the sensitivity of the 75˚C samples was slightly lower compared to the results of the other AT samples.

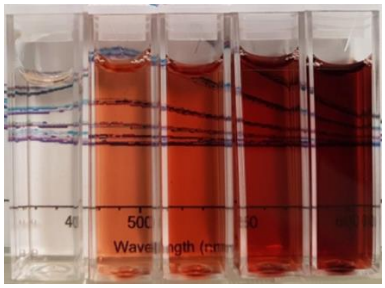

Figure 1 PVA-GTA-I samples irradiated with γ-rays. Doses from left to right: 0(control), 10, 20, 40, & 70 Gy.

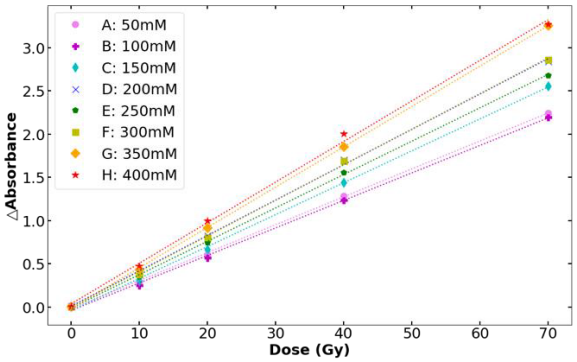

Figure 2 Dose - ΔAbs response of the PVA-GTA-I samples with various GDL molarities.

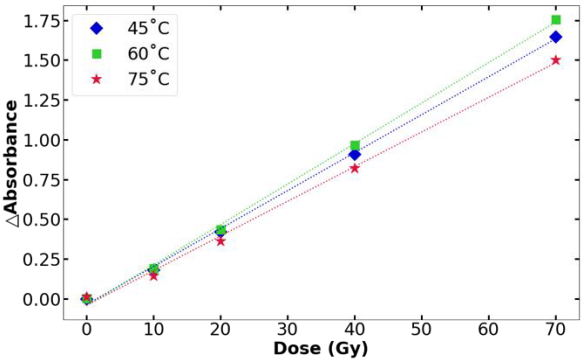

Figure 3 Dose - ΔAbs response of the PVA-GTA-I samples with different annealing temperatures.

Conclusion The researchers hereby report a novel radiochromic gel dosimeter composed of PVA crosslinked with GTA and doped with KI, GDL, and fructose. It was observed that the proton generator concentration increases the sensitivity of the gel dosimeter while maintaining good dose response linearity. Also, the annealing temperature has a minor influence on the radiation sensitivity of the gel dosimeter samples. It is thus expected that this novel gel dosimeter would be a valuable tool for 3D dosimetry in radiotherapy. Supplementary experiments are currently being performed to further investigate its dosimetry characteristics.

Acknowledgment This work is supported by JSPS KAKENHI (Grant Number 17K09072 and 18KK0417).

References

[1] Sunagawa T et al. Development of the Gel Indicator Using PVA and KI. 2017. *Mem*

Fukui Univ Technol (in Japanese). **47** 105–10.
[2] Hayashi S *et al* 2019 *J. Phys.: Conf. Ser.* (in press).
[3] Taño JE *et al* 2019 *J. Phys.: Conf. Ser.* (in press).

Lanthanide and transition metal doped $NaMgF_3$: Radio-photoluminescence and optically stimulated luminescence suitable for non-destructive luminescence-based dosimetry

Joseph J. Schuyt[1]* and Grant V.M. Williams[1]

[1]*The MacDiarmid Institute for Advanced Materials and Nanotechnology, SCPS, Victoria University of Wellington, PO Box 600, Wellington 6140, New Zealand*

Highlights OSL is observed in $NaMgF_3$ doped with Mn, Eu, or Sm and the response to radiation is linear over a wide dose range. PL and optical absorption data show that several radiation-induced defects contribute to the OSL and that these are primarily *F*-type centres. RPL is observed in the form of F-centre/Mn^{2+} complexes for Mn^{2+} doping, and is also observed in cases of lanthanide doping due to electron trapping by the divalent lanthanides. The OSL and RPL properties can be monitored in a complementary way to measure radiation doses.

Key words $NaMgF_3$, luminescence, dosimetry, defects, radiation

Background and Objectives Luminescence-based dosimeters have been extensively studied over the past several decades due to the advantages of optics-based sensing. Additionally, there is a need for tissue-equivalent dosimeters for radiotherapy applications[1)]. In recent years, emphasis has been placed on the development of novel materials that exhibit optically stimulated luminescence (OSL)[1,2)]. OSL occurs in materials post-irradiation, where exposure to radiation produces free electrons and holes that are trapped in various mid-bandgap defect states. Later stimulation of the material with light of a suitable wavelength may liberate the trapped charges, resulting in electron-hole recombination and the emission of light, where the intensity is proportional to the radiation dose[1,2)]. The OSL measurement technique has proven useful as it allows for highly sensitive optical readout. However, as readout involves the de-trapping of charges, the measurements necessarily erase the stored signal. It is therefore of interest to investigate additional radiation-induced luminescence changes, such as variations in the photoluminescence (PL) caused by defects or the transfer of charges, known as radio-photoluminescence (RPL)[2,3)]. Luminescence-based dosimeters capable of coupled RPL and OSL measurements should have improved device accuracy, sensitivity, and versatility. $NaMgF_3$ is a tissue-equivalent compound and is suitable for radiotherapy applications. Therefore, the development of a coupled OSL/RPL system in $NaMgF_3$ is highly encouraged.

Materials and Methods Polycrystalline samples of doped $NaMgF_3$ were synthesized by

stoichiometric mixing of precursor fluorides NaF, MgF_2, and dopants MnF_2, EuF_3, SmF_3, or YbF_3. The mixture was heated in an RF furnace to 1100°C, cooled to 1035°C over one hour, then cooled through the $NaMgF_3$ melting point to 1015°C over 12 hours. This method produced transparent samples. PL and OSL measurements were made using a Jobin-Yvon Fluorolog-3 spectrofluorometer. Transmittance data were obtained using a Shimadzu UV-2600 spectrophotometer. Samples were irradiated using 40 kV X-rays from a Phillips PW1730 X-ray generator operating at 20 mA, such that the dose rate was approximately 0.1 Gys^{-1}.

Results and Discussion All samples exhibited PL characteristic of the intended dopant. Optical absorption and PL measurements before and after irradiation show that several defects are formed during irradiation that contribute to OSL and that these defects are primarily F-type centres. The OSL emission intensity is characterised as a function of radiation dose for Eu^{2+}, Sm^{3+} and Mn^{2+} and shown to be linear over a wide dose range. F-centre/Mn^{2+} pairs are shown to form complexes, where electron interactions result in perturbed, spin-allowed Mn^{2+} luminescence that increases in intensity with radiation dose. The complexes can be probed non-destructively using suitable stimulation wavelengths. Sm^{3+} and Yb^{3+} are shown to act as deep electron traps, resulting in the X-ray induced conversion from the trivalent to divalent states. The conversion is readily detectible via PL and therefore constitutes RPL that is useful for dose monitoring. The large trap depths allow for non-destructive probing of the Sm and Yb luminescence. 405 nm stimulation produces luminescence from both Sm^{3+} and Sm^{2+}, and we demonstrate that the ratio of emissions Sm^{2+}/Sm^{3+} increases with dose up to ~500 Gy. The Sm^{3+} OSL can be coupled with the RPL in order to make cumulative and total dose measurements, with the added benefit of a record of dose history. The Mn^{2+} OSL can be coupled with the F-centre/Mn^{2+} complex RPL in order to make total, cumulative and real-time dose measurements.

Conclusion We demonstrate that both RPL and OSL are observed in variously doped $NaMgF_3$ compounds and characterise these phenomena as a function of radiation dose. Ultimately, we show that the two methods of dose monitoring may be used together in order to improve measurement versatility and accuracy.

References

1) J.J. Schuyt and G.V.M. Williams, Radiat. Meas. **121** (2019) 99-102.
2) J.J. Schuyt and G.V.M. Williams, Mater. Res. Bull. **106** (2018) 455-458.
3) G. Okada, F. Nakamura, N. Kawano, N. Kawaguchi, S. Kasap and T. Yanagida, Nucl. Instrum. Methods Phys. Res. B **435** (2018) 268-272.

OSL measurements with green light stimulation on four varieties of mineral fluorite

Mittani J. C. R.[1]*, Silva M. G.[1]
[1]*Federal São Paulo University, Campus Baixada Santista, Santos, Brazil*

Highlights This work presents OSL measurements using green light stimulation (532 nm) on four varieties of mineral fluorite (green, yellow, purple and yellow with purple highlights). For each sample it was analyzed the OSL intensity as a function of radiation dose and thermal treatment, fading on 24 hour period, and correlation with thermoluminescence.

Key words Fluorite, OSL, green light stimulation, thermoluminescence, fading.

Background and Objectives OSL has become a popular technique nowadays and thus new materials (phosphors) as well new equipments are being studied and developed. Natural or synthetic fluorite base detectors have been studied comprehensively in the last five decades either in their dosimetric or luminescence characteristics[1] and the studies still continue. In OSL, most of the studies have been done using blue stimulation[2-4], so in the present work, OSL measurements and analysis are made on natural fluorite (four varieties) using green light stimulation (532 nm), aiming at its characteristics and implications in radiation dosimetry.

Materials and Methods The mineral fluorite varieties used were green, yellow, purple and yellow with purple highlights as pellets with Teflon as binding agent. The phase of samples was verified by X-ray diffraction measurements using MiniFlex II analyzer from Rigaku. TL and OSL measurements were carried out using a homemade TL/OSL reader, equipped with Hamamatsu PMT, model H7360-2 and optical filter combination of BG-39 (~3 mm thick) and Corning 7-59 (~5 mm thick). The optical stimulation was done using two green laser diodes (532 nm) with a power output of ~100 mW each one. The heating rate used for TL measurements was 5°C/s from room temperature to 280°C. The samples were irradiated with different doses between 1 and 30 Gy using $^{90}Sr/^{90}Y$ source from RISO TL/OSL-DA-20 reader.

Results and Discussion TL measurements of four samples showed in common two TL peaks at ~120°C and 220°C (figure 1A). The green sample had the highest TL glow curve, while the yellow sample the lowest TL glow curve. Similar to TL the green sample also showed the highest OSL signal intensity and the yellow the lowest signal, however, in the last case, the signal showed a re-trapping process (figure 1B). The OSL intensity as a function of

radiation dose was linear for green, purple and yellow with purple highlights while yellow sample showed a supralinear behavior after 5 Gy of radiation dose. The OSL intensity as a function of thermal treatment up to the temperature of 260 °C (with temperature interval of 20°C) showed a small increment in OSL intensity at ~100°C only in the purple and green sample and after a decrease up to 150°C in all the samples, followed by a slight increase in 180-200°C to finally continue with the decrease. TL measurements after and before OSL measurements showed that OSL signal is largely due to the 140°C peak with little contribution of 220°C peak.

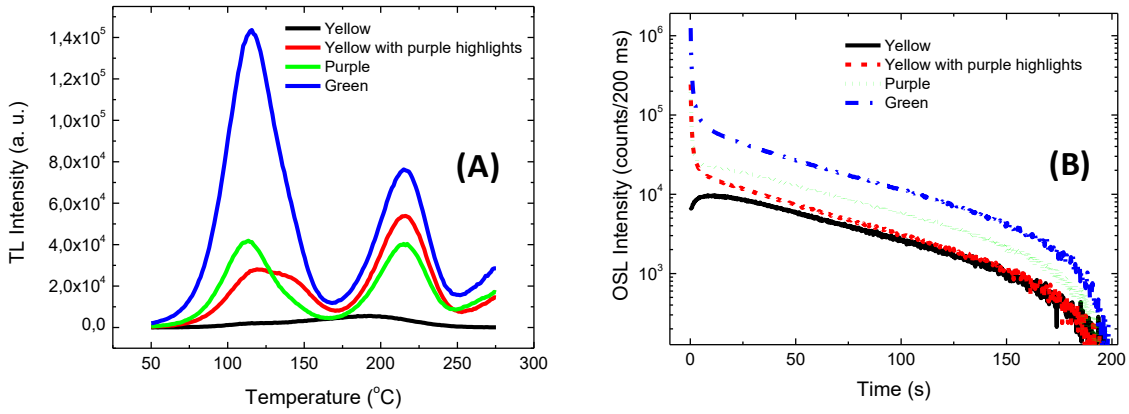

Figure 1. (**A**)TL and (**B**)OSL measurements on four varieties of fluorite mineral after 20 Gy of beta radiation dose.

Conclusion The four natural fluorite samples showed OSL signal with green light stimulation, and the green sample showed the most intense OSL signal among all. The samples showed a linear behavior to radiation doses between 1 and 30 Gy except the yellow sample. The samples presented two TL peaks at 120 and 240 °C and it was verified that most of the luminescence in OSL signal is due to 120 °C TL peak with little contribution of 220°C TL peak.

References

1) S. W. McKeever, M. Moscovitch and P. D. Townsend, Thermoluminescence dosimetry materials: Properties and Uses (Nuclear Technology Publishing, Ashford, England), (1995)
2) M. P. Chougaonkar, B. C. Bhatt, Radiat. Prot. Dosim. 112, 311, (2004)
3) F. A. Ferreira, E. M. Yoshimura, N. K. Umisedo, R. P. Nascimento, Radiat. Meas., 71, 254, (2014)
4) M. Kumar and M. S. Kulkarni, International Journal of Luminescence and applications, 4, 432, (2015)

Luminescence characteristics of Cs_2BaCl_4

Keisuke Takahashi[1]*, Yutaka Fujimoto[1], Masanori Koshimizu[1],
Takayuki Yanagida[2],Keisuke Asai[1]
[1]*Tohoku University, Miyagi, Japan*
[2] Nara Institute of Science and Technology,, *Nara, Japan*

Highlights Cs_2BaCl_4 crystal were fabricated by the Bridgeman method. Cs_2BaCl_4 had a short decay time of 1.2 ns, and the proportion of the first component was approximately 70%. Further, Cs_2BaCl_4 showed a fast component light yield of approximately 1700 photons/MeV. Although the decay time of Cs_2BaCl_4 was only slightly longer than that of BaF_2, the proportion of the fast component was much larger than that of BaF_2. The estimated fast component light yield of Cs_2BaCl_4 was found to be larger than that of BaF_2 in a previous report.

Key words Inorganic scintillator, fast-response scintillator, crystals.

Background and Objectives High-counting-rate measurements of radiation are required for various applications. Development of fast-response scintillators is a promising strategy to address this issue. In this study, we focused on inorganic scintillators. Typically, an inorganic scintillator is known to have high density and exhibit slow decay luminescence. However, several specific inorganic scintillators exhibit fast decay luminescence, including Auger-free luminescence (AFL), self-trapped excitons (STEs), and luminescence at the defect sites. AFL involves the radiative recombination of the outermost-core hole with a valence electron and is a fast process with a typical decay time constant of only a few nanoseconds. For example, several CsCl-based compounds such as CsCl, $CsCaCl_3$, and Cs_2ZnCl_4 show AFL. In particular, $BaCl_2$ is known to exhibit fast decay STEs of a few nanoseconds. Among the abovementioned inorganic scintillators, BaF_2 is the most successful example. The fast component of BaF_2, which is due to AFL, has a decay time constant of 0.8 ns[1)]. In addition, the light yield of the AFL component in BaF_2 is 1400 photons/MeV. However, BaF_2 also has some undesirable characteristics, which are its slow scintillation decay component caused by STEs and short wavelength of AFL. Because of its unfavorable properties, BaF_2 finds limited applications. Therefore, it is necessary to develop alternative materials with better properties.

With the aim of developing new inorganic scintillators that exhibit fast decay luminescence, we focused on Cs_2BaCl_4 in this study. Thus, we fabricated Cs_2BaCl_4 crystals and characterized their luminescence and scintillation properties.

Materials and Methods Crystal samples of Cs_2BaCl_4 were fabricated using the Bridgman method. CsCl and $BaCl_2$ powders were mixed in the desired stoichiometric ratios. For Cs_2BaCl_4, the photoluminescence (PL), X-ray excited radioluminescence (XRL), and γ-ray-

excited pulse-height spectra as well as the scintillation temporal profile were measured.

Results and Discussion Fig. 1 shows the PL spectra for excitation at 180, 150, and 84 nm. The excitation wavelengths correspond to the excitation within the bandgap, interband excitation, and outermost core-level excitation of Cs. No clear band is observed for the 84 nm excitation, which indicates that Cs_2BaCl_4 does not exhibit AFL. Bands at 410 and 480 nm are observed for excitation at 150 and 180 nm, and these can be ascribed to STEs and luminescence at the defects. Fig. 2 shows the XRL spectrum. The bands at 420 and 490 nm correspond to those in the PL spectra, and hence, they are also ascribed to STEs and luminescence at defects. Table 1 shows the decay time constants and proportion of the fast component, and the light yield of the fast components for Cs_2BaCl_4 and BaF_2 as comparison to example of the most successful. Cs_2BaCl_4 shows a short decay time at 1.2 ns, and the proportion of the fast component is approximately 70%. This fast scintillation can be ascribed to the luminescence at defects or STEs, as observed in the scintillation spectra. Although the decay time of Cs_2BaCl_4 is only slightly longer than that of BaF_2, the proportion of the fast component is much larger than that of BaF_2. The estimated fast component light yield of Cs_2BaCl_4 is approximately 1700 photons/MeV, which is larger than that of BaF_2 in a previous report.

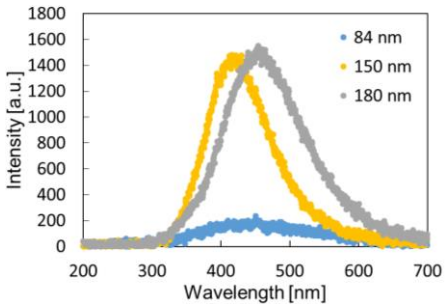

Fig. 1 Luminescence spectra of Cs_2BaCl_4 for excitation at 84, 150, and 180 nm.

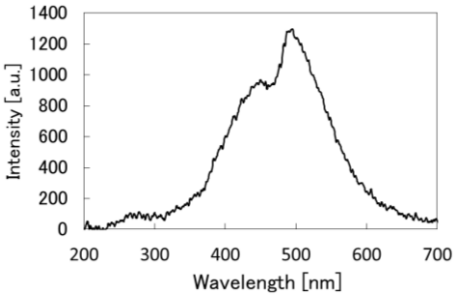

Fig. 2. Scinillation spectrum of Cs_2BaCl_4.

Table 1 Fast component decay time constants and light yields of Cs_2BaCl_4 and BaF_2.

Material	Decay time constant [ns]	Light yield [photons/MeV]
Cs_2BaCl_4	1.2 (70%)	1700
BaF_2	~0.8 (15%)	1400

Conclusion Cs_2BaCl_4 crystals were fabricated using the Bridgeman method. Cs_2BaCl_4 had a fast decay constant of 1.2 ns, and the proportion of the fast component was approximately 70%. Further, Cs_2BaCl_4 showed fast component light yield of approximately 1700 photons/MeV, which was larger than that of BaF_2.

References 1)P. Dorenbos et al., IEEE Trans. Nucl. Sci., 40, 424–430 (1993).

Response Evaluation of LiF-CsI Mixed Powder Neutron Scintillators

Kenichi Watanabe[1]*, Akihisa Ishikawa[1], Yuho Hirata[1], Atsushi Yamazaki[1], Sachiko Yoshihashi[1], Akira Uritani[1]

[1]*Nagoya University, Nagoya, Japan*

Highlights We fabricated the LiF-Tl:CsI mixed powder neutron scintillators. We experimentally evaluated the neutron response and some properties of the fabricated scintillators. The LiF-CsI mixed powder scintillator shows higher light yield for neutron irradiation than the single crystal Eu:$LiCaAlF_6$ scintillator.

Key words neutron scintillator, mixed powder scintillator, LiF, CsI:Tl

Background and Objectives Neutrons are widely used in various fields. Neutron detection is one of the key technologies in these applications. Recently, we are developing some mixed powder neutron scintillators, which are mixed powders between converter materials from neutrons to energetic charged particles and scintillator materials. The most famous mixed powder neutron scintillator is LiF and Ag:ZnS mixed powder. This combination shows quite high light yield but it also has limitation of effective scintillator thickness because of its opacity. This opacity is because of its large difference in the refractive indices between LiF and ZnS. Therefore, we attempted applying powder combination with similar refractive indices. The first candidate was LiF and Eu:CaF_2 combination[1]. However, this combination shows much lower light yield than Eu:$LiCaAlF_6$ scintillator, which is one of the bright, transparent and non-hygroscopic neutron scintillators. As a neutron scintillator, a bright and transparent one is desired. The LiF-Ag:ZnS combination is bright but opaque. On the other hand, the LiF-Eu:CaF_2 combination is translucent but not so bright. Therefore, we would like to attempt other combination to find better one. In this paper, we attempt LiF-Tl:CsI combination. The Tl:CsI scintillator is one of the famous bright scintillator and has lower refractive index than Ag:ZnS. Our goal is to find out the better combination with balance between brightness and transparency.

Materials and Methods We fabricated the LiF-Tl:CsI mixed powder scintillator. We crushed the bulk Tl:CsI scintillator and grinded them into fine powder. The ^6Li in LiF was 95% enriched. The LiF and Tl:CsI powder were mixed with weight ratio of 1:2. The mixed powder was layered on an acrylic plate The layered powder was solidified with transparent resin. The acrylic plate with the LiF-Tl:CsI mixed powder scintillator was

mounted on the entrance window of a photomultiplier tube (PMT). The PMT signal was fed into a digital signal processing multichannel analyzer. In order to evaluate response to neutrons, the fabricated scintillation detector was irradiated with neutrons from a ^{252}Cf source surrounded by polyethylene moderator.

Results and Discussion Figure 1 shows the pulse height spectrum obtained from the fabricated LiF-Tl:CsI mixed powder scintillation detector, which was irradiated with neutrons. For a comparison purpose, the spectrum obtained from the Eu:$LiCaAlF_6$ scintillator. We confirm that the fabricated LiF-Tl:CsI scintillator shows brighter light emission for neutron absorption events. Although they cannot show a peak shape, this LiF-Tl:CsI combination seems to be a promising mixed powder neutron scintillator.

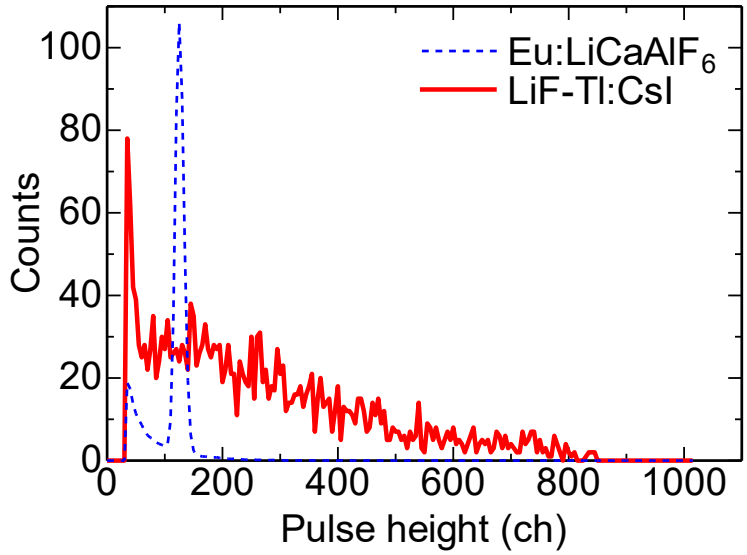

Figure 1. The pulse height spectrum obtained from the fabricated LiF-Tl:CsI mixed powder scintillation detector. The spectrum obtained from the Eu:$LiCaAlF_6$ scintillator is also plotted for a comparison purpose.

Conclusion We fabricated the LiF-Tl:CsI mixed powder neutron scintillator and evaluated its response to neutrons. This combination shows brighter light emission than Eu:$LiCaAlF_6$ scintillator. We concluded that the LiF-Tl:CsI mixed powder will be a promising neutron scintillator material.

References

1) K. Watanabe, N. Mitsuboshi, A Ishikawa, A. Yamazaki, S. Yoshihashi, A. Uritani, N. Kawaguchi, T. Yanagida, K. Fukuda, Basic study on a LiF-Eu:CaF_2 mixed powder neutron scintillator, Nucl. I. Methods Phys. Res. A, in press, https://doi.org/10.1016/j.nima.2018.09.079

Effect of Al_2O_3 on thermally stimulated luminescence of Cu-doped Li_2O-B_2O_3 glasses

Kiyomitsu Shinsho[1*], Hirokazu Masai[2], Risa Shimomura[1], Shin Yanagisawa[1], Daiki Maruyama[1], Hitomi Takagi[1], Morimi Kudo, Yusuke Koba[3]

[1]*Tokyo Metropolitan University, Tokyo, Japan*

[2]*National Institute of Advanced Industrial Science and Technology, Osaka, Japan*

[3]*National Institute of Radiological Sciences, Chiba, Japan*

Highlights We studied the effects of Al_2O_3 on the thermally stimulated luminescence (TSL) of Cu-doped Li_2O-B_2O_3 glasses. The TSL sensitivities of $0.01Cu_2O$-$33.33Li_2O$-$66.66B_2O_3$ glass are enhanced by addition of Al_2O_3. In addition, the glow peak temperature shifted from 420 K to 380 K along with decrease of the glass transition temperature.

Key words Dosimetry, glass, copper, Al_2O_3, thermally stimulated luminescence

Background and Objectives Recently, X-ray CT (Computed Tomography) is very popular in diagnostics. Although it has a good diagnosability, its exposure dose is high compared with other rentgenography. So, patients' medical exposures have been increased. The IAEA (International Atomic Energy Agency) has called for enhanced radiation protection of patients. Accordingly, we have been interested in each organ's risk evaluations for the medical exposure. The important things for this are to measure the doses of each organ. But, we depend on calculations now, because these measurements are technically difficult. Therefore, we are pushing forward the development of an anthropomorphic dosimeter the consists of only TSL materials of slab shape. (Fig. 1) Our TSL reader is able to read in two dimensions(2D).[1)] A human body roughly consists of air, soft tissue and bone. So, we have to develop both soft tissue equivalent and bone equivalent 2D-TSL materials. In this study, we focus on soft tissue equivalent TSL materials, and studied the effects of Al_2O_3 on the TSL of Cu-doped Li_2O-B_2O_3 glasses.

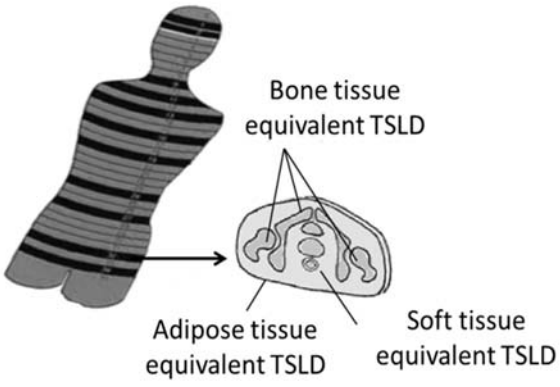

Fig.1 Our plan for an anthropomorphic dosimeter consisting of only 2D-TSL materials.

Materials and Methods The Cu, Al co-doped Li_2O-B_2O_3 glasses were

prepared by a conventional melt-quenching method. The chemical composition of the Cu - doped Li_2O-B_2O_3 (CuLiB) glass is 0.01Cu_2O-33.33Li_2O-66.66B_2O_3 (mol%), and Al_2O_3 was added as an excess component. The starting chemicals were non-enriched (natural) Li_2CO_3, B_2O_3, Cu_2O, and Al_2O_3. These chemicals were mixed and melted by using Pt crucibles at 1223 K for 20 min. After quenching, the obtained glass was annealed at the glass transition temperature, and then polished in order to obtain the mirror surface. The measurements of glow curves were recorded from room temperature up to 600 K at a heating rate of 0.1 K s^{-1} in air. Irradiation was produced by mediXtec Japan Corporation MX-80Labo X-ray equipment at a voltage of 80kV. The X-ray exposure dose was 3 Gy. In the TSL dose-response curve measurements, the doses were 0.5–100 Gy.

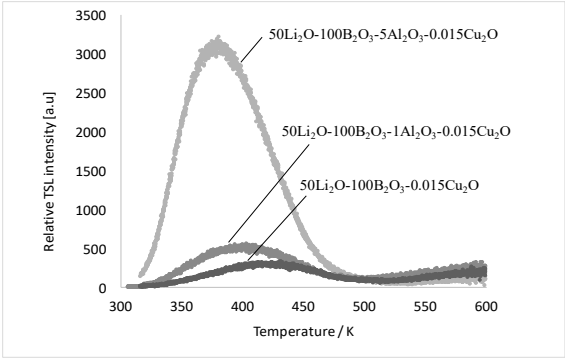

Fig. 2 TSL glow curves of Al_2O_3-doped CuLiB glasses

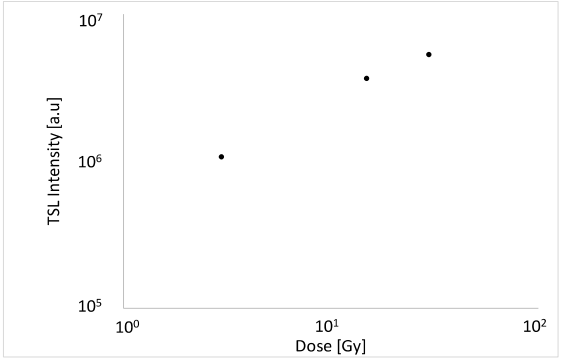

Fig. 3 TSL dose-response curves for x-ray of 3.33Al_2O_3-CuLiB glasses

Results and Discussion The glass transition temperatures of Al_2O_3-doped CuLiB glasses decreased with increasing Al_2O_3 concentration. The TSL glow curves of the Al_2O_3-doped CuLiB glasses exposed to a 3 Gy x-ray radiation dose are shown in Fig. 2. It can be seen that there is one peak in all cases. The glow peak temperatures are 420 K, 400 K and 380 K, when the Al_2O_3 components are none, 0.66Al_2O_3 and 3.33Al_2O_3, respectively. The TSL sensitivity was increased by doping CuLiB glasses with Al_2O_3. Figure 3 shows the TSL dose-response curve for the x-ray of 3.33Al_2O_3-CuLiB glasses. The TSL intensity increased with the dosage. The TSL linearity for dosage was low. Because the glow peak temperature was low, it was affected of the fading at the high dose.

Conclusion Doping of Al_2O_3 for CuLiB glasses increased the TSL sensitivity and the glow peak temperature shifted from 420 K to 380 K. The 3.33Al_2O_3-CuLiB had the highest TSL sensitivity in this study. In the future, we will try to improve the fading property and develop a new 2D-soft tissue equivalent TSLD.

References

1) K. Shinsho *et.al.*, *Appl. Radiat. Isot.* 111 (2016) 117-123.

Silver as an enhancer of the optically stimulated luminescence in gadolinium activated calcium borate

Leonardo V. S. França[1]*, Éder J. Guidelli[1], Oswaldo Baffa[1]
[1]*University of São Paulo, Ribeirão Preto, Brazil*

Highlights Radioluminescence of gadolinium activated CaB_6O_{10}: Gd^{3+}exhibited a sharp UV emission (~ 313 nm), which corresponds to the transition $^6P_J \rightarrow {}^8S_{7/2}$ of Gd^{3+}; The OSL signal showed to be strongly dependent on gadolinium concentration; The incorporation of silver on CaB_6O_{10}: Gd^{3+} has increased the OSL considerably.

Key words OSL, radioluminescence, dosimetry, gadolinium, silver.

Background and Objectives The fact there is only two commercially available materials for OSL dosimetry, i.e., Al_2O_3:C and BeO, encourages us to search for new candidates. Furthermore, that demand is highlighted when dealing with neutron dosimetry. In view of the above, we have explored the luminescence properties of CaB_6O_{10}: Gd^{3+}, since the gadolinium and 10-boron possess high cross-sections for neutrons.

Materials and Methods For preparation of gadolinium activated CaB_6O_{10}, the precursors, i.e., proper amounts of boric acid, calcium carbonate and gadolinium nitrate (0.04 M solution) were dissolved in a 100 mL glass beaker using a magnetic stirrer. Molar concentrations of gadolinium ranged from 0 to 3%. For the sample incorporated with silver, the same procedure was carried out, except for the addition of 5 mL of $AgNO_3$ (0.002 M). In all cases, the resulting white powder was placed in alumina crucible and annealed in a muffle furnace. At the end of annealing, samples were allowed to cool down in air. Later, samples were crushed with agate mortar and pestle.

For OSL measurements, irradiation of samples was carried out in a Magnum 50 kV x-ray source, Moxtek Inc., 0.2 mA maximum current. OSL and RL measurements were both performed in home-made systems.

Results and Discussion The presence of luminescence centers on CaB_6O_{10}: Gd^{3+}, was verified by RL measurements. Figure 1a shows the RL emission (plot in red). Whereas the large band emission between 290 and 590 nm is attributed to the calcium borate (results not shown here), the pronounced emission in the UV region (~ 313 nm) is attributed to $^6P_J \rightarrow {}^8S_{7/2}$ transition of Gd^{3+} [1]. The silver incorporated sample showed the same emission shape,

but exhibited a strengthened UV emission primarily. Furthermore, gadolinium activated CaB_6O_{10} showed to be sensitive to ionizing radiation, under light excitation. Figure 1b exhibits the OSL emitted from sample (plot in red) and the inset depicts the OSL emission dependent on gadolinium concentration. As can be seen, OSL emission effectively increased for lower concentrations and saturated for the highest concentrations, which lead us to adopt the 2% dopant concentration as reference. Using the silver incorporated CaB_6O_{10}: $Gd_{2\%}$, OSL emission increased prominently (plot in black). By total OSL, the emission of the silver incorporated sample was ~ 4 times higher than sample with no silver. Other studies need to be performed to enlighten about the role of silver ions on the luminescence process, i.e., if they are acting as dopant on crystal structure or if silver nanoparticles are formed during synthesis, suggesting the possibility of the plasmonic resonance properties of the silver be responsible for the enhancement of the OSL signal.

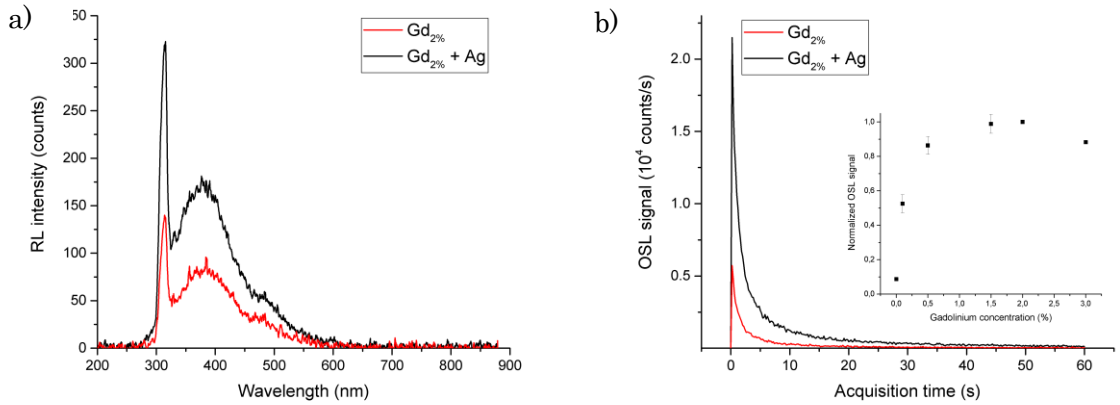

Figure 1: a) RL emission of CaB_6O_{10}: Gd^{3+} with silver and without it. b) Comparison between OSL signals from CaB_6O_{10}: Gd^{3+} with incorporation of silver and without it (dose ~ 100 mGy).

Conclusions Silver incorporation on CaB_6O_{10}: Gd^{3+} showed to be effective on the enhancement of OSL emission, which encourages us to understand the role of silver on the luminescence process. As the 10-boron and gadolinium possess high cross sections for neutron radiation, dosimetric properties of the material can eventually be investigated.

Partial Financial Support: Brazilian Agencies CNPq (407471/2016-2) FAPESP (2013/07699-0, 2009/02069-2) and CAPES Finance Code 001.

References

1) W.T. Carnall et al., Electronic Energy Levels of the Trivalent Lanthanide Aquo Ions. II. Gd^{3+}, J. Chem. Phys., 49 (1968), 4443-4446.

Photon energy dependence of NaCl pellets

Lovisa Waldner[1]*, Jan Lillhök[2], Christian Bernhardsson[1]
[1]*Medical radiation physics, Lund University, Malmö, Sweden*
[2]*Swedish Radiation Safety Authority, Stockholm, Sweden*

Highlights

NaCl pellets show a strong energy dependence at energies below 100 keV. Over response of a factor 15-17 compared to air kerma and personal dose equivalent at 30 keV.

Key words OSL, NaCl, dosimetry, energy response,

Background and Objectives

Ordinary salt, NaCl, has many properties suitable for dosimetry and has previously been suggested for retrospective optically stimulated luminescence, OSL, dosimetry. With greatly improved reproducibility and dosimetric properties when used as compressed solid pellets, NaCl has later been suggested also for prospective dosimetry applications. It has previously been shown that the dose response of the NaCl pellets is linear up to at least 300 mGy and the minimum detectable dose, MDD, is about 10 µGy. The signal fading is negligible over at least 30 days. Here we present the results on another important dosimetric property; the energy dependence of the NaCl pellets. The energy dependence is investigated as the over estimation of the absorbed dose to the NaCl pellets, in relation to air kerma and personal dose equivalent for a wide range of photon energies. With a well-defined energy dependence, possible applications for NaCl pellets include, but are not limited to, radiation dose assessments in radiology, nuclear medicine, radiotherapy, the nuclear industry and environmental monitoring.

Materials and Methods

The energy dependence of NaCl pellets was investigated using two different exposure geometries. In the simplest geometry, the NaCl pellets were irradiated free-in-air. The estimated absorbed dose to the NaCl pellets was compared to the air kerma, K_{air}, at the point of exposure. In the other exposure geometry, the NaCl pellets were placed on an ICRU slab phantom during irradiation to relate the response in the salt to the personal dose equivalent, $H_p(0.07)$ and $H_p(10)$. The estimated absorbed dose to the NaCl pellets was compared to $H_p(0.07)$ and $H_p(10)$ calculated from the K_{air} at the point of exposure, using conversion coefficients from ISO 4037-3.

X-rays with mean energies between 30 keV and 250 keV, and radiation sources with energies 662 keV and 1250 keV were used for irradiations in both exposure geometries. For each energy and geometry, the exposure time was chosen to yield an absorbed dose of about 1 mGy to a

light sealed package containing 10 NaCl pellets. The kerma rates varied between 0.3 μGy/s and 1.4 mGy/s.

Results and Discussion

Because of the difference in material thickness in front of the sensitive point of measurement in NaCl pellets compared to the definition of personal dose-equivalent, and difference in effective atomic number between tissue and NaCl, a significant variation in the energy responses is expected. In particular at low photon energies where, in addition to attenuation differences, the photoelectric effect is the dominant photon interaction. This is evident from the results from both exposure gemoetries.

For the exposure geometry free in air, the estimated absorbed dose is 17 times larger than the air kerma at 35 keV. At 250 keV the overestimation has decreased to 1.45 and above 662 keV the response is close to 1. For the exposure geometry with the slab phantom, the estimated absorbed dose is a factor 15 higher than $H_p(0.07)$ and 16 times higher than $H_p(10)$ at 32 keV. At 250 keV the overestimation is about 65% compared to $H_p(0.07)$ and 60 % compared to $H_p(10)$. For 662 keV the over estimation of the absorbed dose to NaCl is about 20% as compared to $H_p(0.07)$ and $H_p(10)$.

Several dose measurements have been performed in various low photon energy fields commonly used in hospitals and after corrections for the energy dependence, absorbed doses have been successfully estimated.

Conclusion

NaCl has a high over response compared to tissue for energies below 100 keV. To be able to fully use the potential of NaCl pellets for dosimetry, and for a wide range of photon energies, the dosemeter badge must be optimized appropriately.

References

1) Waldner, L., Bernhardsson, C., 2018. Physical and dosimetric properties of NaCl pellets made in-house for the use in prospective optically stimulated luminescence dosimetry applications. Radiat. Meas. 119, 52–57. https://doi.org/10.1016/j.radmeas.2018.09.001
2) ISO 4037-3:1999. X and gamma reference radiation for calibrating dosemeters and doserate meters and for determining their response as a function of photon energy -- Part 3: Calibration of area and personal dosemeters and the measurement of their response as a function of energy and angle of incidence.

Alexandrite Mineral: A Natural OSL Dosimetric Material

Neilo M. Trindade[1], Matheus C.S. Nunes[1], Luan S. Lima[2], Anna L.M.C. Malthez[3], Elisabeth M. Yoshimura[2], Luiz G. Jacobsohn[4,5]*

[1]*Department of Physics, Federal Institute of Education, Science and Technology of São Paulo, São Paulo, SP, Brazil*

[2]*Institute of Physics, University of São Paulo - USP, São Paulo, SP, Brazil*

[3]*Department of Physics, Federal University of Technology – Parana, Curitiba, PR, Brazil*

[4]*Department of Materials Science and Engineering, Clemson University, Clemson, USA*

[5]*NEESRWM - Center for Nuclear Environmental Engineering Sciences and Radioactive Waste Management, Clemson University, Anderson, USA*

Highlights The first investigation of alexandrite mineral ($BeAl_2O_4:Cr^{3+}$) as a natural OSL dosimetric material was executed [1,2]. Moreover, alexandrite powder was used to fabricate composites, and the composite OSL dosimetric response was successfully demonstrated [3].

Key words alexandrite mineral, $BeAl_2O_4:Cr^{3+}$, OSL dosimetry, composite dosimeter

Background and Objectives Presently, there are only two commercially-available OSL dosimeters, BeO and Al_2O_3:C. The chemical nature of the mineral alexandrite, $BeAl_2O_4:Cr^{3+}$, combines two binary oxides, BeO and Al_2O_3, thus naturally suggesting this mineral for OSL dosimetric applications. This fact, together with Z_{eff} = 10.8 value that is lower than that of Al_2O_3:C, made alexandrite an interesting candidate for investigation as a natural OSL dosimetric material. The final goal is the development of a low-cost OSL dosimetric material that can be widely employed.

Materials and Methods 1 mm-thick slices with masses around 50 mg were extracted from the same dark green rock originated from the State of Bahia, Brazil. The chemical composition of the samples was determined by SEM/EDX analysis. Since Be cannot be detected by this technique, the amount of BeO was determined based on the amounts of Al_2O_3, Cr_2O_3, and Fe_2O_3, assuming perfect stoichiometry [1,2]. TL and blue stimulated OSL measurements were executed using a DA-20 Risø TL/OSL reader. Irradiations were performed at room temperature with a $^{90}Sr/^{90}Y$ beta source with dose rate = 10 mGy/s. Photoluminescence (PL) measurements were executed using Horiba Jobin-Yvon FluoroLog spectrofluorometers. Radioluminescence (RL) measurements were executed using a

customer-designed Freiberg Instruments Lexsyg Research spectrofluorometer. Details of these measurements can be found in [1-3].

Results and Discussion Thermoluminescence glow curves of the slices showed five glow peaks, as confirmed by T_m-T_{stop} measurements, all exhibiting first order kinetics within the 1-10 Gy irradiation range (Fig. 1A). The traps depth energy was evaluated by glow curve fitting and the beta method, with both approaches yielding consistent results and energy values between 0.66 and 1.29 eV [1,2]. Composites based on alexandrite powder were fabricated (Fig. 1B) and evaluated in their OSL response, showing a linear response of the integrated intensity signal as a function of the beta irradiation dose within 0.1 and 5 Gy (Fig. 1C, [3]). No fading was observed within a period of 28 days, after a 20% fading within the first hour after irradiation.

(A) (B) (C)

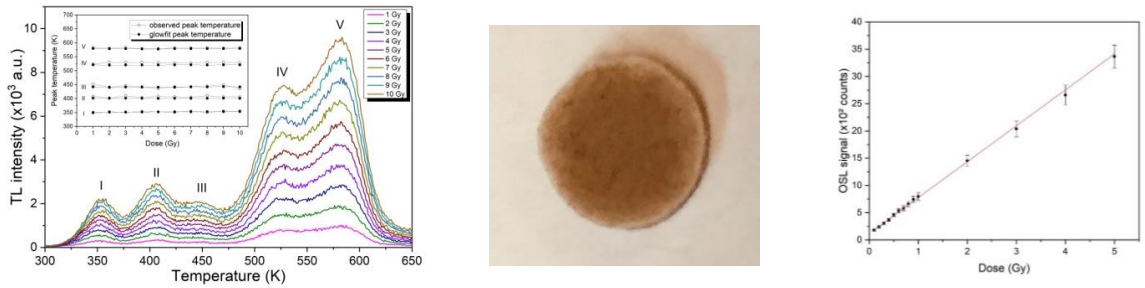

Figure 1A) TL glow curves of alexandrite mineral obtained with different irradiation doses within 1 to 10 Gy [2]; 1B) 5.5 mm diameter alexandrite-based composite [3]; and 1C) linearity of the average OSL signal of six composites as a function of the irradiation dose up to 5 Gy [3].

Conclusion TL analysis of the alexandrite mineral showed first order kinetics of the TL response of all five glow peaks. Composites based on alexandrite powder were successfully fabricated. The OSL response of the composites showed linear variation with the irradiation dose and long-term storage stability. Our results showed alexandrite mineral is a promising natural material for OSL dosimetry. Future work will focus on improving the reproducibility of the response of different pellets.

References

1) N.M. Trindade, H. Kahn, E.M. Yoshimura, Journal of Luminescence **195** (2018) 356-361.
2) N.M. Trindade, M.R. da Cruz, H. Kahn, L.G. Jacobsohn, E.M. Yoshimura, Journal of Luminescence **206** (2019) 455-461.
3) N.M. Trindade, A.L.M.C. Malthez, A.C. Nascimento, R.S. da Silva, L.G. Jacobsohn, E.M. Yoshimura, Optical Materials **85** (2018) 281-286.

This material is based upon work supported by the National Science Foundation, USA, Grant #1653016. The National Council for Scientific and Technological Development (CNPq), Brazil, Grant #307375/2015-3, and the São Paulo Research Foundation (FAPESP), Brazil, Grant #2017/11663-1 are also acknowledged.

Influence of optical bleaching and pre-dose on sensitivity changes in halite

M. Biernacka[1]*, R. Majgier[1], A. Mandowski[1]
[1]*Jan Dlugosz University, Czestochowa, Poland*

Highlights Sensitivity changes in halite were tested using multiple irradiation – OSL readout – bleaching procedure. The effect was reduced by pre-dose or test-dose administration. It was confirmed that both methods stabilized the sensitivity changes.

Key words OSL, sensitivity changes, retrospective dosimetry, sodium chloride, halite

Background and Objectives Sensitization of a material during multiple OSL readouts is an undesirable phenomenon. This can overestimate the dose determined by multiple measurements performed on the same sample. This effect in various types of salts has been previously observed in NaCl[1)], including halite[2)] and in KCl[3)] crystals. The method used for elimination or stabilization of sensitivity changes in the SAR (single aliquot regenerative dose) procedure is a test dose which constitutes a certain percent of the regenerative dose. The method, however, has some limitations. Despite its use some fluctuations of the OSL signal are still being observed. In this work, an experiment was carried out to minimize the salt sensitivity changes by using pre-dose method with a relatively high dose. The idea of this method is based on the assumption that during the initial irradiation the traps responsible for unstable OSL signal are filled with charge carriers. In the next steps (OSL readout, subsequent irradiations, etc.) the carriers from these traps will not be released, which would result in stabilization of the material and thus reduction of the OSL signal fluctuations.

Materials and Methods The investigated materials were natural rock salts (halites) from the Kłodawa salt mine: the youngest pink rock salt (SK4) and the older white rock salt (SK5). As a reference material pure sodium chloride crystals were used. The irradiation was made by beta Sr^{90}/Y^{90} source. The OSL measurements were performed using a dedicated measuring equipment OSL reader Helios the construction of which is shown in the Figure 1.

Results and Discussion The following experiments were carried out on the study of salt sensitivity changes: (1) the repeatable procedure of irradiation – OSL readout – optical bleaching (blue light) was carried out for various bleaching times – 5 min. and 10 min., (2) the above procedure was repeated in weekly cycles (for 3 weeks) with and without using a test dose, (3) the pre-dose method consisting of initial irradiation with a high dose and subsequent procedure of irradiation – OSL readout – optical bleaching (see point 1) was

applied. The signal stabilization effect obtained by the pre-dose method was compared with the effect of sensitization during the irradiation – OSL readout – optical bleaching procedure, which is shown in the Figure 2.

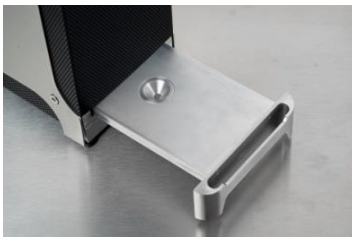

Figure 1. Helios OSL reader system.

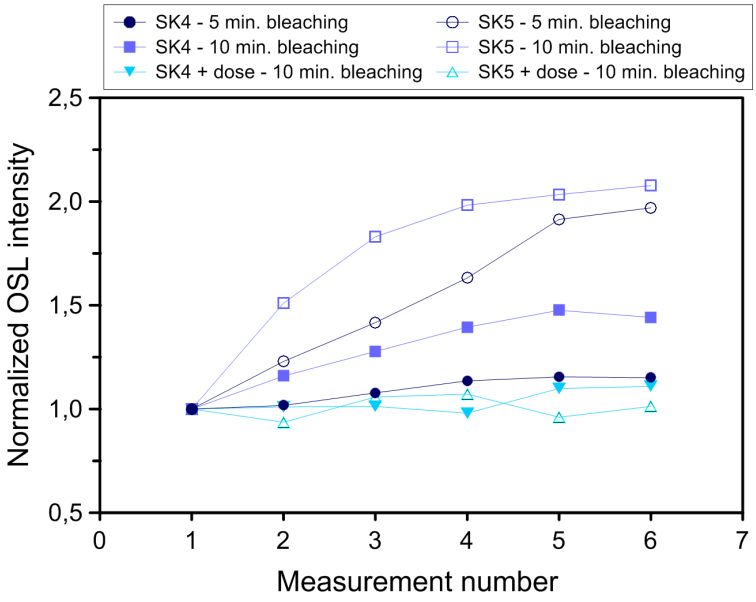

Figure 2. Comparison of sensitivity changes with and without using pre-dose method.

Conclusion The sensitivity changes of halite have been observed during the procedure of repeatable irradiation – OSL readout – optical bleaching procedure. The pre-dose method stabilizes the OSL signal to a similar degree as the test-dose method.

Acknowledgements The research was partly supported by research project no 2014/15/N/ST10/05148 from the Polish National Science Centre.

References

1) Christiansson, M., Bernhardsson, C., Geber-Bergstrand, T., Mattsson, S., Rääf, C. L. (2014). *Household salt for retrospective dose assessments using OSL: signal integrity and its dependence on containment, sample collection, and signal readout*. Radiation and environmental biophysics, 53(3), 559-569.

2) Biernacka, M., Majgier, R., Maternicki, K., Liang, M., Mandowski, A. (2016). *Peculiarities of optically stimulated luminescence in halite*. Radiation Measurements, 90, 247-251.

3) Majgier, R., Rääf, C. L., Mandowski, A., Bernhardsson, C. (2018). *Osl Properties In Various Forms Of Kcl And Nacl Samples After Exposure To Ionizing Radiation*. Radiation protection dosimetry (in press, doi.org/10.1093/rpd/ncy189).

Monte Carlo Simulation of PVCFilms Loaded with $MgB_4O_7$for neutron OSL Dosimetry

M. C. L. Moreira[1], M. C. Alves[1], A. B. de Carvalho Jr[1], S.O. Souza[1], F. d'Errico[2, 3]
[1]*Federal University of Sergipe, São Cristóvão, Brazil*
[2]*Università di Pisa, Scuola di Ingegneria, Pisa, Italy*
[3]*Yale University, School of Medicine, New Haven, CT USA*

Highlights: Monte Carlo simulations using the PHITS code were used to obtain the ideal geometric configuration of PVC loaded with OSL MgB_4O_7microparticles using B-10 and B-11 in different films. By using a water phantom covered with the OSL film, it is possible to detect the differential dose deposited into the films due to the albedo neutrons on the surface of the body.

Keywords:OSL film, PVC films,PHITS, OSL, MgB_4O_7

Background and Objectives: Several aspects of the nuclear fuel cyclerequire operations where the operators' hands are exposed to intense mixed fields of gammas and neutrons. Measurements of these extremity doses are quite complex, particularly when it comes to neutron radiation. Another important problem is the measurement of the *in-vivo* intake dose for patients in radiotherapy in order to minimize unnecessary exposure. For this reason, films of transparent and flexible polymers loaded with luminescent materials sensitive to photons and neutrons have been developed experimentally[1]. Experimental work has been made attempted to load PVC films with MgB_4O_7:Ce,Li for OSL dosimetry because the intense signal emitted by this crystal[2].However, there is a demand for optimizing the shape and arrangement of the crystals in these films. Computational simulation is a useful tool because, through a mathematical formulation, it is possible to perceive several factors that influence the development of the system.
The objective of this work wasto verify if PVC films loaded with micro OSL particles of MgB_4O_7could be used to detect neutrons albedo from an irradiated bodyand differentiate them from gamma irradiation for future development of these devices for application in 2D dosimetry.

Materials and Methods: Monte Carlo simulations using the PHITS(Particle and Heavy Ion Transport Code System)[3] code wereperformed to obtain the energy deposition in the films. This deposition of the energy in the film was measured with a scenario consisting of a radiation source, a PVC film loaded with MgB_4O_7 particles, with (Figure 1-a) and without (Figure 1-b) a water phantom. The film has dimensions of 2.5 × 2.5 cm and a thickness of 0.5 mm. Its geometry is composed of voxels, each measuring 0.01 × 0.01 × 0.01 cm, with a centered MgB_4O_7 sphere with a diameter of 7.5 μm, immersed in PVC evenly distributed in the film. The simulation used a monoenergetic (photon or neutron)radiation sourcefor different energy values. B-10 film, sensitive to photons and slow neutrons, B-11 film, insensitive to these neutrons, were simulated using these correspondent isotopes in the composition of MgB_4O_7loaded into the film to verify the percentage of energy deposited for each material.

Results and Discussion: Tables 1 and 2 show the energy deposited in the B-10 film loaded with microparticles of $MgB_4O_7$by using a photon or a neutron source, respectively.For the photon source, the behavior of the energy depositionwas similar in both simulations, with and without the water phantom, demonstrating that phantom does not interfere decisively in the process with this type of source.For the neutron source, the energy deposited in the B-10 film was lower without the water phantom, with more accentuated differences for higher energies, except for the 25 meV and 1 MeV, where the energy deposited with and without a phantom was of the same order of magnitude (Table 2). Neutrons do not deposit considerable energy in B-11 film.

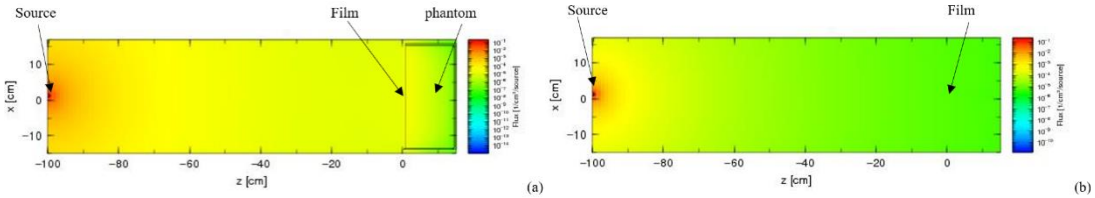

Figure 1: (a) Scenario with the phantom for a neutron source of 1000 eV; (b) Scenario where the phantom is drawn using the same source of neutrons. Since the range on the z-axis is large and the thickness of the small film (0.05 mm) cannot be seen on the image created by PHITS. The image is taken from tally t-track. The same scenarios were created for each photon or neutron energy.

Table 1: Energy deposited in the B-10 film loaded with microparticles of $MgB_4O_7$by using a photon source.

	with phantom		without phantom		difference	
Photon energy	Total energy deposited (MeV/source)	Rel error (%)	Total energy deposited (MeV/source)	Rel error (%)	Total energy deposited (MeV/source)	Rel error (%)
10 keV	2,5377E-07	2,40	2,5362E-07	2,39	1,50E-10	19,31
60 keV	6,1762E-08	1,93	3,2577E-08	1,48	2,92E-08	2,43
100 keV	3,5516E-08	2,22	1,6954E-08	1,46	1,86E-08	2,91
140 keV	3,1464E-08	0,91	1,6559E-08	0,66	1,49E-08	1,19
364 keV	4,8142E-08	0,65	3,8454E-08	0,64	9,69E-09	0,69
511 keV	6,1762E-08	1,93	3,2577E-08	1,48	2,92E-08	2,43
672 keV	7,8246E-08	1,38	6,9928E-08	1,42	8,32E-09	1,04
1250 keV	1,2414E-07	1,40	1,1826E-07	1,42	5,88E-03	9,98E-07

Table 2: Energy deposited in the B-10 film loaded with microparticles of $MgB_4O_7$by using aneutron source.

	with phantom		without phantom		difference	
Neutron energy	Total energy deposited (MeV/source)	Rel error (%)	Total energy deposited (MeV/source)	Rel error (%)	Total energy deposited (MeV/source)	Rel erro (%)
25 meV	3,8569E-07	7,85	2,0116E-07	10,87	1,85E-07	4,55
1 eV	1,8498E-07	11,34	4,3110E-08	23,63	1,42E-07	7,60
10 eV	1,3343E-07	13,26	1,4380E-08	40,94	1,19E-07	9,92
100 eV	1,1443E-07	14,29	7,4372E-09	57,97	1,07E-07	11,25
1000 eV	8,7127E-08	16,46	2,3220E-09	100	8,48E-08	14,17
10 keV	4,6308E-08	22,35	-	-	4,63E-08	22,35
100 keV	6,0725E-08	19,62	-	-	6,07E-08	19,63
1 MeV	3,4068E-08	18,59	-	-	3,41E-08	18,57

Conclusion: By using the photon source, there is no significant difference with the use of the phantom, and the dose deposited is that referring to the photons that enter the film directly from the source. However, the water phantom is responsible for backscattering neutrons that deposit the bulk of the dose in the dosimetric B-10 film. Therefore, films can detect the differentiated dose due to albedo neutrons on the surface of the body.In the near future, the two types of films, with B-10 and B-11, can be used to differentiate the neutron dose in mix fields.

References
1)SOUZA LF. et al. Dosimetric properties of MgB_4O_7:Dy,Li and MgB_4O_7:Ce,Li for optically stimulated luminescence applications. Rad Meas. 2017. 106: 196-9.
2) SOUZA SO. et al. OSL films for in-vivo entrance dose measurements. Rad Meas. 2017: 106: 643-8.
3)PHITS. Available in: <https://phits.jaea.go.jp/>. 2018.

Infrared Optically Stimulated Luminescence of Co-doped CaF_2 Produced by Combustion Synthesis

M.T.S. Medeiros[1], V.S.M. Barros[1], V. K. Asfora[1], H.J. Khoury[1], F. d'Errico[2,3]

[1]*Nuclear Energy Department, Federal University of Pernambuco, Brazil*

[2] *Yale University, School of Medicine, New Haven, CT 06510 USA*

[3] *Università di Pisa, Scuola di Ingegneria, Pisa 56126, Italy*

Highlights The fading curves of infrared stimulated luminescence of co-doped calcium fluoride are described; the material appears suitable for novel applications in safeguards.

Key words Infrared optically stimulated luminescence, CaF_2, safeguards

Background and Objectives This work shows results for infrared optically stimulated luminescence of CaF_2:RE,X (RE=Ce^{2+}, Tm^{3+}, Pr^{3+}, Dy^{3+} or Tb^{3+}; X=Li^+, Al^{3+}, Cu^{2+} or Ag^{3+}) produced by solution combustion synthesis [1] and presenting different fading rates. Infrared stimulation with OSL emission in the visible spectrum is investigated at the Federal University of Pernambuco because it may simplify the construction of OSL equipment, where less optical filtration is required. While the original focus was the search for new dosimetric materials, our current collaborative effort examines the use of these materials as passive, tamper-indicating systems for the detection of the undeclared movement of nuclear materials. Indeed, optically or thermally stimulated materials may serve as tamperproof devices capable of determining the time elapsed since the exposure to nuclear material in motion. In order to time the movement of radioactive these materials a system must be composed of at least two highly sensitive optically stimulated luminescent (OSL) materials with different fading rates.

Materials and Methods Powder samples of calcium fluoride were produced by the Solution Combustion Synthesis (SCS) method with co-doping with a rare-earth element and Li, Al, Cu or Ag. Samples of CaF_2 doped with 0,15% of Ce were prepared by mixing stoichiometric amounts of calcium nitrate $Ca(NO_3)_2$ as oxidant, ammonium fluoride (NH_4F), a rare-earth nitrate (Ce^{2+}, Tm^{3+}, Pr^{3+}, Dy^{3+} or Tb^{3+}) at 0.2 mol%, Li^+ (or Al^{3+}, Cu^{2+} or Ag^{3+}) as nitrates at 2 mol% and urea ($CO(NH_2)_2$) as fuel [1]. Distilled water was added to the mixture, placed in a beaker and heated with a magnetic stirrer until water evaporated. The mixture was then transferred to a muffle furnace (pre-heated to 565 °C) where it spontaneously ignited in one to two minutes resulting in a fluffy white powder. Pellets with a diameter of 6 mm and 1 mm in thickness were prepared using cold pressing. The OSL was measured using an automated Lexsyg Smart OSL reader equipped with an internal $^{90}Sr/^{90}Y$ beta source with a dose rate of

100 mGy/min and a Hamamatsu H7360-02 bialkaline type photomultiplier tube. Blue stimulated Luminescence (BSL) measurements were performed using an illumination with blue LEDs with peak emission at 458 nm and power set to 5 mW/cm^2. For Infrared Stimulation luminescence (IRSL) was performed using a LED with emission peaking at 850 nm, a Wide-Band-Blue filter pack and a power setting of 150 mW/cm^2.

Results and Discussion The results showed that co-doping CaF_2 with Li^+, Al^{3+}, Cu^{2+} or Ag^{3+} both increased and decreased the BLS/IRSL response depending on the rare-earth used. Best results were found for CaF_2:$Tb_{0.1\%}$,$Al_{2\%}$ with a response 6.8 times higher than CaF_2:$Tb_{0.1\%}$ (without Al doping), shown in Figure 1-a. A comparison CaF_2:$Tb_{0.1\%}$,$Al_{2\%}$ to Al_2O_3:C chips (Czochralski grown) showed a 0.71:1 ratio for integrated area. By measuring OSL decay curves after different delays after irradiation, components with distinct fading rates could be observed (Figure 1-b).

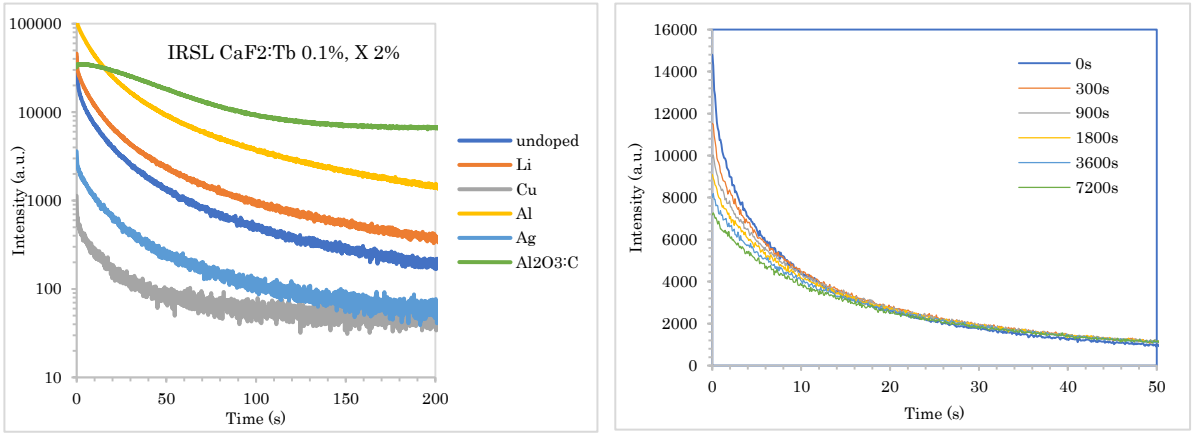

Figure 1. Results for the IRSL for (a) OSL deacy curves of CaF_2:$Tb_{0.1\%}$,$X_{2\%}$ (X=Li, Cu, Al, Ag) and Al_2O_3:C for comparison; and (b) IRSL of CaF_2:$Ce_{0.1\%}$ after different elapsed times after irradiation with 100 mGy beta (Sr^{90}/Y^{90}).

Conclusion An increase in the sensitivity of IRSL was obtained by co-doping with Al rare-earth CaF_2. Results corroborate to the development of IRSL materials for use in elapsed time measurements and detection of the undeclared movement of materials in safeguards applications.

References

1) Asfora et al. Optically Stimulated Luminescence of CaF_2:Tm. Radiation Measurements 85, p. 73-77 (2016).

Scintillation properties of Nd-doped $MSiO_3$(M = Ca, Sr, Ba) single crystals

M. Akatsuka*, D. Nakauchi, N. Kawaguchi, T. Yanagida
Nara Institute of Science and Technology, Nara Japan

Highlights We evaluated Nd-doped $MSiO_3$ single crystals in photoluminescence, scintillation and dosimetric properties. Among the present samples tested, Nd-doped $CaSiO_3$ samples showed the best performance.

Key Words scintillation, dosimetry, near-infrared

Background and Objectives Scintillators are a kind of the fluorescent materials and they have a function to convert the absorbed energy of ionizing radiation (e.g. X-rays) immediately. They are used in various different fields; for examples, medical imaging, security and high energy physics. In recent years, the scintillators emitting near-infrared (NIR) photons have attracted much attention because NIR photons are more suitable for biomedical imaging and probe than ultraviolet (UV) or visible emitting ones due to the high transparency to the human body[1]. However, there have been few reports on NIR emitting scintillators, and there remains a large room for study about this topic. In this study, we synthesized Nd-doped $MSiO_3$ (M = Ca, Sr, Ba) single crystals doped with difference concentrations of Nd by the Floating Zone (FZ) method. After the crystal growth, we evaluated their photoluminescence (PL), scintillation and dosimetric properties.

Materials and Methods 1% Nd-doped $MSiO_3$ single crystals were grown by the FZ method. Raw material powders were CaO (4N), $SrCO_3$ (4N), $BaCO_3$ (4N), SiO_2 (4N), and Nd_2O_3 (4N). After the powders were mixed to the composition as above, they were formed to a cylindrical rod by applying hydrostatic pressure. Then, cylinders were sintered at 1100 °C for 8 hours in air to obtain ceramic rods. Finally, we conducted the melt crystal growth by the FZ method in air. As fundamental luminescence properties, the PL excitation/emission counter spectrum (PL map) and PL quantum yield (*QY*) were measured using Quantauras-QY (C11347, Hamamatsu). PL decay time profiles were evaluated using Quantauras-τ (C11367, Hamamatsu), and excitation and monitoring wavelength were selected on the basis of the obtained PL spectrum. In scintillation properties, we measured X-ray induced scintillation emission spectra[2] and decay times[3]

using our original setup which equipped the pulse X-ray tube. To examine the real time dose monitoring property, the X-ray dose was changed from 1 to 10^4 mGy by integration of NIR scintillation photons, and the dose response was evaluated.

Result and Discussion Figure 1 represents X-ray induced scintillation spectra of all samples measured in the NIR range. The samples showed emission due to the electronic transitions of $^4F_{3/2} \rightarrow {}^4I_{9/2}$ (910 nm), $^4F_{3/2} \rightarrow {}^4I_{11/2}$ (1060 nm), and $^4F_{3/2} \rightarrow {}^4I_{13/2}$ (1320 nm). The emission around 1060 nm was stronger than any other emission and it was well known for laser application[4]. Figure 2 shows the relation between the scintillation intensity and X-ray exposure dose from 1 mGy to 10 Gy in NIR wavelength. All samples showed approximately liner proportional relations. In addition, the only $CaSiO_3$ sample showed approximately liner proportional relations over 5 digits.

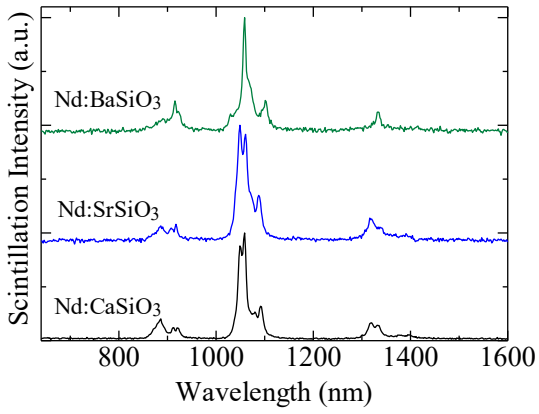

Fig. 1. X-ray- induced scintillation spectra of all samples in the NIR ranges.

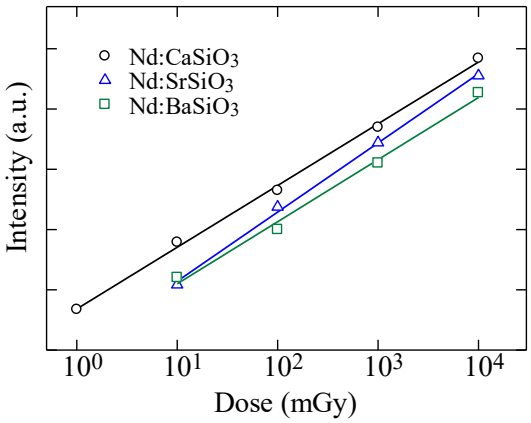

Fig. 2. The relation between the scintillation intensity and X-ray exposure dose from 1 mGy to 10 Gy in the NIR wavelength of all samples.

Conclusion We synthesized 1% Nd-doped $MSiO_3$ single crystals by the FZ method and evaluated their optical and scintillation properties. In the scintillation properties, all samples demonstrated a strong emission peak around 1060 nm owing to $^4F_{3/2} \rightarrow {}^4I_{11/2}$ transitions of Nd^{3+}, and $CaSiO_3$ showed the best performance.

References

1) R. Weissleder: Nat. Biotechnol. 19 (2001) 316.
2) T. Yanagida, *et al*. Opt. Mater., 35, 24802485 (2013).
3) T. Yanagida, *et al*. Appl. Phys. Express, 7, 062401 (2014).
4) X. D. Xu, *et al*. Laser Phys. Lett. 6 (2009) 678.

Photoluminescence response of color centers in lithium fluoride detectors irradiated by proton beams up to 35 MeV

M. Piccinini[1]*, E. Nichelatti[2], A. Ampollini[1], G. Bazzano[1], F. Bonfigli[1], P. Nenzi[1], L. Picardi[1], C. Ronsivalle[1], V. Surrenti[1], E. Trinca[1], M. Vadrucci[1], M.A. Vincenti[1] and R.M. Montereali[1]

[1]*ENEA C.R. Frascati, Fusion and Technologies for Nuclear Safety and Security Department, Via E. Fermi 45, 00044 Frascati (Rome), Italy.*

[2]*ENEA C.R. Casaccia, Fusion and Technologies for Nuclear Safety and Security Department, Via Anguillarese 301, 00123 S. Maria di Galeria (Rome), Italy.*

Highlights The photoluminescence response of stable aggregate color centers in nominally pure lithium fluoride (LiF) crystals, after irradiation with 27 and 35 MeV protons, is linear up to doses just below 100 Gy. Such linearity was confirmed along the whole Bragg curve and the dose distribution with depth was obtained.

Key words LiF, color centers, proton beams, photoluminescence, dose-mapping

Background and Objectives In the framework of the TOP-IMPLART (Oncological Therapy with Protons – Intensity Modulated Proton Linear Accelerator for Radiotherapy) project[1)], ENEA is developing a 150 MeV proton linear accelerator for protontherapy applications. Suitability of LiF-based radiation detectors, either in bulk crystal or polycrystalline thin-film form, for advanced diagnostics of the TOP-IMPLART beam has been recently demonstrated by our team[2,3,4)]. Such passive solid-state detectors exploit the visible photoluminescence (PL) of stable F_2 and F_3^+ color centers created in LiF by proton beam irradiation. From the PL images stored in LiF detectors of both the transversal beam intensity distribution and of the Bragg curve[3,5)], the advanced diagnostics of a high-fluence 7 MeV proton beam was performed by using a simple color center formation model, that allows reconstructing dose maps and depth profiles up to doses higher than 10^5 Gy. A similar experimental approach was applied for the characterization of proton beams at higher nominal energies of 27 and 35 MeV and doses below 100 Gy, where a linear PL response with dose was found.

Materials and Methods Commercially available nominally pure LiF crystals were irradiated in air by 27 and 35 MeV proton beams during the commissioning of the TOP-IMPLART accelerator at several doses below 100 Gy in different irradiation geometries. After irradiation, the F_2 and F_3^+ color centers were simultaneously pumped in their overlapped absorption

bands[6] with a continuous wave 445 nm laser and the PL spectra were acquired by an Andor iDus 401 CCD coupled to a monochromator. The PL images of the Bragg curves were acquired by a Nikon 80-i fluorescence microscope equipped with a Hg-lamp and an Andor NEO s-CMOS camera. The images were processed in ImageJ and MATLAB.

Results and Discussion At the red peak wavelength of the F_2 centers, the PL signal vs. dose was found to be linear up to doses just below 100 Gy at both the nominal proton beam energies. The experimental PL Bragg curves were satisfactorily best fitted by processing in MATLAB linear energy transfer (LET) curves generated by SRIM, provided spread of the proton beam energy, modeled with a Gaussian distribution, was assumed with only two fit parameters[5]: the mean energy and the standard deviation of the energy distribution. From the best-fitting LET curve the dose distribution with depth was obtained, as the fluence was known from experiment.

Conclusion These results show that LiF is a good candidate to be used as a dosimeter by exploiting the visible PL signal of stable radiation-induced F_2 color centers for proton beams in a wide dose range and at different energies. Work is in progress to extend the LiF PL response characterization at energies higher than 35 MeV for dosimetry applications in protontherapy.

References

1) C. Ronsivalle et al., Eur. Phys. J. Plus 126 (2011) 68.
2) M. Piccinini, F. Ambrosini, A. Ampollini, L. Picardi, C. Ronsivalle, F. Bonfigli, S. Libera, E. Nichelatti, M.A. Vincenti and R.M. Montereali, Appl. Phys. Lett. 106 (2015) 261108.
3) M. Piccinini, E. Nichelatti, A. Ampollini, L. Picardi, C. Ronsivalle, F. Bonfigli, S. Libera, M.A. Vincenti and R.M. Montereali, EPL 117 (2017) 37004.
4) M. Piccinini, C. Ronsivalle, A. Ampollini, G. Bazzano, L. Picardi, P. Nenzi, E. Trinca, M. Vadrucci, F. Bonfigli, E. Nichelatti, M.A. Vincenti and R.M. Montereali, Nucl. Instrum. Methods A 872 (2017) 41.
5) E. Nichelatti, M. Piccinini, A. Ampollini, L. Picardi, C. Ronsivalle, F. Bonfigli, M.A. Vincenti and R.M. Montereali, EPL 120 (2017) 56003.
6) J. Nahum and D.A. Wiegand, Phys. Rev. 154 (1967) 817.

MgB_4O_7:Zn,Li glass: A Potential thermoluminescence dosimeter for clinical dosimetry

Muhammad Bakhsh[12]*, Jeannie Hsiu Ding Wong [1], Iskandar Shahrim Mustafa[2]

[1]*Department of Biomedical Imaging, Faculty of Medicine, University of Malaya, Kuala Lumpur, Malaysia*

[2]*School of Physics, Universiti Sains Malaysia, Pulau Penang, Malaysia*

Highlights In this study we explored the dosimetric properties of MgB_4O_7:Zn,Li glass and its potential use for clinical dosimetry. Sensitivity, dose linearity and energy dependence are the dosimetric properties that were explored and reported.

Key words ZnO, MgB_4O_7, glass, thermoluminescence dosimeter, clinical dosimetry

Background and Objectives Potential use of MgB_4O_7 as a thermoluminescence dosimetric material for clinical dosimetry has been intensively explored since it was first proposed by Kazanskaya in 1974 [1]. Magnesium borate based thermoluminescence dosimeters are of great interest for clinical dosimetry due to their nearly tissue equivalent effective atomic number. Numerous attempts are made, recently, by different researchers, to enhance dosimetric efficiency of MgB_4O_7 by introducing different dopants and co-dopants as well as different synthesis route [2-4]. Despite of some remarkable advancements, in recent years, there remain some hurdles, in considering MgB_4O_7 for clinical dosimetry, that needs to be overcame to further enhance the efficiency of this material. The objective of this study was to develop a MgB_4O_7 glass based highly sensitive tissue equivalent TL dosimeter for clinical dosimetry.

Materials and Methods Three glass series with nominal compositions 35 MgO – 65 B_2O_3, 0.4 ZnO – 34.6 MgO – 65 B_2O_3 and 0.08 Li_2O – 0.4 ZnO – 34.52 MgO – 65 B_2O_3 were synthesized through melt quenching method [5]. The samples were irradiated, at reference conditions, using Co-60 teletherapy unit and a LINAC. The TL measurements were performed using a Harshaw TLD reader 3500.

Results and Discussion The effective atomic number for the proposed compositions were 8.57, 9.28 and 8.87 for MgB_4O_7, MgB_4O_7:Zn and MgB_4O_7:Zn,Li, respectively. TL response and Z_{eff} were found to be increasing with the introduction on ZnO as dopant in the glass network. However, introduction of Li_2O as co-dopant reduced the Z_{eff} and enhance the TL response simultaneously at the cost of minimum detectable dose. The energy and dose

response is depicted in figure 1.

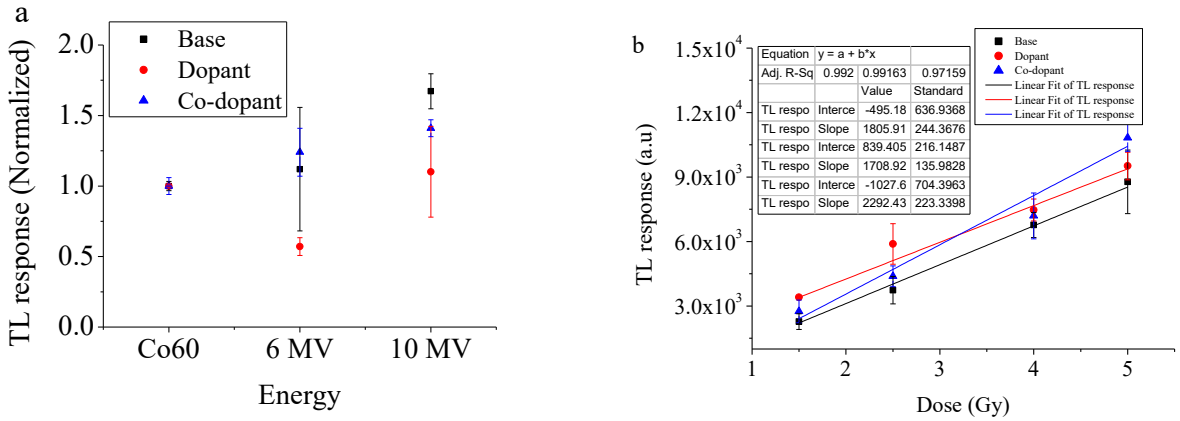

Figure 1: (a) Depicts the energy response and (b) depicts the dose response of the synthesized samples.

Conclusion Based on the findings it could be concluded that the synthesized glass has the potential to be used as TL dosimeter for clinical dosimetry.

References

1. Kazanskaya, V., et al. *Magnesium borate radiothermoluminescent detectors*. in *Proceedings of the fourth international conference on luminescence dosimetry, Krakow-Poland, 27-31 August*. 1974.
2. Yukihara, E.G., et al., *Thermally stimulated and recombination processes in MgB_4O_7 investigated by systematic lanthanide doping.* Journal of Luminescence, 2014. **154**: p. 251-259.
3. Bahl, S., et al., *Synthesis and thermoluminescence characteristics of gamma and proton irradiated nanocrystalline MgB4O7: Dy, Na.* Journal of Luminescence, 2013. **134**: p. 691-698.
4. Annalakshmi, O., et al., *Synthesis and thermoluminescence characterization of MgB4O7:Gd,Li.* Radiation Measurements, 2013. **59**: p. 15-22.
5. Bakhsh, M., et al., *Synthesis, characterisation and dosimetric evaluation of MgB4O7 glass as thermoluminescent dosimeter.* Radiation Effects and Defects in Solids, 2018: p. 1-15.

Soil and bone equivalent detectors based on Si ceramics with a wide range of dose determination for application in environmental monitoring, high-dose radiation dosimetry, medicine and luminescent dating

N. Aluker[1]*, M. Herrmann[2]

[1] *Kemerovo State University, Kemerovo, Russia*
[2] *Pennsylvania State University, PA, USA*

Highlights The characteristics of detectors made of Si ceramics are considered. and analyzed their use for solving various dosimetric tasks.

Key words radiation dosimetry, Si ceramics, environmental monitoring, high-dose radiation dosimetry luminescent dating

Background and Objectives This type of thermoluminescent detectors, based on Si ceramics, was developed in Kemerovo, and a large batch of detectors has been released [1,2]. Both the basic dosimetric characteristics of the detectors and their luminescent characteristics were studied. Detectors are successfully used in solving various dosimetric monitoring tasks.

Materials and Methods Detectors are chips 3 * 3 mm in size, 0.5 mm thick, weighing 11 mg. The sensitivity of the detectors with such minimum dimensions and thickness is comparable to the sensitivity of serial LiF-based detectors with large dimensions. In terms of material, the sensitivity of ceramic Si is 7 times less than the sensitivity of the most effective sensitivity of anion-deficient Al2O3, widely used in thermoluminescent and OSL dosimetry. The amorphous state of the material of the detectors causes a high stability of the dosimetric response in the batch of detectors, i.e. unlike all monocrystalline materials used, no selection of sensitivity detectors is required. A very important dosimetric characteristic of detectors is a record wide range of linearity of the dosimetric response from 10–4 Gy to 103 Gy and a proven absence of dependence on excitation density up to 1011 Gy / s, which gives grounds from the use in technological dosimetry and dosimetry of therapeutic medical radiation. An important characteristic is the equivalence of detectors in Z eff soil, ceramics Bacterial material and bone tissue. This allows the detectors to be widely used in environmental monitoring and thermoluminescent dating to determine both the dose rate in the soils from

which the artifact was withdrawn and for monitoring the dose of laboratory irradiation [3].

Results and Discussion The use of these miniature detectors for patient dosimetry in radiation therapy and diagnostics may be the most debatable. In medical dosimetry applications during therapy, in most cases external penetrating radiation of the whole body is considered. In this case, the magnitude of the individual dose of Hp (10) can be taken as a reasonable approximation for determining the absorbed dose. For X-rays, this is not the case, due to the substantial heterogeneity of the dose distribution over the body (the maximum dose is formed on the irradiated surface and decreases at least 10 times at the exit from the irradiated body). To determine the maximum absorbed dose, which is proportional to the negative effect, the use of miniature detectors is necessary. In the case of irradiation with particles, such as high-energy protons, the maximum dose (approximately 5 times greater than that on the irradiated surface) will be formed at a certain depth of the body, which depends on the energy of the particle. For high-energy electrons, it is important to take into account the dose generated by bremsstrahlung x-rays. All this makes the problem of the dosimetry of patients in medicine important.

Conclusion The use of TLD-K detectors [1-2] made of Si ceramics in technological dosimetry, thermoluminescent dating, and soil environmental monitoring is almost without any alternative. The use of this absolutely non-toxic miniature detector in medical dosimetry is promising because of its potential in vivo use.

References

1) Patent: “Working substance for a thermoluminescent ionizing radiation detector” No. 408900, 01/10/2011. KemSU, Aluker NL, Yurieva Yu.B.
2) Aluker, N. L. Suzdaltseva, Ya. M. Herrman, M. E. Dulepova A. S. Effective thermoluminescent detectors for recording the absorbed doses of ionizing radiation in the environment // *SSN 0020-4412, Instruments and Experimental Techniques, 2016, Vol. 59, No. 5, pp. 733–739.*
3) Aluker, N. L. Suzdal'tseva, Ya. M. Bobrov, V. V. Parameters of traps essential for thermoluminescent dating of archaeological ceramics // Inorganic Materials. – 2015, Vol. 51, No. 2, pp. 182–186. http://elibrary.ru/item.asp?id=23970534

Persistent luminescence properties of Eu^{2+}, Dy^{3+} co-doped calcium aluminate synthesized by combustion method

R. Ruiz-Torres [a], N.J. Zúñiga-Rivera [b], P. Salas-Castillo [c], L.A. Díaz-Torres [d], V. Chernov [e], R. Meléndrez [e] and M. Barboza-Flores [e]

[a] *Departamento de Física, Posgrado en Nanotecnología, Universidad de Sonora, Hermosillo, Sonora, 83000, México.*
[b] *Departamento de Física, Matemáticas e Ingenierías, Universidad de Sonora URS, Navojoa, Sonora, 85880, México.*
[C] *Departamento de Nanotecnología, centro de Física y Tecnología Aplicada y Tecnología Avanzada, UNAM, Juriquilla, Qro. México.*
[d] *Grupo de Espectroscopia de Materiales Avanzados y Nanoestructurados (GEMANA), Centro de Investigación en óptica, Lomas del Bosque 115, Lomas del Campestre, 37150, León, Gto, México.*
[e] *Departamento de Investigación en Física, Universidad de Sonora, Hermosillo, Sonora, 83000, México.*

Highlights We report on the photoluminescence, thermoluminescence and persistent luminescence properties of calcium aluminate synthesized by combustion method using urea as a fuel and co-doped with Eu^{2+} and Dy^{3+}. The phosphor exhibited persistent luminescence immediately after ceasing irradiation exposure with a time decay of the order of hours. The long lasting luminescence was associated to the thermal empting of the traps related to the low temperature TL peaks.

Keywords: persistent luminescence, calcium aluminate, photoluminescence, thermoluminescence,

Background and Objectives The persistent luminescence (PLUM) properties of materials are widely studied due to novel application in signalization, biosensors, detectors, and functional inorganic phosphors. The persistent luminescence is the emission of light of a material after excitation with ionizing or nonionizing radiation, the phenomenon is commonly observed in materials that emit light after the end of excitation with a typical long lasting time decay behavior. Persistent luminescence in $SrAl_2O_4:Eu^{2+},Dy^{3+}$ and $CaAl_2O_4:Eu^{2+},Dy^{3+}$ been investigated previously usually emitting in the blue region [1, 2]. In the present paper we further investigate the persistence luminescence properties of $CaAl_2O_4:Eu^{2+},Dy^{3+}$ phosphor synthesized by combustion method and exposed to beta radiation. Thermoluminescene (TL) analysis allowed to study the trapping and detrapping levels associated to the observed PLUM emission.

Materials and Methods X ray diffraction (XRD) was obtained by a Philips x'pert MPD diffractometer with CuKα source (1.5405 Å). Photoluminescence (PL) measure was obtained in Fluorolog Horiba Jobin-Ybon Model FL-1039 at room temperature from 200 to 900 nm. Thermoluminescence (TL) and Persistent Luminescence (PLUM) were obtained in Risø TL/OSL reader model TL/OSL-DA-20 with β particle radiation source 39 mCi 90Sr-90Y and irradiation dose of 302 Gy/h. The size of particle and semi-quantitative detection of

elements in the sample was obtained by a Microscopy electronic FE-SEM JEOL model JSM-7800F using 5.0 kV of acceleration with carbon conductive tape TED PELLA double coated.

Results and Discussion The synthesized samples displayed a characteristic XRD pattern composed of two crystalline $CaAl_2O_4$ and $CaAl_4O_7$ phases. The photoluminescence spectrum showed a wide band from 380 to 530 nm with a maximum peaked at 438 nm. It corresponds to the allowed transition from the $4f^65d^1$ to the $4f^7$ levels of Eu^{2+} ion under excitation with 338 nm light. The $CaAl_2O_4$: Eu^{2+}, Dy^{3+} phosphor exposed to β particle radiation in the range of 0.8–10.6 Gy presents a wide glow curve with at least three overlapped peaks around 350, 410 and 470 K. The phosphor exhibited persistent luminescence immediately after ceasing irradiation exposure with a time decay of the order of hours. The long lasting luminescence was associated to the thermal empting of the traps related to the low temperature TL peaks. The high TL and persistent luminescence efficiencies of $CaAl_2O_4$: Eu^{2+}, Dy^{3+} phosphor open the possibility of many applications of this material in the field of radiation physics related to sensors, detectors, dosimetry and medical applications.

Conclusion The high TL and PLUM efficiencies of $CaAl_2O_4$: Eu^{2+}, Dy^{3+} phosphor open the possibility of many applications of this material in the field of radiation physics related to sensors, detectors, dosimetry and biomedical applications involving functional inorganic phosphors.

References

1. R. E. Rojas-Hernandez, F. Rubio-Marcos, M.Á. Rodriguez, J.F. Fernandez, Long lasting phosphors: $SrAl_2O_4$:Eu, Dy as the most studied material, Renew. Sustain. Energy Rev. 81 (2018) 2759–2770. Yang Li , et al., Long persistent phosphors: from fundamentals to applications. *Chem Soc Rev*. 45(8), (2016) 2090-2136.
2. T. Aitasalo, J. Hölsä, H. Jungner, M. Lastusaari, and, J. Niittykoski, Thermoluminescence Study of Persistent Luminescence Materials: Eu^{2+}- and R^{3+}-Doped Calcium Aluminates, $CaAl_2O_4$:Eu^{2+}, R^{3+}, *J. Phys. Chem. B* 2006, *110,* 4589-4598.

Reaching reproducibility of Luminescent signal by irradiation-measurements treatment

René Rojas Rocca[1]*, Sonia Hatsue Tatumi[1,2]
[1]*UNIFESP, Federal University of Sao Paulo, Santos, Brazil*
[2]*USP, University of São Paulo, Electric Engineering Department, São Paulo, SP, Brazil.*

Highlights For some dosimeters it is possible to reach reproducibility with low dose irradiation, sensitization with low doses irradiation.

Key words calibration, radiation, dosimetry, low dose sensitizing.

Background and Objectives TL dosimeters are important for measuring radiation, such dosimeters need to satisfy some requirements to be suitable for dosimetry, one requirement is reproducibility. TL signal of quartz has commonly used for dating sediments and it is known that the signal of one aliquot can be modified along several irradiation-measurements (single aliquot regeneration SAR). In order to fix this problem, SAR protocol was performed using a "test dose" to normalize the signal[1)], because the signal of the quartz for many measurements with same dose is not same, it increases for each new irradiation-measurement.
For dosimetry, new materials are been developed for many different procedures as sol gel, combustion, coprecipitation, etc. in some cases heat treatment at high temperature is necessary for enhancing the luminescent signal[2)]. It was observed that these new materials even when heated at high temperature (~1000 ºC) and cooled slowly until room temperature, when two measurements are performed at lower temperature ~500 ºC the signal is not reproducible. For each new measurements the luminescent intensity changes, in some cases this one increases, other cases decreases and some few cases it remain constant as it is expected for dosimetry.

Materials and Methods In this work we present the results for natural quartz (SiO2) and synthetic crystal (CaSiO3), the last one was heated until 1200 ºC, bot samples were submitted to several irradiation-measurement, same dose, using a RISOE TL/OSL reader DA-20 with a beta source coupled, TL signal was recorded in visible region.

Results and Discussion When samples are heated to high temperature we expect they to be stable for reading at low temperature, then two sequential measurements performed under same condition should present same signal. As we can see on Fig 1b two measurements do

not emit same intensity (first and second measurements), this intensity is increasing for each new reading (Fig 1a and b), also it is observed that this increasing is not constant and after several readings it will near to zero, reaching the reproducibility.

For synthetic sample, between the two first measurements the luminescent signal increased 35 %, from 45th to 46th measurement signal increases 0.5 %, for quartz sample also it is observed a similar behavior. Other samples spend more repetition for reaching the stabilization. Fitting with an exponential curve it is possible to know how many times, this sample must pass for this radiation-measurements process in order to reach acceptable reproducibility.

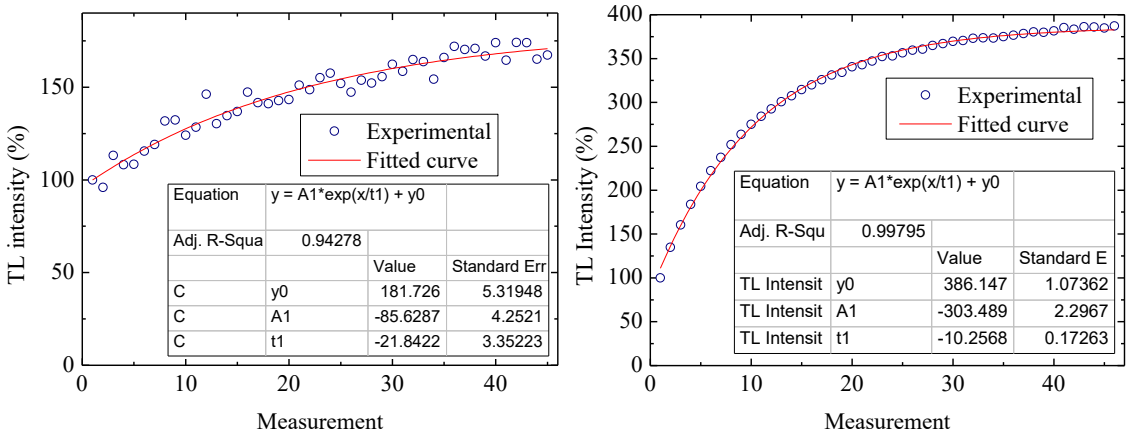

a) b)

Figure 1. TL increasing for each new irradiation-measurements a) natural quartz sample, b) synthetic CaSiO3 sample.

Conclusion It is possible to reach reproducibility for new dosimeter, that do not show this property, carrying on many times the process irradiation-measurement, for quartz sample the intensity was increased ~70% for synthetic sample ~300%, using low doses also is possible to sensitize samples as it is commonly done with high dose. These process can contribute with structure relaxation originating more recombination centers that are not jet stable maybe also filling deep traps at every time.

References

1) Murray, A. S., & Wintle, A. G., Luminescence Dating of Quartz Using an Improved Single Aliquot Regenerative-Dose Protocol. Radiation Measurements, 32 (2000) 57-73.
2) Soares A.F., Tatumi S.H., Mazzo T.M., Rocca R.R., Courrol L.C., Study of morphological and luminescent properties (TL and OSL) of ZnO nanocrystals synthetized by coprecipitation method, Journal of Luminescence 186 (2017)135–143.

The Thermoluminescence Efficiency and the Glow Curves of Cr-doped Al_2O_3 Ceramic TLD in Wide range Linear Energy Transfer

Risa Shimomura[1]*, Yusuke Koba[2], Weishan Chang[2], Masanori Koshimizu[3], Yutaka Fujimoto[3], Hiroki Kawamoto[3], Daiki Maruyama[1], Kazuki Matsumoto[4], Hiroaki Ushiba[4], Takayuki Andoh[5], Kiyomitsu Shinsho[1]

[1] *Tokyo Metropolitan University, Tokyo, Japan*

[2]*National Institute of Radiological Sciences, Chiba, Japan*

[3] *Tohoku University, Miyagi, Japan*

[4]*Chiyoda Technol Co., Tokyo, Japan*

[5]*Chiba Ceramic Mfg. Co.,Ltd., Chiba, Japan*

Highlights We investigated the thermoluminescence (TL) efficiency and the glow curve of Cr-doped alumina (Al_2O_3) ceramic thermoluminescent detectors (TLD).The TL efficiency showed unique trend lines separated by particle beams and the shape of the glow curve remains the same in a wide range linear energy transfer (LET) between 0.5 keV/μm and 128 keV/μm.

Key words Heavy charged particle, thermoluminescent detector, linear energy transfer

Background and Objectives Heavy charged particle (HCP) therapy has the advantage of allowing a higher local control of the tumor and causing less damage to normal tissues. It is necessary to verify that the correct dose is delivered to the tumor. We developed a measurement system of 2D dose distribution using TLD based on Cr-doped Al_2O_3 ceramic. It is reusable and has high reproducibility. We previously reported about the dose linearity and LET dependence of an Cr-doped Al_2O_3 ceramic TLD using several HCP beams[1)]. This study aims at investigating the LET dependence in TL efficiency and the glow curve shape in detail.

Materials and Methods The Cr-doped Al_2O_3 ceramic TLD were composed of Al_2O_3(>99.5wt%) with 0.05wt% Cr_2O_3 added. Their size was 11×11×0.7 mm^3.Irradiation experiments were performed at the Heavy Ion Medical Accelerator in Chiba (HIMAC) at the National Institute of Radiological Sciences. The species of irradiation source and the initial energies are as follows: 160 MeV/u H, 150 MeV/u He and 290 MeV/u C. Irradiated dose was 1 Gy. The distance between source and detector was fixed and energy was changed by the binary filter. LET was calculated by Monte Carlo simulation. The glow curves were measured using our original readout system which consists of a heater and a photon-counter in a dark box. The Cr-doped Al_2O_3 ceramic TLD were heated on the heater with a heating rate of 0.2℃/s from

room temperature to 400℃.

Results and Discussion TL intensity was evaluated using a range of 10℃ centered on the main peak. The TL efficiency is defined as the following equation,

$$\text{TL efficiency} = \frac{(\text{Measured dose}/\text{Irradiation dose})_{\text{LET}}}{(\text{Measured dose}/\text{Irradiation dose})_{\text{X-ray,1Gy}}}$$

Measured dose is the TL intensity multiplied by conversion coefficients in terms of absorbed dose to water in X-ray. Figure 1 shows the TL efficiency of Cr-doped Al_2O_3 ceramic TLD to LET. The TL efficiency showed unique trend lines separated by particle beams. Figure 2 make a comparison of glow curve between a carbon beam (LET: 13.3 keV/μm) and a helium beam (LET: 11.5 keV/μm). The glow curve shape remained the same whereas the TL intensity decrease when LET increases. Some commercial TLDs such as LiF:Mg,Ti have been reported the glow curve is changed by LET[2]. The activation energy is related to the shape of glow peak. Since the glow curve of Cr-doped Al_2O_3 ceramic TLD is not changed by LET, changes of LET may have no connection with trap depth of Cr-doped Al_2O_3 ceramic TLD.

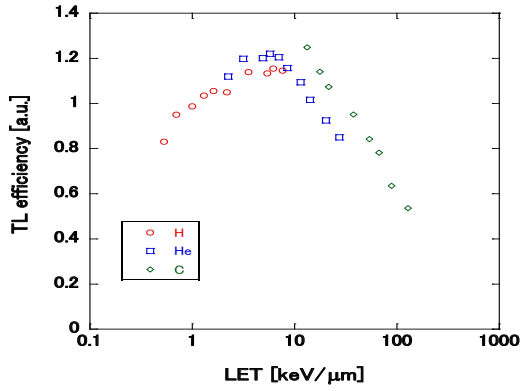

Figure 1 The TL efficiency of Cr-doped Al_2O_3 ceramic TLD to LET

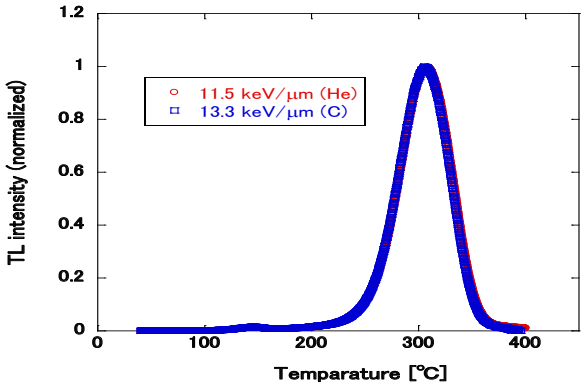

Figure 2 The glow curve of Cr-doped Al_2O_3 ceramic TLD

Conclusion The present study showed the TL efficiency and the glow curves of Cr-doped Al_2O_3 ceramic TLD. The glow curve shape is not changed by LET. Further studies are needed to elucidate what is responsible for the change of TL intensity by LET.

References

1) Koba Y.et al.2018. Dose Linearity and Linear Energy Transfer Dependence of Cr-doped Al_2O_3 Ceramic Thermoluminescence Detector, Sensors and Materials, Vol. 30,No.7, 1599-1604
2) P. Bilski, M. Puchalska. 2010. Relative efficiency of TL detectors to energetic ion beams, Radiation Measurements, 45,1495-1498

Influence of hydrothermal treatment, beta particles irradiation and thermal treatment on the optical properties of $SrMoO_4$ phosphors

R. Künzel[1], N. K. Umisedo[2*], E. M. Yoshimura[2], E. Okuno[2], A. P. A. Marques[1]
[1] *Federal University of Sao Paulo, Diadema, SP, Brasil*
[2] *Institute of Physics, University of Sao Paulo, SP, Brazil*

Highlights The effects of hydrothermal treatment and irradiation with beta particles on the luminescent properties of $SrMoO_4$ phosphors are investigated. Results from TL, OSL and PL data show that hydrothermal treatment affects the optical properties of $SrMoO_4$ materials.

Key words Ceramics, Luminescence, Microwave, Optical Properties

Background and Objectives Strontium molybdate ($SrMoO_4$) exhibits excellent luminescence and structural properties and has emerged as a potential candidate for optoelectronic applications and in the design of scintillators detectors[1]. The light output efficiency and emission profile from $SrMoO_4$ materials depend on the concentration and characteristics of surface defect states[2]. Hydrothermal treatments and/or irradiation with beta particles can affect morphology, particle size, crystallinity and electronic properties of materials[2]. The structural, morphological and optical properties of $SrMoO_4$ samples submitted to hydrothermal treatment and/or irradiation with beta particles are investigated using thermoluminescence (TL), optically stimulated luminescence (OSL) and photoluminescence (PL) measurements.

Materials and Methods $SrMoO_4$ powders were synthesized by a co-precipitation method according to Paradelas et al. (2017)[1]. One sample of the collected solid powder was dried at a temperature of 60 °C whereas another sample was heat-treated using the Microwave-Assisted Hydrothermal (MAH) method (Paradelas et al., 2017)[1]. After this, some samples were irradiated to an absorbed dose of 1.8 Gy with beta particles and/or heat treated. TL and OSL data were registered using a Risø TL/OSL reader, model DA-20, with a built-in $^{90}Sr/^{90}Y$ beta source. The traps depth were determined from TL glow curves using Computerized Curve Deconvolution Analysis (CCDA). PL spectra were acquired using a Fluorolog 3–11 spectrometer coupled with a 450 W xenon arc lamp, with 359 nm excitation wavelength. The morphology of all samples was analyzed using Scanning Electron Microscopy (SEM).

Results and Discussion The shape and intensity of TL glow curves change with the synthesis methodology (Figure 1 (A)). The TL glow curve for the sample submitted to MAH treatment is broader and less intense when compared with those registered for the sample without MAH

treatment. The determined trap depth values are in the range of 0.85 –2.3 eV. Figure 1 (B) depicts the OSL decay curves registered according to the following procedure: (i) after irradiation of the sample (black line), (ii) after the first TL readout and subsequent irradiation (red line), (iii) after the second TL readout and subsequent irradiation (green line). Results show that the shape and intensity of the OSL decay curve change after the thermal treatment. The irradiation of the $SrMoO_4$ samples (without MAH and MAH-treated) modify both the intensity and the wavelength of the maximum PL emission. The recorded SEM images suggest that the samples submitted to irradiation with beta particles and heat treatment exhibit more holes when compared with the non-irradiated samples.

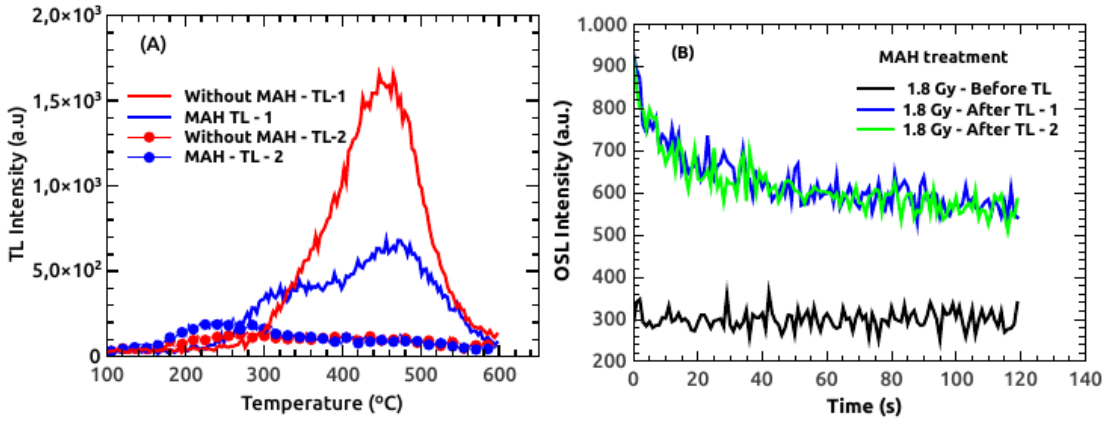

Figure 1. (A) TL glow curves (heating rate 3 ºC/s) from irradiated $SrMoO_4$ samples and (B) OSL decay curves for the sample submitted to MAH treatment. The terms TL-1 stands for the first TL readout from the samples and TL-2 stands for the second one.

Conclusion Results show that the glow curve present in the $SrMoO_4$ materials changes with the MAH treatment. Results give insight that thermal treatment affects the shape and intensity of the OSL profile.

References

1) S. M.V. Paradelas, R. F. Gonçalves, F. V. Motta, R. C. Lima, M. S. Li, E. Longo, A. P. de A. Marques, Journal of Luminescence 192 (2017) 818–826.
2) R. Künzel, R. M. Latini, N. K. Umisedo, E. M. Yoshimura, E. Okuno, A. P. A. Marques, Ceramics International 45 (2019), 7811-7820.

Mechanical and Shielding Properties of Normal Weight Concrete by Incorporating Iron Cutting Waste (ICW)

Saman Shahid[1*], Rehan Amjad[2], Shahid Ali[2]

[1] Department of Sciences & Humanities, National University of Computer & Emerging Sciences (NUCES), Foundation for Advancement of Science & Technology (FAST), Lahore Pakistan.*
Department of Civil Engineering, National University of Computer & Emerging Sciences (NUCES), Foundation for Advancement of Science & Technology (FAST), Lahore Pakistan.
*Email address of *Corresponding author: drshahidsaman@gmail.com*

Highlights: For shielding purposes, concrete is preferred because of its good attenuation property, which can be controlled by its composition. The mechanical and shielding properties of concrete were investigated by replacing some percentage of sand up to 20%, with ICW.

Keywords: Mechanical & Shielding Properties, Iron Cutting Waste, Ionizing Radiation, Concrete, Attenuation Co-efficient, Mean-free Path, Split Tensile Strength

Background and Objectives: There has been large amount of work has already been carried out on the optimization of concrete properties (mechanical and shielding) in both nuclear and medical fields. As concrete made of many natural material of different sizes. More research has been carried out on coarse aggregates and their effects rather than on fine aggregate on the radiation properties of concrete. Most commonly used material for shielding ionizing radiation is concrete. There is a use of concrete in various facilities such as nuclear reactors and medical radiotherapy rooms etc., due to its good attenuation property. A research is in progress to optimize concrete by adding some admixtures in it. There are many elements of concrete which can improve the structural and shielding strength of concrete. This research was aimed to investigate mechanical and shielding properties of concrete by replacing some percentage of sand up to 20%, with iron cutting waste (ICW). Number of cubes, cylinders and beams were casted to evaluate the compressive strength, split tensile strength, flexural strength and attenuation coefficient of concrete-mix incorporating 0% -20% of ICW ([1-4].

Materials and Methods: There were different percentages of iron cutting waste into the mix. Number of cubes, cylinders and beams were casted to test the sample for observing the effect of replacement of sand by iron cutting waste. In this study 0.48 (w/c) water to cement ratio was kept high for casting samples containing the iron cutting waste. This ratio was higher than the ratio used by Ghannam (2016) [(4-5)]. This ratio was set after many trails to achieve the workability of the mix. Concrete was mixed in electric mixer machine. First, mixer machine was cleaned by all the undesired material. Mixer machine was then washed by water for both cleaning and making moist surface of mixer before adding a material in it. All components of mix were weighted on the weight balance and as per the mix design.

Results and Discussion: A better understanding related to the modification of concrete radiation shielding with types of aggregates which is good for radiation community, is illustrated.

Compression Test: Compressive strength of mix was increased maximum by 35% on 10% replacement of sand. On the other hand, the tensile strength increased about 10% on replacing sand upto 10%. And Fluxral strength was increased about 22% from the control mix on 10% replacement for sand. While, the increase in fluxral strength of mix was more prominent then the comepressive or split tensile strength.

Split tensile strength: The tensile strength increased about 10% on replacing sand upto 0-10% with iron cutting waste. On further percent replacement of sand with iron cutting waste from 10%-20%, the split tensile strength of mixes started decreasing from the control mix about 10% on 20% replacement respectively.

Attenuation Result: Mass attenuation coefficient of mix with 20% replacement was higher and increased about 10.5% from the control mix (see Figure 1). This increase in attenuation coefficient was mainly due to the iron waste heavy metal used in the mix.

Mean Free Path Length: The difference in mean free path length for control mix and mix with 20% iron waste was about 0.5cm. Mass attenuation increased with increase in iron waste percentage in the concrete matrix. Maximum mass attenuation achieved on 15% replacement of sand, which was about 7.5% from the control mix [6].

Conclusion: Optimum percentage to replace the sand with iron cutting waste was 10%, considering the mechanical properties of concrete. While, the attenuation properties of concrete increased with increase in iron cutting waste. At 10% replacement of sand with iron cutting waste increased 5% of attenuation coefficient. It is suggested that attenuation properties could be increased by using fine iron cutting waste and its uniform distribution in concrete mix.

Figure 1: measurements of attenuation co efficient in the laboratory

Acknowledgement: We are thankful to the Pakistan Institute of Engineering and Applied Sciences (PIEAS), Islamabad for the assistance in measuring attenuations.

References

1) Stanković, S., Ilić, R., Janković, K., Bojović, D., Lončar, B., Gamma radiation absorption characteristics of concrete with components of different type materials. Acta Physica Polonica A 117 (2010) 812.
2) Akkurt, I., Basyigit, C., Kilincarslan, S., Mavi, B., Akkurt, A., Radiation shielding of concretes containing different aggregates. Cement and Concrete Composites 28 (2006) (2) 153.
3) Dj. Ristic, Absorption-Protection properties of barite concret, IBK-1322, Institute of Nuclear Sciences VINCA, (1975).
4) Ghannam, S., Najm, H., Vasconez, R., Experimental study of concrete made with granite and iron powders as partial replacement of sand. Sustainable Materials and Technologies 9 (2016) 1.
5) Ghannam, S., Flexural strength of concrete-filled Steel tubular beam with partial replacement of coarse aggregate by granite. International Journal of Civil Engineering and Technology 7 (2016) 161.
6) Kirn, F. Kennedy, R. Wyckoff, H., The attenuation of gamma rays at oblique incidence. Radiology 63 (1954) 94.

Characteristics of fluorescence nuclear track detection with Ag^+-activated phosphate glass

Satoshi Kodaira[1]*, Tamon Kusumoto[1], Hisashi Kitamura[1], Yuka Yanagida[2], Yasuhiro Koguchi[2]

[1]Radiation Measurement Research Team, National Institute of Radiological Sciences, National Institutes for Quantum and Radiological Science and Technology, Chiba, Japan

[2]Oarai Research Institute, Chiyoda Technol Corporation, Ibaraki, Japan

Highlights Characteristics of fluorescent nuclear track detection with the silver ion-activated phosphate glass were demonstrated for the application of heavy ion measurement in space.

Key words radiation, dosimetry, fluorescent nuclear track detector, space radiation

Background and Objectives Silver ion-activated phosphate glass has a good potential for application to radiation dosimetry in various radiation fields [1)]. We have demonstrated the radiation dosimetry with three independent signals of radiophotoluminescence, optical absorption and etched nuclear track, which allows the dynamic range of the measured dose and LET (linear energy transfer) to be widened [2)]. The fourth alternative signal of fluorescent nuclear track was recently reported [3)]. However, the LET spectroscopic performance should be addressed for complementing LET range between 10 – 1,000 keV/μm for the application in space radiation dosimetry. The characteristics of fluorescent nuclear track detection in Ag^+-activated phosphate glass irradiated to various energetic heavy ions were demonstrated.

Materials and Methods The Ag^+-activated phosphate glass (51.2wt%O, 31.6wt%P, 11.0wt%Na, 6.1wt%Al, 0.2wt%Ag; AGC Techno Glass Co. Ltd., Japan) was employed. Glass specimens were 8.5 mm x 8.5mm x 1.5mm in size. The Ag^+-glass specimens were irradiated to various ions from protons to iron with energies of <500 MeV/n at HIMAC of NIRS/QST. The beam fluence was 10^6 cm^{-2}. The fluorescent nuclear track signal of around 590 nm emission was detected with the confocal laser microscope (FV-1000, Olympus) exciting by 405 nm laser illumination.

Results and Discussion The fluorescent nuclear tracks were detected and imaged for relatively high LET particles of carbon to iron ions as shown in Figure. The detection threshold was estimated to be 8.5 keV/μm in water, which is insensitive for low LET

particles such as protons and helium. The quenching effect that the fluorescent intensity is decreased by repeating scan was found. Trapped electrons making color center may be released with high intense laser illumination.

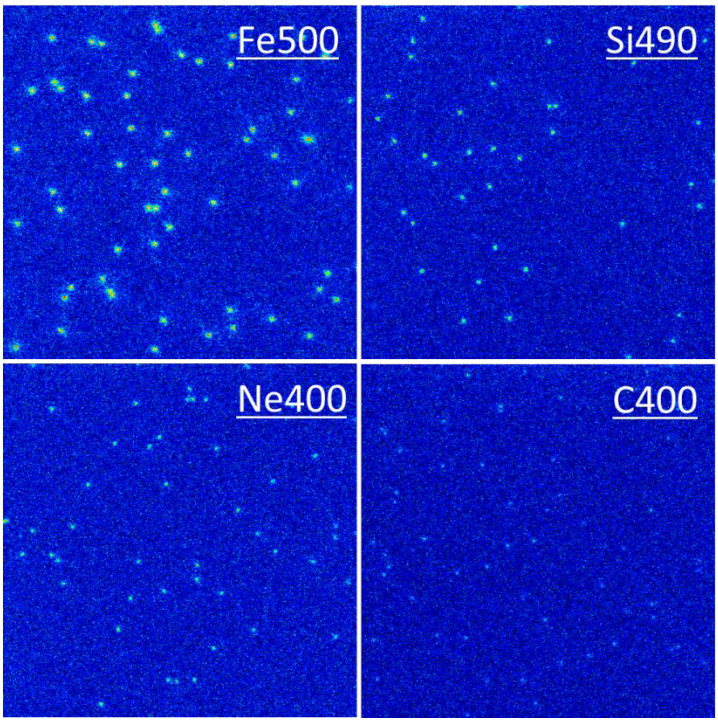

Figure. Fluorescent nuclear track images for Fe 500 MeV/n, Si 490 MeV/n, Ne 400 MeV/n and C 400 MeV/n. The image size is 71 μm by 71 μm.

Conclusion The Ag^{+}-activated phosphate glass has good potential as the fluorescent nuclear track detector for covering high LET range (several 10 – 100 keV μm). The feature of insensitive for low LET particles will allow to measure only high LET radiation in space, where low LET protons and helium ions are occupied. The careful measurement such as one time scan is required due to the quenching effect. More detail study of quenching effect should be investigated for the practical use in radiation dosimetry.

References

1) Y. Miyamoto, T. Yamamoto, K. Kinoshita, S. Koyama, Y. Takei, H. Nanto, Y. Shimotsuma, M. Sakakura, K. Miura, K. Hirao, Radiat. Meas., 45, 546-549 (2010).
2) S. Kodaira, Y. Yanagida, Y. Koguchi, H. Kawashima, H. Kitamura, M. Kurano, K. Ogura, Rev. Sci. Instrum., 89 (2018) 116106.
3) T. Kurobori, Y. Yanagida, S. Kodaira, T. Shirao, Nucl. Instr. Meth., A855, 25-31 (2017).

New luminescent ceramics based on anion-deficient Al_2O_3-BeO for high-dose dosimetry

S.V. Nikiforov, A.D. Borbolin, A.Yu. Marfin, D.V. Ananchenko
Ural Federal University, Ekaterinburg, Russian Federation

Highlights

New anion-deficient Al_2O_3-BeO ceramics were synthesized in vacuum in reducing conditions.
TL glow curve of Al_2O_3-BeO ceramics consists of three TL peaks.
The drop of TL output in TL peak at 520 K is not observed in the samples under study.
TL and OSL dose response is linear from 10 to 300 Gy for gamma-irradiation and is sublinear from 3 to 50 kGy for pulsed electron beam.

Key words Luminescence, High-dose dosimetry, Composite ceramics, Alumina, BeO.

Background and Objectives The increasing use of radiation technologies in industry and science requires the development of detectors for recording high absorbed doses (0.01-100 kGy). Commercial TL and OSL detectors are characterized by an upper limit of recorded doses 1-10 Gy and are not suitable for high-dose dosimetry [1-2]. In this regard the search and creation of new materials suitable for solving this problem is especially relevant.

Nanostructured phosphors are promising materials for the registration of high doses of radiation due to their high radiation resistance [3]. Along with the already known phosphors, it is of interest to investigate the possibilities of using new materials for high-dose dosimetry, in particular, on the basis of ceramic composites obtained from nanopowders of different oxides. The aim of this work is to synthesize anion-defective Al_2O_3-BeO ceramic composites and study their luminescent and dosimetric properties to evaluate the possibilities of their application for the registration of high doses of ionizing radiation.

Materials and Methods We have developed a new method for producing ceramics under study, involves high-temperature treatment (1400-1500 °C, 4 hours) of Al_2O_3 pellets (obtained from nanopowders) in vacuum with the presence of carbon (graphite) in crucibles made from beryllium oxide. It was found by X-ray diffraction that the presence of carbon led to the appearance of BeO phase with a high concentration (about 30%) due to solid-phase reactions during the synthesis of ceramics. In addition, the presence of carbon in the synthesis caused the formation of oxygen vacancies in the ceramics, which was confirmed by pulsed cathodoluminescence measurements.

Results and Discussion TL of the synthesized ceramics exposed to high-dose irradiation contained three peaks at 360 (A), 520 (B) and 720 K (C). Emission at 2.2, 2.4, 3.45 and 3.8 eV associated with oxygen vacancies and their aggregates in Al_2O_3 and BeO were recorded in the TL spectrum of peak B. The TL output of the peak at 520 K did not depend on the heating rate, which may indicate the absence of thermal quenching of luminescence in the samples under study. It was found that the traps responsible for peaks A and B, in contrast to the deep trap C, are subject to optical bleaching during stimulation at a wavelength of 470 nm. At the same time there was a change in the shape and shift of the TL peak B in the high-temperature region. This result, along with the analysis of the TL kinetics by the Tm-Tstop method, shows the presence of the energy distribution of the traps responsible for the specified TL peak. It was established that the range of linearity of the TL dose response after gamma-irradiation is from 10 to 300 Gy. After irradiation with a pulsed electron beam (130 keV), sublinear (k=0.6-0.7) behavior of TL and OSL dose response was observed from 3 to 50 kGy. The variation of TL response in a batch of samples synthesized in one cycle was no more than 10%, in different cycles – no more than 15%. The fading of the obtained ceramics was about 50% for 5 days of storage in the dark. At the same time, it did not exceed 5% for the first 6 hours, which is quite acceptable for the high-dose dosimetry used in radiation technologies.

Conclusion In this paper, new ceramics Al_2O_3-BeO were synthesized by high-temperature treatment of pellets made from nanostructured Al_2O_3 powder under reducing conditions. In this case, the formation of beryllium-containing phases occurs in ceramics as a result of solid-phase reactions between the pressing material (Al_2O_3) and the crucible walls (BeO). The advantage of our synthesis method is the fact that it completely eliminates the handling of highly toxic powders of beryllium oxide. The obtained results show that the synthesized Al_2O_3-BeO ceramic composites have the maximum limit of the recorded doses which significantly exceed limit of commercial detectors based on Al_2O_3 and BeO and not inferior to these detectors in a number of other characteristics.

References

1) S.W.S. McKeever, M. Moscovitch, P.D. Townsend. Thermoluminescence dosimetry materials: properties and uses. Ashford: Nuclear technology publishing, 1995. 204 p.
2) E. Yukihara, S.W.S McKeever. Optically Stimulated Luminescence. Fundamental and Application. Wiley: 2011. 362 p.
3) Kortov V.S. Radiat. Meas. (2010) 45, 512-515.

Influence of Mode Synthesis of Alumina Ceramics Doped with Manganese on Sensitivity to Ionizing Radiation

S.V. Zvonarev[1], V.Y. Churkin[1], V.A. Pankov[1]
[1]*Ural Federal University, Ekaterinburg, Russia*

Highlights The luminescence intensity in the band of 678 nm increases significantly with growth of Mn ions concentration within the range of 0.1-1 wt. %. An intensity of high-temperature peak at 370 °C grows enormously within the sintering temperature range of 1200-1500 °C. Presence of carbon, temperature growth and sintering duration, together with the impurity ion concentration result in the sensitivity increase of Al_2O_3:Mn ceramics to the ionizing radiation.

Key words alumina ceramic, manganese doping, sensitivity to radiation

Background and Objectives Influence of synthesis parameters and structural condition of the material on luminescent and dosimetric properties of low-dimensional nonstoichiometric oxides is an important fundamental and application-oriented task [1]. A special attention is given to the radiation induced defects which contribute to the appearance of the luminescence in similar materials. A change of luminescent and dosimetric properties of these materials can occur as a result of their doping with various impurities. In this work we studied a sensitivity to ionizing radiation of Mn-doped alumina ceramics synthesized at different temperature and time of sintering, dopant concentraions.

Materials and Methods Initial compacts were manufactured by a cold static pressing under a pressure in range of 0.5 GPa from the α-Al_2O_3 powder (purity 99.5 %) with the average particle size of 70 nm. Compacts were immerged in a solution of the manganese (II) nitrate hexahydrate with the ion concentration in range of 0.01-18.77 wt. % duration 30 min after a preliminary drying at the temperature of 450 °C for 30 min. Al_2O_3:Mn ceramics were annealed under vacuum (0.013 Pa) at a temperature range between 1000 °C and 1700 °C for 2 and 4 hours. Some samples were vacuum annealed in the presence of carbon in order to create reducing conditions. SEM, XRD, XRF, pulse cathodo- (PCL) and photoluminescence (PL) methods performed for characterization of samples. Thermoluminescence (TL) measurements by a 'GREY' dosimetry TL system equipped with a Hamamatsu H10722 photomultiplier were made to evaluate a sensitivity of Al_2O_3:Mn ceramics to ionizing radiation. TL curves were obtained at a linear heating with the rate of 1 K/s in range of 300–720 K under radiation of different doses by beans of the electron beam gun and the $^{90}Y/^{90}Sr$ β-source.

Results and Discussion According to the XRD and XRF analysis data high temperature synthesis results in the formation of the two phase structure: corundum and manganese spinel. The luminescence Mn^{4+} ions responsible for the emitting transition $^2E \rightarrow {}^4A_2$ by the luminescence in the 678 nm band [2] is recorded in the PCL spectra. The luminescence intensity in the band mentioned decreases with the sintering temperature growth from 1200 to 1500 °C (for 4 hours) and increases with the temperature growth from 1500 to 1700 °C under the sintering during 2 hours. The luminescence intensity in the band of 678 nm increases significantly with growth of Mn ions concentration within the range of 0.1-1 wt. %. The TL peaks with the maxima at 110-120, 190-200 and 370 °C are recorded during the exposure to high-energy pulse beam of 130 keV and the pulse duration of 2 ns. A low temperature peak at 110-120 °C is not recorded under TL excitation by the $^{90}Y/^{90}Sr$ β-source. Presence of carbon during sintering contributes to the intensity increase of all TL peaks luminescence. In addition an intensity of high-temperature peak TL at 370 °C grows enormously within the sintering temperatures range of 1200-1500 °C. Al_2O_3:Mn ceramics sensitivity to the ionizing radiation increases both with the growth of sintering temperature and with the sintering time under radiation of the test dose equal to 15 kGy for the electron beam and 430 Gy for the β-source. Mn ions concentration increase causes a sensitivity decline of the ceramics under study to the ionizing radiation.

Conclusion Samples of alumina ceramics doped with Mn were synthesized under variation of temperature, sintering time and Mn ions concentration in the solution with the alumina compacts impregnation. Influence of mode synthesis of alumina ceramics doped with manganese on the sensitivity to ionizing radiation was investigated. Presence of carbon, temperature growth and sintering duration, together with the impurity ion concentration resulted in the sensitivity increase of Al_2O_3:Mn ceramics to the ionizing radiation.

Acknowledgments This work was financially supported by the Russian Science Foundation (RSF), project No. 18-72-10082.

References

1) E. de Albuquerque Brocchi, R.N.C. de Siqueira, M.S. Motta, F.J. Moura, I.G. Sol_orzano-Naranjo, Reduction reactions applied for synthesizing different nano-structured materials, Mater. Chem. Phys. 140 (2013) 273–283.
2) S. P. Feofilov, A. B. Kulinkin, A. B. Kutsenko, R. I. Zakharchenya, Selective laser spectroscopy of RE^{3+} and Mn^{4+} in sol-gel technique produced Al_2O_3, J. Lumin. 76–77 (1998) 217–220.

Dosimetric Properties of Undoped and Tb-doped $MgAl_2O_4$ Transparent Ceramics

Takumi Kato[1]*, Noriaki Kawaguchi[1], Takayuki Yanagida[1]
[1]*Nara Institute of Science and Technology, Nara, Japan*

Highlights We prepared undoepd and Tb-doped $MgAl_2O_4$ transparent ceramics by using the SPS technique, and then evaluated the optical and dosimetric properties. The dynamic ranges of the Tb-doped sample as TSL dosimeter was over the range of 0.01 to 100 mGy.

Key words transparent ceramic, $MgAl_2O_4$, Tb, dosimeter, TSL, OSL

Background and Objectives Magnesium aluminate ($MgAl_2O_4$) is a refractory oxide material with good mechanical strength and chemical stability and low electrical conductivity. Hence, $MgAl_2O_4$ is used in various technological applications such as light emitting devices including laser, optical, electrical applications. On the other hand, thermally stimulated luminescence (TSL) properties of undoped $MgAl_2O_4$ single crystal, opaque ceramic and powder forms have been investigated [1,2]. In addition, Tb, Dy and C-doped $MgAl_2O_4$ have been studied as TSL and optically stimulated luminescence (OSL) dosimeter materials [3]. However, these reports did not deal with the transparent ceramic form. In comparison with single crystal, opaque ceramic and powder forms, transparent ceramic dosimeters are considered to have distinct advantages because of defect centers and a transparency. To the best of our knowledge, dosimetric properties of transparent ceramic form of $MgAl_2O_4$ have not studied so far. Therefore, it would of great interest to explore the dosimetric properties of $MgAl_2O_4$ transparent ceramics. In this study, we synthesized undoped and 0.1 % Tb-doped $MgAl_2O_4$ transparent ceramics by the spark plasma sintering (SPS) method and investigated the TSL and OSL dosimetric properties against X-rays. Further, we also studied their photoluminescence (PL) properties in order to revel origins of emission centers. In general, SPS is performed in a highly reductive environment; therefore, oxygen vacancies are effectively generated, and radiation response properties of transparent ceramic are expected to be enhanced compared with those of single crystal. Such effects were observed in different material systems and reported elsewhere [4].

Materials and Methods $MgAl_2O_4$ transparent ceramic samples were prepared by the SPS technique using Sinter Land LabX-100. $MgAl_2O_4$ (99.9 %) and Tb_4O_7 (99.99 %) powders of reagent grade were used. In order to evaluate TSL properties of the undoped and Tb-doped

$MgAl_2O_4$ transparent ceramics, we measured TSL glow curves using a Nanogray TL-2000 after X-ray irradiations with various doses from 0.01 to 1000 mGy. The heating rate was fixed to 1 °C/s for all the glow curve measurements, and the measurement temperature range was from 50 to 490 °C. Moreover, TSL spectra were measured using the CCD-based spectrometer (QE Pro, Ocean Optics) while the sample was heated by an electric heater (SCR-SHQ-A, Sakaguchi E.H Voc) at a constant temperature.

Results and Discussion Figure 1 shows TSL glow curves. The glow peaks of the Tb-doped sample were detected at 75, 230 and 375 °C whereas the ones of the undoped sample were detected at 75, 280 and 400 °C. An integrated TSL intensity from 50 to 490 °C of the Tb-doped sample was 110 times higher than that of the undoped sample. Figure 2 depicts the TSL dose response functions. The tested irradiation dose range was from 0.01 to 1000 mGy. A TSL response of the Tb-doped sample was confirmed to be linear to the X-ray irradiation dose from 0.01 to 100 mGy. Since the glow peak was quite luminous, we could not evaluate higher dose due to the upper detection limit of the instrument.

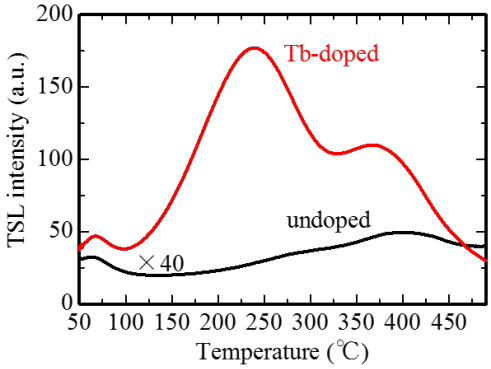

Figure 1. TSL glow curves.

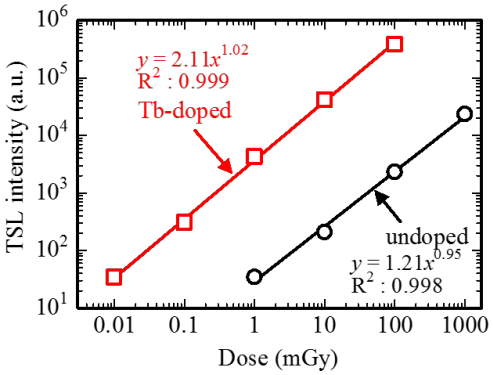

Figure 2. TSL dose response.

Conclusion The Tb-doped sample showed the glow peaks around 75, 230 and 375 °C. The sensitivity of the Tb-doped sample is higher than that of the undoped sample by a factor of 100, and equivalent to the commercial personal dosimeters and the highest sensitivity among reported $MgAl_2O_4$.

References

[1] E.M. Yoshimura and E.G. Yukihara, Radiat. Meas. 41 (2006) 163–169.
[2] A. Ibarra et al., Radiat. Eff. Defects Solids. 119 (1991) 63–68.
[3] S.S. Raj, et al., Radiat. Phys. Chem. 127 (2016) 78–84.
[4] T. Kato et al.,Opt. Mater. 54 (2016) 134–138.

Luminescence Response of MgB_4O_7: Dy prepared by Combustion Synthesis and Solid-State Reactions

B. P. A. G. Nobrega[1], V. K. Asfora[1], V.S.M. Barros[1], R. A. P.,Oliveira[3], W. M. de Azevedo[2],H.J.Khoury[1]

[1]*Nuclear Energy Department, Federal University of Pernambuco,Recife, PE, Brazil*

[2]*ChemistryDepartment, Federal University of Pernambuco, Recife, PE, Brazil*

[3]*Institute of Materials Science, Federal University of São Francisco Valley, Juazeiro, BA, Brazil*

Highlights MgB4O7: Dy prepared by combustion synthesis and solid-state method. Comparison between Infra-red and blue stimulated luminescence.

Key words Luminescence of MgB_4O_7: Dy, combustion, solid-state, radiation detectors

Background and Objectives: Borate based phosphor materials like lithium tetraborate and magnesium tetraborate are widely studied to evaluate its thermoluminescent application for radiation dosimetry. The magnesium tetraborate (MgB_4O_7) doped with rare earth has an effective atomic number equal to 8.4 near human tissue, which is 7.4, and its main TL peak occurs at approximately 200 ° C. Among several synthetically route used to prepare this material the wet reaction (precipitation) and solid-state synthesis stands out. A literature survey showed that there are few studies investigating the OSL response of the magnesium tetraborate and its production by the combustion method. Furthermore, the best temperature of synthesis is not optimized. The aim of this work was to investigate the Thermoluminescence (TL) and the Optically Stimulated (OSL) responses of MgB_4O_7:Dy synthesized by the solid-state and the combustion methods and the luminescent response as a function of the annealing temperature..

Materials and Methods Two routes were used to prepare MgB_4O_7: Dy powder samples: a) solid-state reaction and b) solution combustion synthesis. In both procedures 0.1% mol of $Dy(N_3O_9).5H_2O$ was used as dopants. The procedure used to prepare the solid-state samples follows the procedure described by Porwal et al.[1], while for the combustion procedure follows the methodology described by Vasconcelos et al. [2].The powder prepared by solid-state route was divided in two samples and one was synthesized at 900 °C during 7 h and the second at 900 °C during 4 h + 500ºC during 1h.The powder produced by combustion technique was treated at two different annealing temperatures: a) 900 ºC during 2h and b) 850 ºC during 1h. The structure of MgB_4O_7 samples was confirmed by X-ray diffraction. Pellets with a

diameter of 6 mm and 1 mm in thickness were prepared using teflon as a binder and pressing machine. The TL and OSL signal were measured using an automated Lexsyg Smart OSL/TL reader equipped with an internal $^{90}Sr/^{90}Y$ beta source. TL measurements were performed using a heating rate of 2 °C s^{-1}. The Blue stimulated Luminescence (BSL) curves were acquired under constant illumination intensity mode (CW) with blue LEDs with peak emission at 458 nm using a 380 nm filter pack during 60 s and a channel time of 0.1 s and power setting at 80 mW/cm². For Infrared Stimulation luminescence (IRSL), LEDs with emission peak at 850 nm were used, a Wide-Band-Blue filter pack and power setting at 250 mW/cm².

Results and Discussion: Figure 1 shows the results obtained for the samples irradiated with beta source$^{90}Sr/^{90}Y$ with the dose of 1Gy. It shown that the highest TL and OSL responses is obtained for the sample prepared by combustion route and treated at 900 ^{0}C/2h. This sample presents BSL and IRSL response while the samples prepared by solid-state route don´t present any OSL response.

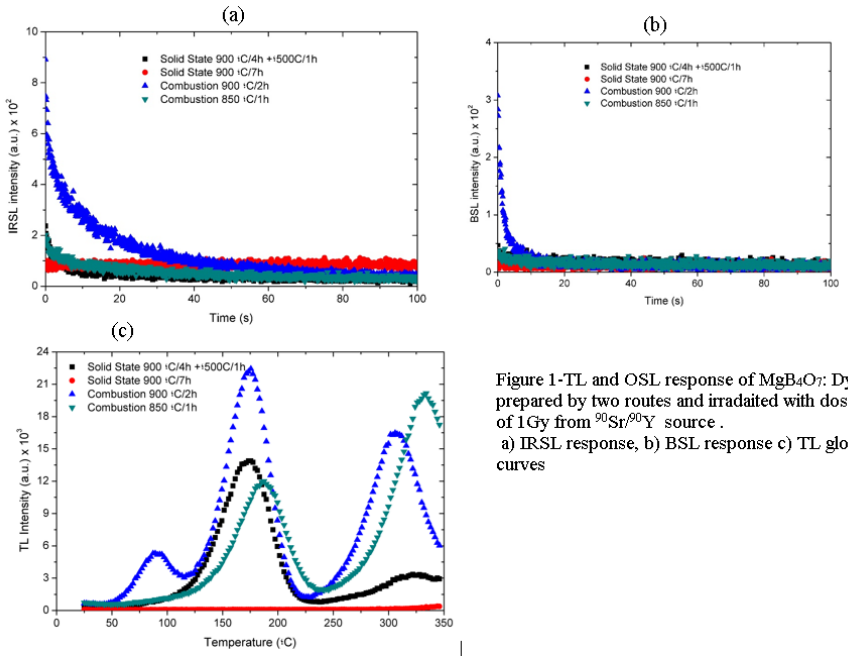

Figure 1-TL and OSL response of MgB_4O_7: Dy prepared by two routes and irradaited with dose of 1Gy from $^{90}Sr/^{90}Y$ source .
a) IRSL response, b) BSL response c) TL glow curves

Conclusion: From the results above It can be conclude that by the combustion route is more suitable technique to prepare MgB_4O_7: Dy samples which presents TL, IRSL and BSL response with sensitivity higher than the produced by solid- state method.

References

[1] Porwal, N. K.; Seshagiri, T. K.; Ntarajan, V. Dhobal, A. R.; Page, A. G. EPR and TSL studies on MgB_4O_7 doped with Tm: role of BO^{2-}_3 in TSL glow peak at 470 K. **Radiat. Measure.** V. 40, p. 69-75, 2005

[2] Vasconcelos, D. A. A.; Barros, V. S. M.; Khoury, H. J.; Azevedo W. M.; Asfora, V. K.; Guzzo, P. L. Synthesis and thermoluminescent response of CaF2 doped with Tm^{3+}. Radiat. Measure**.** v. 71, pp. 51-54, 2014

Radio-photoluminescence and scintillation properties of phosphate glass dosimeter with complexed activator of silver and europium

Wataru Kada[1]*, Yuki Akagami[1], Kazuya Iiduka[1], Daichi Hasegawa[1], Makoto Sakai[2], Raj Kumar Parajuli[2], Masashi Koka[3], Akihito Yokoyama[1,4], Yasuyuki Ishii[4], Takahiro Satoh[4], Kenta Miura[1], Osamu Hanaizumi[1]

[1]*Graduate School of Science and Technology, Gunma University, 1-5-1 Tenjin-cho, Kiryu, Gunma 376-8515, Japan.*

[2] *Gunma University Heavy Ion Medical Center, Gunma University, 3-39-22 Showa-machi, Maebashi, Gunma 371-8511, Japan.*

[3] *Beam Operation Co., Ltd.*

[4]*National Institutes for Quantum and Radiological Science and Technology, 1233 Watanuki-machi, Takasaki, Gunma 370-1292, Japan*

Highlights Fabrication of new type of co-doping activator in phosphate glass radiophoto luminescence (RPL) dosimeter was demonstrated with complex of silver and europium. Through the response of those detector, RPL function was obtained by silver activators as a function of radiation dose, while europium activator constantly emitted the luminescence which could be utilized for in-situ measurement of radiation. Both activators are able to be exist at the same time in same glass substrate.

Key words radio-photoluminescence, scintillation, phosphate glass, co-doping

Background and Objectives Growing interests are being paid for more precise radiation dosimetry as radiotherapy progresses its applications. Dosimeters which equips higher spatial resolution without strong energy dependencies are desired to be implemented to cover the wide range of radiotherapy from X-ray to particle therapy. For quality control and assurance, there also exists a potential demand of in-situ visualization of radiation profile. Radio-photoluminescence (RPL) glass dosimeter is quite comprehensive dosimeter for wide range of radiation [1]. However, build-up effect of RPL prevent us to utilize conventional phosphate glass RPL dosimeter with sliver activator as real time radiation measurement at radiotherapy field [2]. If some of the known luminescent centres as the source of scintillation could coexist with RPL centres of slivers in the same phosphate glass, it could be a solution of this disadvantage. Here we have investigated alternative activators co-doped in phosphate RPL glass dosimeter to accomplish real time radiation measurement.

Materials and Methods House made phosphate glass RPL dosimeters with different activator complex of silver and europium were fabricated to examine such implementation. Industrial-grade powders of sodium metaphosphate ($NaPO_3$) and aluminium metaphosphate ($Al(PO_3)_3$) (Taihei Chemical Industrial Co. Ltd.) were homogenized and placed in crucibles with limited density of additional reagent-grade silver chloride (AgCl) and europium oxide (Eu_2O_3). Appearance of fabricated phosphate glass was illustrated in Fig.1. Phosphate glass dosimeter with two activators remained transparent as conventional RPL glass with silver activator. Photoluminescence from Eu activator was dominantly observed from the samples without irradiation. Those glasses were then exposed X-rays.

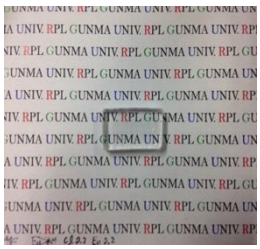

Fig.1.Fabricated glass dosimeter with Ag and Eu co-dopants.

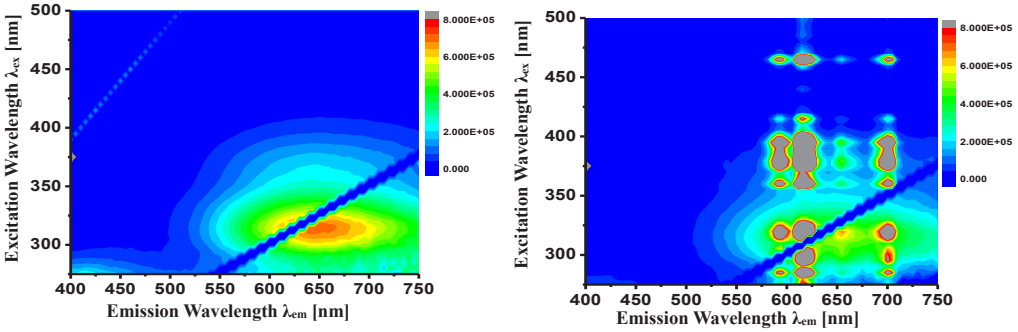

Figs. 2 photo excitation-emission mapping of (left) silver-doped (right) silver and europium co-doped RPL glass exposed with X-ray.

Results and Discussion Typical photo emission-excitation spectrum of fabricated glass was compared with the one with silver, as illustrated in Figs 2. Through the spectrum peak dosimeter function from silver oriented broad peak was observed while PL from europium activator (Eu^{3+} $^5D_0$->$^7F_{2,4}$) sustains its intensity for variety of X-ray exposure time. Those results suggested that RPL-PG with silver and europium co-activators could be utilized for two different functions related with radiation detection in single substrate.

Conclusion Co-doping of different functionalized activator of silver and europium were successfully introduced into well-known phosphate glass substrate. Scintillation from europium had sharp peak while RPL from silver had broad peak in single spectrum.

Acknowledgement Authors deeply thank Dr. Yuichi Kitagawa of Horiba techno service co. ltd for PLE measurements.

References

1) J. A. Perry, RPL Dosimetry, Radiophotoluminescence in Health Physics (Adam Hilger, Bristol, U.K., 1987).
2) T. Kurobori, Performance characterisation of a real-time fiber dosimetry system using radiophotoluminescent glasses, *Jpn. J. Appl. Phys.,* 57 (2018) 106402.

Luminescence enhancement of $LiMgPO_4$ crystal host by trivalent rare-earths ions co-doping

W. Gieszczyk*, P. Bilski, M. Kłosowski, A. Mrozik, B. Marczewska, A. Sas-Bieniarz
Institute of Nuclear Physics Polish Academy of Sciences, Krakow, Poland

Highlights:

- $LiMgPO_4$ crystals were grown from the melt by micro-pulling-down method
- The undoped and rare-earths (REs) ions co-doped crystals were investigated
- The highest luminescence enhancement was observed for Tb, Tm co-doped samples

Key words: $LiMgPO_4$; lithium-magnesium phosphate; rare-earths ions co-doping;

Background and Objectives: The REs doped materials play an important role in the modern optical technologies. Their partially filled f-shells, shielded by the outer filled s- and p- shells, allow spectrally narrow electronic transitions at the wavelengths ranging from the far IR to the vacuum UV. Recently, the REs doped luminescent materials are of increasing interest, because of their possible application for dosimetric purposes, as well as the scintillating materials. A lot of attention is now paid for a lithium magnesium phosphate ($LiMgPO_4$, LMP) compound, as it shows a high radio-sensitivity and a broad linear dose-response range. Radio-luminescence of LMP also allows for real-time measurements. As previous investigations showed that Tm doped LMP crystals possess the highest radio-sensitivity, this work is focused on comparative studies on luminescent properties of REs ions co-doped LMP crystals. The influence of Tb^{3+}, Tm^{3+} ions co-doping on luminescence enhancement of LMP host has been investigated.

Materials and Methods: Within this work the Tb, Tm co-doped $LiMgPO_4$ crystals have been grown from the melt by micro-pulling-down (MPD) method. The luminescent properties of the obtained crystals were investigated by thermoluminescence method after the irradiations with both alpha particles and beta radiation. Incorporation of the doping trivalent REs ions into the host material was confirmed by spectral measurements and their comparison with the spectra of the undoped sample.

Results and Discussion: Figure 1 compares the glow-curves measured for $LiMgPO_4$ crystals with different ions co-doping after the irradiation with the same dose of beta radiation. The undoped sample shows two peaks at around 110 and 180 ºC. It is visible that the addition of RE dopants shifts the second peak to around 300 ºC (peak at around 110 ºC remains unaffected) and also causes a strong increase of luminescence intensity. The highest enhancement was observed for Tb (0.2 mol%), Tm (0.8 mol%) co-doped sample.

An interesting feature was noted in spectrally resolved measurements performed over a broad range of temperatures. At low temperature range (< 300 °C) the luminescence originated mainly from the $^1D_2 \rightarrow {}^3F_4$ transition (460 nm) of Tm^{3+}. At higher temperatures the Tm^{3+} luminescence decreased and $^5D_4 \rightarrow {}^7F_5$ emission (550 nm) of Tb^{3+} started to be dominant in the measured spectra (Fig. 2 left). This behavior is also visible in the shape of glow-curves recorded at 460 and 550 nm (Fig. 2 right), corresponding to the maxima of emission.

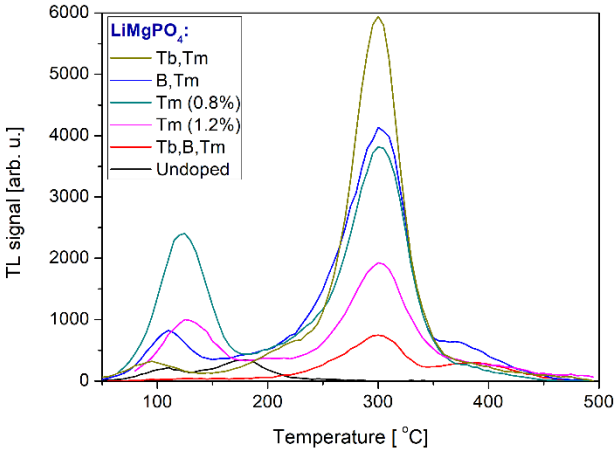

Fig. 1. TL glow-curves of $LiMgPO_4$ host with different doping ions recorded after the same dose of radiation.

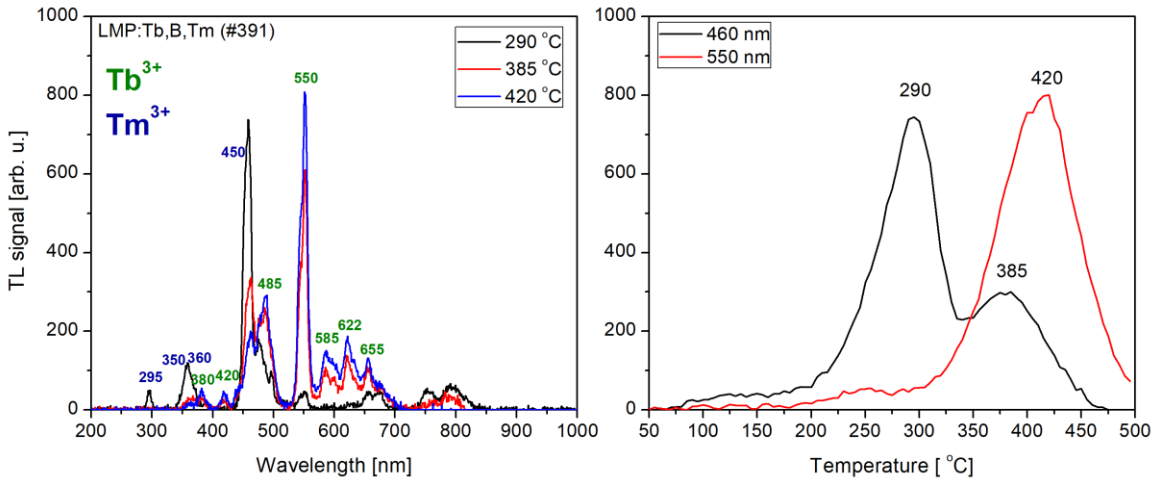

Fig. 2. Temperature dependence of emission of Tb^{3+} and Tm^{3+} ions embedded in $LiMgPO_4$ host (panel left). TL glow-curves recorded at the wavelengths corresponding to the maxima of emission (panel right).

Conclusion: Luminescence enhancement of $LiMgPO_4$ host by RE ions co-doping was studied regarding the response to different radiation qualities. The highest increase of luminescence intensity was observed for Tb (0.2 mol%), Tm (0.6 mol%) co-doped sample. While the different Tm^{3+} concentrations were investigated, the role of Tb^{3+} concentration remains under study.

Acknowledgements: This work was partially supported by the National Science Centre, Poland (contract No. UMO-2016/21/B/ST8/00427)

Development of the composite thermoluminescent detectors based on the epitaxial structures of garnet and perovskite compounds

A. Mrozik[1], W. Gieszczyk[1], P. Bilski[1], S. Witkiewicz-Lukaszek[2], V. Gorbenko[2], Yu. Zorenko[2*]

[1]*Institute of Nuclear Physics Polish Academy of Sciences, Krakow, Poland*
[2]*Institute of Physics, Kazimierz Wielki University, Bydgoszcz, Poland*

Highlights: Composite TL detectors based on the films and crystals of garnet and perovskite compounds were developed using LPE growth method. Difference between TL glow curves of film and crystal-substrate is observed under simultaneous registration of α- and β-particles.

Keywords: composite TL detector, LPE method, garnets, perovskites, Ce and Mn dopants

Background and Objectives: The simultaneous registration of the different components of mixed ionization fluxes strongly demands the development of new types of composite detectors with the ability to separate the signals coming under α- , β-particles and γ-quanta irradiation. Recently we have shown [1, 2] that the epitaxial structures based on the Ce^{3+}, Pr^{3+} and Sc^{3+} doped single crystalline films (SCF) and single crystals (SC) of garnet compounds, prepared using liquid phase epitaxy (LPE) growth method can be successfully applied for this task. The application of composite scintillators presupposes the active mode of *in situ* registration of incoming ionization fluxes. Meanwhile, such a mode of registration is not always possible especially in the case of low doses of radiation and the long-time radiation exposure or due to limitations of analysis of the liquid and gas radioactive materials or high-doses sources.

The above mentioned problems demand consideration of other approaches for producing the composite detectors of ionization radiation. Nowadays we consider the new possibility for simultaneous registration of the different components of mixed ionization fluxes, using differences between the TL glow curves, coming from the film and substrate parts of a composite detector [2]. This work presents the next attempt in creation of such composite TL detectors in the form of the epitaxial structures based on SCs and SCFs of oxide compounds. Namely, we consider in this work the combinations of the Ce^{3+} doped $Lu_3Al_5O_{12}$ and $Lu_2GdAl_5O_{12}$ garnets and Ce^{3+} and Mn^{3+} doped $YAlO_3$ (YAP) perovskites (Fig.1). The choice of mentioned dopants in these materials is due to fact that these ions typically create in oxide compounds the hole and electron trapping centers, respectively. For this reason, the TL glow curves in mentioned materials a priori can be different significantly.

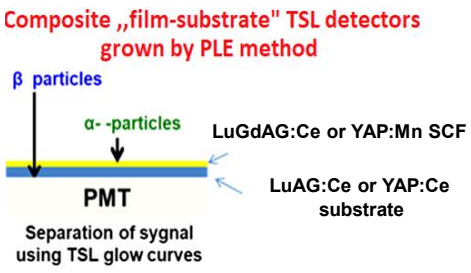

Fig.1 Scheme of composite TSL detector

Materials and Methods: Thermoluminescent detectors, based on the epitaxial structures of Lu_2GdAG:Ce SCF/LuAG:Ce SC garnets and YAP:Mn SCF/YAP:Ce SC perovskites, were grown using the LPE method from the melt-solution based on the $PbO\text{-}B_2O_3$ flux. The cathodoluminescent spectra of SC and SCF part of composite detector were measured using SEM JEOL JSM-820 electron microscope, additionally equipped with Stellar Net spectrometer working in the 200-1100 nm range. For TL measurements we used the Risø TL/ OSL-DA20 reader under α- and β-particles excitation by ^{241}Am and $^{90}Sr/^{90}Y$ sources, respectively.

Results and Discussion: The first results on separation of the TL signals from SCF and SC components for the Lu_2GdAG:Ce SCF/LuAG:Ce SC and YAP:Mn SCF/YAP:Ce SC epitaxial structures after α- and β-excitation are encouraging. We have observed the significant differences in the positions (up to 80-130 degrees) and intensity (more than one order of magnitude) of the main TSL peaks of the glow curves of SCF and SC components of these epitaxial structures after α- and β-particle irradiation. For this reason, we expect that the mentioned combinations of the different garnet and perovskite compounds and/or different dopants, creating of the electrons and hole trapping centers in them, can be considered as the prototypes in the future development of a new generation of composite TL detectors based on the epitaxial structures of different oxide compounds using the LPE growth method.

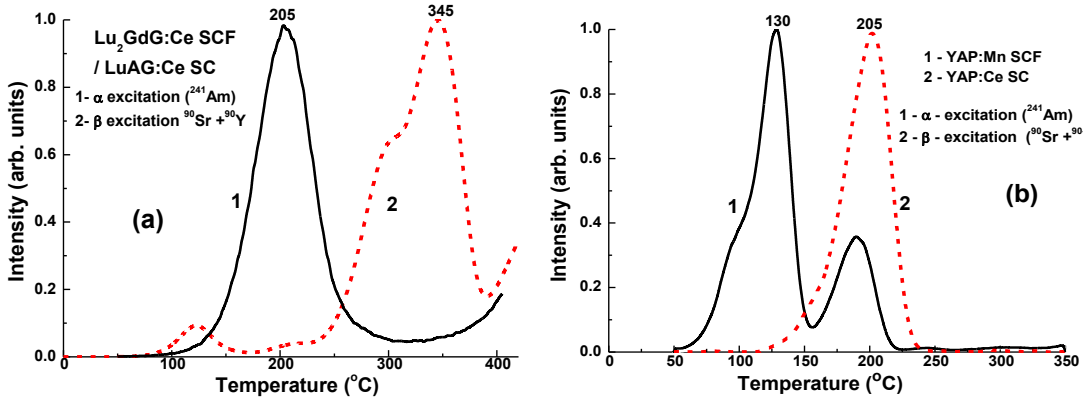

Fig.2 TL glow curves of Lu_2GdAG:Ce SCF/LuAG:Ce SC a) and (b) epitaxial structures under the excitation by α- and β-particles of ^{241}Am (1) and $^{90}Sr\text{-}^{90}Y$ sources (2).

Conclusion: The thermoluminescent properties of composite detectors, based on the LPE grown Lu_2GdAG:Ce SCF/LuAG:Ce SC and YAP:Mn SCF/YAP:Ce SC epitaxial structures were examined under excitation by α- and β-particles of ^{241}Am and $^{90}Sr\text{-}^{90}Y$ sources. The registration of α- and β-particles by the SCF and SC components of composite detectors, respectively, was performed using differences between TL glow curves of SCF and substrate.

Acknowledgements: The work was supported by Polish NCN 2016/21/B/ST8/03200 project.

References

1) S. Witkiewicz-Lukaszek, V. Gorbenko, T. Zorenko, Crystal Growth&Design, 201, 18, 1834.
2) S. Witkiewicz-Lukaszek, V. Gorbenko, T. Zorenko, Yu. Zorenko 2018, IEEE TNS, 65, 2114.
3) S. Witkiewicz-Lukaszek, Yu. Zorenko, P. Bilski, e. a. Radiation Measurment, submitted

Pr^{3+} 5d-4f luminescence in Cs_3PrCl_6 crystalline scintillator

Yutaka Fujimoto[1]*, Daisuke Nakauchi[2], Takayuki Yanagida[2], Masanori Koshimizu[1], and Keisuke Asai[1]

[1]*School of Engineering, Tohoku University, Sendai, Japan*

[2] *Nara Institute of Science and Technology, Ikoma, Japan*

Highlights We studied photoluminescence and scintillation properties of a Cs_3PrCl_6 crystal using by conventional Bridgman–Stockbarger method. The Cs_3PrCl_6 crystal showed an intense scintillation band with a short decay time of 16 and 110 ns in ultraviolet (UV) wavelength region owing to 5d-4f allowed transitions of Pr^{3+}.

Key words Pr^{3+} 5d-4f luminescence, scintillator, chloride crystal

Background and Objectives Scintillation materials plays a central role in the detection and measurement of ionizing radiations such as X-rays and gamma-rays as they provide an efficient means of converting high-energy electromagnetic radiation into UV-visible photons of light that can be detected with photosensitive sensors. For the development of a scintillation detector with good coincidence timing and high count-rate capability, a scintillator with a combination of high light yield and short decay time is strongly required. Some researchers currently focus on CsCl-$CeCl_3$ based self-activated chloride scintillators such as Cs_3CeCl_6 and $CsCe_2Cl_7$ [1] crystals, because of the large atomic number of Ce (Z = 58), as well as their high light yields and short decay times due to the 5d-4f allowed transitions of Ce^{3+}. Thus, in this study, we investigated a newly Cs_3PrCl_6 crystalline scintillator because the decay time of Pr^{3+} 5d-4f luminescence is usually shorter than that of Ce^{3+}. To the best of our knowledge, no other study on the photoluminescence and scintillation properties of crystalline Cs_3PrCl_6 has been reported so far.

Materials and Methods A sample of Cs_3PrCl_6 crystal was grown under vacuum using the vertical Bridgman–Stockbarger method. The excitation and emission spectra were recorded using a Hitachi F-7000 fluorescence spectrophotometer equipped with a xenon lamp as the excitation source. The scintillation spectrum was obtained through X-ray excitation from an X-ray generator (RINT2200, Rigaku) equipped with a copper target at power settings of 40 kV and 40 mA. The scintillation photons from the specimen were counted with a SILVER-Nova multi-channel spectrometer (Stellarnet Inc.), which was cooled to −15°C by a Peltier module through an optical fiber. The scintillation decay time profile, obtained under excitation with pulsed X-rays, was measured using our original set-up with a pulsed X-ray-induced afterglow

characterization system (Hamamatsu Photonics).

Results and Discussion The obtained excitation and emission spectra are shown in Fig. 1. The excitation spectrum, monitored at an emission wavelength of 310 nm, showed at least three excitation bands in the wavelength range from 200 to 275 nm. These excitation bands corresponded to the transitions from 4f ground states to 5d excited states of Pr^{3+} split by the ligand-field interaction and the spin-orbit coupling. Upon UV excitation at 260 nm, the characteristic Pr^{3+} 5d–4f (^3H_J and ^3F_J) emission band was observed at 280 and 310 nm. A shoulder band at around 360 nm is due to allowed transitions from 5d excited state to 4f ($^1G_4$) state. Similar emission bands were reported previously for crystalline $Cs_2LiYCl_6:Pr^{3+}$ [2]. The scintillation spectrum obtained under X-ray excitation is provided in Fig. 2. The spectrum shows two emission bands in the UV region peaked at 280 and 310 nm, which is consistent with the photoluminescence, and can thus be assigned to the transitions from the 5d excited state to the 4f (^3H_J and ^3F_J) ground states owing to Pr^{3+}. Figure 3 shows the pulsed X-ray-induced scintillation decay time profile. The decay time constants were calculated to be approximately 2.3 (13%), 16 (47%), and 110 (40%) ns. The fast decay time component of 2.3 ns is due to an instrumental response function while the other components were due to the Pr^{3+} emission.

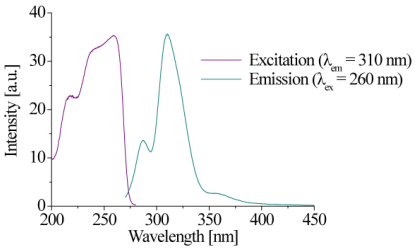

Fig. 1 Excitation and emission spectra of the Cs_3PrCl_6 crystal.

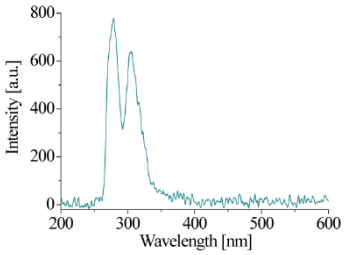

Fig. 2 Scintillation spectrum of the Cs_3PrCl_6 crystal.

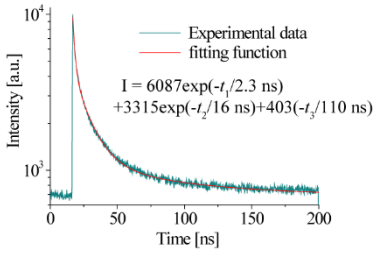

Fig. 3 Scintillation decay time profile of the Cs_3PrCl_6 crystal.

Conclusion We present the results of an initial study of a Cs_3PrCl_6 crystalline scintillator, which was grown using the vertical Bridgman–Stockbarger method. Under excitation by UV light and X-rays, the spectra showed the characteristic Pr^{3+} 5d–4f (^3H_J and ^3F_J) emission bands at 280 and 310 nm. The scintillation decay time constants corresponded to two components, which were approximately 16 and 110 ns.

References

1) M. Zhuravleva, K. Yang, and C. L. Melcher, J. Cryst. Growth, 318, (2011) 809–812.
2) E.V.D. van Loef et al., IEEE Trans. Nucl. Sci., 52(5), (2005) 1819–1822.

Radiation induced change in the optical properties of NaCl:Yb crystal

Yutaka Fujimoto[1]*, Go Okada[2], Dai Sekine[1], Takayuki Yanagida[3], Masanori Koshimizu[1], Hiroki Kawamoto[1], Keisuke Asai[1]

[1]*School of Engineering, Tohoku University, Sendai, Japan*

[2]*Kanazawa Institute of Technology, Nonoichi, Japan*

[3]*Nara Institute of Science and Technology, Ikoma, Japan*

Highlights We reported photoluminescence and radiation-induced photoluminescence (RPL) properties of NaCl:Yb crystals grown by conventional Bridgman–Stockbarger technique. The NaCl:Yb crystals showed an emission band peaking at 435 nm owing to 5d-4f transitions of Yb^{2+} excited at 375 nm. The characteristic Yb^{2+} 5d–4f emission intensity increased after X-ray irradiation.

Key words Yb^{2+} 5d-4f luminescence, radiation-induced photoluminescence (RPL), dosimeter

Background and Objectives Increasing number of applications of ionizing radiation in various fields such as security, radiotherapy, and industry, stimulates a large demand for development of new radiation detection and measurement techniques with superior performance. Some inorganic luminescent materials are commonly used as dosimeter phosphors for ionizing radiation dose measurements due to radiation induced change in the optical properties. There are basically at least three types of dosimeter phosphor; thermoluminescence (TL), optically stimulated luminescence (OSL), and radiation induced photoluminescence (RPL) materials. The TL and OSL arise from the trapping of electrons and holes at metastable levels within host material caused by ionizing radiation irradiation that can be stimulated into recombination by visible-infrared light or heat, respectively. The irradiation dose can be measured with the TL and OSL intensity that is proportional to the concentration of trapped charges. In the case of the RPL, the phenomena arise from a creation of new luminescence center with radiation-induced valence conversion. The RPL intensity that depend on the number of luminescence centers increases as a function of irradiation dose. Although the RPL materials are very interesting because of the high stability of stored dose information, compared with the TL and OSL materials, there are few reports on new RPL materials. In this paper, we present the results of photoluminescence (PL) and radiation-induced photoluminescence (RPL) property measurements on NaCl:Yb crystals as a new RPL material.

Materials and Methods The 0.1 mol% Yb-doped NaCl crystal was grown under vacuum

using the vertical Bridgman–Stockbarger method. The PL spectra were measured with a Hitachi F-7000 fluorescence spectrophotometer equipped with a xenon lamp as the excitation source. The RPL spectra were measured using a HORIBA DeltaFlex fluorescence spectrometer. An X-ray generator (RINT2200, Rigaku) equipped with a copper target was used as the X-ray irradiation source. X-ray irradiation doses of 0.1, 1, 10, and 100 Gy were chosen for the measurements under a controlled voltage (20–40 kV) and current (2–40 mA) of the X-ray generator. The irradiation dose was inferred from air kerma rate at the entrance of sample using an ionization chamber (TN30013, PTW).

Results and Discussion The excitation and emission spectra of the NaCl:Yb (0.1 mol%) crystal are shown in Fig. 1. The excitation spectrum (green line) monitored at an emission wavelength of 435 nm showed at least six bands at 225, 240, 270, 285, 335, and 375 nm. The excitation bands are ascribed to the transitions from $4f^{14}$ ($^1S_0$) ground state to $4f^{13}5d$ excited states of Yb^{2+} split by the ligand-field interaction and the spin-orbit coupling [1]. In the emission spectrum (blue line) under excitation at 375 nm, an intense emission band at 435 nm was observed. The observed blue emission band can be ascribed to the transitions from the $4f^{13}$ ($^2F_{7/2}$) 5d excited states to the $4f^{14}$ ($^1S_0$) ground state of Yb^{2+} [1]. The RPL spectrum (pink line) of the NaCl:Yb crystal exposure to 10 Gy X-rays are shown in Fig. 2. The PL spectrum (blue line) is also presented for comparison. From the spectra, the Yb^{2+} 5d–4f emission intensity was found to increase after X-ray irradiation. The X-ray induced change in the photoluminescence may be attributed to the valence conversion of Yb^{3+} ions that exist in the NaCl host crystal ($Yb^{3+} \rightarrow Yb^{2+}$).

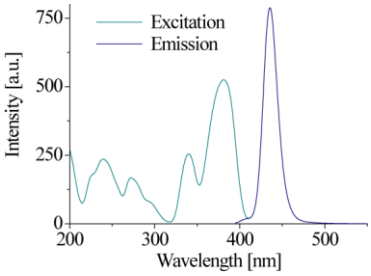

Fig. 1 Excitation and emission spectra of the NaCl:Yb (0.1 mol%) crystal.

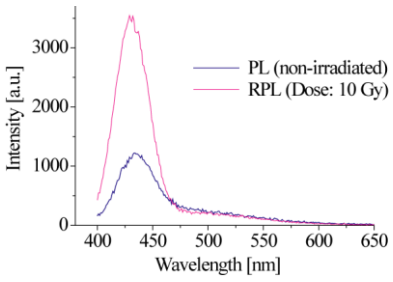

Fig. 2 PL and RPL spectra of the NaCl:Yb (0.1 mol%) crystal.

Conclusion In conclusion, the NaCl:Yb (0.1 mol%) crystal was found to exhibit PL band owing to 5d-4f transitions of Yb^{2+} under excitation at 225, 240, 270, 285, 335, and 375 nm. The X-ray irradiation resulted in an increasing of the PL intensity for Yb^{2+}.

References

1) C. P. An, Volkmar Dierolf and Fritz Luty, Phys. Rev. B, 61, (2000), 6565-6573.

Sponsors

PLATINUM SPONSORS

BRONZE SPONSORS

Sponsors

OTHER SPONSORS/EXHIBITORS

dosilab

PAUL SCHERRER INSTITUT
PSI

Hiroshima Prefecture

The City of Hiroshima

HIROSHIMA

Advanced Fusion Technology

ThermoFisher
SCIENTIFIC

ROTUNDA
SCIENTIFIC TECHNOLOGIES
www.RotundaSciTech.com

Fuji Electric
Innovating Energy Technology

MIRION
TECHNOLOGIES

Jan Dlugosz
University
in Czestochowa

Hiroshima University

ISSDO
International Solid State
Dosimetry Organisation